XXXIX INTERNATIONAL SCIENTIFIC CONFERENCE ON INFORMATION, COMMUNICATION AND ENERGY SYSTEMS AND TECHNOLOGIES

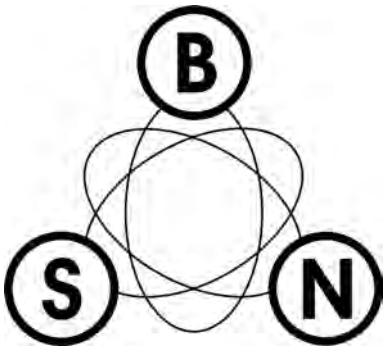

ICEST 2004

Proceedings of Papers

Volume 2

Bitola, 2004

XXXIX INTERNATIONAL SCIENTIFIC CONFERENCE ON INFORMATION, COMMUNICATION AND ENERGY SYSTEMS AND TECHNOLOGIES

-ICEST 2004-

Procedings of Papers – Volume 2 of 2 volumes

Editor: Prof. Dr. Cvetko Mitrovski

Technical Editor: Pargovski Jove

Published by: Faculty of Technical Sciences, Bitola, Macedonia

Printed by: MIKENA, Bitola, Macedonia

Total print run: 260

ISBN: 9989-786-38-0

CIP – Каталогизација во публикација
Матична и универзитетска библиотека
"Св. Климент Охридски", Битола

621.391:004(063)(082)
007.52(063)(082)
004.22(063)(082)
621.397.3:004(063)(082)
621.396.67(063)(082)
004.738.5(063)(082)

INTERNATIONAL scientific conference on information, communication and energy systems and technologies (39 ; 2004 ; Bitola)

ICEST 2004 : proceedings of papers / XXXIX International scientific conference on information, communication and energy systems and technologies ; [editor Cvetko Mitrovski]. - Битола : Технички факултет, 2004. – 2 св.
(XVI, 422 ; XVI, 422 стр.) : илустр. ; 28 см

Библиографија кон трудовите. – Регистар

ISBN 9989-786-38-0
1. Gl. Stv. nasl. 2. Mitrovski, Cvetko
а) Електроенергетски системи – Зборници б) Кодирање – Зборници в) Дигитална обработка на сигнали – Зборници г) Антени – Зборници д) Интернет – Зборници ѓ) Индустриска електроника – Зборници
COBISS.MK-ID 17470017

Dear Colleges,

On Behalf of the Technical Program Committee I was given the pleasure to wish you a welcome on the International Scientific Conference on Information, Communication and Energy Systems and Technology, **ICEST 2004**, which will be held from June 16 through 18, 2004 at the Winter-Summer Tourist Centre "Pelister" near Bitola.

The Conference is organized by the Faculty of Technical Sciences at the Saint Kliment Ohridski University of Bitola, Faculty of Electronics at the University of Nis and by the Faculty of Communications and Communication Technologies at the Technical University of Sofia, in cooperation with IEEE sections of Macedonia, Serbia and Montenegro, and Bulgaria. This year, the Faculty of Technical Sciences-Bitola has an honor for first time to be a host of the Conference under the ICEST acronym and we shall do our best to fulfill the standards established by our partners on the previous two ICEST Conferences.

This year, the Conference Program includes 222 papers for oral and poster presentation which are going to be presented by more than 150 participants of the Conference. Therefore the participants will have rather busy schedule, which I sincerely hope, won't affect their presentations. I also hope that the Conference will be the place where you can strengthen the collaboration among the institutions and the countries you are representing by sharing your ideas and your scientific results.

At last I want to express my gratitude to all our sponsors that has enabled the organization of this conference.

I wish you all a pleasant and a fruitful work on the ICEST-2004!

Assoc. Prof. D-r Cvetko Mitrovski
Conference Chairman

ICEST 2004

XXXIX INTERNATIONAL SCIENTIFIC CONFERENCE ON INFORMATION, COMMUNICATION AND ENERGY SYSTEMS AND TECHNOLOGIES

organized by

Faculty of Technical Sciences
University "St. Kliment Ohridski", Bitola, Macedonia

Faculty of Communications and Communications Technologies
Technical University of Sofia, Bulgaria

Faculty of Electronic Engineering
University of Niš, Serbia and Montenegro.

with support of

- Ministry of Education and Science Macedonia
- Macedonian Science Society-Bitola
- ETAI Macedonia
- ALCATEL Macedonia

in cooperation with

- IEEE Macedonia Section
- IEEE Bulgaria Section
- IEEE Serbia and Montenegro Section

ICEST HISTORY

The ICEST Conference appears to succeed a series of conferences started from 1963 at the Technical University of Sofia under the name "Day of the Radio". In 1977 the name of the Conference was changed into "Communication, electronic and computer systems".
Since 2000 it has become an international conference under the name EIST (Energy and Information Systems and Technologies). The first two EIST Conferences were organized by the Faculty of Communications and Communication Technologies, Sofia and the Faculty of Technical Sciences, Bitola.
In 2002 the Faculty of Electronic Engineering, Niš joined successfully the Conference organizers. Again, the Conference changed its name becoming ICEST (International Scientific Conference on Information Communication and Energy Systems and Technologies).
This year host of the ICEST conference is the Faculty of Technical Sciences, University "St. Kliment Ohridski", Bitola, Macedonia.

ORGANIZERS OF THE CONFERENCE

General Chairman:

C. Mitrovski	*University "St. Kliment Ohridski"- Bitola, Macedonia*

Vice Chairmen:

B. Milovanovic	*University of Niš, Serbia and Montenegro*
R. Arnaudov	*Technical University of Sofia, Bulgaria*

Members:

G. Dimirovski	*University of Skopje, Macedonia*
B. Dimitrijevic	*University of Niš, Serbia and Montenegro*
N. Dodov	*Technical University of Sofia, Bulgaria*
E. Ferdinandov	*Technical University of Sofia, Bulgaria*
M. Gusev	*University of Skopje, Macedonia*
Lj. Kocarev	*University of San Diego, USA*
Lj. Panovski	*University of Skopje, Macedonia*
V. Litovski	*University of Niš, Serbia and Montenegro*
M. Hristov	*Technical University of Sofia, Bulgaria*
L. Jordanova	*Technical University of Sofia, Bulgaria*
G. Milovanovic	*University of Niš, Serbia and Montenegro*
V. Milutinovic	*University of Belgrade, Serbia and Montenegro*
G. Stojanov	*Technical University of Sofia, Bulgaria*
M. Stojcev	*University of Niš, Serbia and Montenegro*
B. Spasenovski	*University of Skopje, Macedonia*
Lj. Trpezanovski	*University "St. Kliment Ohridski"- Bitola, Macedonia*
D. Velickovic	*University of Niš, Serbia and Montenegro*

ORGANIZING COMMITTEE

Chairman:

P. Mitrevski	*University "St. Kliment Ohridski"-Bitola, Macedonia*

Members:

M. Popnikolova-Radevska	*University "St. Kliment Ohridski"-Bitola, Macedonia*
I. Nedelkovski	*University "St. Kliment Ohridski"-Bitola, Macedonia*
G. Trombev	*University "St. Kliment Ohridski"-Bitola, Macedonia*
N. Acevski	*University "St. Kliment Ohridski"-Bitola, Macedonia*
D. Najdenov	*University "St. Kliment Ohridski"-Bitola, Macedonia*
B. Stevanovski	*University "St. Kliment Ohridski"-Bitola, Macedonia*
V. Ceselkoska	*University "St. Kliment Ohridski"-Bitola, Macedonia*
M. Kostov	*University "St. Kliment Ohridski"-Bitola, Macedonia*
M. Stojcev	*University of Niš, Serbia and Montenegro*
L. Lubih	*Technical University of Sofia, Bulgaria*
I. Docev	*Technical University of Sofia, Bulgaria*

CONFERENCE SECRETARIAT

M. Kostov	*University "St. Kliment Ohridski"-Bitola, Macedonia*
M. Atanasovski	*University "St. Kliment Ohridski"-Bitola, Macedonia*

Faculty of Technical Sciences, Bitola, Macedonia
I. L. Ribar, bb, 7000 Bitola
Phone:+389 47 207 701
Fax: +389 47 203 370

TECHNICAL SUPPORT

A. Kolevska	*University "St. Kliment Ohridski"-Bitola, Macedonia*
J. Pargovski	*University "St. Kliment Ohridski"-Bitola, Macedonia*

CONFERENCE INTERNET SITE

For further information, please visit the Conference Internet Site:
http://www. tfb.uklo.edu. mk/icest2004

TABLE OF CONTENTS

VOLUME 2

Control Systems and Robotics

Electronic Components, Systems and Technologies

Telecommunications Systems and Technology

Electrical Machines

Education Quality

Poster Session

Session CSR:

Control Systems and Robotics

Bond Graph Modelling and Simulation of Stochastic Systems using Bondsim – Simulink Tools

Dragan Antić[1], Bratislav Danković[1], Biljana Vidojković[2] and Bojana M. Vidojković[3]

***Abstract* – The extension of the bond graph theory for the modelling of nonlinear stochastic systems is given in this paper. For that purpose the new Bondsim elements are constructed. The efficiency of application of the proposed approach for modelling stochastic dynamic systems is illustrated using an example.**

***Keywords* – Stochastic system, Bond graph, Bondsim library**

I. INTRODUCTION

There are different approaches for deriving mathematical models. The one of them is using the bond graphs [1-4]. The fundamental advantage of this modelling is that it is based on the central physics concept-energy (bond graph consists of components which exchange energy or power using connections which connected them; these connections are bonds). The power is product of two variables: the effort *e* and the flow *f* . The effort (for example: voltage, force, pressure, etc.) and the flow (for example: current, velocity, volume flow rate, etc.) are generalization of similar phenomenon of physics. Therefore, the second advantage is that bond graphs can be used for the different types of systems (electrical, mechanical, hydraulic systems, etc.) and for their combinations (electro-mechanical, mechanical-hydraulic systems, etc.). The third advantage is that complex systems can be divided into simple elements using the bond graphs. The bond graphs give the complete description of dynamical systems and the state space equations can be derived easily. Also, stochastic dynamic systems can be modeled using this modeling technique.

Causes for the stochastic behaviour of a system may be either random excitations from the environment, or statistical variations in the material properties and geometrical configuration of the system itself, or both [5].

Calculation with stochastic dynamic is possible using new stochastic (random) Bondsim elements, which are presented in this paper.

[1]Prof.dr Dragan Antić, dipl.ing is with the Faculty of Electronic Engineering, Beogradska 14, 18000 Niš, SCG, E-mail: dantic@elfak.ni.ac.yu

[1]Prof.dr Bratislav Danković is with the Faculty of Electronic Engineering, Beogradska 14, 18000 Niš, SCG, E-mail: dankovic@elfak.ni.ac.yu

[2]Mr Biljana Vidojković, dipl. ing. is with the Faculty of Science and Mathematics, Višegradska 33, 18000 Niš, SCG, E - mail: biljana@pmf.ni.ac.yu

[3]Mr Bojana M. Vidojković, dipl ing is with the Faculty of Occupational Safety, Čarnojevića 10a, 18000 Niš, SCG, E - mail: bojana@znrfak.znrfak.ni.ac.yu

II. STOCHASTIC SYSTEMS MODELLING

In order to model stochastic systems, bond graph theory must be extended so the stochastic behaviour of a parameter can be incorporated in the model. For such an extension every parameter of a model is assumed to be composed of two parts – the deterministic part and the stochastic part. Thus parameter values for scalar (λ) as well as field $([\lambda])$ bond graph elements, can be approximated to the following form:

$$\lambda = \lambda_d\left(t, \overline{X}(t)\right) + \lambda_S\left(t, \overline{X}(t)\right)V(t) \tag{1}$$

$$[\lambda] = \left[\lambda_d\left(t, \overline{X}(t)\right)\right] + \left[\lambda_S\left(t, \overline{X}(t)\right)\right]\overline{V}(t) \tag{2}$$

where $\lambda_d\left(t, \overline{X}(t)\right)$ and $\lambda_S\left(t, \overline{X}(t)\right)$ represent deterministic and stochastic behaviour of a parameter, respectively, and $V(t)$ is the physical white noise.

The equations of stochastic process motions obtained from a bond graph model can be written in the following form:

$$\frac{d}{dt}\overline{X}(t) = \bar{f}\left(t, \overline{X}(t)\right) + \left[\sigma\left(t, \overline{X}(t)\right)\right]\overline{V}(t) \tag{3}$$

where $\overline{X}(t)$ is a n – dimensional state vector of the response coordinates, $\bar{f}\left(t, \overline{X}(t)\right)$ is a vector function of the state variables, $\left[\sigma\left(t, \overline{X}(t)\right)\right]$ is an $n \times \mu_S$ matrix function and $\overline{V}(t)$ is a μ_S - dimensional independent random processes which influence the model through matrix $\left[\sigma\left(t, \overline{X}(t)\right)\right]$. Eq.(3) is known as *Langevin* equation. The vector $\overline{V}(t)$ is a vector of white noises. The white noise is conceived as a random process with mean value zero and a constant spectral density on the entire real axis. Such a process does not exist in the conventional sense, since it must have the Dirac function as covariance, and hence an infinite variance (and independent values at all points). The white noise is a useful mathematical idealization for describing the random influence that fluctuate rapidly and hence are virtually uncorrelated for different instants at time.

For a system with deterministic parameters, there is no need for any modification of the graph as long as there is no occurrence of differential causality. If some parameters of the system fluctuate randomly with time, then the scheme of causality needs a modification [5]. In bond graph modelling reciprocal of white noise is strictly not allowed. If any of the system parameters exhibits stochastic behaviour and if in the bond graph model the parameter gets inverted, the alternative

measure has to be taken to avoid such reciprocation. The causality assignment of a bond graph model should be such that the multiplications of white noises in the mathematical model do not occur.

The steps for the causality assignment procedure for stochastic models are:

1. Causality is assigned to the port of a source element.
2. Causality may be propagated using elements 0, 1, TF, GY connected to the ports to which causality has been assigned. If any conflict arises at this stage, the model would be declared to be morphologically incompatible and should be modified.
3. Go back to step 1 until all source ports are assigned appropriate causality.
4. Integral causality is assigned to all storage ports.
5. The causality of a stochastic element ports should be assigned so that its parameter does not get inverted.
6. To the remaining element ports and internal bonds the causality should be assigned in order to minimize causal violations at the 0 and 1 junctions.

If any bond graph element has inverted parameter exhibiting stochastic behaviour, new bond graph elements should be added to avoid such reciprocation. Thus the bond graph model becomes more complex.

Further in the paper, the stochastic (random) Bondsim elements are presented. The use of these elements avoids the division with zero which can be appeared because of the stochastic behaviour of parameters.

III. Stochastic Bondsim – Simulink Elements

When the bond graph model is known for a dynamic system, Bondsim Simulink library may be used for directly obtaining of Simulink simulation models from bond graph models, without using the state-space equations. This library was realized for deterministic systems and contains elements (blocks) which were derived from bond graph elements based on the knowledge of the causality and the appropriate functional relations between inputs and outputs. The elements of this library and their application are described in detail in [4], while the method of the direct transformation of causal bond graph models into the block diagrams (Fakri transformation) is described in [3]. In order to get a simpler and more effective direct transformation using the Bondsim tool, a connection with Fakri transformation was proposed [6].

Calculation with stochastic dynamic is possible using new stochastic (random) Bondsim elements given in Fig. 1. On the example of Random Inductance (Ir) Bondsim element, the way for stochastic Bondsim elements obtaining, is described. On Fig.2 the block diagram of Ir element is given. This block diagram realizes the next functional relation between its input and output:

$$f = f(0) + \frac{1}{I_S}\int e dt \qquad (4)$$

where I_S is stochastic parameter:

$$I_S = (1 \pm tol)\cdot I \qquad (5)$$

Parameter I has deterministic value and tol is random number, $0 < tol < 1$, generated by the Uniform Random Number block (Fig.3). This block generates uniformly distributed random numbers over a specifiable interval with a specifiable starting seed. The seed is reset each time a simulation starts. The generated sequence is repeatable and can be produced by any Uniform Random Number block with the same seed and parameters.

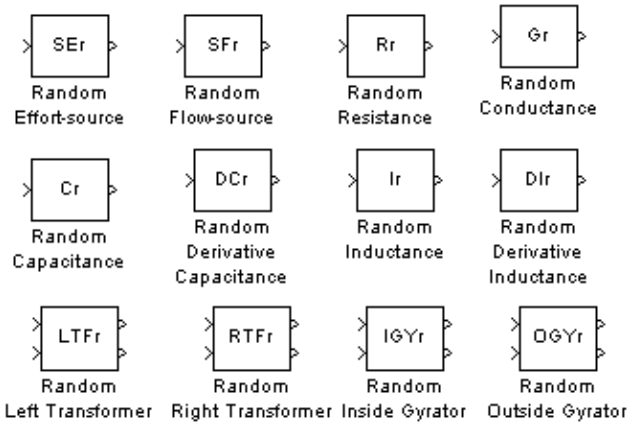

Fig.1. Random Bondsim elements

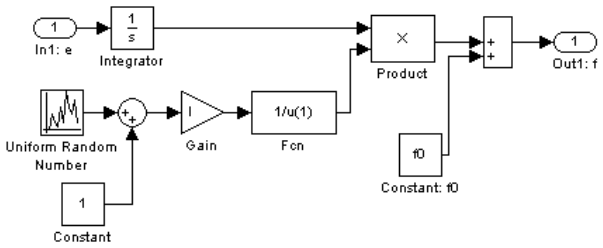

Fig.2. Random Inductance Bondsim element

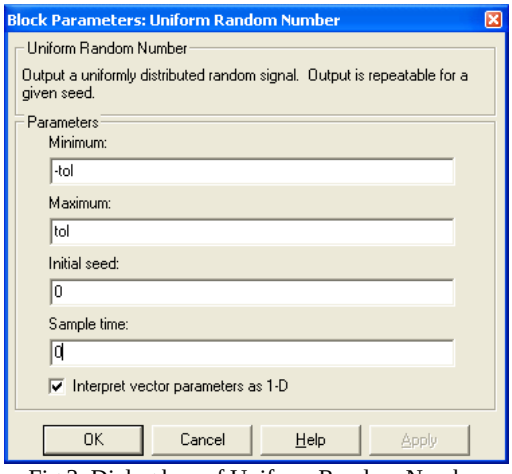

Fig.3. Dialog box of Uniform Random Number

Dialog box of Random Inductance Bondsim element is given in Fig.4.

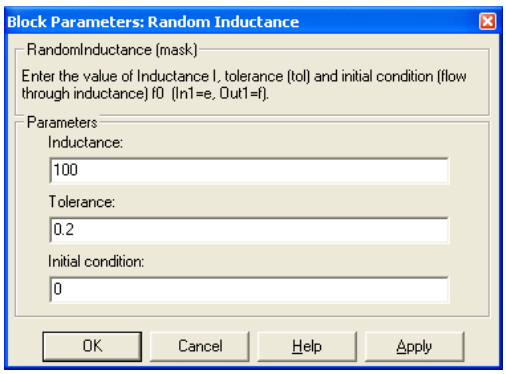

Fig.4. Dialog box of Random Inductance Bondsim element

IV. Simulation Results

The application of stochastic Bondsim elements will be illustrated using an electrical circuit example shown in Fig.5. The parameter values are: I=980A, C=0.351F, n=1963, L=100H, $R_1 = 1/11.6\Omega$, $R_2 = 5000\Omega$ and the initial conditions are: capacitor voltage equal to 0V and coil current equal to 0A.

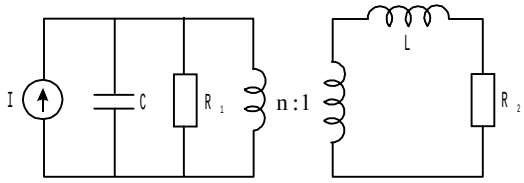

Figure 5. The electrical circuit.

The causal bond graph model of given example is shown in Fig. 6.

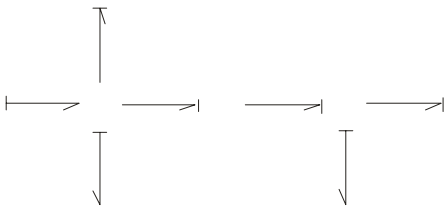

Figure 6. The causal bond graph model.

Two cases are considered: a) stochastic inductivity parameter with parameter tol =0.2 and b) stochastic flow-source with parameter tol=0.05. Bondsim simulation model with Ir element is given in Fig.7.

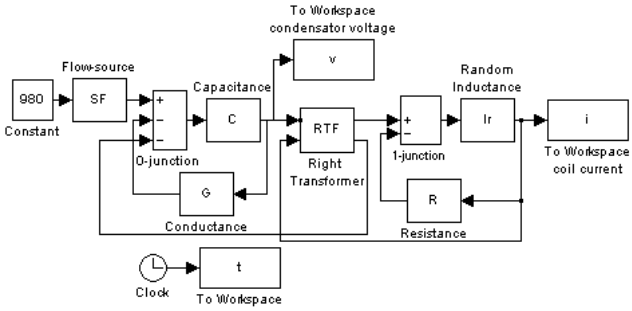

Figure 7. Bondsim simulation model with Ir element

On Figs. 8a) and 8b) the simulation results of coil current for deterministic case (without stochastic) and coil current for stochastic case (with stochastic Ir element) are given respectively.

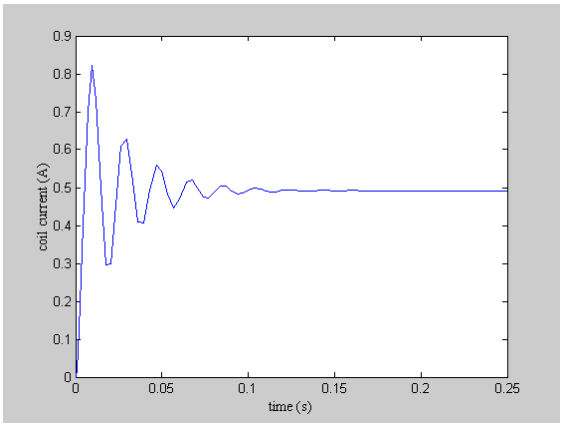

Fig.8a). Coil current for deterministic case (without stochastic)

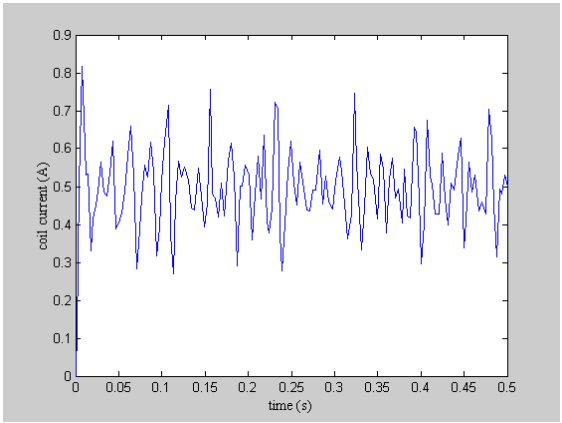

Fig.8b). Coil current for stochastic case (with stochastic Ir element)

The simulation results of capacitor voltage for deterministic case (without stochastic) and capacitor voltage for stochastic case (with stochastic Ir element) are given respectively on Figs. 9a) and 9b).

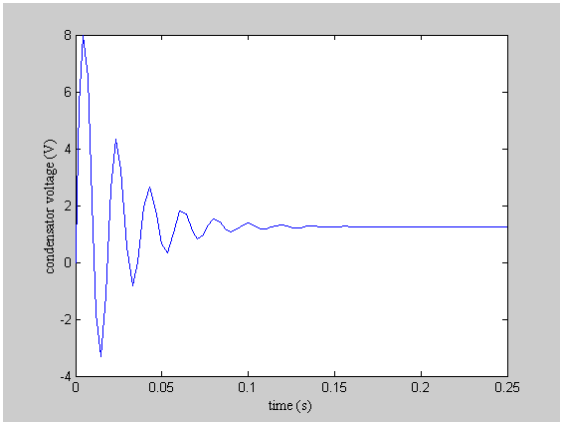

Fig.9a). Capacitor voltage for deterministic case (without stochastic)

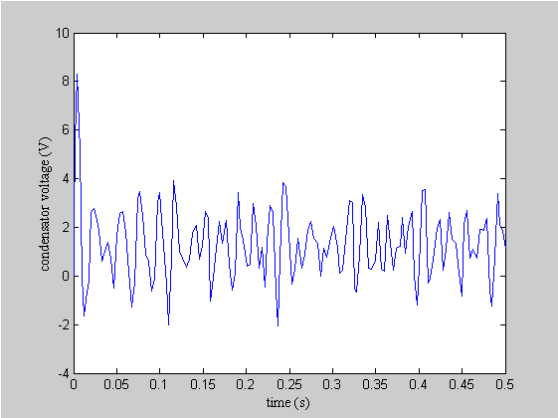

Fig.9b). Capacitor voltage for stochastic case (with stochastic Ir element)

In the second case the stochastic excitation (Random Flow-source) is considered. On Fig.10 the block diagram of SFr element is given.

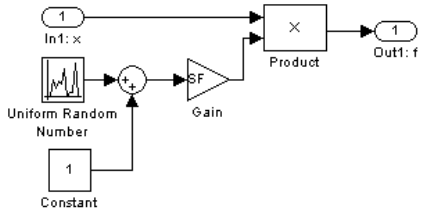

Fig.10. Random Flow-source Bondsim element

Bondsim simulation model with SFr element is given in Fig.11.

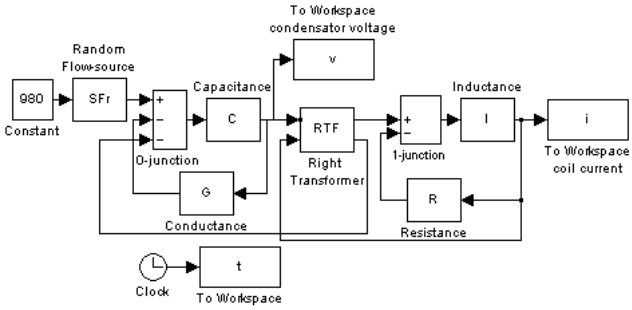

Fig. 11. Bondsim simulation model with SFr element

On Figs. 12a) and 12b) the simulation results of coil current and capacitor voltage for stochastic case (with stochastic SFr element) are given respectively.

V. CONCLUSION

Using the stochastic Bondsim library a visually more distinct simulation model is obtained and it enables simpler manipulation of stochastic elements of the simulation model. The application of stochastic Bondsim library retained the computational as well as the topological structure of the system. The simple application of proposed method is illustrated using a concrete example of modeling and simulation.

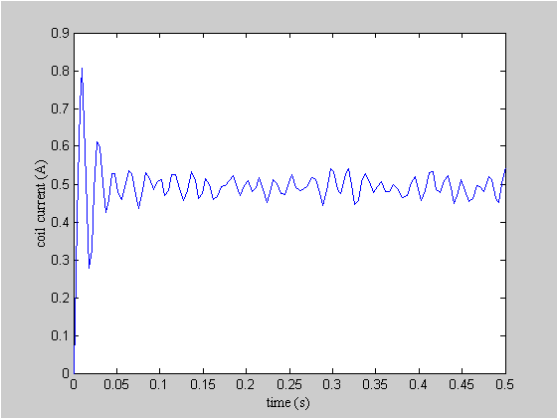

Fig.12a). Coil current for stochastic case (with stochastic SFr element)

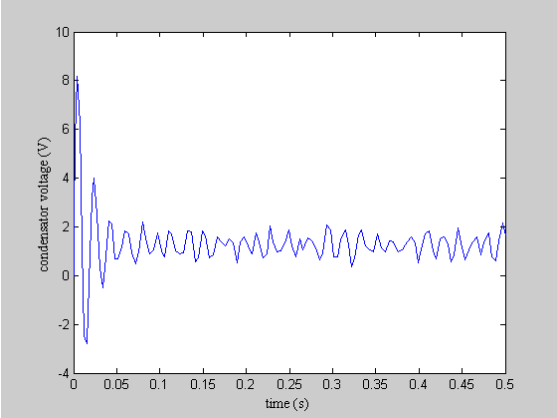

Fig.12b). Capacitor voltage for stochastic case (with stochastic SFr element)

REFERENCES

[1] P. J. Gawthrop, L. Smith, "Metamodelling: Bond graphs and dynamic systems", Prentice Hall International, London, 1996.

[2] J. U. Thoma, "Simulation by bond graphs: Introduction to a graphical method", Springer-Verlag, Berlin, 1990.

[3] A. Fakri, F. Rocaries, A. Carriere, "A simple method for the conversion of bond graph models in representation by block diagrams", *International Conference on Bond Graph Modeling and Simulation (ICBGM'97)*, pp.15-19, Phoenix, 1997.

[4] B. Vidojković, D. Antić, B. Danković, "Bondsim-Simulink tools for bond graph modelling and simulation", *Proc. 7th Symposium of Mathematics and its Applications*, pp.243-248, Timisoara, 1997.

[5] R. Nantu, "Structured Approach to Stochastical System Dynamics", Ph.D. Thesis, Department of Mechanical Engineering, Indian Institute of Technology, Kharagpur, India, July, 1998.

[6] D. Antić, B.Vidojković, "Obtaining System Block Diagrams based on Bond Graph Models and Application of Bondsim Tools", *International Journal of Modelling & Simulation*, Vol 21, Number 4, pp.257-262, 2001.

Modeling and Simulating the Work of Robotics Technologic Modules

Tatyana A. Andonova-Vakarelska[1], Dimcho S.Chakarski[2] and Vania K. Georgieva[3]

Abstract: ***In the conditions of the market economy and restructuring of the economy, the Robotics Technologic Modules (RTM) and systems are an appropriate decision for automation of the small and middle businesses and companies. The pre-modeling and exploration of their work lets to be received preliminary idea for the functions of the system as a whole. The simulation modeling is in effective method exploration of RTM without risks, it makes possible to reveal the simultaneous factors and to determine their places.***

Some schematic decisions are revealed, regarding to the work cycles. For the most used typical decisions, is proposed simulation model for exploring the work state and the effectiveness of RTM. The state of the structural nuits are defined and model scenaria for are revealed.

Key words: robotics technologic module (RTM), structure of RTM, structural elements, simulating, examining.

I..INTRODUCTION

There is a big diversification of the objects and the tasks for their automation. For their solution we have to approach from a point of view of their special features as well as giving an account of the fraternity and the unified methodology for their realization. All this requires certain investment so before their implementation it is good to perform a computer research with time for different variants. As a result of this research we get the whole notion about how RTM function as well as their structural components (experimenting without risk).

The purpose of their development on the basis of existing structures of RTM is, through modeling and simulating, to examine the working of RTM with an eye to the choice of an effective solution.

II. STRUCTURES OF RTM

The Robotics Technologic Modules represent a totality of technologic unit (TU), an industrial robot (IR) and a pallete trolley (automating devices), unified by a general system for automated control.

[1]Tatyana A. Andondva-Vauarelska is with the Faculty of Mechanical Engineering, boul. "Kl. Ohridski" N8, 1756 Sofia, Bulgaria, E-mail: tvakarelska@abv.bg

[2] Dimcho S. Chauarsky is with the Faculty of Mechanical Engineering, boul. "Kl. Ohridski" N8, 1756 Sofia, Bulgaria, E-mail: adp@tu-sofia..bg

[3]Vania K. Georgieva is with the Faculty of Mechanical Engineering, boul. "Kl. Ohridski" N8, 1756 Sofia, Bulgaria, E-mail: vkib@abv.bg

In the flexible automated manufacturing TU has a compulsory digital program control. In general the type of the station defies the difference in the structures. Sort, type size and models can distinguish the structural components.

When setting up the RTM structure attention should be paid to the technical features of the components which construct it and to the cultivating objects. The analysis of the details allows the determination of the working space and the determination of the structural units of the RTM considering the type of the working space, the loading capacity and the type of the IR grip as well as the type of the storage devices.

TABLE I.
TYPES OF STRUCTURAL SCHEMES OF RTM

№	Simptoms	Structure
1	TU = 1 IR = 1 MA = 1 CM-C CM-C	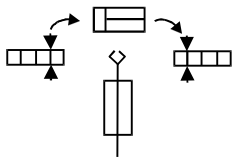
2	TU = 1 IR = 1 MA = 1 CM-C TD	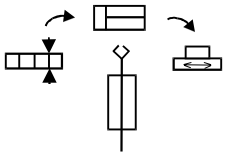
3	TU = 1 IR = 1 MA = 1 CM-C SP	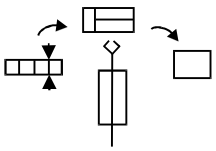
4	TU = 1 IR = 1 MA = 2 CM-C CM-C	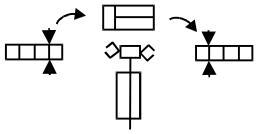
5	TU = 2 IR = 1 MA = 1 CM-C CM-C	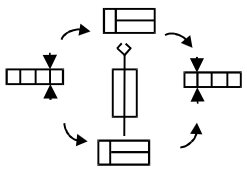

Explanation: MA – mechanic arm (a grip); CM-C – charging magazine collector; CM-C – conveying magazine collector; TD – time device; SP – specialized

Structures of RTM can be built by using the following **basic variation indications:**

- Number of TU

- Number of IR
- Number of grips
- Type of charging magazine devices
- Type of conveying magazine devices
- Position of the structural units
- Type of technologic operations

Additional indications:

- Class of automating device
- Reciprocal disposition of the components; a possibility for connection to other similar RTM;

A structural RTM should be built in the form of a relatively independent system, that has an opportunity for unlimited growing.

In Table.I are shown some of the characteristic structural solutions for RTM.

An important factor when choosing the RTM structure is its productiveness. The cycling productiveness of RTM depends on the cycling time and it does not count the out-of-cycle losses in the time through the fault of instruments, devices, organizing causes and so on. The cycling productiveness Q is determined by this formula:

$$Q_{Ц} = \frac{1}{T_c} = \frac{1}{T_M + T_{s.n..}} \quad (1)$$

Where: T_c - is the time in a cycle;

$T_м$ – mechanic time;

$T_{s.n.}$- Subsidiary non-recovering time, when the machine stops so it can be served by the IR;

It is necessary: $T_{s.n..} \leq T_м$

Through analyzing the productiveness of different structural RTM solutions it can be choose a robotics module with high efficiency and minimal continuance of the subsidiary non-recovering time.

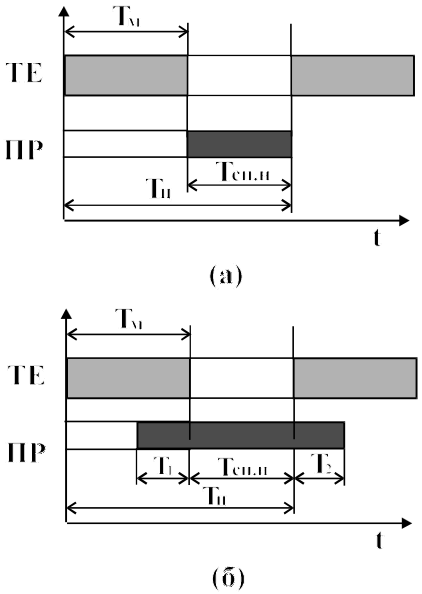

Fig.1. Cyclorama of RTM
a-RTM with IR with a single grip; b – with two grips;
$T_1 + T_2 = T_{s.n}$ subsidiary non-recovering time;

Figure.1. Shows cycloramas for structural variants which were represented in Table.1: (a) - variants of RTM with IR with a single grip; (b) – IR with two grips

In the first case (a) – the time for serving the TU by IR ($T_{t)}$ is equal to the subsidiary non-recovering time: $T_t = T_{s.n.}$

In the case (b) the subsidiary non-recovering time is obligatory decreased which leads to a higher cycling productiveness: $T_t = T_{s.n.} + T_{s.p.}$

Thus a minimum stay of TU is achieved with maximum load of IR

III. STIMULATING THE RTM WORK

The development of the computer technologies has created opportune preconditions for projecting and examining RTM and systems with the help of simultaneous modeling.

The simultaneous modeling is a creative method for examining the accidental operative process and factors in the time. It allows the discovery of accidental operative factors on the work of the robotics system so the results are very close to the actual ones.

The result of the simultaneous modeling is the simultaneous model that serves for the examining of RTM behavior in different situations of work and different disturbances from the outside which can change stochastically. In the simultaneous model more of the dependencies between the parameters are in a vague aspect which makes very difficult their analyzing and the search for the solution.

The mathematic models for simultaneous modeling can be determined and stochastic. More interesting are the stochastic ones. The examinations is made with time when in an arbitrary intervals of time, in the frames of the time for modeling, the state of all structural elements and the system as a whole can be followed. Two types of algorythms are typical for the simultaneous modeling:

- Algorhythms with a constant (determined) step – there is a possibility to follow the condition in a desired interval of every structural element. It is simpler and requires more computer time for completing the examination.
- Algorhythms with an inconstant step – only the intervals of time, where the change is expected to set in the condition of a specific structural component, are examinated.

The robotics systems are determined on the basis of two different multitudes – a multitude of elements and a multitude of the relations between them. Elements of RTM are: TU, IR, PT and more.

For exploring the complex of questions on the examination of RTM and systems the theory of mass servicing (TMS) is used. TMS gives the methods for analyzing the processes of functioning of the manufacturing systems when the time for servicing the applications is a casual quantity and the applications come in accidental moments of time.

The more of the simulation models use casual quantities so they compensate detailed information about what is going to happen in the process of real life. The occurrences, which are modeled in such, ways include: choice, quantities, frequencies, intervals and continuance. Suitable probable apportionment is chosen and the computer is programmed to generate casual quantities from this apportionment.

The following probable apportionments are used: constant, exponential normal, triangular, apportionment of Poisson.

In the mechanical engineering the most broad application find the exponential and the normal (Gauss's) apportionment as in some cases it is possible the application of the constant one.

The stages and the relations between them, when working out the simulation model, are illustrated on Fig.2.

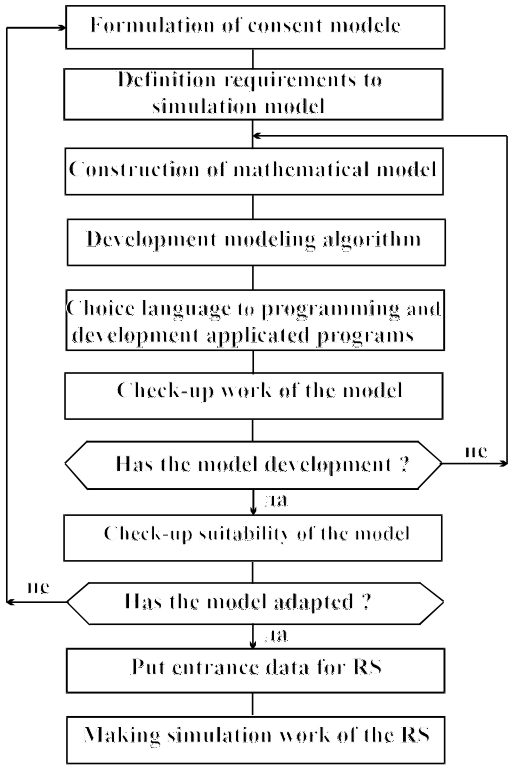

Fig. 2. Block-scheme – stages of working out the simultaneous model

The RTM functioning is considered for an exact interval of time. It can be represented as accidental sequence of discreet moments of time t_i ($i = 1 \div n$), while in every one of these moments changes occur in the state of a single one or some structural elements and in the gaps of time no changes in the state occur. It is necessary to follow the rule: the event that occurs in the t_i can be modeled only after modeling all the events, which have occurred in the moment t_{i-1} . Otherwise the result of modeling can turn out to be false. The mechanism of RTM modeling with determinate step is as follows:

- At the i-step of moment of time t_i all he elements of RTM are examined and it is determined which one of them can change their state in this time.
- All the changes in the state, which can occur in a given moment of time t_i, are modeled
- A transition towards the moment of time is completed $t_{i+1} = t_i + \Delta t$, while the step Δt is performed until the time for modeling is over.

The continuance of the process is interpreted as a casual quantity, put with the function of F (d) or the function of the density of the possibility f (d). For rating the continuance of the process d we use the mathematic expectancy m (d):

$$m(d) = \int_a^b f(d)dd \qquad (2)$$

Where: **a** – is the shortest possible continuance of the process; b – the longest possible continuance of the process.

In general terms the simultaneous model can be represented mathematically in this way:

$$F = f(X_i, Y_i) \qquad (3)$$

Where: F – is the result of the operation of the system; X_i – dirigible changeable parameters; Y_i – non- dirigible changeable parameters, which determine the value of F.

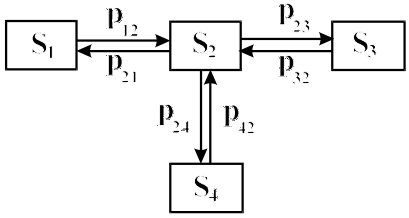

Fig. 3 Similar Markovsky chain for the states of TU

TABLE II.
STATES OF TU

State	Description of the state	Code
S_1	Stops because of lack of blanx	0
S_2	Works	1
S_3	Stops because its own unreliability	2
S_4	Stops for a change of the grip	3

For TU of RTM are determined the following four characteristic conditions, which are shown in the table.II.

The four listed conditions of TU can be described through Markovsky chain - Fig.3.

The matrix of the previous probability for technological unit is:

$$\|p_{ij}\| = \begin{Vmatrix} p_{11} & p_{12} & 0 & 0 \\ p_{21} & p_{22} & p_{23} & p_{24} \\ 0 & p_{32} & p_{33} & 0 \\ 0 & p_{42} & 0 & p_{44} \end{Vmatrix} \qquad (4)$$

The elements of the matrix of the previous probability, when there is no change of the state are defined by the following dependencies:

$$\begin{aligned} p_{11} &= 1 - p_{12} \\ p_{22} &= 1 - (p_{21} + p_{23} + p_{24}) \\ p_{33} &= 1 - p_{32} \\ p_{44} &= 1 - p_{42} \end{aligned} \qquad (5)$$

TABLE.III.
IR STATES

State	Description of the state	Code
S_5	Stops because of lack of blanx	0
S_6	Brings blanx towards TU	0
S_7	Carries worked details towards the palletes	2
S_8	Stops because its own unreliability	3
S_9	Stops for a change of the grip	4

For IR are delimited five conditions – TableIII.

The above given five states of the industrial robot can be represented with the Markovsky chain that is shown on Fug.4.

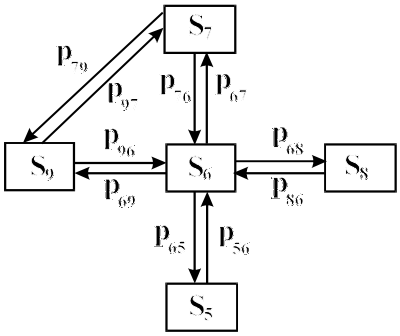

Fig.4. A uniform Markovsky chain of IR states

The matrix of the previous possibility for the industrial robot will look this way:

$$\left\|p_{ij}\right\| = \begin{Vmatrix} p_{55} & p_{56} & 0 & 0 & 0 \\ p_{65} & p_{66} & p_{67} & p_{68} & p_{69} \\ 0 & p_{76} & p_{77} & 0 & p_{79} \\ 0 & p_{86} & 0 & p_{88} & 0 \\ 0 & p_{96} & p_{97} & 0 & p_{99} \end{Vmatrix} \quad (6)$$

The element of the previous matrix, when they do not change their states, is determined by the following dependencies:

$$p_{55} = 1 - p_{56}$$
$$p_{66} = 1 - (p_{65} + p_{67} + p_{68} + p_{69})$$
$$p_{77} = 1 - (p_{76} + p_{79}) \quad (7)$$
$$p_{88} = 1 - p_{86}$$
$$p_{99} = 1 - (p_{96} + p_{97})$$

Modeling the work of RTM is based on the construction of the Petrie's nets, which gives the connections between TU and IR.

On Fig.5. Is shown an exemplary scheme of a Petrie's net for RTM.

In TableIV.are represented some of the results when simulating the mechanic of RTM with the help of computer technology while achieving minimal stops of the TU at maximum load of the IR (the highest coefficient of loading).

TABLE IV.
RESULTS

Stop	Without blax	Dead load	A change in the grip	Summary	Coefficient of loading
ТЕ	61	240	0	301	0,218
ТЕ	181	0	0	181	0,887
ТЕ	301	0	0	301	0,812
ПР	220	60	0	280	0,825
ПР	220	50	0	270	0,815
ПР	220	60	0	280	0,825

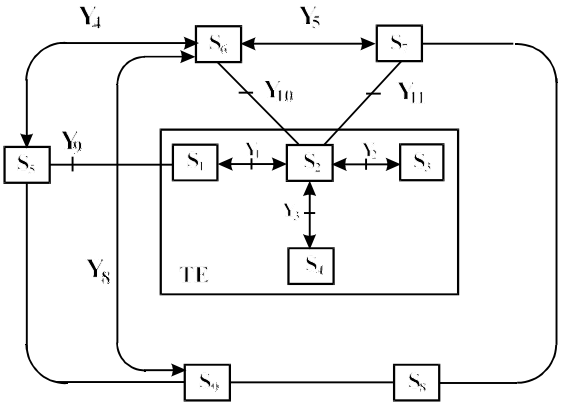

Fig.5. Petrie's net for RTM.
$S_1 \div S_4$ - states of TU; $S_5 \div S_9$ – states of IR; $Y_1 \div Y_3$ - conditions for a change in the state of TU; $Y_4 \div Y_8$ – conditions for a change in the state of IR; $Y_9 \div Y_{11}$ - conditions for a change in the interaction Between TU and IR;

IV. CONCLUSION

When realizing the development the following results were achieved:

- Type-structures of RTM on the basis of the various indications were developed
- The stages and the relations when developing the simultaneous model for RTM were observed.
- A simultaneous model for examining the work of a certain structure of RTM was developed while scrutinizing the states of the structural units and the relations between them were represented using Markovsky chains and Petrie's nets.
- Some of the results completed when simulating RTM were given. They can serve when choosing the effective decision.

REFERENCES

1. Vakarelska, T. "Examining the work of robotics system with the help of computer technologies", A book of reports from a Scientific workshop over "The synthesis and analysis of 2001", Sliven, 2001
2. Chakarski, D. "A method for modeling optimizing while projecting and examining of automating techniques", research work, Sofia, 1999
3. Diulgerov, V. "Robotics modules and systems", Technics, Sofia, 1990.

On A Class of the Discrete Oscillators with Several Attractors

B. Danković[1], Z. Jovanović[2], D. Antić[3]

Abstract – **In this paper a class of discrete nonlinear oscillators is presented, with several steady states. This oscillators has possibility to generate oscillations with different amplitudes and frequencies. Oscillators generate periodical oscillation which are invariant to external disturbances.**

Keywords – **Nonlinear oscillator, discrete attractor, amplitude, frequency.**

I. INTRODUCTION

Continous oscillators which generate harmonic signals with required frequency and amplitude is well known [2,3,4], as linear oscillators and Van der Pole's oscillator. However, these oscillators are sensitive to external disturbances, because each disturbance is a new initial condition. In the paper [1] is presented a class of the nonlinear oscillator with several steady states.

Nonlinear Van der Pole's oscillator has stable oscillations, but this oscillation is not simple periodical.

Oscillator, presented in this paper, can generate plain periodical discrete oscillations with several required amplitudes and frequencies. In other words, oscillator can generate several discrete oscillations, by setting up different initial conditions. These oscillators are robust with respect to external disturbances.

II. NECESSARY CONDITIONS FOR THE EXISTENCE OF OSCILLATIONS OF DISCRETE NONLINEAR SYSTEM

Let consider discrete nonlinear system:

$$\sum_{i=0}^{n} a_i\left(x(k)\right)x(k+i)=0,\;\; a_n\left(x(k)\right)=1 \tag{1}$$

where coefficients $a_i(x)$ are functions of the $x(k)$ i.e.:

$$a_i(x)=\varphi_i\left(x(k)\right)=\varphi_i(x),\;\; i=0,....,n-1 \tag{2}$$

are nonlinear function of state coordinates $x(k)$.

Let consider the linear equation instead equation (1):

$$\sum_{i=0}^{n} a_i x(k+i)=0,\;\; a_n=1 \tag{3}$$

The characteristic polynomial of the (3) is:

$$\sum_{i=0}^{n} a_i z^i=0,\; a_n=1 \tag{4}$$

where a_i are constant parameters. System Eq. (3) is stable if and only if all zeros of the polynomial Eq. (4) is inside unit circle $|z|\le 1$. Stability region of this linear system can be determined by using Schur-Cohn criterion or using the bilinear transformation, $z=\dfrac{s+1}{s-1}$ and Hurwitz criterion. Let us denote stability region in parametric space by S_n (where n is order of system).

Let define a curve $a(x)$ in parametric space by equations:

$$a(x)\Leftrightarrow \begin{array}{c} a_1=\varphi_1(x) \\ a_2=\varphi_2(x) \\ \vdots \\ a_n=\varphi_n(x). \end{array} \tag{5}$$

This is an oriented curve in the direction increase of $|x|$, starting from $x=0$.

The necessary conditions for the existence of attractors are given [1, 5]. Let us denote with l the set of points of the curve $a(x)$, and with $\vec{L}$ the unit tangent vector of curve $a(x)$ in the point $(a_1, a_2,..., a_n)$.

The necessary conditions for the existence of attractors of system (1) are:

$$\begin{array}{l} S_n \cap l \neq \varnothing \\ \vec{L}\,\mathrm{grad}\partial\, \mathrm{S_n} < 0 \end{array} \tag{6}$$

[1]Prof. dr Bratislav Dankovic is with the Faculty of Electronic Engineering, Beogradska 14, 18000 Nis, Serbia and Montenegro, E-mail: dankovic@elfak.ni.ac.yu

[2]Mr Zoran Jovanovic is with the Faculty of Electronic Engineering, Beogradska 14, 18000 Nis, Serbia and Montenegro, E-mail: zoki@elfak.ni.ac.yu

[3]Dragan Antić is with the Faculty of Electronic Engineering, Beogradska 14, 18000 Nis, Serbia and Montenegro, E-mail: dantic@elfak.ni.ac.yu

where $\vec{L} = \left(\frac{\partial \varphi_1}{\partial x}, \frac{\partial \varphi_2}{\partial x}, ..., \frac{\partial \varphi_n}{\partial x} \right)$, while $\varnothing$ is the empty set.

The sufficient condition for the absence of attractors of system (1) is:

$$S_n \cap l = \varnothing.$$
$$\text{or } \vec{L} \, \text{grad} \partial \, S_n > 0 \tag{7}$$

For example, in the case of second order system we obtain characteristic polynomial:

$$z^2 + a_1 z + a_2 = 0 \tag{8}$$

Using the Schur-Cohn criterion can determined stability region S_2:

$$\begin{aligned} a_2 &< 1 \\ a_2 - a_1 &> -1 \\ a_2 + a_1 &> -1 \end{aligned} \tag{9}$$

The stability region S_2 is given in Fig. 1. The oriented curve $a(x)$ is given in the same Figure also.

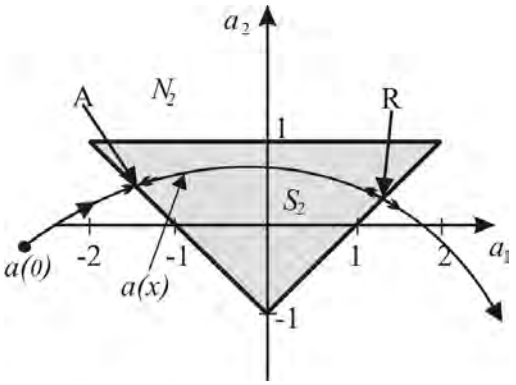

Fig.1 Stability region S_2

where A- attraction point, R- repeller point.

In the case of *n*–th order system, using bilinear transformation $z = \frac{s+1}{s-1}$ we obtain new characteristic polynomial:

$$b_n s^n + b_{n-1} s^{n-1} + \cdots + b_1 s + b_0 = 0 \tag{10}$$

Using the well known Hurwitz criterion, we obtain:

$$D_n = \begin{vmatrix} b_{n-1} & b_{n-3} & b_{n-5} & ... & 0 \\ b_n & b_{n-2} & b_{n-4} & ... & 0 \\ 0 & b_{n-1} & b_{n-3} & ... & 0 \\ 0 & b_n & b_{n-2} & ... & 0 \\ . & . & . & ... & . \\ 0 & 0 & 0 & ... & b_0 \end{vmatrix} \tag{11}$$

The stability region S_n is given with: $D_1 = b_{n-1} > 0$, $D_2 = \begin{vmatrix} b_{n-1} & b_{n-3} \\ b_n & b_{n-2} \end{vmatrix} = b_{n-1} b_{n-2} - b_n b_{n-3} > 0, ...,$ $D_i > 0$, where D_i is *i*-th diagonal minor of D_n.

III. EXAMPLES

Example 1: Consider a discrete nonlinear second order system:

$$\begin{aligned} &x(k+2) + \left(x^2(k) - 1\right)\left(x^2(k) - 4\right)\left(x^2(k) - 9\right)\left(x^2(k) - 16\right) \\ &\left(x^2(k) - 25\right)\left(x^2(k) - 36\right) x(k+1) + x(k) = 0, \end{aligned} \tag{12}$$

Oscillations are given in Fig.2 in phase plain. Note that oscillator can generate six oscillations with different amplitude (denoted by 1, 2, 3, 4, 5 and 6) as shown in the Figure.

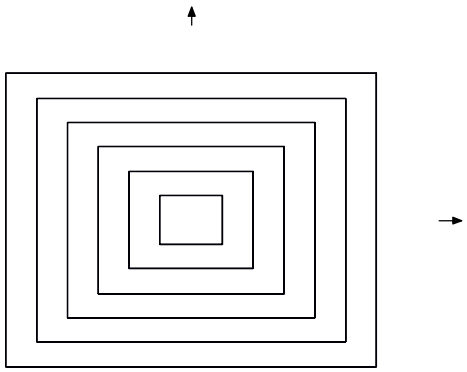

Fig. 2 Oscillations in phase plane

The same oscillations time diagram are given in the Fig.3.

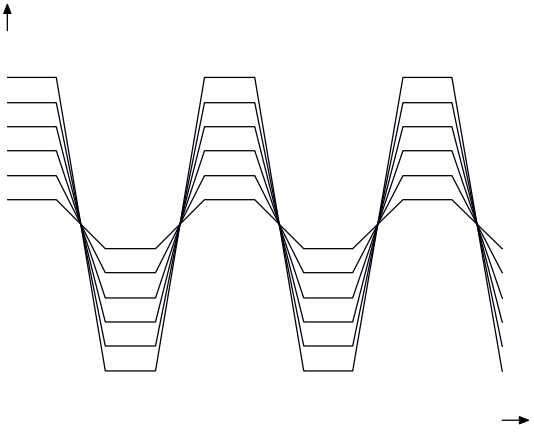

Fig. 3 Oscillations time diagram

Example 2: Let us given discrete time system:

$$\begin{aligned} &x(k+2)+\left(x^2(k)+x^2(k+1)-1\right)\left(x^2(k)+x^2(k+1)-4\right)\\ &\left(x^2(k)+x^2(k+1)-9\right)\left(x^2(k)+x^2(k+1)-16\right)\\ &\left(x^2(k)+x^2(k+1)-25\right)\left(x^2(k)+x^2(k+1)-36\right)\\ &\left(x^2(k)+x^2(k+1)-49\right)x(k+1)+x(k)=0, \end{aligned} \tag{13}$$

Oscillations in the phase plain are shown in Fig.4. The oscillator can generate seven oscillations with different amplitude (denoted by 1, 2, 3, 4, 5, 6 and 7) as shown in the same Figure.

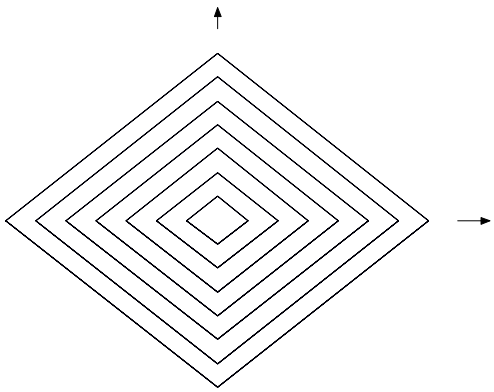

Fig. 4 Oscillations in phase plane

The same oscillations in time diagram are shown in the Fig.5.

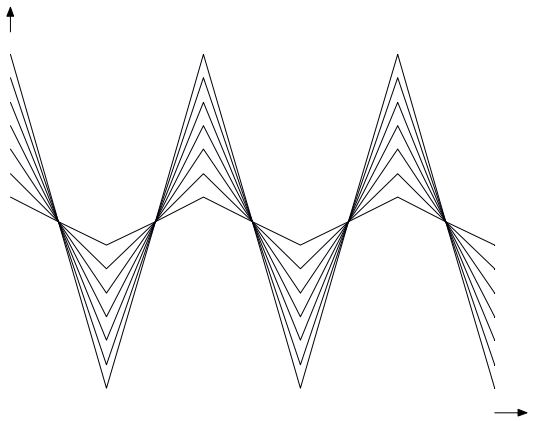

Fig. 5 Oscillations time diagram

IV. CONCLUSION

Discrete nonlinear oscillators which can generate many oscillations with different amplitude and frequencies are considered. Amplitude and frequencies can determine by choosing different initial conditions.

Necessary conditions for existence of steady oscillations and sufficient conditions for absence of the oscillations are given also.

Presented oscillator is able to realized on many different ways. The best solution would be implementation based on microcontroller system, due to its software flexibility the same hardware configuration could be used for various types of oscillators.

REFERENCES

[1] Danković, B., Jovanović, Z., and Mitić, D., "On the Class of Nonlinear Oscillator with Several Steady States", *6th International Conference on Telecomunications in Modern Satellite, Cable and Broadcasting ServicesTELSIKS 2003*, Niš, Serbia and Montenegro, October 1-3, 2003, pp. 802-804.

[2] Leftschetz, S., *Differential Equations: Geometric Theory*, Dover Pub. Inc., New York, 1990.

[3] B.M Dankovic, Z.D Jovanovic., "On the Limited and Asymptotic Quasi-periodical Solutions of Differential Equations", *Proceedings Intern. AMSE Conference "Sygnal and Systems"*, pp.157-161, Warsaw, Poland, July 15-17, 1991.

[4] B.M Dankovic, Z.D Jovanovic, "On stability and Consistancy of Solutions of Diference Equations", *AMSE Review, AMSE Press*, vol. 17, no. 4, pp. 5-10, 1991.

[5] B. Dankovic, B. Vidojkovic, Z. Jovanovic, B. Vidojkovic, "On Conditions for Attractor Existence at Nonlinear Discrete Systems", *Proceedings of XXXVII International Scientific Conference on Information, Communication and Energy Systems and Technologies*, pp , 124-128, Nis, Yugoslavia.

Pseudorandom Position Encoder and Code Conversion Problems

Dragan B. Denić[1], Ivana S. Ranđelović[2] and Milica P. Rančić[3]

Abstract **- Basic methods related to functioning of currently known pseudorandom position encoders with serial code reading are considered. In particular, problems of pseudorandom to natural code conversion are discussed. It is indicated to the possibility of code conversion time reducing in regard to the standard method of serial pseudorandom to natural code conversion.**

Keywords **- position measurement, pseudorandom code, optical encoders**

I. INTRODUCTION

In order to avoid use of large number of code tracks and still obtain high-resolution measurements, a new type of absolute encoders, named pseudorandom absolute encoders, was developed. It considers use of cyclic or serial codes, which possess a feature that two *n*-bit code words that correspond to two successive positions contain an identical sequence of (*n-1*) bits. In other words, the last (*n-1*) bits of the current code word are equivalent to the first (*n-1*) bits of the subsequent code word. A possibility of overlapping of all 2^n code word records on one code track is evident, [2]. To begin with, such encoder has an enormous advantage not only because it solves the problem of increasing the number of code tracks for the purpose of high-resolution system, yet it always has only one code track regardless to the resolution. Due to well-known and simple rules for its later conversion into the natural code, the pseudorandom code is applied. However, we would still need *n* sensors for the instant reading of *n* output code bits, which, in case of high resolutions, becomes a technical problem of allocating *n* sensor heads within a small physical area.

Fortunately, cyclic code properties provide a new way for code bits reading using only one detector, [3]. This method considers code bits collecting into a code-forming shift register. Only one bit is being read for each new position of the movable system and entered into the mentioned shift register. After the initial movement that corresponds to space width of *n* bits, forming of the code word, which corresponds to the current position of the movable system, will be done. For each of the following positions a new bit is being read, and along with (*n-1*) bits of the previous code word, an output code word of the new position is obtained. Evidently, there is a necessity of initial moving after the first plugging in, meaning that the movable system (MS) crosses a distance equivalent to space width of *n* code bits, so that the first valid output *n*-bit code could be formed. This is the reason that these absolute encoders are called virtual absolute encoders. In the case of high-resolution encoders, mentioned distance of initial movement is very small. However, this is still a virtual absolute encoder's disadvantage. This disadvantage becomes almost negligible regarding the new quality that is provided by the virtual absolute encoder. After pseudorandom code reading is done, it is necessary to convert it into the natural code. In the case of high-resolution encoders, the method of parallel conversion using memory elements is not acceptable. Since the pseudorandom code is so specific [1], it is possible to apply serial code conversion method [2]. A disadvantage that comes from the significant code conversion time could be lightened using the code conversion algorithm proposed in the paper.

II. BASIC FUNCTIONING PRINCIPLE OF THE VIRTUAL ABSOLUTE ENCODER

Virtual absolute pseudorandom encoder is nowadays a big hit that, day by day, straightens its position on the market in regard to the classic absolute encoders. So that main problems would be pointed out, a concrete simple example of the virtual absolute encoder will be discussed.

A rotary disc consists of two tracks, Fig. 1. Let us consider that these two tracks consist of transparent and non-transparent segments. Also, let us consider that appropriate optical methods for detection are applied. Interior track is identical to the one of incremental encoder, [4], and it is used in this example for generating two bits in the output code word with the smallest weight. Its main role is providing synchronized code reading and it is often called synchronization or clock or time track, [5].

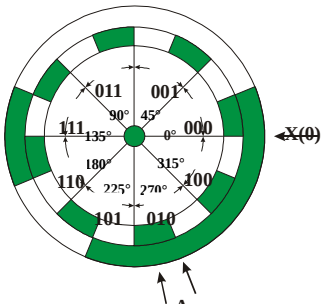

Fig. 1. Virtual absolute encoder disc

In this simple example, which considers 5-bit binary encoder, it is adopted that the space-time width of one incremental cycle is equivalent to the space width of one code track bit. Otherwise, that ratio can change. External code track is coded in a way to provide residual important bits needed for forming

[1] Dragan B. Denić is with the Faculty of Electronic Engineering, University of Niš, Aleksandar Medvedev 14, 18000 Niš, Serbia and Montenegro, e-mail: ddenic@elfak.ni.ac.yu

[2] Ivana S. Ran|elović is with the Faculty of Electronic Engineering, University of Niš, Aleksandar Medvedev 14, 18000 Niš, Serbia and Montenegro, e-mail: rivana@elfak.ni.ac.yu

[3] Milica P. Rančić is with the Faculty of Electronic Engineering, University of Niš, Aleksandar Medvedev 14, 18000 Niš, Serbia and Montenegro, e-mail: milica@elfak.ni.ac.yu

of the complete absolute output code word. Applied cyclic code, named shift register code [1], provides a unique code word for each new position of the encoder, which alludes reading of a new bit from the code track.

For obtaining the output position code, three detectors are being used. Serial bit reading from the code track is done by detector X(0). Obtaining a signal from the synchronized track is realized using two detectors, as in case of conventional incremental encoder, [4].

In this example, classic quadrature signals are required (two sine signals dislocated by 90°), because two additional bits are planned that would magnify the position measurement resolution four times. These two signals are also used for determining the rotation direction of the encoder disc. These signals are then shaped into rectangular signals, and whenever a transition of signal A (with signal B on logical "0") is detected, reading of a new code bit is being performed. In order to entirely explain a principle of serial code reading, an example of realization of electronic block of this virtual absolute encoder is shown in Fig. 2.

A LED diode used as a light source for track synchronization is always actuated and it illuminates two detectors forming quadrature signals A and B at the comparator outputs C_1 and C_2. As said before, code reading is done whenever a transition of the signal A (with signal B on logical "0") takes place. Because of this, signal A goes to the input of a signal edge detection circuit, and then, the output signal of this circuit along with the signal B complement are led to the input of the AND circuit I_1. Whenever an impulse at the logical AND circuit output appears, a new bit reading is done. A simple realization of the signal edge detector is presented here. Rectangular signal A from the comparator output C_1 is brought to both inputs of the same EXOR circuit E_1, but with small delay at one of the inputs. In this case, the delay is generated using integrator in the form of RC circuit.

Whenever an impulse appears at the transistor T base, it leads, whereby the LED diode, which illuminates the code track, is excited. Considering that at that moment the code track detector is located at the middle of the sector that defines current code track bit, reliable reading of that bit can be done. A logical value of the read bit is located at the comparator output C3. That bit is brought to the appropriate shift register input depending on the disc rotation direction. Considering that impulses at the signal edge detector output always appear at the moment immediately after the detected transition on the synchronization track, then, based on the logical value of the quadrature signal A, encoder rotation direction is being determined, Fig. 1. If A equals "1" when the impulse appears, then the rotation direction is clockwise (CW). Then, an impulse appears at the output of the logical AND circuit I_4, shift register shifts to the left and newly read bit is accepted at the appropriate shift register input. In the case of reverse encoder disc rotation, an impulse occurs at the output of the logical AND circuit I_5. After the initial movement of (*n-2*) bits in the same direction, a correct code word is formed and valid position information is at the output. It is obvious, that it is necessary to preconvert a cyclic code at the shift register output into a desired output code, usually into the natural binary code. There are few known methods for code conversion, [6, 7], one of which named parallel conversion method that uses a table memory located in PROM, is applied here. At the end, two bits of the smallest weight are obtained at the quadrature detector output, which consists of one EXOR circuit and one logical NOT circuit.

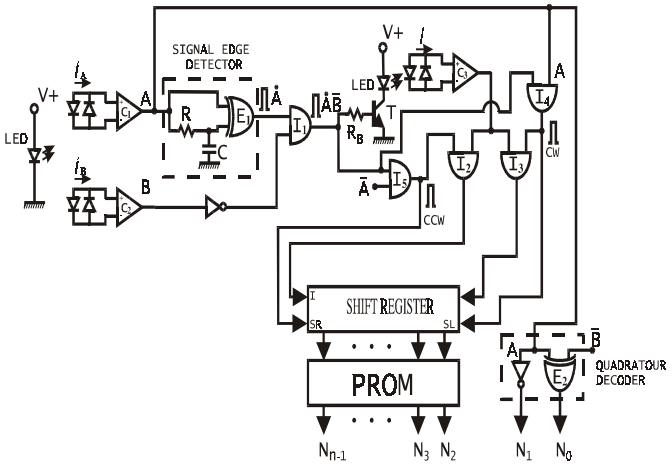

Fig. 2. An example of the virtual absolute encoder electronic block realization

Basic reason for using of the impulse stimulus of the LED diode is that there is one gap for bit reading, in contrast to conventional incremental optical encoders where a number of gaps is used for fine tracks observing (multiple-line slits). Impulse stimulus allows greater pick values for current, whereby greater momentary illumination is achieved and thus, a probability of amplitude loss due to usage of only one gap (single-line slit) is reduced. Only in the case of low-resolution measurements when gap is width enough to provide enough signal amplitude from photo detector, DC activating of the LED diode is possible.

Illustrated example in a simple way presents the manner in which the virtual absolute encoder functions. A possibility of applying the parallel code conversion method is indicated, although, generally, it is not the best solution, especially in the case of encoders for high-resolution position measuring. Therefore, an application of the serial code conversion method is suggested, where the PROM memory, shown in Fig. 2., is simply replaced by the appropriate serial code converter.

III. A NEW SERIAL CODE CONVERSION METHOD

A pseudorandom binary sequence of length 2^n-1 is considered, that is:

$$\{S(p) / \ p = 0,1,.....2^n - 2\} \qquad (1)$$

Since it is written with one bit per sector, a code track is divided in 2^n sectors. Term $S(p)$ represents content of the n^{th} element of the shift register after p shifts to the left. Considering that pseudorandom sequences are periodical, it is of no importance which *n*-bit word is adopted as the initial one.

$$\{S(n-k) / k = n,.....,1\} \qquad (2)$$

Further, it can be considered that the pseudorandom binary sequence is generated using a shift register with a feedback, according to the following algorithm.

$$X(0) = X(n) \oplus c(n-1)X(n-1) \oplus \ldots\ldots\ldots\ldots \otimes c(1)X(1),$$
$$X(i) = X(i-1), \text{ for } i = n,\ldots\ldots\ldots 1,$$

where feedback coefficients $c(n-1)$ are foreclose defined, as shown in Table I.

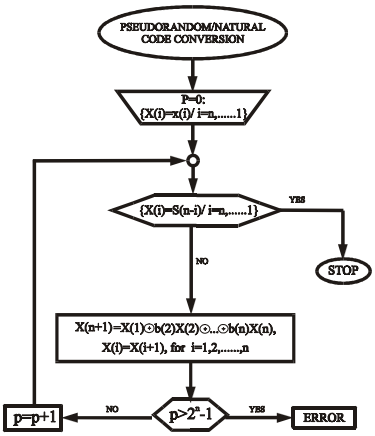

Fig. 3. The code conversion algorithm

$$X(0) = X(n) \oplus c(n-1)X(n-1) \oplus \ldots\ldots\ldots\ldots \otimes c(1)X(1)$$
$$X(i) = X(i-1), \text{ for } i = n,\ldots\ldots\ldots 1,$$

Conversion of these n bits into the natural code, following the serial code conversion method, is performed based on the property of the PRBS generating algorithm that it is reversible. The code conversion algorithm is shown in Fig. 3. The content of the register for code word generating, for the given position p, will be

$$\{S(p+n-k)/k = n,\ldots\ldots,1\}, \qquad (3)$$

for each $p = 0,1,..,2^n - 2$.

It is based on the idea that it is possible to find the actual value of the position p, simply by counting the steps that the shift register with the inverse feedback needs until it reaches the initial state by successively shifting from the read pseudorandom n-bit word (2). Therefore, the code conversion algorithm is started (Fig. 3.) setting the current value with the n-bit quantity "X", which is gained using reading heads. Afterwards, "X" is being cyclically modified in accordance to the inverse generation low given in Table I. The algorithm will be in the cycle until the "X" reaches the defined initial state (2). Finally, when this state is reached, the algorithm stops, and current value of the register represents n-bit natural code of the real position. A new pseudorandom to natural code conversion algorithm is shown in Fig. 4.

In the case of high resolution, the code conversion time becomes a limiting factor for linear moving or rotation speed. The new algorithm reduces the maximum conversion time approximately two times. It is based on the idea that, thanks to PRBS cycling property, the initial state (2) could be reached using feedback relations that are used for either "direct" or "inverse" PRBS generating. Depending on the preceding position of the transporting system it is decided which PRBS generating low would be used for the current code conversion. When the relation for the "direct" PRBS is used, the real position will be 2^n-1-p. Associating to the information about the preceding position is not of big importance, because eventual absence of the information (e.g. when starting the system) does not affect the code conversion accuracy, and it could only exceed the code conversion time.

TABLE I

Shift register length n	Feedback in case of direct PRBS $X(0) = X(n) \oplus c(n-1)X(n-1) \oplus \ldots \otimes c(1)X(1)$
3	$X(0) = X(3) \oplus X(1)$;
4	$X(0) = X(4) \oplus X(1)$;
5	$X(0) = X(5) \oplus X(2)$;
6	$X(0) = X(6) \oplus X(1)$;
7	$X(0) = X(7) \oplus X(3)$;
8	$X(0) = X(8) \oplus X(4) \oplus X(3) \otimes X(2)$;
9	$X(0) = X(9) \oplus X(6)$;
10	$X(0) = X(10) \oplus X(3)$;
11	$X(0) = X(11) \oplus X(2)$;
12	$X(0) = X(12) \oplus X(6) \oplus X(4) \otimes X(1)$
13	$X(0) = X(13) \oplus X(10) \oplus X(6) \otimes X(4)$;
14	$X(0) = X(14) \oplus X(13) \oplus X(8) \otimes X(4)$;
Shift register length n	Feedback in case of inverse PRBS $X(n+1) = X(1) \oplus b(2)X(2) \oplus \ldots \otimes b(n)X(n)$
3	$X(4) = X(1) \oplus X(2)$;
4	$X(5) = X(1) \oplus X(2)$;
5	$X(6) = X(1) \oplus X(3)$;
6	$X(7) = X(1) \oplus X(2)$;
7	$X(8) = X(1) \oplus X(4)$;
8	$X(9) = X(1) \oplus X(3) \oplus X(4) \otimes X(5)$;
9	$X(10) = X(1) \oplus X(3)$;
10	$X(11) = X(1) \oplus X(4)$;
11	$X(12) = X(1) \oplus X(3)$;
12	$X(13) = X(1) \oplus X(2) \oplus X(5) \otimes X(7)$;
13	$X(14) = X(1) \oplus X(5) \oplus X(7) \otimes X(11)$;
14	$X(15) = X(1) \oplus X(5) \oplus X(9) \otimes X(14)$;

Both software and hardware realizations of the pseudorandom to natural code conversion algorithms, shown in Fig. 3. and Fig. 4., could be done. Comparing of software realizations of two algorithms is done using a micro computing development system based on a microprocessor Intel 8051, which operates at 12 MHz. Maximal gained code conversion time for the solution described in [2] is 5.6 ms. Maximal conversion time, for the solution proposed in this paper, is 2.8 ms. This means that applying the hardware realization of the new algorithm, shown in Fig. 5., an improvement would be achieved in regard to the hardware realization of the solution in Fig. 3 [2].

Another bidirectional shift register, depending on the MSB bit of the output binary information of the transporting system preceding position, performs shifting to the left or to the right from the initial state (2). A counter counts those shifts and, in the case of shifting to the right, its output is the actual value of the position. When shifting to the left, the value that corresponds to the actual position is obtained by

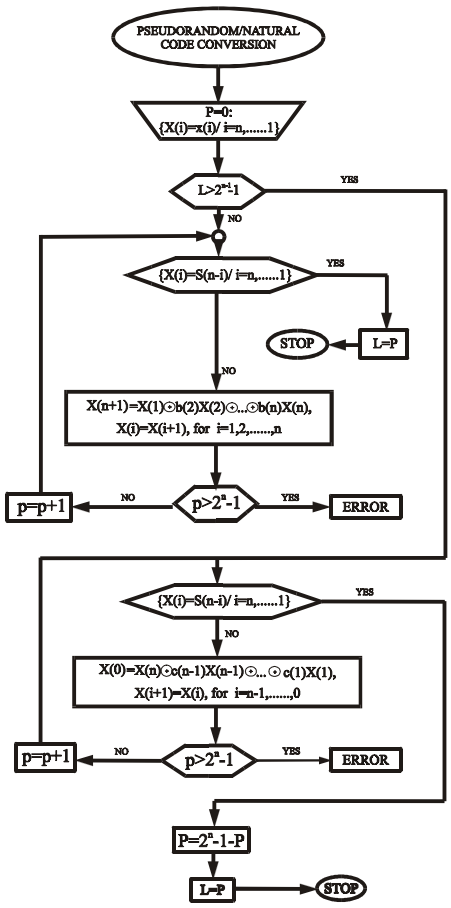

Fig. 4. The new code conversion algorithm

complementing the counter output, which is equal to 2^n-1-p in the algorithm. The problem that occurs because of whether output should be complemented or not, depending on a shifting direction, is simply solved using EXOR circuits, Fig. 5.

At the end, it should be mentioned that the system must involve a functional part, which would, after the system is turned on, signalize that the read code is wrong for the first n quanting steps. There are both software and hardware solutions to this problem. The software solution considers a subroutine that is automatically called for after n information on position. Appropriate hardware solution that uses an additional counter is described in detail in [2].

IV. Conclusion

The virtual absolute encoder is currently the greatest hit, as something new with an entirely new quality. They are especially interesting because they own great number of possibilities for further upgrading of their performance. Their price is less than the one of conventional absolute encoders, in return of great new quality. The system reliability is increased as well as the possibility of providing additional information to the user about the output measuring information validity. An important function that significantly affects pseudorandom encoder performances is pseudorandom to natural code conversion. The pseudorandom to natural code conversion is

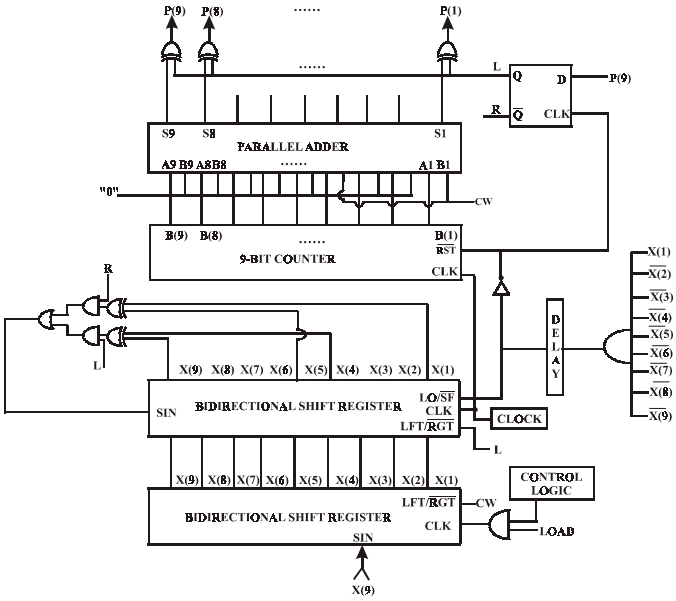

Fig. 5. Hardware realization of the pseudorandom/natural code conversion

one-way and can be performed using a memory with a translation table. However, this method is not practical for pseudorandom binary sequences of relatively long length, so it is of great importance to develop a code conversion method that, even for very long sequences, provides simple conversion into the natural code. A new approach to code conversion suggested in this paper, provides, in a simple way, an acceleration of the code conversion algorithm approximately two times.

References

[1] MacWilliams, F.J., Slone, N.J.A.: "Pseudo-random sequences and arrays", *Proceeding of IEEE*, Vol. 64, No. 12, pp. 1715-1728, December 1976.

[2] Petriu, E.M.: "Absolute-type position transducers using a pseudorandom encoding", *IEEE Trans. Instrum. and Meas.*, Vol. IM-36, No. 4, pp. 950-955, December 1987.

[3] Petriu, E.M., Basran, J.S.: "On the position measurement of automated guided vehicles using pseudorandom encoding", *IEEE Trans. Instrum. and Meas.*, Vol. 38, No. 3, pp. 799-803, June 1989.

[4] Wigmore, T.: "Optical shaft encoder from SHARP", *Elektor Electronics*, pp. 60-62, July/August, 1989.

[5] Petriu, E.M., Basran, J.S., Groen, F.C.A.: "Automated guided vehicle position recovery", *IEEE Trans. Instrum. and Meas.*, Vol. 39, No. 1, pp. 254-258, February 1990.

[6] Petriu, E.M.: "New pseudorandom/natural code conversion method", *Electronics Letters*, Vol. 24, No. 22, pp. 1358-1359, 1988.

[7] John G. Webster: "The measurement, instrumentation and sensors handbook", CRC Press and IEEE Press, 1999.

Sensitivity and Stability of A Level Measuring Device

Ventseslav D. Draganov[1] Iliya T. Tanchev[2] Hristina J. Jekova[3]

Abstract

Experimental research proves the correctness of choice of method and device for controlling the level of bulk material in silos (bunkers) providing high sensitivity and stability when changes of temperature and supply voltage occur.

Key words: **Level of bulk material.**

INTRODUCTION

Module [1] is used for controlling the level of bulk material in silos and stock level in bunkers. *It consists of a primary converter "level - capacity" and a secondary converter "capacity - frequency" which includes a crystal oscillator.* The general scheme (circuit) of the module used for experimental research is shown in Fig.1.

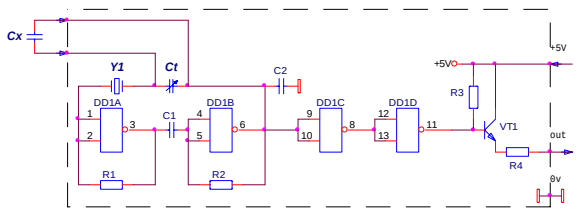

Fig.1. Module for experiments

The primary converter "level - capacity" is represented by the Cx capacitor, connected in series with the crystal resonator. It uses the possibility for slight variations of frequency of the crystal oscillator under the influence of the change of capacity of the capacitor connected in series with the crystal resonator. The trimmer Ct capacitor is connected in parallel with the Cx capacitor.

[1] Ventselav D.Draganov is from the Faculty of Electronics at the Technical University - 1, Studentska Str., Varna, Bulgaria.e-mail address: itta@ms3.tu-varna.acad.bg
[2] Iliya T.Tanchev is from the Faculty of Electronics at the Technical University - 1, Studentska Str., Varna, Bulgaria.e-mail address: itta@ms3.tu-varna.acad.bg
[3] Hristina J. Jekova is from the Faculty of Electronics at the Technical University - 1, Studentska Str., Varna, Bulgaria.e-mail address: itta@ms3.tu-varna.acad.bg

EXPERIMENTAL RESEARCH

The experiments carried out are as follows:

1. Determining the sensitivity and the linearity of the circuit of the converter.

2. Determining the stability of the circuit of the converter during changes of supply voltage and temperature.

Three crystal resonators are used with the following frequencies of the series resonance:

Fs_1 = 1,000.0 kHz; Fs_2 = 3,200.0 kHz;
Fs_3 = 5,000.0 kHz.

1. Results from the experiments on the sensitivity and linearity of the converter

The experiments are carried out at different values of the Cx capacitor - from 0.5 to 20 pF; the Ct capacitor is not connected but exists as a parasite mounted capacity.

The results for each of the three crystal resonators are shown graphically in Fig.2, Fig.3 and Fig.4 respectively.

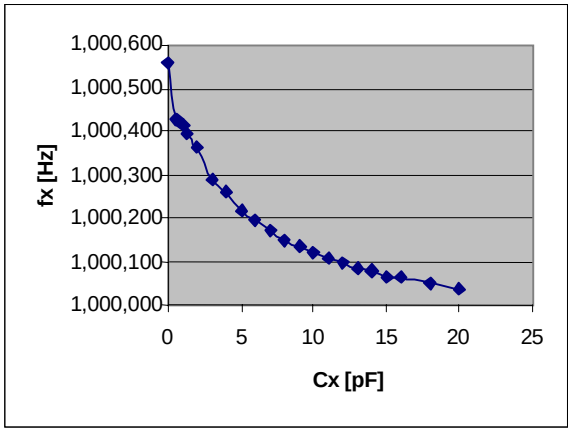

Fig.2. Dependency $f_X = \varphi(C_X)$ for fs_1 = 1,000.0 kHz

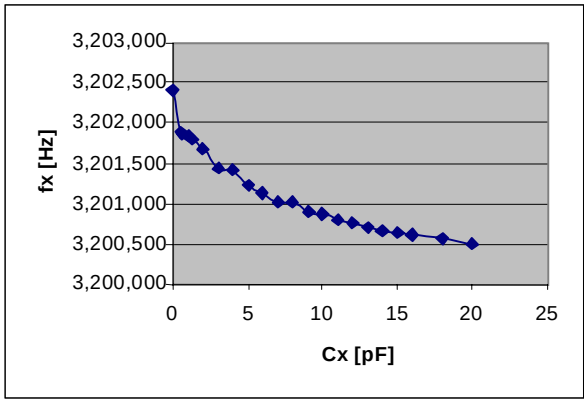

Fig.3. Dependency $f_X = \varphi(C_X)$ for fs_2 = 3,200.0 kHz

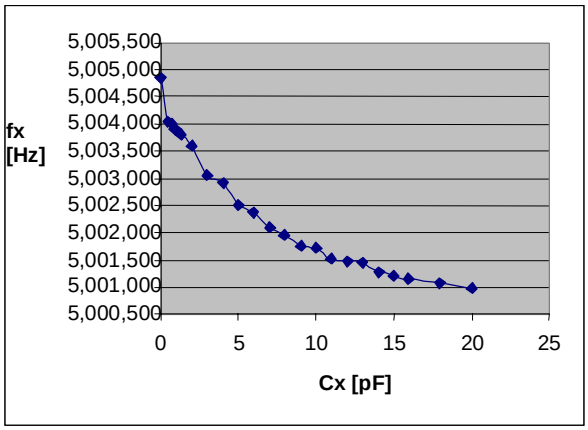

Fig.4. Dependency $f_X = \varphi(C_X)$ for fs_3 = 5,000.0 kHz

Conclusions:

1. The dependency *fx = φ(Cx)* is non-linear.

2. The non-linearity of the characteristic *causes great difficulty in using the capacity converter for uninterrupted control of the level of liquids or bulk material.*

Its use is recommended mainly for control of minimum and maximum levels.

3.The experiment on the dependency of the fx frequency value of the Cx capacitor shows that *the sensitivity of the capacity converter decreases with the increase of the measured Cx capacitor values*.

4. *The exceptionally high sensitivity of the circuit allows its use for controlling even slight changes of capacity (under 1 pF).*

2. Results from the experiment on the stability of the converter circuit.

Circuit stability is tested in two cases - with an available measured capacitor *Cx* = 4 pF and when there is no such capacitor (only the mounted capacitor remains).

2. Results from the experiment on the stability of the converter circuit.

Circuit stability is tested in two cases - with an available measured capacitor *Cx* = 4 pF and when there is no such capacitor (only the mounted capacitor remains).

2.1. Circuit stability when the supply voltage changes – fx = φ (Uo)

The experiment is carried out when the supply voltage changes from 5.25 V to 4.75 V as well as in lower voltage, which allows the circuit to be efficient.

2.1.1.With a lack of Cx capacitor - the instability of the crystal resonator with frequency of the series resonance:

- 1,000.0 kHz is *3 Hz*,
  i.e. $\pm 1.53 \times 10^{-6}$ *% / V* with *(Uo = 5.25 ÷ 3.3 V);*
- 3,200.0 kHz is *1 Hz*,
  i.e. $\pm 0.18 \times 10^{-6}$ *% / V* with (*Uo = 5.25 ÷ 3.6 V*);
- 5,000.0 kHz is *38 Hz*,
  i.e. $\pm 8.94 \times 10^{-6}$ *% / V* with (*Uo = 5.25 ÷ 4.4 V*).

2.1.2. With an available capacitor Cx = 4 pF - the instability of the crystal resonator with frequency of the series resonance:

- 1,000.0 kHz is *1 Hz*,
  i.e. $\pm 0.51 \times 10^{-6}$ *% /.V* with *(Uo = 5.25 ÷3.3 V);*
- 3,200.0 kHz is *1 Hz*,
  i.e. $\pm 0{,}23 \times 10^{-6}$ *% / V* with *(Uo = 5.25 ÷3.9 V);*
- 5,000.0 kHz is *26Hz*,
  i.e. $\pm 4{,}95 \times 10^{-6}$ *% / V* with *(Uo = 5.25 ÷4.2 V*).

Conclusions:

1. *The most stable in terms of the change in supply voltage is the crystal resonator with frequency of the series resonance 3200.0 kHz*. It also has very little dependency on the value of the capacitor connected in series with the crystal resonator.

2. The instability of the oscillator frequency in this case doesn't exceed *±1 Hz* ($\pm 0.23 \times 10^{-6}$ *% / V*), with a change of the supply voltage within 3.9 ÷ 5.25 V. This instability is equivalent to the admissible error in measuring the oscillator frequency *(±1 Hz*). It allows the supply voltage to be connected to the measuring module with wires of considerable length.

3. The connection of the *Cx* capacitor influences the stability of the frequency to a different extent (degree) and in a different direction for each crystal resonator.

2.2. Temperature stability of the circuit

The circuit stability is tested for each of the three crystal resonators with changes in temperature within 20 °C - 60 °C. The data are for the same two cases - with a lack of measured *Cx* capacitor and with an available measured capacitor *Cx = 4 pF*.

The results from the measuring tests when there is no measured *Cx* capacitor are shown in Table 1.

TABLE I

t,°*C* ***f***, *kHz*	20°	30°	40°	50°	60°
1,000	1,000.543	1,000.558	1,000.573	1,000.586	1,000.608
3,200	3,202.741	3,202.718	3,202.705	3,202.700	3,202.696
5,000	5,004.680	5,004.526	5,004.423	5,004.318	5,004.382

The graphic presentation of the results is shown in Fig.5

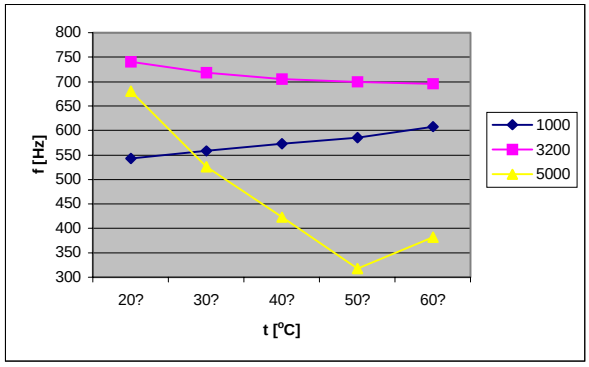

Fig.5. Dependency $f_X = \varphi\ (t)$ without *Cx* capacitor

The results from measuring with an available measures Cx capacitor are given in Table 2.

TABLE II

t,°C ***f***, *kHz*	20°	30°	40°	50°	60°
1,000	1,000.272	1,000.285	1,000.398	1,000.320	1,000.347
3,200	3,201.576	3,201.569	3,201.567	3,201.565	3,201.580
5,000	5,003.017	5,002.994	5,002.953	5,002.895	5,002.836

The graphic presentation is in Fig.6

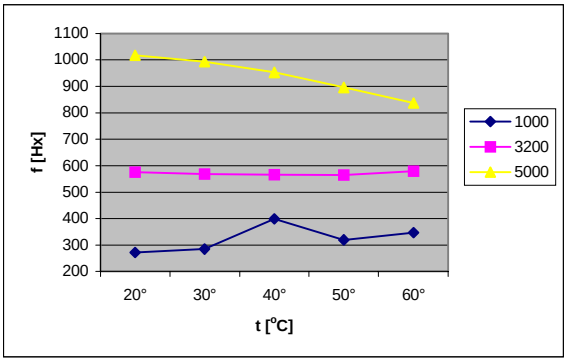

Fig.6. Dependency $f_X = \varphi\ (t)$f with capacitor *Cx* = *4 pF*

The respective frequency changes of the three crystal resonators are as follows:

- For 1,000.0 kHz it increases by *65 Hz* (*without Cx*) and by 75 Hz (with Cx = 4 pF);
- For 3,200.0 kHz it changes by *55 Hz* (*without Cx*) and by 15 Hz (with Cx = 4 pF);
- For 5,000.0 kHz it decreases by *298 Hz* (*with Cx*) and by 181 Hz (with Cx = 4 pF).

The respective temperature coefficients for the three crystal resonators are as follows:

- For 1,000.0 kHz
  - TCF = $+1.62\text{x}10^{-6}$/°C (without Cx);
  - TCF = $+1.88\text{x}10^{-6}$/°C (with Cx=4pF);
- For 3,200.0 kHz
  - TCF = $-0.43\text{x}10^{-6}$/°C (without Cx);
  - TCF = $\pm0.06\text{x}10^{-6}$/°C (with Cx = 4 pF);
- For 5,000.0 kHz
  - TCF = $-1.49\text{x}10^{-6}$/°C (without Cx);
  - TCF = $-0.91\text{x}10^{-6}$ / °C (with Cx = 4 pF).

Conclusions:

1. The most stable in terms of temperature changes is the crystal resonator with frequency of the series resonance *fs* = 3,200.0 kHz. The temperature coefficient *TCF* for it doesn't exceed $\pm0.25\text{x}10^{-6}$/°C.
2. *TCF decreases when the Cx capacitor is connected in series to the crystal resonator*.
3. The selection of values for *Cx* and its temperature coefficient may decrease *TCF* additionally.
4. The low values of *TCF allow measuring very small capacities in a wide temperature span*.

GENERAL CONCLUSION

1. The suggested circuit solution allows the registration of very small changes in capacity (under 1 pF).

2. The dependency *fx = φ(Cx)* is non-linear. The use of this module is recommended mainly for the control of minimum and maximum levels.

3. The circuit sensitivity is maximum at a minimum change of the measured capacity (under 1 pF).

4. The stability of frequency of the crystal oscillator at a wide range of changes in the supply voltage is very high - it doesn't exceed ±1 Hz ($\pm0.23\text{x}10^{-6}$ %/V).

5. On the whole, the temperature stability is very high. The experimental results show that the most stable in terms of the temperature change is the crystal resonator with frequency of the series resonance *fs* = 3,200.0 kHz (the temperature coefficient *TCF* is smaller than $0.5\text{x}10^{-6}$/°C). *TCF* is additionally decreased with the parallel connection to *Cx* of a *Ct* capacitor with a selected value and temperature coefficient.

The results obtained from the tests show the correctness of choice for a method and device for controlling the level of bulk material in silos providing high sensitivity and stability when temperature conditions and supply voltage change.

Given the temperature instability and the one caused by the change of supply voltage a well-grounded choice can be

made of an optimum construction and size of the primary converter "level - capacity" which will be used for controlling the level of bulk material in silos and stock in bunkers.***l***

REFERENCE

[1] V. Draganov, “Device for measuring level”, author's license 45168 (MPC - C 01 G 23/26) from 08.01.1988

[2] V. Draganov, I. Tanchev, “Device for measuring level”, AUTOMATICS-2003, Sevastopol, Russia, 2003

An investigation of GM-estimators for outlier robust regression estimation

Dimitar G. Genov[1] and Nasko R. Atanasov[2]

Abstract - **This paper discusses the class of GM-estimators for outlier robust regression estimation. M-estimators with objective functions of Cauchy, Welsh, Huber, Tukey, Mallows' GM-estimators and Schweppe's GM-estimators are investigated. An accuracy, a convergence and a computational complexity of the algorithms are analyzed. The best model is determined by robust Akaike information criterion.**

Keywords - **Robust estimators, Outliers, Akaike information criterion, Mallows' GM-estimators, Schweppe's GM-estimators.**

I. INTRODUCTION

Consider the linear regression model $y_i = x_i^T \beta + \varepsilon_i, i = 1,\ldots,N$, where x_i is a p-dimensional vector. The class of generalized maximum likelihood (GM) type estimators is defined implicity by the condition

$$\sum_{i=1}^{N} x_i \varsigma\left(x_i, \left(y_i - x_i^T \beta\right)/\sigma\right) = 0 . \qquad (1)$$

The parameter σ denotes the scale of ε_i. The function $\varsigma(\cdot,\cdot)$ depends on both the set of regressors (x_i) and the standardized residual. The most important conditions that must be satisfied by $\varsigma(\cdot,\cdot)$, in order for the GM estimator to have nice asymptotic properties are that for all $x \in R^p$ $\varsigma(x,\cdot)$ has to be continuous and continuously differentiable except in a finite number of points, that $\varsigma(x,\cdot)$ has no vertical asymptotes, and that $\varsigma(x,\cdot)$ is odd. Moreover $\mathrm{E}\left(\left(\varsigma(x_i, \varepsilon_i/\sigma)\right)^2 x_i x_i^T\right)$ and $\mathrm{E}\left(\varsigma'(x_i, \varepsilon_i/\sigma) x_i x_i^T\right)$ must exist and be nonsingular, where $\varsigma'(x_i, r) = \partial\varsigma(x_i, r)/\partial r$, and r denotes standardized residual ε_i/σ [2], [6].

The OLS estimator is obtained as a special case of Eq. (1) by setting $\varsigma(x,r) = r$. Also M-estimators are special case of Eq. (1), namely $\varsigma(x,r) = \psi(r)$ for some function ψ satisfying the above regularity conditions [6].

Instead of defining GM estimators as a solition to a first order condition of the type Eq. (1), one can also define them as the minimand of the objective function

$$\sum_{i=1}^{N} \tau\left(x_i, \left(y_i - x_i^T \beta\right)/\sigma\right), \qquad (2)$$

with $\partial\tau(x,r)/\partial r = \varsigma(x,r)$. The focus in this paper, however, is on the definition as aplied by Eq.(1). Note that the OLS estimator is defined by setting $\tau(x,r) = r^2/2$, while the class of M-estimators is obtained by setting $\tau(x,r) = \rho(r)$ with $d\rho(r)/dr = \psi(r)$ [1],[3].

II. FEATURES OF MALLOWS' GM-ESTIMATORS AND SCHWEPPE'S GM-ESTIMATORS

The easiest way to explain the intuition behind GM estimators is by considering the class of Mallows' GM estimators, given by $\varsigma(x,r) = w_x \psi(r)$, with $\psi(r)$ as intrtoduced above (Section I), and $w_x(x)$ a weight function that assigns weights to the vectors of regressors, $w_x : R^p \to [0,1]$. Using this specification of $\varsigma(\cdot,\cdot)$, Eq. (1) can be rewritten as

$$\sum_{i=1}^{N} w_x(x_i) x_i w_r\left(\left(y_i - x_i^T \beta\right)/\sigma\right)\left(y_i - x_i^T \beta\right) = 0 , \quad (3)$$

$$w_r(r) = \begin{cases} \psi(r)/r & \text{за } r \neq 0 \\ 1 & \text{за } r = 0 \end{cases} . \qquad (4)$$

The functions $\psi(\cdot)$ and $w_x(\cdot)$ can now be chosen such that the weight of ith observation decreases if either $\left(y_i - x_i^T \beta\right)/\sigma$ becomes extremely large (vertical outliers and bad leverage points), or x_i becomes large (leverage points)[6]. In this way, outliers and influential observations automatically receive less weight. For the OLS estimator, $w_x(x) \equiv 1$ and $w_r(r) \equiv 1$, such that all observation receive the same weight.

A disadvantage of Mallows' proposal for GM estimators is that it assigns less weight to both good and bad leverage points, but good leverage points often increase the efficiency of the imployed estimator. As an alternative to Mallows' proposal for GM-estimators, one can consider the proposal of Schweppe. The Schweppe's form of the GM estimator only downweights vertical outliers and bad leverage points, but not good leverage points. This generally increases the efficiency of the Schweppe's estimator over the Mallows' version. The Schweppe's specification of $\varsigma(\cdot,\cdot)$ is given by

[1] Dimitar G. Genov is with the Faculty of Computer System and Automation, Technical University, 9010 Varna, 1 "Studentska" str E-mail:dggenov@yahoo.com

[2] Nasko R. Atanasov is with the Faculty of Computer System and Automation, Technical University, 9010 Varna, 1 "Studentska" str E-mail:nratanasov@yahoo.com

$$\varsigma(x,r) = w_x \psi(r / w_x(x)). \quad (5)$$

Using Eq. (5), Eq. (1) can be written as

$$\sum_{i=1}^{N} x_i w_r \left(\left(y_i - x_i^T \beta \right) / \sigma w_x(x_i) \right) \left(y_i - x_i^T \beta \right) = 0. \quad (6)$$

Assume that $w_x(\cdot)$ and $\psi(\cdot)$ are chosen such that outliers receive less weight. For a leverage point (y,x), $w_x(x)$ will than be small. The weight for the ith observation in the estimation proces is given by $w_r(\cdot)$ in Eq. (6). Note that this weight may be close to one if the standardized residual is close to zero, irrespective of whether the observation is a leverage point or not. The requirement that the standardized residual is close to zero becomes stricter if $w_x(x_i)$ is small, i.e. if x_i is a leverage point.

The Schweppe's version of GM-estimators also has some practical disadvantages. First, the bias in the Schweppe's estimator may be larger than that of the Mallows' estimator. Second, the Schweppe's estimator more easily displays convergence problem than the Mallows' variant, especialy if strongly redescending specification of ψ are used. Even if no convergence problems arise, moderately bad leverage points tend to have a larger influence on the Schweppe's version of the GM-estimators than on the Mallows' version [4],[6].

If the weights on the regressors $w_x(\cdot)$ are dropped, the class of GM-estimators reduces to the class of M-estimators. Thus, the class of GM-estimators contains the class of maximum likelihood type estimators (M-estimators). Therefore, the class of M-estimators is not dealt with, separately.

In the next part of this paper it will be discuss the problem about specification of $\psi(\cdot)$ and $w_x(\cdot)$. The OLS specification for $\psi(\cdot)$, $\psi(r) = r$, is the most familiar one. OLS-estimator is not robust. The most important reason for this is that the function $\psi(r) = r$ is unbounded. Several forms of bounded ψ functions are suggested in the literature,e.g., the Huber, the Cauchy, the Geman-McClure, the Welsch, the Tuke, the Hampel, the Student t specification, etc.[3],[6].

The Huber's function ψ is given by $\psi(r) = median(-c, c, r)$, where c>0 is a tuning constant[1]. The lower *c*, the more robust is the resulting estimator. As a special case of the Huber's estimator, one can obtain the OLS estimator ($c \to \infty$) and the least absolute deviations (LAD) estimator ($c \to 0$). The constant *c* not only determines the robustness of the coresponding estimators, but also its efficiency. For Gaussian ε_i, for example, the efficiency of the estimator is an increasing function of *c*. This illustrates that there is a tradeoff beetween efficiency and robustness. Common value for *c* is 1,345 for the Huber's function. This value produce estimators that have an efficiency of 95% in case ε_i is normally distributed [3].

As a specification for the weight function $w_x(\cdot)$ for the regressors, one usually encounters the specification

$$w_x(x_i) = \sqrt{1 - h_i}, \; i = 1, \ldots, N, \quad (7)$$

with h_i the diagonal elements of the hat matrix H [1],[4]

$$\hat{y} = X\hat{\beta} = X\left(X^T X\right)^{-1} X^T y = Hy. \quad (8)$$

III. The Generalized Procedure for Robust Estimation

GM estimators are mostly computed by means of numerical techniques. Most of these techniques employ iteration schemes. Therefore, an initial estimate is required to start up the iteration. A starting value should, preferably, be easy to calculate. From this perspective, the OLS-estimator usually is used.

Once the starting values have been obtained, one can start an iteration scheme for solving Eq. (1). It is, of course, possible to use general techniques for solwing sets of nonlinear equations. The special structure of Eq. (1), however, also allows a different iteration scheme by means of weigthed and ordinary least - squares.

A very important computational aspect concerns the estimation of scale parameter σ. If σ is omitted from Eq. (1), the GM-estimator is not scale invariant, i.e., the estimates would change if both y_i and x_i were multiplied by a constant k>0. The estimate σ, one cannot safely use the ordinary standard deviation, as this estimator is not robust. An often used alternative is the median absolute deviation, defined as

$$MAD\left(\{\varepsilon_i\}_{i=1}^{N}\right) = median\left|\varepsilon_i - median(\varepsilon_i)\right|. \quad (9)$$

The MAD is usually multiplied by 1,4826 to make it consistent estimator of the standard deviation for Gaussian ε_i. The use of a scale equivariant estimator for σ in Eq. (1) renders the GM-estimator for β scale equivariant [6].

We proposed the generalized procedure for robust estimation includes the sequent stage, listed below:

- choice of estimator's type;
- choice of method for estimation;
- calculation of the model's parameters with chosen set of structures;
- choice of the best structure from this set, with applying of robust Akaike information criterion;
- test for first order autocorrelation in the residuals;
- final choice of the model, after analysis of results from applying of different estimation methods and estimator's types.

IV. Model Selection and Model Diagnostics

The best model among competing multivariate models is determined by robust Akaike information criterion [2]

$$AICR = 2LFR + 2p. \quad (10)$$

The parameter *p* denotes the number of estimated parameters. The robust loss function LFR depends on both the

number of observations (N) and the objective function $\rho(r_i)$ of the standardized residuals

$$LFR = N^{-1}\sum_{i=1}^{N}\rho(r_i). \quad (11)$$

AICCR (robust Akaike information criterion corrected) is used when the ratio $N/p < 40$ [5]

$$AICCR = AICR + \frac{2p(p+1)}{N-p-1}. \quad (12)$$

The Durbin-Watson test for first order autocorrelation in the residuals is used

$$DW = \sum_{i=2}^{N}(r_i - r_{i-1})^2 \Big/ \sum_{i=1}^{N} r_i^2. \quad (13)$$

V. Simulation investigations

It is created an applied software in MATLAB with realization of the sequent varieties:

- estimator's type – Mallows' GM, Schweppe's GM, M-estimator;
- estimation methods – modified residuals, modified weigths, pseudo observations, Huber-Kleiner's method;
- objective function - Huber, Cauchy, Geman-McClure, Welsch, Tuke, "Fair", L_p, L_1.
- scale estimation – MAD or ordinary standard deviation.

Simulation research is made with the model:

$$y = -68 + 13x_1 + 23x_2. \quad (14)$$

Number of the observations is 100. To the output model signal is added Gaussian white noise and the ratio noise/signal is 7,76%. There are simulated 10 additional outliers and as a result the ratio noise/signal increases up to 32%.

The accuracy of the estimations $\hat{b}_j,\ j = 0,\ldots,p$ is defined by relative mean-squared error

$$Qb = \sqrt{\sum_{j=0}^{p}\left(b_j - \hat{b}_j\right)^2 \Big/ \sum_{j=0}^{p} b_j^2}. \quad (15)$$

The parameters $b_j,\ j = 0,\ldots,p$ denote the real values of model's parameters.

Criterion for stopping the iterative procedure is

$$\varepsilon = \left|\hat{b}^i - \hat{b}^{i-1}\right| \le 0{,}0001. \quad (16)$$

Computational complexity of the algorithm is estimated by the cumulative number of floating point operations into MATLAB (flops).

At the estimation of the parameters there is used general regressive model from the type

$$y = b_0 + \sum_{i=1}^{p} b_i x_i + \sum_{\substack{i=1 \\ j>i}}^{p} b_{ij} x_i x_j + \sum_{i=1}^{p} b_{ii} x_i^2. \quad (17)$$

There are made a lot of investigations with the mentioned in Section V eight objective functions. The best results in aspect of convergence and accuracy is given by Huber's function and it is used in the next investistigation Eq. (18).

$$\rho(r) = \begin{cases} r^2/2 & if \quad |r| \le c \\ c|r| - c^2/2 & if \quad |r| > c \end{cases}. \quad (18)$$

TABLE I

CHOICE OF ESTIMATOR'S TYPE AND METHOD

			Q_b	iter	flops
M-estimator	Modified residuals	MAD	.0034	7	13703
		std	.0076	6	78202
	Modified weights	MAD	.0034	6	36744
		std	.0076	5	95422
	Pseudo observetions	MAD	.0034	7	14843
		std	.0076	6	78667
	Huber-Kleiner	MAD			
		std	.0034	8	83893
Mallows' GM	Modified residuals	MAD	.0034	7	79436
		std	.0075	6	79767
	Modified weights	MAD	.0034	6	102143
		std	.0075	5	96674
	Pseudo observetions	MAD	.0034	7	80576
		std	.0075	6	80232
	Huber-Kleiner	MAD			
		std	.0032	9	87859
Schweppe's GM	Modified residuals	MAD	.0034	7	79436
		std	.0075	6	79767
	Modified weights	MAD	.0034	6	102143
		std	.0075	5	96674
	Pseudo observetions	MAD	.0034	7	80576
		std	.0075	6	80232
	Huber-Kleiner	MAD			
		std	.0033	7	83070

The results from experiments are given in Table I. The relative mean-squared error (Q_b), number of iterations for reaching the preassigned accuracy ε (iter) and the computational complexity (flops) are given in accordance with the type of estimators (Mallows' GM, Schweppe's GM and M-estimator), the used method for estimation (modified residuals, modified weigths, pseudo observations, Huber-Kleiner's method) and the chosen scale estimators of residuals (median absolute deviation – MAD or ordinary standard deviation - std).

TABLE II

MODEL SELECTION AND MODEL DIAGNOSTICS

	M1	M2	M3	M4	M5	M6
b_o	-67,28	-73,04	-68,05	-68,04	-67,91	-68,19
b_1		12,77	12,93	12,94	12,96	13,02
b_2	22,68		22,77	22,78	22,79	22,91
b_{12}				0,171	0,118	0,192
b_{11}					-0,135	-0,103
b_{22}						0,252
LFR	35,74	107,4	5,63	5,553	5,481	5,406
AICR	75,49	218,8	17,26	19,11	20,96	22,81
AICCR	75,62	218,7	17,51	19,53	21,60	23,71
DW	1,88	2,065	2,40	2,402	2,408	2,415

Table II displays the estimation parameters, the model selection and diagnostics. The data are simulated with model Eq. 14. Mallows' GM-estimator with modified weights method and MAD as scale estimator is applied. The best model is

$$y = -68.05 + 12.93x_1 + 22.77x_2 .$$

The corresponding values of AICR and AICCR are minimal and DW=2,4. Therefore, there is not first order autocorrelation in the residuals and the estimations are unbiassed.

VI. Conclusion

From the implemented research then can be made some conclusions:

- the minimum error (Q_b=0,0032) is achieved with Mallows' GM-estimator with Huber-Kleiner's method, but This method gives the slowest convergence;
- the rate of convergence, at every forms of the robust estimators, is the greatest with modified weights method, but this method also gives the greatest computational complexity;
- modified residuals method gives the least computational complexity;
- the accuracy with MAD scale estimators is nearly twice as big as than the ordinary standart deviation one;
- the usage of the studentized residuals (it is not given in the Taable I) leads to considerably increasing of the computational complexity of the algorithms (for Schweppe's GM with Huber-Kleiner's method - flops=83070, but for Schweppe's GM with Huber-Kleiner's method with studentised residuals - flops=2664134);
- The equal error (Q_b=0,0034 or Q_b=0,0075) is dued to the application of the same objective function in every estimators – Huber's function Eq. (18).

VII. Appendix

Cosider the problem for investigation of micro motors. There is not completed design theory in this area of knowledge. Therefore, some characteristics must be defined experimentally. This leads to creation of mathematical model.

Factors, their values and steps of variation are given in Table III.

TABLE III
MICRO MOTOR

EP55/110A	L_{rotor} [mm]	L_{stator} [mm]	W_{rotor} [number of wind]	$L_{wavstator}$ [mm]
factors	X_1	X_2	X_3	X_4
Base level	40	40	54	167
step	2,5	2,5	10	5
Upper level	42,5	42,5	64	172
Lower level	37,5	37,5	44	162

It is realized Full Factors Experiment with $N=2^4$. The motor's efficiency is a function of factors $\eta = \eta(x_1, x_2, x_3, x_4)$ and is obtained by applying of Mallows' GM-estimator with modified weight method and MAD for scale estimation.

The best model is

$$\eta = 49.2 - 5.49x_1 + 0.97x_2 + 5.32x_3 - \\ - 0.28x_4 + 0.73x_1x_2 - 4.97x_1x_3 .$$

Indicators, according which the best model is chosen, are: LFR=0,3271; AICR=14,7941; AICCR=28,7941; DW=1,9244.

References

[1] Хьюбер П., Робастность в статистике, Москва, Мир, 1984.
[2] Хампель Ф., и др., Робастность в статистике. Подход на основе функций влияния, Москва, Мир, 1989.
[3] Zhang Zh., M-estimators, www-sop.inria.fr/robotvis/personnel/zzhang/Publis/Tutorial-Estim/node24
[4] Chave A., Thomson D, A bounded influence regression estimator based on the statistics of the hat matrix, J. Roy. Stat. Soc., Series C (Appl. Statist.), 52, 307-322, 2003.
[5] Godinez-Dominguez E., Freire J., Information-theoretic approach for selection of spatial and temporal models of community organization, MARINE ECOLOGY PROGRESS SERIES, Vol.253:17-24, 2003.
[6] Lukas A., A brief intraduction to robust statistics, www.staff.feweb.vu.nl/alucas/thesis.

CAD systems for design and examining of automated technique

Vania K. Georgieva[1], Dimcho S.Chakarski[2] and Tatyana A. Andonova-Vakarelska[3]

Abstract: ***There are multiple objects in the discrete production being subject of automation; differing in shape, mass, dimensions, materials, lot size, technological process, operation's time, technological units etc. Every different solution has its own specifics. Nevertheless the variety present - it is possible to standardize them on the basis of a unified approach to automation of a discrete production.***

In order to optimize the activity of designing an effective solution for automated technique a CAD system is needed.
A model structure of a CAD system for automated technique of a discrete production design and analysis is presented in the paper. The main program modules and menu types are examined. Special attention is devoted to building the database.

Key words: automation, automated technique, a CAD system, projecting, examining.

I. INTRODUCTION:

The discrete production has a range of specific features: the huge diversity of the applied technologic processes, the industrial machines and appliances. The requirements towards the accuracy in the production of the details are huge. For every particular case an enormous count of solutions is possible and this makes very difficult the choice of the most suitable variant for a certain object with correspondence to the set requirements. The seriation of the production is also different; the discrete production of batch and semi-batch character is predominate. The automation imposes the formation of technical means with high productivity and represents accelerated and general implanation of scientific and technical progress in the manufacture. The automation of the manufacture holds the following tasks - an increasement of the efficiency of people's work while increasing its effectiveness. It leads to a new approach and a new vision, reveals big possibilities for positive changes in the part and the function of the person, in the ease of the work, and a change in its character and in its intellectualizing.

The automation is not a concept of a set of technical means but an all round process in choosing the most perspective directions for development, and improvement of the production, the creation of progressive technologic methods and processes, technical means and organizational forms and systems for control.

[3]Tatyana A. Andondva-Vauarelska is with the Faculty of Mechanical Engineering, boul. "Kl. Ohridski" N8, 1756 Sofia, Bulgaria, E-mail: tvakarelska@abv.bg

[2] Dimcho S. Chauarsky is with the Faculty of Mechanical Engineering, boul. "Kl. Ohridski" N8, 1756 Sofia, Bulgaria, E-mail: adp@tu-sofia..bg

[1]Vania K. Georgieva is with the Faculty of Mechanical Engineering, boul. "Kl. Ohridski" N8, 1756 Sofia, Bulgaria, E-mail: vkib@abv.bg

The automation is a powerful means for completing high technical economical indicators of manufacture, while receiving enough quantity of production, achieving growth in industrial produce and improving the vital standard, improving the competitive power of the production, a concern for the environment through the usage of non-scarps technologies and more.The information technologies will develop more and more together with the computer techniques in the whole cycle "examination-projection-production-marketing". The task of the development is to present a structure of a CAD system for computerized projection and examination the work of the automated techniques as choosing the suitable graphic surroundings.

II. CLASSIFICATION OF THE AUTOMATED TECHNIQUE AND TYPES OF TASKS ON AUTOMATION OF THE DISCRETE PRODUCTION

TABLE.I.
CLASSIFICATION OF THE AUTOMATED TECHNIQUE.

Automated technique					
Automated Devices	APM (technologic units)			RTM	Automated complexes
Orientate	Processin	Montagin	Packi	Processing	Flexible
Hopper-type	Mechanical-	Helix-	Proportioning	Dyeing	AC with a hard jointp
Storage-type		Screwing	Foil handing	Hot sticking under	AC with a flexible joint
Transported	Forge-	Pressing		Under pressure	FAMS
Manipulative	Pressing	Askingи	Sticking	Point-welding	Automated sections
Fixing	Welding	Point-	Other	Arc-welding заваряване	Automated departments
Based on and	Founding	Welding		Montage	
Embedded	Them-processin	Flattening downaщи		Packing	
Separatin		Other		Palletizing	
Collective Other				Other	

To complete the various tasks around the automation of the discrete production the automated technique is used. Its systematic conversance allows a qualitative approach when automating these production processes. The automated technique is a general concept that includes whatever techniques perform particular types of functions and operation i.e. this is the technique that ensures the automation of the manufacture. There is a variety of automated technique but four big groups can be differentiated: automated devices, automated production machines (APM), robotics technologic modules (RTM),

flexible production cells (FPC), automated complexes (AC).
On Table I is shown an exemplary classification of the automated technique when from every group are specified the respective types and varieties. One and same production processes can be realized by different types of automated technique.

While projecting and examining the automated technique can be distinguished the following basic types of tasks, regarding the type of the automated technique: marketing researches, prognosis, projecting, engineering, technical preparation, programming the industrial robots, programming the machines with CPS and the robotics technologic modules, exploitation, documentation, design and artwork, preparing export reports, making out offers and assignments for projection and more

For effective solution of the specified tasks the computer technology is used in most of the cases. Industrial packs are applied or specialized program systems. In Table.II. are shown the most used program-industrial packs.

III. POTENTIALITIES OF THE GRAPHIC SYSTEMS AND AREAS OF THEIR APPLIANCE.

Amidst the variety of CAD/CAM products, a practical role in the automating of the manufacture holds the listed in the Table.II. systems (listed alphabetically by the name of their producer company).

TABLE.II

Basic features of the leading CAD/CAM program packs

Company / Product	1	2	3	4	5	6	7	8	9	10	11
AutoDesk / MD Power Pack 5	S	S	S	0	S	S	S	P	P	S	м
Bentley / Micro Station	S	S	0	0	0	p	p	P	P	S	н
Dassault / CATIA V5	S	S	0	0	0	p	p	P	P	S	н
Dassault / SowidWorks	S	S	S	S	S	0	0	0	S	S	м
Matra Datavision / Euclid	S	S	0	0	0	p	S	S	P	S	н
PTC/Pro/Engineer 200i	S	S	S	S	S	S	0	P	P	S	H
Unigraphics Solution / Unigraphics	S	S	S	0	0	p	S	S	P	S	н

1. Surface & Ware frame - planes and netting;
2. Solid – hard modeling;
3. Automated generating of sketches;
4. Check for collisions when montaging;
5. Bifarious suggestiveness between the sketch and the 3D object;
6. A presence of libraries with standardized details;
7. An analysis using the method of the complete elements;
8. Programs for engineering calculations and interface programs;
9. Photo-realistic visualization of the projected articles;
10. Maintenance of WEB – appliances and possibility for sharing file formats; (S) uproot – support, (P) Arial – partially, (0) – no;
11. Class of the product (H – high, M - middle);

Marked are those features of the products in the range of the automated projection of mechanical articles. In the table we see the tendency among the leading companies which produce CAD/CAM products, towards unifying the systems. The main differences are in the prices and the variety of the offered accessory modules. All the specified systems for projection of mechanical articles have the potentialities to a bigger integration of the whole process from the projecting to the analysis of the article and the preparation of the production and their approach to the idea about the construction of an integrated product-information model.

Because of this reason every one of them is suitable for the tasks of the projection on the automated technique. But the biggest popularity among the constructors in Bulgaria holds the program Sowid Works. The choice is made mainly because of the following features: a presence of modules, including the whole process "projecting-producing", a presence of intuitional consumer interface with elements of artificial intellect, a presence of modules for projecting of specific articles such as ones made of sheet plate materials, plastic, die details and more, possibilities for assembling very complex articles (made of few hundred thousands elements), possibilities for different analyses of the details and the constructions as a whole (strain, temperatures, size chains and collisions in the unions and more) when generating the NC-programs, types of treatment and number of operated axes, a presence of graphic and other data libraries.

IV. STRUCTURE OF CAD SYSTEMS FOR PROJECTION AND EXAMINATION OF AUTOMATED TECHNIQUE.

On Figure.1. is given an exemplary scheme of the structure of CAD for projection and examination of automated technique while the scheme is open for accessory modules (program-calculated).

V. GRAPHIC DATABASE OF THE AUTOMATED TECHNIQUE.

Here are discussed the last tendencies in storage and reproduction of graphic objects as database in the range of CAD systems. These are the so-called technologies based on the features of the elements, which a specified detail is consisted of, a technologic process, or other object of the projection activity.

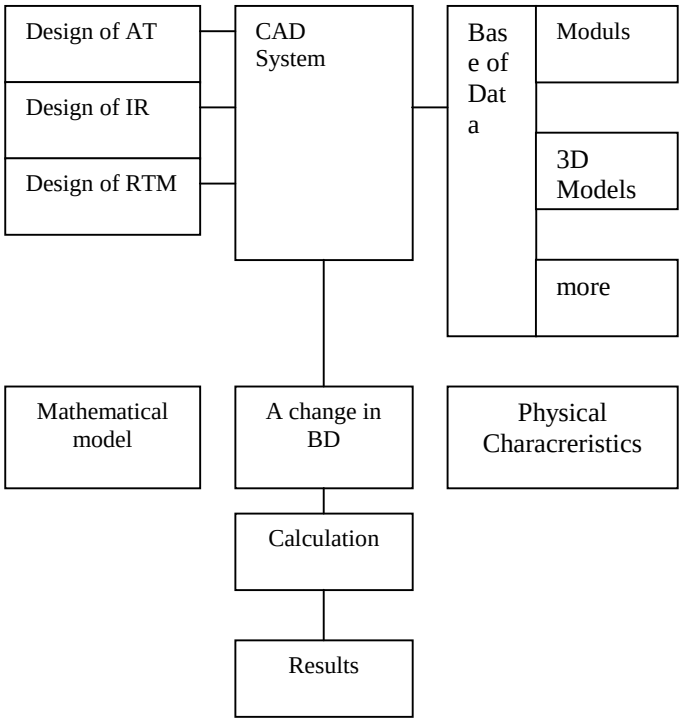

Fig1. Structural scheme of a CAD system

Most generally these database appropriate more knowledge (graphic, dynamic, technologic and more included) of these elements with an aim to get a higher state of integration at the separate stages of projection. On Figure .2. is given such an example: on the left side is shown an element of a geometric form together with its adjoining attributes. On the right side of the figure are shown the technologies which are necessary for the production of this element – a technologic route, the suitable for this case machines and instruments and so on. The parametric database that consists of rigidly shaped objects is constructed through the method of Fitcher's technology that was discussed above when the separate elements from which the model of the projected article is made, hold individual characteristics. From a point of view of the methodology, used by the producer, this is a method for construction, under which the volumetric model of already made elements (stored with their systematic features) are created first and then from it automatically is generated a sketch that is suggestively connected to the model. This means that if the model (respectively on the sketch) some changes are made (size and form of the objects) these changes automatically will be affected on the sketch (respectively in the model). This is shown on Figure .3. A vibrated hopper was given for an example as on Figure .3. is shown the suggestive connection between the sketch and the produced 3D element, and on figure .4. is shown the stiff bond between the diameter of the glass and the base of the vibrated hopper i.e. when a change occurs in some parameter in whichever part (left or right) on the figures, the rest is automatically transformed. This storage of data is called parametrical because the separate objects, from which the detail is constructed, are defined through a conscription of figurative and geometric parameters. Also this way produced models are called Hard making and they can be given and calculated material characteristic like when it comes to actual solid objects.

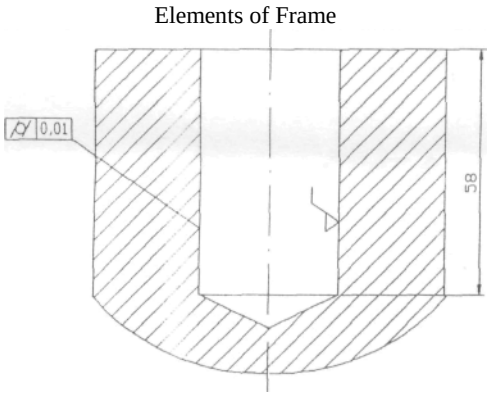

Fig. 2. Scheme of a technologic Feature (hallow hole)

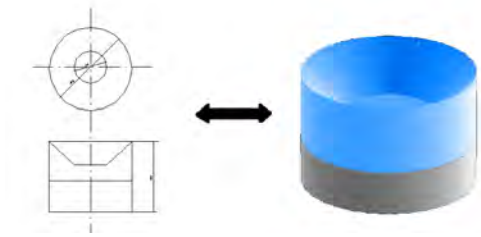

Fig3.Associativeness of the models, a) 2D model (sketch); b) 3D model)

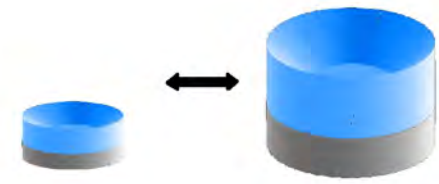

Fig.4.Geometric suggestiveness of the 3D model

On Figure .5. is given an example of storage of graphic database and a parametric access to it. On the figure is illustrated a pneumatic module that holds the features of a rigid object and it is 3D visual.

VI. Conclusions:

- A classification of automated technique is made and the characteristic tasks in the automation of the discrete production have been marked off.
- The possibilities of the graphic systems were analyzed and their features were marked off with a view to their application to the computerized construction of the automated technique
- CAD system of a principle has been given for projection and examination of A structure of a specialized automated technique while there is a connection to graphic surroundings

- A way for construction of a graphic database that is necessary for the realization of a specialized CAD system.

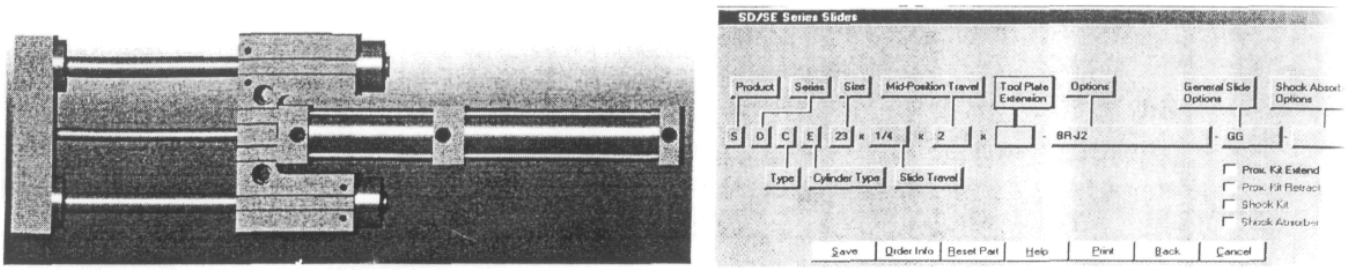

Figure.5. Graphic data bank a) module for translation – 3D, b) parametric access to the graphic database for modules of translation

REFERENCES:

1. Todorov N., D. Chakarski. Automation of the projection in the engineering, S, Technics, 1994
2. Donkov D., CAD/CAM systems in the engineering, A University publishing house, Gabrovo, 2001 eng. Ivo Mihailov Yanakiev
3. Georgieva, V. Typical Solutions for automation productional process of orientation parts. Scientific Nnewsletter of the Union of Mechanical Engineerings. Sofia, 2002.

Two-channel Circuits for Generation of Control Signals with Programmable Duration and Frequency

Hristo Z. Karailiev[1], Valentina V. Rankovska[2], Georgi D. Donev[3]

Abstract – **In this paper digital circuits forming two-channel control signals with programmable duration are described. A simulation and experimental study and comparative analysis of two circuits are made. The circuits can be used as a base in building of precise microprocessor devices intended for test and control of transistor converting devices.**

Keywords – **control signals, programmable duration, generation, simulation, hexadecimal counter**

I. INTRODUCTION

Through the recent years the number of applications requiring more precise and stable forming of signals with various duration and frequency defined from controlled object and it's modes of operation increases. The technical decisions in that area are the following:

1. Analogue methods. Disadvantages of such circuits are poor stability of formed signals parameters, depending on ambient temperature, supplying power, variations of the parameter characteristics in serial production. They require measures for temperature stability, hardware and software corrections of the formed signal parameters.

2. Digital-analogue methods. Some of disadvantages of the analogue methods are eliminated here, but it is difficult to form signals with precise step of the signal changes and requirements for hardware and software corrections of the formed signal parameters exist.

3. Digital methods [1]. They remove most of the disadvantages of the analogue and digital-analogue methods. Also there are possibilities for microprocessor control of the signal parameters, thus allowing programmability, parameters measuring and so on.

II. AIM AND TASKS OF THE PROJECT

The major aim is to develop and analyze digital circuit variants forming two-channel control signals with programmable duration.

The tasks in developing the circuits are as follows:

- development of two-channel circuits forming control signals with programmable duration;
- circuits simulation in a distinct range of parameters values (frequency, pulse duration);
- experimental study of the circuits;
- comparative analysis based on the simulations and experiments.

[1] Hristo Z. Karailiev is from the Technical University, 4 H. Dimitar str. 5300 Gabrovo, Bulgaria, E-mail: hkarailiev@hotmail.com

[2] Valentina V. Rankovska is from the Technical University, 4 H. Dimitar str. 5300 Gabrovo, Bulgaria, E-mail: rankovska@tugab.bg

[3] Georgi D. Donev is from the Technical University, 4 H. Dimitar str. 5300 Gabrovo, Bulgaria, E-mail: donev_g@yahoo.com

III. CIRCUITS AND OPERATION

Variant 1 of circuit forming control signals

- *Circuits and operation*

The first variant of circuit is shown in Fig.1. It consist of two generators: G1 (low frequency) and G2 (high frequency), four D-triggers (U1A, U1B, U7A, U7B), an inverter (U2A), four hexadecimal counters (U3, U4, U5, U6), connected in series and two 3-input AND gates (U8A, U8B).

G2 generates square waves with fixed frequency and period shown in Eq. (1):

$$T_{G2} = \frac{1}{f_{G2}}, \quad (1)$$

determining the step of pause change between the two channels output signals. G1 generates square waves which frequency f_{G1} can be changed with a step of Δf_{G1} in a defined working range and respectively period T_{G1}. The triggers U1B and U1A synchronize the frequencies of G1 and G2 and form two-channel output signals dephased on π (rad).

The counters U4 and U6 and the trigger U7A form programmable pause on the output *Q* of the trigger U7A in the form of logical "0" and duration set by the pins a, b, c and d of the counters U4 and U6. The Eq. (2) gives the duration of the pause:

$$t_{П}=T_{G2}.k_{Д}, \quad (2)$$

$k_{Д}$ is a scaling formed from 8-digit divider realized by the connected in series counters U4 and U6.

The gates U8A and U8B generate two-channel control signals with duration, given in the Eq. (3):

$$T_{yB}=T_{yA}= T_{G1}-t_{П} \quad (3)$$

- *Simulation of the 1 variant working*

The software Protel 99 SE [2] in simulation mode is used for the analysis. The circuit shown in Fig. 1 is used for that purpose. The simulation is made using the following data-in:

- output frequencies $\frac{f_{G1}}{2}$ in the range of 10 kHz to 1 MHz;
- fixed generator frequency of G2 $f_{G2}=20$ *MHz* setting up the change step for the programmable duration;
- setting proper values for the scaling $k_{Д}$ varying in the range from 0 to 255.

For the parameters of integrated circuits (counters, triggers, gates) the typical values from their technical data at normal conditions are set.

Fig. 2 and Table I show the results from the simulation of output signals, where *a* is the first channel output signal and *b* is the second channel output signal.

- *Experimental study of the circuit working*

The results form the experiments with the first circuit variant using the oscilloscope TDS 1002 and generator FG-8102 are shown in Table II, where:

F_y is the output signal frequency

T_y – output signal period

t_{Π} – pause duration

k_{Π} - scaling

$t_{\Pi}^{E/C}$ - pause duration from the experiment /simulation

t_{Π}^{1} - channel 1 pause duration

t_{Π}^{2} - channel 2 pause duration

The comparison of the experimental and simulation results shows that there are slight differences which proves the correct working of the circuit.

Variant 2 of circuits forming control signals

The second variant of a circuit is shown in Fig. 3. In contrast to the first variant it is without two hexadecimal counters and a D-trigger.

The Eqs. (1), (2) and (3) are valid here too. The difference in functioning of this variant in comparison to the first one is that during one period T_{G1} the scaling is load to the frequency dividers U3 and U4 twice at the beginning of each one-half period.

Table III and Table IV show respectively the results of simulation and experiments. It is evident that they are nearly the same.

IV. Conclusion

It is seen from the comparing of the experimental results and two circuits analyses that the parameters of the programmable pauses and output pulses are closer to the ideal ones at the second circuit. Also the number of elements is less, thus determining less expenses in production.

The developed circuits forming programmable pause may be implemented in building two-channel devices for test, control and regulating resonant inverters work.

References

[1] C. Slattery, DDS Circuit Generates Precise PWM Waveforms, www.edn.com, Design Ideas, pp. 85-88, October 2, 2003

[2] Protel 99 SE Designer's Handbook, Altium Limited, 2001

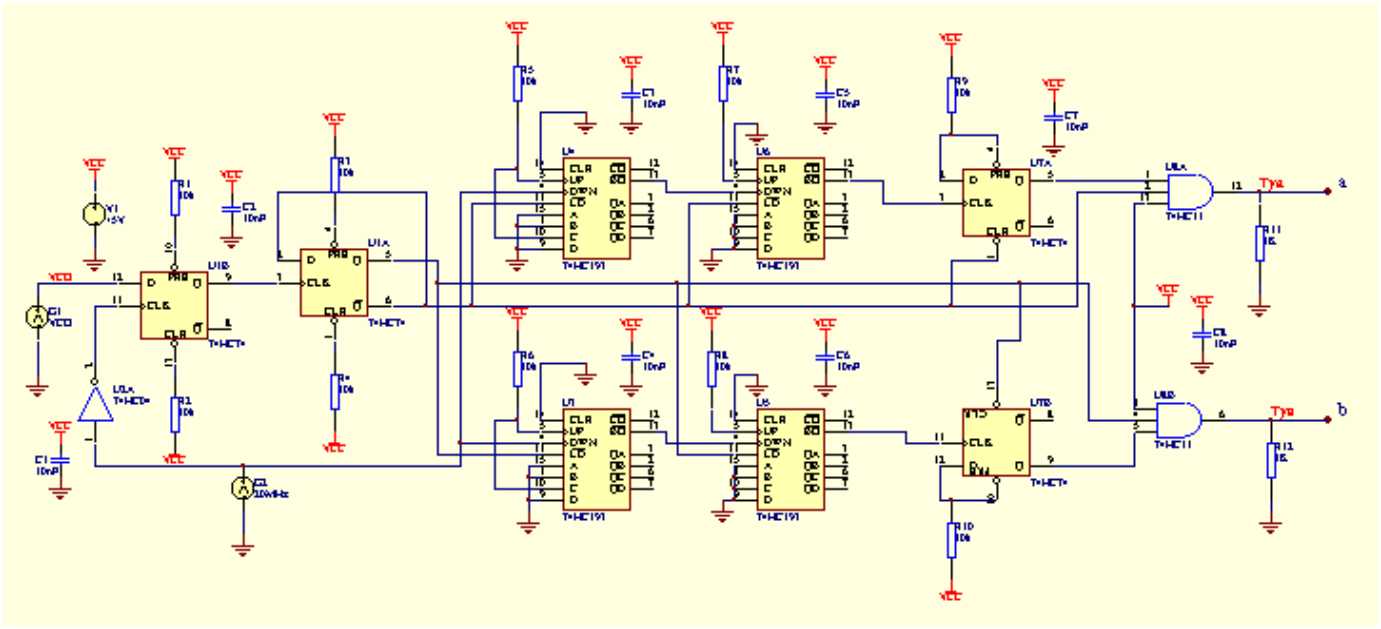

Fig 1 Control signal generating circuit – variant 1

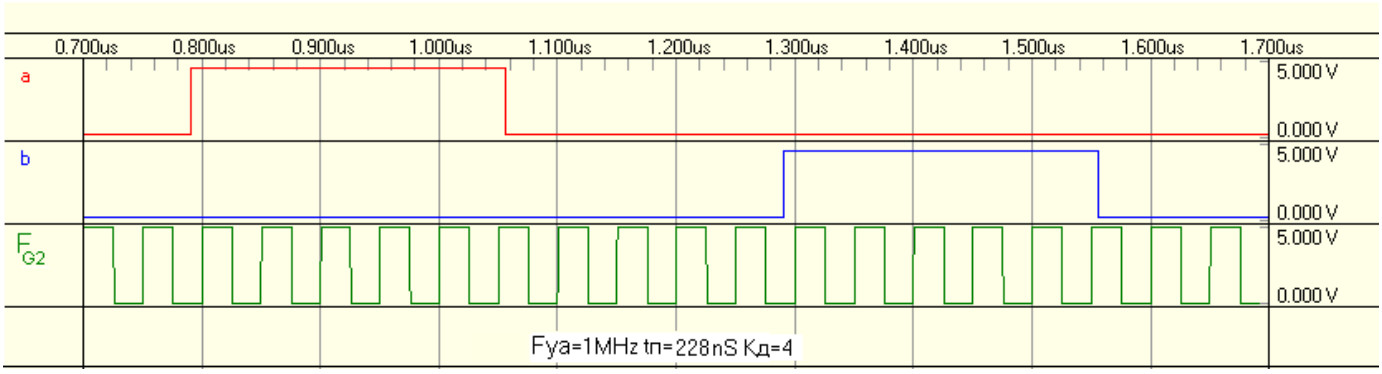

Fig 2 Output signal timing diagram for the circuit 1

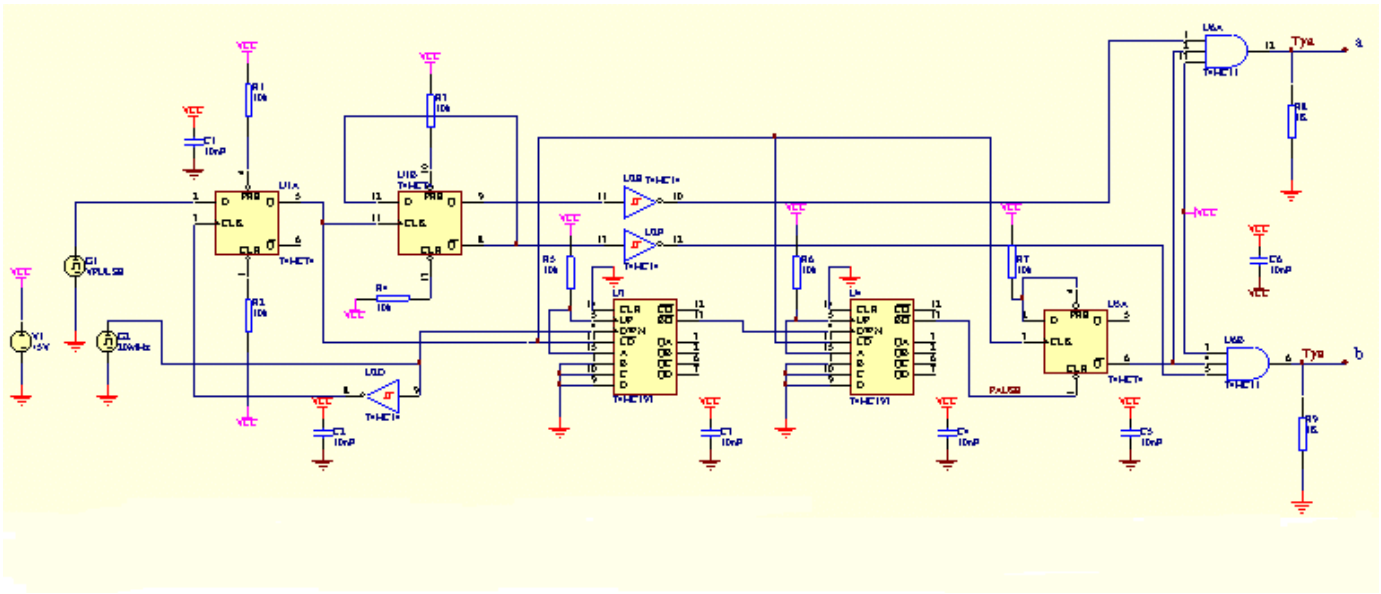

Fig 3 Control signal generating circuit – variant 2

TABLE I

SIMULATION RESULTS FOR CIRCUIT DIAGRAM 1

F_y	T_y	$t_п=K_д.T_п$ [nS]						$K_д$						$t_п^C$ [nS]						$t_и^1$ [µS], $t_и^2$ [µS]					
KHz	µS	t_0	t_1	t_2	t_3	t_4	t_5	t_0	t_1	t_2	t_3	t_4	t_5	t_0	t_1	t_2	t_3	t_4	t_5	t_0	t_1	t_2	t_3	t_4	t_5
10	100	0	50	100	150	200	250	0	1	2	3	4	5	29	78	128	179	230	279	49,95	49,85	49,8	49,75	49,7	49,65
50	20	0	50	100	150	200	250	0	1	2	3	4	5	29	78	128	179	230	278	9,95	9,9	9,85	9,8	9,75	9,7
100	10	0	50	100	150	200	250	0	1	2	3	4	5	29,2	79	129	179	230	278	4,95	4,9	4,85	4,8	4,75	4,7
200	5	0	50	100	150	200	250	0	1	2	3	4	5	29,4	79	130	180	229	278	2,46	2,42	2,36	2,32	2,26	2,21
400	2,5	0	50	100	150	200	250	0	1	2	3	4	5	28,7	78,8	130	179	228	279	1,21	1,17	1,12	1,07	1,02	0,97
500	2	0	50	100	150	200	250	0	1	2	3	4	5	29	79	129	180	230	278	0,97	0,92	0,87	0,82	0,77	0,72
1000	1	0	50	100	150	200	250	0	1	2	3	4	5	30	79	129	180	228	279	0,465	0,418	0,37	0,318	0,27	0,22

TABLE II

EXPERIMENTAL RESULTS FOR CIRCUIT DIAGRAM 1

F_y	T_y	$t_п=K_д.T_п$ [nS]						$K_д$						$t_п^E$ [nS]						$t_и^1$ [µS], $t_и^2$ [µS]					
KHz	µS	t_0	t_1	t_2	t_3	t_4	t_5	t_0	t_1	t_2	t_3	t_4	t_5	t_0	t_1	t_2	t_3	t_4	t_5	t_0	t_1	t_2	t_3	t_4	t_5
10	100	0	50	100	150	200	250	0	1	2	3	4	5	32	82	133	183	233	283	49,991	49,987	49,981	49,978	49,976	49,973
50	20	0	50	100	150	200	250	0	1	2	3	4	5	31	82	132	183	232	282	9,94	9,89	9,84	9,79	9,74	9,68
100	10	0	50	100	150	200	250	0	1	2	3	4	5	32	83	134	182	233	282	4,94	4,89	4,84	4,79	4,74	4,68
200	5	0	50	100	150	200	250	0	1	2	3	4	5	32	83	133	184	233	281	2,44	2,40	2,34	2,30	2,24	2,19
400	2,5	0	50	100	150	200	250	0	1	2	3	4	5	31	81	134	183	234	281	1,19	1,13	1,10	1,05	1,00	0,968
500	2	0	50	100	150	200	250	0	1	2	3	4	5	32	82	132	182	232	283	0,968	0,918	0,868	0,818	0,768	0,718
1000	1	0	50	100	150	200	250	0	1	2	3	4	5	32	81	134	184	233	282	0,463	0,416	0,368	0,316	0,268	0,217

TABLE III

SIMULATION RESULTS FOR CIRCUIT DIAGRAM 2

F_y	T_y	$t_п=K_д.T_п$ [nS]							$K_д$							$t_п^C$ [nS]							$t_и^1$ [µS], $t_и^2$ [µS]						
KHz	µS	t_0	t_1	t_2	t_3	t_4	t_5	t_6	t_0	t_1	t_2	t_3	t_4	t_5	t_6	t_0	t_1	t_2	t_3	t_4	t_5	t_6	t_0	t_1	t_2	t_3	t_4	t_5	t_6
10	100	0	50	100	150	200	250	300	0	1	2	3	4	5	6	1,02	43	94	143	193	242	294	49,99	49,98	49,84	49,81	49,8	49,77	49,69
50	20	0	50	100	150	200	250	300	0	1	2	3	4	5	6	1,02	43	94	144	192	243	294	9,998	9,957	9,906	9,857	9,808	9,755	9,703
100	10	0	50	100	150	200	250	300	0	1	2	3	4	5	6	1,02	42	94	143	193	243	293	4,992	4,952	4,903	4,852	4,803	4,753	4,701
200	5	0	50	100	150	200	250	300	0	1	2	3	4	5	6	1,03	43	95	143	193	243	292	2,492	2,452	2,402	2,352	2,313	2,253	2,202
400	2,5	0	50	100	150	200	250	300	0	1	2	3	4	5	6	1,02	44	94	142	192	244	293	1,242	1,202	1,152	1,102	1,052	1,003	0,957
500	2	0	50	100	150	200	250	300	0	1	2	3	4	5	6	1,02	44	95	144	194	243	293	0,991	0,953	0,902	0,852	0,804	0,754	0,704
1000	1	0	50	100	150	200	250	300	0	1	2	3	4	5	6	1,03	43	94	143	194	244	294	0,499	0,457	0,415	0,352	0,303	0,255	0,204

TABLE IV

EXPERIMENTAL RESULTS FOR CIRCUIT DIAGRAM 2

F_y	T_y	$t_п=K_д.T_п$ [nS]							$K_д$							$t_п^E$ [nS]							$t_и^1$ [µS], $t_и^2$ [µS]						
KHz	µS	t_0	t_1	t_2	t_3	t_4	t_5	t_6	t_0	t_1	t_2	t_3	t_4	t_5	t_6	t_0	t_1	t_2	t_3	t_4	t_5	t_6	t_0	t_1	t_2	t_3	t_4	t_5	t_6
10	100	0	50	100	150	200	250	300	0	1	2	3	4	5	6	2,4	47	98	147	197	247	297	49,99	49,98	49,81	49,8	49,79	49,76	49,68
50	20	0	50	100	150	200	250	300	0	1	2	3	4	5	6	2,2	48	97	147	197	247	297	9,99	9,95	9,9	9,85	9,8	9,75	9,7
100	10	0	50	100	150	200	250	300	0	1	2	3	4	5	6	2,1	48	97	147	198	247	298	4,99	4,95	4,9	4,85	4,8	4,75	4,7
200	5	0	50	100	150	200	250	300	0	1	2	3	4	5	6	2,3	47	97	147	198	248	298	2,49	2,45	2,4	2,35	2,31	2,25	2,2
400	2,5	0	50	100	150	200	250	300	0	1	2	3	4	5	6	2,1	48	97	147	198	248	298	1,24	1,2	1,15	1,1	1,05	1	0,955
500	2	0	50	100	150	200	250	300	0	1	2	3	4	5	6	2,2	48	98	147	198	248	298	0,99	0,952	0,9	0,85	0,802	0,752	0,702
1000	1	0	50	100	150	200	250	300	0	1	2	3	4	5	6	2,2	48	98	147	198	248	298	0,49	0,452	0,4	0,353	0,302	0,252	0,202

Microprocessor System for Control, Testing and Regulation of Transistor Converter Devices

Hristo Z. Karailiev[1], Valentina V. Rankovska[2], Nikolai D. Madjarov[3]

Abstract – **In this paper the structure and the modes of operation of a microprocessor system for control, test and regulation of a class of transistor power converters – resonant inverters is presented. The system allows to set the parameters of the output control signals at a wide frequency and duration range, to receive an information about the resonant inverter operation and to convert, save and indicate it.**

Keywords – **microprocessor system, control, test, regulation, resonant inverter**

I. INTRODUCTION

In recent years together with the quick development of the active and passive elements for the power converters, ambition to synthesize new circuits including principles and operating modes which allow higher frequencies, reducing the mass and dimensions parameters (kW/dm^3) and the price (EURO/kW) of the devices is observed. The successful realization and testing of the power circuit of such devices is determined to a great extent by the availability of a flexible control system allowing a change of control pulses parameters (frequency, amplitude, duration) and watching the output characteristics in order to define and optimize the operating mode [2].

In every separate case development of individual control systems for the transistor power converters is needed because of the various powers, frequencies, operating modes and changes of the load during the technological process. Accumulating an information about the operating modes and determining an advisable limits of change while regulating are also required.

Every time this leads to solve one and the same problem to synthesize a system for control, test, regulation and protection. On one hand the solutions are not always optimal and on the other hand redundant time is lost to develop, make experiments and debug.

II. AIM AND TASKS OF THE PROJECT

The aim of the present report is to develop a universal variant of a microprocessor control system (MCS) allowing to generate control signals at the range from 10 kHz to 1 MHz with a step of 100 Hz and duration changed with step of 50 ns. The system have to control a resonant inverter and to measure the output characteristics and parameters defining the operating modes and advisability of the project.

[1] Hristo Z. Karailiev is from the Technical University, 4 H. Dimitar str. 5300 Gabrovo, Bulgaria, E-mail: hkarailiev@hotmail.com

[2] Valentina V. Rankovska is from the Technical University, 4 H. Dimitar str. 5300 Gabrovo, Bulgaria, E-mail: rankovska@tugab.bg

[3] Nikolai D. Madjarov is from the Technical University, 4 H. Dimitar str. 5300 Gabrovo, Bulgaria, E-mail: madjarov@tugab.bg

The main problems to resolve are the following:

- Defining the main features of the microprocessor system to meet the requirements for universality and intended for a class of converting devices – resonant inverters;
- Synthesizing a block diagram of the control system and description of the purpose and the main features of it's blocks;
- To present the operation of the control device at different operating modes and also the ways to start and stop them.

III. FEATURES OF MICROPROCESSOR SYSTEM

The main features of the presented system are as follows:

- Setting the frequency of the control pulses equal for the two output channels at the range from 10 kHz to 1 MHz with a step of 100 Hz by a keyboard or automatically;
- Generating two-channel sequence of control signals dephased by π (rad) and separated galvanically from the powerful circuit of the inverter;
- Setting a programmable pause at switching over the channels equal for both of them at the range from 50 ns to 12,75 μs with a step of 50 ns by a keyboard or automatically;
- Control menu including commands for debugging, input parameters values, choosing a mode, measuring, saving and indicating currents, voltages, control signal parameters, time durations, etc.;
- Three operating modes of the system:

⇒ setting the parameters of the control signals, choosing the mode of operation, regulating time durations, etc.;

⇒ testing the combined operation of the resonant inverter and the control system. This is achieved by setting control signals with fixed values of the parameters, measuring, saving and indicating currents and voltages which characterizes the mode of operation of the resonant inverter;

⇒ regulating and maintaining automatically the power of the resonant inverter following a particular law of control.

- Measuring, saving and indicating on LCD the working frequency in kHz, the value of the pause in ns, the values of the high frequency current and voltages, the phase difference between the current and the voltage in the resonant circuit of the resonant inverter, time intervals, etc.;

- Blocking the output signals manually by a keyboard or automatically after definite time-out or by the differential protection.
- Indicating on LEDs the current mode of operation, the source power, the differential protection, time-out.
- Reprogramming the program memory of the microcontroller and ability to debug together the monitoring software and the hardware of the system.

IV. Block Diagram of Microprocessor System

The block diagram of the microprocessor control system is synthesizes on the base of the features mentioned above (Fig. 1). The purpose of each of the blocks is following:

CB – Control Block. It is based on an Atmel ATmega128L microcontroller [3]. It's program memory containing the monitoring program is 128kB. The internal data memory is 4 kB and the external data memory is 1 GB. CB is connected with all other blocks of the MCS.

SPI - Serial Programming Input. It is intended for connecting the programmer Atmel STK500 to program and correct the monitor program.

JTAG – input intended for connecting Atmel JTAG ICE to debug the monitor program and the hardware of the MCS.

LED, LCD – Indicator blocks (LEDs and LCD) showing the values of the parameters or the current mode of operation.

K – Keyboard for setting the input parameter values in the first mode and to choose and start a command from the menu.

PTI - Programmable Time Intervals block generating digitally two-channel control signals with programmable duration set manually by the operator or automatically by the regulating algorithm.

TGB – Timing Generation Block setting the step of the change for the programmable interval generated by PTI.

PFB - Programmable Frequencies Block implementing various frequencies of the control signals at the range from 10 kHz to 1 MHz, set manually by the operator or automatically by the regulating algorithm.

GSB - Galvanic Separation Block isolating galvanically the programmable duration control signals from the signals Y1÷Y4 driving the gates of the transistors T1÷T4.

DB – Drivers Block generating and regulating the level of the control signals Y1÷Y4 grouped in couples: Y1 and Y3 sourced by the first channel and Y2 and Y4 sourced by the second channel of the output signal from GSB.

FLS – Block Forming the Levels of the Signals from the voltage transformer (HT) and the current transformers TT1÷TT5 at the range of 0÷3 V and also to generate the phase difference between the current and voltage in the resonant circuit.

DPB – Differential Protection Block applying a control signal for switching off the resonant inverter by stopping the control pulses in an emergency mode – simultaneous operating of the transistors in one and the same side [1].

PS1,2 – Power Sources 1 and 2.

RI – Resonant Inverter

V. Operation Modes of the Control System

Three modes of operation exist:

- "Setting the system" mode

The purpose of the mode is to set the parameters of the signals supplying the operation of the system in the other two modes.

In that mode the system is prepared for the two other modes without starting the operation of the inverter. The system is getting into this mode automatically by default at switching on the power supply.

In this mode possibilities are provided for inputting the parameters of the control signals – operation frequency and duration, the power of the resonant inverter, operating time, time durations for maintenance various values of the output power, etc.

- "Testing, measuring and indicating" mode

The main task of this mode is to control the operation of the resonant inverter at fixed values of the control signals parameters, to measure, save and indicate the values of the characteristics of the resonant inverter. In this way it is possible to accumulate digital information at the various operation modes of the transistors at various fixed values of the frequency and various durations of the control signals.

The starting of this mode is possible from the first mode by the command "Start/Test" from the main menu. The results of the measuring may be saved in the memory of the CB, and also may be indicated on the LCD.

Quitting the mode is possible by two ways:

⇒ Manually, by a command "Stop" input by the operator. The resonant inverter operation is stopped by blocking the control signals;

⇒ Automatically, after a definite time period while the device is operating or switching on the differential protection.

- "Regulating and maintenance the power" mode

The main task of the mode is to monitor the changes of the operation mode according to prior defined control law of the resonant inverter defined by the particular technological process and to maintain it in advisable limits.

This leads to possibilities for realization of the particular technological process maintaining an optimal mode of operation.

The start of the mode is implemented from the first mode by a command "Start regulation". In this mode the parameters values of the RI are monitored automatically and the control signal parameters are changed automatically with a defined step at advisable limits.

Quitting the mode is as at the previous one – manually or automatically.

VI. Conclusion

The suggested analysis approach is characterized with flexible development of the monitor program and leads to reducing the time of development of optimal control system circuits.

The presented microprocessor system is suitable for implementing in development of wide range of transistor resonant inverters, as it allows an easy setting in a wide range the parameters of the transistor control signals. On the other hand it allows measuring the output

characteristics and parameters and precise defining of the modes of operation.

The measuring and saving the values of the main characteristics and parameters of the resonant inverters allows to determine their static and dynamic parameters by the means of analysis.

The system is implemented and tested in laboratory conditions to control the operation of resonant inverters with operation frequency by 500 kHz and power by 3 kW.

REFERENCES

[1] С. Е. Табаков, Х. Е. Алексиев, “Защита на IGBT от късо съединение”, сп. Е+Е, № 5-6, 1995, pp. 8-14.

[2] R. W. Erickson, “Fundamentals of Power Electronics”, Chapman&Hall, NY, 1997.

[3] ATmega128(L) Data Sheet, Atmel Corp., 2003

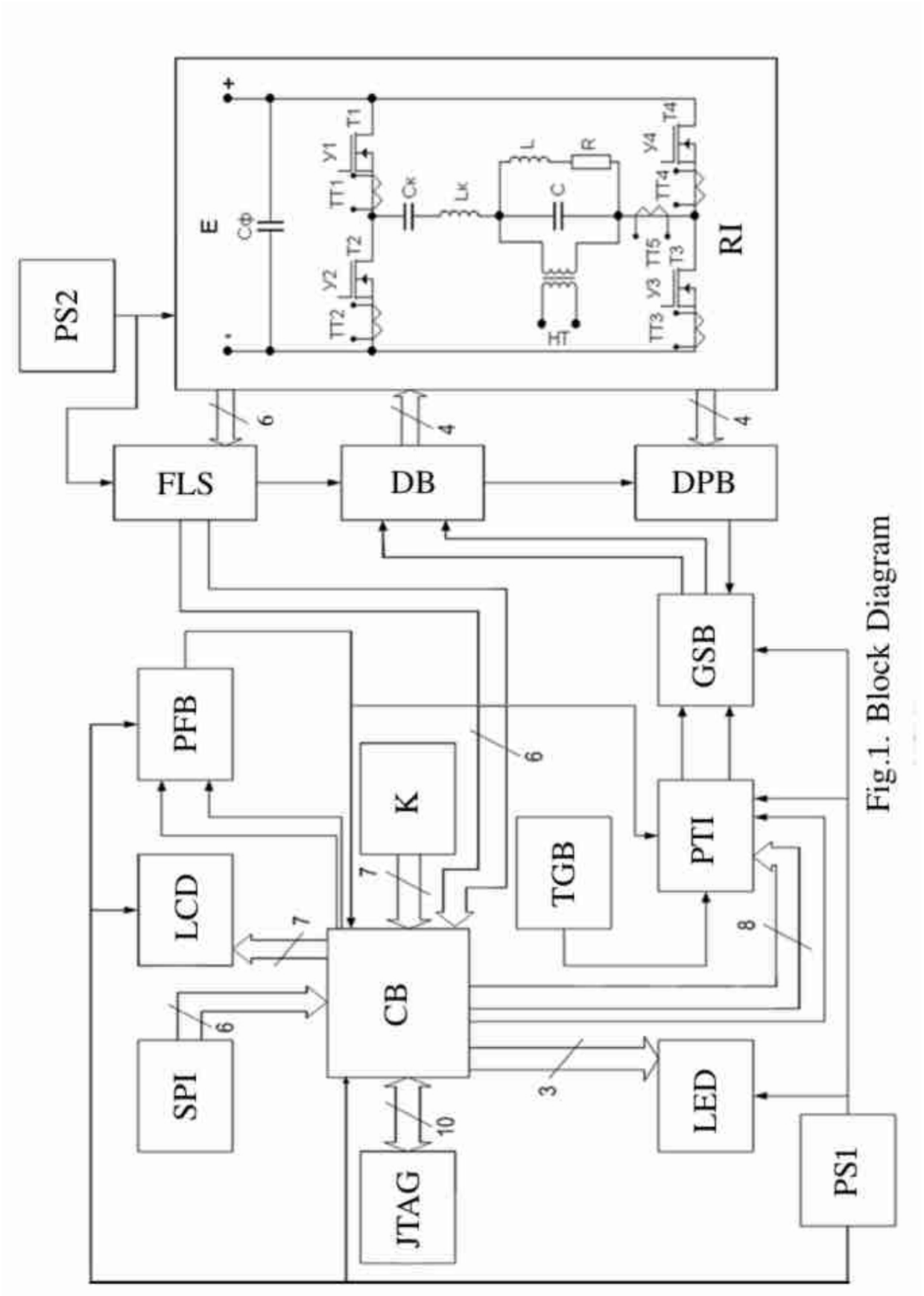

Fig.1. Block Diagram

Modeling and Investigation of a Position Control Drive System

Mikho R. Mikhov[1]

Abstract – **The performance of a permanent magnet synchronous motor drive system with position control is discussed in this paper. Detailed study and analysis have been carried out for different loads at respective dynamic and static regimes. The developed computer simulation models and the results obtained can be used in optimizing and tuning of such types of position drive systems.**

Keywords – **Position control drive, Brushless DC motor drive**

I. INTRODUCTION

In recent years permanent magnet synchronous motors (PMSM) have been used in many high performance applications such as numerically controlled machine tools, robotics, electric vehicles, aerospace, and many more [1], [4], [6], [7].

The increasing interest can be explained by their following advantages:

- low power loss and high efficiency;
- high power-mass ratio;
- good heat dissipation characteristics;
- low rotor inertia and good dynamics;
- high speed capabilities.

Generally, according to the phase current waveforms, PMSM electric drives can be classified as brushless DC motor drives (with rectangular current control) and brushless AC motor drives (with sinusoidal current control) [2].

This paper describes the performance of a brushless DC motor drive system with position control in which a parabolic position controller has been applied. Detailed analysis and study by means of modeling and computer simulation have been carried out for the respective transient and steady state regimes. Some investigation results are presented and discussed.

II. MODELING OF THE DRIVE SYSTEM

The simplified block diagram of the position control drive system under consideration is shown in Fig.1. MS is a three-phase PMSM controlled in brushless DC motor mode [5]. The corresponding notations are as follows: PC - position controller; SC - speed controller; RC - reference current block; CC - current controllers block; IC - inverter control block; VI – six-step voltage source inverter; RF – rectifier; PS - position sensor; PF - position feedback block; SF - speed feedback block; L - load of the electric drive; V_{pr} - position reference signal; V_{sr} - speed reference signal; V_{cr} - current reference signals for the phases *a*, *b* and *c* respectively; $2\Delta i_r$ - reference hysteresis band; V_{pf} - position feedback signal; V_{sf} - speed feedback signal; V_{cf} - current feedback signals; V_d - DC link voltage; C - filter capacitor; ω - angular motor speed; θ - angular position; T_l - load torque applied to the motor shaft.

The simplifying assumptions in the analysis of the electric drive are as follows:

- the motor is unsaturated;
- eddy-current and hysteresis effects in the electric motor's magnetic materials have negligible influence on the stator winding current;
- the motor is a symmetrical three-phase machine;
- there is no saliency and therefore self and mutual inductances are constant and independent of rotor position;
- the devices in the power-electronic circuits are ideal.

The PMSM model and the respective power-electronic circuits are represented in Fig. 2, where $S1 \div S6$ are power electronic switches and $D1 \div D6$ are diodes.

The circuit equation in phase variables is:

$$\begin{bmatrix} v_a \\ v_b \\ v_c \end{bmatrix} = \begin{bmatrix} R_s & 0 & 0 \\ 0 & R_s & 0 \\ 0 & 0 & R_s \end{bmatrix} \begin{bmatrix} i_a \\ i_b \\ i_c \end{bmatrix} + \begin{bmatrix} L_a & L_{ba} & L_{ca} \\ L_{ba} & L_b & L_{cb} \\ L_{ca} & L_{cb} & L_c \end{bmatrix} \frac{d}{dt} \begin{bmatrix} i_a \\ i_b \\ i_c \end{bmatrix} + \begin{bmatrix} e_a \\ e_b \\ e_c \end{bmatrix}, \quad (1)$$

where v_a, v_b, v_c are the voltages applied in stator phases *a*, *b* and *c* respectively; i_a, i_b, i_c - the phase currents; e_a, e_b, e_c - the back electromotive forces (EMFs); $R_s = R_a = R_b = R_c$ - the stator phase resistance; L_a, L_b, L_c - the phase self inductances; L_{ba}, L_{ca}, L_{cb} - the mutual inductances.

The back EMF shape waveforms are expressed by the following equation

$$\begin{bmatrix} e_a \\ e_b \\ e_c \end{bmatrix} = \omega \frac{d}{d\theta} \begin{bmatrix} \Phi_a \\ \Phi_b \\ \Phi_c \end{bmatrix}, \quad (2)$$

where Φ_a, Φ_b, Φ_c are the stator magnetic fluxes of phases *a*, *b*, and *c* respectively.

Assuming there is no change in the rotor reluctance with angular position, then

$$L_a = L_b = L_c = L \quad (3)$$

[1]Mikho R. Mikhov is with the Faculty of Automatics, Technical University of Sofia, 8 Kliment Ohridski Str., 1797 Sofia, Bulgaria, E-mail: mikhov@tu-sofia.bg

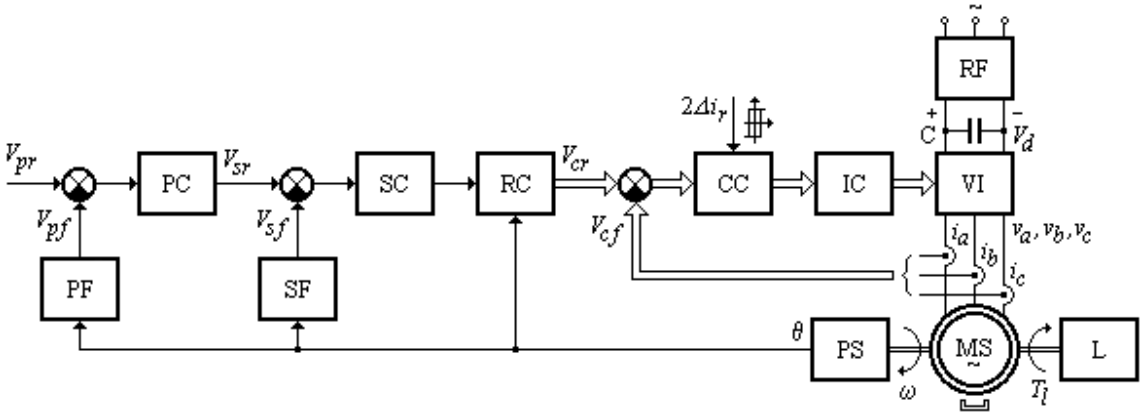

Fig. 1. Block diagram of the drive system under consideration

and

$$L_{ba} = L_{ca} = L_{cb} = M \,. \tag{4}$$

Since the motor windings are star connected, the next relations can be obtained:

$$i_a + i_b + i_c = 0 \,, \tag{5}$$

and

$$Mi_b + Mi_c = -Mi_a \,. \tag{6}$$

Thus, the electric dynamic equations for each motor phase are arranged as follow:

$$\frac{di_a}{dt} = \frac{1}{L_s}\left(v_a - R_s i_a - e_a\right); \tag{7}$$

$$\frac{di_b}{dt} = \frac{1}{L_s}\left(v_b - R_s i_b - e_b\right); \tag{8}$$

$$\frac{di_c}{dt} = \frac{1}{L_s}\left(v_c - R_s i_c - e_c\right), \tag{9}$$

where $L_s = L - M$ is the stator phase inductance.

The motor electromagnetic torque can be expressed as

$$T = \frac{e_a i_a + e_b i_b + e_c i_c}{\omega} \,, \tag{10}$$

and the mechanical dynamics equations are as follows:

$$J\frac{d\omega}{dt} = T - T_l - D\omega \,; \tag{11}$$

$$\frac{d\theta}{dt} = \omega \,, \tag{12}$$

where J is the total inertia referred to the motor shaft; D - the viscous damping coefficient.

The current controllers have programmable hysteresis band $2\Delta i_r$ which determines the modulation frequency of the inverter f_m.

The transfer function of the speed controller is

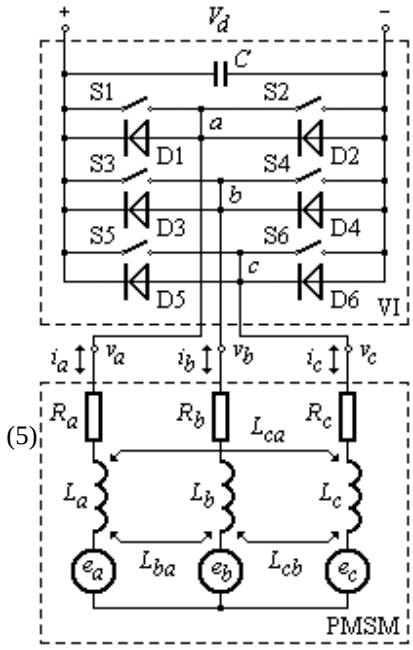

Fig. 2. Model of the motor and respective power-electronic circuits

$$G_{sc}(s) = K_{sc}\left(1 + \frac{1}{\tau_{sc} s}\right), \tag{13}$$

where K_{sc} is the respective coefficient and τ_{sc} is the controller time-constant.

A parabolic position controller is used in the investigated system [3]:

$$G_{pc}(s) = K_{pc}(\Delta\theta) = \frac{K_{sf}}{K_{pf}}\sqrt{\frac{\varepsilon_b}{2\Delta\theta}} \tag{14}$$

where K_{sf} is the coefficient of the speed feedback block; K_{pf} - the coefficient of the position feedback block; ε_b - the

reference deceleration.

The position controller performance is illustrated in Fig. 3, where the following notations are used: $\Delta\theta_{b\max}$ - maximum braking angle; $\Delta\theta_{bs}$ - braking distance at which the controller coefficient value is switched over; $V_{sr\max}$ - maximum speed reference signal.

The motor speed reference signal is determined by the expression

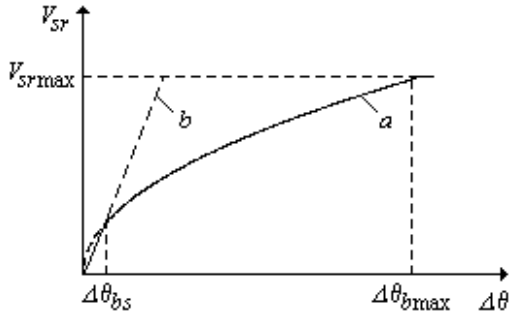

Fig. 3. Illustration of the position controller performance

$$V_{sr} = K_{pc}(\Delta\theta)K_{pf}\Delta\theta \tag{15}$$

After substitution of Eq. 14 in Eq. 15, the following is obtained (Fig. 3, curve *a*):

$$V_{sr} = K_{sf}\sqrt{\frac{\varepsilon_b \Delta\theta}{2}} \tag{16}$$

Reduction of $\Delta\theta$ brings about to increase of K_{pc} up to a value equal to K_{pcs}, calculated according to the admissible overshoot. At $\Delta\theta < \Delta\theta_{bs}$ the $V_{sr}(\Delta\theta)$ ratio coincides with the *b* straight line.

Using MATLAB/SIMULINK software package a number of computer simulation models of electric drives have been developed. A detailed study of the drive system under consideration has been carried out for different loads at transient and steady state regimes.

III. SIMULATION RESULTS

Fig. 4 shows the phase current waveform i_a and the respective trapezoidal back electromotive force e_a obtained at steady state regime for rated load.

Fig 5 illustrates dynamic maintenance of zero phase current.

The programmable hysteresis band influence is shown in Fig. 6 where are represented current waveforms for two reference hysteresis bands.

Fig. 7 represents motor speed stabilization when the load changes. Transient and steady state regimes are represented, as well as the drive system reaction to disturbances expressed in load changes. The load torque acting upon the motor shaft is equal to the rated value $T_{l\text{rat}}$, while the disturbances applied sequentially on the drive are $\pm\Delta T_l = \pm 0.5 T_{l\text{rat}}$. The reference speed is $\omega_r = 157$ rad/s and the starting current is limited to the maximum admissible value $I_{\max}$, which provides maximum starting motor torque.

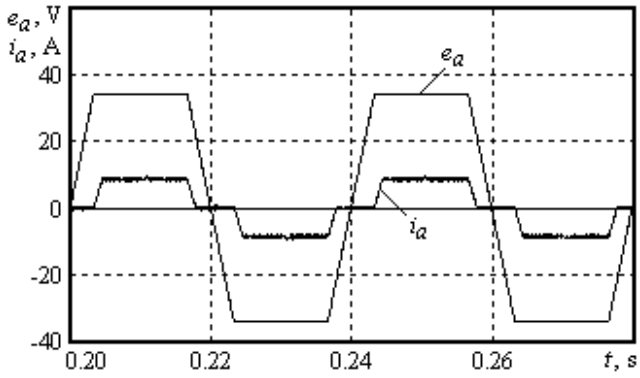

Fig. 4. Phase current and back electromotive force waveforms

Some time-diagrams obtained at reverse speed control with electrical braking are shown in Fig 8. The braking torque of the motor is notated as T_b. The reference speed values in this case are $\pm\omega_r = \pm 100$ rad/s.

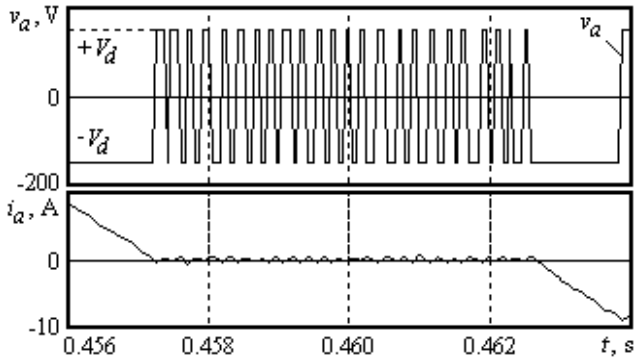

Fig. 5 Dynamic maintenance of zero phase current

Fig. 9 represents simulation results from the investigation of the electric drive system at position control. The motor speed is limited to the maximum value of $\omega_{\max}$, which ensures good dynamics of the drive system.

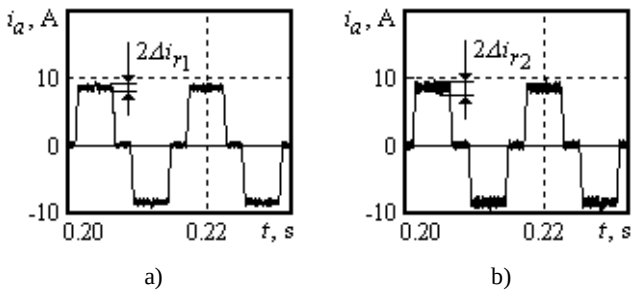

a) b)

Fig. 6. Influence of the current controllers hysteresis band

IV. CONCLUSION

The used motor rated power is $P_{\text{rat}} = 0.6\,\text{kW}$, and the rated speed is $\omega_{\text{rat}} = 157\,\text{rad/s}$.

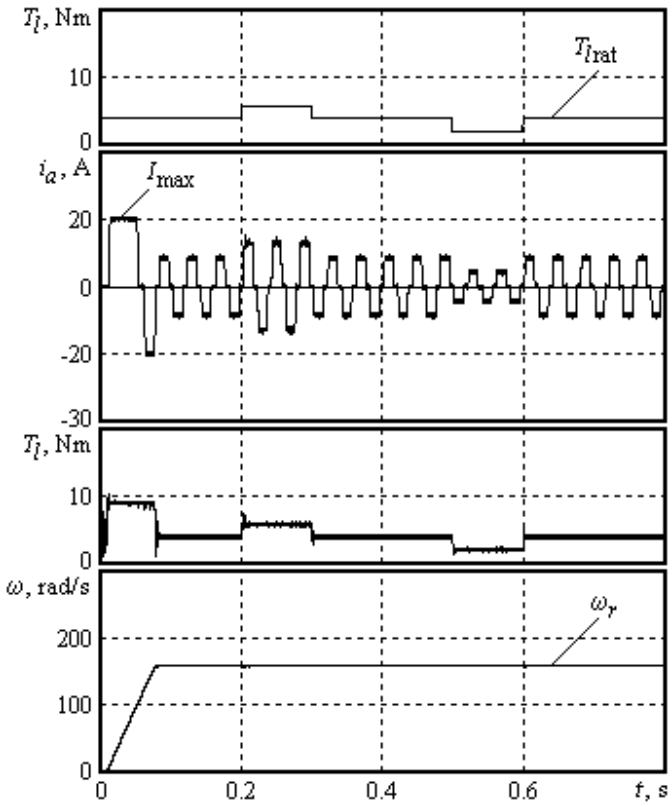

Fig. 7. Motor speed stabilization at load changes

Some specified appropriate setting parameters of the studied electric drive system are as follows: maximum modulation frequency $f_{m\max} = 8\,000\,\text{Hz}$; hysteresis band $2\Delta i_r = 1\,\text{A}$; maximum phase current $I_{\max} = 20\,\text{A}$.

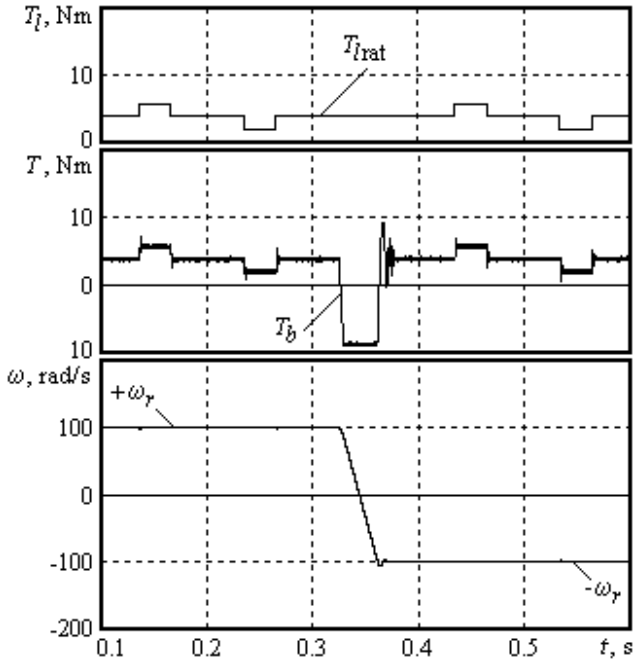

Fig. 8. Diagrams at reverse speed control with electrical braking

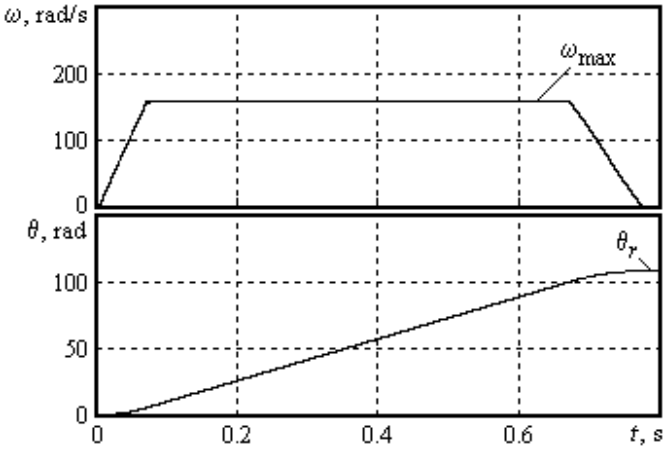

Fig. 9. Time-diagrams at position control of the electric drive

The analysis of the investigated dynamic and steady state regimes shows that the represented electric drive system provides good performance, which makes it suitable for a variety of industrial applications. The developed models and the respective simulation results can be used in optimizing and final tuning of such types of position control drive systems.

ACKNOWLEDGEMENT

This work has been supported by the Bulgarian Ministry of Education and Science, under the project N: 449-8 HK/2004.

REFERENCES

[1] F. Bodin, S. Siala. New reference frame for brushless DC motor drive, *Proceedings of the Conference on Power Electronics and Variable Speed*, pp. 554-559, London, UK, 1998.

[2] I. Boldea, S. A. Nasar, *Electric Drives*, Boca Raton, CRC Press, 1999.

[3] V. I. Klyuchev, *Electric Drive Theory*, Moscow, Energoatomizdat, 1985 (in Russian).

[4] K. Lee, J. Park, H. Yeo, J. Yoo, H. Jo. Current control algorithm to reduce torque ripple in brushless DC motors, *Proceedings of the International Conference on Power Electronics*, pp. 380-385, Seoul, Korea, 1998.

[5] M. R. Mikhov, Investigation of a Permanent Magnet Synchronous Motor Control System, *Technical Ideas*, vol. 38, no. 3-4, pp. 23-34, 2001.

[6] S. K. Safi, P. P. Acarnley, A. G. Jack. Analysis and simulation of the high-speed torque performance of brushless DC motor drives, *IEE Proceedings – Electric Power Applications*, vol. 142, no. 3, pp. 191-200, 1995.

[7] Y. Yoon, D. Kim, T. Lee, Y. Choe, C. Won, A Low Cost Speed Control System of PM Brushless DC Motor Using 2 Hall-Ics, *Proceedings of the International Conference on Mechatronics and Information Technology*, pp. 150-155, Jecheon, Korea, 2003.

On Relation Between Minimum Variance and Sliding Mode Equivalent Control Concepts

Darko Mitic, Cedomir Milosavljevic and Boban Veselic[1]

Abstract **- The paper investigates the connection existing between the minimum variance control and the discrete-time sliding mode equivalent control. It is shown that the minimum variance control represents the counterpart of the discrete-time equivalent control for the input-output based sliding mode control design approaches.**

Keywords **- Variable structure control systems, Discrete-time sliding mode control**

I. INTRODUCTION

Variable structure control (VSC) systems [1] are well-known and well-studied class of nonlinear systems, wherein sliding mode is of particular interest. It happens when a control forces a system state to move along a predefined sliding surface in spite of the actions of external disturbances and parameter perturbations. This is accomplished by a high frequency control signal whose switching is guided by a function also known as the switching function. The switching function, equalized with zero, determines the equation of the above mentioned sliding surface. When the system is in sliding mode, the control can be replaced by the so-called equivalent control [2], a very powerful mean for the analysis of system dynamics. If a system state is on a sliding surface, the equivalent control will ensure a system motions towards the steady-state.

The discretization process and the control algorithm implementation by using a digital signal processor produce a quasi-sliding mode [3] and a discrete-time equivalent control [4]. Regardless of the use of continuous- or discrete-time sliding mode techniques, the equivalent control is based on the system modeling in the state space. For the input-output based control approaches, the combinations of minimum variance and sliding mode controls seem to be more appropriate [5-7].

The aim of this paper is to show that the minimum variance control corresponds to the discrete-time equivalent control for the case when only plant input and output signals are measured to form the control law. As we can see later, this link is settled by the implementation of the techniques for equivalent control derivation on some modified system state-space model.

[1]Authors are with the Faculty of Electronic Engineering, University of Nis, Medvedeva 14, 18000 Nis, Serbia and Montenegro, E-mails: darkom@elfak.ni.ac.yu , milosavljevic@elfak.ni.ac.yu , bveselic@elfak.ni.ac.yu .

The paper is organized as follows. In Section II and Section III, the brief descriptions of the discrete-time equivalent control and the minimum variance control are given, respectively. Section IV presents the procedure which proves that the minimum variance control is really discrete-time equivalent control analog for input-output based VSC systems. This approach is referred to as the input-output based equivalent control concept. In Section V, the illustrative example of the second order system demonstrates the established connections between the minimum variance control and the equivalent control, and explains why the equivalent control algorithm, described in Section IV, can not be used for treating the VSC problems based on measuring of input-output signals.

II. DISCRETE-TIME EQUIVALENT CONTROL

Let us consider a discrete-time state-space model of a single-input-single-output plant of the *n*-th order:

$$\begin{aligned} \mathbf{x}(k+1) &= \mathbf{\Phi x}(k) + \boldsymbol{\gamma} u(k), \\ y(k) &= \mathbf{d x}(k) = x_1(k), \end{aligned} \tag{1}$$

where: $\mathbf{x}(k) = [x_1(k) \quad x_2(k) \quad ... \quad x_n(k)]^{\mathrm{T}}$ is a vector of state coordinates, $u(k)$ is a control input, $y(k)$ is a plant output, $\mathbf{\Phi} = \lfloor \phi_{ij} \rfloor_{nxn}$ and $\boldsymbol{\gamma} = [\gamma_i]_{n\mathrm{x}1}$. We suppose that a system is autonomous, i.e. a reference signal is equal to zero. Notice that $\bullet(k) = \bullet(kT)$ with T as a sampling period. Let the switching function be:

$$s(k) = \boldsymbol{\sigma x}(k), \quad \boldsymbol{\sigma} = [\sigma_0 \quad \sigma_1 \quad ... \quad \sigma_{n-1}], \tag{2}$$

with the coefficients of $\boldsymbol{\sigma}$ forming the Jury's polynomial.

By substituting Eq. (1) in Eq. (2), someone gets:

$$s(k+1) = \boldsymbol{\sigma \Phi x}(k) + \boldsymbol{\sigma \gamma} u(k) . \tag{3}$$

The liner control law that would provide the ideal discrete-time sliding mode, also called the discrete-time equivalent control, is obtained by solving $s(k+1) = 0$ as:

$$u_{eq}(k) = -(\boldsymbol{\sigma \gamma})^{-1} \boldsymbol{\sigma \Phi x}(k), \tag{4}$$

assuming $\boldsymbol{\sigma \gamma} \neq 0$. In other words, if the state of the system is initially on the sliding surface $s(k) = 0$, the control (4) will provide the system motion on $s(k) = 0$ and towards the steady state.

III. MINIMUM VARIANCE CONTROL

The discrete-time model of the plant (1) in *z*-domain is given by:

$$y(k) = \frac{z^{-1}B(z^{-1})}{A(z^{-1})}u(k), \quad (5)$$

where:

$$A(z^{-1}) = z^{-n}\det(z\mathbf{I} - \mathbf{\Phi}), \quad (6)$$

$$B(z^{-1}) = z^{-n+1}\mathbf{d}\,\mathrm{adj}(z\mathbf{I} - \mathbf{\Phi})\boldsymbol{\gamma}, \quad (7)$$

and z^{-1} is a unit delay ($z^{-1} = e^{-sT}$, s is a complex variable).

The switching function is now chosen as:

$$s(k) = C(z^{-1})y(k). \quad (8)$$

The polynomial $C(z^{-1}) = c_0 + c_1 z^{-1} + ... + c_{n-1}z^{-n+1} + c_n z^{-n}$ has all zeros inside the unit disk.

The linear control ensuring $s(k+1) = 0$ is the minimum variance control:

$$u_{mv}(k) = -\frac{F(z^{-1})}{E(z^{-1})B(z^{-1})}y(k). \quad (9)$$

The polynomials $E(z^{-1})$ and $F(z^{-1})$ are the solutions of the so-called Diophantine equation:

$$E(z^{-1})A(z^{-1}) + z^{-1}F(z^{-1}) = C(z^{-1}). \quad (10)$$

It can be easily proved, by implementing Eq. (9) in Eq. (5), taking into account Eq. (10), that $s(k+1) = 0$ is ensured by the control (9), indeed.

IV. Input-output Based Discrete-time Equivalent Control Approach

In order to show that the minimum variance control represents the equivalent control analog for the input-output based VSC systems, we convert the plant model (1) using the following transformation:

$$\mathbf{z}(k) = \mathbf{T}\mathbf{x}(k), \quad (11)$$

where:

$$\mathbf{z}(k) = [\mathbf{z}_1(k) \quad \mathbf{z}_2(k) \quad ... \quad \mathbf{z}_n(k)]^{\mathrm{T}}, \quad (12)$$

$$\mathbf{z}_i(k) = [x_i(k) \quad x_i(k-1) \quad ... \quad x_i(k-n)]^{\mathrm{T}}, \quad (13)$$

and $\mathbf{T}$ is the transformation matrix in the form of:

$$\mathbf{T} = \begin{bmatrix} \mathbf{t} & \mathbf{0} & ... & \mathbf{0} \\ \mathbf{0} & \mathbf{t} & ... & \mathbf{0} \\ \vdots & \vdots & & \vdots \\ \mathbf{0} & \mathbf{0} & ... & \mathbf{t} \end{bmatrix}, \quad (14)$$

$$\mathbf{t} = \begin{bmatrix} 1 & z^{-1} & ... & z^{-n} \end{bmatrix}^{\mathrm{T}}, \quad (15)$$

and we implement the procedure described in Section II for obtaining the discrete-time equivalent control.

The implementation of Eq. (11) in the plant model (1) gives:

$$\mathbf{z}(k+1) = \begin{bmatrix} \mathbf{\Phi_{11}} & \mathbf{\Phi_{12}} & ... & \mathbf{\Phi_{1n}} \\ \mathbf{\Phi_{21}} & \mathbf{\Phi_{22}} & ... & \mathbf{\Phi_{2n}} \\ \vdots & \vdots & & \vdots \\ \mathbf{\Phi_{n1}} & \mathbf{\Phi_{n2}} & ... & \mathbf{\Phi_{nn}} \end{bmatrix}\mathbf{z}(k) + \begin{bmatrix} \boldsymbol{\gamma}_1 \\ \boldsymbol{\gamma}_2 \\ \vdots \\ \boldsymbol{\gamma}_n \end{bmatrix}u(k), \quad (16)$$

with:

$$\mathbf{\Phi_{ij}} = \phi_{ij}\mathbf{I}_{(n+1)\mathrm{x}(n+1)}, \quad (17)$$

$$\boldsymbol{\gamma}_\mathbf{i} = \gamma_i \mathbf{t}, \quad (18)$$

since:

$$\mathbf{T}\mathbf{\Phi} = \begin{bmatrix} \mathbf{\Phi_{11}} & \mathbf{\Phi_{12}} & ... & \mathbf{\Phi_{1n}} \\ \mathbf{\Phi_{21}} & \mathbf{\Phi_{22}} & ... & \mathbf{\Phi_{2n}} \\ \vdots & \vdots & & \vdots \\ \mathbf{\Phi_{n1}} & \mathbf{\Phi_{n2}} & ... & \mathbf{\Phi_{nn}} \end{bmatrix}\mathbf{T}. \quad (19)$$

The model (16) can be rewritten as:

$$\mathbf{z}_1(k+1) = \mathbf{\Phi_{11}}\mathbf{z}_1(k) + \overline{\mathbf{\Phi}}_{\mathbf{12}}\overline{\mathbf{z}}_2(k) + \boldsymbol{\gamma}_\mathbf{1}u(k), \quad (20)$$

$$\overline{\mathbf{z}}_2(k+1) = \overline{\mathbf{\Phi}}_{\mathbf{21}}\mathbf{z}_1(k) + \overline{\mathbf{\Phi}}_{\mathbf{22}}\overline{\mathbf{z}}_2(k) + \overline{\boldsymbol{\gamma}}_\mathbf{2}u(k), \quad (21)$$

where:

$$\overline{\mathbf{\Phi}}_{\mathbf{12}} = [\mathbf{\Phi_{12}} \quad \mathbf{\Phi_{13}} \quad ... \quad \mathbf{\Phi_{1n}}], \quad (22)$$

$$\overline{\mathbf{\Phi}}_{\mathbf{21}} = [\mathbf{\Phi_{21}} \quad \mathbf{\Phi_{31}} \quad ... \quad \mathbf{\Phi_{n1}}]^{\mathrm{T}}, \quad (23)$$

$$\overline{\mathbf{\Phi}}_{\mathbf{22}} = \begin{bmatrix} \mathbf{\Phi_{22}} & ... & \mathbf{\Phi_{2n}} \\ \vdots & & \vdots \\ \mathbf{\Phi_{n2}} & ... & \mathbf{\Phi_{nn}} \end{bmatrix}. \quad (24)$$

$$\overline{\boldsymbol{\gamma}}_\mathbf{2} = [\boldsymbol{\gamma}_\mathbf{2} \quad \boldsymbol{\gamma}_\mathbf{3} \quad ... \quad \boldsymbol{\gamma}_\mathbf{n}]^{\mathrm{T}} \quad (25)$$

From Eq. (21), $\overline{\mathbf{z}}_2(k)$ is calculated as:

$$\overline{\mathbf{z}}_2(k) = \left(z\mathbf{I}_{(n^2-1)\mathrm{x}(n^2-1)} - \overline{\mathbf{\Phi}}_{\mathbf{22}}\right)^{-1}\overline{\mathbf{\Phi}}_{\mathbf{21}}\mathbf{z}_1(k) + \left(z\mathbf{I}_{(n^2-1)\mathrm{x}(n^2-1)} - \overline{\mathbf{\Phi}}_{\mathbf{22}}\right)^{-1}\overline{\boldsymbol{\gamma}}_\mathbf{2}u(k), \quad (26)$$

and substituted in Eq. (20), providing:

$$\mathbf{z}_1(k+1) = \tilde{\mathbf{\Phi}}(z)\mathbf{z}_1(k) + \tilde{\boldsymbol{\gamma}}(z)u(k), \quad (27)$$

with:

$$\tilde{\mathbf{\Phi}}(z) = \mathbf{\Phi_{11}} + \overline{\mathbf{\Phi}}_{\mathbf{12}}\left(z\mathbf{I}_{(n^2-1)\mathrm{x}(n^2-1)} - \overline{\mathbf{\Phi}}_{\mathbf{22}}\right)^{-1}\overline{\mathbf{\Phi}}_{\mathbf{21}}, \quad (28)$$

$$\tilde{\boldsymbol{\gamma}} = \boldsymbol{\gamma}_\mathbf{1} + \overline{\mathbf{\Phi}}_{\mathbf{12}}\left(z\mathbf{I}_{(n^2-1)\mathrm{x}(n^2-1)} - \overline{\mathbf{\Phi}}_{\mathbf{22}}\right)^{-1}\overline{\boldsymbol{\gamma}}_\mathbf{2}. \quad (29)$$

We choose now the switching function to be:

$$s(k) = \tilde{\mathbf{c}}\mathbf{z}_1(k), \quad \tilde{\mathbf{c}} = [\tilde{c}_0 \quad \tilde{c}_1 \quad ... \quad \tilde{c}_n]. \quad (30)$$

Notice that Eqs. (8) and (30) are equal if the coefficients $c_i = \tilde{c}_i$, $i = \overline{0,n}$. As in Section II, the discrete-time equivalent control is obtained by solving:

$$s(k+1) = \tilde{\mathbf{c}}\tilde{\mathbf{\Phi}}(z)\mathbf{z}_1(k) + \tilde{\mathbf{c}}\tilde{\boldsymbol{\gamma}}(z)u(k) = 0, \quad (31)$$

as:

$$u_{eq}(k) = -(\tilde{\mathbf{c}}\tilde{\boldsymbol{\gamma}}(z))^{-1}\tilde{\mathbf{c}}\tilde{\mathbf{\Phi}}(z)\mathbf{z}_1(k), \quad (32)$$

assuming $(\tilde{\mathbf{c}}\tilde{\boldsymbol{\gamma}}(z))^{-1}$ is realizable. Eqs. (9) and (32) have the similar form, representing the digital filters of the same order. This will be shown by the illustrative example given in the next section.

V. Illustrative Example

To promote the conversion procedure given in the previous section and to show that it gives similar digital filter as the minimum variance control technique, we consider the second order plant model whose transfer function is:

$$G(s) = \frac{Y(s)}{U(s)} = \frac{\omega_n^2}{s^2 + 2\zeta\omega_n s + \omega_n^2}, \quad (33)$$

and the continuos-time state-space model:

$$\begin{bmatrix}\dot{x}_1(t)\\ \dot{x}_2(t)\end{bmatrix}=\begin{bmatrix}0 & 1\\ -\omega_n^2 & -2\zeta\omega_n\end{bmatrix}\begin{bmatrix}x_1(t)\\ x_2(t)\end{bmatrix}+\begin{bmatrix}0\\ \omega_n^2\end{bmatrix}u(t) \quad (34)$$

Under the assumption that a control signal is constant during sampling period, $u(t)=u(kT),\ kT\le t\le(k+1)T$,the discrete-time model in the state-space is obtained from (34) as:

$$\begin{bmatrix}x_1(k+1)\\ x_2(k+1)\end{bmatrix}=\begin{bmatrix}\phi_{11} & \phi_{12}\\ \phi_{21} & \phi_{22}\end{bmatrix}\begin{bmatrix}x_1(k)\\ x_2(k)\end{bmatrix}+\begin{bmatrix}\gamma_1\\ \gamma_2\end{bmatrix}u(k), \quad (35)$$

using standard discretization procedure, and in *z*-domain:

$$y(k)=\frac{\gamma_1+(\gamma_2\phi_{12}-\gamma_1\phi_{22})z^{-1}}{1-(\phi_{11}+\phi_{22})z^{-1}+(\phi_{11}\phi_{22}-\phi_{12}\phi_{21})z^{-2}}u(k-1). \quad (36)$$

For $\zeta=0.707$, $\omega_n=10$ and $T=0.01s$, the models (35) and (36) become:

$$\begin{bmatrix}x_1(k+1)\\ x_2(k+1)\end{bmatrix}=\begin{bmatrix}0.9952 & 0.0093\\ -0.9310 & 0.8636\end{bmatrix}\begin{bmatrix}x_1(k)\\ x_2(k)\end{bmatrix}+\begin{bmatrix}0.0048\\ 0.9310\end{bmatrix}u(k), \quad (37)$$

and

$$y(k)=\frac{0.0048+0.0045z^{-1}}{1-1.8588z^{-1}+0.8681z^{-2}}u(k-1). \quad (38)$$

respectively. We also suppose that the switching functions are identical in both cases i.e. $c_0=\tilde{c}_0$, $c_1=\tilde{c}_1$ and $c_2=\tilde{c}_2$ and the polynomial $C(z^{-1})$ is defined as:

$$C(z^{-1})=(1-z^{-1}\exp(-2\pi f_{cut}T))^2 \quad (39)$$

with $f_{cut}=1\text{Hz}$.

The minimum variance control for the plant model (36) is given by:

$$u_{mv}(k)=-\frac{f_0+f_1z^{-1}}{g_0+g_1z^{-1}}y(k), \quad (40)$$

where:

$$f_0=c_1/c_0+\phi_{11}+\phi_{22}=-0.0194, \quad (41)$$

$$f_1=c_2/c_0-\phi_{11}\phi_{22}+\phi_{12}\phi_{21}=0.0138, \quad (42)$$

$$g_0=\gamma_1=0.0048, \quad (43)$$

$$g_1=\gamma_2\phi_{12}-\gamma_1\phi_{22}=0.0045. \quad (44)$$

The implementation of the procedure elaborated in Section IV yields:

$$u_{eq}(k)=-\frac{\tilde{f}_0+\tilde{f}_1z^{-1}}{\tilde{g}_0+\tilde{g}_1z^{-1}}y(k), \quad (45)$$

with:

$$\tilde{f}_0=\phi_{11}=0.9952, \quad (46)$$

$$\tilde{f}_1=-\phi_{11}\phi_{22}+\phi_{12}\phi_{21}=-0.8681, \quad (47)$$

$$\tilde{g}_0=g_0, \quad (48)$$

$$\tilde{g}_1=g_1. \quad (49)$$

It is obvious from Eqs. (40) and (45), that the minimum variance control approach and the procedure based on the classical equivalent control method with the transformed state-space plant model produce, as a result, two similar digital filters of the same order. Accordingly, we conclude that the minimum variance control can really be treated as the equivalent control analog for the input-output based VSC systems.

As one can see, the control (45) represents the special case of the minimum variance control (40) with:

$$c_2=0, \quad (49)$$

$$c_1=c_0\phi_{22}. \quad (50)$$

It is also evident that the control law from Section IV depends only on plant parameters since the vector $\tilde{\mathbf{c}}$ vanishes during the design procedure. Therefore, the system dynamics in sliding mode can not be chosen freely when the control algorithm (32) is implemented. That is the reason why this approach is not used in the input-output based sliding mode control.

The system responses with nominal plant parameters are shown in Figs. 1 and 2 for both control algorithms: (40) and (45). The minimum variance control law gives better dynamic behavior, which is determined by Eq. (39).

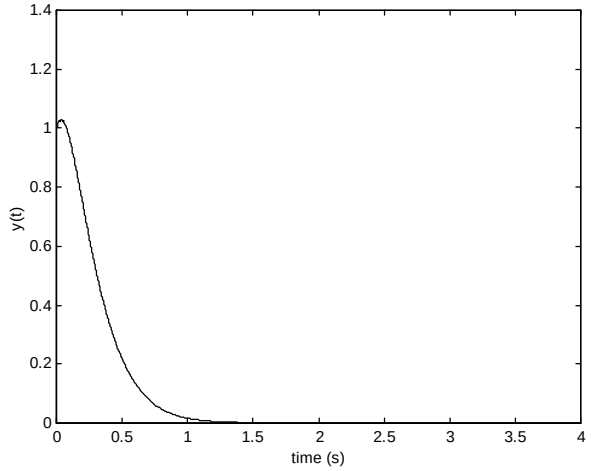

Fig. 1. Response of system with minimum variance control (nominal plant parameters)

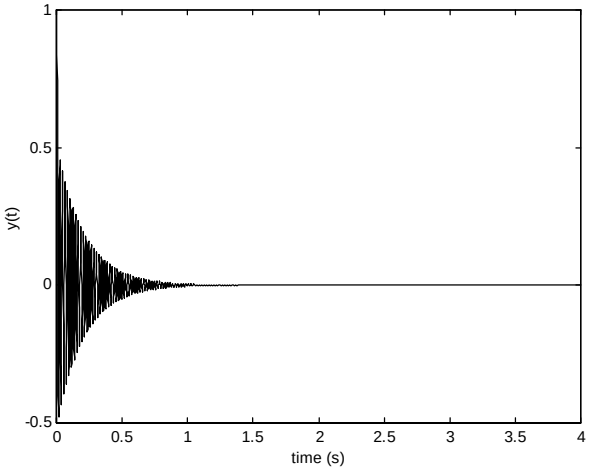

Fig. 2. System response with the control given by Eq. (45) (nominal plant parameters)

The responses of the system with perturbed plant parameters ($\zeta=1$ and $\omega_n=12$) are presented in Figs. 3 (Eq. (40)) and 4 (Eq. (45)). The system with the minimum variance control does not change its response significantly, while the

control law (45) gives unstable system output, what is expected, since the control law (45) depends only on plant parameters, i.e. there is no control mechanism to compensate the parameter variations.

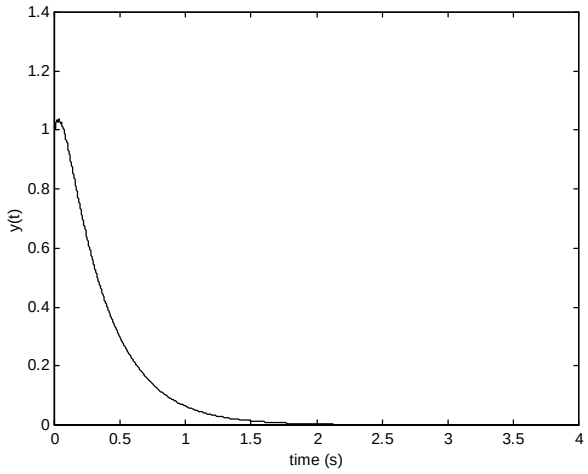

Fig. 3. Response of system with minimum variance control (perturbed plant parameters)

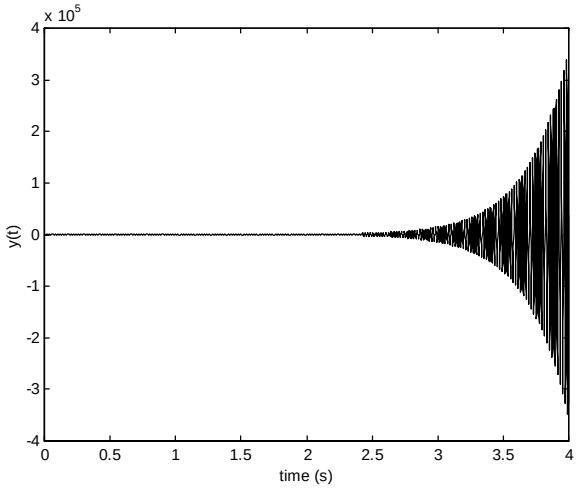

Fig. 4. System response with the control given by Eq. (45) (perturbed plant parameters)

VI. CONCLUSION

The paper establishes the relation between the minimum variance control and the discrete-time sliding mode equivalent control. It is shown that the minimum variance control can be treated as the discrete-time equivalent control analog in the cases when the input-output based variable structure control designs are considered. The proof of this correspondence starts with the transformation of the initial state-space model into the state space model with time-delayed state coordinates. To reduce the obtained model to the model with only plant outputs and its time-delayed values, the *z* transformation is introduced. Then, the standard equivalent control design procedure is implemented, leading to the digital filter of the same order as in the case of the application of the minimum variance control concept. Unfortunately, this approach is limited by a not-freely choice of the system dynamics in sliding mode, since the coefficients of the control algorithm are only dependant on plant parameters. That is the main reason why this approach is not used in the design of input-output based sliding mode control laws.

ACKNOWLEDGEMENT

This paper is a part of the project No. IT0125 at the University of Nis, Faculty of Electronic Engineering, and was supported by the Ministry of Science and Protection of Environment, Republic of Serbia.

REFERENCES

[1] V. I. Utkin, “Variable structure systems with sliding mode”, IEEE Trans. on Automatic Control, vol. 22, no. 2, pp. 212-222, 1977.

[2] B. Dra`enovi}, “The invariance conditions in variable structure systems”, Automatica, vol. 5, pp. 287-295, 1969.

[3] ^. Milosavljevi}, “General conditions of the existence of a quasi-sliding mode on the switching hyperplane in discrete variable structure systems,” Automat. Remote Contr., vol. 46, pp. 307-314, 1985.

[4] Z. Bu~evac, *Design of Digital Discrete Control Systems with Sliding Mode*, Ph. D. Dissertation (in Serbian), Mech. Eng. Faculty, University of Belgrade, 1985.

[5] K. Furuta, “VSS type self –tuning control”. IEEE Trans. on Ind. Elect., vol. 40, pp. 37–44, 1993.

[6] M. L. Corradini, G. Orlando, “Discrete variable structure control for nonlinear systems”, Proceedings of the 3rd European Control Conference, pp. 1465-1470, Rome, Italy, 1995.

[7] D. Miti}, ^. Milosavljevi}, “Sliding mode based minimum variance and generalized minimum variance controls with $O(T^2)$ and $O(T^3)$ accuracy”, Electrical Engineering (Archiv fur Elektrotechnik), vol. Online First, Springer-Verlag, http://www.springer.de, DOI:10.1007/s00202-003-0198-y, 2003

2D-Linear Motion Controller for Step Motors Based on a 8-bit microcontroler

Dejan Mitic[1], Dragan Antic[2], Zoran Jovanovic[3]

***Abstract* – In this paper a solution of motion controller for turning machine with stepper motors is shown. Motion controller is based on 8-bit microcontroller that receives commands from the supervisor computer dedicated to perform CNC program and communicate with operator. Special set of commands has been developed to functionally cover all specific needs for turning machine motions.**

***Keywords* – motion controller, CNC unit, step motor, turning machines**

I. INTRODUCTION

One of the most important machine industry improvements, almost comparable with new technology revolution, is certainly automation of production machines by supplementing them with the computer numerical control unit. CNC machines become, de facto, standard equipment of modern production lines. They are programmed by specially designed and standardized control language that has many 'dialects' depend on type of machine. Interface between computer and machine play a vital role in a control loop. Sensors, like position decoders, indexer, boundary switches, etc. send information about position, temperature and other statuses to the control unit. Accordingly to the control program, control unit acts via a range of actuators as motors, valves, pumps, heaters etc. The most important activity of any machines is motion. Depend on type of motor and motion complexity many type of motion controller has been developed. In this paper we shall present a solution for small and precise turning machine equipped with stepper motors and indexer.

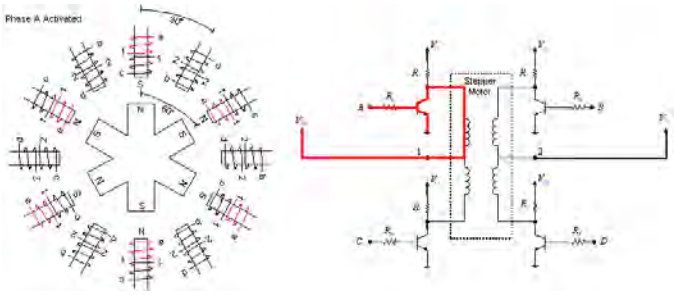

Fig. 1. Stepper motor phases activation

[1]Dejan Mitic is with Tehnopetrol, Sretena Mladenovića 32/10, 18000 Niš, Serbia and Montenegro, E-mail: dmitic@elfak.ni.ac.yu
[2]Prof. dr Drangan Antic is with the Faculty of Electronic Engineering, Beogradska 14, 18000 Nis, Serbia and Montenegro, E-mail: dantic@elfak.ni.ac.yu
[3]Mr Zoran Jovanovic is with the Faculty of Electronic Engineering, Beogradska 14, 18000 Nis, Serbia and Montenegro, E-mail: zoki@elfak.ni.ac.yu

II. DESCRIPTION OF MOTION CONTROLLER HARDWARE

Motion controller is applied for bipolar stepper motor (Fig. 1) control without closed loop.

Solution is based on microcontroller that is networked with other control modules of CNC unit. For that purpose we have chosen 8-bit AT89C2051 microcontroller and dedicate its ports to I/O signals as it is shown on Table I.

TABLE I
I/O SIGNALS ON AT89C2051 MICROCONTROLLER

N.P	Pin	Port	Sig.	N.P	Pin	Port	Sig.
1	RST		SRD	20	VCC		
2	RxD	P3.0	SWR	19		P1.7	DIRX
3	TxD	P3.1		18		P1.6	CLKX
4	XTAL2			17		P1.5	DIRZ
5	XTAL1			16		P1.4	CLKZ
6	!INT0	P3.2	BSY	15		P1.3	NLSX
7	!INT1	P3.3	SIND	14		P1.2	PLSX
8	T0	P3.4	ICLK	13	AIN1	P1.1	PLSZ
9	T1	P3.5		12	AIN0	P1.0	PPSX
10	GND			11		P3.7	PPSZ

Interface signals (Table II) provide connection of motion controller with relevant sensors and actuators.

TABLE II
DESCRIPTION OF THE INTERFACE SIGNALS

Sig.	Description
SRD	Serial read
SWR	Serial write
BSY	Busy
SIND	Indexer start
ICLK	Indexer clock
DIRX	X-axis direction
CLKX	X-axis clock
DIRZ	Z-axis direction
CLKZ	Z-axis clock
NLSX	X-axis negative limit switch
PLSX	X-axis positive limit switch
PLSZ	Z-axis positive limit switch
PPSX	X-axis precise position switch
PPSZ	Z-axis precise position switch

III. Description of Motion Controller Software

We developed software solution that completely meets all specific requirements that motion control for turning machines has.

CONTROL COMMANDS

A set of commands (Table III) has been developed to control the motion controller:

III Table
Control comands

Mnemonic	Description
INIT	Initialization
FMOV	Fast federate move
ZMOV	Move to machine zero
PMOV	Programmed feedrate move
STOP	Stop motion
FFDR	Set fast motion federate
MFDR	Set machining federate
PFDR	Set program federate
DELY	Delay
CSTP	Clock based motion step
ISTP	Indexer based motion step
PSTN	Set position
RDPS	Read position
RDST	Read status

INIT

Initialize the motion controller with default parameters for position and feedrates, clear all queues and put the motion controller in ready state.

FMOV

Fast move to specified position. This command is issued for fast positioning without machining. Usually, it is direct translation of G00 or some complex motion CNC commands.

ZMOV

Fast move to machine zero position defined with limits switches. Usually, command is issued for positioning machine for tool change or final machining position setup.

PMOV

Programmed move to specified position. Command is issued for motion during machining. Usually, it is direct translation of G01 or any other machining motion.

STOP

Abrupt stop movement. Command is issued for abrupt stop commanded by operator.

FFDR

Set fast feedrate used during FMOV and ZMOV command. Command is issued for immediate altering fast feedrate value. It allows to operator continual changing of maximal traverse speed during fast movement.

MFDR

Machining feedrate used during PMOV Command is issued for immediate altering normal feedrate value. It allows to operator continual changing machining speed.

PFDR

Machining feedrate used during PMOV. Command is issued for changing feedrate value upon fetching next motion command.

DELY

Delay machining for specified amount of time. Command is issued usually due to G04 command or during complex movement when there is need for short pause between two consequent movements.

CSTP

Set clock timer as source for stepping. Dedicated to simple motion control. Feedrate depends only on the timer clock. Speed in CNC program is expressed in mm/min.

ISTP

Set indexer timer as source for stepping. Dedicated to thread machining motion control. Feederate depends on speed of the main spindle. It allows special machine motion typical for turning machines, such as motion for producing threads.

PSTN

Set actual position. Command is issued to setup new coordinate. The actual position takes provided arguments values.

RDPS

Read actual position. Command is a request for actual position. Motion controller returns value of the actual position to computer. Usually, such information is presented to operator via appropriate user interface.

RDST

Read motion control status flags. Command is a request for status flags of motion controller. According to these flags computer as well as operator is informed about motion status, potential reaching limit positions or unpredictable situations.

SOFTWARE MODULES

THE PATH PLANNER MODULE covers all motion that turning machine should perform. It is linear motion planner for 24-bit discrete 2D motion space with two timing sources. The clock timing step source allows simple machining motion. The indexer timing step source is using for thread machining. The Bresenham's line algorithm has been used for discretization of motion space. The same algorithm has been used for discretization of the synchronized spindle-tool motion space in case of the indexer-controlled motion. Algorithm allows minimal inaccuracy on motion path caused by discretization. For reason of processing speed algorithm

has been split on two phases: motion preparing and motion executing. First phase is executed immediately upon interpreting command as a motion command. On the end of first phase all calculated data for phase two are saved as parameters of the new pending movement. Phase two is executed in every step cycle while the actual position does not reach final position.

THE PROCESSING MODULE is virtual processor, which fetches calculated data from the first phase of Bresenham's line algorithm and executes motion by following the second phase of the mentioned algorithm. Second phase is executed in determined moments according to motion feedrate and type of timer source (clock or indexer).

```
processing:
if (prosessor.isready()) {
      cmd = fetch();
      start(cmd);
}
if                (!processor.isstopped())
processor.run();
goto processing;
```

THE MODULE FOR ASYNCHRONOUS SERIAL COMMUNICATION runs input and output communication queues with error-free communication protocol. This protocol provide link between computer and motion controller as well as other microcontroller sustems dedicated to other tasks of control.

```
async_comm:
if (mssg_received()) {
      if (validate()) {
            cmd = extract_cmd();
            cmdq.put(cmd);
      } else {
            send(NAK);
      }
}
if (mssg_ready() == true) {
      send(mssg);
      while (ackn() == NAK) resend(msg);
}
goto async_comm;
```

THE INTERPRETER MODULE is supplied from pipelined command queue, which could accept three commands in advance, feeding interpreter continuously. It allows smooth motion changes to succeeding path. Also interpreter is able to find in advance commands that have to be executed immediately upon receiving (STOP, RDPS, RSST, etc).

```
interpret:
if (cmdq.isempty()) goto interpret;
while (cmdq.isimmcmd()) {
      icmd = cmdq.getimmcmd();
      processor.execute(icmd);
}
if (processor.ispend()) goto interpret;
processor.put(cmdq.getcmd());
goto interpret;
```

IV Conclusion

In this paper we shown practical realization of 2D-linear motion controller for stepper motor based on 8-bit microcontroller AT89C2051 and supplemented with unique software solution based on set of commands that cover all specific requirements of turning machine motion. Achieved results met all expectations. Implementation of preprocessing and preparing motion command in advance gave smooth transition between adjacent trajectories and resulting in high quality machining.

References

[1] Douglas W.J., *Control of Stepping Motors*, 5.2.10, 10.8, 10.9 and 10.10 of the Handbook of Small Electric Motors edited by W. H. Yeadon and A. W. Yeadon, McGraw-Hill, 2001.

[2] Koren, Y., *Control of Machine Tools and Robots*, Applied Mechanics Reviews, Vol. 39, No. 9,Sept. 1986, pp. 1331-1338.

[3] Kramer R.T., Proctor M.F., Messina E., *The NIST RS274NGC Interpreter*, Intelligent Systems Division National Institute of Standards and Technology, Technology Administration U.S. Department of Commerce, Gaithersburg, Maryland 20899, NISTIR 6556, August 17, 2000

Nonlinear State Observation in a Didactic Magnetic Levitation System

Milica B. Naumović

Abstract **- The magnetic levitation control system of a metallic sphere is an interesting and visual impressive device successful for demonstration many intricate problems for control engineering research. The dynamics of magnetic levitation system is characterized by its open-loop instability, highly nonlinearity and complexity. In this paper an approach to the nonlinear velocity estimation in the control system for positioning of the levitating sphere is addressed. Results of several simulation runs are given to verify the analytical investigations.**

Keywords **- Nonlinear observer, Magnetic levitation system, Control engineering education.**

I. INTRODUCTION

Magnetic levitators not only present intricate problems for control engineering research, but also have many important applications, such as high-speed transportation systems and precision frictionless magnetic bearings. From an educational viewpoint, this process is highly motivating and suitable for laboratory experiments and classroom demonstrations, as reported in the engineering education literature [1]-[9].

The classic magnetic levitation control experiment is presented in the form of laboratory equipment given in Fig. 1. The complete purchase of the Feedback Instruments Ltd. Maglev System 33-006 [10] was supported by WUS (**W**orld **U**niversity **S**ervice [11]) – Austria under Grant CEP (**C**enter of **E**xcellence **P**rojects).

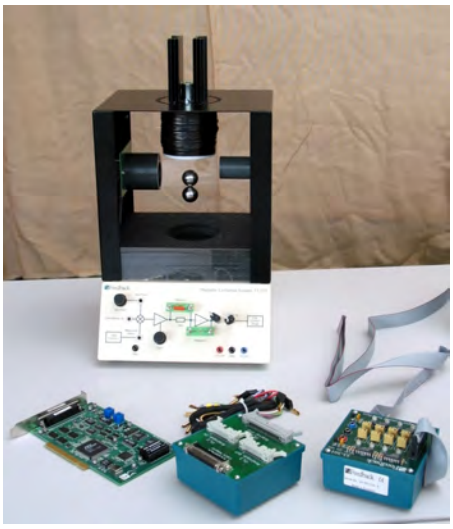

Fig. 1. Photograph of magnetic levitation system

Milica B. Naumović is with the Faculty of Electronic Engineering, University of Niš, Aleksandra Medvedeva 14, 18000 Niš, Serbia and Montenegro, E-mail: nmilica@elfak.ni.ac.yu

This attraction-type levitator system is a challenging plant because of its nonlinear and unstable nature. The suspended body is a hollow steel ball of 25 mm diameter and 20 g mass. This results in a visually appealing system with convenient time constants. Both analogue and digital control solutions could be implemented. In addition, the system is simple and relatively small, that is portable.

In order to obtain smooth and sufficiently accurate position and speed signals, an observer structure is often implemented. The observer processes the voltage command and position signal from transducer as it is shown in Fig. 2.

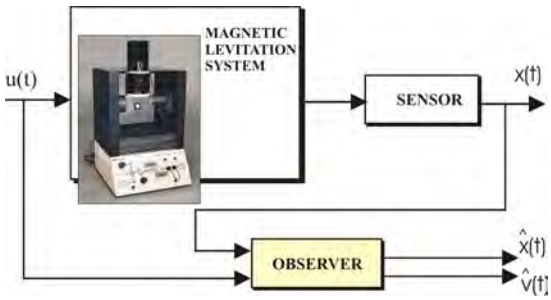

Fig. 2. Block diagram of the plant with observer

In this paper, referring to the problem of ball positioning beneath an electromagnet, the possibility of employing the Lie-algebraic method [12] in nonlinear velocity estimator design is considered. In the proposed method a nonlinear transformation is found, that brings the system into a canonical form, from where observer design is facilitated.

II. SYSTEM DESCRIPTION

The Magnetic Levitation System (Maglev System 33-006 given in Fig. 1) is a relatively new and effective laboratory set-up very helpful for control experiments. The basic control goal is to suspend a steel sphere by means of a magnetic field counteracting the force of gravity. The Maglev System consists of a magnetic levitation mechanical unit (an enclosed magnet system, sensors and drivers) with a computer interface card, a signal conditioning unit, connecting cables and a laboratory manual.

In the analogue mode, the equipment is self-contained with inbuilt power supply. Convenient sockets on the enclosure panel allow for quick changes of analogue controller gain and structure. The bandwidth of lead compensation may be

changed in order to investigate system stability and time response. Moreover, user-defined analogue controllers may be easily tested. Note, that the position of the sphere may be adjusted using the set-point control and the stability may be varied using the gain control.

In the digital mode, the Maglev System operates with MATLAB® /SIMULINK® software. Feedback Software for SIMULINK® is provided for the control models and interfacing between the PC and the Maglev system hardware.

III. MAGNETIC LEVITATION DYNAMICS

The modeling of the electromagnetic levitation system is based on its electrical, mechanical, and electromechanical equations [6]-[9] , as follows

$$\begin{aligned} \frac{\mathrm{d}x}{\mathrm{d}t} &= v \\ \frac{\mathrm{d}^2x}{\mathrm{d}t^2} &= g - \frac{C}{m}\frac{i^2}{x^2} \\ \frac{\mathrm{d}i}{\mathrm{d}t} &= -\frac{R}{L}i + \frac{2C}{L}\frac{i}{x^2}\frac{\mathrm{d}x}{\mathrm{d}t} + \frac{e}{L} \quad , \end{aligned} \tag{1}$$

where m, x and v denote the ball's mass, position and velocity, i is the current in the coil of the electromagnet, e is the applied voltage, R is the coil's resistance, $L(x)$ is the coil's inductance, g is the gravitational constant and C is the magnetic force constant. Note that the inductance $L(x)$ is a nonlinear function of the ball's position with some typical approximation that can be found in the literature [9].

Adopting $x(t)$, $v(t)$ and $i(t)$ as state variables, and voltage e as control signal, the equation of motion for the magnetic levitation system can be written as

$$\begin{aligned} \frac{\mathrm{d}x_1}{\mathrm{d}t} &= x_2 \\ \frac{\mathrm{d}x_2}{\mathrm{d}t} &= g - \frac{C}{m}\frac{x_3^2}{x_1^2} \\ \frac{\mathrm{d}x_3}{\mathrm{d}t} &= -\frac{R}{L}x_3 + \frac{2C}{L}\frac{x_2x_3}{x_1^2} + \frac{u}{L} \quad . \end{aligned} \tag{2}$$

IV. NONLINEAR OBSERVER DESIGN

Nonlinear observer form is defined to be a canonical form for which an observer can be constructed with a linear error dynamics. Such a concept has emerged as a dual to the feedback linearization problem known in nonlinear control systems theory [13]. The system can be transformed into a nonlinear observer form via a coordinate change. The Lie-algebraic method has be proved to be an effective means of coordinate transformation map obtaining.

Consider the vector-valued functions

$$\mathbf{f}: \Re^n \to \Re^n \quad \text{and} \quad \mathbf{g}: \Re^n \to \Re^n .$$

Definition 1. The Lie bracket is defined by

$$[\mathbf{f},\mathbf{g}](\mathbf{x}) = \frac{\partial \mathbf{f}}{\partial \mathbf{x}}(\mathbf{x})\mathbf{g}(\mathbf{x}) - \frac{\partial \mathbf{g}}{\partial \mathbf{x}}(\mathbf{x})\mathbf{f}(\mathbf{x}) \ , \tag{3}$$

where $\partial\mathbf{f}/\partial\mathbf{x}$ and $\partial\mathbf{g}/\partial\mathbf{x}$ are the Jacobian matrices of $\mathbf{f}$ and $\mathbf{g}$, respectively.

Using an alternative notation, we can represent the Lie bracket as

$$[\mathbf{f},\mathbf{g}] = \left(\mathrm{ad}^1\mathbf{f},\mathbf{g}\right) \ . \tag{4}$$

We also define

$$\left(\mathrm{ad}^i\mathbf{f},\mathbf{g}\right) = \left[\mathbf{f},\left(\mathrm{ad}^{i-1}\mathbf{f},\mathbf{g}\right)\right] \tag{5}$$

with $\left(\mathrm{ad}^0\mathbf{f},\mathbf{g}\right) = \mathbf{g}$.

Let $\mathrm{d}h$ denotes the gradient of scalar function h with respect to $\mathbf{x}$, that is $\mathrm{d}h = \nabla^{\mathrm{T}}h$. Let $\langle\cdot,\cdot\rangle$ denotes the inner product on $\Re^n$.

Definition 2. $\mathrm{L}_{\mathbf{f}}h$ represents the Lie derivative of h with respect to $\mathbf{f}$ and is defined by

$$\mathrm{L}_{\mathbf{f}}h = \langle \mathrm{d}h,\mathbf{f}\rangle \ . \tag{6}$$

We shall employ the following notation

$$\mathrm{L}_{\mathbf{f}}{}^i h = \mathrm{L}_{\mathbf{f}}\left(\mathrm{L}_{\mathbf{f}}{}^{i-1}h\right) \tag{7}$$

where $\mathrm{L}_{\mathbf{f}}{}^0 h = h$.

With these definitions, the Lie derivative of $\mathrm{d}h$ with respect to the vector field $\mathbf{f}$ takes the form

$$\mathrm{L}_{\mathbf{f}}(\mathrm{d}h) = \left(\frac{\partial(\mathrm{d}h)^{\mathrm{T}}}{\partial\mathbf{x}}\mathbf{f}\right)^{\mathrm{T}} + (\mathrm{d}h)\frac{\partial\mathbf{f}}{\partial\mathbf{x}} \ . \tag{8}$$

One may easy verify that so defined Lie derivatives are realated by the following so-called Leibnitz formula

$$\mathrm{L}_{[\mathbf{f},\mathbf{g}]}h = \langle \mathrm{d}h,[\mathbf{f},\mathbf{g}]\rangle = \mathrm{L}_{\mathbf{g}}\mathrm{L}_{\mathbf{f}}h - \mathrm{L}_{\mathbf{f}}\mathrm{L}_{\mathbf{g}}h \ . \tag{9}$$

Note that the following relation is valid

$$\mathrm{d}\mathrm{L}_{\mathbf{f}}h = \mathrm{L}_{\mathbf{f}}(\mathrm{d}h) . \tag{10}$$

Consider the class of time-invariant nonlinear single-input/single-output systems described by

$$\begin{aligned} \dot{\mathbf{x}} &= \mathbf{f}(\mathbf{x}) \\ y &= h(\mathbf{x}) , \end{aligned} \tag{11}$$

where $\mathbf{x}\in\Re^n$, $y\in\Re$, and $\mathbf{f}$ and h are n-dimensional vector and scalar function, respectively. We desire to find a nonlinear transformation $\mathbf{P}: \Re^n \to \Re^n$, where

$$\mathbf{x} = \mathbf{P}(\mathbf{x}^*) , \tag{12}$$

such that, in the new coordinate, system (Eqs. (11)) is

represented as

$$\dot{\mathbf{x}}^* = \begin{bmatrix} 0 & \cdots & 0 & 0 \\ 1 & \cdots & 0 & 0 \\ \vdots & \ddots & \vdots & \vdots \\ 0 & \cdots & 1 & 0 \end{bmatrix} \mathbf{x}^* - \begin{bmatrix} f_0^*(x_n^*) \\ f_1^*(x_n^*) \\ \vdots \\ f_{n-1}^*(x_n^*) \end{bmatrix} = \mathbf{f}^*(\mathbf{x}^*) \qquad (13)$$

$$y = \begin{bmatrix} 0 & \cdots & 0 & 1 \end{bmatrix} \mathbf{x}^* \quad .$$

It is convenient to utilize Lie-algebraic notation [12], [13], as follows

$$\dot{\mathbf{x}} = \frac{\partial \mathbf{P}}{\partial \mathbf{x}^*} \mathbf{f}^*(\mathbf{x}^*) \ , \qquad (14)$$

where

$$\frac{\partial \mathbf{P}}{\partial \mathbf{x}^*} = \begin{bmatrix} \frac{\partial \mathbf{P}}{\partial x_1^*} & \cdots & \frac{\partial \mathbf{P}}{\partial x_n^*} \end{bmatrix} . \qquad (15)$$

It is straightforward to show that all the columns of $\partial \mathbf{P} / \partial \mathbf{x}^*$ is possible to express in terms of the single "starting vector" $\partial \mathbf{P} / \partial x_1^*$ as

$$\frac{\partial \mathbf{P}}{\partial \mathbf{x}^*} = \begin{bmatrix} \left(\mathrm{ad}^0 \mathbf{f}, \frac{\partial \mathbf{P}}{\partial x_1^*} \right) & \left(\mathrm{ad}^1 \mathbf{f}, \frac{\partial \mathbf{P}}{\partial x_1^*} \right) & \cdots & \left(\mathrm{ad}^{n-1} \mathbf{f}, \frac{\partial \mathbf{P}}{\partial x_1^*} \right) \end{bmatrix} . \qquad (16)$$

To obtain an expression for the starting vector, the equation $y = h(\mathbf{x}) = x_n^*$ is used, and by repeated application of Leibnitz's formula given by Eq. (9), one may show that

$$\begin{bmatrix} \mathrm{L}_{\mathbf{f}}^0 (\mathrm{d}h)(\mathbf{x}) \\ \mathrm{L}_{\mathbf{f}}^1 (\mathrm{d}h)(\mathbf{x}) \\ \vdots \\ \mathrm{L}_{\mathbf{f}}^{n-1} (\mathrm{d}h)(\mathbf{x}) \end{bmatrix} \frac{\partial \mathbf{P}}{\partial x_1^*} = \begin{bmatrix} 0 \\ 0 \\ \vdots \\ 1 \end{bmatrix} . \qquad (17)$$

The system form given by Eq. (13) is called nonlinear opserver form and the matrix

$$\mathrm{O}(\mathbf{x}) = \begin{bmatrix} \mathrm{L}_{\mathbf{f}}^0 (\mathrm{d}h)(\mathbf{x}) \\ \mathrm{L}_{\mathbf{f}}^1 (\mathrm{d}h)(\mathbf{x}) \\ \vdots \\ \mathrm{L}_{\mathbf{f}}^{n-1} (\mathrm{d}h)(\mathbf{x}) \end{bmatrix} \qquad (18)$$

is termed the observability matrix of the system defined by Eq. (11). The starting vector $\partial \mathbf{P} / \partial x_1^*$ is equal to the last column of the matrix $\mathrm{O}^{-1}(\mathbf{x})$.

Note that it is not easy to obtain in general the coordinate transformation map since it requires one to solve a set of partial differential equations. However, the advantage of employing the preceding technique of putting the system into observer form, is that observer design in the new coordinate system is extremely simplified. Namely, for the case of a single-output system consider now the observer state equations

$$\dot{\hat{\mathbf{x}}}^* = \begin{bmatrix} 0 & \cdots & 0 & 0 \\ 1 & \cdots & 0 & 0 \\ \vdots & \ddots & \vdots & \vdots \\ 0 & \cdots & 1 & 0 \end{bmatrix} \hat{\mathbf{x}}^* - \begin{bmatrix} f_0^*(x_n^*) \\ f_1^*(x_n^*) \\ \vdots \\ f_{n-1}^*(x_n^*) \end{bmatrix} - \mathbf{K}(\hat{y} - y), \qquad (19)$$

where $\hat{y}$ and the gain matrix $\mathbf{K}$ are defined as $\hat{y} = \begin{bmatrix} 0 & \cdots & 0 & 1 \end{bmatrix} \hat{\mathbf{x}}^*$ and $\mathbf{K} = \begin{bmatrix} k_0 & \cdots & k_{n-1} \end{bmatrix}^{\mathrm{T}}$.

If the error vector is defined as

$$\mathbf{e}^* = \hat{\mathbf{x}}^* - \mathbf{x}^* , \qquad (20)$$

it follows that the homogeneous differential equation becomes

$$\dot{\mathbf{e}}^* = \begin{bmatrix} 0 & \cdots & 0 & -k_0 \\ 1 & \cdots & 0 & -k_1 \\ \vdots & \ddots & \vdots & \vdots \\ 0 & \cdots & 1 & -k_{n-1} \end{bmatrix} \mathbf{e}^* \quad . \qquad (21)$$

Hence, if $\mathbf{K}$ is chosen so that the system in Eq. (21) is asymptotically stable, the reconstruction error will always converge to zero. Via an appropriate selection of $\mathbf{K}$, it is easy to assign the spectrum of the characteristic polynomial of the Eq. (21) given by

$$\Delta_o(s) = k_0 + k_1 s + \cdots + k_{n-1} s^{n-1} + s^n \quad . \qquad (22)$$

V. Observer Design Problem Solution

Note, that in most cases some, but not all, of the state variables can be measured. In this case, we need to estimate the unmeasured state variables and the estimated values can be used to perform the adequate control. In the considered magnetic levitation system the ball's position and velocity will be estimated. Namely, we choose the state variables $x_1 = x$ and $x_2 = v$; for the plant output (y) we take ball's position which is controlled by the applying voltage (input u).

According to the consideration given in [5], we have for the plant parameters: the ball's mass $m = 2.12 \times 10^{-2}$ kg, the gravity acceleration $g = 9.81 \mathrm{m/s^2}$, the electromechanical conversion coefficient $k = 1.2 \times 10^{-4} \mathrm{Nm^2/A^2}$ as well as the current/voltage coefficient $\rho = 0.166 \mathrm{A/V}$ obtaining constant $C = k\rho^2 = 3.307 \times 10^{-6} \mathrm{Nm^2/V^2}$. These parameters lead to the elements of the vector function $\mathbf{f}(\mathbf{x})$ in Eq. (11) given by

$$f_1(\mathbf{x}) = x_2$$

$$f_2(\mathbf{x}) = 9.81 - 1.56 \times 10^{-4} \frac{u^2}{x_1^2} \quad . \qquad (23)$$

A straightforward calculation given in the previous section yields transformation $\mathbf{P}: \Re^2 \to \Re^2$, where

$$\mathbf{x} = \mathbf{P}(\mathbf{x}^*) = \begin{bmatrix} 0 & 1 \\ 1 & 0 \end{bmatrix} \mathbf{x}^* \qquad (24)$$

such, that the system given by Eqs. (11) and (23) may be

transformed into observer form as

$$\dot{\mathbf{x}}^* = \begin{bmatrix} 0 & 0 \\ 1 & 0 \end{bmatrix} \mathbf{x}^* + \begin{bmatrix} 9.81 - 1.56\times 10^{-4} \dfrac{u^2}{x_2^{*2}} \\ 0 \end{bmatrix} = \mathbf{f}^*(\mathbf{x}^*) \quad (25)$$

and

$$y_1 = \begin{bmatrix} 0 & 1 \end{bmatrix} \mathbf{x}^* = x_2^* \ . \quad (26)$$

For the system given in the canonical coordinates by Eqs.(25) and (26), the observer can be constructed with a linear error dynamics, i.e.

$$\dot{\hat{\mathbf{x}}}^* = \begin{bmatrix} 0 & 0 \\ 1 & 0 \end{bmatrix} \hat{\mathbf{x}}^* + \begin{bmatrix} 9.81 - 1.56\times 10^{-4} \dfrac{u^2}{x_2^{*2}} \\ 0 \end{bmatrix} - \begin{bmatrix} k_0 \\ k_1 \end{bmatrix} \left(\hat{y}_1 - y_1 \right). \quad (27)$$

The continuous domain observer in the original coordinates is obtained as

$$\dot{\hat{\mathbf{x}}} = \begin{bmatrix} 0 & 1 \\ 0 & 0 \end{bmatrix} \hat{\mathbf{x}} - \begin{bmatrix} 0 \\ 9.81 - 1.56\times 10^{-4} \dfrac{u^2}{x_1^2} \end{bmatrix} - \begin{bmatrix} k_1 & 1 \\ k_0 & 0 \end{bmatrix} \left(\hat{y} - y \right) \quad (28)$$

$$\hat{y} = \begin{bmatrix} 1 & 0 \end{bmatrix} \hat{\mathbf{x}} \ ,$$

with characteristic polynomial of linear error equation given by

$$\Delta_o(s) = k_0 + k_1 s + s^2 \quad . \quad (29)$$

VI. Simulation Results

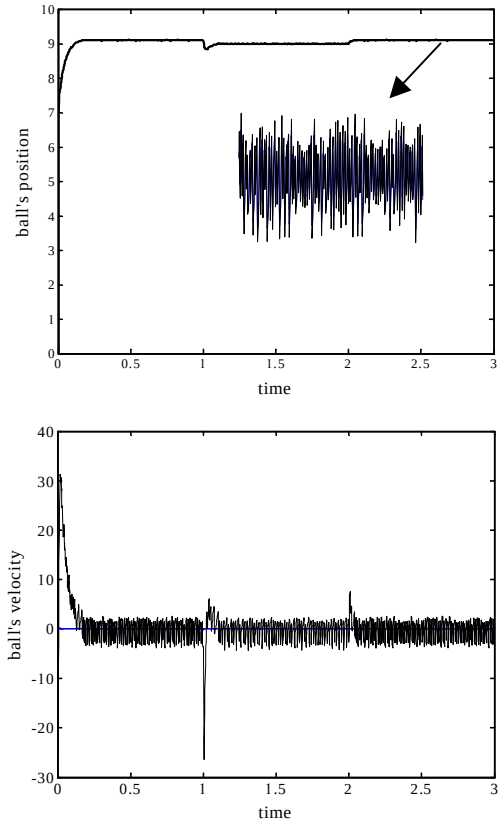

Fig. 3. Estimation results derived by observer (Eq. (28))

Results of analytical design given above are verified by several simulation runs. The system is exited by the pulse generator signal with period of $2\,\mathrm{s}$. The traces of position and velocity signals in Fig. 3 show the ability of observer given by Eq. (28) $\left(k_0 = 6.4\times 10^5, \ \ k_1 = 1.6\times 10^3\right)$ to estimate the state variables. Note that the system has been simulated in all details, taking into account the limited resolution (8-bit, as the worst case) of position sensor.

VII. Conclusion

Using the magnetic field to levitate a steel ball, the Magnetic Levitation System as a teaching aid enables the theoretical study and practical investigation of basic and advanced approaches to control of nonlinear unstable systems. The simple structure of nonlinear state estimator, proposed in this paper, is verified by the computer simulation. In the suggested observer the observation error vector is multiplied by the observer gain matrix which is obtained after a special coordinate transformation map. Note that finding a suitable nonlinear transformation requires the precise knowledge of the system nonlinear dynamics.

References

[1] T. H. Wong, "Design of a Magnetic Levitation Control System – An Undergraduate Project", IEEE Trans. on Education, Vol. E-29, No.4, pp. 196-200, November 1986.

[2] W.G. Herley and W.H. Wölfle, "Electromagnetic Design of a Magnetic Suspension System",IEEE Trans.on Education,Vol. E-40,pp. 124-130,1997.

[3] V.A. Oliveira, E.F. Costa and J.B. Vargas, "Digital Implementation of a Magnetic Suspension Control System for Laboratory Experiments", IEEE Trans. on Education, Vol. E-42, pp. 315-322, 1999.

[4] A.El Hajjaji and M. Ouladsine, "Modeling and Nonlinear Control of Magnetic Levitation Systems", IEEE Trans. Ind. Electron., Vol. 48, No.4, pp. 831-838, August 2001.

[5] R. K. H. Galvão, T. Yoneyama, F. M. Ugulino de Araújo, and R. G. Machado, "A Simple Technique for Identifying a Linearized Model for a Didactic Magnetic Levitation System", IEEE Trans. on Education, Vol. 46, No.1, pp. 22-25, February 2003.

[6] M. B. Naumović, "The Magnetic Levitation System – A Laboratory Equipment",TELFOR2002,Conference Proceedings, pp. 604-605, Beograd, Yugoslavia, 2002 (in Serbian).

[7] M.B.Naumović, "Magnetic Levitation System Analysis–A Laboratory Approach", INFOTEH-JAHORINA 2003, Symposium CD Proceedings, Vol.3, Ref.A-1, pp.1-5, Jahorina, Republica Srpska-BA, 2003 (in Serbian).

[8] M. B. Naumović, "Modeling of a Didactic Magnetic Levitation System", ETRAN2003, Conference Proceedings, pp.231-234, Herceg Novi, Serbia and Montenegro, 2003 (in Serbian).

[9] M. B. Naumović, "Modeling of a Didactic Magnetic Levitation System for Control Education", TELSIKS2003, Conference Proceedings, pp. 783-786, Niš, Serbia and Montenegro, 2003.

[10] Feedback Instruments Limited http://www.fbk.com/

[11] http://www.wus-austria.org

[12] B. L. Walcott, M. J. Corless, and S. H. Žak, "Comparative study of non-linear state-observation techniques", *Int. J. Control*, Vol. 45, no. 6, pp. 2109-2132, 1987.

[13] A. Isidori, *Nonlinear Control Systems - An Introduction*, Heidelberg, Springer-Verlag, 1989.

Controllability of a Small Hydro Power Plant

Sotir Panovski[1] and Gordana Janevska[2]

Abstract – **The paper presents the analysis of controllability theory for hydroenergetic installation of the Small Hydro Power Plant "Strezevo" using mathematical algebra. The analysis is based on the linear mathematical model of this plant treated as an object of automatic control.**

Keywords – **Controllability, Linear mathematical model, Small hydro power plant.**

I. INTRODUCTION

Kalman introduced the notion of controllability in 1960. **Controllability** is an important property of a control system. This property plays a crucial role in many control problems, such as stabilization of unstable systems by feedback, or optimal control.

At the power industrial objects the primar task, before the task of controller synthesis, is the analysis of the object's controllability. If we suppose that the mathematical model which represents the object's dynamic behavior is known, then the question is: Is it possible for every state of the system to find a define action (control vector) that brings it into the desired state? Roughly, the concept of controllability denotes the ability to move a system around its entire configuration space using only certain admissible manipulations.

An example of its applicability is a water turbine. The electrical network loading changes disturb the current steady state of the turbine and this results in decreasing or increasing the turbine angular speed, which is not plausable. Therefore, the turbine controller should provide a control action which will annulate these disturbances.

The above example is about the state controllability, but in most cases we are interested in the output controllability. The *state controllability* is usually taken to mean that it is possible, by admissible inputs, to steer the states from any initial value to any final value within some time window. A linear controllable system may be defined as a system which can be steered to any state from the zero initial state. *Output controllability* means the ability to manipulate the outputs of a system by admissible inputs. For a system with several outputs, it might not be possible to manipulate these outputs independently by the admissible inputs, in which case the system is not output controllable.

[1] Sotir Panovski is at the Faculty of Technical Sciences, I.L.Ribar bb, 7000 Bitola, R. Macedonia
E-mail: sotir.panovski@uklo.edu.mk

[2] Gordana Janevska is at the Faculty of Technical Sciences, I.L.Ribar bb, 7000 Bitola, R. Macedonia
E-mail: gordana.janevska@uklo.edu.mk

II. MATHEMATICAL MODEL

A linear mathematical model of a hydro energetic installation (Fig. 1) consists of an accumulation, a supply tunnel, a compression pipeline, a water chamber, a hydroelectric generating set and electric net is derived.

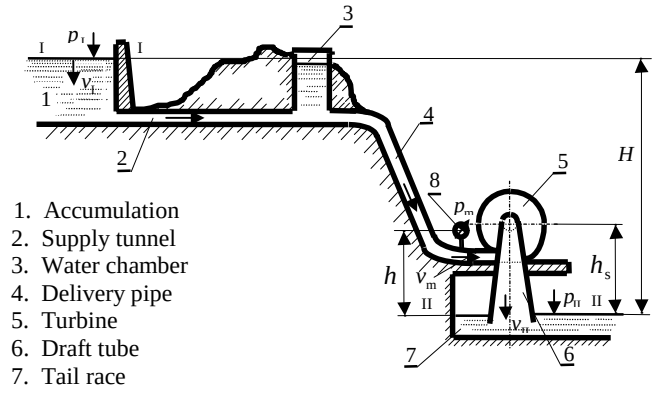

Fig. 1. Hydro electrical power plant

The block diagram of the hydro power plant as an object of automatic control is given in Fig. 2.

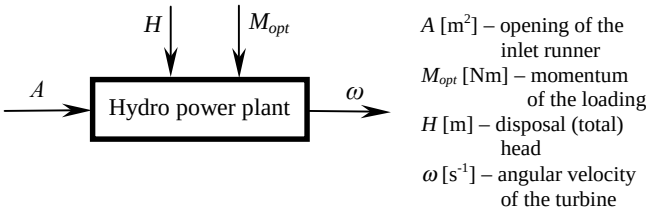

Fig. 2 Block diagram of HPP

Analyzing the dynamics of each constructive part (subsystem) of the general system, the mathematical model is developed. The model is linearised based on realistically adopted and critically studied assumptions and the following equations are obtained:

- Equation of the supply tunnel

$$\Delta \dot{\bar{q}}_{\mathrm{t}} = -\frac{2\left(C_{\mathrm{t}}+C_{\mathrm{v}}\right)}{T_{\mathrm{t}}}\cdot\Delta\bar{q}_{\mathrm{t}} - \frac{1}{T_{\mathrm{t}}}\cdot\bar{h}_{\mathrm{v}} + \frac{1+C_{\mathrm{t}}}{T_{\mathrm{t}}}\cdot\Delta\bar{H}_{\mathrm{br}} \qquad (1)$$

- Equation of the surge tank

$$\dot{\bar{h}}_{\mathrm{v}} = \frac{1}{T_{\mathrm{v}}}\cdot\Delta\bar{q}_{\mathrm{t}} - \frac{1}{T_{\mathrm{v}}}\cdot\Delta\bar{q}_{\mathrm{c}} \qquad (2)$$

- Equation of the delivery pipe

$$\dot{\Delta \bar{q}}_c = \frac{2C_v(1+C_c)}{T_c}\cdot \Delta \bar{q}_t + \frac{(1+C_c)}{T_c}\cdot \bar{h}_v - \frac{2C_c e_1 + 1}{T_c e_1}\cdot \Delta \bar{q} + \\ + \frac{e_7}{T_c e_1}\cdot \Delta \bar{f} + \frac{e_2}{T_c e_1}\cdot \Delta \bar{A} \qquad (3)$$

- Equation of frequency of the electricity
  - For isolated SHPP

$$\dot{\Delta \bar{f}} = -\frac{K_v}{T}\cdot \Delta \bar{A} + \frac{K_q}{T}\cdot \Delta \bar{q} - \frac{e}{T}\cdot \Delta \bar{f} - \frac{1}{T}\cdot \Delta \bar{P}_L \qquad (4)$$

  - For SHPP in parallel electrical network

$$\dot{\Delta \bar{f}} = -\frac{K_v}{T_{sa}}\cdot \Delta \bar{A} + \frac{K_q}{T_{sa}}\cdot \Delta \bar{q} - \frac{e_a}{T_{sa}}\cdot \Delta \bar{f} - \frac{1}{T_{sa}}\cdot \Delta \bar{P}_{\kappa a} \qquad (5)$$

This system of equations is obtained in normal form, which is most convenient for transfer into state space form and allows direct choice of the state values, control value, controlled and disturbance values. Choosing:

- State vector $\mathbf{x} = \left[\Delta \bar{q}_t \quad \bar{h}_v \quad \Delta \bar{q}_c \quad \Delta \bar{f}\right]^T$
- Input vector $\mathbf{x}_u = \left[\Delta \bar{H}_{br} \quad \Delta \bar{A} \quad \Delta \bar{P}_L\right]^T$
- Control vector $\mathbf{u} = u = \Delta \bar{A}$
- Disturbance vector $\mathbf{z} = \left[\Delta \bar{H}_{br} \quad \Delta \bar{P}_L\right]^T$
- Output vector $\mathbf{x}_i = x_i = \Delta \bar{f}$

the mathematical model into state space form is obtained:

$$\dot{\mathbf{x}} = \mathbf{A}\,\mathbf{x} + \mathbf{B}\,\mathbf{u}$$
$$\mathbf{x}_i = \mathbf{C}\,\mathbf{x} \qquad (6)$$

and the particular matrices are given below:

- For isolated SHPP

$$\mathbf{A} = \begin{bmatrix} -\frac{2(C_t + C_v)}{T_t} & -\frac{1}{T_t} & 0 & 0 \\ \frac{1}{T_v} & 0 & -\frac{1}{T_v} & 0 \\ \frac{2C_v(1+C_c)}{T_c} & \frac{1+C_c}{T_c} & -\frac{2C_c e_1 + 1}{T_c e_1} & \frac{e_7}{T_c e_1} \\ 0 & 0 & \frac{K_q}{T} & -\frac{e}{T} \end{bmatrix}$$

$$\mathbf{B} = \begin{bmatrix} 0 & 0 & \frac{e_2}{T_c \cdot e_1} & -\frac{K_v}{T} \end{bmatrix}^T$$

$$\mathbf{C} = [0 \quad 0 \quad 0 \quad 1] \qquad (7)$$

- For SHPP in parallel electrical network

$$\mathbf{A} = \begin{bmatrix} -\frac{2(C_t + C_v)}{T_t} & -\frac{1}{T_t} & 0 & 0 \\ \frac{1}{T_v} & 0 & -\frac{1}{T_v} & 0 \\ \frac{2C_v(1+C_c)}{T_c} & \frac{1+C_c}{T_c} & -\frac{2C_c e_1 + 1}{T_c e_1} & \frac{e_7}{T_c e_1} \\ 0 & 0 & \frac{K_q}{T_{sa}} & -\frac{e_a}{T_{sa}} \end{bmatrix}$$

$$\mathbf{B} = \begin{bmatrix} 0 & 0 & \frac{e_2}{T_c \cdot e_1} & -\frac{K_v}{T_{sa}} \end{bmatrix}^T$$

$$\mathbf{C} = [0 \quad 0 \quad 0 \quad 1] \qquad (8)$$

III. THE CONTROLLABILITY CRITERIA

Definition 1. A linear system is said to be *completely controllable* if, for all initial times t_0 and all initial states $\mathbf{x}(t_0)$, there exists some input function that drives the state vector to any final state $\mathbf{x}(t_1)$ at some finite time $t_1 > t_0$.

Matrices **A** and **B** determine controllability of the system. According to the well known algebraic criteria the system

$$\dot{\mathbf{x}} = \mathbf{A}\,\mathbf{x} + \mathbf{B}\,\mathbf{u}$$
$$\mathbf{x}_i = \mathbf{C}\,\mathbf{x}$$

is state-controllable if and only if the controllability matrix

$$\mathbf{P} = \left[\mathbf{B} \quad \mathbf{A}\,\mathbf{B} \quad \mathbf{A}^2\,\mathbf{B} \quad \ldots\ldots \quad \mathbf{A}^{n-1}\,\mathbf{B}\right] \qquad (9)$$

has full rank.

This criterion represents the test for state controllability of a linear system.

Another kind of controllability may be useful from a practical perspective, namely, complete *output controllability*, which is defined as the ability to drive the output vector to the origin in finite time. This property involves all matrices **A**, **B**, **C.** The **output controllability** matrix of the system is

$$\mathbf{Q} = \mathbf{C}\cdot\mathbf{P} = \left[\mathbf{C}\,\mathbf{B} \quad \mathbf{C}\,\mathbf{A}\,\mathbf{B} \quad \mathbf{C}\,\mathbf{A}^2\,\mathbf{B} \quad \ldots\ldots \quad \mathbf{C}\,\mathbf{A}^{n-1}\,\mathbf{B}\right] \qquad (10)$$

The sufficient condition for complete output controllability of the system is that the rank(**Q**) is equal to the number of outputs.

IV. CONTROLLABILITY ANALYSIS FOR SPECIFIC HPP

Controllability analysis is performed for the Small Hydro Power Plant "Strezevo" taken as a specific HPP in this paper. SHPP "Strezevo" belongs to the group of SHPP with the powerhouse located at the base of a dam. This SHPP is located on the main canal of the Strezevo dam and affords energy utilization of the hydrological potential of the water from the reservoir Strezevo. Namely, the artificial lake Strezevo is a part of the Hydro System "Strezevo", which provides required quantities of water for irrigation of 20.200 ha of agricultural land in Bitola region of Pelagonia Valley,

Republic of Macedonia. Apart from irrigation, this hydro-system provides water to additionally supplement the required quantities of unprocessed water for water supply, supplying technological water for one part of the industry, energy utilization of the hydrological potential of the water, as well as flood control.

Using the project data for the SHPP "Strezevo":

Accumulation	112 000 000 m^3
Installed discharge	3 x 2,67 = 8 m^3/s
Installed power	3 x 0,8 = 2,4 MW
Turbine Francis	
Nominal net head	30 m
Turbine speed	750 min^{-1}
Diameter of turbine wheel	600 mm

the numerical values for the time constants and other coefficients in the mathematical model are determined. Thus, the linear mathematical model for this specific SHPP is obtained in the form given by the Eq. (6), where the particular matrices have had the following values:

- For isolated SHPP

$$\mathbf{A}=\begin{bmatrix} -0{,}0083 & -3{,}5714 & 0 & 0 \\ 0{,}0026 & 0 & -0{,}0026 & 0 \\ 0{,}0017 & 1{,}7100 & -3{,}2918 & -0{,}1282 \\ 0 & 0 & 0{,}4578 & -0{,}0545 \end{bmatrix}$$

$$\mathbf{B}=\begin{bmatrix} 0 \\ 0 \\ 2{,}5641 \\ -0{,}2644 \end{bmatrix} \qquad \mathbf{C}=\begin{bmatrix} 0 & 0 & 0 & 1 \end{bmatrix} \qquad (11)$$

- For SHPP in parallel electrical network

$$\mathbf{A}=\begin{bmatrix} -0{,}0083 & -3{,}5714 & 0 & 0 \\ 0{,}0026 & 0 & -0{,}0026 & 0 \\ 0{,}0017 & 1{,}7100 & -3{,}2918 & -0{,}1282 \\ 0 & 0 & 0{,}0223 & -1{,}109 \end{bmatrix}$$

$$\mathbf{B}=\begin{bmatrix} 0 \\ 0 \\ 2{,}5641 \\ -0{,}0129 \end{bmatrix} \qquad \mathbf{C}=\begin{bmatrix} 0 & 0 & 0 & 1 \end{bmatrix} \qquad (12)$$

The state space dimension *n* for this mathematical model is 4, so that, the system is state controllable if the rank of matrix **P** (Eq. 9) is equal to 4. According to its mathematical model, the number of outputs for this specific system is equal to 1; thus, the output controllability test means that the system is output controllable if the matrix **Q** (Eq. 10) has rank equal to1.

The controllability test for the considered SHPP is performed using the mathematical software package MATLAB. The calculation results are given below.

- For isolated SHPP

$$\mathbf{P}=\begin{bmatrix} \mathbf{B} & \mathbf{A}\mathbf{B} & \mathbf{A}^2\mathbf{B} & \mathbf{A}^3\mathbf{B} \end{bmatrix}$$

$$\mathbf{P}=\begin{bmatrix} 0 & 0 & 0{,}0238 & -0{,}0783 \\ 0 & -0{,}0067 & 0{,}0219 & -0{,}0715 \\ 2{,}5641 & -8{,}4066 & 27{,}5091 & -90{,}0155 \\ -0{,}2644 & 1{,}1883 & -3{,}9133 & 12{,}8070 \end{bmatrix}$$

$$rank(\mathbf{P}) = 4$$

$$\mathbf{Q}=\begin{bmatrix} \mathbf{C}\mathbf{B} & \mathbf{C}\mathbf{A}\mathbf{B} & \mathbf{C}\mathbf{A}^2\mathbf{B} & \mathbf{C}\mathbf{A}^3\mathbf{B} \end{bmatrix}$$

$$\mathbf{Q}=\begin{bmatrix} -0{,}2644 & 1{,}1883 & -3{,}9133 & 12{,}8070 \end{bmatrix}$$

$$rank(\mathbf{Q}) = 1$$

- For SHPP in parallel electrical network

$$\mathbf{P}=\begin{bmatrix} \mathbf{B} & \mathbf{A}\mathbf{B} & \mathbf{A}^2\mathbf{B} & \mathbf{A}^3\mathbf{B} \end{bmatrix}$$

$$\mathbf{P}=\begin{bmatrix} 0 & 0 & 0{,}0238 & -0{,}0786 \\ 0 & -0{,}0067 & 0{,}0219 & -0{,}0721 \\ 2{,}5641 & -8{,}4389 & 27{,}7584 & -91{,}3034 \\ -0{,}0129 & 0{,}0715 & -0{,}2675 & 0{,}9156 \end{bmatrix}$$

$$rank(\mathbf{P}) = 4$$

$$\mathbf{Q}=\begin{bmatrix} \mathbf{C}\mathbf{B} & \mathbf{C}\mathbf{A}\mathbf{B} & \mathbf{C}\mathbf{A}^2\mathbf{B} & \mathbf{C}\mathbf{A}^3\mathbf{B} \end{bmatrix}$$

$$\mathbf{Q}=\begin{bmatrix} -0{,}0129 & 0{,}0715 & -0{,}2675 & 0{,}9156 \end{bmatrix}$$

$$rank(\mathbf{Q}) = 1$$

According to the presented results, it can be concluded that the treated SHPP is state and output controllable.

V. Conclusion

Based on the known controllability criteria, in this paper we perform a controllability test for specific SHPP. We introduce the mathematical model of SHPP as an object of automatic control given in state space form. For a specific SHPP "Strezevo" we use the mathematical model to explore the contolability of this SHPP for isolated work, as well as for work in parallel electrical network. The results gained from controllability analysis confirm that the SHPP "Strezevo" as an object of automatic control is complete state and output controllable.

Appendix - List of symbols

$\Delta\bar{q}_t$ - supply tunnel water flow in relative coordinates;

$\bar{h}_v$ - water level in the surge tank in relative coordinates;

$\Delta\bar{q}_c$ - delivery pipe water flow in relative coordinates;

$\Delta\bar{f}$ - electrical network frequency in relative coordinates;

$\Delta\bar{A}$ - opening of the inlet runner in relative coordinates;

$\Delta\bar{P}_L$ - generator loading disturbance in relative coordinates;

$\Delta\bar{H}_{br}$ - disposal (total) head in relative coordinates;

e_1 - relative change of flow q as a function of the net head H at $\omega = const$ and $A = const$;

e_2 - relative change of flow q as a function of the inlet runner opening A at $\omega = const$ and $H = const$;

e_3 - relative change of the efficiency coefficient η as a function of the net head H at $\omega = const$ and $A = const$;

e_4 - relative change of the efficiency coefficient η as a function of the inlet runner opening A at $\omega = const$ and $H = const$;

e_p - self-regulation loading coefficient;

C_t - loss coefficient for the supply tunnel;

C_v - coefficient of the kinetic energy;

C_c - loss coefficient for the delivery pipe;

T_v - time constant of the surge tank;

T_t - time constant of the supply tunnel;

T_c - time constant of the delivery pipe;

T_a - time constant of the turbine and generator mechanical inertia.

REFERENCES

[1] L. Borel, *Stabilite de reglage des installations hydroelectrigues*, Dunod, Paris, 1960.

[2] R. Kalman, "On the General Theory of Control Systems", Proc. First IFAC Congress, Moscow, vol. 1, pp.481-493, 1960.

[3] B. Pivovarov, *Proektirovanie i rasčet sistem regulirovanie gidroturbin*, Mašinostroenie, Leningrad, 1973.

[4] S. Panovski, "Controllability and Observabillity of Hydro-Energetic Systems", JUREMA, Conference Proceedings, pp.69-72, 1980.

[5] Milic Sojic, *Kontinualni sistemi automatskog upravljanja*, Naučna knjiga, Beograd, 1990.

[6] G. Janevska, *Mathematical Modeling of Dinamics of Hydro-energetic Plants*, Master's thesis, Faculty of Mechanical Engineering, Ss. Cyril and Methodius University, Skopje, Republic of Macedonia, 1998.

[7] *Technical Documentation of SHPP "Strezevo"*.

Advanced CAD/CAM System for Robotic Filament Winding

Aleksandar Markoski[1], Blagoja Samakoski[2], Zlatko Sokoloski[3], Kire Mrceski[4], Zoran Petreski[5]

Abstract **- In this paper CAD/CAM system for designing and manufacturing composite parts with robotic filament winding is presented. System provides automatic designing of mandrel shape, creating radial, helical and transition layers with great flexibility for changing winding angle, covering degree, and winding pattern with complete simulation of the winding process. Final result of the presented CAD/CAM system is complete G-code for controlling the individual axes of the industrial robot for filament winding.**

Keywords **– CAD/CAM, filament winding, simulation, G-code,**

I. INTRODUCTION

The filament winding process is efficient technique used commonly in the mass production of fibre-reinforced composite components such as pipes, pressure vessels, water tanks, rocket motor cases, lunch tubes, shafts, and other different axis and non-axisimetrical parts. The process is relatively simple involving the winding of continuous fibers, that are either impregnated or have been immersed into a epoxy resin bath onto a mandrel mould, to produce a polymeric composite component (Fig. 1.).

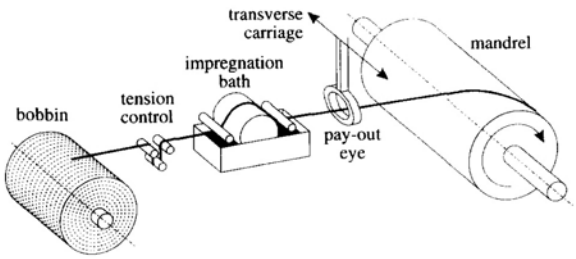

Fig. 1. Basic Filament Winding Process

[1]Aleksandar Markoski is with the Faculty of Technical Sciences, Ivo Lola Ribar bb, 7000 Bitola, Macedonia, e-mail: aleksandar.markoski@uklo.edu.mk

[2]Blagoja Samakoski is with the Faculty of Technical Sciences and Mikrosam, Krusevski pat bb, 7500 Prilep, Macedonia, e-mail: bsamak@mt.net.mk

[3]Zlatko Sokoloski is with the Mikrosam, Krusevski pat bb, 7500 Prilep, Macedonia, e-mail: zlatkos@mikrosam.com.mk

[4]Kire Mrceski is with the Mikrosam, Krusevski pat bb, 7500 Prilep, Macedonia, e-mail: kirem@mikrosam.com.mk

[5]Zoran Petreski is with the Mikrosam, Krusevski pat bb, 7500 Prilep, Macedonia, e-mail: zoranp@mikrosam.com.mk

The shape of the final part is determined by the shape of the mandrel, and the thickness of the part is controlled by the number of circuits wound (number of layers). The reinforcement configuration is determined by controlling the winding angle which is the angle formed between the tangent to the filament end the tangent line to the intersection line of the surface to be wound with the plane parallel to the running axis of winding. For a body of revolution it will be the angle between the filament and the wind axis. By varying the angle of filament it is possible to control the reinforcement fiber angles within the same layer and through the thickness of the composite wall.

In the simplest filament winding machines with 2 to 3 axes, control of the movements and speed of the axes is done by rigid kinematical coupling (usually gears or chains). With modern winding machines up to 6 axes (with 3 rotational and 3 linear axes) different motions can be regulated individually with greater accuracy by computer control (Fig. 2.).

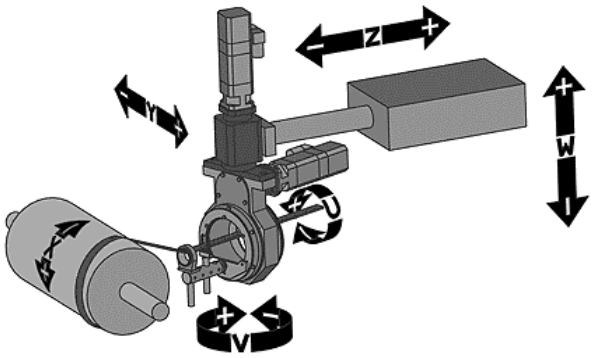

Fig. 2. Axis for Robotic Filament Winding: 1-mandrel X, 2-carriage Y, 3-cross-carriage Z, 4-vertical W, 5-Yaw Rotation V, 6-Eye Rotation U.

II. ROLE OF CAD/CAM SYSTEMS IN FILAMENT WINDING

Creation of the programs for the FW machines is not a simple task. The main problem in the control of the robotic filament winding is the synchronization of the axes. In the past the most common practice was using “trial and error” and teach method. Starting from 20 years ago a different algorithms were developed for off-line programming [2], [4], [6] and several software packages (CADWIND, CadFill, Composite Designer, FiberGrafix) are introduced and widely used in filament winding industry. All of these packages offers different level of flexibility, accuracy, adaptability and user friendly environment.

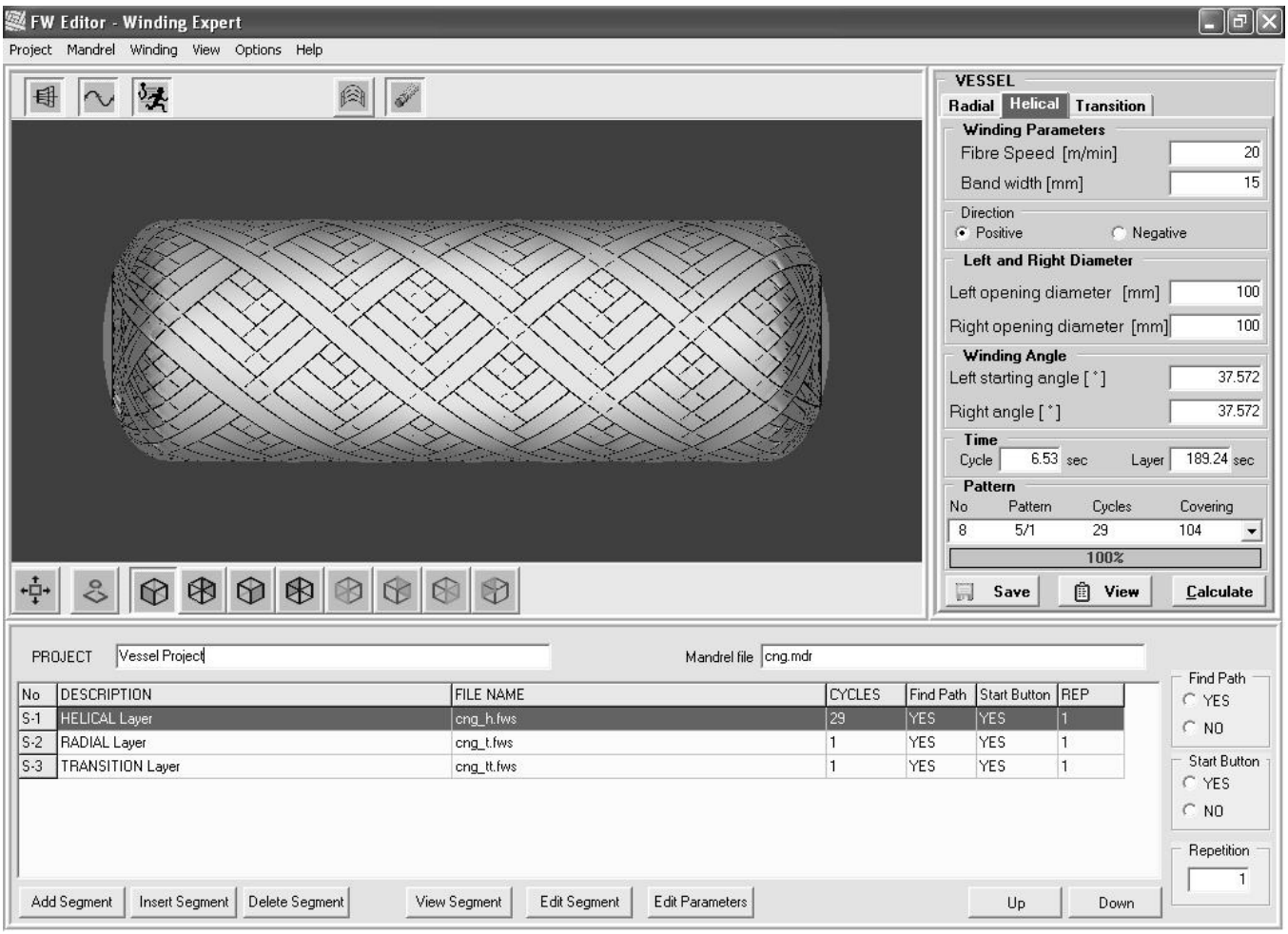

Fig. 3. Winding Expert Main Screen

The main features of the programs are: (i) the calculation of possible winding paths for rotationally-symmetric components; (ii) searches for covering patterns; (iii) updating of the geometry between successive layers; (iv) the performing of simple strength and stiffness analyses of the resulting laminate; (v) the transfer of laminate data to FEM-programs for detailed analysis; and (vi) the transfer of data for the generation of control files for filament-winding machines. All previous mentioned software packages provides main features on different level of implementation, but also there are gaps whish must be filled with the new generation of software. Improvements can be made in these fields:

- Real time simulation and rotation of mandrel instead of predefined views,
- Accurate calculation of winding path in the opening diameter regions,
- Integration of all patterns for the composite product into single file,
- Integration of smoothing algorithms directly in generation of axis movements,
- Maximum flexibility for different FW machines and motion controllers.
- Intuitive Human Machine Interface

III. ADVANCED CAD/CAM SYSTEM - WINDING EXPERT

Starting from 1999 a research group from Faculty of Technical Sciences and Mikrosam – Prilep began with development of new advanced CAD/CAM system, which will incorporate the latest achievements in filament winding technology, compatibility with PC Based controller for Robotic Filament Winding [3], maximum flexibility for use in different motion controllers and improved user friendly interface. In this paper is presented a new, advanced CAD/CAM system for Robotic Filament Winding – Winding Expert.

In Fig. 3 is shown the main screen of the Winding Expert (WE). The upper left part is Simulation window in which user can see in real time mandrel shape and created winding patterns. Upper right part is for winding parameters, which are used as input in calculation of patterns, and for showing the possible patterns and their characteristics. Depending of the winding mode this part can be different. In lower part (Project window) are all necessary information's and all patterns for specific composite part.

Design of composite structures and appropriate programs for manufacturing on FW machines requires 6 steps:

1. Creation of Mandrel
2. Designing of the composite layers by creating filament winding segments
3. Winding simulations

4. Export data for Finite Element Analyses
5. Creation of the Winding Project
6. Post processing and creating the executable G-code

Mandrel can be designed using standard forms with parameters for most frequent used shapes: pipe, vessel and cone. For the rotational bodies mandrel can be created by importing the profile from DXF file created with CAD program.

Composite layers are designed by creating different filament winding segments using a panel with winding parameters which appears in upper right part of the screen for chosen mandrel shape (Fig 4.), using different algorithms which ensure a large number of achievable patterns with avoidance of fiber slippage [6].

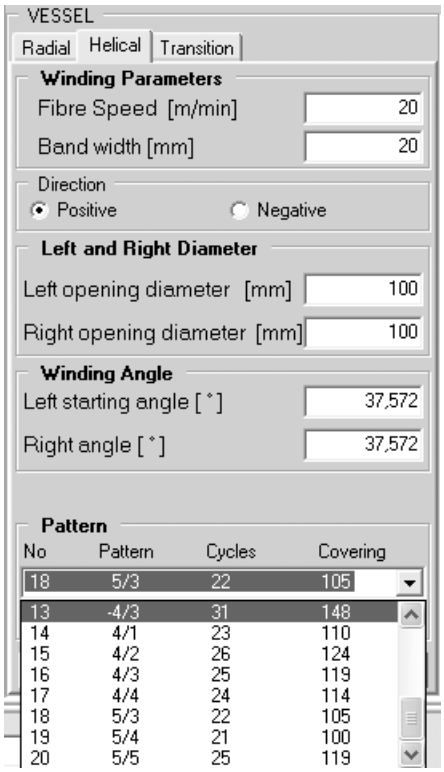

Fig. 4. Winding parameters for Vessel

For Vessel winding for example, user can choose radial, helical and transition layer, with different fiber width and speed, can vary opening diameters, and angles of the composite, and also can chose between different winding patterns with specific characteristics (number of cycles, degree of covering, etc.).

User has complete control of creating composite structure. Using the Simulation window he can create a lot of different patterns (Fig. 5), with different characteristics, and he can choose the most appropriate for his project.

The next step in creating the composite structure is Finite Element Analyses. Software will provide an export file with all data necessary for input in FEA software (NISA, NASTRAN, ANSIS etc.). If the structure does not satisfy the real conditions (resistance to strain, forces, pressure, temperature) user can change (increase) the number of layers (thickness of the composite), angles and patterns, until the structure reaches the appropriate characteristics.

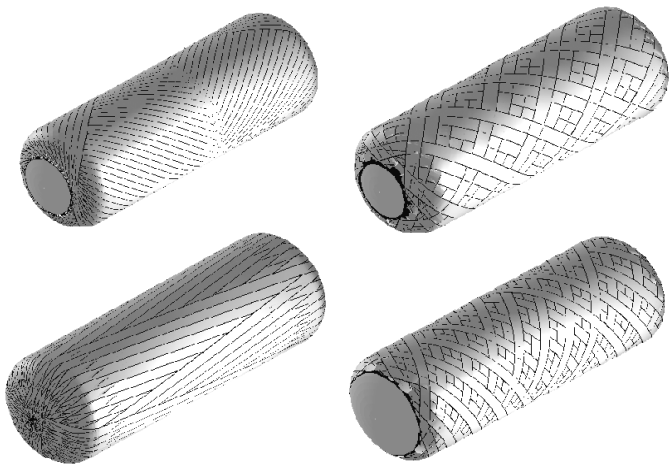

Fig. 5. Different helical patterns for vessel winding

Combination of different layers can be done in the Project Window, the lower part of the screen. User can use the following options:

- *Add Segment* – Add filament winding segment in project
- *Insert Segment* – Insert filament winding segment in project
- *Delete Segment* – Remove segment from project
- *View Segment* – View segment code
- *Edit Segment* – Edit segment code in Segment Form
- *Edit Parameters* – Edit parameters in segment window
- *Up* – Move the segment up in the grid
- *Down* – Move segment down in the grid

After creating the composite structure, thus means that Winding Project is created. This is very important in mass production of composite parts (for example CNG tanks) where the composite structure always is created with combination of different number of radial and helical layers connected with radial-to-helical and helical-to-radial transition layers. This concept ensures that the whole part will be manufactured at once without stopping the FW machine.

The last step is post processing and creating the executable code for different FW machines with different motion controllers and CNC control systems. For the post processing module it is necessary to provide a lot of machine parameters:

- Number of active axes (max 6)
- Reference coordinates (or angles) for each axis
- Dimensions of each axis
- Maximum velocities for each axis
- Maximum acceleration for each axis
- Resolutions of each axis

One of the main features in Winding Expert is jerk elimination algorithms incorporated in post processing module, which ensures smooth movement without strokes at high speeds (up to 1.7 m/s for carriage). As a default option post processing module is creating standard ISO G-Code for 6 axes, which can be viewed, edited and corrected (Fig. 6.) if it is necessary to make some adjustments in real conditions.

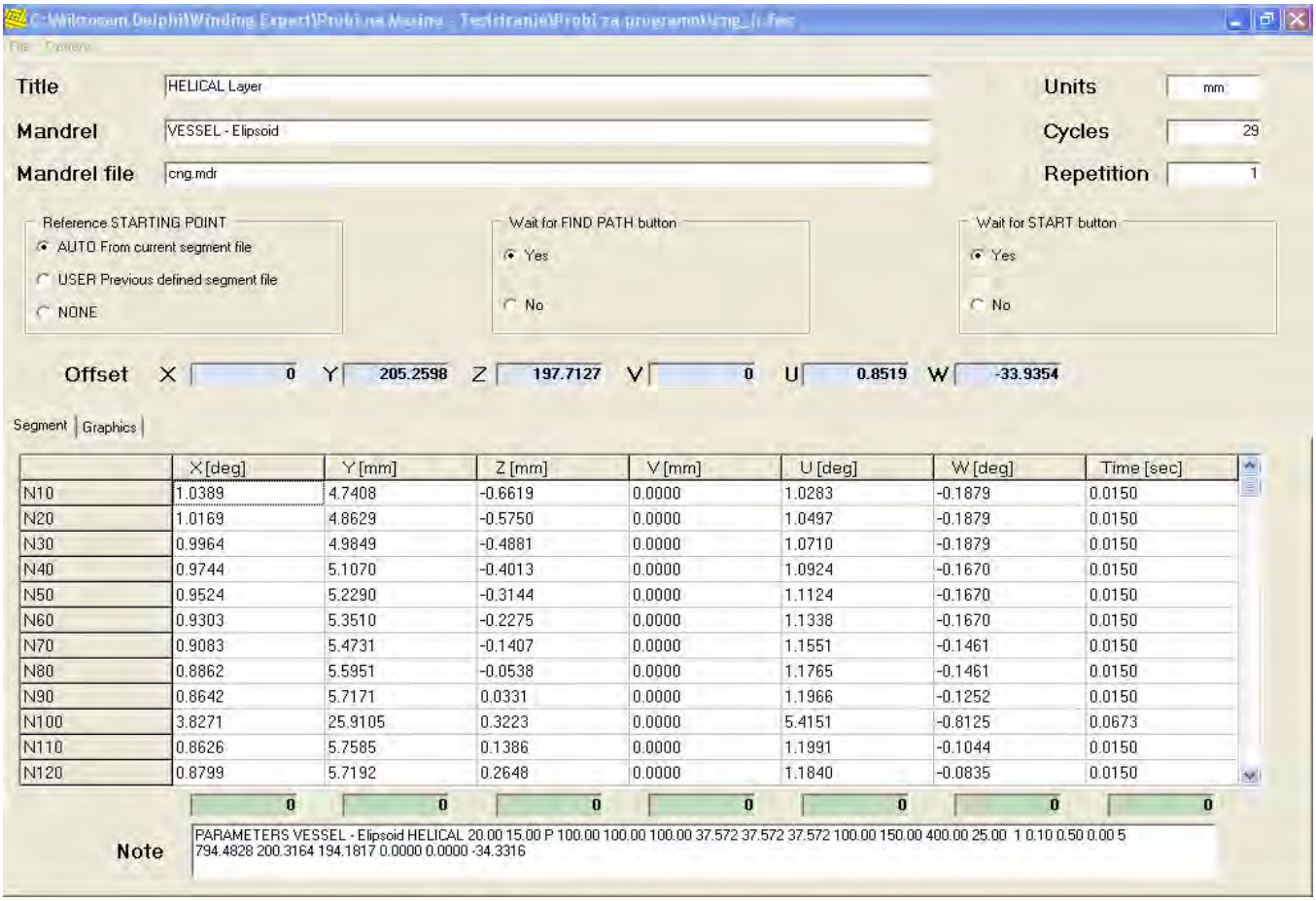

Fig. 6. Editing of G-Code

Also if it is necessary to ensure pause or break between segments (for applying reinforcement or different material between layers) user can chose the appropriate options for different pushbuttons supported by the control system. These settings can be different for the development phase and for the manufacturing phase of the composite production.

IV. Conclusion

Advanced CAD/CAM system for designing and manufacturing of composite parts with robotic filament winding is presented. System provides automatic design of mandrel shape, radial, helical and transition layers and offers great flexibility for changing of all winding parameters: winding angle, covering degree, opening diameters and winding patterns with complete simulation of the winding process. Smoothing algorithm ensures smooth movements of the machine without strokes at high speed. Final result of the presented CAD/CAM system is complete G-code for the industrial filament winding robot.

References

[1] S. Chan, M. Munro, A. Fahim, “Accuracy-speed relationships of a robotic filament winding cell”, Robotics and Computer-Integrated Manufacturing, Vol 12. No 1, pp. 3-13, 1996.

[2] B.S. Johansen , A. Lystrup , M.T. Jensen, “CADPATH: a complete program for the CAD-, CAE- and CAM-winding of advanced fibre composites”, Journal of Materials Processing Technology, vol. 77, pp. 194–200, 1998.

[3] Markoski, B. Samakoski, Z. Sokoloski, Z. Petreski, K. Mrceski, “PC-Basec CNC system for Roboric Filament Winding, 4th CiiT Conference on Informatics and Information Technology, Bitola, Macedonia, 2003.

[4] Markoski, K. Mrceski, “FW Editor - Winding Expert”, *User Manual*, Mikrosam, Prilep, 2003.

[5] J.Scholliers, H.V. Brussel, “Design and off-line programming of a robotic tape winding cell”, Robotics and Computer-Integrated Manufacturing, Vol 12. No 1, pp. 93-98, 1996.

[6] D. Trajkovski, “GENWIND – Algorithms for pattern creation on rotational symetrical parts”, Mikrosam, 2002.

Controlling the Rikitake's nonlinear system with chaotic behaviour by means of synchronization

Radoslav H. Radev[1], Elena D. Monova[2] and Dragomir P. Chantov[3]

Abstract – **In this paper the problems about relay-based control of the nonlinear Rikitake's system are discussed. The control laws are designed on the basis of the necessary condition of the maximum principle. These laws are formed by the state space variables of a second (response) system, which is synchronized with the first (drive) system. The results are confirmed by computer simulation.**

Keywords – **chaos, synchronization, control, conditional Lyapunov exponent.**

I. Introduction

The chaos is a special type of dynamical behaviour of systems, possessing a number of specific features which in essence determine the concept *chaos*. These features are [3, 10]:

- strong sensitivity to tiny variations of the initial conditions and/or the system parameters which means that small differences in the initial conditions lead to substancial differences in the system behaviour;
- the 'motion' of the system in the state space is performed over orbits, which are restricted in a definite area, possessing at the same time a positive Lyapunov exponent;
- these systems have continuous frequency spectrum.

A lot of processes in physics, chemistry, technics, biology, medicine, ecology and economics possess such behaviour [10].

The mathematical model of these systems is a system of nonlinear differential equations of the type:

$$\dot{\mathbf{x}} = \mathbf{f}(\mathbf{x},\mathbf{p}), \tag{1.1}$$

where:

- $\mathbf{x} \in \Re^n$ is the state vector;
- $\mathbf{f}(\mathbf{x},\mathbf{p}) = [f_1(\mathbf{x},\mathbf{p}),\ f_2(\mathbf{x},\mathbf{p}),\ \dots,\ f_n(\mathbf{x},\mathbf{p})]^T$
- $\mathbf{p} \in \Re^m$ - is the vector of the variable parameters for which the $m \le n$ condition is satisfied. The change of at least one of the vector elements leads to bifurcations in the system.

It is a characteristic feature of the systems with chaotic behaviour that the linearized system is unstable in all equilibrium points $\mathbf{x}_i^*$, which are the solution of the equation:

$$\mathbf{f}(\mathbf{x}^*,\mathbf{p}) = \mathbf{0}. \tag{1.2}$$

[1]Radoslav H. Radev is with the Technical University of Gabrovo, 4 H. Dimitar Str., 5300 Gabrovo, Bulgaria, E-mail: radev@tugab.bg

[2]Elena D. Monova is with the Technical University of Gabrovo, 4 H. Dimitar Str., 5300 Gabrovo, Bulgaria, E-mail: elena@tugab.bg

[3]Dragomir P. Chantov is with the Technical University of Gabrovo, 4 H. Dimitar Str., 5300 Gabrovo, Bulgaria, E-mail: dchantov@yahoo.bg

1.1. Synchronization of chaotic systems.

The synchronization is a process [1], when two or more connected systems, equivalent or not by structure and parameters, adjust their dynamics to each other. In actual fact this phenomenon is reproducing the state of one of the systems by the other on the basis of information received through a connecting signal.

When dealing with synchronization, two systems S_{dr} (*drive*) and S_{resp} (*response*) are considered:

$$S_{dr}: \quad \dot{\mathbf{x}} = \mathbf{f}(\mathbf{x}) \tag{1.3}$$

and

$$S_{resp}: \quad \dot{\tilde{\mathbf{x}}} = \tilde{\mathbf{f}}(\tilde{\mathbf{x}}), \tag{1.4}$$

with the corresponding solutions $\mathbf{x}(t, t_0, \mathbf{x}(t_0))$ and $\tilde{\mathbf{x}}(t, t_0, \tilde{\mathbf{x}}(t_0))$, where $\mathbf{x} \in \Re^{n_1}$ и $\tilde{\mathbf{x}} \in \Re^{n_2}$ and initial conditions $\mathbf{x}(t_0)$ and $\tilde{\mathbf{x}}(t_0)$.

For $n_1 = n_2$ and $\tilde{\mathbf{f}}(\tilde{\mathbf{x}}) = \mathbf{f}(\mathbf{x})$, the systems S_{resp} and S_{dr} are *identical*.

The solutions $\mathbf{x}(t, t_0, \mathbf{x}(t_0))$ and $\tilde{\mathbf{x}}(t, t_0, \tilde{\mathbf{x}}(t_0))$ of the S_{dr} and S_{resp} systems with initial conditions $\mathbf{x}(t_0)$ and $\tilde{\mathbf{x}}(t_0)$ are *asimptotically synchronized* in relation to a chosen function Q_t, if

$$\lim_{t\to\infty} Q_t[\mathbf{x}(t), \tilde{\mathbf{x}}(t)] = 0. \tag{1.5}$$

For identical systems the function most frequently is chosen of the type

$$Q_t = \|\mathbf{e}(t)\|, \tag{1.6}$$

where

$$\mathbf{e}(t) = \mathbf{x}(t, t_0, \mathbf{x}(t_0)) - \tilde{\mathbf{x}}(t, t_0, \tilde{\mathbf{x}}(t_0)) \tag{1.7}$$

is the difference between S_{dr} and S_{resp}.

Generally the synchronization of chaotic systems is realized by two methods – through one-way and through two-way coupling. In case of one-way coupling the first system is *free* and it *leads* the second, which tracks the dynamics of the first, while in the case of two-way coupling the influence over the two systems is mutual.

In the case of one-way coupling of two autonomous

identical systems, which are the subject of the present investigation, most frequently a decomposition of the system to two subsystems (Pecora-Carroll method) is searched [8]:

$$\mathsf{S}_{dr}: \begin{cases} \dot{\mathbf{x}}_1 = \mathbf{f}_1(\mathbf{x}_1, \mathbf{x}_2), \\ \dot{\mathbf{x}}_2 = \mathbf{f}_2(\mathbf{x}_1, \mathbf{x}_2), \end{cases} \tag{1.8}$$

and

$$\mathsf{S}_{resp}: \begin{cases} \dot{\tilde{\mathbf{x}}}_1 = \mathbf{f}_1(\tilde{\mathbf{x}}_1, \tilde{\mathbf{x}}_2), \\ \dot{\tilde{\mathbf{x}}}_2 = \mathbf{f}_2(\mathbf{x}_1, \tilde{\mathbf{x}}_2), \end{cases} \tag{1.9}$$

where $\mathbf{x}_1 \in \Re^l$, $\mathbf{x}_2 \in \Re^m$, $\tilde{\mathbf{x}}_1 \in \Re^l$, $\tilde{\mathbf{x}}_2 \in \Re^m$, $m + l = n$. The state subvector $\mathbf{x}_1$ of the first subsystem of S_{dr} is applied to the second subsystem of the system S_{resp} for achieving synchronization.

1.2. *Lyapunov exponents.*

A quantitative evaluation of synchronization of chaotic systems is carried out on the basis of the Lyapunov exponents λ_i [1, 3, 8, 9], which are an analogue to the eigenvalues of the linear systems. These exponents are a measure of the convergence or the divergence of the nonlinear systems. A main index for the presence of chaos is the maximum Lyapunov exponent, which is positive. In general case there is no analytical solution for computing the maximum Lyapunov exponent and it is calculated by means of a numerical procedure by the following expression:

$$\lambda = \lim_{t\to\infty} \frac{1}{t} \lim_{|e(t)|\to 0} \frac{|\mathbf{e}(t)|}{|\mathbf{e}(0)|}. \tag{1.10}$$

By the Pecora&Carroll synchronization method

$$\mathbf{e}(t) = \mathbf{x}_2(t) - \tilde{\mathbf{x}}_2(t) \tag{1.11}$$

is the difference between S_{dr} and S_{resp} with initial conditions

$$\left\|\mathbf{x}_2(0) - \tilde{\mathbf{x}}_2(0)\right\| \neq 0.$$

The evaluation of the decomposition-type synchronization is carried out by the so called *conditional Lyapunov exponents* (*CLE*), which are calculated by (1.10) with the substitution of the difference (1.11).

II. Control Synthesis

A relay based control of the type:

$$\dot{\mathbf{x}} = \mathbf{f}(\mathbf{x}, \mathbf{p}) + \mathbf{B}u \tag{2.1}$$

has to be determined for the system (1.1).

The Hamilton function for the system (2.1) is:

$$\mathscr{H}(\mathbf{x}, u, t, \boldsymbol{\lambda}) \overset{\Delta}{=} \boldsymbol{\lambda}^{\mathrm{T}}(t)\left[\mathbf{f}(\mathbf{x}, \mathbf{p}) + \mathbf{B}u\right] \tag{2.2}$$

and according to the maximum principle the following conditions for the n-dimensional auxiliary vector $\boldsymbol{\lambda}(t) = [\lambda_1(t) \quad \cdots \quad \lambda_n(t)]^{\mathrm{T}}$ have to be satisfied:

1. For each t (with the exception of the interruption points of $\mathbf{f}$ and u) the Hamiltonian function takes a maximum over the optimal trajectory, i.e.:

$$\frac{\partial \mathscr{H}}{\partial u} = 0. \tag{2.3}$$

2. For each t (with the exception of the interruption points of $\mathbf{f}$ and u) the following condition for the vector $\boldsymbol{\lambda}(t)$ over the optimal trajectory is satisfied:

$$\frac{d\boldsymbol{\lambda}(t)}{dt} = -\frac{\partial \mathscr{H}(\mathbf{x}, u, \boldsymbol{\lambda})}{\partial \mathbf{x}}. \tag{2.4}$$

3. If there is no limitation for the duration of the transient process an additional condition is imposed:

$$\mathscr{H}(\mathbf{x}, u, \boldsymbol{\lambda}) = 0. \tag{2.5}$$

It follows from (2.3) that the control is relay based of the kind:

$$u = \operatorname{sign} s_i(\mathbf{x}), \tag{2.6}$$

where with taking to consideration of (2.4) and the necessary condition for a nonzero vector $\boldsymbol{\lambda}$, the control function over the i-th input $s_i(\mathbf{x})$ for third-order systems is obtained from the following equation:

$$\det\begin{bmatrix} f_l(\mathbf{x}) & f_k(\mathbf{x}) \\ -\dfrac{\partial f_l(\mathbf{x})}{\partial x_i} & -\dfrac{\partial f_k(\mathbf{x})}{\partial x_i} \end{bmatrix} = 0 \quad \text{for} \quad k \neq i \text{ and } l \neq i \tag{2.7}$$

and it has the form:

$$s_i(\mathbf{x}) = f_k(\mathbf{x})\frac{\partial f_l(\mathbf{x})}{\partial x_i} - f_l(\mathbf{x})\frac{\partial f_k(\mathbf{x})}{\partial x_i} = 0. \tag{2.8}$$

It is accepted that the control function (2.8) is formed from the state variables of S_{resp} and the control is active when the system trajectory enters a given region $\mathscr{L}_i$ in the state space (as shown on fig.1) for which the following condition is satisfied:

$$\mathbf{x}_i^* \in \mathscr{L}_i \in \mathscr{A}. \tag{2.9}$$

$\mathscr{A}$ is the system attractor and the region $\mathscr{L}_i$ is a sphere

$$\mathscr{L}_i = \left\{\mathbf{x} \in \Re^n : \left\|\mathbf{x} - \mathbf{x}_i^*\right\| \leq R\right\} \tag{2.10}$$

around the equilibrium point $\mathbf{x}_i^*$ with a radius R, which has to be such that the condition

$$\mathscr{L}_i \cap \mathscr{A} \neq \varnothing \tag{2.11}$$

to be performed.

This is the *so called* local control [9].

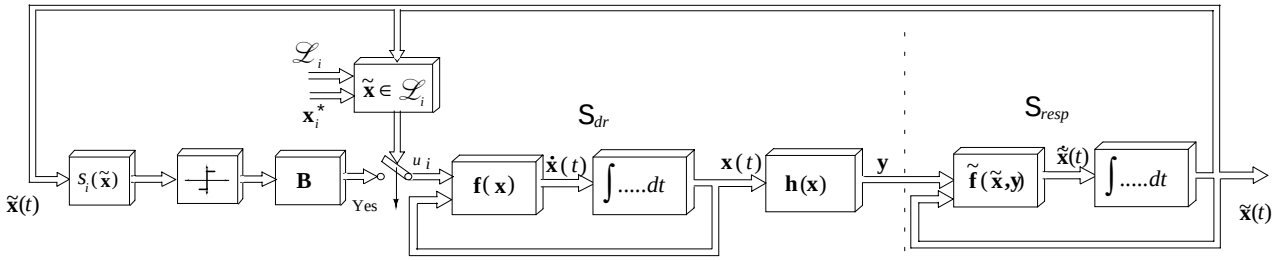

Fig. 1.

III. Rikitake's system

The Rikitake's system [4] represents a model of a double-disk dynamo system and is described by the following equations:

$$\begin{aligned} \dot{x}_1 &= -\mu x_1 + x_2 x_3, \\ \dot{x}_2 &= -\mu x_2 + (x_3 - \mu A) x_1, \\ \dot{x}_3 &= b - x_1 x_2, \end{aligned} \qquad (3.1)$$

where $A = \left(K^2 - K^{-2}\right)$.

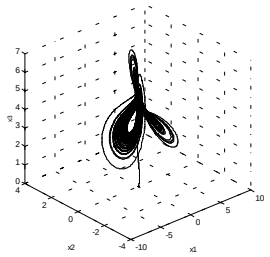

Fig. 2

The system attractor is shown on fig.2. The system has two equilibrium points with the following coordinates:

$$\mathbf{x}_{1,2}^* = \begin{bmatrix} \pm K\sqrt{b} \\ \pm K^{-1}\sqrt{b} \\ \mu K^2 \end{bmatrix}, \qquad (3.2)$$

which for parameter values $\mu = 1, \quad K = 2, \quad b = 1$ are

$$\mathbf{x}_{1,2}^* = \begin{bmatrix} \pm 2 \\ \pm 0.5 \\ 4 \end{bmatrix}.$$

The Jacobian of the system (3.1) in the equilibrium points $\mathbf{x}_j^*$ is

$$\mathbf{A}_j = \begin{bmatrix} -\mu & x_{j3}^* & x_{j2}^* \\ x_{j3}^* - \mu A & -\mu & x_{j1}^* \\ -x_{j2}^* & -x_{j1}^* & 0 \end{bmatrix}. \qquad (3.3)$$

Evaluation of the possibility to drive the system into $\mathbf{x}_j^*$ is made by the rank of the matrix

$$\mathbf{Q}_i = \left[\mathbf{B}_i \quad \mathbf{B}_i\mathbf{A}_j \quad \mathbf{B}_i\mathbf{A}_j^2\right]. \qquad (3.4)$$

The analysis shows that

$$\operatorname{rank}\mathbf{Q}_i = 3 \quad \forall\ i \text{ and } j, \qquad (3.5)$$

from which follows that the system is completely controllable in the equilibrium points.

The control functions for the i-th input control by taking into consideration the state variables of S_{resp} are:

$$s_1(\mathbf{x}) = b(x_3 - \mu A) - \mu x_2^2$$
$$s_2(\mathbf{x}) = b x_3 - \mu x_1^2$$
$$s_3(\mathbf{x}) = \mu\left(x_1^2 - A x_1 x_2 - x_2^2\right)$$

The Pecora&Carroll synchronization method is proposed for the Rikitake's system. Table 4.1 shows the three possible decompositions of the system by the given method as well as the calculated according to [12] conditional Lyapunov exponents.

Табл. 4.1.

Controlled system	Connec-ting variable	Conditional Lyapunov exponent
$\dot{\tilde{x}}_2 = -\mu\tilde{x}_2 + (\tilde{x}_3 - \mu A)x_1$ $\dot{\tilde{x}}_3 = b - x_1\tilde{x}_2$	x_1	$\lambda_{1,2} = -0.5$
$\dot{\tilde{x}}_1 = -\mu\tilde{x}_1 + x_2\tilde{x}_3$ $\dot{\tilde{x}}_3 = b - x_1\tilde{x}_2$	x_2	$\lambda_{1,2} = -0.5$
$\dot{\tilde{x}}_1 = -\mu\tilde{x}_1 + \tilde{x}_2 x_3$ $\dot{\tilde{x}}_2 = -\mu\tilde{x}_2 + (x_3 - \mu A)\tilde{x}_1$	x_3	$\lambda_1 = -4.76$ $\lambda_2 = 2.76$

Synchronization of the *response* system with the *drive* system is only possible with x_1 and x_2 as driving variables since one of the conditional Lyapunov exponents in the case of x_3 as driving signal is positive.

III. Experimental results

Synchronization with x_1 and x_2 as driving variables is done. A control function is then applied to the first, to the second and to the third input of the original system using the state variables of the synchronized response system. The following figures show the errors (the differences) by synchronization with x_1 and x_2 and control over the three inputs.

- First-input control, synchronization by x_1.

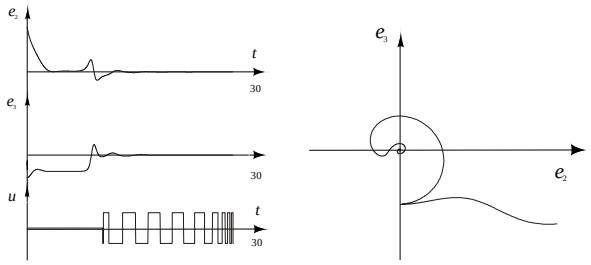

Fig. 3

- First-input control, synchronization by x_2 .

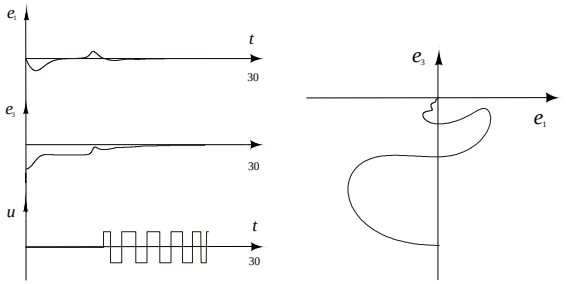

Fig. 4

- Second-input control, synchronization by x_1

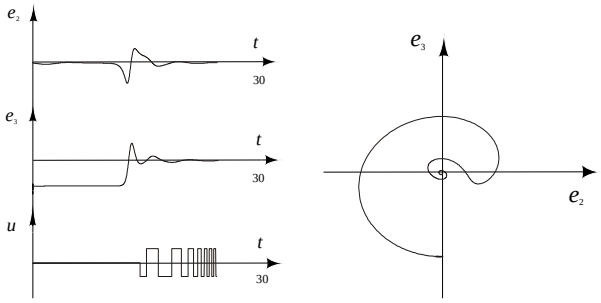

Fig. 5

- Second-input control, synchronization by x_2

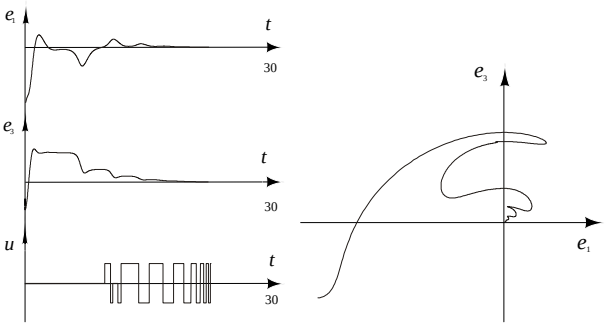

Fig. 6

- Third-input control, synchronization by x_1

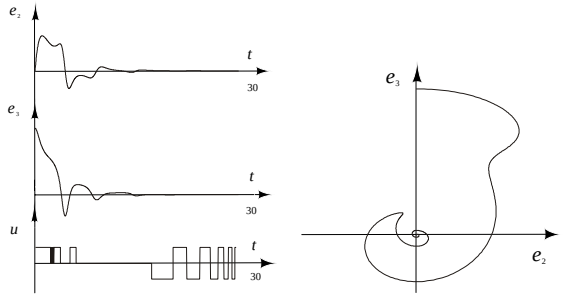

Fig. 7

- Third-input control, synchronization by x_2

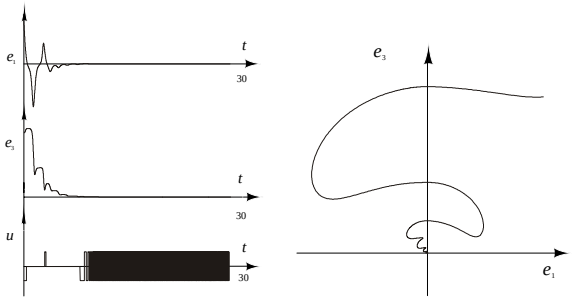

Fig. 8

III. Conclusion

In this paper control through synchronization for the Rikitake's system is proposed. The investigations made show that this control in essence little differs from the control through direct use of the state vector.

References

[1] Boccaletti, S., J.Kurths, G.Osipov, D.L.Valladares, C.S.Zhou, The synchronization of chaotic systems, Physics Reports 366 (2002), pp.1 –101.

[2] Chen, G., Control and Synchronization of Chaotic Systems, (Bibliography), Dep. of Electrical and Computer Engineering, University of Houston, 1997 **www.ee.cityu.edu.hk/~gchen/chaos-control.html**

[3] Chen, G., X. Dong, From chaos to order: perspectives, methodologies and applications.World Scientific, Singapore, 1998.

[4] Cook, A.E., P.H.Roberts, The Rikitake two-disc dynamo system, Proc. Cambridge Phil. Soc., 68,1970, pp.547-569.

[5] Fradkov, A.L., Chaos Control Bibliography (1997 - 2000).Russian Systems and Control Archive (RUSYCON), **www.rusycon.ru/chaos-control.html**

[6] Fradkov, A.L., H. Nijmeijer, A.Yu.Pogromsky, Adaptive observer based synchronization, in Chen G., (Ed.), Controlling Chaos and Bifurcations in Engineering Systems, CRC Press, Boca Raton, FL, 1999, pp.417-435.

[7] Hsu, J., A. Meyer, Modern Control Principles and Applications, Mc.Graw- Hill Book Comp., N.Y., 1968.

[8] Pecora, L.M., T.L. Carroll, Synchronization in Chaotic Systems, Phys. Rev. Lett., vol. 64, No 8, 1990, pp. 821-824.

[9] Richter, H., K.Reinschke, Local control of chaotic systems- a Lyapunov approach, ***IJBS***, Vol.8, No 7(1998), pp.1565-1573.

[10] Панчев, Ст., Теория на хаоса, Акад. Изд. "Проф. М. Дринов, София, 1996.

[11] Понтрягин, Л., В.Болтянский, Р.Гамкрелидзе, Е. Мищенко, Математическая теория оптимальньх процессов, Физматгиз, Москва, 1961.

[12] Guemez, J., C.Martin, M.Matias, Approach to the synchronized state of some driving methods, Phys.Rev.E, Vol.55, No1, pp.124-134.

Input-output based discrete-time disturbance estimator using sliding mode approach

Boban Veselić[1], Čedomir Milosavljević[2] and Darko Mitić[3]

***Abstract* – This paper proposes input-output based discrete-time disturbance estimator structure, in which conventional passive digital filters are replaced with an active digital sliding mode controlled subsystem. In ideal sliding mode, complete disturbance rejection occurs and plant output follows nominal system. Estimator robustness is actively gained by providing sliding mode existence conditions. Simulation results show effectiveness of the proposed disturbance estimator.**

***Keywords* – Disturbance estimator, external disturbances, model uncertainties, sliding mode, robustness.**

I. INTRODUCTION

In almost every control environment the presence of external disturbances and model uncertainties is inevitable, which has significant impact on the performance of a controller. Hence, the performance of a control system is evaluated through its disturbance rejection ability and robustness to model uncertainties.

One approach in handling external disturbances and model uncertainties, which is usually regarded as an equivalent or generalized disturbance, is an employment of disturbance observers. The concept of disturbance observer is that the disturbance action can be efficiently compensated by feedback of the observed disturbance. Thus, disturbance observer enables real plant to behave like the nominal plant.

Generally, there are two methods in a disturbance observer design. The first is the design of a state space disturbance observer, which requires disturbance model to be employed in an augmented state observer. This approach is suitable for simple disturbances, such as bias and periodic disturbances. It is hardly used for arbitrary disturbances. However, it is proposed in [1] a design of discrete-time robust control system, containing a state space disturbance observer, in which modeling of disturbances is not required.

The other method of a disturbance observer design is based on transfer function approach. Conventionally, the disturbance observer is designed using inverse dynamic of a plant, [2]. Disturbance observer efficiency is dependent on the design of the so-called Q filter, which is essentially utilized for the causality of the observer. Q filter determines robustness and disturbance rejection performance, which is proved to be contradictory requirements, [3].

This approach may be viewed from the aspect of internal model concept. The IMPACT (Internal Model Principle And Control Together) structure incorporates both internal models of nominal plant and disturbances, in order to obtain rejection of known class of disturbances, robustness to parameter perturbations and desired dynamic response. Compensation of an arbitrary external disturbance may be obtained by on-line adaptation of disturbance internal model, [4]. A simplified IMPACT controlling structure [5] may be treated as a disturbance estimator.

As a nonlinear robust control strategy, which is theoretically insensitive to model uncertainties and external disturbances, variable structure systems (VSS) with their associated sliding mode behavior are very attractive for perturbed system control. Sliding mode control (SMC) essentially utilizes a switching control law to drive the state of the concerned system to a predefined sliding surface in the state space and to maintain the sliding motion along the surface into the equilibrium point [6]. Due to digital realization of VSC algorithms, analysis of discrete-time sliding mode control (DSMC) systems shows that in general only quasi-sliding modes can be achieved, i.e., the system trajectories are in a small bounded vicinity of the sliding surface.

Among many versatile applications, SMC has found its role in a system state observation [6], and thereby in disturbance observers. Discontinuous disturbance estimators, where VSS equivalent control theory is employed in disturbance estimation, are proposed in [7,8].

This paper proposes sliding mode controlled input-output based discrete-time disturbance estimator. Conventional passive digital filters responsible for estimator robustness and disturbances rejection are replaced with an active DSMC structure, due to its emphasized robustness property. If an ideal sliding mode is established, complete disturbance rejection occurs and plant output follows nominal system. Estimator robustness (stability) against model uncertainties is actively gained by providing sliding mode existence conditions. Thus, robustness and good external disturbances rejection property are no longer contradictory requests.

II. DSMC BASED DISTURBANCE ESTIMATOR

Consider a single-input single-output continuous time dynamic system described by the state space model

[1] Boban Veselić is with the Faculty of Electronic Engineering, Medvedeva 14, 18000 Niš, Serbia and Montenegro, E-mail: bveselic@elfak.ni.ac.yu

[2] Čedomir Milosavljević is with the Faculty of Electronic Engineering, Medvedeva 14, 18000 Niš, Serbia and Montenegro, E-mail: milosavljevic@elfak.ni.ac.yu

[3] Darko Mitić is with the Faculty of Electronic Engineering, Medvedeva 14, 18000 Niš, Serbia and Montenegro, E-mail: darkom@elfak.ni.ac.yu

$$\dot{\mathbf{x}}(t)=\mathbf{A}\mathbf{x}(t)+\mathbf{b}u(t)+\mathbf{j}v(t),\ y(t)=\mathbf{c}\mathbf{x}(t), \quad (1)$$

where the state $x\in R^n$, the control $u\in R^1$, the external disturbance $v\in R^1$ and the output $y\in R^1$; $\mathbf{A}$, $\mathbf{b}$, $\mathbf{j}$, $\mathbf{c}$ are the constant matrix and vectors of appropriate dimensions. The discrete time representation of the dynamic system (1) is obtained by applying u through a zero-order-hold,

$$\mathbf{x}(k+1)=\mathbf{E}\mathbf{x}(k)+\mathbf{f}u(k)+\mathbf{w}(k),\ y(k)=\mathbf{c}\mathbf{x}(k), \quad (2)$$

where T is a sampling period and

$$\mathbf{E}=e^{\mathbf{A}T},\ \mathbf{f}=\int_0^T e^{\mathbf{A}t}\mathrm{d}t\mathbf{b},\ \mathbf{w}(k)=\int_0^T e^{\mathbf{A}t}\mathbf{j}v(kT+T-t)\mathrm{d}t. \quad (3)$$

By assuming zero initial conditions, Z-transform of (2) yields

$$Y(z)=\mathbf{c}(z\mathbf{I}-\mathbf{E})^{-1}\mathbf{f}U(z)+\mathbf{c}(z\mathbf{I}-\mathbf{E})^{-1}\mathbf{W}(z). \quad (4)$$

Using Eq. (4), the system output y in terms of the control u and the external disturbances d may be expressed as

$$y(k)=G(z)u(k)+d(k), \quad (5)$$

where

$$G(z)=\frac{z^{-1}B(z^{-1})}{A(z^{-1})},\ d(k)=\frac{z^{-1}\mathbf{H}(z^{-1})}{A(z^{-1})}\mathbf{w}(k),$$
$$A(z^{-1})=z^{-n}\det(z\mathbf{I}-\mathbf{E}),\ B(z^{-1})=z^{-n+1}\mathbf{c}\,\mathrm{adj}(z\mathbf{I}-\mathbf{E})\mathbf{f}, \quad (6)$$
$$\mathbf{H}(z^{-1})=z^{-n+1}\mathbf{c}\,\mathrm{adj}(z\mathbf{I}-\mathbf{E})=\left[H_1(z^{-1})\quad H_2(z^{-1})\right].$$

The polynomials $A(z^{-1})$ and $B(z^{-1})$ are assumed to be stable and relatively prime, where z^{-1} denotes unit-delay operator.

The main concept is to compensate action of the equivalent disturbance, consisting of model uncertainties and external disturbance, by feedback of the observed equivalent disturbance, and thereby to obtain nominal model behavior. Consider the control structure proposed in Fig. 1., which is composed of the real plant (5) and the disturbance estimator in the local loop. The extraction of the equivalent disturbance q in the disturbance estimator is obtained using discrete transfer function of the nominal model $G_n(z)$. The mismatch between the real plant and nominal model inevitably exists due to uncertainties of the plant parameters. The real plant may be reliably described by

$$G(z)=G_n(z)(1+\delta G(z)), \quad (7)$$

where its perturbation is limited by the multiplicative bound of uncertainties $|\delta G(e^{j\omega T})|\le\gamma(\omega),\ \omega\in[0,\pi/T]$. According to Eq. (7) and Fig. 1., the extracted equivalent disturbance is

$$q(k)=d(k)+G_n(z)\delta G(z)u_k(k). \quad (8)$$

In order to improve disturbance estimator robustness, an active controlling structure is employed instead of conventionally used passive digital filter. A reasonable choice is a DVSC system due to its emphasized robustness property. Signal $\hat{q}$ is an estimation of the compensated equivalent disturbance portion. If DSMC ensures $\hat{q}=q$ (an ideal sliding mode occurs), the control signal may be described as $u_{sm}(k)=G_n^{-1}(z)q(k)$. It can be easily proved that the system output behaves as a nominal model $y(k)=G_n(z)u(k)$. Since DSMC systems enables only quasi-sliding mode, certain but small bounded error between q and $\hat{q}$ will exist, whose value depends on the employed control algorithm.

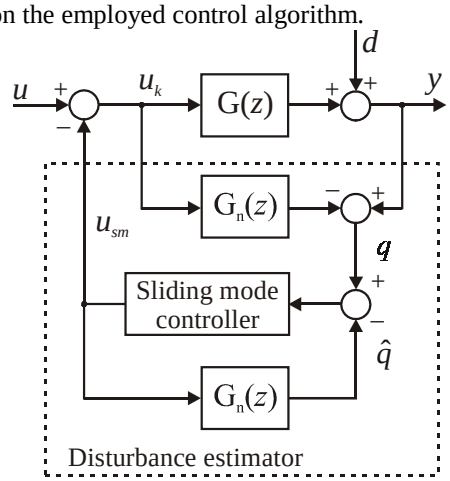

Fig. 1. Structure of DSMC based disturbance estimator

Robustness against model uncertainties is actively gained by providing sliding mode existence conditions. Thus, robustness and good external disturbances rejection property are no longer contradictory requests. From the control design aspect, the proposed method of equivalent disturbance compensation may be treated as a discrete-time tracking control problem with measurable but unknown in advance reference signal $q(k)$. Since digital controller steers a nominal model not a real plant, all state variables are available. This enables variety of DSMC algorithms to be utilized, which successfully handle this control task.

III. DSMC Design

Robust chattering-free DSMC algorithm [9] based on state-space approach is chosen for the digital sliding mode controller. Controller design is demonstrated on the second order system. Consider a discrete-time nominal model.

$$\mathbf{x}(k+1)=\mathbf{E}\mathbf{x}(k)+\mathbf{f}u_{sm}(k),\ y(k)=\mathbf{c}\mathbf{x}(k), \quad (9.a)$$

$$\mathbf{E}=e^{\mathbf{A}T}=\begin{bmatrix}e_{11}&e_{12}\\e_{21}&e_{22}\end{bmatrix},\ \mathbf{f}=\int_0^T e^{\mathbf{A}t}\mathrm{d}t\mathbf{b}=\begin{bmatrix}f_1\\f_2\end{bmatrix},\ \mathbf{c}=\begin{bmatrix}1&0\end{bmatrix}. \quad (9.b)$$

It is more convenient to consider tracking error dynamics, which may be obtained using coordinate transformation. A new state space vector $z(k)=[z_1\quad z_2]^{\mathrm{T}}$ is introduced, defined as $z_1(k)=q(k)-x_1(k),\ z_2(k)=z_1(k)-z_1(k-1),\ \hat{q}(k)=x_1(k)$, which has to be driven to zero by the control force $u_{sm}(k)$. The discrete-time model (9) is transformed to

$$\mathbf{z}(k+1)=\mathbf{E}_x\mathbf{z}(k)+\mathbf{f}_x u_{sm}(k)+\mathbf{h}x_2(k)+\mathbf{g}q(k+1)+\mathbf{p}q(k),$$
$$\mathbf{E}_x=\begin{bmatrix}e_{11}&0\\e_{11}-1&0\end{bmatrix},\mathbf{f}_x=\begin{bmatrix}-f_1\\-f_1\end{bmatrix},\mathbf{h}=\begin{bmatrix}-e_{12}\\-e_{12}\end{bmatrix}, \quad (10)$$
$$\mathbf{g}=\begin{bmatrix}1\\1\end{bmatrix},\mathbf{p}=\begin{bmatrix}-e_{11}\\-e_{11}\end{bmatrix}.$$

The basic sliding mode control philosophy comprises global stabilization of the control system by steering system states onto predefined sliding surface, and maintaining

subsequent motion along that surface into the state space origin. Let the switching function be

$$s(k)=\boldsymbol{\sigma}\mathbf{z}(k),\ \boldsymbol{\sigma}=[\sigma\quad 1] \tag{11}$$

Control law $u_{sm}(k)$ should be determined which provides the desired motion constrained into the quasi-sliding domain, defined as small bounded vicinity of the sliding line $s(k)=0$. Sliding line parameter σ defines sliding mode dynamics, that is, compensation dynamics of the equivalent disturbance. An adequate adoption of the slope σ should provide stable system eigenvalues with desired dynamics.

According to Eqs. (11) and (10), system motion toward the sliding line is presented by

$$\begin{aligned}s(k+1)=s(k)+\boldsymbol{\sigma}[(\mathbf{E}_x-\mathbf{I})\mathbf{z}(k)+\mathbf{f}_x u_{sm}(k)\\ +\mathbf{h}x_2(k)+\mathbf{g}q(k+1)+\mathbf{p}q(k)].\end{aligned} \tag{12}$$

Let the control signal be in the form

$$\begin{aligned}u_{sm}(k)=\frac{-1}{\boldsymbol{\sigma}\mathbf{f}_x}\{\boldsymbol{\sigma}[(\mathbf{E}_x-\mathbf{I})\mathbf{z}(k)+\mathbf{h}x_2(k)+(\mathbf{p}+2\mathbf{g})q(k)\\ -\mathbf{g}q(k-1)]+\operatorname{sgn}(s(k))\min(|s(k)|,\alpha T)\},\end{aligned} \tag{13}$$

under constraint $\boldsymbol{\sigma}\mathbf{f}_x\neq 0$. Control signal has two modes. The first mode, nonlinear with respect to $s(k)$ and active outside the region $|s(k)|<\alpha T$, ensures reaching the region in a finite number of steps; afterwards, the second linear mode provides reaching the quasi-sliding domain in one step. Thus, a discrete-time sliding mode is achieved employing smooth control signal, [9].

To prove that the proposed control law (13) ensure above described motion, and to determine the related switching gain as well as the width of the quasi-sliding domain, the following two supportive lemmas are given.

Lemma 1, [10]**:** *System trajectories described by*

$$s(k+1)=s(k)+f(k+1)-\alpha T\operatorname{sgn}(s(k)) \tag{14}$$

where $f(k)$ *is some bounded function and* $\alpha>|f(k+1)|/T$, $\forall k\in N$, *will reach region* $|s(k)|<\alpha T$ *from any initial state* $s(0)$ *in finite number of steps.*

Lemma 2, [10]**:** *If* $q(t)$ *is an arbitrary smooth function with bounded time derivative* $|\ddot{q}(t)|\le R$, *then the following discrete time inequality holds* $|q(kT+T)-2q(kT)+q(kT-T)|\le 2T^2R$.

The designed discrete time variable structure controller is summarized by the following theorem.

Theorem: *Consider the discrete time system (10) under the action of the control signal (13), where the switching function is chosen as (11). If the switching gain satisfies*

$$\alpha>2TR|\boldsymbol{\sigma}\mathbf{g}|, \tag{15}$$

the discrete-time quasi-sliding mode will arise from any initial state in a finite number of steps in the domain defined by

$$|s(k+1)|\le 2T^2R|\boldsymbol{\sigma}\mathbf{g}|. \tag{16}$$

Proof: Since the system motion starts outside the region $|s(k)|<\alpha T$, by virtue of Eq. (13), Eq. (12) becomes

$$s(k+1)=s(k)-\alpha T\operatorname{sgn}(s(k))+\boldsymbol{\sigma}\mathbf{g}[q(k+1)-2q(k)+q(k-1)]. \tag{17}$$

Under condition (15), according to lemmas 1 and 2, system trajectories (17) will reach the region in a finite number of steps. Governed further by the linear phase of the control (13), system motion is described by

$$s(k+1)=\boldsymbol{\sigma}\mathbf{g}[q(k+1)-2q(k)+q(k-1)], \tag{18}$$

indicating that the quasi-sliding domain is entered in the next step, whose width (16) is proved by (18) and lemma 2. □

It is evident from (16) that $s(k+1)=0$ if $\ddot{q}(t)=0$, implying that the proposed sliding mode based disturbance estimator completely rejects step and ramp like equivalent disturbances. In all other cases, when $R\neq 0$, it provides $O(T^2)$ accuracy.

VI. Simulation Results

The effectiveness of the proposed DSMC based disturbance estimator has been investigated by simulation. The plant is a DC motor, whose continuous-time model (1) is defined with

$$\mathbf{x}=\begin{bmatrix}\omega\\ i_r\end{bmatrix},\ \mathbf{A}=\begin{bmatrix}0 & k/J\\ -k/L_r & -R_r/L_r\end{bmatrix},\ \mathbf{b}=\begin{bmatrix}0\\ 1/L_r\end{bmatrix},\ \mathbf{j}=\begin{bmatrix}-1/J\\ 0\end{bmatrix},\ \mathbf{c}^{\mathrm{T}}=\begin{bmatrix}1\\ 0\end{bmatrix} \tag{19}$$

The nominal plant (model) parameters are: $R_{rn}=1\Omega$, $B_n=0$ $L_{rn}=2.5\cdot 10^{-3}H$, $J_n=3.267\cdot 10^{-3}kgm^2$, $k_n=0.33$. Using the discrete-time model (2) with the sampling time $T=10^{-3}s$ the following nominal discrete transfer function is obtained according to Eqn. (6)

$$G_n(z)=\frac{z^{-1}(0.0177384+0.0155257z^{-1})}{1-1.65934z^{-1}+0.67032z^{-2}}. \tag{20}$$

The plant is subjected to parameter and external disturbances. Load torque, shown in Fig. 2., acts as an external disturbance. Model uncertainty, i.e., the mismatch between the real plant and the nominal model, is defined by the following values: $R_r=R_{rn}\cdot 1.3$, $L_r=L_{rn}\cdot 1.2$, $J=J_n\cdot 2$, $k=k_n\cdot 1.1$. Consequently, the real plant discrete transfer function is

$$G(z)=\frac{z^{-1}(0.00805062+0.00696901z^{-1})}{1-1.64289z^{-1}+0.648344z^{-2}}. \tag{21}$$

Parameters of the digital sliding mode controller have been selected as: $\alpha=10$, $\sigma=10$. The main control loop contains linear digital controller $G_r(z)=(1-0.985z^{-1})/(1-z^{-1})$, which involves an integral action. The controlled DC motor is subjected to a step angular velocity reference.

Step responses of the controlled systems with and without disturbance estimator are shown in Fig. 2, as well as the load torque. Due to the integral action of the main loop controller, the uncompensated system output $y_0(t)$ has zero error only in the section of step like disturbance action. In other sections, system error is significant. The compensated system output $y(t)$ demonstrates an excellent disturbance rejection performance.

According to the enlarged scale of the switching function plotted in Fig. 3., it is confirmed the complete rejection of step and ramp like disturbances by the proposed disturbance estimator. The deviation from the zero value in other sectors is significantly small.

Error signal of he compensated system is shown in Fig. 4. in the enlarged scale also. It may be noticed that the system

has no error in the case of step, ramp and parabolic like disturbance action. This is a result of the combined action of the disturbance estimator and the main controller with integral action.

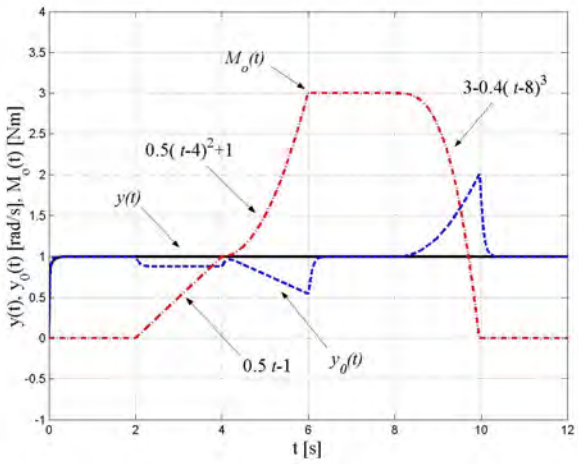

Fig. 2. Step responses of uncompensated system $y_0(t)$, compensated system $y(t)$; and external disturbance $M_o(t)$.

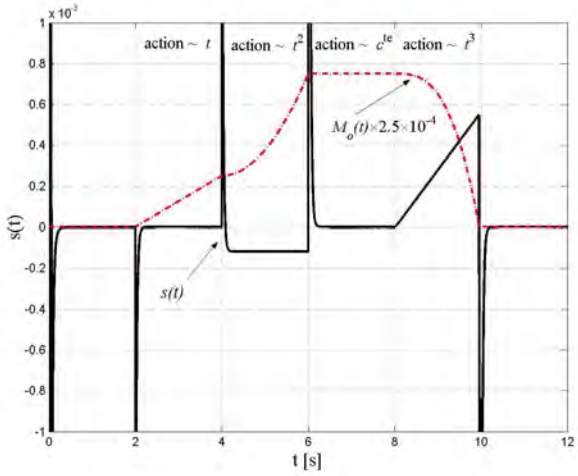

Fig. 3. Switching function $s(t)$.

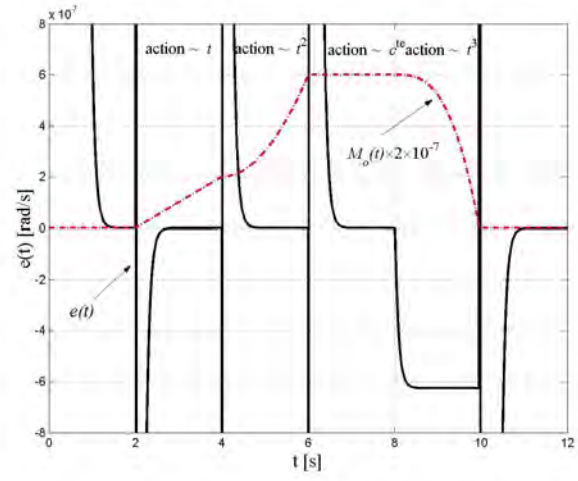

Fig. 4. Error signal $e(t)$ of the compensated system.

V. Conclusion

The proposed input-output based discrete-time disturbance estimator structure, where conventional passive digital filters are replaced with active DSMC subsystem, inherits recognized sliding mode properties with respect to internal and external perturbations. Estimator robustness against model uncertainties is actively gained by providing sliding mode existence conditions. Thus, robustness and good external disturbances rejection property are no longer contradictory requests.

From the control design aspect, the proposed equivalent disturbance compensation method may be viewed as a discrete-time tracking control problem with measurable but unknown in advance reference signal. Sliding mode digital controller governs a nominal model not a real plant, where all state variables are available, offering variety of DSMC algorithms to be utilized. The applied state-space DSMC algorithm enables complete rejection of step and ramp like equivalent disturbances. In all other cases it provides an $O(T^2)$ accuracy.

References

[1] S.M. Suh, C.C. Chung and S.H. Lee, "Discrete-time track following controller design using a state space disturbance observer", Microsystem Technologies, no. 9, pp. 352-361, 2003.

[2] S. Komada, K. Nnomura, M. Ishida and T. Hory, "Robust force control based on compensation for parameter variations of dynamic environment", IEEE Trans. Industrial Electronic, vol. 40, no. 1, pp. 89-95, 1993.

[3] Y. Chou, K. Yang, W.K. Chung, H.R. Kim and H. Suh, "On the robustness and performance of disturbance observers for second-order system", IEEE Trans. Automatic Control, vol. 48, no. 2, pp. 315-320, 2003.

[4] M.R. Stojić and M.S. Matijević, "Structural design of digital control system with immeasurable arbitrary disturbances", The th Mediterranean Conference on Control and Automation, Proceedings of Conference, Dubrovnik, Croatia, 2001.

[5] M.R. Stojić, M.S. Matijević and S. Korać, "Design of IMPACT controlling structure with conventional digital controllers", (invited paper), XLVII ETRAN Conference, Proceedings of Conference, vol. 1, pp. 263-268, Heceg Novi, Serbia and Montenegro, 2003.

[6] V.I. Utkin, *Sliding Modes in Control and Optimization*, Berlin, Springer-Verlag, 1992.

[7] P. Korondi, K.K.D. Young and H. Hashimoto, "Discrete-time sliding mode based feedback compensation for motion control", 1996 IEEE Workshop on Variable Structure Systems, Proceedings of Conference, pp. 127-131, Tokyo, Japan, 1996.

[8] X. Chen, S. Komada and T. Fukuda, "Design of nonlinear disturbance observer", IEEE Trans. Industrial Electronics, vol. 47, no. 2, pp429-437, 2000.

[9] G. Golo and Č. Milosavljević, "Robust discrete-time chattering free sliding mode control", Systems & Control Letters, vol. 41, pp. 19-28, 2000.

[10] B. Veselić, G. Golo and Č. Milosavljević, "Discrete time sliding mode approach to synchronization of modulated two-phase harmonic oscillator", Electrical Engineering, (in press) DOI 10.1007/s00202-003-0209-z, http://dx.doi.org/10.1007/s00202-003-0209-z.

Session ECST:

Electronic Components, Systems and Technologies

Noise Modeling and Analysis of a BJT Common – Emitter Stage

Pesha D. Petrova[1]

Abstract **- Accurate noise modeling is a prerequisite for circuit noise simulation. In this paper, a noise model for Bipolar Junction Transistor (BJT) common – emitter stage using input voltage and current equivalent generators is presented. Noise analysis of a model is performed. Analytical equations for input equivalent generators of a stage, as well as, for optimum noise factor and for optimum source resistance are worked out. MATLAB simulation results are presented.**

Keywords **– noise modeling, noise analysis, noise factor, BJT common – emitter stage, MATLAB**

I. INTRODUCTION

Noise behavior is an important characteristic of electronic circuits, as it usually determines the fundamental limit of the performance of circuits. Circuit noise is generated within resistors, devices, and interconnections. Mathematically, noise is characterized in terms of mean and autocorrelation in the time domain, or the power spectral density in the frequency domain. The most important noise sources in circuit devices are thermal noise, shot noise and flicker noise [1].

The spectral density function of thermal noise, $i_{NT}^2 / \Delta f$, can be given by

$$\frac{i_{NT}^2}{\Delta f} = \frac{4kT}{R} \quad , \tag{1}$$

where k is Boltzman's constant ($k = 1.374x10^{-23}\ J/K$), T is the absolute temperature in degrees Kelvin, R is the resistance in ohms, and Δf is a circuit bandwidth in Herts.

The noise spectral density of shot noise, $i_{NS}^2 / \Delta f$, can be described by

$$i_{Ss}^2 / \Delta f = 2qI \tag{2}$$

where q is the electron charge ($q = 1.6x10^{-19}\ C$), and I is the average junction current.

The spectral density of flicker noise, $i_{Nf}^2 / \Delta f$, can be determined by

$$\frac{i_{Nf}^2}{\Delta f} = KF \frac{I^{AF}}{f} \tag{3}$$

where KF is a constant for a particular device and AF is a constant in the range from 0.5 to 2.

[1]Pesha D. Petrova is with the Department of Communication Equipment and Technologies, Technical University of Gabrovo, 5300 Gabrovo, 4, Hadji Dimitar St.,Bulgaria, E-mail: daneva@tugab.bg

II. INPUT NOISE GENERATORS AND NOISE FACTOR OF ELECTRONIC CIRCUITS

A general noise model of an electronic circuit can be obtained by reflecting all internal noise sources to the input. In order for the reflected sources to be independent of the source impedance, two noise sources can be used – a series voltage source and a shunt current source. Furthermore, the noisy circuit can be presented as shown in Fig. 1(a), and the noiseless one can be presented as shown in Fig. 1(b). The representation in Fig. 1(b) is valid for any impedance, if correlation between the noise generators is considered.

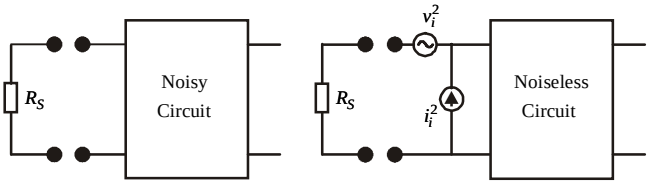

(a) (b)

Fig. 1. A noisy (a) and a noiseless (b) circuit.

The equivalent noise input voltage v_{iN} can be considered as the voltage in series with v_S (see Fig. 3) that generates the same noise voltage at the output as all noise sources in the circuit [2].

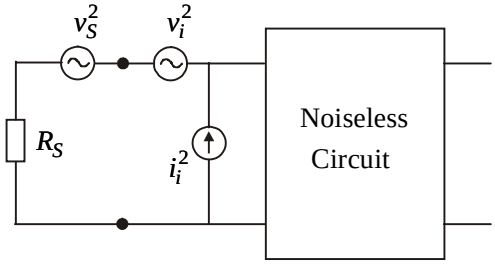

Fig. 3. A circuit with equivalent input noise generators.

The mean-square value of the total input equivalent noise can be found by

$$v_{iN}^2 = v_S^2 + v_i^2 + i_i^2 R_S^2 \quad , \tag{4}$$

where v_S^2 is the thermal noise of R_S.

In most practical circuits the correlation between v_i and i_i is small and may be neglected. If either v_i^2 or i_i^2 dominates, the correlation may be neglected in any case.

The value of v_i^2 can be found by shorting the input ports and equating the output noise in each case. In a similar

manner, the value of i_i^2 can be found by opening the input ports and equating the output noise in each case.

Assuming no correlation between v_i^2 and i_i^2, is obtained

$$\frac{N_a}{N_i}=\frac{v_i^2+i_i^2R_S^2}{v_S^2} \quad . \tag{5}$$

Thus, the noise factor fop the two – port circuit is

$$F=1+\frac{N_a}{N_i}=1+\frac{v_i^2}{4kTR_S\Delta f}+\frac{i_i^2R_S}{4kT\Delta f} \quad . \tag{6}$$

It is obvious, that for small R_S, v_i^2 dominates, whereas for large R_S, i_i^2 dominates.

There is an optimal R_S for minimum F. Solving Eq. (7), as a result $R_{S,opt}$ is found.

$$\frac{dF}{dR_S}=-\frac{v_i^2}{4kTR_S^2\Delta f}+\frac{i_i^2R_S^2}{4kTR_S^2\Delta f}=0 \quad . \tag{7}$$

$$R_{S,opt}=\frac{v_i^2}{i_i^2} \quad . \tag{8}$$

Substituting Eq. (8) into Eq. (6) gives

$$F_{opt}=1+\frac{i_i^2R_S}{2kT\Delta f} \quad . \tag{9}$$

IV. Noise Modeling and Analysis of a BJT Common – Emitter Stage

A. BJT Noise Model

A key element in most analog circuits is a bipolar junction transistor. From various BJT models [3], [4], [5] for noise modeling and analysis of analog circuits a model shown in Fig. 4 is the most suitable.

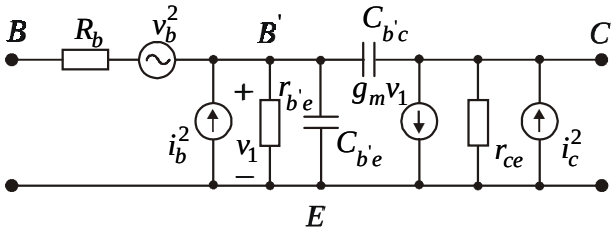

Fig. 4. BJT noise model.

Thermal noise du to the resistance R_b can be modeled by a thermal noise source

$$v_b^2=4kTR_b\Delta f \quad . \tag{10}$$

Base and collector currents are considered to be independent. Therefore, the shot noise can be described by

$$i_b^{'2}=2qI_B\Delta f \tag{11}$$

at the base and

$$i_c^2=2qI_C\Delta f \tag{12}$$

at the collector.

The total *1/f* noise of the transistor is described by a noise source in parallel with base – emitter contact. This leads to the noise source at the base following

$$i_b^2=2qI_B\Delta f+KF\frac{I_B^{AF}}{f}\Delta f \quad . \tag{13}$$

B. Noise Model of BJT a Common – Emitter Stage

Using BJT model in Fig. 4, a noise model for common – emitter stage, shown in Fig. 5, is synthesized.

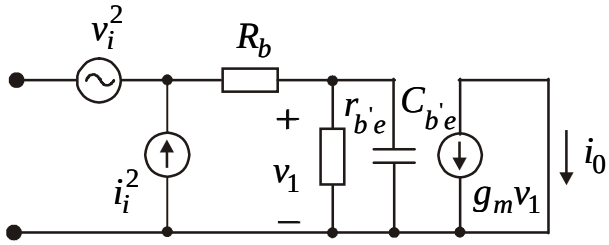

Fig. 5. BJT common-emitter stage noise model

A noise voltage generator v_i^2 and a noise current generator i_i^2 model the noise in a common - emitter stage.

By shorting the input ports, is obtained

$$i_o=g_mv_b+i_c=g_mv_i \quad . \tag{14}$$

Since r_b is small, i_b is neglected. Thus, from Eq. (14) follows that

$$v_i^2=v_b^2+\frac{i_c^2}{g_m^2} \quad , \tag{15}$$

and

$$\frac{v_i^2}{\Delta f}=4kT\left(r_b+\frac{1}{2g_m}\right)=4kTR_{eq} \quad . \tag{16}$$

In Eq. (16) R_{eq} is the equivalent input resistance and

$$R_{eq}=r_b+\frac{1}{2g_m} \quad .$$

Similarly, by opening the input ports, as can be seen from Fig. 5,

$$i_o=\beta(j\omega)i_b+i_c=\beta(j\omega)i_i \tag{17}$$

from where the current of the input noise generator can be expressed by

$$i_i^2=i_b^2+\frac{i_c^2}{|\beta(j\omega)|^2} \quad . \tag{18}$$

Thus

$$\frac{i_i^2}{\Delta f}=2q\left[I_B+KF'\frac{I_B^{AF}}{f}+\frac{I_C}{|\beta(j\omega)|^2}\right]=2qI_{eq} \tag{19}$$

where

$$KF'=\frac{KF}{2q}, \quad \beta(j\omega)=\frac{\beta_0}{1+\beta_0\dfrac{C_{b'e}+C_{b'c}}{g_m}j\omega} \quad .$$

From Eq. (19) it is obvious that the equivalent input shot noise current I_{eq} can be expressed as

$$I_{eq} = I_B + KF^{'}\frac{I_B^{AF}}{f} + \frac{I_C}{\left|\beta(j\omega)\right|^2} \quad .$$

C. Total Equivalent Noise Voltage of a BJT Common - Emitter Stage

Substituting Eqs. (16) and (19) into Eq. (4) and taking into consideration that $v_S^2 = 4kTR_S$, the total equivalent noise voltage with a source resistance R_S is found as

$$\begin{aligned} v_{iN}^2 &= \left(4kT(R_S + r_b + \frac{1}{2g_m}\right)\Delta f \\ &+ R_S^2 2q\left(I_B + KF^{'}\frac{I_B^{AF}}{f} + \frac{I_C}{\left|\beta(j\omega)\right|^2}\right)\Delta f \\ &= 2qR_S^2(A+B)\Delta f \end{aligned} \qquad (20)$$

where

$$A = \frac{2\varphi_T}{R_S^2}\left(R_S + r_b + \frac{1}{2g_m}\right)$$

$$B = I_B + KF^{'}\frac{I_B^{AF}}{f} + \frac{I_C}{\left|\beta(j\omega)\right|^2}$$

and $\varphi_T = kT/q$.

D. Noise Factor of a BJT Common - Emitter Stage

Neglecting flicker noise and substituting $I_C = I_B/\beta_F$ into Eq. (19) gives

$$\frac{i_i^2}{\Delta f} = 2q\left(\frac{I_C}{\beta_F} + \frac{I_C}{\left|\beta(j\omega)\right|^2}\right) \quad . \qquad (21)$$

Using Eqs. (6), (16) and (21) the noise factor of a BJT common – emitter stage is obtained as

$$\begin{aligned} F &= 1 + \frac{1}{R_S}\left(r_b + \frac{1}{2g_m}\right) \\ &+ R_S\left[\frac{g_m}{2\beta_F} + \frac{g_m}{2\beta_o^2}\left(1 + \beta_o^2\left(\frac{\omega}{\omega_T}\right)^2\right)\right] \end{aligned} \qquad (22)$$

where $\omega_T = 1/f_T$ (f_T - transition frequency).

For high - frequency circuits, if $\omega/\omega_T >> 1/\beta_o$ and $\omega/\omega_T >> 1/\beta_F$

$$F \approx 1 + \frac{1}{R_S}\left(r_b + \frac{1}{2g_m}\right) + R_S\frac{g_m}{2}\left(\frac{\omega}{\omega_T}\right)^2 \quad . \qquad (23)$$

Solving equation $dF/dg_m = 0$ for fixed R_S and ω_T gives

$$g_{m,opt} = \frac{1}{R_S}\frac{\omega_T}{\omega} \quad . \qquad (24)$$

and

$$F_{opt} = 1 + \frac{r_b}{R_S} + \frac{\omega}{\omega_T} \quad . \qquad (25)$$

Similarly, from equation $dF/dR_S = 0$, for fixed g_m and ω_T, are determined

$$R_{S,opt} = \sqrt{\frac{2r_b}{g_m} + \frac{1}{g_m^2}}\,\frac{\omega}{\omega_T} \quad , \qquad (26)$$

and

$$F_{opt} = 1 + \sqrt{2r_b g_m + 1}\,\frac{\omega}{\omega_T} \quad . \qquad (27)$$

For low – frequency circuits, if $\omega/\omega_T << 1/\beta_o$ and $\omega/\omega_T << 1/\beta_F$

$$F \approx 1 + \frac{1}{R_S}\left(r_b + \frac{1}{2g_m}\right) + R_S\frac{g_m}{2}\frac{1}{\beta_F} \quad . \qquad (28)$$

Applying optimization procedure to Eq. (28), the following equations for $g_{m,opt}$, $R_{S,opt}$ and F_{opt} are obtained:

$$g_{m,opt} = \frac{1}{R_S}\sqrt{\beta_F} \quad , \qquad (29)$$

$$F_{opt} = 1 + \frac{r_b}{R_S} + \frac{1}{\sqrt{\beta_F}} \qquad (30)$$

for fixed R_S and β_F,
and

$$R_{S,opt} = \sqrt{\frac{2r_b}{g_m} + \frac{1}{g_m^2}}\;\sqrt{\beta_F} \quad , \qquad (31)$$

$$F_{opt} = 1 + \sqrt{2r_b g_m + 1}\;\frac{1}{\sqrt{\beta_F}} \qquad (32)$$

for fixed g_m and β_F.

E. Demonstration example

In order to demonstrate the effectiveness and the accuracy of the above stated approach a MATLAB file for computation and simulation the noise of a common – emitter stage is written. Assume that a NPN BJT type 2N2222A is used in the stage. Computed results for optimum source resistance's, on condition that f = 1kHz and varying collector current I_C, are given in Table I.

TABLE I
OPTIMUM VALUES FOR SOURCE RESISTANCE

I_C, mA	1.00	0.50	0.10	0.05
$R_{S, opt}$, Ω	150	200	2000	4000

The results of the simulations are shown in Figs. 6 and 7. In Fig. 6 the frequency dependence of noise factor with varying the values of collector current and optimum source resistance, is presented. Fig. 7 is the result of noise factor versus source resistance simulation.

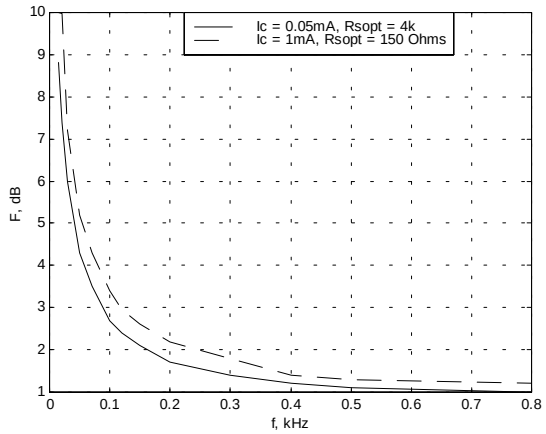

Fig. 6. Noise factor as a function of frequency.

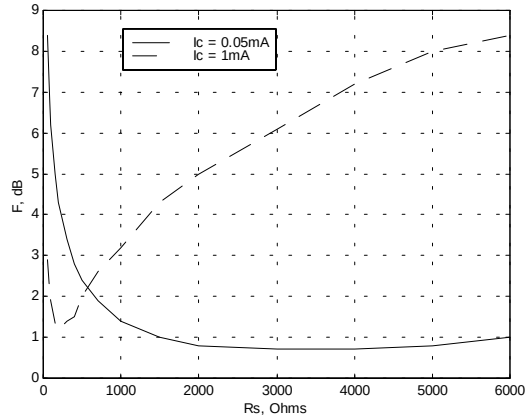

Fig. 7. Noise factor as a function of source resistance.

The calculation and simulation outcomes of the BJT common - emitter stage coincide with the values given in manufacturer' s data books [6].

IV. CONCLUSION

A simple but effective approach for noise modeling and analysis of a BJT common – emitter stage is developed. Noise generators are used to model the total input noise of a stage. Analytical equations for noise factor and source resistance of low and high–frequency circuits are obtained. The calculation and simulation outcomes of a common – emitter stage by implementing various BJT types support the efficiency and fidelity of the approach proposed in this paper. This approach can be applied successfully to the other BJT configurations. The equivalent input noise generators of a common – base stage or emitter follower are the same as those of a common – emitter stage. For the common – base configuration, since its current gain ≈ 1, any noise current at the output is referred directly back to the input without reduction. For the emitter follower, since its voltage gain ≈ 1, any noise voltage at the output, including noise due to Z_L, is transformed unchanged to the input.

REFERENCES

[1] F. Sischka, Noise Modeling for Semiconductors, Agilent Technologies GmbH, Munich, 2002.

[2] Jieh-Tsorng Wu, Noise Analysis and Modeling, National Chiao-Tung University, 2001.

[3] G. Massobrio, P. Antognietti, Semiconductor Device Modeling with SPICE, McGraw-Hill, New Jork, 1993.

[4] F. X. Sinnesbichler, M. Fischer, G. R. Olbrich, "Accurate Extraction Method for 1/f-Noise Parameters Used in Goomel-Poon Type Bipolar Transistor Models", IEEE MTT-S Symposium, Baltimore, 1998, pp. 1345-1348.

[5] Pesha D. Petrova, "Noise Modeling of Semiconductor Devices", TELSIKS'03, Proceedings of Papers, vol. 2, pp.577-580, Nis, Yugoslavia, 2003.

[6] Motorola Semiconductor Technical Data, Motorola, Inc, 1999-2003.

Trends in Modeling and Simulation for Power Electronics Convertors

Ekaterina N. Dimitrova[1], Vencislav C. Valchev, [2]
Nikolay R. Nikolov[2], Dimitar M. Kovachev[2]

***Abstract* – The simulation of Power Electronics Systems (PES) enables to predict its behavior before any hardware to be built. It allows checking various options, unusual operating or failure conditions and protection operating. These checks are difficult to realize in practice. The simulations allow also increasing the quality of students teaching. The current and future trends in the simulation of PES are discussed here. A comparison of the three most useful simulators for PES – MATLAB/SIMULINK, SABER and PSPICE is given. Power semiconductor models and magnetic models for PSPICE and SABER are compared and evaluated.**

***Keywords*: PSPICE, SABER, MATLAB/SIMULINK, Power semiconductor models, magnetic models**

I. INTRODUCTION

The general trend in the simulations in power electronics is the remarkable increase in its application. The State-of-the-art power electronics laboratory set up along with supporting simulation laboratory is an important part of modern education process. Some curses in power electronics education are simulation supported [2].

Usually, general purpose electronics software is used for power electronics, rather than software specifically designed that application. In this case, the proper choice of the relevant simulation tool is important in power electronics design.

In this article, current and future trends in PES simulation, simulation software tools and device modeling are described.

II. CURRENT AND FUTURE TRENDS IN THE SIMULATION OF PES

Background to SPICE, SABER, and MATLAB

With one notable exception, almost all commercially analogue simulation tools for electronics are based on the SPICE [3] program. Its algorithms are robust, powerful and thus, SPICE became an industry standard tool and the most commonly used simulator for power converter circuits. The main disadvantage of SPICE is inflexibility of the embedded models, which are difficult to adapt to the particular tasks in power device modeling.

SABER [4] is a relatively new simulator in which the models are separated from the simulator. Thus, one can readily create a library of accurate models, specifically designed for power devices. For many engineers, SABER remains unfamiliar and expensive compared to the available versions of SPICE.

SIMULINK is a simulation tool based on the popular MATLAB package. The equations of the system are essentially modeled using a wide range of graphical building blocks including control system notation, s-plane, state-space representation, etc. Users can add their own C programs too.

Mixed-Mode Simulation

One of the most significant developments in simulation technology, which affects the world of PES, is the advent of True Concurrent Mixed Analogue and Digital Simulation (TCMADS). Many switch-mode power supplies are based on integrated circuits that contain digital logic as part of the switching control circuitry. As the "pure analogue simulation" time increases exponentially with the size of circuit model for such circuits, it is sensible to look for techniques that reduce the model size while keeping the accuracy of the model. Opposite to the commonly known approaches based on model simplifications, TCMADS runs an analogue and digital simulators as separate processes in a multi-tasking environment, passing information between them at run time.

State Averaging Techniques (SAT)

SAT is based on characterization of the switching and the control circuitries as behavioral models rather than as combination of discrete components. Such technique provides an accurate model of the behavior of the power supply in response to variations in load without having to simulate each switching cycle individually and thus, it eliminates the great deal of data due to very small time step of simulation, which may vary down to picoseconds. This method can reduce the simulation time hours down to a matter of seconds.

Device models

In addition to the techniques described above, the modeling of the circuit at the component level is critical for the success of the simulation. One of the greatest problems here is the availability of device models. While the manufacturer's data provides a "starting point" for modeling the devices, it falls short in at least two aspects.

Firstly, the parameters provided by the manufacturer do not map easily into the internal SPICE parameters. A lot of models for typical small signal devices are available directly from manufacturers. However, for power devices and less commonly used components, these models are sadly lacking.

Secondly, the manufacturers tend to provide the kind of parameters that designers use in an average application. Their models often fall short, when an accurate simulation is required, especially in the cases when the devices work on the edge of its specification. Furthermore, often the only

[1] Dept. of Electronics, Technical University of Varna 9010, Bulgaria, E-mail: katy@ieee.bg
[2] Dept. of Electronics, TU of Varna 9010, Bulgaria

parameters that are provided are nominal values with no tolerance specifications.

The solution of the described problems lies in the increased use of simulation by Original Equipment Manufacturers (OEMs). This "positive feedback" results in providing the more necessary data in relevant formats. Nevertheless, if the information required is not available from the manufacturer, then the only solution is to measure the device parameters.

High –Voltage, High Current, Layout and EMC

A number of specific problems occur in high power applications modeling, such as welding. They are caused by the extreme values of process parameters (100s of volts, 100s of amps, switching times of 50-100ns, etc) combined with the large number of very small parasitic capacitance effects and transmission line effects. These make the modeling of the equivalent electrical circuit very dependent on the mechanical dimensions of components, mountings and interconnect. Shortcomings in device models also cause problems in this area. At this sort of level, the only real solution is to provide a simulator that solves electromagnetic field effects and converts them into an equivalent circuit. With the advent of EEC wide regulations on electromagnetic emissions we can expect to see much work being done in this area to solve a pressing problem.

III. A COMPARISON OF THREE POPULAR PACKAGES

Although there are areas of overlap between the simulations, each has some particular qualities. Sometimes the tools are used in a complementary manner. For example, MATLAB can be used to calculate parameters for a SABER model or even, vice versa, SABER can be used to derive parameters for a SIMULINK model.

MATLAB/SIMULINK

The simulation engine is based on MATLAB' s powerful matrix processing core and several fixed and variable time step solving algorithms are available. The full power of MATLAB is available for graphing and post processing. SIMULINK is mainly useful for application level modeling since it contains a wide variety of control system models.

SABER

SABER, from Analogy Inc., was developed as an engineering simulation tool. The library of models covers several technologies, not just electrical/electronic. All the models can be mixed in the same simulation. Users can create their own models (if the required function is not in the library) using Analogy's proprietary Hardware Definition Language, MAST. SABER is also compatible with SPICE models.

The simulation engine has separate simulators for the analogue and digital domains and a patented algorithm ensures synchronization of two simulations when required. This is especially important for modeling wide range of switching circuits. The analogue simulator engine has a variable time step algorithm with various simulation controls available to the user. Graphical display of the simulation is good, with an intuitive user interface. A variety of post processing tools are available including waveform measurements and a waveform calculator. Some work has been done using MASAT/SABER to develop a range of physics based power device models [1].

PSPICE

PSPICE is one of the most popular of the commercial SPICE-based simulation packages. Models are created by schematic capture or by text editing of a netlist. Large numbers of models are available since SPICE models are interchangeable between all SPICE based simulation tools. Unlike SABER, PSPICE is only aimed at electronic engineering applications, although it is possible to develop analogues models using electrical elements (R, C, and L) for non-electrical problems e.g. Heat dissipation. Graphical display of the simulation output is good, with a reasonable user interface. A variety of post processing tools are available including waveform measurements and FFT.

Table I compares basic features of the packages.

IV. POWER SEMICONDUCTOR MODELS

The specially developed power semiconductor device models for SPICE are compared and evaluated in this section.Table II presents the generic and special SPICE models for power devices. Note that no models exist for several of the devices, and that most of the models have major limitations. The comments about DIODE and BJT are illustrated on Fig.1 and Fig.2 respectively.

Table III compares three simulations: GENERIC SPICE, a typical ENHANCED SPICE, and SABER for their relative capability in modeling phenomena relevant to power semiconductor devices

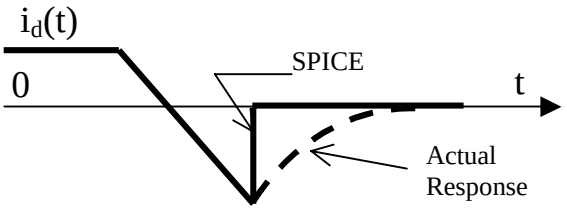

Fig.1. Diode Turn-OFF Waveform

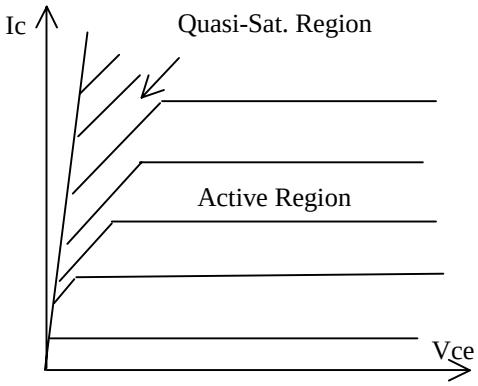

Fig.2. BJT Collector Characteristics Showing Quasi-Saturation Region

Table I. Comparisons between MATLAB, SABER and PSPICE

PROPERTY	MATLAB/SIMULINK	SABER	PSPICE
VERSION	5.2/2.2	4.3	9.2
Supplier	The Mathworks Inc	Analogy Inc.	Orcad
Platforms	PC (Windows 98/NT or Linux), Unix Systems, Apple	PC (Windows 98/NT), HP and Solaris Unix systems	PC (Windows 98/NT)
Circuit Entry	Schematic or text	Schematics or text	Schematics or text
Simulation Engine	Based on Matlab' s matrix solving algorithms; Various solving algorithms available (both fixed and variable step)	Variable time step. Separate analogue and digital simulation engines with synchronized interface.	Spice 2
Available Simulations	DC, time domain	DC, time domain, frequency domain, parameter sweep (nested), Monte Carlo	DC, time domain, frequency domain, parameter sweep, Monte Carlo
Display of Results	Uses Matlab's Graphing Functions which include 3D. Wide range of functions available but not user friendly.	Only 2D graphs available. User interface very good. Frequency domain results can be shown as Bode or Nyquist plots	Only 2D graphs available. User interface fair.
Availability of Models	Increasing. Several "block sets" representing components are now available, including the Power System Block set aimed for modeling of power generation and distribution. Users can interface own C or FORTRAN routines.	The generic template library gives a good coverage. Good coverage of electronic components used in the automotive industry. The user group has a library of templates donated by Saber users. Users can interface their own C or FORTRANE routines	Very large availability of models due to the wide Spice user base.
Post-Processing	All Matlab functions available since results stored as matrices: FFT, Filtering, waveform extraction and calculations. Data can be saved in ASCII format.	Waveform calculator allows manipulation of data: arithmetic, parameter extraction, FFT. Waveform measurements available. More functions available in AIM macro language including matrix arithmetic. Data can be saved in ASCII format.	Calculations can be performed on waveforms e.g. calculate power from V and I. FFT available. Data can be saved in ASCII format
Documentation of results	Graphs can be annotated with user information. Graphs can be saved for later recall. Wide variety of graphical formats and printer support available (PS, BMP, TIFF and JPEG)	Graphs can be annotated with user information and measurements. Graphs can be saved for later recall. Limited number of graphical formats and printer support: basically Postscript, PCL and MIF.	Graphs can be annotated with user information. Graphs can be copied to the Windows clipboard and then passed into word processor, spreadsheet etc. Graphs cannot be saved as files.
Batch Processing	Simulink can be controlled from a Matlab M-script.	The simulation engine can be rum in true batch mode on Unix systems. Simulator can be controlled using a command line script (which is separate from the netlist) or an Aim script.	All parts of the tool (schematic, simulator and results analysis) can be run separately. The simulator is controlled from commands embedded in the netlist. These can be inserted via the schematic GUI or by editing the netlist.
Add-ons	Additional Matlab toolboxes are available covering wide range of applications. DSpace real-time simulator	Sensitivity and stress analysis. Linear system (pole/zero) analysis. Magnetic system design tool. Links to other simulation tools.	PCB layout tool
Customization	Matlab contains a range of GUI. Creation commands which allow users to create their own applications/ interfaces	The AIM macro language is a superset of TCL/Tk which includes a full range of GUI creation commands. AIM is a powerful tool which includes comm.-ands for waveform manipulation, graph creation and controlling the simulator. However, it is not well documented.	Users can create their own measurement functions.

TABLE II. POWER SEMICONDUCTOR DEVICE MODELS FOR SPICE

COMPONENT	GENERIC MODEL	POWER MODEL	COMMENTS
DIODE	Charge Control	Yeung &Shackleton; Xu & Schrőder	Lacks "soft" recovery and forward recovery. Requires complex subcircuit
BJT	Ebers-Moll and/or Gummel- Poon	Bowers et al.; Getreu; Yeung et al.	Lacks quasi-saturation and dynamic saturation
MOSFET	Frohman-Grove	Neinhaus,Bowers Lauritzen& Shi Wheatley, Ronan,Dolny Fay& Sutor Hancock Yee & lauritzen Simas, Piedade,Freire Xu & Schrőder Cordonnier	Basic Model, Const. Cgd. Unusable for BVdss>80V. Inaccurate on Turn-OFF. Const. Cgd, internal info req. Cgd:switched. Accurat e, but complex Cgd:2C values plus switch. Cgd:3C values plus switch. Insufficient information to evaluate. Cgd: 1C value plus diode C.
JFET or SIT	Shichman & Hodges	None	The power JFET is called the Statistic Induction Transistor SIT.
SCR, GTO	None	Xu & Ki Avant&Lee Wong &Lin McMurray	All models have same dynamic deficiencies as DIODE and BJT models. Includes cond. Modulation.
IGBT	None	McDonnald&Fossom	Uses SPLICE (special SPICE)
BJT Darlington	2 BJT models	None	Model for integrated Darlington is needed

TABLE III. SIMULATOR COMPARISON FOR DEVICE MODELING

MODELING CAPABILITY	TYPICAL SIMULATORS		
	GENERIC SPICE	ENHANCED SPICE	SABER
1. Provides Two Levels of Accuracy			
Basic	YES	YES	YES
High Accuracy	?	YES	YES
2. High Voltage Device Phenomena			
Diode Recovery and Turn-ON	?	YES	YES
Quasi –Sat., Dynamic Sat. in BJTs	NO	?	YES
Wide Cgd Capacitance Swing in MOSFETs	?	YES	YES
Tail Currents in GTOs, IGBTs	?	YES	YES
3. Temperature Effects			
T as Independent Device Parameter	NO	NO	YES
T as function of Device Dissipation	NO	?	YES
T as Func. Of Heat Sink Dynamic Thermal Impedance	NO	?	YES
4. Power Ics and Control ICs	Subcircuit only	Behav. model	Behav. model

Of the inductor and transformer models developed for SPICE and SABER, only the Pei & Lauritzen and Meares models listed in Table IV will work with ordinary versions of SPICE. They both simulate saturation well, but not the variation of hysteresis or losses with frequency. These models are based on empirical curve fitting. Teegardin has recently implemented a physical model, the Jiles-Atherton model on SABER. However, the Jiles-Atherton equations are probably too complex for simulation on SPICE

TABLE IV. MAGNETIC DEVICE MODELS FOR SPICE AND SABER

AUTHOR	FEATURES	COMMENTS
Pei & Lauritzen	Saturation and hysteresis simulated by non-linear controlled sources on SPICE	Good for constant freq. excitation
Mears	Saturation and hysteresis simulated by diodes and voltage sources on SPICE	Complex sub circuit;
Tabrizi[]	Closed model, Insufficient information to evaluate	Works on Analog Workbench SPICE only

Models available in a public domain:
http://www.orcadpcb.com/PSPICE/models.

V. CONCLUSIONS

Although the analog circuit simulators currently available such as SPICE or SABER contain elementary semiconductor and magnetic device models, these models fail to simulate important power (high voltage) device phenomena. Thus, many power device types such as thyristors or IGBTs are omitted from these model libraries. New device types and combination devices such as Darlingtons also need to be included.

The new simulator SABER offers a number of special features for modeling of power devices from their fundamental equations. However, some enhanced versions of SPICE also allow direct insertion of the special device equations for modeling.

However, building good models is not simple. The efforts to create models for power devices have just begun.

In the paper we give the current and future trends in the development and improvements of some most widely spread simulators. A comparison of the three most useful simulators for PES – MATLAB/SIMULINK, SABER and PSPICE is given. The specific features and advantages of each of the discussed simulators are given. Thus, the designer can benefit reading the results of that comparison and to make the right choice of the most appropriate simulator.

REFERENCES

[1] Lauritzen P. O, Subramamanin Y, Bi Y, Green L. "An Efficient Way to Implement Electrical and Thermal Device Models in MAST", North American ASSURE Meeting, March 1997

[2] Batarseh, I.; Kemnitz, D.A**,** " Undergraduate education in power electronics"-Southcon/94. Conference Record , 29-31 March 1994

[3] Paul W. Tuinenga- "SPICE- AGuide to Circuit Simulation & Analysis using PSPICE.

[4] SABER, Analogy,Inc., P.O. Box 1669, Beaverton OR 97075

Temperature sweep modeling of the electronic elements in medium and deep vacuum conditions

Dr. Eng. Ivan Evstatiev[1], Dr. Eng. Dimitar Dimitrov[2]

Abstract **- The description of heat exchange of the electronic elements in medium and deep vacuum conditions is a priority based on the radiant heat exchange.**
The approximating hypotheses for building the model are stated (grounded) in the publication. Special attention is put on the relations describing the radiant heat exchange. Considered are the basic connecting relations used in the publication.
Synthesized a logarithmic model by developing algorithm describing the relations of the basic physical dependencies. The modeling is based on the final differences' method. Given is a graphic interpretation of modeling process.

Key words: **mathematical model, electronic elements, vacuum.**

The work of the electronic devices in the medium and deep vacuum conditions is typical for rocket and military industry. The temperature regime of the electronic devices in these conditions is basic circumstance for their standard (normal) exploitation.
The task of this publication is modeling of the temperature regime of the electronic elements, set as a electronic module, situated in a closed area in medium and in deep vacuum.
Hypothesis and basic thermodynamic dependencies.
The work of the electronic module situated in a closed area in vacuum presumes that the basic heat exchange is radiant. Transfer of energy through heat emitting and heat conductance are ignored.
Starting conditions are: temperatures of the electronic module and the surface of the closed area are equal. Besides this the temperature of the closed area is constant.
The electronic product is considered as a printed circuit board average specific heat capacity and specific area.
The electric energy consumed by the module is being transferred into heat. It is well known that for a period of time $\Delta\tau$, S, the liberated energy over the model is:

(1) $W_{EL} = U.I.\Delta\tau$, J,

where U is the voltage of the source, V;
I – current, consumed by the module, A.

The change in the temperature of the electronic module for the period of time $\Delta\tau$, S, is calculated on the basis of the following calorimetric equation [1, 3]

(2) $Q = m_{EL}.c_{EL}.(t_2 - t_1)$, J,

where m_{EL} is the mass of the electronic module, kg;

c_{EL} – average specific heat capacity of the electronic module, $J.kg^{-1}.K^{-1}$;

t_1, t_2 – temperatures respectfully in the beginning and after the energy reception, ^0C.

The radiant energy exchange is calculated with the following subjection [1]:

(3)

$$Q = \Delta\tau.\varepsilon_P.c_0.F_{EL}.\left[\left(\frac{273{,}16 + t_{EL}}{100}\right)^4 - \left(\frac{273{,}16 + t_{PR}}{100}\right)^4\right]$$

, J,

where ε_P is the given rate of black. It is defined regarding [1].

(4) $$\varepsilon_P = \frac{1}{\frac{1}{\varepsilon_{EL}} + \frac{F_{EL}}{F_{PR}}\left(\frac{1}{\varepsilon_{PR}} - 1\right)},$$

where

ε_{EL} and ε_{PR} are respectively the rates of black of the electronic module and the wall of the closed area;

F_{EL} and F_{PR} - respectively the areas of the surfaces of the electronic module and closed area, m^2;

c_0 - coefficient of the radiation of the absolute black body, $c_0 = 5{,}67$, $W.m^{-2}.K^{-4}$;

t_{EL} and t_{PR} - respectively temperatures of the surfaces of the electronic module and closed area, ^0C.

PROCESS MODELING

An algorithm is established on the basis of the upraised hypothesis, the basic thermodynamic dependencies and the energy balance, describing the change in the temperature regime of the electronic module (Fig. 1).
In block 1 are given the basic conditions. Blocks 2 and 6 do organize the time change. The energy changes are calculated in block 3, 4 and 5.

[1] Ivan Evstatiev, University of Russe "Angel Kanchev", Faculty of Electro technique, Electronics and Automatics. e-mail: ievstatiev@ecs.ru.acad.bg address: Bulgaria, Russe 7017, ul. "Studentska" 8.
[2] Dimitar Dimitrov, Technical University – Sofia, Faculty of Coommunications and Communication Technologies, e-mail: ddim@tu-sofia.bg address: Bulgaria, Sofia 1000, bul. Kliment Ohridski 8.

RESULTS

Described are approximating hypothesis and basic thermodynamic dependencies, modeling energy processes in vacuum conditions.

Mathematic-algorithmic model is synthesized, simulating the change of the temperature in a time function of the electronic module working in vacuum conditions.

CONCLUSIONS

The given model is appropriate for examination of the temperature regime of the electronic devices working in rocket and military industry.

LITERATURE

1. Velev, D. Technical thermodynamic and heat exchange. Technics, Sofia, 1984.

2. Stamov, S. Manual on heating, ventilation and climate conditioning. Part I. Basis of heating and ventilation. Technics, Sofia, 1990.

3. Holman, P. Jack, John R. Llpoyd. Fundamentals of Engineering Thermodynamics. International Editions, 1992.

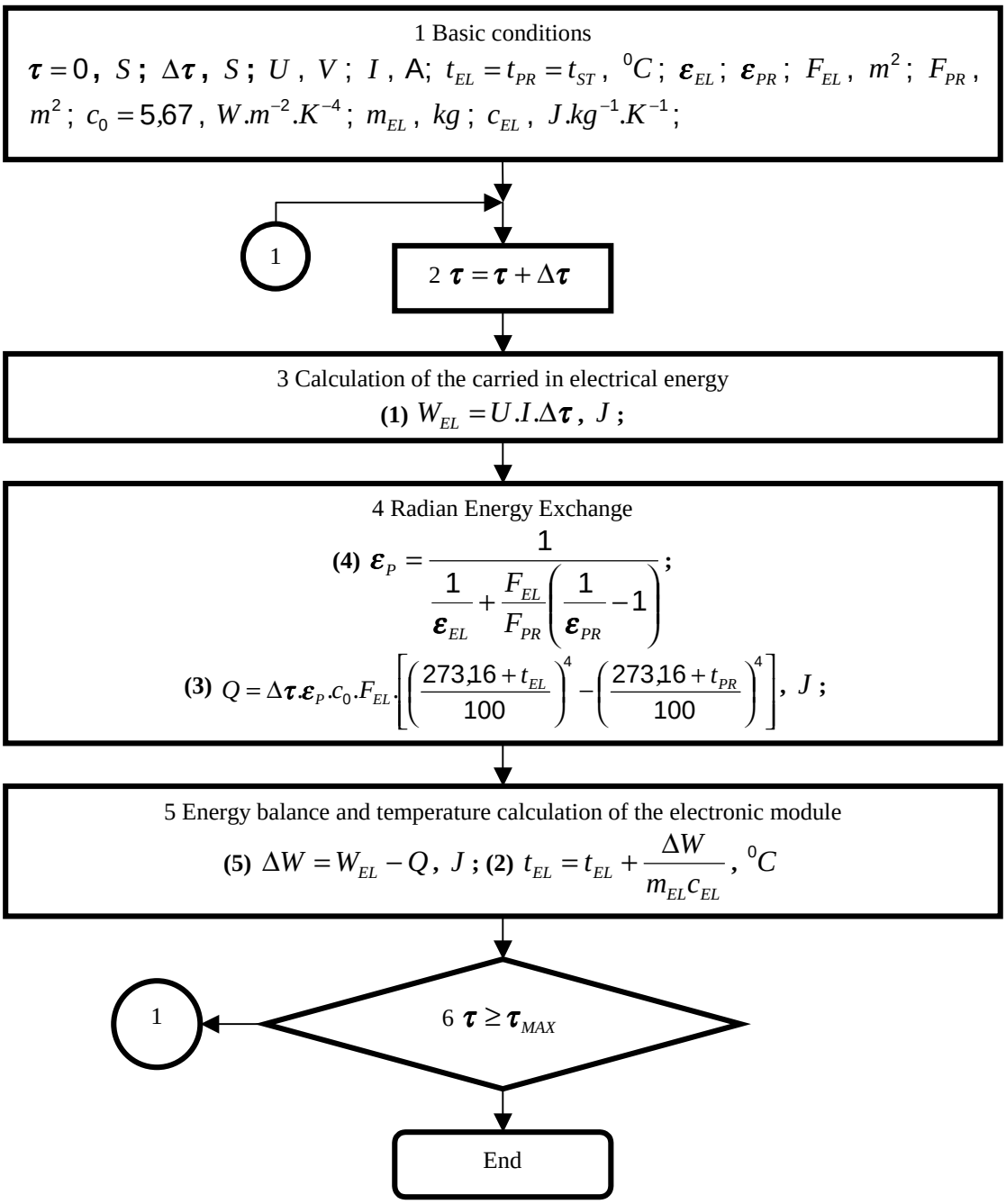

Fig. 1. Algorithm of the temperature regime of an electronic module working in vacuum conditions

Voltage Controlled Active Delay Element

Goran S. Jovanović[1] and Mile K. Stojčev[2]

***Abstract* – Variable delay elements are often used in different types of high-speed integrated circuits mainly intended for delay compensation, skew equalization, etc. These circuits are realized as hybrid, composed of digital and analog controlled parts. Digital part is used for coarse-grain while the analog for fine-grain delay variation. In this paper is propose a new analog delay element architecture and develop analytical equation for the delay of the circuit. The proposed circuit has linear transfer function, delay in term of control voltage in a full range of regulation.**

***Keyword* – Delay, CMOS circuit design, programmable delay element, current starved delay element.**

I. INTRODUCTION

Variable active delay elements have numerous applications in semiconductor VLSI IC's technology. Typically in meet them, as constituents, in Delay Locked Loops (DLL) [1-9], time-to-digital converters (TDC) [6], frequency multipliers [8], poly-phase clock generators [2], etc.

Active delay elements can broadly classified as digital or voltage controlled. Digitally controlled delay elements are usually realized as series of elements of variable length. The number of elements determines the amount of the delay. These kinds of delay elements are suitable for coarse-grain delay variation in a wide range of regulation. Analog voltage controlled delay elements are usually realized using shunt capacitor [1,3,5] or current starved delay elements [1-3,6-7]. Shunt capacitor delay element is capacitive loaded inverter, where a transistor, connected as a linear resistor, defines the charging and discharging current of the load capacitor. This type of delay element has the following disadvantages: a) the output capacitor occupies large silicon area; b) delay value and regulation range is small. Current starved delay elements are implemented with current supplied inverters. Varying the charging and discharging currents of the output parasitic capacitor we can control the propagation delay of these elements. Analog delay elements are suitable for fine-grain delay variation in limited range of regulation. Therefore, a combination of analog and digital delay elements, called hybrid, is used in many applications as an optimal solution [4,7].

Within the range of regulation, digitally controlled delay elements are linear, i.e. each delay element involves equal delay. Contrary to this, analog delay elements are non-linear, i.e. delay variation in terms of control voltage is non-linear function [1]. This means that for identical voltage increment constant delay difference, in a full range of voltage variation, is hardly to achieve.

Having this in mind, in this paper we focus our attention towards realization of linear hybrid delay line in a full range of voltage regulation. In our proposal, as digital controlled delay element we adopt the solution described in [7]. So, in the next all our efforts will be directed towards realization of linear voltage controlled analog delay element. The proposed solution is based on modification of the current starved delay elements. Improved linearity is achieved by involving symmetric load circuits. Simulation results which relate to 1.2 μm CMOS double-poly double-metal technology show that the proposed delay element has linear transfer function, delay in term of control voltage, in the full range of voltage regulation.

This paper is organized as follows: In Section II, we briefly explain the standard realization of the current starved delay element. In Section III, the proposed version of the modified current starved delay element is presented. Also, a detailed analysis of the modified circuit, which includes: results of simulation; testing linearity of the delay element and an analytical model of the propagation delay. Finally, Conclusion is presented in Section IV.

II. CURRENT STARVED DELAY ELEMENT – STANDARD REALIZATION

In order to explain our proposal, concerning modification of the current starved delay element, in the sequel, we will first briefly explain its standard realization [1], given in Fig. 1.

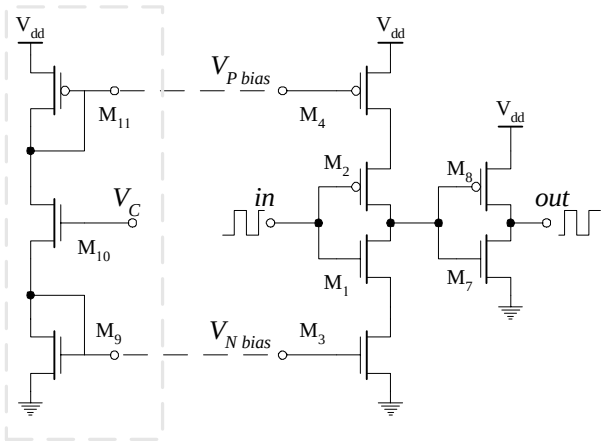

Fig. 1. Current starved delay element

[1] Goran S. Jovanović is with the Faculty of Electronic Engineering, Beogradska 14, 18000 Niš, Serbia and Montenegro, E–mail: joga@elfak.ni.ac.yu

[2] Mile K. Stojčev is with the Faculty of Electronic Engineering, Beogradska 14, 18000 Niš, Serbia and Montenegro, E–mail: stojcev@elfak.ni.ac.yu

As can be seeing from Fig. 1, the voltage controlled delay cell is implemented as a two–stage inverter. Transistors M_1 and M_2 are constituents of the first stage, while transistors M_7 and M_8 form the second stage. Transistors M_3 and M_4 act as current sink and source, respectively. Currents of transistors M_3 and M_4 represent discharging and charging currents of the output parasite capacitance, during rising and falling edge of the pulse, respectively. Voltages V_{Pbias} and V_{Nbias} regulate currents of M_3 and M_4, respectively. The bias circuit, composed of transistors M_9, M_{10} and M_{11}, provides correct polarization for transistor M_3 and M_4. The second inverter composed of transistors M_7 and M_8 involves some small constant delay. Also, second inverter improves rising and falling edge of the clock pulse at the output of delay element. It increases the slope of the rising and falling edges of the output pulse, too.

In Fig. 2, the propagation delay of the starved delay element (from Fig. 1.) in term of control voltage V_c is given. This curve is obtained using Spice simulation for transistor models of 1.2 μm CMOS technology, at supply voltage V_{dd}=5V. As can be seen from Fig. 2, the range of delay variation is large but nonlinear, and is analytically defined as [7]:

$$t_p = \frac{C_L \cdot V_{dd}}{K_p (V_C - V_t)^2} \qquad (1)$$

where: C_L - output load capacitance; V_{dd} – supply voltage; K_p – technology parameter $\mu C_{ox}(W/L)$; V_t - threshold voltage; and V_C - control voltage.

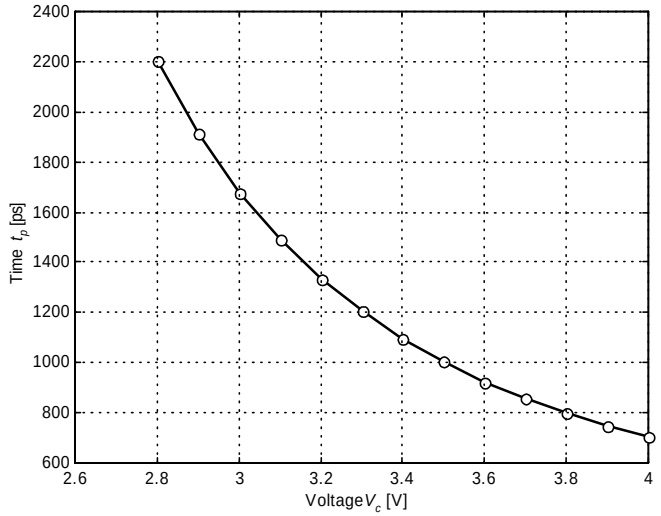

Fig. 2. Propagation delay t_p in term of control voltage V_c

III. CURRENT STARVED DELAY ELEMENT WITH SYMMETRIC LOAD

The modified version of the current starved delay element is pictured in Fig. 3. In parallel with transistors M_3 and M_4, symmetric load circuits, transistors M_5 and M_6, are added. By involving symmetric load circuits we provide a condition that transistors M_3, M_4, M_5 and M_6 operate in saturation mode. Also, the charging and discharging currents of parasitic capacitor C_L, are increased. This modification results to shorter propagation delay in respect to standard current starved delay element (Fig. 1.).

In order to derive an analytical model of the signal propagation delay trough the delay element we will use schematic given in Fig. 4. Here we assume that transistors M_1 and M_2 (Fig. 3.) are ideal switches, M_3 and M_5 act as current sinks, and M_4 and M_6 as current sources.

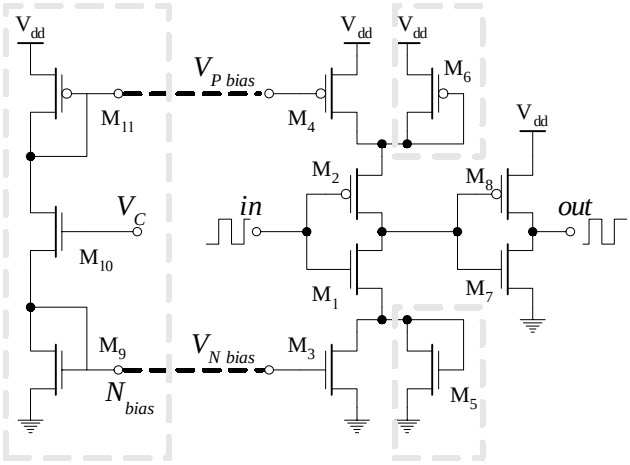

Fig. 3. Current starved delay element with symmetric load

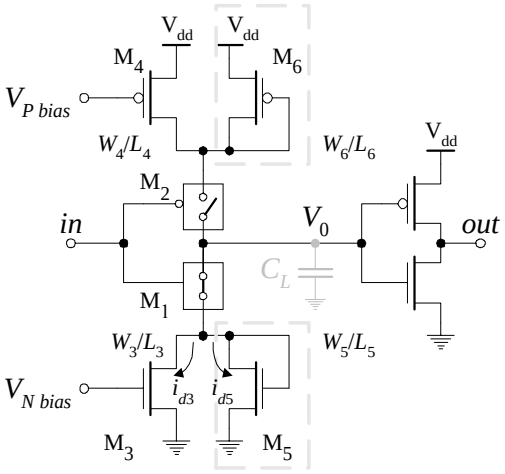

Fig. 4. Simplified scheme of the current starved delay element with symmetric load

If at the input *in* rising pulse edge is present, transistor M_1 act as closed switch. The parasitic capacitor C_L, at the output of first inverter stage, discharges from V_{dd} to 0V. The capacitor discharging current consists of i_{d3} and i_{d5}, and the following is valid:

$$-C_L \frac{dV_0}{dt} = i_{d3} + i_{d5} \qquad (2)$$

where i_{d3} i i_{d5} a currents of transistors M_3 and M_5 respectively. Both transistors M_3 and M_5 operate in saturation mode, so that the following is valid:

$$-C_L\frac{dV_0}{dt}=\frac{k_n}{2}\frac{W_3}{L_3}(V_g-V_t)^2+\frac{k_n}{2}\frac{W_5}{L_5}(V_0-V_t)^2 \\ =k_1(V_g-V_t)^2+k_2(V_0-V_t)^2 \quad (3)$$

Eq. (3) can be simplified by involving following substitutions: $k_1=(k_n/2)(W_3/L_3)$ and $k_2=(k_n/2)(W_5/L_5)$. By solving the differential eq. (3) on obtain

$$\int\frac{d(V_0-V_t)}{\frac{k_1}{k_2}(V_g-V_t)^2+(V_0-V_t)^2}=-\frac{1}{\tau}\int dt \quad (4)$$

where $\tau=C_L/k_2$. For initial values t=0 and $V_0=V_{dd}$, Eq. (4) has the following solution:

$$t=\frac{\tau}{\sqrt{\frac{k_1}{k_2}}(V_g-V_t)}\left[\arctan\frac{V_{dd}-V_t}{\sqrt{\frac{k_1}{k_2}}(V_g-V_t)}-\arctan\frac{V_0-V_t}{\sqrt{\frac{k_1}{k_2}}(V_g-V_t)}\right] \quad (5)$$

Using the well know trigonometric transformation

$$\arctan u+\arctan v=\arctan\frac{u+v}{1-uv} \quad (6)$$

we obtain following form

$$t=\frac{\tau}{\sqrt{\frac{k_1}{k_2}}(V_g-V_t)}\arctan\frac{(V_{dd}-V_0)\sqrt{\frac{k_1}{k_2}}(V_g-V_t)}{\frac{k_1}{k_2}(V_g-V_t)^2+(V_0-V_t)(V_{dd}-V_t)} \quad (7)$$

The propagation delay of the first inverter t_{p1} is derived when the logical threshold voltage is $V_0=V_{dd}/2$, and is equal to:

$$t_{p1}=\frac{\tau}{\sqrt{\frac{k_1}{k_2}}(V_g-V_t)}\cdot\arctan\frac{\frac{V_{dd}}{2}\cdot\sqrt{\frac{k_1}{k_2}}(V_g-V_t)}{\frac{k_1}{k_2}(V_g-V_t)^2+\left(\frac{V_{dd}}{2}-V_t\right)\cdot(V_{dd}-V_t)} \quad (8)$$

where: k_1 and k_2 are constants determined by technology parameters and transistor geometry; V_g - corresponds to gate to source voltage of transistors M_3 and M_4; V_t – threshold voltage; V_{dd} – voltage supply.

The total delay time is obtained as a sum of the propagation delays, that correspond to both inverters, i.e. $t_p=t_{p1}+t_{p2}$. Propagation delay time of the first inverter t_{p1} depend of gate to source transistors voltage V_g, and is given by Eq. (8). Time delay of the second inverter is independent of V_g and is defined by [10]:

$$t_{p2}=\frac{C_L}{K_p(V_{dd}-V_t)}\left\{\ln\left[4\left(\frac{V_{dd}-V_t}{V_{dd}}\right)-1\right]+\frac{1}{2}\right\} \quad (9)$$

where: C_L - output load capacitance; V_{dd} – supply voltage; K_p – technology parameter $\mu C_{ox}(W/L)$ and V_t - threshold voltage.

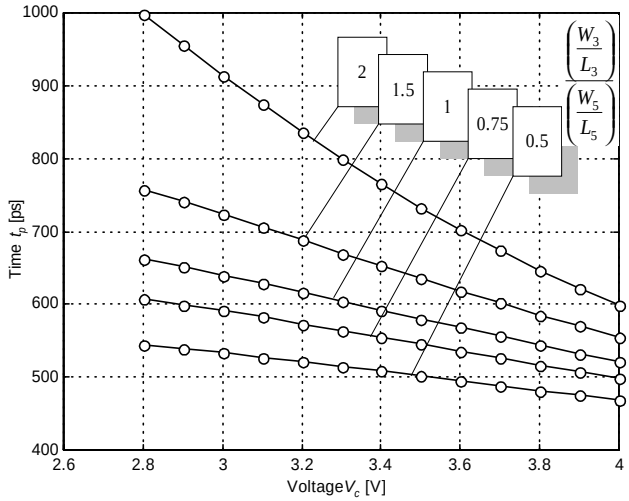

Fig. 5. Time delay in term of control voltage for current starved delay element with symmetric load

In Fig. 5, simulation results for the proposed circuit are given. For Spice simulation transistor models for 1.2 μm CMOS technology and supply voltage V_{dd}=5V are used. Sketched curves relate to different ratios $(W_3/L_3)/(W_5/L_5)$ and $(W_4/L_4)/(W_6/L_6)$. Where W_3, W_4, W_5 and W_6, and L_3, L_4, L_5 and L_6 correspond to channel width and length of transistors M_3, M_4, M_5 and M_6 respectively. As can be seen from Fig. 4, the range of delay regulation, in respect to standard current starved delay element (Fig. 2.) is decreased, but the linearity is drastically improved. According to the Fig. 4, one can conclude that for greater ratio $(W_3/L_3)/(W_5/L_5)$ and $(W_4/L_4)/(W_6/L_6)$ we obtain greater range of delay regulation. This means that if dimensions of transistors M_3 (M_4) are greater then that of M_5 (M_6) the range of delay regulation increases, in contrary it decreases.

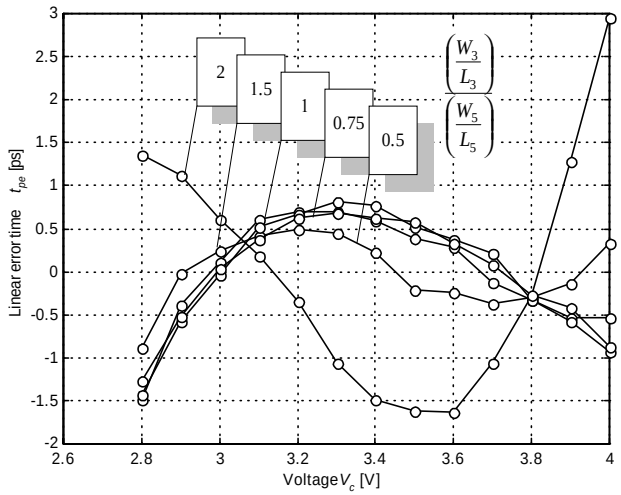

Fig. 6. Delay linearity errors in term of control voltage for different ratios $(W_3/L_3)/(W_5/L_5)$ and $(W_4/L_4)/(W_6/L_6)$ as parameters

In Fig. 6, linearity errors of the modified circuit (Fig. 3.) for different ratios of $(W_3/L_3)/(W_5/L_5)$ and $(W_4/L_4)/(W_6/L_6)$ are given. In general, in worst case errors are small (<1%) and depend of the ratio $(W_3/L_3)/(W_5/L_5)$ and $(W_4/L_4)/(W_6/L_6)$.

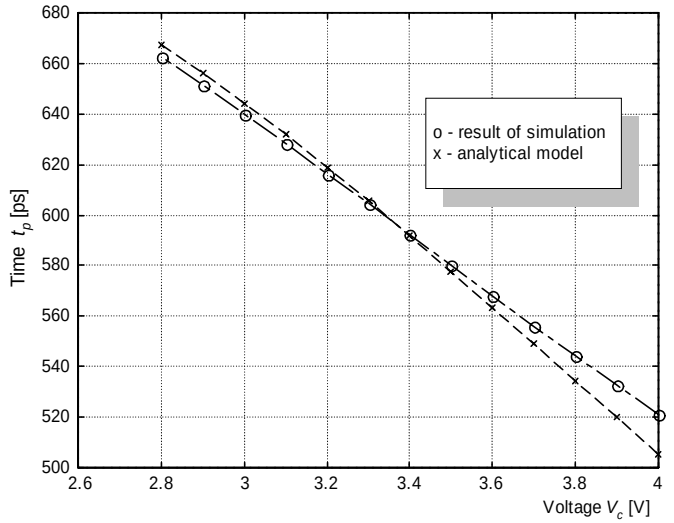

Fig. 7. Results of simulation and analytical model for time delay in term of control voltage

In Fig. 7, result of simulation and derived analytical model, Eq. (8), for fixed ratios $(W_3/L_3)/(W_5/L_5)=1$ and $(W_4/L_4)/(W_6/L_6)=1$, i.e. $k_1/k_2=1$, are given. As can be seen from Fig. 7, good agreement (<5%) between the analytical model and result of simulation exists.

IV. CONCLUSION

In this paper we propose new architecture for an analog voltage controlled delay element. This circuit represents a modified version of the current starved delay element with symmetric load. Analytical model of propagation delay is derived. The circuit is implemented in CMOS 1.2 μm double-poly double-metal technology. The obtained simulation results show that the circuit has linear transfer function, delay in term of control voltage in a full range of regulation. Delay linearity error is less then 1%. Agreement between analytical model and simulation results is good, i.e. the error is less then 5%.

REFERENCES

[1] Mark Johnson, Edwin Hudson, "A Variable Delay Line PLL for CPU-Coprocessor Synchronization", IEEE Journal of Solid-State Circuits, vol. 23, No. 5, pp. 1218-1223, October 1988.

[2] Yongsam Moon, Jongsang Choi, Kyeongho Lee, Deog-Kyoon Jeong and Min-Kyu Kim, "An All-Analog Multiphase Delay-Locked Loop Using a Replica Delay Line for Wide-Range Operation and Low-Jitter Performance", IEEE Journal of Solid-State Circuits, vol. 35, No. 3, pp. 377-384, March 2000.

[3] Mohammad Maymandi-Nejad Manoj Sachdev, "A digitally Programmable Delay Element: Design and Analysis", IEEE Transactions on Very Large Scale Integration (VLSI) Systems, vol. 11, No. 5, October 2003.

[4] Stefanos Sidiropoulos, Mark Horowitz, "A Semidigital Dual Delay-Locked Loop", IEEE Journal of Solid-State Circuits, vol. 32, No. 11, pp. 1683-1692, November 1997.

[5] Feng Lin, Jason Miller, Aaron Schoenfeld, Manny Ma, and R. Jacob Baker, "A Register-Controlled Symmetrical DLL for Double-Data-Rate DRAM", IEEE Journal of Solid-State Circuits, vol. 34, No. 4, pp.565-568, April 1999.

[6] Piotr Dudek, Stanislaw Szczepanski, John V. Hatfield, "A High-Resolution CMOS Time-to-Digital Converter Utilizing a Vernier Delay Line", IEEE Journal of Solid-State Circuits, vol. 35, No. 2, pp. 240-247, February 2000.

[7] Yeon-Jae Jung, Seung-Wook Lee, Daeyun Shim, Wonchan Kim, Changhyun Kim, Soo-In Cho, "A Dual-Loop Delay-Locked Loop Using Multiple Voltage-Controlled Delay Lines", IEEE Journal of Solid-State Circuits, vol. 36, no. 5, pp. 784-791, May 2001.

[8] Chain G., *Low-Noise Design Techniques using a DLL- based Frequency Multiplier for Wireless Application*, Ph. Thesis, University of California, Berkeley, 2000.

[9] John G. Maneatis, "Low-Jitter Process-Independent DLL and PLL Based on Self-Biased Techniques", IEEE Journal of Solid-State Circuits, vol. 31, No. 11, pp. 1723-1732, November 1996.

[10] Richard C. Jaeger, *Micro electronic Circuit Design*, International Edition, McGraw-Hill, 1996.

Quick designing methods for power current inverters with electrotechnology application

*Assoc. prof. PhD. Rumen D.Karov[1], eng. Radoslav I. Trendafilov[2],

Abstract. **Comfortable equations are derived from this work, because of the starting conditions' optimization in the parallel current inverter curcuit, and they are used for different current inverter designing (series-parallel, parallel-series), which have electrotechnology application.**

Unificated methods are obtained for a variety of different curcuits, based on the parallel and series substitution inverter curcuit.

Formula unification and optimization give possibility for quick current power inverter designing with electrotechnology application. The given examples and simulations show the design methods' application ability.

Keywords: **Current inverter, analysis, simulation**

Introduction

Quick method for power current inverters calculation with electrotechnology application is shown in the paper and method comparison is made to the simulation data. The result of the comparison helps to method accuracy evaluation having in mind the simple methodology. Because of the equations complexity, describing the current inverter processes, some assumptions for close to real regimes are made, which are optimal towards maximal voltage, commutation conditions, defasing angle β between output current and output voltage. The paper includes practical equations, results and example calculations at active-inductance load work, characterized with small $\cos\varphi_т$ in electrotechnology applications (as induction metal melting).

Analysis

A coefficients choice for current inverter analysis is recommended [2] by the well know methodologies, which puts indeterminacy in the calculations and slows the procedure.

*TU - Sofia, branch Plovdiv, Electrotechniques and Electronics, tel. 032/659713, e-mail: [1]r_karov@mail.bg, [2]radoslav_t@abv.bg

Because of the made workouts for current equation [1,3] of

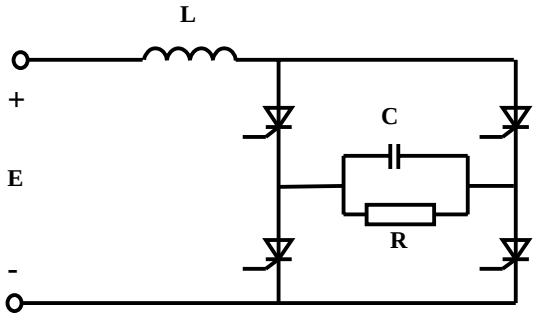

Fig.1

parallel inverter (fig.1), we have:

$$i(t)=\frac{E}{R}+\left(\frac{E+U_{C0}}{\omega L}-\frac{\delta}{\omega}.\frac{E}{R}+\frac{\delta}{\omega}.I(0)\right)e^{-\delta t}\sin\omega t+ \\ +\left(I(0)-\frac{E}{R}\right)e^{-\delta t}\cos\omega t \quad (1)$$

Parallel current inverter modeling methodology is based on the conduction:

$$I(0)=\frac{E}{R} \quad (2)$$

If we substitute $I(0)=\frac{E}{R}$ (2) into current equation i(t) (1), which is obtained for close to optimal regimes, angle $\beta\approx30^0$ and limit regime, where:

$$\sqrt{\frac{L}{C}}=2R \quad (3)$$

then for current in (1) we have:

$$i(t)=\frac{E}{R}\left(1+e^{-\delta t}\sin\omega t\right) \quad (4)$$

For maximal thyristor voltages and power supply voltage, following equations are obtained:

$$E=\frac{U_{изх}}{\sqrt{1.64\eta}},\ U_m=\sqrt{2}U_{изх} \quad (5)$$

The output current phase shifting to voltage and thyristor recovery time can be determined from:

$$\beta=\arccos\frac{\pi}{2\sqrt{2}\sqrt{1.64\eta}},\ t_q=\frac{\beta}{\omega} \quad (6)$$

The equivalent active resistance value in respect to inverter output and currents offer processing is:

$$R = \frac{U_{изх}^2}{P_{изх}},\ I_0 = \frac{1.64E}{\eta R} \text{ and } I_{AV} = \frac{I_0}{2} \quad (7)$$

The connection between equivalent and active load resistance is:

$$R_T = R\cos^2\varphi_T \quad (8)$$

For load inductance we have:

$$L_T = \frac{R_T tg\varphi_T}{\omega} \quad (9)$$

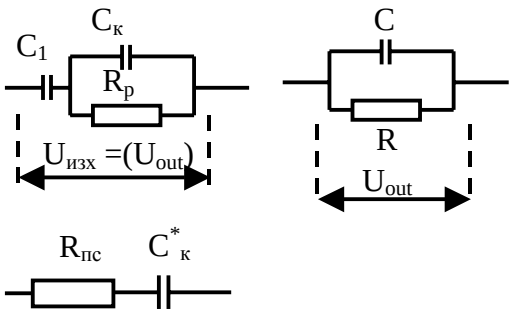

Fig.2

When the output circuit is substituted by series equivalent circuit (fig. 2), the active resistance value is:

$$R_{пс} = R\cos^2\beta \quad (10)$$

Minimal required input inductance and parallel capacity values are:

$$L = 4R^2C \quad (11)$$

$$C_T = \frac{L_T}{RR_T} \quad (12)$$

The same theoretical base can be used for series – parallel current inverter the necessary circuit processing (fig.2).

The parallel capacitor is divided into two components – inductive character compensating one ($C_т$) and compensating one ($C_к$).

The series parallel inverter circuit is shown on fig.3 and its elements can be expressed simply by the substituting circuit as it is shown on fig.2.

As (1) is used and assumption (2), is made, which is applicable for the case, for necessary supplying voltage we have (5).

Thyristor recovery time by the use of β is (6).

Output inverter active resistance and current are (7).

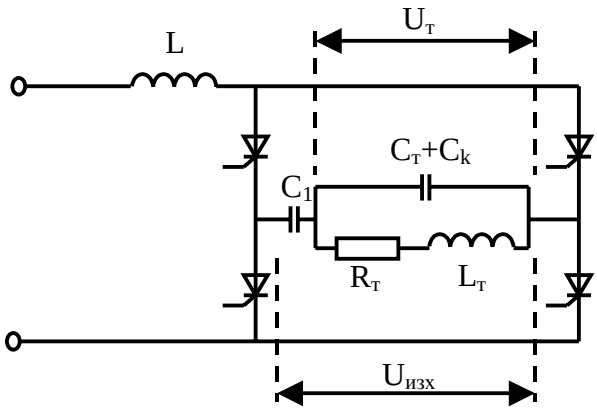

Fig.3

R_p value (fig.2) is:

$$R_p = \frac{U_т^2}{P_{изх}} \quad (13)$$

$U_{изх}$ and $U_т$ ratio is determined by angles γ and β:

$$\frac{U_{изх}}{U_т} = \sqrt{\frac{R}{R_p}} = \frac{\cos\gamma}{\cos\beta},\ \cos\gamma = \frac{U_{изх}}{U_т}\cos\beta \quad (14)$$

As output circuit processing is used, capacitor values can be determined by equations after equivalent capacity towards inverter output is calculated:

$$\omega CR = tg\beta,\ C = \frac{tg\beta}{\omega R} \quad (15)$$

The necessary commutating capacitor, giving enough recovery time is:

$$\omega C_k R_p = tg\gamma,\ C_k = \frac{tg\gamma}{\omega R_p},\ C = \frac{tg\beta}{\omega R} \quad (16)$$

Then for series capacitor we have:

$$C_1 = \frac{1}{\frac{1}{C}\sin^2\beta - \frac{1}{C_k}\sin^2\gamma} \quad (17)$$

and active load component:

$$R_т = R_p\cos^2\varphi_т \quad (18)$$

Here – similar to parallel inverter, when output circuit is substituted by series equivalent circuit, active resistance and load inductance values are:

$$R_{пс} = R_p\cos^2\gamma = R\cos^2\beta,\ L_т = \frac{R_т tg\varphi_т}{\omega} \quad (19)$$

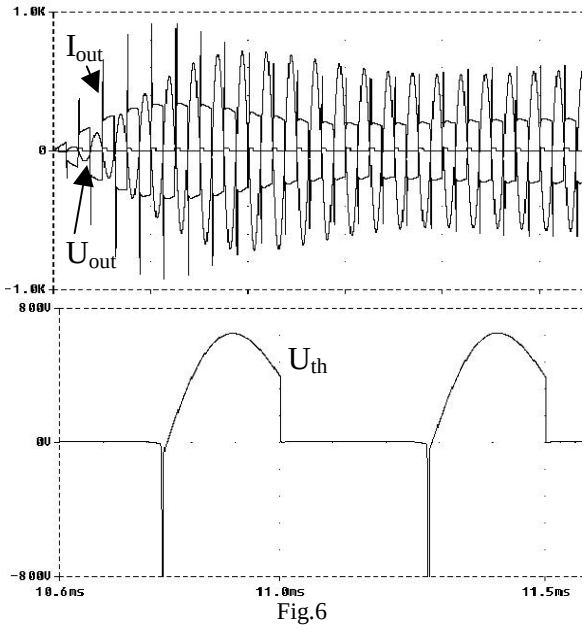

Fig.6

Minimal input inductance is (11), but necessary input inductance reactor is:

$$L = \frac{R_{пс}}{R_T} L_T \qquad (20)$$

Compensating load inductance component is:

$$C_T = \frac{L_T}{R_p R_T} \qquad (21)$$

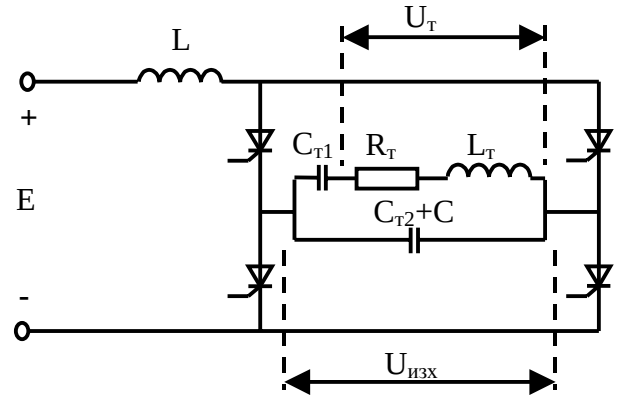

Fig.4

For parallel-series current inverter (fig.4) modeling also begins with the help of (5), (6), (7) and $U_{изх}/U_т$ ratio is determined by angles φ_e and $\varphi_т$:

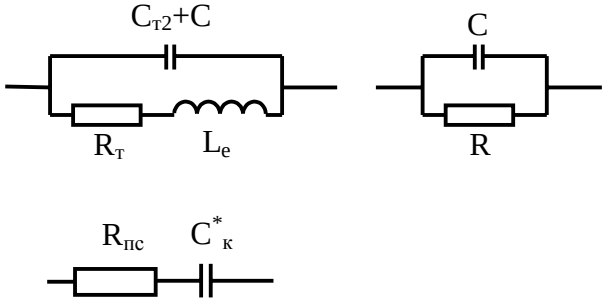

Fig.5

$$\frac{U_T}{U_{изх}} = \frac{\cos\varphi_e}{\cos\varphi_T},\ \cos\varphi_e = \frac{U_T}{U_{изх}}\cos\varphi_T,\ R_T = R\cos^2\varphi_e,$$

$$L_T = \frac{R_T \operatorname{tg}\varphi_T}{\omega} \qquad (22)$$

from where equivalent inductance L_e (fig.5), $C_{т1}$ and $C_{т2}$ are determined.

$$L_e = \frac{R_T}{\omega}\operatorname{tg}\varphi_e,\ C_{T1} = \frac{1}{\omega^2(L_T - L_e)},\ C_{T2} = \frac{L_e}{RR_T} \qquad (23)$$

C and L values are determined from (15) and (20).

Calculations and simulation results.

Calculations and simulation of series-parallel current inverter for electrotechnology application are made according to the following output data: cosφ=0,1; $U_{изх}$=500V; f=2kHz; η=0,95; $U_т$=450V. Data comparison is made on Table 1.

Table 1. Results

	E	$U_{th\,max}$	I_0	t_q	β	γ
Calculated values	400V	700V	250A	38μS	27°	9°
Simulation values	400V	650V	230A	33μS	24°	7°

	C_1	$C_т+C_k$	$R_т$	$L_т$	L
Calculated values	93μF	376μF	0,02Ω	15μH	1,48mH
Simulation values	100μF	400μF	0,02Ω	15μH	1,5mH

Inverter curcuit simulation graphics is shown on fig.6.

Conclusions: By the use of the shown calculations a current inverter for electroechnology applications can be modeled with quick methodology at different ratio of inverter circuit and input inductance parameters. Used switching elements type can also be determined the base of maximal work current and voltage.

References:

[1] Karov R. – Comparison for the condition of resonance and aperiodical regime for series and parallel current inverter, Conf. “Electronics 2003” Sozopol, Bulgaria.

[2] Hinov N., M. Bobcheva, N. Gradinarov – Methodology for series-parallel current inverter research, “Electrotechniques and Electronics”, 3-4, 2000, Bulgaria.

[3] Chudnovsky V., B. Axelord, A. Shenkam “An approximate analysis of a starting process of current source parallel inverter with a high Q induction heating load “IEEE Transaction on Power Electronics”, vol.12 no.2 pp.294.305, 1997.

Condition identification system for rechargeable batteries

Hristo S. Kilifarev[1]

***Abstract* – In this paper are described the base characteristics of different types rechargeable batteries and some of functional possibilities of some real systems for their analysis. The base methods for defining of some important parameters of rechargeable batteries are shown. A general scheme of a device is presented which own the functional possibilities to make identification (analysis) of rechargeable batteries, to charge them and to make their service maintenance.**

***Key words* – rechargeable batteries analyzer, charge-discharge curves, characteristics of rechargeable batteries.**

I. INTRODUCTION

In the present moment in the life of the contemporary man there are many devices, which have rechargeable batteries like power source. Mostly these devices are comparatively with small sizes and they are movable. Typical applications are the cell phones and the mobile radio devices, the camcorders, the laptop computers and the measurement devices, many handheld electrical tools and etc. Usually in the devices of that kind there are comparatively little rechargeable batteries in size, with small amount of capacity and little number of cells.

Other group batteries are these, which are used in stationary devices or in different type of vehicular machines. These rechargeable batteries are with comparatively big size, large amount of capacity and are with big number of cells. Typical applications are in backup power sources and in the automobiles.

A common property of the all kinds of rechargeable batteries is that after some exploitation period their parameters become worse. And it is necessary then to replace the batteries with a new. If the battery is comparatively cheap, but there is need from often replaces, or the change with a new battery is big amount of expenses, or if the batteries are big number – this procedure is economical disadvantage. In these cases it is good to take care to prolong the exploitation period of rechargeable batteries. This can be done with appropriate maintenance and when needed – to recover (revive) the batteries with worse parameters.

There are many different kinds of rechargeable batteries according to the used chemistry, the mechanical characteristics, the production parameters and the environment where they are used. Because of these reasons there exist many different algorithms to charge / discharge the different kinds of rechargeable batteries – every one kind of rechargeable battery requires special mode to be charged /discharged. From essential interest are the algorithms which achieve the recharge procedure in shortest time periods, but which give guarantee for saving their parameters (or make them betters) for entire exploiting period.

Very often the reason rechargeable batteries to be destroyed are the charging devices, which are used.

In the market for electrical devices can be found chargers with a big variety - they are with very different parameters, with different principles to work and construction, and their price is different too. The biggest part of these chargers are cheap, they can support only one type of rechargeable battery and the way to do the charging is done mostly by use of one or two algorithms. A less part of the chargers in the market have some kind of protection circuits in their construction - in example protection circuit for the highest permissible temperature of the rechargeable batteries. For now in the very little part on the market there are chargers, which have abilities to make some 'intelligent' identification (analysis) for the current state of the rechargeable battery before and through the time of charging /discharging, and can adjust themselves according to the type of battery. The last described chargers have one disadvantage – they are comparative expensive devices and for that reason they are not appropriate for the mass user.

In this paper is propound a general solution for scheme of a state identification system for rechargeable batteries (in short a battery analyzer) and a charge device. The identification of rechargeable batteries is done in two stages. On the first stage the measurements and calculations of the all parameters, which can be obtained, are done. On the second stage in the base of firstly collected statistical data and the entered data by user, an appraisal is obtained for the current state of the rechargeable battery. The other functionality of this scheme to charge / discharge the batteries can be applied then, accordingly to obtained appraisal, to the measured / calculated parameters and the wishes of the user. A decision can be given by the device for the mode of work (normal charging, fast charging, discharging, maintenance, recover and etc.) and accordingly decision for the algorithms which will be used.

The same device can collect the statistical data used for the first stage – just the different types of rechargeable batteries and in different condition must to be analyzed and the data stored in the memory. This statistical data can be transferred to the device by the connection to a computer. The processing over the measured parameters by the device can be done with the computer in the same way.

II. DEFINITION OF THE BASE TERMS AND PARAMETERS FOR RECHARGEABLE BATTERYES

Cell – electro-chemical device, capable to deliver energy, which is a result from an internal chemical reaction to an external electrical circuit. The cell's general construction consists of two electrodes and a electrolyte between them. The

[1]Hristo S. Kilifarev is with Technical University – Gabrovo, 4 H. Dimitar str., 5300 Gabrovo, Bulgaria, E-mail: hri_100@abv.bg

negative pole is *cathode* and the positive pole – *anode*. The electrolyte is a substance, which ensures ion-exchange conductivity between the electrodes.

Battery – it is build by one or more cells which can be connected serially (to increase the voltage), in parallel (to increase the current) or in combination. Often part of the battery is a special circuit for protection from higher temperatures of the package, from higher charging / discharging currents, from discharging to the level of cut off voltage and other events.

Chemistry – in the construction of the rechargeable batteries different materials are used which give them the different characteristics. Most important are the materials of the used electrodes, which give the name of the batteries. In the present time mostly used chemistries are Lead-Acid (LA), Ni-Cd, Ni-MH and Li-Ion (Li-Polymer batteries was developed soon and because of this they are not considered in this paper).

C – the unit for measurement of the battery (or the cell) capacity, which is related with the amount of energy that the battery can store and deliver. This unit is presented as Ah or mAh and is the value of the current, which the battery can deliver for 1 hour - before the voltage drops to the point of cut off voltage. The charge and discharge currents are given as function of C. In example for battery with capacity 1000 mAh if the charging current is 100 mA, then the battery will be charged for 10 hours and this current may be presented as 1/10 C or C/10. For the same battery, if the current is 1C (or 1000 mA), then the battery will reach full charge for 1 hour.

Middle voltage – this is the nominal voltage over the cell and this is the measured voltage over the cell, when it is discharged to 50% from the maximal capacity.

Cut off voltage (end of life voltage) – this is the measured voltage over the cell in the end of operating cycle when discharging. Under this point this is so called zone of *deep discharge*. It is possible as a result to have inverse polarity over the weaker cells in the battery which can make nonreversible chemical reactions in these cells and therefore to drop down overall performance of the battery. The good side of deep discharge is that with some limits removes the memory effect (see below).

Top voltage – this is the maximal voltage over the cell in its operational cycle and corresponds to fully charged battery. When continuing the charge after this value this is called *overcharge* and leads to rising of the temperature, and also to destroying of electrodes, vaporizing of electrolyte and other damages.

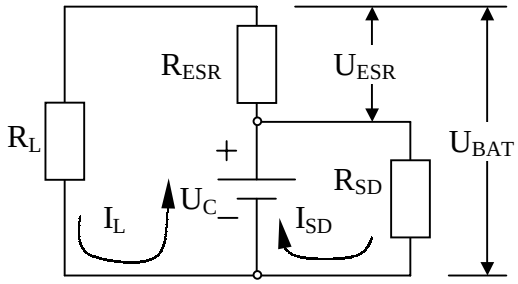

Fig.1. The equivalent scheme of a rechargeable battery

The voltage over the battery U_{BAT} is presented in Eq. (1) as:

$$U_{BAT} = I_L.R_L \quad (1)$$

But this voltage is equal to Eq. (2) too:

$$U_{BAT} = U_C - U_{ESR} \quad (2)$$

The drop of voltage over the equivalent serial resistance of the battery R_{ESR} is:

$$U_{ESR} = I_L.R_{ESR} \quad (3)$$

And the dissipation of the energy over R_{ESR} is:

$$P_{ESR} = I_L{}^2.R_{ESR} \quad (4)$$

From Eqs. (1), (2) and (3) can be obtained the next:

$$I_L.R_L = U_C - I_L.R_{ESR} \quad (5)$$

From where can be concluded that:

$$I_L.(R_L + R_{ESR}) = U_C \quad (6)$$

ESR (Equivalent Serial Resistance) – this resistance is the sum of the internal resistance of serial connected cells in the battery. This resistance appears to be serially connected to the resistance of the load (or the charging device), hence the current flow I_L is the same in the both. In the equivalent scheme in Fig. (1) this is presented as the resistor R_{ESR}. In consequence of this over this resistor appears the voltage drop U_{ESR} , which is proportional to values of I_L and R_{ESR} - Eq. (3). The energy dissipation then is in quadratic dependence from the value of the current flow, Eq. (4). When high amounts of dissipated energy P_{ESR} is reached, the battery temperature is rising and in some cases can result as ignition or explosion of the battery. The voltage drop over ESR is with inverse polarity in relation to the polarity of the battery U_C, which brings to lowering or to rising of the battery's voltage U_{BAT} respectively to rising of discharge current or rising of charge current. ESR depends from used chemistry, from the mechanical characteristics and form the age of the battery (see below for cycle life parameter).

In the Table I are shown typical values for ESR for the most widespread rechargeable batteries. Especially big influence over the battery's ESR has the temperature. When the temperature is lowered the ESR rising and over the high temperatures – ESR drops down.

Self discharge – this is a process of discharge, when there is not connected load. This is consequence from rising of the conductivity through the electrolyte. For Ni-based batteries this process is with the highest rate as can be seen in the Table I. This process is strongly nonlinear – batteries, which loose 30% of its capacity for one month, loose about 15-20% in the first 24 hours after the charging. The values in Table I are taken for 20ºC temperature. The rising with only 10ºC lead to doubling of self discharge rate. In the equivalent scheme from Fig. (1), the effect of self discharge is presented with the resistor R_{SD}.

Memory effect – this effect is typical for the rechargeable batteries with Ni-based chemistry (NiCd, NiMH). The cause for this effect is the lowering of effective surface of the electrodes when the crystalline structures of Ni compounds rising in size. The situations when this happened are after long time of inactivity or when the charge process is started before full discharge of the battery. The memory effect is reversible process with some limits through the *forming mode*. In the forming mode there have to be made up to 5 full cycles of charge – discharge. Other ways for repairing of the memory effect are the deep discharge and the charging in the mode with negative pulse (see below).

Cycle life – this value presents the number of charge-discharge cycles that can be completed and after which the performance of the battery drops so much so that the battery must to be replaced with a new one. Only the parameters of Li-Ion batteries do not depend from the number of charge-discharge cycles. The life of one such battery is about 1-3 years and depends from manufacturer and the way of usage. The influence of the cycle life over the batteries is related to dry out of the electrolyte (from leaks or from vaporizing), lowering of effective surface of the electrodes (destroying, oxidation, memory effect and etc.), mechanical changes (destroying of the separator, changes in the form of electrodes and etc.) and other defects. These defects are evince for the age of battery and can be revealed mostly as lowering of the maximal capacity, rising of ESR and curtail of time period for self discharge.

Charge-discharge curves profile – this is the shape of the curve which according to changes in the voltage, when a constant charge / discharge current is applied in dependence from the amount of energy in the battery (or the time). This curve is defined mostly by the chemistry type of the battery, the rate of charging / discharging, its internal resistance and from the temperature. In Fig. 2 are presented the typical charge curve profiles of the different battery types according to their chemistry. Here the profile for Li-Ion battery is received, when constant voltage method is used with current limiting (see below).

TABLE I
GENERALIZED PARAMETERS OF RECHARGEABLE BATTERIES BY THEIR CHEMISTRY

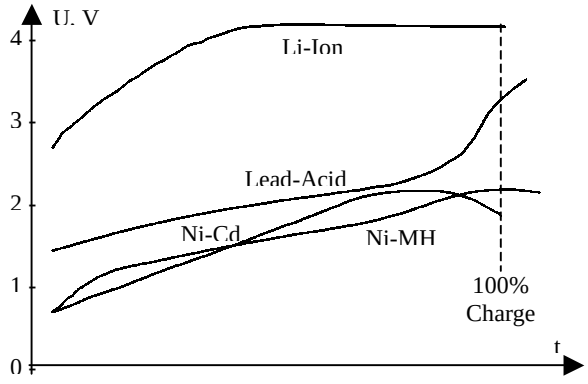

Fig. 2. Typical charge profiles of different batteries by the type of the chemistry

A *constant-voltage charger (C-V)* is a circuit that charges a battery by sourcing only enough current to force the battery voltage to a fixed value. Usually the maximal current is limited to some value.

A *constant-current charger (C-C)* is a circuit that charges a battery by sourcing a fixed current into the battery, regardless of battery voltage.

A *negative pulse charger* is a circuit that charges a battery like C-C method but there are short negative pulses in the current's shape.

III. METHODS FOR DEFINING OF COMMON PARAMETERS FOR RECHARGEABLE BATTERYES

The common parameters that characterizing rechargeable batteries and can be measured / calculated are:

1. Capacity – the reading is the most accurate when the full charge discharge cycle is done and the amount of discharged energy is calculated. The lower rates of discharge give more accurate results. Usually the rate of discharge currents is with about C/20.

2. Chemistry – it is possible to be recognized trough tracking of the charge and discharge profiles and also after comparison of some parameters values, which are peculiar for given rechargeable battery's type of chemistry with the stored statistical data.

3. Internal resistance – the reading of this parameter can be done after applying the sequence showed in Fig. 3 about 20 times and to take the middle value from the calculations results. The voltage over the battery is measured when through the sequence duration a constant current is applied. The sequence has positive and negative parts, which are symmetrical each other, and the duration of every step is about 10ms (the step 5 is about 200ms long). This is because the rising of the temperature or the level of capacity must be avoided. The calculation of internal resistance can be obtained with Eq. (7).

$$R_{ESR} = \frac{U_1 - U_4}{I_1 - I_4} \quad \text{, where} \qquad (7)$$

U_1 is the measured voltage through the positive current pulse duration – step №1 in the figure;

Chemistry Parameter	LA	NiCd	NiMH	Li-Ion
ESR, [mOhm]	100 - 200	100 - 200	200 - 300	150 - 250
Self discharge, [% per month]	5	10 – 20	20 - 30	<10
Top U, [V]	2.4	1.35	1.4	4.1
Nominal U, [V]	2	1.2	1.2	3.7
Min. U, [V]	1.8	0.9	0.9	2.9
Cycle life	300	1500	500	500
Memory Effect	No	Yes	Yes	No
Overcharge Tolerate	high	middle	low	very low

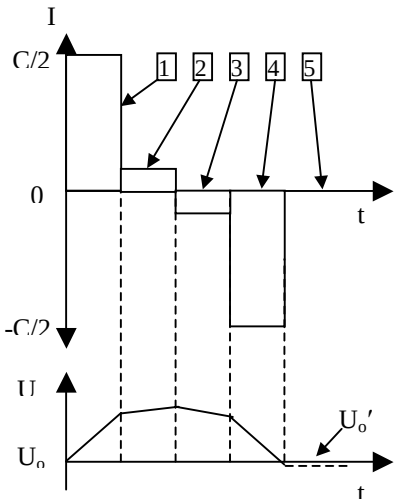

Fig. 3. Method for measurement of internal resistance and performance

U_4 is the measured voltage through the negative current pulse duration – step №4 in the figure.

4. Performance – this is appraisal for the energy expense necessary for the battery charging in relation to the amount of energy, which is stored in the battery. The same sequence from Fig. 3 is used to do this measurement, but here the pulses are with 1 to 5 minutes duration, the current rate is about C/5 to C/10, and the measurements are made less times. The relation between the voltages of the battery in the end of the sequence U_O' and this voltage in the beginning U_O, multiplied by 100 is the value of this parameter in percents.

5. Self discharge – this parameter approximately can be read if the rate of voltage falling is measured for period of several hours (or days) without connected load to the battery and after applying corrections for nonlinearity of this process.

6. Temperature – it is measured through a thermal sensor, which is mounted closely to the battery's case. This parameter is very important, because of his strong influence over the all battery's parameters and hence the need of corrections in measurements and calculations.

7. Charge level – this is the current level of stored energy in relation to the maximal amount of energy that can be stored. This parameter can be taken from charge-discharge profiles, current level of the voltage and internal resistance after comparison with statistical data.

8. State of health – appraisal for the battery's overall efficiency in the base of comparative analysis with stored statistical data and all obtained parameters.

IV. A GENERAL SCHEME SOLUTION

The propound for a general scheme solution is showed in Fig. 4. The main role is assigned to one programmable microcontroller, which common tasks are: 1) control over LCD display and keyboard – to bring out the information, navigate through the menus and data entering; 2) PWM for control over the power switches for charge and discharge of the batteries; 3) control and readings from one 5-channel ADC; 4) reading and writing from/to the memory chip; 5) digital control over adjustable power supply; 6) communication with the computer; 7) other tasks.

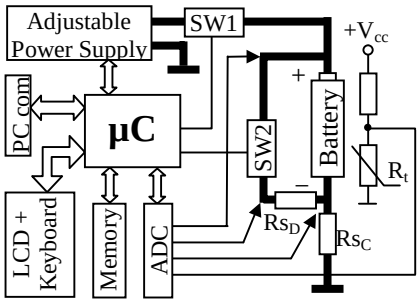

Fig.4. A general scheme solution for rechargeable batteries identification system

The algorithms for analyzing (identification) of rechargeable batteries are realized in the software, hence their changes and the addition of new functionality is not related to more hardware expenses.

V. CONCLUSION

The propound scheme solution is comparatively low self price but with high functionality. The computer communication extends this device and gives it more flexibility. The universality and low self price was the main purposes of this project.

REFERENCES

[1] Buchmann I. "Understanding your batteries in a portable world" Cadex Electronics Inc. http://www.cadex.com/

[2] Buchmann I. "Choosing a battery that will last" Cadex Electronics Inc.

[3] Simpson, C. " Battery Charging ", National Semiconductor

Comparison of Energy Factors of Transistor Invertors for Induction Heating Using PSpice

G. Kunov[1], M. Popov[2], E. Gadjeva[3]

***Abstract*: In the present paper *PSpice* computer models are developed for the basic transistor inverter types – series, series-parallel and current-fed parallel inverters. Based on the same conditions - voltage across and current through the transistors, output power comaprison has been made within the different inverter topologies. The computer simulation allows a detailed investigation of the commutation processes in the inverter circuits taking into account the real characteristics of the active components. The commutation processes are simulated, and the static and dynamic dissipated power on the transistors is calculated.**

***Keywords:* Power Electronics, Transistor Invertors, Induction Heating.**

I. INTRODUCTION

The transistor inverters are widely used in the high-frequency induction heating technologies for power greater than 10 kW and frequency above 20 kHz. From the great variety of transistor inverters being used in the field of high frequency induction heating, the bridge topologies are the most widely used [1].

The point of study in the current article is: bridge series resonant inverter, series-parallel resonant inverter and bridge parallel current-fed inverter. These topologies (Fig.1a,b,c) have been *PSpice* analyzed.

The commutation processes are specific for each inverter circuit type, and their adequate modeling is of significant importance for the transistor driver circuit composition. These processes of the active and passive components are simulated, and the static and dynamic dissipated power on the transistors is calculated.

Examples are given, illustrating the validity, the specific features and the efficiency of the developed *PSpice* models. The simulation is performed using the *OrCAD PSpice* simulator.

The major processes in the series resonant inverters are widely analyzed and described in the engineering literature like [1], [2] ect.

The waveforms of the voltage (V_{AB}) across and the current (I_{Rs}) through the diagonal of the bridge are *PSpice* simulated and shown in Fig.2.

[1] Technical University of Sofia, Faculty of Electronic Engineering and Technologies, Department of Power Electronics, Sofia 1797, Bulgaria, e-mail: gkunov@tu-sofia.bg

[2] Technical University of Sofia, Faculty of Electronic Engineering and Technologies, Department of Power Electronics, Sofia 1797, Bulgaria, e-mail: mariannp@dir.bg

[3]Technical University of Sofia, Faculty of Electronic Engineering and Technologies, Department of Electronics, Sofia 1797, Bulgaria, e-mail: egadjeva@tu-sotia.bg

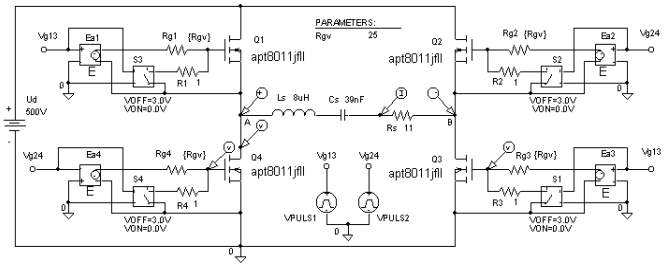

a)

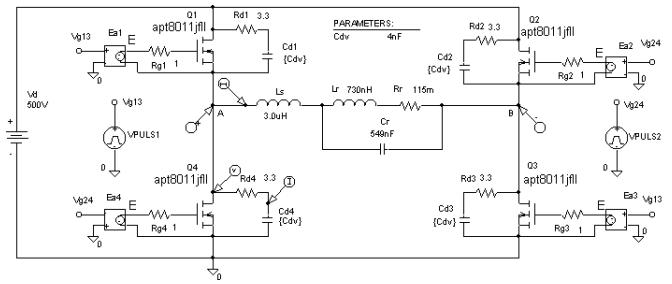

в)

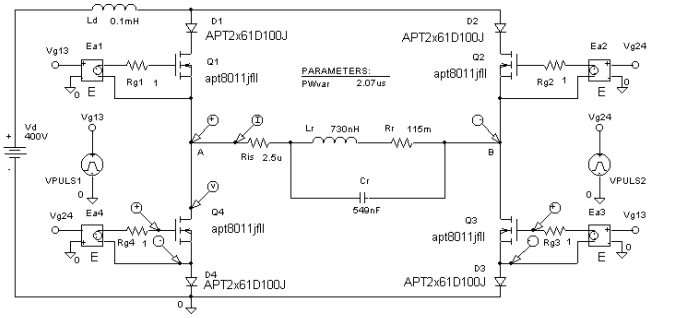

c)

Fig. 1. The basic investigated inverter circuits

The shape of the voltage waveform is rectangular and the magnitude equals the value of the supply voltage (V_d). The shape of the current is a sine wave. When the frequency of the gate drive pulses (VPULSE1,2) equals the resonant frequency of the series oscillation loop ($f_{sw} = f_o$), then the transistors are commutated at zero current ZCS.

The operation of the series-parallel resonant inverter at active load is analyzed in [2] while the simulation at complex load is analyzed in [4] and [5]. A characteristic feature is the rectangular shape of the inverter voltage waveform (V_{AB}), which magnitude is equal to the value of the supply DC voltage. The diagonal current waveform (I_{LS}) resembles trapezoid shape (Fig.3). The inductance L_s makes sure the inverter operates in inductive mode while the load is fully compensated. When having enough dead time between the gate-drive pulses, this mode ensures that the switches are commutated at zero voltage (ZVS).

Unlike the SCR [6], the transistor inverters are recommended to be operated in inductive mode of the load oscillator loop ($f_{sw} < f_o$). This mode eliminates the current in the body diodes.

The shape of the voltage across the diagonal (V_{AB}) is a sine-wave. The current (I_{Ris}) is rectangular (Fig.4).

For comparison purposes the same supply voltage, load, operation frequency (250kHz), maximal voltage across and maximal current through the switches are selected. In this way the similar working conditions give the possibility to compare the power characteristics of the different topologies i.e. the active power in the load and the power loss in the switches.

II. EVALUATION CRITERIA BASED ON THE MAXIMUM POWER DISSIPATED IN THE LOAD

In this evaluation, the approach used in [3] is applied. The output power is defined as a multiplication of the inverter voltage, current through the diagonal and $\cos(\beta)$, where β is the phase angle between these two parameters.

In the case of *series resonant inverter* the amplitude of the rectangular inverter voltage in the diagonal of the bridge is equal to the max. voltage across the switches i.e. $V_{AB} = V_{Dm}$. The RMS value of the inverter voltage is defined by the equation:

$$V_{AB(RMS)} = \frac{4V_{Dm}}{\pi\sqrt{2}}.$$

The RMS value of the current across the diagonal is defined by the equation:

$$I_{AB(RMS)} = \frac{I_{Dm}}{\pi\sqrt{2}}.$$

Because these two parameters are phased, the power equation will be as follows:

$$P_S = \frac{4V_{Dm}}{\pi\sqrt{2}}\frac{I_{Dm}}{\sqrt{2}} = \frac{2V_{Dm}I_{Dm}}{\pi} = 0.636V_{Dm}I_{Dm} \qquad (1)$$

In the case of *series parallel resonant inverter* the RMS voltage is the same as in the previous case. The RMS value of the trapezoid current is defined by the equation:

$$I_{AB(RMS)} = \frac{4I_{Dm}\sin(\beta)}{\pi\beta\sqrt{2}},$$

where β is the rise time from zero to max and vise versa of the current in Radians [RAD]. In fully compensated mode of operation this angle matches the phase angle between the inverter current and voltage.

Consequently the equation of the power will be stated as follows:

$$P_{SP} = \frac{4V_{Dm}}{\pi\sqrt{2}}\frac{4I_{Dm}}{\beta\pi\sqrt{2}}\sin(\beta)\cos(\beta) = 0.729V_{Dm}I_{Dm} \qquad (2)$$

The following parameters can be defined in Fig. 3: t_β=250ns which is equal to β=22.5° or 0.393 rad [5] for switching frequency of 250kHz.

In the case of *parallel current-fed inverter* the equations of inverter voltage and current are the same as in the series resonant inverter but their positions are swapped.

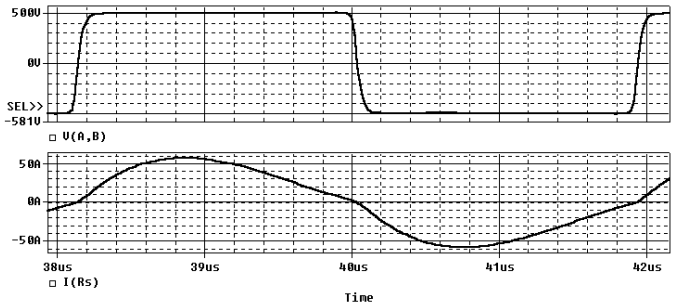

Fig. 2. The waveforms of the voltage V_{AB} and the current I_{Rs} of the series resonant inverter

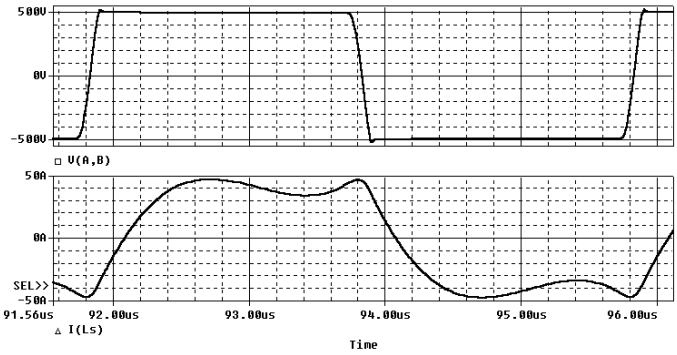

Fig. 3. The waveforms of the voltage V_{AB} and the current I_{Ls} of the series parallel resonant inverter

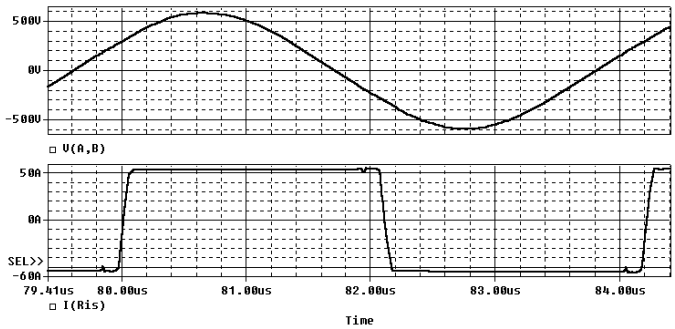

Fig. 4. The waveforms of the voltage V_{AB} and the current I_{Ris} of the parallel current-fed inverter

When β=22.5° then:

$$P_P = \frac{V_{Dm}}{\sqrt{2}}\frac{4I_{Dm}}{\pi\sqrt{2}}\cos(\beta) = 0.588V_{Dm}I_{Dm} \qquad (3)$$

From (1) , (2) and (3) becomes evident that at identical initial conditions, the series parallel inverter will deliver the biggest power, while the parallel will deliver the smallest power in the load.

III. PSPICE SIMULATION AND POWER LOSS EVALUATION DURING THE TRANSITION OF THE SWITCHES

Duding this simulation and evaluation, *PSpice* models of the following transistors and diodes are used:
Switch: APT8011JFLL
Diode: APT2x61D100J
Manufacturer: Advanced Power Technology [9].

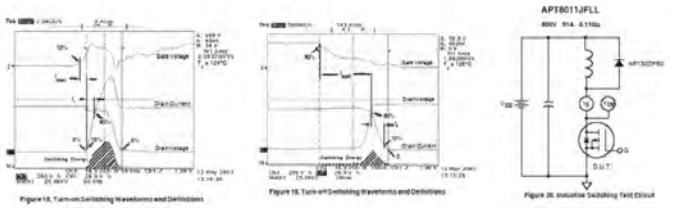

Fig. 5. The test setup for the power loss during transition given by Advanced Power Technology manufacturer

All manufacturers use the test setup shown in Fig.5 to measure the power loss during transition.

It is a severe mode for the transistor, when hard switching is applied. In this case additional power loss is encountered during the saturation of the switch, caused by the free willing current running through the body diode.

The purpose of the following *PSpice* simulations is the measurement of the power loss into the real applications.

In the case of *series resonant inverter* specific commutation features in each leg of the inverter bridge characterize ZCS in bridge resonant inverter. The input and reverse capacitance of the conducting transistor are zero charged at the end of each current sine wave. At that time the capacitance of the opposite transistor in the same leg is charged to the value of the supply voltage. When this transistor is turned on the current running through, is initially discharging its own capacitance while charging the capacitance of the other transistor in the same leg. The capacitance current running at the end and the beginning of each current sine wave, determine the loss during transition.

This simulation was done in parametric mode analysis. The value of the gate resistor **{Rgv}** is the variable parameter. This resistor is limiting the value of the charging current in the input capacitance. It results in decreasing du/dt and di/dt. This approach is used in [7] and [8] as well. The results from this simulation are shown in Fig. 6.

Increasing the value of *Rg* will result in smoother transition through active mode. The benefit is the decrease of the maximum value of power loss and du/dt across the switch.

As seen in Fig. 7 the total power (sum of commutation and static power) decreases when *Rg* increases. In this example this value is equal to 120W when $Rg = 20\,\Omega$.

In the case of *series parallel resonant inverter* the inductive character of the load in the diagonal of series-parallel inverter is a typical case of ZVS. Installing an additional capacitor drain to source (C_{dv}) will split a part of the current out of the switch during turn off. The bigger the ratio C_{dv}/C_{ds} is, the bigger part of the current is split out. This results in decreasing the maximum power dissipated across the switch (Fig. 8).

The transistor power loss in this inverter is mostly concentrated in the turn off cycle. In this example Cd= 6nF which results in equal power loss as within series inverter (Fig.9).

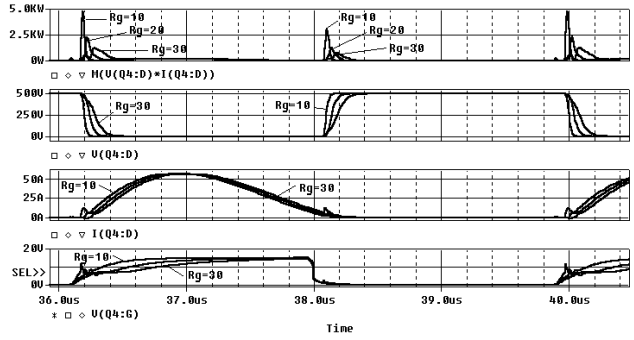

Fig. 6. The results of *PSpice* simulation of the commutation processes for series resonant inverter

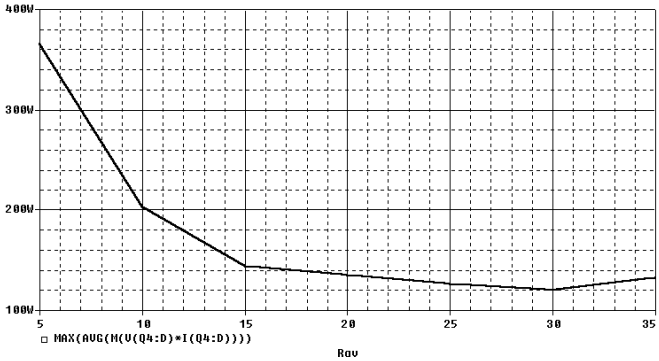

Fig.7. The dependence of switching losses on R_{gv} for series resonant inverter

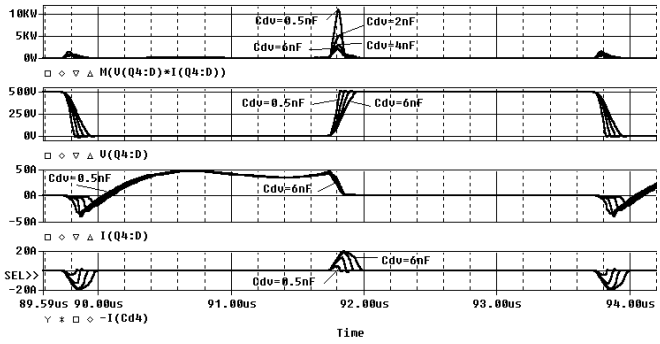

Fig. 8. The results of *PSpice* simulation of the commutation processes for series parallel resonant inverter

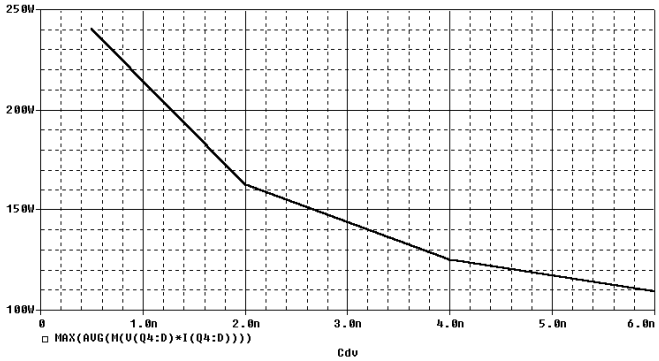

Fig. 9. The dependence of switching losses on C_{dv} for series parallel resonant inverter

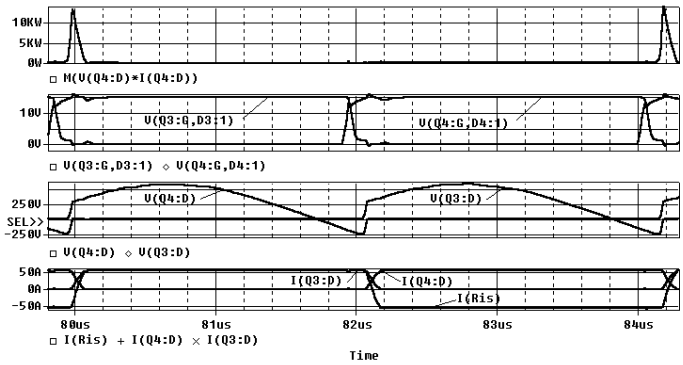

Fig. 10. The results of *PSpice* simulation of the commutation processes for parallel current-fed inverter

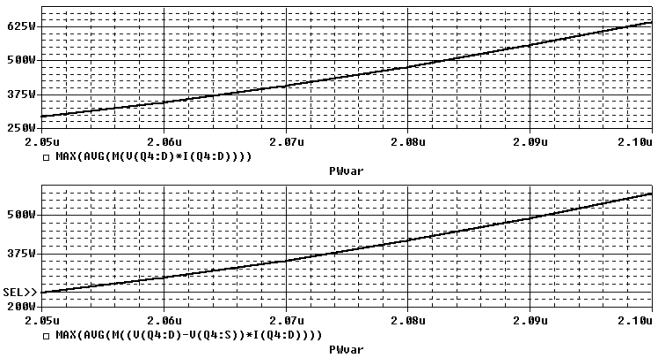

Fig. 11. The dependence of switching losses on f_{sw} for parallel current-fed inverter

Because the *parallel current-fed inverter* is powered by a current source, no time interval when all switches are turned off is acceptable. The inductive mode of the oscillating load loop ($f_{sw} < f_o$) ensures smooth current transition in the inverter legs (Fig.10).

As seen from the simulation results, commutation loss is observed just during turn on of the switch. The amplitude of this loss is relatively high. Increasing the inductive mode (decreasing the switching frequency will result in power loss increase (Fig. 11).

This topology encounters the most power loss compared to the other two topologies.

IV. Conclusions

Resulting the analysis of the research, the following statements can be concluded:

1. The series-parallel inverter delivers the highest output power to the load.

2. Concerning the power loss in the switches, the series and the serial-parallel inverter are equal while the parallel inverter encounters the highest power loss.

3. By optimal selection of the gate resistor in the serial inverter and by increasing the value of the additional drain to source capacitor, the power loss can be optimized.

The less possible inductive mode of the oscillating load loop must be applied with the parallel inverter.

References

[1] C.J.Ericson,"Handbook of Electrical Heatig for Industry",IEEE-IAS Press , 1994

[2] F. Labrique, G.Seguer, R. Bausiere, "Les Convertisseurs de Puissance", Vol.4, "La Convertion Continu-alternatif, Technique et Documentation", Lavoisier, Paris, 1995.

[3] F. Brichant, "Electronique de Puissance". Edition Techniques et Ssciantifiques Francaises, 1977.

[4] G.Kunov,E.Gadjeva,I.Eftov,"Modeling of Selfoscillating Control System of a Transistor Oscillator for Tube Welding Using Spice",ICEST-2002,1-4 October 2002, Nis,Yugoslavia

[5] G. Kunov, E. Gadjeva, "Desin and simulation of working in parallel transistor invertors", 12th International Symposium on Power Electronics-Ee 2003, Novi Sad, Serbia&Montenegro, November 5th-7th, 2003.

[6] N. Moham, T. Underland, W. Robin, "Power Electronics", Wiley&Sons Inc. , 1989.

[7] C. Gerster, P. Hofer,"Gate-controlled dv/dt-and di/dt-limitation in power IGBT converters", EPE Journal, Vol.5, No3/4, January 1996, page 11-16

[8] N. Idir, J.J. Franchaud, R. Bausiere, "How to reduce EMI generated by IGBT and MOSFETs.New control technique achieves low di/dt and dv/dt.",PCIM-EUROP, Power Electronics, No2, February 2000, pp.28-30

[9] http://www.advancedpower.com

Calculating the Thickness of Thin Films, Produced by Different Kinds of Evaporators

Dimiter D. Parashkevov[1]

Abstract **- The thickness uniformity of thin films, deposited on different substrates is very important with a respect to the quality of the layers and the output of the technological process. It has to be proofed, when a new vacuum equipment is first set in operation. The present work predicts the thickness of the produced layers using some idealized models and shows the way for calculating it by a real sputtering process.**

Keywords **– cathode sputtering, mathematical models, NiCr, erosion profile.**

I. INTRODUCTION

A standard B-55 vacuum plant is supplied additionally with a magnetron sputtering system in order to produce NiCr resistive layers. We have to consider according to the new arrangement in the chamber and some technological parameter – for instance the sputtering rate some models, which are suitable for calculating the thickness distribution of the film over the substrate.

II.BASIC CONCEPTS AND QUANTITIES

We suggest a cos law of distribution for the sputtered atoms. They reach the substrate without hindrance and all of them condense there.

A basic concept in the models is the parallel disposition between the motionless substrate and target.

The main quantities we use in our considerations are shown on Fig.1. Here denote the symbols the following: dA_e – the elementary emitting surface, dA_r – the elementary surface on the substrate, φ - the sputtering angle, θ - the condense angle, α - the angle between the Y axis and the radius vector to dA_e, h – the distance target-substrate, s – radius, r – the distance between dA_e and dA_r, l – the distance between the centre of the substrate and the point, where the thickness d is calculated.

III.MODELS FOR CALCULATING LAYER'S THICKNESS

A.SMALL SURFACE EVAPORATOR

The thickness of the layer d_e from the small emitting surface dA_e on an infinite small surface dA_r of the substrates by randomly oriented to each other substrate and target is given with [1]:

$$d_e = \frac{m_1}{\pi.\rho}\frac{\cos\varphi.\cos\vartheta}{r^2}dA_e \qquad (1)$$

where ρ is the density of the sputtered material. The meaning of m_1 is the mass of the sputtered material, produced from one sputtered surface unit in one second, that is so to say the mass velocity (intensity) of sputtering.

Assuming a *plain substrate, planar to the emitting surface* of the target we get (Fig. 1):

$$\varphi = \theta,\ \cos\varphi = \cos\theta = \frac{h}{r},\ \ dA_e = s.d\alpha.ds \qquad (2)$$

$$d_e = \frac{m_1}{\pi.\rho}\frac{h^2}{r^4}.s.ds.d\alpha \qquad (3)$$

We can get the distribution of the final thickness d of the layer over the substrate when we integrate (3):

$$d = \iiint_{t,s,\alpha} d_e = \iiint_{t,s,\alpha} s.\frac{m_1}{\pi.\rho}\frac{h^2}{r^4}.ds.d\alpha \qquad (4)$$

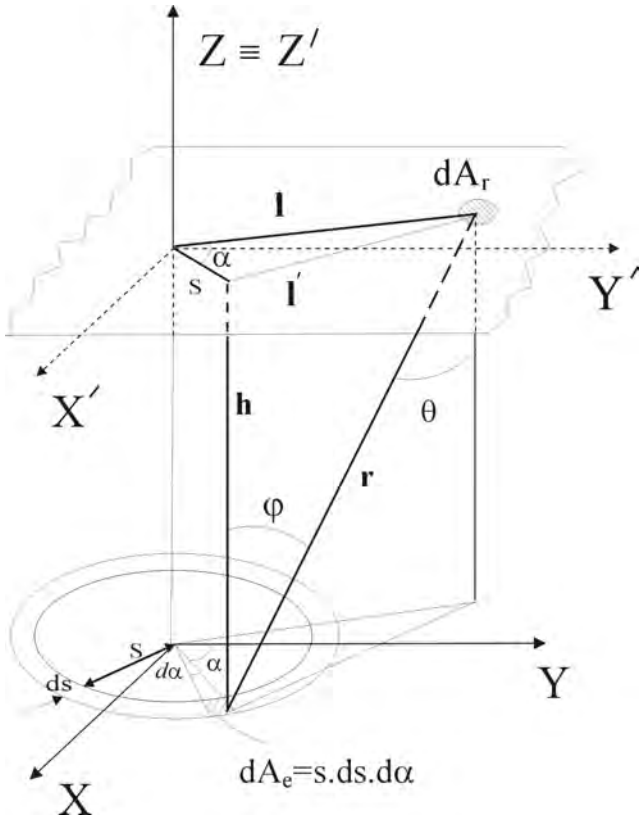

Fig.1: Geometric arrangement substrate-sputtering target

According to the relationships between the quantities on Fig.1 we get:

[1]Dimiter D. Parashkevov,Physics Department,Bourgas Prof. Assen Zlatarov University,1 Prof. Yakimov Str., Bourgas 8010, Bulgaria,E-mail: parashkevov@btu.bg and paraskkevov@abv.bg

$$r^2 = h^2 + l'^2 = h^2 + (l^2 + s^2 - 2l.s.\cos\alpha) \quad (5)$$

Then:

$$d = \iint_{t,s} \frac{h^2 m_1}{\pi\rho}.s.ds.dt \int_{\alpha} \frac{d\alpha}{(h^2 + l^2 + s^2 - 2l.s.\cos\alpha)} =$$

$$= \frac{h^2}{\pi\rho} \iint_{t,s} m_1.s.ds.dt \int_{\alpha} \frac{d\alpha}{(h^2 + l^2 + s^2 - 2l.s.\cos\alpha)} =$$

$$= \frac{h^2}{\pi\rho} \iint_{t,s} m_1.s.ds.dt.\Im \quad (6)$$

$\Im$ means here:

$$\Im = \int_0^{2\pi} \frac{d\alpha}{(h^2 + l^2 + s^2 - 2l.s.\cos\alpha)} \quad (7)$$

Substituting:

$$b = h^2 + l^2 + s^2\ ;\ c = 2l.s\ ;\ a = \frac{c}{b} \quad (8)$$

we get for $\Im$:

$$\Im = \frac{1}{b^2} \int_0^{2\pi} \frac{d\alpha}{(1 - a.\cos\alpha)^2} = \frac{1}{b^2}.I \quad (9)$$

The integral I is a sum of four integrals, two of the kind I' $= \int_0^{\frac{\pi}{2}} \frac{dx}{(1 - a.\cos x)^2}$, the rest - $I'' = \int_0^{\frac{\pi}{2}} \frac{dx}{(1 + a.\cos x)^2}$.

We unite all them in one integral within the same limits and after some transformations we receive:

$$I = \frac{2\pi}{(1 - a^2)^{\frac{3}{2}}} \quad (10)$$

Substituting (10) in (9) and using (8) we get for $\Im$:

$$\Im = 2\pi \frac{(h^2 + l^2 + s^2)}{\left[(h^2 + l^2 + s^2)^2 - 4.h^2.l^2\right]^{\frac{3}{2}}} \quad (11),$$

and for d:

$$d = \frac{2h^2}{\rho} \iint_{t,s} m_1 \frac{(h^2 + l^2 + s^2)}{\left[(h^2 + l^2 + s^2)^2 - 4.h^2.s^2\right]^{\frac{3}{2}}} s.ds.dt \quad (12)$$

The expression (12) is for the case of a small surface evaporator.

Further on the calculation for a certain point of the substrate of the full (final) thickness of the layer d depends on:

- The kind of the evaporating source
- The dependency $m_1 = m_1(s,t)$

B.THIN RING EVAPORATOR

An evaporator in the form of a thin ring with radius s is considered. Assuming m_1= const(t) and $m_1 \neq m_1(s)$, we receive from (12) after double integrating:

$$d = \frac{M_r}{\pi\rho h^2} \frac{1 + (l/h)^2 + (s/h)^2}{\left\{\left[1 + (l/h)^2 + (s/h)^2\right]^2 - 4(s/h)^2\right\}^{3/2}} \quad (13)$$

M_r here means the total evaporated mass from the thin ring evaporator.

$$M_r = 2\pi s.ds \int_t m_1 dt = 2\pi s ds \tau \quad (14)$$

C.DISK EVAPORATOR

The same procedure in the case of a disk evaporator by the same conditions (m_1= const(t) and $m_1 \neq m_1(s)$ gives for d the expression:

$$d = \frac{M_d}{2\pi\rho s^2} \left\{1 - \frac{1 + \left(\frac{l}{h}\right)^2 - \left(\frac{s}{h}\right)^2}{\sqrt{\left[1 + \left(\frac{l}{h}\right)^2 + \left(\frac{s}{h}\right)^2\right] - 4\left(\frac{s}{h}\right)^2}}\right\} \quad (15)$$

In (15) M_d stands for the total amount of the sputtered mass from the disk:

$$M_d = \pi s^2 \int_t m_1 dt = \pi s^2 m_1 \tau \quad (16)$$

IV.REAL EXPERIMENTAL MODEL

The equations (14) and (16) show, that the sputtering rate m_1 is assumed to be invariable during the whole time of evaporation - τ . This is reasonable when we keep up a constant power of the generator. When we calculate d in the case of a thin ring evaporator (13) or a disk evaporator (15), *we regard m_1 as a constant over the whole surface* of evaporation as well. Otherwise m_1 would take part in the integration over s.

Actually m_1 varies over the surface of the evaporator. The real dependence $\mathbf{m_1 = m_1(s)}$ is connected with the concrete technological equipment and the kind of the target.

A good proof for the above mentioned are the *erosion profiles* of long used targets (cathodes). Their erosion surfaces repeat the dependence $m_1 = m_1(s)$ and are not ideal responding to the models *B* and *C*.

The main interest in our experiments was in the thickness of the deposited resistive films over the substrate. They were produced by sputtering a NiCr (Ni:Cr = 80:20) target. After a long time of sputtering the cathode looks like this shown in Fig. 2.

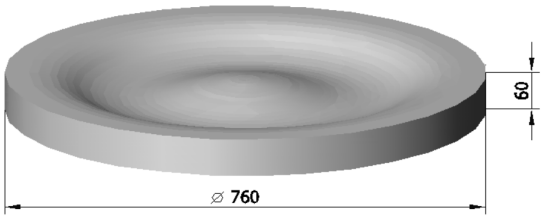

Fig. 2: The view of a NiCr target after a long use, mm.10

When new the target is a regular disk with ϕ = 76 mm, h = 6 mm.

The sputtering profile of NiCr target as a result of measurements and interpolation is shown as curve *1*on Fig. 3:

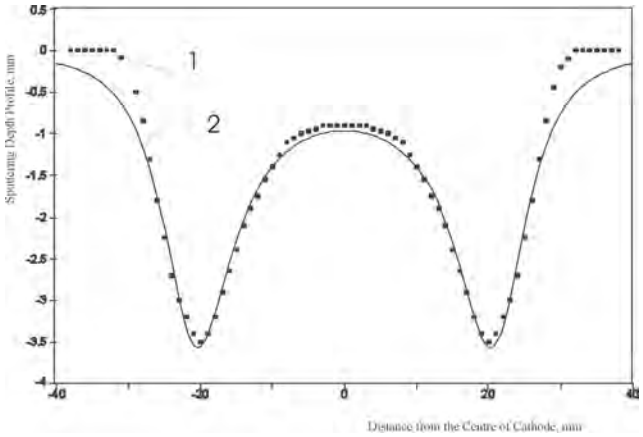

Fig. 3: Measured erosion profile – *1* and fitting curve to it – *2* of a long used NiCr target

It can be seen from Fig.3, that the profile is sharp with a minimum by distances $\pm$ 20 mm from the centre of the target. The edges of the target are practically not sputtered, but the centre is sputtered with some little rate.

The fitting curve (Fig. 3, curve *2*), witch corresponds best to the measured profile can be found with the help of an appropriate software program. We have used TableCurve2d program to reveal the analytical form of the dependence $m_1(s)$. So we got for m_1 a function of a kind:

$$m_1(s) = (a + b.s + c.s^2 + d.s^3 + e.s^4)^{-1} \quad (17),$$

where:

$$a = -1.0284864,\ b = -1.715905.e^{-6},\ c = 0.0036083349,$$
$$d = 4.3724109.e^{-9},\ e = -4.3472891.e^{-6} \quad (18)$$

The integral, which has to be solved in our case is:

$$d = \frac{2h^2\tau}{\rho} \int_{-38}^{38} \frac{m_1(s)(h^2 + l^2 + s^2)}{\left[\left(h^2 + l^2 + s^2\right)^2 - 4h^2.s^2\right]^{3/2}}\, s.ds \quad (19)$$

In the last equation $m_1(s)$ comes from (17), the coefficients in it from (18), h and l are technological parameters. Equation (19) can be numerically calculated with a suitable program, for example with the mentioned TableCurve.

V.CONCLUSIONS

In the present work we consider some idealized models for calculating thickness of sputtered layers. In the reality we can't ignore the influence of the different rate of evaporation over the target on the thickness distribution. A model which takes into consideration this different sputtering rate is proposed.

A comparison between calculated and experimental results for the layer's thickness distribution over the substrate using different models will be a subject of an other work [2].

REFERENCES

[1] Leon I. Maissel and Reinhard Glang, *Handbook of Thin Film Technology*, McGRAW HILL COMPANY, 1970.
[2] D. Parashkevov, in preparation

Noise Wave Model of RF MOSFETs - Development and Software Implementation

Olivera R. Pronić, Vera V. Marković

Abstract — **Noise wave model of RF MOSFETs based on *T* representation of transistor intrinsic circuit is derived in this paper. The presented modeling procedure is based on circuit theory concepts and on similar kind of analysis we proposed earlier for MESFETs / HEMTs noise modeling. The noise wave temperatures are introduced as empirical parameters of the model. The complete noise modeling procedure is implemented in microwave circuit simulator Libra. Noise parameter values modeled by proposed procedure are verified by the comparison with the measured ones for a typical RF MOSFET.**

Keywords – **MOSFET, noise parameters, noise wave temperatures**

I. INTRODUCTION

For decades, the high-frequency properties of silicon integrated circuits have been considered inferior comparing to the GaAs counterpart. The situation is now changing. Namely, by scaling down the CMOS technology, the RF gain and noise performance of deep and ultradeep sub-micrometer MOSFET are improved so that it can be used for wireless communications, [1]. The advantages of MOSFET-based technology are: low cost, low power consumption, small dimensions and weight, high reliability, high-level integration possibility and ability to combine digital, analog and RF circuits on the same chip [2]. Because of that, today ultradeep-submicrometer CMOS technology is considered as the most promised technology for 3G mobile terminals and other wireless products such as GPS, Home RF, Bluetooth, etc.

For these new wireless applications, designers need reliable RF small signal models, which are easy to extract and use. In some cases MOSFET noise models are also requiered. Physical models, like the well-known models of the BSIM family, for instance BSIM3v3, [3], are not quite adequate for RF and microwave MOSFETs. In addition, their application is time consuming, requiring much technological data. Because of that, many efforts were made during the last few years, in order to develop the appropriate empirical device models that can be implemented into the microwave CAD tools, [4].This task still remains a challenge because mechanisms of noise generating and other effects inside the short-channel MOSFETs are complex and even not yet completely explained. Therefore, there is still an interest for new results in the field of RF MOSFET modeling.

Olivera R. Pronić and Vera V. Marković are with the Faculty of Electronic Engineering, University of Niš, Beogradska 14, 18000 Niš, Serbia and Montenegro, E-mails: oljap@elfak.ni.ac.yu, vera@elfak.ni.ac.yu

On the other hand, during the last two decades, much more work has been done for developing small-signal and noise models of the traditionally used microwave FET transistors, like MESFETs and HEMTs. Small-signal equivalent circuits of MESFETs and MOSFETs are very similar. Consequently, having a great experience in noise modeling of MESFETs, in previous papers we applied the similar kind of analysis to RF MOSFET noise parameter modeling, [5], [6].

In this paper we present a new noise wave model for microwave MOSFETs based on *T* representation of transistor intrinsic circuit. Namely, for high frequency circuit applications a wave interpretation of noise is advantageous since it allows the use of scattering parameters for noise computations, [7], [8]. The complete microwave MOSFETs' noise modeling procedure proposed in this paper is based on circuit theory concepts and therefore is very convenient for implementation in microwave CAD programs.

II. NOISE WAVE MODEL OF RF MOSFET

We considered a typical MOSFET small-signal equivalent circuit, as shown in Fig. 1. The intrinsic part of the circuit is denoted by the dashed line.

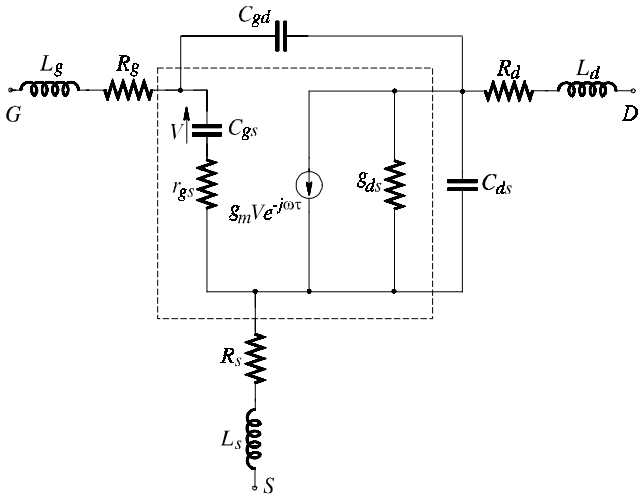

Fig. 1. MOSFET small-signal equivalent circuit

Noise in linear two-port networks can be characterized in many different ways, [9]. Any noisy linear two-port can be replaced by the noiseless two-port network and two additional correlated noise sources. Noise is typically characterized using equivalent voltage and current sources, or a combination of both. Therefore, impedance and admittance matrix representations, chain matrix representation and a few others are often used in CAD of noisy networks. On the other hand, in the noise wave representation, a noisy two-port network is

described by using a noiseless linear equivalent circuit and the waves that emanates from its port.

It is known that a linear noisy two-port component can be characterized by a noise temperature T_n (or, alternatively, by a noise figure, F, defined as $F = 1 + T_n/T_0$, where T_0 is standard reference temperature of 290K), in following way:

$$T_n = T_{n\min} + 4T_0 \frac{R_n}{Z_0} \frac{\left|\Gamma_g - \Gamma_{opt}\right|^2}{\left|1+\Gamma_{opt}\right|^2 \left(1-\left|\Gamma_g\right|^2\right)}, \quad (1)$$

where Z_0 is normalization impedance (Z_0 =50 Ω).

Eq. (1) gives the depedence of device noise temperature on four noise parameters: minimum noise temperature $T_{n\min}$ (alternatively, minimum noise figure, $F_{min} = 1 + T_{min}/T_0$, can be used), magnitude and angle of optimum reflection coefficient, $\Gamma_{opt} = \left|\Gamma_{opt}\right| e^{j\varphi_{opt}}$, and noise resistance, R_n. The set of four noise parameters describe inherent behavior of the component and are independent of a connected circuit.

The noise parameters of transistor intrinsic circuit can be determined in terms of noise waves in the following way:

We consider *T* representation of a transistor intrinsic circuit. In this case, noisy two-port is represented by a noiseless two-port defined by transfer scattering parameters, [*T*], and two noise wave sources a_n and b_n referred to the input, as shown in Fig. 2.

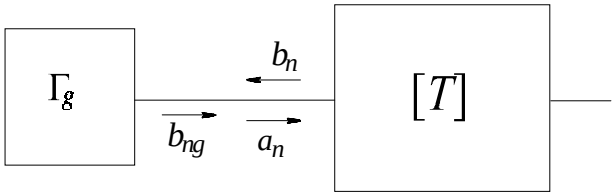

Fig. 2. *T* representation of a linear noisy two-port

The linear matrix equation describing this noisy two-port is:

$$\begin{bmatrix} a_1 \\ b_1 \end{bmatrix} = \begin{bmatrix} T_{11} & T_{12} \\ T_{21} & T_{22} \end{bmatrix} \begin{bmatrix} b_2 \\ a_2 \end{bmatrix} + \begin{bmatrix} a_n \\ b_n \end{bmatrix}, \quad (2)$$

where a_i and b_i, i=1, 2, are incident and output waves at the i-th port.

Generally, the noise wave sources a_n and b_n are correlated and characterized by a correlation matrix $\boldsymbol{C_T}$ given by

$$\boldsymbol{C_T} = \begin{bmatrix} \langle |a_n|^2 \rangle & \langle -a_n b_n^* \rangle \\ \langle -b_n a_n^* \rangle & \langle |b_n|^2 \rangle \end{bmatrix}, \quad (3)$$

where the brackets $\langle\rangle$ indicate time average of the quantity inside and * indicates complex conjugation.

It is very convenient to use the noise wave temperatures as empirical noise model parameters, [8]. In this way, the correlation matrix $\boldsymbol{C_T}$ can be expressed by

$$\boldsymbol{C_T} = k\Delta f \begin{bmatrix} T_a & |T_c| e^{j\varphi_c} \\ |T_c| e^{-j\varphi_c} & T_b \end{bmatrix}, \quad (4)$$

where k is the Boltzmann's constant and Δf is the noise bandwidth (it is assumed that Δf=1Hz). In this way the noise performance of a two-port network is completely characterized by two real temperatures T_a and T_b and a complex correlation temperature $T_c = |T_c| e^{j\omega\tau_c}$.

The expressions for noise wave temperatures could be derived considering the representation of a noisy two-port as shown in Fig. 2. A source of reflection coefficient $\Gamma_g = \left|\Gamma_g\right| e^{j\varphi_g}$ and noise wave b_{ng} is connected to the input of noiseless two-port. The total noise wave that is incident on the input of noiseless two-port is

$$a_{ng} = a_n + \Gamma_g b_n + b_{ng}. \quad (5)$$

Assuming no correlation between source and two-port noise, after some elementary mathematical transformations, [8], [10], the noise temperature is obtained as

$$T_n = \frac{T_a + \left|\Gamma_g\right|^2 T_b - 2|T_c|\left|\Gamma_g\right| cos\left(\varphi_g - \varphi_c\right)}{1-\left|\Gamma_g\right|^2}. \quad (6)$$

Comparison of the Eqs. (6) and (1) yields to the following expressions for the noise parameters:

$$\Gamma_{opt} = \left(\frac{T_a + T_b}{2|T_c|} - \sqrt{\left(\frac{T_a + T_b}{2|T_c|}\right)^2 - 1} \right) e^{j\omega\tau_c}, \quad (7)$$

$$R_n = Z_0 \frac{|T_c|}{4T_0\left|\Gamma_{opt}\right|} \left[1 + 2\left|\Gamma_{opt}\right| cos\,\phi_{opt} + \left|\Gamma_{opt}\right|^2 \right], \quad (8)$$

$$F_{min} = 1 + \frac{T_a - T_b}{2T_0} + \frac{1}{2T_0}\sqrt{(T_a + T_b)^2 - 4|T_c|^2}. \quad (9)$$

III. NUMERICAL EXAMPLE

The numerical results presented in this paper are related to the modeling of RF MOSFETs fabricated by 0.35 μm technology, [11]. The MOSFET small-signal and noise simulations are performed by using microwave circuit simulator Libra, [12]. The modeling of *S* parameters is done in the frequency range of (1 - 20) GHz. The noise parameters are modeled in the frequency range of (2 - 10) GHz, for which the experimental data for noise parameters were available.

At the beginning, the equivalent circuit element values are extracted from the scattering parameter data. For this purpose, the optimization routine of the circuit simulator Libra was

used. In order to obtain as accurate small-signal model as possible, an extended set of optimization goals (*S* parameters, input and output reflection coefficients, stability factor and maximum available gain) was used, [13]. In that way the following element values were extracted: R_g=5.68Ω, L_g=2.83pH, R_d=4.11Ω, L_d=6.86pH, R_s=0.05Ω, L_s=0.1pH, g_m=8.73mS, τ=3.12ps, C_{gd}=14.72fF, R_{gs}=0.6Ω, C_{gs}=157.1fF, R_{ds}=1368.9Ω and C_{ds}=140.2fF.

The comparison of simulated *S* parameters (MOD) and referent data (REF) taken from [11], is shown in Fig. 3. It can be seen that all simulated parameters are in good agreement with the referent data.

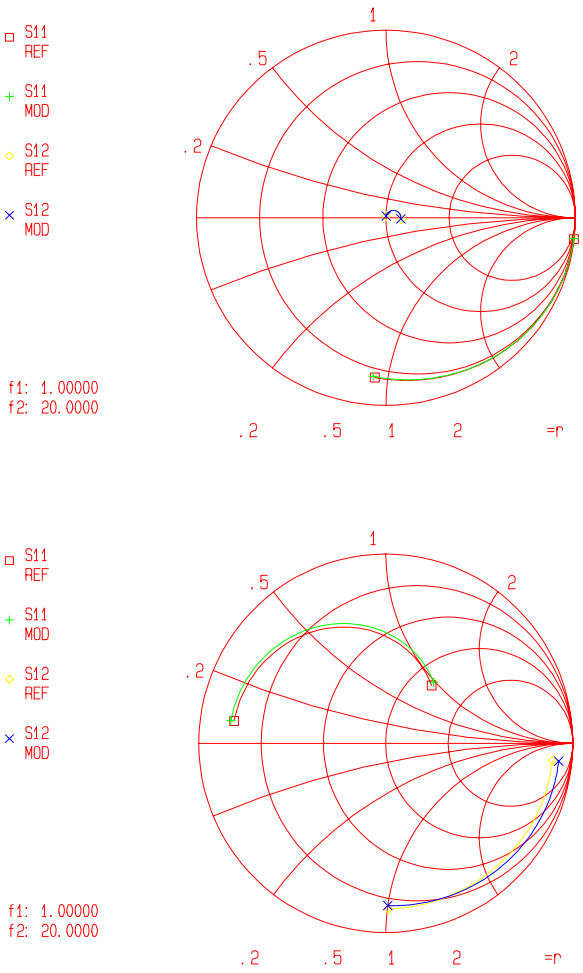

Fig. 3. *S* parameters

In order to determine all model parameters, after the extraction of the small-signal equivalent circuit elements, it is also necessary to determine the noise wave temperatures. The noise wave temperatures are also obtained by using the optimization capabilities of microwave circuit simulator Libra, in the following way: First, the expressions for the intrinsic circuit noise parameters (Eqs. (7) - (9)) are programmed using the "equation" capability of the applied circuit simulator and assigned to the intrinsic circuit by the corresponding statement. After that, all parasitic elements are connected and the topology of the entire transistor is described. Finally, the noise wave temperatures are optimized with the aim that the complete model fits the measured noise parameters. In that way, the following values of noise wave temperatures are extracted: T_a=1714 K, T_b=1649 K, $|T_c|$=1677 K, τ_c=14.7 ps. It can be observed, that the noise wave temperatures obtained for RF MOSFET are much higher than those typically obtained for microwave MESFETs / HEMTs, [10].

Using the obtained model and circuit simulator Libra, the noise parameters for the complete transistor over the frequency range 2 - 10 GHz were computed. The results are presented in following figures.

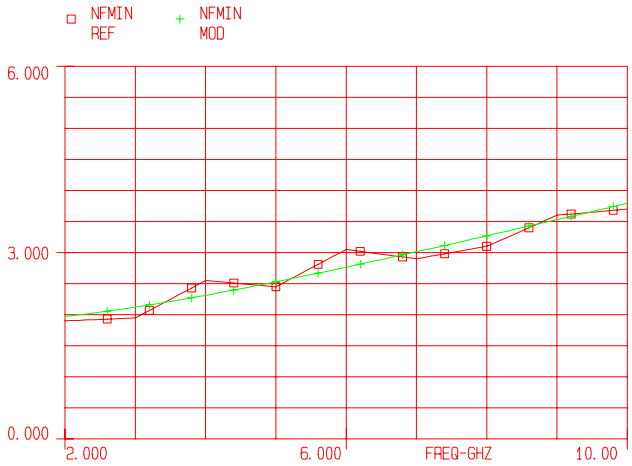

Fig. 4. Minimum noise figure

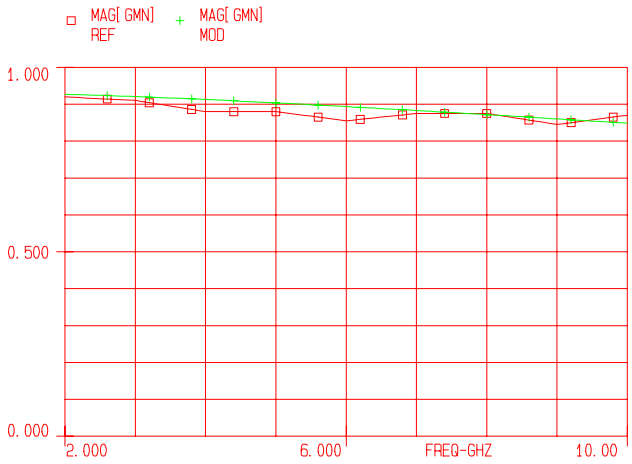

Fig. 5. Magnitude of optimum reflection coefficient

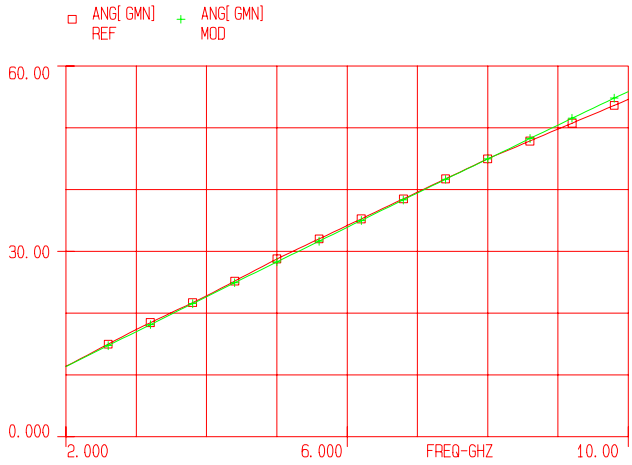

Fig. 6. Angle of optimum reflection coefficient

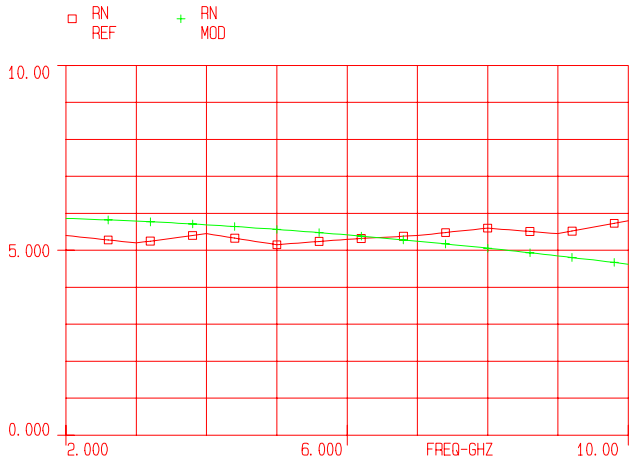

Fig. 7. Normalized noise resistance

For all four noise parameters, the curves obtained by using the model proposed in this paper are denoted by MOD. Minimum noise figure is shown in Fig. 4, magnitude and angle of optimum reflection coefficient are shown in Figs. 5 and 6, respectively, and normalized noise resistance is presented in Fig. 7. In the same figures the simulated noise parameter characteristics are compared with those based on referent data [11] (denoted by REF). Quite a good agreement can be observed for all noise parameters.

IV. CONCLUSION

A noise wave model of MOSFETs for RF and microwave low-noise wireless applications is proposed in this paper. The presented procedure is very convenient for CAD applications, enabling a simple, fast and reliable prediction of noise parameters over a wide frequency range.

The modeling procedure is based on an empirical approach, in a similar way we proposed earlier for the other technology microwave transistors. A noise wave representation based on transfer scattering parameters (T) is used. The expressions for the noise parameters of transistor intrinsic circuit are derived in terms of three equivalent noise wave temperatures. These temperatures are extracted on the basis of experimental data by using a simple procedure incorporated within a standard microwave circuit simulator. Having the values for three noise wave temperatures in addition to the other equivalent circuit elements, the model is completed and can be used for simulation.

In the presented example, S and noise parameter characteristics obtained by the proposed method were compared with the referent ones and quite a good agreement was achieved.

REFERENCES

[1] T. E. Kolding, Review of CMOS Performance and Future Process Innovations, *Technical Report R98-1014*, October 1988.

[2] B. Razavi, “CMOS Technology Characterization for Analog and RF Design”, *IEEE Journal of Solid-State Circuits*, Vol. 34, pp. 268-276, March 1999.

[3] *BSIM3v3 Manual*, Department of Electrical Engineering and Computer Science, University of California, Berkeley, 1995.

[4] C. Enz, “An MOS Transistor Model for RF IC Design Valid in All Regions of Operation”, *IEEE Trans. Microwave Theory Tech.*, vol. MTT-50, pp. 342-359, January 2002.

[5] O. Pronić and V. Marković, "New Small Signal & Noise Model for MOSFETs", Mediterranean Microwave Symposium MMS'2003, Conference Proceedings, pp. 107-110, Cairo, Egypt, 2003.

[6] O. Pronić and V. Marković, "RF MOSFETs Noise Modeling - the Wave Approach", *TELSIKS 2003*, Conference Proceedings, pp. 449-452, Niš, Serbia and Montenegro, 2003.

[7] S.W. Wedge, D.B. Rutledge, "Wave techniques for noise modeling and measurement", *IEEE Trans. Microwave Theory Tech.*, vol.MTT-40, pp. 2004-2012, November 1992.

[8] R. P.Meys, “A wave approach to the noise properties of linear microwave devices”, *IEEE Trans. Microwave Theory Tech.*, MTT-26, pp. 34-37, 1978.

[9] J. A. Dobrowolski, *Introduction to Computer Methods for Microwave Circuit Analysis and Design*, London, Artech House, 1991.

[10] O. Pronić, *Development of empirical noise models of microwave transistors using the wave approach*, PhD thesis, Faculty of Electronic Eng., University of Niš, 2002.

[11] A. Pascht, M. Grözing, D. Wiegner, M. Berroth, “Small-Signal and Temperature Noise Model for MOSFETs”, *IEEE Trans. Microwave Theory Tech.* Vol.50, No.8, pp. 1927-1934, 2002.

[12] *Touchstone and Libra Users Manual*, EEsof, Inc., 1990.

[13] C. Giusto, C. White, “Techniques for small-signal modeling”, *Applied Microwave and Wireless*, Vol.12, No.5, pp. 42-46, 2000.

Optimize the Models about Temperature and Transitional Process by Numerical Elements

Ilya T. Tanchev[1] Ventceslav D. Draganov[2]
Nevena A. Avramova[3] Behidje K. Hacu[4]

ABSTRACT

This paper examines problems of simulation elements electronic in integrated area. After theoretical materials of principal work simulate processor ways and means - models, computers language at mathematic mean (numerical mean) suggest hold out method of optimization work point with simulate transistor poly-emission. Improvement takes only temperature interval for someone value, but method applicable for other parameters. In this manner it wise range.

Key word: **delay, retardation, transitional process, simulation.**

INTRODUCTION

By experience in any case delay is important by each logical operation. From theirs reality reflects subjection originality result of simulation. Still more logical operations ought, to one at this distance of time at delay of this operation. Once again that at work from

In

[1] Ilya T. Tanchev, Technical University of Varna, - department of Electronic – Varna, Studentska Str. №1, Bulgaria, E-mail: itta@ms3.tu-varna.acad.bg

[2] Ventceslav D. Draganov, Technical University of Varna, - department of Electronic – Varna, Studentska Str. №1, Bulgaria, E-mail: itta@ms3.tu-varna.acad.bg

[3] Nevena A. Avramova, ms Department Telecom, Technical University of Varna, E-mail: newenka@abv.bg

[4] Behidje K. Hacu, ms Department Telecom, Technical University of Varna, E-mail: newenka@abv.bg

logic operation they follow one a trace another and delay from it too grow.

Every time slight error of heaping and calculation set a task of error, inaccuracy at simulation. In practice oneself apply by discreet process simulation let optimize similar function. If models is digital, (numerical data) et description by means of VHDL, to work is difficult of access if need to standard function width at most just to the original. Partially determination of problem whit delay in models is theirs description in parts. This is enable to parts descript in standard in VHDL languish function

For every discreet element et his model in any case use the concrete kind. For example, to connected electrical elements in system present in one model else connected models.

Basic conception for description of digital electronic circuit scheme with electrical undone model is this en VHDL. This conception has an effect in many level of abstraction – from one logical element to total system hardware.

Per example: Management structure in VHDL is management port with reality value.

```
BEGIN
    word <= 00000, wait 10ns
    word <= 00001, wait 10ns
    word <= 00011, wait 10ns
    word <= 00111, wait 10ns
    word <= 11111, wait 10ns
END PROCESES
```

In environment VHDL there are two species retardation: momentum and transport. Delay in variable type or not lineal in VHDL not support. List roll is restricted by:

wait: - Process not activity from operation to finish
wait: **on** (follow list fro work)
wait: until (execute by condition)
wait: for (execute after definite time)

In many times necessary delay deferent in standard VHDL procedure. In that case procedure in VHDL takes standard value. In example present delay who answer in function but in the lab is indefinite, especially this lab is divide in phase et his is important.

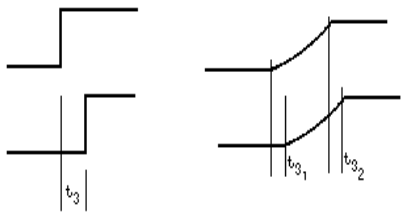

fig. 1. Transitional process

Serious dimension there are tension limit in models et time for this models via is it work. ect. (tu).

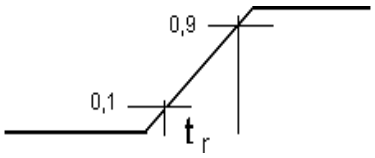

fig. 2. Transitional tension

In this paper suggest description on transitional process by divide this process in lab. A description is in dynamic work area, et account is standard functions in VHDL.

By descriptions in models used value et parameter function with who approach parameter in reality. In this way prevent some failing in investment procedure in program.

- Influence in temperature

With temperature variance in each elements of model set in considerable change in algebraic calculation in work the models. Par example for transistor - description mathematics by work model joint in ten characteristic equation and 29 parameters per each. [9]

Parameters is: $D_1, D_2, \alpha_{N0} I_1,$ $\alpha_1 I_2, G_{CE},$ $R_{BB^8}, R_{EE^8}, R_{CC^8}, Z_m I_B, C_{DE}, C_{DC}, C_{TE}, C_{TC},$ $I_{E0}(I_{C0}), M_E(M_C), T_E(T_C), \alpha_{N0}(\alpha_I), A_0, A_1, A_2, A_3$ $, G_0, G_1, G_2, C_{TE0}(C_{TC0}),$ $\varphi_E, n_E(\varphi_C, n_C), \tau_E(\tau_C),$ $T_0, T_1, T_2.$

with:

- If temperature not read $\Delta t^\circ = 0$ and many other parameters take on trust work out compromise and simplification of the model. Consequently decrease number of characteristic equation end many parameters in them is coefficient.
- If give an account temperature $\Delta t^\circ \neq 0$, have full number of characteristic equation.

WORK PROBLEM

Models and digital circles for digital simulation.

Models are abstract or materials system in spirit realization. This system reflected objects and be able to replacement. A reality object and replacement description is model. Make a study of information by object give norm for principal work models.

Models is categorize in differing indication, example: 1) by methods of reflection or else way re-create objects; 2) by methods of models work (law of the work); 3) by specific characteristic in original who investigate or reproduce in model e.t.c.

Classification of models according to construct is two big groups. : ideally and material.

1) Ideally model exist only in memory persons. To article pass in phase mental models. Each model in first exists in consciousness of the man as an image valid object, as the any theoretical circuit. All models who are created of the man except for that they imaginary they also are ideal independently that outward fixture in marks, figure, drawing or circuit. Are ideal character in model is caused in that all calculations in them are done(made) only in memory. Models in memory it interstitial product for construction material models. These models can a life in more full independent and that can not realize. It is a lot of ideal models can not realized actually.

2) Material models его of which all models use on is ready or with which are created artificial from the man. To material models of model be constructed from computers, it so are named numerical model. These models are usually actually and they are divided into three basic groups: spatial (geometric) kind, pphysically kind and mathematical kind.

- Spatial (geometric) models reflect spatial properties and attitude(relation) in the original. Similarity between sampler and original is based on geometrical similarity.
- Ratio between sampler and the object at physical similar samplers is based on physical similarity witch present identical physical law.
- At mathematical similar samplers similarity is based on mathematical analogy witch might be structural or functional.

This publication is searching for similarity by element's mathematical process. For example: it's used multiemitter transistor.

THEORETICAL VINDICATION

Let we look at the universal, non-linear constantan current transistor's sampler in two rates; static and dynamic.

It's made on the base of injection Eber-Mol's samplers witch is developed and refreshed as approach the mapping and mathematical description and characteristically parameter. The equivalent circuit of the universal sampler consists of elements witch expresses important physical effect and processes in transistor's structure. Mathematical sampler's description is by 10 characteristically equations with 29 parameters.

A part of constant current sampler's descriptions equations are the following:

$$I_1 = I_{E0} e^{T_E \Delta t^\circ} (e^{U_1 / M_E U_T} - 1) \quad (1)$$

$$I_2 = I_{C0} e^{T_C \Delta t^\circ} (e^{U_2 / M_C U_T} - 1) \quad (2)$$

$$\alpha_{N0}(t^\circ) = \alpha_{N0}^{(25^\circ)} + T_A \Delta t \quad (3)$$

$$\alpha_{N0} = A_0 + A_1 U_1 + A_2 U_1^2 + A_3 U_1^3 \quad (4)$$

$$G_{CE} = G_0 + G_1 I_1 + G_2 I_1^2 \quad (5)$$

Temperature potential U_T and temperature increasement Δt° are performed like diode (9) and (10).

Knowing of parameter's numerical value for certain type transistor gives a chance to perform all graphic transistors' characteristics by modulating equations during definite environment temperature. The mistake in the in to modulating of those dependences is under 5%.

In difference of transistor the ideal semiconductor diodes sampler with a junction and its VA characteristics are performed by the following equations:

$$I_d = I_s\left(e^{U_D/U_T} - 1\right), \tag{6}$$

където:

I_d , U_D diod's currents [A] and diod's voltage [V];

I_s - diod's saturation current (reverse current) [A];

U_T - temperature potential. It's definite by the formula (7):

$$U_T = \frac{kT}{q}, \tag{7}$$

where: k – Bolcman's constant ($k = 1{,}3810.10^{-23}$ [J/K]); T – absolute temperature, K; q – charge of electron; e – constant e = 2,71828 at indoor temperature (300 K), $U_T \approx 26$ mV.

Mathematical description to the diod's sampler uses equations for real diode:

$$Id = Ido.e^{Kd\Delta t}\left(e^{Ud/MdU_T} - 1\right), \tag{8}$$

$$\Delta t^{\circ} = t^{\circ} - 25^{\circ}, \tag{9}$$

$$U_T = \frac{t^{\circ} + 273}{11600}, \tag{10}$$

$$Rd = Q_0 + Q_1 Id + Q_2 Id^2 + Q_3 Id^3, \tag{11}$$

$$Rdy = \frac{Ud^{=}}{Id^{=}}, \tag{12}$$

Equation (9) is taking in to consideration the temperature's **t°** increase above the normal temperature 25° and gives a chance to be performed quantitative diod's temperature qualities with know approximation.

The parameter **Md** is emissitive and expresses constructive junction's specialties (special features).

EXPERIMENTAL INVESTIGATIONS

Has to a kind of the equation for calculations of the transistor and his about the diode - the temperature difference Δt is defined(determined) to one and too method. [9].

For change of temperatures for three value (15°, 25° ,35°,) is often equation vary in the following a kind [3]:

$$\alpha_{N0} = \alpha_{N0}^{(25^{\circ})} - 10T_A \tag{13}$$

$$\alpha_{N0} = \alpha_{N0}^{(25^{\circ})} \tag{14}$$

$$\alpha_{N0} = \alpha_{N0}^{(25^{\circ})} + 10T_A \tag{15}$$

The results can will be presented graphically if the temperature difference is measured correctly. On fig. 3. is presented $\Delta x'$ and $\Delta x''$ accordance +10 and -10 than $\alpha_{N0}^{(25^{\circ})}$. Within the framework of that range it is possible to make of optimization for models with which inspected.

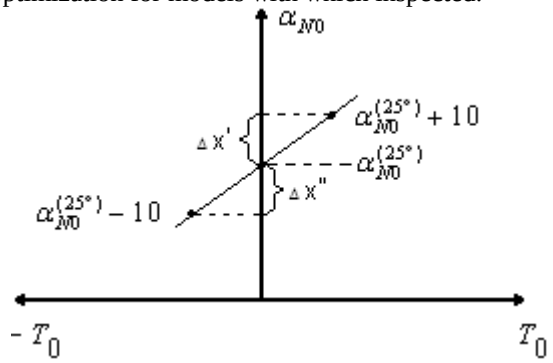

fig. 3. Temperature interval

INFERENCE

This means enable give a chance for process of mathematical calculation in optimization in models.

Element T_A by 25° is eliminate in participation by mathematical calculations.

Existence of coefficient T_A is necessary in fixed temperature interval. So itself reach many large (exact) approaches. Restriction is conditionally. (indicated three temperature is random elected).

CONCLUSION

In the publication is offered model semiconductor multiemitter transistor in which give additional parameters, in this case temperature difference. Which method is offered it is possible using and for other parameters in model of the transistor.

1. Optimization to concern to one exacted approach of transient (the description of transient for analog elements in digital environment).

2. With this way it is possible the interval watches (keeps up) of temperatures in is very much limited and then it is possible will receive 3D the image graphics. It is very important specialty for reception and calculation on thermal models and such working on integrated environment

REFERENCE

[1] Танчев Ил., В. Драганов, "Оптимизиране на преходни процеси при дискретни модели за симулация чрез VHDL в електрониката" , *Юбилейна конференсия на ТУ*, ТУ Варна , България, 2003 г.

[2] Танчев Ил., В. Драганов, Хр. Жекова, "Оптимизиране процесите за симулация". ТУ-Габрово , България, 2003

[3] Танчев Ил., " Оптимизиране закъсненията при дискретни модели чрез VHDL". ВТУ – Каблешков *13-конференция* TRANSPORT-2003, България

[4] Танчев Ил. , Моделиране на непрекъснати сигнали чрез дискретни модели в интегрирана среда, *6-та конференция Еко-Варна*, ТУ Варна, 2003г,.

[5] Райковска Л., И. Танчев, В. Драганов, П. Иванова " Интегрирана среда за проектиране, анализ и документиране на аналогови електронни схеми на базата на OrCAD и PSpice" *Юбилейна конференсия на ТУ Варна*, 1993г. ТУ Варна , България

[6] Uyemura P. , Circuit design for CMOS VLSI, Kluwer Academic , 1993

[7] Weste N. K. Eshraghian, Principles of CMOS VLSI Design, 1993

[8] Ayeres F. , VLSI Silicon Compilation and the art of automatic Microchip design, Prentice-Hall, 1983.

[9] Боянов, Й., Л. Райковска., В. Фурнаджиев. Автоматизация на проектирането и конструирането в електрониката. Техника, София, 1991г.

[10] Боянов,Й., Л. Райковска, Д. Механджийска, Ръководство по автоматизация на проектирането в електрониката, София, Техника, 1993.

ISCAS-85 Netlist Translator into VHDL Code

Neša P. Tomić[1] and Mile K. Stojčev[2]

***Abstract* – Benchmark circuits are mainly intended to support the research in the area of high-level automatic test pattern generation during production of VLSI ICs. For ease of development of new test tool, the benchmarks have to be standardized both in term of description styles and languages. The VHDL language has been adopted as one of the standard for description of electronic circuits. ISCAS-85 are the most popular benchmark circuits used for performance evaluation and testing of VLSI ICs, but they are described in a netlist format which is inconvenient for CAD tools. In this paper we describe an algorithm for ISCAS-85 benchmark circuit netlist translation into VHDL code.**

***Keywords* – Benchmark, ISCAS-85, VHDL, Translator.**

I. INTRODUCTION

Benchmarks are important vehicles that let industry and academia to develop new tools, compare and contrast different methodologies, and research new algorithms and techniques [1]. During the last thirty years, there have been many attempts to create and use neutral benchmarks for tool evaluation and comparison.

We will define here, benchmark as a standardized problem (circuit or circuit segment) used to compare performance of different tools and algorithms in term of speed, effectiveness, and quality of the result [2]. Typically, a benchmark set consists of a collection of circuits in a common format, which attempt to represent a range of problems for evaluating algorithms and tools within an important problem domain [3].

Nowadays, several benchmark sets are widely used. Among them, ISCAS-85, ISCAS-89, ITC'99, and Politecnico di Torino, are the most popular. In this paper we will focus our attention to ISCAS-85, especially to conversion its netlist into VHDL code, because these benchmarks represent a wide variety of problem domains and are by far the most frequently cited of all benchmarks [3].

Namely, as designers we will use reverse engineering approach in order to determine system specifications, output functions, or other design characteristics from an existing implementation, in a form of VHDL code, for a given set of benchmark circuits.

ISCAS-85 benchmark set of circuits are industrial designs whose functions and high-level designs have not been published, both for confidentiality reasons and to allow them to be viewed as random logic circuits with no significant high-level structure [4]. In this way, instead of using ISCAS-85 netlists, we will use corresponding VHDL codes, which allow us better understanding of benchmark circuit's hardware structure.

The rest of the paper is organized as follows: Section 2 gives a short overview of benchmark circuit types. Section 3 deals with ISCAS-85's netlist format example. In Section 4 the proposed algorithm concerning ISCAS-85 to VHDL code translation is given. Finally, Section 5 is Conclusion.

II. OVERVIEW OF POPULAR BENCHMARK SETS

In the sequel, we will describe briefly some of the most popular benchmark sets.

ISCAS-85: consists of collection of 10 benchmarks contributed by the number of individuals and organizations over a period of 20 years. These benchmark circuits are well-defined, high-level structures and functions based on common building blocks such as MUXs, ALUs, decoders, counters, etc [4].

ISCAS-89: These are a set of 31 digital sequential circuits. Each circuit is described in two files: a generic gate-level netlist and a list of equivalence-collapsed faults. A simple translator is included to read/write the netlist. There are no schematic diagrams [5].

ITC'99: This set of benchmarks provides a realistic example circuits to stress current automatic test-pattern generation (ATPG) algorithms, to provide impetus for the development of new automatic test-pattern generation and design for testability (DFT) algorithms, and to encourage research into fundamental DFT problems for large, complex designs [3]. They are written in either of two hardware description languages: Verilog or VHDL.

Politecnico di Torino: These high-level benchmarks are represented in synthesizable register transfer level (RTL). For their description VHDL is used.

Analog and mixed signal: This set currently include amplifier, filters, an analog/digital converters, PLL, switches and additional circuits that can be added to the set [7].

Other useful benchmark sets are available at various universities and institutes worldwide: Texas Formal Verification Benchmark, IFIP WG10.5, STEED, etc [3].

III. ISCAS-85 NETLIST FORMAT EXAMPLE

The ISCAS-85 netlist format was never formally documented, but it becomes viable despite its shortcomings, since it contains information not present in most other netlist formats.

The netlist format of a small ISCAS-85, six-NAND-gate benchmark circuit, known as "c17" [6] is listed below (see

[1] Neša P. Tomić is with the Faculty of Electronic Engineering, Beogradska 14, 18000 Niš, Serbia and Montenegro, E–mail: nesto@eunet.yu

[2] Mile K. Stojčev is with the Faculty of Electronic Engineering, Beogradska 14, 18000 Niš, Serbia and Montenegro, E–mail: stojcev@elfak.ni.ac.yu

Fig. 1), for which in Section 4, a corresponding VHDL code will be presented.

As can be seen from Fig. 1 each line consists of several columns, which are mutually separated by delimiters (space, tab, new line). Naming of each column with its description is given in Table I.

```
* These first five lines are comments.
* The comment character is the "*" (asterisk).
* The comment character may appear anywhere on a
* line and remains in effect until the end of
                    * the line is reached.
  1    1gat inpt   1   0           >sa1
  2    2gat inpt   1   0           >sa1
  3    3gat inpt   2   0    >sa0 >sa1
  8    8fan from    3gat          >sa1
  9    9fan from    3gat          >sa1
  6    6gat inpt   1   0           >sa1
  7    7gat inpt   1   0           >sa1
 10   10gat nand   1   2           >sa1
  1    8
 11   11gat nand   2   2  >sa0 >sa1
  9    6
 14   14fan from   11gat          >sa1
 15   15fan from   11gat          >sa1
 16   16gat nand   2   2  >sa0 >sa1
  2   14
 20   20fan from   16gat          >sa1
 21   21fan from   16gat          >sa1
 19   19gat nand   1   2           >sa1
 15    7
 22   22gat nand   0   2  >sa0 >sa1
 10   20
 23   23gat nand   0   2  >sa0 >sa1
 21   19
```

Fig. 1. ISCAS-85 netlist format for c17 benchmark circuit

Table I. Description of column notation

Address	Unique number for given node
Name	Descriptive string of characters related to the corresponding node
Type	Function performed by a given node (inpt, and, nand, or, nor, xnor, xor, buff, not, from)
Fanout	Number of gates connected to the output of given node
Fanin	Number of nodes which represent inputs to the given node
Fault(s)	Stuck-at-fault(s) on given node that are included in the fault set. Possible values are >sa0 for stuck-at-zero and >sa1 for stuck-at-one

Three types of lines in the netlist (Fig. 1) can be identified. The first, so called **node line** (typical for line 1-Fig. 1), gives basic information about the node. The second, referred as **fanin line** (the first line after node address 10), corresponds to the list of node addresses that drive inputs for a given node. This line appears immediately after node line with *fanin* value greater than 0. The number of addresses that appear in fanin line is identical to the *fanin* number in corresponding node line. The third type of line is called **fanout branch line** (the line with node address 8). This line use similar notation like node line, except the field *type* always takes value *from*, and information from which address this branch starts. This line appears immediately after corresponding node line (and its fanin line).

Each node has *fanout* value greater than 0, excluding primary circuit outputs that have *fanout* value 0.

More details about netlist syntax can be found in [6].

IV. Description of Translation Algorithm

Usually, when engineers create new design, they use standard building blocks for which they know functionality and hardware structure. On the other hand, benchmark circuits are “anonymous neutral circuits” of unknown functionality, but they are mainly used for efficient objective testing of the implemented algorithms. The main disadvantage of ISCAS-85 benchmark circuits is that their descriptions are given in netlist format. Such format is inconvenient for designers, who more prefer high-level or schematic circuit description.

Let us note that ISCAS-85 benchmark circuits are complex circuits with 160 to 3500 gates, 36 to 207 inputs and 7 to 140 outputs. For explanation of the proposed algorithm, without violating its generality, we have chosen one simple circuit, primarily due to limited space of this paper.

In order to obtain a descriptive readable format, acceptable for designer, a code translator has been developed. The translator accepts ISCAS-85 netlist as input, and generates VHDL code as output. The program was developed using Microsoft Visual Basic 6.0.

At the beginning of the program, a start form appears on a display (see Fig. 2), with command button for input ISCAS-85 netlist file selection (upper command button). This file must be textual (with .txt extension).

After file has been selected, we can see the message on the form, which file was chosen.

Fig. 2. Start Form

The translation process starts since the second command button is pressed (lower command button). After that, the name for the VHDL code file must be entered, the entity name for the whole circuit, and the architecture name (software offers default name as the entity name).

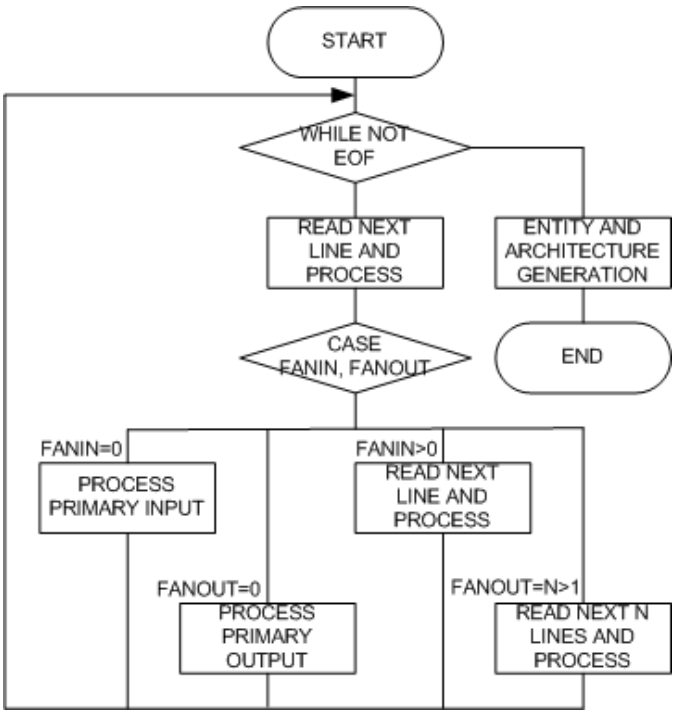

Fig. 3. Translator Algorithm

Program reads line by line, recognizes the type of line and parses data according to text delimiters (tab or space). Empty lines and lines which start with "*" (comment lines) are not taken into consideration, and software continues with reading of the next line. Parsed data are stored in corresponding dynamic data arrays, where each array represents one column from the netlist.

When one line is read, *fanin* and *fanout* values are analyzed (see Fig. 3). These values determine the type of line. If the *fanin* value is 0, this line represents node which corresponds to primary circuit input. If the *fanout* value is 0, than that line represents primary circuit output. If the *fanin* value is greater than 0, program reads the next line, where addresses of nodes, as inputs of a given node, are specified. These addresses, together with node address and its fanin number, are stored in auxiliary dynamic matrix, which is used later for port mapping.

If the *fanout* value is $n>1$, the program reads the n following lines, that represent nodes as branches from node, for which *fanout* value was n. These node addresses are also used for internal signal generation in VHDL code.

Since all lines from netlist are read, according to data structure from dynamic arrays, a VHDL code is generated. In the header of this VHDL code, the list of all gates that appear in the netlist is cited. After generation of entity definition (all primary inputs and outputs are identified), created program begins with architecture definition generation. First of all, the list with all internal signals is generated (all nodes with *fanout* greater or equal to 1). After that algorithm creates port mapping section (gate inputs connected to other gates outputs) for each node (gate), according to data structure stored in auxiliary dynamic matrix. At the end of VHDL code generation, a final message about successful translation finalization and location of the generated file (see Fig. 4) is reported to the designer.

Fig. 4. Final Message

The listing of the VHDL code which correspond to the c17 netlist is presented in Fig. 5.

```
------------------------------------------------
-- In this circuit the following gates are present
-- and must be added into CAD tool in order to complete
analysis:
--
--          nand2   -->        nand     with number of inputs 2

------------------------------------------------


library IEEE;
use IEEE.STD_LOGIC_1164.all;

entity c17 is
        port (
                1gat_in_port : in STD_LOGIC;
                2gat_in_port : in STD_LOGIC;
                3gat_in_port : in STD_LOGIC;
                6gat_in_port : in STD_LOGIC;
                7gat_in_port : in STD_LOGIC;
                22gat_out_port : out STD_LOGIC;
                23gat_out_port : out STD_LOGIC
            );
end entity c17;

architecture c17 of c17 is
signal int_10gat, int_11gat, int_16gat, int_19gat :
std_logic;
begin
  10gat : entity work.nand2(nand2)
    port map (1gat_in_port, 3gat_in_port, int_10gat);
  11gat : entity work.nand2(nand2)
    port map (3gat_in_port, 6gat_in_port, int_11gat);
  16gat : entity work.nand2(nand2)
    port map (2gat_in_port, int_11gat, int_16gat);
  19gat : entity work.nand2(nand2)
    port map (int_11gat, 7gat_in_port, int_19gat);
  22gat : entity work.nand2(nand2)
    port map (int_10gat, int_16gat, 22gat_out_port);
  23gat : entity work.nand2(nand2)
    port map (int_16gat, int_19gat, 23gat_out_port);
end architecture c17
```

Fig. 5. VHDL code for c17 ISCAS-85 benchmark circuit

According to the VHDL code listed in Fig. 5, the designer now can draw a schematic of the circuit, analyze its function. In our case, the schematic of c17 is given in Fig. 6.

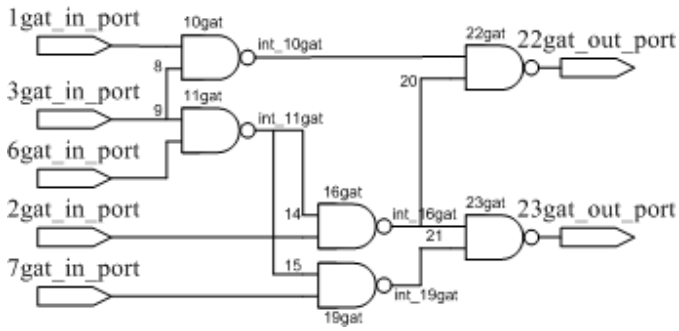

Fig. 6. c17 Schematic

The generated VHDL code obtained from ISCAS-85 benchmark circuit netlist can be used for testing some other application specific circuits. In order to realize that analysis, it is necessary to add all gates cited in the header of created VHDL code, into the VHDL project, i.e. to give their entity and architecture description.

V. Conclusion

Effective high-level automatic test pattern generation tools are increasingly needed as an essential element in the quest for reducing as much as possible the designer work on gate-level descriptions. One of the crucial parameters for speeding up and making more effective the design evolution process in any technical research is the availability of suitable and meaningful benchmark.

ISCAS-85 are one of the most popular benchmark circuits used for performance evaluation and testing of VLSI ICs. Unfortunately, they are described in a netlist format which is inconvenient for CAD tools and designers themselves. Having this in mind, in this paper we describe a suitable algorithm for ISCAS-85 benchmark circuit netlist translation into VHDL code, which, in our opinion, will be of great benefit for VLSI IC designer, during the phase of testing and performance evaluation of their solutions.

References

[1] Basto L., “First Result of ITC’99 Benchmark Circuits”, IEEE Design & Test Computers, Vol. 17, No. 4, pp. 54-59, 2000.
[2] Davidson S., Harlow J., “Introduction: Benchmarking for Design and Test”, IEEE Design & Test Computers, Vol. 17, No. 4, pp. 12-14, 2000.
[3] Harlow J., “Overview of Popular Benchmark Sets”, IEEE Design & Test Computers, Vol. 17, No. 4, pp. 15-17, 2000.
[4] Hansen M., Yalcin H., Hayes J., “Unveiling the ISCAS-85 Benchmarks: A Case Study in Reverse Engineering”, IEEE Design & Test Computers, Vol. 16, No. 4, pp. 72-80, 1999.
[5] http://www.cbl.ncsu.edu/pub/Benchmark_dirs/ISCAS89/DOCUMENTATION/iscas89.ps.
[6] http://www.cbl.ncsu.edu/pub/Benchmark_dirs/ISCAS85/DOCUMENTATION/iscas85.ps.
[7] http://www.ee.washington.edu/research/mad/benchmarks/benchmarks.html.

Most Possible Zones for Discharge Initiation in a Vacuum Interrupter under Test

Raina Tzeneva[1] and Peter Dineff[2]

Abstract **- Nowadays, the best method to measure the pressure inside a vacuum circuit interrupter designed to operate at pressures of 10^{-4} Torr and lower is the magnetron. A cold-cathode magnetron ionization principle is employed to measure pressure within the vacuum interrupter through the use of the existing interrupter elements as the principal parts of an ionization gauge and by immersing the vacuum apparatus in a magnetic field.**

The role of a metallic vapor-condensing shield of tubular configuration as a collector of positive ion current for creating the characteristic torus-shaped plasma regions in the internal space of a vacuum apparatus is revealed by appropriate modeling of the electric and magnetic fields.

Keywords **- Cathode magnetron ionization principle, Magnetron pressure measurement method, Metallic vapor-condensing shield, Vacuum circuit interrupter.**

I. INTRODUCTION

Measuring the pressure in a *vacuum circuit interrupter* (*VCI*) has always been a great problem for manufacturers of vacuum switchgear. A factory-made *VCI* is not able to maintain its internal pressure forever, yet its shelf life is longer than ten or twenty years and customers want to be sure that pressure in the vacuum envelope won't increase considerably during this period. Thus, one needs a technique that can provide detection of residual pressure alteration in *VCI*, [6].

Nowadays, the best method of measuring the pressure inside a vacuum envelope is the magnetron. A cold-cathode magnetron ionization principle is employed for measuring the pressure within the vacuum interrupter by using the existing interrupter elements as the principal parts of an ionization gauge and by immersing the vacuum circuit apparatus in a magnetic field.

The *VCI* comprises an evacuated sealed envelope, a pair of separable contacts or electrodes within the envelope, which are movable from an engaged position to a spaced-apart position to define an arcing gap therebetween, and a *metallic vapor-condensing shield* (*MVCS*) of tubular configuration surrounding the gap and electrically isolated from at least one of the electrodes by an evacuated space surrounding said electrode [3, 6, 7].

[1]Raina T. Tzeneva is with the Faculty of Electrical Engineering, Department of Electrical apparatus, Blvd. Kliment Ohridski 8, 1000 Sofia, Bulgaria, E-mail: tzeneva@tu-sofia.bg

[2]Peter D. Dineff is with the Faculty of Electrical Engineering, Technical University of Sofia, Blvd. Kliment Ohridski 8, 1000 Sofia, Bulgaria, E-mail: dineff_pd@abv.bg.

There are four possible cases of realizing a diode ionizing gauge for measuring the pressure inside the *VCI* vacuum envelope with the participation of *MVCS* as a cathode of a cold-cathode ionizing gauge, Fig. 1, or as an anode – not shown as an execution variant in Fig. 1:

♦ As a cathode *MVCS* performs the part of a collector for measuring the ion current, and the two contacts of *VCI* are closed and have the same potential, i. e. they represent an anode, Fig. 1a;

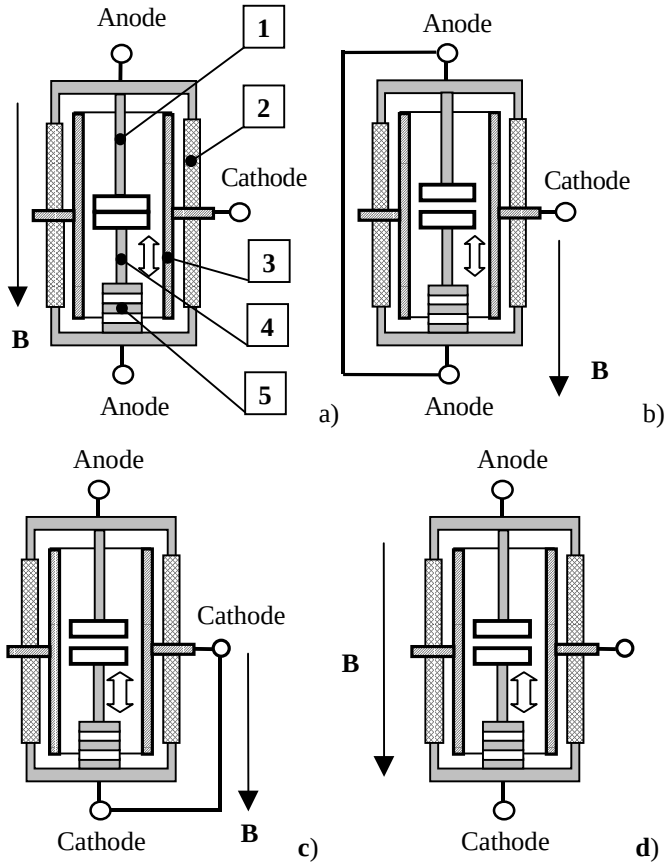

Fig. 1. Principal parts of a vacuum circuit interrupter performing the part of a diode ionization gauge (a) for measuring the pressure inside the vacuum sealed envelope and the way of participating of the metallic vapor-condensing shield (*MVCS*): **a** – for a closed electrode system and negative potential at *MVCS*; **b, c** - for an opened electrode system and negative potential at *MVCS*; **d** – for an opened electrode system, *MVCS* having a floating potential.

1 – fixed electrode; **2** – insulation cylinder; **3** - metallic vapor-condensing shield; **4** – movable electrode; 5 - bellows.

♦ *MVCS* may be a cathode again, depending on its electrical connection to one of the two electrodes, Fig. 1c;

♦ *MVCS* participates indirectly in the measurement, remaining with a floating potential, fig. 1d. This case is

characteristic for *VCI*, the *MVCS* of which has no terminal outside the vacuum-sealed envelope of *VCI*.

T. Lee (1957) patented a triode ionizing gauge for measuring the pressure, but these technical solutions dropped off in the subsequent development of this issue, [6].

All variants shown are realizable only in the presence of an electric terminal of *MVCS* outside the vacuum envelope.

In all described cases of measurement *MVCS* performs the part of a cathode that collects positive ions moving towards it. The arrival of these positive ions at the cathode results in a current flowing through the cathode. The magnitude of this current is indicative of the pressure in the interrupter, Fig. 1.

THE TASK of the present work consists in revealing the participation of the metallic vapor-condensing shield in the occurrence and maintenance of a cold-cathode magnetron discharge in the space between the anode and the cathode of an ionizing gauge inside the evacuated envelope of *VCI*.

II. GENERAL FORMULATION OF THE INVESTIGATIONS

From the theory of Penning's discharge it is well known that at using weak magnetic fields – having minimal magnetic flux density **B** below 20 mT – and at pressures below 10^{-4} Torr a maximally uniform distribution of the negative volumetric charge is obtained. Under these conditions the discharge exists in its steady state without any electromagnetic radiation. The percentage of the electron component in the cathodic (discharge) current does not exceed a few hundredths. The theoretical model agrees well with the results from the experimental investigations, [1].

Discharge current I_p varies with applied anode potential V_a in the following manner [1]:

$$I_p = M\left[2(V_a - V_0) - V_0\left(r_a \big/ l^2\right)\right] a\ p\ l_a \qquad (1)$$

$$M = \frac{1 + \left(1 - \beta^2 \big/ 2\omega^2\right)^{0.5}}{2\left(1 - \beta^2 \big/ \omega^2\right)^{0.5}} \qquad (2)$$

$$\beta^2 = 2\,e\,(V_a - V_0)/\,m_e\,r_a{}^2 \qquad (3)$$

$$\omega = e\,B\,/\,2\,m_e \qquad (4)$$

where p is the pressure; a – a constant that depends on the nature of the gas; V_0 – the potential at the center of the *Penning's cell*; e, m_e – the electron charge and mass; r_a, l_a – radius and length of the *Penning's cell.*

From Eq. (1) it follows a conclusion, which is important for the measurement of pressure p, namely that the intensity of Penning's discharge is constant in the so-called first regime of burning:

$$I_p \big/ p = const \ \text{ or } \ I_p = k\ p\,, \qquad (5)$$

where k is a coefficient depending on gauge construction.

This relationship lies at the basis of the operation of the ionization vacuum gauges of the so-called Penning's vacuum gauges, [5].

There are also patented proposals of including the cold-cathode ionization gauge as a separate measurement element in the construction of *VCI*, [3, 6].

Measuring the pressure in a sealed envelope by means of the contact system of *VCI* transforms the Penning's gauge into a magnetron-type diode ionization gauge, Fig. 2.

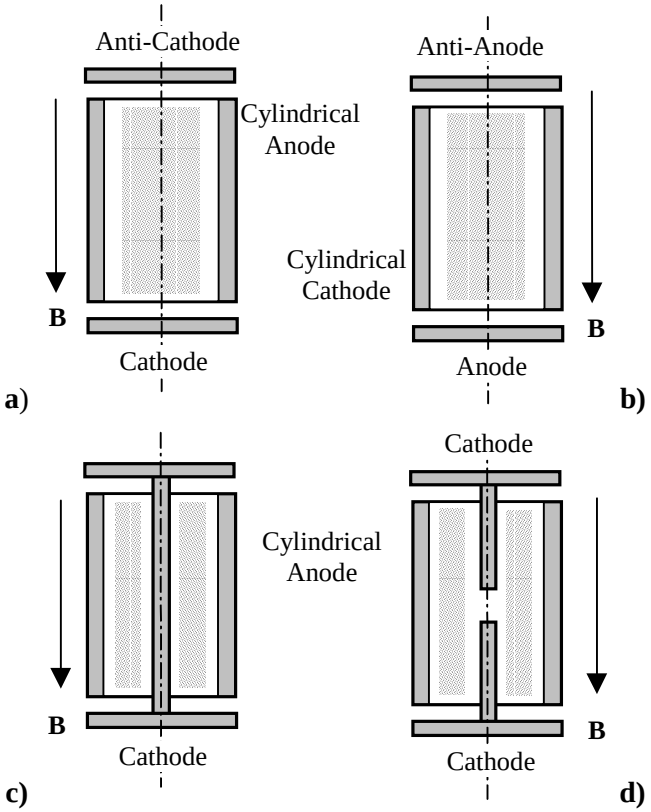

Fig. 2. Principal configurations of Penning's discharge - basic (**a)** and inverse (**b**), and of the magnetron ionizing discharge - basic with one cathode (**c**) and basic with a two-part cathode - cathode and anti-cathode (**d**) in a diode ionizing gauge.

The principle of permanence of discharge intensity I_p remains in force also for the basic and inverse cold-cathode magnetron ionization discharge, which allows performing the pressure measurement in *VCI* under the same conditions.

The difference consists in the manifestation in this case of a power law instead of the linear one [3, 7]:

$$I_p \big/ p^n = const \ \text{ or } \ I_p = k\ p^n\,, \qquad (6)$$

where n is the exponent, the value of which most often is $n = 1.1$ in the most frequently used constructions.

As Eq. (6) has been obtained empirically from the investigation of real constructions, it should be assumed the understanding of the fact that the increase in exponent *n* mirrors not only the transition to magnetron ionization discharge, but also the rotational non-cylindrical form of *MVCS*, the creation of a labyrinth transition from the space inside *MVCS* to the volume in front of the insulation cylinders with the purpose of protecting it against metal vapors, etc., Fig. 4.

Lucek and *Pearce* [3], have already informed about the fact that modifying the construction of flanges with the purpose of creating the labyrinth transition leads to instability of the magnetron discharge and cathodic current. Our investigations performed on such modern constructions indicate that in this case it is most appropriate to use the circuit of inverse magnetron ionizing discharge, i. e. *MVCS* becomes a cathode in accordance with Fig. 1a.

III. RESULTS AND DISCUSSION

The *MVCS* role is examined in two basic cases of measurement: ♦ the measurement circuit or the first model in accordance with Fig. 1a and ♦ the measurement circuit or the second model in accordance with Fig. 1d.

A vacuum circuit interrupter is immersed in the magnetic field of two Helmholz's coils located co-axially with respect to each other, the magnetic flux density of which is directed along the axis of the vacuum device, Fig. 3a.

Using modern software products, simulation is conducted for the 2D-distribution of the axially symmetrical magnetic field of Helmholz's coils, in which *VCI* is immersed.

The technical solution selected creates a relatively uniform magnetic field all through the volume of the vacuum sealed envelope, which ensures the same conditions for the manifestation of the cathode magnetron ionization principle in different regions of discharge burning, Fig. 3b.

This allows estimating the effect of the three characteristic zones of the magnetron ionizing discharge in the volume of *VCI* upon the magnitude of the positive ion current consisting respectively of three components, each of them corresponding to one of the following discharge regions:

♦ higher region of discharge between the fixed contact flange and the top part of *MVCS* – in the region of the upper labyrinth sealing;

♦ central region of discharge between the contacts that touch each other and *MVCS* for the first model of measuring or in the intercontact region and between the opened contacts and the middle part of *MVCS*;

♦ lower region of discharge between the movable contact flange, bellows and bottom part of *MVCS* – in the region of the lower labyrinth sealing, Fig. 4.

By using software products based on the numerical method of finite elements, two distributions of electric field intensity |**E**| are obtained. Each of these distributions corresponds to the selected variant of pressure measurement performed by measuring the positive ion current, Fig. 4.

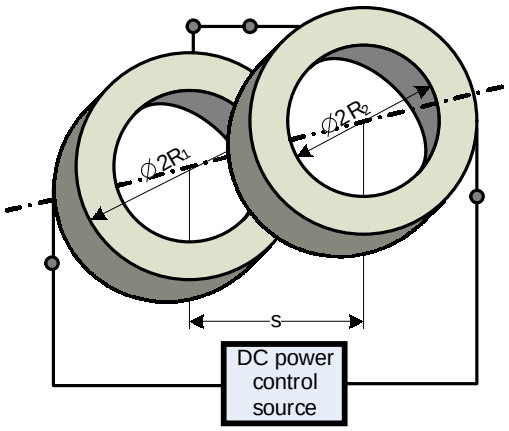

a)

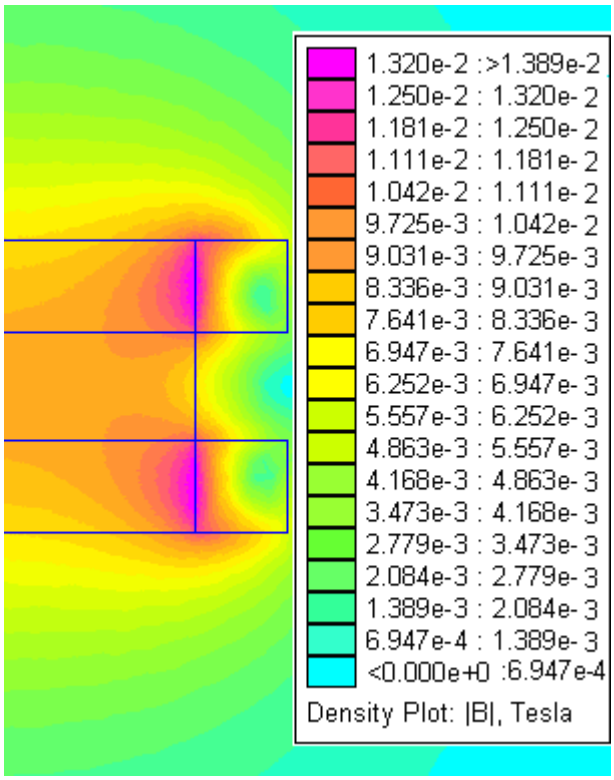

b)

Fig. 3. Modeling the distribution of the magnitude of magnetic flux density **B** along the axis of the two Helmholz' s coils (**a**), one of which is placed under the other and which create a relatively uniform magnetic field (**b**) in the whole volume of the vacuum circuit interrupter.

The relatively uniform electric field makes visible the regions of burning of the magnetron ionizing discharge, which form the common ion current. Moreover, from the magnitude of the intensity of electric field **E** in the corresponding region it is possible to estimate, although roughly, the contribution of each region to the value of the common ion current.

In both cases of participation of *MVCS* in the circuit of measuring the pressure in *VCI*, as a basic element of the magnetron ionization gauge, it is possible to take into account the strong influence exerted by the two regions of labyrinth transitions of the vacuum sealed envelope upon the cathodic current.

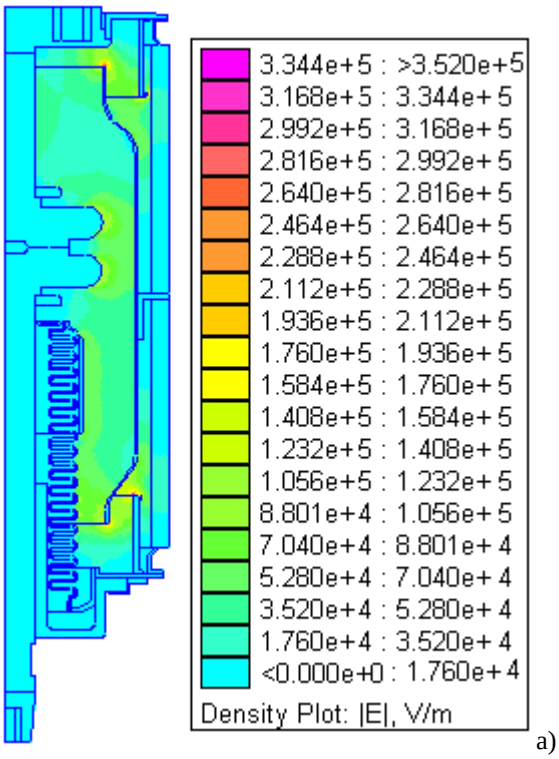

a)

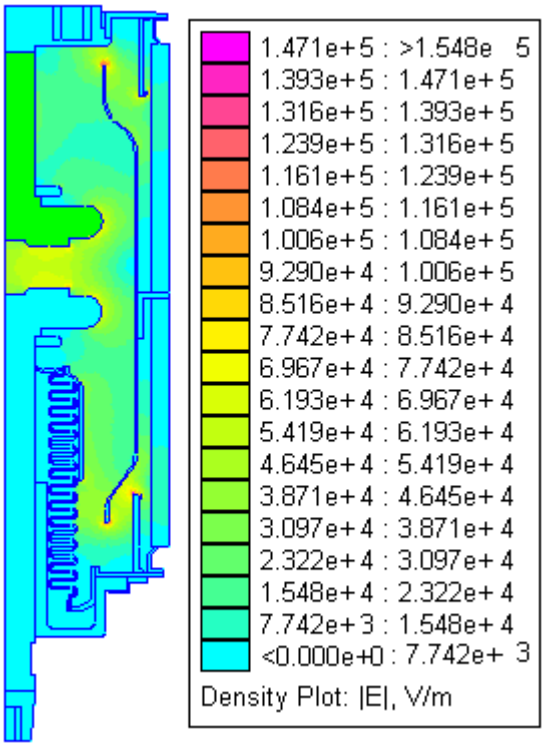

b)

Fig. 4. Distribution picture for the magnitude of the electric field intensity |**E**| in the volume of *VCI* for a closed contact system and *MVCS* electrically powered as a cathode (**a**) and left in the state with floating potential (**b**).

The maximal values of intensity |E| of the electrical field in the corresponding regions of the magnetron ionizing discharge are shown in Table 1.

In both cases of investigation it is obvious that the contribution of the lower labyrinth transition and the bellows region to the magnitude of discharge current is considerably higher – with 91 percent (model 1) and with 64 percent (model 2) – with respect to the central region of the discharge.

TABLE 1.

REGION OF MAGNETRON IONIZING DISCHARGE	MAXIMAL VALUE OF ELECTRICAL FIELD INTENSITY, V/m
MODEL OF MEASURING 1	
Higher discharge region	219
Central discharge region	121
Lower discharge region	232
MODEL OF MEASURING 2	
Higher discharge region	134
Central discharge region	86
Lower discharge region	142

For the labyrinth transition shown above this difference is considerably smaller – respectively with 80 percent (model 1) and with 56 percent (mode 2), Table 1.

The difference between the two central zones of the magnetron discharge amounts to about 41 percent in favor of the circuit with *MVCS*-cathode.

IV. CONCLUSION

Watrous (1971) patented a magnetron circuit for direct pressure measurement with local action of the magnetic field in the central zone of *VCI*, [7].

The investigation performed indicates that this may be even more successfully carried out locally also in the zone of each of the two labyrinth transitions.

The simultaneous involving of the three characteristic discharge regions with the participation of *MVCS* increases sharply the sensitivity of the magnetron method of pressure measurement.

REFERENCES

[1] G. L. Saksaganski, Electro-physical vacuum pumps, Moscow, Energoatomizdat, 1988 (in Russian).
[2] J. D. Cobine and J. M. Lafferty, Vacuum device gas measurement apparatus and method, US-Patent Appl. No 3,495,165, Patented Feb. 10, 1970.
[3] J. R. Lucek and W. J. Pearce, Apparatus and method for measuring the pressure inside a vacuum circuit interrupter, US-Patent Appl. No 188,991, Patented July 26, 1966.
[4] P. Dineff, Electrotechnology. Introduction to electrotechnology. Technical University, Sofia, Bulgaria, 2000 (in Bulgarian)
[5] P. A. Redhead, Ionization vacuum gauges, US-Patent Appl. No 3,051,868, Patented Aug. 28, 1962.
[6] T. H. Lee, Pressure measuring arrangement for a vacuum circuit interrupter, US-Patent Appl. No 2,864,998, Patented Dec. 16, 1958.
[7] W. W. Watrous, Method and apparatus for measuring pressure in vacuum interrupters, US-Patent No 3,575,656, Patented Apr. 20, 1971.

Metrological Support of Electronic Energy Meters Production

Bozidar B. Dimitrijevic[1], Ivana S. Randjelovic[2] and Milica P. Rancic[3]

Abstract **- An automated calibration procedure developed for metrological assurance of the gauging procedure in electronic energy meters production is described in this paper. In the framework of the project sponsored by the Ministry of science and technology in Serbia, mentioned gauging procedure is developed using a PC control software tool LabVIEW and 8-channel acquisition card PCI-NI 6713. Advantages of virtual instrumentation software opposite to standard programming methods are used for evaluation of measuring uncertainty, especially the component introduced by the DAQ card, which is specifically analyzed. Controlled performance of each function and component of the system is provided, as well as their analyzed influence on the accuracy of the whole system.**

Keywords **- automated calibration, virtual instrumentation, gauging energy meters**

I. INTRODUCTION

Rapid growth in key technologies, such as information technologies, involves more accurate measurements over much wider value and parameters range, as well as reduction of time needed for measurement procedure to be fulfilled. Improvement of calibration systems in electric energy meter production is especially important for industry as well as for energy traffic manager centers. Investment in development of these systems is economically reasonable because of falling costs in quality control procedure during the production process.

Besides all advantages that automation calibration procedure offers, many known designed calibration systems use expensive etalon energy meters regardless to the applied level of automation [1]. In that case, employed computer is not shared for attaining adequate accuracy class of the produced energy meters under test. A recalibration system without etalon energy meter that involves a computer becomes an intelligent measurement station in the production process that scopes automated test procedures and higher throughput and capacity.

Various systems of this kind are employed worldwide, with a final goal of complete automation. Automated process, based on application of the PC computer and virtual instrumentation software would significantly save time needed for calibration and presentation of results obtained during that process. There are already few completely automated systems employed in the world, and in our country, with similar characteristics [2,3]. For example, the System Century Controls Company from India now offers a fully automatic energy meter calibration [4].

In the framework of our project an automated system for gauging of new type of kWh meters, which are produced in the Ei - "Professional Electronics" factory in Niš, is being developed. The principal goal of our project is to develop a new traceability/calibration procedure for metrological assurance of the automated gauging system in the production of a new type of electronic kWh meters.

II. PRELIMINARY REQUIREMENTS AND TECHNICAL CHARACTERISTICS

Necessary conditions for rising technological quality of kWh meters to a higher level are accomplished by designing and realizing of the automated gauger using modern information technologies in the field of measurements. In addition, optimization regarding the needed time and testing expenses in accordance with up-to-date requirements of domestic and foreign market is also provided. Use of the PC computer and virtual instrumentation software significantly saves time needed for calibration and presentation of results obtained during that process, as well as it provides secure level of quality, reliability, and accuracy appointed by the corresponding standards for measuring of electrical energy.

Fig. 1 depicts symbolic logic connection of IBM PC and its needed peripheral hardware devices (PCI-NI 6713, SCB-68) as a constituent part of automated calibration system. The Calibrator Metratop53 is used periodically according to issued rules for the legal traceability. Using a software procedure further described in the paper, calibrated voltages as references for energy meters gauging are obtained at six analogue outputs of the 68-Pin Shielded Connector Block (SCB-68). The accuracy of calibrated voltage and current references is reduced due to subsequent analogue processing in the gauger. Correction of the reduced accuracy of set magnitude and phase of three-phase voltages and currents that are brought to energy meters under test is achieved by embedded self-calibration technique.

A global functional scheme of the automated gauger and its working principle are shown in Fig.2. Preliminary requirements, which concrete modules should fulfill, are defined and are as follows:

The gauger is designed for automated and semiautomatic simultaneous calibration and gauging up to twenty kWh meters of following types:

- Direct mono-phase kWh meters for reactive and active electrical energy measurement;
- Direct three-phase kWh meters for reactive and active electrical energy measurement;
- Indirect kWh meters for reactive and active electrical energy measurement;

[1] Božidar B. Dimitrijević is with the Faculty of Electronic Engineering, University of Niš, Aleksandra Medvedeva 14, 18000 Niš, Serbia and Montenegro, e-mail: dimitrijevic@elfak.ni.ac.yu

[2] Ivana S. Ranđelović is with the Faculty of Electronic Engineering, University of Niš, Aleksandra Medvedeva 14, 18000 Niš, Serbia and Montenegro, E-mail: rivana@elfak.ni.ac.yu

[3] Milica P. Rančić is with the Faculty of Electronic Engineering, University of Niš, Aleksandra Medvedeva 14, 18000 Niš, Serbia and Montenegro, E-mail: milica@elfak.ni.ac.yu

There is a possibility of simultaneous calibration of kWh meters with same characteristics and of different type, e.g.:

- Mechanical kWh meters which obtain the information about the measured energy using optical reading head;
- Electronic kWh meters which obtain the information about the measured energy at the test output;
- Digital kWh meters, which obtain the information about the measured energy at the optical port.

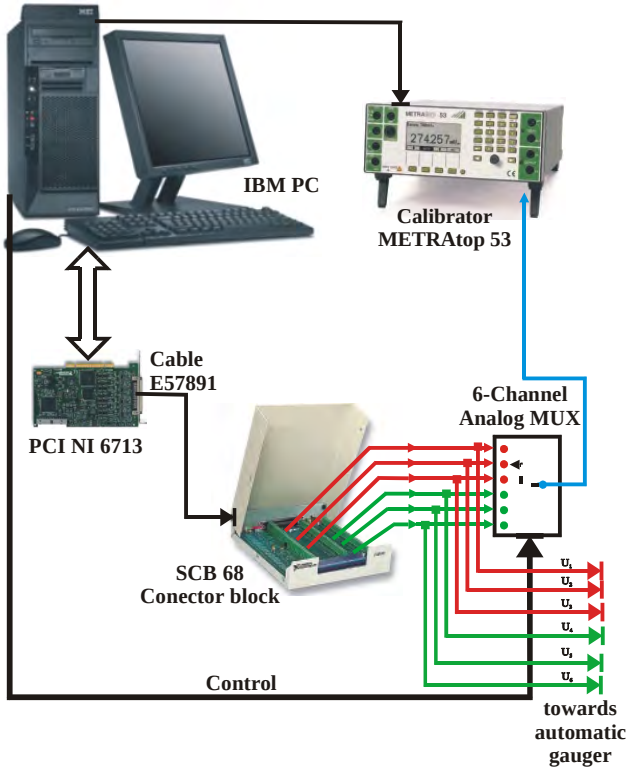

Fig. 1. Virtual instrument with programmable generator

The gauger consists of:

- PC computer, which provides communication between the user and the system, pools and controls parts of the whole system and makes a database of obtained results during the gauging. Based on those results, daily and monthly reports are presented and filed for each of the tested energy meters in all points of the protocol.
- Programmable generator of voltage and current (distributive electrical network simulator) which generates three voltage outputs (U_R, U_S, U_T) and three current outputs (I_R, I_S, I_T);
- Data logger that simultaneously and precisely gathers information about the measured energy from the tested kWh meters and voltage and current references (AC dividers outputs and current shunts). Gathered data are sent to the PC computer, where performance accuracy of tested energy meters is evaluated and all necessary corrections are performed.
- A rack with (20 + 20) locations for linking and testing of kWh meters of different type and floor plan, whereas each tested spot is equipped with a mechanism for maintaining and controlling the optical reading head, local error indicator and connector through which a RS 232 interface can be realized between the tested energy meter and the PC computer.

TABLE I

Voltage sources	
Nominal voltage	$U_{n1} = 57.73\,V$ $U_{n2} = 230\,V, 50\,Hz$
Programmable adjustment	2-120% U_n
Voltage stability	≤ ±1%
Voltage phase difference	$0\text{-}120^0$
Phase error	≤ ±1%
Maximal output load/phase	200 VA
Current sources	
Programmable current adjustment	20 mA-120 A
Current stability	≤ ±1%
Current phase difference	$0\text{-}120^0$
Phase error	≤ ±1%
Maximal output load/phase	1 kVA
Phase angle between U and I	
Adjustment of the Phase angle between U and I	$0 - \pm 180^0$
Phase angle stability	$\leq 2^0$
Frequency adjustment	
Frequency band	45-65 Hz
Stability of the set frequency	±2%

Standard technical requirements of the gauging system that must be met are listed in Table I. In accordance with technical specifications, an automated system for gauging, which contains a PC computer in the feedback circuit, is being developed. Output information from the current shunt as well as those from AC dividers, across the ADC converter, are returned to the PC computer where the kWh parameter correction is done. Using a multi-channel microcomputer card PCI-NI 6713 [9], for referent voltage and current generating, eight digital/analogue output channels are provided. DAQ card outputs are connected to the system through SCB-68 (68-Pin Shielded Connector Block).

It should be mentioned that the Commission of the European Communities has published *Directive 2004/22/EC of the European Parliament and of the Council on measuring instruments* [5]. Our future work should consider complete accordance with requirements proposed by this Commission.

III. METHOD FUNDAMENTALS

Using a software package LabVIEW [6], based on virtual instrumentation, amplitude and phase corrections of current/voltage channels are performed, which fulfills requirements and technical characteristics of the programmable voltage and current generator. A program sequence developed using a graphical program language LabVIEW, is shown in Fig.3. A program provides a possibility for changing amplitude and phase of all voltage and current channels. Using a portable calibrator METRAtop 53 [7], metrologically verified using a technique given in [8],

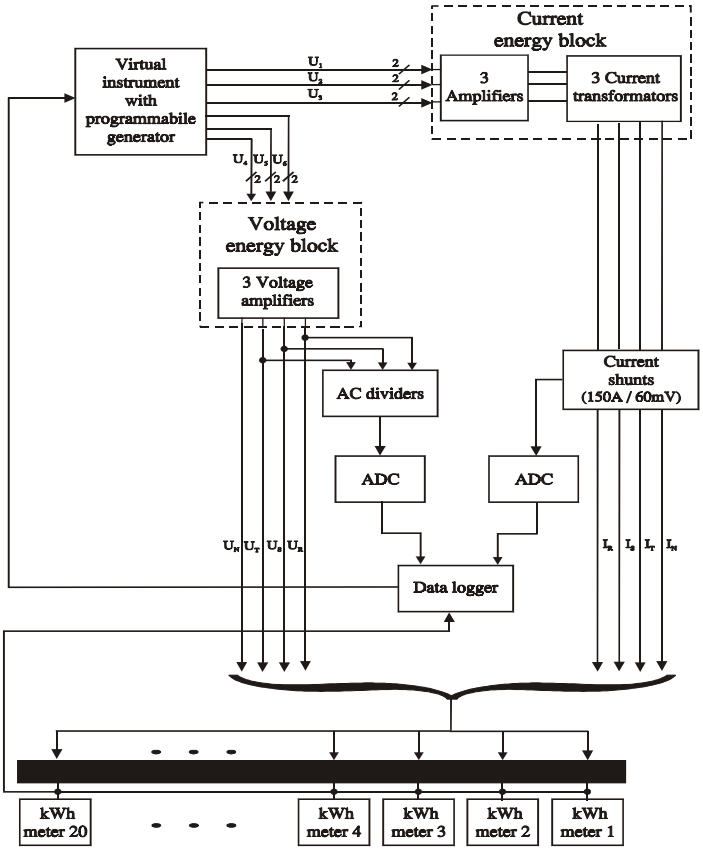

Fig.2. Block scheme of the measuring system

which is connected to the PC computer through the RS-232 interface, output levels are measured and then returned to the computer for further analyzing. Based on obtained results, any of known methods for uncertainty evaluation can be applied, such as Monte Carlo method that considers the following procedure, [10]:

The first step is characterization of metrological performance featured by each component of the measuring system. The information concerning the uncertainties can be achieved by means of either statistical methods applied to experimental tests (type A evaluation, according to [10]) or, more frequently, by exploiting accuracy specifications provided by the manufacturer (type B evaluation), for any device included in the system [12,13]. Both kinds of uncertainty evaluations are based on probability distributions. If the evaluation of type B is applied and there is not any available information on distribution, each contribution to uncertainty is considered a random variable. It has a uniform distribution on an interval centered at zero, whose lower and higher limits are defined by accuracy specifications given in data sheets.

Since the distribution function is defined, the Monte Carlo procedure can be applied in order to determine standard uncertainty. The procedure can be generalized and automated using a program sequence developed under the software package LabVIEW. Generalization considers a possibility to generate sets of random variables of desired statistical parameters. As a result, a large number of variable sets is obtained. Now, different types of tests can be performed on these variables. In each test, values of input data are being changed and, for known relationship between the input and the output quantities, corresponding sets of output data are obtained. Statistical parameters that describe obtained output data, such as mean, standard deviation, mean square value, etc, are calculated.

Described method shows that numerical approach can be applied to a large number of practical situations. In the case of analogue signal conditioning systems, the accuracy specifications mainly concern gain, offset, harmonic distortion, slew rate, noise, bandwidth, etc. In the case of sampling and A/D devices, other uncertainty sources also have to be taken under consideration, such as time jitter, nonlinearity, quantization, etc, [10]. In order to fulfill required specifications, this procedure must be repeated a number of times N, [11]. As mentioned above, the A/D conversion system can also be a significant source of uncertainty because of quantization, offset, gain, and nonlinearity errors. Therefore, an evaluation of the uncertainty, which could be introduced by this system part, must be performed using the method described above.

IV. CONCLUSION

The contribution of accurate gauger in production now has a lot preferences and primary among them is to maintain both energy meters quality and optimization costs of the final control of this kind of products. Therefore, it is essential that

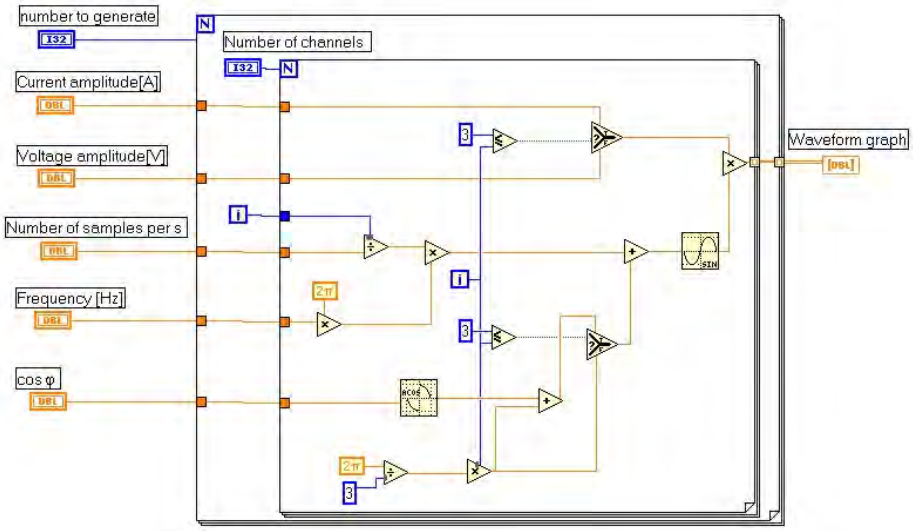

Fig. 3. A program sequence developed using LabVIEW

all subjects concerned with electric energy measurement quality are ensured, and that the right standard for calibration service is obtained in order to achieve and maintain proposed quality requirements.

In the framework of our project an automated calibration system for gauging of new type of kWh meters, which are produced in the Ei - "Professional Electronics" factory in Niš, is being developed. The principal goal of our project was to develop a traceability/calibration procedure for metrological assurance of the automated gauging system in kWh meters production. Based on the preliminary requirements and technical characteristics of a new energy counter, a new solution for the automated calibration procedure is designed using available modern measurement means in our metrological laboratory.

As the traceability for automated systems must be provided by regular re-calibration, which would be based upon an approved procedure including details of how the system software controls the traceability and self-calibration procedure, the proposed laboratory project provides two principal mutual dependence functions: traceability and re-calibration. All known automated systems of gauging use the PC and realized software as a programmable generator and all eventual corrections are done apart from the computer system. In our case, all referent as well as measured values are led to the computer through the feedback, where all necessary corrections are automatically performed. Self-re-calibration of automated gauging equipment within the system is performed under virtual instrumentation control (LabVIEW software), against higher echelon laboratory standards, such as portable calibrator MetraTop53 and the acquisition card PCI-NI 6713.

REFERENCES

[1] Matavulj Lj. et all, "A Device for Automated Accuracy Test of Electrical Energy Meters (energy counter)", First Yugoslav Conference on Electrical Distribution Networks, Zlatibor, 1998, (in Serbian).

[2] Fluke Corporation, Using the 6100A Electrical Power Standard to calibrate energy meters, Application Note.

[3] Cronin L. B., Electrical measurement accreditation of automated calibration systems.

[4] Fully Automatic Energy Meter Calibration, System Century Controls, 28/2, 2nd Main Road, Seshadripuram, Bangalore 560 020, India.

[5] Commission of the European Communities, "Directive 2004/22/EC of the European Parliament and of the Council on measuring instruments", Official Journal of the European Union, pp. 49-52, March 31, 2004, Brussels.

[6] LabVIEW, User's Manual, National Corporation, USA, 2000.

[7] Benchtop Multimeter and Calibrator, Operating Instructions, Gossen Metrawat Camillebauer, Germany, 2001.

[8] Đurić V., Dimitrijević B., Ranđelović I., "Managing Calibration Confidence in Calibration Process", ICEST 2003, Conference proceedings, pp. 398-401, 16-18 October 2003.

[9] DAQ 6711/6713/6715 User Manual, Analogue Voltage Output Device for PCI/PXI/CompactPCI/PCMIA/1394 Bus Computers, National Corporation, 2003, USA.

[10] Locci N., Muscas C., Peretto L., "Numerical Approach to the Evaluation of Uncertainty in Nonconventional Measurements on Power Systems", IEEE Transactions on Instrumentation and Measurement, vol .51, no. 4, pp.734-739, August 2002.

[11] Ferrero A., Lazzaroni M., "A Calibration Procedure for a Digital Instrument for Electric Power Quality Measurement", IEEE Transactions on Instrumentation and Measurement, vol .51, no. 4, pp.716-721, August 2002.

[12] Taylor B., Kuyatt C.,"Guidelines for Evaluating and Expressing the uncertainty of NIST Measurement Results", 1994.

[13] Engineering Statistic Handbook, "Instrument calibration over a regime", vol. 2.3.6., NIST, 2002.

Temperature Measurement Using Bridge Transducer ADC

Georgy Sl. Mihov[1], Emil N. Dimitrov [2], Nencho G. Nenov[3]

***Abstract* – The topic of the paper is a temperature measurement on purpose for correction the result from a force sensor, built on strain gauges. A specialized bridge transducer AD7730, transforming the resistance of the PT100 into a voltage does the measurement. A proper methodology for temperature measurement treatment by linear and second order polynomial dependency has been proposed. An algorithm for measurement device calibration has been created. Practical experiments of error estimating have been done.**

***Keywords* – PT100, Temperature measurement, Resistance transducer, Polynomial interpolation.**

I. INTRODUCTION

The topic of the paper is a problem of a temperature measurement on purpose for correction the result from a force sensor, built on strain gauges which measure the deformation of a specimen.

There exist a lot of methods for temperature measurement. Most of them measure the resistance of a temperature sensitive element. The measurement is done mostly with a DC current [1, 2].

A Resistive Temperature Device (RTD), like PT100, is suitable for measurement the temperature of the strain gauge environment. The PT100 is situated at the place where the gauge bridge is mounted. In our case, the signal from the gauge bridge is threaded by a specialized bridge transducer AD7730 (Analog Device). The AD7730 has got two measurement channels, using common reference voltage. The gauge bridge engages one of the channels and the second one is free. So, we decided to use the second channel for the temperature measurement.

Temperature measurement devices, using similar of the AD7730 transducers (AD7709, AD7719, AD7731 e.t.c.), are offered in [3]. Fig. 1 shows a fragment of a temperature measurement application for the AD7731 with a PT100. The arrangement is a four-lead RTD configuration. In the application shown, the external 400 μA current source provides the excitation current for the PT100 and it also generates the reference voltage for the AD7731 via resistor R1. Resistor R2 is required to set the common-mode voltage within the allowable range for the AD7731.

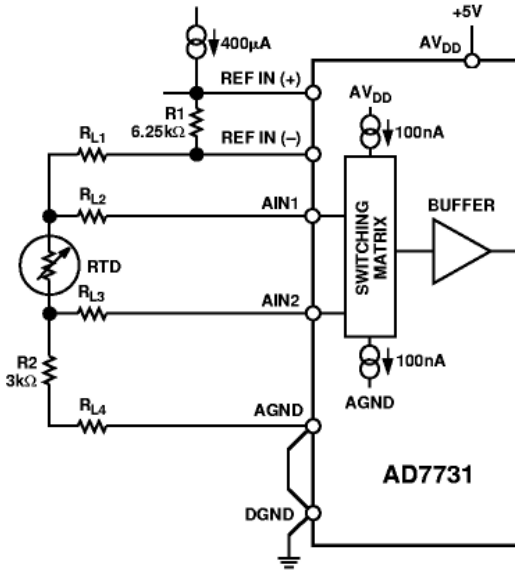

Fig. 1. Temperature measurement using PT100

In our case of the AD7730 using, a considerable changes in the measurement scheme are needed, according to the used transducer working mode:

– the AD7730 uses just one voltage reference for both channels. This requires the device for the temperature measurement to use the same voltage reference;

– the AD7730 could dynamically change, during the measurement, the polarity of the reference voltage, to reduce the value of polarization voltages. The device for the temperature measurement has to be consistent with this mode.

II. TEMPERATURE MEASUREMENT SCHEME

The classical method for a temperature measurement by transforming the resistance of the PT100 into a voltage has been chosen. The external current source provided the excitation current for the PT100. The current is defined by:

$$I = \frac{V_{i\,max}}{R_{max} - R_0}, \qquad (1)$$

where R_{max} and R_0 are values of the PT100 resistance at maximal temperature and at 0^0C respectively. The V_{imax} is the input voltage range of the second channel of the AD7730. The resistor R shifts the input voltage in purpose to reduce the

[1]Georgy Sl. Mihov is with the Faculty of Electronic Engineering, and Technologies, TU – Sofia, 1797, Sofia, Bulgaria, E-mail: gsm@tu-sofia.bg

[2]Emil N. Dimitrov is with the Faculty of Electronic Engineering, and Technologies, TU – Sofia, 1797, Sofia, Bulgaria, E-mail: edim@tu-sofia.bg

[3]Nencho D. Nenov is with the Higher School of Transport, 1574, Sofia, Bulgaria, E-mail: rector@vtu.bg

common-mode voltage and is calculated by:

$$R = \frac{V_R}{2I}. \quad (2)$$

The voltage of the PT100 is measured via the second channel of the AD7730. The current source is proportionally depended by the reference voltage, so its variations do not affect the result due to the ratiomertically method of the AD7730 measurement. Fig. 2 shows the flow char of the measurement device.

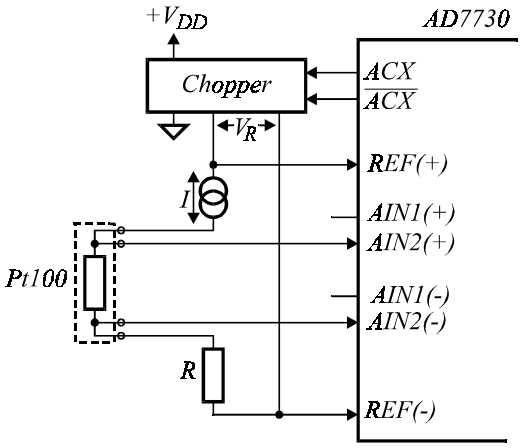

Fig. 2. Flow char of the temperature measurement device with the bridge transducer AD7730

In our case, the bridge transducer AD7730 is controlled by a 68HC11 microconroller unit [4]. The microcontroller threats the result from the gauge measurement as well as from the temperature measurement.

The combined circuit for the force and the temperature measurements is shown in Fig. 4. The external current source is realized by the amplifier TL081 and resistors R4, R5 and R6. Those resistors must have a low temperature coefficient to avoid errors in the reference current via the PT100 over temperature. The resistor R6 defined the value of the current, according the Eq. (1). In our case it is 250μA.

Variations in the reference voltage do not affect the circuit as the current via PT100 and the input voltage vary ratiometrically with the reference voltage.

Due to the four-lead connections, voltage drops across lead resistances do affect the input voltage.

II. Temperature Measure Treatment

The relationships between the temperature and the resistance for platinum thermometry is strongly defined [5].

The followed linear dependency is proposed for a short temperature range:

$$\Delta R = R_t - R_0 = R_0 \alpha t,\ \alpha = 0.00385\ ^0C^{-1},\ R_0 = 100\Omega. \quad (3)$$

For a large temperature range (from 0^0C to 850^0C) should be used the relationship:

$$R_t = R_0(1 + At + Bt^2); \quad (4)$$

$A = 3.9083\times10^{-3}$, $^0C^{-1}$; $B = -5.775\times10^{-7}$, $^0C^{-2}$.

We have decided to modeled the recurrent dependency by a second order polynomial relationship:

$$t = b.\Delta R + a.\Delta R^2, \quad (5)$$

Defining $\Delta R / t = R_0(A + Bt)$ from Eq. (4) and $t / \Delta R = b + a.\Delta R$ from Eq. (5), it can be written:

$$b + a.\Delta R = \frac{1}{R_0(A + Bt)}. \quad (6)$$

Replacing $\Delta R = 0$ at $t = 0$ in Eq. (6) the coefficient b is calculated:

$$b = \frac{1}{R_0 A}, \quad b = 2.5587,\ ^0C/\Omega. \quad (7)$$

Replacing Eq. (7) in Eq. (6) the coefficient a is defined as:

$$a = -\frac{Bt}{R_0 A(A + Bt)\Delta R}. \quad (8)$$

We suggest, the coefficient a to be calculated according the temperature range, e.g. at the maximal temperature t_{max}, corresponding to the value ΔR_{max}.

For example, for the temperature range from 0^0C to $+125^0$C $a = 0.001$, $^0C/\Omega^2$. The same coefficients are calculated using the table array $\{R_i, t_i\}$ of the relationship for the PT100 in the environment for the temperature range from -40^0C to $+125^0$C. The result is shown in Fig. 3. A small difference exists for the coefficient b.

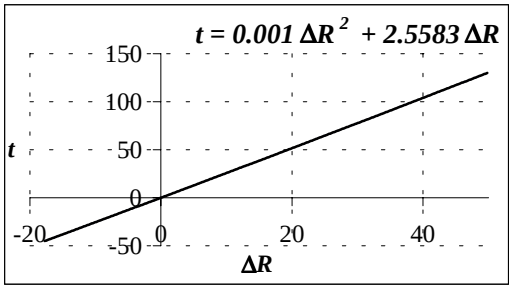

Fig. 3. The table relationship between the temperature and the PT100 resistance

III. Temperature Measurement Calibration

The temperature measurement calibration is similar to the AD7730 calibration for the force measurement purpose [6]. The process of the calibration consists of two stages. A resistance magazine, connected instead of the PT100 element simulates the temperature.

The first stage does the zero-scale calibration. The stage is performed at the temperature 0^0C. Followed procedures are sequentially performed:

– setting of the internal digital-to-analog converter (DAC);

– setting of the internal offset.

The first procedure aims to compensate in large steps the zero-scale shifting (each bit of the DAC has got the value of 2mV). A special algorithm, which applies the method of the successive approximation, is developed. It defined the new content of the selected DAC Register.

The second procedure compensates fine the zero-scale shifting. Hundred measurements are done, averaged and the result is subtracted from the content of the selected Offset Register.

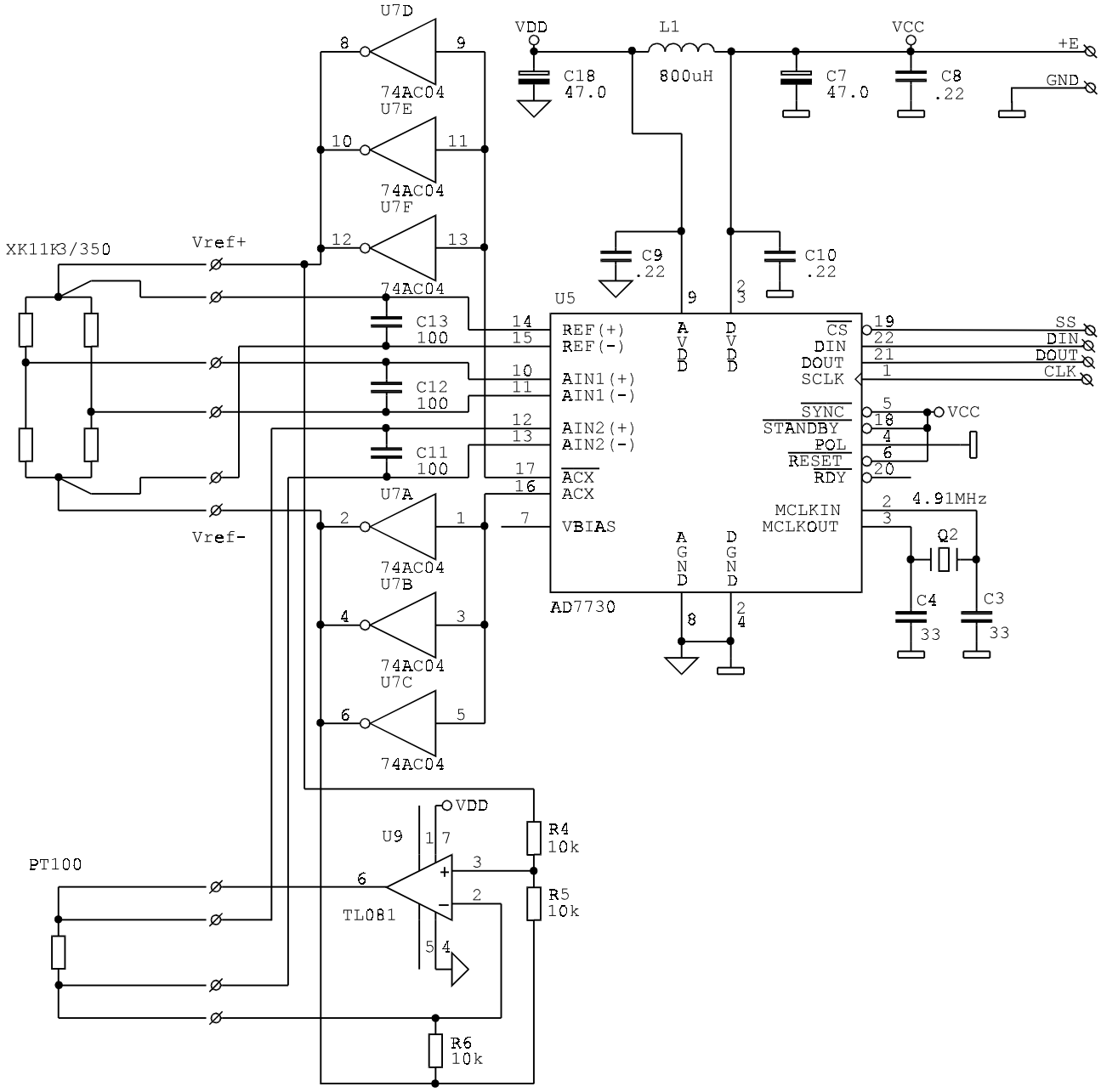

Fig. 4. Combined circuit for a the force and for the temperature measurements, using the bridge transducer AD7730

Determined during the first stage new contents of the selected DAC Registers and Offset Registers are stored into the internal EEPROM of the embedded microcontroller.

The second stage does the full-scale calibration. It determines the transfer factor k of the measurement. The factor k defined the relationship between the calculated number N by the measurement and the linear part of the measured temperature:

$$b.\Delta R = kN, \tag{9}$$

Resistance of the PT100 is simulated at the maximal temperature, e.g. it is ΔR_{max}. New hundred measurements are done, averaged and the result N_{max} is substituted in (9). The factor k is calculated by:

$$k = \frac{b.\Delta R_{max}}{N_{max}}. \tag{10}$$

The AD7730 calculates N according the relation $N = GU$, where U is the input voltage, and G is the value of the internal gain coefficient. So, $kN = kGU$. A correction of the G is done in the way $G^* = kG$, and the new value N_S of the measured result is $N_S = kN = G^*U$.

The calculated value G^* is the new content of the selected Gain Register and it is also stored into the internal EEPROM of the microcontroller.

Stored in the EEPROM new values of the DAC Register, Offset Register and Gain Register are updated in the AD7730 each time a new measurement is performed.

According to the Eqs. (5), (9) and (11), the value of the real

temperature is calculated by:

$$t = N_S + K_2 N_S^2, \quad (11)$$

where $K_2 = \frac{a}{b^2}$ is a constant.

IV. Experiments

Experiments have been done for the measurement errors estimating. The resistance of the PT100 has been emulated by specialized DC bridge P333 (Russia – 1991, class 0.5) used as a resistor magazine. The results are shown in Table 1.

TABLE 1
TEMPERATURE MEASUREMENT ERRORS

R	*t-tbl*	*t-clc*	*t-ms1*	*t-ms1*	Δ*t-ms1*	Δ*t-ms2*	Δ*t-clc*
84	-40.675	-40.683	-41.559	-40.746	-0.884	-0.071	-0.008
88	-30.564	-30.560	-31.161	-30.603	-0.597	-0.039	0.003
92	-20.411	-20.405	-20.787	-20.431	-0.377	-0.021	0.004
96	-10.225	-10.218	-10.395	-10.233	-0.17	-0.008	0.006
100	0	0	-0.015	-0.015	-0.015	-0.015	0
104	10.256	10.250	10.416	10.276	0.16	0.02	-0.005
108	20.538	20.533	20.801	20.567	0.263	0.029	-0.004
112	30.846	30.848	31.197	30.888	0.351	0.042	0.002
116	41.184	41.195	41.588	41.241	0.404	0.057	0.011
120	51.564	51.574	51.975	51.629	0.411	0.065	0.011
124	61.973	61.984	62.347	62.034	0.374	0.061	0.011
128	72.421	72.427	72.736	72.475	0.315	0.054	0.006
132	82.894	82.902	83.125	82.953	0.231	0.059	0.008
136	93.394	93.409	93.523	93.451	0.129	0.057	0.015
140	103.947	103.948	103.911	104.013	-0.036	0.066	0.001
144	114.526	114.518	114.301	114.571	-0.225	0.045	-0.007
148	125.131	125.121	124.706	125.161	-0.425	0.03	-0.009

R – Emulated resistance of the PT100;
t-tbl – Corresponding temperature by the table [6];
t-clc – Calculated temperature by Eq. (5);
t-ms1 – Measured temperature, applying linear dependency;
t-ms2 – Measured temperature, applying polynomial dependency;
Δ*t-xxx* – Absolute temperature measurement errors.

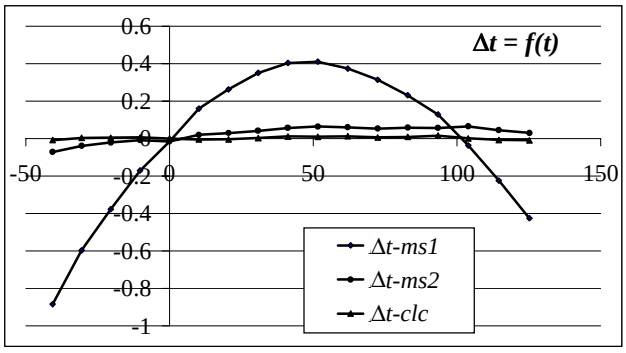

Fig.5. Allocation of the temperature measurement errors

The emulating resistance *R* of the DC bridge is fixed of each 4Ω for the range from 84Ω to 148Ω, that corresponds to the temperature range from -40^0C to $+125^0$C. The absolute error Δ*t* is calculated in comparison of the corresponding from the table value of the temperature *t* for the PT100. Allocations of the temperature measurement errors are graphically shown in Fig. 5.

V. Conclusions

The topic of the paper is a problem of a temperature measurement on purpose for correction the result from a force sensor, built on strain gauges which measure the deformation of a specimen.

A Resistive Temperature Device (PT100) has been chosen for temperature measurement of the strain gauge environment. In the presented case, a specialized bridge transducer AD7730 (Analog Device) threads the signal from the gauge bridge. This is the reason the same transducer to be applied for the temperature measurement.

The classical method for a temperature measurement by transforming the resistance of the PT100 into a voltage has been chosen. A proper scheme for the platinum element supplied has been built. It is adapted to the specific features and the modes of the bridge transducer AD7730.

A proper methodology for temperature measurement treatment by linear and second order polynomial dependency has been proposed. An algorithm for measurement device calibration has been created. Practical experiments of error estimating have been done.

References

[1] I. Stoyanov, "Measurements in Electronics", Technical University – Sofia, Sofia, 2000 (in Bulgarian).

[2] G. Stoilov, N. Nikolov, S. Ovcharov, "Method and Scheme for DC Resistance Measurement", Proceedings of the VMEI – Sofia, vol. 34, b. 1, pp. 183-190, Sofia, Bulgaria, 1975 (in Bulgarian).

[3] http://www.analog.com/

[4] G. Mihov, E. Dimitrov, V. Gunev. "Industrial Controller for Weight Measurement", The International Scientific Conference ENERGY AND INFORMATION SYSTEMS AND TECHNOLOGIES. vol. III, pp. 649-654. Bitola, Macedonia, 2001.

[5] N. Nenov, T. Rouzhekov, G. Mihov, E. Dimitrov, "Strength Sensor for Dynamic Wheel Load Measuring of Railway Carriages", 26th International Spring Seminar on Electronics Technology, pp. 260-265, ISBN 0-7803-8002-9, High Tatras, Slovakia, Czech Republic, 2003.

[6] International Temperature Scale IEC 751:1983 (BS EN 60751:1996).

[7] N. Nenov, T. Ruzhekov, G. Mihov, E. Dimitrov, "Technology for Dynamic Wheel Load Measuring of Railway Carriages", The Twelfth International Scientific and Applied Science Conference ELECTRONICS ET'2003, Book 1, pp. 64-69, ISBN 954-438-374-3, Sozopol, Bulgaria, 2003.

[8] K. Hoffman, "Ursachen temperaturabhängiger Nullpunkts und Empfindlichkeitsänderungen bei Dehnungsmeßstreifen-Aufnehmern" VDI-Berichte, Nr. 137, S. 23/27, VDI-Verlag GmbH, Düsseldorf, 1970 (in German).

Automated Measurement System for Characterization of CATV Components and Devices

Mladen Ranđelović[1], Aleksandar Atanasković[2], Bratislav Milovanović[3]

***Abstract* – This paper presents the automated measurement system for characterization of CATV components and devices. The automatisation of measurement system enables the control of the instruments using the computer. This kind of measuring makes controlling measurement devices easier and more efficient, as collecting, analysis and presentation of the results.**

***Keywords:* CATV measuring, CATV amplifiers, HP VEE.**

I. INTRODUCTION

What is considered under cable distribution system is antenna system for reception and distribution of radio diffusive programme via cable distribution net to the blocks of buildings, towns and cities.
The primary task of cable distribution system is to enable the signal of continual and permanent quality for all the customers, where servicing means the distribution of radio and TV programme as well as the joint data services. Cable TV presents the most significant system for the TV programme distribution and different largescale services accomplishment. More than 70% of the population in the USA has access to cable TV, whereas in some European countries the number is even higher (Belgium, the Netherlands about 98%). In our country cable TV has been expanding in recent years, so that there are over 300.000 on-line customers, and the number of users is increasing for about 10.000 each month.

II. THE PURPOSE OF AMPLIFIER MEASURING

With the large expansion of new technologies and services in the sphere of cable distribution systems, there is an increasing demand for the improvement of the performance of some components in CATV which would further provide a better quality of video as well as audio signal for each subscriber. CATV amplifier as an active device is a key element of the CATV system structure, therefore it is necessary to get to know it and if possible improve its performances. CATV amplifier has a role to:

- make the signal stronger in the largescale range for multichannel signal distribution
- enable minimum distortion and fluctuations of frequency characteristics
- have an input and output impedance of 75 Ω
- enable signal distribution in both directions (bidirectional component)
- have changeable amplification which can be altered in accordance with the changes of environmental conditions.

The basic role of the amplifier is to compensate for the losses of the strength of a signal while it is being disturbed and in that way to improve the quality of the signal before sending it eventually to the subscriber (Fig.1). The losses added because of the cable distribution, given in the relation to the frequency are:

$$Losses(f) = a * f + b * \sqrt{f} + c \qquad (1)$$

, where the *losses(f)* are, in fact, the cable losses over the length measuring unit (dB/km), *f* is the frequency in MHz, while *a*, *b* and *c* are the constants which correspond the cable characteristics.

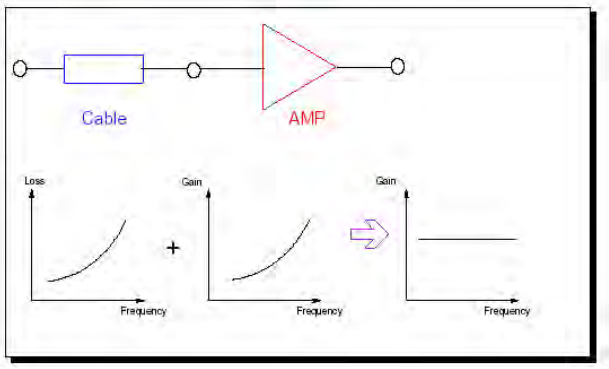

Fig. 1. Amplitude vs. frequency characteristics of cable and amplifier

Electrical characteristics [1-2] of the amplifier is because of that really essential, and it is gained by vectoral and spectral measurements. In order to do measurings effectively, it is necessary to have the measuring equipment which will enable:

- precise amplitude and phase measuring
- a low level noise and distortion when measuring the level
- fast measuring with a high resolution

[1] Mladen Ranđelović is with the Faculty of Electronic Engineering, Beogradska 14, 18000 Niš, Serbia and Montenegro, E-mail: mladen@elfak.ni.ac.yu
[2] Aleksandar Atanasković is with the Faculty of Electronic Engineering, Beogradska 14, 18000 Niš, Serbia and Montenegro, E-mail: beli@elfak.ni.ac.yu
[3] Bratislav Milovanović is with the Faculty of Electronic Engineering, Beogradska 14, 18000 Niš, Serbia and Montenegro, E-mail: bata@elfak.ni.ac.yu

III. GRAPHIC PROGRAMMING AND HP VEE

Necessary measuring with CATV components and devices can be carried out directly (by hand) but higher accuracy and validity is achieved by fully automated measuring. Automate measuring with CATV amplifiers is carried out by using HP VEE developing environment which is made on the principle of graphic programming.

Graphic programming [4] differs in many ways from a traditional programming because it is graphically carried out while the programme and data processing go on. HP VEE programme is made by connecting icons together using a mouse; whereas with textual languages we use a keyboard applying syntax rules. The outcome with HP VEE resembles a diagram of data processing which is easier to use and understand than traditional coded lines and there is no tiresome process of edit-compile-link-done. The programme is created by using objects and lines. The lines represent data, while the objects create, analyze and display data. The objects have different functions like I/O operation, analysation and display. All the objects have input and output pins which are located in this way: the data input pin on the left; the data output pin on the right; the sequence input pin is on the top and the sequence output pin is at the bottom of the object. Each object can be shown as an icon or in its open view. The open view is larger and more elaborate.

HP VEE provides three easy ways to control instruments: panel drivers, "Direct I/O" object, and PC I/O libraries. There are panel drivers that offer a simple user interface for the instrument control from computer screen. These are provided by HP with VEE and cover over 450 instruments from different vendors, or you can use VXI plug&play drivers to call C functions to control instruments. These are provided by HP and other vendors with their instruments for support. Panel drivers have two purposes with HP VEE :

- they allow defining of measure state that describes all the performing functions of instruments. When the panel driver is in operation, the adequate instrument is automatically programmed to be set with the state defined by the panel driver.
- operate as control panels for interactive control of instruments. This is useful during the programme development and debugging and when the instrument has no physical front panel.

The open view of a panel driver contains graphical control panel for connecting the instruments. If the instrument is connected with a computer in a specified way, the instrument can be controlled by pressing some area on the graphic control panel. In addition to that, some measurements can be shown on numerical or XY display. Direct I/O objects allow the distribution of commands and the reception of data via one of the supported interfaces.

It can be concluded that the process of creating a programme by using a graphic programming is quite simple [6-7]. Graphic programming can be easily understood and maintained by the author himself as well as any other user. Due to the characteristics that the objects can be selected from the falling menus, it is possible to make a valid and usable code. Most objects used so far would require hundreds or even thousands of lines of traditional code. The processing of the performing programme and processing data can be easily seen from a diagram which represents a programme itself. There are fewer possibilities for human factor erring, and it is easier to detect a problem.

IV. MEASURING SYSTEM AND THE MEASUREMENT RESULTS

For the realization of the measuring system for measuring with CATV components and devices the following equipment, which is available at the Faculty of Electronic Engineering, Laboratory for Microwave technique and satellite television, is used:

- HP8970B Noise Figure Meter,
- HP8757A Scalar Network Analyzer,
- HP8753C Vector Network Analyzer,
- HP8350B Sweep Oscilator,
- HP437B Power Meter,
- HP5350B Microwave Frequency Counter,
- Power supply and switch matrica
- Signal generators
- HP 82341 HP-IB card for PC (system controler),
- HP VEE enviroment, software for developing applications for measurement automatisation.

For the sake of automising the realized measuring system, the adequate software is created for control and measuring equipment handling by using HP VEE developing environment. The created software is primarily intended for characterization of CATV amplifiers and it can support the following types of measuring with amplifiers:

Vectoral measurements:

- Amplitude characteristics (amplification)
- Phase characteristics (group delay)
- The standing wave ratio and return losses
- The noise factor

Spectral measurements:

- The distortion of the secondary order
- The distortion of the third order
- Cross modulation distortion
- Intermodulation distortion
- Hum modulation distortion

By means of the available measuring equipment the measuring of the amplitude frequency characteristics, return losses, and the standing wave ratio, noise factor and power level are measured. A part of the programme for the automation of the realized measuring system is shown in the Fig. 2. This diagram would be analogue to the original code of the main procedure in some of the textual languages. From this part of the programme the calling of subprogrammes needed for the correct performance of corresponding types of measuring is done.

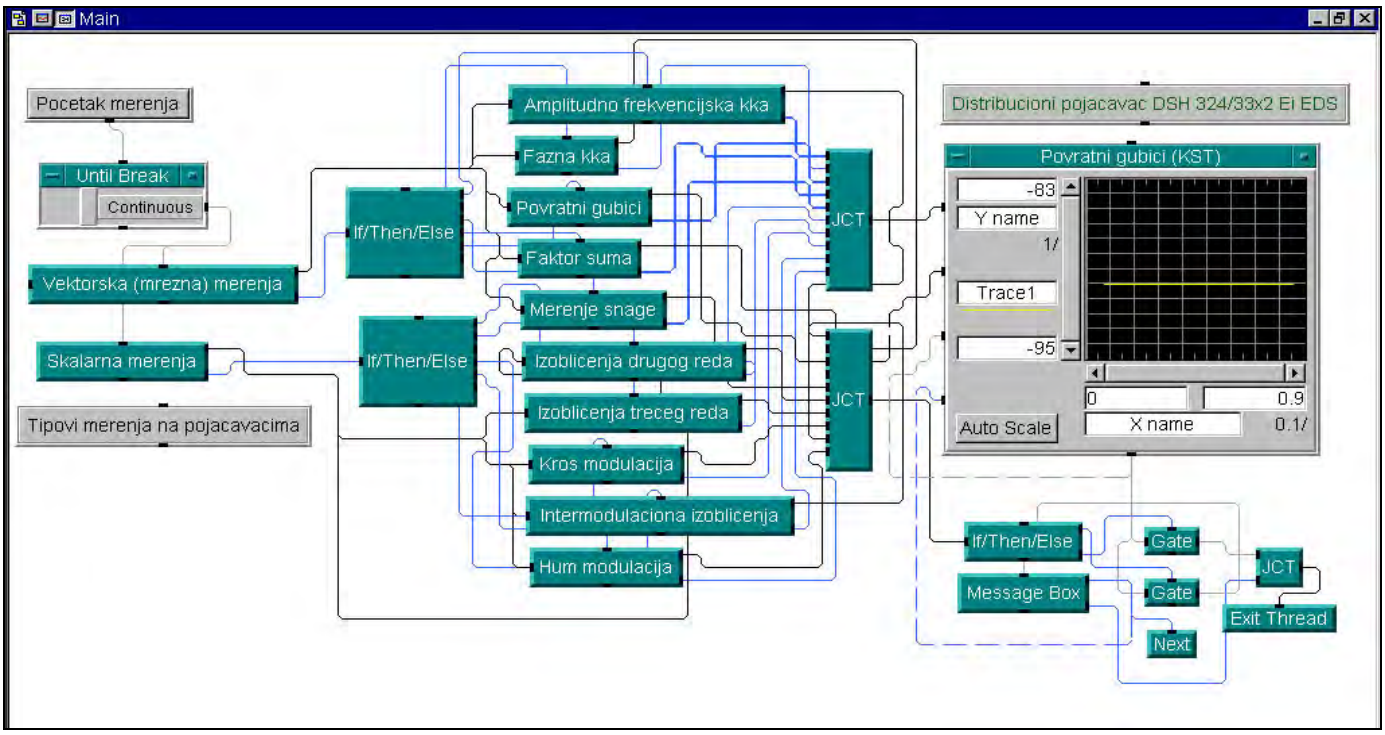

Fig. 2. Part of the designed programme for automatisation of the measurement system

The basic screen (Fig. 3) contains two measuring groups: vectoral (net) and scalar (spectral). From the measuring group a particular measuring is selected from the falling menus. On the right, there is a screen showing the data. There is a possibility of changing the name of asis as desired. There is also a possibility of changing unit range on both sides, which enables zooming of particular characteristics of interest (the size of peaks at particular frequencies as well as frequencies can be determined with higher accuracy). The option of *Auto Scale* enables adjustment of the size of the graphic on a display. The option *Start Measure* signifies that the choice of measuring is completed and that a corresponding procedure can start. In order to verify software, some measuring procedures have been performed at corresponding amplifiers and the gathered results have been compared with factory specifications. The results of measuring for the distribution amplifiers DSH 324/33x2 made by Electronics Industry Co. in Nish are shown in Figs. 3, 4 and 5.

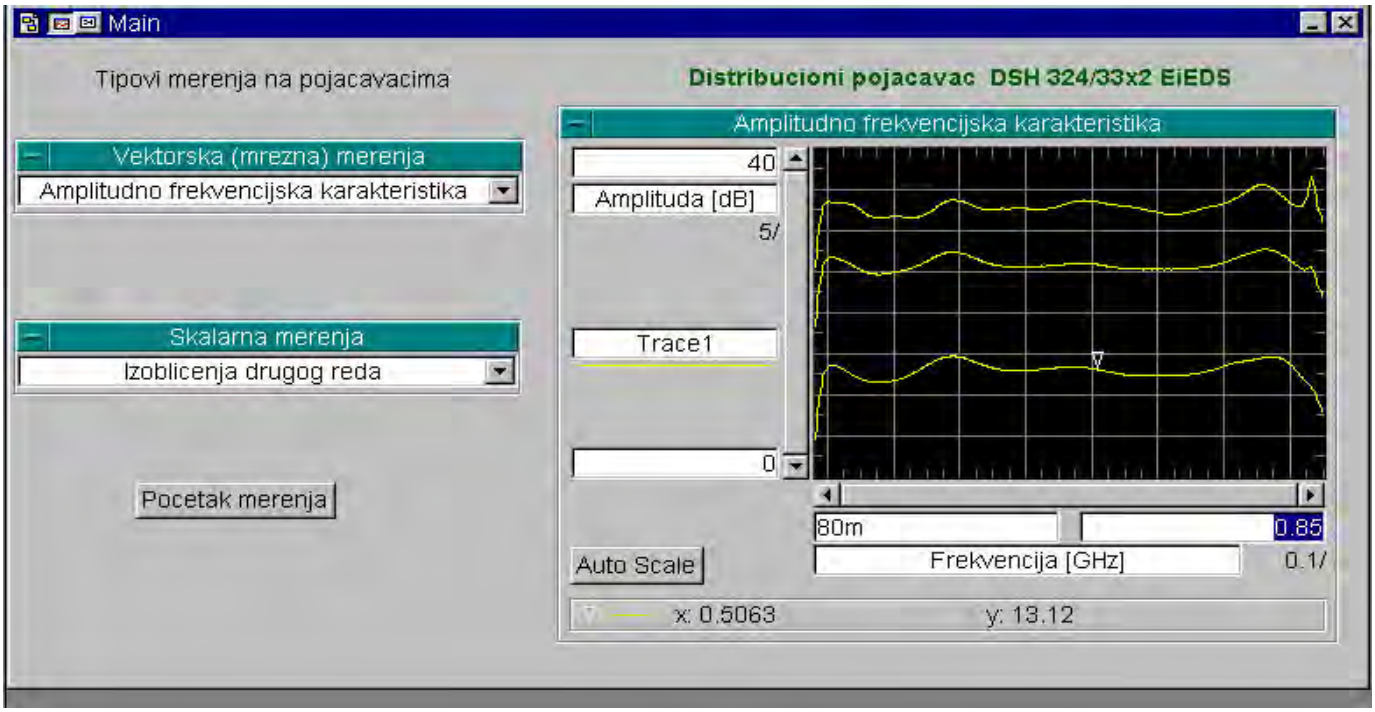

Fig. 3. Display of the measument results of amplitude-frequency characteristics

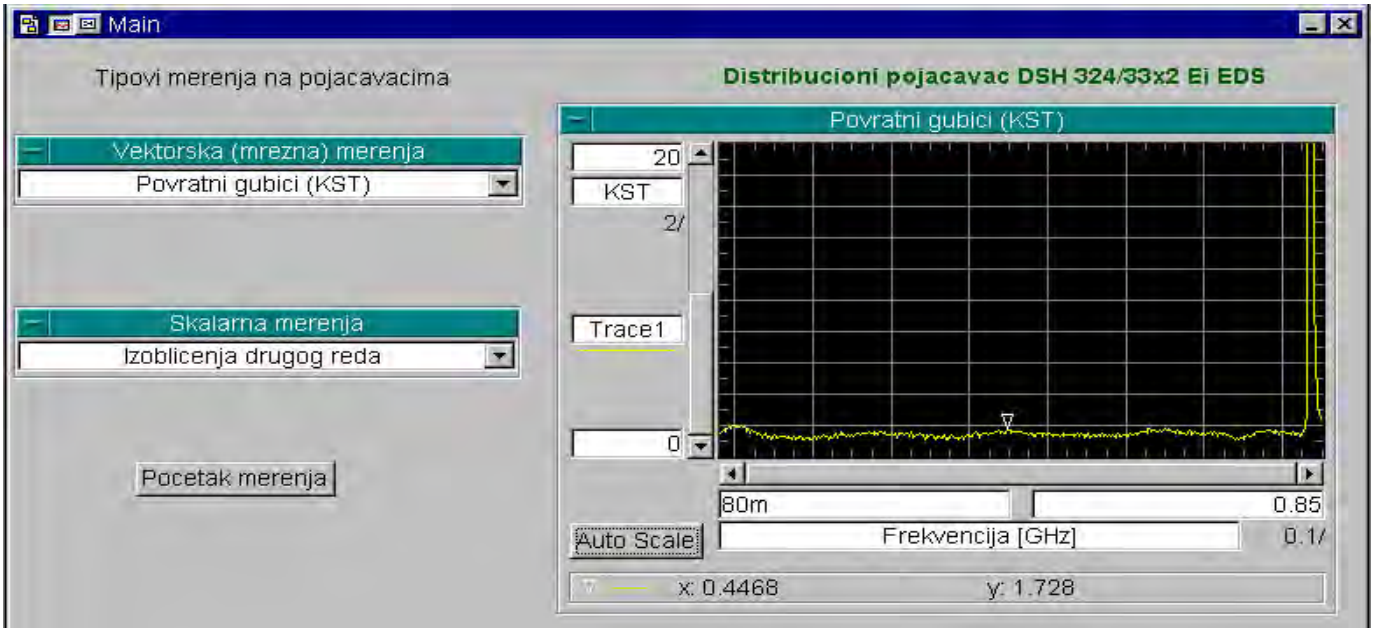

Fig. 4. Display of the measurement results of standing wave ratio

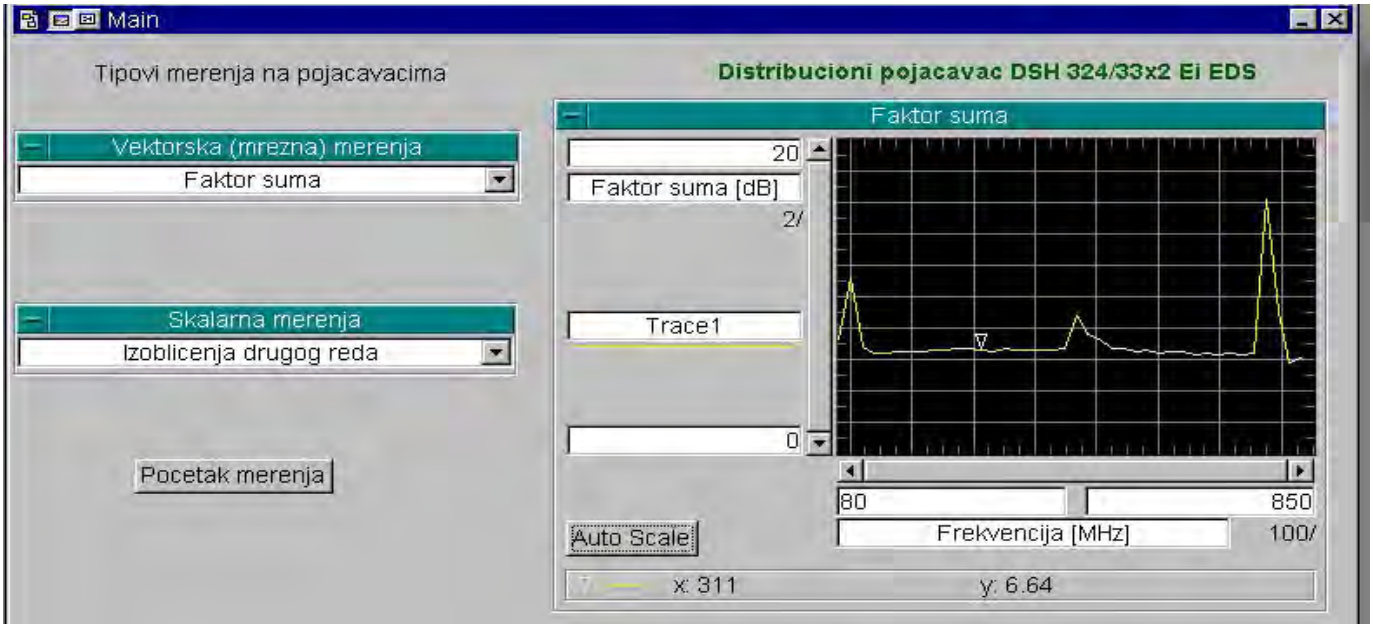

Fig. 5. Display of the maesurement results of the noise factor

V. Conclusion

Characteristics measurement of CATV amplifiers can be often large, difficult to check up and control and poor as far as the outcome results are concerned. For the sake of overcoming shortcomings we have turned to automated measuring by creating a corresponding software in HP VEE environment. This particular software enables not only an easier equipment handling (only by a computer which is the sole comanding component), but its advantages take place both in the measuring process and the process of gathering results (the characteristics drawing, table generating and so on).

References

[1] "*How to Characterize CATV Amplifiers Effectively*", Application Note 1288-4, Hewlett Packard

[2] International standard IEC 60728-3, Second edition, 2000-10

[3] Zbornik izlaganja, Stručni seminari, Telsiks'97, Niš, oktobar 1997.

[4] R.Helsel, "*Visual Programming with HP VEE* ", Second Edition, Prentice Hall PTR, New Jersey, March 1997.

[5] G.Donić, B.Milovanović, V.Stanković, J.Bogdanović, S.Ivković, B.Narančić, "TUNTEST - Programme Package for TV Tuner Characteristics Automated Measuring", 42nd ARFTG Conference digest, pp.23-31, San Jose, USA, 1993.

[6] S.Ivković, B.Milovanović, A.Atanasković, V.Tasić, ″Automatization of Permittivity Measuring Using Microwave Culindrical Cavity″, TELSIKS'99, Niš, Yugoslavia, 1999, pp.218-221.

[7] A. Atanasković, V. Tasić, S. Ivković: "Automatization of the Complex Dielectric Constant Measurement", TELSIKS 2001, Niš, Yugoslavia, Vol.2, pp.691-694, 2001.

A New Method for Accurate Noise Modeling of Microwave FET Transistors

Olivera Pronić, Vera Marković, Gordana Mitić, Jovana Ranđelović

Abstract - **A new procedure for noise parameter modeling of microwave MESFETs / HEMTs is proposed in this paper. The proposed modeling procedure presents a modification of Pospieszalski's noise model with the aim to improve the model accuracy. For this purpose, frequency-dependent error correction functions are determined and incorporated into the Pospieszalski's noise equations. Due to this, more accurate noise prediction is obtained. It will be shown that initially calculated error correction functions can be used for efficient transistor noise parameter prediction for various bias conditions.**

Keywords – **MESFET, noise modeling, error correction function**

I. INTRODUCTION

As the performance of modern communications systems improves, the noise of devices becomes the limiting factor for overall system. Therefore, much work has been done for developing noise models of microwave transistors that enable accurate estimation of noise behaviour.

There are different opinions about the most appropriate transistor noise model. Since the physical models are complex and may deviate from measured data, the empirical noise models are used more often, [1], [2], [3]. The two-parameters Pospieszalski`s model turns out to be the most suitable for implementation into the standard commercial circuit simulators, as Libra or ADS. Pospieszalski's noise model is based on simple expressions for noise parameters of transistor intrinsic circuit as the functions of transistor intrinsic circuit elements and two frequency independent parameters called equivalent gate and drain temperature. This model generally shows good agreement with measured data, but some deviations still can be observed. One of the ways for improving the accuracy is including some additional effects into the model.

In the original Pospieszalski's model, the correlation between two noise sources it completely ignored. However, it has been found that the inaccuracy caused by this approximation is not negligible at higher frequencies.

Olivera R. Pronić, Vera V. Marković, Gordana B. Mitić and Jovana B. Ranđelović are with the Faculty of Electronic Engineering, Niš, Beogradska 14, 18000 Niš, Serbia and Montenegro, E-mails:{oljap, vera, goca, jovanar}@elfak.ni.ac.yu.

In [4], the correlation is taken into account by defining the third equivalent temperature, called correlation temperature.

The other empirical noise models, like those proposed by Gupta [1] or Fukui [2], give the results for noise parameters that also deviate in some extent from experimental data. A procedure for improving the Fukui's empirical model by some correction functions is proposed in [5].

In this paper a simple procedure for more accurate noise modeling of MESFETs / HEMTs, starting from Pospieszalski`s model, is suggested. In order to achieve a better agreement between simulated and experimental data, the novel error correction functions are incorporated into the Pospieszalski`s equations for noise parameters. The possibility for using the same error correction functions for various bias conditions is investigated in this paper as well.

II. DESCRIPTION OF MODELING PROCEDURE

The schematic of GaAs FET package model equivalent circuit is shown in Fig.1. Transistor intrinsic circuit, which is common for the most of microwave models, is denoted by the dashed line. It consists of capacitor C_{gs}, resistors R_{gs} and R_{ds} and voltage controlled current source $g_m V$, where $g_m = g_{m0} e^{-j\omega\tau}$ is transconductance, and V is the voltage on C_{gs}. The remaining extrinsic elements, embedded in the circuit, represent parasitic effects of device. The equivalent circuit for MESFET / HEMT chip is denoted by dotted line.The effects of package are modeled by including transmission lines T_1, T_2 and T_3, capacitors C_{gsp}, C_{gdp} and C_{dsp} and inductances L_1, L_2 and L_3.

The resistors R_{gs} and R_{ds} determine thermal noise of intrinsic circuit. In MESFET noise model proposed by Pospieszalski, [3], equivalent gate noise temperature, T_g, and drain noise temperature, T_d, are assigned to these resistances. The noise contributions of these resistors are represented by voltage noise source e_{gs} and current noise source i_{ds}, respectively.

The noise parameters of intrinsic transistor circuit: minimum noise figure F_{min}, optimal source impedance $Z_{opt} = R_{opt} + jX_{opt}$ and noise resistance R_n can be calculated over wide range of frequencies as follows [3]:

$$F_{min} = 10 log\left(1 + \frac{T_{min}}{T_0}\right), \quad (1)$$

$$T_{min} = 2\frac{\omega C_{gs}}{g_m}\sqrt{r_{gs}T_g g_{ds}T_d + \left(\frac{\omega C_{gs} r_{gs} g_{ds} T_d}{g_m}\right)^2} + 2\left(\frac{\omega C_{gs}}{g_m}\right)^2 r_{gs} g_{ds} T_d \,, \quad (2)$$

$$X_{opt} = \frac{1}{\omega C_{gs}}, \quad (3)$$

$$R_{opt} = \sqrt{\left(\frac{g_m}{\omega C_{gs}}\right)^2 \frac{r_{gs}T_g}{g_{ds}T_d} + {r_{gs}}^2}, \quad (4)$$

$$R_n = \frac{T_g}{T_0} r_{gs} + \frac{T_d g_{ds}}{T_0 {g_m}^2}\left(1 + \omega^2 {C_{gs}}^2 {r_{gs}}^2\right), \quad (5)$$

$$\Gamma_{opt} = \frac{Z_{opt} - Z_0}{Z_{opt} + Z_0}. \quad (6)$$

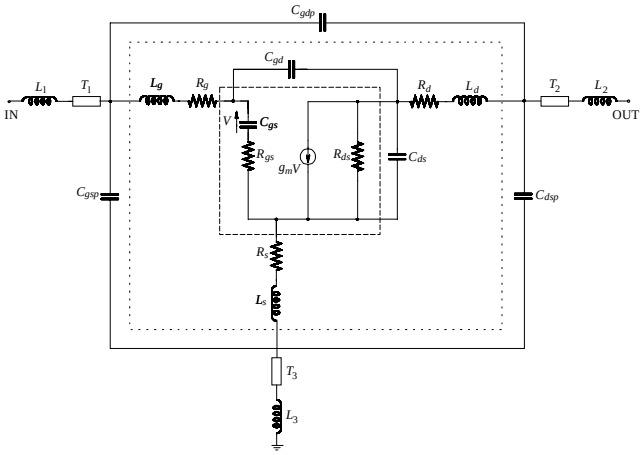

Fig.1. Equivalent circuit for FET packages

It is shown that noise parameters calculated in this way do not perfectly match measured noise parameters. In order to minimize deviations that exist between measured and modeled noise parameters, a correction procedure based on incorporation of frequency-dependent error correction functions into the Pospieszalski`s noise equations is applied.

At the beginning, for each of four noise parameters, the ratio of the experimental and simulated noise parameter values is calculated over the entire frequency range. Then, curve fitting procedure is applied on these sets of data, in order to obtain suitable frequency dependences. In this way, corresponding mathematical functions are chosen for all four noise parameters: F_{min}, $Mag(\Gamma_{opt})$, $Ang(\Gamma_{opt})$ and $r_n = R_n / 50$. These functions represent error correction functions for improving the Pospieszalski's noise model. Namely, standard noise equations (1-6) are modified by including error correction functions $y_1(f), y_2(f), y_3(f)$ and $y_4(f)$. As a result, new equations for transistor intrinsic circuit noise parameters become:

$$F_{minnew} = F_{min} \cdot y_1(f), \quad (7)$$

$$Mag(\Gamma_{opt})_{new} = Mag(\Gamma_{opt}) \cdot y_2(f), \quad (8)$$

$$Ang(\Gamma_{opt})_{new} = Ang(\Gamma_{opt}) \cdot y_3(f), \quad (9)$$

$$r_{nnew} = r_n \cdot y_4(f). \quad (10)$$

It is shown that the most suitable form of error correction function for the minimum noise figure is the exponential one:

$$y_1 = m + ne^{-\frac{f}{l}}, \quad (11)$$

where f is the frequency, and m, n and l are the constants.

Error correction functions for $Mag(\Gamma_{opt})$, $Ang(\Gamma_{opt})$, and r_n has the form:

$$y_i = a_i + b_i f + c_i f^2 + d_i f^3, \quad i = 2,3,4 \quad (12)$$

where a_i, b_i, c_i, d_i are the constants.

III. NUMERICAL EXAMPLE

Numerical results related to small-signal and noise modeling of HP GaAs FET packaged microwave transistor, type ATF 21186, are presented in this paper. All simulations are performed using microwave circuit simulator ADS (Advanced Design System), [6].

With the aim to predict the noise parameters using the proposed model, the equivalent circuit element values are determined at the beginning. The two-step optimization procedure is used for the efficient determination of circuit elements. Firstly, the extraction of equivalent circuit elements is done in order to achieve the best possible agreements between measured and modeled scattering parameters. Next, the equivalent noise temperatures T_g and T_d are extracted by fitting measured and modeled noise parameters. As referent data, manufacturer's S parameter and noise parameter data for various bias conditions in the frequency range (0.5 – 8) GHz, are used, [7]. Extracted component values, for ambient temperature equals 25°C and bias condition I_{ds}=20mA, V_{ds}=2V, are: R_{gs}=1.81Ω, τ=0.0099ps, L_s=0.084nH, L_g=0.772nH, L_d=0.388nH, R_s=0.61Ω, R_g=2.25Ω, R_d=0Ω, C_{ds}=0.156pF, C_{gd}=0.137pF, C_{gs}=0.326pF, g_{m0}=68.28mS, R_{ds}=101.4Ω, C_{dsp}=0.150pF, C_{gdp}=0.093pF, C_{gsp}=0.224pF, L_1=0.41nH, L_2=0.034nH, L_3=0.93nH. Transmission lines segments are characterized by following: physical lengths LNG_1=29.183mil, LNG_2=10.151mil, LNG_3=18.91mil, characteristic impedances Z_1=80.82Ω, Z_2=65.482Ω,

Z_3=63.86Ω, effective dielectric constant k=7, attenuation A=0.001dB/mil and scaling frequency for attenuation f=1GHz. The extracted equivalent noise temperatures are: T_d = 3244K, T_g = 246K.

The comparison of experimental (squares) and simulated S parameters(triangles) is shown in Fig. 2. It can be observed that, despite of a great number of variables, a satisfied agreement with referent data is achieved.

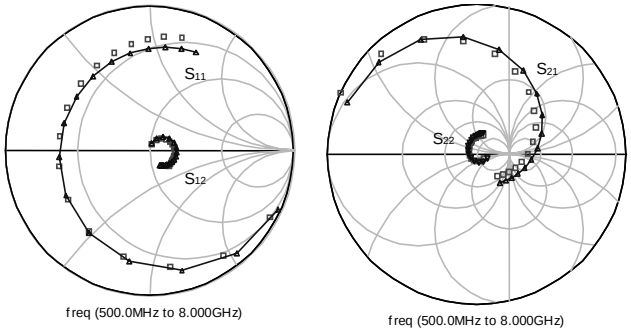

Fig. 2. Comparison between simulated and referent S-parameters

Noise parameter characteristics obtained by Pospieszalski's approach (denoted by MOD1), together with those based on measured data (denoted by MEAS) are presented in Fig. 3. Inaccuracy in noise modeling, specially for F_{min} and $Mag(\Gamma_{opt})$ can be observed.

In order to minimize deviations that exist between measured (MEAS) and modeled (MOD1) values of noise parameters, the error correction functions are included, as described in previous section. Evaluated constants in exponential function for minimum noise figure (Eq.(11)) are:

$$m=0.63,\quad n=3.95,\quad l=7.904\ 10^{7},$$

The parameters of polynomial functions (Eq.(12)) for $Mag(\Gamma_{opt})$, $Ang(\Gamma_{opt})$ and r_n are given in Table I.

TABLE I

	a	*b*	*c*	*d*
y_2	1.017	-5.93e-11	1.055e-20	0
y_3	0.973	5.643e-12	0	0
y_4	3.078	-1.7e-9	3.521e-19	-2.17e-29

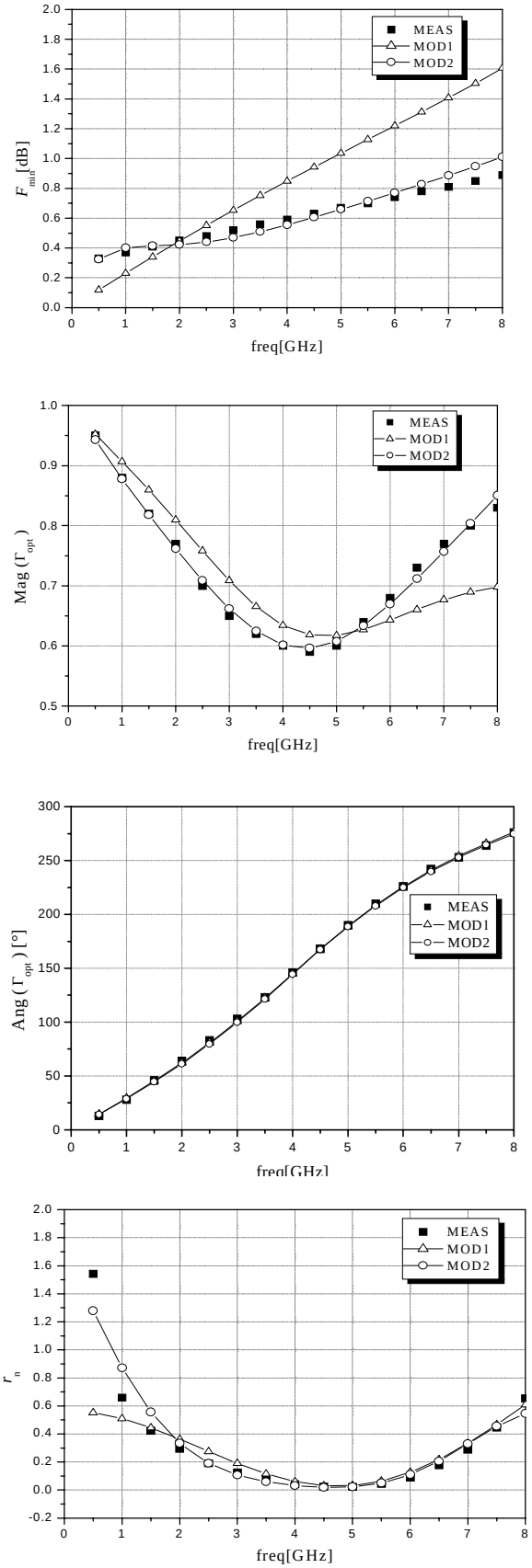

Fig. 3. Noise parameters for bias condition I_{ds}=20mA, V_{ds}=2V

Modified frequency dependences of noise parameters are also shown in Fig. 3. Corresponding curves are denoted by MOD2. It is obvious that significantly better agreement between measured and modeled parameters is now achieved.

The main advantage of the proposed model is that the error correction functions calculated for one bias condition can be used for efficient noise parameter modeling of the same transistor for other bias conditions. Since measured values of *S* parameters, as well as noise parameters, are different for various bias conditions, it is only necessary to repeat extraction procedure of equivalent circuit elements and equivalent temperatures. However, once determined error correction functions can be applied in the same form for various bias conditions.

As example, noise modeling of the same transistor is also done for new bias conditions: I_{ds}=15mA, V_{ds}=2V. Frequency dependences of the noise parameters obtained by proposed procedure using previously determined error correction functions (MOD2), are compared with measured values (MEAS) and shown in Fig. 4. A very good agreement is achieved in this case, too.

IV. CONCLUSION

New noise model of microwave FET transistors that presents modification of Pospieszalski's model is suggested in this paper. Modification is done by including the error correction functions to the Pospieszalski's standard noise equations. Due to this, deviations that exist between measured and modeled data are significantly reduced, and therefore better noise prediction is achieved. It is also shown that once determined error correction functions enable efficient noise modeling of the same transistor for various bias conditions. Proposed noise modeling procedure is applicable to any other MESFET / HEMT noise model presented in literature.

REFERENCES

[1] M.S. Gupta, O.Pitzalis, S.E.Rosenbaum, P.T.Greiling, "Microwave Noise Characterization of GaAs MESFETs: Evaluation by On-Wafer Low-Frequency Output Noise Current Measurement", *IEEE Trans. Microwave Theory Tech.*, vol. MTT-35, pp. 1208-1218, December 1987.

[2] H.Fukui, "Design of Microwave GaAs MESFET's for Broadband Low-Noise Amplifiers", IEEE Trans. Microwave Theory Tech., vol. MTT-27, pp. 643-650, July 1979.

[3] M.W.Pospiezalski, "Modeling of noise parameters of MESFET and MODFET and their frequency and temperature dependence" IEEE TransMicrowave Theory Tech, vol. MMT-37, pp.1340-1350, Sept. 1989.

[4] V.Marković, B.Milovanović, N.Maleš-Ilić, "MESFET Noise Model Based on Three Equivalent Temperatures", Proceedings of 27th European Microwave Conference, pp. 966-971, Jerusalem, Israel, Sept. 1997.

[5] P. Ratna and V.S.R. Kirty, A novel technique for accurate noise modeling, Proceedings of APMC2001, Taipei,Taiwan, pp.730-734.

[6] Advanced Desing System-version 1.5, Agilent Eesof EDA, 2000.

[7] Communications Components Desingner's Catalog, Hewlett Packard, 1997.

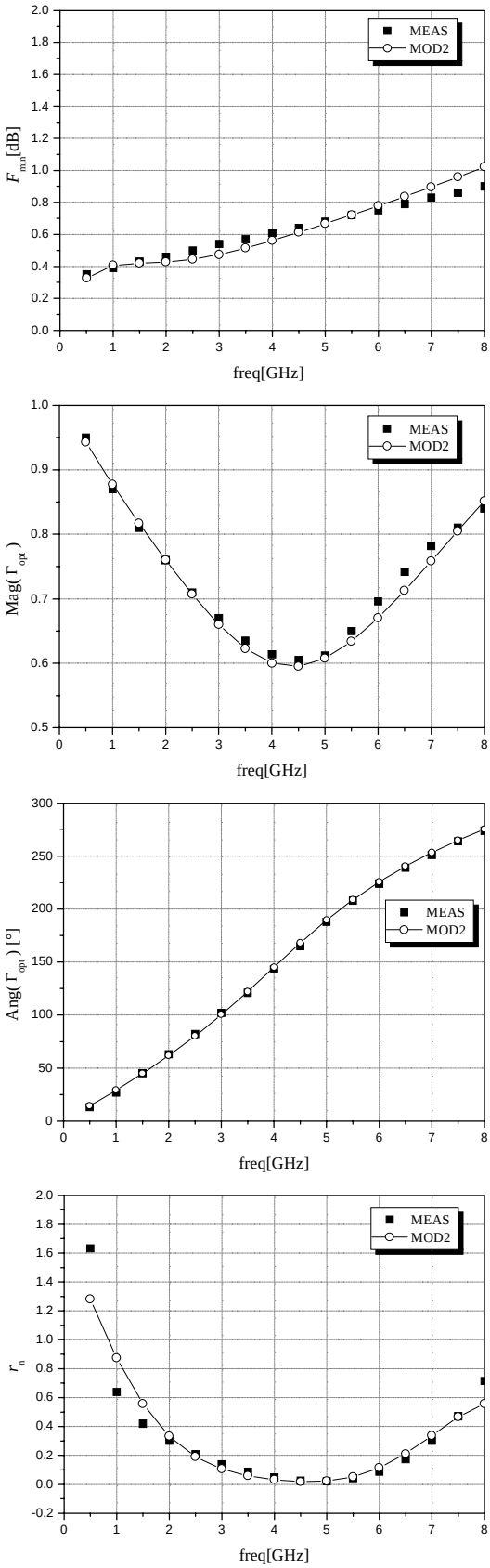

Fig. 4. Noise parameters for bias condition I_{ds}=15mA, V_{ds}=2V

Session TST:

Telecommunications Systems and Technology

Mobility management modeling with the use of an object-oriented approach

Ivaylo Atanasov[1], Evelina Pencheva[2]

Abstract - **The paper presents an object-oriented approach to modeling mobility management (MM) procedures in cellular networks. MM procedures are offered as services on Intelligent network (IN) platform. GSM mobility procedures incorporate common signaling blocks like authentication, new TMSI assignment, ciphering and database updating. Defining these blocks as Service Independent Building Blocks (SIBs) it is possible to offer MM services composed by an appropriate set of SIBs. Furthermore comparing MM procedures in GSM with those in GPRS and UMTS, it is possible to use almost the same SIBs in mobility services creation. Of course some of the SIBs defined for GSM have to be modified for GPRS and UMTS and some new ones have to be defined.**

Keywords – **Intelligent network services, SIBs, objects, mobility management**

I. Introduction

An intelligent network (IN) is "a communication network that is controlled by a software services layer enabling new services to be developed without the need to modify the network switching nodes".

ITU standardized IN in a continuous process and froze the standards at regular intervals, called capability sets (CSs). IN was initially designed for fixed voice telephony networks. CS-1 standard was powerful and simple, but it was disabled to meet the requirements for mobile communications. The mobile networks incorporate some kind of intelligence like mobility management and in-call mobility. In case of a mobile terminating call the network has to contact with the subscriber and therefore to keep track of where his telephone is at that time. During a call, it is possible that a subscriber will move out of reach of the antenna to which he or she is connected. The network must be able to reconnect the subscriber as quickly as possible to the closest available new antenna without breaking the call. So to lift some of the limitations of CS-1, CS-2 was defined. CS-2 allows user interactions to take place outside the context of a call. CS-2 allows call-related and call-unrelated interactions to use out-channel signaling connections. So new mobility management services (MM) can be offered on the IN platform.

IN recognizes the need for efficient creation of new services. It defines services as composition of features, which in turn are composed out of elementary building blocks, SIBs. There is commonality or a "red thread" in all the scenarios the mobile telephone is involved. Some individual blocks in signaling procedure are applied to all: mobile originating, mobile terminating and location updating. Defining these individual blocks as SIBs it is possible to offer MM services composed by an appropriate set of SIBs.

Furthermore comparing MM procedures in GSM with those in GPRS and UMTS, it is possible to use almost the same SIBs in mobility services creation. Of course some of the SIBs defined for GSM have to be modified for UMTS and some new ones have to be defined. The paper investigates the common parts in MM procedures in GSM, GPRS and UMTS and presents an object-oriented approach to defining SIBs that can be used in mobility services creation.

II. Service creation in a mobile IN network

Before presenting details on how IN mobility services can be defined, some signaling procedures for MM in GSM, GPRS and UMTS are considered in brief. In order to simplify the descriptions we will restrict the MM procedures to location area update (LAU) and routing area update (RAU). Nevertheless the identified steps are common for all: IMSI attach, LAU, RAU, mobile originating call and mobile terminating call.

In a possible architecture of an IN structured mobile network the MSC implements the service switching function (SSF) and the call-unrelated service function (CUSF); the HLR is integrated with the service data function (SDF) and in addition to mobile subscriber data it contains an information about IN services; the SCP resides the logic of the services and implements the service control function (SCF).

Let us assume that there is a signaling link between the mobile telephone (MT) and the radio access network. Before providing the required service the MSC requests authentication data. Receiving the necessary information the MSC starts authentication procedure. If authentication succeeds the MSC activates ciphering, which is followed by new TMSI assignment. The next step depends on the requested service.

[1] Ivaylo Atanasov is with Faculty of Communications, Technical University of Sofia, 8 Kl. Ohridski Blvd., 1000 Sofia, Bulgaria, e-mail iia@tu-sofia.bg

[2] Evelina Pencheva is with Faculty of Communications, Technical University of Sofia, 8 Kl. Ohridski Blvd., 1000 Sofia, Bulgaria, e-mail enp@tu-sofia.bg

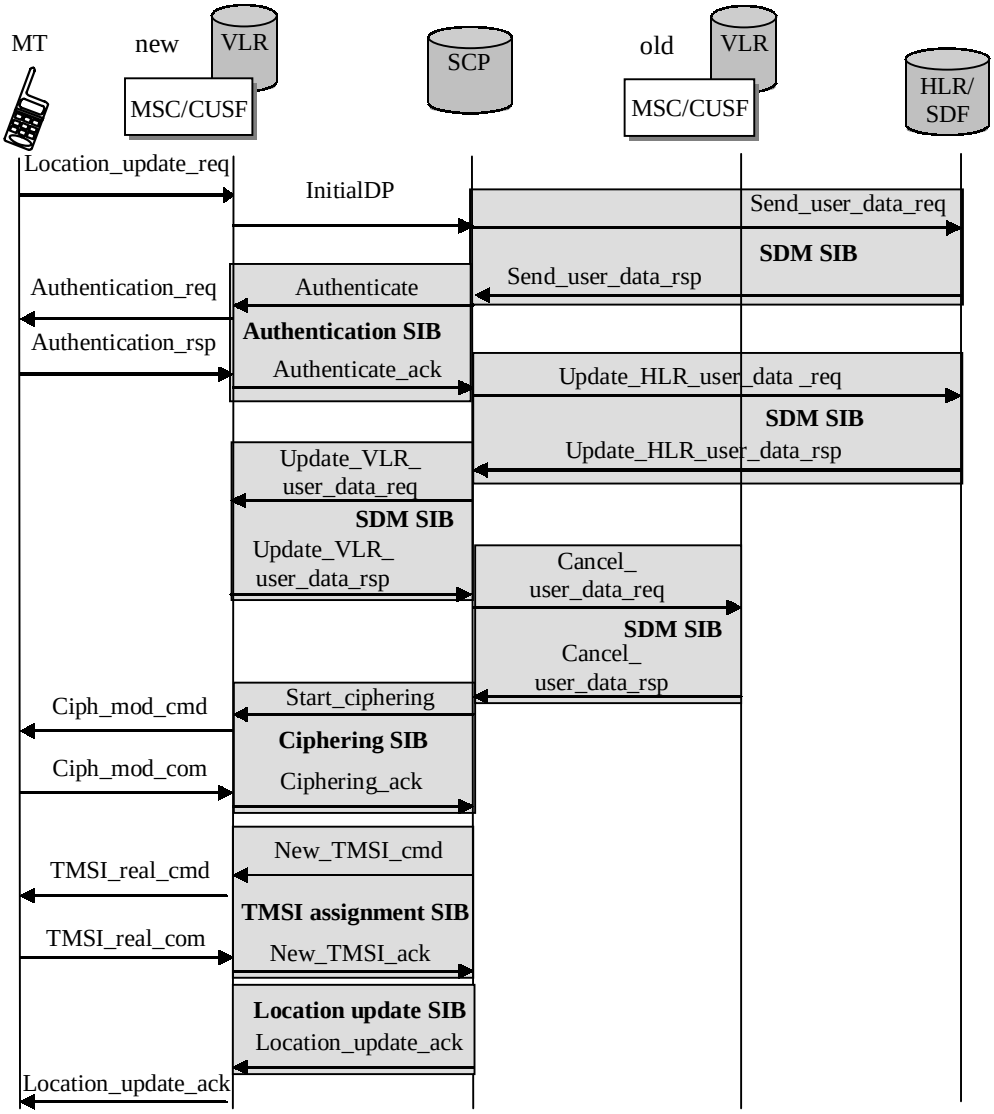

Figure 1 Inter-MSC LAU service with the use of SIBs

By modularizing the MM procedures in this way we can define SIBs corresponding to the identified common blocks. So, the following SIBs are necessary to offer GSM/GPRS/ UMTS mobility functionality:

- Authentication SIB – generates data required for authentication and checks the calculated value against the returned value.
- Ciphering SIB – instructs the radio access network to cipher a channel to the MT.
- TMSI assignment SIB – issues a new TMSI to the MT.
- Service data management SIB – used for creating, updating and deleting records on database. This SIB is defined in CS-1 and can be adapted for mobile subscriber data management.

In order to define service specific parts some more SIBs have to be defined.

- Location update SIB – if LAU procedure is successful, then the user is informed accordingly or else the SIB is used to process any errors that may have been occurred during the procedure.
- Mobile originating SIB – checks the compatibility service requested by the user with the subscription for the user. Instructs the MSC capture a radio channel to the MT and forwards instructions on call completion to SSF.
- Mobile terminating SIB – instructs the SSF to check compatibility of incoming call with the mobile terminal and capture a radio channel to the MT;
- Paging SIB – instructs radio access network to page a MT in a specified area.

Figure 1 illustrates the inter-MSC LAU provided as IN service using the defined SIBs.

The MT detects that coverage is provided by a new location area and initiates the location update procedure. It transmits a *Location_update_req* message. The MSC/CUSF treats the message as an IN service trigger and requests instructions from the SCP how to proceed. The SCP invokes LAU service and requests authentication data for the subscriber from the

HLR/SDF (SDM SIB). The HLR/SDF returns authentication data for the user. The SCP invokes Authentication SIB and instructs MSC to send the *Authentication_req* message to the MT. The MT returns the authentication result. If authentication succeeds the SCP invokes the SDM SIB to update user location data in the HLR. In order to create a new user record on the new VLR the MSC initiates the SDM SIB. The SDM SIB is also used to delete the user record on the old VLR. Ciphering is activated with the use of the Ciphering SIB. The SCP invokes the TMSI assignment SIB to issue new TMSI to the MT. The service ends with the Location update SIB to inform the MT that LAU update is accepted.

III. An object-oriented approach to SIB definition

The described services cover the main steps in LAU procedure in GSM, GPRS and UMTS as a whole. However the Authentication sub-procedure in UMTS is more complicated than that in GSM (not discussed here) and there are some differences in massage parameters for the three systems. The SIB functionality, which is common, can be defined as an object type. The specific message parameters require redefinition of the corresponding SIB.

The object type for the generic Inter-MSC LAU service is presented in Figure 2 using the object-oriented concepts in SDL[3]. The common SIBs are defined by virtual SDL services. To adapt this generic service to GSM or GPRS the virtual SDL services have to be redefined. Following the object orientation the identified SIBs can be used for example in combined RAU/LAU in case of intra-SGSN RA update or in case of inter-SGSN RA update.

Figure 3 shows the specialization of the generic Inter-MSC LAU service for the combined RA/LA update in case of intra-SGSN RA update. The service is triggered by SGSN/ CUSF when the *RA_update_req* message is received. The message parameters indicate if the location area is changed with the routing area updating. The redefined start makes some settings specific for the GPRS MM procedure. As in this scenario the SGSN is involved, the SDM virtual services which requests authentication data and the Authentication virtual service have to be redefined. A new SDM virtual service associated with the SDM SIB is defined to update user data in the SGSN. A new RA update SIB is identified. If the RAU procedure is successful then the user is informed accordingly or else the SIB is used to process any errors that may have been occurred during the procedure. The RA update SIB is presented by the RA_update virtual service.

To apply the defined object types to combined RAU/LAU in case of inter-SGSN routing area update procedure new SIBs have to be defined, for example:

- SGSN context SIB – provides MM and PDP contexts for the subscriber;
- Update PDP context SIB – updates the existing PDP contexts for the subscriber in GGSN.

As in the former cases some of the SIBs have to be redefined.

[3] Specification and description language

Following the same approach common parts in GSM IMSI attach procedure and in GPRS/IMSI attach procedure can be identified and the corresponding SIBs can be defined.

- Attach SIB - informs the user about the successful IMSI attach procedure otherwise the SIB is used to process an exception situation during the procedure;
- Delete PDP context SIB – deletes the PDP contexts. This SIB may be used also in detach procedures.

IV. Conclusion

By modularizing the GSM mobility procedures it is possible to identify commonality within the various procedures. These common parts are defined as SIBs. The SIBs can be combined to create IN mobility service. Furthermore following the resemblance between the mobility management procedures in GSM, GPRS and UMTS it is possible to redefine the generic SIBs and to define some new ones. An object-oriented approach is used to define SIBs for generic mobility services and to redefine the SIBs according to the specifics in GSM, GPRS and UMTS. As object-oriented programming has become the industrial standard and the envisaged architecture of the future telecommunication networks is IN structured this approach can provide an elegant way in defining mobility services for next generation networks.

Reference

[1] ITU Q.1223, IN Global Functional Plane Architecture for Capability Set 2.
[2] ETSI TS 123 121, Universal Mobile telecommunications System, Architectural Requirements for Release 1999
[3] ETSI TS 123 060, General Packet Radio Service, Service Description.
[4] Gunnar Heine, GSM Networks: Protocols, Terminology, and Implementation, 1999

Virtual process type

<<block type LA_service>> Updating

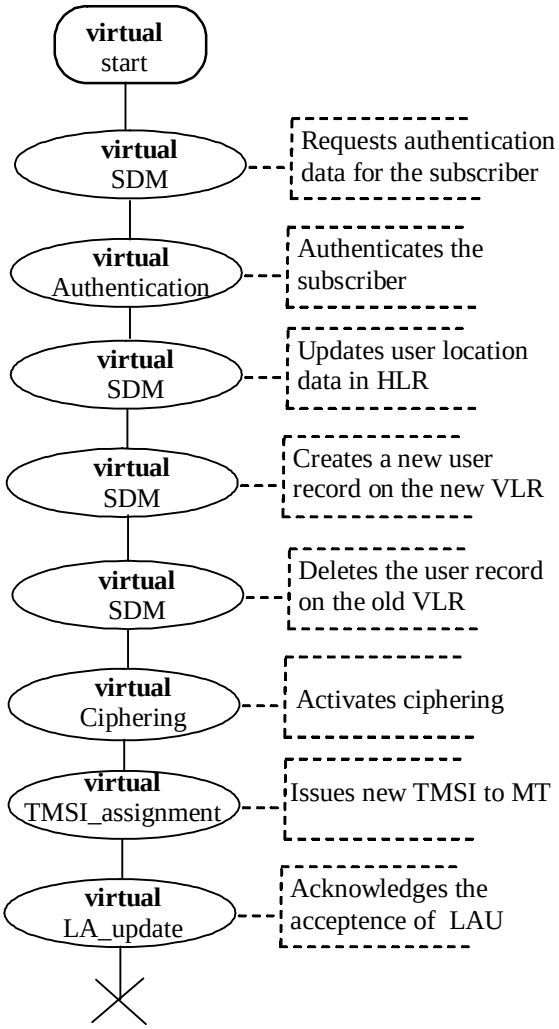

Figure 2 Generic inter_MSC Location update service, presented as SDL virtual process type

Redefined process type

<<block type RA_LA_service>> Updating inherits <<block type LA_service>> Updating adding

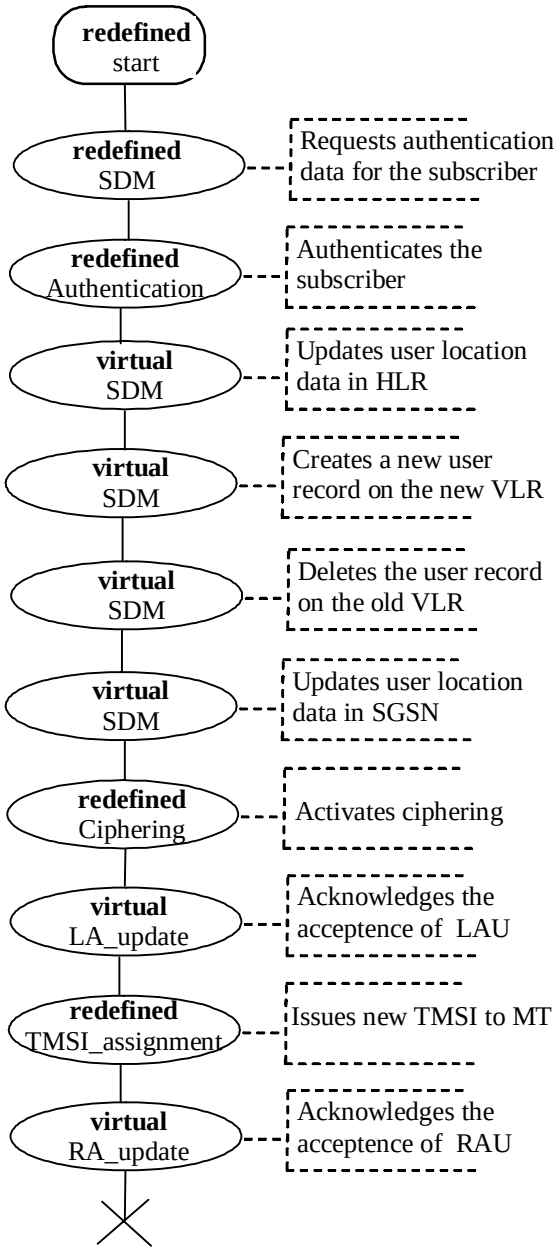

Figure 3 Specialised combined RA/LA update service in case of intra SGSN RA update prosedure, presented as SDL virtual process type

An Object-Oriented Approach to Mobility Service Creation

Ivaylo Atanasov[1]

Abstract - **The paper presents an object-oriented approach to modeling mobile value-added services. Service capabilities are set of building blocks that can be used to implement value-added services. The service capability features are common utility features that provide such things as authentication, authorization, registration, and notification services. The paper investigates how security features can be implemented using an object-oriented approach on the Intelligent network platform. It exploits the Service independent building block (SIB) concept of the IN conceptual model for service creation.**

Keywords – **Intelligent network services, SIBs, objects, authentication, ciphering**

I. Introduction

The three service classes (bearer services, teleservices and supplementary services) are all standardized in 2G and 3G mobile networks and their functionality is strictly specified. This means that no matter which operator provides them, they are always the same from the subscriber's perspective. Operators have longed for a set of tools which to build unique services, a means to distinguish themselves from the competition. Service capabilities are set of building blocks that can be used to implement value-added services. As the value added services themselves are not standardized, but only the building blocks, it is possible to implement them in a way that produces unique services. Service capabilities are accessible to applications via a standardized application interface. Various toolkits and mechanisms such as the SIM Application Toolkit (SAT), Mobile station Execution Environment (MExE), Customized Application for Mobile Enhanced Logic (CAMEL) and Intelligent network (IN) provide them.

Framework service capability features are common utility features that are used by nonframework features. They provide such things as authentication, authorization, registration, and notification services. Nonframework features are used by the applications as building blocks for value-added services. These features should be as generic as possible, so that the applications using the features are easily portable.

The paper investigates how security nonframework features may be implemented using an object-oriented approach on the Intelligent network platform.

To create services the IN conceptual model uses the Service independent building block (SIB) concept. It defines services as composition of features, which in turn are composed of elementary SIBs. An IN service creation environment allows even inexperienced service engineers to create services by clicking together elementary SIBs in a plug-and-play fashion.

II. SIBs supporting mobility procedures

By modularizing the GSM mobility procedures it is possible to identify commonality within the various procedures. Examples of common sub-procedures are authentication, new TMSI assignment, ciphering and database updating. These sub-procedures are self contained and identical irrespective of the mobility procedure using it. Each of these sub-procedures may be converted to a Service independent building block (SIB). The following list of SIBs may be identified:

- Authentication SIB – generates data required for authentication and checks the calculated value against the returned value.
- Ciphering SIB – instructs the radio access network to cipher a channel to the mobile telephone (MT).
- TMSI assignment SIB – issues a new TMSI to MT.
- Service data management SIB (SDM SIB) – used for creating, updating and deleting records on database.
- Location update SIB – if location area updating procedure is successful then the user is informed accordingly or else the SIB is used to process any errors that may have been occurred during the procedure.
- Mobile originating call SIB (MOC SIB) – checks the compatibility service requested by the user with the subscription for the user. Instructs MSC capture a radio channel to the MT and forwards instructions on call completion to Service Switching Function (SSF).
- Mobile terminating call SIB (MTC SIB) – instructs SSF to check compatibility of incoming call with the mobile terminal and capture a radio channel to the MT.
- Paging SIB – instructs radio access network to page a MT in a specified area.

For example, the mobile terminating call service in GSM uses Paging SIB, SDM SIB, Authentication SIB, Ciphering SIB, TMSI assignment SIB and MTC SIB. It proceeds in the following way. Receiving an *Initial address message* from the GMSC the MSC/SSF treats it as a service trigger and sends an *InitialDP message* to the Service Control Point (SCP). The SCP starts service logic with the Paging SIB in order to contact with the MT. The SCP also sends a *requestReport* message to the SSF, indicating the detection point (DP) where it wants to be notified. When the MT answers the paging, the SSF sends an *eventReport* message. The SCP proceeds with

[11] Ivaylo Atanasov is with Faculty of Communications, Technical University of Sofia, 8 Kl. Ohridski Blvd., 1000 Sofia, Bulgaria, e-mail iia@tu-sofia.bg

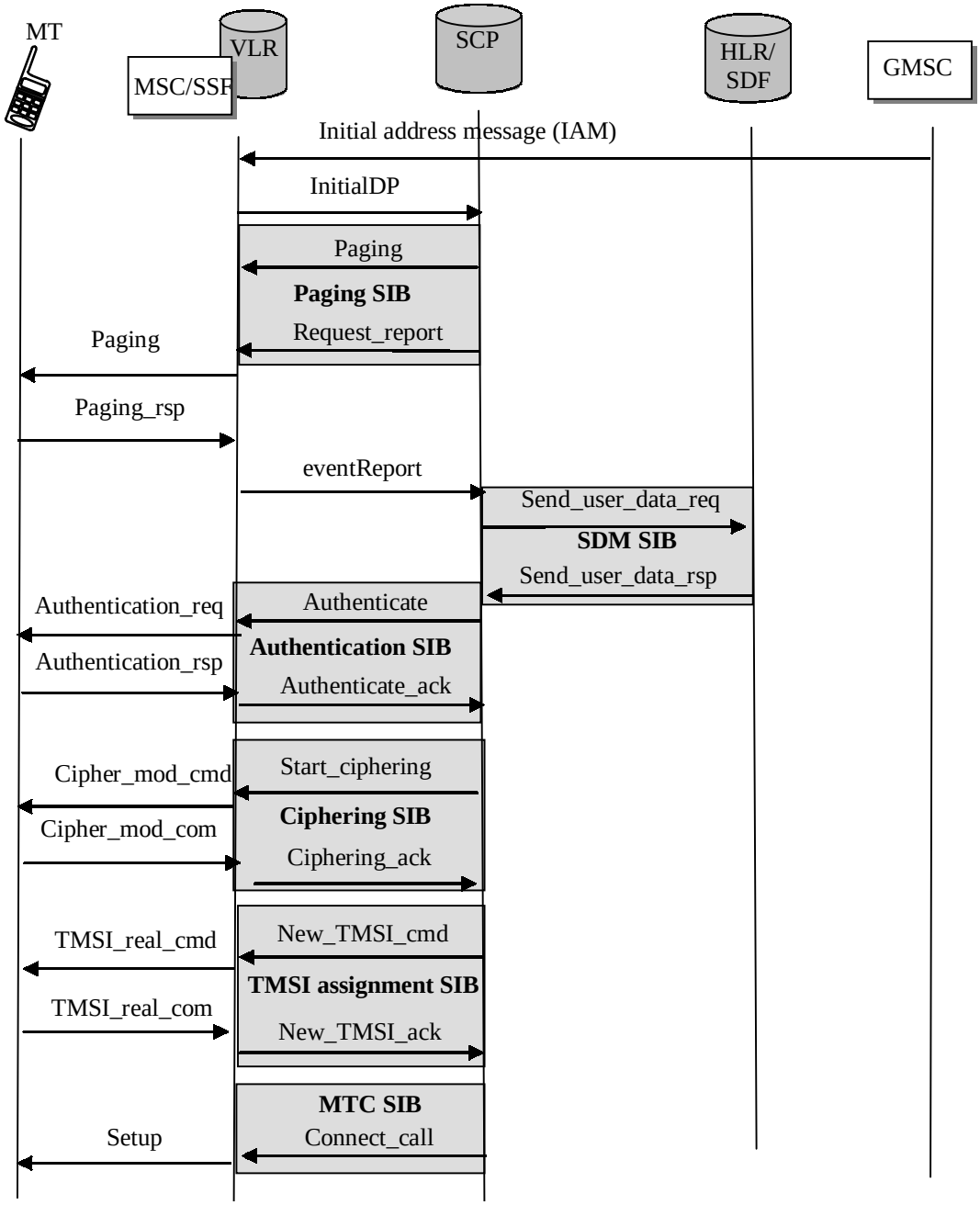

Figure 1 Mobile terminating call service by the use of SIBs supporting mobility

service logic execution starting the SDM SIB to request authentication data for the subscriber from the HLR/SDF. Having the needed information the SCP invokes the Authentication SIB and instructs the MSC to send *Authentication_req* message to the MT. The MT returns the authentication result. If authentication succeeds the SCP invokes the Ciphering SIB which instructs the MSC to start ciphering over the air interface. A new TMSI is assigned to the MT by the use of the TMSI assignment SIB. The SCP instructs the SSF to check compatibility of the incoming call with the MT and capture a radio channel to the MT using the MTC SIB. Figure 1 shows the mobile terminating call service created with the use of identified SIBs.

The appropriate SIB set can be used to create the mobile originating call service and the location update service.

The mobility procedures in GPRS and UMTS follow almost the same steps as those in GSM. The main deference is in the security sub-procedure, which is more complicated in UMTS. UMTS uses mutual authentication, more advanced radio access network encryption and integrity protection.

III. Security in mobile environment

The most important security features in the GSM system are:

- Authentication of the user
- Encryption of communication in radio interface
- Use of temporary identities.

As GSM system became more and more successful, the usefulness of these basic security features also becomes more and more evident. Naturally, it has been a leading principle in specification work of UMTS security to carry these features over to the new system.

The success of GSM also emphasised finally the limitations of its security. A popular technology is also tempting for intruders. The properties of GSM that have been most criticized on the security front are the following:

- Active attacks towards the network are possible in principle: it refers to somebody who has the required equipment to deviate communication from legitimate network/ terminal equipment.
- Sensitive control data, e.g. keys used for radio interface ciphering, are sent between different networks without ciphering.
- Some parts of the security algorithms are kept secret but they trend to be revealed sooner or later.
- Keys used for radio interface ciphering become eventually vulnerable to massive attacks where somebody tries all the possible keys until one matches.

In UMTS countermeasures for perceived weaknesses in GSM are developed. The most important security features of UMTS are the following:

- Mutual authentication of the user and the network
- Use of temporary identities
- Radio access network encryption
- Protection of signaling integrity inside UTRAN.

Publicly available cryptographic algorithms are used for encryption and integrity protection. Algorithms for mutual authentication are operator-specific.

IV. From SIBs to objects

Defining the generic functionality of GSM mobility procedures by the use of SIB object types, it is possible to extend the model with GPRS and UMTS mobility procedures. For example, a new UMTS object type can inherit basic properties from an already existing GSM type and extend it with new features. Common objects as the TMSI assignment SIB and the Service data management SIB can be reuse in many service scripts.

The focus in the paper is on security sub-procedures: Authentication SIB and Ciphering SIB.

Considering the common parts in GSM and UMTS security functions the following object types can be defined.

- *User identity request* object type– allows the identification of a user on radio path by means of IMSI. The mechanism should be invoked by the serving network when the user registers for the first time in a serving network or when the serving network cannot retrieve the IMSI from the TMSI. This object types is used to negotiate whether the authentication is necessary. For GSM and UMTS the specializations use CKSN (Cipher key sequence number) and KSI (key set identifier) accordingly.
- *User authentication* object type - generates user authentication vector that is temporary authentication and key agreement (AKA) data enabling a VLR/SGSN to engage AKA with a particular user. The specializations of this object types are for GSM and UMTS authentication procedures. GSM authentication vector consists of three elements: a) network challenge RAND, b) an expected user response SRES and c) a cipher key Kc. UMTS authentication vector consists of five elements: a) network challenge RAND, b) an expected user response XRES, c) a cipher key CK, d) an integrity key IK and e) network authentication token AUTN.
- *Security algorithm decision* object type – for GSM determines which ciphering algorithm is to be used and for UMTS which UMTS Encryption algorithms (UEAs) and UMTS Integrity algorithms (UIAs) are allowed to be used in order of preference.
- *Start security mode* object type – sends a start security command to the BSC/SRNC. For GSM to activate ciphering the value Kc and the reference to the chosen A5/X algorithm is sent. For UMTS an ordered list of allowed UEAs and IK to be used are sent. The message contains the ordered list of allowed UEAs and CK to be used too.
- *Start ciphering* object type – starts ciphering.
  - For GSM at BSS the Kc and information about cipher algorithm is retrieved and a message is forwarded to MT. This message triggers the MT to enable ciphering of all outgoing data and deciphering all incoming information. The MS confirms the change to ciphering mode to the MSC/VLR.
  - For UMTS the SRNC decides which algorithm to use, generates a random value FRESH and initiates downlink integrity protection. The SGSN sends a security mode command message including user equipment security capability, the UIA and FESH to be used. Before sending this message the SRNC generates the MAC-I and attaches this information to the message. At reception of the message the MT controls that the user equipment security capabilities received is equal to the user equipment security capabilities sent in the initial message. The MT verifies the integrity of the message by calculating the XMAC-I. If all controls are successful, the MT compiles a message that confirms the security mode and generates MAC-I for this message. At the reception of response message the SRNC verifies the data integrity of the message by comparing the received MAC-I with the generated XMAC-I. The SRNC acknowledges the security mode to the VLR/SGSN.

The Authentication SIB can be defined as a generic object type composed of the *User identity request* object type and the *User authentication* object type. The Ciphering SIB can be defined as a generic object type composed of the *Security algorithm decision* object type, the *Start security mode* object type and the *Start ciphering* object type. Figure 2 illustrates the generic definitions of the Authentication SIB and the Ciphering SIB.

For GSM and UMTS these generic object types are inherited by specializations representing the specific features of the security procedures.

For example, the GSM Authentication SIB is composed of the *GSM User identity request* object type that inherits the *User identity request* object type and the *GSM User authentication* object type that inherits the *User authen-*

tication object type. The GSM Ciphering SIB is composed of the *GSM Security algorithm decision* object type that inherits the *Security algorithm decision* object type, the *GSM Start security mode* object type that inherits the *Start security mode* object type and the *GSM Start ciphering* object type that inherits the *Start ciphering* object type. Figure 3 illustrates the adopted approach.

Similar definitions of the UMTS Authentication SIB and UMTS Ciphering SIB can be done.

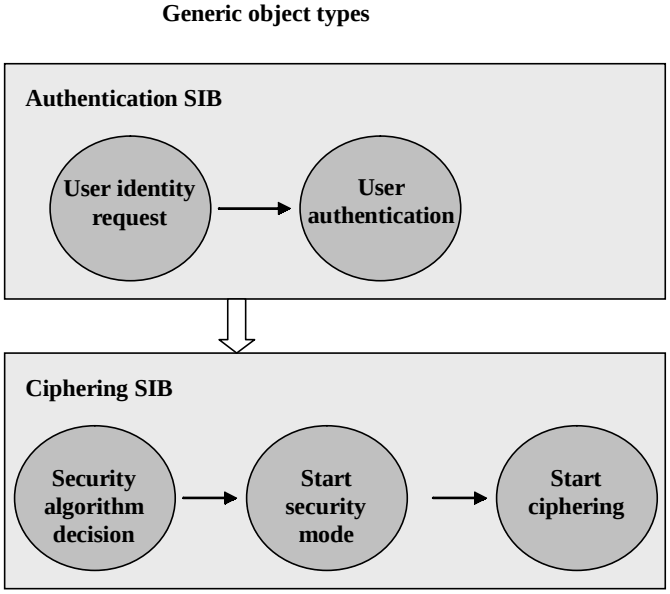

Figure 2 The generic object types:
Authentication SIB and Ciphering SIB

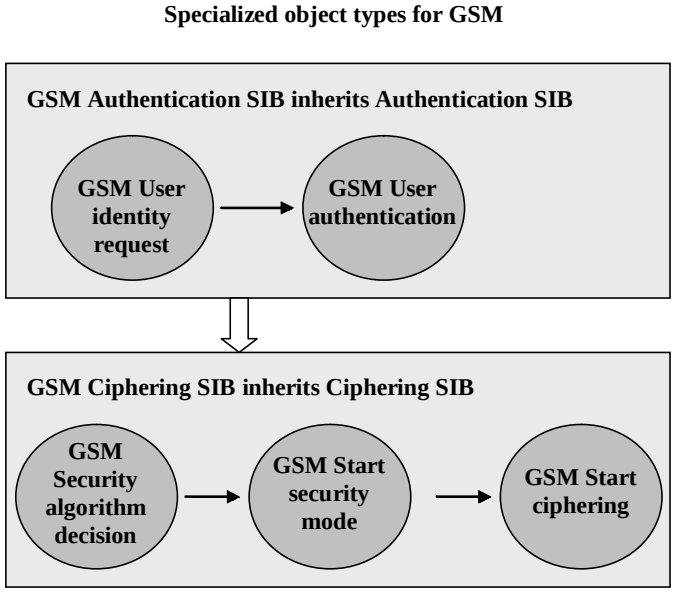

Figure 3 The specialized object types:
GSM Authentication SIB and GSM Ciphering SIB

V. Conclusion

A new approach to provisioning mobile value-added services is suggested. The service capabilities can be offered as a composition of SIBs defined as object types. The generic object types represent the common parts in mobility management procedures for GSM, GPRS and UMTS systems. The specific parts are defined by the use of specialized object types that inherit communality in the generic object types. The approach is illustrated with concern of the security procedures in GSM and UMTS. Both systems apply common security functions as: authentication of the user, encryption of communication in radio interface, use of temporary identities. Adding to that, UMTS applies integrity check of the signaling data. By identification of common parts some generic object types are defined and to consider the specifics for GSM and for UMTS some object types are redefined and new ones are defined.

The approach suggests a flexible way of capability service feature implementation that exposes all the advantages of object-oriented programming.

Reference

[1] ITU Q.1223, IN Global Functional Plane Architecture for Capability Set 2.
[2] ETSI TS 123 121, Universal Mobile telecommunications System, Architectural Requirements for Release 1999
[3] ETSI TS 123 060, General Packet Radio Service, Service Description.
[4] Gunnar Heine, GSM Networks: Protocols, Terminology, and Implementation, 1999.

Evaluation of QOS Enhancements Provided by EDCF Medium Access Scheme in IEEE 802.11 WLAN

Zoran Dimitrovski[1] and Liljana Gavrilovska[2]

Abstract - **This paper presents an evaluation of the effects that have the prioritizing parameters introduced by the EDCF access scheme (adopted in an upcoming IEEE 802.11e standard) on QoS improvements versus DCF medium access scheme, defined with the legacy 802.11 standard. Also we analyze the impact of the frame length and the contention-free burst (CFB) mechanism on QoS performances produced by the EDCF.**

Keywords - **WLAN, QoS, IEEE 802.11e, EDCF, simulation**

I. Introduction

The support of higher data rates and widespread use of multimedia applications push the demand of IEEE 802.11 WLANs to support both traditional data and multimedia applications in the same infrastructure. However, legacy IEEE 802.11 MAC specification, which follows the best-effort paradigm, doesn't provide any traffic prioritization to meet the QoS requirements imposed by multimedia applications such as real time voice, audio and video. Therefore, the IEEE Task Group E is currently working on a new IEEE 802.11 MAC specification, named IEEE 802.11e [4], which will enhance legacy MAC specification to support QoS sensitive multimedia applications. The legacy IEEE 802.11 MAC specification [2] defines two access schemes: DCF (Distributed Coordination Function) and PCF (Point Coordination Function). DCF uses CSMA/CA (Carrier Sense Multiple Access with Collision Avoidance) algorithm and it is contention-based access scheme supporting asynchronous data transfer, while PCF uses a central-controlled polling method to support synchronous data transmission. The IEEE 802.11e standard introduces two additional access schemes: *EDCF (Enhanced Distributed Coordination Function)* and *HCF (Hybrid Coordination Function)*. EDCF is an extension to the DCF contention-based access scheme which provides service differentiation via prioritization of traffic supporting prioritized QoS, while HCF is a modification to the PCF for more efficient polling method supporting both prioritized and parameterized QoS.

Recently, several authors [1, 5, 6, 7] have shown interest in evaluation of QoS enhancements provided by the new access schemes defined with IEEE 802.11e. Performance analysis show that EDCF can support better QoS than DCF [9], but as the network load is increased QoS improvements of EDCF are diminished, especially for high demand QoS sensitive traffic, such as video. The main reason for this is inadaptable EDCF prioritizing parameters to the network conditions. This paper presents simulation-based evaluation of QoS enhancements provided by the EDCF over the DCF access scheme through analysis of the effects that have the EDCF prioritizing parameters on the QoS performances of high priority traffic flows. Furthermore, this paper analyses the effects of the frame length and the contention-free burst (CFB) mechanism [8] on QoS provided by the EDCF access scheme for given EDCF prioritizing parameters. Simulation model based on Microsoft Visual Basic and SQL Server 2000 is utilized to investigate effects of the EDCF prioritizing parameters, the frame length and the CFB mechanism on two QoS parameters of traffic flows: throughput and MAC frame delay.

The paper is organized as follows: Section II gives short descriptions of the legacy 802.11 MAC/DCF and 802.11e MAC/EDCF. Section III describes the simulation scenarios, while in Section IV are given results and analysis. Conclusions are outlined in Section V.

[1] KJP "Niskogradba"-Bitola, Bul. 1vi Maj bb, PO Box 183, 7000 Bitola, Macedonia, E-mail: dimzor@sonet.com.mk

[2] Faculty of Electrical Engineering, Karpos II bb, PO Box 574, 1000 Skopje, Macedonia, E-mail: liljana@etf.ukim.edu.mk

II. DCF and EDCF

DCF is basically listen-before-talk access scheme. According to DCF, each station senses the medium before initiating a frame transmission. If the medium is found idle for a time interval longer than DCF InterFrame Space (DIFS), then the station can transmit frame immediately. Otherwise the station shall defer until medium has been detected idle for at least DIFS interval and after deferral, the station will start backoff procedure setting its backoff timer at value between zero and current Contention Window (CW) size as follows:

$$BackoffTime = Rnd(0, CW) \times SlotTime \qquad (1)$$

where $Rnd(0,CW)$ is a pseudorandom integer drawn from a uniform distribution over the interval $[0,CW]$ and *SlotTime* is constant which depends on the PHY layer type. During backoff procedure, the station shall sense the medium to determine whether there is activity during each backoff slot. If the medium is free the station shall decrement its backoff timer by *SlotTime*. Otherwise, the backoff timer is paused and is resumed after the medium has been sensed idle for duration of at least DIFS interval. As soon as the backoff timer expires, the station is authorized to access the medium and transmit the pending frame. Since in wireless environment collision detection is impossible due to significant difference between transmitted and received power levels, the DCF uses method of positive acknowledgment to notify the sending station that the transmitted frame has been successfully received. The transmission of the acknowledgment is initiated at a time interval equal to Short InterFrame Space (SIFS) after the end of the successful reception of frame. If the acknowledgment is not received, the sending station assumes that the transmitted frame was lost and starts the backoff procedure again. To reduce the probability of collisions, after each unsuccessful transmission attempt, the *CW* is doubled according to:

$$CW_k = 2^{k+p-1} - 1 \quad (2)$$

where k is the number of attempts to transmit the frame, and p is constant (which depends on PHY layer type) defining the minimum contention window for the first attempt, $CW_{min}=2^p-1$. For each unsuccessful transmission, contention window is doubled until a maximum value CW_{max} is reached. After successful transmission, the backoff procedure is also performing for the next frame but contention window is reset to a fixed minimal value CW_{min}. According this, the value of CW that should be used in setting backoff timer Eq.(1) depends on the current attempt to transmit the frame for which the backoff procedure is performed, and $CW_{min} \leq CW \leq CW_{max}$.

EDCF is simply enhancement of DCF access scheme with possibility of traffic prioritization, thus in what follows we will pay attention on main difference between DCF and EDCF. As it can be seen from DCF access scheme, described above, at least two contention parameters can be used to provide medium access prioritization: DIFS and CW used in calculation of backoff timer. Generally, lower DIFS and CW values will give higher priority for medium access. Following this idea, EDCF allows traffic to be classified into different Traffic Categories (TC) with different values of the above contention parameters. Classification is performed according priority value in the MAC frame header.

Instead of waiting a DIFS interval before trying to access the medium, or continuing to decrement backoff timer after it was paused as in DCF, an interframe space called Arbitration InterFrame Space (AIFS) is used for each TC. The AIFS interval for TC i is set according to the following formula:

$$AIFS(TC_i) = DIFS + \Delta TC_i \times SlotTime \quad (3)$$

where ΔTC_i is integer and $\Delta TC_i \geq 0$. This means that TC using large ΔTC_i (large AIFS) will have lower priority than TC using small ΔTC_i (small AIFS), since it will wait longer before trying to access the medium or continuing to decrement backoff timer after it was paused. Note that minimal AIFS interval according Eq.(3) is equal to DIFS.

To be able to further differentiate between TCs, the contention window from which the backoff timer is calculated is different for each TC. The backoff timer for TC i is calculated as follows:

$$BackoffTime(TC_i) = Rnd(1, CW(TC_i)+1) \times SlotTime \quad (4)$$

where $Rnd(1,CW(TC_i)+1)$ is a pseudorandom integer drawn from a uniform distribution over the interval $[1,CW(TC_i)+1]$. $CW(TC_i)$ is current contention window size for TC i, $CW_{min}(TC_i) \leq CW(TC_i) \leq CW_{max}(TC_i)$, where $CW_{min}(TC_i)$ and $CW_{max}(TC_i)$ is minimal and maximal value of the contention window for TC i. Choosing a smaller CW_{min}/CW_{max} for a given TC will cause generating shorter backoff intervals for that TC, thus gaining priority over a TC with larger CW_{min}/CW_{max} which generates longer backoff intervals.

According, optional contention-free burst (CFB) mechanism [7, 8], a station that has gained access to the medium can send more then one frame without contending for the medium again. After getting access to the medium, the station is allowed to send multiple frames from given TC, as long as the total access time does not exceed the TXOPLimit parameter for that TC.

III. Evaluation

In order to evaluate influence of the EDCF prioritizing parameters: AIFS and CW_{min}, the frame lengths and the CFB mechanism on the QoS improvements of EDCF over DCF access scheme, an event-driven simulator with support of both DCF and EDCF has been implemented. The simulator was built by using Microsoft Visual Basic and SQL Server 2000. Simulation model assumes ideal PHY channel with negligible propagation delay and no transmission errors, so eventually frame retransmission is a result of collision. We consider an infrastructure-type WLAN where all traffic flows generated from wireless stations are directed to the AP. All PHY dependent MAC parameters were set assuming 802.11b [3] DSSS 11 Mbps PHY layer, i.e. DIFS=50μs, SIFS=10μs, SlotTime=20μs, and for DCF the CW_{min} and CW_{max} are set to 31 and 1023, respectively. Table I describes simulated scenario. Three different types of traffic are considered: voice, video and data.

Table I: Traffic types and *default* EDCF parameters

Traffic type	*Inter-arrival frame time*	*Frame Size (bytes)*	*Data Rate*	*default EDCF parameters*		
				ΔTC_i	CW_{min}	CW_{max}
Voice	Const.(0.025s)	200	64kbps	0	7	15
Video	Const.(0.004s)	1000	2Mbps	0	15	31
Data	Exp. (0.012s)	1500	1Mbps	1	31	1023

Each station generates only a single type of traffic, and hence, we refer to a station according the traffic type that it generates, i.e., the station that generates data traffic we refer as data station. In order to simulate high-load network environment, in considered scenario we simulate with four voice, three video and four data stations, generating total offered load of 10.256Mbps. Furthermore, because each station generates only a single type of traffic, stations are modeled with a single transmission queue (MAC buffer) of infinitive size. Table I also shows *default* EDCF parameters for each traffic type according draft version 4.0 [7] for voice, video and data traffic.

IV. Simulation Results

A. Effects of the EDCF parameters: AIFS, CW_{min}

To evaluate QoS improvements for the prioritized voice and video traffic flows provided by EDCF, we perform simulations of described scenario for both DCF and EDCF access schemes. Furthermore, to examine effects that have solely AIFS or CW_{min} parameter on the QoS performances of the traffic flows we perform series of simulations under EDCF varying AIFS and CW_{min} parameter of the data flows, but keeping *default* EDCF parameters for the voice and video flows and *default* values of $CW_{min/max}$ and AIFS for data flows, respectively. Figs. 1 and 2 show Cumulative Distribution Function (CDF) of MAC frames delay for the voice flows, as the AIFS and CW_{min} for the data flows are varied. MAC frame delay is measured as a time interval between the moment when the frame enters the MAC buffer

and the moment when ACK is received for that frame. Time dependence of throughput achieved by the video stations as the AIFS and CW_{min} for the data flows are varied, are shown on Figs. 3 and 4. Points in throughput characteristics represent mean throughput achieved by all stations generating video traffic. Note that in all simulations the data stations are activated in the 5-th second of simulation time. In graphs AIFS is represented by a number instead of time, the actual AIFS in time is determined if the given value of AIFS is substituted as ΔTC_i in Eq.(3).

By observing CDF of frame delay for the voice flows we can notice that as the AIFS and CW_{min} for the data flows are increased, CDF characteristics become steeper indicating that maximum delay is reduced and more frames have a delay with in small range of values, meaning jitter is reduced. Increasing the AIFS and CW_{min} for data flows, also increase throughput of the video flows and reduce their throughput variance. Analyzing throughput characteristic of the video flows we can notice that there is some saturation in the QoS improvements as the values of AIFS or CW_{min} for data flows are increased.

B. Effects of frame length of the prioritized flows

To analyze the effects of the video frame length on the QoS performances provided by EDCF, simulations of described scenario under EDCF are performed for different lengths of frames generated by the video stations. Note, that in all simulations for voice, video and data flows are set *default* EDCF parameters. Fig. 5 shows CDF of MAC frame delay for the voice flows, while throughput for the video flows is shown on Fig. 6. By observing results for the video flows we can notice that increasing the length of video frame improve their QoS performances. However, increased video frame length has negative impact on QoS performances of the voice flows Decrease of slope for CDF voice delay characteristic indicate that increase of video frame length, also increase jitter and maximum delay of voice frames. This degradation of delay performance for the voice flows is due to extended transmission times of video stations by using longer frames.

C. Effects of Contention-Free Burst (CFB) mechanism

Results from simulation performed in order to evaluate the effect of the CFB mechanism on EDCF QoS performances are presented in this section. Because previous analysis show that QoS performances of the video flows, are far more degraded than QoS performances of the voice flows for low values of the EDCF parameters, in performed simulations, contention-free bursting is enabled only for the video stations. TXOPlimit parameter was set on value of 3.5ms which allows transmitting a burst of up to four video frames with length of 1000 bytes in one access to the medium. Note that again *default* EDCF parameters are set for all traffic flows. Fig. 7 show CDF of MAC frame delay for the voice flows, while on Fig. 8 is presented throughput for the video flows.

From the presented results we can conclude that enabled CFB mechanism for the video flows significantly improve their QoS performances. For the same EDCF prioritizing parameters utilizing CFB, the video flows achieve almost constant throughput with value nearly 2Mbps. CFB also improve the overall throughput for the whole WLAN because the overhead of backoff and deference is reduced. Namely, according simulation results overall throughput without CFB for video was 7.2Mbps; while with enabled CFB for video overall throughput was increased on 7.9Mbps. However, similar like increasing frame length of the video flows, CFB introduces degradation in delay and jitter of the voice flows.

V. Conclusion

This paper presents evaluation of QoS support provided by EDCF medium access scheme, adopted in an upcoming 802.11e standard. Simulation results show that EDCF can provide prioritized channel access, which results in improvements over DCF in the QoS performances for traffic flows categorized as high priority by means of the EDCF prioritizing parameters. However, EDCF can "hardly" provide suitable QoS performances for high-demand prioritized traffic flows, such as video flows, in high-load network condition. In order to provide acceptable QoS performances for the video flows, the EDCF prioritizing parameters (AIFS and CW_{min}) for the low priority data flows should be set on high values, which results in their significant performance degradation. Also, above some value of AIFS or CW_{min} parameter there is a drastic improvement in the QoS performances of the high-demand video flows. Further increasing of AIFS and CW_{min} introduces minimal QoS improvements. Comparing effects of AIFS and CW_{min} we can conclude that AIFS has stronger prioritizing effect than CW_{min}, but simulations show that both have stronger impact on the delay characteristic than on the throughput of the traffic flows. Utilizing longer video frames or enabling CFB for the video flows improve QoS performances for them even at lower values of AIFS and CW_{min} for the data flows, but results in degradation of performances for the other priority flows (voice flows) with shorter frame length. CFB also provide better channel utilization, increasing global throughput in system. Taking into account effects of increased frame length and CFB on QoS provided by EDCF, we can conclude that these methods can be used to provide better QoS performances for high-demand QoS sensitive traffic with fixed low values of the EDCF parameters for low priority traffic.

VI. References

[1] D. Gu, J. Zhang, "QoS enhancement in IEEE 802.11 wireless local area networks", *IEEE Commcations Magazine*, Volume: 41 Issue: 6, Page(s): 120-124, June 2003

[2] IEEE std 802.11-1999, Part 11: Wireless LAN Medium Access Control (MAC) and Physical Layer (PHY) specifications, 1999

[3] IEEE std 802.11b-1999, Higher-Speed Physical Layer Extension in the 2.4 GHz Band, 1999

[4] IEEE 802.11e draft/D2.0, Medium Access Control (MAC) Enhancements for Quality of Service (QoS), November 2001

[5] P. Garg, R. Doshi, R. Greene, M.Baker, M. Malek, X. Cheng, "Using IEEE 802.11e MAC for QoS over Wireless" *The Proceedings of the IPCCC 2003*, Phoenix, Arizona, April 2003

[6] S. Mangold, S. Choi, P. May, O. Klein, G. Hiertz, L. Stibor: ″IEEE 802.11e Wireless LAN for Quality of Service (invited paper)", *Proceedings of the European Wireless*, Vol. 1, pp. 32-39, Florence, Italy, February 2002

[7] S. Choi, J. del Prado, S. Shankar, S. Mangold, ″IEEE 802.11e Contention-Based Channel Access (EDCF) Performance

Evaluation" *Proceedings of the ICC 2003*, Anchorage, AL, USA, May 2003

[8] S. Choi, J. del Prado, A. Garg, M. Hoeben, S. Mangold, S.Shankar, W. Menzo, "Multiple Frame Exchanges during EDCF TXOP," *IEEE 802.11-01/566r3*, January 2002.

[9] Z. Dimitrovski, L. Gavrilovska, "QoS Evaluation of EDCF Medium Access Scheme," CiiT *2003*, Bitola, Macedonia, December 2003

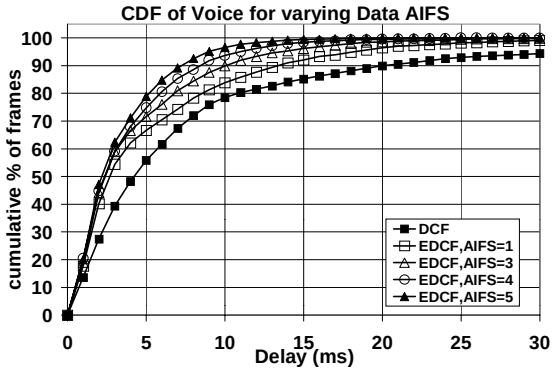

Fig.1. Effects of data AIFS on delay of voice frames

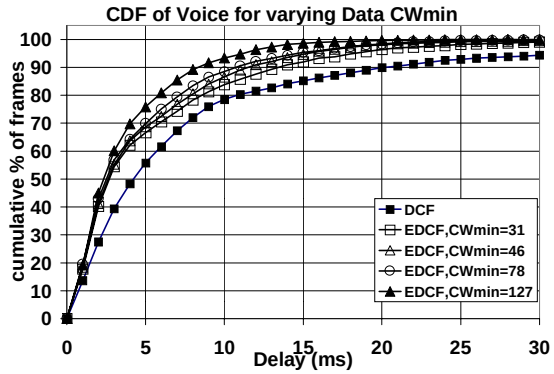

Fig.2. Effects of data CW_{min} on delay of voice frames

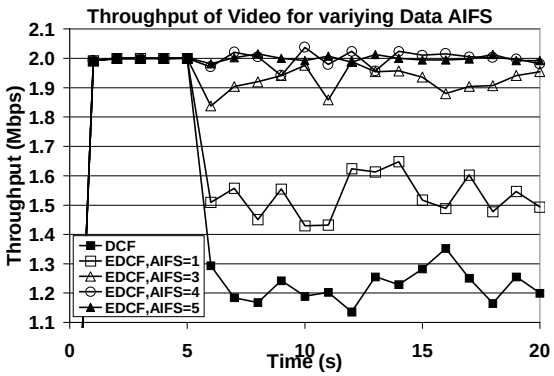

Fig.3. Effects of data AIFS on video throughput

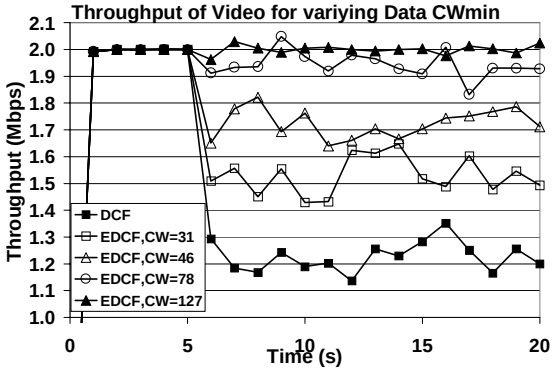

Fig.4. Effects of data CW_{min} on video throughput

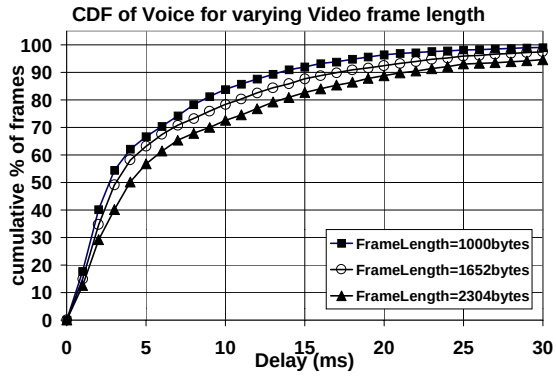

Fig.5. Effects of video frame length on voice delay

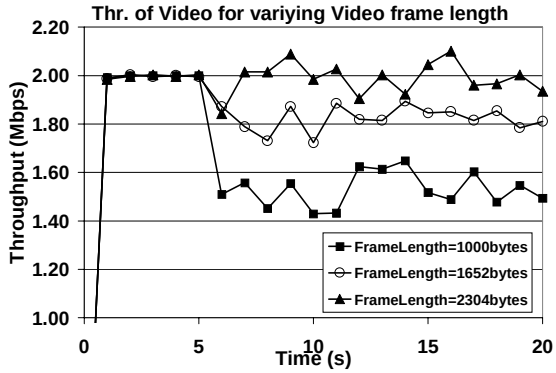

Fig.6. Effects of video frame length on video throughput

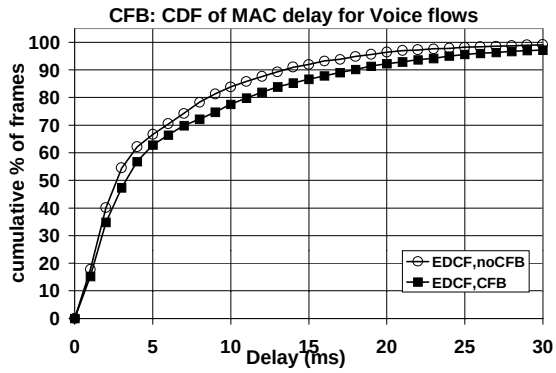

Fig.7. Effects of CFB for video on voice delay

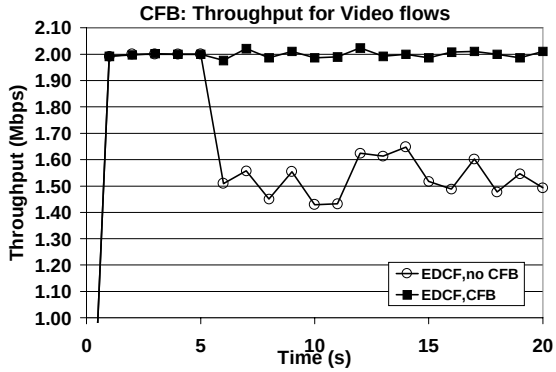

Fig.8. Effects of CFB for video on video throughput

Performance Improving Of HF Modem Using TCM

Saša Đorđević[1], Aleksandar Đorđević [2]

I

Abstract - This paper deals with a problem of upgrading performance of an existing HF modem, by use of a trellis-coded modulation (TCM). Modification consists of replacement of existing DQPSK modulation with a trellis-coded 8PSK (TCM 8PSK) modulation. Also, some of the modern DSP algorithms are used to attain better performances. By introducing these solutions, much better performances can be achieved without major hardware upgrades. Performances of modified modem acquired by means of simulation are compared with commercial modems of similar design and data rate.

Keywords – HF modems, TCM modulation, Parallel tone modem

I. INTRODUCTION

Since the beginning of data transmission, HF band was very interesting for both civil and military use. Its main advantage is possibility of relatively long-range transmission with limited power. Another advantage is large number of 3 kHz voice channels in this band. But, harsh and time variable conditions of HF radio channel rendered it unsuitable for data transmission until development of DSP technology and modern error-controlling codes.

There are many commercial products that operate over HF radio channel. Over the years, different protocols, modulations and error-correcting techniques were used, with one goal in mind: more robust modems with higher data rates. Currently, data rates up to 2400 bps are most common. But, for special services (military, navy, etc.) higher and non-standard data rates are needed. In this paper a commercial HF3618 3000 bps HF modem will be discussed [1]. This modem has been developed by the end of 1980's and uses rather old techniques and can be upgraded by using more up-to-date knowledge of information theory.

[1]Saša Đorđević is with Mihailo Pupin Institute of Tecnology, Volgina 15, Belgrade, Serbia and Montenegro,
e-mail: sasha@kondor.imp.bg.ac.yu
[2]Aleksandar Đorđević is with Mihailo Pupin Institute of Tecnology, Volgina 15, Belgrade, Serbia and Montenegro,
e-mail: sasha@kondor.imp.bg.ac.yu

In the next chapters concept of an N-tone parallel HF modem will be presented. Also, there will be given some methods of modification, which should greatly improve robustness of this particular modem. Finally, the results obtained by simulation are compared with other solutions.

II. THE N-TONE PARALLEL TONE MODEM

Current 2400 bps modems are 16-tone modems. Basically, the signal is composed of 17 OFDM tones. (16 data carriers and one Doppler-shift correction pilot tone). Pilot tone is set on 605Hz and is 7dB larger then the data carriers creating SNR loss of 1.7dB. Data carriers reside in spectral area from 935 to 2585 Hz with spacing of 110 Hz between each of the signaling tones. The signaling tones are modulated with Differential Quadrature PSK (DQPSK) with a symbol rate of 75 baud. Total bit rate is: $16 \times 75 \times 2 = 2400$ bps.

HF3618 3000 bps modem uses 20 data carriers with DQPSK modulation and signaling rate of 75 baud per carrier. The signal structure of this modem is given in figure 1.
This modem uses larger part of the voice band, thus making it more efficient for data transmission, but effectively reducing power of each signaling tone for approximately 1 dB.
Doppler shift correction is done by sending three pilot tones set in second, eleventh and twentieth channel (605 Hz, 1595 Hz and 2585 Hz respectively) in period of 0.5 seconds prior to data transmission. This method does not reduce SNR, but procedure for establishing connection is longer for 0.5 seconds. Maximum frequency offset which can be overcame by this method can be in range of ±75 Hz

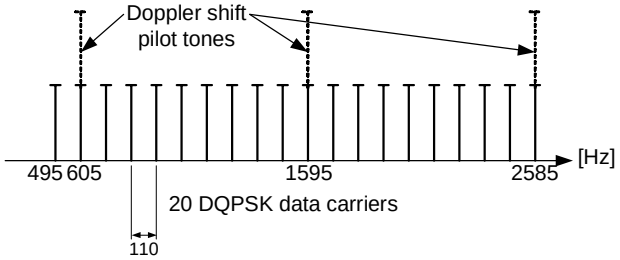

Figure 1. HF3618 signal format

Transmitted composite OFDM signal *s(t)* in *n*-th symbol interval can be represented as in:

$$s(t) = \sum_{n=-\infty}^{\infty} \sum_{k=0}^{N_t-1} c_{n,k}\, g_k(t - n \cdot (N_t T_s)) \qquad (1)$$

where $c_{n,k}$ is symbol transmitted in *n*-th symbol period with length of T_s over *k*-th of N_t carrier tones.
OFDM complex subcarrier tones can be defined as:

$$g_k(t) = \begin{cases} e^{j2\pi f_k t} & , \quad t \in [0, N_t \cdot T_s] \\ 0 & , \quad other \end{cases} \qquad (2)$$

Because of the intersymbol interference (ISI) there is a "guard time" after each signaling period. Active signal period is 9 ms and the guard time is 4.5 ms as shown in Figure 2. Due to this time, effective SNR in HF modem is 1.8dB less than in ideal system.

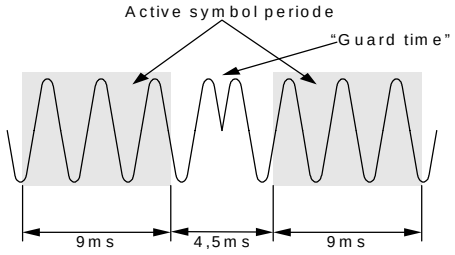

Figure 2. Signaling period and "guard time"

Modem is using one of the following two types of error-correction, depending on channel condition:

- BCH code (code length 255)
- Reed-Solomon code (symbol length 8 bits)

III. HF CHANNEL CHARACTERISTICS

HF channels are known to be very hostile environment even for an analog voice communication, let alone digital data transmission. It is known that its main characteristics are very slow Rayleigh fading, time varying impulse response and strong impulse noise, produced either by lightning or man-made machines. Reason for time variation in impulse response is the way the transmitted signal propagates.

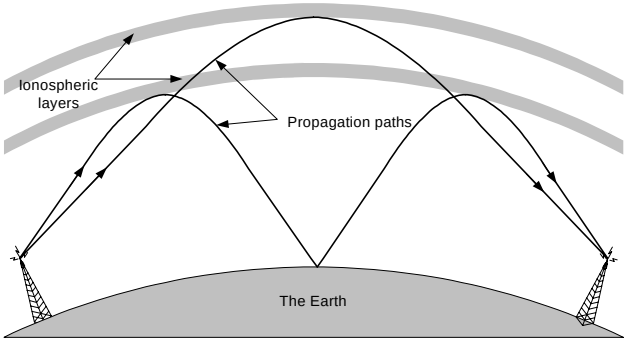

Figure 3. HF propagation paths

There are two basic propagation paths that are shown in figure 3. Due to the time variant nature of ionosphere layers there is a time dependency of channel characteristics of transmission channel.

On the receiver end, these two signals (or even more if there is a case of multiple reflections) make one composite signal with a frequency offset and slow fading. Since there is no direct wave, this is the only signal which can be received. Fading is so dominant in HF channel, that the mere effect of fading was first noticed in radio broadcast over HF on the early stage of radio communication.

There are many HF channel simulators, but the most used is Watterson simulator. Although this simulator has many flaws, it is widely used as a standard for modeling HF channels [3]. Another way is "replay simulator", which consists of a database obtained by measuring the HF channel propagation characteristics over a long time. Replay simulator is more exact, but it takes a long time to be created and is less flexible [4].
CCIR gave two definitions of HF channel for digital communication: *Good* and *Poor* [5]. Main characteristics of these two channels are given in Table 1.

Table I

Characteristics of CCIR HF channels

	Good channel	*Poor* channel
Fade rate f_d [Hz]	0.1	1
Interpath delay t_d [ms]	0.5	2

Time and space variation of signal can be diminished by using time and space diversity. This can be accomplished through time interleaving and using two or more receive points (antennae). These two methods exclude each other and can be used according to the nature of transmission. If voice transmission is used, long interleaving blocks cannot be tolerated, thus urging the use of space diversity. In data communication, time gap is not of great importance so interleaving can be used. Long interleaving blocks cannot be used if modem is part of an ARQ system.
Although interleaving can decrease error rate, it can also make periodic error bursts. These errors then must be retransmitted, thus reducing an overall data rate. Due to this reasons simulation is done using very short interleaving blocks. It is shown that space diversity can considerably decrease BER without need for long data interleaving [2]. This combination of space diversity and short interleaving blocks are ideal for both voice and data transmission.

IV. USE OF TRELLIS-CODED MODULATION

Trellis-coded modulation (TCM) is commonly used in modern digital communications. A 16-tone modem with TCM scheme is presented in [2] and is used as a reference for comparison with TCM modification of 3000 bps 20-tone parallel modem.

Use of TCM implies inserting redundancy bits, thus decreasing data rate. As maintaining data rate of 3000 bps is imperative, other modulation must be used. Since every tone carries two bits of information in DQPSK it is logical to use convolutional code that uses two input bits, like 2/3 rate convolutional code. If 2/3 rate convolutional codes for TCM are used, 8PSK constellation is imposed as logical choice as it uses three input bits per symbol. This way we still have two bits per symbol throughput, while introducing inherent error-correction. 8PSK TCM schemes are known for some time now, since famous Ungerböck's paper from early 80's [6].

Choice of an 8PSK trellis code was the next step. Main criteria for choosing a particular code were relatively low computation load for DSP processor (existing modem was made around TMS320C25 DSP platform), good performance over slow fading and possibility to work in presence of the impulse noise. After considering multiple trellis-coding schemes [6,7,8,9] it was decided that a 2/3-rate 8PSK trellis with 256 states have shown a good performance over low fading channels. This code is optimized for use on slow fading AWGN channels, but has no inherent protection from impulse code. As HF channel is non-AWGN channel finding adequate trellis code is another interesting area of research. Detail description of this code is given in [6] with the following parameters used:

- h_0=417
- h_1=573
- h_2=612

A 2x8DPSK modulation scheme is also considered but due to its complexity it was dropped out of consideration [9].

As a result of a very slow Rayleigh fading it is important to have interleaving of up-to 20 seconds, although to completely overcome effects of slow fading this value can be as high as 60 seconds. However, simulation was done with minimum interleaving of 2 seconds on assumption that space diversity is used. This combination of time/space diversity is good for both voice and data transmission.

Doppler shift correction tones are also omitted, enabling faster modem handshaking. Doppler shift can be overcome by the use of FFT that gives 20 equally spaced phasors, regardless of amount of Doppler shift.

By eliminating the pilot tone it is possible to use lower portion of voice band for additional data carriers, raising data rate to 3600, by the loss of only 1.8dB of SNR. This modem, using 8DPSK TCM modulation, should give much better performance than a 3600 bps modem described in [2], making this modem yet another interesting area of research.

Results obtained by this simulation were compared with following HF modems:

- Single tone 2400 bps HF modem (described in MIL-ST-188-110A)[10]
- 16-tone 2400 bps modem with 8PSK TCM (described in [2])
- 16-tone 3600 bps modem with 16PSK TCM (also presented in [2])

V. DISCUSSION OF SIMULATION RESULTS

In following figures (4 and 5) simulation results are given. HF3618 3000 bps modem is compared with similar modems described earlier. Results for these modems are taken from [2].

In Figure 4 performance of HF modems over CCIR *Good* channel are given. This figure shows that parallel tone modems are more robust than single tone.

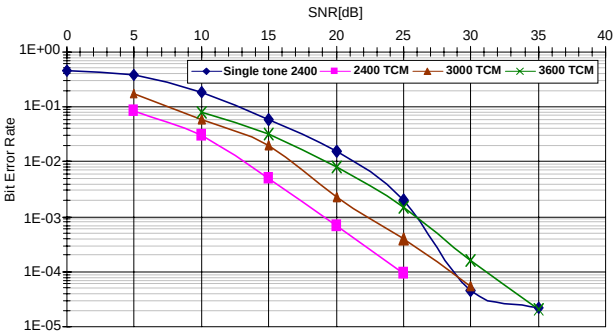

Figure 4. Performance over CCIR Good channel

It can be shown that even 50% higher data rate can be used over same channel with the same if not better results. The only area where single-tone modem has better performance than 3600 bps is that of SNR>25dB. A 3000 bps modem has lower performance than 2400 bps modem by some 3.5dB lower SNR.

Figure 5 represents performance of these modems over CCIR *Poor* HF channel. Over *Poor* channel single-tone modem has the lowest overall drop of performance and on some SNR values it almost reaches performance of 2400 TCM modem.

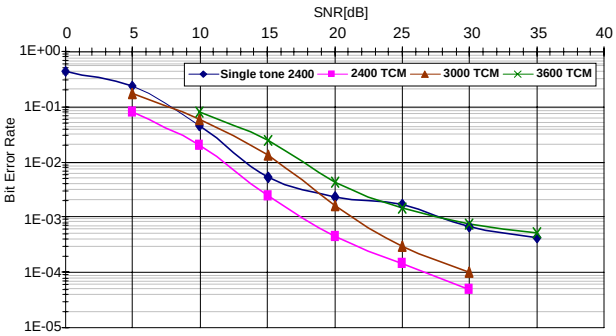

Figure 5. Performance over CCIR *Poor* channel

A 3000 bps TCM modem has performance that was expected, although on some SNR's (10-20dB) it has worse performance in comparison with single-tone modem.

Overall, results are as expected, with performance of 3000 bps modem between those of 2400 and 3600 bps modems.

VI. CONCLUSION

This simulation shows that by using TCM in some of existing HF modem techniques (such as 16 or 20-tone parallel modem) quality and robustness of data transmission can be improved significantly without decreasing data rate. Also, using modern DSP algorithms a Doppler correction pilot tone can be omitted, thus enabling a lower portion of the voice spectrum to be used for data carriers. In case of HF3618 modem, omission of the Doppler correction tones can lower channel setting time by some 0.5seconds. By adding additional tones data rate of the HF modem can be increased by losing a small amount of overall performance. Using other MPSK schemes are also in consideration. Some companies are already producing 4800 bps HF modems, which are obviously 16-tone non-TCM 16PSK modems. The biggest benefit of parallel tone modem with (or without) TCM is possibility to improve current modems with small, if any, modification of hardware, enabling simple upgrade by "flashing" new DSP code into processor. In modern systems this is a big advantage, because algorithms are changing much faster than actual design of devices. It also gives possibility to create so called "multirate" modems, with selection of modulation type during initial handshaking of modems according to channel characteristics. This is the principle which is used in wired modem communications for some time now. At present, this paper is just a study, with a goal to be used in real upgrade of the existing HF modem.

There are many possibilities that should be accounted for, whether the goal is improving performance or data rate. It is sure that, by applying newly acquired knowledge in DSP and information theory, data rate will increase, as it is sure that a HF band would remain interesting for both military and civil services.

REFERENCES

[1] http://www.telecom.imp.bg.ac.yu/services_products/pr_radio.htm

[2] *M.C. Gill, S.C. Cook, T.C. Giles and J.T. Ball* "A 300 To 3600 Bps Multi-Rate HF Parallel Tone Modem", Proc. IEEE MILCOM '95, also on http://www.s3.kth.se/~tim/pub_list.html

[3] *Watterson C.C.* "Experimental Confirmation Of An HF Channel Model", IEEE Trans of Com, Tecnol.COM-18 (DEC), 1970, pp. 792-803

[4] *Giles T.C. & Preiss M.*, "On the Design of a Voiceband HF Replay Channel Simulator", The Proceedings of the Eighth International Conference on HF Radio Systems and Techniques, University of Surrey, Guildford, UK, 10-13 July 2000

[5] *CCIR* "Use Of High Frequency Ionospheric Channel Simulators", Rec. 520-1, Recommendations and Reports of the CCIR, Vol 3, 57-58, ITU, Geneva

[6] *G.Ungerböck* "Channel Coding With Multilevel/Phase Signals", IEEE Trans. of Information Theory, IT-28, 1, 55-67

[7] *J. Du and B. Vučetić* "New MPSK Trellis Codes for Fading Channels", Electronic letters vol 26, No 16, 1992, 395-399

[8]*F. Edbauer* "Performance of Interleaved Trellis-Coded Differential 8PSK Modulation Over Fading Channels", IEEE Journal on selected areas in communications, vol. 7, No.9, December 1989, pp. 1340-1346

[9] *S. Đorđević* " Differential 8-PSK Code With Multisymbol Interleaving", Proc. TELSIKS '99 Niš pp. 596-599

[10] *MIL-STD-188-110A* "Interoperability and Performance Standards for Data Modem", US military standard, 1991.

Optimization of the performance of the hybrid fiber-coax network

Dobri M. Dobrev[1] and Lidia T. Jordanova[2]

***Abstract* – In this paper is represented an optimization method of performance of hybrid fiber-coax network. Analytical results and plots are used for an estimation of the received optical power and the level of RF modulation signal that are required for a given signal to noise ratio (SNR) and intermodulation distortions. The variation limits of output signal level of the wideband coaxial line amplifier are defined. It is shown a signal power distribution in downlink and uplink of CATV distribution network.**

***Keywords* – Attenuation in fiber optic/coaxial cable; Effectiveness of optical transmitter/receiver; Gain of optical link; Noise and distortion in a CATV network; optimal output level of an amplifier in CATV network.**

I. INTRODUCTION

The development of CATV distribution networks up to the present was passing through the three generations. The first generation is one-way and only analog signals are transmitted. It is build by coaxial cables and the coverage area is limited by the noises and the distortions in the trunk amplifiers. The next generation is the hybrid fiber–coax (HFC) networks that use a fiber optic to convey a signal from the headend to local area coaxial distribution network. In this way, the coverage area is significantly increased. Further, these networks transmit both analog and digital signals that result in a growth of the number of the transmitted TV channels by eight times.

The special feature of the third generation CATV networks is the two-way capability. This allows additional services to be provided by a control of subscribers access. For example, video films by order, security services, paid TV channels, VoIP and Internet. The third generation CATV networks are composed of main and secondary optical rings, Hubs, transmitters and receivers for uplink and downlink and digital signal processing (DSP) devices. Service of the subscribers of an area under construction is performed by peripheral coaxial distribution networks.

II. CONFIGURATION OF CATV NETWORK

The object of the analysis is a part of hybrid fiber-coax (HFC) networks that includes optical trunk link and several coaxial distribution networks. Optical transmitter that is located in the headend or in a given HUB feed the optical trunk link. The optical signal is divided between *n* feeder links then passes to nodes that convert it into electrical signal and feed the local area coaxial distribution networks.

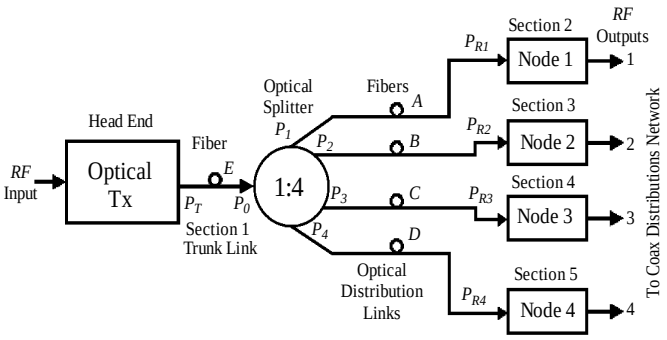

Fig. 1 The "star-shape" topology of the optical part of HFC network

At the present, two main topologies of the optical part of the HFC network are imposed – "star-shape" and "tree-and-branch". In the first topology, the distribution of the signal between several feeder links is performed in one point by optical divider. In the "tree-and-branch" topology the signal power from the optical backbone is diverted to the feeder links in several points. On Fig. 1 and Fig. 2 are shown block diagrams of the two topologies of CATV optical trunk networks.

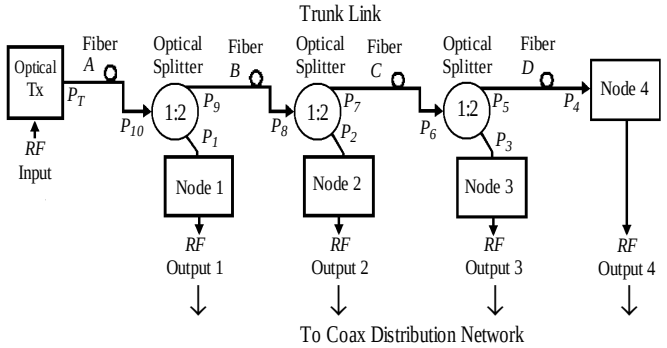

Fig. 2 The "tree-and-branch" topology of the optical part of the HFC network

[1] Dobri M. Dobrev is with Faculty of Telecommunications of TU-Sofia, 8 "Kl. Ohridski" blvd., 1756 Sofia, Bulgaria, E-mail: dobrev@tu-sofia.bg

[2] Lidia T. Jordanova is with Faculty of Telecommunications of TU-Sofia, 8 "Kl. Ohridski" blvd., 1756 Sofia, Bulgaria, E-mail: jordanova@tu-sofia.bg

The classical coaxial CATV networks are realized by three-stage scheme that consists: trunk link, distribution network and subscriber drop. Along the trunk link at intervals of 400-600m, a wideband amplifier is included due to the great losses inherent to coaxial cables.

In view of fact that each amplifier introduces additional noises and distortions, the number of amplifiers is limited and this reduces the coverage area of the coaxial CATV network.

III. OPTIMIZATION OF THE PERFORMANCE OF THE OPTICAL NETWORK

The design performance of CATV network is estimated by the parameters of the end signals of the network and it must be ensured a predefined quality of the received information. The end of an optical trunk network is the receiver in the optical node and in a coaxial distribution network – subscriber point. The carrier-to-noise ratio (CNR) and the intermodulation distortion – composite second order (CSO) and composite triple beat (CTB) – estimate the quality of the received signal. The levels of CSO and CTB products are given relative to the level of the carrier and denoted by CIR_{CSO} and CIR_{CTB}. In the subscriber point these ratios must be CNR > 43 dB, CIR_{CSO} > 54 dB and CIR_{CTB} > 54 dB.

First, it is necessary to be distributed the acceptable worsening of the quality between the optical part and the coaxial part of the HFC network. This is performed taking into account that the greater noise and intermodulation are inherent to the coaxial part. Furthermore, in an optical trunk network the levels of the intermodulation distortion CSO and CTB are defined by the parameters of the transmitter. The laser transmitters on the market have great margin with respect to these distortions and hence no need to concern about these parameters in the optimization procedure.

The ratio CNR in the output of the receiver of an optical node can be expressed by

$$CNR = \frac{i_{pd}^2}{i_{sh}^2 + i_{th}^2} = \frac{\left(P_R R_{pd}\right)^2}{\left[4kT/R_l + 2e\left(P_R R_{pd} + I_d\right)\right]B}, \qquad (1)$$

where i_{pd} – the average photoelectric current through the load R_l; i_{sh} and i_{th} – the average currents caused by the shot and the thermal noise in the photodiode receiver; P_R – the input optical receiver power; R_{pd} – the sensitivity of the photodiode (typically 0,75 mA/mW); B – the receiver bandwidth; I_d – the current of darkness; $k = 1{,}38.10^{-20}$, mW/[Hz.K] – the constant of Boltzman; T – the temperature in K (290 K ambient); e – the charge of electron.

On Fig. 3 are shown curves of the ratio CNR versus the received power P_R for different number of TV channels. If the ratio CNR is given for each optical node then by the aid of these curves it can be determined the necessary received optical power. Let we assume that the number of TV channels is 79, "star-shape" topology is used for the optical trunk network and the required values of the ratio CNR in the feeder links as follows: $(CNR)_2$ = 48 dB, $(CNR)_3$ = 49 dB, $(CNR)_4$ = 50 dB, $(CNR)_5$ = 51 dB. Then the received optical power must be as follows: P_{R1} = – 3,3 dBm, P_{R2} = – 2,5 dBm, P_{R3} = – 1,8 dBm and P_{R4} = – 1,0 dBm.

The level $U_{RF\,in}$ of the modulating RF signal is the next important parameter for optimization. In VSB-AM systems this level is adjusted in such a way so that the depth of the modulation to be about 4%. When the modulating signal has lower values of magnitude then the ratio CNR is made worse. If there is too strong signal then an undesirable non-linear distortions occur. Let, the third order distortion CIR_{CTB} (in dB) and the number of the TV channels n are given then the maximum allowed power of the modulating signal $P_{RF\,in}$ (in dBm) can be derived from

$$CIR_{CTB} = 2\left(IIP3 - P_{RF\,in}\right) - \left(6 + 10\lg x\right), \qquad (2)$$

where IIP3 is the input intercept point of the third order in dBm (it can be read from the specifications of the laser transmitter), and the term x for $n > 16$ is given by $x \approx (3/8)n^2$.

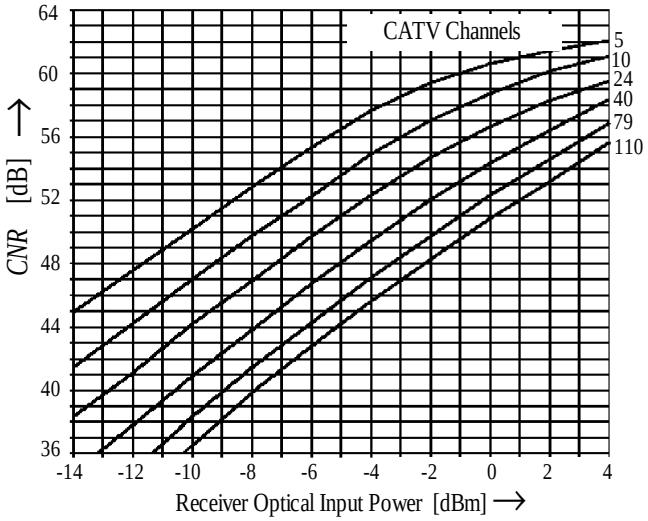

Fig. 3 The signal-to-noise ratio CNR versus the received optical power P_R

According to the equation (2) Fig. 4 is drawn. This plot can be used for an estimation of the optimum level of the modulating signal $U_{RF\,in}$ (in dBmV), when the output power of the laser transmitter P_T (in dBm) and the number of TV channels n are given. Let, we look again at the "star-shape" topology and try to estimate the acceptable output power P_T of the transmitter. Just for that, we must know the losses in the feeder, the trunk links and the four-way divider. The losses L_i in a fiber optic cable with length l_i and attenuation constant α (for λ = 1310 nm α is 0,5 dB/km and for wavelength λ about 1550 nm α is 0,25 dB/km) are defined by $L_i = \alpha l_i$. Let, we assume that the computed value of P_T is 12 dBm and n = 79 then the acceptable level of the modulating signal is $U_{RF\,in}$ = 11 dBmV. The coaxial distribution network requires a level of the RF signal about 50 dBmV, whereas the optical transmitters need comparatively low level of the input signal (usually, from 10 to 20 dBmW).

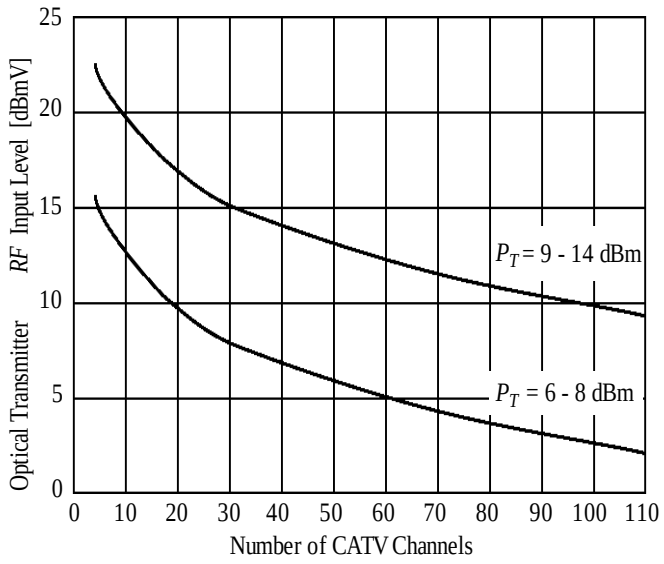

Fig. 4 Plot for an estimation of the modulating RF signal level

The next important parameter for optimization in this part of the HFC network is the gain of the optical link. The optical link is defined as all components of the network between the modulating input of the optical transmitter and the output of the optical receiver. The gain of this link can be expressed by

$$G = \left(I_{out}/I_{in}\right)^2\left(R_{out}/R_{in}\right) = \left(\eta_T \eta_R / L\right)^2\left(R_{out}/R_{in}\right). \quad (3)$$

The parameter $\eta_T = P_T/I_{in}$, [mW/mA] gives an account of the efficiency of the optical transmitter transformation of the input current I_{in} in a modulated output optical power P_T and $\eta_R = I_{out}/P_R$, [mA/mW] – the efficiency of the inverse receiver transformation of the received optical power P_R in a RF output current I_{out}. These parameters can be seen in the specifications of the transmitter and the receiver. The total loss in the optical link $L = P_R/P_T$ includes both the attenuation in the fiber optic and the losses in the passive components (optical divider and connectors).

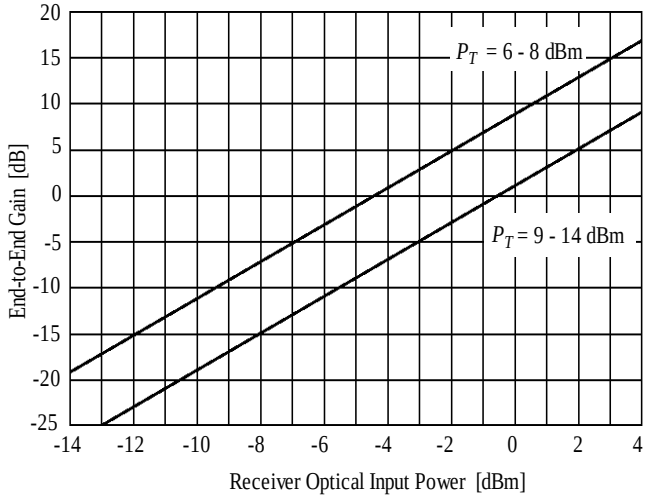

Fig. 5 Plot for an estimation of the optical link gain

Usually in the specifications are shown the relations between the gain of the optical link G and the output optical power of the transmitter P_T and the power of the received optical signal P_R (Fig. 5). For example, the gain of the first optical link shown on Fig. 1 is about 2.5 dB (P_T =12 dBm and P_{R1} = – 3.3 dBm) and the fourth optical link gain is about 7 dB (P_{R4} = – 1,0 dBm). The level of the output RF signal of the node when the optical link gain is known can be calculated from the equation

$$U_{RF\ out}[dBmV] = U_{RF\ in}[dBmV] + G[dB]. \quad (4)$$

In the previous example $U_{RF\ in}$ = 11 dBmV and hence, the level of the output RF signal varies from 13,5 dBmV (73,5 dBμV) to 18 dBmV (78 dBμV).

IV. A LIMITATION DUE TO THE NOISES AND THE DISTORTIONS IN THE COAXIAL NETWORK

The attenuation of the signals in the coaxial CATV network is compensated by a great number of wideband amplifiers and this result in an increase of the noises and distortions. In order to ensure the required signal quality in the subscriber point the amplifiers output level is supported in certain limits. These limits are defined by the minimum ($U_{A\ min}$) and the maximum ($U_{A\ max}$) level of the amplifier output signal. The minimum level is related to the required signal-to-noise ratio CNR and the maximum is to the acceptable non-linear distortion.

The limits $U_{A\ min}$ and $U_{A\ max}$ in dBμV for the ith amplifier in succession are given by

$$U_{A\min} = 2 + NF + K + CNR + 10\lg i \quad (5)$$

$$U_{A\max} = U_{A(k)} - 7{,}5\lg(n-1) - 20\lg i, \quad (6)$$

where NF and K (in dB) are the noise figure and the gain of the amplifier, respectively; $U_{A(k)}$ – the maximum amplifier output level according to the specification (in dBμV); n – the number of the TV channels. In equation (5), the noise caused by the coaxial (about 2dBμV) is included. Automatic Gain Control (*AGC*) circuitry controlled by a pilot signal supports the output level in the acceptable limits.

If the number of the TV channels n and the numbers of consecutive amplifiers are increased then the value of $U_{A\ min}$ approach to $U_{A\ max}$ and for given amplifier they coincide. Exactly, in this point is defined the optimum signal level in the coaxial distribution network that must not be smaller than the minimum acceptable level in the subscriber point (63 dBμV). In view of the attenuation of the coaxial cables on the market and the parameters of the wideband amplifiers, it is estimated that the longest coaxial trunk link is about 7 km and the number of the amplifiers along the line could be no more than 10 ... 15. In [2] the optimization of the performance of coaxial CATV network is described in details.

V. SUPPORT OF THE OPTIMAL PARAMETERS IN THE SUBSCRIBER POINT

It must give an account of two conflicting requirements choosing the distribution network topology. First, it is used as possible as shorter coaxial cables. On the other hand, the coupling between the subscriber points must be smaller. Then only an intentional or unintentional change of the parameters of the subscriber point (interruption or short) has no influence on the signal quality of the other subscribers.

The "tree-and-branch" topology of the distribution network is cheapest, but it has a great disadvantage: the subscriber has a free access to the line that feed a group of subscribers. The subscriber's access to the feeder link is entirely restricted when the "star-shaped" topology is used. However, this topology is very expensive, a great amount of cables is used. The "star-shaped" topology has an important advantage: the possibility for remote control of the subscriber signals. For example, the joint/disjoint to CATV network, collecting of an information about the number and the kind of channels that the subscribers watch on television, restricted access to coded TV channels and etc.

The main problem in the distribution network design is the different attenuation of the passive components that build the downlink and the uplink. For example, the loss in coaxial cables for the maximum uplink frequency (65 MHz) is about 4 times smaller than the losses for 860 MHz (the maximum downlink frequency). In the uplink frequency band, the losses of the taps (directional couplers) and the dividers are about 60% of the losses in the downlink frequency band. Other grave problem is so called funnel effect that is an accumulation of the noise and the interference of the subscriber and another devices in the headend. In addition, problems are caused by the ferrite cores of the taps and the dividers that make non-linear distortions of the downlink signals when the cable modems transmit great powers. This effect can be prevented by the blocking capacitors in the input and the output of these passive devices.

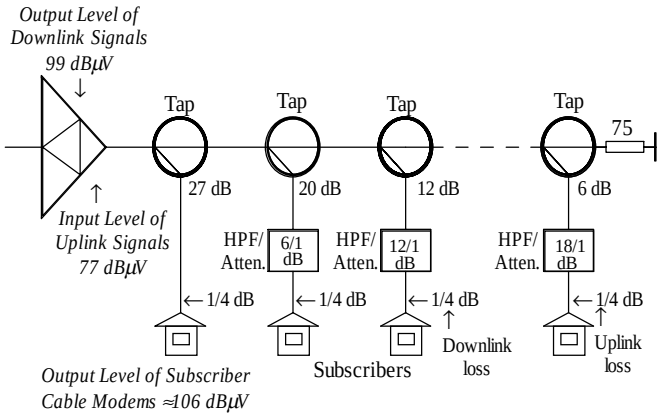

Fig. 6 The signal distribution in the uplink and the downlink of coaxial distribution network.

On Fig. 6 it is shown an example for the distribution of the signal power between several subscribers taking into account the different attenuation in the downlink and the uplink. In order to avoid the noise and the interference infiltration into the CATV network, the high pass filters (HPF) are included in the taps output of subscribers that no use of the uplink. The required level in the subscriber point is ensured by the (forward) coupling of the tap. Attenuators (Atten.) are used for alignment of the subscriber modem levels in the uplink. Attenuation in the passive components in the distribution network are given by two digits, the first is used for uplink signals and the second for the downlink.

VI. CONCLUSIONS

In this paper was described an optimization method of very important parameters of the coaxial and the fiber-optic part of the HFC network. It was the attenuation of trunk and feeder links; the output power of the laser transmitter; the sensitivity of the optical node receivers; the level of *RF* modulating signals; the limits of variation of amplifier output levels; the coupling of taps and etc.

REFERENCES

[1] Д. Добрев, Л. Йорданова. Приемане на радио и телевизионни програми чрез спътници и по кабел. С., Електронинвест, 1996.

[2] Д. Добрев, Л. Йорданова. Проектиране на кабелна разпределителна мрежа. Радио, телевизия, електроника, No 1-3, 4-6, 1997.

[3] Л. Йорданова, Д. Добрев. Осигуряване на качествено приемане на радио- и телевизионни програми в колективни системи. Proceedings of the ISC on EIST'2001, vol II, pp 405-410, Bitola, june 2001.

[4] Application note AN132A. Force, Incorporated, www.forceinc.com

[5] Fiber Optic FIBT Design Tool. Fiber Optic Design Guide, Blonder Tongue Laboratories, INC, www.blondertongue.com

[6] CATV and other fiber-optic networks. Sergiusz Patela 2001, Other_nets.pdf

[7] William Grant. Cable Television. Third Edition, SCTE, Inc., Exton, PA, 1994.

Modeling of Impulsive Noise in PLC Systems Using Middleton Class A Noise Model

Vesna M. Golubovic[1], Zoran R. Petrovic[2], Jasmina Mandic-Lukic[3]

Abstract **– Power line communications (PLC) represent technology for transmission of information along the existing electric utility infrastructure. This is technology with great potential to enable reliable high-speed data communications over low-voltage power distribution network or existing indoor power lines. In order to achieve high-speed data transmission using PLC, high carrier frequencies must be considered (within the range from 500kHz to 20MHz). One of the major disadvantages in this frequency range is influence of impulsive noise and narrowband interference. In this paper Middleton Class A noise model is implemented for modeling of this kind of disturbances. Simulation model is developed and compared with theoretic results. Theoretic expression for BER (Bit Error Rate) in case of BPSK (Binary Phase Shift Keying) signal transmission in presence of Class A noise is derived. Simulation model is also implemented for determining BER and results are compared with theoretic ones. Finally, concluding remarks are given with some suggestions for possible future work.**

Keywords **–PLC channel, impulsive noise, simulation model.**

I. INTRODUCTION

There is constantly growing demand for systems that would enable reliable high-speed data communications. Solutions that are easy for implementation and don't require too much of investments are of great interest [1]. PLC technology has natural potential to develop power distribution network into economic and convenient communication medium. Main advantage of PLC technology is that it uses highly developed and widely available infrastructure for data transmission. Furthermore, since many communication devices are normally plugged into an electric outlet, unification of these two networks is very attractive combination. There are two main applications for PLC systems. The first application is broadband Internet access. This kind of Internet access could help overcoming problems concerning covering of rural areas. Alternative access solution usually doesn't exist there and investment in new infrastructure is not feasible. PLC systems can also be used as alternative for local network, as power plugs are available in almost every room.

[1]Vesna M. Golubovic is with Faculty of Electrical Engineering, Department of Telecommunications, Bulevar kralja Aleksandra 73, Belgrade, Yugoslavia, e-mail: vesna.golubovic@etf.bg.ac.yu .
[2]Zoran R. Petrovic is with Faculty of Electrical Engineering, Department of Telecommunications, Bulevar kralja Aleksandra 73, Belgrade, Yugoslavia, e-mail: zrpetrov@etf.bg.ac.yu .
[3]Jasmina Mandic-Lukic is with the Energoprojekt, Bulevar Mihaila Pupina 12, Belgrade, Yugoslavia, email: jmlukic@ep-entel.com .

Although PLC represents potentially "no new wire" solution, there are a number of technical issues that should be addressed. Power lines are not originally designed as data transmission medium. In fact, PLC channel suffers from a number of occurrences that are not desirable during the data transmitting. In order to design appropriate system that can cope with very hostile nature of power line channel it is necessary to develop channel model with sufficient accuracy. The problem of modeling PLC channel is very complex; as it is cited in [2] "there is no universally recognized power line channel model available". PLC channel is disturbed by various noise types, but in the frequency range of interest it is mostly dominated by impulsive noise [3], [4], [5].

In Section II PLC channel characteristics are given and importance of impulsive noise is emphasized. In Section III memoryless Class A Middleton noise model is described in details and proposed as model for impulsive noise, interference and background noise in PLC channel [6]. Simulation model is developed and implemented in case of determining Class A noise PDF (probability density function). In Section IV theoretic BER formula is derived for the case of transmitting BPSK signal in the presence of Class A noise. Simulation model is also used for determining BER. It is shown that simulation and theoretic results fit very well in both implementations. Finally, some concluding remarks are given with suggestions for possible future work.

II. PLC CHANNEL

In order to achieve high-speed communications over power line channel, higher carrier frequencies within the range of 500kHz to 20MHz should be considered. In frequency range of interest signals are mostly degraded due to effects of multipath propagation, various kinds of noise and frequency dependent cable attenuation [5]. PLC channel characteristics are also very time and frequency dependent.

Multipath effect in power line channel is consequence of signal propagation along more than one path. During transmission signal exhibits reflections and cancellations caused by impedance mismatches at joints and points where equipment is connected to the network. Multipath nature of PLC channel is described in [5] for frequency range from 500kHz to 20MHz. Transfer function of PLC channel given is given in [5], in the form of transversal filter with frequency dependent attenuation. As PLC channel is very dependent on location and network topology, variable number of propagation paths is implemented, depending on channel peculiarities.

On contrary to many other communication channels, noise in PLC channel cannot be described with AWGN (Additive White Gaussian Noise) noise type. There are various types of noise, colored background noise, asynchronous impulsive

noise, and narrowband interferers. As noted in [3], in a frequency range from several hundred kilohertz up to 20 MHz PLC channel is mostly dominated by narrowband interference and asynchronous impulsive noise. Asynchronous impulsive noise is caused by unavoidable switching transients in the network [3].

Impulsive disturbances can cause bit or burst errors that can significantly degrade system performances. Thus, properly describing of impulsive noise for purpose of designing system that can efficiently combat this kind of noise is of great interest.

There are a number of papers that are dealing with problematic of impulsive noise in PLC channels. In [3] Gilbert–Elliot model is proposed as a simple PLC channel model. This channel model is not memoryless and therefore it is very suitable for modeling burst of errors [7]. For more accurate channel model, partitioned Markov chain approach with variable number of states is also proposed. Markov chain parameters are evaluated according to statistics obtained by real channel measurements. Disadvantage of this model is that Markov chain values have to be individually determined in each separate scenario and do not represent general channel model.

One of suitable models for this type of noise is memoryless additive Class A noise channel model [2], [8], [9]. It is usually used as model for a man-made impulsive noise.

III. CLASS A MIDDLETON NOISE MODEL

Class A discrete model PDF is given by [6]

$$\mathrm{PDF}(z)=\sum_{m=0}^{+\infty} P_m(A)\cdot\frac{1}{\sqrt{2\pi\sigma_m^{\,2}}}\cdot e^{-\frac{z^2}{2\sigma_m^{\,2}}} \qquad (1)$$

where $P_m(A)$ are coefficients of Poisson distribution, given by

$$P_m(A)=e^{-A}\cdot\frac{A^m}{m!} \qquad (2)$$

Thus, Class A PDF is given by infinite sum of weighted additive white Gaussian noise distributions with increasing variances. Variance of each distribution is given by

$$\sigma_m^{\,2}=\sigma^2\cdot\frac{m/A+\Gamma}{1+\Gamma} \qquad (3)$$

where σ^2 is total noise power. Parameter Γ describes ratio of the Gaussian noise power $\sigma_G^{\,2}$ to the impulsive noise power $\sigma_I^{\,2}$, and is equal $\Gamma=\sigma_G^{\,2}/\sigma_I^{\,2}$ (total noise power is $\sigma^2=\sigma_G^{\,2}+\sigma_I^{\,2}$). So, Class A noise always includes background noise with power $\sigma_G^{\,2}$, and can additionally include a number of impulsive sources. Number of additional sources is distributed according to Poisson distribution (with mathematic expectation equal A). Probability of having one additional source is equal $P_1(A)$ and total noise power in that case is $\sigma_1^{\,2}=\sigma_G^{\,2}+\sigma_I^{\,2}/A$. Similarly, probability of having m additional impulsive sources is equal $P_m(A)$ and total noise power in that case is $\sigma_m^{\,2}=\sigma_G^{\,2}+m\sigma_I^{\,2}/A$ [6], [10].

The other parameter used in Eq. (1) is called Impulsive Index. Small A (say A=0.01) describes highly structured channel interference and therefore impulsive channel. Large A means large overlap with a corresponding approach to Gaussian PDF [6], [10].

Class A model is memoryless, so noise sample at the moment t_k is not dependent on previous channel states. States are taken independently for every noise sample. Noise model obtained in this way is the most critical for evaluating system performances, as it represents the most critical case because of its memoryless character.

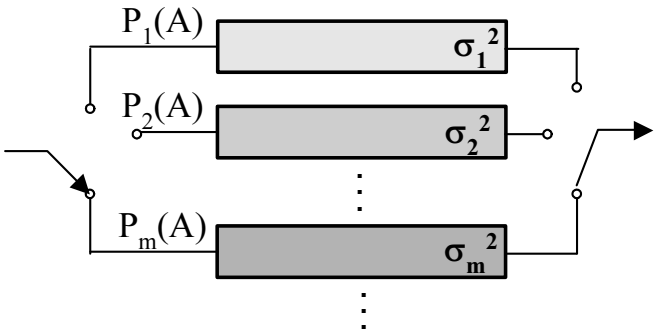

Fig. 1. Equivalent Middleton Class A channel model

This model can be graphically represented by equivalent model that comprises infinite number of parallel channels, as it is shown in Fig. 1. In each moment t_k only one channel is active. Probability of m^{th} channel being active is distributed according to Poisson distribution and is equal $P_m(A)$. Therefore, $P_m(A)$ is also probability that signal at the receiver is influenced by Gaussian noise with power $\sigma_m^{\,2}$.

TABLE I
POISSON COEFFICIENTS FOR DIFFERENT PARAMETER VALUES

	A=0.01	A=0.1	A=1	A=10
m=0	0.99	0.9048	0.3678	$4.54\cdot10^{-5}$
m=1	$9.9\cdot10^{-3}$	$9.05\cdot10^{-2}$	0.3678	$4.54\cdot10^{-4}$
m=2	$4.95\cdot10^{-5}$	$4.52\cdot10^{-3}$	0.1839	$2.27\cdot10^{-3}$
m=3	$1.65\cdot10^{-7}$	$1.51\cdot10^{-4}$	0.0613	$7.56\cdot10^{-3}$
m=4	$4.12\cdot10\text{-}^{10}$	$3.77\cdot10^{-6}$	$1.53\cdot10^{-2}$	$1.89\cdot10^{-2}$
m=5	$8.25\cdot10^{-13}$	$7.54\cdot10^{-8}$	$3.06\cdot10^{-3}$	$3.78\cdot10^{-2}$
m=6	$1.37\cdot10^{-15}$	$1.25\cdot10^{-9}$	$5.1\cdot10^{-4}$	$6.3\cdot10^{-2}$
m=7	$1.96\cdot10^{-18}$	$1.79\cdot10^{-11}$	$7.3\cdot10^{-5}$	$9\cdot10^{-2}$
m=8	$2.4\cdot10^{-21}$	$2.24\cdot10^{-13}$	$9.12\cdot10^{-6}$	0.1126
m=9	$2.7\cdot10^{-24}$	$2.5\cdot10^{-15}$	$1.01\cdot10^{-6}$	0.125

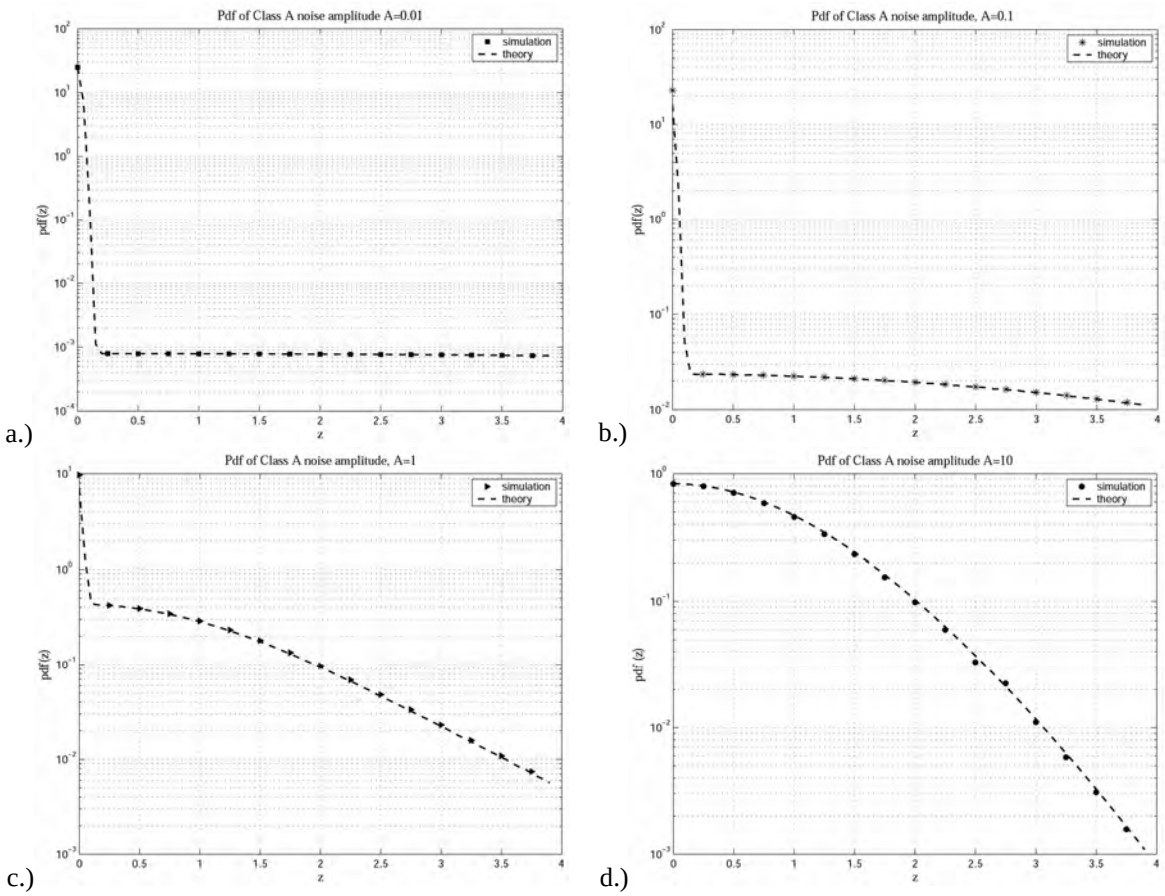

Fig. 2. Class A noise PDF for various A values (a. A=0.01, b. A=0.1, c. A=1, d. A=10)

Poisson coefficients are given in Table I for various A values. For values A≤1, Poisson coefficients decrease with m (on contrary to behaving of variance σ_m^2 with m) and channels with large variances σ_m^2 have small probabilities of realizations.

For very small A (A=0.01), $P_m(A)$ coefficient decrease very fast with m, while for A=10 coefficient values get their maximum for m=9 and m=10, and then decrease for m>10.

As Class A channel model consists of infinite series of Gaussian components, it's not convenient for computer simulations. Therefore, approximation that takes into account finite number of Gaussian distributions should be used. According to Table I, the number of component comprised by model should be smaller for small values of A. Similarly, the number of components should be larger for large A values.

Class A noise is simulated using Monte Carlo simulations. Depending on region that comprises value of uniformly distributed variable, Gaussian variable with appropriate variance is generated. Regions for decision are proportional to values of Poisson coefficients. In simulations, parameter Γ has value Γ=0.001. Results of simulations are given in Fig. 2 for four different A values (A=0.01, A=0.1, A=1 and A=10). In case of A=0.01 first 5 channels are taken into account, and for evaluating theoretic values m<100 in Eq. (1) are taken into account. Similarly, for large A, large m is needed for sufficiently precise results. For A=10, first 25 channels are considered for simulation model. Theoretic and simulated curves fit very well for all values of A.

IV. ERROR PROBABILITY FOR BPSK

Observe BPSK transmission in the presence of Class A noise type. If m^{th} channel is realized in moment t_k, probability of error is equal

$$P_{e,m} = \int_U^{+\infty} \frac{1}{\sqrt{2\pi\sigma_m^2}} \cdot e^{-\frac{z^2}{2\sigma_m^2}} dz = \frac{1}{2}\operatorname{erfc}\left(\frac{U^2}{2\sigma_m^2}\right) \qquad (4)$$

where U represents BPSK signal amplitude. BER in the presence of Class A noise can be found as mathematical expectation of probability of error given by Eq. (4), for all possible channel realizations. Therefore it is given by:

$$P_{e,tot} = \sum_{m=0}^{\infty} P_m(A) \cdot P_{e,m} = \frac{e^{-A}}{2} \sum_{m=0}^{\infty} \frac{A^m}{m!} \operatorname{erfc}\left(\frac{U^2}{2\sigma_m^2}\right) \qquad (5)$$

Simulation model described in Section III is implemented for determining BER. In Fig. 3. theoretic results obtained by Eq. (5) are compared with simulation results. Results are shown for different values of A (A=0.01, A=0.1, A=1 and A=10). Theoretic BER curves determined by Eq. (5) are given for upper bound of m equal 100. As there is almost no difference between theoretic and approximate values, it can be concluded that the use of simulation model is approved. Thus, this model can be used as a base model for computer evaluation of system performances when influence of Class A impulsive noise exists.

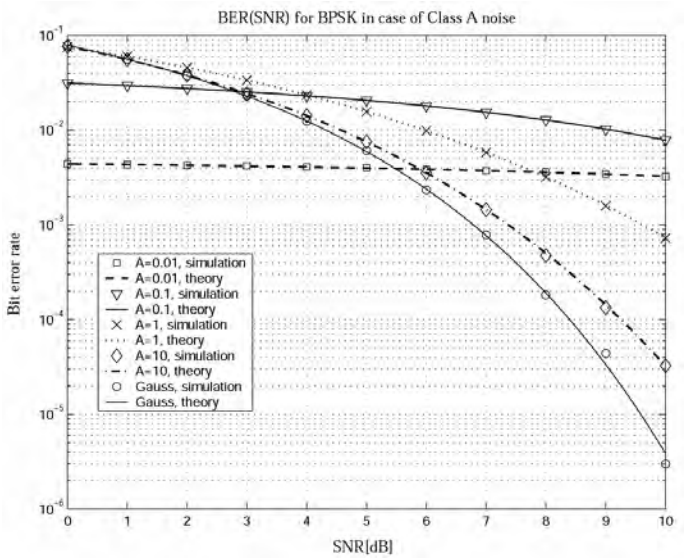

Fig. 3. Theoretic and simulation BER curves for case of BPSK transmission in the presence of Class A noise

V. CONCLUDING REMARKS

Class A discrete model given by [6] is suitable for modeling impulsive noise and narrowband interference in PLC systems [2], [4], [8], [9]. One of main advantages is that it represents the most critical case for system performance evaluation because of memoryless character of Class A channel model. Furthermore, because of its generality it's applicable in theoretic evaluations and simulations of systems performances.

Contribution of this paper is in developing efficient simulation model for Class A impulsive noise. This model is implemented for determining Class A impulsive noise PDF. Simulation results are compared with results obtained using theoretic PDF formula. Simulation model is also implemented for determining BER in BPSK system influenced by Class A noise. Theoretic expression for BER is derived. Theoretic and simulated results are compared for several different specific values of channel model parameter A. According to results obtained in this paper, it is clear that use of simulation method is approved and can be easily implemented in more complex systems.

Subject of future work will be channel model that comprises multipath nature of PLC channel and frequency selective attenuation, as well as its impulsive nature. Different modulation and coding schemes can be implemented [2], [4]. As various types of DSL (Digital Subscriber Line) systems suffer from similar disturbances [1], [4], solution can be found in modulation and coding schemes similar to those used in this systems, but adapted to specific characteristic of PLC channel.

REFERENCES

[1] M. Jankovic, Z. Petrovic ,"*Broadband ISDN – access networks*", Academic Mind, Belgrade, in Serbian, 2002.

[2] E. Biglieri, "Coding and Modulation for Horrible channel", IEEE Communications Magazine, May 2003.

[3] M. Zimmermann, K. Dostert "Analysis and Modeling of Impulsive Noise in Broad-Band Powerline Communications", , IEEE Transactions on Electromagnetic Compatibility, Vol 44 No, February 2002.

[4] Huaiyu Dai, H. Vincent Poor ,"Advanced Signal Processing for Power Line Communications", IEEE Communications Magazine, May 2003.

[5] M. Zimmemann, K. Dostert, "Multipath Model for the Powerline Communications", IEEE Transactions Communications, vol. 50, no. 4, April 2002.

[6] A. D. Spaulding, D. Middleton "Optimum Reception in as Impulsive Interference Environment – Part I: Coherent Detection", IEEE Transactions on Communications, Vol. Com-25, No. 9, September 1977.

[7] V. Golubovic, P. Ivanis, "The use of concatenated codes for error correction in channel with influence of strong impulsive noise", TELFOR 2003.

[8] C. L. Giovaneli, P. Farrell, B. Honary "Space-Time Block Codes with Rate ≥1 for Power Line Channels".

[9] J. Haring, A. J. H. Vinck, "Coding for Impulsive Noise Channel", International Symposium on Power-Line Communications, ISPLC 2001.

[10] Y. Nakano, D. Umehara, M. Kawai, Y. Morihoro, "Viterbi Decoding for Convolutional Code over Class A Noise Channel".

Influence of Multiple Co-channel Interference on Hard-Limited Channel with Application of Convolutional Codes and Soft Decision Viterbi Decoding

Predrag N. Ivaniš[1], Goran T. Đorđević[2], Vesna M. Golubović[1], Aleksandra M. Cvetković[2]

Abstract **- This paper presents the simulation analysis of BPSK (Binary Phase Shift-Keying) signal transmission over satellite system in the presence of multiple uplink and downlink co-channel interferences. The CC (convolutional codes) (2,1,3), (2,1,5) and (2,1,7) are used with soft decision Viterbi decoding. The emphasis is placed on determining the *BER* (bit error rate) improvement in the case of these codes implementation in the satellite system influenced by multiple co-channel interferences that can be very often the predominant destructive influence in such system.**

Keywords **- Satellite communications, Co-channel interference, Convolutional coding, Bit error probability.**

I. INTRODUCTION

The co-channel interference is one of the predominant limiting factors in the performance of digital satellite communication systems, [1-6]. This co-channel interference is usually produced by adjacent satellite or terrestrial radio relay links operating on the same carrier frequency. In addition, in order to double the information capacity of satellite systems, two orthogonally polarized electromagnetic waves are transmitted over the same radio frequency channel; i.e. the carrier frequencies of these waves are the same. Under real conditions in satellite communication systems, it is not possible to totally separate these two waves in the receiver; i.e. there is crosstalk between these orthogonally polarized waves. In other words, there is typical co-channel interference in the receiver, [1-6]. This interference can appear both at the satellite input (over uplink) and at the receiver ground station input (over downlink).

The influence of these interferences was considered in [5-6]. In those papers, the analysis included one interference per uplink and one interference per downlink, and numerical results were presented. The general method for analyzing the influence of multiple co-channel interference can be easily derived from previously mentioned papers, and other ones appeared in the literature. But, using this analytical approach including numerical integration, it is very difficult to obtain concrete numerical results for several co-channel interferences (greater than one per up- and down-link) because it must be compute multidimensional numerical integration over some special functions with considerable accuracy. In addition, the analyses in those papers were concerned only uncoded modulation formats.

The contribution of this paper is in determining the bit error probability P_e (*BER*) in detecting BPSK signal transmitted over a satellite link influenced of any number of co-channel interference (for example the results for ten interferences are presented). Except taking the uncoded BPSK signals into account, we also apply the convolutional coding with soft decision Viterbi decoding, since it is the standard technique for today's satellite communications, [4], and clearly present the improvements of system performance. The co-channel interference is modeled sufficiently general by unmodulated sinusoidal wave with constant amplitude and stochastic varying phase uniformly distributed in $(-\pi,\pi]$, [5-7]. The satellite station amplifier is modeled by a hard-limiter, [8], (the assumption is that input power-output power (AM/AM) and input power-output phase (AM/PM) conversion effects are compensated). Convolutional coding and soft Viterbi decoding algorithms are applied, as described in [9], [10].

II. SYSTEM MODEL AND ANALYSIS

After signal processing in the transmitting ground station (encoding data by classical convolutional encoder [9], and modulation process), the signal is emitted from transmitter to the satellite station. The bandpass filter at the satellite station input is wide enough to pass the useful signal without distortion and to limit the uplink noise to a bandwidth that is small compared to the filter central frequency. Other interferences that not occupy the same frequency range as the useful signal are cancelled by this filter. For our analysis we assume that the filter bandwidth is sufficient to not cause intersymbol interference. The satellite input signal can be written as, (Fig. 1),

$$s_i(t) = A_u \cos(\omega_0 t + \phi_0) + \sum_{j=1}^{N_1} A_{iuj} \cos\left[\omega_0 t + \theta_{iuj}(t)\right] + \\ + n_{Cu}(t)\cos(\omega_0 t) - n_{Su}(t)\sin(\omega_0 t) \quad , \quad (1)$$

where A_u, ω_0 and ϕ_0 are the useful signal amplitude, carrier frequency and phase, respectively. In the case of the BPSK modulation format application, ϕ_0 is 0 or π depending on binary one or binary zero is transmitted; A_{iuj}, ω_0 and $\theta_{iuj}(t)$ are the amplitude, carrier frequency and phase of the j-th co-channel interference $i_{uj}(t)$ (j=1,2,...,N_1) (there are N_1 co-channel interferences over uplink). Since we observe the influence of so-called co-channel interference, it should be noticed that the carrier frequencies of the useful signal and co-channel interference are quite equal. The co-channel

[1]Predrag N. Ivaniš and Vesna M. Golubović are with the Faculty of Electrical Engineering, Bulevar kralja Aleksandra, Belgrade, Serbia and Montenegro, E-mail: predrag48@kondor.etf.bg.ac.yu; vesna.golubovic@etf.bg.ac.yu

[2]Goran T. Đorđević and Aleksandra M. Cvetković are with the Faculty of Electronic Engineering, Beogradksa 14, 18000 Nis, Serbia and Montenegro, E-mail: goran@elfak.ni.ac.yu; alekmi@elfak.ni.ac.yu

interference amplitude is constant, while its phase is random variable uniformly distributed in (-π, π], [5-7],

$$p(\theta_{iuj}) = \frac{1}{2\pi}, \qquad -\pi < \theta_{iuj} \le \pi, \qquad j = 1,2,..., N_1. \quad (2)$$

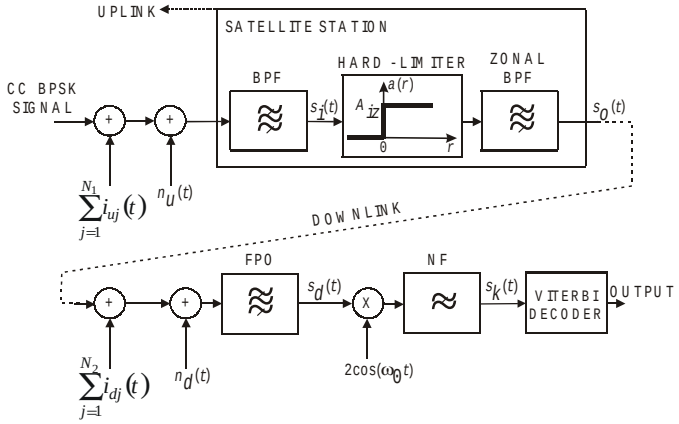

Fig. 1. Model of satellite system for transmission of convolutional encoded BPSK signals in the presence of multiple uplink and downlink co-channel interferences

$n_{Cu}(t)$ and $n_{Su}(t)$ are the quadrature components of the uplink narrowband zero-mean white Gaussian noise with bilateral power spectral density denoted by $N_0/2$.

The signal given by (1) can be re-written in the form

$$s_i(t) = r(t)\cos[\omega_0 t + \gamma(t)], \quad (3)$$

where

$$r(t) = \left\{ \left[A_u \cos\phi_0 + \sum_{j=1}^{N_1} A_{iuj} \cos(\theta_{iuj}(t)) + n_{Cu}(t) \right]^2 + \left[A_u \sin\phi_0 + \sum_{j=1}^{N_1} A_{iuj} \sin(\theta_{iuj}(t)) + n_{Su}(t) \right]^2 \right\}^{1/2},$$

$$\tan(\gamma(t)) = \frac{A_u \sin\phi_0 + \sum_{j=1}^{N_1} A_{iuj} \sin\theta_{iuj}(t) + n_{Su}(t)}{A_u \cos\phi_0 + \sum_{j=1}^{N_1} A_{iuj} \cos\theta_{iuj}(t) + n_{Cu}(t)}. \quad (4)$$

$r(t)$ and $\gamma(t)$ are the envelope and phase of the sum of the narrowband useful signal, N_1 co-channel interferences and Gaussian noise with zero mean value and bilateral power spectral density $N_0/2$. The ratio "useful signal energy per bit/noise power spectral density" over uplink is denoted by

$$(E_b / N_0)_u, \quad (5)$$

The total ratio "useful signal power/co-channel interferences power" over uplink is denoted by

$$SIR_u = \frac{A_u^2}{\sum_{j=1}^{N_1} A_{iuj}^2}. \quad (6)$$

The ideal zonal bandpass filter at the satellite station output totally removes the parasite spectral components produced by hard-limiter. Hence, all amplitude fluctuations of the output signal $s_o(t)$ are removed, while the phase of this signal is not distorted. The satellite output signal

$$s_o(t) = A_{iz} \cos[\omega_0 t + \gamma(t)]. \quad (7)$$

is re-emitted to the receiver ground station. At the receiver front end, this signal is influenced by zero-mean white Gaussian noise with bilateral power spectral density $N_0/2$, and N_2 co-channel interferences. The receiving ground station input signal has the form

$$s_d(t) = A_d \cos[\omega_0 t + \gamma(t)] + \sum_{j=1}^{N_2} A_{idj} \cos[\omega_0 t + \theta_{idj}(t)] + n_{Cd}(t)\cos(\omega_0 t) - n_{Sd}(t)\sin(\omega_0 t) \quad (8)$$

where the second term in the previous expression is the sum of N_2 downlink co-channel interferences. As in the case of the uplink, the j-th co-channel interference $i_{dj}(t)$ (j=1,2,...,N_2) amplitude is constant while its phase $\theta_{idj}(t)$ is stochastic variable uniformly distributed in (-π, π], [5-7].

$$p(\theta_{idj}) = \frac{1}{2\pi}, \qquad -\pi < \theta_{idj} \le \pi, \qquad j = 1,2,..., N_2. \quad (9)$$

$n_{Cd}(t)$ and $n_{Sd}(t)$ are the quadrature components of the narrowband Gaussian noise $n_d(t)$.

The ratio "signal energy per bit/noise power spectral density" over downlink is denoted by

$$(E_b / N_0)_d, \quad (10)$$

The total ratio "signal power/co-channel interferences power" over downlink is denoted by

$$SIR_d = \frac{A_d^2}{\sum_{j=1}^{N_2} A_{idj}^2}. \quad (11)$$

Under assumption that reference carrier signal in the receiver is $2\cos(\omega_0 t)$, [5-6], the signal at the Viterbi decoder input is

$$s_k(t) = A_d \cos[\gamma(t)] + \sum_{j=1}^{N_2} A_{idj} \cos[\theta_{idj}(t)] + n_{Cd}(t). \quad (12)$$

The soft Viterbi decoding, [9-10], is performed and decision is made.

III. Simulation Results and Discussion

On the basis of the analysis presented in Section II, using Monte Carlo simulation method, [11], numerical results are obtained and presented in Figs. 2-5 and Tables 1-4.

Fig. 2 and Table 1 illustrate how the system performance is influenced by different number of co-channel interferences. It can be noticed that if the number of interferences increases from 2 to 4, the *BER floor* decreases 6.5 times, while if the number of interferences increases from 8 to 10, the *BER floor* decreases 1.41 times, that is much less then in the previous case. It can be noticed that the total interference power (over up- and down-link) is constant, and that power is parted to different number of co-channel interferences.

On the basis of the Fig. 3 and Table 2, it is evident that even for relatively high values of bit error probability in the case of uncoded BPSK modulation format application, by using proper convolutional code scheme it is possible to decrease the bit error probability to the acceptable level for practical proposes.

Fig. 4 and Table 3 give the answer how much the downlink energy per bit/noise power spectral density ratio should be in order to achieve the desired bit error rate. In the case of uncoded signal application it is not possible to achieve the bit error probability of 10^{-4} regardless of increasing $(E_b/N_0)_d$ (for example, $P_e=1.44\cdot10^{-4}$ even for $(E_b/N_0)_d$=26dB). But with application of CC(2,1,3), CC(2,1,5) or CC(2,1,7) it is quite possible to reach even less values of bit error probability for very low values of $(E_b/N_0)_d$, that is illustrated in Fig. 4 and Table 3.

And finally Fig. 5 and Table 4 clearly illustrate improvements in bit error rate by applying CC(2,1,3).

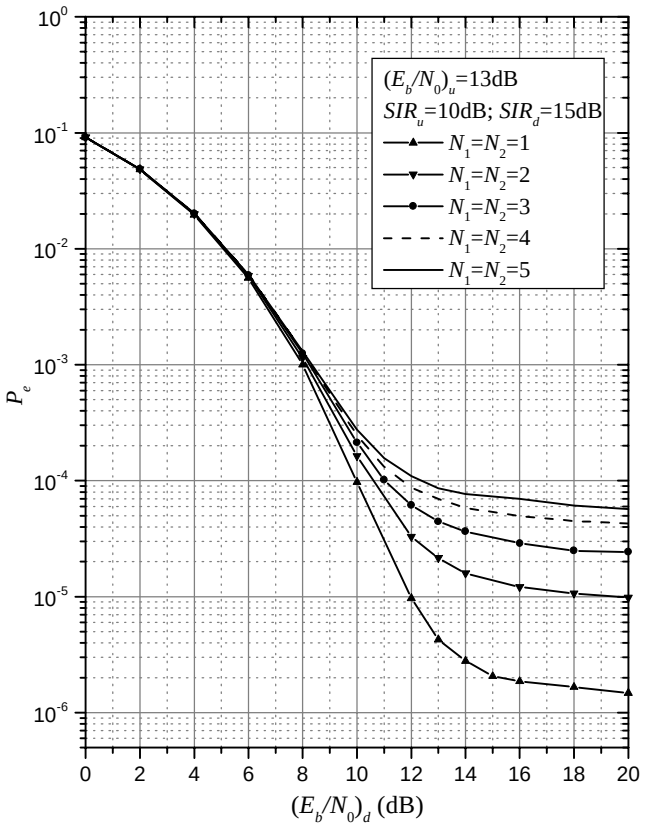

Fig. 2. System performance for various number of co-channel interferences

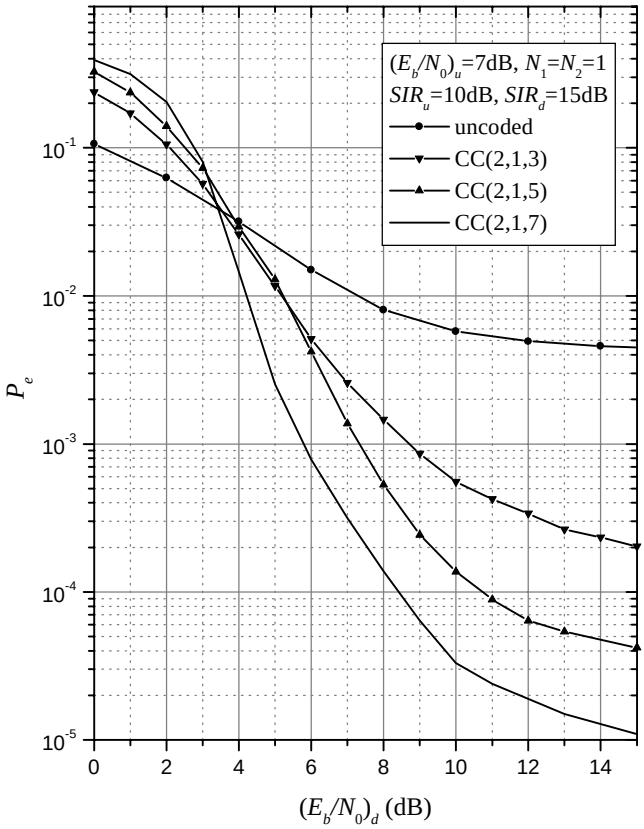

Fig. 3. System performance for various convolutional codes

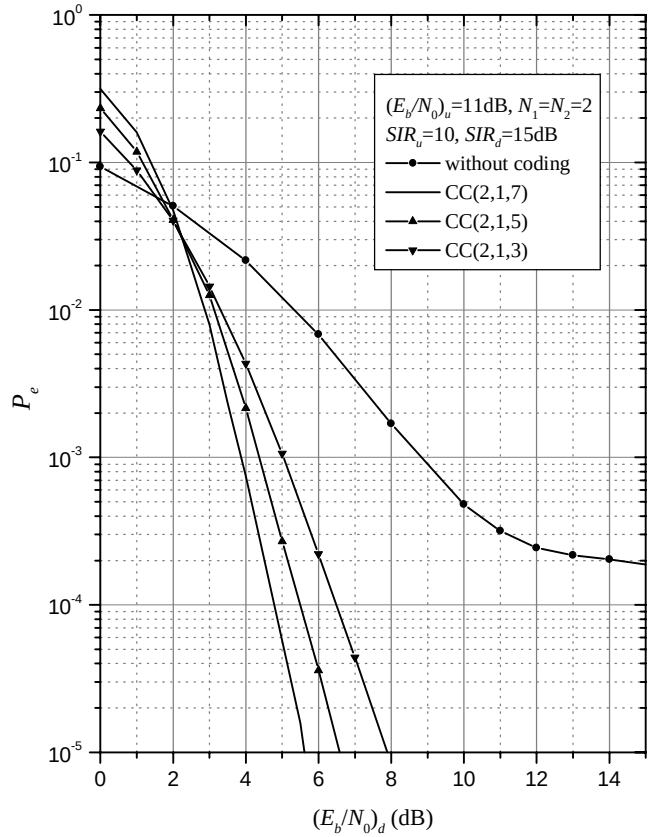

Fig. 4. System performance for various convolutional codes

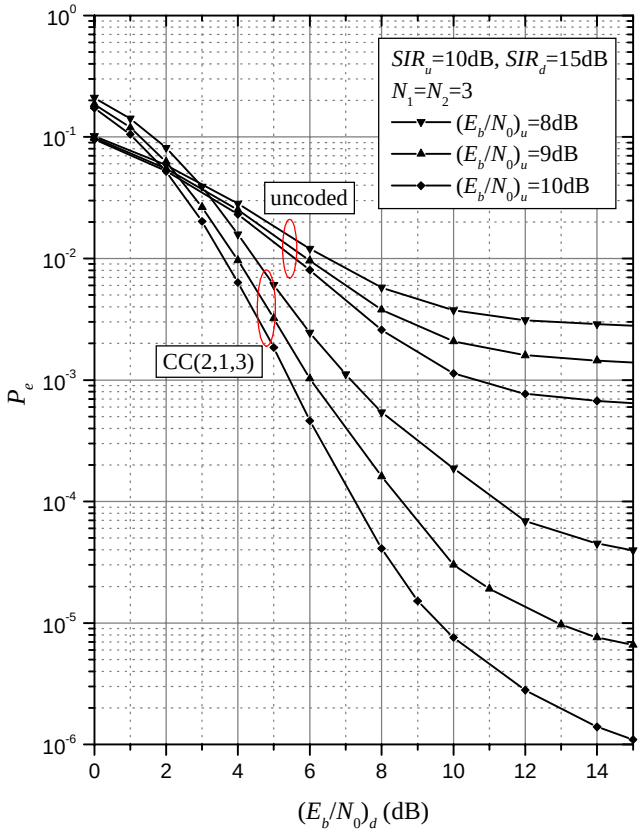

Fig. 5. Performance improvement using CC (2,1,3) in comparison with uncoded BPSK signal

TABLE 1

BER VALUES FOR DIFFERENT NUMBER OF CO-CHANNEL INTERFERENCES ($(E_b/N_0)_u$=13 dB , $(E_b/N_0)_d$=16 dB, SIR_u=10 dB, SIR_d=15 dB)

N_1=N_2	1	2	3	4	5
P_e	$1.9\cdot10^{-6}$	$1.2\cdot10^{-5}$	$2.9\cdot10^{-5}$	$4.9\cdot10^{-5}$	$7.0\cdot10^{-5}$

TABLE 2

SOME *BER* VALUES FOR UNCODED AND CC ENCODED BPSK SIGNALS ($(E_b/N_0)_d$=7 dB, $(E_b/N_0)_d$=12 dB, SIR_u=10 dB, SIR_d=15 dB, N_1=N_2=1)

uncoded	CC(2,1,3)	CC(2,1,5)	CC(2,1,7)
$4.94\cdot10^{-3}$	$3.38\cdot10^{-4}$	$6.40\cdot10^{-5}$	$1.87\cdot10^{-5}$

TABLE 3

NEEDED $(E_b/N_0)_d$ (dB) FOR REACHING SOME *BER* VALUES IN THE CASE OF DIFFERENT CC CODES ($(E_b/N_0)_u$=11 dB, SIR_u=10 dB, SIR_d=15 dB, N_1=N_2=2)

P_e	uncoded	CC(2,1,3)	CC(2,1,5)	CC(2,1,7)
10^{-4}	impossible	6.51 dB	5.50 dB	4.73 dB
10^{-5}	impossible	7.89 dB	6.58 dB	5.58 dB

TABLE 4

BER VALUES FOR UNCODED AND CC(2,1,3) BPSK SIGNALS ($(E_b/N_0)_d$=14 dB, SIR_u=10 dB, SIR_d=15 dB, N_1=N_2=3)

$(E_b/N_0)_u$ (dB)	8	9	10
uncoded	$2.88\cdot10^{-3}$	$1.45\cdot10^{-3}$	$6.73\cdot10^{-4}$
CC(2,1,3)	$4.51\cdot10^{-5}$	$7.60\cdot10^{-6}$	$1.40\cdot10^{-6}$

IV. CONCLUSION

In this paper we present simulation approach in determining the performance of hard-limited satellite system in the presence of multiple uplink and downlink co-channel interferences. Using the real-life system energetic parameters, we determine the error probability in detecting both uncoded and convolutional encoded BPSK signals with soft Viterbi decoding. We give relevant discussions and notes regarding the results presented in the paper, that show how much the system performance can be improved by applying different CC codes in the observed satellite system.

All simulations were performed using software MATLAB 6.5 and Digital Visual Fortran Version 6 on PC Pentium 4 with Intel processor of 1.8 GHz and RAM of 256 MB. The developed simulator is very flexible and efficient and can be used in the further scientific researches that will include implementation of concatenation of Reed Solomon code as outer code and CC as inner code.

REFERENCES

[1] R. M. Gagliardi, *Satellite Communications*, Van Nostrand Reinhold, New York, 1991.

[2] V. K. Bhargava, D. Haccoun, R. Matyas, P. P. Nuspl, *Digital Communications by Satellite - Modulation, Multiple Acces and Coding*, Krieger Publishing Company, Malabar, Florida, 1991.

[3] G. Maral, M. Bousquet, *Satellite Communication Systems - Systems, Techniques and Technology*, John Willey & Sons, 1996.

[4] International Telecommunication Union (ITU), *Handbook on Satellite Communications*, A John Wiley & Sons, Inc., Geneva, Switzerland, 2002.

[5] M. C. Stefanovic, G. T. Djordjevic, "BPSK and QPSK Nonlinear Satellite Communication System Performance in the Presence of Cochannel Interference", International Journal of Satellite Communications and Networking, pp. 285-297, Vol. 21, No. 3, May-June 2003.

[6] G. T. Djordjevic, M. C. Stefanovic, "Influence of Co-Channel Interference and Imperfect Reference Signal Extraction On Transmission Of *M*PSK Signal Over Nonlinear Satellite System", Invited paper, *Proceedings of the XI Telecommunications Forum TELFOR 2003*, paper 5-24.pdf, Belgrade, November 2003.

[7] J. Wang, A. Yongacoglu, "Performance of Trellis Coded-8PSK with Cochannel Interference", IEEE Transactions on Communications, COM-42, No. 1, pp. 6-10, January 1994.

[8] M. C. Stefanovic, G. T. Djordjevic, I. B. Djordjevic, "Performance of Binary CPSK Satellite Communication System in the Presence of Noises and Noisy Carrier Reference Signal", International Journal of Electronics and Communications (AEUE), Vol. 53, No. 2, pp.70-76, 1999.

[9] S. B. Wicker, *Error Control Systems for Digital Communication and Storage*, Prentice Hall, Englewood Cliffs, NJ 07632, 1995.

[10] D. J. Costello, Jr., J. Hagenauer, H. Imai, S. B. Wicker, "Applications of Error-Control Coding", IEEE Transactions on Information Theory, Vol. 44, No. 6, pp. 2531-2560, October 1998.

[11] M. C. Jeruchim, P. Balaban, K. S. Shanmugan, *Simulation of Communication Systems - Modeling, Methodology and Techniques*, Kluwer Academic/Plenum Publishers, New York, 2000.

QOS Analysis of IEEE 802.11 Wireless LAN

Toni Janevski[1] Vasil Maljanovski[2]

Abstract - **In this paper we present a new approach for performance analysis of IEEE 802.11 Wireless Local Area Network (WLAN). Our analysis is targeted to the Quality of Service experienced by the user. Main QoS parameters in these analyses are throughput and packet delay, which are evaluated using simulation methodology.**

***Keywords* – QoS, 802.11 WLAN, Throughput, Delay**

I. INTRODUCTION

Wireless Local Area Networks (WLAN) are gaining momentum today, either as corporate wireless networks or public hot-spots that provide higher data rates than current cellular networks. To provide an efficient and robust network in a wireless environment, the IEEE has chosen the Carrier Sense Multiple Access with Collision Avoidance (CSMA/CA) protocol as the basic standard protocol at Medium Access Control (MAC) layer for 802.11 WLAN. There has been significant research on the evaluation of its performance. However, performance evaluation of the IEEE 802.11 WLAN under realistic traffic conditions has been considered difficult. Therefore, many analyses have assumed simpler traffic conditions such as Poisson sources with fixed size data frames [1].

In telecommunication networks like WLAN is very important to obtain the behavior of the system with varying number of users and at different transmitting bit rates. If we want to maintain defined Quality of Service (QoS) level, we need to keep the number of users that simultaneously communicate, their throughput and packet delay in acceptable limits [2]. If we suppose that characteristics of wireless link do not vary in time and space and if we do not consider mobility of users, which are main sources of appearance of transmission errors, then we should focus out attention to analysis of throughput and packet delay in a given service area.

In this paper we consider the 802.11 standard that is world wide deployed today, that is 802.11b [3]. This WLAN standard is created to provide users with maximum of 1; 2; 5.5 or 11 Mbps, which is dependent upon the physical layer (i.e. multiple access and modulation scheme). To be complete, we should mention the other two existing WLAN standards today, 802.11a and 802.11g, which are using different physical layer than 802.11b with aim to achieve higher data rates up to maximum of 54 Mbps. Also, there is ongoing work to develop other 802.11 standards, such as 802.11e for QoS support, 802.11i for better security etc.

[1]Dr. Toni Janevski is an Ass. Professor at the Faculty of Electrical Engineering, Karpos 2 bb, 1000 Skopje, Macedonia, E-mail: tonij@cerera.etf.ukim.edu.mk

[2]Vasil Maljanovski is a graduate student at the Faculty of Electrical Engineering, Karpos 2 bb, 1000 Skopje, Macedonia, E-mail: maljanovski@hotmail.com

The paper is organized as follows. In Section 2 we present WLAN model used in the analysis. Section 3 we show and discuss the results from the simulations. Finally, Section 4 concludes the paper.

II. MODEL OF IEEE 802.11 NETWOKS

In the IEEE 802.11 standard there are defined two access methods: Distributed Coordination Function (DCF), which provides basic method for contended access based on CSMA/CA; and Point Coordination Function (PCF), which provides uncontended access by allocating part of the bandwidth to some users. We are interested to analyze the most commonly available access method, and that is CSMA/CA. In this paper we refer in our analysis to this basic access method, which is shown in Fig. 1.

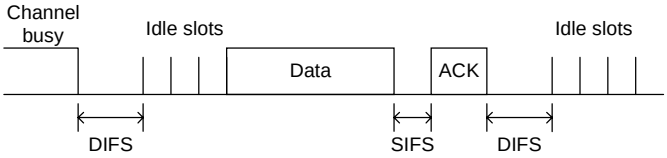

Fig. 1. IEEE 802.11 basic access method

The period that is observed here is Contention Period (CP) that is the period when MUs content for an access to the wireless channel. Mobile users transmit and receive packets using one access point (AP) that first buffers packets and then transmits them. In our analysis we observe only the upstream case, which is more sensitive to collisions. Also, we use finite size buffers in the simulations, so we may have losses due to a packet arrival in a full buffer. Packets are generated from users randomly. Inter-arrival time between two packets is modeled as a stochastic variable following the exponential distribution:

$$P_\lambda(t) = \lambda e^{-\lambda t} \tag{1}$$

where $P_\lambda(t)$ is the probability distribution function (pdf), and λ is the average packet arrival rate. Then, mean value of the inter-arrival time equals to $t_{ia}=1/\lambda$. For example, if a user transmits with bit rate of R=1Mbps and packet length is 1500 bytes, then he would generate packets with rate of λ=1048576bps/(1500*8 bits/packet)=87.38 packets/s. In this example average time between two successive packets would be 1/87.38=11.44 ms (Eq.2). This means that on average every 11.44 ms comes one packet. If the user's bit rate or/and packet length are different then this value is also changed.

$$t_{ia} = \frac{packet\,length}{R} \tag{2}$$

If two or more users are sending packets at the same time then a collision occurs. To avoid collisions mobile users in IEEE 802.11 WLAN utilize the CSMA/CA method. The CSMA/CA

protocol is a random access protocol that is targeted to prevent or minimize collisions. In the case of a collision, each mobile station executes so-called Binary Exponential Backoff retransmission algorithm to resolve the collision and maintain the stability of the wireless channel.

At first MU senses the wireless channel. If it is busy, MU waits until it gets free. After that moment MU waits additional interval called DIFS (DCF-IFS Distributed Coordination Function - Inter Frame Space). The value of DIFS is taken to be 30 μs. Critical moment is at the end of this interval. After that every user that has packets to transmit will send and a collision will occur. However, to avoid such situation, which is undesired due to scarce wireless medium, 802.11 WLAN uses Backoff Algorithm. According to it, MU waits supplementary time that is a product of randomly generated number and a given time interval called time slot (TS). Randomly generated number can belong to the interval [0, CW-1], where CW stands for "Contention Window" and it has an integer value from interval [CWmin, CWmax]. Typical values for CWmin and CWmax are CWmin=8 and CWmax=1024. TS is defined as time that is needed for a station to detect a transmission of another station, and its standardized value is TS=20 μs.

After DIFS interval ends, every MU backs off a time period that can be from one time slot to 7 time slots. For example, if exist 3 users and they generate extra time of 2 TSs, 4 TSs and 4 TSs correspondingly then first user can use the channel and other will have to wait until first user finishes with transmission. But if the order is: 2 TSs, 2 TSs and 5 TSs then first and second MU will collide. The program code for this simulation is written so that collision is registered and after that, mobile users that collide (in this example 2 of them, 1st and 2nd) will generate random number from 0 to 15. So, probability of colliding after this action is diminished. If once again this happens then randomly generated number would have values from 0 to 31 and so on. In the simulation random number for the backoff algorithm are generated by uniform probability distribution function.

After successful packet reception in the buffer, AP waits time interval called SIFS (Short Inter Frame Space) and then transmits message called ACK to let the user know that its packet is received [4]. SIFS represents time interval during which MU is changing its regime from a transmitter to a receiver. In the simulation SIFS=10 μs and ACK transmission time is 210 μs [3].

In our analysis we refer to several different QoS parameters, such as: packet delay, throughput per user, number of collisions, number of rejected packets and number of passed packets, using different traffic conditions (i.e. bit rate) and different number of users served buy a single AP. The packet length is 1500 bytes.

Packet delay is defined as time interval between the instant when the packet enters into the buffer (which, in fact, is the same moment when it is generated by the user because air propagation time is ignored) and instant when the same packet leaves the AP. Packet delay is a sum of its waiting time in the buffer and serving time. For packet length of 1500 bytes and link speed of 11 Mbps the serving time is calculated as:

$$t_{\mu} = \frac{1500 * 8bits}{11534336bits / s} \approx 1.04ms \qquad (3)$$

Throughput for one user presents number of his packets that left AP multiplied by packet length (expressed in bits) divided with time interval that is difference between moment when last packet of the same user left AP and moment when first packet of the same user left AP.

Number of rejected packets is the number of those packets who tried to enter into the buffer while it was full. It depends upon the buffer size (how many packets the buffer can accept), packet length, number of users, and bit rate.

Number of occurred collisions is the number of events when two or more users at the same time tried to send packets. Of course this depends on number of users.

III. Simulation results

We have performed several simulation experiments with aim to obtain QoS behavior of 802.11 WLAN. In first set of simulations we are changing the bit rate per user for the case with single user, and for the second case with two users served by one AP (in the latter case both users are transmitting at the same rate). In the second set of simulations we change number of users served by a single AP.

The results of the first set of experiments regarding the behavior of throughput per user, packet delay, number of rejected packets, number of occurred collisions and number of passed packets versus transmitting bit rate of users, are shown in Figures 2-6, respectively. In the simulations the link speed is set to 11 Mbps (802.11b standard), packet length is 1500 bytes and buffer length expressed in number of packets that can be received is 5 times greater than number of users.

In the first case there exists only one user that varies his transmission bit rate from 1 Mbps to 11 Mbps. We observed that his throughput at source bit rate equal to the wireless link capacity (i.e. 11 Mbps) and assuming error-free wireless environment, is not 11 Mbps, but it is approximately 8 Mbps (Fig. 2). However, this result can be shown via analytical approach as well. For instance, the time for the transmission of a single packet is equal to [5]:

$$T_{sin\,gle} = t_{pr} + t_{tr} + SIFS + ACK + DIFS \qquad (4)$$

where t_{pr} is the preamble time (144 μs), t_{tr} is the frame transmission time (packet length/transmitting bit rate), SIFS=10 μs, DIFS=30 μs, ACK is the ACK transmission time (210 μs). If user's transmitting bit rate is 11 Mbps it means that t_{tr}=1500*8/11534336=1.04 ms. So, the proportion r of useful bandwidth is 0.725, which is calculated using the following relation:

$$r = \frac{t_{tr}}{T_{sin\,gle}} \qquad (5)$$

Then, the throughput of the user is 0.725*11=7.975 Mbps, which is exactly the same as the results from the simulation analysis.

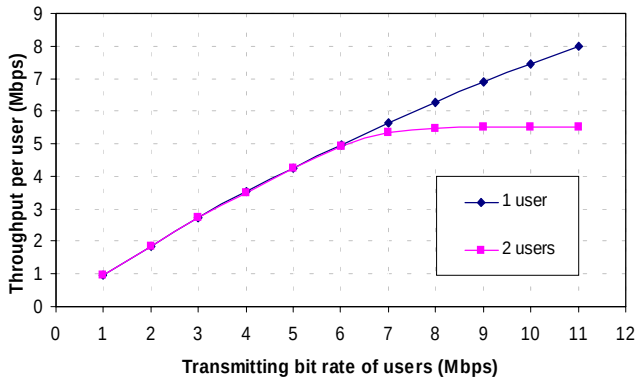

Fig. 2: Throughput per user for different values of transmitting bit rate

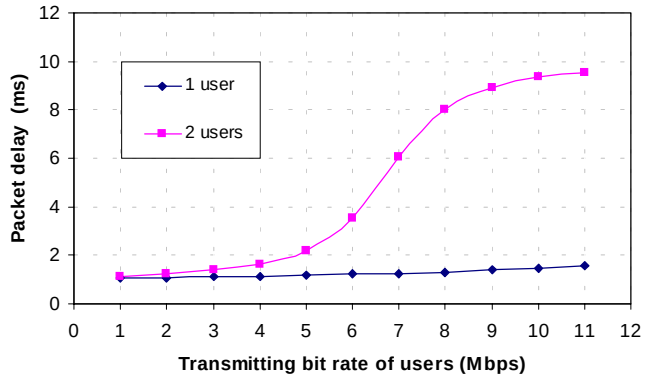

Fig. 3: Packet delay for different values of transmitting bit rate

For example, if user transmits at bit rate of 2 Mbps, then t_{tr}=12000bits/2097152bps=5.72 ms, r=5.72ms/6.114ms=0.936 and his throughput would be 0.936*2 Mbps=1.872 Mbps (refer to Fig. 2).

In the second case there exist two users that transmit simultaneously and with equal bit rates. One can notice from the results shown in Fig. 2 that when transmitting rate reaches 7 Mbps throughput per user, then the average throughput per user stabilizes around 5.5 Mbps. So, we get that we have higher utilization of the wireless link in the case of multiple users compared to the case with a single user.

In this simulation experiment number of rejected packets is relatively small. But, if the buffer size is less than the one used in this simulations, then the number of rejected packets would increase and the throughput of the user would decrease.

In the case with single user average packet delay is increasing with the transmitting bit rate (Fig. 3). When transmitting bit rate reaches infinity, the buffer will be full all the time (for any finite size), and hence packet delay will be equal to the maximum waiting time in the buffer. In our case, buffer size is set to 5 packets (including the serving one), so maximum delay will be 5*1.04ms=5.2 ms. Also, in the case with single user it is trivial to say that number of occurred collisions is zero (Fig.5). In the case of two users packet delay increases, but starts with saturation (due to finite buffer size of 10 packets) near transmitting bit rate of 11 Mbps (Fig.3). This is the result of collisions between the two users.

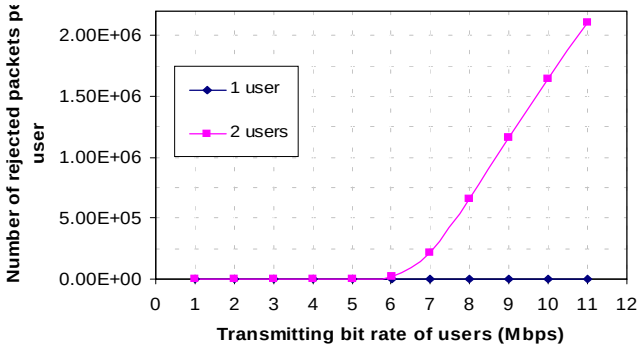

Fig. 4: Number of rejected packets per user for different values of transmitting bit rate

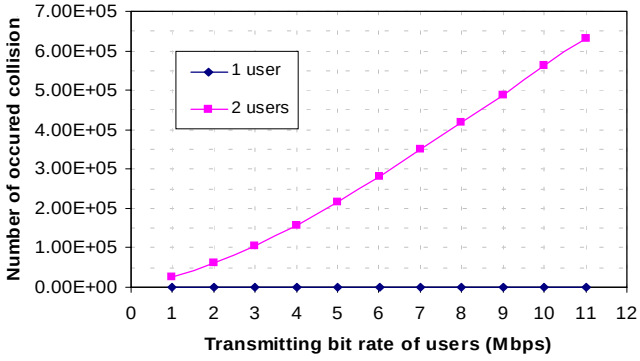

Fig. 5: Number of occurred collisions for different values of transmitting bit rate

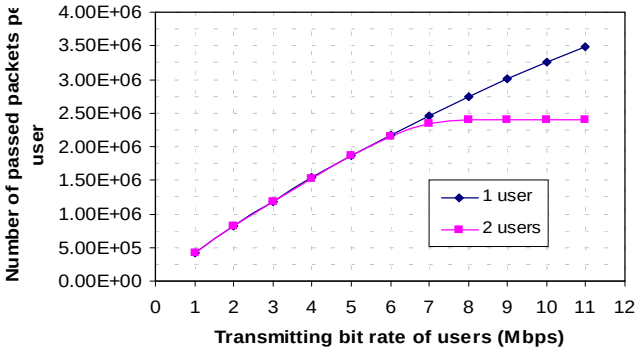

Fig. 6: Number of passed packets per user for different values of transmitting bit rate

So, packet delay would be theoretically 10*1.04ms=10.4ms. This value is asymptotical and can be reached when transmitting bit rate of users reaches infinity. Simulation was done for transmitting bit rates in range 11-20 Mbps (for transmitting bit rate of 20 Mbps packet delay is 10 ms) and the results confirms that packet delay very slowly achieves that theoretical value, which is maximum for the packet delay under previously given assumptions.

While there are no rejected packets or collisions when there is only one user, for the case with two users served by single AP number of rejected packets and collisions are increasing due to finite buffer size (Fig.4-5). Due to statistical multiplexing of traffic from multiple users, number of passed

packets is increasing as well (Fig. 6). Because wireless link speed is 11 Mbps t_{μ}=1.04 ms (Eq.3). This means that for an interval of 1 second one AP can serve maximum 1/1.04 ms=961.5 packets. Simulation lasts 5000 seconds, so maximum number of passed packets can be around 4807692. This value is not achieved for the bit rate of 11 Mbps because t_{ia} is not 1.04 ms, but t_{ia}=1.04+0.394=1.434 ms. For higher user's bit rate that value can be reached.

In Fig. 6 number of passed packets starts to get saturated at value of 2400000 packets when transmitting bit rate reaches near 7 Mbps (it is similar to the throughput behavior, as one should expect) which is half of the previously mentioned maximum number of passed packets.

In the second simulation experiment, we vary the number of users served by single AP. In Figs. 7, 8 and 9 are shown analyses of throughput per user, packet delay and occurred collisions, using variation of number of users and total emitting bit rate (T.E.B.R.). We use three different T.E.B.R. values, and they are: 5.5, 11 and 16.5 Mbps, i.e. 50%, 100% and 150% of the wireless link speed. This means that, for example, if there are 10 users and T.E.B.R. is 16.5 Mbps then each one of them will transmit with 1.65 Mbps. From Fig. 7 can be seen that when 1 user transmits his throughput is shorten accordingly to Eq.5 and when number of users increases value of throughput per user decreases due to the increased number of collisions (Fig.9). Packet delay (Fig.8) also rises because buffer size is 5 times greater than number of users.

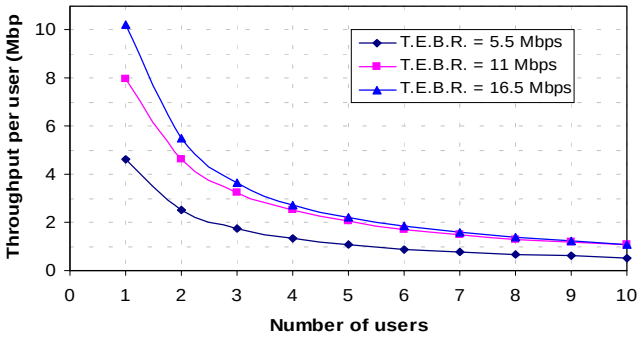

Fig. 7: Throughput per user for different number of users

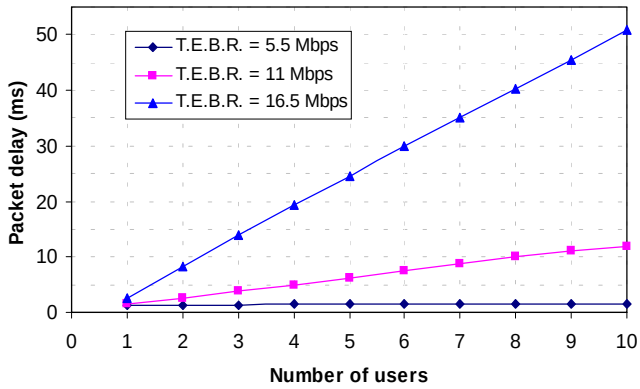

Fig. 8: Packet delay for different number of users

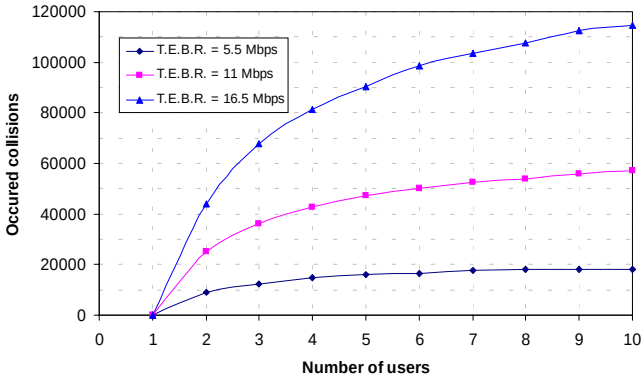

Fig. 9: Occurred collisions for different number of users

IV. Conclusions

In this paper we have performed performance analysis of IEEE 802.11 WLAN regarding mainly the MAC protocol specification. Our analysis targeted QoS parameters, such as throughput and packet delay under different traffic conditions in the network. In the analysis we have used simulation methodology.

The results showed that due to access method in 802.11 WLAN, the efficiency of utilization of wireless link capacity is around 73%. We have shown that more users increases the utilization of the bandwidth, but on the other side increases the average packet delay and number of collisions and rejected packets as well. Additionally, we have also shown that too many users will degrade the performance of the WLAN.

References

[1] Chuan Heng Foh, Moshe Zukerman, "Performance Analysis of the IEEE 802.11 MAC Protocol", European Wireless 2002, Florence, Italy, February 2002.

[2] Toni Janevski, "Traffic Analysis and Design of Wireless IP Networks", Artech House, 2003.

[3] IEEE standard 802.11b, "Wireless LAN Medium Access Control (MAC) and Physical Layer (PHY) specifications", 1999.

[4] Brian P. Crow, Indra Widjaja, Jeong Geun Kim, Prescott T. Sakai, "IEEE 802.11 Wireless Local Area Networks ", IEEE Communications Magazine, September 1997.

[5] Antonio Garcia-Macias, Franck Rousseau, Gilles Berger-Sabbatel, Leyla Toumi and Andrzej Duda; "Quality of Service and mobility for the wireless internet", wireless networks 9, 341–352, 2003, 2003 kluwer academic publishers.

Adaptive Admission Control Strategy for Multimedia Mobile Packet Networks

Tomislav Kartalov[1], Toni Janevski[2]

***Abstract* – In this paper we propose a strategy for adaptive admission control in multimedia cellular networks. The proposed strategy uses adaptive adjustment of threshold values for voice and video traffic by monitoring the network performance, which is measured through performance parameters such as packet loss probability on a packet-level, as well as new call blocking and call dropping probability on a call-level basis.**

***Keywords* – Admission control, Mobile, Quality of Service, Video, Traffic**

I. INTRODUCTION

Mobile networks, due to their cellular structure, are characterized with different traffic characteristics than wired networks. The coverage area is divided in smaller areas called cells. In our analysis we consider packet-based traffic in the mobile network. In such case, during a single ongoing call a subscriber is allowed to handover from its current cell to another neighboring cell. In the handover process the user is releasing the certain amount of bandwidth in the old cell and occupies another same amount in the target cell.

Third generation (3G) mobile networks [1] and beyond (e.g. 4G), as well as Wireless LANs, have many times higher bandwidth than cellular networks in the past (e.g., up to 2 Mbps in 3G, and up to 54 Mbps in 802.11 family of WLANs). Higher bandwidth provides possibility for service providers to offer multimedia services (e.g., video streaming) besides voice service. In such case, we are facing new challenges considering dimensioning and efficient resource utilization in multimedia mobile networks. To gain from statistical multiplexing we should use the same wireless channels for voice and video traffic. However, there are different bandwidth and Quality of Service (QoS) requirements from each of these two traffic types [2, 3]. For example, a voice call demands smaller bandwidth compared to a video call. On the other side, voice is conversational bidirectional traffic which is very sensitive to delay, while video streaming is basically unidirectional and therefore can tolerate higher packet delays (they can be compensated by buffering at the receiving end).

In this paper we propose a novel strategy for adaptive call admission control in mobile multimedia networks, considering voice and video traffic, based on active monitoring of the network performances, defined through packet loss probability, call-dropping probability (P_d) and call-blocking probability (P_b).

[1]Tomislav Kartalov is with Faculty of Electrical Engineering, Karpos 2 bb, 1000 Skopje, Macedonia, E-mail: kartalov@cerera.etf.ukim.edu.mk

[2]Toni Janevski is an Ass. Professor at the Faculty of Electrical Engineering, Karpos 2 bb, 1000 Skopje, Macedonia, E-mail: tonij@cerera.etf.ukim.edu.mk

The paper is organized as follows. In the next section we define the network model that we use in simulations. Section III presents the principles of the network operation. Section IV gives the simulation results. Finally, Section V concludes the paper.

II. NETWORK MODEL

We created a simulation environment in Matlab. Here, we briefly report on our simulation model.

The coverage area of the mobile network is divided into hexagonal cells. Every cell is assigned a certain bandwidth, which presents the capacity of that cell for call handling. The subscribers can be served only by one cell at a moment.

Speed of each subscriber in mobile state is modeled with normal (Gaussian) distribution truncated at 0. Position of each subscriber is represented with 2 coordinates (x and y), and may be in two possible states: moving or stationary. Subscriber movement is defined in the following manner: in every step of the simulation, each subscriber is allowed to move in either x and y directions or in both. The length of the trajectory is dependent upon the subscriber speed.

In our work we consider two call types, voice calls, randomly generated by given traffic parameters, and video calls, intentionally implemented as downlink video streams in a monitored cell. Voice calls, and voice packets have higher priority, but only when voice traffic intensity is lower than a given threshold. One of the issues of this paper is the choice of a criterion for assigning that threshold, and the influence of its value over the network performance.

We model voice call arrival process with Poisson distribution [4]. Each traffic class is given call arrival rate λ (calls/hour/user). Furthermore, call duration time is modeled with exponential distribution, and we denote with t the mean call duration.

In a packet cellular network we may distinguish among three main types of losses:

- Blocking of a new voice call: it occurs when subscriber attempts to make a new call, but there are no free resources in the target cell, and the network rejects that call.
- Dropping of a voice call: it happens when there are no free resources in the target cell at handover events.
- Lost packets (for both voice and video flows): they occur when packets are lost due to full buffers. We assume that the wireless link is error-free.

We denote new call blocking probability and call dropping probability for voice calls with P_b and P_d, respectively. Furthermore, we use Pl_{VI} and Pl_{VO} to denote packet loss probability for video and voice, respectively.

In our network model, we use the policy "blocked calls cleared", that is, an already blocked new call, dropped handover or lost packet is cleared from the system.

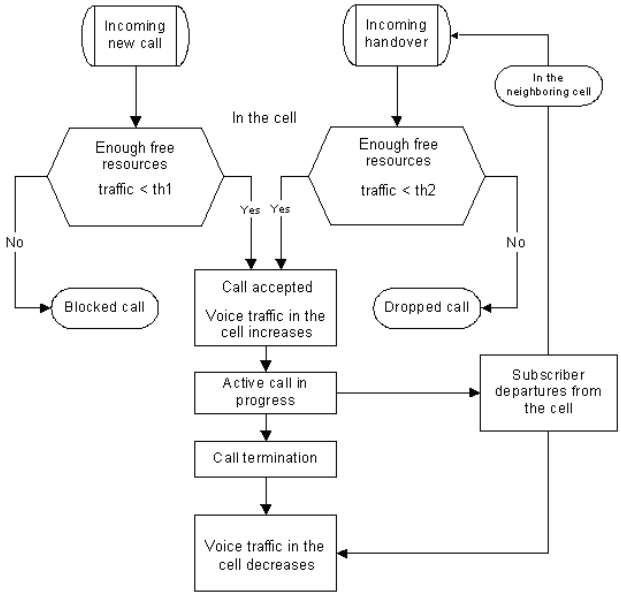

Fig. 1. General principle of network operation

III. The Principles of Network Operation

As written above, in our simulated network we implemented randomly generated voice calls, and few deterministic video streams (1, 2 or 3 video streams). Voice calls bandwidth requirements are fixed to 10 kbps (enough for 3G wireless networks), with exponentially distributed ON-OFF periods. Mean value for these periods is equal to 0.35 s (ON period), and 0.65 s (OFF period). Video streams are PAL (25 fps) video sequences with resolution 316x288 pixels, encoded with MPEG-4 encoder engine. The average bit rate of each of these sequences is approximately 520 kbps. The capacity of a single cell is set to 2048 kbps (2Mbps). From the cell bandwidth certain fractions are assigned to both types of calls (voice and video).

The estimation of the assigned fractions of bandwidth is following few rules:

- Voice calls, once accepted, are of highest priority in the network, and fractions are estimated according to voice bandwidth requirements.
- Video streams, if any, are of lower priority, but have guaranteed minimal fraction of bandwidth, which varies in different simulation scenarios.
- Guaranteed minimal fraction for video is reached with a definition of so-called "threshold" level for voice traffic intensity. This threshold is compared with voice traffic intensity and has the same dimension (bytes/second, or bits/second).
- The control of overwhelming voice traffic (above the "threshold" level) is obtained rather with rejecting new calls, than with terminating active ones. That problem is solved with assigning two different thresholds, one slightly higher than the other. The higher one is valid for the incoming voice handovers, and the lower is for the new calls.

Explained behavior of the system is presented in Fig. 1, where conditions and situations in which one call may be lost (dropped or blocked) are shown. Threshold levels are denoted with *th*1, for new calls, and *th*2 for handovers.

In this work we analyzed three different criteria for determining the threshold levels, as follows:

- *No threshold* (NT): Voice traffic is absolutely of higher priority and can occupy the whole cell bandwidth, if necessary.
- *Fixed threshold* (FT): The fixed fractions of bandwidth are assigned to voice and video traffic (e.g., half of the bandwidth to each one). Voice traffic can occupy the whole bandwidth only when video traffic is not present in that cell. Otherwise, it will use only its portion of the bandwidth.
- *Adaptive threshold* (AT): For each video stream, the system reserves fraction of the bandwidth equal to average bit rate of that video stream. Voice traffic occupies the rest of the bandwidth. Calculation of the video average bit rate is performed on the last few frames of the stream. The system in this case involves prediction, assuming that the next frame will have an average frame size. Concerning the number of frames taken into account for the prediction of the bitrate in near future, we tried several experiments, and concluded that the optimal number is around 100 (10 is too small for getting real average, and 1000 is too large: requires more computational power, and there are problems at the start and at the end of a certain video stream)

By the 3rd criterion, it may seem that video traffic has the priority over the voice, but these reservations are not "hard" reservations, i.e. with reserved bandwidth. It is a "soft" reservation, more like recommendation to the system not to allow more voice calls to enter the system when voice traffic reaches the threshold. However, the fractions of bandwidth are still estimated according to voice traffic, and once accepted, the voice call still has the highest priority.

IV. Simulation Results

We performed several simulation experiments in which we obtained dependence of mobile network performances upon various traffic parameters and upon the three defined threshold estimation criteria.

Because there are many traffic parameters that influence in the same manner traffic intensity, we defined so called "traffic coefficient" T. The bigger this traffic coefficient is, the higher is the traffic intensity. We obtained the value of $T = U \lambda t$ by multiplying three traffic parameters: Number of subscribers per cell U, average call arrival rate λ [calls/hour/subscriber], and mean call duration (holding time) t [s].

In this simulation experiment, we performed two groups of simulations, using different threshold policies. In each group, we worked with two different scenarios, i.e. with two and three MPEG-4 video streams activated in the monitored cell. In each scenario, for various traffic parameters (various T) we performed several simulations, examining the influence of traffic intensity on the network performance.

Video streams in the system are not always active, but they are introduced one by one. For example, if we have three video streams, the simulation will run for a certain time only

with voice, and then sequentially we introduce the three video streams, one after other, as shown in Fig. 2. In the scenario with two video streams we use the first two streams.

We present the simulation results in a particular order with aim to notice the dependence of QoS on our three threshold policies. The results for one video stream (light video traffic), because of the small network load, and small losses, were not illustrative enough, and they will not be shown in this paper. Also, it is important to state that in FT (Fixed Threshold) policy, the threshold level was optimized for medium video traffic intensity, i.e. for two video streams.

In Fig. 3 to 8 we show the packet losses in the system in the case with two video streams.

From Fig. 3 we can observe highest losses of voice packets with NT (No Threshold) strategy, which is odd at first sight because the NT policy gives the highest priority to voice traffic. But, these losses are consequence exactly of that behavior. Uncontrolled acceptance of new voice calls and incoming handovers overwhelms the server buffers in the system, and probability of appearance of lost packets increases. In other words, voice traffic is jamming itself, especially at high traffic intensity in the system, because in that case even the whole bandwidth of the cell is not enough to transfer all the voice calls.

On the other hand, with NT policy we have very few blocked and dropped calls (unrestrained acceptance), which can be seen in the Fig. 7 and 8. The NT policy gives highest packet loss probabilities for video packets too. This results also from high acceptance rate of voice calls. As written above, the bandwidth quotas are estimated according to voice requirements, so in this case we note high packet loss probability for video at higher network load, as shown in the Fig. 4.

Concerning AT and FT policies, the FT policy gives lower losses for both voice and video traffic. This is due to higher acceptance rate in system with AT. If the threshold is fixed (FT), when there is only one active video stream, the system still rejects new voice calls when the traffic is above the fixed threshold, although the rest of the bandwidth may be more than enough for one video stream. As shown in Fig. 5, after introducing the first video stream, the voice traffic is reduced to its value defined by the threshold level. With AT, that problem is solved, and system adaptively recalculates the threshold allowing higher voice traffic intensity, but this also means higher probability of buffer overload and lost packets. As we can see from Fig. 6, with AT scheme voice traffic reduction occurs only after the acceptance of the second video stream in the system. Thus, with AT we have slightly more lost packets, but we avoid unnecessary blocking of new or handover voice calls, which can be seen from Fig. 7 and 8, where both P_b and P_d have smaller values for AT strategy compared to FT.

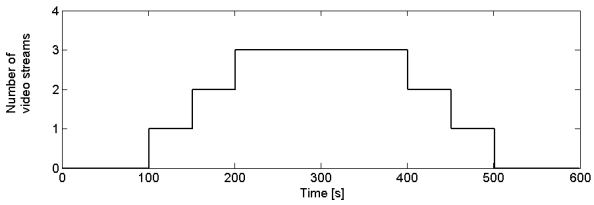

Fig. 2. Introducing video streams in the simulation

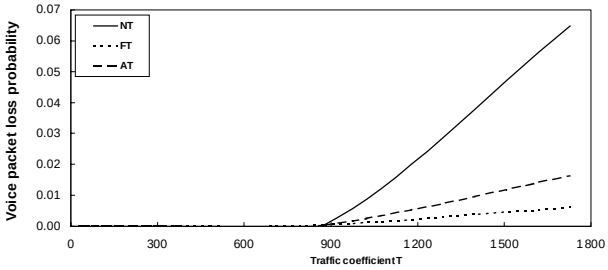

Fig. 3. Voice packet loss probability vs. traffic intensity (2 video streams)

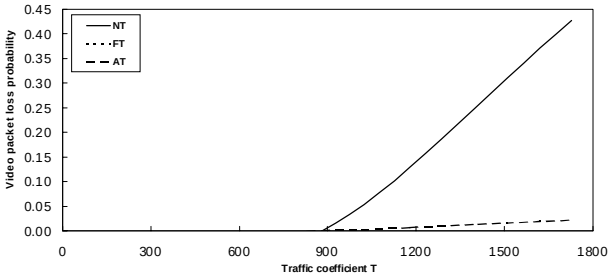

Fig. 4. Video packet loss probability vs. traffic intensity (2 video streams)

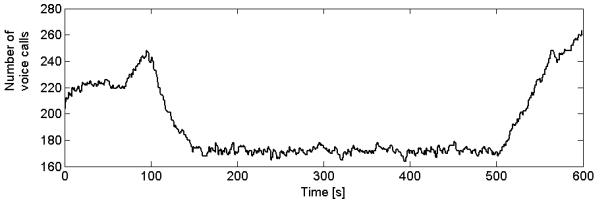

Fig. 5. Number of active voice calls over time (FT)

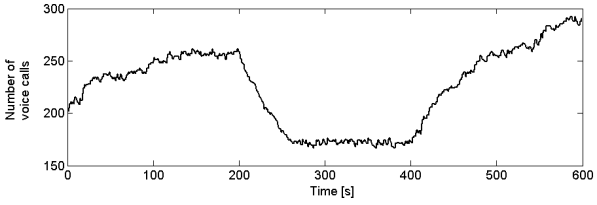

Fig. 6. Number of active voice calls vs. time (AT scheme)

Fig. 9 and 10 presents the losses with three video streams (heavy video traffic) in the system. From these Figures we can derive the same conclusions about high packet losses, and low blocking and dropping probabilities with NT policy. Higher video packet loss probability for FT is the result of the fact that fixed threshold is optimized for medium video traffic intensity (2 video streams), and at heavy video traffic the video bandwidth requirements are not satisfied. At expense of

video packets, the voice packets have lower loss probability with FT, but that is negligible comparing to difference in video packet losses.

V. CONCLUSIONS

In this paper we introduced different strategies for handling two types of traffic (voice and video) in multimedia mobile networks. The strategies include various methods of estimating the "threshold", parameter which determines the bandwidth quotas for each of the call types. The performance of the network was considered through its Quality of Service (QoS), defined by new call blocking and call dropping probabilities, and by probability of packet losses. We investigated different strategies upon traffic conditions in the cell, i.e. voice traffic intensity, and different number of video streams.

Using simulation analysis we showed that network performance is highly dependent on chosen threshold strategy for call admission. But, which one is the most optimal with lowest level of losses? The answer to that question is dependent upon the priorities established in a certain system. For example, if we create a system with constraints on call blocking and dropping probabilities, regardless of the lost packets, we could use the NT strategy (with lower quality of accepted connections). On the other hand, if the constraint is packet loss, the use of FT strategy is recommended because of its simplicity and time independence. However, the most flexible solution appears to be AT strategy.

REFERENCES

[1] E. Dahlman et al. "WCDMA-The radio interface for future mobile multimedia communications," IEEE Trans. on Veh. Tech., vol. 47, no. 4, Nov. 1998.

[2] D. Wu, Y. Hou, Y.-Q. Zhang, and W. Zhu, "Adaptive QoS Control for MPEG-4 video communication over wireless channels", in Special Issue selected from ISCAS 2000 Workshop and Exhibition on MPEG-4, IEEE Trans. on Circuit and System for Video Technology, vol. 11, 2000.

[3] Q. Zhang, W. Zhu, G. J. Wang, and Y.–Q. Zhang, "Resource allocation with adaptive QoS for multimedia transmission over W-CDMA channels," IEEE WCNC, Chicago, Sept. 2000.

[4] Toni Janevski, "Traffic Analysis and Design of Wireless IP Networks", Artech House Inc., 2003.

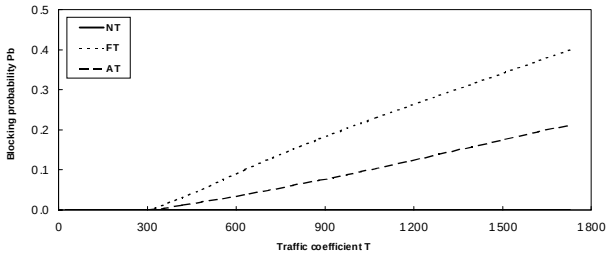

Fig. 7. Call blocking probability vs. traffic intensity (2 video streams)

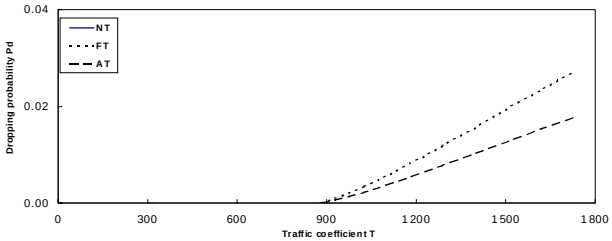

Fig. 8. Call dropping probability vs. traffic intensity (2 video streams)

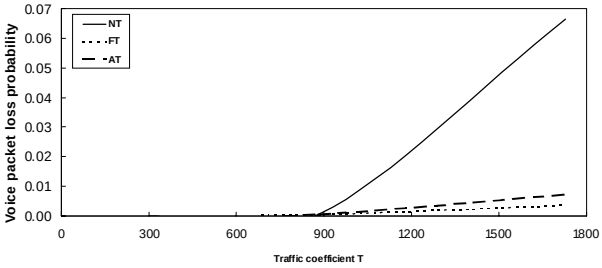

Fig. 9. Voice packet loss probability vs. traffic intensity (3 video streams)

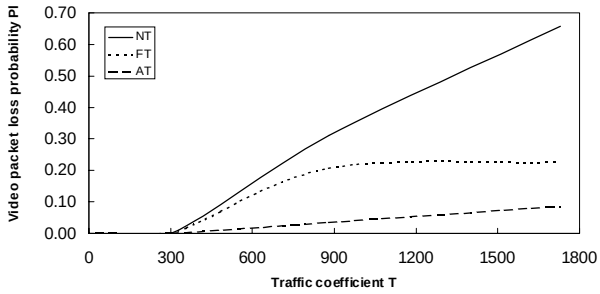

Fig. 10. Video packet loss probability vs. traffic intensity (3 video streams)

Investigation of the Impact of Disturbances in Transmitting Digital Data Along the Return Channel in CATVs

Kiril Koitchev[1], Stanimir Sadinov[2]

Abstract: **In CATVs the range between 0-47 MHz is used to create interactive systems fir transmission of data and is revered to as reverse channel or return channel.**

Cable lines, which are used to transmit data along the return channel of CATVs, undergo a certain amount of disturbances, which causes the quality of transmitted data to deteriorate. The quality of transmitted digital signals is characterized by error coefficient within a certain section of cable track. This coefficient could be expressed as a ratio of the number of error characters received at the end of a certain cable section versus the total number of transmitted characters-BER.

Calculation of BER for most frequently used modulations M-PSK and M-QAM is performed either by estimating the probability for character error or by means of evaluating upper and lower limits of noise level. Precise analysis of BER system is often difficult to achieve and, usually, the results should be processed further.

This paper proves that the signal/noise ratio *R* is a function of probability *P* and is numerically equal to the error coefficient BER. In this way it is possible to calculate the required ratio signal/noise *R* by analytical estimation, which used a preset error coefficient BER.

Further it is proved that heat noises appear to be a key factor that limits the length between two cable amplifiers. The paper also contains deduced relationships, which allow to determine the permissible length between two highway amplifiers *l* depending on the noise arising in the line. Graphic presentations show relationships between the length of individual cable sections and the rate of transmission of digital signals along different types of coaxial cable lines; the permissible error coefficient for particular section being 10^{-9} and kilometer attenuation in coaxial lines for frequency of 1 MHz.

Keywords - **CATV network design, return channel; M-PSK and M-QAM), BER coefficient**

I. INTRODUCTION

CATV networks allow for two-way transmission of signals; from the main station to a large number of subscribers and , conversely, from subscribers to the main station via a narrower channel. Frequency range from 80 to 862 MHz is used for the straight channel whereas the reverse channel will use from 5 to 47 MHz. Cable lines which are used to transfer digital information along the reverse channel are impacted by disturbances which lower the quality of transferred data.

[1]Asoc. Prof. Ph.D. Kiril R. Koitchev is with the Department of Communications Technology and Equipment, Technical University of Gabrovo, Bulgaria, 5300 Gabrovo, str."Hadji Dimitar" № 4 Bulgaria, E-mail: koitchev@tugab.bg

[2]Ass. Stanimir M. Sadinov is with the Department of Communications Technology and Equipment, Technical University of Gabrovo, Bulgaria, 5300 Gabrovo, str."Hadji Dimitar" № 4 Bulgaria, E-mail: murry@tugab.bg

Transferred digital signals' quality is characterized by error coefficient at a certain section of the cable track. This coefficient could be expressed as a ratio between the number of erroneously received characters at a certain section of the cable track and the total number of transferred symbols – BER

Calculation of BER for most frequently used modulations M-PSK and M-QAM is performed either by estimating the probability for character error or by means of evaluating upper and lower limits of noise level. The precise analysis of BER for any particular system is often difficult to achieve which usually entails further processing of results[4, 5, 6].

The reason for errors in digital signals is found in noise and disturbances whose instantaneous voltages exceed permissible limits thus causing the occurrence of redundant pulses or disappearance of pulses. To avoid errors it is necessary to keep a correct signal/noise ratio at the amplifier input which is hooked up to the CATV reverse channel [1].

Permissible values of noise voltage are determined by the magnitude of the "lowest possible eye-opening of the diagram" B_0 and should not exceed the value $0{,}5B_0$ [2]. Error coefficients of individual amplifiers are determined by the probability of exceeding that value.

II. EXPOSITION

Noises which occur in the communication channel, as well as the heat and those which are caused by mutual impact, have normal (Gauss) distribution. Therefore, the probability of exceeding the permissible noise voltage value will be determined by the integral of probabilities. In this particular case the character 0 should not exceed any absolute voltage value($B_0/2$). The probability for bilateral excess over P_2 of this value . (i.e. $B_0/2$ и + $B_0/2$) will be equal to

$$P_2 = 1 - \frac{1}{\sqrt{2\pi}} \int_{-b_0}^{+b_0} l^{-b^2/2} db = \frac{2}{\sqrt{2\pi}} \int_{+b_0}^{\infty} l^{-b^2/2} db, \quad (1)$$

where $b=u/Us$; u-instantaneous voltage value of the noise (random variable); U_s - effective value of noise voltage; $b_0=B_0/2U_s$.The probability for unilateral excess over values $+B_0/2$ (or - $B_0/2$), which occur in case of character –1 (or +1)will be equal to the half of values determined in (1), i.e.

$$P_1=P_2/2 \quad (2)$$

Since in dual signal characters 0 and 1 occur with equal probability, which equals ½, then it follows that when using bipolar signal the probability for occurrence of 0 will be

$$P_0=1/2 \quad (3)$$

Then the probability for the occurrence of characters –1 and +1 will be

$$P_{-1}=P_{+1}=1/4 \qquad (4)$$

Error occurrence probability will be expressed by the following relationship

$$P=P_0P_2+ P_{-1}P_1+ P_{+1}P_1= P_2[P_0+(P_{-1}+P_{+1})/2]$$

So after taking account of (1) it will be

$$P = [P_0 + \frac{1}{2}(P_{-1} + P_{+1})].\frac{2}{\sqrt{2\pi}} \int_{+b_0}^{\infty} l^{-b^2/2} db = \\ = \frac{3}{4}\frac{2}{\sqrt{2\pi}} \int_{+b_0}^{\infty} l^{-b^2/2} db \qquad (5)$$

In (5) the value P determines the probability of noise voltage u to exceed the value $B_0/2$ at a point of solution which, consequently, will cause an error. In order for the error probability to be lower the effective value of noise voltage U_s should be lower,too, and consequently there should be lower probability of occurrence of noise whose instant value of b_0 exceeds U_s with a number of times thus reaching a permissible value $B_0/2$, i.e.

$$b_0\, U_s= B_0/2$$

hence

$$b_0 = B_0/2\, U_s \qquad (6)$$

occurs as the boundary of integration which is indicated above in (1). Assuming that the permissible amplitude of the $B_0/2$ pulse may obtain various values, then the probability expressed in (5) will occur as function of the value B_0.

$$P(b_0) = \frac{3}{4}\frac{2}{\sqrt{2\pi}} \int_{+b_0}^{\infty} l^{-b^2/2} db \qquad (7)$$

Signal/noise relationship occurs as a unit of measuring amplifier's noise resistance

$$R=20 \lg B_0/ U_s, \, [dB] \qquad (8)$$

By taking (6) into account we get

$$R=20 \lg 2.b_0 \qquad (9)$$

In this way the signal/noise relationship determined by (9) occurs as a function of probability P which is expressed through (7) and numerically equal to the error coefficient BER By using expressions (7) and (9) it is possible to calculate the required signal/noise relationship R by employing a preset error coefficient P.

The results are presented in a table 1.

In coaxial cables operating cable temperature appears to be the main source of noise. Hence temperature generated noises are the reason for limiting interamplifier sections l depending on the noise occurring within the line. In [1] we have the deduced formula of the power of heat noises N:

$$N = R.T_0 \int_0^{f_T} F_\omega(f) g_\omega(f) df \quad , \qquad (10)$$

where $F_\omega(f)$ is the resultant noise coefficient of sequentially started amplifiers and adjusters; $g_\omega(f)$- is the total coefficient of transfer of both amplifier and adjuster; f_T- is thepulse frequency.

Tabl. 1

P	R_p[dB]	P	R_p[dB]	P	R_p [dB]
10^{-3}	16,1	10^{-7}	20,5	10^{-11}	22,6
10^{-4}	17,7	10^{-8}	21,1	10^{-12}	23,0
10^{-5}	18,8	10^{-9}	21,7	10^{-13}	23,4
10^{-6}	19,7	10^{-10}	22,2	10^{-14}	23,7

From (10) it is possible to determine the permissible length of amplifiers' sections l for dual signals

$$\frac{e^x}{x} = \frac{P_u}{2kT_0F_1Q\Phi} \qquad (11)$$

and

$$x = 2\alpha_0 l\sqrt{\Phi / f_0} \quad , \qquad (12)$$

where P_u-stands for the maximum signal power, [W]; $k=1,38.10^{-23}$ W.C/K-Boltzmann constant; $T_0=290$ K-absolute temperature, at which noise parameters are determined; $F_1=3,162$-coefficient of amplifier's noise; Q-relationship between signal maximum power and the power of heat noise upon the same load; Φ-rate of transmission *[bit/s]*; α_0-kilometre attenuation of cable *[Np/km]* with frequency of f_0 *[Hz]*; l-length of regenerating section *[km]*.

To simplify calculations, it is assumed that the transmission coefficient of power amplifier does not depend on frequency

$$g_u= e^{\alpha_0 l\sqrt{f_T / f_0}}$$

and the adjuster's transmission coefficient is frequency dependent:

$$g_k = e^{\alpha_0 l\sqrt{f / f_0}} e^{-\alpha_0 l\sqrt{f_T / f}}$$

After integrating above expressions we obtain the expression for heat noises power of amplifiers and adjusters which are connected in series.

$$N = 2kT_0F_1 f_T \frac{e^x}{x} .$$

By introducing new parameters $Q=P_u/N$ and $\Phi=f_T$ we get simpler expressions for (11) and (12) and by assuming that the maximum voltage of signal (character l) U_{max} is 3V over the wave resistance of line $z=75\Omega$

Then the maximum power of signal in [mW] will be.l:

$$P_u=U^2_{max}/z=3^2.1000/75=120$$

And the signal/noise relationship

$$R=10.lgQ$$

hence

$$Q=10^{R/10}$$

Rate of transmission of dual signals

$$\Phi =f_T =2f_0$$

- kilometer attenuation of cable for frequency f_0 [*MHz*] is $\alpha_0 = \alpha_1 \sqrt{f_0}$, where α_1 is kilometer attenuation for frequency of 1 *MHz*.

a) For normal coaxial cable(Bulgarian make) type PK 75 with pairs 1,37/9,0 mm

$$\alpha_1 = 2{,}34 \text{ dB/km}$$

b)For coaxial cable with pairs 0,68/4,6 mm

$$\alpha_1 = 5{,}31 \text{ dB/km}$$

c) For coaxial cable with pairs 0,68/2,2 mm

$$\alpha_1 = 8{,}86 \text{ dB/km}$$

where f_T and f_0 are in *MHz.*

Relationships (11) and (12) appear as (rate of transmission Φ is expressed in *kbit/s*).

$$\frac{e^x}{x} = \frac{4{,}74.10^{12}}{10^{R/10}\Phi}$$

$$x = 2\alpha_1 l\sqrt{\Phi} \quad [Np]$$

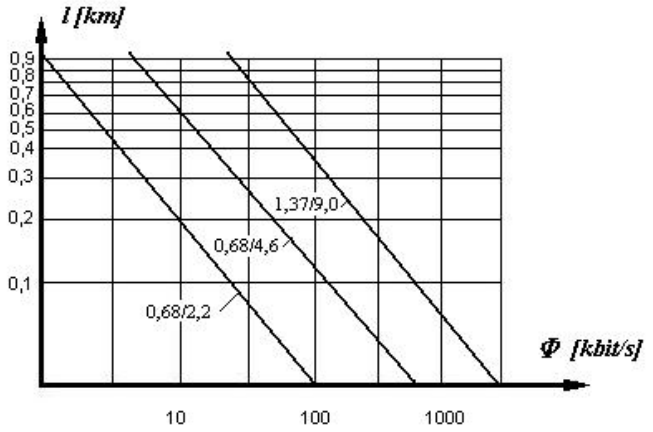

Fig.1. Amplified section length related to the rate of transmission of digital signal with permissible error coefficient 10^{-9} and kilometer attenuation for three types of coaxial cables at frequency of 1*MHz*.

Fig 1 presents the dependences for the length of regeneration section l on the rate of digital signal transmission which are abstained by means of the expressions that have been analyzed so. The permissible value of error coefficient 10^{-9} corresponds to $R=21{,}7$ *dB*. Taking margined from the tolerance of the regenerator 3 dB and , also, taking in consideration the level of disturbances from previous impacts and heat noises, R is to be increased to *4,8 dB* (*10*.lg *3*) and then

$$R=21{,}7+3+4{,}8=29{,}5 \text{ dB}$$

III. CONCLUSIONS

Drawing upon Fig. 1 it follows that for a particular rate of transmission Φ_1 the length of the regenerating section l_1 for the corresponding coaxial cable is to be selected in such a way so that the point with coordinates (Φ_1, l_1) is located below the the straight line that corresponds to the type of coaxial cable used. Accordingly, the error coefficient of the regeneration section with length of l does not exceed the value 10^{-9}. For example, if the rate of transmission of digital data is 500 *kbit/s* the length of cable section should be 300*m* if coaxial cable with pair of 1.37/9.0 *mm* is used and with pairs of 0,68/4,60 *mm* and rate of Φ =200 *kbit/s* the length should not exceed 250 *m.* Since the length of regeneration section is about 600 *m* when highway amplifiers are used ,the optimum rate of transmission is reached at 300 *kbit/s* for trunk cables with pair of 1,37/9,0 *mm*.

REFERENCES

1. Койчев К., С. Садинов. Проектиране на кабелни телевизионни мрежи. "АЛМА МАТЕР Интернационал", Габрово 2001. ISBN 954 9577 81 3

2. Кабельное ТЕЛЕВИДЕНИЕ справочник. 1999 ÷ 2000

3. Койчев К., С.Садинов, С.Немцов. Оценка на BER характеристиките за M-QAM модулации използвани в обратния канал на кабелните телевизионни мрежи.ТЕЛЕКОМ-2003

4. Koitchev K., S. Nemtsov, S. Sadinov. Studies on The Realiability of Two-way Cable TV Network. 6th International Conference on Telecommunications in Modern Satellite, Cable and Broadcasting Services - TELSIKS 2003

5. Koitchev K., Sadinov St. Maximum Value Determination of Non-linear Products in Cable Television Networks. IEEE Transactions on Broadcasting, March 2003

6. Koitchev K., S. Sadinov, S. Nemtsov, "Suggested Method for Composite Frequencies Allocation", 5th International Conference on Telecommunications in Modern Satellite, Cable and Broadcasting Services TELSIKS 2001, Proceedings of Papers, volume 2, pp. 541-543.

The Effects of Interchannel Interference on Optical FSK Systems Influenced by Phase Noise

D. Milić, M. Stefanović

Abstract:- **Moments approach is generally considered a systematic way to perform analysis of coherent optical systems. In this paper, we extend the method to a wider class of systems to include the cases where interchannel interference may be significant. We derive essential equations in matrix form and compare the moments approach with numerical simulation and Fokker-Planck approach. To illustrate the results, we apply the moments method to two-channel optical heterodyne FSK system with dual-filter receiver structure, and evaluate required channel spacing to have less than 1 dB penalty due to crosstalk.**

Keywords:- **Phase noise, optical communication, envelope detection, interchannel interference, frequency shift keying**

I. INTRODUCTION

Considerable efforts have been devoted to theoretical description of coherent optical systems, in order to account accurately for the influence of laser phase noise on the system performance. During the past decade, several solutions to the problem have been presented in the literature [1-5]. Among the solutions, the most widely used are the results of Taylor expansion method [1] and the moments approach [3, 4].

There have been previous attempts to include the impact of interchannel interference on the FSK system performance, using the moments approach [6, 7]. However, potentials of the moments approach were not used to the maximum, and the results are mostly qualitatively valid. In most cases, the effects of time shift between the interfering channels were neglected, and only the systems with ideally synchronized channels were considered. A comprehensive worst-case analysis of ASK systems, which includes the aforementioned effects is outlined in [8]. However, the proposed method uses the leading order Taylor expansion to account for the phase noise influence, together with an approach based on the inverse Fourier transform to compute the bit-error rate, as opposed to conditional error probability approach [7] which is generally more accurate. In this paper, we outline a procedure that combines the good sides of both the approaches -the worst-case analysis of [8], and the conditional error probability approach [7]- to yield the results that should be in closer agreement with the real system performance. We apply the procedure to heterodyne dual-filter FSK receiver, and calculate the required channel separation for a two-channel system.

The authors are with the Faculty of Electronic Engineering, A Medvedeva 14, 18000 Nis, Serbia and Montenegro. E-mail: milko, misa@elfak.ni.ac.yu

II. MOMENTS EVALUATION

Analysis of coherent optical system performance, including the effects of interchannel crosstalk, requires the knowledge of probability density function (pdf) of the following random variable:

$$\frac{1}{\tau}\int_0^{\tau}\left(e^{j\varphi(t)}+e^{j(\theta+2\pi d_{el}t+\phi(t))}\right)dt\,, \tag{1}$$

or -in envelope detection schemes- its squared modulus. Random phase processes $\varphi(t)$ and $\phi(t)$ are considered independent [3] Brownian motions [1] with diffusion constants $2\pi\Delta\nu$, d_{el} is channel separation and θ is interference offset phase - constant over the one bit duration. Using Taylor expansion of the interference, the leading asymptotic behavior is obtained as [6, 8]:

$$\frac{1}{\tau}\int_0^{\tau}e^{j\varphi(t)}dt+je^{j\theta}\frac{1-e^{j2\pi d_{el}\tau}}{2\pi d_{el}\tau}+e^{j\theta}\frac{\phi(\tau)e^{j2\pi d_{el}\tau}-\phi(0)}{2\pi d_{el}\tau} \tag{2}$$

In the above equation, it is convenient to identify the interference as a Gaussian random variable with mean r, and variance $\frac{\Delta\nu\tau}{2\pi(d_{el}\tau)^2}$. Therefore, it is possible to include the last term of the previous equation with other Gaussian noise contributions, such as shot and receiver noises [6, 7]. However, the deterministic interference term r is more complicated to account for.

Let the moments $\hat{\mu}_{m,n}$ of X be defined as

$$\hat{\mu}_{m,n}=E\left[X^m\overline{X}^n\right]. \tag{3}$$

where the overbar stands for complex conjugation. Exact moments $\mu_{i,j}$, of the filtered phase-noisy signal without the influence of interference, are known in symbolic form [2, 3, 4], and they can be used to express $\hat{\mu}_{m,n}$, as we will show.

By introducing the notation $X = r + z$, where

$$r=e^{j(\theta+\pi d_{el}\tau)}\frac{\sin(\pi d_{el}\tau)}{\pi d_{el}\tau}\,, \tag{4}$$

$$z=\frac{1}{\tau}\int_0^{\tau}e^{j\varphi(t)}dt\,, \tag{5}$$

according to Eq. (2), the moments $\hat{\mu}_{m,n}$ are written as:

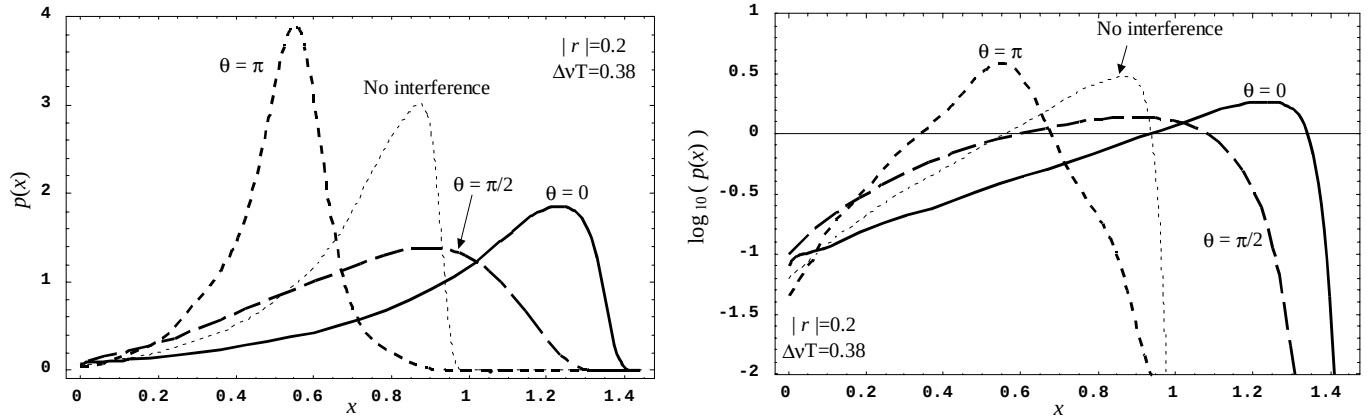

(a) (b)

Fig. 1. Probability density functions of the envelope detector output, with and without deterministic interference. Curves are reconstructed from the first 12 moments using maximum entropy approach.

$$\hat{\mu}_{m,n} = E\left\{(r+z)^m(\bar{r}+\bar{z})^n\right\} = \sum_{i=0}^{m}\sum_{j=0}^{n}\binom{m}{i}\binom{n}{j}\mu_{i,j}\, r^{m-i}\,\bar{r}^{\,n-i} \tag{6}$$

It is convenient to write the equation in the matrix form:

$$\hat{\mu}_{m,n} = \langle\bar{\rho}\rangle_{m+1}\langle M\rangle_{n+1,m+1}\langle\rho\rangle_{n+1}^{T} \tag{7}$$

where $\langle M\rangle_{n,m}$ denotes the moment-matrix of the random variable z, namely:

$$\langle M\rangle_{n,m} = \left[\!\left[\,\mu_{i-1,j-1}\,\right]\!\right]_{\substack{i=1,2,\ldots,n\\ j=1,2,\ldots,m}}, \tag{8}$$

The row-vector $\langle\rho\rangle_k$ is defined as $\langle\rho\rangle_k = [\,r_i\,]_{i=1,2,\ldots,k}$, where r_i are given by:

$$r_i = \binom{k-1}{i-1} r^{k-i}. \tag{9}$$

The moments $\hat{\mu}_{k,k}$ are in fact moments of random variable $|X|^2$ and they are relevant in performance analysis, since the dual-filter FSK receiver uses envelope detection.

Described procedure may be generalized to yield the following result:

$$\left\langle\hat{M}\right\rangle_{k,k} = \langle\bar{R}\rangle_{k,k}\langle M\rangle_{k,k}\langle R\rangle_{k,k}^{T} \tag{10}$$

where the matrix $\langle R\rangle_{k,k}$ is defined as

$$\langle R\rangle_{k,k} = \left[\!\left[\,r_{i,j}\,\right]\!\right]_{i,j=1,2,\ldots,k} \tag{11}$$

and the $r_{i,j}$ are given by

$$r_{i,j} = \begin{cases}\binom{i-1}{j-1} r^{i-j} & , \quad j \le i\\ 0 & , \quad j > i\end{cases}. \tag{12}$$

The moment-matrix $\left\langle\hat{M}\right\rangle$ of the random variable X may not be real, as this is obvious from Eqs. (4) and (6). However, the moments on the main diagonal, which represent moments of the random variable $|X|^2$, are real. Figs. 1 and 2 illustrate the results and their validity.

Define: $\xi_m = \sum_{i=1}^{m}|X_i|^2$, and $\eta_{m+1} = |X_{m+1}|^2$. Moments of the sum of m+1 independent variables $|X_i|^2$ may be obtained by the following recurrence approach:

$$\zeta_n^{\Sigma(m)} = E\left\{\left(\sum_{i=1}^{m}|X_i|^2\right)^n\right\} = E\left\{\xi_m^n\right\} \tag{13}$$

$$\begin{aligned}\zeta_n^{\Sigma(m+1)} &= E\left\{\left(\sum_{i=1}^{m}|X_i|^2 + |X_{m+1}|^2\right)^n\right\} = E\left\{(\xi_m+\eta_{m+1})^n\right\}\\ &= E\left\{\sum_{k=0}^{n}\binom{n}{k}\xi_m^{n-k}\eta_{m+1}^{k}\right\} = \sum_{k=0}^{n}\binom{n}{k}\zeta_{n-k}^{\Sigma(m)}\hat{\mu}_k^{(m+1)}\end{aligned} \tag{14}$$

Again, the matrix formulation is convenient because the recursion process can be replaced by the multiplication of m matrices. The matrix equation is expressed as:

$$\begin{aligned}\left\langle\zeta^{\Sigma(m+1)}\right\rangle_k &= \left\langle\zeta^{\Sigma(m)}\right\rangle_k \cdot \langle W_{m+1}\rangle_{k,k}\\ &= \left\langle\zeta^{\Sigma(m-1)}\right\rangle_k \cdot \langle W_m\rangle_{k,k}\cdot\langle W_{m+1}\rangle_{k,k}\\ &= \ldots = \left\langle\mu^{(1)}\right\rangle_k \cdot \prod_{i=2}^{m+1}\langle W_i\rangle_{k,k}\end{aligned} \tag{15}$$

where $\left\langle\zeta^{\Sigma(m)}\right\rangle_k$ denotes the moment row-vector of the sum of m variables, defined as:

$$\left\langle\zeta^{\Sigma(m)}\right\rangle_k = \left[\zeta_{i-1}^{\Sigma(m)}\right]_{i=1,2,\ldots,k}, \tag{16}$$

$\left\langle\hat{\mu}^{(i)}\right\rangle_k$ is the moment row-vector of a single variable $|X_i|^2$, and the matrix $\langle W_n\rangle_{k,k}$ is defined as

$$\langle W_n\rangle_{k,k} = \left[\!\left[\,w_{i,j}(n)\,\right]\!\right]_{i,j=1,2,\ldots,k} \tag{17}$$

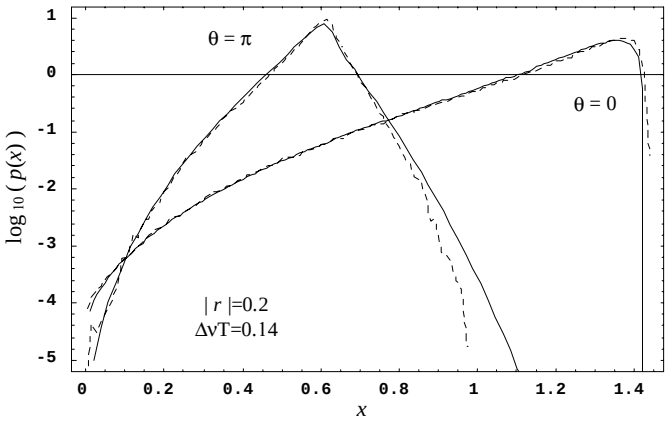

Fig. 2. Pdf of the envelope detector output with "best" and "worst" case interference, in logarithmic scale. Curves: full - Fokker-Planck approach, dashed - numerical simulation of the random variable *X*.

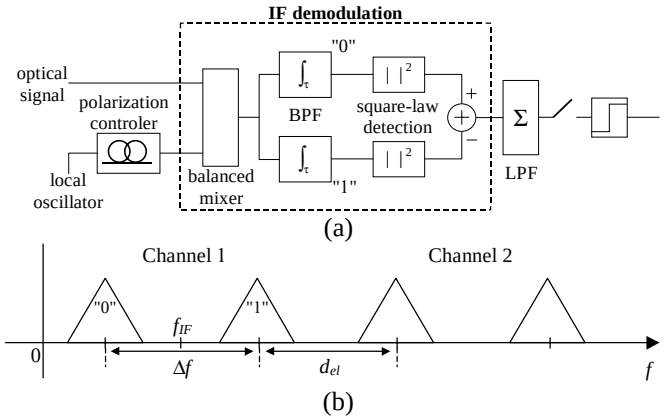

Fig. 3. (a) Block diagram of a FSK receiver model and (b) the schematic of channels after balanced detection

with elements

$$w_{i,j}(n) = \begin{cases} \binom{i-1}{i-j} \hat{\mu}_{i-j}^{(n)} & , \quad j \le i \\ 0 & , \quad j > i \end{cases} . \qquad (18)$$

By proceeding one step further from Eq. (15), it is easy to identify that the moment vector $\left\langle \zeta^{\Sigma(m)} \right\rangle$ equals the first row of the matrix $\prod_{i=1}^{m} \langle W_i \rangle$.

III. Application to FSK System

The moments may be used in a detailed performance analysis, as we will show on the FSK system example. We consider a receiver model shown in Fig. 3. It is a heterodyne polarization control receiver with dual-filter structure. Frequency deviation of the incoming FSK signal is considered large and the correlation effects between the two receiver branches are neglected. IF filtering is performed using equivalent integrate-and-dump filters with central frequencies tuned to the FSK signal frequencies, and with integration time τ. Postdetection filter is a summation device that averages *Md* consecutive detected samples during the bit interval. Shot noise is considered the dominant Gaussian noise factor; other Gaussian noise contributions can also be easily included in the analysis. Under these conditions, the error probability is computed as derived in [7] or [9].

We consider a two-channel heterodyne model with low intermediate frequency and ideal envelope detection. Interchannel interference is therefore the crosstalk from the other channel which is separated in the electrical domain by the spacing d_{el}. The crosstalk has different influence during the transmission of binary "0" and "1". When binary "0" is transmitted, the crosstalk can never be constructive since its squared modulus in the other branch impairs the decision variable; hence the interference phase is irrelevant. The amount of crosstalk changes with channel spacing and with time shift between the data, as explained in [8]. During the transmission of binary "1", the effect of crosstalk additionally depends on the relative signal phase in the interfering channel. Depending on the interference phase, the crosstalk can be either constructive or destructive (see Fig. 1).

For the given system model, worst-case error probability is:

$$P_e = \frac{1}{2} P(0/1) + \frac{1}{2} P(1/0) \qquad (19)$$

where $P(0/1)$ is the worst-case probability of detecting "0" when binary "1" is transmitted, and vice-versa for $P(1/0)$. The probabilities are computed based on the results of [7], which have been modified to reflect the differences in system models and to include the more accurate statistics of phase-noisy signal with crosstalk. Worst-cases are then found by numerical search over the crosstalk time and phase shifts.

The following steps outline the procedure of performance evaluation of the FSK receiver:

1) Compute the error probability for the single-channel system as in [7]. Optimize the integration time and the number of samples to obtain the best performance for the given total laser linewidth.
2) With *Md* optimized in the previous step, and for the given channel spacing, compute $P(1/0)$ for the worst-case time shift $\tau_2 = 1/(2d_{el})$ [8], during the last sample.
3) Compute $P(0/1)$ for arbitrary time shift, initial phase and transition sample, taking into account the interference phase shift over each sample [8]. For this purpose, use Eqs. (10) and (15) to compute the appropriate moments. Using the computer search over the variables, find the worst-case performance.
4) Using Eq. (19) and two previous steps, find the sensitivity penalty relative to the ideal single-channel case with no phase noise.

Step 3 requires the use of derived matrix equations to describe the sumation of signal samples with appropriate crosstalk phase shift during each of *Md* samples. Once the appropriate moments are calculated, a Gaussian quadrature rule can be constructed in order to compute the performance [7]. The procedure is also applicable to step 2, with simpler conditions of no interference in the signal branch, i.e. all W_i are equal.

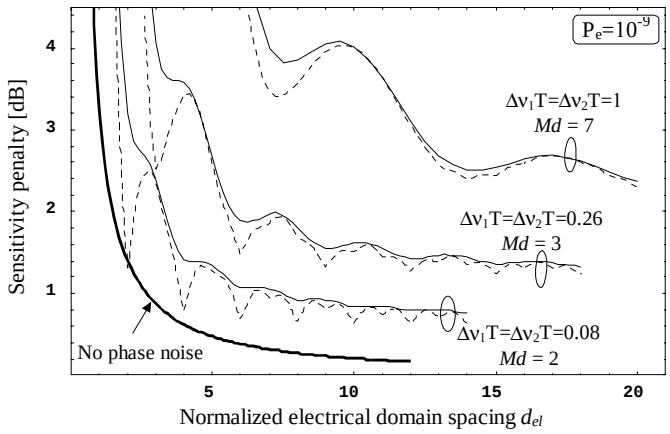

Fig. 4. Worst-case sensitivity penalty for FSK receiver. Curves: full - non-synchronized channels; dashed - synchronized channels.

IV. Numerical Results and Discussion

In Fig. 1, we compare the pdf's at the square-law envelope detector output, with, as well as without interference. The curves are reconstructed using maximum entropy method and first 12 moments. We have also obtained the densities using the Fokker-Planck equation [1, 2] to find the joint density of real and imaginary parts of *z*, and then numerically computed the densities of $|X|^2$ for the same *r* values. In Fig. 2, we show the pdf resulting form Fokker-Planck approach compared to the results of numerical simulation of variable *X*. The agreement is apparent and general behavior of the pdf curves is close to Fig. 1.

Fig. 4. shows sensitivity penalty of the FSK receiver due to phase noise and interchannel crosstalk. Penalties are calculated relatively to the sensitivity of the single channel receiver without phase noise, which is 40 photons per bit. In the limit of no phase noise, the two-channel system requires channel separation d_{el} of 2.7 times the bit rate in order to operate within 1 dB penalty. Phase noise generated by the lasers with total linewidth of 8% of the bit rate causes further sensitivity degradation. Wider bandwidths are required to contain the signals and the best single-channel sensitivity is obtained for *Md*=2, resulting in about 0.6 dB penalty without any crosstalk. Additional penalty due to crosstalk from the second channel is under 1 dB when the channel separation is above 3.6 times the bit rate. However, if the two channels are operated with exactly the same bit rate, and are synchronized, it should allow closer channel separation of about 2 times the bit rate. The situation is also beneficial for a system without phase noise, where channel spacing equal to the bit rate would suffice (not shown in Fig. 4).

When total linewidth equals 26% of the bit rate, optimum *Md* value is 3 and required channel spacing is about 5.5 times the bit rate. In this case, the synchronization of the channels can not reduce the required channel separation, although somewhat smaller penalties are expected. For linewidth equal to the bit rate, optimum *Md* is 7 and required channel separation rises to about 12, while the effects of synchronization are less noticeable. Therefore, synchronization may enable closer channel separation only when laser linewidths are relatively small. When the linewidths are close or even larger than the bit rate, the difference between synchronized and non-synchronized systems becomes negligible.

System performance are computed asymptotically accurate as long as local laser and neighboring channel transmitting laser have negligible linewidths with respect to the transmitting laser. Moreover, if the neighboring channel transmitter linewidth is not negligible, yet small, the leading order asymptotic description of interference is expected to be valid. However, in a real system, all lasers are expected to have same linewidths, and the results of this paper should be considered approximate. Nevertheless, this is a reasonable degree of accuracy, somewhat better than in other aproaches.

V. Conclusion

In this paper, we have presented a procedure that enables the use of moments approach in detailed analysis of coherent optical systems impaired by phase noise and interchannel interference. Furthermore, we have set up a model of a heterodyne FSK receiver and applied the procedure to performance evaluation of the two-channel system. We have found that the required channel spacing for 1 dB crosstalk penalty is about 2.7 times the bit rate in the worst-case situation without any influence of phase noise. When total laser linewidth equals the bit rate, the required channel spacing rises to at least 12 times the bit rate. Somewhat closer channel spacing may be achieved by synchronizing the two channels, but the operation is expected to yield significant results only if the laser linewidths are relatively small.

References

[1] G. J. Foschini and G. Vannucci, “Characterizing Filtered Light Waves Corrupted by Phase Noise”, *IEEE Trans. Inf. Theory.*, vol. 34, pp. 1437-1448, Nov. 1988.

[2] I. Garret, D. J. Bond, J. B. Waite, D. S. L. Lettis and G. Jacobsen, "Impact of Phase Noise in Weakly Coherent Optical Systems: A New and Accurate Approach", *IEEE J. Lightwave Technol.*, vol. 8, pp 329-337, Mar. 1990.

[3] G. L. Pierobon, L. Tomba, "Moment characterization of Phase Noise in Coherent Optical Systems", *IEEE J. Lightwave Technol.*, vol. 9, pp 996-1005, Aug. 1991.

[4] I. T. Monroy and G. Hooghiemstra “On a Recursive Formula for the Moments of Phase Noise”, *IEEE Trans. Communications.*, vol. 48, no. 6, pp. 917-920, June 2000.

[5] M. Stefanovic, D. Milic, "An Approximation of Filtered Signal Envelope with Phase Noise in Coherent Optical Systems", *IEEE J.Lightwave Technol.*, vol. 19, pp. 1685-1690, Nov. 2001.

[6] R. Corvaja, L. Tomba, "Crosstalk Interference in FSK Coherent Optical Systems", *IEEE J. Lightwave Technol.*, vol. 12, pp 670-677, Apr. 1994.

[7] M.-J. Hao and S. B. Wicker, “The effect of error control coding in multichannel FSK coherent lightwave communication system influenced by laser phase noise”, *IEEE J. Lightwave Technol.*, vol. 14, pp. 2648-2656, Dec. 1996.

[8] G. Jacobsen and I. Garret, “The Effect of Crosstalk and Phase Noise in Multichannel Coherent Optical ASK Systems”, *IEEE J. Lightwave Technol.*, vol. 9, no. 8, pp. 1006-1018, Aug. 1991.

[9] M. Stefanovic, D. Milic, N. Stojanovic, "Evaluation of Optimal Bandwidth in Optical FSK System Influenced by Laser Phase Noise", *IEEE J. Lightwave Technol.*, vol. 16, pp 772-777, May 1998

Performance Analysis of UMTS WCDMA Rake Receiver

Nenad Milošević[1], Bojan Dimitrijević[2], Zorica Nikolić[3], Đorđe Paunović[4]

Abstract – **In this paper we present a theoretical analysis of a number of channel estimation schemes for UMTS WCDMA Rake receiver. In general these schemes are data aided/decision directed and consist of two blocks, channel sample preselection and channel predictor. The first block is introduced to minimize the impact of incorrect data decisions on the channel estimator. This is what makes our schemes different from the solutions known so far. The result of channel predictor (the second block) is used to generate the data estimate for the next sampling interval which is an element used for these purposes by a number of authors.**

Keywords – **UMTS, WCDMA, Rake receiver, channel estimationn**

I. INTRODUCTION

A Rake receiver synchronization in a CDMA system includes, code delay estimation for each path and complex channel coefficient estimation (amplitude and phase) to be used in rake combiner. Code delay estimation is a well elaborated field and a number of references can be found in the open literature covering this issue [2-4]. In this work we will assume that the code delays are already estimated and we focus only on estimating the channel coefficients.

In [5] a ML based algorithm for multiuser (MU) channel estimation is discussed. The second order statistics was used so that the information about the phase could not be extracted. Due to complexity of the likelihood function only single path propagation model has been considered. Further modification of the cost function should be introduced in order to make possible the multipath channel coefficient estimation. Some options, described in [5], remain still to complex to be considered for practical applications.

An algorithm for joint detection and estimation of amplitudes, but with known delays, was developed in [6]. In that paper a tree-search method was used together with least-squares estimation.

A neural-network based algorithm [7] implicitly estimates delays and amplitudes using backpropagation algorithm. This kind of algorithm is rather slow, and can not be used for tracking fast fading parameters.

A recursive signal processing using the Viterbi algorithm for joint tracking of amplitudes and delays was described in [8]. An extended Kalman estimator is used to update the amplitude and delay estimates for each survivor sequence in Viterby Algorithm. The Nyquist samples are used as sufficient statistics. The resulting algorithm requires storage of the survivor sequences and is difficult to simplify.

In the case of advanced CDMA receivers, a rough channel estimates could be found by subtracting the estimated overall MAI from the matched filter outputs, removing the modulation by pilot or estimated symbols and then additionally filtering the result of such preprocessing.

In systems with high processing gain, power control and low crosscorrelations between the users the output of the matched filter of the *k*th user synchronized to the *l*th path, can be considered separately as a digital phase modulated signal in flat fading and Gaussian noise.

For such channels, it was shown even in classical literature, the optimum receiver results in a structure that follows Kailath's separation theorem. In order words, the optimum receiver consist of an estimator that delivers MMSE estimates of the fading distortion and a detector that utilizes these estimates. In [10] a pilot tone signaling to provide channel amplitude and phase information for the detection and the adaptive control of the transmitter, is used.

If the pilot symbols are not available a possible approach is to perform detection using an old channel estimate and then use the detected data to update the channel estimate in a decision-feedback manner.

The main problem of using decision-aided channel estimators comes form the two stochastic processes "data" and "channel" being involved simultaneously.

An alternative is a data aided approach, were a sequence of channel estimates ("snapshots") is obtained via training segments multiplexed into the data stream.

The above solutions are based on using training sequence with or without additional exploitation of the feedback decisions. The existing UMTS standards support such solutions by providing pilot symbols and this approach is the basis for the algorithms used in this paper.

II. SYSTEM MODEL

In W-CDMA (UMTS FDD Mode), the data transmission is organized in frames of 10ms, each divided in slots of 0.625 ms. The slot structure in the uplink is well known and may be seen in [1]. It consists of both data bits (dedicated physical data channel-DPDCH) and control information (dedicated physical control channel-DPCCH): The number of data bits per slot N_d depends on the data rate of the link and varies from 10 to 640. The number of control bits is fixed to 10. It consists of pilot symbols for channel estimation, transmit power control (TPC) bits and transport frame indicator (TFI) bits. The data bits $d(i)$ of the DPDCH are spread with an orthogonal variable spreading factor (OVSF) sequence $s_d(k)$

[1]Autor is with the Faculty of Electronic Engineering, Beogradska 14, 18000 Nis, Serbia and Montenegro, nemilose@elfak.ni.ac.yu

[2]Autor is with the Faculty of Electronic Engineering, Beogradska 14, 18000 Nis, Serbia and Montenegro,

[3]Autor is with the Faculty of Electronic Engineering, Beogradska 14, 18000 Nis, Serbia and Montenegro,

[4]Autor is with the Faculty of Electrotechnics, 11000 Belgrade, Serbia and Montenegro,

(channelization sequence for data) with chip rate of 4.096 Mcps. For the fixed chip rate, the spreading factor N is determined by the number of bits per slot and varies from 4 to 256. The control bits $d_c(i)$ of the DPCCH are spread by factor N_c= 256 by using the code $s_c(k)$ (channelization code for control channel, orthogonal to $s_d(k)$).

The chip streams of data and control channel are I/Q multiplexed and scrambled with the complex scrambling sequence $s_{scr}(k)$. Thus the transmit signal can be represented as

$$t(k) = s_{scr}(k)\{s_d(k)d(\lfloor k/N \rfloor) + js_c(k)d_c(\lfloor k/N \rfloor)\} \quad (1)$$

The channel impulse response is defined as

$$h(t,\tau) = \sum_l C^{(l)}(t)\delta(t-\tau_l) \quad (2)$$

In the analysis we use the channel model specified by Rec.ITU-R M.1225. For the channel coefficient correlation function we use the Jack's model where $\rho_c(\tau) = J_0(\omega_D\tau)$.

The general block diagram of Rake receiver may be seen in [1]. A direct sequence spread spectrum signal (DSSS) after propagation through a multipath channel, will be despread in L Rake fingers, and the output of the lth despreading circuit will have the form

$$y_k^{(l)} = C_k^{(l)} \cdot d_k + n_k^{(l)} \quad (3)$$

This operation is performed separately in both, data and control channel. We assume a perfect code synchronization per finger. In (3) k is the sampling index, l = 1, … L is the path index, $C_k^{(l)}$ is the complex channel coefficient, d_k=$d(k)$ for data channel and d_k=$d_c(k)$ for control channel. Parameter $n_k^{(l)}$ is the overall noise in the l-th Rake finger including residual multipath interference (MPI), multiple access interference (MAI), inter-channel interference (ICI) and thermal noise. All together, this component will be approximated as Gaussian noise with zero mean and variance $\sigma^{(l)2}$.

As it was explained above, in the DPCCH channel the pilot symbols are used to facilitate the channel estimate. A sequence of N_p bits is periodically inserted into the control channel stream and used as preamble for channel estimation. In the remaining interval the tentative decisions can be used to remove the modulation from the signal components $y_k^{(l)}$.

III. Performance Analysis

Detailed explanation of channel estimation algorithm, as well as some simulation results, may be found in [1]. In this paper, a theoretical analysis of sustem performance is given.

In general signal $\overline{C}_k^{(l)}$, that will be used for further processing (predictor) can be represented as

$$\overline{C}_k^{(l)} = C_k^{(l)} + \varepsilon_k^{(l)} + n'_k \quad (4)$$

where $\varepsilon_k^{(l)}$ is error due to preprocessing and $n'_k = S(n_k^{(l)})$ is the noise sample after preselection processing. The error and noise will be considered as an equivalent noise of zero mean and variance $\sigma_n^2 = \sigma_\varepsilon^2 + \sigma^2 + 2\rho_{n\varepsilon}\sigma_\varepsilon\sigma$. Parameter $\rho_{n\varepsilon}$ characterizes correlation between the input noise (variance σ^2) and preprocessing error ε (variance σ_ε^2). In this analysis we do not intend to find an exact relation for $\rho_{n\varepsilon}$ but rather use upper and lower bounds on the performance for $\rho_{n\varepsilon}$ = 0 and $\rho_{n\varepsilon}$ = 1 respectively. In the sequel we discuss this parameter for different preselection functions.

 # No preselection

$$\begin{aligned} &\overline{C}_k^{(l)} \Rightarrow C_k^{(l)}(1-2P_e) \\ &\sigma_\varepsilon^2 = 2P_e\sigma_c^2 \end{aligned} \quad (5)$$

#1 Hard decision

Let us use notation $1-P_d = P(v_k^{(l)} < th) = P_c$ for preselection correct decision. Then we have

$$\begin{aligned} &\overline{C}_k^{(l)} \Rightarrow \\ &C_k^{(l)}(1-P_e)P_c + 0(1-P_e)P_d - 0P_eP_c - C_k^{(l)}P_eP_d = C_k^{(l)} + \varepsilon \\ &\varepsilon \Rightarrow -C_k^{(l)}(P_e+P_d) \\ &\sigma_\varepsilon^2 = (P_e+P_d)\sigma_c^2 \end{aligned} \quad (6)$$

#2 Interpolation

$$\begin{aligned} &\overline{C}_k^{(l)} \Rightarrow \\ &C_k^{(l)}(1-P_e)P_c + C_{k-1}^{(l)}(1-P_e)P_d + C_{k-1}^{(l)}P_eP_c - P_eP_dC_k^{(l)} = C_k^{(l)} + \varepsilon \end{aligned} \quad (7)$$

By introducing $C_k^{(l)} = C_{k-1}^{(l)} - \Delta C_k^{(l)}$ we have

$$\begin{aligned} \varepsilon \Rightarrow &-(P_e+P_d-P_eP_d)C_k^{(l)} + (1-P_e)P_d(C_k^{(l)} + \Delta C_k^{(l)}) \\ &+ P_eP_c(C_k^{(l)} + \Delta C_k^{(l)}) - P_eP_dC_k^{(l)} \\ &= -2P_eP_dC_k^{(l)} + (P_e+P_d-2P_eP_d)\Delta C_k^{(l)} \\ \sigma_\varepsilon^2 = &\,2P_eP_d\sigma_c^2 + (P_e+P_d-2P_eP_d)\sigma_{\Delta c}^2 \end{aligned} \quad (8)$$

#3 Substitution

$$\begin{aligned} &\overline{C}_k^{(l)} \Rightarrow \\ &(1-P_e)P_cC_k^{(l)} + (1-P_e)P_d\hat{C}_k^{(l)} + P_eP_c\hat{C}_k^{(l)} - P_eP_dC_k^{(l)} = C_k^{(l)} + \varepsilon \end{aligned} \quad (9)$$

By introducing $\hat{C}_k^{(l)} = C_k^{(l)} + \bar{\varepsilon}$ we have

$$\begin{aligned} \sigma_\varepsilon^2 &= 2P_eP_d\sigma_c^2 + (P_e+P_d-2P_eP_d)\sigma_\varepsilon^2 \\ &= \frac{2P_eP_d}{P_e+P_d-2P_eP_d}\sigma_c^2 \end{aligned} \quad (10)$$

#4 Alternation

$$\begin{aligned} &\overline{C}_k^{(l)} \Rightarrow \\ &(1-P_e)P_cC_k^{(l)} - (1-P_e)P_dC_k^{(l)} + P_eP_cC_k^{(l)} - P_eP_dC_k^{(l)} = C_k^{(l)} + \varepsilon \\ &\varepsilon \Rightarrow -2P_d \\ &\sigma_\varepsilon^2 = 2P_d\sigma_c^2 \end{aligned} \quad (11)$$

The input signal in a Rake finger is

$$y = Cd + n \quad (12)$$

After multiplication by the estimated value of the channel coefficient we have

$$\begin{aligned} f &= (Cd+n)(C^*+\Delta C^*) \\ &= CC^*d + (C\Delta C^*d + nC^* + n\Delta C^*) \end{aligned} \quad (13)$$

The first term is the useful signal. The remaining terms are an equivalent noise.

So, the signal to noise ratio in a finger is

$$SNR_f = \frac{\sigma^2_{signal}}{\sigma^2_e} \tag{14}$$

where

$$\begin{aligned}
\sigma^2_{signal} &= E^2\{(C)(C^*)\} = \sigma_c^4 \\
\sigma^2_e &= E\{(C\Delta C^* d + nC^* + n\Delta C^*)(C\Delta C^* d + nC^* + n\Delta C^*)^*\} \\
&= E\{C\Delta C^* C^* \Delta C\} + E\{C\Delta C^* n^* C\} + E\{C\Delta C^* n^* \Delta C\} \\
&+ E\{nC^* C^* \Delta C\} + E\{nC^* n^* C\} \\
&+ E\{nC^* n^* \Delta C\} + E\{n\Delta C^* C^* \Delta C\} \\
&+ E\{n\Delta C^* n^* C\} + E\{n\Delta C^* n^* \Delta C\}
\end{aligned} \tag{15}$$

To evaluate the second term we use the relation

$$\begin{aligned}
E\{x_1x_2x_3x_4\} = {} & E\{x_1x_2\}E\{x_3x_4\} + E\{x_1x_3\}E\{x_2x_4\} + \\
& + E\{x_1x_4\}E\{x_2x_3\}
\end{aligned} \tag{16}$$

Losses are defined as

$$LS = \frac{SNR_f(\Delta C = 0)}{SNR_f} \tag{17}$$

Bearing in mind that $\rho_{cn} = 0$ for a real signal we have

$$\begin{aligned}
\sigma^2_e = {} & 2(\rho_{c\Delta c}\sigma_c\sigma_{\Delta c})^2 + \sigma_c^2\sigma^2_{\Delta c} + \sigma_c^2\rho_{n\Delta c}\sigma\sigma_{\Delta c} + \\
& + 2\rho_{c\Delta c}\sigma_c\sigma_{\Delta c}\rho_{n\Delta c}\sigma\sigma_{\Delta c} + \rho_{n\Delta c}\sigma\sigma_{\Delta c}\sigma_c^2 + \sigma^2\sigma_c^2 + \\
& + \sigma^2\rho_{c\Delta c}\sigma_c\sigma_{\Delta c} + 2\rho_{n\Delta c}\sigma\sigma_{\Delta c}\rho_{c\Delta c}\sigma_c\sigma_{\Delta c} + \\
& + \sigma^2\rho_{c\Delta c}\sigma_c\sigma_{\Delta c} + 2(\rho_{n\Delta c}\sigma\sigma_{\Delta c})^2 + \sigma^2\sigma^2_{\Delta c}
\end{aligned} \tag{18}$$

Like in the previous case we have no intention to go into a detailed analysis of correlation functions in the previous equation. Instead we will deal again with upper and lower bounds of σ_e^2 obtained for ρ_{ab} equal one and zero, respectively.

Simillary, in the case of a complex signal we get

$$\begin{aligned}
\sigma^2_e = {} & 4\rho_{c\Delta c}\rho_{nc}\sigma\sigma_c^2\sigma_{\Delta c} + 2\rho_{c_1c_2}\rho_{\Delta cn}\sigma_{\Delta c}\sigma\sigma_c^2 + \\
& + 2\rho_{c\Delta c}\sigma^2\sigma_{\Delta c}\sigma_c + 4\rho_{\Delta cn}\rho_{cn}\sigma_{\Delta c}\sigma^2\sigma_c + \\
& + \sigma_c^2\sigma^2_{\Delta c} + 2\rho^2{}_{c\Delta c}\sigma_c^2\sigma^2_{\Delta c} + \sigma^2\sigma_c^2 + 2\rho_{nc}{}^2\sigma^2\sigma_c^2 + \\
& + \sigma^2\sigma^2_{\Delta c} + 2\rho^2_{n\Delta c}\sigma^2\sigma^2_{\Delta c} + 2\rho_{nc}\sigma\sigma^2_{\Delta c}\sigma_c + \\
& + 4\rho_{\Delta cn}\rho_{c\Delta c}\sigma^2_{\Delta c}\sigma\sigma_c
\end{aligned} \tag{19}$$

For the channel model we accept

$$C_k = \rho C_{k-1} + n_{ck} \tag{20}$$

where n_{ck} is modeling error (zero mean Gaussian variable with variance $\sigma_c^2(1-\rho^2)$.

The channel is estimated using a smoother, adaptive linear predictor with LMS algorithm and with Kalman filter.

The channel smoother is producing

$$\hat{C}_k = \frac{1}{K}\sum_{i=1}^{K}(C_{k-i} + n_{k-i}) \tag{21}$$

The Rake finger output signal is

$$\begin{aligned}
& y_k\hat{C}_k^* = (C_k + n_k)\left\{\frac{1}{K}\sum_{i=1}^{K}(C^*_{k-i} + n^*_{k-i})\right\} = \\
& \frac{C_k}{K}\sum_i C^*_{k-i} + \left\{\frac{C_k}{K}\sum_i n^*_{k-i} + \frac{n_k}{K}\sum_i C^*_{k-i} + \frac{n_k}{K}\sum_i n^*_{k-i}\right\}
\end{aligned} \tag{22}$$

The useful signal power can be represented as

$$\sigma^2_{signal} = E^2\left\{\frac{1}{K}C_k\left(\sum_i C^*_{k-i}\right)\right\} = \frac{\sigma_c^4}{K^2}\left(\sum_{i=1}^{K}\rho_c(i)\right)^2 \tag{23}$$

One can show that the equivalent noise power for a real signal is given as

$$\sigma_e^2 = \frac{\sigma^2(\sigma^2 + \sigma_c^2)}{K} + \frac{\sigma^2\sigma_c^2}{K^2}\sum_{i=1}^{K}\sum_{l=1}^{K}\rho_c(i-l) \tag{24}$$

and the signal to noise ratio per finger is given again by (28)

In the case of a complex signal we have

$$\sigma_e^2 = \frac{\sigma^2\sigma_c^2}{K} + \frac{\sigma_c^2\sigma^2}{K^2}\sum_i\sum_l(\rho_c(i-l)) + \frac{1}{K}\sigma^4 \tag{25}$$

For a transversal filter with coefficients

$$\mathbf{W}_k = (w_k, w_{k-1}, w_{k-2}, ..., w_{k-L}) \tag{26}$$

and channel sample vector

$$\mathbf{C}_k = (C_k, C_{k-1}, C_{k-2}, ..., C_{k-L}) \tag{27}$$

the steady state tracking error variance (minimum mean square error) is given as

$$\sigma_\varepsilon^2 = E\{|C_k|^2\} - \mathbf{P}^T\mathbf{W}_o = \sigma_c^2 - \mathbf{P}^T\mathbf{W}_o \tag{28}$$

where $\mathbf{W}_o$ is the optimum solution for the prediction coefficients obtained from

$$-2\mathbf{P} + 2\mathbf{R}\mathbf{W}_o = 0 \tag{29}$$

and the vector $\mathbf{P}$ and the matrix $\mathbf{R}$ are defined as

$$\begin{aligned}
& \mathbf{P}^T = E[C_k\mathbf{C}_k] \\
& \mathbf{R} = E[\mathbf{C}_k\mathbf{C}_k^T] = [\rho(k-m)], \quad k,m = 1,..L
\end{aligned} \tag{30}$$

Parameter SNR_f is given by eq(28) with σ_ε^2 given by eq(28).

For Kalman filter the estimation error is solution to Ricatti equation [18] which for this case can be expressed as

$$\sigma_\varepsilon^2 = \frac{\sigma^2\left[\rho^2\sigma_\varepsilon^2 + (1-\rho^2)\sigma_c^2\right]}{\rho^2\sigma_\varepsilon^2 + (1-\rho^2)\sigma_c^2 + \sigma^2} \tag{31}$$

and the SNR_f is given again by eq(14).

For the BER we use the standard results for the diversity of order L [9].

Expressions for SNR_f per finger should be further modified by modifying the equivalent noise to include interference between different paths and different users. It can be shown that, in case of QPSK modulation, BER may be expressed as

$$BER = \frac{1}{2}\sum_{k=1}^{L}\pi_k\left[1-\sqrt{\frac{\bar{\gamma}_k}{2+\bar{\gamma}_k}}\right] \tag{32}$$

where

$$\pi_k = \prod_{\substack{i=1 \\ i\neq k}}^{L}\frac{\bar{\gamma}_k}{\bar{\gamma}_k-\bar{\gamma}_i} \tag{33}$$

and $\bar{\gamma}_k$ is the average *SNR* for the *k*-th path.

IV. Numerical Results

Fig. 1. shows bit error probability as a function of receiver velocity. Signal to noise ratio per bit is chosen to be SNR = 5 dB, and sample preselection/modification function is *substitution* with th=0.

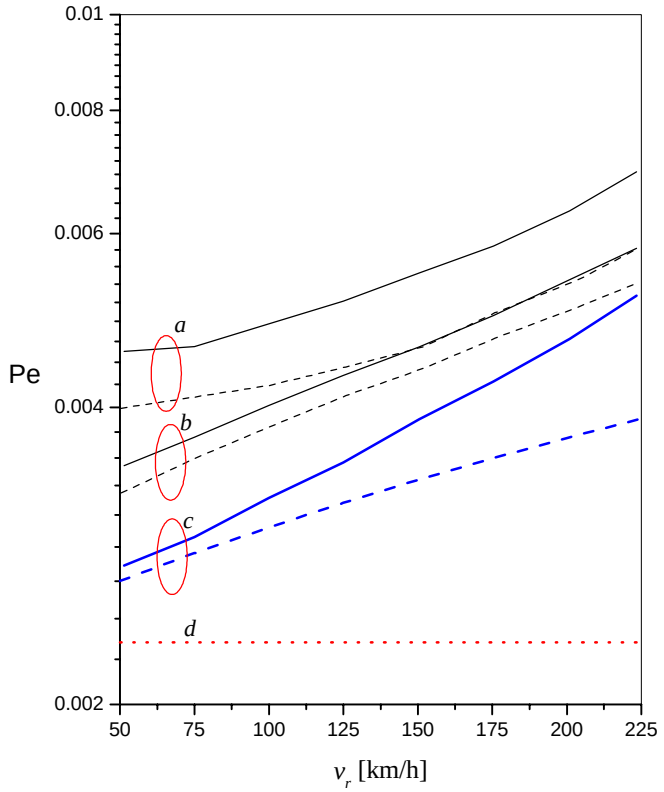

Fig. 1. Bit error probability as a function of receiver velocity
– – – – – theoretical results
——— simulation results

There are results for different channel estimators (*a* – Smoother, *b* – adaptive linear predictor with LMS algorithm, *c* – Kalman filter), as well as for the case if there is a perfect channel estimation (*d*). It can be seen that the theoretical results are very simillar to the simulation ones, especially for low receiver velocity. As expected Kalman filter has the best performances, and the smoother has the worst ones.

V. Conclusions

In this paper we presented a approximate theoretical analysis of a number of channel estimation schemes for UMTS WCDMA Rake receiver. The results show that theoretical performances are in high agreement with the simulation ones. The agreement is higher for low receiver velocities. Since Kalman filter has more information about the channel than the other estimators, its performances are the best. Smoother has the poorest performances, but it is a acceptable solution if we need a simple estimator.

References

[1] B. Dimitrijević, N. Milošević, Z. Nikolić, "Procena feding kanala kod UMTS WCDMA Rake prijemnika", *Proceedings of TELFOR 2003*, Beograd, Novembar 2003.

[2] Polydoros, A., and C. L. Weber, "A Unified Approach to Serial Search Spread-Spectrum Code Acquisition—Part 1: General Theory," *IEEE Transactions on Communications*, Vol. 32, No. 5, May 1984, pp. 542-549.

[3] Polydoros, A., and C. L. Weber, "A Unified Approach to Serial Search Spread-Spectrum Code Acquisition—Part II: A Matched-Filter Receiver," *IEEE Transactions on Communications*, Vol. 32, No. 5, May 1984, pp. SSO-560.

[4] A. Polydoros and S. Glisic - Code Synchronization: A Review of Principles and Techniques - In S.Glisic and P.Leppanen ed. *Code Division Multiple Access*, Kluwer Academic Publishers, 1995

[5] J. S. Bensley and B. Aazhang, " Subspace-Based Channel Estimation for Code Division Multiple Access Communications & Systems", *IEEE Transactions on Communications*, vol. 44, No. 8, pp. 1009-1020, August 1996.

[6] Z. Xie, C. Rushforth, R. Short and T. Moon, "Joint signal detection and parameter estimation in multiuser communications," *IEEE Transactions on Communications*, vol. 41, pp. 1208-1216, Aug. 1993.

[7] B. Aazhang, B. Paris and G. Orsak, "Neural networks for multiuser detection in code-division multiple-access communications," *IEEE Transactions on Communications*, vol. 40, pp. 1212-1222, July 1992.

[8] R. lltis, "A digital receiver for demodulation of CDMA waveforms with a-priori unknown delays and amplitudes," in *Proceedings of the IEEE Military Communications Conference*, (McLean, VA), pp. 113-116, Nov. 1991.

[9] Proakis, *Digital Communiactions*, Mc GrawHill, 1998

[10] T. Kailath, "A general likelihood formula for random signals in Gaussian noise," *IEEE Trans. Inform. Theory*, vol. IT-15, May 1969.

Analysis of MPLS Network

Seferin T. Mirtchev[1] and Natalia V. Vesselinova[2]

***Abstract* – Analysis of wireless cellular MPLS network is performed in this paper. The convolution algorithm is used to obtain the dependence of carried traffic from the size of the overlapping area of cells. The increase of the amount of carried traffic reaches saturation point after certain level of overlapping.**

***Keywords* – carried traffic, overlapping area, MPLS.**

I. INTRODUCTION

There are many efforts underway to incorporate IP based technologies into wireless cellular systems because of the increasing user demand for Internet, providing IP-based multimedia services over wireless. Such networks are expected to provide efficient packet transfer and support of quality-of-service (QoS). In the core of networks, Multi-Protocol Label Switching (MPLS) is used as a technology of choice to facilitate teletraffic engineering (TE) and QoS support. In this paper, an architecture with label switching is considered and the effect of overlapping cells is studied, since the efficient utilization of resources in wireless networks is of importance as well.

The paper is organized as follows. In next section we define the system model used in the analysis. Numerical results are presented in Section 3. Finally, Section 4 concludes the paper.

II. SYSTEM MODEL

In [1] a hierarchical architecture for label-switched networks supporting wireless users is described. We use the proposed system architecture to develop our analysis.

The considered network consists of base stations (BS), connected to label switching nodes (LSN), along with the components of the standard MPLS network (LSRs, LERs). LSN provides service to BSs and supports fast handoff and location management mechanisms [1]. A routing area (where the location information of the mobiles is stored) is defined to effectively limit the registration traffic and routing updates when the subscribers cross cell boundaries. Another means to further reduce the updates is to group some LSRs and LSNs.

There is one router in each group, which communicates topology information with other representative group routers and thus forming another level of hierarchical label-switched network architecture.

[1] Seferin T. Mirtchev is with the Faculty of Communications and Communication Technology, Technical University of Sofia, blvd. "Kl. Ohridski" 8, 1000 Sofia, Bulgaria, E-mail: stm@tu-sofia.bg.

[2] Natalia V. Vesselinova is with the Faculty of Communications and Communication Technology, Technical University of Sofia, blvd. "Kl. Ohridski" 8, 1000 Sofia, Bulgaria, E-mail: nvesselinova@tu-sofia.bg.

III. NUMERICAL RESULTS

We consider two cells in a cellular label switched network. The two cells overlap each other, Fig. 1. Subscribers in area 1 (the region covered by BS1) have access to all its channels n_1, subscribers in area 2 (the region covered by BS2) have access to all n_2 channels, and subscribers in the overlapping area 12 have access to n_1+n_2 channels. The subscribers in area 12 are expected to experience smaller blocking probability due to the larger number of channels.

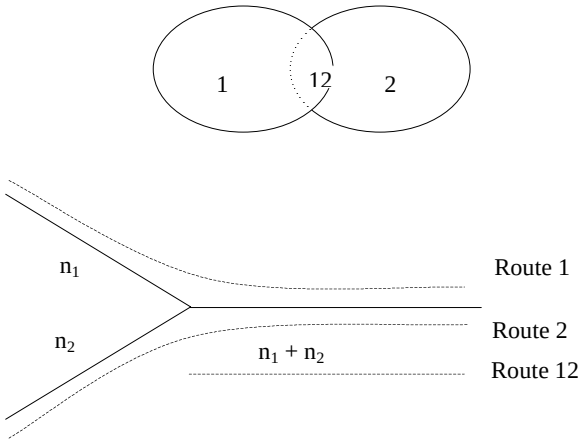

Fig. 1. Two overlapping cells and equivalent routes in a circuit-switched network with direct routing

If we denote the number of existing connections in area i with m_i, then the restrictions are as follows:

$$0 \le m_1 \le n_1 \quad (1)$$

$$0 \le m_2 \le n_2 \quad (2)$$

$$0 \le m_1 + m_2 + m_{12} \le n_1 + n_2 \quad (3)$$

This is equivalent to the circuit-switched network with direct routing [2] shown in Fig. 1. The convolution algorithm proposed by V. Iversen can be applied to networks with direct routing [3].

The convolution becomes multi-dimensional, the dimension being the number of links in the network.

In Fig. 2, a system with three cells, which are mutually overlapping, is illustrated. Subscribers in the overlapping areas (also known as diversity areas) have access to two base stations, but not three. When the subscriber is in the area 23 e.g. and all the channels in area 2 are busy, then we can handover the connection to BS3 if it has enough capacity. Therefore, subscribers in the diversity areas will experience a smaller blocking probability then those in the separate areas. The described model (with restrictions on the number of

simultaneous calls similar to Eqs. (1), (2) and (3)) is equivalent to a circuit-switched communication network with direct routing [3]. In the table shown on Fig. 2, the restrictions are denoted as links and the number of separate areas as routes. For the example regarded, the number of routes becomes 6 (there is no overlapping 123 between three cells). The algorithm allows calculation of time congestion, call congestion, and traffic congestion for BPP traffic.

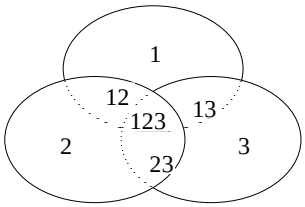

Route

Link	1	2	3	12	13	23	123
1	1	0	0	0	0	0	0
2	0	1	0	0	0	0	0
3	0	0	1	0	0	0	0
12	1	1	0	1	0	0	0
13	1	0	1	0	1	0	0
23	0	1	1	0	0	1	0
123	1	1	1	1	1	1	1

Fig. 2. Three overlapping cells and equivalent circuit-switched network with direct routing

For the purpose of the analysis we considered the case of a system with three cells. Each base station can service a number of 15 subscribers at most, each subscriber occupying only one channel simultaneously. We have assumed that the arrival process is Poisson and that the offered traffic per cell is 15 erl. The subscribers are evenly distributed in the region covered by the three base stations. The PC-tool ATMOS [4], in which the convolution algorithm was implemented was used for the calculations. The results obtained are shown in Fig. 3.

Carried traffic per cell (A_c) increases with the percentage of overlapping area to some extent. The amount of A_c can not be increased after a certain point of overlapping in the systems discussed. This point in our case (for the conditions we set preliminary) is at about 20 – 30 %, when saturation is observed.

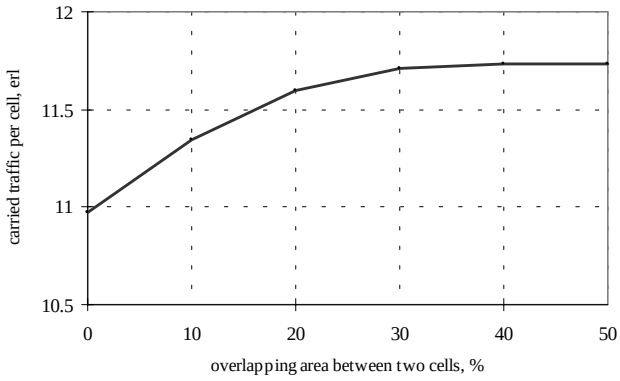

Fig. 3 System with three mutually overlapping cells

In [5] an analytical model of system behaviour, based on the architecture mentioned, is created. It is shown that the overload probability depends on the size of the diversity area in a similar way as the function in Fig. 3.

IV. CONCLUSIONS AND FUTURE WORK

In this paper we applied the convolution algorithm to calculate the carried traffic per cell when cells overlap and the effect of overlapping (to what extent the performance of the system is improved when the size of the diversity area is increased). The algorithm we used is appropriate for small systems. Real systems are usually larger, with base stations maintaining greater number of simultaneous calls. Future work should include simulation study of the behaviour of a larger label-switched network supporting multilink technique.

REFERENCES

[1] B. Jabbari, R. Papneja, E. Dinan, “Label Switched Packet Transfer for Wireless Cellular Networks”, IEEE WCNC’2000, no. 1, September 2000, pp. 958 – 962.

[2] V. Iversen, “Traffic Engineering of Cellular Wireless Communication Systems”, Modeling and Simulation Environment for Satellite and Terrestrial Communication Networks, Proceedings of the European COST Telecommunications Symposium, September 2000.

[3] V. Iversen, “Traffic Engineering: Chapter 10 – Multi-Dimensional Loss System”, ITU – D, December 2003.

[4] H. Listov-Saabye and V. Iversen, “ATMOS: a PC-based tool for evaluating multi-service telephone systems”, IMSOR, Technical University of Denmark, 1989, pp. 75.

[5] S. Mirtchev, N. Vesselinova, “Architecture and Performance for Wireless Cellular Networks with Label Packet Switching”, TELECOM’2003, Varna, Bulgaria, October 2003.

A Research Of Maintenance-Effect Failures With Markov's Modelling

Georgi D. Nenov[1] and Borislav D. Boiadjiev[2]

***Abstract* – To ensure the properly work without failures of the communication and railway signalling systems is recommended to maintain them. But the preventive maintenance has not only advantages because after it there are some failures caused of work within systems. These failures are called "Maintenance-effect failures".**

To analyze these failures there must be an appropriate model. The maintenance will be optimized with assistance of this model. The research of maintenance-effect failures with Markov's modelling is used in the paper.

***Keywords* – Maintenance-effect failures, Markov's models, pre-failures, sudden and parametric failures.**

The communication and railway signalling systems ensure railway traffic against accidents and they must work properly without failures. This is the reason to maintain these systems.

The preventive maintenance of the technical systems is introduced to avoid the parametric (gradual) and to repair the sudden failures, with ensuring of maximum availability of the systems to perform its function algorithm. But it has as well disadvantages because of some failures caused when working within systems. These failures are called "Maintenance-effect failures".

To analyze the mentioned failures there must be an appropriate mathematical model and the preventive maintenance will be optimized with assistance of it. The Markov's modelling for researching of all types of failures and the process of the maintenance of the systems is offered in this paper.

Suggested model is shown on Fig. 1. It has three states: S_0 – a fault-free state; S_1 – pre-fault state and S_2 – a fault state. The states S_0 and S_1 reflect the availability state of the system and S_2 – reflects the unavailability state.

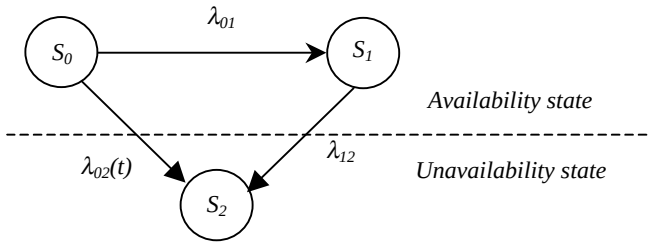

Fig. 1. Three states Markov's model

The model includes an additional fictitious "pre-fault" state (S_1), emulating the "hidden" failures appearing in the system, they are discovered and removed in the preventive maintenance. These hidden failures are identified as "pre-faults". If the system is in the "pre-fault" state, it is still available, since a hidden failure is not yet discovered. The removal of the "pre-fault" state on time prevents arising another one. If the "pre-fault" state is discovered before the preventive maintenance, it arises in the unavailability state. These types of failures are parametric failures and they are emulated by transition intensities $\lambda_{01} = const$ and $\lambda_{12} = const$.

The research of the "maintenance-effect failures" is possible by including the time dependence in the parameter $\lambda_{02}(t)$, which is the transition intensity from the state S_0 to the state S_2. This intensity is

$$\lambda_{02}(t) = \lambda_{02} + \lambda_m \left\{ \frac{1}{1+(t-T_m)^2} \right\}, \qquad (1)$$

where $\lambda_{02} = const$ is intensity of the sudden failures; $\lambda_m = const$ and T_m are respectively the maximal failure intensity and the time after the end of maintenance when the negative effects of it are maximal.

The characteristic of $\lambda_{02}(t)$ is shown on Fig. 2.

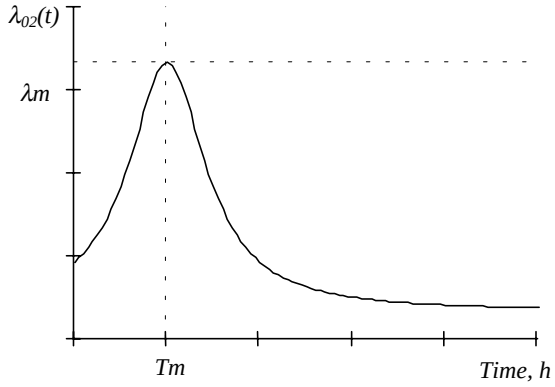

Fig. 2. The $\lambda_{02}(t)$ characteristic

Thus obtained model emulate three type of failures: the sudden failures – with intensity $\lambda_{02}(t)$; the parametric failures – with intensities λ_{01} and λ_{12}; and the "maintenance-effect" failures – through $\lambda_m(t)$ and T_m.

To analyse the above mentioned model, is necessary to solve its system of differential equations:

[1] Georgi Dimitrov Nenov, is with the Department of Communication and Railway Signalling Engineering in "Todor Kableshkov" Higher School of Transport. 158 Geo Milev Street, Sofia 1574, Bulgaria.

[2] Borislav Draganov Boiadjiev, is with the Department of Communication and Railway Signalling Engineering in Todor Kableshkov Higher School of Transport. 158 Geo Milev Street, Sofia 1574, Bulgaria. E-mail: bboiadjiev@vtu.bg.

$$\begin{cases} \dfrac{dP_0(t)}{dt} = -\left[\lambda_{01}+\lambda_{02}+\lambda_m.\left(\dfrac{1}{1+(t-T_m)^2}\right)\right].P_0(t), \\ \dfrac{dP_1(t)}{dt} = \lambda_{01}.P_0(t)-\lambda_{12}.P_1(t), \\ \dfrac{dP_2(t)}{dt} = \left[\lambda_{02}+\lambda_m\left(\dfrac{1}{1+(t-T_m)}\right)\right].P_0(t)+\lambda_{12}.P_1(t), \\ P_0(t)+P_1(t)+P_2(t)=1. \end{cases} \quad (2)$$

with the following initial conditions:

$$P_0(0)=1; \quad P_1(0)=0; \quad P_2(0)=0. \quad (3)$$

The first equation of the system given in Eqs. (2), is solved as following:

$$\frac{dP_0(t)}{dt} = -\left[\lambda_{01}+\lambda_{02}+\lambda_m.\left(\frac{1}{1+(t-T_m)^2}\right)\right].P_0(t), \quad (4)$$

$$\frac{dP_0(t)}{P_0(t)} = -\left[\lambda_{01}+\lambda_{02}+\lambda_m.\left(\frac{1}{1+(t-T_m)^2}\right)\right].dt, \quad (5)$$

$$\int\frac{dP_0(t)}{P_0(t)} = -\int\left[\lambda_{01}+\lambda_{02}+\lambda_m.\left(\frac{1}{1+(t-T_m)^2}\right)\right].dt, \quad (6)$$

$$\ln P_0(t) = -\left[(\lambda_{01}+\lambda_{02})t+\lambda_m.arctg(t-T_m)+C\right] \quad (7)$$

When $t=0$ it is got C, i.e:

$$\ln P_0(0) = -\left[\lambda_m.arctg(-T_m)+C\right], \quad (8)$$

$$0 = -\lambda_m.arctg(-T_m)-C, \quad (9)$$

$$C = -\lambda_m.arctg(-T_m) = \lambda_m.arctg(T_m). \quad (10)$$

And for $P_0(t)$ is got:

$$\ln P_0(t) = -(\lambda_{01}+\lambda_{02}).t - \\ -\lambda_m.arctg(t-T_m)-\lambda_m.arctg(T_m), \quad (11)$$

$$P_0(t) = e^{-\lambda_m.arctg(T_m)}.e^{-\left[(\lambda_{01}+\lambda_{02}).t+\lambda_m.arctg(t-T_m)\right]}. \quad (12)$$

The second equation of the system given in Eqs. (2), is solved under initial condition $P_1(0)=0$, since at the initial moment the system is fault-free (it is in S_0 state). This equation is a linear differential equation:

$$\frac{dP_1(t)}{dt}+\lambda_{12}.P_1(t) = \lambda_{01}.P_0(t), \quad (13)$$

It is solved by means of the formula given in [2] and it is got:

$$P_1(t) = e^{-\lambda_{12}.t}.[C_1+\int\lambda_{01}.P_0(t).e^{\lambda_{12}.t}dt]. \quad (14)$$

$P_0(t)$ is replaced from Eq. (12) and it got:

$$P_1(t) = e^{-\lambda_{12}.t}.[C_1+\lambda_{01}.e^{-\lambda_m.arctg(T_m)}* \\ *\int e^{-(\lambda_{01}+\lambda_{02}+\lambda_{12}).t}.e^{-\lambda_m.arctg(t-T_m)}dt]. \quad (15)$$

The exponent $e^{-\lambda_m.arctg(t-T_m)}$ in Eq. (15) is expanded in a row, using the known formula [2]:

$$e^{-\lambda_m.arctg(T_m)} \approx 1+(-\lambda_m.arctg(t-T_m)) = \\ =1-\lambda_m.arctg(t-T_m). \quad (16)$$

Then, for $P_1(t)$ is got:

$$P_1(t) \approx e^{-\lambda_{12}.t}.\{C_1+\lambda_{01}.e^{-\lambda_m.arctg(T_m)}* \\ *\int e^{-(\lambda_{01}+\lambda_{02}+\lambda_{12}).t}.[1-\lambda_m.arctg(t-T_m)]dt\} \quad (17)$$

After solving the integral in Eq. (17), it is got the following:

$$P_1(t) \approx e^{-\lambda_{12}.t}.\left\{C_1+\frac{\lambda_{01}.e^{\lambda.t-\lambda_m.arctg(T_m)}}{\lambda}*\right. \\ *\{1-\lambda_m.\{arctg(t-T_m)- \\ \left.-\frac{1}{\lambda.[1+(t-T_m)^2]}-\frac{2.(t-T_m)}{\lambda.[1+(t-T_m)^2]^2}\}\right\} \quad (18)$$

where, $\lambda = \lambda_{12}-\lambda_{01}-\lambda_{02}$.

The C_1 constant is got when $t=0$ and the initial condition for $P_1(t)$:

$$\Rightarrow C_1 = \frac{\lambda_{01}.e^{-\lambda_m.arctg(T_m)}}{\lambda}.\left\{\lambda_m.\left[\frac{2.T_m}{\lambda.(1+T_m{}^2)^2}-\right.\right. \\ \left.\left.-\frac{1}{\lambda.(1+T_m{}^2)}-\lambda_m.arctg(T_m)\right]-1\right\}. \quad (19)$$

Finally for $P_1(t)$ the following expression is got:

$$P_1(t) \approx \frac{\lambda_{01}.e^{-[\lambda_{12}.t+\lambda_m.arctg(T_m)]}}{\lambda}\left\{e^{\lambda.t}.\{1-\lambda_m.\{arctg(t-T_m)-\right. \\ \left.-\frac{1}{\lambda.[1+(t-T_m)^2]}-\frac{2.(t-T_m)}{\lambda.[1+(t-T_m)^2]^2}\}\right\}+ \\ \left.+\lambda_m.\left[\frac{2.T_m}{\lambda.(1+T_m{}^2)^2}-\frac{1}{\lambda.(1+T_m{}^2)}-\lambda_m.arctg(T_m)\right]-1\right\}. \quad (20)$$

Then the probability that the system is in availability state $P_{av}(t)$ is:

$$P_{av}(t) = P_0(t)+P_1(t). \quad (21)$$

The probability that the system is in the unavailability state $P_2(t)$ is got from fourth equation, given in Eqs. (2).

CONCLUSION

The submitted Markov's model of the process of the failure development, describes both sudden and parametric failures, as well as failures deriving from preventive maintenance – the "maintenance-effect" failures. That can be used for solving a number of special problems, related to reliability, efficiency and safety of communication, railway interlocking and signalling systems, as well as for researching the problem of preventive maintenance optimisation.

REFERENCES

[1] Boiadjiev, B. A Model For Analysis Of Maintenance-Effect Failures. Zel 2002 9th International Symposium Railways on the Edge of the 3rd Millennium, Zilina (Slovak Republic), 28- 29 May 2002.

[2] Bronshtein, I.N., K.A. Semendiaev. Spravochnik po matematike dlya ingenerov. Moskva, Nauka, 1986 (in Russian).

[3] Alexandrov, G. Diagnostika i tehnichesko obsluzhvane na osiguritelnata tehnika v zhelezoputniya transport, VVTU "Todor Kableshkov", Sofia, 1993 (in Bulgarian).

MQAM Interference Rejection Using LMS Algorithm in UWB Radio System

Zorica Nikolić[1], Vladimir Milošević[2], Bojan Dimitrijević[3], Nenad Milošević[4]

Abstract – **Performances of UWB system using PPM in the presence of MQAM interference are considered in this paper. Interference rejection is performed using a adaptive transversal filter (ATF). A ATF parameter (filter length) optimization is performed in this paper.**

Keywords – **UWB, adaptive filtering, interference rejection**

I. INTRODUCTION

Ultra-wideband (UWB) technology has been recently proposed as a viable solution for high-speed indoor short range wireless communication system, because of its robustness to severe multipath conditions and low cost and low power implementation.

Time Hopping combined with pulse position modulation (TH-PPM) has been the original proposal for UWB systems [1]. An analysis of this modulation and multiaccess scheme performance in terms of bit error rate has been proposed in [1] for AWGN channel. In [1] a method to evaluate the bit error rate performance of time hopping TH-PPM in the presence of multiuser interference and AWGN channel is proposed. Gaussian quadrature rules are used in this approach.

In this paper TH-PPM UWB radio system performance in the presence of MQAM interference will be determined. The receiver uses a ATF for the interference rejection. Filter weights are adapted using the LMS algorithm.

II. SYSTEM MODEL

The signal transmitted by the desired user is modeled as:

$$s(t) = \sum_i b(t - iNT_f - (1 - a_i)\Delta)\cos\ \omega_c t \qquad (1)$$

where

$$b(t) = \sum_{n=0}^{N-1} g(t - nT_f - h(n)T_c) \qquad (2)$$

ω_c is channel carrier frequency. $g(t)$ represents basic pulse shape (rectangular pulse) and T_f represents frame duration during which there is only one pulse T_c seconds wide. The sequence $h(n)$ is the user's time-hopping code and its elements are integers taking values in the range $0 \le h(n) \le N - 1$. The parameter T_c is the duration of an addressable time bin. In other words, the right hand side of (2) consists of a *block* of N time-hopped monocycles. a_i represents information bits (0,1). Equation (1) says that, if a_i were all zero, the signal would be a repetition of $b(t)$-shaped blocks with period NT_f. Δ may be viewed as the time shift impressed by a unit data symbol on the monocycles of a block. It is clear that the choice of Δ affects the detection process and can be exploited to optimize system performance. To summarize, the transmitted signal consists of a sequence of $b(t)$-shaped position-modulated blocks. The code sequence restarts at every data symbol.

The receiver block diagram is shown in Fig. 1. When several time-hopping signals are simultaneously transmitted over a channel with L_c paths, the composite waveform at the output of the receiver antenna may be written as:

$$r(t) = \sum_{l=1}^{L_c} \left(\gamma_l^{(I)} s(t - \tau_l)\cos\omega_c t + \gamma_l^{(Q)} s(t - \tau_l)\sin\omega_c t\right) + n(t) + j(t) \qquad (3)$$

$$r^{(I)}(t) = r(t)\cos\omega_c t, \quad r^{(Q)}(t) = r(t)\sin\omega_c t \qquad (4)$$

where $n(t)$ is noise, and $j(t)$ is the total interference, $\gamma_l = \gamma_l^{(I)} + j\gamma_l^{(Q)}$ is the complex attenuation and τ_l is the delay in l-th path.

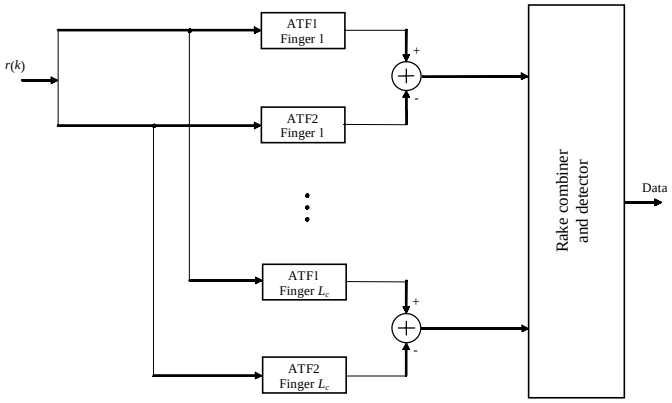

Fig. 1. Receiver block diagram

If we consider signal sampled at chip interval T_c we have:

$$r(k) = r^{(I)}(k) + jr^{(Q)}(k), \quad k = \frac{t}{T_c} \qquad (5)$$

[1]Autor is with the Faculty of Electronic Engineering, Beogradska 14, 18000 Nis, Serbia and Montenegro, E-mail: zora@elfak.ni.ac.yu

[2]Autor is with the Faculty of Technical Sciences, Trg Dositeja Obradovica 6 , 21000 Novi Sad , Serbia and Montenegro, E-mail: tlk_milos@uns.ns.ac.yu

[3]Autor is with the Faculty of Electronic Engineering, Beogradska 14, 18000 Nis, Serbia and Montenegro, E-mail: dbojans@ptt.yu

[4]Autor is with the Faculty of Electronic Engineering, Beogradska 14, 18000 Nis, Serbia and Montenegro, E-mail: nemilose@eunet.yu

The interference is rejected using two two-sided adaptive transversal filters of length 2M, denoted as ATF1 and ATF2. In order to predict the interference signal, sampling is performed at frame rate, and the adaptation of filter weights using LMS algorithm is performed at bit rate.

The filter weights are adapted using the LMS algorithm and for ATF1 and ATF2 we have, respectively:

$$W_m(i+1) = W_m(i) + \frac{\mu e_1^l(i)\left(S1_m^l(i)\right)^*}{\sum_{j=-M}^{-1}\left(S1_j^l(i)\right)^2}, \quad \begin{matrix} -M \le m \le M \\ m \ne 0 \end{matrix} \tag{6}$$

$$W_m(i+1) = W_m(i) + \frac{\mu e_2^l(i)\left(S2_m^l(i)\right)^*}{\sum_{j=1}^{M}\left(S2_j^l(i)\right)^2}, \quad \begin{matrix} -M \le m \le M \\ m \ne 0 \end{matrix} \tag{7}$$

where μ denotes the adaptation factor, and :

$$\begin{aligned} S1_m^l(i) &= \sum_{n=iN}^{(i+1)N} A_m^l(n), \\ S2_m^l(i) &= \sum_{n=iN}^{(i+1)N} B_m^l(n), \end{aligned} \quad -M \le m \le M \tag{8}$$

$e_1^l(i)$, $e_2^l(i)$ may be calculated as:

$$\begin{aligned} e_1^l(i) &= S1_0^l(i) - \sum_{\substack{m=-M \\ m\ne 0}}^{M} S1_m^l(i) W_m(i)), \\ e_2^l(i) &= S2_0^l(i) - \sum_{\substack{m=-M \\ m\ne 0}}^{M} S2_m^l(i) W_m(i)) \end{aligned} \tag{9}$$

i represents the sequence number of the considered bit.

Therefore, variables $A_m^l(n)$ and $B_m^l(n)$ from Eq. (9), belonging to filter 1 and filter 2, respectively, may be calculated as

$$\begin{aligned} A_m^l(n) = &\sum_{k=n\frac{T_f}{T_c}-\frac{\tau_l}{T_c}}^{(n+1)\frac{T_f}{T_c}-\frac{\tau_l}{T_c}} r^{(I)}(k) g(k - n\frac{T_f}{T_c} - \frac{\tau_l}{T_c} - h(n) - m) \\ &+ j \sum_{k=n\frac{T_f}{T_c}-\frac{\tau_l}{T_c}}^{(n+1)\frac{T_f}{T_c}-\frac{\tau_l}{T_c}} r^{(Q)}(k) g(k - n\frac{T_f}{T_c} - \frac{\tau_l}{T_c} - h(n) - m) \end{aligned} \tag{10}$$

$$\begin{aligned} B_m^l(n) = &\sum_{k=n\frac{T_f}{T_c}-\frac{\tau_l}{T_c}}^{(n+1)\frac{T_f}{T_c}-\frac{\tau_l}{T_c}} r^{(I)}(k) g(k - n\frac{T_f}{T_c} - \frac{\tau_l}{T_c} - h(n) - m - \frac{\Delta}{T_c}) \\ &+ j \sum_{k=n\frac{T_f}{T_c}-\frac{\tau_l}{T_c}}^{(n+1)\frac{T_f}{T_c}-\frac{\tau_l}{T_c}} r^{(Q)}(k) g(k - n\frac{T_f}{T_c} - \frac{\tau_l}{T_c} - h(n) - m - \frac{\Delta}{T_c}) \end{aligned} \tag{11}$$

n designates the considered frame index (n = 0, N-1), and m is ATF weight index.

The detection variable in the first Rake receiver finger is:

$$d(i) = \sum_{l=1}^{L_c} (\mathrm{Re}\{D^l(i)\} * \mathrm{Re}\{T^l(i)\} + \mathrm{Im}\{D^l(i)\} * \mathrm{Im}\{T^l(i)\}) \tag{12}$$

where

$$\begin{aligned} \mathrm{Re}\{D^l(i)\} &= \mathrm{Re}\{e_1^l(i) - e_2^l(i)\}, \\ \mathrm{Im}\{D^l(i)\} &= \mathrm{Im}\{e_1^l(i) - e_2^l(i)\} \end{aligned} \tag{13}$$

$$\begin{aligned} \mathrm{Re}\{T^l(i)\} &= \overline{\mathrm{Re}\{e_1^l(i)\} + \mathrm{Re}\{e_2^l(i)\}}, \\ \mathrm{Im}\{T^l(i)\} &= \overline{\mathrm{Im}\{e_1^l(i)\} + \mathrm{Im}\{e_2^l(i)\}} \end{aligned} \tag{14}$$

and i is again the sequence number of the considered bit.

The error probability is computed using Monte-Carlo simulation.

III. Numerical Results

Fig. 2. shows error probability as a function of filter length. Interference bit duration is chosen to be $T_j = 1000T_c$. Signal to noise ratio is SNR = 10 dB, and interference to signal ratio is J/S = 20 dB.

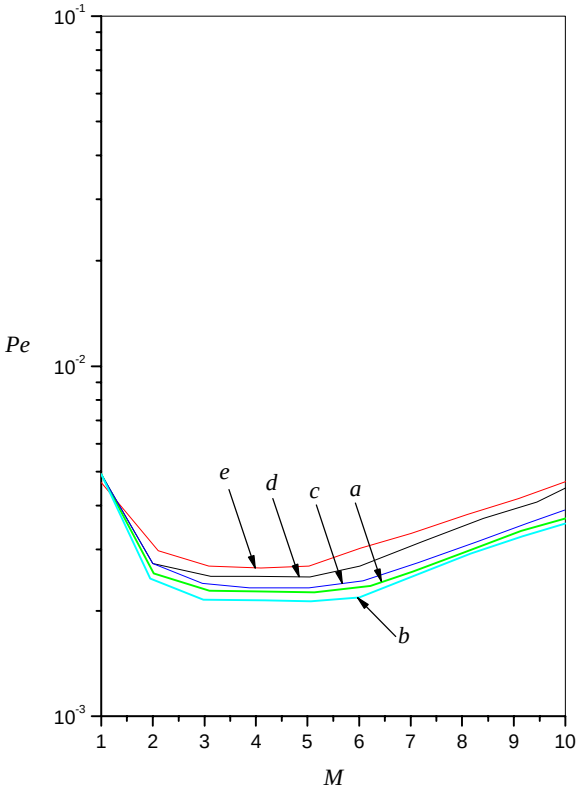

Fig. 2. Error probability as a function of filter length
a – PSK interference; *b* – 4QAM interference
c – 16QAM interference; *d* – 64QAM interference
e – 256QAM interference

It can be noted that there is a range of ATF lengths for which the error probability is minimal, regardless of interference

constellation (PSK, 4QAM, 16QAM, 64QAM, 256QAM). The smallest filter length that meets the requirements for the minimal error probability is M = 4, and it was chosen to be optimal.

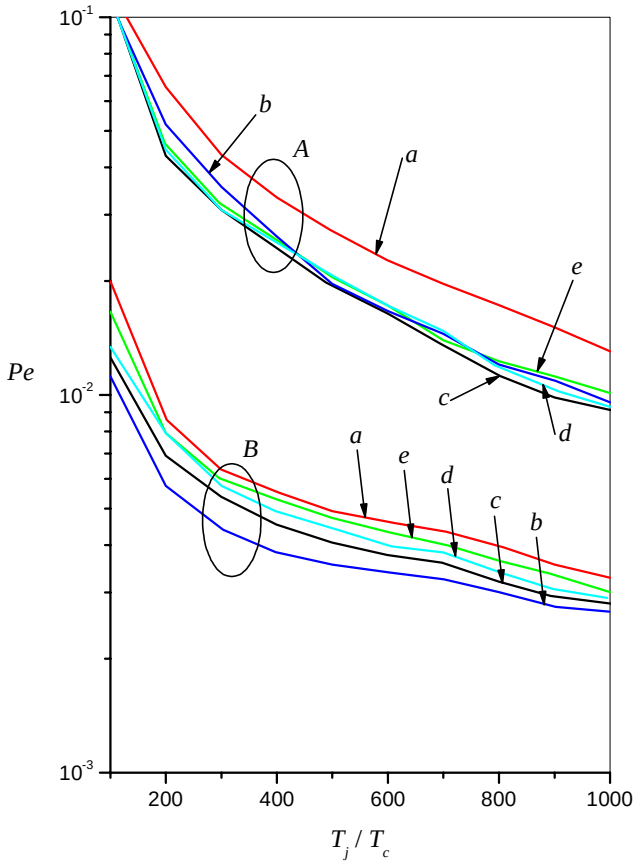

Fig. 3. Error probability as a function of interference bit duration
A – without interference rejection
B – with interference rejection with ATF
a – PSK interference; *b* – 4QAM interference
c – 16QAM interference; *d* – 64QAM interference
e – 256QAM interference

Fig. 3. shows error probability as a function of interference bit duration. Filter length is chosen to be M = 4. Signal to noise ratio is SNR = 10 dB, and interference to signal ratio is J/S = 20 dB.Curves labeled with *A* stand for the case is there is no interference rejection with ATF, and curves *B* represent the performance of the system if there is ATF. The figure shows that interference suppression with ATF at TH-PPM UWB radio brings the decrease of error probability for almost one order of magnitude compared to the case if there is no interference rejection.

IV. Conclusion

In this paper we consider TH-PPM UWB radio system error probability. Interference rejection is performed using adaptive transversal filter. The ATF length optimization is also done in this paper. A significant performance drop may be noticed with the interference rate increase. The interference suppression with ATF at TH-PPM UWB radio system brings the decrease of error probability for almost one order of magnitude, regardless of the interference bit rate.

References

[1] M.Win and R. Scholtz, "Ultra-wide bandwidth time hopping spread-spectrum impulse radio for wireless multiple-access communications," *IEEE Trans. Commun.*, Vol.48, No.4, April 2000, pp. 679-691

[2] G. Durisi and S. Benedetto, "Performance evaluation of TH-PPM UWB systems in the presence of multiuser interference," *IEEE Communications Letters*, Vol.7, No.5, May 2003, pp. 224–226.

[3] M. Win and R. Sholtz, "Impulse Radio: How It Works," *IEEE Communications Letters*, Vol.2, No.2, February 1998, pp. 36–38.

[4] Z. Nikolić, B. Dimitrijević and N. Milošević, "Rejection of PSK Interference in DS-SS/QPSK System Using Complex Adaptive Filter and Nonlinear Correlation Receiver," *Electronics Letters*, Vol.33, No.4, February 1997, pp. 268–270.

About a Possible Way of Optimizing the Number of Amplifiers in CATVs

Stanimir Sadinov[1], Kiril Koitchev[2]

Abstract - **One of the essential stages in CATV network design or that of larger networks for corporate reception is the proper calculation of voltage level within distribution nets, which must provide good quality of TV signal in the subscriber unit. A major quality factor is the relationship signal/noise as well as signal/required level of retaining of retaining of combination frequencies of the third order in the TV channel at the output of the subscriber's contact (CTB). Level increase at the input (i.e. the first active element) and output of the amplifier will cause a corresponding increase in the signal/noise (S/N) relationship. Voltage level rise at the output will increase the impact of combination frequencies.**

All calculations contribute to the proper determination of input and permissible output levels of voltage in broad band amplifiers so that the required relation-ship signal/noise (S/N) could be ensured along with the influence of combination frequencies (CTB) of the third order in CATV.

By way of programming it is possible to optimise either the number of amplifiers, i.e. the required coefficient of amplification k_{nom}, or the cost of the individual amplifier. Within this procedure the largest possible number of steps is calculated N_{max} by means of comparing noise levels with non-linear deviations (CTB), i.e. the minimum and maximum output level.

Keywords - **CATV network design, signal/noise (S/N), combination frequencies (CTB), non-linear deviations, coefficient of amplification k_{nom}.**

I. INTRODUCTION

Non-linear distortions in the network normally depend on the features of amplifiers which are connected in series in the preliminary tract, the level of their input signals and the number of TV and radio channels which are transmitted along the network. These distortions result in products with new frequencies. The input signal in CATV can be rendered by the following simplified expression:

$$U_{in} = \sum_{i=1}^{M} U_i \cos\left(\omega_i t + \varphi_i\right) \qquad (1)$$

where M is the number of all bearing oscillations by means of which all TV and radio channels are transferred.

Assume that AF characterization of a particular cable amplifier is approximated by power polynomial of the kind:

$$U_{out} = f\left(U_{in}\right) = \sum_{i=0}^{m} k_i U_{in}^i \qquad (2)$$

In such cases heterodyne frequencies are formed at the output which are of the kind $b_1\omega_1 + b_2\omega_2 + ... + b_n\omega_n$, where coefficients $b_1 \ldots b_n$ are positive integers. The levels of nonlinear components obtained at the amplifier output should be low enough to prevent deterioration of picture and sound quality at subscriber's end. The permissible level of each component is determined in relation to the bearing oscillations of desired signals and is defined as a minimum distance whose value, expressed in – 60 dB, is recorded in standard specifications.

Thermal noise is of basic importance to CATV and is defined by means of Niquist's formula:

$$U_{Noise} = \sqrt{4kTR\Delta f}$$

where: k– is Boltzmann constant; T– is absolute thermodynamic temperature, K; R– input amplifier resistance, Ω; Δf– is the frequency band, Hz.

This noise has a uniform frequency range and is referred to as white noise.

Major guiding criterion in building CATVs is reducing of non-linear distortions and the level of noise as well.

These are the conclusions that can be drawn when designing and constructing CATV [1]:

1. Increasing (decreasing) the level of output signal by 1dB will improve (deteriorate) the signal/noise (S/N) ratio by 1dB ; increasing(decreasing) of intermodulation products of the second order (IMD2, CSO) by 1dB and those of third order (IMD3, CTB) by 2 dB.

2. Cumulation of intermodulation products of second order(CSO) along the highway is implemented according to the law of power one(analogous to noise power) whereas the the products of third order (CTB) follow the squared law. Physically this means that when two identical amplifiers are cascade connected and have equal individual values for S/N , CSO , and CTB then there will be lower values of S/N and CSO by 3dB and CTB will be lower by 6dB.

[1]Ass. Stanimir M. Sadinov is with the Department of Communications Technology and Equipment, Technical University of Gabrovo, Bulgaria, 5300 Gabrovo, str."Hadji Dimitar" № 4 Bulgaria, E-mail: murry@tugab.bg

[2]Asoc. Prof. Ph.D. Kiril R. Koitchev is with the Department of Communications Technology and Equipment, Technical University of Gabrovo, Bulgaria, 5300 Gabrovo, str."Hadji Dimitar" № 4 Bulgaria, E-mail: koitchev@tugab.bg

3. In terms of economy the coefficient of amplification will depend on the length of highway. Greater length of trunkline should correspond to a smaller coefficient of amplification. For traditional type of trunklines amplifiers of class not lower than B are to be used (this in accordancewith EN 50083) with amplification coefficient 28÷38dB. For main trunklines or longer ones it is recommendable to use amplifiers of class A with amplification coefficient 20÷27dB. When dimensionong a CATV system it is expedient to leave a margin of 2÷3dB according to the coefficient of amplification

These conclusions can be observed by virtual analysis by means of program application which is the objective of this paper.

II. DEVELOPMENT AND IMPLEMENTATION OF CABLE TV DESIGNER PROGRAM

Individual Windows application of Delphi has been developed This program is designed to calculate all basic parameters of CATV.

Fig 1. Presents the graphic interface of the related program application

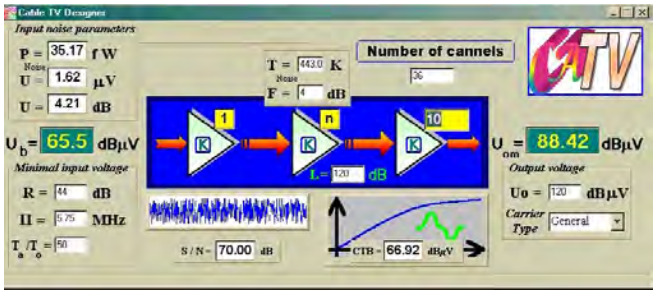

Fig 1. Graphic interface of the Cable TV Designer

Here follows the methodology which underlies Cable TV designer that facilitates computer aided design of cable TV.

It is a well known fact that the relationship between voltages can be expressed in dB by the following:

$$U_{12} = 20.\lg \frac{U_1}{U_2}, \quad dB \qquad (4)$$

Engineering practice has adopted measurements of voltages and power of signals to be in dB. Obviously that is possible if a fixed datum for U_2. Is defined. When designing cable networks it is assumed that U_2=1µV i.e. the levels of signals are measured by the unit dBµV. This is the record used in the standard specifications and the service forms and records of communications technology for cable TV

Correlation with the measuring units of SI is expressed by (2):

$$U\ [dB\mu V] = 20.\lg U\ [\mu V] \qquad (5)$$

All relationships of two similar values can be expressed in dB unambiguously For example, the signal /noise relationship:

$$S/N = 20.\lg U_S/U_N, \qquad (6)$$

where the levels of signal U_S and noise U_N are recorded in random equal units of voltage(normally µV)

A. *Input Parameters:*

F – noise coefficient of individual amplifier, dB

T_{Noise} – noise temperature, K;

R = 44 dBµV – standard protection ratio S/N;

Π – effective noise frequency band of TV channel, MHz;

SECAM --> Π = 5,75 MHz; PAL --> Π = 4,75 MHz

Ta/To <= 50 – relative noise temperature of TV antenna;

M – number of active channels;

N – number of amplifier steps connected in series;

L – losses along the line, dBµV;

U_O – Rated voltage of amplifier with guaranteed CTB ≤ 60 dB (set by the manufacturer), dBµV;

B. *Output Parameters:*

U_b – minimum level of input voltage, dBµV;

U_{Om} - maximum level of output voltage, dBµV;

S/N – signal /noise relationship at the output, dB;

CTB – non-linear distortions (Composite Triple Beat), dBµV;

U_{Noise} – noise voltage at the input, dB;

K_{opt}–optimum coefficient of amplification of particular amplifier, dB.

C. *Methods of Estimation:*

Estimation of input noise parameters

$$T_{Noise} = T_0(F - 1) \qquad (7)$$

$$P_{Noise} = k\Pi T_{Noise} \qquad (8)$$

$$U_{Noise} = \sqrt{k\Pi T_0 R_0 (F-1)}, \quad \mu V \qquad (9)$$

$$U_{Noise[dB]} = 20\lg U_{Noise}, \ dB\mu V \quad , \qquad (10)$$

where:

k = 1,38 x 10^{-23} J/K – Boltsmann constant;

T_0 = 293 K – normal noise temperature;

R_0 = 75 Ω – input resistance.

Calculation of input level

$$U_b = R + N_r + 10\lg[(N + 2)10^{0.1F} + T_a/T_0] \qquad (11)$$

where:

$N_r = 10\lg(kT_0\Pi/P_0) = 2.4$ dBμV–thermal noise of TV channel;

$P_0 = 1/75$ pW, power over 75 Ω, with voltage of 1 μV;

Calculation of non-linear distortions

$$CTB = 31{,}13 + 23\lg M \qquad (12)$$

Calculation of output level

$$U_{Om} = U_0 - \Delta U_M - \Delta U_N - (CTB - 60)/2\ , \qquad (13)$$

where:

$\Delta U_M = x.\lg(M - 1)$

x = 10 / synchronous carriers /;

x = 5 / asynchronous carriers /;

x = 7.5 most frequently used value.

$\Delta U_N = y.\lg N$

y = 17 /N < 24/;

y = 20 /N ≥ 24/.

Adjustment according to CTB should be applied only for N≥18.

Calculation of signal/noise relationship at line output

$$S/N = U_{Om} - K_{nom} - F - N_r \qquad (14)$$

After optimizing the number of used amplification steps the program calculates the required optimum coefficient of transmission.:

$$K_{opt} = L / N \qquad (15)$$

This program allows for the optimisation of the number of amplifiers. i.e. the required coefficient of amplification or the cost of individual amplifier. Maximum permissible steps o are calculated N max meanwhile comparing the levels of noise (S/N) and non-linear distortions (CTB) that is, the maximum and minimum output level (see fig 2)

Fig 2 presents signal /noise relationship dependence as well as the dependence of non-linear distortions on the number amplification steps Consequently the optimum number of amplifiers is automatically determined according to a preliminary assigned permissible value of signal/noise relationship. Amplification coefficient of individual amplifier is then optimised by using (15). Also accessible are the dependences of signal/noise relationships and the non-linear distortions on the number channels which are transmitted in the network (see Fig 3) Signal output level is explored as a function of S/N and CTB (see Fig 4). Fig 5 presents the algorithm which is executed by the presented program application.

This program features totally interactive performance and suggests contextual back up information on all input data and estimated parameters of CATV. Application is error protected by continuous control over the values entered by the user. This program application was developed largely with the help of Delphi [3].. Graphic data could be recorded in vector format or raster(bitmap)

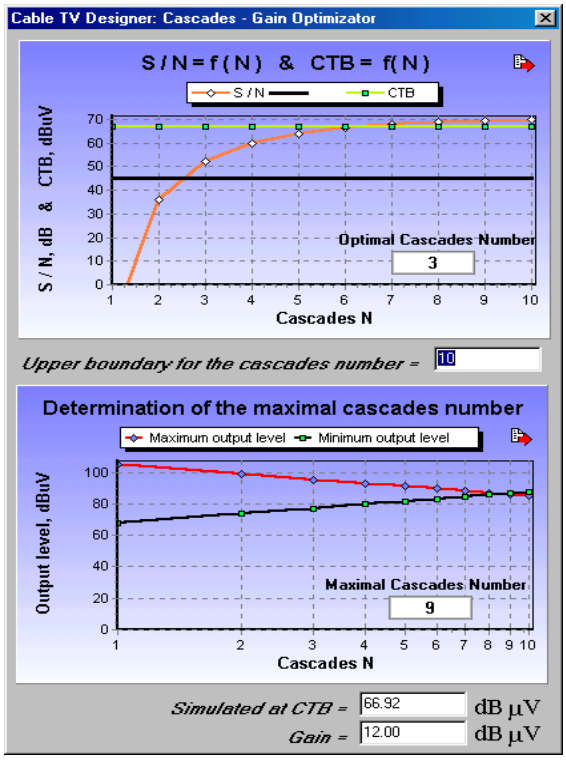

Fig 2 Window of the optimizer for the number of used amplifiers

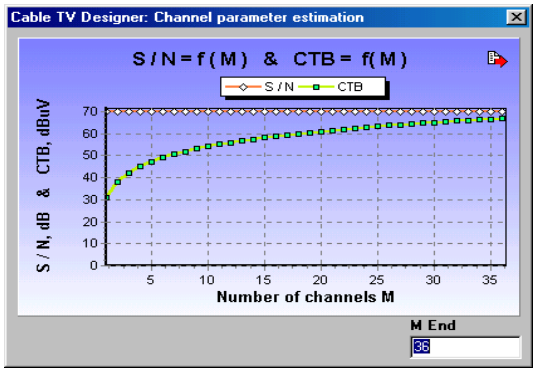

Fig 2 Window of the optimizer for the number of used amplifiers

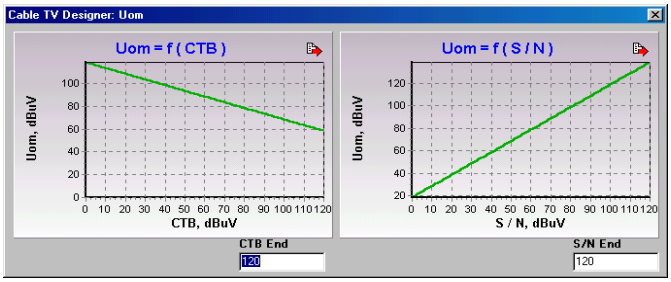

Fig4. Study of the output level dependence on the non-linear distortions and signal/noise relationship

III. CONCLUSIONS

➢ A special purpose program application has been designed called “Cable TV Designer” which is employed in estimating basic parameters determined by standards, specially applicable in engineering designs of CATV. This program enables computer aided methods of design. [1,2];

➢ Impact of model parameters has been studied with reference to:

- the impact of the number of employed amplifiers(N) (fig.2)
  - Non-linear distortions remain constant : they are determined solely by the non-regularity of AF characterization (set by the standard as manufacturer’s parameter of amplifiers) and the number of transmitted channels(carriers)
  - Concerning the impact on the signal level as compared to that of noise S/N it should be given a comprehensive regard Optimisation is effected by selecting a pattern with minimum amplification coefficient when output signal is at its peak level[2].
- Concerning the impact of the number of channels(M) (fig 3):
  - The noise level does not change Thermal noise retains the same level throughout the whole frequency range
  - Non-linear distortions grow in number along with the increase in the number of transmitted carriers due to their interaction
- Output level dependence on the S/N relationship and CTB(fig 4)
  - Increase of the non-linear distortions level entails adjustment of output level(decrease) so that the 60dB standard level could be reached.
  - As already noted, the increased output level ensures performance with high signal/noise relationship

The large number of model parameters necessitates the development of computer aided engineering design of CATVs. This program, along with the relevant current standards and manufacturers’ manuals, contributes to a large extent to the solution of such engineering tasks.

REFERENCES

1. Койчев К., С. Садинов. Проектиране на кабелни телевизионни мрежи. “АЛМА МАТЕР Интернационал”, Габрово 2001. ISBN 954 9577 81 3

2. Кабельное ТЕЛЕВИДЕНИЕ справочник. 1999 ÷ 2000

3. Marco Cantu. Mastering™ Delphi™ 5. Vol. I & II“SoftPress”, S. 2000. ISBN 954-685-082-9

4. Koitchev K., S. Nemtsov, S. Sadinov. Studies on The Reliability of Two-way Cable TV Network. 6th International Conference on Telecommunications in Modern Satellite, Cable and Broadcasting Services - TELSIKS 2003

5. Koitchev K., Sadinov St. Maximum Value Determination of Non-linear Products in Cable Television Networks. IEEE Transactions on Broadcasting, March 2003

6. Koitchev K., S. Sadinov, S. Nemtsov, “Suggested Method for Composite Frequencies Allocation”, 5th International Conference on Telecommunications in Modern Satellite, Cable and Broadcasting Services TELSIKS 2001, Proceedings of Papers, volume 2, pp. 541-543.

Centers 130 For Faults Maintenance In BTC

K. SHWERTNER
CITS-BTC, Sofia 1574, 69Shipchenski prohod, tel.8 705 076, e-mail:shvertner.cits@btc.bg

Abstract **- The report presents centers 130 for fault service, data analysis and fault management to support qulity of service in fixed telecommunication distribution network.**
The main achievements of the presentation are:
- precise analysis of the quantitative quality of service data;
- data evaluation for a support of quality of service of fixed telecommunication network.

Key words **- Fault Maitenance, Telecommunication, QoS.**

I. INTRODUCTION

Telecommunication Network is a complex technical system, which has developed chronologically with the level of technology available in the moment of building. The main goal of the telecommunication network is to provide quality communication for exchanging information.

In telecommunication network have applied different stage of technology developments. There are used wireless technologies, satellite technologies, optical cables, coacsial cables and copper cables. Fast technology changing and new services lead to building of many complex telecommunication networks. In contemporary networks are connected different type and different generation of element and equipment, which must join suitable in order to provide subscriber services based on a connection end to end in the network. There are different type of elements and equipment digital and analogical, that means, it is increased complex functionality of network. It is important to provide for QoS (Quality of Services) of telecommunication network.

The new high technologies, which are applied in telecommunication don't support high quality of services of telecommunication network, because the level are determined of the oldest technological elements in network.

Telecommunication network requirements for reliability are very high and reestablishment (in case of faults) must be done fast. Its main components are in generally the following: subscriber cable net, cable net between exchanges, main cable net between towns, commutation equipments, transportation equipments, electricity units. To support of high quality of telecommunication services it is need to maintain parameters and functions of each of the main components of telecommunication network in the given boundaries. It is necessary continual control and supervision of parameters and processes in separate components of the net.

Digital exchanges have many function and software programs, which allow to do control and supervision of base net parameters and functions. Siemens analogiue exchanges A-29 have electrical-mechanical elements and their maintenance in good technical condition require doing continual preventive and technical survey.

II. CENTER 130 COMPONENTS

Center 130 is hardware-software product that combines communications and data processing technology to enable an organization to implement critical fault management strategies in telecommunication. Physically, Center 130 is a place where a group of people handles large volumes of incoming or outgoing calls for the purpose of customer service, fault management, technical support, or other specialized business activity. Center 130 is organized in every BTC region. The components of BTC Centers 130 include fault tests, fault management and rehabilitation.

III. CENTER 130 FUNCTIONAL STRUCTURE

Customers are usually given a free call number to ask questions about products or services. Functional structure of Centers 130 includes the following ways in depending operational implements:

- Oracle application for initial subscriber calls;
- Oracle application for fault management;
- Hardware-software application for rehabilitation.

Order processing Center 130 with the appropriate call management/tracking software can improve the customer service and the quality of service of telecommunication network. There are four phases:

Phase 1: Start test It is tested the status of subscriber line using distance automatic test. The start test includes measurement of electrical parameter of subscriber line and evaluation toward giving limited values. If only one of the parameter value don't satisfy the limit conditions, it is accept a fault.

Phase 2: Fault Localization It is executed the search algorithm, applied to the telecommunication network object, which can be out of order. As a result it is found at least one object in fault.

Phase 3: Fault Identification All hypotheses, connected with the object from previous phase, are tested and evaluated to fine exactly hypotheses.

Phase 4: Control test and rehabilitation After reparation the status of subscriber line is tested and the object is permitted to ordinary work.

IV. FAULT MANAGEMENT APPLICATION SYSTEM

In research center of BTC was developed integrated hardware-software system, which maintains Center 130 for fault requests, test, diagnosis and faults remove management. The system works in all regions of Bulgaria.

The system provides the following main functions:

- Acceptance of single call requests and their registration in Data Base (DB);
- Order calls and making faults diagnosis;
- Faults repair management and reestablishment;
- Automatic assignment;
- Support network data;
- Network maintenance;
- Supervision and telecommunication network quality of services (QoS).

Main system components, supporting the previous functions are the following:

- Access data module;
- Test module includes three components:

A/ automatic exchange test, which makes a list of telephone numbers with parameters out of prescribed default limits;

B/ test of single telephone number in exchange and subscriber lines (personal subscriber elements and units) or test of some network elements and equipments;

C/ intelligent software module for evaluation the test results.

- Faults management module;
- Network support module;
- Exchange and subscriber data support module.

There is a special module for testing and analyses the faults, which leas to a group of subscriber failures in the same net area, for example more than 20 pairs faults in one cable.

- The system support different work places:
- In Center 130 for faults diagnostic – there are some operators who work with entry-requests screen form, accept subscriber telephone calls and faults requests, start testing and save the information in DB.
- In exchanges and maintenance services, which are in different building for different exchange there are technical operators, who make additional tests, dispatching faults and control the process, print reports.
- System administrators, who control and supervise all system modules and support DB, aided with SQL program language can have access to the whole DB. The system creates and maintains centralization DB as Oracle DB.

The computer system for Center 130 is developed using Oracle Server 8.1.7, Designer/2000, Developer/2000 (Forms 6.0 and Reports 6.0), Discoverer 3.0, C++. The first realization is a client-server application. The second realization is developed as web application and it is used Oracle 8i, Web Application Server.

Data base structure is most complexity. Objects are used for modeling and representation of data and knowledge in the system. Knowledge is used for creating a suitable object structure, which design the subject area. The objects are all net elements and units. The data, which is need for system work, can separate to incoming data and system data. The incoming data include data for objects in the system, as the system data formulate and reflect the work environment of the computer system. Incoming data is taken into the system in the installation process. The system data is part of the system, but only part of it can update in current system environment.

Program realization is module designing, flexible and parameter ability. The system is prepared to different configurations and application using parameters. The system is prepared to different test units, digital exchanges and structures in BTC.

V. DATA ANALYSIS

In the system for Center 130 there are accepted, received, updated and saved many data and it allows the survey of both the statistical data processions of the test results of single call tests and automatic exchange tests. Using data criteria faults data supply the data to be grouped in error groups as the quality indexes, character and causes of failures.

There is created a quality matrix, which allows a full view to the operator by the testing network. The rows of the quality matrix are the subscribers calling, the columns are the units, which are called and tested. Quality matrix is generated when the tested values exceed the given limit values. Excess is given by three parameters: absolute error number, error rate and time interval. They can be defined individually in each test selectively to each error–group. Excess of limit occurs if in a given time interval the absolute error number or the calculated error rate of the incoming test results is greater than the relevant parameter. To the efficient use of the quality matrix adds that not only the excess limit but their display can be selected individually in each test and error-group. Consequently, information on a given problem (for example switching faults of domestic trunk calls in high traffic period) can be treated separately.

Here an overall analysis of calls ending up with a busy tone will be presented. It must be underlined that a busy tone can have three causes:

- Congestion while the call is being built up (it is due to the actual traffic load);
- Time out release while the call is being built up (it is due to a technical failure);
- The called telephone number is engaged (it is excluded by the system operation program in the testing network, the telephone number is not allowed to be busy by another “internal” incoming call).

In the course of the analysis congestion and timeout can be distinguished by the distribution of the built-

up time (the time passing until the ringing tone) of the successful calls. The distribution of the build-up time, the separation value is 12 sec.

Results of the processing by statistical programs are as follows:

- A summary table comprising the absolute number of calls and errors and the percentage error rate related to error-groups and calling-called party exchange pairs;

- Sorted lists by calling exchanges, called exchanges and error rates of the tests;

- Diagrams for the calls ending up with a busy tone by calling-called exchange type pairs; Matrices of test calls ending up with a busy tone with error rate arrangement according by calling and called exchanges in different traffic conditions such as:

A/ the total of the test calls;

B/ congestion in high traffic period;

C/ time-out in high traffic period;

D/ congestion in low traffic period;

E/ time-out in low traffic period;

Of the presented results the most important are the sorted lists, as they show the worst exchanges and relations on the top, therefore the work has to be started with them. The location of the weaker points of the network is supported by the matrices, they supply the join test results of the calling exchange to different called parties. If the error rate is similar in the direction of all called parties then the error detection has to be turned to the calling exchange. The matrix is in the same way useful to detect faults in the called exchange.

Instead of giving a presentation of how actual failures are located, a few actual failures are listed below to indicate their nature and variety:

- The call has reached the called party, a few minutes later the route has been cut off. The failure in the direction analogical exchange – mobile network in some exchanges has been witnessed with the occurrence of 90%. The failure was caused by a short time-out adjustment in the analogical exchanges (in the fixed network it did not cause any problems);

- In some cases the digital exchange did not sent a tariff signal to the analogical exchange. The failure was caused by the transient signal sent from the analogical exchange to the digital exchange following the answering signal;

- In case of calls from the digital to the analogical exchanges wrong number occurred in proportion of 1-2 % of the calls. The failure was due to insufficient transient protection solution embed by a software in the digital exchange;

- In calls following the directions of analogical exchange -> digitally transferred stage -> digital exchange -> international exchange, cut off was quite frequent after the call had been built up. The failure was the result of incorrect timing to accept the tariff receipts in the digital exchange.

- Level adjustment problems. Besides switching technology related problems they cause serious speech intelligibility problems (echo) especially in the new modern radio system applications.

The tests have shown that the failures are not significant of one system but they occur consequent to the introduction of new systems, software modification, etc. and are especially frequent at the interfaces of different systems. They can come up later in the real traffic even if the new systems have been thoroughly tested prior the installation. One of the results for this is, for example, that in a low capacity network of 100 thousand lines 50 million calls have to be handled monthly. Even if discrepancies occur only in 10 of a thousand calls, in amounts to about 5000failures. That how many of these failures will turn to be complaints, depends on the character and concentricity of the failures. Obviously, if a smaller range of the callers is concerned, the complaints will be growing in number.

An overall outcome of the test is that failures are not consequent to hardware faults but to software anomalies, which only occur under certain traffic conditions in certain exchanges or traffic routes in a certain phase of the call being built up. Due to the software nature of the deficiencies after they have been detected and impaired network improvement is expected to be long lasting. Failure detection in parallel with other tests and with investigations of complaints should be done continuously following a thorough planning of the work.

Further general experience is that congestion and overload is not caused by lack in circuits, but the congestion of common controlling and signaling transmitting-receiving circuits (software), and this is due to software malfunctions. Network overload, therefore in many cases in only illusive, thus solving these problems does not need costly network extensions.

VI. CONCLUSION

The developed computer system to support Center 130 in telecommunication network is useful to improve the quality of services of the network. The main achievements of the system are:

- Faster and precise subscriber service;

- Faster and precise processing of the failure data;

- Central acceptance and automatic test of subscriber lines, net elements and units, exchanges etc;

- Automatic track-keeping of the failures (the character and causes of them) and making of the necessary lookups;

- Access of the technical personnel to the Data Base through the use of suitable screens sets on a new

quality base the control of the quality of the technical services in telecommunication nets;

- The regular building-up of data and knowledge about failures enables analysis for finding of segments and elements of the net, which work unreliably and generate failures.

For this purpose Oracle Database was used for a full description of the elements of the telecommunication nets, the alterations in the network and their causes and all data about failures in the nets.

REFERENCES

[1] P. Grogono, A.Preece, R. Shinghal, and C.Suen. Evaluation of expert systems in telecommunications. Expert Systems with Applications, 5(2/3), 395-401,1992

[2] A. Katel, Magdi N. "A Prototype Rule Based Front End Expert System for Integrity Enforcement in relational Data Bases', Expert Systems with Applications: An International Journal 8(1),1995

[3] P. Gray, A.Preece, N. Fiddian, W. A. Gray, t. Bench-Capon, M.Shave, N.Azarmi, M.Wiegand e al. Knowledge Fusion from Distributed Databases and Knowledge bases. Eighth International Workshop on Database and Expert System Applications (DEXA-97), pages 682-691, IEEE Press, 1997

[4] Beck A., Usage Specification and Statistical Testing, Alcatel Telecommunications Review, 1, 1999

[5] Dodd A.Z., The Essential Guide to Telecommunications, New York, Printice-Hall, 2000

[6] Labbe T.,A.Mohammed, J.P.Streck, M.V.Vouk, Alcatel – North Carolina State University virtual laboratory for end_to_end quality of service (QoS) engineering, Alcatel Telecommunications Review, 3,2001, pp. 227-230

A Global Concept for Remote Railway Digital Video Surveillance

Ivaylo P. Topalov[1] and Borislav P. Avramov[2]

***Abstract* – An investigation of the technical possibilities to create railway digital video surveillance system based on united network conception with GSM-R is done. For that reason a different computers, telecommunication and fail-safe technologies are applied, the software and hardware requirements are discussed.**

***Keywords* – GSM-R, digital video surveillance, railway.**

1. INTRODUCTION

In recent years the digital signal processing became a main direction in developing of the video surveillance systems. The digital video recording (DVR) is playing the leading role in expansion of safeguard systems using the last technologies.

The nowadays development of a rail transport in Bulgaria and Europe leads a speed increasing and the relevant developing of a fail-save control systems. They can be improved by implementation of a different computer and telecommunication technologies such as digital video surveillance and digital wireless communication.

From the beginning of 90-ty years the Europe UIC started standardization based on investigation of an applied digital radio communication. Experts from 32 European railways administrations signed a memorandum for agreement on GSM-R technology and developed the project named EIRENE [1]. An elaborated catalogue of requirements was developed based on the ground of the executing MORANE project [2]. The new system is already tested to confirm all requirements up to 500 km/h. A frequency band with 19 canals around 900MHz is reserved for GSM-R voice communication and fail-safe ETCS data transmission [3]. Some of the most common user's services available on GSM and ISDN networks were accepted in GSM-R railway radio systems [4] [5]. Such communication platform gives the opportunity to elaborate a mobile digital video surveillance system to observe the railroad, trains traffic and station platforms [6] [7].

2. DIGITAL VIDEO SURVEILLANCE (DVS) TECHNOLOGY

The DVS is a PC based network observation system recording still or moving images in a specified area. Using the network browser a selected users can remotely monitor in a real time through the network different TV-cameras and clips. The selected event will send an alarm request to the control centre alerting the safeguard and /or will swiftly send a message. It can also record the event in an audio/video file. Other useful functions are [6] [7]:

Motion detection to save time for data retrieval;

Wavelet compression for better image quality;

Programmable multiple detection zones for each camera;

Point-to-point or multicast transmission of live video via Internet/LAN;

Web-based user interface for easy operation;

Send message to monitoring units or communication devices when detect event;

Motion detection, Round-the-Clock, or by Schedule recording mode;

Interaction with UPS device;

Multiple passwords to view permitted cameras;

Playback while monitoring;

Remote playback, remote recording;

Unlimited users view from remote without taking extra bandwidth (LAN).

Using standard for unified voice and video compression MPEG-4 the coded files are up to 300 times less then original. It is possible a video frames to be transferred through the computer network and via telecommunication canals and base station to reach a wireless terminal.

To guarantee authentication and the security of the sent images like digital copiers a digital watermarking is available for application. Special software marks the unvisible points onto the video image and so the specific point constellation should be detected in the received end. The advantages are three:

- Elimination of the opportunity the frame passing through the INTRANET or INTERNET to be fake;
- The recorded video information with actual date and time can be used as a piece of evidence;
- The point's constellation is put into every frame leads to increasing of the data reliability and authentication of the observed screen image.

The system controls simultaneity a lot of video servers and is possibly to interact with other information systems in a network environment. For an example if a request for video processing is received from local computer video control (LCVC) but is not serviced, it will be forwarded to the next free server.

[1]Ivaylo Penev Topalov, is with the Department of Communication and Railway Signalling Engineering in Todor Kableshkov Higher School of Transport. 158 Geo Milev Street, Sofia 1574, Bulgaria. E-mail: ivo_topalov@hotmail.com

[2]Borislav Petrov Avramov, is with the Department of Communication and Railway Signalling Engineering in Todor Kableshkov Higher School of Transport. 158 Geo Milev Street, Sofia 1574, Bulgaria. E-mail: b.avramov@vtu.bg

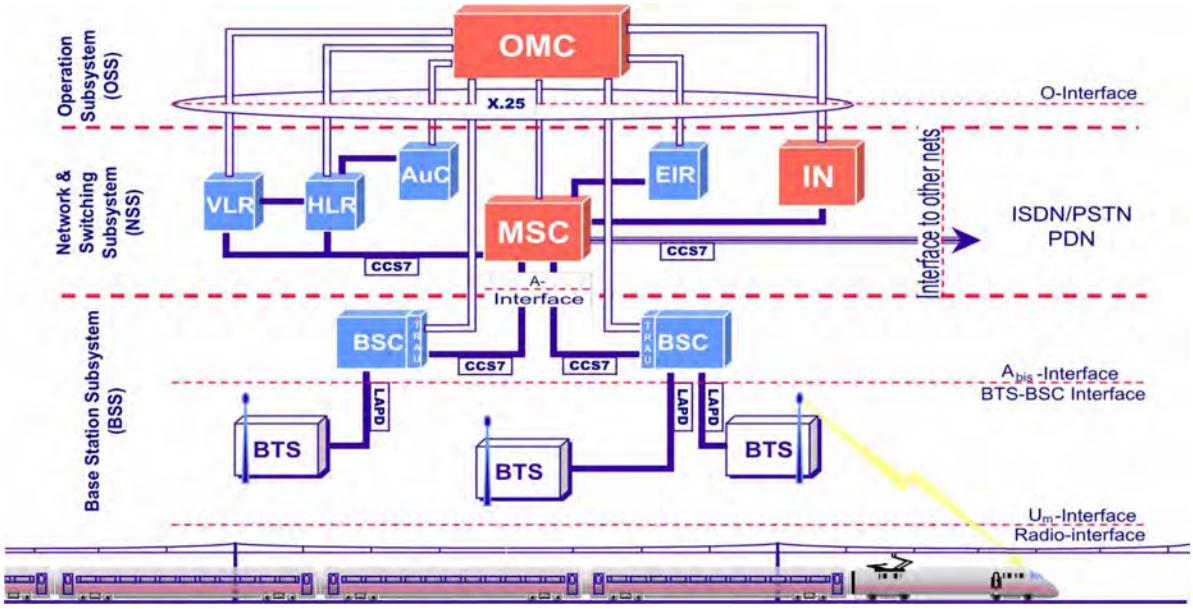

Fig. 1. GSM-R Architecture

3. GSM-R NETWORK PLATFORM

GSM-R is a railway radio communication system using different information processes and personal for transmission of high reliable data to control the railway traffic. Signal information from and to the trains is directed to the locomotive drivers such way that on future developing of the system will be possible to implement an automatic train control (ATC) system. This shows the direct dependence of the railway traffic from the specifications of radio communication platform to support end-to-end secure communication [4].

3.1. Specific fail-safe requirements.

To guarantee the necessary fail-safe requirements in radio communication and signalling control systems on GSM-R in some network elements a hardware redundancy is applied. The physical connection from the fixed network to the wireless interface is with extended accessibility and reliability compared with common use systems. So in the whole accessibility of the system the weakest section in the chain is critical for the security and every element of the structure is reliable weighted. To guarantee the reliability requirements for an outdoor work the minimal received level on the train cab should be better than -85 dBm and the electromagnetic cover probability should be better then 95% along any GSM-R section. The accessibility of the transmission canal in the network should be better then 98.5%. So the train radio transmitters and the receivers should be hot reserved.

To provide the software reliability a special algorithm for system errors processing and remote control diagnostic is applied. In case of partial malfunction the reserved units will support only the main user and test functions. The application of routers with physical and software redundancy is another media sets to reach high accessibility and reliability.

Network elements such as MSC, BSC and BTS would be connected with reliable digital connections through copper or fibre optic cables. The maintenance and control in GSM-R network is organized from network management centre (NMC) or network operation maintenance centre (OMC) [7].

3.2. Evolution of Radio data transfer.

GSM-R supports most of standard GSM user's sets of voice and data services and the decreased number of canals in cells gives the opportunity of high quality High Speed Circuit Switched Data transmission (HSCSD) [9]. So it's possible to transmit near real time a video frames from the railway path to the locomotive cab in a united digital data stream. It will prepare the ground for the next step in GSM evolution – Enhanced Data rates for Global Evolution (EDGE).

4. GLOBAL CONCEPT FOR REMOTE RAILWAY DIGITAL VIDEO SURVEILLANCE.

4.1. Futures and requirements.

The design of the DVS system as a network configuration is based on a structure characteristics of GSM-R communication platform [4]. So that way is possibly to implement a universal radio data transmission system with soft control and multifunctional services of the whole transport processes and will decrease the maintenance expenses of railway equipment. To improve the safety traffic condition only the forward directed pictures are transmitted to the second driver in locomotive cab [10]. The implementation of widely used standards allows utilization of cheaper and worked off technologies. Additional price discount can be achieved by adoption the existing network software.

On Fig. 2 the general scope for railway remote DVS application is given. The traction surveillance control is a conventional computer based network system connected by a copper or fibre optic cables. It collects and records in DVS centre the video clips of the real railroad traction near the dangerous path points. Only a vehicle movement activates the cameras and the OMC/NMC operator observes on terminal the composition traction (Fig. 3).

The passenger terminals control is an integrated security and safety control system. The real time images from station

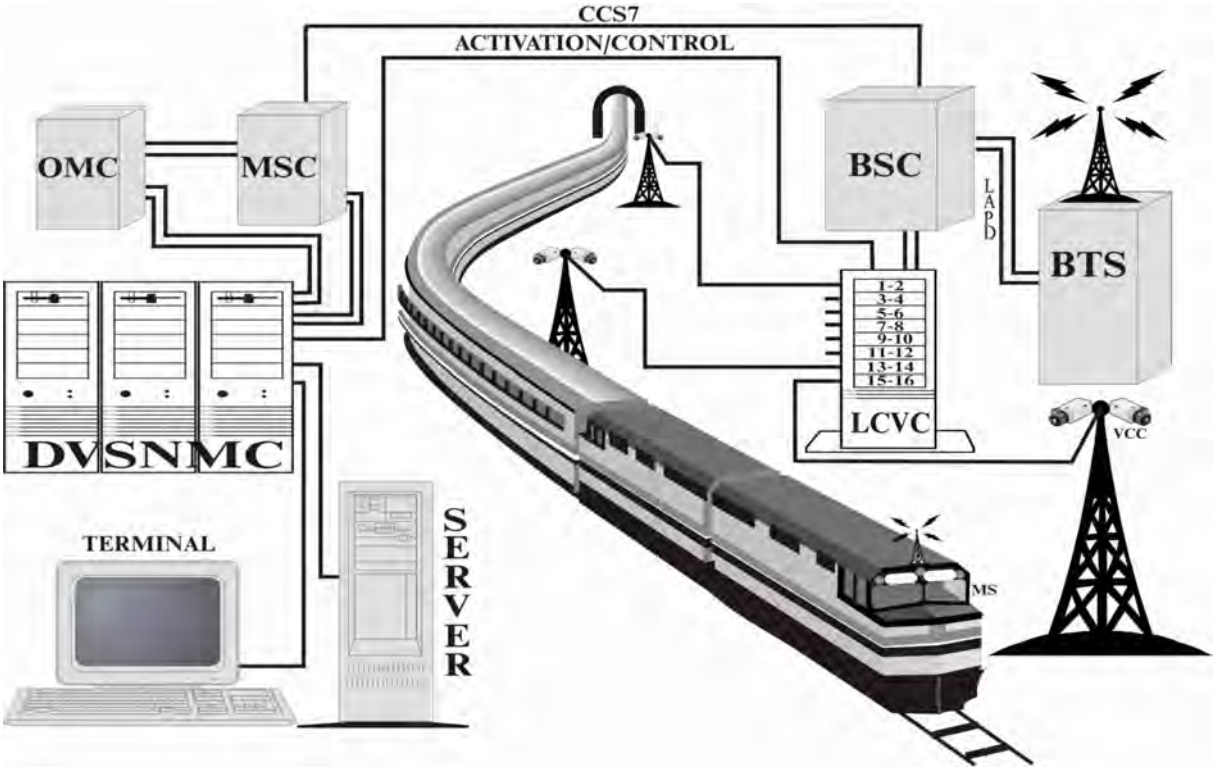

Fig.3: Mobile Concept for Railway Remote Digital Video Surveillance

platform are sent simultaneously to the railway dispatcher, security guard and to the departing/arriving train driver. Meanwhile the video information not concerned with the security or a movement is not available for routing without permission. The wireless transmission uses the reserved in GSM-R HSCSD canals [9]. In case of cell overload the connection returns to a standard data transmission mode with reduced image resolution.

Fig. 2. Global railway DVS solution

The vehicle control is carried out mainly on the train. The local train DVS computer collects data from the wireless cameras, placed inside and outside according to the trainload. The information is at train chef and/or train guard disposal and by needs they send it to the locomotive cab. The DVS dispatcher can retrieve it by the GSM-R downlink to resolve an arising problem.

4.2. Structure and connections.

The Railway Remote Digital Video Surveillance System (RRDVSS) will contain remote computer part for local two-way video surveillance of railway path and part of server connected via INTRANET (Fig. 3). The (LCVC) will scan the video control cameras (VCC) continuously and will save the compressed data on disk.

On first vision it looked not economically to store such large volume of information, but the coded images takes only about 150MB per day. Simultaneity with the recording the video data the information will be send to the Digital Video Surveillance Network Management Centre (DVSNMC). By using the wire interconnection in GSM-R network the time delay of the video packets will be less then one second.

Along the railroad, communication points should be arranged to connect the LCVC to the fixed GSM-R network. The connection between BSC and LCVC should be organized by ISDN links with LAPD. LCVC is necessary to be fixed nearly BTS and using the resources and functional redundancy of the system. Some of the temporary unused canals should be directed to LCVC.

The compressed information from VCC should be transferred to the DVSNMC. DVSNMC is controlling the video services according to the railway traffic and sends a command to the appropriated VCLC to transmit the local frames in BTS with actual date and time. Using the GSM-R radio canales the video frames are reaching the locomotive receiver connected to the mobile computer terminal (MCT) and the actual pictures from the forward path are displayed. For that purpose a work canal is reserved for uninterrupted data transfer with conformation. According to the fact that the GSM data stream is limited to 9.6kb/s [4] [5] is felicitous to work with packets containing the complete images in JPEG format. To constrain the unused data stream in cases of not passing locomotives along observed railroad is necessarily to elaborate train position software. Such program will be reading the actual cell position of MT from HLR and this allows sending the observed picture according to the train speed and direction. Meanwhile the images with the train composition movement taken from the backwards TV-

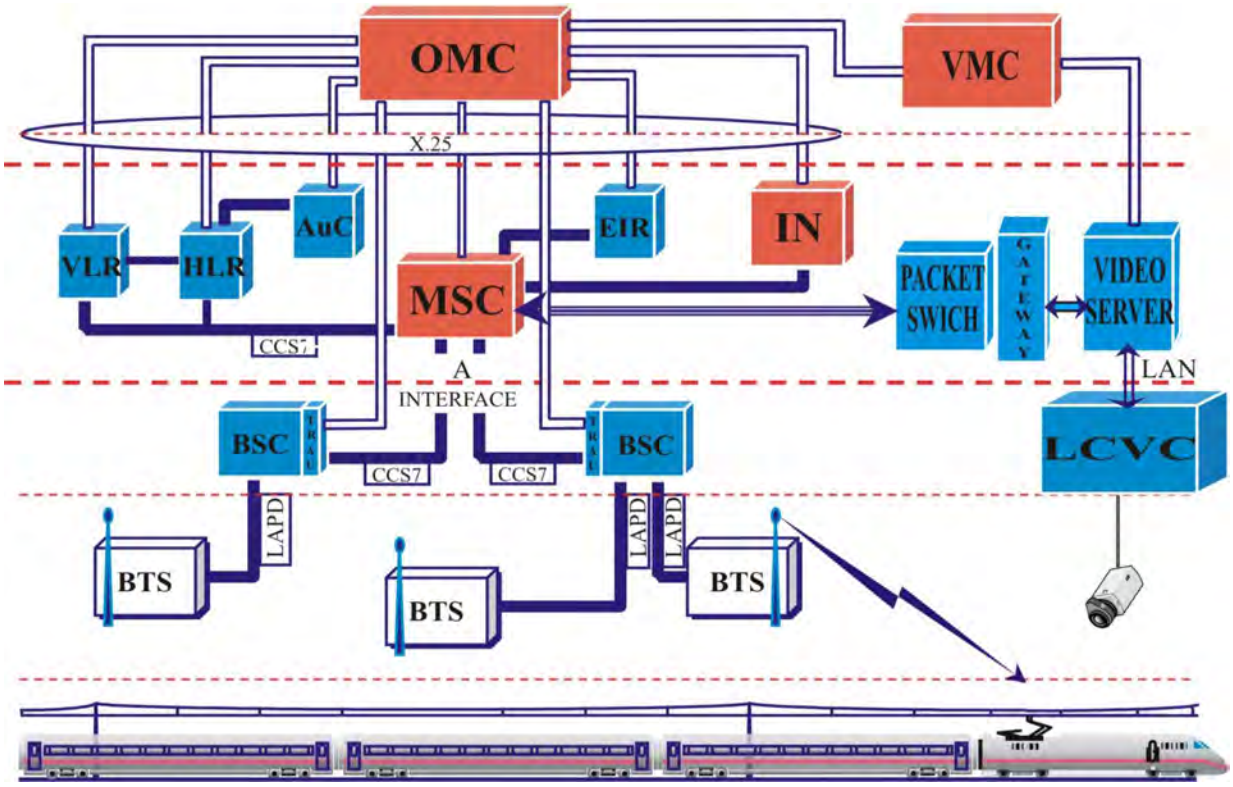

Fig. 4. GPRS video data transfer over GSM-R network

cameras will be transported to DVSNMC and in case of need it will e transferred in locomotive cab. The beginning of the digital recording ought to start from motion detection program after that the clip will be saved on the system server. In the same manner will be treated the transferred to the MCT and confirmed with reports frames. To guarantee authentication of the received data an installation on LCVC a digital watermarking program is needed and only the checked frames should be transmitted. In case of disparity the clip should be rejected and an alert command would be send to the DVSNMC terminal.

CONCLUSION

An investigation of the possibilities to implement a GSM-R global concept for remote railway digital video surveillance based on unified optical and wireless network is done. For that reason a different computers, telecommunication and fail-safe technologies are combined, so the appropriate software and hardware requirements are discussed. As a result, the highlight features of Global Mobile Concept for Railway Remote Digital Video Surveillance are described. The necessary structure was analyzed and some figures pointed out the practical realization of RRDVSS project on already builded GSM-R network can be realized on available price. The nowadays GSM data transfer technology can be enhanced with HSCSD to approach a real time remote observation.

The periodical received frames in locomotive cab from the railway path and the train composition will decrease the risk of arising incidents. By that time such situations are unavoidably in case of limited visibility and/or vehicle brake length.

And something more - the continuous video frames data transmission is convenient for calculation of BER and block errors to give a statistical base for reliability evaluation.

REFERENCES

[1] EIRENE Draft System Specification, version 7.0 UIC EPT, 1996.

[2] MORANE Sub-System Requirements Specification, A 04/02 T 6002, 1996.

[3] HÖRMANN, Digitales Betriebsfunknetz, Machbarkeitsstudie für Planung, Errichtung und Betrieb eines digitalen Betriebsfunknetzes auf Grundlage des GSM-Standards für Eisenbahnen Entwurf, 2000.

[4] TS-GSM 01.02 European digital cellular telecommunications system (Phase 2): General description of a GSM Public Land Mobile Network (PLMN).

[5] TS-GSM 09.02 European digital cellular telecommunication system (Phase 2) Mobile Application Part (MAP) specification.

[6] Topalov I., B. Avramov, Izsledvane na vasmojnostite za distancionno nabludenie na jp dvijenieto po GSM-R mreja, Telecom 2002, Varna, Bulgaria, 2002.

[7] Topalov I., B. Avramov, Osobenosti na terminalnite ustroistva za GSM-R slujebni komunikacii, XII Nauchna konferencia s mejdunarodno uchastie “TRANSPORT 2002”, vol. 1 pp. 479-484, Sofia, Bulgaria, 2002.

[8] Topalov I., B. Avramov, Isledvane vasmojnostite za GPRS prenos na video kadri po GSM-R mreji, Telecom 2003, Varna, Bulgaria, 2003.

[9] Topalov I.P., B.P. Avramov, Mobile Concept for Railway Remote Digital Video Surveillance, “INFOTRANS 2003, Pardubice, Chech Republic, 2003.

Study Of The Genetic Algorithm – Parameters In Telecommunications Network Planning Process

Aleksandar Tsenov[1]

Abstract: **The Genetic Algorithm is a heuristic approach witch is being used in wide areas of optimization works. In the last years this approach is also widely implemented in Telecommunications Network Planning. In order to solve less or more complex planning problem it is important to find the most appropriate parameters for initializing the function of the algorithm.**

There are six important parameters of the Genetic Algorithm witch define the normal and successful function and the obtaining of optimal decisions of the problem – Number of individuals in the initial population, number of populations in the process, usage of mutation, usage of additional local search, type of selection and type of replacement of the individuals. The variation of each of them causes different results.

The goal of this work is to define the optimal values of the parameters in dependence of the problem witch must be solved.

I. INTRODUCTION

The problem of optimally designing a network in order to meet a given set of specifications (such as prescribed traffic requirements, achieving a desired level of reliability, respecting a given maximum transit time), while minimizing total cost, arises in a wide variety of contexts: computer networks, telecommunications networks, transportation networks, distribution systems.

Network design algorithms draw an increasing amount of attention nowadays. Considering the complexity, high cost factor and fast deployment times of today's communications systems (such as IP and ATM backbones, optical networks, numerous types of access structures etc.), network operators can benefit a lot from the use of network design tools.

These tools can help speeding up and 'automating' the design process, ensuring superior quality (i.e. lower cost and/or better Quality of Service) and more justifiable solutions. Network design tools typically incorporate a wide range of functionality, such a geographical database handling, traffic estimation, link dimensioning, cost calculation, equipment configuration databases etc.

The real benefit of using these tools, however, comes from the possibility of using the algorithmic network optimization approaches. In this way, there arises a possibility for finding solutions of better quality in much shorter time, as compared to the manual network design.

II. PARAMETERS OF THE GENETIC ALGORITHM

Initial Population

The genetic algorithm begins by creating a random initial population. There is very important to obtain the optimal number of individuals in the initial population in order to:

- give the algorithm enough genetic material for creating "fit" offsprings;
- reduce the working time by finding the optimal solution of any problem.

The number of the individuals depends in most cases of the representation of the problem and of the number of the genes in the chromosome.

Number of Populations

The number of populations in the algorithm is also important for finding the best solution of a definite problem. This number must be large enough to obtain the optimal solution, and at the same time it must be not too large, because of the computing time and the production of too many unused solutions. The number of population depends of the complexity of the problem.

Selection

The selection method determines how individuals are chosen for mating. If you use a selection method that picks only the best individual, then the population will quickly converge to that individual. So the selector should be biased toward better individuals, but should also pick some that aren't quite as good (but hopefully have some good genetic material in them).

In selection the individuals producing offspring are chosen. The first step is fitness assignment. Each individual in the selection pool receives a reproduction probability depending on the own objective value and the objective value of all other individuals in the selection pool. This fitness is used for the actual selection step afterwards.

The most popular selection schemes are:

- rank – based assignment;
- roulette wheel selection;
- tournament selection;
- stochastic remainder sampler;
- stochastic uniform sampler.

Some of the more common methods include roulette wheel selection (the likelihood of picking an individual is proportional to the individual's score), tournament selection (a number of individuals are picked using roulette wheel selection, then the best of these is (are) chosen for mating), and rank selection (pick the best individual every time). Threshold selection can also be effective.

Replacement

Replacement schemes are used by genetic algorithms with overlapping populations to determine how the new individuals will be assimilated into the population. Replace-worst and replace most-similar are the only really useful replacement schemes. Sometimes replace-parent can be effective, but usually when the parents are similar to the offspring, and this is just replace-most-similar.

[1]Aleksandar Tsenov is with Telecom Department at Technical University of Sofia, "Kliment Ohridsky Blvd 8, 1756 Sofia, Bulgaria, E-mail: akz@tu-sofia.bg

The most popular replacement schemes are:

- replace worst;
- replace best;
- replace parent;
- replace random;
- replace most similar (crowding).

Mutation

The mutation is the recombination operator, which randomly changes the value of a separate gene in the chromosome. This appears with a low probability. The probability of the mutation must be chosen very carefully because of two reasons: if too high the algorithm will operate with non stabile genetic material, and if too low – the algorithm will achieve too rapidly a limited decision, without using the whole genetic material in the generations.

Local search

The local search by applying the genetic algorithms includes an estimation if the effect of small changes over the decision – if a change leads to a better result, it will be accepted, if not – the change will be rejected. There are two possible strategies for realizing the local search in the network planning:

- exchange of customers between nodes;
- exchange of the node, serving a group of customers.

III. EXPERIMENTAL METHOD

In order to find the most appropriate application values of the parameters two experiments were made. The planning problem is to find the optimal topological solution for a real town area by applying the following initial requirements:

- the network is a Passive Optical Network;
- the network to be optimized is a three level network – primary nodes, secondary nodes (splitters) and end nodes (customers);
- the problem is of type UCPL (Uncapacitated Concentrator Plant Location) – the splitters have unlimited capacity;
- two primary nodes, located on fixed positions;
- 12 secondary nodes (as a result obtained in [7]), located on positions in the terrestrial infrastructure equipment - ducts;
- 63 end nodes;

The experiments were fulfilled using a application, developed by the author and called PonOpt.

Experiment 1

The experiment includes 8 test by using the following initial conditions:

- Individuals in the initial population – 20, 50, 100, 200, 250, 500;
- Number of populations – respectively 20, 50, 100, 200, 250, 500 for every number of individuals;
- The algorithm were started 50 times for every combination;
- The algorithm was started 50 times for every combination of the algorithms parameters;

The tests performed in this experiment are:

- Test 1 – mutation, random selection, local search, replace parent;
- Test 2 – mutation, random selection, local search; replace – worst (50%);
- Test 3 – no mutation, random selection, local search, replace parent;
- Test 4 – no mutation, random selection, local search, replace worst (50%);
- Test 5 – mutation, best selection (rank-based assignment), local search, replace parents;
- Test 6 – mutation, best selection (rank-based assignment), local search, replace worst;
- Test 7 – mutation, random selection, no local search, replace parent;
- Test 8 – mutation, random selection, no local search, replace worst (50%);

Figure 1 represents the optimal solution obtained with the application PonOpt for experiment 1.

Fig. 1: The optimal topological decision for experiment 1

Table 1 shows the computational results for all the tests. The dark grey fields contain the lower price of the network.

TABLE 1
COMPUTATIONAL RESULTS FOR EXPERIMENT 1

		Mutation	NoMutation	RandSelection	BestSelection	LocalSearch	NoLocalSearch
Replace Parents	20-20	2819.10	2593.98	2818.10	2908.16	2819.10	3838.33
Replace Worst	10	3322.55	2988.13	3322.55	3322.27	3322.55	3973.31
Replace Parents	50-20	2492.76	2214.84	2492.76	2391.93	2492.76	3792.37
Replace Worst	25	2855.21	2413.41	2855.21	2838.81	2855.21	3750.71
Replace Parents	100-20	2436.86	2145.78	2436.86	2445.79	2436.86	3835.41
Replace Worst	50	2458.00	2130.64	2458.00	2409.52	2458.00	3877.40
Replace Parents	200-20	2495.15	2142.16	2495.15	2446.67	2495.15	3820.05
Replace Worst	100	2430.00	2126.39	2430.00	2383.00	2430.00	3739.68
Replace Parents	250-20	2399.72	2140.12	2399.72	2159.17	2399.72	3794.41
Replace Worst	125	2470.89	2086.66	2470.89	2330.00	2470.89	3799.59
Replace Parents	500-20	2332.21	2129.00	2332.21	2106.92	2332.21	3837.88
Replace Worst	250	2349.74	2046.67	2349.74	2277.00	2349.74	3773.53
Replace Parents	20-50	2564.91	2293.60	2564.91	2550.00	2564.91	3569.47
Replace Worst	10	3090.00	2907.84	3090.00	3190.00	3090.00	3627.52
Replace Parents	50-50	2166.04	2021.42	2166.04	2020.33	2166.04	3625.71
Replace Worst	25	2465.00	2224.50	2465.00	2640.00	2465.00	3534.71
Replace Parents	100-50	2030.48	1989.54	2030.48	2004.74	2030.48	3570.57
Replace Worst	50	2109.50	2081.70	2109.50	2203.64	2109.50	3650.02
Replace Parents	200-50	2035.85	1989.54	2035.85	2058.00	2035.85	3593.16
Replace Worst	100	2052.46	2006.44	2052.46	2076.00	2052.46	3660.85
Replace Parents	250-50	2038.85	1989.54	2038.85	2006.77	2038.85	3663.22
Replace Worst	125	2050.84	2014.93	2050.84	2019.77	2050.84	3657.35
Replace Parents	500-50	2024.42	1989.54	2024.42	1990.72	2024.42	3603.02
Replace Worst	250	2016.14	1991.15	2016.14	1989.54	2016.14	3667.54
Replace Parents	20-100	2359.13	2315.27	2359.13	2762.19	2359.13	3281.27
Replace Worst	10	2996.00	3036.31	2996.00	3296.40	2996.00	3457.83
Replace Parents	50-100	2060.33	2044.41	2060.33	2029.34	2060.33	3286.49
Replace Worst	25	2533.86	2354.35	2533.86	2694.07	2533.86	3281.27
Replace Parents	100-100	1992.29	1991.19	1992.29	2030.28	1992.29	3385.00
Replace Worst	50	2080.75	2036.82	2080.75	2096.55	2080.75	3278.06
Replace Parents	200-100	2002.52	1989.54	2002.52	1996.28	2002.52	3362.00
Replace Worst	100	2003.97	2051.59	2003.97	2005.67	2003.97	3375.45
Replace Parents	250-100	1995.82	1989.54	1995.82	2004.96	1995.82	3523.42
Replace Worst	125	2008.37	1989.54	2008.37	2015.47	2008.37	3570.10
Replace Parents	500-100	1998.63	1989.54	1998.63	1993.89	1998.63	3434.00
Replace Worst	250	2001.07	1989.54	2001.07	1990.71	2001.07	3448.16
Replace Parents	20-250	2339.00	2234.00	2339.00	2604.23	2339.00	3179.60
Replace Worst	10	2957.00	2944.31	2957.00	3295.00	2957.00	3541.86
Replace Parents	50-250	2015.01	2030.47	2015.01	2027.47	2015.01	3214.02
Replace Worst	25	2494.61	2445.41	2494.61	2535.46	2494.61	3472.11
Replace Parents	100-250	2000.94	1989.54	2000.94	1999.98	2000.94	3005.65
Replace Worst	50	2009.57	2065.00	2009.57	2121.46	2009.57	3366.99
Replace Parents	200-250	1989.54	1989.54	1989.54	1989.54	1989.54	3112.98
Replace Worst	100	2006.68	2036.97	2006.68	2022.75	2006.68	3232.86
Replace Parents	250-250	1989.54	1989.54	1989.54	1989.54	1989.54	3256.65
Replace Worst	125	1989.84	2015.88	1989.84	1999.55	1989.84	3335.78
Replace Parents	500-250	1989.54	1989.54	1989.54	1989.54	1989.54	3185.96
Replace Worst	250	1989.54	1989.54	1989.54	1989.54	1989.54	3102.45
Replace Parents	20-500	2315.14	2220.00	2315.14	2706.46	2315.14	3291.48
Replace Worst	10	2933.97	3144.50	2933.97	3317.00	2933.97	3581.36
Replace Parents	50-500	2006.65	2008.62	2006.65	2035.38	2006.65	3001.01
Replace Worst	25	2483.53	2561.72	2483.53	2460.20	2483.53	3476.22
Replace Parents	100-500	1989.84	1989.54	1989.84	1989.54	1989.84	3111.22
Replace Worst	50	2004.00	2018.54	2004.00	2122.21	2004.00	3302.56
Replace Parents	200-500	1989.54	1989.54	1989.54	1989.54	1989.54	2999.89
Replace Worst	100	2008.61	2007.97	2008.61	2011.32	2008.61	3105.00
Replace Parents	250-500	1989.54	1989.54	1989.54	1989.54	1989.54	2845.23
Replace Worst	125	1989.54	1995.89	1989.54	1998.96	1989.54	2962.30
Replace Parents	500-500	1989.54	1989.54	1989.54	1989.54	1989.54	2781.94
Replace Worst	250	1989.54	1989.54	1989.54	1989.54	1989.54	2889.31

Figures 2 to 9 show the graphical results for all the tests in experiment 1 – the left side of each figure shows the cost dependence of the number of populations, and the right side – of the number of individuals in the populations.

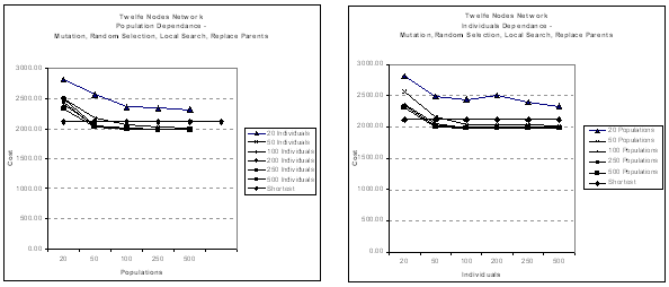

Fig. 2: Experimental results of Test 1

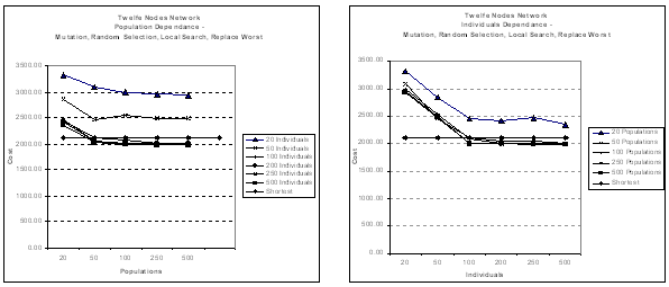

Fig. 3: Experimental results of Test 2

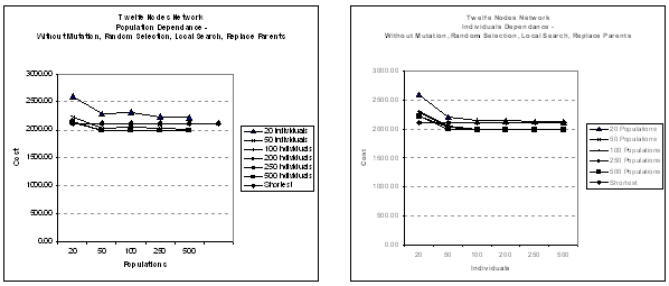

Fig. 4: Experimental results of Test 3

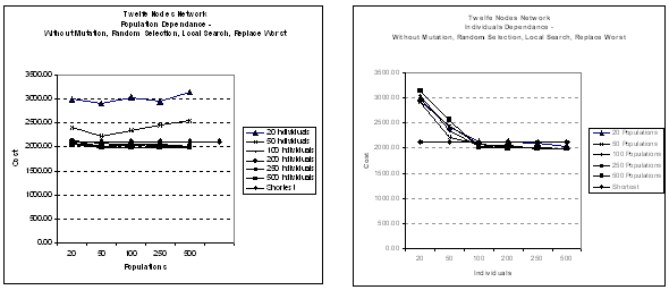

Fig. 5: Experimental results of Test 4

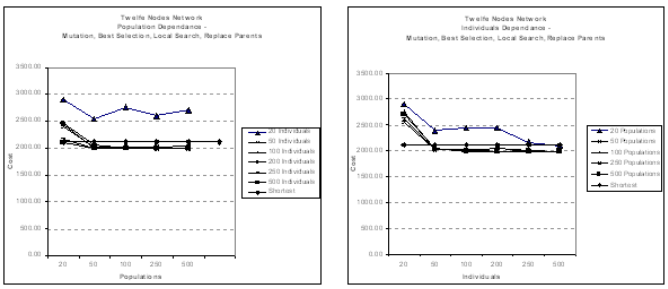

Fig. 6: Experimental results of Test 5

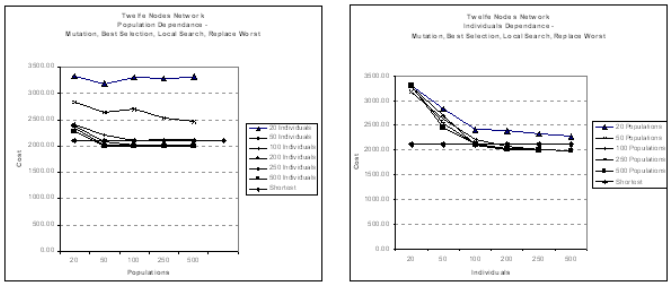

Fig. 7: Experimental results of Test 6

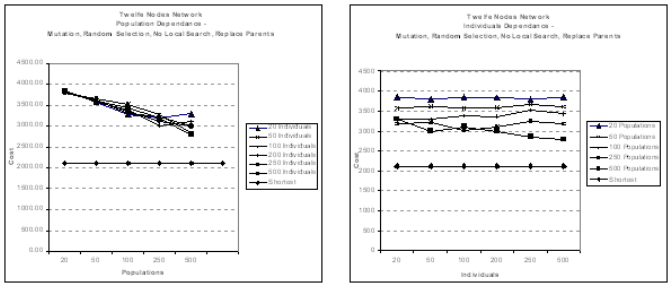

Fig. 8: Experimental results of Test 7

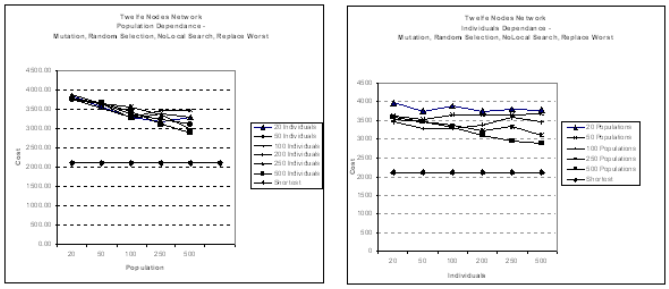

Fig. 9: Experimental results of Test 8

The straight line, presented as "shortest" represents the solution of the problem using the shortest path algorithm. This is shown for a comparison between the algorithms.

The results may be generalized as follows:

- the number of the individuals must be great enough (approximately N*M/2, where N is the number of splitters and M is the number of the end nodes) in order to create a good initial population;
- the number of the populations can be presented by the same mathematical representations – in some cases the algorithm finds the best solution more earlier, but in most cases it needs grater number of populations;
- the local search is very important element of the algorithm – test 7 and test 8 show bed results, especially in cases with small number of individuals;
- the replacement procedure have also an important influence over the results – the parent replacement leads the algorithm a little bit backwards, according to the computational time, the worst replacement makes the algorithm faster, but in some cases not enough reliable – the best solution may be let trough;
- the selection method has no influence on the computational time, but in case of best selection there are too much "bed" solutions in the population.

Experiment 2

The results of experiment 1 give the initial data for experiment 2:

- number of populations – 500;
- number of individuals in the population – 500;
- studied variants:
  - o mutation, random selection, local search, replace parents;
  - o mutation, random selection, local search, replace worst;
  - o mutation, best selection (rank-based assignment), local search, replace parents;
  - o mutation, random selection, no local search, replace parents;

The algorithm was started 10 times per variant in order to find the common and the specific characteristics for each case.

The results are graphically represented on figures 10 to 13.

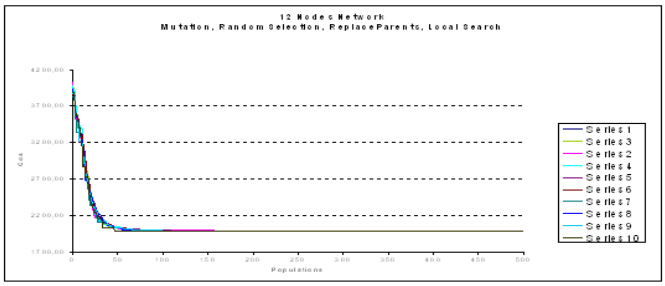

Fig. 10: Experimental results for variant 1 in Experiment 2

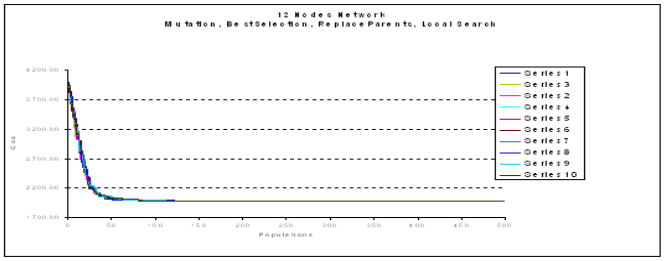

Fig. 11: Experimental results for variant 2 in Experiment 2

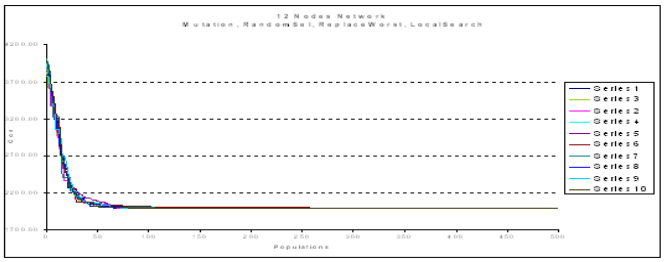

Fig. 12: Experimental results for variant 3 in Experiment 2

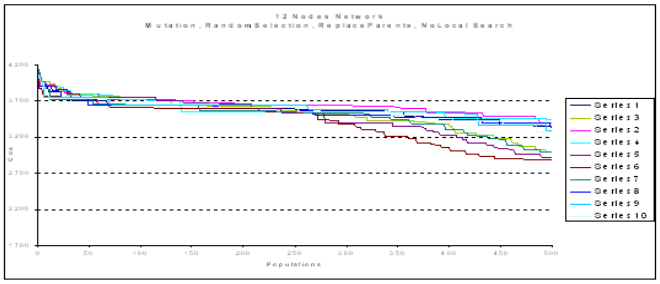

Fig. 13: Experimental results for variant 4 in Experiment 2

IV. CONCLUSIONS

The results of this experimental study can be generalized as follows:

- The number of the individuals and the number of the populations must be at least N*M/2. So there are enough initial solutions, which will be used later for producing of next generations. There is enough genetic material available for obtaining more of the possible decisions and at the same time the algorithm has enough possibilities to reach the best solution;
- There is no possibility to find the optimal solution without applying local search. This is so because the first solution for a single point is accepted, independently of other possible solutions by little local changes;
- The best selection approach leads very fast to the lowest price for a problem, but this is not ever the optimal price. This is because of the great number of "bed" individuals which are manipulated;
- The replace worst approach leads to two disadvantages – first: the computational time becomes longer and second: the used genetic material is limited.

The initialization of the genetic algorithm depends also on the capacity of the network to be planed, of the required computational time, of the required price. The results of this work will be used later for future studies in order to increase the performance of the genetic algorithm for solving of most complex network planning problems.

REFERENCES

[1] Tsenov A., "Presentation of location problems", ICEST 2002, pp. 299 - 302, Nish, Yugoslavia, 2- 4 October 2002

[2] Tsenov A., "Application Of Genetic Algorithms In Access Network Planning", XXXVIII International Scientific Conference ICEST 2003, p. 158-161, Sofia, Bulgaria, (2003)

[3] Routen T., "Genetic Algorithms and Neural Network Approaches to Local Access Network Design", Proceedings of the 2nd International Workshop on Modeling, Analysis and Simulation of Computer and Telecommunications Systems, 1994

[4] Kratica J., V. Filipovitch, V. Ljeljum, D. Toljijg "Solving of the Uncapacitated Warehouse Location Problem Using a Simple Genetic Algorithm", Proceedings of the XIV International Conference on Material handling and warehousing, 3.33-3.37, Belgrade, 1996

[5] Kratica J., "Improvement of Simple Genetic Algorithm for Solving the Uncapacitated Warehouse Location Problem", Proceedings of the 3rd On-line World Conference on Soft Computing (WSC3), 1998

[6] P. Chardaire, A. Kapsalis, J.W. Mann, V.J. Rayward-Smith and G.D. Smith, "Applications of Genetic Algorithms in Telecommunications". In J. Alspector, R. Goodman, T.X. Brown (Eds.), Proceedings of the 2nd International Workshop on Applications of Neural Networks to Telecommunications, pp. 290-299, 1995

[7] Tsenov A., "Concentrator location using Simulated Annealing" , Electronics & Electrotechnics, ISSN 0861-4717, issue 5 -6, p. 10 - 15, 200

Study of the Simulated Annealing – Parameters in Telecommunications Network Planning Process

Aleksandar Tsenov[1]

Abstract: **The Algorithm of Simulated Annealing unifies the local search algorithms. In addition – Simulated Annealing allows acceptation of moves in the search space witch lead to decisions with higher cost in order to attempt to overcome any local minima obtained.**

There are four important parameters of the Simulated Annealing Algorithm witch define the normal and successful function and the obtaining of optimal decisions of the problem – Initial temperature, temperature coefficient, number of iteration on each step and stop criterion. The variation of each of them causes different results.

The goal of this work is to define the optimal values of the parameters in dependence of the problem witch must be solved.

Keywords: ***Simulated Annealing, Network planning, Concentrator location problems***

I. INTRODUCTION

Planning of telecommunications networks

The planning of telecommunications networks can be defined as follows: it must be realized the functionality of the lower 4 levels of the OSI (Open System Interconnection) reference model by fulfilling the necessary and preliminary specified technological requirements [1] [4].

These are the function which realize: the physical connectivity between the networks and between the subscribers and the network; the procedures for reliable transfer of information and signalization; the establishment, the control and the release of the connections in the network; the logical connection and the transfer of separate information blocks.

According to some works [4] there are 4 stages in the network planning process:

- building the topological structure;
- synthesis of the network;
- traffic load assignment;
- realization.

The four stages define an iterative process which has to find an optimal solution for a predefined cost function according to the geographical network plan.

The cost function may be defined in conformity with several network characteristics – realizations cost, life cycle cost, connection lengths, reliability.

Location – Allocation problems

On the first stage of the planning process the telecommunication equipment must be located and the customers must be allocated.

[1]Aleksandar Tsenov is with Telecom Department at Technical University of Sofia, "Kliment Ohridsky Blvd 8, 1756 Sofia, Bulgaria, E-mail: akz@tu-sofia.bg

The one possible way to find an optimal decision for this problem is to use cheaper communication equipment. In most cases this equipment consists of simple multiplexers - concentrators. This leads to the idea of implementing of optical technology in the concentrator networks. One possible solution is the so called PON (Passive Optical Network) [2]. The problem is – an appropriate hierarchical structure of the network to be proposed.

There are many known concentrator location problems. One of them is the UCPL (Uncapacitated Plant Location) problem, which will be used in this work.

UCPL

The mathematical model of UCPL is as follows [6]:

$$\min \sum_{i \in I} \sum_{j \in J} c_{ij} x_{ij} + \sum_{j \in J} f_j y_j \qquad (1)$$

$$\sum_{j \in J} x_{ij} = 1 \qquad (2)$$

$$x_{ij} - y_j \le 0, \qquad i \in I, j \in J \qquad (3)$$

$$x_{ij} \in \{0,1\}, \qquad i \in I, j \in J \qquad (4)$$

$$y_j \in \{0,1\}, \qquad j \in J \qquad (5)$$

where:

I is the location area;

J is set of sub areas for location of the concentrators, while $J \in I$;

C_{ij} is the cost function – it represents the cost for connecting the end node i to the concentrator j;

f_j is the cost for connecting the concentrator j to a node from the higher network level.

For the parameters x_{ij} and y_j may define:

$x_{ij} = 1$, when end node i is connected to concentrator j;

$x_{ij} = 0$, when end node i is not connected to concentrator j;

$y_j = 1$, when concentrator j is located;

$y_j = 1$, when concentrator j is not located;

The equation (1) guaranties the connectivity of one end node to one and only one concentrator. The equation (2) defines the connection of end node I to concentrator j only when the concentrator j exists.

Simulated annealing

The algorithm of the Simulated Annealing (SA) is an approach that integrates most of the local search algorithms [3]. These algorithms accept the next step only when it reduces the cost. So they reach a local minimum and stop searching.

An essential feature of simulated annealing is that it can climb out from a local minimum, since it can accept worse neighbors at the next step. Such an acceptance happens with a probability that is smaller if the neighbor quality is worse.

The probability of the acceptance can be presented as follows:

$$P\{accept\} = \begin{cases} 1, \text{ if } \Delta \le 0 \\ \exp\{-\Delta/T\}, \text{ if } \Delta > 0 \end{cases} \quad (6)$$

Δ is the cost change, and T is a control parameter that is called temperature.

The algorithm of SA has the following form:

```
Begin
  Initialize   T, Nt, Ni, s;
  for temperature step = 1 to Nt do
     for iteration = 1 to Ni do
       generate s';
       Δ = C(s') – C(s);
       if Δ ≤ 0 then
         s = s';        /*P{accept} = 1*/
         else
           s = s' with P{accept}= exp {- Δ/T};
       end if
     end for
   T = T*k;
   end for
End.
```

where:

T – temperature of the process;

Nt – number of temperature steps;

Ni – number of iterations (moves) on each temperature step;

S,s' – solutions;

C(s), C(s') – cost of solutions s and s';

K – cooling coefficient.

There are four problems by the initializing of the algorithm – defining the initial temperature, defining the cooling schedule, defining the number of iterations on each temperature step and stop criterion.

Initial temperature

The initial temperature is very important parameter and must be defined very carefully. When the initial temperature is too high the algorithm will work too long without reduce of cost, specially at the beginning of the process. The too low temperature leads to a very quick end of the process without finding the global minimum of the cost.

Often the initial temperature is being defined intuitively. In this work an optimal value of the temperature for UCPL will be searched.

Cooling procedure and cooling coefficient

In [7] there are three cooling procedures presented.

The simplest one is the geometrical cooling procedure – each next value of the temperature arise by multiplying of the old value with coefficient that is smaller than 1.

The other one is the logarithmic procedure – the new temperature depends on the decreasing speed of the temperature and on the variation of the cost by the old temperature value.

The third one is the so called exponential cooling procedure. The parameters of this procedure are the cost variation and an exponential coefficient.

II. EXPERIMENTAL METHOD AND RESULTS

In this work the initial data for the UCPL are:

- real town area;
- number of end nodes – 63;
- search space – Euclidian area – 200x200;
- three level PON with two primary nodes on fixed locations;
- initial number of concentrators – 2 to 63;
- two variants of the concentrator location – free in the search space and in the existing ducts.

The experiments are made with a computer application written by the author and called PonOpt.

Three series of test were performed in order to obtain the most appropriate values of the most important algorithms parameters. The cost is normalized with a lowest cost value because the optimum is not known.

Test 1 – Finding the optimal temperature for the process

For UCPL the optimal value is being searched between 10 000 and 1 000 000. In comparison with other similar tasks these values are low. This is because of the absence of limits for the capacity of the concentrators. The results of the test are shown on figure 1.

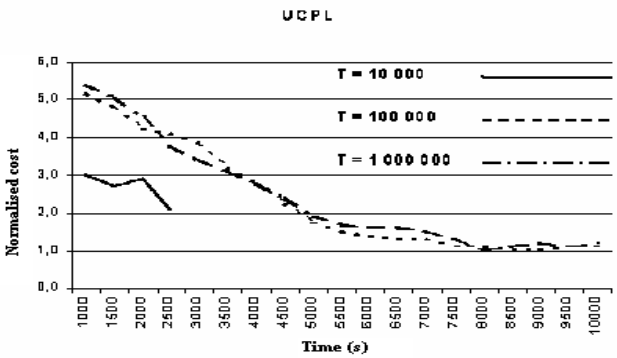

Fig. 1: The experimental results of test 1

By usage of too low temperature the process "freezes". That means – the algorithm reaches a deep local minimum and can not go any farther.

This case is presented with not dashed line on the figure.

For the next tests a value for the temperature of 500 000 is accepted, because, as shown on the figure, the optimal solution is found in very broad bounds of the initial temperature.

Test 2 – Finding the optimal cooling coefficient

The test is performed by using a geometrical cooling procedure. The values are 0.7, 0.8 and 0.9. The results are presented on the Figure 2.

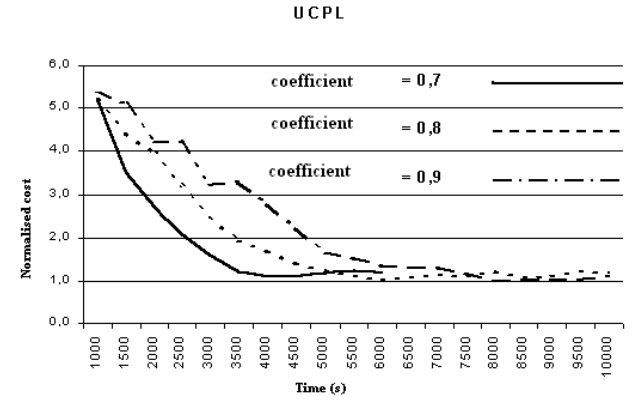

Fig. 2: The experimental results of test 2

The little coefficient value provokes a short working time without finding an optimal solution. The best results are obtained by cooling coefficient 0.9. The working time is practically the same as by coefficient 0.8. It was performed a test with coefficient 9.9 (not shown in this work). The working time is this case were 3 times longer then by 0.9 and the obtained cost was not much better.

Test 3 – Finding the optimal number of iterations (moves) on every temperature step

In order to find the optimal number value a series of tests are performed. The values that were studied are 10, 50, 200, 400 and 600 by initial temperature 500 000 and cooling coefficient – 0.9.

The most general conclusion that can be made is: the grater is the number of iterations the longer works the algorithm because of the large amount of equal solutions and the cost reduction is very slow.

The number of iterations has to be defined in dependence of the number of nodes that must be located and connected and of the search space.

The results of test 3 are shown on figure 3.

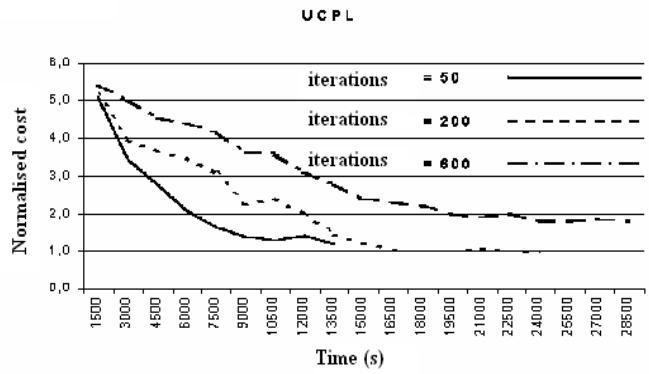

Fig. 3: The experimental results of test 3

The results of a three test are now used for solving the concrete planning problem. The initial structure of the area to be planed is shown as a text map file on the figure 4. There are primary nodes, secondary nodes (concentrators) and end nodes (customers) specified with their coordinates. The algorithm may add or remove concentrator nodes in order to find the better solution. Figure 5 shows the graphical representation on the work screen of the application PonOpt.

```
'Primary node description
'P x        y
'Secondary node description
'S x        y
'Customer description
'Cx         y
'Duct description
'D          x1        y1        x2        y2        ..
'Primary nodes
P 30        195
P 110       45
'Secondary nodes
S 110       45
S 30        195
'Customers
C 130       60
C 150       60
C 230       65
C 120       70
C 160       70
……..……..
C 50        230
'Ducts
D 230       55        230       135
D 220       135       220       240
D 200       85        200       125
D 140       60        140       95
……..
D 90        130       110       90
D 90        135       100       130
D 100       130       200       125
```

Fig. 4: The map file for planed area

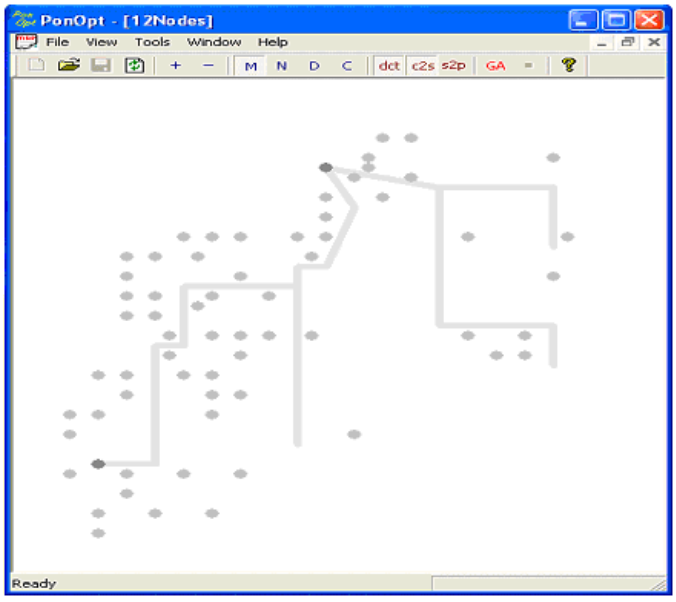

Fig. 5: The graphical presentation of the planed area with ducts

The application was started 10 times with the following parameters:

- initial temperature – 500 000;
- number of iterations – 200;

- cooling coefficient – 0.9.

In 8 of the case one and the same optimal solution was found. That proves the good definition of the initial parameters of the algorithm. The optimal solution of the planning problem is shown on figure 6.

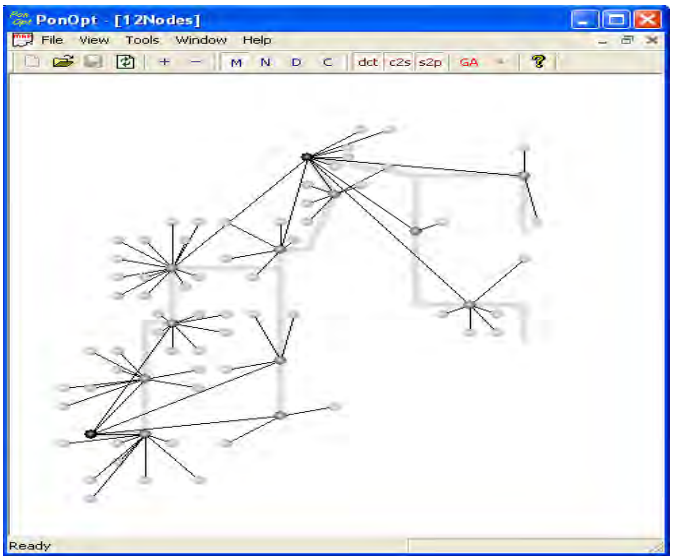

Fig. 6: The optimal solution of the planning problem

III. CONCLUSIONS

The initialization of the algorithm of Simulated annealing is very important in order to find the best solution of any optimization problem. Therefore it is necessary to spend some time to find the most appropriate values of the algorithms parameters.

The results in this work and in some other works make clear that the choice of the initial temperature of the process must give the algorithm the possibility to find the best solution in acceptable time and in conjunction with this to avoid "freezing" of the process or production of too many equal solutions.

From the results is also clear that the cooling coefficient must have a value that in not too low – the process may freeze, and at the same time not too high – the process becomes almost endless and not effective.

The optimal number of iterations on every temperature step depends on the network size and on the type of the problem. For UCPL the number of iterations is approximately equal to N*M*K (where N is the number of the primary nodes, M is the number of the secondary nodes and K is the number of the customers).

One very interesting problem may be to find an appropriate approach for dynamic (adaptive) definition of the main parameters of Simulated Annealing. That might stand for:

- finding optimal number of iterations for every single temperature step in dependence of different constraints (customer density, possible concentrator locations, concentrator capacity);
- finding optimal cooling coefficient in dependence of the results on the last temperature step.

The search for new, nontraditional methods for solving of topological problems in network planning is at the time too new for Bulgaria.

The liberalization of the telecommunications market, the existence of new network operators and their objectives (large number of services with high quality), lead to the applying of more effective approaches and algorithms for realizing of high performance networks. These approaches must be studied in near future according to their applicability in the telecommunications network planning.

REFERENCES

[1] Mirtchev S.T., Teletraffic engineering, TU-Sofia, 1999, ISBN 954-438-235-6.

[2] Aarts E. & J. Korst, Simulated Annealing and Boltzmann Machines. John Wiley & Sons Ltd., 1989.

[3] Aarts E. & J. Lenstra (Eds.), Local Search in Combinatorial Optimization. Wiley & Sons Inc., 1997.

[4] Girard Andre, Routing in dimensioning in circuit – switched networks, Addison – Wesley Publishing Company, 1990, ISBN – 0-201-12792-X.

[5] Kirkpatrick S., C.D. Gelatt Jr., M.P. Vecchi, Optimization by Simulated Annealing. Science, 220, 671-680,1993.

[6] Nurmela K. J., Constructing Combinatorial Design in local Search, Series A: Research Reports, Helsinki University of Technology – Digital System Laboratory, ISSN 0783-5396, ISBN 951-22-1857-7, 1993.

[7] Spears W. M., Simulated Annealing for Hard Satisfiability Problems, AI Center – Naval Research Laboratory, Washington, 1998, D.C. 20375-5320.

[8] Tsenov A., "Concentrator location using Simulated Annealing" , Electronics & Electrotechnics, ISSN 0861-4717, issue 5 -6, p. 10 - 15, 2003

[9] Jшrgensen, N. M., Simulated annealing in FWA-network, Master thesis on Informatics and Mathematical Modelling, TU-Denmark, September (2001)

[10] Pjataev O.W, A.W. Semashko, Formalization of optimization problem for campus networks, Electronic Journal "Studied in Russia", pp. 950-952, (2001)

[11] Orljansky I.W. contemporary approaches and methods of global optimization, Electronic Journal "Studied in Russia", pp. 2097-2108, (2002)

A Modified Approximation Algorithm for the Small Communication Time Scheduling Problem (MAASCT)*

Vassil G. Guliashki[1]

Abstract – **The paper presents a modified approximation algorithm MAASCT, designed to solve the small communication time scheduling problem. The proposed algorithm is a modification of the recently published AASCT algorithm [2], improving its efficiency through reducing the number of computational operations, necessary in the worst case, and saving the same solution quality.[1]**

Keywords **– scheduling, makespan, communication delays**

I INTRODUCTION

The real problems for scheduling a finite number of tasks on limited number of processors require consideration of communication delays between two consecutive tasks when they are not assigned performance to one and the same processor. For convenience it is assumed that a precedence relation between two tasks i and j is available if task i needs data from task j before being started.

The paper considers the problem for making a schedule to perform n tasks on m processors, for which the task duplication is not allowed, the communication between any two processors is possible and the communication delays depend only on the corresponding tasks. The precedence constraints and the processing times are arbitrary. The objective is to find the schedule that minimizes the overall finishing time, or the "makespan". Let ρ denotes the ratio of the greatest communication delay to the smallest processing time and let the greatest communication time between any two different processors be smaller than the processing time, needed for the completion of the smallest task, i. e. $\rho \leq 1$. This problem is known as Small Communication Time problem (SCT problem).

There are surveys studying scheduling problems (see for example [1], [8], [14]), where some theoretical results about this problem are presented. As it is mentioned in [1] Picouleau has proven in 1992 that this problem is *NP*-hard. Jakoby and Reischuk have shown in [7] that the special case with unlimited number of processors and unit processing time is *NP*-hard even when the in-degree of each node is at most two. Using a similar reduction, they also proved that for a binary tree, unit processing times and arbitrary communication times the problem is *NP*-complete. For fixed $m \geq 3$, no algorithms which ensure optimal schedules are known yet. For this reason different kind of approximation algorithms have been developed (see for example [3], [5], [6], [10], [12], [13]). The parallelism of multiprocessor problem in combination with the communication delays causes difficulties at the design of approximation algorithms, because the problem is combinatorial one. The worst-case performance of all of them is as bad as possible (see [5]), especially if a great number of processors are assumed. The performance ratio for the known approximation algorithms varies around 2 and tends to 3 when the number of processors - m is fixed. The best known approximation algorithms for this problem are those presented in [10] and [5] with performance ratio $\frac{7}{3}$, and $\frac{7}{3} - \frac{4}{3m}$ correspondingly. For the problem with unlimited number of processors Hanen and Munier (see [5]) have created an approximation algorithm with $\frac{4}{3}$ performance ratio. The aim of this paper is to present the approximation algorithm MAASCT, which improves the efficiency of the algorithm AASCT [2] by means of some modifications of its steps. The new algorithm also avoids to a great extent the "anomalous behavior", arising when the number of processors increases. The computational time complexity of MAASCT algorithm is $O(\gamma n^2)$.

II PRELIMINARIES

Some symbols are introduced to define the SCT task system. The set of n tasks will be denoted by T and the corresponding processing times by $p_1, \ldots, p_n$. Let $G = (T,E)$ be a directed acyclic graph (DAG). An arc $(i,j) \in E$ corresponds to the data transfer from task i to task j, that occurs after i has been finished and before the start of j. The duration of this data transfer is a constant delay, equal to c_{ij} in case i and j are performed by different processors and 0 if i an j are performed by one and the same processor. The task system $\Im(T, p, G, c)$ is called SCT task system, if the following constraint on the communication delays holds:

$$\rho = \frac{\max_{(ij) \in E} c_{ij}}{\min_{i = 1,\ldots,n} p_i} \leq 1 \qquad (1)$$

[1] Vassil G. Guliashki is with the Institute of Information Technologies – Bulgarian Academy of Sciences, Bulgaria, Sofia 1113, "Acad. G. Bontchev" Street, Bl. 29 A, E-mail: vgoul@iinf.bas.bg, vggul@yahoo.com .

* This study is partly supported by the Ministry of Education and Science - National Science Fund, contract № I-1203 / 2002, Sofia, Bulgaria.

In some cases (see [2], [10]) the SCT system is defined by weaker conditions, but the algorithm presented in section 3 is based on condition (1).

Here is considered the problem of scheduling n tasks of the SCT task system on m processors under condition (1), where n and m are finite numbers.

A schedule $S = (t, \pi)$ assigns a starting time t_i and a processor π_i to each task i, so that

1) for any pair of tasks (i,j) if $\pi_i = \pi_j$, then $t_i + p_i \le t_j$ or $t_j + p_j \le t_i$;

2) for any arc (i,j) of G, if $\pi_i = \pi_j$, then $t_j \ge t_i + p_i$; else $t_j \ge t_i + p_i + c_{ij}$;

3) if m processors are available: $\forall\, i \in T$, $\pi_i \in \{1,\ldots,m\}$.

The makespan of the schedule is denoted by ω:

$$\omega = \max_{i \in T} (t_i + p_i) \qquad (2)$$

The optimal (minimal) makespan is denoted by ω_{opt}.

It will be assumed that the task i precedes task j if there is a path in G from i to j. The task i is called predecessor of j and the task j is called successor of i. This relation will be denoted by $i \rightarrow j$. A task i is said to be an immediate successor (resp. predecessor) of a task j if there is an arc (j,i) (resp. (i,j)) in G. For any task i we denote by $\Gamma^+(i)$ (resp. by $\Gamma^-(i)$) the set of immediate successors, (resp. predecessors) of i. In case one of immediate successors of a task j satisfies the following condition:

$$t_j < t_i + p_i + c_{ij} \qquad (3)$$

j is called the favorite successor of i. It follows from (1) that there is only one favorite successor j of i. Similarly i is called a favorite predecessor of j.

The usual approximation algorithms used for scheduling tasks on m processors, called list scheduling (LS) algorithms, build a schedule by means of a greedy process, that schedules a new task at each iteration. Assuming a partial schedule is already built for the time period $[0,t_{k-1}]$, the greedy algorithm scans each processor to find a task that is ready for it at the moment t_k and if any, to assign to it the first ready task in the list at this moment. Graham (see [3]) has proposed such algorithm for the problem without communication delays. For this case he obtained the performance ratio $\omega/\omega_{opt} = 2 - \frac{1}{m}$. Rayward-Smith has shown in [13] that any list scheduling algorithm with unit execution times and unit communication times (UET-UCT) satisfies $\omega < (3 - \frac{2}{m})\omega_{opt} - (1 - \frac{1}{m})$.

When general communication delays are considered (not necessarily SCT), an extension of the usual schema has been proposed [6], called ETF (i.e. earliest task first) that can be outlined as follows:

While there remains an unscheduled task, the set of ready tasks R (the predecessors of which have been already scheduled) is determined. Then for each couple (i, π), $i \in R$, $\pi \in \{1,\ldots,m\}$, the earliest starting time of task i on processor π, denoted by $e(i, \pi)$ is computed. Then the earliest starting time $e = \min_{(i,\pi)} e(i, \pi)$ is determined and a task i, for which there is a couple (i, π) with $e(i,\pi)=e$ is chosen and scheduled at time e. Finally a processor, for which $e(i,\pi)=e$ is assigned to i.

The ETF algorithm is analyzed in [6] and its performance ratio has the following bound: $\omega/\omega_{opt} \le 2 - \frac{1}{m} + \rho$.

As commented in [5] and [6] the relative performance of ETF can be decomposed in two parts. One of them is the Graham's bound $2 - \frac{1}{m}$ and the other is the contribution of communication delays along a path of the graph, i. e. the ratio ρ. The time complexity of ETF (see [6]) is $O(mn^2)$.

Hanen and Munier [5] proposed an approximation algorithm called FS, based on an algorithm for unlimited number of processors and on a modification of ETF algorithm. They have proved that the performance ratio of their algorithm has the following worst-case bound:

$$\omega/\omega_{opt} \le \frac{4+3\rho}{2+\rho} - \frac{2+2\rho}{m(2+\rho)} .$$

Möhring, Schäffter and Schulz [10] proposed another approximation algorithm, that is simpler than the algorithm in [5]. They first compute a schedule that regards all constraints except for the processor restrictions. This schedule is then used to construct a provable good feasible schedule for a given number of processors and as a tool in the analysis of the algorithm. The performance ratio of this algorithm is: $\omega/\omega_{opt} \le \frac{7}{3}$. In the next section is presented an approximation algorithm that in contrast to the above mentioned algorithms not is not based on a greedy procedure.

III THE MODIFIED APPROXIMATION ALGORITHM FOR THE SMALL COMMUNICATION TIME PROBLEM (MAASCT)

The algorithm MAASCT like the algorithm in [2] is based on the idea, that the arcs (i,j) of G having great c_{ij}–values should connect tasks performed by one and the same processor. In this way the tasks become favorite successors and the great delays are eliminated, which leads to reducing the greatest processing time and minimizing the makespan.

At the first step of MAASCT a consequence of tasks (chain) is constructed, beginning with the root of the spanning tree of G, so that to the current task i is added the task j for which the c_{ij} –value is maximal. In case there are many arcs having one and the same c_{ij} –value, then task j, for which p_j is maximal, is chosen as a next in the chain under composition. If there are many tasks, having one and the same processing time, then the task with smallest index is chosen. In case the current chain is composed (i.e. no more tasks can be added to it), the chain is assigned to the next processor in the list of idle processors. If there is not available idle processor, then assign the composed chain to the first processor which becomes idle. In case the starting task of the current chain needs data transfer from a task assigned to another processor, the corresponding

communication delay should be added. A new graph G' is created by removing all tasks in this chain from G. Then graph G is replaced by G' and this step is repeated until no more tasks are available for composing new chains.

At the second step the starting times for each task are calculated. At the third step are computed the finishing times for all processors. At the fourth step the processor with greatest finishing time (equal to the makespan) is determined. At the fifth step an attempt is made to rearrange the tasks on each processor in order to reduce the finishing times and the makespan. At the sixth step the replacing of groups of tasks on different processors is checked in order to reduce the makespan. At the seventh step an attempt is made to rearrange the places of tasks on the processor with greatest finishing time, trying to assign the last task on it to another processor and to reduce the makespan. Almost at each step $O(n)$ mathematical operations are performed. Steps 3÷5 may be repeated n times, and steps 2÷6 may be repeated γ times, where γ is a small positive integer. Hence there are necessary $O(\gamma n^2)$ mathematical operations for the performance in the worst case.

Step 5 and step 6 are modifications of step 3 and step 2 in AASCT algorithm (see [2]) correspondingly. Step 1 is the same as in the AASCT algorithm.

Description of MAASCT:

Step 0. Initialize $G' \equiv G$, $T' = T$, $n' = n$, s' is an empty chain. Set $icount = 0$ and $ic = 0$.

Step 1. Chose an initial task i from T' (the root of G') and add it to the current chain s'.
For j=1,…,n'; ($j \neq i$, $i \in s'$) add the task j to s', where $c_{ij} = max_{ij \in E'} \{ c_{ij} \}$. If there are many arcs (more than one), having the same c_{ij}-values, add the task j, having greatest p_j, to s'(or if there are many tasks with the same p_j, add the first j in the list to s').
Repeat the **For** cycle until there are not available successors of the last task in the chain.
If there are idle processors available, assign the chain s' to the first processor π in the list of idle processors, otherwise assign s' to the first processor, which will become idle.
Remove all task in s' and their connecting arcs from G'. Initialize s' as an empty chain.
Repeat Step 1. until there are no more unassigned tasks .

Step 2. Compute the starting time t_i for each task i on π_j as follows: $t_i = \max(f_k + c_{ki})$, where f_k are the final times for the tasks $k \in \Gamma^-(i)$ and k not assigned to π_j.

Step 3. Compute the finishing time for each processor π_i, (i=1,…,m;).

Step 4. Find the processor π_g, having the greatest finishing time T_g after processing all tasks assigned to it.

Step 5. On each processor π_l, (l=1,…,m;) rearrange all tasks, having one and the same predecessor in such order, so that the task with the smallest starting time t_i is performed first, then the task with next greater t_j *value* and so on to the task having greatest starting time t_k. In case the makespan has not been changed during this step go to Step 6. Otherwise set $ic = ic+1$. If $ic \leq n$, go to Step 3, otherwise proceed Step 6.

Step 6. For each task i on π_g, find the task j on each processor π_k, (k=1,…,m;), such that $f_i \leq t_j$. Make an attempt to reduce the makespan replacing the corresponding subchains s''_k and s''_g after the tasks j and i. In case this attempt is successful, set $icount = icount+1$. If $icount < \gamma$ go to Step 2, otherwise go to Step7.

Step 7. Try to change the place of the task before the last on π_g, and to assign the last task to another processor, reducing the makespan.

Step 8. Stop the computations (End of MAASCT).

Theorem: The time complexity of MAASCT is $O(\gamma n^2)$, where n is the number of tasks and γ is small positive integer correspondingly.

Proof: Each from the steps 1, 2, 3, 5 and 6 requires $O(n)$ mathematical operations. Since steps 3 ÷ 5 may be repeated no more than n times, and steps 2 ÷ 6 may be executed no more than γ times, the worst case performance of MAASCT algorithm requires $O(\gamma n^2)$ mathematical operations.

IV BASIC FEATURES OF MAASCT

In [3] and [13] is mentioned that when the number of processors increases, sometimes the performance of the approximation algorithm degrades ("anomalous behavior"). This is due to the essence of greedy procedures used. At Step 1. of MAASCT algorithm (like in the AASCT algorithm [2]) the composed chains are dispatched uniformly to all processors, so that the anomalous behavior is reduced to a great extent. Step 5 and Step 6 try to reduce the makespan changing the starting time of a task on the same processor and replacing tasks on different processors correspondingly. In this way they contribute anomalous behavior to be avoided.

Another important feature of MAASCT algorithm is that it has polynomial time complexity, which is better than that one of AASCT approximate algorithm for the same class of problems. In case $\gamma \leq m$, MAASCT algorithm has better or the same time complexity as the ETF algorithm (see [6]).

The mentioned features lead to the good performance of MAASCT as it is demonstrated in the next section.

V AN ILLUSTRATIVE EXAMPLE

Here is considered the illustrative example used in [5]:

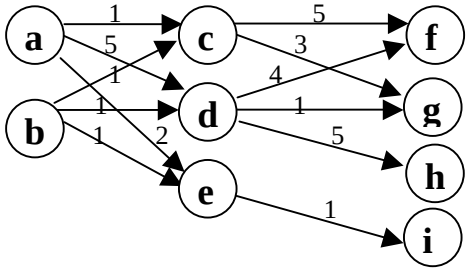

Fig. 1. Graph G with communication delays

The corresponding SCT task system for the example on Fig. 1. is presented in Table 1:

Table 1
SCT task system for the graph *G* from Fig. 1.

a	b	c	d	e	f	g	h	i
6	7	9	8	10	6	6	10	6

On Fig. 2 and Fig 3. are presented two schedules as shown in [5].

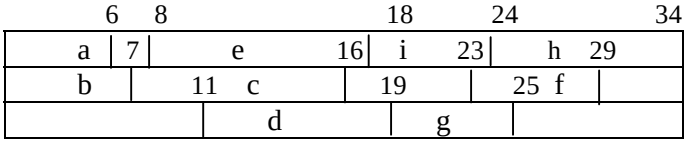

Fig. 2. An ETF schedule (3 processors)

Obviously the ETF algorithm creates a schedule with makespan (maximal finishing time) equal to 34. For the same example FS algorithm (see [5]) creates schedule with makespan equal to 29.

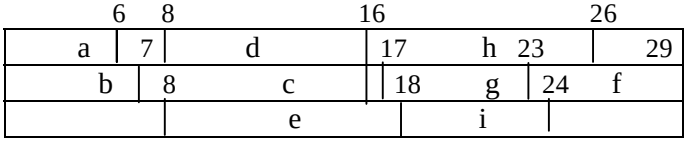

Fig. 3. A FS and MAASCT schedule (3 processors)

The MAASCT algorithm obtains the same result as the FS algorithm (see Fig. 3). Taking into account that each task can be started after it receives the necessary data from all its predecessors, the algorithm AASCT [2] obtains the same result. After Step 1 MAASCT schedules on first processor tasks *a*, *d* and *h*; on second processor – tasks *b*, *c*, *f* and *g*; and on the third processor – tasks *e* and *i*, starting *e* at moment t=8 (Step 2). The makespan is equal to 32 on the second processor (Step 4). After Step 5 MAASCT obtains the result on Fig. 3 with makespan equal to 29. At Step 6 and Step 7 the algorithm can not find new order of tasks, reducing the makespan.

On Fig. 4 is presented the result obtained by MAASCT algorithm for the same example but on two processors. After Step 1 the task schedule for the first processor is *a*, *d*, *h*, *g*; and for the second processor: *b*, *c*, *f*, *e*, *i*; The makespan is 42. After Step 6 tasks *c* and *f* are replaced by tasks *e* and *i*. The makespan is equal to 39. After Step 7 the makespan is reduced to 38 as shown on Fig. 4.

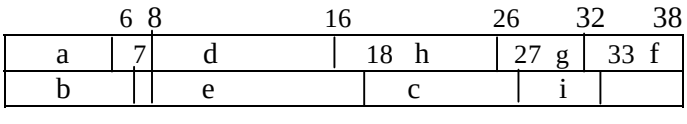

Fig. 4. A MAASCT schedule (2 processors)

VI CONCLUSIONS

An approximation algorithm called MAASCT is presented in this paper. Its time complexity is $O(\gamma n^2)$. For comparison the algorithm AASCT (see [2]) has $O(\gamma n^2(n\text{-}m))$ and ETF (see [6]) has $O(mn^2)$ time complexity. In case $\gamma \leq m$, MAASCT algorithm has better or the same time complexity as the ETF algorithm. It has also a better efficiency than the AASCT algorithm [2]. The known approximate algorithms in the literature have polynomial time complexity, but some of them have "anomalous behavior" (see [3], [13]) due the use of greedy heuristics. The algorithms AASCT [2] and MAASCT dispatch the tasks uniformly to all processors, so that the anomalous behavior is reduced to a great extent. They don't use artificial delays (see [5]). It is expected that the MAASCT algorithm will have better performance in comparison to ETF algorithm, as well as to some other approximation algorithms, based on greedy procedures.

REFERENCES

[1] Chrétienne P., C. Picouleau (1995) „*Scheduling Theory and its Applications*", P. Chrétienne, E. G. Coffman, J. K. Lenstra and Z. Liu (Eds.), 1995, John Wiley & Sons Ltd, pp. 65-90.

[2] Guliashki V., (2003) "An approximation algorithm for scheduling problem on a finite number of processors with communications delays", Proceedings of the XXXVIII International Scientific Conference ICEST'2003, held in Sofia, Bulgaria, pp. 333-336.

[3] Graham R. L. (1969) „Bounds on multiprocessing timing anomalies", *SIAM J. Appl. Math.*, Vol. 17, No. 2, pp. 416-429.

[4] Hanen C., A. Munier (1994) „Performance of Coffman-Graham schedules in presence of unit communication delays", http://citeseer.nj.nec.com/hanen94performance.html

[5] Hanen C., A. Munier (1995) „An approximation algorithm for scheduling dependent tasks on *m* processors with small communication delays", Preprint, Laboratoire Informatique Théoretique et Programmation, Institute Blaise Pascal, Université Pierre et Marie, Curie.

[6] Hwang J. J., Y. C. Chow, F. D. Anger, and C. Y. Lee (1989) „Scheduling precedence graphs in systems with interprocessor communication times", *SIAM J. Comput.*, Vol. 18, No.2, pp.244-257.

[7] Jakoby A., R. Reischuk (1992) „The Complexity of Scheduling Problems with Communication Delays for Trees", *Lecture Notes in Computer Sciences*, No. 621, Vol. 3, pp. 165-177 Springer, Berlin.

[8] Liu Z. (1995) „Worst-case analysis of scheduling heuristics of parallel systems", N° 2710, Institut National de Recherche en Informatique et en Automatique, http://citeseer.nj.nec.com/cache/papers/cs/1573/ftp:zSzzSzftp.inria.frzSzINRIAzSzpublicationzSzpubli-ps-zzSzRRzSzRR-2710.pdf/liu95worstcase.pdf

[9] Moukrim A., A. Quilliot (1998) „Scheduling with communication delays and data routing in message passing architectures", http://ipdps.eece.unm.edu/1998/scoop/moukrim.pdf

[10] Möhring R., M. Schäffter, A. Schulz (1996) „Scheduling jobs with communication delays: using infeasible solutions for approximation",http://citeseer.nj.nec.com/cache/papers/cs/5233/http:zSzzSzwww.math.tu-berlin.dezSzcogazSzpeoplezSzformer_ members_pageszSzschaeffterzSzPaperszSzExtendedAbstract517.pdf/schedu

[11] Munier A., C. Hanen (1995) „Using duplication for scheduling unitary tasks on *m* processors with unit communication delays", http://citeseer.nj.nec.com/munier95using.html

[12] Munier A., J-C. König, (1997) „A Heuristic for a scheduling problem with communication delays", *Operations Research*, 45 (1), pp. 145-148.

[13] Rayward-Smith V. J. (1987) „UET Scheduling with unit interprocessor communication delays", *Discrete Applied Mathematics* 18, 1987, pp. 55-71.

[14] Veltman B., B. J. Lageweg and J. K. Lenstra (1990) „Multiprocessor scheduling with communication delays", *Parallel Computing* 16, pp. 173-182.

Statistical Optimization of Filters in Radiocommunication Systems in IESD Simulator

Galia I. Marinova[1] and Dimitar I. Dimitrov[2]

Abstract - The papers presents the methodology for statistical design of band pass filters set in radiocommunication systems. The function constraints are defined from norms. Monte Carlo simulations and optimizations are performed with the statistical simulator IESD and Orcad PSpice. Both design centering and optimal tolerancing optimizations are considered.

Keywords - Band pass filters; Norms for radiocommunication systems; Statistical optimization; Monte Carlo simulation

I. INTRODUCTION

A research was performed to develop specific methodologies for statistical optimization of different types of electronic circuits. The general methodology for statistical design using the statistical simulator IESD [3] and the PSpice tool is proposed in [4]. Specific applications of this methodology were developed for a voltage regulator circuit in [2] and for a TV module in [5]. The paper presents a new specific application of the general statistical optimization methodology developed for a set of band pass filters in radiocommunication systems. A set of band pass filters for community antennas system was proposed in [1]. First the design from [1] is estimated through nominal AC and noise simulations in PSpice. An improved solution was proposed to fit better the frequency band constraints for the radio and TV channels studied. The constraints for the band pass filters in the community antenna are taken from the norms given in [6] by Bulgarian telecommunications company. Then the specific statistical optimization methodology is developed. The statistical optimization goal function is defined. Statistical analysis in AC(NOISE) and TIME domain are performed. Circuit parameters, yield and fail are estimated. Two statistical optimization methods [4,7]: design centering and optimal tolerancing are performed.

II. SPECIFIC METHODOLOGY FOR STATISTICAL OPTIMIZATION OF BAND PASS FILTERS FOR COMMUNITY ANTENNA SYSTEMS

The steps of the specific statistical design methodology are:

- Nominal simulation, estimation and adjusting of the initial design for the set of band pass filters corresponding to the frequency band constraints for the radio and TV channels.
- Constraints definition following the norms for radiocommunication systems in [6].
- Nominal analysis and estimation of the circuit performance.
- Definition of critical performance parameters for each filter.
- Statistical optimization of each filter with objective 100% yield and 0% Fail through:
  - Design centering
  - Optimal tolerancing.
- Statistical estimation of the optimized design

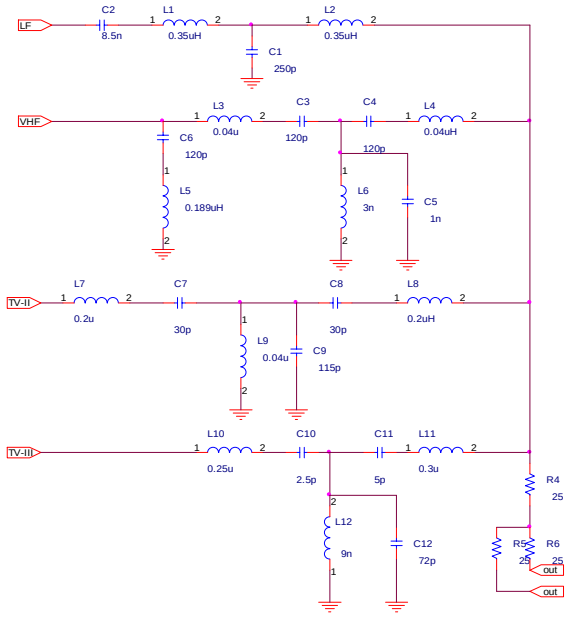

Figure 1. New design for the Band pass filters set for community antenna systems from [1] obtained after nominal simulations in ORCAD (PSpice)

III. NOMINAL DESIGN

The four band pass filters separate 4 channels:
2 radio channels LF (+ MF, HF,with amplitude modulation) , with frequency band **ΔF=(150kHz-26MHz)** and VHF (with frequency modulation) with **ΔF=66MHz-108MHz**,
and 2 TV channels TV-II with **ΔF=(47MHz-100MHz)** and TV-III with **ΔF=(173MHz-230MHz).**

PSpice simulation of the original circuit with the C_i, L_i values from [1] doesn't meet the frequency band constraints for the 4 channels. New design values were defined and the design was corrected as presented in Table I. The set of filters from [1] with the parameters values from Table I is presented on Figure 1. Figure 2 presents the 4 filters in the set, separated from each other in order to perform the nominal and statistical simulations in PSpice and IESD tools.

[1]Galia I. Marinova is with the Faculty of Communications and Communications Technologies, Technical University-Sofia, Kliment Ohridski 8, 1000 Sofia, Bulgaria, e-mail: gim@tu-sofia.bg
[2] Dimitar I. Dimitrov is with the Faculty of Communications and Communications Technologies, Technical University-Sofia, Kliment Ohridski 8, 1000 Sofia, Bulgaria, e-mail: ddim@tu-sofia.bg

TABLE I

Correction of the nominal design from [1] after ORCAD (PSpice) simulation

a) New values for the capacitors

C	C1	C2	C3	C4	C5	C6	C7	C8	C9	C10	C11	C12
Value from [1]	150pF	Not available	33pF	33pF	120p	18pF	10pF	10pF	100pF	3.9pF	3.9pF	72pF
New value	250pF	8.5nF	120pF	120pF	1nF	120p	30p	30pF	115pF	2.5pF	5pF	22pF

b) New values for the inductors

L	L1	L2	L3	L4	L5	L6	L7	L8	L9	L10	L11	L12
Value from [1]	0.226µH	0.226µH	0.189µH	0.133µH	0.189µH	0.189µH	0.174µH	0.149µH	0.023µH	0.066µH 0.066µH 0.131µH	0.089µH	0.131µH
New value	0.35µH	0.35µH	0.04µH	0.04µH	0.189µH	3nH	0.2µH	0.2µH	0.04µH	0.25µH	0.3µH	9nH

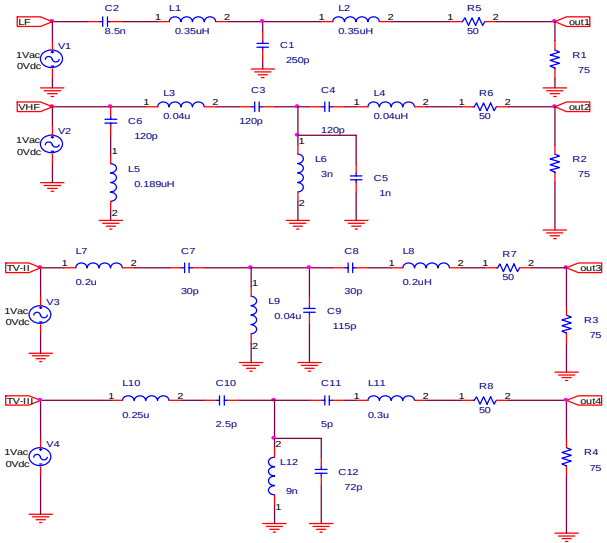

Figure 2. Four band pass filters for simulations with IESD and PSpice

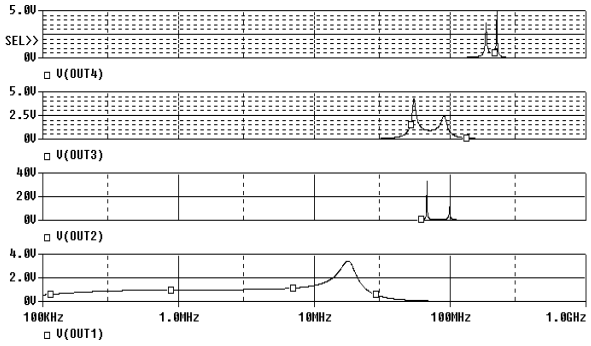

Figure 3. Output voltage curves in the different channels

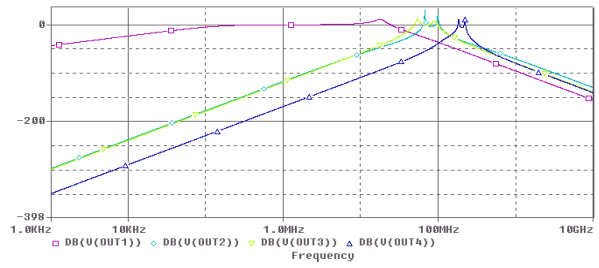

Figure 4. Output voltage in [db]

Nominal simulations in AC(Noise) domain for the set of band pass filters is performed in PSpice. Figure 3 presents the output voltage curves and Figure 4 presents the output voltage in [db]. Figure 5 presents the output noise and the S/N ratios in frequency domain for the 4 channels. Figure 6 presents the group delays. Table 2 presents the nominal values of the circuit parameters for the 4 filters as well as the limit imposed on the circuit. The limits for the TV pole gains, S/N ratio and group delay for the TV channels I and II are taken from the norms in [6].

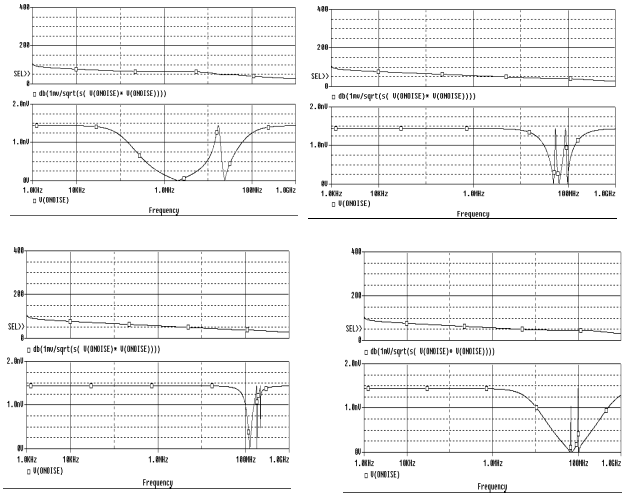

Figure 5. Output noise and S/N ratio for the four band pass filters

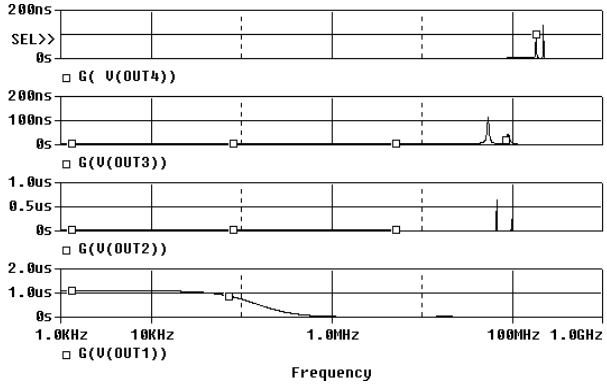

Figure 6. Group delays of the four band pass filters

TABLE II
Circuit parameters from nominal simulation and norm limits

Filter	LF (+MF,HF)	VHF	TV – II channel	TV – III channel	Limits
Frequency band ΔF (fL-fH)	150kHz-26MHz	66MHz-108MHz	47MHz-100MHz	173MHz-230MHz	**fL ± 10%** **fH ± 10%**
Pole gain	Before R5: P1=10.657dB At node out1: P1=6.27db	Before R6: P1=30dB P2=18.544dB At node out2: P1=20.88dB P2=16dB	Before R7: P1=11dB P2=3.39dB At node out3: P1=8.15dB P2=3.54dbdB	Before R8: P1=11db P2=14db At node out4: P1=6.6dB P2=8.37dbdB	Norms for TV channels II, III from [6] **Strongest limit ≤6db** **Lightest limit ≤16db**
S/N ratio for the lower and higher limit frequency in ΔF	S/N(fL)=66db S/N(fH)=49db	S/N(fL)=45db S/N(fH)=45db	S/N(fL)=42db S/N(fH)=41db	S/N(fL)=36db S/N(fH)=35db	Norms for TV channels II, III from [6] **Strongest limit ≥57db** **Lightest limit ≥ 48db**
Group delay	VG(fL)=535ns VG(fH)=8.5ns	VG(fL)=26ns VG(fH)=1.22ns	VG(fL)=10ns VG(fH)=6.7ns VGmax=112ns (154MHz)	VG(fL)=3.34ns VG(fH)=1ns VGmax=136ns (220MHz)	Norms for TV channels II, III from [6] **Strongest limit ≤100ns** **Lightest limit ≤ 200ns**
Slope 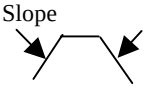	20db/dec -60db/dec	60db/dec -60db/dec	60db/dec -60db/dec	60db/dec -60db/dec	-

For the LF (+MF,HF) band pass filter the S/N ratio is 57db at 11MHz and at that frequency it goes down fast with about 10db. The S/N ratios for the channel TV-II are at the lowest deterioration limit permitted in [6] (48-7)db. The S/N ratios for the channel TV-III are out of the norms and some design improvement has to be performed on the circuit for these parameters. More powerful emitter has to be used for TV- III.

IV. STATISTICAL OPTIMIZATION METHODOLOGY

A. Definition of the goal function

The objective is to perform design centering and optimal tolerancing to the circuit in order to obtain 100% Yield and 0% Fail with the given constraints from Table II.

The goal function for the statistical optimization of the band pass filters set is defined as follows:

Opt Val(C_i, i=1,12, L_j=j=1,12) and Max Tol(C_i, i=1,12, L_j, j=1,12), Yield=100%, Fail=0%,
{fL(LF+MF,HF)=150kHz±10%,
fH(LF+MF,HF)=26MHz±10%,
fL(VHF)=66MHz±10%, fH(VHF)=108MHz ±10%,
fL(TV-II)=47MHz±10%, fH(TV-II)=100MHz±10%,
fL(TV-III)=173MHz±10%, fH(TV-III)=230MHz±10% ,
minP_1(LF+MF,HF), min $P_{1,2}$(VHF), $P_{1,2}$(TV-II)≤16db, $P_{1,2}$(TV-III) ≤16db,VG(TV-II) ≤200ns, VG(TV-III) ≤200ns, S/N(fL)≥48db, S/N(fH))≥48db}

The design centering and optimal tolerancing are illustrated for the LF(+MF,HF) band pass filter. The goal function for the LF(+MF,HF) band pass filter is defined as:

Opt Val($C_{1,2}$, $L_{1,2}$) and Max Tol($C_{1,2}$, $L_{1,2}$), Yield = 100%, Fail=0%, fL(LF+MF,HF)=(135-165)kHz, fH(LF+MF,HF)=(23.6-28.6)MHz,
min P1, S/N(fL)≥48db, S/N(fH))≥48db}

B. Design centering of the LF(+MF,HF) channel filter

The design centering is performed in order to decrease the pole gain in the allowed frequency band and S/N ratio. A Monte Carlo AC analysis with 10% tolerances and uniform distribution for C1, C2, L1, L2 is performed. The runs with the smallest results for P1 are considered and the frequency band ΔF are considered for each case. The gain in P1 was decreased from 10.558db to 10.05db, with frequency band ΔF=148kHz – 26MHz which corresponds to the constraints. The pole gain decrease is very strongly related to the value of ΔF, so that solution is a reasonable compromise.

TABLE III
Results for the element values after design centering

Element	C_1	C_2	L_1	L_2	P_1	fL	fH	S/N(fL)	S/N(fH)
Initial value	250pF	8.5nF	0.35μH	0.35μH	**10.657**	150kHz	26MHz	66db	49db
Optimized value	234pF	9nF	0.38μH	0.33μH	**10.05**	148kHz	26MHz	66.7db	48.7db

C. Optimal tolerancing of the LF(+MF,HF) channel filter

Table IV presents the statistical optimization steps for the optimal tolerancing of the LF (+MF,HF) band pass filter. The optimal tolerancing objective is to select the maximal tolerance values that guarantee 100% yield and 0% Fail. The statistical simulation data show that the S/N ratio and the group delay are not sensitive to tolerances and their values correspond to the constraints. The critical parameters for the statistical optimization are the frequency band limits fL and fH, and the pole gains.

TABLE IV
Steps in optimal tolerancing procedure

Element Value Parameter	Tolerances at step1	Step2	Step3	Step4	Step5	Step6	Step7
C1	1%	2%	5%	5%	**10%**	10%	10%
C2	1%	2%	5%	10%	**5%**	5%	5%
L1	1%	2%	5%	5%	**5%**	10%	5%
L2	1%	2%	5%	5%	**5%**	5%	10%
P1	(9.895-10.21)db	(9.772-10.29)db	(9.4-10.697)db	(8.917-11.01)db	**(9-10.45)db**	(8.75-11.1)db	(8.95-10.5)db
fL	(141-148.5)kHz	(138.6-151)kHz	(135-159)kHz	(121-162)kHz	**(136-156)kHz**	(131-159)kHz	(129-159)kHz
fH	(25.731 -27.05)MHz	(25.7-27)MHz	(25.3 -28)MHz	(23.85 -27.8)MHz	**(24.4-28.5)MHz**	(23.6-30)MHz	(24-29.5)MHz
S/N(fL)	(66.6-66.7)db	(66.5-66.7)db	(66.4-66.8)db	(66.3-66.8)db	**(66.6-67.2)db**	(67-67.1)db	(67-67.1)db
S/N(fH)	(48.6-48.7)db	(48.5-48.8)db	(48.3-49)db	(48.3-49.1)db	**(48.2-49.1)db**	(48.3-49)db	(48-49)db
VG(fL)	(530-532)ns	(530-532)ns	(529-532)ns	(517-536)ns	**(526-535)ns**	(529-532)ns	(529-533)ns
VG(fH)	(8-8.5)ns	(7.5-8.5)ns	(5.9-10)ns	(48.3-49.1)ns	**(6.5-13.1)ns**	(6.9-10)ns	(8-10.1)ns
Yield/ Fail	Yield100% Fail 0%	Yield100% Fail 0%	Yield100% Fail 0%	Yield 67% Fail 33% on FL	**Yield100% Fail 0%**	Yield 60% Fail 40%	Yield 60% Fail 40%

The optimal solution for the LF (+MF,HF) band pass filter is:

C1=234pF±10%,C2=9nF±5%, L1=0.38μH±5%, L2=0.33μH±5%

Figure 7 illustrates the statistical time domain response for the output voltage of the LF (+MF,HF) band pass filter with an unitary input pulse with 1μs period (the frequency 1MHz ∈ ΔF[LF+MF,HF]). This simulation can be the basis for rise time and pulse peaks estimation, as defined in the norms from [6].

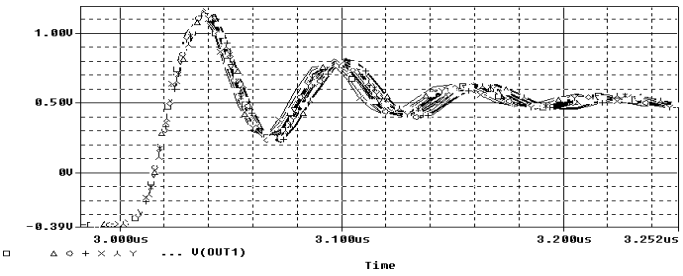

Figure 7. Monte Carlo simulation of the output voltage in Time area with an unitary input pulse, 1μs period.

The three other filters are optimized nominally and statistically following the same methodology.

CONCLUSION

The paper presents a methodology for statistical optimization of a set of band pass filters in community antenna system. Starting from a previously published initial circuit, nominal and statistical estimations and optimizations are performed in order to obtain performance corresponding to the constraints from the radiocommunication systems norms, 100% yield and 0% fail. The new approach defined permitted to improve the high sensitive band pass filters system following the very strict and strongly correlated constraints. The statistical design methodology developed for the band pass filters system completes the previously developed methodologies for voltage regulator circuits and TV modules. It confirms again the advantages of the statistical design approach in design for manufacturing in radiocommunications systems. The methodology can be implemented for other selective circuits. The general approach will be specified for other types of circuits.

ACKNOWLEDGEMENT

The authors acknowledge the National Science Fund for the financial support of the research on the project I-1203/02 and Dr. Vassil Guliashki for his precious advices.

REFERENCES

[1] D. Dimitrov, H. Shadura, A. Mindov, "Band pass filters for community antenna systems", *"Radio, Televizia, Elektronika"*, Year XXIX, N°6, 1980, pp.10-11

[2] G. Marinova, D. Dimitrov, "Statistical analysis and optimization of voltage regulator circuit using IESD and ORCAD environment", *Proceedings of XXXVIII International Scientific Conference on Information, Communication and Energy Systems and Technologies ICEST'2003*, Sofia, Bulgaria, 2003, pp. 478-482.

[3] G. Marinova , "Statistical design simulator for electronic design – IESD", *The European Design and Test Conference, Users Forum*, Paris, March 11-14, 1996, pp. 297

[4] G. Marinova, "Statistical optimization of electronic circuits in the simulator IESD", Proceedings of "Prilojenie na matematikata v tehnikata", Sofia, 1992, pp. 144-148, (in bulgarian)

[5] G. Marinova, "Statistical optimization of TV modules in IESD", TELSIKS'2003, Serbia and Montenegro, October 1-3 2003, pp.143-146

[6] Ts. Vassileva, St. Popov, "Bulgarian Telecommunications Company methodology for estimation of the technical performances of the radio and TV equipment and systems and the quality of the transmitted and emitted signals ", Sofia, 1999

[7] Zhang J. C., Styblinski M. A., "Yield and variability optimization of integrated circuits", Klewer Academic Publisher 1999

Session EM:

Electrical Machines

Parallel Operation Of Transformers - Conditions, Application And Economics

Jovce Doneski[1] and Nikolce Acevski[2]

Abstract **- Parallel operation means transformers connected to the same power systems on the input side and on the output side. There are two forms of parallel operation: in parallel with bus, and in parallel with system. This paper deals with the conditions of the parallel operation of transformers, as well as the conditions for the parallel operation with minimum power losses, i.e. optimal parallel operation.**

Key words **- Three phase transformer, vector group, equalizing current, impedance voltage, parallel operation.**

1. GENERAL REQUIREMENTS FOR PARALLEL OPERATION

1.1. Vector groups of similar phase displacement

The connections of three-phase transformers mean the interconnections of the phase windings on the input or output sides to form star, delta or zigzag connections. The vector group is a notation indicating the connection of the phases of two windings of a transformer and their relative phase displacement. Transformers with vector groups of similar phase displacement are suitable for parallel operation. The terminals with similar notation must be interconnected. However, it is also possible to operate certain other transformers with vector groups of different phase displacement in parallel if the phase connections are interchanged appropriately. Fig. 1 shows the possible connections for parallel operation of transformers with the commonly used numerical indices 5 and 11.

1.2. Approximately equal voltage ratio and tapping range

When the voltage ratios are equal, the total load is distributed between the parallel-connected transformers in direct proportion to the transformer powers and in inverse proportion to their impedance voltages. When the input voltages of two parallel-connected voltage transformers are equal, and the output voltage unequal, an equalizing current flows through both transformers; it can be determined from the following approximate formula:

$$I_{Equal\,Tr1} \approx \frac{|\Delta u|}{u_{Z(r)1} + u_{Z(r)2} \cdot \frac{S_{r1}}{S_{r2}}} \cdot 100 \qquad (1)$$

$I_{Equal\,Tr1}$ - Equalizing current as % of rated current of transformer 1

$|\Delta u|$ - Absolute value of voltage difference as % of output voltage of transformer 1 at no-load

$u_{Z(r)1}$, $u_{Z(r)2}$ - Impedance voltages at rated current or for certain tappings and/or deviations from the rated induction for transformers 1 and 2

$\frac{S_{r1}}{S_{r2}}$ - Ratio of rated powers

The equalizing current is completely independent of the load and of the distribution thereof; it also flows when there is no load.

When there is load, the load current is added geometrically to the equalizing current. If the load current has an inductive power factor, this results in an increased total current in the transformer with the higher secondary voltage and a decreased total current in that transformer with the lower secondary voltage.

Example 1:

	No-load output voltage [V]	Rated power [kVA]	Impedance voltage (at rated current) [%]
Tr. 1	400	250	4
Tr. 2	390	400	4

$$|\Delta u| = \left| \frac{400 - 390}{400} 100 \right| = 2.5\ \%$$

$$\frac{S_{r1}}{S_{r2}} = \frac{250}{400} = 0.625$$

$$I_{Equal\,Tr1} \approx \frac{2.5}{4 + 4 \cdot 0.625} \cdot 100 \approx 38.5\%$$

[1] Jovce Doneski is with the EMO OHRID Transformer Factory, P.O. BOX 118, 6000 Ohrid, Macedonia,
E-mail: djovce@yahoo.com
[2] Nikolce Acevski is with Faculty of Technical Sciences, I. L. Ribar bb, 7000 Bitola, Macedonia,
E-mail: nikola.acevski@mofk.gov.mk

In example 1, it is unfortunately the smaller transformer which has the higher secondary voltage and therefore must carry the higher total current. Referring to this example, this means that when the equalizing current is 38.5%, a load current of only 61.5% is permitted in order for the rated current of transformer 1 (=100%) not to be exceeded. Therefore, the whole transformer set can be operated at only 61.5% of its total power of 250+400=650 kVA, i.e. approximately 400 kVA. When the load power factor is less than 0.9, this approximate calculation gives sufficiently accurate values, but when the power factor exceeds 0.9 the increasing vectorial differential raises the permitted total power.

Under certain circumstances, changing the setting of the tapping switch on one transformer can improve the load capacity. If, in the case of the 250 kVA transformer in example 1, it were possible to select a higher tapping on the high-voltage side (e.g. 5% more turns), it would give a low voltage reduced by 1/1.05, i.e. 381 V instead of 400 V, owing to the reduced induction with connection to the same high voltage. If this method were to produce too low a distribution voltage, an alternative (if possible) would be to select a lower tapping on the high-voltage side of the 400 kVA transformer (e.g. 5% fewer turns) which would give a low voltage increased by 1/0.95, i.e. 411 V instead of 390 V, owing to the greater noise, core temperature rise and no-load current).

When the voltage setting is changed it must be remembered that the impedance voltage also changes. With EMO transformers conforming to IEC, indirect voltage adjustment associated with a change in induction alters the impedance voltage in approximate proportion to the percentage of increased or decreased turns. The calculations of example 1 are now repeated using a 5% lower tapping on the high voltage winding on the 400 kVA transformer (example 2).

Example 2:

	No-load output voltage [V]	Rated power [kVA]	Impedance voltage (at rated current) [%]
Tr.1	400	250	4
Tr. 2	411	400	3.8 (≈ 95% of 4)

$$|\Delta u| = \left| \frac{400-411}{400} 100 \right| = 2.75\ \%$$

$$\frac{S_{r1}}{S_{r2}} = \frac{250}{400} = 0.625$$

$$I_{Equal\,Tr1} \approx \frac{2.75}{4 + 3.8 \cdot 0.625} \cdot 100 \approx 43\%$$

Now, that transformer 2 has the higher no-load secondary voltage, it carries the combined load current and equalizing current and therefore determines the permitted total load of the parallel units.

The equalizing current referred to transformer 2 then becomes:

$$I_{Equal\,Tr2} = I_{Equal\,Tr1} \cdot \frac{S_{r1}}{S_{r2}} \qquad (2)$$

$$I_{Equal\,Tr2} = 43 \cdot \frac{250}{400} = 26.9\%$$

The permitted load current for transformer 2 is therefore 100%-26.9%=73.1% of the rated current. Consequently, when the load power factor is less than 0.9 ($\cos\varphi<0.9$), the transformer set can be operated approximately 73.1% of its total power of 650 kVA, i.e. roughly 475 kVA.

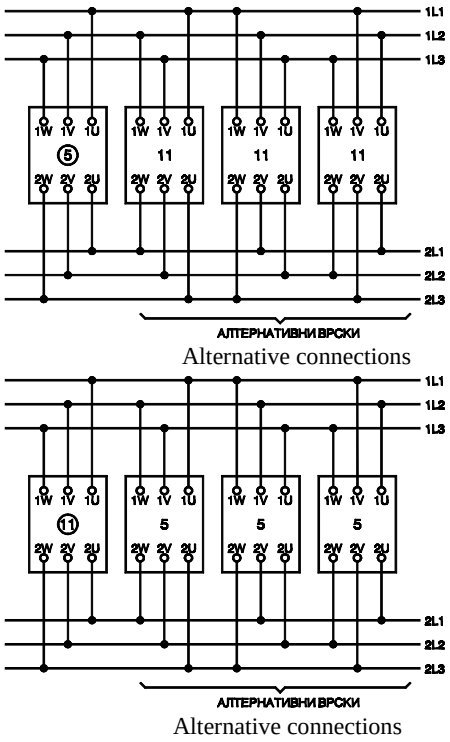

1L1, 1L2, 1L3 - High voltage
2L1, 2L2, 2L3 - Required index 5

Alternative connections

1L1, 1L2, 1L3 - High voltage
2L1, 2L2, 2L3 - Required index 11

Alternative connections

Fig. 1 Alternative connections for the parallel operation of transformers with vector-group numerical indices 5 and 11

1.3. Approximately equal impedance voltage

The impedance voltages of the individual transformers should not deviate by more than ±10% from the mean value of all the transformers to be operated in parallel. If $S_{r1}, S_{r2}, ..., S_{rp}$ are the rated powers of the parallel transformers, and $u_{Z(r)1}, u_{Z(r)2}, ..., u_{Z(r)p}$ are their impedance voltages at rated current (the lowest subscript 1 corresponding to the lowest impedance voltage etc.) the maximum possible total load S can be worked out according to the following approximation formula:

$$S \approx S_{r1} + S_{r2} \cdot \frac{u_{Z(r)1}}{u_{Z(r)2}}$$

$$+ S_{r3} \frac{u_{Z(r)1}}{u_{Z(r)3}} + ... + S_{rp} \cdot \frac{u_{Z(r)1}}{u_{Z(r)p}} \qquad (3)$$

At identical rated power levels, the part loads are inversely proportional to the impedance voltages.

Example 3:

	Rated power [kVA]	Impedance voltage (at rated current) [%]
Tr. 1	250	3.6
Tr. 2	250	4.0
Tr. 3	250	4.4
Transformer 1 $250 \cdot \frac{3.6}{3.6} = 250\,kVA$ (100% of S_r)		
Transformer 2 $250 \cdot \frac{3.6}{4.0} = 225\,kVA$ (90% of S_r)		
Transformer 3 $250 \cdot \frac{3.6}{4.4} = 205\,kVA$ (82% of S_r)		
Total load S=380 kVA (=91% of theoretical total power of 3x250=750 kVA)		

Whereas transformer 1 can carry 100% load, transformer 2 can only be operated at 90% of rated load and transformer 3 at only 82%. The transformer with the lower impedance voltage carries more load than that with the higher impedance voltage.

Deviations in the impedance voltage between 10% and 20% are generally still economically acceptable if the transformer with the lower rated power has the higher impedance voltage. In the opposite case even a 1:3 ratio of the powers of the parallel-connected transformers can lead to uneconomical operation.

As a remedial measure, a paralleling reactor can be connected on series with the too highly loaded transformer, e.g. on the low-voltage side. Its function is simply to increase the impedance voltage, and it is not suitable for limiting the short-circuit current owing to the saturation of the reactor core which occurs.

Perfectly satisfactory parallel operation is possible under the above-mentioned conditions.

2. ECONOMICS OF PARALLEL OPERATION

When a group of several parallel-connected transformers is subjected to a varying load over a specified period of time, minimum total losses can be attained by the connection or disconnection of individual transformers. The load loss varies as the square of the load, i.e. the sum of the load loss and the no-load loss when the load is distributed between several transformers can be less (under certain circumstances) than when only a few transformers are used.

In order to avoid a complicated comparison of the losses of the parallel-connected transformers, the part-load at which the switching-in of a further identical transformer (the p^{th} transformer) becomes economical can be calculated as follows:

$$\text{Part-load factor } n = \frac{\text{Part load}}{\text{Rated power}} \qquad (4)$$

Power of the group:

$$S_{group} = n \cdot S_r \qquad (5)$$

S_r - Rated power of the individual transformer

The part load factor for the economical switching-in of a further identical transformer (the p^{th} transformer) can be calculated using the following formula:

$$n = \sqrt{\frac{p \cdot (p-1) \cdot P_0}{P_k}} \qquad (6)$$

p - number of transformers to be connected in parallel

Calculation example for three identical EMO transformers to be connected in parallel:

Rated data		
Rated power	S_r	630 kVA
No-load ratio	u_r	10/0.4 kV
Vector group		Dyn 5
Rated frequency	f_r	50 Hz
No-load losses	P_0	1300 W
Load losses	P_k	6500 W
Impedance voltage at rated current	u_{Zr}	4 %

with p = 2

$$n = \sqrt{\frac{2 \cdot 1 \cdot 1300}{6500}} = 0.632$$

$$S_{group} = 0.632 \cdot 630 = 398\,kVA$$

with p = 3

$$n = \sqrt{\frac{3 \cdot 2 \cdot 1300}{6500}} = 1.095$$

$$S_{group} = 1.095 \cdot 630 = 690\,kVA$$

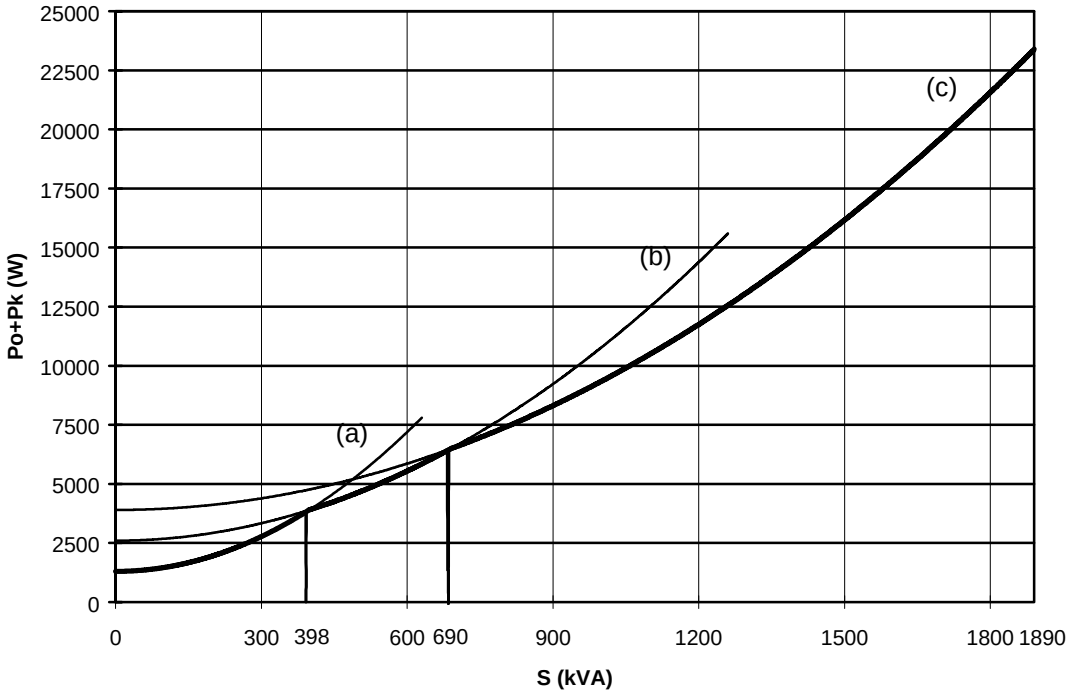

Fig. 2 Curves of total losses of parallel-connected 630 kVA transformers:
(a) 1 transformer; (b) 2 transformers; (c) 3 transformers

Therefore, it is most economical to switch in the second transformer at 398 kVA and the third at 690 kVA, a figure precisely 11.5% over the rated power of one transformer. This is also shown in the diagram (Fig. 2).

3. CONCLUSION

By determining the total losses of parallel connected transformers it is possible to establish the transformers' limit load. During such load, the operation of one transformer is switched to parallel operation of two, three etc. transformers, in order to enable minimum total losses, i.e. parallel operation to be economical.

REFERENCES

[1] ”Three-phase Distribution Transformers 50 to 2500 kVA - Technical Notes” - SIEMENS.
[2] ”IEC 76 Power Transformers” - International Standard
[3] Г.Н. Петров, ”ЭЛЕКТРИЧЕСКИЕ МАШИНИ”, Москва, 1974.
[4] Hrvoje Pozar, ” Visokonaponska Rasklopna Postroenja” , Tehnicka Kniga, Zagreb, 1973.

Method Of Determining The Most Economical Transformer

Jovce Doneski[1] and Nikolce Acevski[2]

Abstract - **Whenever offers are received from several manufacturers it is essential to compare the efficiency of the transformers as well as their technical features, their quality and their reliability. The efficiency of a transformer is measured in terms of its purchase price and the cost of losses occurring during operation.**

Key words - **No-load loss, load loss, transformer loss evaluation.**

1. INTRODUCTION

To permit the manufacturer of design the most economical transformer for his customer's needs, the latter must provide the data required for calculating efficiency. With this data, the manufacturer can determine and offer the transformer with the lowest overall costs during its expected service life.

2. TECHNICAL APPRAISAL

Most of the characteristics of industrial transformers are specified in national or international product standards for distribution transformers. The application of standards can be legally required, or by specific reference in the purchase contract.

For distribution transformers purchased in the European Union, three levels of standards are applicable:

- World-wide standards (IEC, ISO)
- European standards and regulations (EN, HD)
- National standards (e.g. DIN, BSI, NBN, NF)

European Harmonisation Documents (HD) are initiated if there is a need for a European standard. The draft HD is a compilation of the different national standards on the subject. The HD is finalized by eliminating as many national differences as possible. Usually, the HD is the predecessor of an European standard (EN), which must be adopted as a national standard in the EU member countries. Thus, purchase orders which refer to national standards (EN) are compatible with European standards (EN) and/or harmonisation documents (HD). Among the many international standards for distribution transformers, two main European Harmonisation Documents specify energy efficiency levels:

- HD 428: Three phase oil-immersed distribution transformers 50 Hz, from 50 to 2500 kVA, with highest voltage for equipment not exceeding 36 kV;
- HD 538: Three phase dry-type distribution transformers 50 Hz, from 100 to 2500 kVA, with highest voltage for equipment not exceeding 36 kV.

Table 2 gives the limits for load losses fore some important types of oil-immersed and dry-type distribution transformers according to HD 428.1 and HD 538.1 for the preferred rated power range of the transformers. For oil-filled distribution transformers, the HD allows a choice of energy efficiency levels, A, B and C. The no-load losses (iron losses) for the same range of transformers are given below. For oil-filled transformers, the HD offers a choice between three efficiency levels, A', B' and C'.

HD 428 therefore allows customers to choose between three levels of no-load losses and three levels of load losses. In principle, there are a total of 9 possible combinations, ranging from the lowest efficiency, (B-A'), to the highest, (C-C'), which may be regarded as providing a high practical standard of energy efficiency for a distribution transformer. There appears to be a "league table" of national standards for distribution transformer losses specified by the electricity utilities of various European countries. Switzerland and Scandinavian countries are said to set the highest standards, with France and Italy amongst the lowest (A-A'). Others are somewhere in the middle.

Table 1. League table for distribution transformer efficiency levels in Europe

Country	Utility Distribution Transformer Loss Levels
Belgium	C-C'
France	A-A' and B-B'
Germany	A-C' and B-A' and C-C'
Italy	B-C'
Netherlands	Better than C-C'
Spain	50% meet C-C'
UK	Uses capitalization values

[1] Jovce Doneski is with the EMO OHRID Transformer Factory,
P.O. BOX 118, 6000 Ohrid, Macedonia,
E-mail: djovce@yahoo.com
[2] Nikolce Acevski is with Faculty of Technical Sciences,
I. L. Ribar bb, 7000 Bitola, Macedonia,
E-mail: nikola.acevski@mofk.gov.mk

Table 2 Distribution transformer loss standards

	Load Losses for Distribution Transformers				No-Load Losses for Distribution Transformers			
RATED POWER	OIL-FILLED (HD 428) UP TO 24kV			DRY TYPE (HD 538)	OIL-FILLED (HD 428) UP TO 24kV			DRY TYPE (HD538)
	LIST A	LIST B	LIST C	12kV PRIMARY	LIST A'	LIST B'	LIST C'	12kV PRIMARY
kVA	W	W	W	W	W	W	W	W
50	1100	1350	875	N/A	190	145	125	N/A
100	1750	2150	1475	2000	320	260	210	440
160	2350	3100	2000	2700	460	375	300	610
250	3250	4200	2750	3500	650	530	425	820
400	4600	6000	3850	4900	930	750	610	1150
630 (4%)	6500	8400	5400	7300	1300	1030	860	1500
630 (6%)	6750	8700	5600	7600	1200	940	800	1370
1000	10500	13000	9500	10000	1700	1400	1100	2000
1600	17000	20000	14000	14000	2600	2200	1700	2800
2500	26500	32000	22000	21000	3800	3200	2500	4300

Table 3

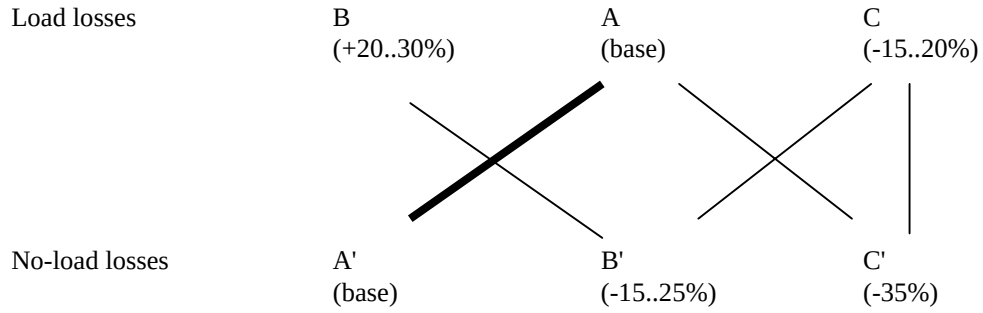

HD 428 defines five preferred combinations of these losses. These combinations are shown in Table 3 where the combination A-A' is chosen as the base case (shown as a bold line - the percentages refer to this combination).

3. DETERMIMING OVERALL COSTS

Overall costs are normally calculated for a one-year period. Consequently, allowance will have to be made for any changes in operating conditions likely to occur during the expected service life of the transformer.

Overall costs can be broken down as follows:

- Capital cost
- Cost of no-load losses
- Cost of short-circuit losses

Any transformer maintenance costs should be included with those of the installation as a whole, so that they will not be included in the present calculations.

3.1. Capital cost K_A

The following formula is used to calculate capital cost:

$$K_A = \frac{A \cdot r}{100} \text{ [Euro p.a.]} \quad (1)$$

where A is the purchase price of the transformer in Euro and r the redemption factor in % p.a.

The redemption factor r is calculated with the formula:

$$r = \frac{p \cdot q^n}{q^n - 1} \quad (2)$$

where p - interest rate (% p.a.), $q = 1 + \frac{p}{100}$ - interest factor, n - the depreciation period in years.

The redemption factor r will therefore depend on the interest rate and the depreciation period. The capital cost K_A is therefore equal to the annual amounts required to repay capital A borrowed at an interest rate of p% for a period of n years.

3.2. Cost of no-load loss C_{P0}

No-load losses will give rise to costs throughout the transformer's entire operating life. The annual cost of no-load losses is calculated as follows:

$$K_{P_0} = (k_L + k_a \cdot T_B) \cdot P_0 \ \text{[Euro p.a.]} \qquad (3)$$

where
k_L - cost of power in Euro/kW p.a.;
k_a - energy costs in Euro/kWh;
T_B - operating time in hours p.a. (8760 hours maximum);
P_0 - no-load losses in Kw.

The power costs k_L include the cost of providing electric power (capital and operating costs of the installation) and the costs of power used. These are known to the customer, e.g. from the power supply contarct.

3.3. Cost of short-circuit losses K_{Pk}

The costs incurred through short-circuit losses are somewhat more difficult to calculate since they are in proportion to power squared, and the transformer is subject to wide load fluctuations in the course of a year. Instead of making a curve of the actual load as it occurs in the course of one year, which is quite irregular, the operating times at the various particular power levels are added together (power=ordinate, operating time=abscissa) and shown in an adjusted annual load curve.

At this point it is necessary to introduce some new terms.

The utilization period for the year, T_m, is the period of time during which the transformer would have had to be operated at full load P_{max} (active component corresponding to the adjusted annual load curve) in order to generate the same amount of energy in the year A_W (active component) as it did with the variable load).

The ratio $\frac{T_m}{T_B}$ is the load factor m.

$m = \frac{T_m}{T_B}$; $m = \frac{A_W}{T_{max.} \cdot T_B}$ from which it follows

$$T_m = \frac{A_W}{P_{max.}} \ \text{[hours p.a.]} \qquad (4)$$

A_W - year's energy [kWh p.a.];
$P_{max.}$ - peak value of the adjusted annual load curve [kW].

This value $P_{max.}$ [kW] from the adjusted annual load curve is to be converted into $S_{max.}$ [kVA] for the following calculation of the cost of short-circuit losses.

Peak value of the adjusted annual load curve [kVA]

$$S_{max.} = \frac{P_{max.}\ \text{[kW]}}{\cos\varphi_{max.}}. \qquad (5)$$

Here is the essential to know the value of $\cos\varphi$ at peak load $P_{max.}$.

In many publications, the energy loss factor δ is also introduced to calculate the short-circuit losses more accurately. The energy loss factor δ is a function of the load factor m. For the calculation of the cost of short-circuit losses performed here it certainly suffices to assume that δ is the same as m^2, and than use m^2 instead of δ in calculations. If other influencing factors are introduced, e.g. the inclusion of the tolerances of the stated losses or of the figure for peak load in the adjusted annual load curve $S_{max.}$, this results in deviations which are greater than the inaccuracy of results obtained by the present simplified form of calculation.

The ratio $\frac{S_{max.}\ \text{[kVA]}}{S_N\ \text{[kVA]}}$ is designated the relative peak load h_r. The short-circuit losses P_k [kW] is proportional to the square of this ration, which can vary considerably from transformer to transformer (distribution transformer, network transformer, generator transformer) and will also depend on the conditions under which the transformer operates. The figure may also vary quite considerably in the course of years of operation, especially in the case of distribution transformers. When purchased, a transformer may have a very low figure for h_r, e.g. 0.5, and by the end of its service life, it may even rise above 1, depending on the type of use.

If the above mentioned figures are known, the cost of annual short-circuit losses may be calculated according to the formula given below:

$$K_{P_k} = (k_L + k_a \cdot m^2 \cdot T_B) \cdot h_r^2 \cdot P_k \ \text{[Euro p.a.]} \qquad (6)$$

The influence of the overlapping factor is ignored here.

Result: The sum total of costs incurred during one year (capital cost K_A cost of no-load losses K_{P0} and short-circuit losses K_{Pk}) are lowest for the most economical transformer. For the sake of completeness, however, it should be pointed out that overall costs should also include the cost of magnetizing reactive power and auxiliary features (cooling installations).

4. THE CAPITALIZATION OF THE COSTS

The convenient method of determining the most economical transformer is used when figures are available for no-load and short-circuit losses. Calculations are again based on annual overall costs.

The annual no-load loss costs K_{P_0} are divided by P_0, the annual short-circuit loss costs are divided by P_k. This yields the annual costs of no-load losses and short-circuit losses per kW, as shown in the formulae below:

$$b_{P_0} = \frac{K_{P_0}}{P_0} = k_L + k_a \cdot T_B \ [\text{Euro/kW p.a.}] \quad (7)$$

$$b_{P_k} = \frac{K_{P_k}}{P_k} = \left(k_L + k_a \cdot m^2 \cdot T_B\right) \cdot h_r^2 \ [\text{Euro/kW p.a.}] \quad (8)$$

These annual loss costs per kW [P_0 and P_k] are now multiplied by the factor $\frac{100}{r}$. This yields the capitalized value of the annual cost of losses per kW P_0 and P_k for the transformer at date of purchase. Below are given the values applied by the operator for no-load and short-circuit losses:

$$B_{P_0} = b_{P_0} \cdot \frac{100}{r} \ [\text{Euro/kW}] \quad (9)$$

$$B_{P_k} = b_{P_k} \cdot \frac{100}{r} \ [\text{Euro/kW}] \quad (10)$$

A direct comparison with the purchase price A of the transformer is now possible since the annual costs of losses were capitalized by multiplication with the factor $\frac{100}{r}$.

The capitalized price for comparison is obtained by adding the transformer's purchase price A, the assessment of the no-load losses · value of no-load losses and assessment of the short-circuit losses · value of short-circuit losses, as follows:

$$K_{VG} = A + B_{P_0} \cdot P_0 + B_{P_k} \cdot P_k \ [\text{Euro}].$$

Example: Distribution transformer 630 kVA, 10/0.4 kV

	Type 1	Type 2
P_0 [kW]	1.3	0.86
P_k [kW]	6.5	5.4
A [Euro]	6175	8160
$B_{P_0} \cdot P_0$ [Euro]	3900	2580
$B_{P_k} \cdot P_k$ [Euro]	9750	8100
K_{VG} [Euro]	19825	**18840**

(Note: $B_{P_0} = 3 \frac{\text{Euro}}{\text{kW}}$; $B_{P_k} = 1.5 \frac{\text{Euro}}{\text{kW}}$)

5. CONCLUSION

The most economical transformer is the one with the lowest total.

$$\left(\begin{array}{c}\text{Purchase prise}\\ +\\ \text{capitalised cost}\\ \text{of losses}\end{array}\right)_{\min} = \text{the most economical transformer}$$

Once the transformer manufacturer has assessed the cost of losses, it will possible for him to design the transformer with optimal losses. The other advantage of this method of determining capital value lies in the fact that valuation data does not lead to the disclosure of information relating to the operator's own internal calculations. This method is therefore often given preference over other methods which require records to be kept of the actual annual costs incurred.

REFERENCES

[1] Hans De Keulenaer, M.J. McDermott, "The scope for saving in the EU through the use of energy-efficient electricity distribution transformers", IWCC Technical Seminar, Italy, September 1999.
[2] W.T.J. Hulshorst, J.F. Groeman, "Energy saving in industrial distribution transformers", KEMA report reference 40130017-TDC 02-24226A, May 2002.
[3] The assessment of transformer losses - investments compared" - Trafo-Union GmbH.

Current State Regulator of Asynchronous Motor Commanded by Field Orientation

Pencho Georgiev[1], Simeon Neykov[1], Pavlik Rahnev[2], Silvija Letskovska[2], Kamen Seymenliyski[2], Marina Uscheva[2]

Abstract -**The object of the present work is development and investigation of the current stator regulator of the asynchronous electromotor commanded by field orientation.**

The deviation of the current from the gives values in the state mode is reduced to zero using integrated regulators, separately for flux – determining $\underline{i}_{sd}$ and moment - determining $\underline{i}_{sq}$ component of the vector of the stator current $\underline{i}_s$ in the coordinate system synchronized with rotor fool magnetic flux.

Key words - **regulators, electro motors, vector current, stator current.**

I. Introduction.

One of the most modern methods to control the asynchronous electric motors is based on the determined type of field orientation [2]. In this case good dynamic of an electrical movement depends, first of all, on the chosen method for regulation of the stator vector current different components. Comparatively good results in the fixed work are received using different PI regulators in synchronous with field coordinate system [2]. The given discrete models for the state [1] allow the synthesis of different variants of vector regulators [4]. Another way, based on these models, is the regulation of the current in the space of the state.

The object of this report is the synthesis of such kind regulation circuit, synchronized with field coordinate system, named below with the term regulator of the current state.

II. Theory.

The generalized model of the controlled object is presented with Eq.1:

$$\underline{i}_s(k+1) = \underline{\Phi}_{11}\underline{i}_s(k) + \underline{\Phi}_{12}\underline{\psi}'_r(k) + \underline{H}_1\underline{u}_s(k) \qquad (1)$$

where:

- $\underline{i}_s$ – is a vector of stator current;
- $\underline{u}_s$ - vector of the stator voltage;
- $\underline{\psi}_r$ - vector of the rotor fool magnetic flux, $\underline{\psi}'_r=\underline{\psi}_r/L_m$. ($L_m$ is a manual inductance).

The matrices $\underline{\Phi}_{11}$, $\underline{\Phi}_{12}$ and $\underline{H}_1$ are expressed using the parameters of T form equivalent circuit of the electric motor in the synchronized with field coordinate system according the Eq. 2 ÷ 4:

$$\underline{\Phi}_{11} = \underline{\Phi}^1_{11} = \begin{bmatrix} f_{11} & f_{12} \\ f_{21} & f_{22} \end{bmatrix} = \begin{bmatrix} 1-\frac{T}{\sigma}\left(\frac{1}{T_s}+\frac{1-\sigma}{T_r}\right) & \omega_s T \\ -\omega_s T & 1-\frac{T}{\sigma}\left(\frac{1}{T_s}+\frac{1-\sigma}{T_r}\right) \end{bmatrix} \qquad (2)$$

$$\underline{\Phi}_{12} = \underline{\Phi}^f_{12} = \begin{bmatrix} f_{13} & f_{14} \\ f_{23} & f_{24} \end{bmatrix} = \begin{bmatrix} \left(\frac{1-\sigma}{\sigma}\right)\frac{T}{T_r} & \left(\frac{1-\sigma}{\sigma}\right)\omega' T \\ -\left(\frac{1-\sigma}{\sigma}\right)\omega' T & \left(\frac{1-\sigma}{\sigma}\right)\frac{T}{T_r} \end{bmatrix} \qquad (3)$$

$$\underline{H}_1 = \underline{H}^f_1 = \begin{bmatrix} T/\sigma L_s & 0 \\ 0 & T/\sigma L_s \end{bmatrix} \qquad (4)$$

where:

- T – duration of the fact;
- T_r – time constant of the rotor;
- T_s – time constant of the stator;
- ω’ – electric angle speed of the rotor. If the mechanic angle speed of the rotor is ω’ and the number of the couple poles of the motor is z_p, it means $\omega' = z_p\,\omega$.

The coefficient σ is presented by the Eq. 5:

$$\sigma = 1 - \frac{L_m^2}{L_s L_r} \qquad (5)$$

where:

- L_s – inductance of the stator;
- L_r – the rotor's inductance.

From the model [1] for the stator voltage gives:

$$\underline{u}_s(k) = \frac{1}{\underline{H}_1}\left[\underline{i}_s(k+1) - \underline{\Phi}_{11}\underline{i}_s(k) - \underline{\Phi}_{12}\underline{\psi}'_r(k)\right] \qquad (6)$$

If the part dependant on the current in the Eq. 6 is separated as an output factor for the designed regulator, of means that for the stator voltage the equation is validated:

[1]Pencho Georgiev is with of Tehnical University Gabrovo, pencho_georgiev2001@yahoo.com

[1]Simeon Neykov is with of Tehnical University Gabrovo, Bulgaria, simeon.neykov@kkservice.bg

[2]Pavlik Rahnev is with of Burgas Free University, Alexandrovska 101, 8000 Burgas, Bulgaria, E-mail rahnev@bfu.bg

[2]Silvija Letskovska is with of Burgas Free University, Alexandrovska 101, 8000 Burgas, Bulgaria, E-mail silvia@bfu.bg

[2]Kamen Seimenliyski is with of Burgas Free University, Alexandrovska 101, 8000 Burgas, Bulgaria, silvia@bfu.bg

[2]Marina Uscheva is with of Burgas Free University, Alexandrovska 101, 8000 Burgas, Bulgaria, E-mail silvia@bfu.bg

$$\underline{u}_s(k) = \frac{1}{\underline{H}_1}\left[\underline{y}(k-1) - \underline{\Phi}_{12}\underline{\psi}'_r(k)\right] \quad (7)$$

Than for the output factor of the current state regulator the equation is:

$$\underline{y}(k-1) = \underline{i}_s(k+1) - \underline{\Phi}_{11}\underline{i}_s(k) \quad (8)$$

Using Laplas transformation for discrete signals the Eq. 8 will have a form:

$$z^{-1}\underline{y}(z) = \left(z\underline{I} - \underline{\Phi}_{11}\right)\underline{i}_s(z) \quad (9)$$

where I is single matrices.

The generalized block circuit of the current state regulator is given in Fig. 1, where $\underline{\mathbf{i}}^*_s(k)$ is a vector of the determined value of the stator's current.

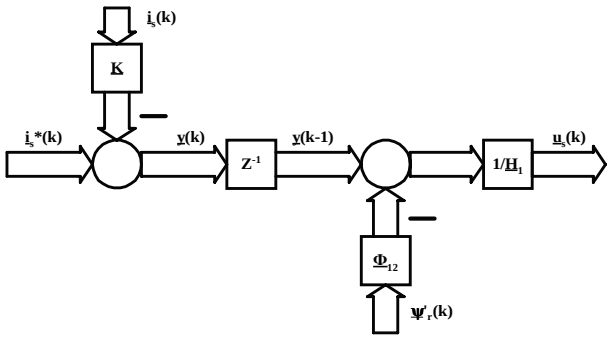

Fig. 1.

In accordance with the circuiting Fig. 1 for the output factor $\underline{y}(k)$ for the designed state regulator is obtained:

$$\underline{y}(k) = \underline{i}^*_s(k) - \underline{K}\underline{i}_s(k) \quad (10)$$

where K is a reflexive regulation matrices and it determination is the goal of this work. In Z – area from the Eq. 10 follows:

$$\underline{y}(z) = \underline{i}^*_s(z) - \underline{K}\underline{i}_s(z) \quad (11)$$

The matrices K must be determined is such away to realize the desirable dynamic behavior of the system, expressed by Eq. 12 [14]:

$$\underline{i}_s(z) = z^{-2}\underline{i}^*_s(z) \quad (12)$$

The Eq. 12 shows the regulator transmission function in relation with the given regulated factor and it describes that, the real value mast reach the substitution of Eq. 12 in Eq. 11 and after than Eq. 11 in Eq. 9 the result is:

$$\underline{\Phi}_{11} - \underline{K}z^{-1} = \underline{0} \quad (13)$$

That, for the reflexive regulating matrices the equation is:

$$\underline{K} = z\underline{\Phi}_{11} \quad (14)$$

After the substitution of Eq. 14 in Eq. 11 for the output vector of the designed regulator, the z - area is:

$$\underline{y}(z) = \underline{i}^*_s(z) - z\underline{\Phi}_{11}\underline{i}_s(z) \quad (15)$$

The Eq. 15 in the time area is:

$$\underline{y}(k) = \underline{i}^*_s(k) - \underline{\Phi}_{11}\underline{i}_s(k+1) \quad (16)$$

Disadvantage of the above describe method for formation of the commanding effect $\underline{\mathbf{y}}$ is the residual current deviation $\underline{\mathbf{x}}_\mathbf{w}$ in the settled mode. This problem could be removed using additional integrated regulators, as it is shown in Fig. 2.

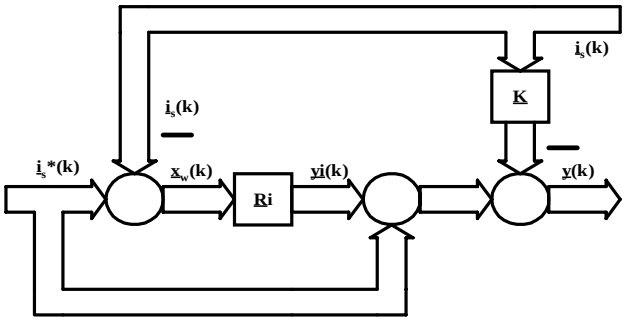

Fig 2. $\underline{x}_w(k)$ is the stator current deviation from the set value; $\underline{R}_i$ and $\underline{y}_i(k)$ are integrated regulator with its output factor.

The output factor of the state regulator in this case is given by Eq. 17, and for the integrated regulator by Eq. 18:

$$\underline{y}(k) = \underline{i}^*_s(k) - \underline{\Phi}_{11}\underline{i}_s(k+1) + \underline{y}_i(k) \quad (17)$$

$$\underline{y}_i(k) = \underline{V}_i\underline{x}_w + \underline{y}_i(k-1) \quad (18)$$

Where $\underline{V}_i$ gives the amplifying parameters of the integrated regulators. In this situation, according the above explained, the regulation of the current in the state space could be realized with next steps:

1. Calculation the value of the stator current $\underline{i}_s(k+1)$ is for one tact before using the model (Eq. 1) where the values $\underline{u}_s(k)$ and $\underline{i}_s(k)$ are derived from measurements, and $\underline{\psi}'_r(k)$ is given using a model with input values measured current and turns revolutions [1, 4];
2. Calculation the integral parts using Eq. 18;
3. Forming the output factor of the state current regulator according to an Eq. 17. The received values is memorized for one tact and it is used for calculation of the stator voltage in the next tact;

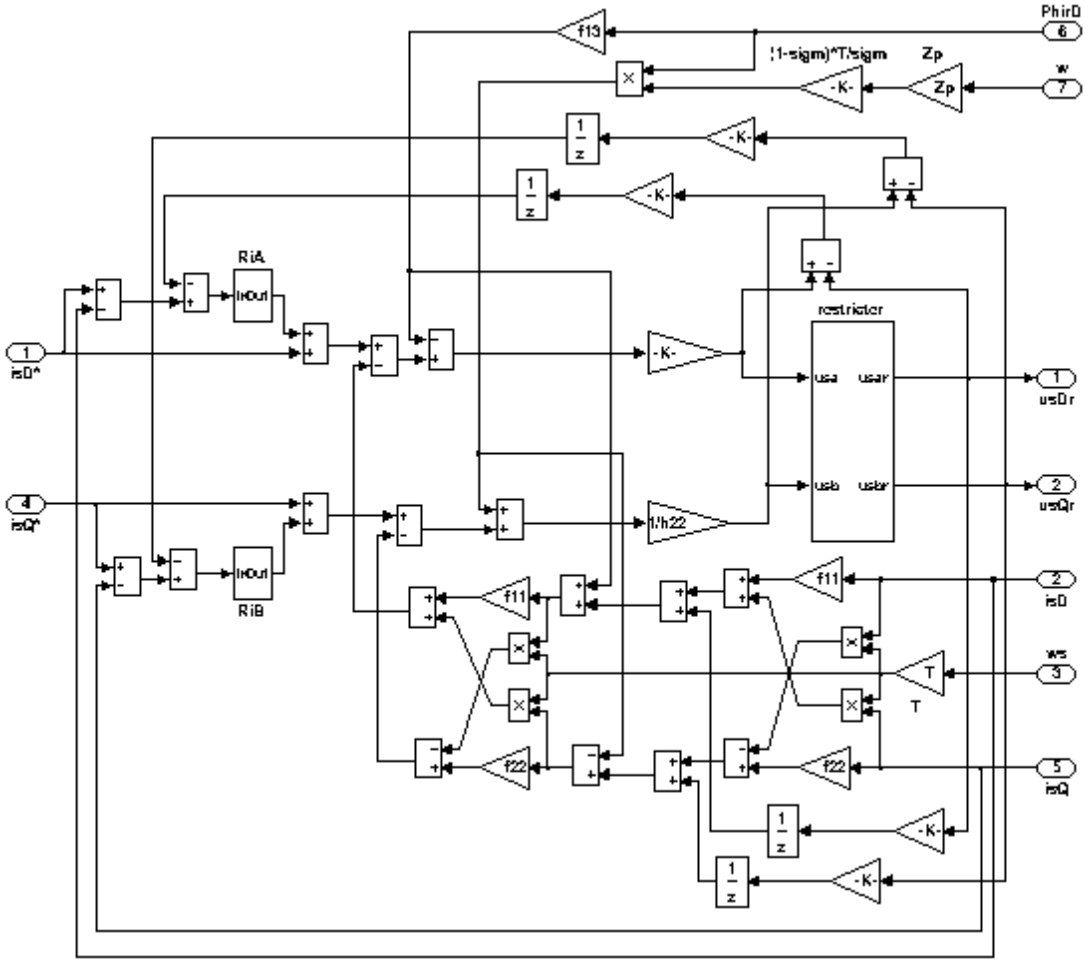
PhirD
6
f13
(1-sigm)*T/sigm
Zp
-K-
Zp
w
7
1
z
-K-
1
z
-K-
RiA
InOut
restrikter
1
isD*
usa
usar
1
usDr
usb
usbr
2
usQr
4
isQ*
f1/h22
f11
f11
2
isD
ws
3
T
T
InOut
RiB
f22
f22
5
isQ
1
z
-K-
1
z
-K-

Fig 3.

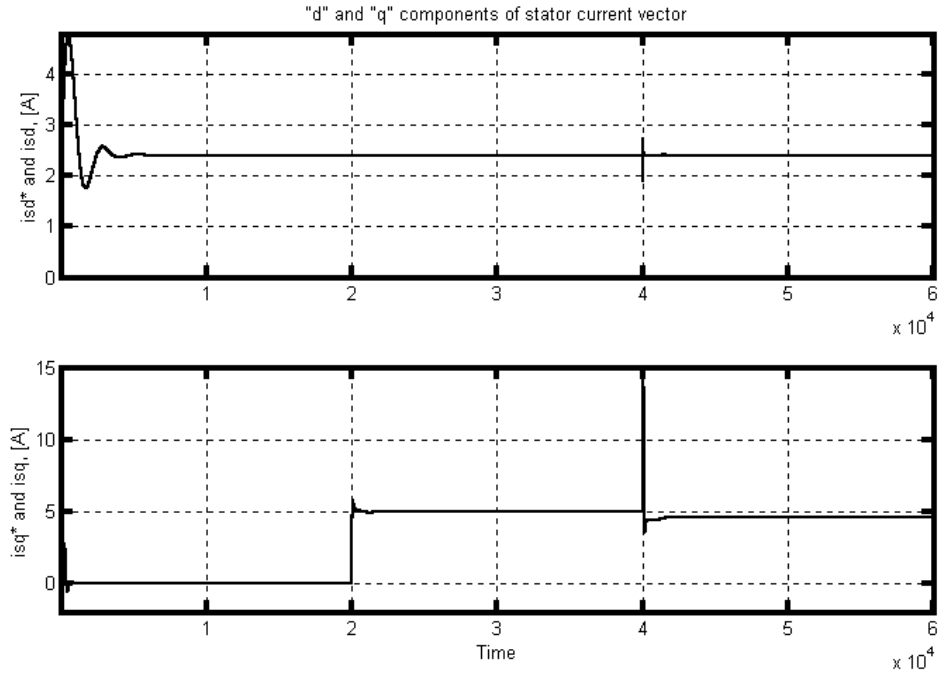
"d" and "q" components of stator current vector
isd* and isd, [A]
0
1
2
3
4
1
2
3
4
5
6
x 10^4
isq* and isq, [A]
0
5
10
15
1
2
3
4
5
6
Time
x 10^4

Fig.4.

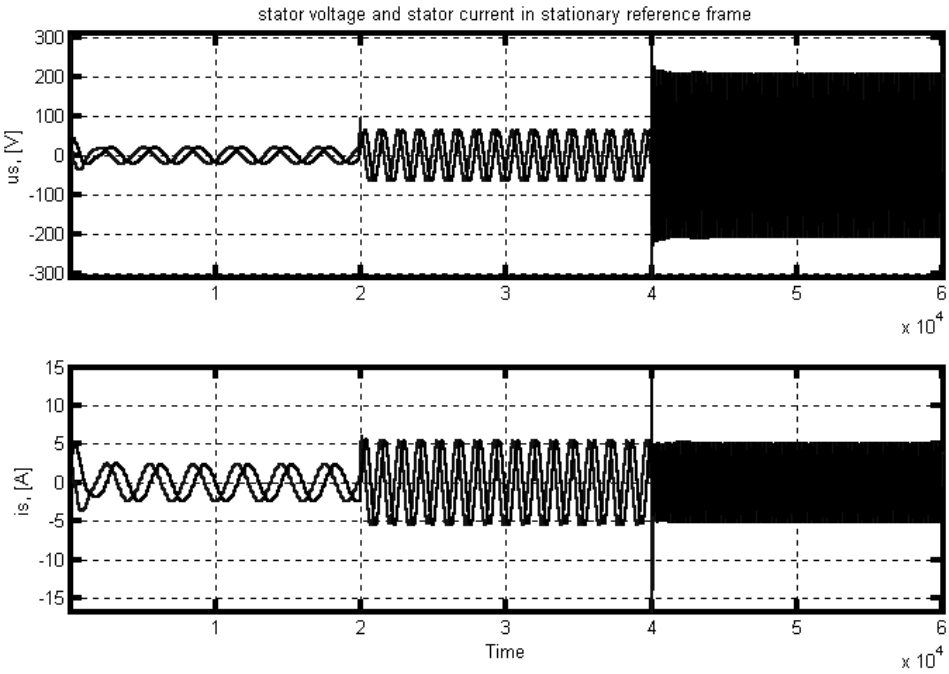

Fig. 5.

4. n the running tact the stator voltage calculates with the help of Eq. 7.

In [4] the particularities and one possible approach for limitation of the stator voltage components are described. Than the presented, up to now, steps for current regulation are illustrated in Fig. 3.The circuit is synthesis and analyzed with MATLAB/SIMULINK software. The simulations are provided for the motor next parameters:

- Tape T90L - 4 ("Elma" – Trojan)];
- Power P_n = 1.5kW;
- Nominal current I_n = 3.8A;
- Nominal phase voltage U_n=220V/50Hz;
- J = 0.00278kgm^2;
- z_p=2;
- n = 1400rpm;
- mM = 10.23Nm;
- L_m = 0.291H;
- L_s = 0.304H;
- L_r = 0.3066H;
- T_r = 0.0726s;
- T_s = 0.0544s.

The simulation is done in next conditions:

- Time 6s, 1s = 10000steps, T = 0.0001s;
- Static resistive moment mW changes steeply from 0 for 10.23Nm in the moment t = 2s;
- The determined speed of rotor's rotating n changes steeply from 100 to 1000 rpm in the moment t = 4s.

Fig. 4 shows the given and measured values of the stator currents i^*_{sd}, i_{sd} и i^*_{sq}, i_{sq}, in the coordinate system synchronized with the field. Fig. 5 presents the stator voltage an a stator current in the common coordinate system.

References

[1] Georgiev P. V., S. V. Neykov, Development of discrete model of the asynchronous motor state in the coordinate system with *dq* synchronous with field, X – International Conference ET'2001, Sozopol, Bulgaria, 2001.

[2] P. V. Georgiev, Electronic regulators for electric machines, University Editor "V. Aprilov", Gabrovo, Bulgaria, 1999.

[3] Openchaim A.V., A. C. Wilsky, Jan T. Jang, Signals and systems, "Techniques", Sofia, Bulgaria, 1993.

[4] S. V. Neykov, P. V. Georgiev, Circuit for current regulation in the coordinate system synchronistic with field for vector commanding of a an asynchronous electromotor, International Conference "UNITEX' 02", Gabrovo, Bulgaria, 2002.

An Optoelectronic Method of Machine Diagnostics

Assoc. Prof. Totyo Iliev, Ph.D

INTRODUCTION

Correct assessment of current and prospective operating order of technical objects involves the use of technical diagnostics.Using systems and equipment for technical diagnostics which employ objective quantitative criteria will have, on the one hand, a positive impact on decision making related to the correct selection of the right operation mode of a particular electric machine and , on the other hand ,will determine its performance capacity.. Various well known methods of technical diagnostics of electric machines include parameter-based diagnostics ,simulation diagnostics, high frequncy test diagnostics , impact-pulse diagnostics, flaw detection, etc.

Two major aspects of application are derived from these methods: manufacturing and performance.

This paper presents an option which employs optoelectronic method of diagnostics that eliminates direct contact with the object. Further advantage of this method is the possibility to ensure motor control as well.

EXPOSITION

In electric machines there are parameters which do not lend themselves easily to measuring in the process of their diagnostics, running and control. To meet the challenge it is necessary to resort to optoelectronics in order to effect relevant control over the current in stator and rotor coils, temperature of both coils, machine vibrations, air gap, and bearing of the machine under diagnostics.

General tests of electric machines require that a large number of auxiliary devices should be connected to the electric motor which is being tested. This encumbers to a considerabale extent the procedure of diagnostics especially when the motor is running.

The paper reviews a feasible method of automated flaw detection and visual control whereby various defects and flaws in the tested electric machine are possible to detect without any use of instruments such as brakes and sesnors, which are usually connected to the machine, and also of electrical and mechanical parameters. Readings obtained by this method are best combined with the readings obtained in analyzing signals resulting from a signal spreading in a solid noise medium. In this way it would be possible to detect and recognize a large group of mechanical flaws as well as some flaws in the bearings. By using digital classifiers it will be well possible to detect various electromechanical distortions and deviations from the normal mode of operation which, consequently, may cause serious corruption of both electrical and physical parameters of the object. These parameters are compared with model parameters corresponding to a particular aspect and mode of operation. The quality of these parameters will largely depend on the reference (preset) parameters.

A new type of system for diagnostics is introduced which employs highly error sensitive filter : Systematization of parameters is based on the selection of model and methods applied to the tested object. Using this new approach will lead to a novel method of classifying damage parameters. Based on the classical methods in time and frequency range, a new approach should be established for evaluation of defects in bearings, air gap, as well as some other flaws which correspond to these defect parameters.

Evaluation of these detected flaws is supported by additional measurements made by alternative means on general type of electric motors.

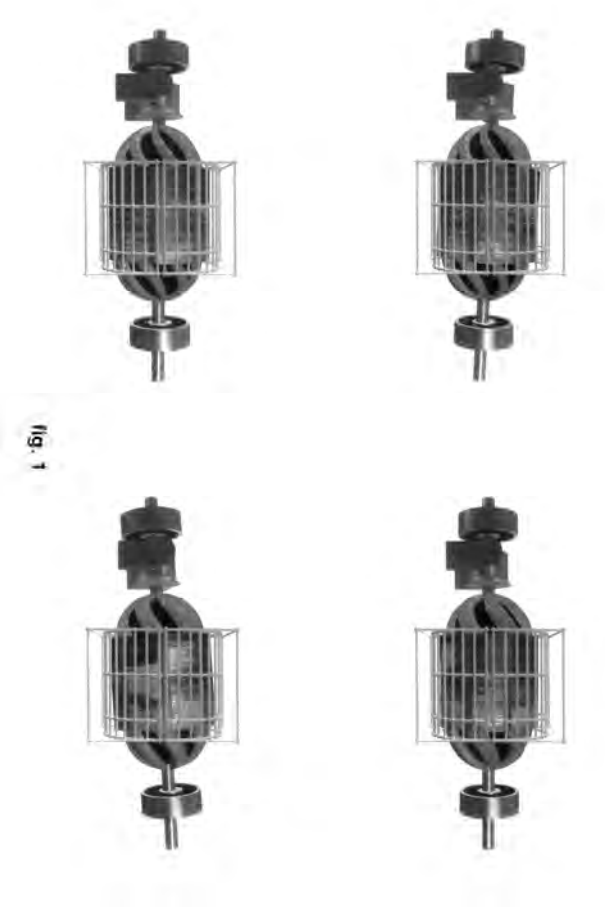

Fig 1 presents results based on 3D modeling by means of which information obtained through optoelectronic elements is visualized.The figure helps to properly analyze moments of displacement and rotation of the rotor in relation to the stator. Based on that analysis it is possible to determine the air gap and the level of arcing(in commutator machines). Selected objects are transformed into 3Ds with appropriate scaling and change of the object in relation to time. This approach allows annimation of serial frames with regard to time.

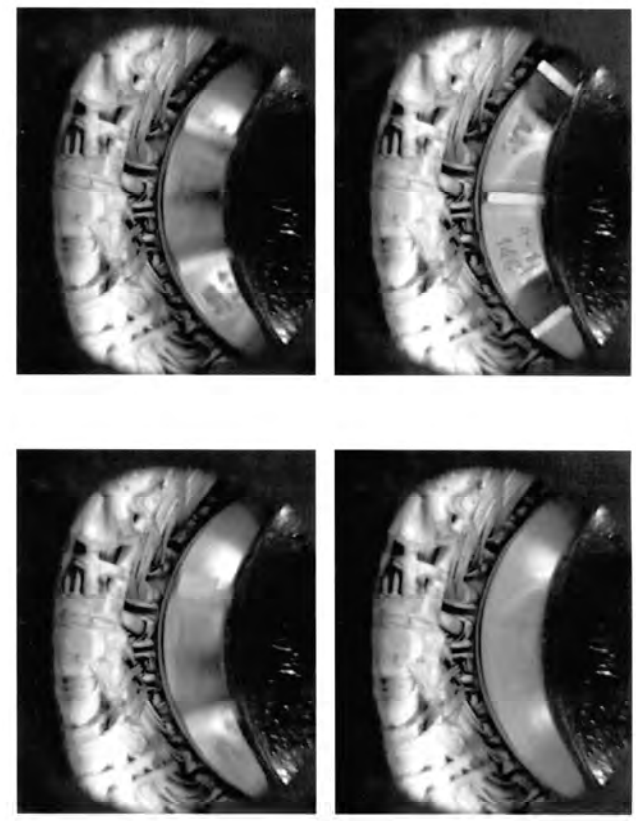

fig. 2

Fig .2 presents a digital image of the change in the air gap of the tested machine both in turning and stationary state. The author has used his CCD colour camara. Photos display different positions of the movable part. Readings obtained by this measurement are processed by proper software

CONCLUSION

So far diagnostics of electro-mechanical objects has been based largely on the experience of control experts. In order to avoid the impact of human factor and ensure objective outcomes it is necessary to employ automated diagnostic tests.Diagnostics approaches revealed in this paper involve methods of evaluation that are based on state of –the- art ways of obtaining relevant information. They are not confined solely to the data concerning the original cause for the flaws because problems with system's sensitivity are already eliminated by digital filters. Objects of display are based on experimental results and moreover appear as problematic when a certain malfunction is to be properly identified. By classifying these results , it is possible to spot electric or mechanical malfunctions by means of a cost effective system for diagnostics.

REFERENCES

1) G.Bozhilov . "Notes on technical diagnostics". Sofia. 1992
2) Tenekedjiev K. Technical diagnostics and sample identification. Varna .1994
3) Gemke R. Malfunctions of electrical machines. L. 1988
4) Fleuder Esat. Bautzner Str. 147. A D-01099. Dresden

Reliability of work of large synchronic turbogenerators

Natasa D. Mojsoska[1] and Dimitar L. Najdenov[2]

Absract - **The generators are the one of the most important elements of electrical energetic system EES and of their accuracy depends pogon security of EES. Insulating system of generators performed the weakest point.**

Security of work of large synchronic generators depends on many factors which during the exploatation and annual maintenance are contraled, measured, examined and followed.

In this work are elaborated factors which influence on IS of synchronic generators in feromagnetic material, stators and rotors wires, exposed to influence of external factors (mechanical load, atmospheric influences - humidity, dust, gases etc.) and internal factors (structure of material). During the exploatation of turbogenerators the insulation "grows old" thanks to different exertions as voltage, temperature, mechanical and chemical

Keywords - **generator, reliability, insulating system, rezistance**

I. INTRODUCTION

Insulating system of generators is exposed to friction, oscilations, vibrations, electromagnetic and mechanical forses and also to electrical, mechanical and aerodinamic infuence.

In this paper is analized and mesured insulating system of synchronic turbogenerator on block 3 in REK - Bitola in 1997 till 2003 year. It was mesured temperature performance before and after the repair, condition of magnetic core, impedances, inductances, insulating rezistance, koeficient of apsorpcion and factor of dielectric power loses wich depends by voltage $tg\delta=f(U)$ during the annual repair.

On the base of prophylactic examination of the parametars of insulating system in period of more years are made comparisons and is observed insulation in exploatation conditions. Where a big diference beetwen mesured and factory allowed values is noticed is recomended a detailed examinations of that parametars of insulating system.

A final result is that insulating system of turbogenerator in block 3 in REK Biotola have extremly quolity insulating, but it is not made any particulary documentation about this prophylactical following and there are no special analyses. It is recomended to do special documentation of this examinations.

[1] Natasa D. Mojsoska is with the Faculty of Technical Sciences, I.L.Ribar bb. 7000 Bitola, Macedonia E-mail: natasamojsoska@yahoo.com

[2] Dimitar L. Najdenov is with the Faculty of Technical Sciences, I.L.Ribar bb. 7000 Bitola, Macedonia

II. FACTORS ON WHICH DEPENDS REALIBILITY OF LARGE SYNCHRONIC TURBOGENERATORS

Repairs in block 3 in Rek - Bitola are made every year as regular and every five years as capital. Program for those repairs consist of:

- prepearing work for putting block in repair
- timing plan for repair
- suplies of parts and spare material
- purpose of mechanical thermal operation examination
- organization of examination
- operation of work during the complex examination
- control of mesured instruments
- complex pogon thermal and mechnical examinations
- elaborates, protocols and referats
- pripearing for putting on work of the blok after finishing the repair and turning on the block on the EES of Macedonia.

Preparation work for putting on the block in work consist of the following actions:

- organizations of educated team who will do the repair,
- back up excitation is checked and examined
- turbogenerator is gradually switched off and put in the no-load state
- research of short-circuit and no-load characteristic and influence of protection relay
- examing of rotor impedence of turbogenerator as a function of speed and voltage

Timing plan for the repairing actions consists of:

- exact date and hour of begining and the end of repair
- exact date and hour of begining and the end of repair on: generator plant, protection of worked and back up excitation, mesuring system, controlled system and G.V.Z.

Parts and spare material for carrying out of repair are:

- brushes for the generator, working and back-up excitation
- insulating material, pump material,
- sprays, cleaning materials, alchohol, colors, towels, conducters, bulbs, bateries ect.

III. ACTIVITIES WHICH ARE MADE TO GET RELIABILITY OF WORK FOR ONE YEAR FOR LARGE SYNCHRONIC TURBOGENERATORS

Purpose of pogon thermal- mechanical research is to record the real condition of the main equipment before and after the repair. That will provide blok working till next repair and have reliability for at least one year.

Organization of examination is with complete profesionality and responsibility of all participans in the repair. People who work on the blok are in groups from different profiles and they exactly know the hierarhy and who is responsible for what.

Operations of work during the complex examination are:

- unloading of TG and calling the person in sharge for turning on/off in EES of R. Macedonia
- power and nesesery operation of work: no-load, short circuit, load by 225MW; 200MW; 175MW and 150MW with time of 2 hours till 4h with posibility for some specific situation time increase for 90 min.

Control of mesured instruments mostly consists of:

- voltage and curent measuring transformers
- wattmeter and warmeter
- voltmeters, ammeters
- measurers of primary and secondary vapour, water into turbine and into cotel
- measuring temperature and presure of coolant
- mesured instruments of woking and back-up excitation.

Control of thermal and mechanical condition of main equipment consist of control of: power and producing of electric energy, electrical recording instruments, control of coal,ash, content of CO and O_2, smoke gases, vibration. Also are examinated the atmospheric influences like humidity, pressure, temperature.

Electrical parametars are exzamined with laboratory instrument with accuracy of 0.5 or smaller. Usualy is measured:

- active and reactive power and apparent power is calculated
- currents and voltages on stator and rotor of turbogenerator, main and additional exitater of working and back-up excitation

When all researches and examination are finished, protokols and referats are made. That shows if there is necessity for more researches and how is state of insulating system at this moment.

After finishing of the all repairing work the block is putts on probe and regular wokr on the network. That preparation consist of:

- observation of functionality of worked and back-up excitation
- rotating of the turbine
- observation of rotor impendance of turbogenerator as a function by speed of rotation
- mesuring of short-circuit and no-load characteristis of TG with all following manipulations for grounding and sepparating in substation
- parametars for manual sinchronization during the putting on the network.

In this paper are given the results from last seven years for blok 3 in Rek - Bitola. For active rezistance of stator winding rezults are sistemized according to years and that is the essential for prophylactical following of insulating system.

IV. ANALYSES OF THE RESULTS OF ACTIVE REZISTANCE OF STATOR WINDING ON TURBOGENERATOR ON BLOCK 3 IN REK BITOLA

In experimental part of this paper insulating system on sinchronous turbogenerator in blok 3 in Rek - Bitotla is mesured and special attention is given to the results of measuring of active rezistance of the stator winding. Sistematization is given in table 1.

TABLE I
VALUES FOR ACTIVE REZISTANCE OF STATOR WINDING ON TURBOGENERATOR IN LATELY YEARS

number	**$1C_1$ - C_4**	**$2C_1$ - C_4**	**$1C_2$ - C_5**	**$2C_2$ - C_5**	**$1C_3$ - C_6**	**$2C_3$ - C_6**
factory value R_{15}° mΩ	3.26	3.19	3.23	3.31	3.18	3.27
R_{15}° mΩ 1997	3.272	3.202	3.242	3.307	3.213	3.285
R_{15}° mΩ 1998	3.274	3.205	3.243	3.308	3.215	3.288
R_{15}° mΩ 1999	3.294	3.223	3.226	3.329	3.229	3.291
R_{15}° mΩ 2000	3.312	3.237	3.277	3.343	3.243	3.323
R_{15}° mΩ 2001	3.318	3.240	3.285	3.353	3.209	3.331
R_{15}° mΩ 2002	3.299	3.224	3.260	3.327	3.230	3.306
R_{15}° mΩ 2003	3.289	3.214	3.255	3.322	3.227	3.301

On the basis of the prophylactic followings so far the parametars on the insulating system in period of more years it is made a comparison of insulating values and is evaluated the efficiency of insulation in exploatation condition. For some parametars detal research is recomended.

From analyses and comparisons the mesured and calculated results as the methods of following, it is obvious the recomended acceptable way of prophylactical followings on insulation and continuing the --- of the exploatation wich is the benefit of this research.

The previous table shows that in all years, active rezistance of stator winding is moving to allowed values time. Compared to the factory value never has been bigger then 2% (1.94%) . Also the criteria for differences between max and min measured values do not exceed the value of 5%.

CONCLUSION

The subject of examination in this paper is insulating system on synchronous generators, detailed active rezistance of stator windings, its efficiency in exploatation as its prophylactic following. More characteristics on the insulating system are observed which are given the real state. There are: electrical insulating rezistance R_{iz}, coeficient of apsorpcion K_a, factor of dielectric power loses in function of voltage $tg\delta=(U)$, intensity of partial discharge, current in the insulating system with high d.c. voltage and dielectrical hardness on insulation with test voltage (---, inducated and sparcover voltage).

It is very important to take a special care for accuracy of the generator as the one of the most important components in EES on what depends the pogon security.

The failure on insulating system are the most often in generators and it is performed the weakest point in exploatation.

State of the insulating system on generators depends of external factors such as mechanical load, atmospheric influences: humidity, dust, gases and internal factors: material structure,athesive material etc.

During exploatation insulating system " grows old " and change the characteristic under the influence of those factors. "Growing old" is manifestated by permanent changes of one or more characteristic compared to some previous known state. It is nessesery "growing old" to be under control.

Insulating system must satisfy the following characteristics: big electrical insulating rezistance, small dielectrical losses, low level of partial discarge, positive mechanical, temperatural and chemical characteristic and big stabillity of all characteristic by the time of use.

The basic electrical load are under the influence of the voltage which define a flowing of electric current in the insulating system. Current creates dielectric loses which increase the temperature in insulating system. Thus insulating rezistance fall down and the current, too. That make loses increase their value. This process in insulating systems in god condition ends with making a balance, but the IS with bed state keep going (continued) and a short-circuit will happen.

Following the "growing old" of the insulating system is making with measuring of the curent, insulating rezistance, dieletric loses by a variabile value of voltage.

Criterias for evaluation of efficiency of insulating system in exploatation all over the world as here are based on anylises of prophylactical following of examination of synchronic generators. On the base of that research there are three groups of qulity of the insulating system:

1. Insulating system in god condition, it has pure and dry insulation wich normal geting old and it can work and stay in operation.
2. Insulating system have a little change in insulating characteristics, it is in pogon state, but it is nessesery detale anylises for reasons for variations. It can stay in work one year till next repair when will be elaminated the reasons for changes..
3. Insulating system who work but have big variations in insulating characteristics that can be expected its failureand can not stay in work one year. It require an anylizes for bed insulating state and determinating way for acting for removed the couses of variations. Additional repair had to done for replasing the demage insulation.

REFERENCES

[1] Prof. d-r Damjan Hristovski - Ispituvanje na elektricni masini , ETF ZONIK kompjuteri - Skopje 1996 god.

[2] Elaborati, godisni izvestai i protokoli od redovnite godisni i kapitalni remonti na turbogeneratorot na blok 3 vo REK Bitola

[3] Najdenova Natasa dipl.el.ing. - " Ispituvanje na izolacioniot sistem na sinhroni turbogeneratori" seminarska rabota, ETF Skopje 1999g.

[4] Najdenova Natasa dipl.el.ing. - "Teoretsko i eksperimentalno profilaktiko istrazuvahje na efikasnosta vo eksploatacija na sinhroniot turbogenerator blok 3 vo REK Bitola " magisterska rabota, ETF Skopje 2001 g.

Modern PWM drives voltage sags sensitivity

Milutin Petronijević[1], **Vojkan Kostić**[2], **Nebojša Mitrović**[3], and **Borislav Jeftenić**[4]

Abstract – **In this paper it is presented investigation in modern PWM drives voltage sags sensitivity. The simulation results, presented below, were collected from the variable speed drives with different control algorithms: simple V/Hz control, indirect rotor flux oriented control and direct torque control. The achieved results refer to various types of symmetrical and asymmetrical voltage sags and show the significant influence of PWM inverter control algorithm.**

Keywords – **voltage sag, adjustable speed drive, power quality, control**

I. INTRODUCTION

According to the appropriate IEC and IEEE standards (IEC 61000-2-8 and IEEE 1159-1995) voltage sags are defined as a temporary short duration voltage magnitude reduction in any or all of the phase voltages (in single or poly-phase electrical network). Beside voltage thresholds, voltage sags are expressed by time duration (0.5 cycles – 60 seconds) and type of voltage sag variation: the three-phase balanced and the different unbalanced. Basically, voltage sags are classified in two ways: in the first of them it is taken into consideration the number of sagged phases and the presence of asymmetries; and the second one divides sags into several ranges regarding to sag duration and/or magnitude ([1], [2]). The newest proposals for voltage sags classification and presentation taking into consideration phase shifts and points on wave at the sag initiation and at the voltage recovery, sag shape, etc.

The fact that adjustable speed drives (ASD) with induction motors are highly sensitive to voltage sags can cause long re-start delays and production losses. An extra increase of expenses (for example in continuous processes as paper industry, glass production, etc.) caused by ASD voltage sags sensitivity which also leads to a numerous experimental and simulation studies. The main aim of the studies mentioned above is to determine the sensitivity factors, and to propose prevention of the ASD's from tripping as a result of voltage sags.

[1]Milutin Petronijević is with the Faculty of Electronic Engineering, Beogradska 14, 18000 Nis, Serbia & Montenegro, E-mail: milutin@elfak.ni.ac.yu

[2]Vojkan Kostić is with the Faculty of Electronic Engineering, Beogradska 14, 18000 Nis, Serbia & Montenegro, E-mail: vkostic@elfak.ni.ac.yu

[3]Nebojša N. Mitrović is with the Faculty of Electronic Engineering, Beogradska 14, 18000 Nis, Serbia & Montenegro, E-mail: nesa@elfak.ni.ac.yu

[4]Borislav I. Jeftenić is with the Faculty of Electrical Engineering, Kralja Aleksandra 73, 11000 Belgrade, Serbia & Montenegro, E-mail: jeftenic@etf.bg.ac.yu

This paper presents the effects of the influence of the different control algorithms on ASD voltage sag sensitivity. Using basic library blocks from Matlab/Simulink and SimPowerSystem toolbox, power converter and supply network model are built and also presented three different control algorithms: open loop V/Hz, speed closed loop indirect field oriented control (IFOC) and speed closed loop direct torque control (DTC). Various types of symmetrical and asymmetrical voltage sags are used in simulations with different loading and operating drive conditions. It was also presented simple methods on each at a time, by which speed drops were reduced during voltage sag.

II. ASD AND VOLTAGE SAGS

There are three reasons for tripping ASD's because of voltage sag. The first one is that the control electronics power supply of the drive also sensitive to voltage sag. If the power supply cannot obtain adequate voltage for the control electronics, the drive has to be shut down as a safety measure against losing control of the drive. It is necessary the drive to be equipped with an uninterruptible power supply (UPS) for the control electronics. In industrial plants it is the most common approach by which control electronics operation is obtained during voltage sag or interruption.

The second reason is that DC voltage drop under predefined minimum level or output motor currents go through the over-current limit. DC voltage drop under minimum level can lead to the appearance of the high inrush input current when the power-up again.

The third reason is that some processes with ASD (for example multi-motor and speed synchronized drives) cannot tolerate the loss of accurate speed or torque control, even for a few seconds due to damage the final product or halt of the process.

Figure 1 show a typical PWM ASD equipment topology, which consists of a three-phase diode rectifier, DC-link and an inverter. There are two basic types of rectifiers: the uncontrolled (diode) and the controlled (thyristor or IGBT) rectifiers. In this paper we only considered a diode rectifier.

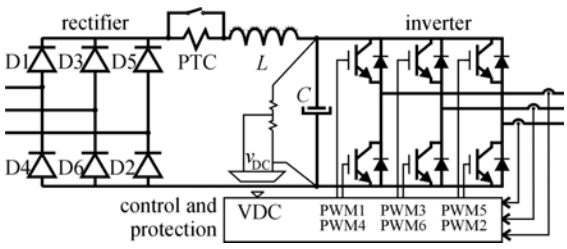

Fig. 1. Typical PWM frequency converter

The DC-link consists of LC filter for smoothing the pulsating DC voltage and the charging circuit suppresses high inrush current during converter power-up. ASD's typically have between 75 and 360 mF of capacitance per kW of drive rating and the DC-link inductor (typically, 2%-5%). The inverter controls the frequency of the motor voltage according to signals (pulses) from control circuit. The control and protection circuit can transmit and receive signals to/from rectifier, the intermediate circuit and the inverter.

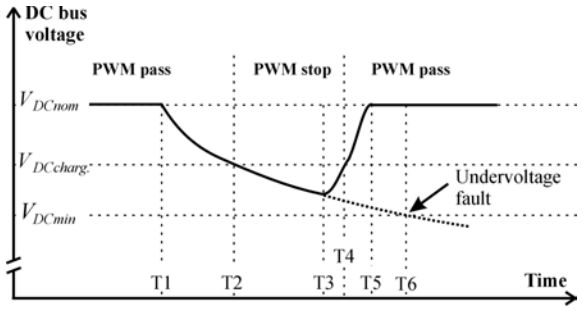

Fig. 2. DC link voltage during voltage sag

In the Figure 2 is shown important occurrences to explain ASD sensitivity to voltage sag. At T1 period the voltage sag is appeared and, due to reverse bias of input diodes, DC bus voltage begins to drop rapidly. When $V_{DCcharg}$ value is reached (level where the drive goes into pre-charge) output to the motor is stopped. Between T2 and T3 the rate of decay on the bus voltage is much slower because the drive is not producing output power to the motor.

If the line voltage is restored at T3 period, the DC bus voltage will begin to rise. Between T3 and T4 the input line current is limited by the pre-charge circuit. This prevents high inrush currents and DC bus over-voltage. At T4 the PWM inverter control starts and output to the motor resumes. If the line voltage not restored at T3, a line loss fault or under-voltage fault could occur at T6 (DC bus voltage falls below a minimum level V_{DCmin}). This minimum DC voltage level may be the lowest safe point when the internal control power supply can be in operation.

The voltage sag type (single-phase, two-phase or three-phase) and duration of the sag influence drive sensitivity. Loading and operating conditions of both the drive and controlled motor also have significant influence on drive behaviour during the sag. Thus, different load types, variations in loading torque and operation with reduced motor speeds should be also regarded as the factors of influence in the assessment of the PWM drive sensitivity.

Adjustable speed drive complexity, numerous of influential parameters and request for special equipment usage (voltage sag generator, programmable load and measurement equipment) make difficult the experimental investigation of ASD voltage sag sensitivity. According to Ref. [6] appropriate simulation model must have the following important parameters: a) the DC link components; b) the power consumption of the load (loading torque including induction motor *qd*-model); c) under-voltage / over-current protection settings including current/voltage sampling effects and RMS calculation; and d) control algorithm. The importance of the influence of the last mentioned parameter is stressed in this paper.

III. MODELLING AND SIMULATION

Complete ASD model with the power supply voltage sag generator is built in Matab/Simulink software. In control circuit we modelled three different control algorithms: open loop V/Hz with stator resistance voltage drop compensation ([3]), speed closed loop indirect rotor field oriented control (IFOC) ([4]) and speed closed loop direct torque control (DTC) ([5]). All parameters of the power unit and control circuit of the frequency converter are shown in Table 1.

TABLE 1. POWER UNIT AND CONTROL CIRCUIT PARAMETERS OF THE FREQUENCY CONVERTER ([5]).

Power unit	Input	3~, 400V, diode bridge rectifier
	Output	3~, IGBT inverter, I_{outnom}=9.5A
	DC link	C=2x640μF in series, (dis)charging time 17ms, L=1.5mH
Protection settings	Under-voltage protection	$V_{DCcharg.}$=320V (57% of V_{DCnom}=560V); sampling period T_s=250μs
	Fast over-current protection	I_{outmax}=20.4A rms, (215% of I_{outnom}=9.5A), $f_{bandwidth}$=5kHz
Control methods	V/Hz control	switching frequency f_{SW}=7.5kHz, with stator resistance voltage drop compensation
	IFOC	speed closed loop, f_{SW}=7.5kHz, torque limit T_{max}=160% T_{nom}.
	DTC	speed closed loop, f_{SW}=7.5kHz, torque limit T_{max}=160% T_{nom}.

In this paper we used induction motor with the following parameters: 3x230/400V, D/Y, 50Hz, nominal speed n_n=1440rpm; rated power: P_n=4kW; stator and rotor leakage inductance: L_{ls}=L_{lr}=0.013mH; mutual inductance L_{lm}=0.130mH; stator and rotor resistance: R_s=1.13Ω, R_r=0.9Ω; inertia J_m=0.015.

Firstly we tested ASD sensitivity against three-phase symmetrical voltage sags with different load torque values and with nominal reference speed. Achieving results are presented in Fig. 3. All drives have identical settings of protection control circuit and in a speed control schemes PI speed controller parameters are adjusted equally.

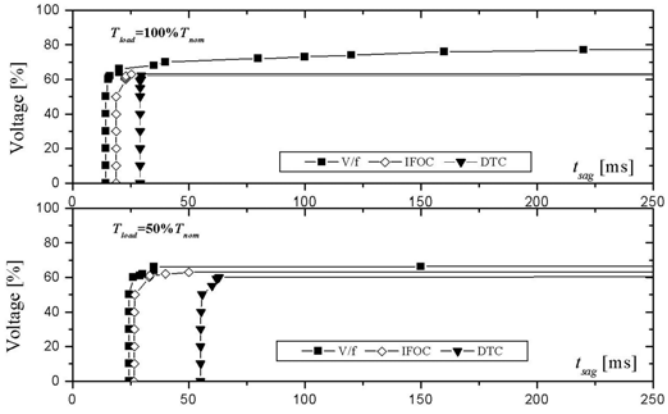

Fig. 3. Sensitivity of ASD drives to symmetrical three-phase sags with different load torque values: T_{load}=100%T_{nom} (top); T_{load}=50%T_{nom} (bottom)

The vertical parts of the drive voltage-tolerance curves are determined under-voltage protection response. Small difference between drives is the consequence of different DC voltage ripple and motor electromagnetic torque (stator currents) during sag. If the supply voltage recovers before the DC bus voltage reaches the under-voltage protection level, a high charging current is drawn from the supply network and may blow the fuses. If this possible, high inrush current can flow to induction motor and activate over-current protection. In V/Hz drive, horizontal part of the voltage-tolerance curve represents this effect. Due to the torque limit (torque limit is set on 160% of nominal torque) drives with IFOC and DTC are not able to cause fast over-current reaction.

Figure 4 compares voltage-tolerance curves obtained in simulations for three-phase voltage sags with different motor speeds. Decreasing the adjusted motor speed also results in lower drive sensitivity.

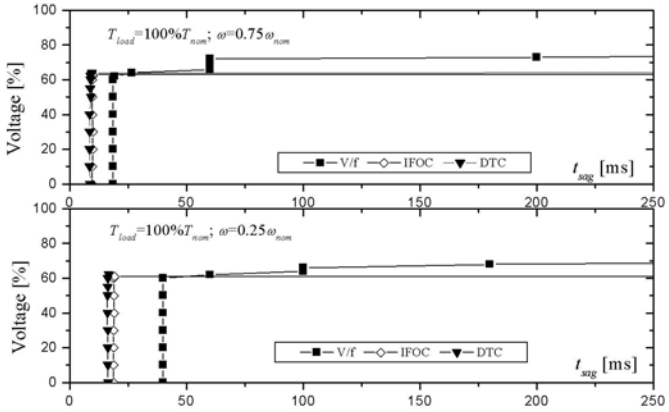

Fig. 4. Influence of different motor speeds on sensitivity of PWM drive to symmetrical three-phase voltage sags.

In Fig. 5 are shown voltage-tolerance curves for two-phase voltage sags with rated voltage in un-sagged phase and with different motor speeds (constant torque load type and rated loading torque value). The similar behaviour is identified in this case - decreasing of the adjusted motor speed results in lower drive sensitivity. Two-phase voltage sag characteristic is DC bus voltage ripple and a significant torque ripple increase (for example, in DTC drive thereabout 300% of rated regime values).

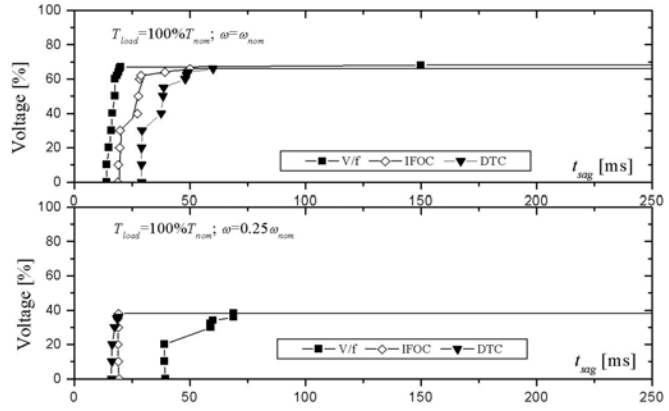

Fig. 5. Sensitivity of VSD drive to two-phase sags.

For single-phase sags with rated voltage in un-sagged phases no-trip occurs in all types of drives.

IV. MOTOR SPEED DROP

Some processes driven by the motors, like multi-motor drive application (speed synchronization or torque load sharing regulation) will not be able to tolerate the drop in speed or the torque variations due to the sag.

In ASD with IFOC the problem of adequate adjusting flux-producing stator current component (i_{ds}) is appeared. Before voltage sag, this component is equal to nominal value i_{dsnom}, as in the period after voltage dropping. During the voltage sag flux-producing current component can be adjusted according to: 1) the rated value; 2) the value which is appropriate to DC bus voltage value during the sag; 3) the dynamic *d*- and *q-axis* current sharing strategy which obtain higher transient torque and minimum speed deviation.

A sudden step supply voltage decrease takes place next, at time instant zero, leading to the operation of the inverter at the maximum allowed stator current value i_{smax}:

$$i_{s\max} = \sqrt{i_{ds}^{*2} + i_{qs}^{*2}} \ . \qquad (1)$$

The available current is to be distributed into *d*- and *q-axis* current. Here asterisk denotes commanded (reference) values and indices *d* and *q* remark *d-q axis* components of the stator currents. The algorithm that is developed here is characterized with the following rules:

$$i_{ds}^{*} = 0 \qquad i_{qs}^{*} = i_{s\max} \qquad \text{for } 0 < t < t_1 \qquad (2)$$

$$i_{ds}^{*} = k \cdot i_{dsnom} \qquad i_{qs}^{*} = \sqrt{i_{s\max}^{2} - i_{ds}^{*2}} \ \text{ for } t_1 < t < t_2 \,, \qquad (3)$$

where: t_1 is the time when the *d-axis* motor current component drops to the decreased value which is matched with the sagged DC bus voltage, t_2 is the time of the power-up and $k = V_{DC} / V_{DCnom}$. V_{DC} and V_{DCnom} denote actual and nominal DC bus voltages. After sag ending, flux-producing current component resets to the nominal value. Developed simulation model takes into account sampling times and frequency bandwidths for currents and voltages measurement loops.

In Fig. 6 is presented the comparison of the simulation results, for three methods mentioned above, in case of symmetrical three-phase voltage sag.

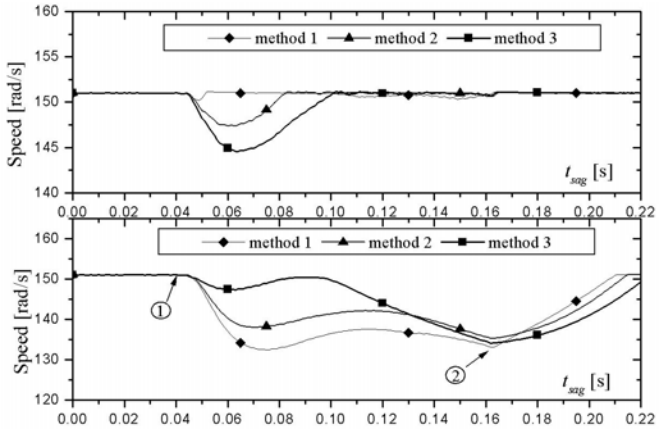

Fig. 6. Motor speed drop during voltage sag in drive with IFOC (① - point of sag start, ② - point of sag end): U_{sag}=80%U_n (top); U_{sag}=70%U_n (bottom)

As it can be seen in Fig. 6, the proposed method of the dynamic current sharing of the inverter maximum current, leads to the minimum speed drop. The adjustable speed drive with IFOC where the third method is implemented reacts faster than the first two ones because of forcing torque-producing current component. It should be noted that in practice there is a problem of the proposed algorithm in detection of the voltage sag magnitude value. Beside the simulated rectangular voltage sag, the experimental researches present that voltage sags which are neither rectangular in most cases nor voltage magnitude is constant during the whole period. This can make problems in practical implementation, which will be target in future research.

In the case of ASD with DTC is modelled very simple algorithm where is the commanded value of the stator flux chosen according to the following equation:

$$\psi_s^* = k \cdot \psi_{snom}^* , \tag{4}$$

Where: ψ_s^* and ψ_{snom}^* actual and nominal stator flux reference value, respectively. In the simulation ψ_s^* is reached as output from look-up table with V_{DC} as an input. More detailed explanation of the simulation model of ASD with DTC can be found in [5] or in request of the first author. In Fig. 7 are shown simulation results in speed drop for DTC classical model (without stator flux correction) and for model in which Eq. (4) is implemented.

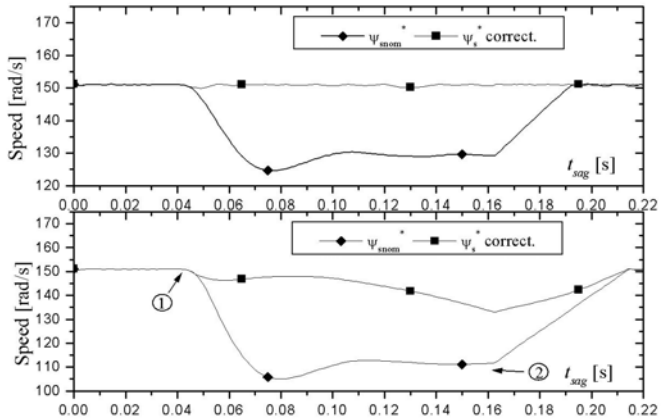

Fig. 7. Motor speed drop during voltage sag in drive with DTC (① - point of sag start, ② - point of sag end): U_{sag}=80%U_n (top); U_{sag}=70%U_n (bottom)

Flux and torque hysteresis controller in DTC bring to excellent dynamic performances in transients. Response rapidity will be dominant determined by low-pass filter transfer function in DC-bus voltage measurement loop.

Having in mind that the induction motor, whose parameters are given in this paper, with small pull-out torque (177%T_{nom}), for all voltage sags with voltage magnitude less than 77% of nominal supply voltage, leads to the motor torque less than nominal load torque and speed drop is unavoidable. Generally, induction motors have pull-out torque greater than 200% of rated torque; so it is the way when speed drops during voltage sags at 70% of nominal value can be avoided.

V. CONCLUSION

PWM inverter drives will shut down at voltage sag, initiated by their under-voltage or over-current protection scheme. As can be seen from the results shown previously the type and magnitude of symmetrical and asymmetrical voltage sags have significant influence to the ASD sensitivity. Also, different motor loading conditions and different motor speeds influence on ASD voltage sag sensitivity. It should be stressed that the presented results of simulation show significant influence of control algorithms to adjustable speed drives sensitivity. Modern adjustable speed drives (IFOC and DTC) demonstrate lower voltage sag sensitivity especially due to impossibility of the over-current reaction (if the user settable maximum current/torque values lower than maximum protection ones).

In this paper is also presented the voltage sag influence on the drop of speed. Regular control algorithms are able to cause the drop of speed which cannot be accepted in some industrial application. Control algorithms in IFOC and DTC drives can be simple modified to maintain speed drop at a minimum. Very good dynamic performances are found in regard to speed drop in both speed closed loop ASD's. Having in mind motor speed drop, DTC drive is simple to adapt to voltage sag than one with IFOC. Future researches will be faced to practical implementation of the proposed algorithms for speed drop minimization during voltage sag and speed synchronization in multi-motor drives along and after the voltage sag.

REFERENCES

[1] S. Ž. Djokić, J. V. Milanović, D. J. Chapman, M. F. McGranaghan, "Shortfalls of Existing Methods for Classification and Presentation of Voltage Reduction Events", (to be published in IEEE Trans. On Power Delivery)

[2] M.H.J. Bollen, "Characterisation of voltage sags experienced by three-phase adjustable-speed drives," *IEEE Trans. Power Delivery*, vol. 12, no. 4, pp. 1666-1671, oct. 1997.

[3] W. Leonhard, "Control of Electrical Drives," *Springer - Verlag*, Berlin, 1996.

[4] I. Boldea and S. A. Nasar, "Vector Control of AC Drives," CRC Press, 1992.

[5] V. Kostic, N. Mitrovic M. Petronijevic and B. I. Jeftenic, "Direct Torque Control", 12th International symposium on Power electronics, Novi Sad, Serbia and Montenegro, T2-1.5, CD-ROM, 2003.

[6] S. Ž. Djokić, J. V. Milanović, K. Stockman and R. Belmans, "Voltage-tolerance Curves of PWM Drives: Comparison of Simulations and Measurements", 12th International symposium on Power electronics, Novi Sad, Serbia and Montenegro, T6-1.3, CD-ROM, 2003.

Session EQ:

Education Quality

An Approach to the Quality Rating of the Bachelor and Master's Curricula

Peter T. Antonov [1]

Abstract - **This paper presents an approach to the quality rating of the Bachelor and Master's curricula. It is based on the estimation and analysis of the courses eligibility level and can be used to compare different curricula. A suitable curriculum model is offered too.**

Keywords - **Bachelor, Master, curriculum, eligibility, quality.**

I. INTRODUCTION

As it is known, the main purpose of the educational system lays in the preparation of qualified and skilled persons, required by the society, with a realization of full value. Nowadays, in relation to the sweeping changes in business and politics, new necessary qualities become topical in order to get a high-paid job and for a successful professional career [1]. This requires considerable changes in the educational content, first of all, in the used educational technologies. It strongly affects the higher education field, which has to adapt itself fast to high technologies and the changing market and labour conditions.

According to the new Regulations for State Requirements for receiving a university degree in Bulgaria, training in each speciality (major) must be carried out under certain curriculum [2], which includes compulsory, elective and optional courses. The compulsory academic courses must provide fundamental training in the chosen professional field, the elective ones - necessary specific knowledge and competencies in the chosen subject field.

The eligibility of courses is one of the most significant indicators of the curricula quality and it becomes the main prerequisite for providing internal and international students' mobility and specifying their preparation in the desired direction. These goals are completely in unison with the UNESCO recommendations [3,4] for higher education improvement and quality increasing.

Having in mind the above-mentioned facts, this paper treats a developed approach to quantitative estimation of the Bachelor and Master's curricula quality. It is based on the analysis and evaluation of the level of course eligibility, comprised in these curricula. At the same time, the paper offers a model for design and presentation of such curricula, which is completely suitable for usage. Its accepting will provide the unification, larger transparency and clearness as well as more efficient control on the quality of the process of academic studying.

II. A MODEL FOR CURRICULA PRESENTATION

It is advisable to mark each course with a *code for the particular curriculum* (*curriculum code*) and a *common code* (*department code*) used in all academic curricula at university, where it is included. It is suitable for the *course code for the particular curriculum* to contain short names of the academic degrees (for instance: B - for Bachelor, M - for Master) and the major, also the number course position in this curriculum. The common code should contain the short name of the department, providing this course, and the number of the course within the frames of the corresponding department. Opposite the pointed out codes, it is logical to write "elective course from:" or a particular title, if the course is not elective. For example,

…..		
B_CST_25	CSE_18	Computer Nets
….		
B_CST_33	E	An elective course from:
	MAT_09	Operations Research
	TEM_12	Numerical Methods
….		
B_CST_44	E	An elective course from group A
B_CST_45	E	An elective course from group B
B_CST_46	E	An elective course from group C
….		

Courses from group A

CSE_36	Cryptography and Data Protection
CSE_42	Internet Technologies
COM_31	Optical Communications
ELC_28	Measurements in Electronics

Courses from group B

CSE_38	Net-based Programming

The first line in the example with B_CST_25 is the code for *Computer Networks* course in the particular curriculum and it means, that the curriculum is for Bachelors' training, the major is CST (Computer Systems and Technologies) and the

[1] Peter T. Antonov is with the Faculty of Computing and Automation, 1 Studentska Str. Varna 9010, Bulgaria, E-mail: peter.antonov@ieee.org

course position in this curricula is 25. In this case the common code CSE_18 shows that the department, providing a certain course, is CSE (Computer Science and Engineering) and its code within the department frames is 18.

The course B_CST_33 is elective (E) from the courses *Operations Research* and *Numerical Methods.* The Department of Mathematics (MAT) provides the first course, The Department of Theoretical Mechanics (TEM) - the second one. The adopted codes of these courses within the frames of the departments are respectively 09 and 12.

B_CST_44 is a curriculum code in the discussed example for an elective course from group A, which includes 4 courses, provided by different departments and so on.

It is obvious that, in order to implement the above-described model in a particular university for curricula design, it will become necessary to acquire common short names of majors and departments in the corresponding native language and in English, and also codes for all courses, provided and offered by different departments. It is quite clear that in dependence on the desired detail of the curricula design, each line in the above-discussed example can be complemented with usual necessities such as final procedure, number of classes, type of classes, week loading and ECST (European Credit Transfer System) credits.

III. Estimation of the Eligibility Level in the Curricula

In order to estimate the level of eligibility in the curricula, the introduction of *coefficient of eligibility* is offered. It can be determined for each individual course, separate semester, groups and the whole curriculum,

The *coefficient of eligibility* for each course C_e can be estimated simply by number n of the offered courses, one of which the student has to chose as compulsory.

Thus, if a certain course is not elective in l-position of the curriculum, but compulsory, it will be denoted with its title and its coefficient of eligibility C_e will be equal to 1, since n=1 in this case. If, for example, the following is written in position *l:*

l) An elective course from

<course 1>
<course 2>
<course 3>,

the coefficient of eligibility C_e in this case will be $C_e = n = 3$. On analogy, in the above-mentioned example, the coefficient of eligibility of the B_CST_33 course is equal to 2, the B_CST_44 - to 4.

Therefore, the coefficient of eligibility for each semester C_s can be defined from the following expression:

$$C_s = \frac{m}{M} + \frac{\sum_{j=1}^{M} C_e^{(j)}}{M} \qquad (1)$$

where

$C_e^{(j)}$ - coefficient of eligibility of j-course in certain semester;
j - index of courses in a semester;
M - total number of courses in a semester;
m - number of the elective courses in a semester

Then the coefficient of eligibility of the whole curriculum (programme) can be defined on analogy with the expression

$$C_c = \frac{q}{Q} + \frac{\sum_{h=1}^{Q} C_s^{(h)}}{Q} \qquad (2)$$

where

Q - number of semesters in the curriculum;
$C_s^{(h)}$ - coefficient of eligibility per semester h;
h - index of semesters in the curriculum;
q - number of semesters with elective courses.

As it has already been mentioned, the introduced coefficient of eligibility equals 1 for all compulsory courses from the curriculum. If elective courses are not offered, i.e. all courses are only compulsory ones, then m=0 and the coefficient of eligibility C_s for that particular semester will also equal 1. On analogy, if there are no semesters with elective courses, then q=0 and the coefficient of eligibility of the whole curricula C_c will also receive a value of 1, following the offered formula (2).

When a particular semester from the curriculum has several or all elective courses to be chosen from a common group of offered courses, then the coefficient C_e for each course is advisable to be calculated as:

$$C_e = \frac{G}{g} + \frac{G - g}{G} \qquad (3)$$

where

g - number of the elective courses to be chosen from a corresponding common group of offered courses (obviously, $g \leq m$);
G - number of offered courses in the common group from which g courses have to be chosen

The second part $[(G-g)/G]$ in the proportion (3) logically allows increasing the eligibility estimation of individual courses in comparison to the alternative case, when each elective course is compared to one of its subgroups in the group of offered courses G.

For example, let g=2, G=4 and the corresponding writing in the curriculum for the discussed semester be the following:

l) An elective course from group H
l+l) An elective course from group H

Courses from group H

<course 1>
<course 2>
<course 3>
<course 4>

In the alternative case the writing in the curricula will appear in the following type:

l) An elective course from
<course 1>
<course 2>

l+l) An elective course from
<course 3>
<course 4>

According to formula (3), the coefficient of eligibility C_e = [4/2+(4-2)/4]=2.5 is received in the first case for each of both elective courses (in position *l* and *l+l*), while in the alternative situation the coefficient is $C_e = n$=2.

The higher value of C_e is logically due to the greater variability of students' choice. It is evident that the number of variants in this case equals the number of combinations in the second level of all 4 elements, i.e. $C_4^2 = 6$, in the other case the variants for course choice are 4.

IV. An Example

The coefficients of eligibility will be defined as an example in the curricula of three Master's programmes (*Programming Systems and Technologies*, *Informatics*, *Computer Systems and Nets*) at the Department of Computer Science and Engineering (CSE) at the Technical University of Varna, Bulgaria. They are presented in [5]

The curricula of each of the above-mentioned Master's programmes contain two academic semesters and the third one is for diploma project and its defense. During each academic semester five courses have to be studied and they are selected from the corresponding groups, containing 10 offered courses. For instance, the curriculum of the first Master's programme at the CSE Department (*Programming Systems and Technologies*) includes the following courses:

1st semester
Five elective courses from

- Systems Analysis
- Numerical Methods
- Parallel Algorithms and Systems
- Parallel Programming
- Language Processors
- Web Design
- Designing Java Applications
- Programming with C# and Visual Studio.Net
- Neural Nets and Applications
- Manager Decisions

2nd semester
Five elective courses from

- Web Applications with C# and Visual Studio Net
- Distributed and Net Databases
- Net-based Programming
- Expert Systems
- Program Diagnostics
- WAP Information Technologies
- Distributed and Net Operating Systems
- Designing Object-oriented Applications
- Integrated Computer Systems and Nets
- Risk Analysis

3rd semester
Diploma project and its defense

In this case g=5, G=10 and the coefficients of eligibility of different courses during each individual semester of Master's programmes are received according to the formula (3) as C_e =[10/5+(10-5)/10]=2.5

The coefficient of eligibility for each semester is received following the formula (1), at $m=M=g$=5, when C_s=3.5. According to (2), C_c = 4.5 for each one of the three Master's programmes is defined for each semester at $q=Q$=2

The values of C_s and C_c show that the eligibility level in the discussed Master's programmes is of a very high level. What is more, it actually reaches the maximum, since it can be increased in this case only by ungrounded further increase of the G value.

References

[1] Пейперт, С. Образование для общества знания. – Международный практический семинар ИИТО ЮНЕСКО "Проектирование национальных и региональных программ информатизации образования. – М.: ИИТО ЮНЕСКО, 21-24 февраля 2001.

[2] Наредба за държавните изисквания за придобиване на висше образование на образователно-квалификационните степени "специалист", "бакалавър" и "магистър". – София, Държавен вестник, брой 76/2002.

[3] Word Declaration on Higher Education for the 21. Century: Vision and Action and Framework for Priority Action for Change and Development in Higher Education adopted by the World Conference on Higher Education. – Paris, UNESCO, 9 October 1998.

[4] Report on Trends and Developments in Higher Education in Europe. – UNESCO, Meeting of Higher Education Partners, Paris, 23-25 June 2003.

[5] Антонов, П. Нови учебни планове на катедра "Компютърни науки и технологии" в Технически университет – Варна. – София, Автоматика и информатика, 2003, бр.2.

Web-Based Tutorial Of Computer Networks And Web Design

Boriana Deliiska[1], Peter Manoilov[2] and Neno Petrov[3]

Abstract — **In this paper the objectives and the structure of web-based tutorial and practical training manual of computer networks and web design are given. The tutorial is developed with a view to introduce students to networking, distributed computing technologies and WWW.**

Keywords — **web-based tutorial, computer network, Internet, web design**

INTRODUCTION

The dynamic development of the computer networks and Internet technologies vastly anticipates the publishing of hard-copy tutorials, practical training manuals and other educational printouts. The continuously increased number of the computer network users of a different age and qualification demands the creation of popular simple-structured web-based tutorials in this area.

In the other hand, the acquiring of skills in the networking is impossible without some preliminary knowledge and experience in the offline computer technologies.

OBJECTIVES

There are many educational courses about computer networks and web technologies published in the web space. Many of them are professional or about concrete business network products. Other ones are payed. Very popular free courses in this area are [1], [2], [3], [4].

The main objectives of the present web-based tutorial is to provides basic knowledge about the nature, purpose, structure, elements, services and terminology in the area the local and global computer networks. The basics of the web technologies and the web design are included too.

With a view to unprofessional users no familiar with the computer English, the tutorial is compiled in Bulgarian but the basic terms in English are given too.

STRUCTURE

The tutorial and the manual cover about 45 training hours – 15 hours lectures and 30 hours practice.

The main page of the tutorial is shown on fig.1.

There are 7 headings in the left menu – lectures, practical training, syllabus, calendar plan, examen, references and authors.

fig.1. Main page

The list of lectures is shown on fig.2.

№	СЪДЪРЖАНИЕ НА ЛЕКЦИИТЕ	бр.ч.
I	ГЛОБАЛНИ ТЕЛЕКОМУНИКАЦИОННИ СИСТЕМИ. РАЗВИТИЕ. КЛАСИФИКАЦИЯ И ПРИНЦИПНА СТРУКТУРА. ОСНОВНИ ПОНЯТИЯ 1. Телекомуникационни системи. Класификация. Същност и предназначение. 2. Историческо развитие. 3.Принципна структура на локални и глобални компютърни мрежи.	2
II	МРЕЖОВИ ОПЕРАЦИОННИ СИСТЕМИ 1. Същност и определение за МОС. Класификация. 2. Слоеве и протоколи. Потребителски интерфейс. 3. Мрежови функции в операционна система.	2
III.	МЕТОДИ И ПРОГРАМНО-ТЕХНИЧЕСКИ СРЕДСТВА ЗА ДОСТЪП В ГЛОБАЛНИ КОМПЮТЪРНИ МРЕЖИ 1. Обзор и характеристики на методи и програмно-технически средства за връзка в глобални компютърни мрежи. 2. Потребители и начини за включването им към Интернет. Протоколи.	2
	ЕЛЕКТРОННА ПОЩА И ЕЛЕКТРОНЕН ОБМЕН НА СЪОБЩЕНИЯ. ПОЩЕНСКИ СПИСЪЦИ	

fig.2. Content of the lectures

The titles of the lectures (fig.2) are links to its contents. The lectures material is divided on 7 themes:

- the basic concepts and classification of the computer networks, network configurations;
- network operating systems, the principles and the layers of the Open System Interconnection (OSI), client/server architecture;
- software, hardware and methods for network connections and protocols;
- structure of Internet and domain name system (DNS);
- the main network services (e-mail, forums, FTP, Telnet, www);
- the content and the structure of web pages and the nature and elements of web design;
- the basic elements of HTML.

[1] Boriana P. Deliiska is with the Department of Computer Science and Informatics of the University of Forestry, Sofia 1756, bul. Kl.Ohridski 10, Bulgaria, e-mail: delijska@mail.bg

[2] Peter G. Manoilov is with Department of Computer Science of the Technical University Sofia 1756, bul. Kl.Ohridski 8, e-mail: manoilov@mail.bg

[3] Neno P. Petrov is with Faculty of Management of the University of Forestry, Sofia 1756, bul. Kl.Ohridski 10, Bulgaria, e-mail: nenopetrov@abv.bg

In the preparation of lectures some elements of [5], [6] and [7] are used.

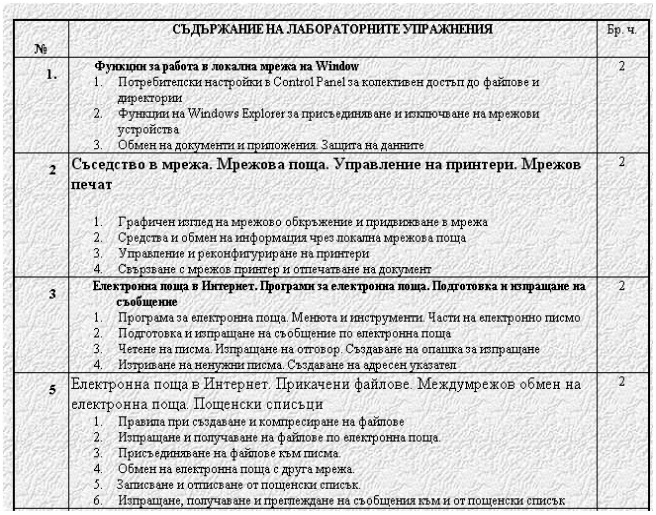

№	СЪДЪРЖАНИЕ НА ЛАБОРАТОРНИТЕ УПРАЖНЕНИЯ	Бр. ч.
1.	**Функции за работа в локална мрежа на Window** 1. Потребителски настройки в Control Panel за колективен достъп до файлове и директории 2. Функции на Windows Explorer за присъединяване и изключване на мрежови устройства 3. Обмен на документи и приложения. Защита на данните	2
2	**Съседство в мрежа. Мрежова поща. Управление на принтери. Мрежов печат** 1. Графичен изглед на мрежово обкръжение и придвижване в мрежа 2. Средства и обмен на информация чрез локална мрежова поща 3. Управление и реконфигуриране на принтери 4. Свързване с мрежов принтер и отпечатване на документ	2
3	**Електронна поща в Интернет. Програми за електронна поща. Подготовка и изпращане на съобщение** 1. Програма за електронна поща. Менюта и инструменти. Части на електронно писмо 2. Подготовка и изпращане на съобщение по електронна поща 3. Четене на писма. Изпращане на отговор. Създаване на опашка за изпращане 4. Изтриване на ненужни писма. Създаване на адресен указател	2
5	Електронна поща в Интернет. Прикачени файлове. Междумрежов обмен на електронна поща. Пощенски списъци 1. Правила при създаване и компресиране на файлове 2. Изпращане и получаване на файлове по електронна поща. 3. Присъединяване на файлове към писма. 4. Обмен на електронна поща с друга мрежа. 5. Записване и отписване от пощенски списък. 6. Изпращане, получаване и препращане на съобщения към и от пощенски списък	2

fig.3. Content of practical training manual

The practical training manual (fig.3) provides developing of skills about:

- connecting to local area network (LAN) and wide-area network (WAN);
- the rules and the etiquette of behaviour in the network;
- the methods of optimal access to information in different areas;
- the methods of saving and protection of personal data and software;
- the choice of e-mail system, creation of e-mail address, structure of e-letter, composing, sending and receiving of e-letters, file attaching, support of address books etc;
- the remote access to applications (Telnet);
- the methods of file downloading and uploading (FTP);
- the software and methods of access, registration and participation in forums (newsgroups or discussion groups);
- the optimal setting and working with web browsers;
- the structuring and developing of web pages;
- using of web page editors and filters;
- the publishing of personal web pages.

In the calendar plan the dates and the places of concrete course are given.

Under reference there are literature issues and useful web links.

This course is intended for the students of the University of Forestry, Sofia, Bulgaria but could be used for other beginners in area of computer networks.

REFERENCES

[1] A Beginner's Guide to HTML, http://archive.ncsa.uiuc.edu/General/Internet/WWW/HTMLPrimerAll.html

[2] M. Isaacs, "Online tutorial system TONIC-NG" copyright of Netskills, University of Newcastle, UK, http://www.netskills.ac.uk/TONIC

[3] B. Mitchell, "Wireless/networking", http://compnetworking.about.com/mlibrary.htm

[4] Yechiam Yemini, "The network book", http://www1.cs.columbia.edu/netbook/

[5] Е. Кастро, "HTML за WWW", София, Инфодар, 1999

[6] И.Маджаров, "Интернет за PC", София, Статист. издателство, 1998

[7] Интернет. Пълен справочник, София, Софтпрес, 200

Using PC Sound Blaster as a Digital Oscilloscope

Rangel Dinov[1], Plamen Shterev[2]

Abstract - **Computer interfacing software has taken advantage of faster processing, development of user-friendly languages for integrating machines and computers. The purpose of this research work is to describe a powerful, widely applicable approach to interfacing that uses object-oriented programming and the concept of "virtual instruments" and to show how this approach can be used in the research laboratory and in practice. The proposed method can be used in engineering education and in web based distance learning.**

Key words – **Digital oscilloscopes, Virtual instruments, Education, Distance education.**

I. INTRODUCTION

In our days many functions, such as communication, data display, data output, human interface, memory, data processing in a measurement instruments system, and signal processing, are gradually taken in by improvement in the data-processing capability of a personal computer. Measurements systems can be customized comparatively free according to a user intention.

The development of powerful personal computers and workstations has transformed the way scientists work. Increased processing speed and available memory have led to the development of highly sophisticated programs that perform intricate calculations and handle large data sets.
[1]

Electronic signal processing can now often be replaced by digital computer processing. Windows and graphical user interfaces have made it possible for computers to perform multiple tasks simultaneously and have made it easier for scientists to analyze and display data as well as to write papers, manage references, and so on.

II. DIGITAL OSCILLOSCOPES

Digital oscilloscopes and waveform digitizers sample signals using a fast analog-to-digital converter (ADC). At evenly spaced intervals, the ADC measures the voltage level and stores the digitized value in high-speed dedicated memory. The shorter the intervals, the faster the digitizing rate and the higher the signal frequency that can be recorded. The greater the resolution of the ADC, the better the sensitivity to small voltage changes. The more memory, the longer the recording time. What are the benefits of this digital technology? Multiple signals associated with intermittent and infrequent events can be captured and analyzed instantly.
Complex problems can be quickly identified by viewing waveform data that precedes a failure condition (pre-trigger data).Captured waveforms can be expanded to reveal minute details such as fast glitches, overshoot on pulses, and noise. These captured waveforms can be analyzed in either the time or frequency domains.
Some oscilloscopes will:

- Monitor parameters such as amplitude fluctuations, timing jitter, risetime, etc., and display worst-case values.
- Provide histograms of parameter measurements to accurately identify important signal characteristics.
- Let you use the full screen as a signal viewing area.
- Allow signals to be saved or recalled from PC card devices such as portable hard drives, ATA Flash Cards, or IC memory cards.

III. VIRTUAL DIGITAL OSCILLOSCOPES

There are a lot of types of digital oscilloscopes made especially for personal computers. All they utilize a PC interface card which has an analog-to-digital converter that manages the incoming analog waves and converts them into a digital sequence. Next, there is special software that manipulates the data and visualizes it on the screen. The most common types use the PCI bus and are quite cheaper compared with the traditional digitizers. The price of such an oscilloscope is about 650EUR while the price of one digital scope is in the range of 1500 to 2000 EUR and has no significant advantages compared with the PC based model. Contemporary PCI based oscilloscopes have 8, 12 and some of them even 16 bit ADC and have the sampling rate of 5GS/s which can guarantee very good measurement results.

One cheap solution to construct a PC based digital oscilloscope is to use as an analog-to-digital converter the PC sound blaster. From microphone or line-in input, a sound card receives a signal in its native format, a continuous analog signal of a sound wave that contains frequencies and volumes that are constantly changing. The sound card can handle more than one signal at a time, allowing us to record signals in stereo or to construct two channel oscilloscopes. It has two inputs one mono input for microphone with amplitude voltage range: 0 – 2mV and frequency range: 20Hz – 20kHz and one stereo input with amplitude voltage range: 0 – 500mV and frequency range: 20Hz – 20kHz. Here is one limitation of this kind of scope as it will work only with frequencies in the sound spectrum from 20Hz to 20kHz. The sound card uses the Sigma-Delta analog-to-digital converter. It is the same as the ADCs used for measurements purposes and has resolution of 16 or even 24 bits. Sigma-Delta Analog-Digital Converters (. ADCs) have been known for nearly thirty years, but only recently has the technology existed to manufacture them as inexpensive monolithic integrated circuits. One of the most

[1]Rangel Dinov is with the Faculty of Communications and Communications technologies, Technical University of Sofia, Kliment Ohridski 8, 1000 Sofia, Bulgaria; E-mail: rdinov@tu-sofia.bg

[2]Plamen Shterev is with the English Language Department of Engineering, Technical University of Sofia, Kliment Ohridski 8, 1000 Sofia, Bulgaria; E-mail: plamensht@abv.bg

advantageous features of the sigma-delta architecture is the capability of noise shaping, a phenomenon by which much of the low-frequency noise is effectively pushed up to higher frequencies and out of the band of interest. As a result, the sigma-delta architecture has been very popular for designing low-bandwidth high-resolution ADCs for precision measurement. Also, since the input is sampled at a high "oversampled" rate, unlike the other architectures described in this paper, the requirement for external anti-alias filtering is greatly relaxed.

Next the digital data is sent to the DSP of the sound card and after that goes to the CPU of the computer and can be manipulated by the application software. This software can be made easily with LabView (fig.1).

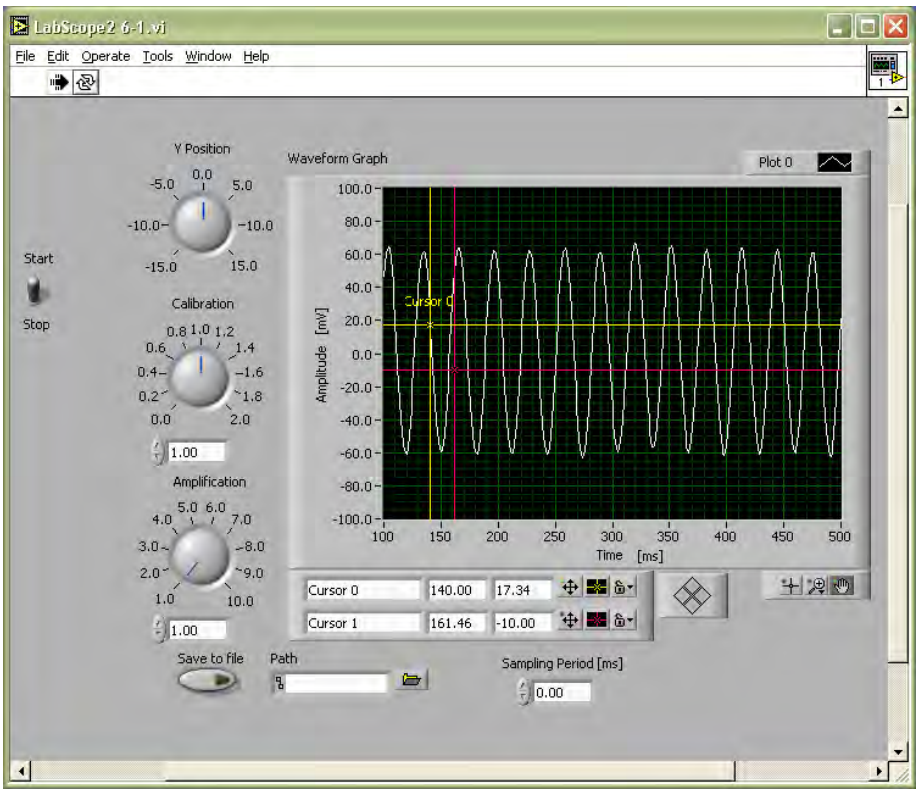

Fig. 1. Front panel

A block diagram of a simple program for this purpose is shown in fig. 2.

The initialization of the program starts with Sound Input Configuration module (fig. 2). Here it is configured which sound device will be used and the format of the incoming sound waves. "Device 0" means that the first sound card will be used. If there is a second sound card it will be addressed as "Device 1". In this case it is used Sound Card 1. The format of the sound can be mono or stereo. Next is the bit rate it can be 8000, 11025, 22050 or 44100. We set it to be 11025. The last adjustment in this block is the bits per sample. They can be 8 or 16. In the LabScope we use 16 bits.

The next block of the program is Sound Input Start module. It prompts the sound input device to begin accumulating incoming data. If the device is running already, calling this block has no effect. Following the SI Start is a block which reads data from the sound input device and sends it for further processing. If data has arrived in the device buffer, it returns that data after buffering, otherwise it waits until data arrives. If for some reason, the unbuffered data is overwritten, no data is returned, and instead, an overwrite error is reported. After the sound is read the SI clear closes the sound input device associated with the task ID in and returns all the resources the device uses to the system.

From the SI Read block the signal is sent to the waveform graph. But before displaying it to the screen the signal passes through a calibration block to adjust it for proper visualization according to the type of the sound card used. This it necessary because different types of sound cards have different voltage levels of input and output signals. It is good practice before starting the first measurement to use a predefined cali-

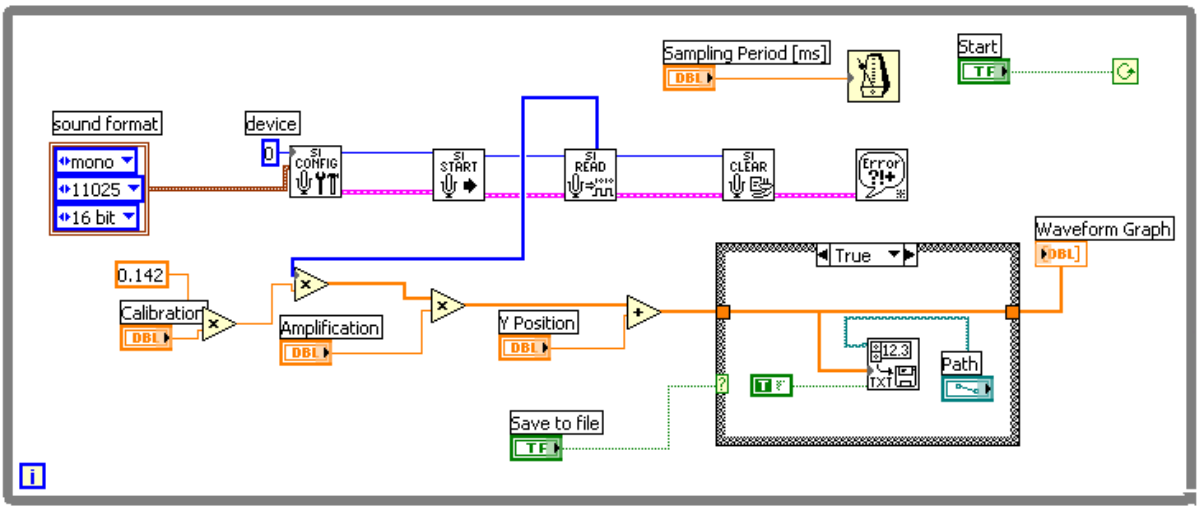

Fig. 2. Block diagram

brating signal to adjust the scope for the concrete sound card input and then we can be sure that the measured results are correct. Next there are some options for the signal: to be amplified from 1 up to 10 times depending on the position of the amplification knob 1 or/and to be added or subtracted 15 units in order to be better visualized. After this adjustment and calibration the data is passed to one cycle which checks the state of the "Save to file" button and if button is not pressed sends the data directly to the waveform graph. In case the button is pressed the data is sent to the waveform graph and to the file writing module. It converts a 2D or 1D array of single-precision numbers to a text string and writes the string to a new byte stream file or appends the string to an existing file, depending on the state of the "Append" input. If the "Append" input is true the new data is written at the end of the same file, otherwise each new group of data is saved in a separate file.

The functioning of the whole program is controlled by one While cycle which executes all of the above operations when the Start/Stop switch is in the true state. When the user turns off the main switch the While cycle receives False command and the operation of the LabScope program is terminated.

The limitation of the sound card is the input voltage range: 2mV for the mono input and 500mV for the stereo input. Range can be extended using the following very simple input buffer. It is used to protect the inputs of the PC sound card from the unwanted from the high voltage of the measured signal and thus it extends the voltage range to ±10V.

The principle of operation of the input buffer (fig. 3) is as follows:

By resistor of R1=1MΩ we ensure high input impedance thus we will not disturb the functioning of the investigated circuit. The input impedance of 1MΩ is typical for most oscilloscopes. The capacitors C1 and C2 are used to reject the signals with frequencies lower than 20Hz and higher than 20kHz e.g. these signals that are outside the range of the sound card. Their values are as follows: C1=10nF and C2=20pF.

The next part of the buffer is the input protection of 150V overvoltage (fig.3). The resistor R2 limits the input current of the operational amplifier in the next stage of the circuit. That's why it is necessary this resistor to be able to dissipate power of 0,5W. Its value of 47kΩ is most commonly used in the frequency range of 20Hz-20kHz. R2 is connected in parallel with one capacitor of 100pF. This capacitor is called accelerating capacitor because it accelerates the high frequency components of the signals and thus straightens shape of the pulses.

The three diodes D1, D2 and D3 are used for protection in case the input voltage of the operational amplifier is larger than 12V. If there are some peaks of the signal, which are higher than 12V the diode D1 opens and sends the overvoltage signal back to +12V terminal. In case the signal is lower than -12V the diode D2 opens and sends the signal to the ground.

Next we place one non-inverting amplifier (fig. 3) to made possible very low signal to be amplified 10 times. For amplifier we use the Operational amplifier TL082. It is connected with two resistors R4=27kΩ and R5=3kΩ. When the switch SW1 is closed the amplification factor A becomes:

$$A = \frac{R4}{R5} + 1 = \frac{27}{3} + 1 = 10$$

When the switch SW1 is open the circuit repeats the input signal without any amplification.

At the output of the amplifier we place one additional trimmer (fig. 3) to adjust more precisely the amplitude of the voltage that will be forwarded to the 2 mV sound card microphone input. It is realized with the one resistor of R6 = 300K and one trimmer of 1K for fine adjustment of the signal.

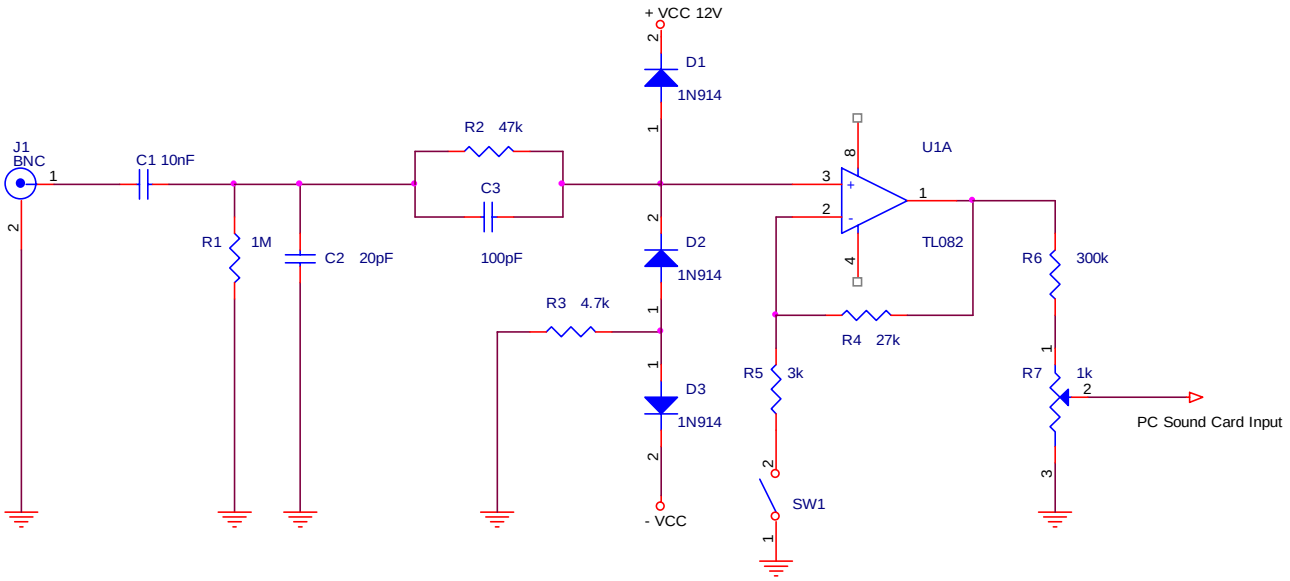

Fig. 3. Buffer circuit

IV. CONCLUSION

In the present project is created one virtual measuring system which can be used as a digital oscilloscope. It uses data acquisition techniques to send the results from the measurements to the personal computer. As a data acquisition board is used an ordinary PC sound card which makes the utilization of such kind of measuring instrument very cheap. That type of oscilloscope is suitable to be used for educational purposes and in research laboratories for low voltage measurements of AC signals.

Application software is worked out for Windows 95/98, NT and XP to handle the incoming data from the sound card microphone input, make it in the form suitable for visualization and display it on the PC screen.

It is designed an input buffer circuit which has two functions: first it is used to protect the input of the sound card from the incoming high voltage peak signals and its second function as an oscilloscope probe and has the ability to multiply 10 times the low voltage signals.

The realized digital oscilloscope has several advantages compared with the traditional analog scopes. On the first place is the possibility to store the data from the measured wave and to record it into a spreadsheet file and thus makes it possible the data to be further processed and analyzed by the standard programs for data analysis. There is no flickering of the waves on the screen. At every time the visualization can be paused in order to be taken some measurements and analysis.

REFERENCE:

1. White R., "How Computer Works", QUE 1998
2. Mueller S., "Upgrading and repairing PC's 13th edition", QUE 2002
3. LabView Measurements Manual, National Instruments 2000
4. Smith S., "The Scientist and Engineer's Guide to Digital Signal Processing", California Technical Publishing 1999
5. Park S., "Principles of Sigma-Delta Modulation for Analog-to-Digital Converters", Motorola Digital Signal Processors, 2001
6. Kester W., J. Bryant, J. Buxton, ADCs for signal conditioning
7. "Data Acquisition Fundamentals", National Instruments 1999
8. "Fundamentals of Digital Oscilloscopes and Waveform Digitizing", LeCroy 2001
9. "Analog/Mixed-Signal Products Designer's Guide", Texas Instruments August 2000
10. Ögren J., "The Hardware Book", 2000
11. Dinov R., E. Popov, N. Kolev, "Electronics", Sofia 1999
12. Takayama S., K. Kariya, "Measurement Education through User Navigation Interface of Virtual Instrument", Ritsumeikan University 2001
13. Müller H., A.Bogaerts, "A millenium approach to Data Acquisition: SCI and PCI",
14. Duarte M., B. Butz, "An Intelligent Universal Virtual Laboratory", Electrical & Computer Eng. Department Temple University, 2002 IEEE
15. Gulota M., "Teaching Computer interfacing with Virtual instruments in an Object-Oriented Language", Biophysical Journal Volume 69 November 1995
16. McCarthyy L., J. Neuendor, S. Sachs, "Reprogrammable Platforms for High-speed Data Acquisition", November 4-7, 2001, Asilomar Hotel Conference Grounds, CA

Method for Evaluating the quality of Web-based courses

Boyka J.Gradinarova

***Abstract* - A methodology for evaluating on collaborative learning processes is proposed. The underlying hypothesis is that three elements affect the quality of online courses: learning quality, content quality, and interaction quality. Evaluation derives from examination of all products that the online learning process yields. The methodology comprises a set of parameters that indicate the quality of online courses and a set of conceptual and technological tools that can be adopted. The paper presents results from the case study wherein the methodology is applied to a Web-based educational course.**

***Keywords* - Web-based education, collaborative learning, evaluation, quality assessment**

I. INTRODUCTION

Conventional distance education frees learners from the need to be present in a particular place at a particular time, but it seldom offers the opportunity for collaborative learning. The reason for this may lie either in the lack of necessary technological resources or in underestimation of the importance that the social aspect has in learning. By contrast, co-operation and interaction among participants is fundamental in online courses. What is more, text-based communication conducted in intense message exchange allows the whole collaborative process to be saved and reconstructed. This makes it possible to review design methods and evaluate the course itself. We can observe also the influence of intensity of the dialogue on the learning results of the students.

In this paper we propose a methodology for evaluating online collaborative learning processes; this is based on a holistic approach in that it takes into consideration a wide spectrum of quality-related characteristics. The main aim is to define a quality management system that will make it possible not only to evaluate learners' performance and knowledge acquisition but also (and especially) to determine whether the course in question effectively meets the needs it was designed to satisfy.

The underlying hypothesis is that three elements affect the quality of online courses:

[1]Boyka J. Gradinarova is with the Department of Computer Sciences & Engineering at TU-Varna, 1, Studentska Str. Varna, Bulgaria

learning quality, correlated to the products that the participants develop collaboratively during the course; content quality, seen in the exchanges and discussions that participants engage in; and interaction quality, meaning the quality of the communication processes set in motion. So evaluation derives from examination, from the three above-mentioned perspectives, of all the messages and products that the online learning process yields.

Finally, a case study will be described wherein the methodology is applied to an online course dealing with environmental education.

II. ONLINE COURSE MODEL

In online courses three main elements can be identified:

- the virtual community comprising students, tutors, experts, observers and technical staff;
- set of material regarding course organization and running, the technology adopted and the course contents;
- new technology used mainly for performing communication functions, accessing and sharing of information, and collaboration.

We wish to focus on a few aspects related to the communication platform and the functions it performs in an online course, given the close link between it and the evaluation methodology.

The communication platform supporting a collaborative learning environment should permit many-to-many interaction among remote users via e-mail or some conferencing systems. They use asynchronous (or deferred) communication, sometimes incorporating synchronous functions such as chatting or videoconferencing.

Computer conferencing environments differ from traditional uses of e-mail in that they are closed and feature controlled access.

The computer conferencing system provides the following interaction modes:

- information exchange, knowledge sharing, group design and development of products;
- co-decision making and negotiation;
- familiarization activities;
- access to external sources;
- access to multimedia learning material.

Module structure

Online collaborative activities call for careful planning, together with timely co-ordination and synchronization efforts on the part of tutors, who play the critical role of stimulating, moderating and mediating. Learning modules are divided into five main phases.

1. *Tutors' stimulus messages*
2. *Local group activities*
3. *Group reply messages*
4. *Analysis and call for discussion*
5. *Discussion among the remote groups*

III. A METHODOLOGY FOR EVALUATING THE QUALITY OF WEB-BASED LEARNING PROCESSES

In this section we will seek to identify what to evaluate and how to evaluate an online course. Finally, we will outline the

chief aspects regarding instrumentation and operating procedure.

What is to be evaluated is the quality of online courses. So, we should first define what is meant by quality in learning processes in general and quality in online courses in particular.

Online learning is chiefly based on collaborative learning strategies; a number of researchers have sought to define what collaborative learning actually means. A broad definition of collaborative learning might be individuals' acquisition of knowledge, skills or behavior as a result of group interaction, or to put it simply, individual learning resulting from group processes see (2) and (3).

Processes of this kind are primarily linked to theories that regard individual learning as a result of social interaction (4). We shall therefore correlate the quality of online courses to both the learning gained by the individual participants and to the interaction that has taken place within the group involved. In online courses, interaction largely centers on a certain knowledge domain. The quality of that interaction will depend on two main elements: the quality of the dialogue that takes place within the group and the quality of the contents dealt with in that dialogue.

Hence, quality is not an absolute value, but is to be considered in relation to the evaluator's interpretation of the context based on predefined learning objectives.

On this basis, our methodology correlates quality in online courses to three elements, that can be thought of as independent components in a three-dimensional quality space Fig. 1:

1. learning gained by the individual participants;
2. interaction, that will be evaluated in relation to the context in which that interaction occurs and on the basis of predefined aims;
3. course contents: the contents of an online course, partly provided to the participants and partly developed by them, should also be evaluated in terms of the context of the dialogue between participants.

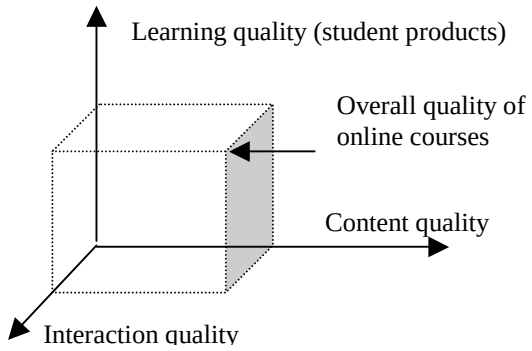

Fig. 1. Overall quality of online courses

The key idea in proposed methodology is to grade each message and each product according to predefined values and attributes (quality parameters). Online courses are divided into a number of conferences, which are composed of chains of messages known as threads, which in turn are made up of individual messages. Accordingly, overall course quality is measured by tallying the quality of the conferences. Conference quality is calculated on the basis of thread quality, which in turn sums up message quality. It is worth noting that all course products, whether they be reports or messages, contribute to determine course quality.

The quality parameters of a message are its:

- Contextual congruency?
- Formal congruency: e.g. does a reply incorporate the relevant parts of the original message?
- Appropriateness of codes.
- Building new knowledge: the educational and cognitive contribution within the context of course objectives.
- Contribution to interaction: does the message prompt discussion and does it keep it alive?
- Correctness of contents: are the contents of message in line with the activities the tutors set?
- Timeliness: are participants promptly responding to tutors' proposals and reacting to the messages of the other members of the community?

IV. INSTRUMENTAL AND OPERATIONAL ASPECTS

In this section we shall describe the tools (both conceptual and technological) and the phases comprising the evaluation methodology. This model is the framework for the database that is used for online course evaluation.

The main elements in the database are:

· community member, which may be a single student (individual student), a group or a tutor.
· conference, which identifies the individual course module.
· message, which comprises a number of attributes:
  - the function performed (persuasive, informative, metalinguistic, etc.);
  - the subject of the contents (CMC system, course-related topics, etc.);
  - the thread that the message belongs to; it should be noted that, in the extreme case, a thread may be no more than one message long, where this message has received no reply or comment;
  - the type: this is the broadest category, and is primarily based on content;
  - the quality parameters described earlier.
· documents.

This last category is distinct from the preceding one in that documents contain material which is not necessarily the fruit of course communication and which has a purpose beyond that context. Examples of such documents include student products, reference material that the tutors or experts have made available in digital form, files in formats which are incompatible with that of messages (graphics, electronic spreadsheets, databases, etc).

One interesting aspect here is that document sharing can stimulate community discussion, and this is even truer of collaborative document development: the tutors can use a provocative article to stimulate debate; draft products may require repeated revision and refinement before agreement can be reached on a final version.

The database is compiled semi-automatically. Objective data such as the attributes' sender, receiver and date related to each message are imported from the CMC server. Conversely,

subjective data like message type, function and quality are determined by the evaluator on the basis of the discussion context, and are stored in the database using an appropriate input form. Quantitative measurement values derive from weighted averages, whereby each element that helps determine the average is duly weighted. By setting the weight of the various parameters, the evaluator can tune the evaluation process in accordance with each conference's objectives. For example, the code correctness parameter may be attributed greater importance in a topic-based conference, or lesser importance in a conference for collecting reference material.

Conference interaction quality in turn depends on thread quality, but also on factors like thread length (distinguishing between messages sent by students or tutors), their temporal duration, and the prevalent type of interaction.

Similarly, thread quality is derived by summing the quality levels for each constituent message. The final element related to the quality of overall course interaction is message quality, which results from the values given to each of the quality parameters.

Interaction quality is only one of the three components comprising course quality. Learning quality (related to student products) is expressed by two quality parameters applied to each conference: formal congruency and content congruency.

Clearly, the usefulness of such a system is not limited to the calculation of a single numerical value expressing the degree of overall course quality. It is often fruitful to compare partial quality measurements, such as those of two topic-based conferences, or the same conference in two different editions of the same course.

V. A CASE STUDY IN THE APPLICATION OF THE PROPOSED METHODOLOGY

One of the primary aims of this work has been to test the validity of the above-described evaluation methodology. This has been done by applying the elements that emerged in the theoretical phase to an actual online course.

The testing has involved a study of messages exchanged through the Course Support System – WebCT, by the students during the distance learning course conducted entirely online. The theme of the course was "Information and Communication Technologies in Education".

As already stated, our methodological approach is based on detailed analysis of every single message, considered as the basic component of the online interaction process. For each conference, an outside observer attributes a value (from 1 to 10) to the quality indicators on the basis of the conference's objectives. Once data input had been completed, we proceeded to formulate database queries. The first step was to extrapolate the elements comprising overall quality of an online course, seen as a function of content quality, interaction/communication quality and learning quality. The description below shows the main logical steps that led to defining and obtaining the overall quality value of the course in question.

A. Query: interaction/communication quality

These data were obtained by applying the analysis criteria illustrated earlier and by careful weighting not only of the quality parameters applied to individual messages but also of the conferences themselves. It is possible to endow each conference with a weight vector, i.e. a value expressing the relative importance of the topic dealt with in that conference, in terms of the overall objective of the online course. The interaction /communication quality peaks in the middle sections of the course and in the laboratory conference (the latter can be explained by the intense message exchange arising from the numerous technical problems experienced during the course).

B. Query: content quality

Values for content quality were obtained from the weighted sum of the quality parameters content correctness and new knowledge. Content quality appears evenly distributed across the various discussion areas but peaks in the Library, where documents related to the course topic are stored.

C. Query: learning (product) quality

This value was obtained through analysis of the students' products. As with content quality, it corresponds to the weighted sum of two quality parameters, in this case formal congruence and content correctness. These are related to the files attached to messages and to messages that the evaluator considers as student products. The quality levels for products peak in the last module of the course.

D. Query: overall quality

The overall quality level of the course derives from the relationships between the levels of interaction quality, content quality and learning (product) quality. So we can define the course overall quality level as a point in a three-dimensional space, where the three axes are represented by the three quality measurements cited above.

VI. COMPARISON WITH CONVENTIONAL EVALUATION METHODS

Besides the evaluation carried out using our methodology, the course was also evaluated in a more traditional manner. Let us compare the findings. The outcome of the online questionnaire is based on responses from 16 participants (out of a total of 40 people, divided into eight groups). The respondents expressed satisfaction with the course, although complained about the amount of time it demanded of them. They were also happy about the communication/interaction that took place with tutors, experts and other participants. In addition, most of the respondents were satisfied with the role played by the tutors, though it was felt that they were overactive (9 respondents out of 16). Intense tutor activity was borne out in our findings as well, comparing the participation levels of all learning community members. Tutor co-operation, feedback and support was not the only positive finding from the questionnaire responses. The teaching approach adopted was also judged to have helped participants

as they progressed through the course. They were happy with the CMC system, both in terms of the user-friendliness of the interface and the innovative learning style. Overall we can conclude that the findings obtained from the online questionnaire confirm the results of our global quality evaluation, namely that the course was a success.

Another important finding from the observation was the influence of intensity of the dialogue on the learning results of the students. Fig.2 shoes the results.

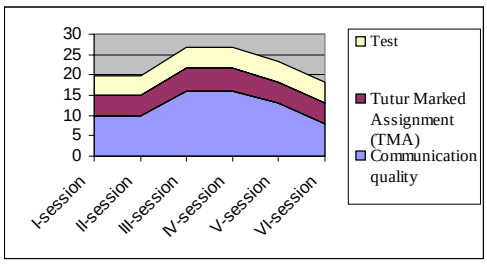

Fig.2. Influence of the dialogue on the learning results of the students.

VII. CONCLUSIONS

This article has presented an approach for evaluating online collaborative learning processes, one based on quantitative measurement of quality parameters related to three aspects of the course: the products developed by the participants, the contents provided and produced, and the interaction that took place. The methodology proposed draws on data management techniques that make it possible to compare the quality levels of different sections of the course, different student groups, and different editions of the same course. The testing carried out so far has highlighted the effectiveness of the approach, which is confirmed by comparison with the findings gained using conventional evaluation methods.

REFERENCES

[1] Midoro, V. (1999) Modelling On-Line Education. *Proceedings of Comned 99 IFIP WG3.1 and 3.2 Open Conference*, Aulanko, Finland, June 13 - 18.

[2] Kaye, A. R. (1991) Learning together apart. In Kaye A. R. *Proceedings of the NATO Advanced Research Workshop on Collaborative Learning and Computer Conferencing, Series F:Computer and System Sciences '90*. Berlin: Springer-Verlag.

[3] Briano, R., Manca, S., Midoro, V., Persico, D. & Sarti, L. (1999) On-Line Teacher Training in Environmental Education across Europe. In *Proceedings of the Telecommunications for Education and Training 1999 - TET99 Conferences.* Gjшvik, Norway, June 8 - 11.

[4] Vygotsky, L.S. (1978) *Mind in society: the development of higher psychological processes*. Harvard.

Importance of 3D Transformations for Displaying of Medical Images

Penka Tz.Isaeva[1]

Abstract - **In this paper the types of 3D transformations in displaying of real medical images are given.**

Keywords - **Medical images, Education on treatment medical signals and images, Distance education**

I. INTRODUCTION

The creation of real 3D medical images is the combination from two fundamental processes – modeling (defining geometry of medical objects) and representing (displaying) these mathematical models. Transformations can be used to rotate, translate or scale an image to obtain an understanding of its 3D shape. This is particularly important in medicine in which the medium for displaying pictures is the two-dimensional display screen on which depth information may not be obvious. Techniques for expressing 3D transformations are represented by extending the 2D techniques. Right-handled coordinate systems are used. A point in 3D space (x, y, z) is represented by a four-dimensional position vector (x, y, z, w). This point may then be transformed by the following matrix operation:

$$\begin{bmatrix} x' \\ y' \\ z' \\ w' \end{bmatrix} = \begin{bmatrix} a & b & c & d \\ e & f & g & h \\ i & j & k & l \\ m & n & o & p \end{bmatrix} \cdot \begin{bmatrix} x \\ y \\ z \\ w \end{bmatrix} \qquad (1)$$

II. TYPES OF 3D TRANSFORMATIONS

In order to obtain the 3D coordinates from the transformed homogeneous point, the x-, y-, z- components are divided by w- component:

$$x''=x'/w'; \quad y''=y'/w'; \quad z''=z'/w'; \qquad (2)$$

Translation - the matrix to perform 3D translation of a medical image is:

$$\begin{bmatrix} 1 & 0 & 0 & d \\ 0 & 1 & 0 & h \\ 0 & 0 & 1 & l \\ 0 & 0 & 0 & 1 \end{bmatrix} \qquad (3)$$

Matrix element **d** is the displacement added to x-coordinate, **h** – is the displacement added to y- coordinate, and **l** is added to the z- coordinates.

Scaling – 3D scaling is performed by the element on main diagonal of the matrix:

$$\begin{bmatrix} a & 0 & 0 & 0 \\ 0 & f & 0 & 0 \\ 0 & 0 & k & 0 \\ 0 & 0 & 0 & p \end{bmatrix} \qquad (4)$$

The x-, y-, and z- scale factors are given by **a**, **f**, and **k** respectively. The element **p** provides overall scaling by a factor of 1/p. The scaling is used to change the size of images.

Rotation – the terms in the upper-left 3x3 component matrix control 3D rotation of the medical images:

$$\begin{bmatrix} a & b & c & 0 \\ e & f & g & 0 \\ i & j & k & 0 \\ 0 & 0 & 0 & 1 \end{bmatrix} \qquad (5)$$

The basic 3D rotations are: rotation about the x- axis, rotation about y- axis and rotation about z- axis.

A rotation about z- axis is equivalent to 2D rotation about the origin. Hence the x and y terms of the matrix may be write down straight away. Since the rotation is about z- axis, the z-coordinates should not be changed, and so the z- row and column should both be [0 0 0 1] (as in the identity matrix). Similarly for rotation about x and y , the row and column corresponding the axis of rotation are taken from the identity matrix. The cosine and sine terms are then used to fill the remaining elements of the 3x3 component matrix. The matrices for rotation about the three axes are:

[1]Penka Tz. Isaeva is with the Faculty of Communications and Communications Technologies, Technical University, Kliment Ohridski 8, 1000 Sofia Bulgaria, E-mail: pepi_is@abv.bg

$$\begin{bmatrix} 1 & 0 & 0 & 0 \\ 0 & \cos\alpha & -\sin\alpha & 0 \\ 0 & \sin\alpha & \cos\alpha & 0 \\ 0 & 0 & 0 & 1 \end{bmatrix}$$ Rotation about the x-axis; (6)

$$\begin{bmatrix} \cos\alpha & 0 & \sin\alpha & 0 \\ 0 & 1 & 0 & 0 \\ -\sin\alpha & 0 & \cos\alpha & 0 \\ 0 & 0 & 0 & 1 \end{bmatrix}$$ Rotation about the y-axis; (7)

$$\begin{bmatrix} \cos\alpha & -\sin\alpha & 0 & 0 \\ \sin\alpha & \cos\alpha & 0 & 0 \\ 0 & 0 & 1 & 0 \\ 0 & 0 & 0 & 1 \end{bmatrix}$$ Rotation about the z-axis; (8)

Shearing – The off – diagonal elements in the upper – left 3x3 component matrix produce 3D shearing effects:

$$\begin{bmatrix} 1 & b & c & 0 \\ e & 1 & g & 0 \\ i & j & 1 & 0 \\ 0 & 0 & 0 & 1 \end{bmatrix} \quad (9)$$

In 3D shear in x may be obtained as a function of the y- and z- coordinates. This is controlled by matrix elements **b** and **c** respectively. Similarly elements **e** and **g** control shearing in y as a function of x and z elements, **i** and **j** control shearing in z as a function of x and y.

Combination of basic 3D transformations of the medical images. A common requirement is to rotate an object about an arbitrary axis rather than one of coordinate axes. A 3D rotation about an arbitrary axis involves transforming the object and axis of rotation so that the axis coincides with one of the coordinate axes, followed by a rotation about the coordinate axis and finishing with a transformation which is the inverse of the first. The individual steps are as follows:

- Translate so that axis of rotation passes through the origin;
- Rotate medical object so that axis of rotation coincides with one of the coordinate axes;
- Perform the specified rotation about appropriate coordinate axis;
- Apply inverse rotation to bring axis of rotation back to original orientation;
- Apply inverse translation to bring rotation axis back to original position;

III. Perspective Transformations Of 3D Medical Images

All of the 3D transformations matrices examined so far have been of the form

$$\begin{bmatrix} a & b & c & d \\ e & f & g & h \\ i & j & k & l \\ 0 & 0 & 0 & p \end{bmatrix} \quad (10)$$

i.e. elements **m**, **n**, and **o** are equal to zero. This section looks at the the effect achieved when one or more of these values is non-zero. Consider the following transformation

$$\begin{bmatrix} x' \\ y' \\ z' \\ w' \end{bmatrix} = \begin{bmatrix} 1 & 0 & 0 & 0 \\ 0 & 1 & 0 & 0 \\ 0 & 0 & 1 & 0 \\ 0 & 0 & \gamma & 1 \end{bmatrix} \cdot \begin{bmatrix} x \\ y \\ z \\ w \end{bmatrix} =$$

$$= \begin{bmatrix} x \\ y \\ z \\ \gamma.z+1 \end{bmatrix} \quad (11)$$

After homogeneous division the real 3D coordinates of the transformed point of the medical image are (x", y", z") where

$$\begin{aligned} x'' &= x / (\gamma.z+1) \\ y'' &= y / (\gamma.z+1) \\ z'' &= z / (\gamma.z+1) \end{aligned} \quad (12)$$

As homogeneous z–coordinates tends to infinity

$$x''\rightarrow 0;\ y''\rightarrow 0;\ z''\rightarrow 1/\gamma$$

Hence, after transformation of medical image lines originally parallel to the z- axis will appear to pass through the point (0, 0, 1/γ), known as the **vanishing point**. This kind of transformation is known as a **perspective** transformation of medical objects.

A perspective transformation has a distorting effect which gives the transformed medical object a natural appearance, similar to that which would be seen by eye from the point (0, 0, -1/γ). This is known as a **centre of projection**.

Different types of perspective transformation of medical objects are obtained if the other two elements of the bottom row are set. For example, the matrix

$$\begin{bmatrix} 1 & 0 & 0 & 0 \\ 0 & 1 & 0 & 0 \\ 0 & 0 & 1 & 0 \\ \alpha & 0 & 0 & 1 \end{bmatrix} \quad (13)$$

would create perspective transformation with a vanishing point for lines originally parallel to the x- axis at (1/α, 0, 0) and centre of projection at (-1/α, 0, 0). Similarly the matrix

$$\begin{bmatrix} 1 & 0 & 0 & 0 \\ 0 & 1 & 0 & 0 \\ 0 & 0 & 1 & 0 \\ 0 & \beta & 0 & 1 \end{bmatrix} \qquad (14)$$

would create a perspective transformation with a vanishing point for lines originally parallel to the y- axis at (0, 1/β, 0) and centre of projection at (0, -1/β, 0). Perspective transformations with only one vanishing point are known as one-point perspective transformation. If two or three of the matrix elements are non-zero together, a two or three point perspective transformations are obtained.

IV. Points Behind The Eye Point

In this section is shown a perspective transformation applied to point (x, y, z) with the eye point at (0, 0, c):

$$\begin{bmatrix} x' \\ y' \\ z' \\ w' \end{bmatrix} = \begin{bmatrix} 1 & 0 & 0 & 0 \\ 0 & 1 & 0 & 0 \\ 0 & 0 & 1 & 0 \\ 0 & 0 & -1/c & 1 \end{bmatrix} \cdot \begin{bmatrix} x \\ y \\ z \\ w \end{bmatrix} =$$

$$= \begin{bmatrix} x \\ y \\ z \\ (c-z)/c \end{bmatrix} \qquad (15)$$

The value of w' varies depending on the value of the original z- coordinate: $z < c \rightarrow w' > 0$; $z = c \rightarrow w' = 0$; $z > c \rightarrow w' < 0$;

This is illustrated in Fig.1.

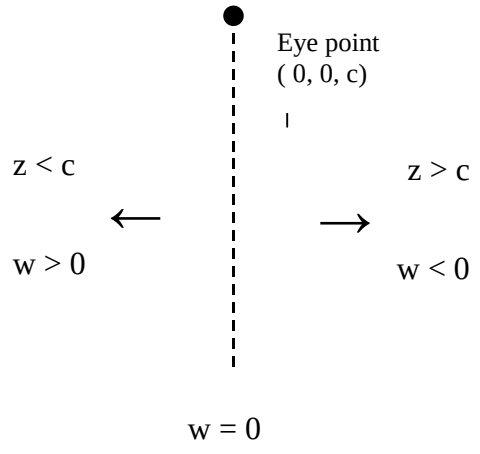

Fig. 1 - Variation of w' with original z- coordinates in a perspective transformation

Consider a line which joins the points $\mathbf{p_1}$ and $\mathbf{p_2}$ which are positioned on either side of the eye point ($\mathbf{p_1}$ has z<c and $\mathbf{p_2}$ has z>c). After transformations $\mathbf{p_1}$ will have a positive w value and $\mathbf{p_2}$ will have a negative w value. Fig. 2 shows the transformed line in homogeneous coordinate space. Homogeneous division then project the transformed points $\mathbf{p_1'}$ and $\mathbf{p_2'}$ onto the w =1 plane. The resulting line however is not the line joining the projected points $\mathbf{p_1''}$ and $\mathbf{p_2''}$. In Fig. 3 other points along the line $\mathbf{p_1'}$ $\mathbf{p_2'}$ are projected onto the w = 1 plane. It can be seen from this that the projected line is actually in two parts: $\mathbf{p_1''}$ to positive infinity and negative infinity to $\mathbf{p_2''}$. These are known as *external line segments* and is the correct interpretation of the application of a perspective transformation to a line joining points on either side of the eye point.

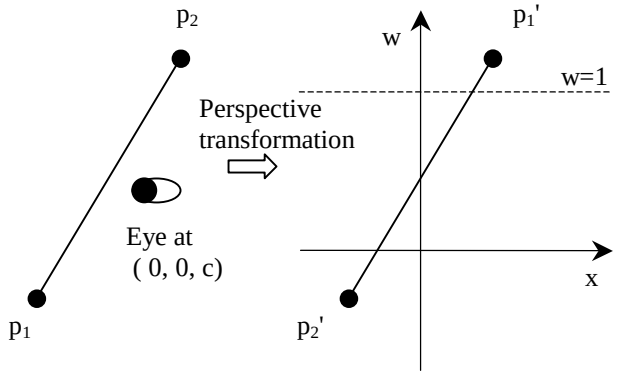

Fig.2 – Perspective transformation of the line p_1p_2

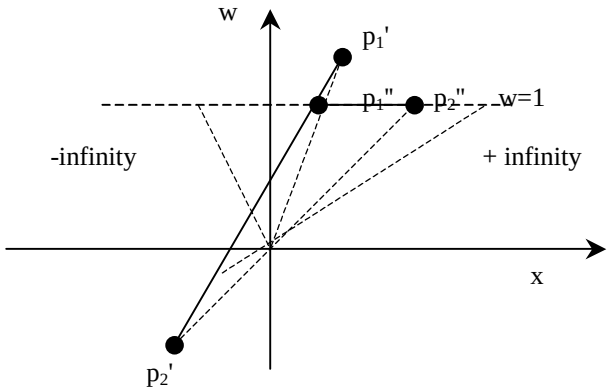

Fig.3 – Projecting line $\mathbf{p_1'}$ $\mathbf{p_2'}$ onto the w = 1 plane

Clipping – In general the results of a perspective transformations simulate what the eye would actually see when medical objects are displaying. Since the eye can only see objects in front of it, items behind the eye should be clipped out. This can be done in one of two ways:

• Clip before the perspective transformation by removing all those parts with $z \geq c$.

• Clip after perspective transformation but before homogeneous division, in this case remove parts with $w \leq 0$.

After the homogeneous division it is impossible to distinguish between points which were originally behind in front of the eye.

V. CONCLUSION

The main methods for transformation of points of 3D medical images are translation, scale, rotation and shear.

The 3D transformations of the medical objects are useful as a tool for creating and subsequently altering an image. They can also help to visualize the three-dimensional shape of the resulting medical image.

For objectives of education these methods can be used in simulations of real processes at training and examining.

REFERENCES

[1] Hearn D. and Baker M. P. , Computer Graphics, Prentice – Hall, 1986.

[2] Blinn J. F. and Newell M. E. , Clipping Using Homogeneous Coordinates, Proceedings of SIGGRAPH , pp. 245 – 251.

[3] Foley J. D. , van Dam A. , Feiner S. K. and Hughes J. F. , Computer Graphics : Principles and Practice (2nd Edition), Addison Wesley, 1990.

Physical and Mathematical Modeling of an Optical Medium – Quartz Fiber

Ivan S. Kolev and Ivelina S. Stoeva

***Abstract* – Nowadays the most often used optical medium is the quartz fiber. Fibers are divided into one-mode and multimode fibers. The multimode fibers on their part are divided into step and gradient fibers. The target of the present paper are the quartz multimode fibers with a step profile of the index of refraction.**

➢ **Keywords – Optical fibers, Mode dispersion; Wave (spectral) dispersion, Quartz Fiber.**

I. OPERATION MODES

The following media are used as optical media in communications:

- Air and vacuum;
- Optical fibers (Quartz or polymer);

There are three main factors which influence the change of the output pulse parameters towards the input pulse:

- Mode dispersion;
- Wave (spectral) dispersion;
- Delay of the fastest mode of the output signal towards the input.

All these three factors have been mathematically described by means of links with pure delay and two aperiodic links.

A physical model of the optical fiber has been developed on this basis. A mathematical expression of the slowest mode towards the fastest has been worked out. This expression contains parameters accessible for the company - introducer.

The time of delay has been optimized towards the indices of refraction of the core and the fiber Digital expressions of the parameters have been assigned and the values received have coincided with a certain allowance with these cited by leading companies. An expression of the maximum operating frequency of the optical fiber directly related to the signal expansion has been derived.

The expressions derived have been checked for polymer multimode fibers with a step profile of the index of refraction.

The transfer function, the pulse transition function and the amplitude-frequency characteristic of the quartz fiber have been derived.

Ivan S. Kolev. Department of Electronics, Technical University – Gabrovo, Street "Hadji Dimiter" No. 4, 5300 Gabrovo, Bulgaria, phone: +359 66 801064.

Ivelina St. Stoeva – post-graduate student/worker; Department of Electronics, Technical University – Gabrovo, Street "Hadji Dimiter" No. 4, 5300 Gabrovo, Bulgaria, phone: +359 66 223-433, e-mail: ivstoeva@tugab.bg

As a result of the expressions worked out, it can be recommended to change the known refractive indices of the fiber and the core in order to widen the frequency band of the fiber.

The expressions derived allow for a computer simulation of the optical fiber operation. This is a subject our team is working on at present.

$$P(L) = P(0).10^{\frac{-aL}{10}}, W \qquad (1)$$

Where:
P(0) – optical power in W set in the beginning of the fiber;
L – length in km;
A – coefficient, measure of attenuation in dB per unit of length in km.

$$A = a.L.10\lg\frac{P(0)}{P(L)}, dB \qquad (2)$$

Where A is an optical attenuation
hence, the coefficient of optical attenuation A is

$$a = \frac{A}{L} = \frac{10}{L}\lg\frac{P(0)}{P(L)}, dB/km$$

The pulse dispersion (expansion) on the output will be:

$$\tau(L) = \sqrt{t_{изх}^2 - t_{вх}^2} \qquad (3)$$

$t_{изх}$ - pulse duration on the output
$t_{вх}$ - pulse duration on the input

II. THE FREQUENCY BAND FOR MULTIMODE FIBERS

The frequency band for multimode fibers can be defined by the following expression:

$$f_{\max} = \frac{0{,}44}{\tau} \qquad (4)$$

$$\tau = \sqrt{t_{изх}^2 - t_{вх}^2} = \mathrm{M}(\lambda).\Delta\lambda_{FRMS}.L, ps \qquad (5)$$

M(λ) – dispersion at maximum spectral radiation, ps/(nm.km)

$$\Delta\lambda_{FRMS} = \frac{1}{\sqrt{\ln 4}} = \Delta\lambda.0{,}85 \qquad (6)$$

Conclusion: Dispersion influences the frequency band. (4)

III. REFRACTIVE INDEX OF THE CORE AND REFRACTIVE INDEX OF THE FIBER COATING

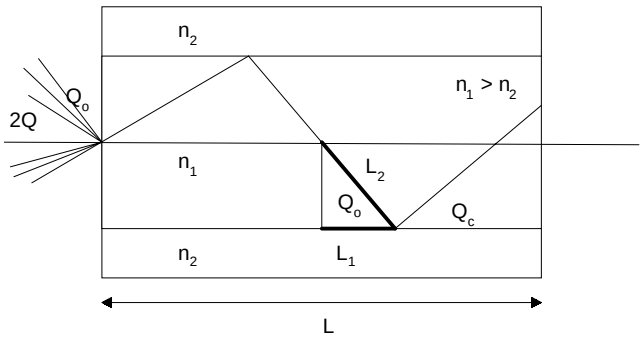

Fig.1

2Q – angle of the beam, entering the core (entrance angle)

$$\sin Q_o = \sqrt{n_1^2 - n_2^2} \qquad (7)$$

n_1 - refractive index of the core

n_2 - refractive index of the fiber coating

$Q_c = ar\cos\frac{n_2}{n_1}$ - critical angle

$$\frac{L_1}{L_2} = \cos Q_c$$

the shortest way (mode L' arrives fastest)

$L'=\Sigma L_1$

the slowest mode (mode L˝ arrives most slowly)

$L''=\Sigma L_2$

If the fastest mode covers the distance L, the slowest mode will cover the distance L+ΔL

The speed of each mode (each beam) is equal at n_1=const,

$$\frac{L}{\cos Q_c} = \frac{L}{(n_2/n_1)} = \frac{L.n_1}{n_2} \approx L + \Delta L$$
$$\Delta L = \frac{L.n_1}{n_2} - L = L\frac{(n_1 - n_2)}{n_2} \qquad (8)$$

The speed of the mode $V = \frac{C}{n_1}$, where C – velocity of light =300 000km/s

The time lag of the slowest mode towards the fastest mode is:

$$\Delta t = \frac{\Delta L}{V} = \frac{L(n_1 - n_2)}{\frac{n_2}{C/n_1}} = \frac{Ln_1(n_1 - n_2)}{C.n_2} = \frac{L}{C}\frac{n_1}{n_2}(n_1 - n_2)$$

Example: L=1km; n_1=1,48; n_2=1,46; C= 300 000km/s

The signal expansion is:

$$\Delta t = \frac{1km}{300000km/s}.\frac{1,48}{1,46}(1,48 - 1,46) = 67,5ns \qquad (9)$$

(multimode quartz fiber)

The delay of the fastest mode per 1κm of length is:

$$t_d = \frac{L}{C/n_1} = \frac{1km}{300000/1,48} \approx 4,93\,\mu s \qquad (10)$$

The delay of the slowest mode is: $t_d+\Delta t$, i. e. 4,93μs+67,5ns=4,9975μs.

The form of the input and the output signal is shown in Fig.2

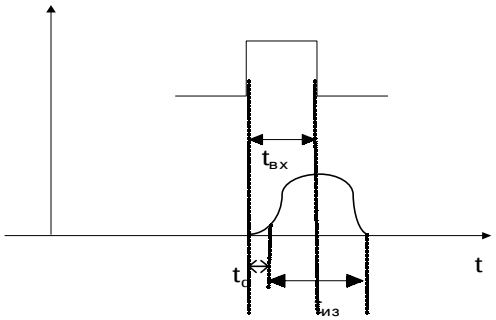

Fig.2

An example of plastic multimode step fibers:

L=1km; n_1=1,492; n_2=1,417; C= 300 000km/s

$$\Delta t = \frac{1km}{300000km/s}.\frac{1,492}{1,417}(1,492 - 1,417) = 263ns$$

Conclusion: The frequency band is

$$f_{\max} = \frac{0,44}{\sqrt{(t_{вх} + \Delta t)^2 + t_{вх}^2}} \qquad (11)$$

We have taken into account only the mode dispersion so far. The other factor for pulse expansion is the dispersion of λ (wave dispersion).

Conclusions:

The output signal differs from the input signal as follows:

1. Pure delay of the signal (t_d) from the mode transition time
2. Dispersion of the output signal towards the input, determined by two factors:

- Mode dispersion
- Wave (spectral) dispersion.

On this basis, the electron model of the optic mean (quartz fiber) is built. It consists of three components (Fig. 3):

IV. DELAY COMPONENT

$W_1(P) = e^{-pT_1}$ (It reads the pure delay of the signal- Fig. 4)

Aperiodic component (gives the mode dispersion – Fig. 5)

$W_2(P) = \frac{k}{1 + p.T_2}$ - Transfer function

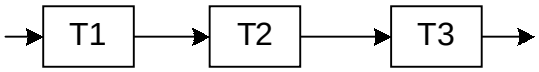

Fig.3

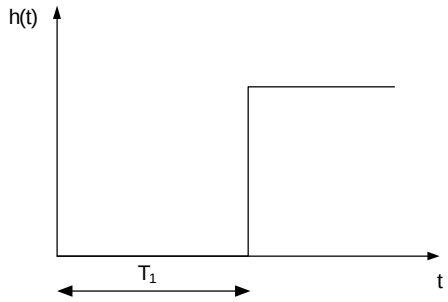

Fig.4

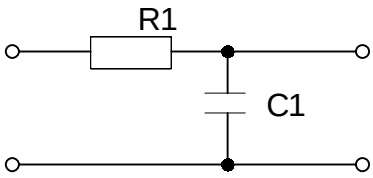

Fig.5

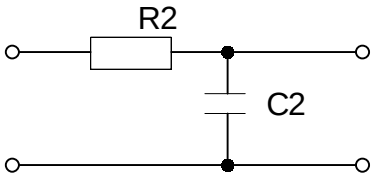

Fig.6

$h(t) = k(1 - e^{\frac{-t}{T_2}}).1(t)$

Pulse transition function

$L(w) = 20\lg\frac{k}{\sqrt{1 + w^2 T_2^2}}$

Logarithmic amplitude-frequency characteristic

$W_2(P) = \frac{k}{1 + p.T_2}$ Se $W_2(P) = \frac{k}{1 + p.T_2}$ - Second (aperiodic) component reads the wave dispersion

$W_3(P) = \frac{1}{1 + p.T_3}$ - (Third aperiodic) component – Fig. 6

$W(P) = \frac{k.e^{-p.T_1}}{(1 + p.T_2).(1 + p.T_3)}$ Common transfer function

Therefore:

$$T_1 = \frac{L}{C / n_1} = \frac{L.n_1}{C}$$

$$T_2 = \frac{L}{C}.\frac{n_1}{n_2}(n_1 - n_2)$$

$$T_3 = M(\lambda).\Delta h.0,85.L$$

VI. CONCLUSION

The results of this paper will be used for lectures and seminars with students in the programmes of "Optoelectronics", "Optoelectronic systems" and "Optoelectronics and Optical Communications".

REFERENCES

[1]. Колев И.С., Инфрачервена оптоелектроника. Унив. изд. „В. Априлов" 2004.
[2]. Колев И.С., Оптоелектронни системи. Унив. изд. „В. Априлов" 2003.
[3]. Колев И.С., Оптоелектроника. III прераб. изд. „В. Априлов" 2003.
[4]. Conrad Electronic. Electronic Welt, 2004.
[5]. Шойкова, Е., Г. Моллова, Г. Матеев, Ил. Хинков, Б. Толев. Компю-търно-интегрирани среди за синтез и изследване на електронни схеми, С., ВМЕИ, 1989.
[6]. General Electric, Optoelectronics, 1991.
[7]. Рабов, С. С., Л. Л. Христов. Оптични комуникации. С., Нови знания, 1989.
[8]. Honeywell. Fiber optic products, 1995.
[9]. Siemens. Optical Information Technology. Data Book, 1996.
[10]. Siemens. Optoelectronics. Data Book, 1993.
[11]. Wandel&Goltermann. High performance, portable fiber optics test equipment, 2000.

Virtual Communication among Teachers and Students in Mathematics Computer Based Learning

Tsvetanka Kovacheva[1]

Abstract **- The paper considers methods of organization and implementation of virtual communication among lecturers and students in mathematics computer based learning on the basis of Internet technologies applied in practical conditions with available resources. This allows rousing of student's activities to improve and consolidate their knowledge of mathematics. The opportunity to extend the existing web site of Mathematics Department in Technical University (TU) Varna is examined.**

Keywords **– information technologies, virtual communication, Internet.**

1. INTRODUCTION

The communication is an important factor in student's training. The use of Internet allows a new interaction among lecturers and students – Web Communications or bi-directional Internet interactions. They allow real time telephone connections, addition of images, sounds, video clips and movies. The conversations can be effected as series of consecutive messages or in real time with the help of text based facilities. It is possible to exchange texts, files, audio and video programs.

Such kind of training provides the students with online information for independent training, synopses, thematic plans, implementation of test papers and course projects as well as opportunity to ask questions and receive answers.

This establishes conditions to increase the interest to the subjects and to make the schooling more active. The lecturer can check faster the learning level of each student and might introduce corrections in the training process, if it is necessary.

[1]Kovacheva Ts. is with the Department of Mathematics, 1 Studetska str. 9010 Varna, Bulgaria, E-mail: ts_kovacheva@hotmail.com

The resources of the so-called Computer Based Learning, which represents a structured and purposeful use of electronic systems or computers to assist the learning process, effect the communication between lecturers and students. It allows presentation of the educational material on various subjects by Internet, audio and videotapes, satellite programs, interactive television and CD – ROM. The Internet mathematical resources such as mathematical programs, libraries, articles, books, etc., can be used as well [3,4].

2. SOME METHODS OF VIRTUAL COMMUNICATION AMONG LECTURERS AND STUDENTS DURING THE TEACHING PROCESS OF MATHEMATICS

Electronic Mail (E-mail). E-mail is the most widely used and accessible way of communication, which allows asynchronous active correspondence of the lecturer with the students (and among the students) by sending/receiving text format messages.

It is assumed that each lecturer and student are possessing E-mail address and Internet page. The process of interaction among them is as follows: The teacher passes all necessary information into Internet. The exchange of messages is made by E-mal, while the larger files are sent by FTP-Protocol. The initially prepared new materials are in text only format. The reformatted texts are transformed then in HTML-files and are published in Web pages. The whole process of exchange of messages is logged. This allows making quality and efficiency analysis of the student's, as well as of the lecturer's work. The mathematics teaching by E-mail reduces the volume of the printed materials. On the other hand, this opportunity is particularly useful for part-time (correspondent) and distant training students.

E-mail provides the following additional advantages:

- ✓ Correspondent conferences by dissemination of full flow of messages from each one to all students included in the list of the students (Mailing List);
- ✓ Automated generation of correspondence flow, supported by environments providing such kind of correspondence and possession of all advantages of the techniques for electronic processing of documents.

One of the best ways of training is to explain the problem to somebody else. That is why the establishment of a Discussion Forum (DF) in Internet helps to improve the preparation of the students (by asynchronous communication on a certain topic). Each student can, during the semester, put his/her questions in a Notice Board (NB) – somebody else can read it and answer the question or start new discussion on the topic. However, the information can remain only few weeks there. Netscape or Internet Explorer can be used to write/read questions or messages in NB. DFs are organized in few general categories and one of them – *sci* (science) category, can be used for topics of scientific interest.

Different types of DFs are:

- ✓ Internet: Usenet: newsgroups are placed on a public news server;
- ✓ Internet: Discussion Forum: newsgroups are placed on a www page (Web based);
- ✓ Internet/ Intranet/ Extranet: Restricted for a specific community, news server or Web based (e.g. only students of one course).

It is possible by DF to: subscribe to, or unsubscribe to, one or more newsgroups, search for newsgroups or messages, reply to Group, to all users or directly to the sender of the message, post attachments like Word, Excel, PowerPoint etc.

files, use automatic signature sending a message to different newsgroups in a time, etc. By this way of interaction the students actually become aware about their knowledge and accumulate good experience to manage in other situations, as during examination for example. Answer to the remaining unclear issues could give the lecturer by E-mail, few days before the examination. E-mail is the basis for communication among lecturer and students.

DF is a fast way of communication, easy to reach the knowledge of people and can create specific groups with a lot of in detail and in-depth conversations. However, it is hard to start up an active forum by DF, especially if a lecturer has a small group of students. Sometimes the forums are full of non-relevant discussions (although a lecturer can solve this problem).

Participation of students in DF can stimulate knowledge sharing among students. They can check the forums before they ask questions. This is a place for informal contacts and furthermore, activates and focuses the students through discussions, for the next subject.

Chat provides a way for students with similar interests to communicate in a synchronous way. When a student chats on the Internet, he "talks" to others using text messages. This informal communication among students (improving atmosphere and mutual relationships) helps sessions with lecturer on a particular question or formal sessions between a lecturer and a small group of students. If a student wants to participate in chatting, he enters a so-called "chat room". This is a virtual environment where he/she can talk to one or more participants. Chat tools can be integrated in his webpage as his learning environment or separate environments could be established.

Different types of chatting include:

✓ Web based chat: a student enters a chat room and starts directly talking with other
chatters in the chat room. In a virtual classroom, this type is used very often.

✓ Instant messaging: a lecturer can create a list of students with similar interest and see whether they are online at any time. He can start talking to them immediately. Famous free instant messaging applications are ICQ and MS Instant Messenger.

✓ Graphical Chat: some chat programs have software to create a graphical chat room, where chatters are displayed as comic book figures or the chatting takes place in a specific environment like a bar.

Chat allows private conversation (one to one), group conversation (many to many), chat request, use of different colors per chat participant, use of sounds and audio-chat. Some applications also support: sending URLs, sending e-mail, sending voice messages, sending files. It is fast, cheap, gives possibility to talk to many, eases the building of relationships (informal way of communicating) and if somebody can see that others are using the learning environment at the same time, he feels part of community. There are some drawbacks however, if it tells too much of your personal life; firewalls are often a hurdle because they keep ports closed; some tools might not function; talking with many will result in a very fragmented conversation (so 4 or 5 students is the maximum); learners can disturb each other by contacting all the time, etc.

3. Extension of the Web-site of Department of Mathematics

Mathematics is one of the basic subjects the students face in the first two years of their tuition in TU. The quality and efficiency of mathematics learning process could be significantly improved by application of up-to-date information technologies. Resources are available – the presence of Web-servers in TU and in the Department of Mathematics in particular, allow building of such structure. All lecturers and students of the University have a real access to Internet.

The use of databases (DB) for storage of information, provides solutions on a qualitative higher level to many real tasks of the organization of the tuition and the scientific work of the students. Necessity arises to extend the Web-site of the department to allow implementation of this communication for student's training and improvement of the mathematics teaching process. A System for Management of DataBases (SMDB) is used for program support of the training process. Internet provides regulated access to it. DB contains information about the training process, which is regularly updated. DB can be accessed by arbitrary requests. The information is read-only for the users. The DataBase contains the following *information*:

- *For lecturers:*

✓ Brief biographical data for each lecturer – education, academic rank, position, professional experience and skills, personal interests, membership in scientific organizations, etc.;

✓ Lectures - List of the subjects of Mathematics delivered by the lecturers, specialties, credits and annotation;

✓ Directions of scientific work – topics, interests, wishes for contacts ant joint research in specific scientific areas;

✓ Papers and monographs;

✓ Contact information

- *For students:*

✓ General reference information – subjects studied during the semester, deadlines of the semester and session, holidays, vacation, University events;

✓ Special reference information - consultations, lectures of visiting professors, extraordinary students forums, etc.;

✓ Academic information – methodic materials – text books published by the department, collections, systematical manuals, as well as addresses of useful and interesting Internet sites – electronic libraries, textbooks, reference books and magazines, data bases, synopses, thematic plans of seminar and laboratory exercises, methodical instructions for laboratory exercises, tests and course projects, list of recommended literature, questions for examinations, knowledge tests, evaluation criteria and system of knowledge control, possibilities for dispensation from examination, results of the systematic control during the semester, printed materials with mostly used formulae, exemplary models of mathematical problems, tests for preparations, etc.;

✓ Information about the life and contributions of renowned mathematicians, especially whose work is related to the

syllabus of mathematics – Euler, Euclid, Newton, Leibnitz, etc.;

- *For foreign students* – it is desirable to translate in English all information for Bulgarian students, with the development of this training;

- *For candidate students* – date of competitive examination on mathematics, solution of examination mathematical problems of previous years, evaluation criteria, reference book, courses in mathematics.

5. CONCLUSIONS

The studied chapters of mathematics are among the most suitable subjects for development of generalized knowledge, skills and habits, required by the engineering practice. That is why the correct organization and enrichment of the forms and ways of information exchange with the students contributes to improve the efficiency of the training process in mathematics, the level of awareness and preparation, the development of creative thinking and is an incentive for independent work. This sets up a requirement to the lecturers to study the various ways of communication and to apply them efficiently.

The proposed way of virtual communication, among the lecturers of the department and the students on the level of educational process of mathematics and the respective informational support, allow:

- ✓ transition to dialog interaction among lecturers and students, which leads to decrease of the costs of the training;
- ✓ decrease of the volume and hence the material expenses for synopses, thematic plans, laboratory and course projects, tests;
- ✓ Solution of the problem with the shortage of printed textbooks and books of mathematical problems, by supplying students with electronic tuition materials and E-books, necessary for the training process and the preparation for examinations in mathematics.

The transition from the traditional presentation of knowledge to the joint (lecturer-student) creative approach to work with contemporary virtual means, contributes to achieve a high quality and efficient training process.

References

[1] Information Technologies in Science and Education http://osu.tpu.ru/edu/tech/

[2] Education http://www.insead.fr/Encyclopedia/Education/

[3] Interactive Math Lessons http://www.mathgoodies.com/

[4] Technology of Educational Resources http://www.webuniversity.ru/

[5] G. Grams “Internet – fast and easily”, “Macropoint”, Sofij, 1998.

[6] Young M., Muder D., Kay D., Warfel K., Barrows A.”Internet: The Complete Reference” Kiev, “Irina”, BHV, 2001.

[7] State Institute of Information Technologies and Telecommunications www.informika.ru

Inteligent Manufacturing Systems And Mechatronics – An Educational Approach

Todor Neshkov [1]

Ab*stract:* The new demands of the industry and educational trends have caused the appearance of the new course of Mechatronics in the Technical University – Sofia in Bulgaria. The discipline of Inegligent Manufacturing Systems (IMS) has been integrated in it, as well as in other specialties. This approach is one of the various ones that have been developed throughout the world.

1. INTRODUCTION

The new demand on engineers for interdisciplinary skills and knowledge and the ability to produce fresh ideas and products for the fast changing market caused the development of educational programs in IMS and Mechatronics in many countries around the world. These programs vary to some extent in their concepts and contents. Different universities offer whole undergraduate or graduate courses or just separate disciplines in these specialties. However almost all educating institutions stress on the integration of the basic engineering areas: Mechanical, Electrical, Computer and Control Engineering. Another common feature of the proposed programs is the need for hands-on experience that allows the students gain the ability to design intelligent manufacturing systems and mechatronic systems on their own and the perspective to start promising engineering careers. There are differences in the number and kind of taught disciplines, the instruction approach, and the structure of laboratory exercises, the projects tasks and requirements. This paper reviews attitudes toward and program features of IMS and Mechatronics education in some countries. It also presents the concepts and the curriculum of the course of Mechatronics in the Mechanical Engineering Department in Technical University – Sofia in Bulgaria and the IMS discipline incorporated in this course.

2. IMS AND MECHATRONICS EDUCATION AROUND THE WORLD

The broad areas of IMS and Mechatronics education provide for the different approaches of preparing students for the dynamic market of highly integrated products. Some universities organize such education programs within a given department (Mechanical, Electrical, and Control Engineering Department) or with the cooperated efforts of several departments. Some programs include subjects not from all four basic engineering areas or are concentrated around one spinal discipline (e. g. control engineering). The differences are caused by the views of the educating bodies and by the needs of the local industries.

Craig (2001) puts the stress on the "balance between modeling/analysis skills and hardware implementation skills". He also asserts the need for mechanical engineers to be proficient in control design in order to produce novel concepts in their design activities. They should include modeling, simulation, analysis, and mathematics together with their former hardware experience in generating new prototypes together with engineers from other areas. There are two senior elective courses in the Rensselaer Polytechnic Institute, "Mechatronics" and "Mechatronic System Design", each lasting for one semester. Craig describes the programs as helpful for the engineers in learning how to apply the classical control designs as an incorporated part of their own design. Students are taught with an emphasis on understanding the physical and mathematical fundamentals. The main issues are Modeling and Analysis of Dynamic Systems, Feedback Control of Dynamic Systems, analogue and digital electronics and control implementation and simulation with latest software products. The first course includes lab exercises with five mechatronic systems, while the second one includes projects for four-person teams that fully develop mechatronic systems and present them in written and oral form. Craig also emphasizes on the need of experience of the instructing stuff in order to teach modeling.

Wikander et al. (2001) claim that a new mechatronic approach is needed where a shift from mechanical hardware to computer software to be established in implementation of functionality. According to them the older subsystem-based approach of designing the separate homogeneous subsystems and interfacing them afterwards does not provide the full integration of the design process of a given mechatronic system. They propose as an educational approach the system in the Swedish Royal Institute of Technology with a five-year curriculum where interdisciplinary courses are integrated in an existing program of mechanical engineering. The courses usually deal mostly with the design process and the acquired knowledge of the various engineering disciplines by the students is achieved by problem-based learning, with team organization. Examples of courses in the Institute above following the given principles are: "Microcomputers in Embedded Systems", "Advanced Course in Mechatronic System Design", "Real-Time Control and Programming". Alciatore (2001) asserts restructuring the core mechanical engineering undergraduate curriculum toward mechatronics program, as well.

Siegwart (2001) provides a discussion on mechatronics education in the Swiss Federal Institute of Technology of Lausanne (EPFL) and ETHZ, Zurich, and particularly the "Smart Product Design" course in the latter one. Students there "bond" their basic interdisciplinary knowledge of elements of mechatronic systems, electric circuits, sensors, actuators, controllers, control and artificial intelligence, etc. with the help of design, system integration, teamwork, project management, communication and controlling activities. They gain all the skills through projects where theory meets practical illustration. The projects consist of building mobile robots, where every student team receives a kit ("smartROB design kit") and an assignment for the tasks the robot should be able to fulfill. Before starting, the participants in the "Smart Product Design" course have both lecture and laboratory work. Various subjects are covered that are not all familiar to the students and the latter communicate with engineers from different areas in order to achieve the integration required in the mechatronic system design. In the end of each course, all robots from the projects participate in a contest. This element adds more motivation to the studies.

The practical education is an emphasis also in the Ritsumeikan's Department of Robotics (Nagai, 2001). The exercises in the courses of advanced robotics there are held from the second until the last year in the university. As for the previous case system, integration is a basic purpose for the students to achieve. Despite the great difficulties they meet, they receive background knowledge and experience in order to proceed with their careers and research in robotics.

Tomizuka (2002) states:

[1] Todor Neshkov is with the Technical University – Sofia, Bulgaria *Faculty of Mechanical Engineering*

"Issues surrounding integration as well as working in team cannot be taught in lecture courses. Students must experience them, and in this regard laboratory courses are essential in mechatronics education."

In addition, he emphasizes on the need for drawing the attention of students toward mechatronics at an early stage (high school and college) and that IT tools have to be broadly incorporated into engineering education. Tomizuka describes a 15-week course in mechatronics design that covers various disciplines and ends with the presentation of projects developed by 3-4-person teams.

Brown and Brown (2002) express their preference toward the approach of project based practical engineering and to support it with theoretical learning. They place the basic questions concerning mechatronics education about the owner of this type of courses, the contents, and the way to "teach such a different philosophy with such a wide range of diverse subjects". The solution attained at Hull University is the control engineering part to be the spinal subject and other subjects come from other departments. The four-year mechatronics program contains mostly project work and supporting lectures. Active learning and quick adaptation are aimed by solving a large-scale design problem, which is put in place of traditional predetermined laboratory exercises. According to the representatives of the university above, self-reliance, motivation, creativity and understanding are built in students by following that approach.

Mechatronic education at the University of South Carolina is being developed together with programs of Smart Structures and Adaptive Materials in the Mechanical Engineering Department in cooperation with the departments of Electrical Engineering and Computer Science and Engineering. Giurgiutiu et al. (2002) discuss the work at that university toward finding methods to teach multidisciplinary courses and organizing multidisciplinary project working teams. They state:

"Today's and tomorrow's products are intertwined blend of mechanisms, sensors, actuators, electronics, and information technology. The ideal graduate should be able to hit the ground running in all these areas concurrently in order to achieve maximum performance with minimum training/adaptation time. … Of course the "ideal graduate" is not a physical reality but a graduate with a broad Mechatronics education will come pretty close to it."

A track system, similar to that in the University of Washington, is proposed, where the courses are to be covered by the Electrical and Mechanical Engineering Departments and the one of the tracks is Mechatronics.

The course sequence in Mechatronics in the University of Arkansas at Little Rock described by Wright (2002) is a supplementary one for the system-engineering program there. The pursued task is to teach mechanical design to the students of that program. The multidisciplinary character of this type of undergraduate education is formed by the following sequence: Introduction to Engineering, C Programming, Elements of Mechanical Design, Circuits and Systems, Digital Systems, Control Theory, Instrumentation and Measurements, and Mechatronics (in the senior level) together with CAD/CAM laboratories and lectures. The design skills are the target of a free-form design project where students have to develop, analyze, simulate and produce a prototype, concerning also cost and budgets. A special competition (US FIRST design competition) in building a teleoperated mobile robot in 42 days is an additional task for the students of the university to enhance their training in cooperation with pre-college students.

The graduate Mechatronics course in the Woodruff School of Mechanical Engineering at Georgia Institute of Technology (Ume et al., 2002) is concentrated on the microprocessors and microcontrollers in mechanical systems. The course contains considerable part of hands-on design and work (usually in teams of couples of students) and ends with a final project also organized in teams. Computer programming and electrical engineering disciplines are mostly covered. Laboratories have large workspace and are devoted to particular skills. The projects are given additional time so that the students can develop proper aesthetic and packing features of their mechatronic products.

An open-ended project is developed for the undergraduate mechatronics course of Stanford University. Carryer (2002) describes it and states:

"The intent is to teach mechanical Engineering students enough about electronics and software so that they will be able to be effective interdisciplinary team members and leaders. The philosophy is that the best way to learn the capabilities of the technology is to actually learn to apply them oneself."

One-quarter course contains this project, while a four-quarter sequence in Mechatronics is provided at the same university at the same graduate level.

3. IMS AND MECHATRONICS IN TECHNICAL UNIVERSITY – SOFIA, BULGARIA

The education in IMS and Mechatronics emerged gradually in Bulgaria during the last six years in the Mechanical Engineering Department and the English Language Department of Engineering (ELDE) of Technical University – Sofia. This academic year the former department offers a graduate program in Mechatronics. IMS is taught within the course in CIM. The graduate program of ELDE in Industrial Engineering provides a one-semester course in both disciplines.

The basics of IMS and Mechatronics have been seeded during the last decade with the fast changing demands of engineering specialists in automation and computer integrated manufacturing. Still in 1991 an educational concept in this area exists although the interdisciplinary idea is not yet well estimated. An emphasis in this concept is placed on the students' preparation for increased computer technology application, broad technical knowledge, and design skills concerning functionality and improvement tendencies, CAD, manufacturing processes development and control, basic economic knowledge. The educational process is proposed to be more problem-oriented and less specialized. A training complex is integrated in the training programs that contains modules for producing and assembling small wooden or plastic parts and is used to simulate a real computer integrated manufacturing system. The discipline of adaptive control has been included in the education program of the Mechanical Engineering Department with the help of the Chair of Automation of Discrete Manufacturing, and the disciplines of Technical Image Processing and Artificial Intelligence in Manufacturing have been developed with the help of TEMPUS projects. There has been useful collaboration within the TEMPUS program with CCTA – Wales and De Monfort University, Leicester, UK that have been supplying the department with modern computers, software didactic materials and scientific literature.

In February 2000, a symposium has been held in Sofia on the theme of "Mechatronics Education". The participants have been from: the Departments of Mechanical Engineering and Electrical Engineering, Technical University - Sofia, the Departments of Mechanical Engineering of Technical University - Illmenau, Germany, Technical University - Nish, Yugoslavia, and Technical University - Skopie, Macedonia. The reports have been connected with the research and educational experience of the different universities. A mutual intention has appeared for the creation of a net of universities to cooperate in this area. The purpose of the future cooperation is to provide for the basis of Mechatronics education aimed at application in the machine building, automatic and precise devices, as well as in micro-technologies and bio-technologies. Another important purpose is to create a common taxonomy for teaching Mechatronics.

Some professors in the Chair of Automation of Discrete Manufacturing participate in a project financed by DAAD (a German organization for academic exchange), in the part of "Mechatronics" with its leader - Professor Helmut Vurmus. An enlargement of this cooperation is planned connected with the Institute of Fine Mechanics and Optics in Technical University - Budapest, Hungary.

The Chair of Automation of Discrete Manufacturing has training and research laboratories in CAD, Assembly Automation, Control Systems and CIM class where most of the practical exercises are held. The training in IMS and Mechatronics is combined with intensive use of information technologies, multimedia, teamwork, and reports preparation, making successful presentations.

Strategies for IMS and Mechatronics education have been blended with those for CIM course. Some special modules introduced there are Hardware and Software CIM Platforms, Integrated Manufacturing, Non-automated Factory of the Future, Multimedia Technologies in Design, Concurrent Engineering, and Low Cost CIM for Small and Medium Enterprises. The existing teaching experience is proposed to be transferred to IMS courses concerning the following problems: the use of systematic approach for successful and effective automation; application of optimization techniques; analysis of artificial intelligence application in manufacturing systems in the aspects of adaptive control in production and assembling, artificial vision, intelligent CAD/CAM/CAE systems.

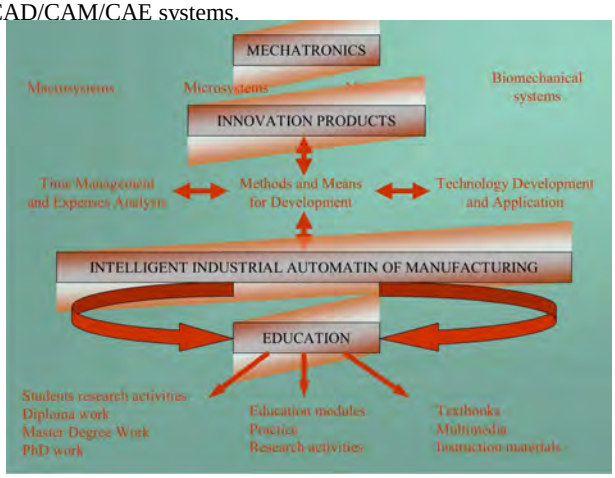

Figure 1. The Concept of the Future Activities in the Mechatronics Education

The Mechatronics program at the Mechanical Engineering Department is aimed at: providing students with interdisciplinary knowledge and skills, integrated design approach, manufacturing and maintenance of products and processes. More precisely the topics that are to be covered in this program include: system design (selection of sensors, actuators, electronic components and computer simulation), microprocessor technology (system architecture, digital systems, memory storage devices, input/ output devices), interfacing techniques, digital communications, software development, and control systems. IMS education is incorporated as a subject in the course of Mechatronics in the department above and in the graduate course of ELDE.

Training in IMS and Mechatronics are supported still in the undergraduate level in both departments mentioned above. The first two years provide knowledge of fundamental principles of engineering sciences with the disciplines of Mathematics, Physics, Theory of Machines and Mechanisms, Electrical and Electronics Engineering, Computing, etc. the next two years provide special topics and some disciplines are elective. The Mechanical Engineering Department offers for example Low Cost Automation, Design of Automatic Machines, Computer Science, Quality Control, Technology of Discrete Production, Computer Integrated Manufacturing, Control Systems, etc. The ELDE program ends with Bachelor Degree in Manufacturing Engineering and interdisciplinary subjects in the second two years include: Control Engineering, Measurement and Instrumentation, Elements of Industrial Automation, Computing, Industrial Electronics, Manufacturing Design with projects and course works, CIM, CAD, Advanced Control Theory, etc.

IMS and Mechatronics in the graduate course of ELDE are taught as two separate modules of one and same subject in the Bulgarian Academy of Sciences by professors from the Institute of Mechanics and Biomechanics and the Central Laboratory of Mechatronics and Instrumentation.

The IMS discipline is incorporated in the Mechatronics course and is taught during the third semester. Here follow details about the Mechatronics course in the university (Fig. 2).

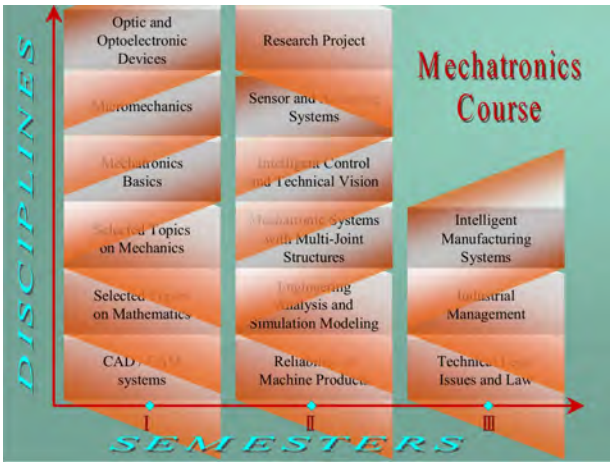

Figure 2. The Mechatronics Course Program in the Mechanical Engineering Department of Engineering

The purpose of the CAD/CAM Systems subject is to get the students familiar with the development and application of these systems and provide them with the ability to choose the suitable system for a given task. The laboratory exercises are devoted to work with AutoCAD, Mechanical Desktop and SolidWorks, as well as to the use of the corresponding CAM systems and the generation of the program code for a given CNC machine. The Selected Topics in Mathematics are aimed at the increased practical knowledge of set theory, images, mathematic statistics, experiment planning, graph theory, probability theory, etc. Selected Topics on Mechanics is an extension of the “Mechanics I and II” from the undergraduate program. It contains topics from the analytical mechanics and vibrations theory, and discrete multimass systems connected with the design and analysis of transport and hoisting machines, building machines, robots and manipulators.

The Basics of Mechatronics course provides knowledge of the structure, functions, environment of the mechatronic systems, as well as their basic elements. An emphasis is placed on the methods for mechatronic systems design; concept preparation, planning, object design, etc. The theoretical bases for mechatronic systems modeling and different models of mechanical building elements, electric actuators and machines are reviewed. Various technologies and technological processes are taught in the Micromechanics subject, which are used for the production of micromechanical structures. Technological equipment for their production and operations control means is reviewed. The design methods of micromechanical elements, the production technology development, and assembly methods are covered. The laboratory exercises provide an analysis of the available equipment design, optimal technological parameters settings of the equipment, and concrete

production operations of the students for preparing micromechanical modules.

The theoretical issues of the optical and optoelectronic devices and specific solutions of some groups of such devices are covered in the subject Optic and Optoelectronic Devices. There are included the principle schemes of the basic types of optical, optoelectronic and laser systems that are used in industry and for research, the typical units of these systems, optical and fiber-optical sensors. The laboratory exercises give the students some skills in the operation in the use of optical and optoelectronic equipment, the ability to choose the right one for a given task in their future engineering careers, and to communicate with specialists in the given area.

The lecture material in Reliability of Machine Products deals with the problems and methods for planning, determining, normalizing, providing the reliability of products during their design, manufacturing and exploitation. Some issues here are basic reliability models, Markov models and processes application, processes that impede reliability and the influence of design and technology on them, methods for diagnostics of machines, systems and processes, etc. The laboratory exercises include some the investigation of the processes that impede reliability, calculation methods and the creation of algorithmic methods for reliability modeling and analysis, as well as diagnostic experiments with specialized equipment and software. The discipline of Engineering Analysis and Simulation Modeling covers the types of models, their application in engineering analysis, practical problems in machine and appliance building through static and dynamic models, stochastic processes, experiment data analysis, regression analysis, dispersion analysis, correlation analysis, experiment planning, simulation methods. Students are provided with skills in working with the basic software products in this area.

The purpose of the subject Mechatronic Systems with Multi-joint Structures is to introduce the students with the kinematics and dynamics of these mechatronic systems, the method of impedance control, mechatronic systems with closed multi-joint structures, and new types of mechatronic systems. The experimental work is carried out with software programs for dynamic modeling and simulation and analysis of the results is made. Intelligent Control and Technical Vision subject covers topics on the methods of modeling, identification, and simulation of incompletely defined structures, digital, adaptive and intelligent control, synthesis and optimization in control problems, increase of system autonomy through artificial intelligence and acquisition of sensor information, technical vision systems, object recognition, video information processing, communication and integration of these systems with the other components of the mechatronic systems. Both laboratory models and industrial devices and software are used. Sensor and Actuating Systems contains issues on acquisition, conversion and processing of information from sensors, integrated sensor schemes, integration of sensor, actuator and control systems. The laboratory exercises improve the understanding of the theoretical material.

The subject of Technical Legal Issues and Law presents basic knowledge about the application of normative acts in two directions: the normative order of the firms and economic units according to the issues of the civil and trades law; the obligatory and the voluntary regulations for manufacturing and selling safe ant qualitative machine products. The purpose of the Industrial Management discipline is to provide knowledge about the basic problems in managing the industrial organizations, management thinking and functions. The lectures review also the contemporary concepts and systems for the effective business management. The practical exercises are in the form of cases, tests and problems.

Intelligent Manufacturing Systems provides the students with knowledge about the application of artificial intelligence and the integration of manufacturing and computer systems. Main issues are: historical development and today's problems of artificial intelligence, data bases, and knowledge bases connected with machine building, expert systems, IMS in robotics, etc. An emphasis is placed on the application of IMS as a base for the "Factory of the Future".

ACKNOWLEDGEMENTS

We would like to express our acknowledgements toward professor Dr. Eng. Helmut Wurmus, coordinator of DAAD project "Suedosteuropa – Mechartonik" and National Scientific Council of Bulgaria – project 1008/00 for the financial and methodological support.

CONCLUSION

The most important features of the education in Mechatronics concerning the world experience according to the information we have gathered are: project-oriented programs, team working and communication with engineers from different areas, systems integration in the design process, competitive approach in pursuing project tasks.

The education in IMS and Mechatronics in Technical University – Sofia has started its development, but it still lacks the hands-on approach because of the economic difficulties that all the country meets today.

It is extremely useful for us to become familiar with the foreign programs and experience and to implant them in our programs for Mechatronics and IMS engineers. It is essential for our university to have cooperation in the education of such specialists. Furthermore, our graduate and undergraduate students can work on projects connected with their own studies in Bulgarian and foreign firms in our country. These initiatives are the steps we can make to produce competitive Mechatronic engineers.

REFERENCES

Boyadjiev, I. K., T. D. Neshkov (1995). Erfahrungen auf dem Gebiet der Intelligenten Fertigungssysteme. *DAAAM-95, 6. Internationales DAAAM Symposium*, Krakow, Poland, pp.039-040

Brown, N. J., O. T. Brown (2002). Mechatronics "a Graduate Perspective". *Mechatronics*, **Vol. 12**, pp. 159-167

Carryer, J. E. (2002). March Madness: a Mechatronics Project Theme. *Mechatronics*, **Vol. 12**, pp. 383-391

Craig K. (2001). Finding a Balance between Modeling/Analysis Skills and Hardware Implementation Skills Is Key to Mechanical Engineers Becoming Successful Mechatronics Engineers. *IEEE Robotics & Automation Magazine*, **June 2001**, pp. 12-19

Ganovski, V., I. K. Boyadjiev, T. D. Neshkov (1991). Eine Konzeption für Ausbildung von Fachleuten auf dem Gebiet der Komplexautomatisierung und CIM. *Ingenieurpädagogik'91, 20. Internationales Symposium*, Dresden, Germany, pp. 721-726

Giurgiutiu, V., A. E. Bayoumi, G. Nall (2002). Mechatronics and Smart Structures: Emerging Engineering Disciplines for the Third Millennium. *Mechatronics*, **Vol. 12**, pp. 169-181

Kostadinov K., (1997) Mechatronics. An Approach to go inside, *Lecture notes*, Universsitatea "Dunarea de Jos", din Galati, Romania, p.59.

Nagai, K. (2001). Enabling Students to Acquire the Knowledge and Experience Necessary to Produce Advanced Technologies. *IEEE Robotics & Automation Magazine*, **June 2001**, pp. 39-43

Neshkov, T. D., V. Ganovski, I. K. Boyadjiev (1997). Computer Integrated Manufacturing – Basis for Building Intelligent Manufacturing Systems. *6th International Conference on Flexible Technologies, MMA'97*, Novi Sad, Yugoslavia, pp. 831-837

Neshkov, T. D., C. Velkov (1998). Automation, Production Systems and Computer Integrated Manufacturing in Education. *The Tenth International IFIP WD 5.2/5.3 conference Prolamat 98*, Trento, Italy

Neshkov, T. D. (2000). Mechatronic and Computer Integrated Manufacturing – an Educational Approach. *Symposium Mechatronik*, Sofia, pp. 66-72

Siedwart, R. (2001). "Hands-on Education Best Enables Students to Integrate Knowledge from the Many Disciplines Involved in Designing and Building the Mechatronics Product of Today. *IEEE Robotics & Automation Magazine*, **June 2001**, pp. 27-34

Tomizuka, M. (2002). Mechatronics: from 20th to 21st Century. *Control Engineering Practice*, **Vol. 10**, pp. 877-886

Ume, I. C., A. Kita, S. Liu, S. Skinner (2002). Graduate Mechatronics Course in the School of Mechanical Engineering at Georgia Tech. *Mechatronics*, **Vol. 12**, pp. 323-335

Wikander, J., M. Törngren, M. Hanson (2001). Emphasizing Team Building in a Problem-Based Curriculum to Meet the Challenges of the Interdisciplinary Nature of this Field. *IEEE Robotics & Automation Magazine*, **June 2001**, pp. 20-26

Wright, A. B. (2002). Planting the Seeds for a Mechatronic Curriculum at UALR. *Mechatronics*, **Vol. 12**, pp. 271-280

Virtual Physical Laboratory and its Intranet Application

Mariya Nikolova[1] and Pavlina Todorova[2]

Abstract – **The goal of the paper is to present Web based exercises in physics. An algorithm for determining the sound's velocity in air by the method of standing waves is described**

Keywords – **Web Application**, **Distance Education, Intranet Application**

I. INTRODUCTION

The module "Physical laboratory" is a part of a Web book in physics for training the students and cadets from Naval Academy "N. J. Vaptsarov". It is in the process of development and has the following structure: list of the laboratory exercises, the choice of one of them leads to the following blocs: theory of the physical phenomenon, scheme (photography) of the laboratory setting, tasks for observation, research and measuring, demo version (animation, film or interactive model), table for the experimental data, form for survey, control tests and links to the calculator and graphical program.

The paper presents a software realization of the laboratory exercise "Determining of the sound's velocity by the method of the standing waves".

II. SUMMARY OF THE EXERCISE

The task of the exercise is to determinate the sound's velocity in dry air by the method of standing waves.

The experiment setting consists of a glass tube with a piston. A loudspeaker, connected to a high-frequency generator is attached to the left end of the tube. A microphone is attached to the other end of the tube and it is connected by means of an amplifier to an ampermeter.

The method of the standing wave consists in [1]: the standing wave in the air column closed at both ends springs up from the interferention of the traveling and the reflected longitudinal waves. It can be received in two ways and they are used for determining the sound's velocity.

First method. The frequency ν is fixed and the length of the tube L is changing until the standing wave starts in the tube. The length of the standing wave is equal to the distance between two neighbouring nodes. The task is to register two neighbouring nodes of the piston, determining the length of the tube, for which for the given frequency the standing wave starts. The sound's velocity will be equal to:

$$V = 2(L_2 - L_1)\nu \quad (1)$$

The places of the nodes are localized according to the situation of the condensing and dispersing of the dots, alternating with the change of phase. Attentive students will also easily localize the nodes by the dots with minimal amplitude.

Second method. The length of the tube L is fixed and the frequency is changing. The task is to find two consecutive resonance frequencies. The difference between them is equal to the basic natural frequency. The sound velocity will be:

$$V = 2(\nu_2 - \nu_1)L \quad (2)$$

III. DESCRIPTION OF THE ALGORYTHM OF THE INTERACTIVE MODEL OF THE EXERCISE

A Web page of the interactive model of the exercise from the first task is presented on fig. 1. The Web page of the second task is analogical, and each row of the table containing one measurement of the length of the tube and two measurements of the frequency.

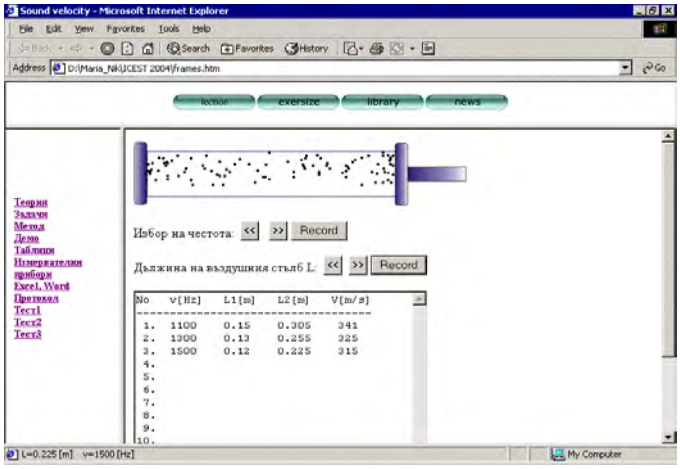

Fig. 1. Web page of the site

At the beginning of the Web page a computer simulation is made of the movement of the dots in the sound wave, spreading in the glass tube.

For each one of 100 dots with random initial position along the tube a movement along the horizontal line is given according to the formula:

$$y = 2A\sin kx\cos 2\pi\nu t \quad (3)$$

where **y** is the distance from the initial position **x**, **A** is the

[1]Mariya Nikolova is with the Department of "Mathematics and Informatics", Naval Academy "N. J. Vaptsarov, 73 Vassil Drumev St., 9026 Varna, Bulgaria, E-mail:mpn@abv.bg

[2]Pavlina Todorova is with the Department of "Mathematics and Informatics", Naval Academy "N. J. Vaptsarov, 73 Vassil Drumev St., 9026 Varna, Bulgaria, E-mail:pawtod@abv.bg

amplitude, $k = 2\pi / \lambda$, **t** is the time, V - is the frequency.

The image of the tube is realized through GIF-file, included in the code of HTML. The dots are realized through GIF–file with a small size as objects with unique names, initial position and visibility, included in the tag <DIV>. The initialization of the objects and the movement of the dots is carried out through two functions, written in Java Script [4] setVariables() and startMove() respectively. They are loaded consecutively in the tag <BODY> by the attribute ONLOAD. Initialization of part of the variables used in startMove() is carried out before its calling.

The algorithm of the function startMove(), through which the computer animation on the screen is realized, includes the following steps:

1. Choice of **L** and V . Visualization of their values in the status bar. Setting the step of time deltat=T/20, by which the new position of each dot is computed (each period is described in 20 steps).

2.Computing the **y** values for the 100 dots – array y[j] and the absolute coordinate of each of the objects xstep[j]

3. Using the function eval of Java Script for determining the movement of each dot to position xstep along the horizontal.

4.Increase of t with deltat and check if t≤T? If yes – calling of setTimeout function with parameters startMove() and 100 - interval of time 100 ms (the movement velocity of all dots on the display is given in this way) and returning to step 1. If no – initialization of variables, calling of setTimeout and returning to step 1.

With the help of “Choice of frequency” and “Length of air column L” buttons, students can change the values of the frequency V and the tube length L. Clicking each of the buttons Record (fig. 1) leads to the automatic writing of the values chosen in the table and to automatic computing of the sound velocity by formula (1). The values in frequency are in [Hz] and change in the interval [1000, 2000] by step 25 [Hz], while the values of L are changed from 0.100 [m] to 0.500[m] with a step of change 0.001[m]. After three or more measurements the average velocity $\bar{V}$ and the mean error ΔV are computed. There is a possibility of correction of the input values of L. Every click of the RECORD button places alternate with the value input before. Inserting a new row in the table is made only by clicking the button for frequency record. There is a possibility for the student to give up a certain measurement (row), for which the computed velocity differentiates with a mean error of than $3\Delta V$ from the average value, as this difference is considered to be a rough error. The mean error ΔV is computed by the formula (4):

$$\Delta V = \sqrt{\frac{\sum_{i=1}^{n} (V_i - \bar{V})^2}{n(n-1)}} \qquad (4)$$

Canceling a measurement is carried out by choosing the number of row in the table by a drop-down menu under the table, including the numbers from 1 to 10 (maximum number of measurements is 10). Then the button DELETE should be clicked. The row with the number chosen is deleted and the following rows automatically go up.

The visualization and processing of the table data is realized by the function Inform, written in Java Script within the body of each of the function zapisf() and zapisL(). These functions process the event OnClick of each of the buttons Record for the frequency and the wave length respectively.

IV. Tests with the exercises of the virtual physical laboratory

The tests are developed in Java Script и HTML. After clicking on the hyperlink for test, a random choice of test from several variants is realized. There could be several true answers to one question. The realization of the test is by HTML form. Besides a clock is visualized, which counts the time in minutes, during which the student should finish the test in order to get a maximum grade. The number of minutes is determined by the professor depending on the complexity of the test. At the bottom of the form is the button “Grade”, which should be clicked by the student to show the grade. Clicking this button, the student starts the function written in Java Script, which “checks” the answers of the test and visualized a grade between 2 and 6, formed on the basis of the number of true and false answers and the algorithmically determined importance of the questions.

In the presence of database on Apache surver [3] in the Intranet, including names, grades and other student’s data, the grade is supposed to be directly recorded back in the database. In this case it is necessary to use MySQL и PHP [2].

V. Conclusion

The laboratory exercise described above as an element of the virtual physical laboratory can be used for:

- introduction to an exercise in real experiment setting;
- instead of a real laboratory exercise, when its setting is impossible;
- as an exercise for self-training for distance education.

References

[1] Georgiev P., Jordanova I., Marinov K., Prokopieva S., Physics – course book for Technical university of Varna, Bulgaria, 1997

[2] Jay Greenspan, Brad Bulgar, MySQL/PHP database applications, AlexSoft, Bulgaria, 2001.

[3] Nikolova M., Automation of some activities of the educational process in the Intranet, Varna, 2003 /under printing/

[4] Tom Negrino and Dori Smith, Visual QuickStart Guide. Java Script for the World Wide Web, InfoDAR, Bulgaria, 1999.

European Higher Education Area

Assoc. Prof. Rumen Pranchov*

The European Ministers of education in Bologna on 19th of June 1999 signed the Joint Declaration. This declaration, known as Bologna Declaration, started the Bologna Process which goal is creation of European Higher Education Area (EHEA) by 2010 (see Appendix).

The European Higher Education Area has the aim to help the free movement of people as one of the four priorities of the European Union, to increase the attractiveness of the European higher education institutions and to establish knowledge based society.

SORBONNE DECLARATION [1]

The four Ministers of Education for France, Germany, Italy and United Kingdom signed Joint declaration on harmonisation of the architecture of the European higher education system on 25th of May 1998 in Sorbonne. A Europe of Knowledge is the main goal in this declaration. The necessity of the creation of the intellectual, cultural, social and technical dimensions of our continent is underlined. The Universities in a large extent have shaped the basic elements of the common European higher education system and continue to play a pivotal role for their development.

Actually with the Sorbonne declaration has started the process known later as Bologna process.

BOLOGNA DECLARATION [2]

Many European Ministers expressed later with letters their approval of the initiative started with the Sorbonne declaration. Next year a meeting of the European Ministers of education took place in Bologna. Between the two meetings the Joint Declaration draft was prepared. The declaration was entitled European Higher Education Area. 29 ministers signed the Bologna declaration. In this declaration the basic parameters of EHEA was described:

- Adoption of a system of easily readable and comparable degrees, also through the implementation of the Diploma Supplement, in order to promote European citizens employability and the international competitiveness of the European higher education system.
- Adoption of a system essentially based on two main cycles, undergraduate and graduate. Access to the second cycle shall require successful completion of first cycle studies, lasting a minimum of three years. The degree awarded after the first cycle shall also be relevant to the European labour market as an appropriate level of qualification. The second cycle should lead to the master and/or doctorate degree as in many European countries.
- Establishment of a system of credits - such as in the ECTS system - as a proper means of promoting the most widespread student mobility.
- Promotion of student mobility.
- Promotion of European co-operation in quality assurance with a view to developing comparable criteria and methodologies.
- Promotion of the necessary European dimensions in higher education.

SALAMANCA CONVENTION [3]

Over 300 European higher education institutions and their main representative organisations gathered in Salamanca on 29-30 March 2001. Their purpose was to prepare their input to the Prague meeting of the Ministers in charge of higher education in the countries involved in the Bologna process. The document called “Shaping the European Higher Education Area” was signed.

The basic principles for EHEA building up were defined – autonomy with accountability; education as a public responsibility; research based higher education and organising diversity (future depends on its ability to organise this valuable diversity effectively to produce positive outcomes rather than difficulties, and flexibility rather than opacity).

PRAGUE COMMUNIQUÉ [4]

European Ministers in charge of higher education, representing 32 signatories, met in Prague on 19th may 2001. The meeting ended with the signing of a Communiqué entitled Towards the European Higher Education Area. Ministers reaffirmed their commitment to the objective of establishing the European Higher Education Area by 2010. The Ministers recognised the six objectives from the Bologna Declaration, approved the next activities and added three new objectives:

- Lifelong learning is an essential element of the European Higher Education Area. Lifelong learning strategies are necessary to face the challenges of competitiveness and the use of new technologies and to improve social cohesion, equal opportunities and the quality of life.
- Higher education institutions and students - the involvement of universities and other higher education institutions and of students as competent, active and constructive partners in the establishment and shaping of a European Higher Education Area is needed and welcomed.
- Enhancing attractiveness of European higher education to students from Europe and other parts of the world. Together with the higher education expansion a market for higher education services with all elements – competition, quality and prise. This enforce the ministers to take action so that to enhance the attractiveness of EHEA throughout the world.

BERLIN COMMUNIQUÉ [5]

The next meeting of the European Ministers of Education took place in Berlin on 19th September 2003. This meeting reaffirmed the objectives of the Bologna process, accepted in the declarations from Bologna and Prague, rearranged some of them and added three new:

* Faculty of Communications & Communications Technologies, Technical University - Sofia

- European Higher Education Area and European Research Area

- two pillars of the knowledge based society. The Doctor degree must become identification mark of the EHEA;

- Stocktaking - with a view to the goals set for 2010, it is expected that measures will be introduced to take stock of progress achieved in the Bologna Process. The results will be presented at the next ministers meeting in 2005. In this way the stocktaking exercise will provide the possibility to take corrective measures, if appropriate.

The Quality Assurance is the first priority in the Berlin Communiqué. The quality of higher education has proven to be at the heart of the setting up of a European Higher Education Area. The quality assurance system has to develop at institutional, national and European level. It is necessary to develop mutually shared criteria and methodologies on quality assurance. The primary responsibility for quality assurance in higher education lies with each autonomous higher education institution itself.

With the view to introducing the two-cycle system the Berlin communiqué report that a comprehensive restructuring of the European landscape of higher education is now under way. All participants in the Bologna process are convinced to having started the implementation of the two-cycle system by 2005.

The member-states are encouraged to elaborate a framework of comparable and compatible qualifications for their higher education systems, which should seek to describe qualifications in terms of workload, level, learning outcomes, competencies and profile. They also undertake to elaborate an overarching framework of qualifications for the European Higher Education Area.

In the planned stocktaking process are included the next priorities: quality assurance, two-cycle system and comparable and compatible qualification degrees.

EUROPEAN COMMISSION AND BOLOGNA PROCESS

The European Commission launched ten concrete measures to help the nine objectives from the Bologna and Prague Declarations and supported by Socrates programme. Some of them are:

- A wide-scale introduction of the Diploma Supplement, increasing substantially the understanding and recognition of degrees at all levels.
- A broad pilot scheme to test a European Credit Accumulation System builds on the European Credit Transfer System (ECTS) experience.
- The Socrates-Erasmus Student Charter - a one page leaflet or card stating clearly the rights and obligations of mobile students.
- The creation of models of European Virtual Universities.
- A special action to promote a "quality culture" within universities. This pilot scheme would help universities to introduce internal quality assurance mechanisms;
- A Pilot Scheme on European higher education quality evaluation in order to experience what European transnational evaluation would mean;
- Define and support European (joint) Masters and Doctoral Courses.

European University Association started project entitled “Developing an internal quality culture in European universities” known as Quality Culture Project [6], financed by Socrates programme with the participation of many universities throughout Europe including universities from countries, which do not participate in the Socrates programme. In the Berlin communiqué also is stressed on the internal (university) quality assurance systems as the most important element of the whole quality assurance system in higher education.

PROBLEMS IN THE CREATION OF EHEA

The Bologna Process is not carrying out smoothly in all national higher education systems. Some of the elements of EHEA contradict to the national traditions in organising and realising of the higher education. The two-cycle system is not at all widespread in the European countries with one exception – United Kingdom. External and internal quality evaluation couldn’t be considered as a long time practice in the European countries. Higher education expansion contradicts the elite character of many European Universities. The globalisation makes the educational institutions accessible throughout the world, that why the competition becomes important part of EU higher education policy. Creation of knowledge based society means in great extent that the higher education converts in service and in this way could be inserted in the General Agreement for Trade and Services (GATS). The country-members in the Bologna process are divided regarding the higher education transformation into service and in this way its commercialisation. It is noticed that some countries from northern part of Europe tend to accept commercialisation process and some countries mainly from southern part of Europe continue to insist that the higher education is a public good and as such it couldn’t be subject of commercialisation. On the other hand in the Graz Declaration “Forward from Berlin: the role of universities”, adopted at a meeting organised by the European University Association, very clear is written that the higher education is first and the most important public responsibility.

The world trends towards higher education expansion, decrease of the public expenditure for higher education and competition for attracting more students bring to behaviour change of the autonomous universities in their aspiration for developing and quality increasing.

The results from a study of the Bologna process, done by S. Reichert and C. Tauch [7], entitled Progress towards the European Higher Education Area (Trends III) are showing clear aspiration of the country-participants in the Bologna process to establish and participate in the EHEA. It is also clear the differences in the approach, achievements and eagerness of the country and higher education institutions. Very clear are shown the differences in the adoption of Bologna process objectives between the academic and administrative staff and the students from one hand and the institution managing bodies from the other hand. Reforms are difficult to be carried out in autonomous institutions with elected managers – they

easily become hostages of their voters, which are in great extent affected from the reforms.

Next results cited in the study are giving a good idea for the passing status of the one of the most important objective – implementation of the two-cycle system (bachelor/master-doctor). 80% of the countries-participants in the Bologna process are having the legal possibility for implementing or at the very moment are implementing this system. In the other 20% of the countries the necessary legal changes for introduction of the two-cycle system are creating now. 53% of the higher education institutions implemented or are implementing the two-cycle system and 36% are planing to do so. Or almost 90% of the higher education institutions in the countries-participants in the Bologna process are implemented or are implementing the two-cycle system. About 55% of the higher education institutions in Southeast Europe are not implemented this system yet.

THE BULGARIAN HIGHER EDUCATION SYSTEM AND BOLOGNA PROCESS

In 1995 the Higher Education Act (HEA) was voted by the Bulgarian Parliament [8]. The act introduces a two-cycle system – bachelor/master-doctor. This is a very important element of the higher education system (HES), which afterwards will be a basic element of the reform in many European countries as a part of the Bologna process and creation of the EHEA. In 1999 some amendments were voted in the Parliament with which was given answer to the requirements of the European legislation – Aquis Communitaire and to the good practices in the member-countries. The most important amendment was the abolition the double standard towards the Bulgarian University admission – the so-called "paid education" was abolished. Instead tuition fees were introduced for all students. The tuition fees couldn't be more than 30% of the real education cost in the respective professional field.

Thanks to the HEA amendments introduced it became possible a Chapter 18 "Education and Training" from the negotiations for the EU accession to be closed in 2000.

The two-cycle system was accepted from the Bulgarian universities without specific opposition. The first students with bachelor degree graduated in 2001 and two years later – the first students with master degree appeared.

The National Evaluation and Accreditation Agency (NEAA) was established in 1996. The Agency is independent structure established for independent external quality evaluation and quality legitimisation through accreditation procedures. The accreditation is institutional and programme. Education in certain programme is allowed and financed only after the respective programme accreditation. The institutional accreditation precedes the programme accreditation and represents preliminarily condition for budget financing of the state universities.

The Higher Education Act requires every university to establish the Internal Quality Assurance System with which they will realise their responsibility for the quality of the higher education proposed. The external evaluation represents verification of the Internal Quality Assurance System operation. All Bulgarian universities (state and private) passed the first accreditation cycle and now some of them started the second cycle.

In the HEA amendments from 2004 the basic elements of the national credit accumulation system created on basis of the ECTS. The Diploma Supplement as the European Commission defines it is introduced.

The participation in the Socrates programme (Bulgaria is in the programme from 1999) is an important part of the Bologna process. Many of the programme activities are supporting the EHEA establishment.

The reforms undertaken in the last 10 years create the necessary preconditions for Bulgarian higher education system inclusion in the European Higher Education Area.

REFERENCES

1. Sorbonne Joint Declaration on harmonisation of the architecture of the European higher education system by the four Ministers in charge for France, Germany, Italy and the United Kingdom, Paris, the Sorbonne, 25 May 1998. (www.bologna-berlin2003.de)
2. "The European Higher Education Area" - Joint declaration of the European Ministers of Education Convened in Bologna on the 19 June 1999. (www.bologna-berlin2003.de)
3. "Shaping the European Higher Education Area" - The Salamanca Convention of European Higher Education Institutions, Salamanca, 30 March 2000. (www.bologna-berlin2003.de)
4. "Towards The European Higher Education Area" - Communiqué of the meeting of European Ministers in charge of Higher Education in Prague on May 19th 2001. (www.bologna-berlin2003.de)
5. "Realising the European Higher Education Area" - Communiqué of the Conference of Ministers responsible for Higher Education in Berlin on 19 September 2003. (www.bologna-berlin2003.de)
6. Developing an internal quality culture in European universities: Report on the Quality Culture Project, 2002 – 2003, European University Association. (www.eua.be/eua/en/projects_quality.jsp)
7. Sybille Reichert and Christian Tauchp. Trends 2003 Progress towards the European Higher Education Area − Bologna four years after: Steps toward sustainable reform of higher education in Europe, A report prepared for the European University Association, July 2003. (www.bologna-berlin2003.de)
8. Bulgarian Higher Education Act (www.minedu.government.bg).

Appendix

BOLOGNA PROCESS

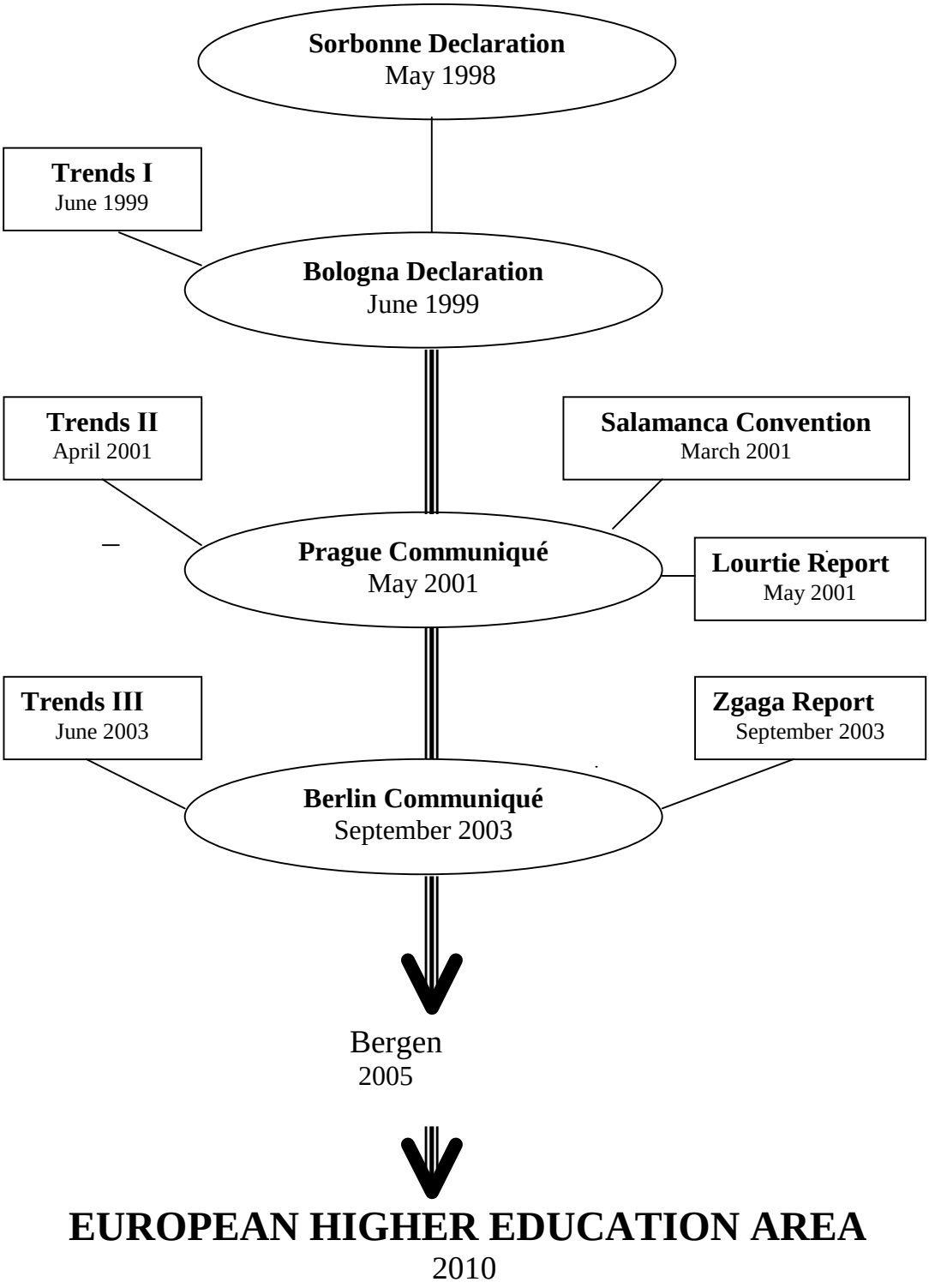

Using multimedia in education of children with special needs

Leonid Stoimenov[1], Bratislav Predić[2]

Abstract – **In this paper we present the possibilities of using multimedia application in education of children with hearing impairment. We believe that this technology enables teaching and hearing aids to be as unobtrusive as possible while allowing the system to adopt itself to individual's needs and characteristics. The ultimate goal is to create a system that can successfully integrate a child with hearing impairment into regular education environment.**

Keywords – **hearing impairment, education, multimedia, computer assisted**

I. INTRODUCTION

Schools specialized in education for the children with hearing impairment face a number of difficulties. Generally, the most important and difficult task is to achieve a degree of interactivity in education process. A number of helping tools like books, musical instruments, toys, picture books etc. are used. All these aids are of non technological nature. Specialized devices for filtering and transmitting sound to the children are also used.

Children with hearing impairment usually do not differ from the children with regular hearing in terms of learning capabilities. Unfortunately, in the standard education system majority of learning material is communicated to the pupil using voice. This method is inapplicable to children with hearing difficulties. To compensate for a loss of one sense these children are usually visual types and have good perception of space. This characteristic should be exploited in the learning process by presenting information visually or as an audio / visual combination. It is important to teach the children to use the remains of their hearing system and to learn how to pronounce words in order to be able to communicate with other people with normal hearing capabilities.

Usage of computer technology and multimedia applications can eliminate or at least alleviate most of the problems children with hearing difficulties today face in education system[1]. With their successful education we can help them integrate in society.

This paper represents an introduction to efforts we have made to envision and design an audio enhancement system aimed at children with mild and intermediate hearing impairment. The audio processing part, which is the basis, is enriched with multimedia content. However, it is not just a question of inserting audio or video clips. It needs to be done within learning structure in order to achieve proper results.

The system's target group are children ages 6 to 12. We can freely say that this is the generation of the "digital age". The children are not intimidated by computer technology and can utilize its advantages to its full extent.

Second section of this paper presents similar systems commercially available and describes their characteristics in short. Third part describes the system we propose, "Multimedia System for Education of Children with Hearing Impairment" or shortly MEDOS. Fourth section proposes types of multimedia applications that are planned to be implemented in the first phase of this project. We give final remarks in the fifth and final section.

II. RELATED WORK

Teaching methodologies currently in use can be improved both conceptually and technologically. Irreplaceable component of any teaching system aimed at children with hearing impairment is some sort of audio processing and amplification device. That component cannot be removed. Different children have various characteristics of impairment. Therefore the first step in any sort of education process is to determine characteristics of the impairment across the audible frequency spectrum. That task is performed by an array of filter amplifiers. The result of this measurement process is a graph that represent hearing loss for certain frequency ranges. Structure of human language defines a set of standard frequency ranges that can be grouped together forming channels. Resulting graph consists of amplification amount needed for each channel for a specific child. That is a sort of "user profile" that can be stored and reused later in education process. System that was the basis for our research is a manual, analog filtering / amplification device. The process of measuring a child's hearing loss consisted of a teacher repeating a sentence into the microphone and manually adjusting parameters for frequency and amplification. At a later time, when a teacher is working with that particular child, he needs to manually enter the measured parameters into the amplification system again and again. This manual process is tedious and error prone. It is tedious not only for a teacher but for a child too which loses concentration and motivation very quickly.

Technical aids available today are mostly hardware devices that mainly deal with transport and amplification of sound.[2] Software tools are virtually non existent, let alone integrated hardware / software solutions [3].

[1]Leonid Stoimenov is with the Faculty of Electronic Engineering, Beogradska 14, 18000 Niš, Serbia and Montenegro, E-Mail: leni@elfak.ni.ac.yu

[2]Bratislav Predić is with the Faculty of Electronic Engineering, Beogradska 14, 18000 Niš, Serbia and Montenegro, E-Mail: bpredic@elfak.ni.ac.yu

Standard hearing aids are usually worn by the listener. They are designed to work best in quiet, structured settings, where the sound source is no more then a few meters away and extraneous noise is minimized. These aids can be supplemented with some sort of frequency modulated amplification system. The FM transmission device functions as a direct line between the teacher and the pupil. This combination minimizes background noise and is widely known as auditory trainer.

FM auditory trainers suffer from radio interference. Sound transmission can be further improved with infrared systems. Infrared systems transmit clean and clear sound invisibly to the listeners. Their main drawback are problems with line-of-sight and limited distance.

III. MEDOS SYSTEM

In cooperation with the specialized school for children with hearing difficulties "Bubanj" CG&GIS Laboratory is trying to solve problems previously noticed in education process implemented at that school. MEDOS is conceived as integrated hardware / software solution enriched with multimedia content.

We can notice a couple of areas in the method currently in use that can be improved. Firstly, we can substitute the analog filter / amplification device with a computer with the audio processing capability. All sound data can be stored digitally. As we stated previously, the analysis and teaching process consists of numerous repetitions of a small number of sentences. When these sample sounds are stored digitally they can be repeated identically regardless of the number of repetitions. This is increasing the accuracy of measurement and at the same time removing some workload from the teacher. The measured data (hearing impairment graph) is stored centrally in a database. This approach increases accessibility of the user profiles and enables comparative analysis of the data over time. This analysis can give the teacher an assessment of the child's improvement or deterioration. Therefore the teaching process can be modified and adjusted "on the fly" perfectly fitting the child's needs.

There are other advantages of multimedia which were unavailable with the previously described method of education. Children with special needs display a lack of motivation and lose interest in lecture contents very quickly. A number of papers describe this problem[4]. Multimedia enables the lecturer to structure the presented information in a dynamic and interactive way. A child is more involved in the learning process and presented material is acquired and retained more quickly this way.

Finally, the teaching system as we have envisioned it is adoptable, being able to follow the child at child's own pace, and in the form that is the most appealing to that specific individual. Generalized conceptual model of the interactive multimedia system is given in the figure 1.

In the following text we will present models for integrated multimedia systems designed for usage in both individual and group education for children with varying degree of hearing impairment. MEDOS can be used within multimedia classroom as a group device or individually. As an individual device it is used by children independently or together with their parents within their home environment. Parents can also use the system as a source of information on methodologies used in school.

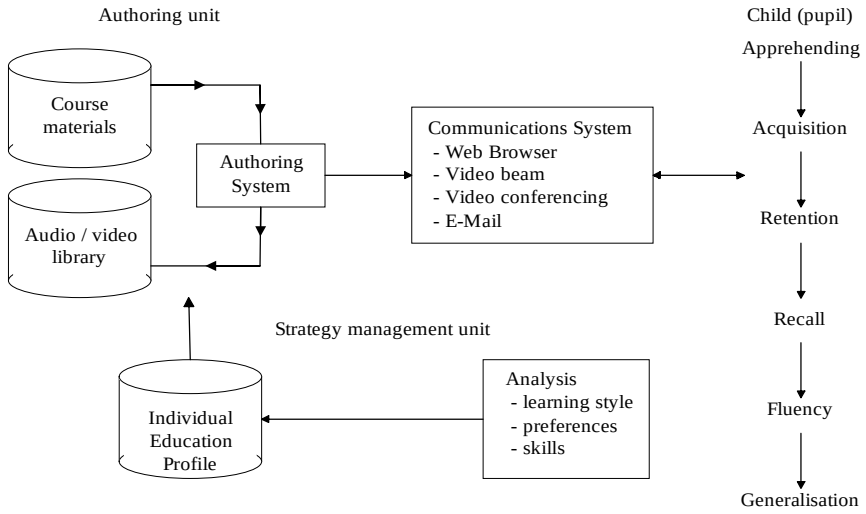

Fig. 1. Conceptual model for interactive multimedia system

Wireless transmission of the sound from the teacher to the listeners is the most important improvement our proposed system offers. Children are not tied anymore to their assigned workplaces and are free to move around the classroom, interact with other children and participate in lecture presentation.

Video subsystem's role is to present lecture material in a manner that will focus children's attention and keep them involved. Audio subsystem contains database of audio data, certain important and characteristic sentences and terms children should learn how to pronounce and understand. Before transmission, audio data is filtered and specifically suited to the characteristics of the child's impairment.

Therefore every child in the classroom hears the same sentence or word but with certain frequency ranges separately amplified. As we previously explained relating frequency ranges are grouped together forming channels. Needed amount of amplification per channel is set up separately for each child fitting the child's impairment characteristic. This is making MEDOS system flexible and adoptable.

Wireless microphone is a part of child's unit. It is enabling loopback in the system. Loopback is very important in education process. Regardless of its position in the classroom or activity the child can react to the presented lecture material and give feedback to the teacher. Further, and more importantly, the sound loopback allows the child to hear its own pronunciation and adjust it accordingly. This proved to be the most effective method for a child to learn or correct its speaking skills.

Software components of the MEDOS system are:

- Multimedia device support software
- Multimedia tools and applications

Device support software is indispensable part of the system but is almost invisible to the end user. Its role is to synchronize operation of the whole system through implemented functions. Another task support software performs is to enable execution of included multimedia content.

MEDOS offers to the educator a container for multimedia content. Multimedia files can be created and prepared using multimedia tools. Each lesson can reference a number of different multimedia sets. Education staff can choose appropriate one and thus make the lesson unpredictable and more interesting. Presentation form of multimedia content is controlled by multimedia applications. As education progresses the staff can notice possible problems with lecture structure and correct or modify it's structure. This is making the system open. It represents a sort of framework that is helping but not limiting the teacher. Being so flexible it adopts not only to the children's needs but also to individual teacher's style of work.

The part of the system that integrates all described software subsystems is user profiles database. Information about all potential users of the system is stored locally and centrally. Simply by linking correct profile with selected headphone / microphone set the teacher can set up the classroom for work with the group of children without regard of the set children choose or their location in the room.

Other type of medical information for each patient is also stored centrally like name, degree of impairment per different channels etc. Information of medical importance can be updated regularly. This way, a sort of medical history for each patient can be recalled at any time and analyzed.

More detailed schematic of the classroom equipped with MEDOS system is given in figure 2.

First phase of the project plans for development of core sound filtering and amplification system and definition and creation of multimedia content. Created content is supposed to support learning process for the children of pre elementary school age. All methodology steps involved in standard, previously used, education process will be covered with new material. Sections that will benefit mostly out of this new

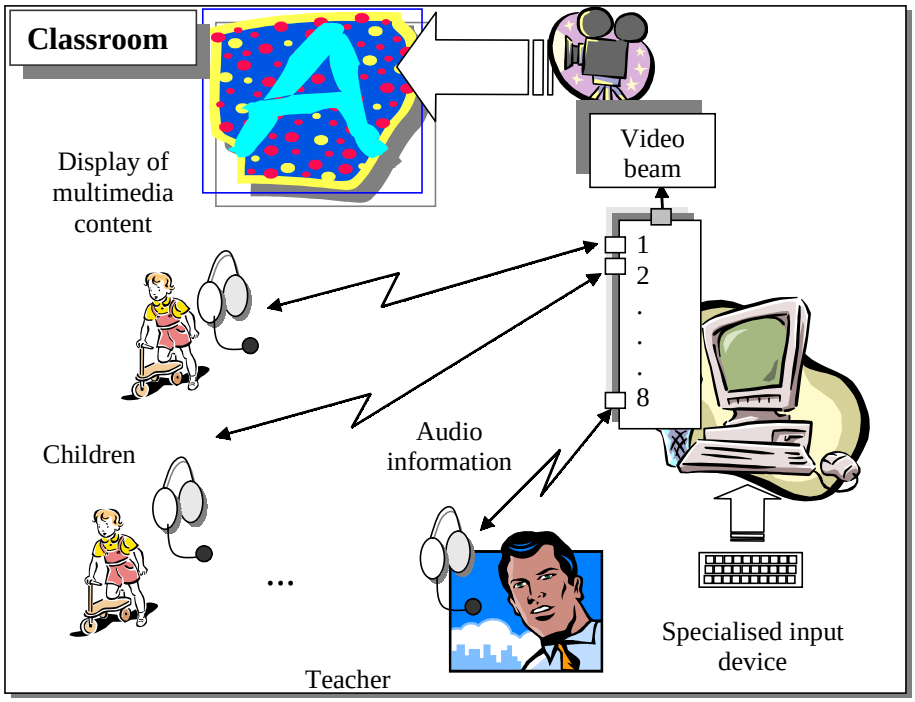

Fig. 2. Multimedia classroom based on MEDOS system

approach are reconstruction of speaking capabilities and improvement of pronunciation. A sample screenshot taken from one of multimedia applications supporting hearing exercises is shown in figure 3.

Fig. 3. Sample screenshot from one of multimedia applicatiopns

Multimedia additions will be available for:

- Breathing exercises
- Listening exercises
- Onomatopoeias
- Vocals pronunciation
- Knowledge retention through games and fun

IV. Concluding Remarks

With the lack of similar systems we believe MEDOS will bring considerable improvement in quality of education for children with hearing impairment. We expect an increase in children's interest and involvement in learning speech and gestures. Today, children with hearing difficulties are usually educated to perform simple manual jobs (bakers, tailors etc.). This is unfortunate because these children can demonstrate above average intelligence [5].

Characteristics of the proposed system can be summarized:

- Wireless transmission of sound gives children additional freedom.
- Centralized management of user profiles allow constant monitoring of children's improvement and medical status.
- Audio loopback allows self correcting procedure.
- Less tedious process of impairment measurement.

References

[1] Au, G. , "Can Multimedia Help People Learn Faster?", International Conference on Multimedia Computing and Systems, Washington, USA, 1995.

[2] Edwin P. Christman, Roxanne R. Christmann, "Technologies for students with special needs", Science Scope, p. 50-53, March 2003.

[3] Green, D.W. , "The Benefits of Multimedia Computer Software for Students with Disabilities", Doctoral Seminar in Topics in Special Education, Binghamton University, NY, ED382172, 1995.

[4] Lynne Parfitt, Dr. Jun Jo, Anne Nguyen, "Multimedia in Distance Learning for Tertiary Students With Special Needs", ASCILITE 98, Wollongong, Australia, December 1998.

[5] Ted S. Hasselbring, Candyce H. Williams Glaser, "Use of Computer Technology to Help Students with Special Needs", The Future of Children, CHILDREN AND COMPUTER TECHNOLOGY vol. 10, no 2, Fall/Winter 2000.

Educational Web Site "Research of the Behavior of Functions with Pseudo asymptotes and Asymptotes"

Anna Tomova[1] and Maria Nikolova [2]

Abstract – **The goal of the paper is to present a Web site for the research of the behavior of functions with pseudo asymptotes and asymptotes by using a system for computing algebra MATHEMATICA 4.0. A criterion for existence of pseudo asymptotes and asymptotes of differentiable functions is announced.**

Keywords – **Criterion for the existence of the pseudo asymptotes and asymptotes of differentiable functions, systems for computing algebra**

I. WHY WAS THIS SITE CREATED?

The educational site was created to teach of students and cadets a practical exercise titled "Research of the behavior of functions with pseudo asymptotes and asymptotes". It was written in HTML by using the editor Macromedia Dream weaver MX.

II. SUMMARY OF THE SITE

At figure 1 the site's navigation toolbar is presented.

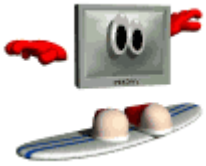

Home page | Introduction | Definitions | Criterion for pseudo asymptotes and asymptotes | Class of functions with pseudo asymptotes and asymptotes | Plan for a practical exercise | Graphics of functions with pseudo asymptotes | Graphics of functions with asymptotes | Conclusions | Literature

Fig. 1. Navigation toolbar of the site

The description of the Web pages is given below:

Page **Introduction** presents an overview of the Web site.

Page **Definition** gives a definition of the concept pseudo asymptote of functions of one independent variable [2], [3], that is not presented in the classic courses in mathematical analysis [1]. We point out the important fact that the logarithmic function is an example for such a function (its pseudo asymptote is the x-axis).

[1]Anna Tomova is with the Department of "Mathematics and Informatics", Naval Academy "N. J. Vaptsarov, 73 Vassil Drumev St., 9026 Varna, Bulgaria, E-mail: anna_bg_2000@yahoo.com

[2] Mariya Nikolova is with the Department of "Mathematics and Informatics", Naval Academy "N. J. Vaptsarov, 73 Vassil Drumev St., 9026 Varna, Bulgaria, E-mail: mpn@abv.bg

Thereby the use of logarithmic tables is explained in a different way: big numbers are avoided.

Page **Criteria for pseudo asymptotes and asymptotes** announces a criterion for the existence of pseudo asymptotes and asymptotes of differentiable functions. This criterion separates the twice-continuous differentiable functions into three groups: functions without asymptotes, functions with pseudo asymptotes and functions with asymptotes. The proof of this criterion in details is made in [3]. Because of the importance of this criterion we describe it here:

Criterion (enough condition) for the existence of pseudo asymptotes and asymptotes of differentiable functions:

Theorem: $f : R \to R$ *is twice continuously differentiable function. Then:*

1) If $f''(x) \geq \frac{1}{1+x}$ *,*$x \geq 0$*,function f(x) has no asymptotes for* $x \to \infty$ *;*

2) *If* $\frac{1}{1+x^{1+l}} \geq f''(x) \geq \frac{1}{1+x^2}, x \geq 1,$ $0<l<1$ *f(x) has pseudo asymptote, but it has not asymptote;*

3) If $0 < f''(x) \leq \frac{1}{1+x^{2+l}}, l > 0, x \geq 0$ *f(x) has asymptote for* $x \to \infty$ *.*

Remark: By analogy we can formulate and prove a theorem for criteria (enough condition) for the existence of pseudo asymptotes and asymptotes of differentiable functions when $x \to -\infty$

Page **Class of functions with pseudo asymptotes and asymptotes** presents formulae for classes of special functions with pseudo asymptotes and asymptotes by using of the system for computing algebra MATHEMATICA 4.0 after integrating twice.

Page **Plan for a practical exercise** includes:

1. Theoretical part: the students have preliminarily attended lecture and have been acquainted with the theme and proof of the criterion. The professor accents the basic ideas and points out the existence of an extra wide class of partial and special functions with pseudo asymptotes He emphasizes the complexity of the calculations and the practical advantage of the systems for computing algebra for finding the formulas.
2. The professor suggests that the students themselves find formulae for functions with pseudo asymptotes and asymptotes.
3. The students draw graphics for the functions received in step 2.

4. Comparisons are made between the functions' graphics and the differences in their behavior toward their pseudo asymptotes and asymptotes are explained.
5. If several systems for computing algebra are installed, comparisons are made between the results received by identical tasks.
6. Conclusions: The possibility is debated of making errors and inaccuracies when working with the systems for computing algebra, finding and eliminating the errors. The advantage of work with the systems for computing algebra is emphasized for receiving and illustration of serious mathematical results.

Page **Graphics of functions with pseudo asymptotes** enables student by using of drop-down menu to choose between two functions with pseudo asymptotes, to consider their formulas and to explain their graphical behavior toward their pseudo asymptotes in intervals of different length of change of the independent variable x. In Figure 2 and Figure 3 two such graphics are visualized for the case of $f''(x) = \frac{1}{1 + x^{1,25}}$, i.e. for l = ¼. The function has a pseudo asymptote, but has not an asymptote.

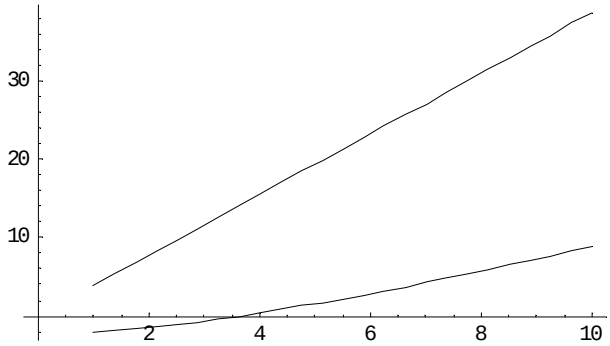

Fig. 2. When x is changed in the interval [0, 10], it is clearly visible that the function graphic has moved away from such graphic of its pseudo asymptote when x grows up.

It can be proved that the difference between the values of function and its pseudo asymptote for the same unlimited large values of x tends to $-\infty$.

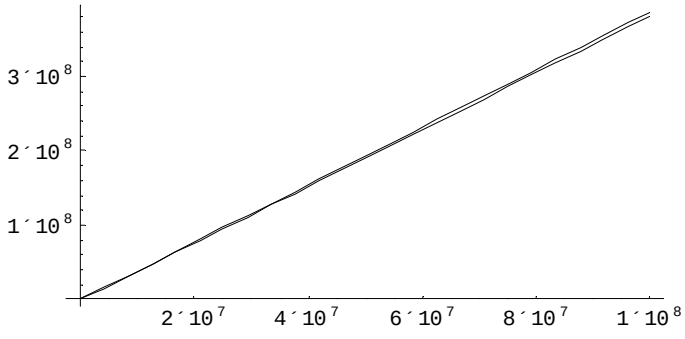

Fig. 3. For very large x the two graphics: of the function and its pseudo asymptote are almost indiscernible.

Page **Graphics of functions with asymptotes** enables student by drop-down menu to choose between two functions with asymptotes, to consider their formulas and to explain their graphical behavior toward their asymptotes in intervals of different length of change of the independent variable x. We consider the case: $f''(x) = \frac{1}{1+x^4}$, i.e. when l = 2. The function is with asymptote. At figure 4 the graphic of the function and its asymptote is shown. As expected for comparatively little x, the difference between the two graphics is slight.

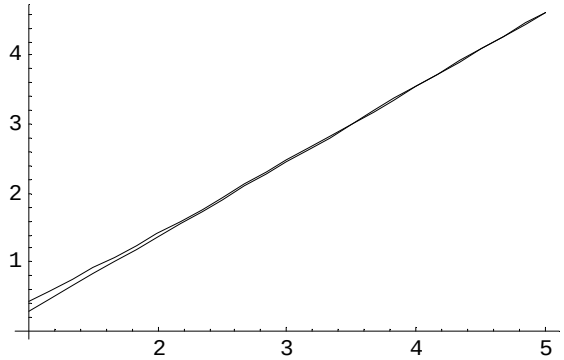

Fig. 4. For the x-values in the interval [0, 5] the difference between two graphics is slight

Page **Conclusions** presents the conclusions made when we compare the functions with pseudoasymptotes and asymptotes described in the previous pages. As expected only for large values of the argument, the graphic of a function with pseudo asymptote and such graphic of its asymptote are indiscernible, while for the functions with asymptote this is observed for considerably smaller x-values.

III. CONCLUSION

The proof of the criteria for existence of functions with pseudo asymptotes and asymptotes is made analytically. Drawing the graphics and finding the described functions is made by the system for computing algebra MATHEMATICA 4.0 The application of the systems for computing algebra realizes still more the receiving of serious mathematical results, as well its use of illustration visual aids and in this sense it must be demonstrated to the students at all levels by the professors.

REFERENCES

[1] Fichtenholc G. M., Course of differential and integral calculations, Russian, 1975.

[2] Tomova A., Notes about the behavior of some functions with pseudo asymptotes. Mathematical Forum, ISSN 1311-297, Volume 5, Issue 2, March-April, 2003 г., pp. 55- 57, Bulgarian

[3] Tomova A., A criterion for the existence of pseudo asymptotes and asymptotes of differentiable functions. Notes about the behavior of some classes of functions with pseudo asymptotes and asymptotes, Scientific proceedings of Naval Academy "N. J. Vaptsarov, 2004, Bulgarian (under printing)

Distance Education System

d-r V. Trajkovik[1], d-r D. Davcev[1]

Abstract - **The primary goal of this paper is to present a system for support of distance education that can be used within the Virtual University. This work represents the attempt for transferring the infrastructure of traditional educational systems (classroom, library, laboratory, student services) into digital world.**

Keywords - **Distance education, education quality**

I. INTRODUCTION

In order to support mainly the adult wishes to continue with education, some universities have offered Bachelor, Masters and Doctoral degrees through distance studies. This concept has evolved from simple educational material exchange to more sophisticated interaction between the user and the distributed resources [1].

The term "Distance Education" has many definitions in the literature. One of the most complete definitions of distance education is given by Keegan in 1986 [2]. According to this author, distance education has following features: The instructor and the student are separated during the most of the educational process, the educational curriculum is controlled by certain educational institution, educational materials are exchanged via different media in order to overcome the physical distance between the instructor and the students, and different forms of two way communications among the participants of educational process are supported.

Students in the higher education are especially common with using Internet resources for their studies and research. This fact opens the possibility of creating an effective education environment, using the Internet as a medium for human interaction. The idea of creating such environment is a challenge of redesigning the user interface systems in order to mimic the classical educational environment, as much as a challenge of improving the education process by implementing options and techniques that are hard to implement in the traditional teaching systems.

The primary goal of this paper is to present a system for support of distance education that can be used within the Virtual University.

[1]Both authors are with the Ss. Cyril and Methodius University, Faculty of Electrical Engineering , Karpos 2 bb, Skopje, R.Macedonia, E-mail: [trvlado|etfdav] @etf.ukim.edu.mk

Educational principles that need to be incorporated within the system for the support of distance education will be given in the second section of this study. Social, economical and institutional preconditions needed for establishment of distance education systems will be also discussed in this section. Several educational materials aimed for distance students created for this study will be presented in the third section. Fourth section will contain the general description of functionalities of distance learning components. The system influence on the efficiency of the learning process will be elaborated in the fifth section. The last section will conclude the study.

II. DISTANCE EDUCATION PRINCIPLES AND PRECONDITIONS

Learning within traditional teacher - centred education systems is based on deficit student model. The educational system tends to identify student's deficiencies and weaknesses. Based on those deficiencies, students are tracked and categorized. It is more important for the student to reproduce teacher's knowledge then to build personal knowledge on certain subject.

Distance education is based on human behavioural educational theories. It should be noted that nowadays traditional education also accommodates concepts from behavioural educational theories. One of the basic educational theories of this type is the Constructivist educational theory. According to this theory, learning is active process, in which the students construct new ideas or concepts based on their current knowledge. Relevant contributors to this theory are Brunner [3], Vygotsky [4] and Piaget [5]. The Constructivist theory is a base for several educational theories. The most quoted theory of that kind is the theory of "Active Learning" [6], which incorporates different educational forms: Inquiry Learning, Problem Based Learning, Learning by doing, etc.

The common element for the above educational theories is the shift from teaching centred education to learning centred education. The education is student centred active process. The teacher's role is to canalize and enable the learning process and thus he/she becomes a trainer or instructor. Students should take initiative in the learning process whenever

possible. In that way, the general concepts which are the subject of learning become the part of students' experiences. Learning is a natural process, which can take different patterns depending on students' affinities, backgrounds and interests. The Learning is social process and thus different forms of communication and collaboration among students should be encouraged. Students should find their own facts related to the educational subject. The knowledge is created through the real world activities rather then reproduced.

The development of the Distance Education support system requires: human resources, educational platform, educational materials, communication tools, administrative support, network of educational professionals and experts.

Distance Education can be treated as a service to the community. When establishing a new service several questions should be answered. Who will be its users? Which are and how huge are the target groups? Why would they be interested in the service (distance education)? How long will demand for the service last?

According to [7], educational system costs can be divided in two groups: fixed costs (staff salary, infrastructure costs, educational material development costs, etc) and variable costs (distribution costs, rental costs, and other costs that depend on number of students). Distance education system has higher fixed costs and lower variable costs. Higher fixed costs are a result of complexity of distance education support systems and higher costs of development of educational material aimed for distance education. Lower variable costs are a result of non campus based learning. However, it is important to be mentioned that the total cost of distance education is smaller than the cost of the traditional education, once certain number of students is reached. The number of students that is needed for this financial benefit of distance education depends on regional low and economical factors.

Technological solutions for distance education support systems can be compared in two manners. The first one is comparison between the levels of the instructor - student interaction and the student interaction with educational materials. The graphical representation of that comparison is given on figure 1. It should be noted that, when using different technologies, the level of interaction does not increase. It is equal to the maximum level of interaction of used technologies. The recommended technology for development of distance education support systems from this point of view is internet technology. The second comparison manner is comparison between availability of educational materials and their development cost (see figure 2). The traditional correspondence distance educational materials are most favourable in this manner. Establishment of Open distance learning centres can increase the score of internet based materials by increasing the availability of internet technology to the student.

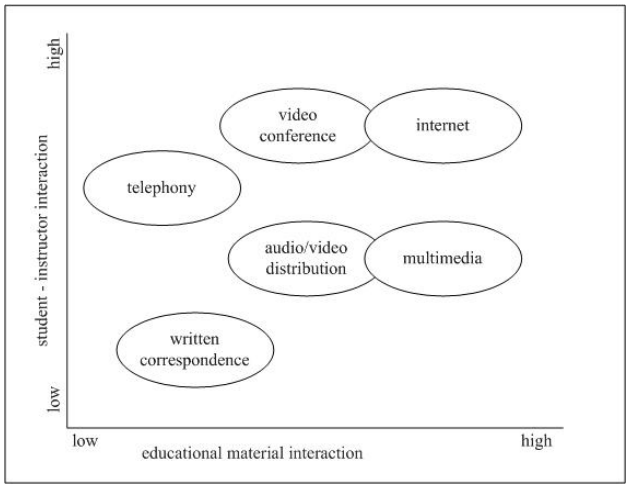

Figure 1 Comparison between the levels of the instructor - student interaction and the student interaction with the educational materials

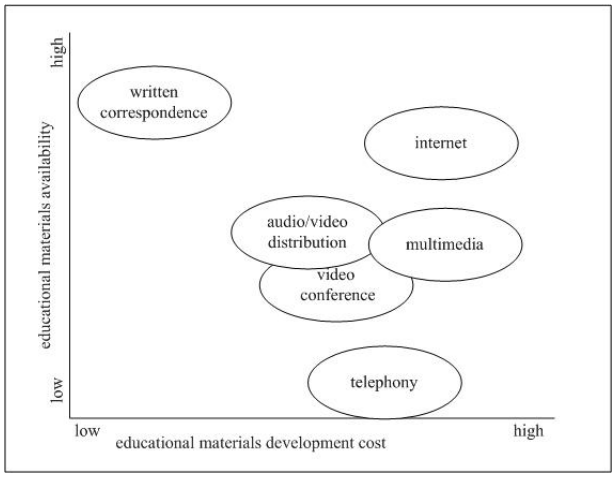

Figure 2 Comparison between availability of educational materials and their development cost

III. EDUCATIONAL MATERIALS

Educational materials for distance education are built in following phases: Analyses of target students' needs, common goals and social background, creation of educational material, upgrade of the way the material is presented depending on student evaluation and the changes in student target group. These phases are presented on figure 3.

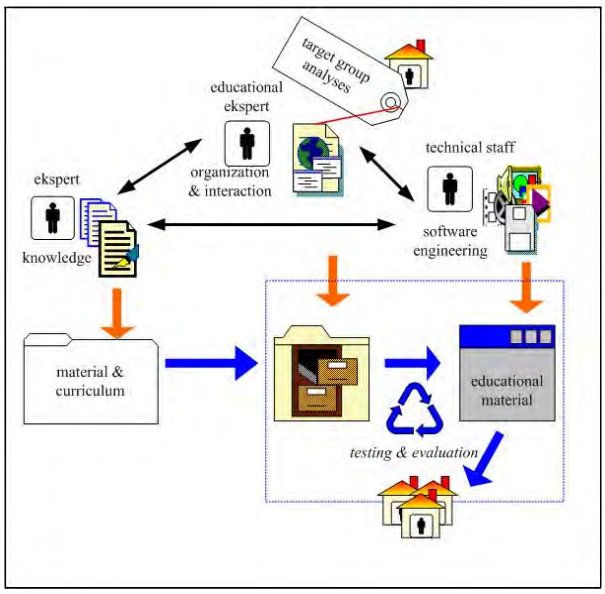

Figure 3. Phases in building distance education learning material

Principles for development of distance educational materials are not related to the expertise knowledge of the material. They give suggestions for the educational approach that can be used when creating educational material aimed for distance education [8].

Educational material should state in a very clear way what is the main contribution for the students and what kind of students it is intended to. Examples should be familiar to the student target group. Cooperative work and different forms of communication between the actors of the educational process should be stimulated by providing discussion groups, chat facilities, virtual tables and other communication support tools.

Educational material has to be divided in entities named "knowledge portions". They should be organized in hierarchy in such way that the whole course can represent one big knowledge portion. Each knowledge portion should contain information about its importance within the educational material, what knowledge is expected from student before its consumption, what knowledge student will gain after its consumption as well as average time needed for the consumption. Student should be also suggested the projects he/she is capable of doing and the way the knowledge could be enhanced.

Within this research, several web based educational materials have been developed. The subject "Databases and data structures" from the regular studies of the Faculty of Electrical Engineering in Skopje is supported with web educational materials where besides the theory students can find solved examples enriched with animations and perform a self testing. Almost all principles for building distance web based learning materials are incorporated in the English version of UML (Unified Modeling Language) web course aimed to all interested computer science students. We received request for translation of this course in Spanish language.

IV. Distance Education System Components

Distance education support systems are complex systems. They should keep track of student history, educational materials content and history and enable easy access to that content. Clear mapping with traditional educational system should be enabled where possible [9]. An example of a distance education support system was developed within this research [10]. The users of this system need only to have internet connection and internet browser installed on their machines. Some of the modules are developed using agent based technology [11]. There are three general groups of the activities that should be supported by this kind of system: institutional administrative activities, student service activities and student activities. Institutional administrative activities are administrative activities of the educational institution. These activities depend on the state regulative and were not be considered by this research. Student service activities are related to educational process by supporting it. Examples of such activities are: lecture scheduling, general information about the subjects, course enrolling, exam enrolling, and administrative library services. Student activities are represented through access to educational materials, consultation activities, discussion activities, laboratory work, project work, self testing. Although not directly related to student activities, instructor supported activities should be included in the distance education support systems. Examples of such activities are: publishing of the exams' results, different kinds of student notifications, educational material creation guide.

V. Distance Education Support System Evaluation

Evaluation of efficiency of the education was done according to the principals given in [12]. The data collected from the Faculty of Electrical Engineering at the Ss Cyril and Methodius University in Republic of Macedonia were collected in order to give input about the quantity, quality and the status of achieved education. Performed analyses indicate the influence of the usage of distance education modules for increasing the efficiency of the education. The correctness of the approach was confirmed with the

conventional and distance education converging trends stated in [13].

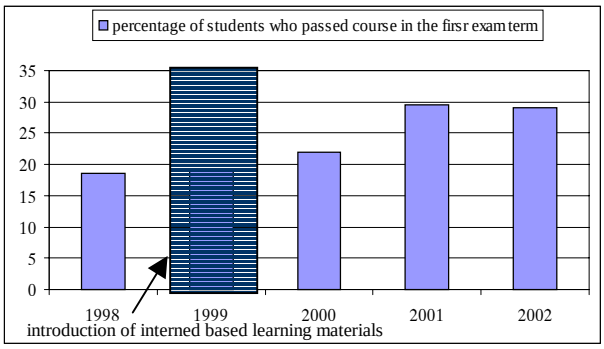

Figure 4. Percentage of students who passed "Databases and data structures" course in the first exam term

The quality of education can be evaluated through the time needed for it to be achieved or that can be indicated with the number of students that are able to pass the exam in the firs exam term. Figure 4 gives the percentage of students that passed "Databases and data structures" course in the first exam term over last five years.

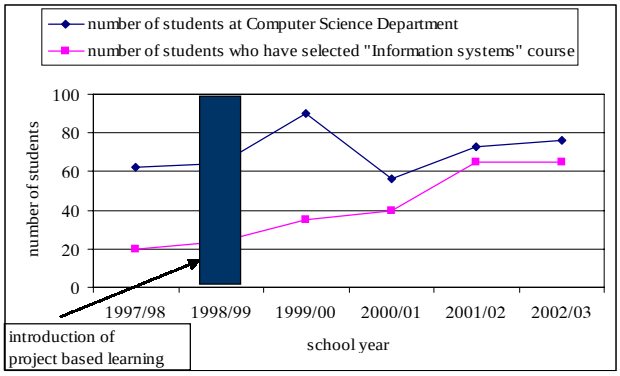

Figure 5. Number of student who have selected "Information Systems" course

The status of the achieved learning can be measured with its real work applicability. The course "Information Systems" (that can be selected from the students from the last year of the studies) introduced the distance based project work for the students in the year1998/99. The projects are done in cooperation with different IT companies in Macedonia. In that way, the course became more difficult to pass. Never the less, the number of the students who select that course increases every year. Figure 5 gives graphical representation of those facts. The survey made with 60 students that were asked why they have selected this course, ended with 75% of students giving one of two typical answers: "Opportunity to use the knowledge in the real world situation", "It will help me to find a job".

VI. Conclusion

The primary goal of this paper is to present an internet based system for distance education support. Distance education has social, economic and technical prerequisites. The developed system has object-oriented architecture. It supports different forms of student-student and student-instructor interactions that are important for providing active learning environment.

The developed distance education support system's influence to efficiency of education was evaluated within this research. Performed analyses for evaluation of efficiency of education indicate the positive influence of the usage of distance education modules for increasing the efficiency of the education.

References

[1] Holmberg, B. "Growth and Structure of Distance Education", Beckenham, UK, Cromhelm, 1986;
[2] Keegen, D. "Foundations of Distance Education", New York, Routledge, 1996;
[3] Brunner, J. "Acts of Meaning", Cambridge, MA, Harvard University Press, 1990;
[4] Vygotsky, L.S., "Mind in Society", Cambridge, MA, Harvard University Press, 1978;
[5] Jean Piaget Society, http://www.piaget.org;
[6] Schank, R.C., "Active Learning through Multimedia", IEEE Multimedia 1(1), pp. 69-78, 1994;
[7] Rumble, G. "Why distance education can be cheaper then conventional education", Distance Education 8 (1), pp.72-94, 1987;
[8] Eisenstadt, M. and Vincent, T. (eds) " The Knowledge Web: Learning and Colaboration on the Net"; Knowledge Media Institute, London, Kogan Page, 2000;
[9] Trajkovik, V., Davcev, D., Kimovski, G., Petanceska, Z . "Web - Based Virtual Classroom", In Proc. 34th International Conference on Technology of Object - Oriented Languages and Systems", Santa Barbara, USA, July 30 - August 4, pp. 137 - 146, 2000;
[10] Kulakov, A., Trajkovik, V., Davcev, D. "Virtual Classroom and Virtual Laboratory", In Proc. of the 20th World Conference on Open Learning and distance Education, Dusseldorf, Germany, April 01-05, CD Rom Publication, 2001;
[11] Vasileva T., Trajkovik, V., Davcev, D., " An Agent - based Model of Web - based Distance Educational System", In Proc. of the IAESTED International Conference on Computers and Advanced Technology in Education, Philadelphia, USA, May 6 - 8, 1999;
[12] Belanger, F., Jordan, D.H. "Evaluation and Implementation of Distance learning: Technologies, Tools and Techniques", London, UK, Idea Group Publishing, 2000;
[13] Tait, A., Mills, R., (eds) "The Convergence of Distance and Conventional Education", NewYork, Routledge, 1999;

WEB based template for communication applications and teaching

Nikolay T. Kostov[1] and Slava M. Yorfdanova[2]

***Abstract* – The learning program gives the opportunity to the student to understand the product very well and has the possibility for checking the knowledge by tests. The test may be realized for certain time because of the integrated timer..**

Keyword – **WEB based template, Communication, Application, Teaching.**

I. INTRODUCTION

According to the penetration of new communication application for work in different companies and organizations, the question is about the teaching the staff. In this issue we propose a leaning program that has recent information about new working communication application. The learning program gives the opportunity to the student to understand the product very well and has the possibility for checking the knowledge by tests. The test may be realized for certain time because of the integrated timer..

II. REALIZATION OF THE PROGRAM

For the presentation of the work of this applet, is used a communication application SARS that is designed to run on Windows 98 or NT based systems. SARS also could use Microsoft LAN Manager and IBM LAN Server. Each station in the net with one or more serial ports has to have installed SARS Server. Each station that will use this share port has to have installed SARS Client.[1,2,3]

This application I realized by Microsoft Visual Studio. Net. The controls and the classes that dotNet gives possibility for development of web pages, are part of the Internet functionality, in VB.NET. They are known as ASP.NET. On fig.1 is shown block scheme of the project.

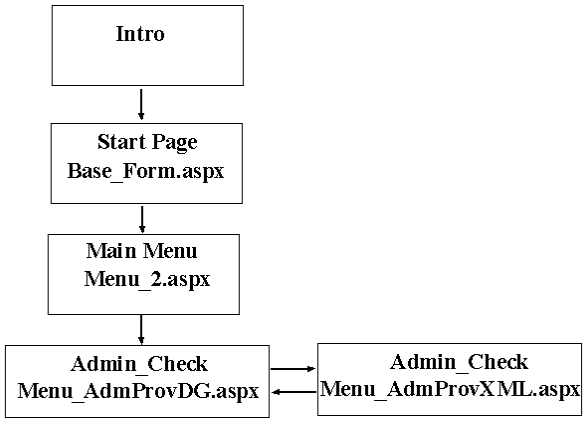

Fig.1 Block – scheme of the project

The realization of the program “Base_Form.aspx” is basis of the first page of the project. It consists of HTML, VB, Net code and server controls, needed for entering user information. The design is stylish because of maximum easy work and quick navigation.[2] The organization of the page is as follows:

- In the title part is defined a logo;
- The fields for entering user information are realized with controls of the type “Combo Box”, with possibility of choosing the needed resource;
- For complete control of the entered information are used controls of the type “Validation control”;
- Are used controls of the type “Label” for maximum understanding and learning of the dynamic fields;
- Is used a button of type “Reset” for removing eventual errors made during the entering of the information;
- Through processing of the event “Click”, to the button “Record”, is made a record of the actual information in the database..

[1]Nikolay T. Kostov is with the Technical University of Varna, Department of Radio engineering, Studentska Street 1, Varna 9010, Bulgaria, E-mail: n_kostov@mail.bg

[2]Slava M. Yordanova is with the Technical University of Varna, Department of Computer Science and Technologies, Studentska Street 1, Varna 9010, Bulgaria, E-mail: slava@windmail.net

The education and test program is developed with the use of application “DreamWeaver”. The database is realized with Microsoft DB Accass. The connection is realized with OleDbProvider 4.0. The installation comes step by step by pressing the certain link that is situated on the main form. The installation is visualized with the needed screenshots.

The educational programs are very popular at this time. Now many educational systems are made and integrated in whole spheres of the real modern life. Is needed a on time education of the staff of the corresponding company for work with the new products. The proposed educational system is developed especially for communication applications. It gives possibility to the user to learn visually the information with the multimedia product and after this to fill the test to check his knowledge. The test is recorded in database so the assigner could check the learning of his employees.

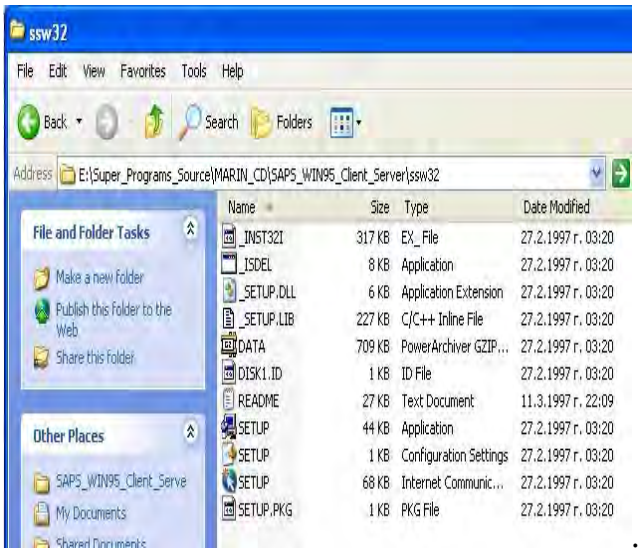

Fig 2 Needed installation files for Server part

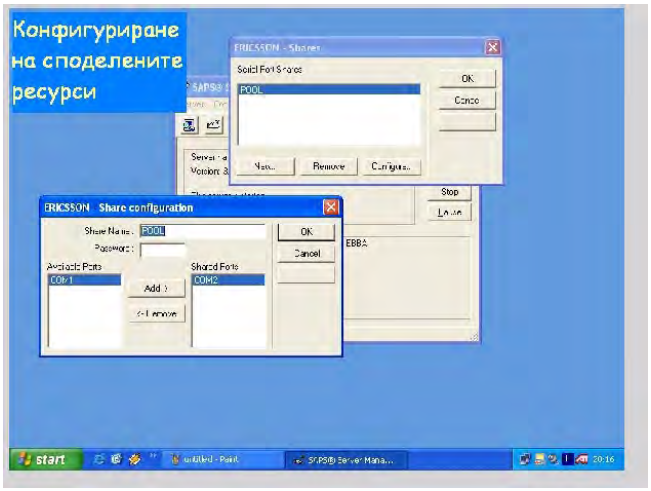

Fig.3 Configuration of the shared resources.

After the user of the company receives certain knowledge, using this product, he fills the test that is recorded in the database. There are possibility for correction of wrong answers from the user by pressing the button “ Cleaning the values”. These corrections could be made only before the button “Record” is pressed.

III. Conclusion

The educational programs are very popular at this time. Now many educational systems are made and integrated in whole spheres of the real modern life. Is needed a on time education of the staff of the corresponding company for work with the new products. The proposed educational system is developed especially for communication applications. It gives possibility to the user to learn

References

[1] Sorrow B. “ Multimedia Activities for students” McFarland&Company 2002

[2] Steinmetz R, Nahrsteedt K “Multimedia& compuring, communication and application”, Prentice Hall. 1999

[3] Microsoft Windows, Microsoft Acces.

Staff Education Cycle for Organization Development in Hi-Tech Companies

Ivaylo Simeonov

Abstract: **This paper discusses the staff education cycle for organization development in hi-tech companies to the competitiveness improvement and the company advance. The training evaluation process is also considered as the main part of the chosen strategy and the human resource management.**

Keywords: **staff education cycle, organization development**

1. Introduction

When the new high-tech technology is available, the only variable parameter to give competitive advantages to organizations appears to be the quality of its human resource [1]-[2]. The implementation of the new technology is often accompanied by a dramatic change in human resource policy and implementation of various types of R&D programs for future product research and investigation.

Industry as well as publicly funded research organizations is facing challenges which are dramatically changing their features. Industry faces increased international competition, increased customer demand, shorter product life and increased complexity of the new product. Publicly funded research organizations face governmental and industrial pressure to become more financially independent, more commercial in operation and adopt the more business-like principles [3]. It is the value creation in today's faster changing knowledge economy. Training, education and learning organization and a knowledge-based organization requires focusing on business strategy and results, teamwork and cooperation, and willingness to undertake the training process and learning activities in innovation ways [4].

The hi-tech companies are becoming the leading ones in the market, because the core of the knowledge economy is innovation. This innovation adds a high value to the products and services, and provides them to the competitive advantages, making it possible for the companies to enjoy the sustainable development. The organization development is based on the realization of the of the benign evolution pattern of "innovation – efficiency - reinnovation" in the hi-tech companies [5]. So the key sustainable development factor is identified as a staff education process.

Ivaylo Petrov Simeonov - ivosim@abv.bg
Technical University of Sofia, 8 Kl. Ohridski Blvd
Faculty of Management

Our previous work [6]-[7] are focused to the human resource development and staff education. This paper discusses the staff education cycle for organization development in hi-tech companies to the competitiveness improvement and the company advance. As the main part of the education cycle description is discussed in our previous work [6], this paper will discuss the relationship between the particular parts of the cycle and the valuation criteria of the education process.

2. Education cycle description

The advent of the knowledge economy era, knowledge has become a determinative in the fierce competition and knowledge capital. The staff education process possesses the following 3 aspects [6]:

- Education (knowledge improvement, study of the basic courses, etc.)
- Training (innovation acquirements, study of the specific courses, etc.)
- Development (sustainable improvement, competitiveness growth, etc.)

The R&D process in the hi-tech companies requires a continuous and high level education to provide a sustainable organization development and innovation improvement. The main factors of the staff education cycle are connected with the information access and defense of the intellectual properties.

The education cycle (fig.1) is a very complicated and long-time process. It requires significant financial resources to ensure the continuity and the quality of the process. The first step of the education cycle begins with the definition of the education needs. This stage is the most important step of the education process, because it forms the cycle frame and defines the required financial resources, education duration and number of the involved participants.

The next two stages specify the education objectives and goal to prepare the particular education plan and programs. The key factor in the program preparation appears as a current plan and program update according to the environment changes and company strategy. The successful program should be based upon the staff's full knowledge of the company development strategy and the vacancy post status. It should pay attention to the vertical and horizontal development as the both parts had to be included equally in the prepared plans. So, a flexible education programs should be drawn up according to the company needs and innovation technology requirements.

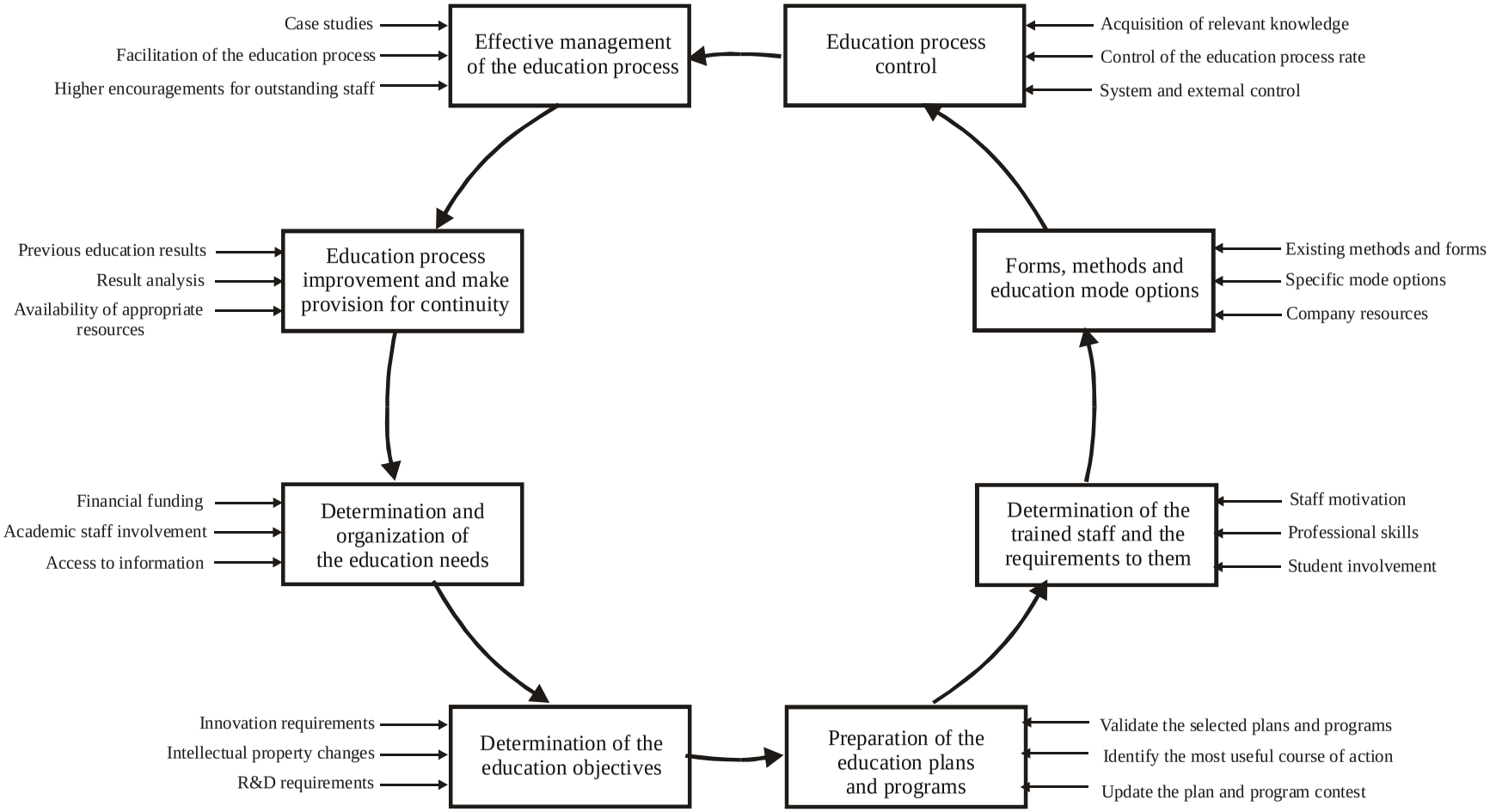

Fig.1. Staff education cycle diagram

The third education stage defines the trained staff and the basic requirements to the participants. To ensure the sustainable development of the hi-tech companies, the human resource managers had to include the students and other academic staff in the education process. This fact is conditioned by the primary goal of the universities, which perform applied research. To attract the attention of this division, the companies had to stimulated publishing and bring their staff in contact with professional networks.

The other main part of the education cycle is distinguished as an education control process. The most important factor of the education success is identified with the training evaluation process since the human factor is the critical one in the high-technology development. Evaluation is undertaken for several purposes, which are:

- To determine whether a program is accomplished its objectives
- To identify the strengths and weaknesses of the human resource development process
- To determine the cost/benefit ratio of an human resource development program
- To test the clarity and validity of the tests, questions and exercises
- To establish a database, which can assist management in decision-making process

The control process allows comparing the education results of every participant from the previous and current cycle and the manager body had to take steps to ensure the high quality of the process. The successful participants are invited to take part in the second level of the company education process.

The education success is based on the staff motivation. It includes higher encouragements and carrier possibilities for the outstanding staff, extra payments for extraordinary education results and financial distribution according to the company section growth. The trained staff is encouraged to mould some parts of the program specifications to motivate them to take part in the active discussions during the education cycle.

The enormous financial resources for the education evaluation process require appropriate criterions to protect the company interests. The practice shows that sometimes the trained staff relinquishes their positions and begins the regular work to the rival companies. To avoid this situation, the manager staff had to include the financial forfeits at the beginning of the second level of the education process and to prohibit the start job in the alternative companies for the preliminarily defined period.

3. Conclusion

This paper discusses the staff education cycle for organization development in hi-tech companies to the competitiveness improvement and the company advance. The training evaluation process is also considered as the main part of the chosen strategy and the human resource management. It is shown that the hi-tech company should accept student and academic staff involvements to provide the sustainable organization development. Also the appropriate programs should be prepared, which pay attention to the vertical and horizontal development and high motivation procedures are required during the education process to guarantee the high education results.

The high education cost insists on the appropriate criterions to protect the company interests. So the relevant financial condition had to be set at the second level of the education process while the company know-how is included in the education process.

References:

[1] Ramsumair Singh - Human resource management: The key to the competitive advantages, *Engineering Measurement Journal*, June 1992, pp.116-120

[2] Ivaylo Simeonov, Boryana Kolchagova – Management model for the organization development of the hi-tech production,

[3] S.W.F. (Omo) Omta and Jo M.L. van Engelen – Enhanced staff motivation in publicly funded research and industrial R&D,

[4] Abdullah Lin and Reha Abdul Razak – The effectiveness and practical application of human resource development (HRD) programs in the semiconductor industry – A case study of SilTerra Malaysia Sdn Bhd, *IEEE/SEMI Advanced Manufacturing Conference*, 2003, pp.175-187

[5] Chen Jin, Wang Li-Ying – Flow and retention of Intellectual employees in Hi-tech companies, pp.176-180

[6] Ivaylo Simeonov – Organization development improvement through the staff education,

[7] Ivaylo Simeonov – Human Resource development: The key to the organization development, Sozopol, 2-5 June, 2004

Theory of Learning and the Brain

Violeta B. Teofilova[1]

Abstract - **An understanding of learning based on the structure and function of the brain. Learning occurs if the brain is not from fulfilling its normal processes. Every person is born with a brain that is an immensely powerful processor. Schooling often inhibits learning by discouraging, ignoring or punishing the natural learning processes of the brain**

Key words - **Learning, Theory, Brain, Schooling, Education**

I. INTRODUCTION

The first part of this paper describes what is a learning in general, and the equation for the learning rate is derived. I also discuss topics concerning the brain because obviously the brain is an integral part of the learning mechanism. However, except for the initial discussions on how the brain develops with age and how that development affects learning.

B. The core principles of brain based learning

- The brain is a "parallel" processor;
- Learning engages the whole physiology;
- The search for meaning is innate;
- The search for meaning comes through patterning;
- Emotions are critical to patterning;
- The brain processes wholes and parts simultaneously;
- Learning involves both focused attention and peripheral perception;
- Learning involves both conscious and unconscious processes;
- We have two types of memory: spatial and rote;
- We understand best when facts are embedded in natural, spatial memory;
- Learning is enhanced by challenge and inhibited by threat;
- Each brain is unique;

The three instructional techniques associated with brain-based learning are: **orchestrated immersion**, where learning environments are created that fully immerse students in a learning experience; **relaxed alertness**, where an effort made to eliminate fear while maintaining a highly challenging environment;
and **active processing**, where the learner consolidates and internalizes information by actively processing it.

II. BRAIN BASED LEARNING

The way the brain works has a significant impact on the kinds of learning activities that are most effective. We need both to help students have appropriate experiences and to help them capitalize on the experience. Three interactive elements are essential to this process:

- Teachers need to orchestrate the *immersion of the learner in complex, interactive experiences* that are both rich and real. A good example is the use of immersion in the teaching of a second language. We need to take advantage of the brain's ability to process in parallel.
- There must be a personally meaningful challenge. This is the intrinsic motivation that is part of the state of mind that we identify as realized alertness.
- There must be intensive analysis so that the learner gains insight about the problem, about the ways in which it could be approached, and about learning generally. We call this the active processing of experience.

Feedback is best when it comes from reality, rather than from an authority figure. We learn best when solving realistic problems. The big picture can't be separated from the details. Because every brain is different we should allow learners to customize their environments. Designers of educational tools should notice parallels between how they approach teaching and how artists approach their craft. ***Educators need to be artists*** in the way they design brain-friendly environments**.** The best way to learn is not through lecture, but by participation in realistic environments that let learners try new things in safe environments.

III. THEORY OF LEARNING AND THE BRAIN

Science is fundamentally not math, physics or equations. It is about human interactions that empower other humans. Can someone totally untrained in science read the following and instantly start using the scientific approach? Most probably not. There is no easy recipe except to study science. You will see that the requirements and complexities of the scientific method will present insurmountable obstacles to most
people. Before we embark on defining science, lets examine a common example of how people misunderstand science because this will help to establish why we need a definition

[1]Violeta B. Teofilova is with Technical University – Gabrovo, 4 H. Dimitar str., 5300 Gabrovo, Bulgaria, E-mail: violeta_teofilova@abv.bg

A. Scientific Approach

Learning: algebra, mechanics, economics, etc., — what do these things have in common? They are all scientific disciplines and therefore share a large number of basic principles in common. It will explain many of the important principles of the scientific method how they are needed in order to produce a useful product. “Science is fundamentally not math, physics or equations. It is about human interactions that empower other humans” [1].

The common example of how people misunderstand science because this will help to establish why we need a definition. Another way of defining science is that it makes previously impossible tasks possible and simplifies difficult tasks. From this point of view, science benefits the less knowledgeable among us more than the better informed who can figure things out for themselves.

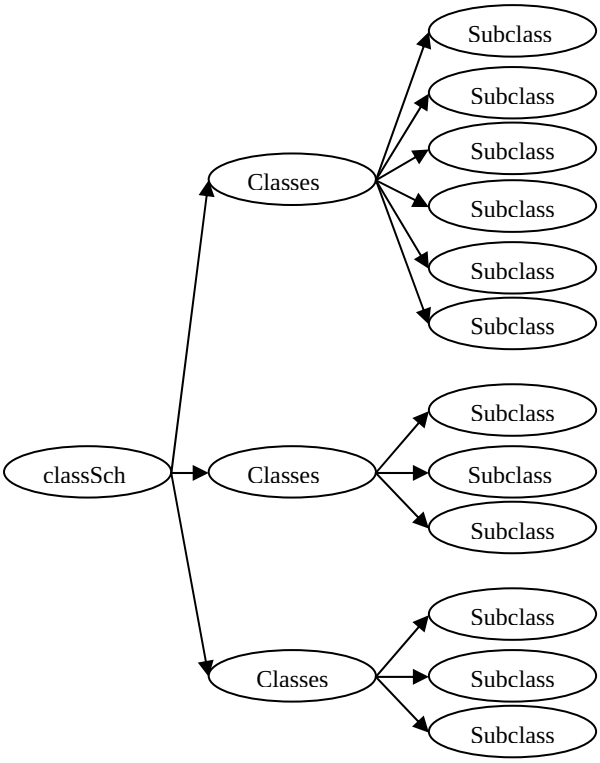

Fig 1: Classification scheme- relationships

The definitions of the scientific method given above do not provide any direct information on how to execute a scientific project. The most general working definition of the scientific approach is that it is a set of uniquely defined objects and the relationships among them. One of the most useful relationships is a classification scheme, which places the objects into classes and subclasses.

Objects must be defined in such a way that they are useful, and in such a way that the relationships between them can be described precisely. And all of these definitions and relationships must be scientifically correct (thats where non-scientists run into problems).

The main ingredient of the scientific method is knowledge but knowledge alone is not enough. That knowledge must be assembled into a structure such that we can see, understand, and exploit the relationships between the objects. Without these relationships, you dont know if you have all the necessary parts or even how to use them. The most common way of building that superstructure is a classification scheme.

In scientific research, you perform experiments, get the data, and write up the results in such a way that others can understand what you did and can reproduce your results. it impossible to put all the ideas together in a coherent way. Once the parallel set concept was introduced, it led naturally to the parallel set exercises.

B. Basic Theory

Scientific results must always be based on some theory or principle that can be verified
by others. Very few concepts stand alone, independently of anything else. In other words, anything that someone claims works, better have a good explanation of why it works; otherwise, it is suspect. The ***explanations*** are often more important than the procedures they explain. Of course, there are always a few concepts that defy explanation, and it is extremely important to clearly classify them as “valid principles without explanations”. In those cases, how are we to know that they are valid? They can be considered valid only after establishing an undeniable record of experimental verification. It is important to label these clearly because procedures without explanations are more difficult to apply and these procedures are subject to change as we learn more and understand them better. The nicest thing about methods that have good explanations is that we don’t need to be told every detail about how to execute the
procedure—we can often fill in the details ourselves from our understanding of the method. This is not only because of the high probability of such procedures being wrong, but also because it is the explanation that helps us to use the procedure correctly. Most instructions on how to do something without any explanation of why they work have little value in a scientific approach. This is not only because of the high probability of such procedures being wrong, but also because it is the explanation that helps us to use the procedure correctly. . In any real life procedure, it is nearly impossible for anyone to describe all the necessary steps of a procedure under all contingencies. It is an understanding of why it works that allows each person to alter the procedure to meet the specific needs of individuals and changing
circumstances. As teachers become more educated, they should be able to replace more dogma with a deeper understanding of the underlying principles. This should significantly enhance efficiency and ease of learning for the student. Most people are aware that scientists must study all their life, not only when they are in college working for their degrees. However, most are unaware of the extent to which scientists devote their time to education, not only to learn but also to teaching everybody else, especially fellow scientists. A scientist therefore often evolves into more of a teacher than say, a piano or school teacher because of the broader range of “students” they encounter as well as the breadth of the subjects that they must cover. It is truly astounding, how much you need to know in order to make just a small new discovery.

The physical principle we use to derive our learning equation is the linearity with time. Such an
abstract concept may seem to have nothing to do with piano and is certainly non-biological, but it turns out that, that is exactly what we need. Let's explain the concept of "the linearity with time". It simply means proportional to time. For example, if we learn an amount of technique L (stands for Learning) in time T, then if we repeat this process again a few days later, we should learn another increment L in the same T. Thus we say that L is linear with respect to T in the sense that they are proportional; in 2T, we should learn 2L. Of course, we know that learning is highly non-linear. If we practice for 4 hours, we are likely to gain a lot more during the first 30 minutes than during the last 30 minutes. However, we are talking about an optimized practice session averaged over many practice sessions that are conducted over time intervals of years. If we average over all of these. learning processes, they tend to be quite linear

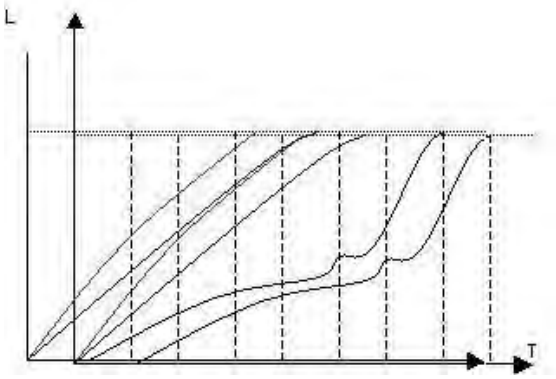

Fig 2: Relationship between learning and time

Certainly within a factor of 2 or 3, linearity is a good approximation, and that amount of accuracy is all we need. Note that linearity does not depend, to first approximation, on whether you are a fast learner or a slow learner; this canges only the proportionality constant. Thus we arrive at the first equation, (1):

$$L = kT \tag{1}$$

where L is an increment of learning in the time interval T and k is the proportionality constant. What we are trying to find is the time dependence of L, or L(t) where t is time (in contrast to T which is an interval of time). Similarly, L is an increment of learning, but L(t) is a function. We have control over L; if we want 2L, we simply practice twice. But that is not the L that we retain because we *lose* some L over time after we practice. Unfortunately, the more we know, the more we can forget; that is, the amount we forget is proportional to the original amount of knowledge, L(0). Therefore, assuming that we acquired L(0), the amount of L we lose in T is , (2):

$$L = -kTL(0) \tag{2}$$

where the k's in equations (1), (2) are different, but we will not re-label them for simplicity. Note that k has a negative sign because we are losing L. (2) leads to the differential equation, (3):

$$\frac{dL(t)}{dt} = -kTL(t) \tag{3}$$

where d stands for differential (this is all standard calculus), and the solution to this differential equation
is (4):

$$L(t) = Ke^{-kt} \tag{4}$$

where e is a number called the natural logarithm which satisfies. (3) and K is a new constant related to k (for simplicity, we have ignored another term in the solution that is unimportant at this stage). (4) tells us that once we learn L, we will immediately start to forget it exponentially with time if the forgetting process is linear with time. Since the exponent is just a number, k in Eq.(4) has the units of 1/time. We shall set k = 1/T (k) where T(k) is called the characteristic time. Here, k refers to a specific learning/forgetting process. Therefore, determining accurate values for T(k) for each process is generally not possible, so in the numerical calculations, we will have to make some "intelligent guesses". Then Eq (4) becomes (5):

$$L(i,t,k) = K_i e^{-k\frac{t_i}{T(k)}} \tag{5}$$

for each repetition i and learning/forgetting process k.
Let's examine some relevant examples (for example- piano playing). Suppose that practicing 4 parallel drill for 10 minutes. We assign i = 0 to one parallel set execution, which may take only about half a second. You might repeat this 10 or 100 times during the 10 minute practice session. You have learned L(0) after the first parallel set. But what we need to calculate is the amount of L(0) that we retain after the 10 minute practice session. In fact, because we repeat many times, we must calculate the cumulative learning from all of them. According to Eq. 1.5, this cumulative effect is given by summing the L's over all the parallel set repetitions, (6):

$$L_{Total} = \sum_i K_i e^{-\frac{t_i}{T(k)}} \tag{6}$$

IV. Conclusion

The consider issues are insignificant part of problems, which are discuss with some science - psychology, pedagogy, instructional design. The computer communications and technologies have grown and a learning have got to discuss and in this aspect.

V. References

[1] Caine R. "Making Connections: Teaching and the Human Brain"
[2] Chuan C. "Fundamentals of Piano Practice"

Session PO:

Poster

On the effect of cochannel interference on average symbol error probability of MQAM in Nakagami fading channels

Perić Zoran[1] , Nikolić R. Jelena[2] , Aleksić R. Danijela[3]

Abstract –**In this paper the analytic expression is derived for the average symbol error probability of M-ary quadrature amplitude modulation (MQAM) in Nakagami fading channels in the presence of additive white Gaussian noise (AWGN). Using this expression numerical results are obtained and are shown in graphical, which represent the effect of cochannel interference on average symbol error probability for three constellations: 4-QAM, 16-QAM i 64-QAM.**

Keywords - **MQAM, cochannel interference, average symbol error probability, Nakagami fading channels.**

I INTRODUCTION

During the transmission of digital modulated signals through communication channels, multipath propagation causes the amplitude fluctuation of received signal in short term of time. This effect is known as a fading. Development of wireless mobile communications requires transmission of data with speed in range from few tenth to hundred Mb/s. One of several problems which appears as following effect is intersymbol interference which is caused by multipath fading. This problem increase equally with increasing of transmission speed. In different modulation schemes the transmission speed of information could be effectively increased if we accept two elementary signals, thereby the multilevel modulation schemes became standards in a many of telecommunication systems [1].

In reference [1] is shown a process for determining the average symbol error probability for M-ary quadrature amplitude modulation (MQAM) scheme. This is the modulation scheme often used in the terrestrial microwave and satellite communication systems. In this paper we directly use the known symbol error probability results for MQAM [3] valid for additive white Gaussian noise (AWGN) as the conditional error probability before averaging over the probability density function (pdf) of the (SIR) signal-to-interference ratio for Nakagami fading [2].

[1]Perić Zoran, is with the Faculty of Electronic Engineering, Beogradska 14, 18000 Niš, Serbia and Montenegro
e-mail: peric @elfak.ni.ac.yu
[2]Nikolić R. Jelena, is with the Faculty of Electronic Engineering, Beogradska 14, 18000 Niš, Serbia and Montenegro
e- mail: njelena @elfak.ni.ac.yu
[3]Aleksić R. Danijela is with the Telekom Srbija, Kosovska 47, 11000 Belgrade, Serbia and Montenegro
e- mail: danijelaal@telekom.yu

II SYSTEM MODEL

In this paper the effects of cochannel interference and multipath fading on the symbol error probability are considered for Nakagami fading channels. Nakagami channel model is more general than the Rayleigh channel model and is commonly used to characterize the urban and digital mobile radio environment. Considerations of system performances, which are limited by the interference in Nakagami fading environment, are based on the calculation of probability of error [2]. It is of interest, therefore, to consider the effect of cochannel interference on the average symbol error probability in Nakagami fading channels.

The desired signal power in a Nakagami fading channel is a gamma distributed random variable with probability density function (pdf) [2] given by Eq.(1)

$$p_s(x)=\left(\frac{m_S}{\Omega_S}\right)^{m_s}\frac{x^{m_s-1}}{\Gamma(m_s)}\exp(-\frac{m_s}{\Omega_s}x) \qquad (1)$$

where are:

Ω_s - the average signal power

m_s - Nakagami fading parameter

$\Gamma(a)=\int_0^\infty e^t t^a dt$ is gamma function

We assume that L mutually independent Nakagami faded interference signals are also present at the receiver. When the interferers are at approximately the same distance from the mobile station, they can also be assumed to have the same average power. The probability density function of the total interference power [2] is given by Eq.(2)

$$p_I(x)=\left(\frac{m_I}{\Omega_I}\right)^{m_I L}\frac{x^{m_I L-1}}{\Gamma(m_I L)}\exp(-\frac{m_I}{\Omega_I}x) \qquad (2)$$

where are:

Ω_I - the average interference power

m_I - Nakagami fading parameter for the interference signals

In a typical microcellular environment in which the desired signal as well as the interfering signals undergo Nakagami fading, it is reasonable to assume that the cochannel interferers experience much deeper fading than the desired signal. Therefore is $m_s \geq m_I \geq 1/2$. In an interference-limited system the effect of noise may be ignored. In this case it can

be shown that the signal-to-interference ratio $\gamma = S/I$, has the pdf [2] given by Eq.(3)

$$p_\gamma(\gamma) = \frac{\Gamma(m_s + m_I L)}{\Gamma(m_s)\Gamma(m_I L)} \left(\frac{m_s}{q_{SIR} m_I} \right)^{m_s} \frac{\gamma^{m_s - 1}}{\left(\frac{m_s}{q_{SIR} m_I} \gamma + 1 \right)^{m_s + m_I L}} \quad (3)$$

where the ratio $q_{SIR} = \Omega_s / \Omega_I$ is the average-signal to average interference ratio (SIR), which is useful in determining the average symbol error probability.

III AVERAGE SYMBOL ERROR PROBABILITY

In an interference limited environment, the average symbol error probability of M-ary quadrature amplitude modulation (MQAM) in Nakagami fading channels [3] can be shown in Eq.(4)

$$P_e = \int_0^\infty P_e(\gamma) p_\gamma(\gamma) d\gamma \quad (4)$$

$P_e(\gamma)$ is the conditional probability of error for a given SIR, γ ($\gamma = S/I$) for additive white Gaussian noise (AWGN) channels [3]. This is given by Eq.(5)

$$P_e(\gamma) = \frac{q}{2} \, erfc\left(\sqrt{\frac{\gamma}{p}} \right) - \frac{q^2}{16} \, erfc^2\left(\sqrt{\frac{\gamma}{p}} \right) \quad (5)$$

where are:

$$q = 4\left(1 - \frac{1}{\sqrt{M}}\right)$$

$$p = 2\frac{(M-1)}{3\log_2 M}$$

$erfc\,(x)$ is the complimentary error function.

For rectangular MQAM in which $M = 2^k$, where k is even, the signal constellation is equivalent to two pulse amplitude modulation (PAM) on quadrature carriers, each having $\sqrt{M} = 2^{k/2}$ signal points.
Eq.(6) is derived by using substitution of Eqs.(3) and (5) in Eq.(4)

$$P_e(\gamma) =$$

$$\frac{\Gamma(m_s + m_I L)}{\Gamma(m_s)\Gamma(m_I L)} (\beta)^{m_s} \frac{q}{2} \int_0^\infty erfc\left(\sqrt{\frac{\gamma}{p}} \right) \frac{\gamma^{m_s - 1}}{(\beta\gamma + 1)^{m_s + m_I L}} d\gamma$$

$$- \frac{\Gamma(m_s + m_I L)}{\Gamma(m_s)\Gamma(m_I L)} (\beta)^{m_s} \frac{q^2}{16} \int_0^\infty erfc^2\left(\sqrt{\frac{\gamma}{p}} \right) \frac{\gamma^{m_s - 1}}{(\beta\gamma + 1)^{m_s + m_I L}} d\gamma \quad (6)$$

where is $\beta = \frac{m_s}{q_{SIR} m_I}$.

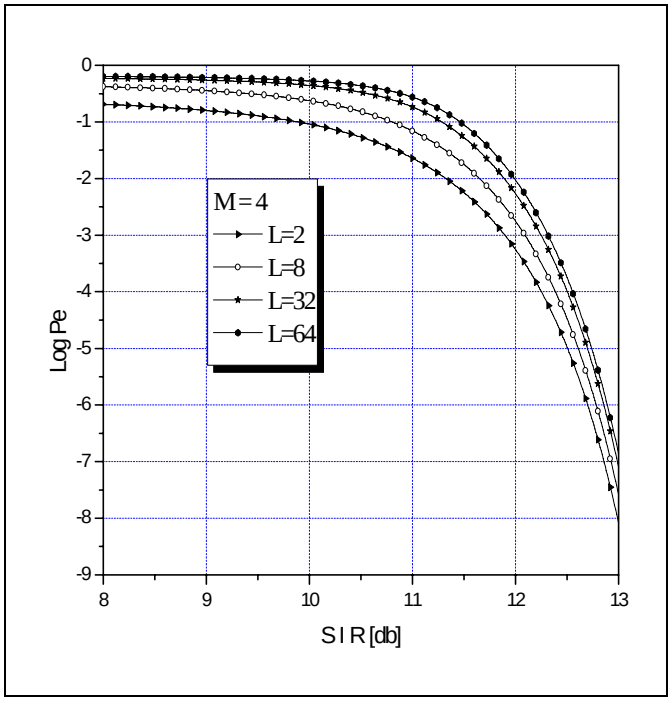

Fig.1. P_e of 4-QAM in Nakagami fading channels in the presence of AWGN for L=2, L=8, L=32, L=64 (m_s =0.8 i m_I =0.6)

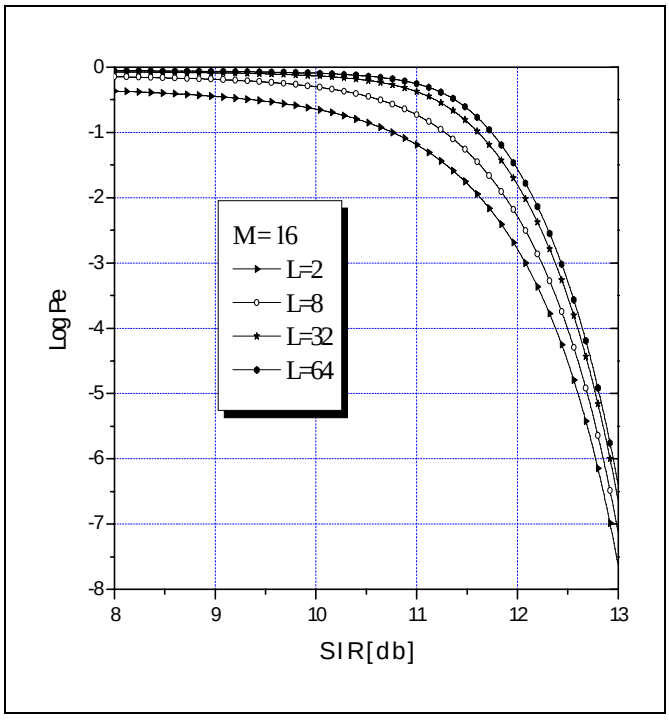

Fig.2. P_e of 16-QAM in Nakagami fading channels in the presence of AWGN for L=2, L=8, L=32, L=64 (m_s =0.8 i =0.6)

IV NUMERICAL RESULTS

Using Eq.(6) and accepting the value of Nakagami fading parameters m_s i m_I , m_s =0.8 i m_I =0.6 we obtain numerical results, which can be illustrate on graphics. These results are represented in Fig.1., Fig.2., Fig.3. The exact average symbol error probability (P_e) curves of MQAM in Nakagami fading for various L, mutually independent Nakagami faded interference signals presented at the receiver, and various M, computed from Eq.(6), as a function of SIR, in dB, $(SIR = 10\log q_{SIR})$ are shown in Fig.1., Fig.2., Fig.3.

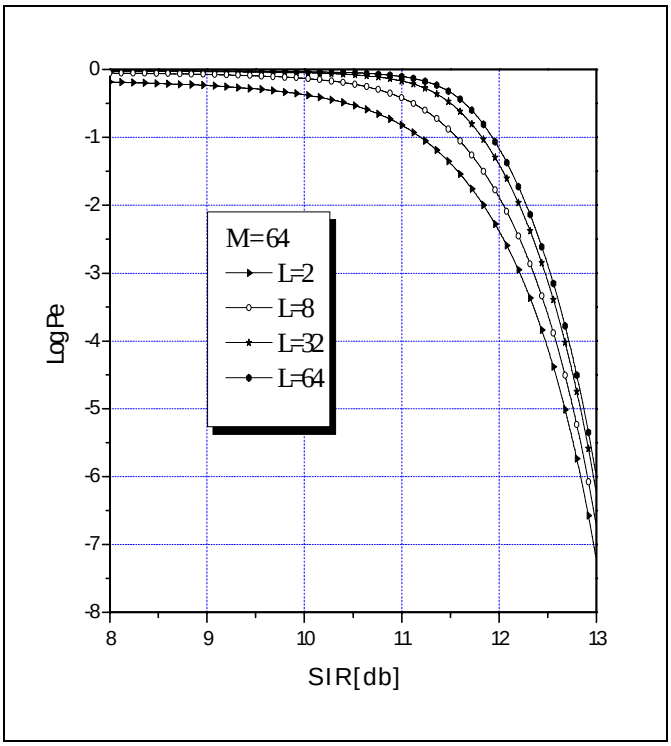

Fig.3. P_e of 64-QAM in Nakagami fading channels in the presence of AWGN for L=2, L=8, L=32, L=64 (m_s =0.8 i m_I =0.6)

The values of k in Fig.1., Fig.2., Fig.3. are 2, 4, 6 respectively and in this cases M are 4, 16, 64. We noted that the results given by Eq.(6) are exact for $M = 2^k$ when k is even. On the other hand, when k is odd, there is no equivalent $\sqrt{M}$ -ary PAM system. From the figures we observe that for a given average symbol error probability P_e, increasing the L, increases the required SIR. Rapidly decreasing of value P_e with increasing of SIR can be noticed for $SIR \geq 10db$.

V CONCLUSION

In this paper the analytic expression is derived for the average symbol error probability of M-ary quadrature amplitude modulation (MQAM) in Nakagami fading channels in the presence of additive white Gaussian noise (AWGN). The numerical results are shown in graphical form. The results represent influence of cochannel interference on average symbol error probability in following cases 4-QAM, 16-QAM i 64-QAM. For constant values of Nakagami parameters, m_s =0.8 and m_I =0.6 and for M=4, 16, 64 respectively, the values of average symbol error probability, P_e are computed from Eq.(6). It is shown that increasing the SIR, decreases the required P_e. Also is shown that increasing the L, increases the required P_e for a given SIR.

REFERENCES

[1] J. G. Proakis, *Digital Communication*, 3rd ed. New York: McGraw-Hill,1995

[2] Valentine A. Aalo and Jingjun Zhang ''On the Effect of Cochannel Interference on Average Error Rates in Nakagami-Fading Channels'', IEEE Communications letters, Vol. 3. No. 5.May 1999

[3] J. Lu, T. T. Tjhung, and C. C. Chai, ''Error Probability of L-Branch Diversity Reception of MQAM in Rayleigh Fading'', IEEE Transactions on Communications, Vol. 46. No. 2. February 1998

Chirped Gaussian Pulse Propagation Along Anomalous Dispersive Optical Fiber in the Presence of Interference

Mihajlo Č. Stefanović[1], Dragan Lj. Drača[1], Aleksandra S. Panajotovic[1] and Aleksandra Ž. Jovanović[1]

***Abstract* – Basic task of all telecommunication systems is that a signal propagation from transmiter to receiver is as good as possible. There are many factors, in optical telecommunication systems, which disable such transmission. Dispersion is one of them. Optical fiber can work under normal or anomalous dispersive regime, but anomalous dispersive regime is better for signal propagation. It is the reason why we study linear chirped Gaussian signal propagation along such fiber. Influence of coherent interference on transmission quality is also studied in this paper. That influence is shown by pulse shape at the reciver, i.e. at the end of optical fiber. Nonlinear Schrödinger equation is solved to get pulse shape along optical fiber. Interference can appear anywhere along the fiber and therefore we determined to what extent appearing place of interference affects signal propagation and transmission quality.**

***Keywords* - Chirped Gaussian signal, Interference, Dispersive optical fiber, Nonlinear Schrödinger equation.**

I. INTRODUCTION

Intermodal dispersion results from refractive index and mode propagation constant frequency dependence and it leads to pulse deformity, i.e. pulse broadening when pulse propagates along optical fiber [1]. Dispersion coefficient β_2 is a parameter that shows magnitude of dispersion. It defines dispersive regime of optical fiber, too. If $\beta_2>0$, then optical fiber works under normal dispersive regime. On the contrary, when $\beta_2<0$ then we can say that optical fiber is exposed to anomalous dispersion [1,2]. It is optimal that optical fiber works under anomalous dispersive regime because dispersive influence can be reduced and soliton transmission can be realised under determinate conditions in such optical fiber. When optical fiber is linear, pulse broadening is the same in cases when absolute value of dispersive coefficients β_2 are equal [3]. Because of that it does not matter if linear optical fiber work under normal or anomalous dispersive regime.

[1]Mihajlo Č. Stefanović is with the Faculty of Electronic Engineering, Beogradska 14, 18000 Niš, Serbia and Montenegro, E-mail: misa@elfak.ni.ac.yu

[1]Dragan Lj. Drača is with the Faculty of Electronic Engineering, Beogradska 14, 18000 Niš, Serbia and Montenegro, E-mail: draca@elfak.ni.ac.yu

[1]Aleksandra S. Panajotović is with the Faculty of Electronic Engineering, Beogradska 14, 18000 Niš, Serbia and Montenegro, E-mail: alexa@elfak.ni.ac.yu

[1]Aleksandra Ž. Jovanović is with the Faculty of Electronic Engineering, Beogradska 14, 18000 Niš, Serbia and Montenegro, E-mail: sanda@elfak.ni.ac.yu

Interference is one kind of disturbance that appears in optical telecommunication system and it is the cosequence of crosstalking, reflection, etc... [2,4,5]. It can be coherent or noncoherent, i.e. it can be of the same or different frequency in relation to a useful signal and it can appear anywhere along the optical fiber. Coherent interference is more important because it cannot be eliminated by optical filtering in reciver. It is the reason why such a kind of interference is discussed in the paper [6,7].

There are many ways to resolve signal transmission problems discussed above. They can be solved numerically or analytically. Great mathematical knowledge is needed for analytical solving and it is simpler to solve problem numerically using some programs.

II. PROPAGATION SHRÖDINGER EQUATION

Pulse propagation along nonlinear-dispersive optical fiber can be described by equation [1]:

$$\frac{\partial A}{\partial z}+\beta_1\frac{\partial A}{\partial t}+\frac{i}{2}\beta_2\frac{\partial^2 A}{\partial t^2}+\frac{\alpha}{2}A=i\gamma|A|^2A \qquad (1)$$

where $A(z, t)$ is slowly varying amplitude of pulse, α is optical losses, $\beta_1=\left.\frac{\partial\beta}{\partial\omega}\right|_{\omega=\omega_0}=\frac{1}{v_g}, \beta_2=\left.\frac{\partial^2\beta}{\partial\omega^2}\right|_{\omega=\omega_0}$, β is mode-propagation constant, v_g is group velocity and γ is nonlinearity coefficient that is defined as:

$$\gamma=2\pi n_2/(\lambda A_{eff}) \qquad (2)$$

n_2 is nonlinear index coefficient, λ is wavelength of signal and A_{eff} is effective core area. If we introduce the following normalization:

$$\tau=\frac{T}{T_0}=\frac{t-\beta_1 z}{T_0},\ U=\frac{A}{\sqrt{P_0}} \qquad (3)$$

where T_0 is half-width, i.e. time when signal power declines to $1/e$ of its top value, P_0 is peak power of useful signal and if we introduce the following changes [1]:

$$L_D=\frac{T_0^2}{|\beta_2|},\ L_{NL}=(\gamma P_0)^{-1} \qquad (4)$$

where L_D is dispersive length and L_{NL} is nonlinear length, then Eq. (1) becomes:

$$\frac{\partial U}{\partial z} = -i\frac{\operatorname{sgn}(\beta_2)}{2L_D}\frac{\partial^2 U}{\partial \tau^2} + \frac{i}{L_{NL}}|U|^2 U \tag{5}$$

Optical losses are neglected in Eq. (5), i.e. α=0, because they are very small for λ=1.55 μm [1]. Equation (5) is well-known as nonlinear Schrödinger equation. There are many methods, numerical or analytical, for its solving. Symmetrical split-step Fourier method is used in this paper for solving Schrödinger equation because of the fact that it is very fast and very accurate method [1].

Parameter that defines working regime of optical fiber is:

$$N^2 = \gamma P_0 L_D = \gamma P_0 T_0^2 / |\beta_2| = L_D / L_{NL} \tag{6}$$

When N^2<<1 then dispersive effects dominate optical fiber. In case when $N^2 \approx 1$ then dispersive and nonlinear effects establish balance among themselves [1].

III. Chirped Gaussian Pulse Propagation along Optical Fiber In the Presence of Interference

Chirped Gaussian pulse is very often found as useful signal in optical telecommunication systems [1,6,8]:

$$U(0,\tau) = a\exp(-(1+iC_1)\tau^2/2)$$
$$s(0,\tau) = U(0,\tau)\cos\omega_r\tau \tag{7}$$

where value of parameter a depends on transmited information (1 or 0), C_1 is chirp of useful signal and $\omega_r = \omega T_0$ is normalized frequency.

Coherent interference is of the same frequency as useful signal and there is time and phase shift in relation to useful signal. Interference at the place of appearance is:

$$s_i(z_i,\tau) = U_i(z_i,\tau)\cos(\omega_r\tau + \varphi),$$
$$U_i(z_i,\tau) = a_i\exp(-(1+iC_2)(\tau-b)^2/2) \tag{8}$$

where b i φ are time and phase shift, respectively. z_i is place along optical fiber where interference appears, C_2 is chirp of interference and value of parameter a_i depends on magnitude of interference. Interference can be chirped although useful signal is not linearly chirped and it depends on the kind of interference [7]. Envelope and phase of resulting signal at the place of interference appearance are [6]:

$$U_r(z_i,\tau) = \sqrt{U^2(z_i,\tau) + 2U(z_i,\tau)U_i(z_i,\tau)\cos\varphi + U_i^2(z_i,\tau)} \tag{9}$$

$$\psi(z_i,\tau) = arctg\frac{U_i(z_i,\tau)\sin\varphi}{U(z_i,\tau) + U_i(z_i,\tau)\cos\varphi} \tag{10}$$

All time shapes of signals both along and at the end of optical fiber, that are showed in following figures, are gained by solving Schrödinger equation (5) by symmetrical split-step Fourier method [1,9,10,11] whereby initial conditions are modificated, at the place of interference appearance. The following values of parameters are used in all cases: T_0=4 ps, A_{eff} =80 μm^2, λ=1.55 μm, , n_2=32·10^{-16} cm^2/W and β_2=-19 ps^2/km.

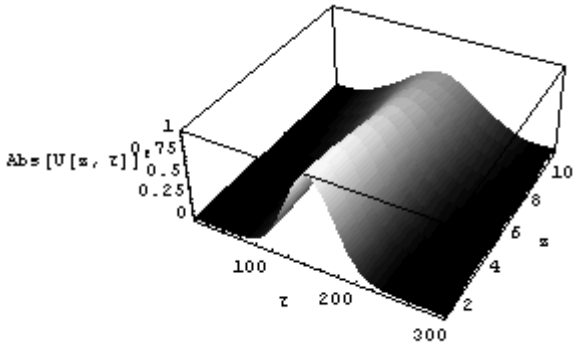

Fig. 1. Nonchirped Gaussian signal propagation along dispersive optical fiber (N^2<<1)

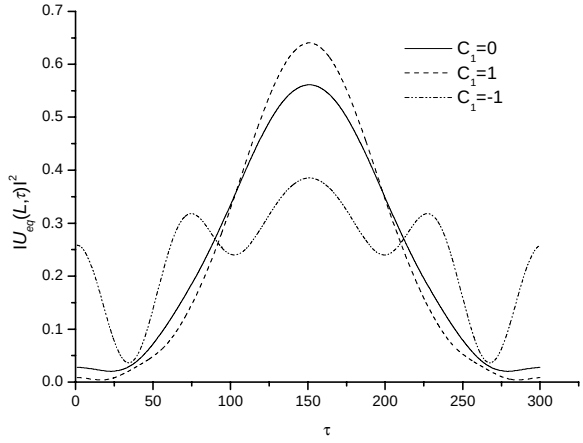

Fig. 2. Useful signal shape at the end of optical fiber in the absence of interference

Nonchirped signal propagation along dispersive optical fiber is displayed in Fig. 1 and it shows to what extent dispersion affects signal expansion. We can see that this dispersion influence is quite great and it is proved in Fig. 2 that shows signal shapes at the reciever for both chirped and nonchirped useful signal. It is known that if optical fiber and signal have such parameters that $\beta_2 C_1$<0 is valid, then signal narrows until determined length of optical fiber and after that signal starts

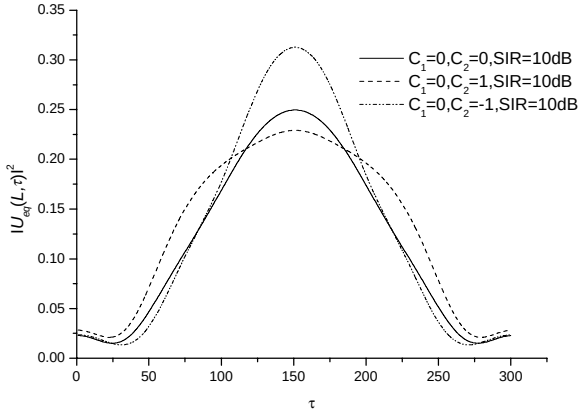

a)

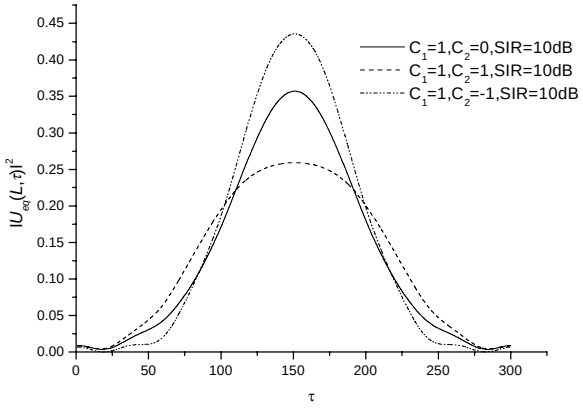

b)

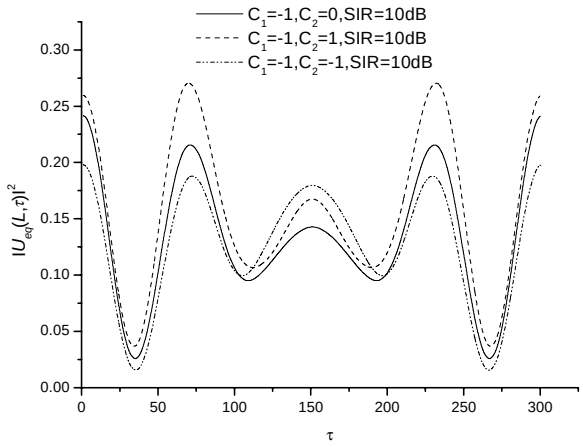

c)

Fig. 3. Signal shapes at the end of optical fiber in the presence of interference (z_i=0.3L)
a) C_1=0 *b*) C_1=1 *c*) C_1=–1

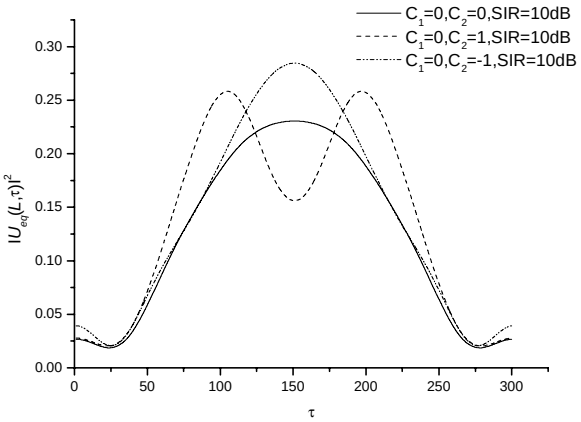

a)

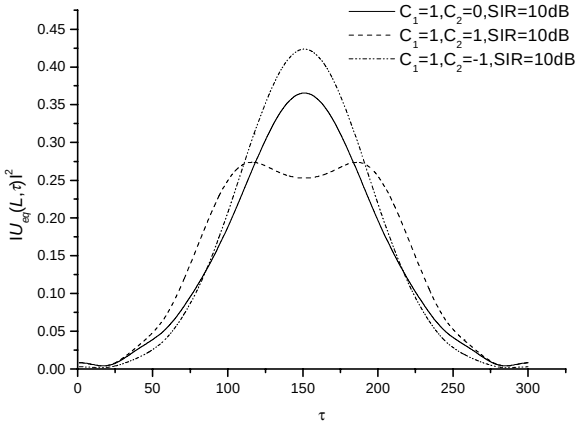

b)

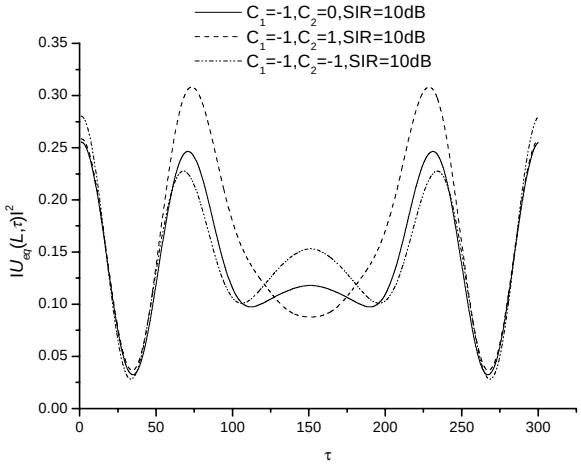

c)

Fig. 4. Signal shapes at the end of optical fiber in the presence of interference (z_i=0.6L)
a) C_1=0 *b*) C_1=1 *c*) C_1=–1

broadening to the end of optical fiber [1]. It is documented in Fig. 2, too. Signal with minimal expansion along optical fiber is signal which has such a chirp that the condition above is realised. Maximal signal deformation is in case when $\beta_2 C_1 > 0$.

Figs. 3 and 4 show signal shape at the end of optical fiber in the presence of interference along optical fiber. If we look at Eq. (8), we can conclude that time and phase shift are random values and that they can have any values ranging from [-1/(2*B*), 1/(2*B*)], i.e. [0, π] respectively (B – bit rate), but in this paper we have considered the worst case, i.e. b=0 and φ=π. We concluded, comparing Figs. 2, 3 and 4, that maximal deformation, i.e. maximal pulse expansion happens in case of C_1=-1 because of condition $\beta_2 C_1>0$ (β_2=-19 ps^2/km). This appearance is more pointed up in the presence of interference. Then, signal loses its shape and big error can be made at the reciever in detection process in the presence of jiter (Figs. 3*c* and 4*c*). The least pulse deformation, bacause of dispersive effects and presence of interference, happens when C_1=1. Reason for that is signal behaviour which narrows along the first part of optical fiber and expands along the second part of optical fiber [1]. We can see that, under such condition, signal is more immune to place of interference appearance, too. It is interesting that signal broadening is quite less for case C_1=1 and C_2=-1 then when C_1=1 and C_2=1. It can be explained by opposite action of chirps such as opposite action of chirp which is made by dispersion and initial chirp which enable pulse narrowing (Fig. 2).

IV. CONCLUSION

Dispersion is inevitable phenomenon in optical telecommunication systems and because of that its influence on chirped Gaussian signal propagation is considered in this paper. First, we showed that influence of dispersion depends on chirp sign of useful signal and dispersive regime optical fiber works under. Since interference which can be anywhere along the fiber appears as one of the disturnabces in optical telecommunication systems, we considered useful signal immunity to it and its place of appearance. From these results we concluded that the signal with negative initial chirp is the least immune to interference and its appearing place in case when optical fiber works under anomalous dispersive regime. All the problems considered in the paper we resolved by using programming package Mathematica 4.

REFERENCE

[1] Govind. P. Agrawal, *Nonlinear Fiber Optics*, Academic Press INC., Boston-San Diego-New York-London-Tokyo-Toronto, 1995.

[2] Drača D., Panajotović A., Stefanović M., Antonijević J., ″Super Gaussian Pulse Propagation along Nonlinear-Dispersive Optical Fiber in the Presence of Interferen*je*″, ETRAN 2003, Sveska II, p. 157-160, Igalo, 2003.

[3] Panajotović A., *Performance of optical system in Base Band in the Presence of Interference*, Master thesis, 2003.

[4] P. J. Legg, M. Tur, I. Andonović, ″Solution Paths to Limit Interferometric Noise Induced Performance Degradation in ASK/Direct Detection Lightwave Networks″, Journal of Lightwave Technology, Vol. 14, No. 9, p. 1943-1954, 1996.

[5] J. Wangg, A. Yongacoglu, ″Performance of Trellis Coded-8PSK with Cochannel Interference″, Transaction on Communications, Vol. 42, No. 1, p. 6-10, 1994.

[6] Stefanović M., *Performance of Digital Telecommunication System*, Monograph, University of Niš, 2000.

[7] Drača D., Panajotović A., Jovanović A., Martinović D., ″Influence of Interference Chirp on Gaussian Signal Propagation along Nonlinear Dispersive Optical Fiber″, TELFOR 2003, Belgrad, 2003.

[8] Lukatela G., *Statistical Telecommunication Theory and Information Theory*, Građevinska knjiga, Belgrad, 1981.

[9] Stefanović M., Drača D., Panajotović A., Spalević P., ″The influence of crosstalk signal interference to signal propagation along nonlinear and dispersive fiber″, Journal of Optical Communications, German, 2002 (accept for printing JOC #844).

[10] Stefanović M, Drača D., Spalević P. and Panajotović A., ″Performance of IM-DD Optical System in the Presence of Interference at Input of the Fiber″, Nonlinear Phenomena in Complex System, Vol.6, No.4, 870-878, 2003.

[11] Wolfram S., *Mathematica*, Addison-Wesley Publishing Company,1988.

A Method For Creation Of An Autonomous Synchronization With Forecasting Of Random Fluctuations Of The Delay Of Radiocommunication Systems With Frequency Hopping Signaling

Antonio Andonov [1]

Abstract - This paper presents a new frequency synthesizer to realize coherent communication in frequency hopping spread spectrum and algorithm for the synchronization.

Keyword- Spread spectrum communication systems

I.COHERENT RADIOCOMMUNICATION SYSTEMS FREQUENCY HOPPING SIGNALING

If a sinusoidal signal of frequency f is transferred through the device, the gain and phase shift are given by [1]:

$$G = \exp\left\{-n\varepsilon\left[1-\cos\left(\frac{2\pi f}{f_c}\right)\right]\right\}$$

and

$$\nabla\theta = -n\varepsilon\left\{\left(\frac{2\pi f}{f_c}\right)-\sin\left(\frac{2\pi f}{f_c}\right)\right\} \quad (1)$$

where ε is the transfer inefficiency of CCD and f_c is the clock frequency.

The proposed synthesizer consists of a standard signal source, a CCD delay line and a switching circuit.

The proposed method gets the signal with different angle frequency from the standard signal with the same angle frequency ω_0. Many signals (called primitive signals) with the same angle frequency of the standard signal and the phases shifted θ-sequentially are prepared. These primitive signals are guided to the output through a switching circuit in the phase shifting order. The circuit is synchronized to one of the primitive signals and switching after each *k* cycle of the primitive signal is done.

Let T_s, called sampling interval, be the time interval between switching. The synthesized signal s(t) is expressed by (2):

$$s(t)=\sum rect(t-kT_s)\sin(\omega_0 T+k\theta) \quad (2)$$

For simplicity, the amplitude of the synthesized signal is unity. The phase difference between the synthesized signal and standard signal increases by θ per time T_s. Therefore the synthesized signal through this method can approximate the signal with angle frequency $\omega_{0+}\theta/T_s$. Let ω_d be the object angle frequency of desired signal, then sequential phase shift amount θ should be determined by (3):

$$\omega_d = \omega_{0+}\theta / T_s \quad (3)$$

Especially when θ= 2π/N, N=2,3,4,… synthesized signal can be maintained for arbitrary timelength by using N primitive signals iteratively.

Since $-2\pi<\theta<2\pi$, the synthesizable angle frequency satisfies (4):

$$\omega_0 - \frac{2\pi}{T_s} < \omega_d < \omega_0 + \frac{2\pi}{T_s} \quad (4)$$

The synthesized signal has a type of distorted wave. Through Fourier expansion, the desired signal component has calculated. Supposing $\theta=2\pi/N$, the period T_d of synthesized signal s(t) is equal to Nt_s and its Fourier expansion is given by (5):

$$s(t)=\sum_{k=1}^{\infty} a_k \sin\frac{2k\pi}{T_d}+\sum_{k=1}^{\infty} b_k \cos\frac{2k\pi}{T_d} \quad (5)$$

In synthesized signals, only frequency components corresponding to k=(K+1)N±1, 1= 0, ±1, ±2,…. exist [1]. Their angle frequency $\omega_1^{\pm}$ is expressed by (6), using $\theta=2\pi/N$, $T_d=NT_s$, $\omega_0 T_s=2k\pi$;

$$\omega_1^{\pm}=\frac{2\pi}{T_d}k=\frac{2\pi}{T_d}KN\pm\frac{2\pi}{T_d}IN=\omega_0\pm\frac{\theta}{T_s}+\frac{2\pi}{T_d}I \quad (6)$$

Substituting I=0, ω_0 equals the desired angle frequency ω_d. Then, the amplitude of the desired signal included in the synthesized signal A_d is evaluated by (7), [1]:

[1] Antonio Vladimirov Andonov is witch the Higher School of Transport, Geo Milev Str.158, 1584 Sofia, Bulgaria, e-mail : a.andonov@infotel.bg

$$A_d = \sqrt{a_{KN+1}^2 + b_{KN+1}^2} = \frac{\sin(\theta/2)}{\theta/2} \quad (7)$$

The phase of the synthesized desired signal φ is determined by the phase of primitive signal at the synthesis start time.

$$\varphi = arctg\left(\frac{b_{KN+1}}{a_{KN+1}}\right) = \frac{\theta}{2} \quad (8)$$

The phase of the desired signal can be varied by starting synthesis using a primitive signal with the corresponding phase. Letting the phase of a primitive signal be nθ, the phase of the desired signal φ also is shifted by nθ,

$$\varphi = \left(n - \frac{1}{L}\right)\theta \quad (9)$$

Since a switching circuit is synchronized to one of primitive signals, the desired signal with the same phase is obtained every time the synthesis start. Thus this method can control the phase of the synthesized desired signal, freely and always reproduces the phase. An interval $1/T_s$ exist between the desired signal and each spurious component. If T_s is small enough, the spurious components are put out of the communication channel band. That is, T_s should be set satisfying (10):

$$T_s<1/F \quad (10)$$

Thus no spurious components are considered to exist within the communication channel band.

Let the delay time be m cycle of primitive signal, $2m\pi/\omega_0$, m=1, 2, 3,….., and N taps be placed at an equal interval. If m and N are prime to each other then all the N waves of primitive signals satisfying $\theta=2\pi/N$ an be obtained. If m and N have common divider except for one, duplication exists among N waves of primitive signals. Especially if m=IN±1, (I=0, 1, 2,..), the shifting order of primitive signals by θ and the tab sequence order agree.

Using all these primitive signals sequentially, a desired signal with angle frequency θ_d satisfying (2) can be synthesized. If every other primitive signal is selected, then each phase is shifted by 2θ. The angle frequency in this case differs by θ/T_s from the former case. In general, if primitive signals are selected so that each phase is shefted by nθ , then the angle frequency of synthesized signal ω_d I, trough (3), evaluated by (11):

$$\omega_d = \omega_0 + \frac{n}{T_s}\theta \quad (11)$$

II. ALGORITHM FOR THE SYNCHRONIZATION IN RADIO COMMUNICATION SYSTEMS

The described algorithm is applied in publication [2]. On the basic of Markov-theory of optimal non-linear filtration a problem is set and being researched for the estimation and maintenance of autonomous synchronization in the system for radio communication among remote moving objects.

REFERENCES:

[1] Andonov A. The problem of functional stability of the systems of mobile radioconnections. Sofia, VTU, 1996

[2] Andonov A., V.Kadrev Algorithm for the synchronization in radio-communication systems with coherent discontinuous variation of the working frequency. ICEST 2002

Theoretical analysis of Frequency, Pulse and Transitional characteristics of Loudspeaker (Part I)

Atanaska A. Angelova [1], Ekaterinoslav S. Sirakov [2] and Georgi K. Evstatiev [3]

***Abstract* - In the work, a researching pulse response of an electrodynamic loudspeaker with a direct radiating is considered. The given method for measuring the system displays: the frequency response, the pulse and the transitional characteristics using the program MathCad. These characteristics are particularly important for the sound quality of the loudspeaker.**

***Keyword* – Loudspeaker, Frequency response, Pulse response.**

I. INTRODUCTION

The Loudspeaker can be described with the lineal four-plus [1].We can describe the lineal four-plus, using linear fluxional equation to the n-th degree where x(t) is an admission of the loudspeaker and y(t) - an outlet signal or a sound level on the radiating axis of the loudspeaker at a distance of one meter.

$$b_0 y(t) + b_1 \frac{dy(t)}{dt} + b_2 \frac{d^2 y(t)}{dt^2} + \ldots + b_m \frac{d^m y(t)}{dt^m} = a_0 x(t) + a_1 \frac{dx(t)}{dt} + a_2 \frac{d^2 x(t)}{dt^2} + \ldots + a_n \frac{d^n x(t)}{dt^n} \quad (1)$$

Equation (1) in an operative form (in the frequency area) is:

$$\left(b_0 + b_1 p + b_2 p^2 + \ldots + b_m p^m\right) y(p) = \left(a_0 + a_1 p + a_2 p^2 + \ldots + a_n p^n\right) x(p) \quad (2)$$

Equation (2) leads to the transfer function of the loudspeaker, presented by the ratio between the created sound pressure and the fed level.

$$K(p) = \frac{y(p)}{x(p)} = \frac{a_0 + a_1 p + a_2 p^2 + \ldots + a_n p^n}{b_0 + b_1 p + b_2 p^2 + \ldots + b_m p^m} \quad (3)$$

When we present the numerator and the denominator we get:

$$K(p) = \frac{a_n.(p - p_{a1}).(p - p_{a2}).\ldots.(p - p_{an})}{b_m.(p - p_{b1}).(p - p_{b2}).\ldots.(p - p_{am})} \quad (4)$$

Where p_{a1}, p_{a2},…, p_{an} are roots of the numerator called zeroes of the transfer function, p_{b1}, p_{b2},…, p_{bm} are roots of the denominator called poles of the transfer function [3].

[1]Atanaska A. Angelova is with the Department of Radio engineering, Faculty of Electronics, Technical University-Varna, Studentska Street 1,Varna 9010, Bulgaria, E-mail: lz4hi@yahoo.com

[2]Ekaterinoslav S. Sirakov is with the Department of Radio engineering, Faculty of Electronics, Technical University-Varna, Studentska Street 1, Varna 9010, Bulgaria, E-mail: katio@mail.bg

[3]Georgi K. Evstatiev is with the Department of Radio engineering, Faculty of Electronics, Technical University-Varna Studentska Street 1, Varna 9010, Bulgaria, E-mail: evstatg@mail.bg

II. THEORETICAL BACKGROUND

The coefficient of transition $K(j\omega)$ can be defined by the Fourier transform:

$$\varphi(t) = \frac{1}{2\pi} \int_{-\infty}^{+\infty} x(\omega).e^{j\omega t} d\omega \quad (5)$$

Spectrum thickness [4]:

$$s(\omega) = \int_{-\infty}^{+\infty} \varphi(t).e^{j\omega t} dt \quad (6)$$

or just when we replace it with the complex variable quantity $p = \sigma + j\omega$. Then:

$$K(j\omega) = \frac{y(j\omega)}{x(j\omega)} = \frac{a_0 + ja_1\omega - a_2\omega^2 - ja_3\omega^3 \ldots + a_n(j\omega)^n}{b_0 + jb_1\omega - b_2\omega^2 - jb_3\omega^3 \ldots + b_m(j\omega)^m} \quad (7)$$

$$K(j\omega) = |K(j\omega)|.\exp[j\varphi(\omega)] = \mathrm{Re}(\omega) + j\,\mathrm{Im}(\omega)$$

The module of the transfer function is expressed by:

$$|K(j\omega)| = \sqrt{\mathrm{Re}(\omega)^2 + \mathrm{Im}(\omega)^2} \quad (8)$$

and the phase is expressed by:

$$\varphi(\omega) = arctg\left[\frac{\mathrm{Im}(\omega)}{\mathrm{Re}(\omega)}\right] \quad (9)$$

The amplitude – frequency responses (fig.1-3):

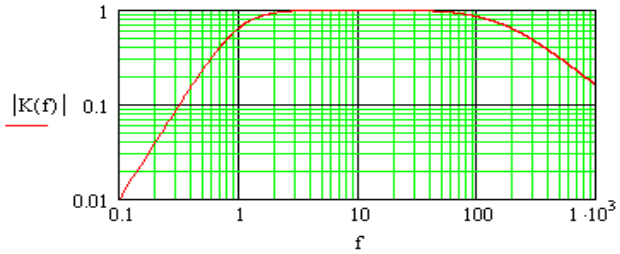

Fig.1 Normalized amplitude – frequency response of the sound pressure created by the loudspeaker

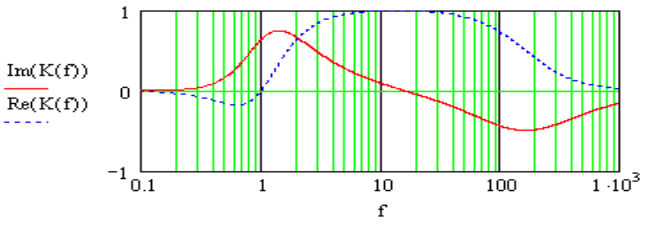

Fig.2 Amplitude – frequency response of the real and the imaginary part

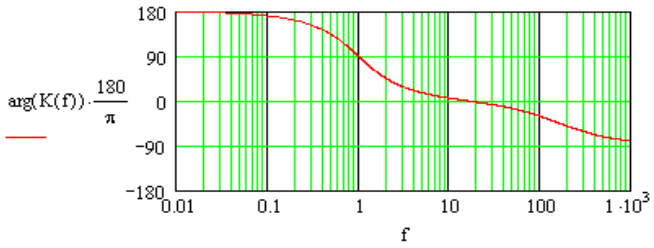

Fig.3 The phase of Amplitude – frequency response

At an analysis of the temporary area, grounded on the impulse response of the loudspeaker g(t) (fig.4) [2] determines the following:

$$g(t) = \frac{1}{2\pi}\int_{-\infty}^{+\infty} \dot{K}(j\omega)e^{j\omega t}d\omega \qquad (10)$$

When we replace the math's expression (7) into (10) we get:

$$g(t) = \frac{1}{\pi}\int_{0}^{+\infty} |K(\varpi)| e^{j(\omega t+\varphi(\varpi))}d\omega$$

$$= \frac{1}{\pi}\int_{0}^{+\infty} \mathrm{Re}(\varpi)\cos\varpi t d\omega - \frac{1}{\pi}\int_{0}^{+\infty} \mathrm{Im}(\varpi)\sin\varpi t d\omega \qquad (11)$$

The simple part is a connection between the real and the imaginary part of the coefficient of transfer:

$$\frac{1}{\pi}\int_{0}^{+\infty} \mathrm{Re}(\varpi)\cos\varpi t d\omega = -\frac{1}{\pi}\int_{0}^{+\infty} \mathrm{Im}(\varpi)\sin\varpi t d\omega \qquad (12)$$

The impulse response has a real and an imaginary part g(t):

$$\mathrm{Re}\, g(t) = \frac{2}{\pi}\int_{0}^{\infty}\frac{\mathrm{Re}(\omega)}{\omega}.\sin(\omega t).d\omega$$

$$\mathrm{Im}\, g(t) = K(0) + \frac{2}{\pi}\int_{0}^{\omega}\frac{\mathrm{Im}(\omega)}{\omega}.\cos(\omega t).d\omega \qquad (13)$$

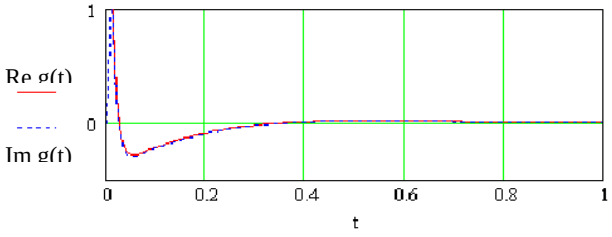

Fig.4 An impulse response

At the computer design of the impulse response it is appropriate to limit the upper border of the integrals to a real cost (fig. 2) at which the graphic images of Re g(t) and Im g(t) for $t > 0$ coincide. The normalized step response with MathCad coincides with the theoretical analysis [1, pp.809, fig.6] and the real results, presented by the producers of loudspeakers.

Since the impulse response g(t) is a reaction of x(t), the transitional response h(t) is designed by the integral of g(t) [2]:

$$h(t) = \int_{0}^{t} g(t)dt\,, \qquad (14)$$

or it is expressed by the transfer function:

$$h(t) = \frac{1}{\pi}\int_{0}^{\infty} K(j\omega).e^{j\omega t}d\omega \qquad (15)$$

If we use the real and the imaginary part, we can present the transitional response with the expressions (fig.5):

$$h(t) = \frac{2}{\pi}\int_{0}^{\infty} \mathrm{Re}(\omega).\cos(\omega t).d\omega$$

$$h(t) = \frac{2}{\pi}\int_{0}^{\infty} \mathrm{Im}(\omega).\sin(\omega t).d\omega \qquad (16)$$

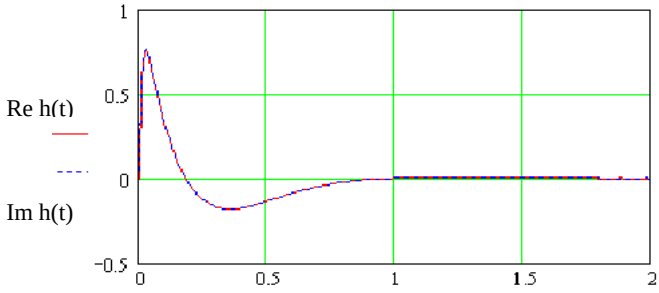

Fig.5 A transitional response

At the computer design of the impulse and the transitional responses, the precision of the graphic design at costs of t at the beginning of the transitional process $t \to 0$, are defined from the chosen step and the computing possibilities of the computer and the program which is used.

CONCLUSIONS

The presented method gives wide opportunities for an investigation of the transitional and the impulse characteristics of the loudspeakers, as well as for a valuation of their qualities and abilities compared with the catalogue data.

REFERENCES

[1] Small R. H., "Closed-Box Loudspeaker Systems Part I: Analysis," J. Audio Eng. Soc.,, vol. 20, Number 10, pp. 798-808, (1972 Dec.).

[2] Poularikas Al. D, *The Handbook of Formulas and Tables for Signal Processing*, CRT Press LLC, 1999.

[3] Angelova Atanaska A., Ekaterinoslav S. Sirakov and Georgi K. Evstatiev, Electrodynamics Loudspeaker described with Band pass' Model , Akustika 2003, TU-Varna, 7 October 2003, Varna, Bulgaria, pp. 38÷43

[4] Sirakov Ekaterinoslav S.,Atanaska A. Angelova and Georgi K. Evstatiev, Transitional characteristics of the Loudspeaker systems, ICEST 2003, 16-18 October 2003, Sofia, Bulgaria, pp 241÷242.

Time-And-Space Filtration By Polarization Of Free Electromagnetic Waves

Georgi D.Nenov[1] and Galina P.Cherneva[2]

Abstract- The paper proposes to use the linear angle polarization for implementing time-and-space filtration. The signals in the form of waves with horizontal polarization are independent from signals, which consist of waves with vertical polarization. The two signals are orthogonal in relation to the real space where the wave propagation takes place. The polarity changes in time under the influence of pseudo-random sequence. Thus the specter is widened and the protection against interferences and non-allowed access is provided.

Key words- polarized wave, noise-like sequences, widened spectrum, switching-able polarization.

The polarization of electromagnetic waves propagating in free space has been used for a long time to divide signals or to filtrate them from interferences caused by other sources. These interferences are often signals from other radio stations. They occupy the same frequency band or a part of it. The division of signals according to frequency or time has been done in order to use one and the same line (medium). The division by linear polarization has been applied in the radio relay lines. The frequency bands are with horizontal or vertical polarization.

The paper proposes to use the linear polarization for time-and-space filtration. The signal in the form of a wave with horizontal polarization is undependable from the signal emitted through a wave with vertical polarization. The two signals are orthogonal in relation to the real space where the waves propagation takes place. Throughout the time polarization is changed under the impact of the pseudorandom sequence. Thus the spectrum is widened and the protection against interferences and unapproved access is provided.

The structural diagram of a radio communication system using the electromagnetic waves polarization for a time-and-space filtration is shown in Fig. 1. The modulation of an appropriate type takes place in the radio transmitter.

The modulated oscillations obtained have been switched in relation to the polarization. In that case switching from horizontal to vertical polarization and vice versa is provided. As a result, the radio waves of relevant polarization have been emitted into the space. The commutation is controlled by a generator of a pseudo-random sequence NLS (Noise-like Signal). The choice of the code sequence is made as it is made with the systems of FH (Frequency Hopping). Its length is of substantial significance. The rapid action of the generator is subjected to transient processes with switching of the modulated high-frequency oscillations. That is determined by the time of transition of displacing register from one condition to another and by the time of signal propagation in the feedback circuit. The time of switching related to the polarization is also in connection with the

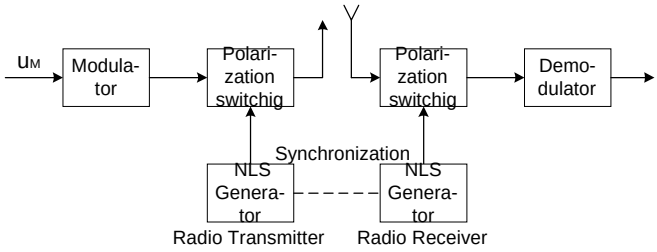

Fig.1

transient process. Both problems are solvable with the means of modern equipment within the microwave band.

The transmitting and receiving aerial are with markedly directed action. That limits the usage of the filtration proposed from the condition of preserving polarization with radio waves propagation. The examination on the process in a more general aspect will probably impose the generalization about a multiple access on the base of polarization and coding, i.e. as a variety of CDMA (Code Division Multiple Access). On its side, it gives a base to consider the radio communication system shown in Fig. 1 as a Spread-Spectrum-System with spreading by polarization switching (PS).

The opposite process takes place in the radio receiving set. First, the spectrum shrinks, then demodulation is carried out. To shrink the spectrum, it is necessary to have available NLS generator for a sequence that is the same as the one used in the radio transmitter. The synchronization of the two sequences is a necessary condition. Various concrete solutions of the problem are possible.

The usage of the linear polarization provides rapid division of the signals, which are emitted into the space in the form of radio waves and correspond to the random code sequence symbols. That is valid for a normal medium of wave propagation. For a complicated situation, it is necessary to develop a precise problem solution supported by a theoretical analysis and experimental confirmation.

The proposed time-and-space filtration is characterized with the following more important peculiarities:

[1] Georgi Dimitrov Nenov is witch the Higher School of Transport, Geo Milev Str.158, 1584 Sofia, Bulgaria
[2] Galina Petkova Cherneva is witch the Higher School of Transport, Geo Milev Str.158, 1584 Sofia, Bulgaria

1. It widens the possibilities of using the frequency resource whose saving is extremely necessary due to the intensive increase of users.

2. The spectrum expansion is a prerequisite to protect it against interferences and some disadvantages with multi-ray radio wave propagation.

3. The usage of random sequences does not admit non-approved access.

4. The effect of filtration depends to a great extent on the conditions of radio wave propagation, as far as they could change the plane of polarization.

The proposed method of time-and-space filtration with switching to linear polarization by a random code sequence can find application in creating radio communication systems with widened spectrum.

REFERENCES:

[1] Hristov, H.D., E.S. Altimirski. Radio Engineering Electrodynamics and Electromagnetic Waves Propagation, Tehnika, Sofia, 1990 (in Bulgarian).

[2] Wideband CDMA Special Issue.IEEE Communications Magazine, vol.36, No 9, September, 1998.

[3] Blake R. Electronic Communication SystemsDelmar-Thomson Learning,2002.

A novel hybrid ARQ scheme using randomly interleaved product codes

Nikolay T. Kostov[1] and Slava M. Yorfdanova[2]

Abstract - **A novel hybrid automatic repeat request (HARQ) scheme using randomly interleaved two-dimensional product codes is proposed. Throughput and bit error rate (BER) performance of the proposed scheme are studied through simulations and compared to the conventional forward error correction scheme.**

Keyword – **Automatic repeat request, product codes, simulation.**

I. INTRODUCTION

The possible implementations of automatic repeat request (ARQ) protocols fall into different categories [1], all of which include automatic requests for retransmission of data that are deemed unreliable by the receiver. A hybrid ARQ (HARQ) scheme [2] uses a forward error correction (FEC) code in conjunction with a retransmission scheme. Typically a cyclic redundancy check (CRC) code is used for frames error detection and this is an example of a so-called two-code approach since two different error control schemes are used for HARQ purpose [3]. Another HARQ method is the so-called one-code approach since only one error control code is used to identify some sort of reliability information within the decoding process that can be used to determine whether a retransmission is needed or not [4].

In this paper a novel one-code approach HARQ scheme based on randomly interleaved product codes (RIPC) is proposed. The performance (throughput and bit error rate) of the proposed HARQ scheme on additive white Gaussian noise channel (AWGN) is studied through simulations and compared to the conventional forward error correction scheme.

II. SYSTEM MODEL

Let us first consider the encoding/decoding processes of the conventional randomly interleaved product code (RIPC) [5]. The data frame to be transmitted (a square block of $(n-1)\times(n-1)$ bits) is first encoded by the component single parity check codes of a single two-dimensional product code (2D-PC), then it is randomly interleaved end re-encoded by the same 2D-PC. The overall RIPC is composed from the original data bits and all parity bits from the single parity check codes. The code rate R_c of the considered RIPC is

$$R_c = \frac{(n-1)^2}{2n-(n-1)^2}, \qquad (1)$$

where n is the length of the component single parity check codes and $(n-1)^2$ is the number of information bits in the encoded frame. Now, consider binary phase shift keying (BPSK) transmission via an AWGN channel. The decoding process is as follows: the original (non interleaved) noisy frame is first decoded using a soft-input/soft-output (SISO) decoding method [6] for a single decoding cycle, then the interleaved data frame is SISO decoded also for a single decoding cycle and so on. The two constituent decoders exchange the so-called extrinsic information (the error correction term gained from the decoding) at each full iteration and the decoding iterations are executed until a predetermined stopping criteria is satisfied. The final soft decision Λ_i of the *i*th data bit is given by

$$\Lambda_i = L_i^{ch} + L_i^1 + L_i^2, \qquad (2)$$

where L_i^{ch} is the noisy channel observation for the *i*th data bit and L_i^1, L_i^2 are the extrinsic information terms from the first and second decoder, respectively. The corresponding hard decision a_i of the *i*th data bit is

$$a_i = \begin{cases} 1, \; if \; \Lambda_i > 0 \\ 0, \; if \; \Lambda_i < 0. \end{cases} \qquad (3)$$

Let us now consider the proposed HARQ based on the described RIPC. The decoding algorithm is as follows:

1. Apply SISO iterative decoding (with a predetermined maximum number of iterations) on the received RIPC frame, checking all parity equations of the component single parity check codes after each full iteration. If all parity equations are satisfied (e.g., the stopping criterion is fulfilled) go to 3. Else go to 2.
2. Request a retransmission of the decoded frame by sending a negative acknowledgement to the transmitter via the feedback channel. If the maximum number of retransmissions is reached, go to 3.
3. Output hard quantized data.

It can be observed that with this decoding algorithm the frame error detection (and consequently the retransmission request) in the proposed HARQ is based on the single parity check equations satisfaction of the overall randomly interleaved product code. Because of the random interleaving, a significant improvement in terms of undetected erroneous frames rate can be expected for the considered error control scheme as compared to the conventional two-dimensional product codes. Further, using the proposed HARQ scheme an overall performance improvement in terms of post-decoded bit error rate (BER) and frame error rate (FER) can be obtained as compared to the RIPC alone.

[1]Nikolay T. Kostov is with the Technical University of Varna, Department of Radio engineering, Studentska Street 1, Varna 9010, Bulgaria, E-mail: n_kostov@mail.bg

[2]Slava M. Yordanova is with the Technical University of Varna, Department of Computer Science and Technologies, Studentska Street 1, Varna 9010, Bulgaria, E-mail: slava_yordanova@mail.bg

III. PERFORMANCE RESULTS

A MATLAB-based Monte Carlo simulation was executed in order to estimate the performance of the considered HARQ scheme. The simulation of the considered error control scheme assumes BPSK signaling over an additive white Gaussian noise (AWGN) channel with at most two retransmissions allowed end error-free feedback channel. Two HARQ schemes were studied: HARQ1 with parent code rate $R_c \approx 3/4$ and HARQ2 with parent code rate $R_c \approx 4/5$. The normalized effective throughput R_{eff} of the HARQ scheme is defined in this paper as

$$R_{eff} = \frac{R_h}{R_c}, \quad (4)$$

where R_h is the HARQ scheme code rate at a given signal-to-noise ratio (SNR) and R_c is the parent scheme (e.g., the randomly interleaved 2D-PC) code rate. Notice that $R_h \le R_c$ and $R_{eff} = 1$ only in case of no retransmissions. The retransmission efficiency R_{ret} (at a given SNR) of the proposed HARQ scheme can be defined as

$$R_{ret} = \frac{N_s}{N_s + N_u} \times 100 \quad [\%], \quad (5)$$

where N_s is the total number of successful retransmissions and N_u is the total number of accepted erroneous frames including undetected bad frames. The retransmission efficiency versus the SNR of the considered HARQ schemes is shown in Figs. 1.

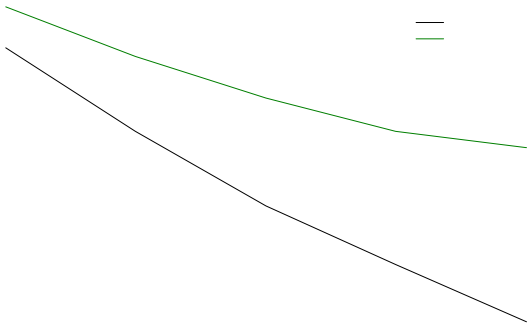

Fig.1. Retransmission efficiency versus the SNR of the HARQ1 end HARQ2 schemes.

According to Fig.1 the retransmission efficiency of the HARQ2 scheme is significantly better than those of the HARQ1 scheme over all range of SNRs of interest. This is due to the better post-decoding frame error rate of the HARQ2 scheme as a result of the larger frame size and interleaving used. It should be mentioned that there is a threshold SNR value of about 4.0 dB over which both HARQ schemes start to outperform the corresponding parent codes. The required SNRs for the HARQ schemes to achieve typical bit error rates (BERs) are shown in Table I. In Table I the BER performance of the parent codes is also given.

TABLE I

ESTIMATED HARQ AND RIPC SCHEMES PERFORMANCE

	HARQ1	RIPC1 $R_c \approx 3/4$	HARQ2	RIPC2 $R_c \approx 4/5$
SNR(dB) for $BER = 10^{-5}$	4.75	5.25	4.25	4.85
SNR(dB) for $BER = 10^{-6}$	5.3	5.8	4.85	5.5

As can be observed from Table I, a coding gain of at least 0.5 dB is obtained with the considered HARQ schemes over the conventional RIPC schemes. Another coding gain of approximately 0.5 dB can be obtained by using higher rate HARQ2 scheme instead of HARQ1 scheme. At $BER \le 10^{-5}$ the normalized effective throughput R_{eff} of both HARQ schemes is close to one (e.g., $R_h \approx R_c$) because of the small overall number of retransmissions.

IV. CONCLUSION

In this paper a novel one-code approach HARQ scheme is proposed. A coding gain of 0.5 dB or higher is obtained over the corresponding parent FEC schemes with practically no bandwidth expansion for moderate-to-high SNR values. The BER performance of the considered HARQ schemes is dominated by the undetectable erroneous frames and no significant performance improvement can be expected with more than two retransmissions allowed.

REFERENCES

[1] S. Lin, D. J. Costello Jr. and M. J. Miller, "Automatic-repeat-request error control schemes", IEEE Communications Magazine, vol. 22, no. 12, pp. 5-16, December 1984.

[2] J. M. Wozencraft and M. Horstein, "Coding for two-way channels", Research Laboratory of Electronics, MIT, MA, Technical Report 383, 1961.

[3] S. Lin and D. J. Costello Jr., *Error Control Coding: Fundamentals and Applications*, Prentice-Hall, Inc., N.J., 1983.

[4] H. Yamamoto and K. Itoh, "Viterbi decoding algorithm for convolutional codes with repeat request", IEEE Transactions on Information Theory, vol. 26, no.5, pp.540-547, September 1980.

[5] D. Rankin and T. A. Gulliver, "Randomly interleaved SPC product codes", in Proc. ISIT, pp. 88 Sorrento, Italy. June 2000.

[6] B. Sklar, "A primer on turbo code concepts", IEEE Communications Magazine, pp. 94-102, December 1997.

Algorithm And A C++ Program For CCS Of Binary Sequences With Primary Lengths

Dimitar M. Kovachev[1], Ventsislav Valchev[2], Ekaterina Dimitrova[2]

Abstract **- This paper focuses on the calculation of cross-correlation functions of binary sequences with maximal length, precisely in the case when lengths are prime numbers. Algorithm has been developed and C++ program has been written and its performance has been compared with those of a convolution and a DFT. The results have been discussed. The programs developed have been used in a program generator for FPGA-based generators of MS.**

Keywords**: FPGA, PRS, DFT**

I. INTRODUCTION

The sequences with a maximum length (M-sequences, or MS) are widely used in radio-location for creating signals with a complex shape [1], in different audio and acoustic measurements [2], in systems of wireless communication [3] and so on.

Their main advantage is excellent auto-correlation properties - binary auto-correlation function (ACF) with a single maximum, surrounded by side lopes with an insignificant level [4.]:

$$\vartheta(k) = \begin{cases} N, \rightarrow k \equiv 0 \bmod N, \\ -1, \rightarrow k \not\equiv 0 \bmod N. \end{cases}, \qquad (1)$$

where N denotes the length of the sequence, $\vartheta(k)$ - the value of ACF at shift k.

If we denote two MSs as vectors $\boldsymbol{x_i}$ and $\boldsymbol{x_j}$, their periodic cross-correlation function (CCF) is received after (2):

$$\vartheta_{ij}(k) = N - 2w(x_i \oplus T^k x_j) \qquad (2)$$

where $w(\bullet)$ is the weight of the vector after Hemming (the number of ones in it), T^k is an operator for k-multiple cyclic shift to the right [4].

If $A_k = A(x_i, x_j)_k$ denotes the positions in which vectors x_i and $T^k x_j$ coincide, and $D_k = D(x_i, x_j)_k$ - the number of their non-coincidences, thus:

$$\vartheta(k) = A_k - D_k, \qquad (3)$$

In most practical applications, a binary sequence is actually transmitted as a sequence of unit amplitude, positive and negative pulses, obtained by replacing each 1 by a –1 and each 0 by a +1. As the expression (2) is suitable only for cases with binary sequences of {0,1}, the most commonly used expression to determine ACF and CCF in engineering literature is (3) [4]. (3) is often calculated by convolution for short sequences, but with the increase of length the time for defining CCF significantly increases. In such cases it is usual to move to the frequency area and use fast convolution.

[1] Dept. of Electronics, Technical University of Varna 9010, Bulgaria, E-mail: dimiter_98@yahoo.com

[2] Dept. of Electronics, Technical University of Varna, 9010, Bulgaria

When processing necessitates the calculation of the periodical CCF of two different MSs, as it is during the correlation processing of the reflections from moving targets, the maximum value of CCF is more significant than its particular values.

One of the possibilities to define CCF is by fast convolution [5], using the direct and reverse discrete Fourier transform (DFT). But when the MS length is a prime number, the calculation time greatly increases (the square of the length). That is why it is necessary to design special algorithms for these cases.

The paper treats an algorithm and a program for determination of the CCF values for MSs with lengths of a prime number by using the Rader conversion.

The response time is estimated in relation to the direct application of DFT. The program has been used as part of programming system for generating FPGA-based (Field Programmable Gate Array) generators of MSs, whose CCF has values lower than the pre-set limiting value.

II. SETTING THE TASK

The calculation of ACF or CCF of MSs differs merely because in the second case two different sequences are used. Hence, the calculation procedure is completely equivalent, the difference lays in the preparation of the input data. For that reason the procedure execution can be carried out despite its particular designation.

On the other hand, in this case not the particular values of CCF are to be considered, but the achieved maximum value. At the same time CCF receives relatively small number of different values. In order to facilitate the processing and discussion, and - on analogy with [4] - for the purposes of compact writing, we introduce the *spectrum of CCF*, and it means different values, included in CCF, and the number of their appearance. The developed algorithm and the program of its implementation are used to extract sets of MSs when the CCF determination is combined with the process of determining their spectrums, denoted as cross - correlation spectrums (CCS).

Therefore, in order to determine CCS we have to define the CCF of both sequences, and after that to count the number of its appearances for each received value.

During the CCF calculation, the operation of convolution is realized as multiplication of Fourier transforms of the involved sequences. For that purpose it is done within the frequency area by element-by-element multiplication of the two Fourier representations and then the CCF is found by a reverse Fourier transform.

III. SOLVING THE TASK

In order to work out the calculations in the frequency area 2 algorithms have been implemented, taking into

consideration the fact, that the length N of the MS cannot be a power of 2.

The first algorithm is implemented as a Fourier transform for compound lengths. A C-program version [6] has been used as a basis, then it has been revised considering the particular peculiarities - multiple cyclic usage of one and the same lengths, usage of one and the same algorithm for direct and reverse transform and so on. If N is non-factorable (i.e. it is a prime number) the program realizes DFT, whose number of operations is O(N^2).

Since the time of the algorithm operation increases significantly for big lengths, that are prime numbers, a version has been developed and implemented, in which a Rader method [7] is applied for DFT with a length of N (N is a prime number) by cyclic convolution for the length $N_1 = N - 1$.

As it is known [5, 6, 7], if the length N of DFT can be presented as $N = N_1 N_2$, where N_1 and N_2 are mutually prime numbers, DFT can be put down as (4):

$$y[k] = \sum_{n=0}^{N-1} x[n]\xi^{nk} \Rightarrow y[k_1 + N_1 k_2] =$$

$$= \sum_{n_2=0}^{N_2-1} \xi^{k_1 n_2} \left[\sum_{n_1=0}^{N_1-1} x[N_2 n_1 + n_2] \xi_1^{k_1 n_1} \right] \xi_2^{k_2 n_2}, \qquad (4)$$

where : $\xi_1 = \xi^{N_2}$ are primitive roots of unit from order N_1 and N_2; $n = N_2 n_1 + n_2$ and $k = N_1 k_2 + k_1$ can be obtained by using the algorithm for the remainders [5], that gives us the correspondence:

$$\begin{array}{ccc} n & \Leftrightarrow & (n_1, n_2) \\ 0 \le n < N & & 0 \le n_1 < N_1 \quad 0 \le n_2 < N_2 \end{array}.$$

Starting from this record, but for the non-factorable length, we observe $(\xi^k)^n$ as a sequence with a length of N, that can be put down as a series after the powers of ξ, i.e. as in (5), then the DFT is defined by the equation (6).

$$\varsigma = \{\xi^j\}, \; j \in \{0, N-1\} \qquad (5)$$

$$y[k] = \sum_{n=0}^{N-1} x[n]\varsigma[kn \bmod N] \qquad (6)$$

If we choose r to be a primitive root of N, then the sequence (7) is a set of numbers $\{1, N-1\}$, i.e.:

$$\{r^0, r^1, ..., r^{N-2}\} \qquad (7)$$

In this case the sequence (5) can be reordered in (8):

$$\zeta = \{\xi^{r^k}\}, \; r = \{0, N-2\}. \qquad (8)$$

Except the element 1, the sequences (5) and (8) are the same, but just reordered. If we put down:

$$n = r^{-m} \bmod N, \; k = r^s \bmod N \qquad (9)$$

and use the Fermat's theorem, according to which

$$r^{-m} \bmod N = r^{N-1-m} \bmod N, \qquad (10)$$

we can rewrite DFT as (11):

$$Y_c[s] = x[0] + (x_c[m] \otimes \zeta[s-m]) \bmod (N-1), \qquad (11)$$

where $x_c[m] = x[r^{-m} \bmod N]$, $\otimes$ denotes cyclic convolution with a period $(N-1)$ and $Y_c[s] = Y[r^s \bmod N]$.

Therefore, the received in such a way $Y_c[s]$ consists of the elements of the searched $Y[k]$, but in a permuted order (sequence ζ is used for the re-arrangement). Only the value of $Y[0]$ is defined on its own by $Y[0] = \sum_0^{N-1} x[n]$.

The algorithm for DFT implementation at lengths of sequences - prime numbers is shown in Figure 1 and it has been developed following the above mentioned formulae.

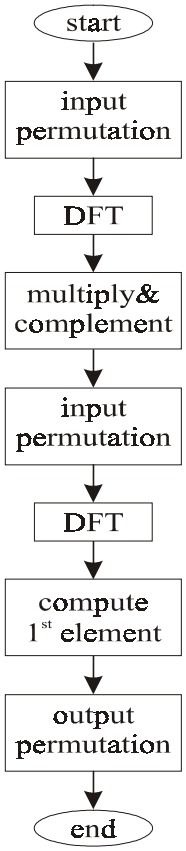

Fig.1. Prime-Factor Algorithm (PFA)

Since the purpose of our investigation is to calculate CCS of the sets of MSs, permutations of the input and output data are implemented once, not in the shown algorithms, and the received re-arrangements are used for re-addressing of the given input data, which accelerates the processing.

The particular implementation is used for finding the CCS, which allows reporting a number of specific peculiarities, such as the necessity of multiple processing of DFT of different sequences, but at the constant length. In this case the processes of factorization and re-arrangement at the input and output (that is compulsory at moving from linear to cyclic convolution and vice versa) are implemented as a common procedure to a certain extend. Figure 2 shows the designed and implemented algorithm for defining CCS.

The designed programs are included as part of a program system for defining FPGA-based generators of MS [8]. Table 1 contains the received results for the response time of a particular C++ implementation of PFA, together with those, obtained during the calculation of the same CCS but by a direct convolution, as well as by DFT.

TABLE 1
TIME FOR CALCULATING CCS

Time / Length	Convolution	DFT	PFA
7	0.015873	0.015873	0.016369
15	0.015873	0.015873	
31	0.015873	0.015873	0.016369
63	0.015873	0.015873	
127	0.015873	0.016865	0.016865
255	0.016865	0.016865	
511	0.020833	0.020337	
1023	0.034226	0.022321	
2047	0.0899	0.038075	
4095	0.3	0.042512	
8191	1.18333	4.933333	0.12949
16383	4.83333	0.275	
32767	19.7333	0.616667	
65535	77.7857	1.733333	
131071	308	*	5.875

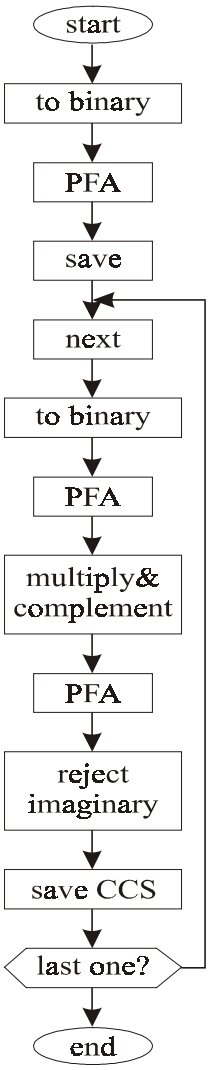

Fig.2. Cross-Correlation Spectrum Algorithm

The calculations are carried out on a computer with a Pentium IV processor, 1.8GHz, 512MB RAM. Symbol "*" denotes quite a long time (considerably increasing that in the previous column). The blank fields are for the lengths, which are not prime numbers.

IV. RESULTS

These data leads us to the conclusion that during the calculation of the mentioned MCS, the response time of the implementation (i.e. at which the calculations are carried out by the help of direct convolution) is comparable with that of the frequency one up to the lengths of $N = 2^{10} - 1 = 1023$. The times for small lengths are almost equal, which is obviously due to the implemented common auxiliary activities – data preparation, defining of the spectrum and sorting its values, file operations, etc.

The actual time for small lengths is much shorter, but it requires averaging in a great number of spectrums for its defining, and during that the number of file operations, operations of dynamic reserve and memory release increases.

V. CONCLUSION

An algorithm for DFT calculation for lengths of prime numbers has been designed and implemented. It has been applied in a designed and implemented algorithm for CCS calculation of MS sets.

The response time of the designed algorithms is compared to the results from the implementation of the same calculation operations, but with the use of convolution and DFT with an factorization of the length. The expected decrease in the time for calculation for cases in which the lengths of MS are non-factorable (prime) numbers is obtained.

The implementations are in a programming C++ language and are incorporated in the designed programming system for automated synthesizing of FPGA-based generators of MS.

REFERENCES

[1] M.I. Skolnik (editor in chief) – RADAR Handbook, 2nd edition, McGraw-Hill, Inc, 1990

[2] N. Xiang, M.R. Schroeder – Reciprocal maximum-length sequence pairs for acoustical dual source measurements, J.Acoust. Soc. Am. 109, 2001, pp.2418

[3] T. Rapparport - Wireless Communications: Principles and Practice, Prentice–Hall Inc., 1996

[4] Д.В.Сарвате, М.Б.Персли – Взаимно-корреляционные свойства псевдослучайных и родственных последовательностей, ТИИЭР, т.68, 5, 1980

[5] R. Tolimieri, M. An, Ch. Lu – Algorithms for Discrete Fourier Transform and Convolution, 2bd Ed., Springer-Verlag, New York, Inc., 1997

[6] http://hjem.get2net.dk/jjn/fft.htm

[7] H.J. Nussbaumer – Fast Fourier Transform and Convolution Algorithms, New York, Springer-Verlag, 1982

[8] Dimitar M.Kovachev - A Method for Automated Synthesis of FPGA-based Generators of Non-intersected Sets of M-sequences, IJCI Proceeding of International Conference on Signal Processing, ICSP 2003, ISSN 1304-2386, Volume 1, Number 2, Sept. 2003, pp:76-81, Canakkale, Turke

Sampling factors and amplitude errors during the sinusoidal and cosinusoidal signal conversion

Petre Tzvetanov Petrov

Abstract**: It is discussed a new approach to amplitude errors calculation during the analog to digital signal conversion due to non sampling the analog signal into its maximal value and in particular during the sinusoidal and co-sinusoidal signal conversion. Formulas for calculating the sampling factor, the sampling frequency Fd and the converter bits n are given.**

Keywords**: amplitude errors, sinusoidal and cosinusoidal signal conversion, sampling factor N**

I. Introduction

The conversion of the analog signal into digital codes and the conversion of the digital codes into analog signals (or more precisely conversion of the analog signal into analog staircase function) are two of the most important problems during the digital signal processing. In order to resolve these problems a number of parameters should be calculated. In this paper we will concentrate on calculating the sampling factor N, sampling frequency Fd and number of converters bits n in order to obtain a given accuracy or amplitude error.

II. Sampling factor N=Fd/Fs

We will introduce a parameter called "sampling factor" ("encoding factor" or "dicsretization factor") with the formulas:

1. For sinusoidal signal (SS) or cosinusoidal signal (CS)

$$N=Fd/Fs>0 \text{ or} \quad (1)$$

2. For band wide signal

$$N=Fd/Fmax>0 \quad (2)$$

Where

Fd is the discretization (sampling, encoding) frequency

Fs is the signal frequency (in this case the frequency of the SS or CS)

Fmax is the maximum frequency of interest in the signal band

Petre Tzvetanov Petrov in an engineer in radio-electronics with "Microengineering"-Sofia, Bulgaria. Emails: ppetre@caramail.com и ptzvp@yahoo.fr.

In the present paper we will deal with sampling factor N=Fd/Fs>=2 because the evaluation of the errors and the reconstruction of the sampled signal is simpler that in the case with N<2.

III. Basic test analog signals and theirs parameters

The basic analog test signals in the electronics are: direct current (DC), SS, CS, triangular, trapezoidal and rectangular (usually with Thighlevel=Tlow level=0.5*Tperiod) signals.

We will discuss the amplitude error during the SS and CS signals conversion into digital codes with ADC, because with acceptable from the practical point of view accuracy most of the analog signals could be considered as an algebraic sum of DC, SS and CS signals. Moreover, the SS and CS are the basic alternative current (AC) test signals.

As it is well known the SS and CS with DC component are characterized with five basic "parameters": amplitude Am, function (sinus or cosinus), frequency (F or ω), phase (φ) and direct current component B and are given with the followings equations:

$$A = Am * \sin(2*\pi*F*t+\varphi)+B \quad (3)$$

$$A = Am * \cos(2*\pi*F*t+\varphi)+B \quad (4)$$

There are two main approaches for analog signal reconstruction from its digital samples:

- Mathematical approach. The parameters of the analog signal are calculated using mathematical methods (models) from the digital samples. Additional points (samples) could be calculated and then the signal is reconstructed. In order to simplify the problem we will admit that the function, represented with the signal (sinus or cosinus in particular) is known. In this case in order to find the four basic parameters Am, F, φ and B a system with four unknowns and four equations should be resolved and a set of four samples A1, A2, A3 and A4 during one period should be used:

$$A1 = Am * \sin(2*\pi*F*t+\varphi)+B \quad (5)$$

$$A2 = Am * \sin(2*\pi*F*t+\varphi)+B \quad (6)$$

$$A3 = Am * \sin(2*\pi*F*t+\varphi)+B \quad (6)$$

$$A4 = Am * \sin(2*\pi*F*t+\varphi)+B \quad (7)$$

- Direct approach. During the direct signal reconstruction the digital samples (codes) are send directly to the DAC and the produced signal (the analog staircase function) or the "copy" is compared with the "original" analog signal at the ADC input.

In this paper we will use the second approach because it is simple, useful and easy for implementation in electronic equipment.

If the function of the signal (for example sinus or cosinus) is known only four basic "parameters" of the signal will be converted into digital codes and it could be estimated that at least four samples during one period are needed for direct reconstruction of SS or CS (Table 1).

Table 1.
Supposition about the minimum number of samples for arithmetic calculation of "parameters" of the sinusoidal and cosinusoidal signals

"Unknown parameters"	Formula for SS	Nmin
Amplitude, frequency, phase, direct current component B	A = Am * sin (2*π*F*t+φ)+B	4
Amplitude, frequency, phase	A = Am * sin (2*π*F*t+φ)	3
Amplitude, frequency	A = Am * sin (2*π*F*t)	2
Amplitude	A = Am * const	1

Notes: 1. (*) With enough amplitude of the samples.
2. Nmin =Fdmin/Fs= supposed minimal number of samples per period to reconstruct directly signal "parameters".

It should be noted that the staircase approximation of the analog signal during the analog to digital conversion depends on three basic factors: 1/ the sampling factor N=Fd/Fs, 2/ the number of the converters bits and 3/ the angle of the first sample φ0.

Moreover, the analog to digital converter could be called "Analog to Staircase Function Converter/Approximater" (ASFC or ASFA) and the block built by an analog to digital converter and a digital converter could be called "Analog to Analog Staircase Function Converter" (AASFC).

IV. Calculating the maximum amplitude error during the SS and CS conversion

When we know the sampling factor N we could calculate the maximum possible amplitude error Emax, and when we have the maximum allowed amplitude error Emax during the signal conversion we could calculate the sampling factor N=Fd/Fs. This "bi-directional" approach is illustrated with the formulas illustrated in the Table 2.

Table 2.
The "bi-directional" relation between the sampling factor N=Fd/Fs and the maximum amplitude error Emax when sampling sinusoidal and cosinusoidal signal.

Analog Signal	Sampling factor N=Fd/Fs
SS	N= 180(90-arcsin(1-Emax))>=2
CS	N= 180/arccos (1-Emax) >=2
	Amplitude Error Eamax
SS	1>=Emax = (1-sin(90-(180/N))>=0.
CS	1>=Emax = (1-cos (180/N))>=0.

Note: The formulas are valid for SS and CS with N>=2 and with an ideal converter. When N<2 a different approaches should be used.

Once the sampling factor N is calculated it is possible to calculate the sampling frequency Fd with the formula

$$Fd = N*Fmax = N*Fs \qquad (8)$$

The utility of the formulas given in Table 2 could be seen in Table 3 and Table 4.

Table 3.
The relation between the maximum amplitude error Emax and the sampling factor N=Fd/Fs from 2 to 5 with step 1 during the SS or CS conversion with ideal ADC (φd/2=αmax)

N	φd	A(αmax)	A(αmax) %	Emax[%]
2.0(!)	180	0	0	100 (!)
2.1	171.4	0.0747	7.47	92.5
2.2	163.6	0.142	14.2	85.8
2.3	156.5	0.203	20.3	79.1
2.4	150	0.259	25.9	74.1
2.5	144	0.309	30.9	69.1
2.6	138.5	0.355	35.5	64.5
2.7	133.3	0.396	39.6	60.4
2.8	128.6	0.434	43.4	56.6
2.9	124.1	0.468	46.8	53.2
3.0	120	0.50	50	50
3.1	116.1	0.529	52.9	47.1
3.2	112.5	0.556	55.6	44.4
3.3	109.1	0.581	58.1	42
3.4	105.9	0.603	60.3	39.7
3.5	102.9	0.623	62.3	37.7
3.6	100	0.643	64.3	35.7
3.7	97.2	0.661	66.1	33.9
3.8	94.7	0.677	67.7	32.3
3.9	92.3	0.693	69.3	30.7
4.0 (!)	90	0.707	70.7	29.3 (!)
4.1	87.8	0.721	72.1	27.9
4.2	85.7	0.733	73.3	26.7
4.3	83.7	0.745	74.5	25.5
4.4	81.8	0.756	75.6	24.4
4.5	80	0.766	76.6	23.4
4.6	78.3	0.776	77.6	22.4
4.7	76.6	0.785	78.5	21.5
4.8	75	0.793	79.3	20.7
4.9	73.5	0.801	80.1	19.9
5.0	72.0	0.809	80.9	19.1

Notes: 1/ When N=2 Emax could be from 0% to -100%.
2/ When N=4, Emax could be from 0% to –29.3%.

According the Table 2 it easy to calculate the sampling factor N when the maximum amplitude error Emax is known and vice versa. In Table 2 and Table 3 the following abbreviations are used:

- N =Fd/Fs is the sampling factor
- φd=360/N is the sampling angle (the angle between two successive samples)

- φd/2=αmax =360/(2*N) is the angle of the maximum deviation from the maximal value of the SS or CS (the angle of the maximal amplitude error Emax)
- A(αmax) – is the maximum value of the guaranteed digital code (sample) when a converter with infinity number of bits (n→ ∞) and with the conversion error equal to zero (Eadc=0 or Edac=0) is used.
- A(αmax) % is A(αmax) in percentage of the maximum value (100%) of SS or CS
- Emax[%] = 100% - A(αmax)% is the maximum amplitude error or the maximum deviation from the maximal value of the sampled SS or CS

Table 4.
The relation between Emax and N=Fd/Fs with step 2 to 39 with step 1.

N from 2 to 19			**N from 20 to 39**	
N	Emax [%]		N	Emax [%]
2	100		21	1.11
3	50		22	1.02
4	29.3		23	0.9314
5	19.1		24	0.856
6	13.4		25	0.789
7	9.9		26	0.729
8	7.61		27	0.676
9	6.09		28	0.629
10	4.89		29	0.586
11	4.05		30	0.548
12	3.40		31	0.513
13	2.91		32	0.482
14	2.51		33	0.453
15	2.18		34	0.427
16	1.92		35	0.403
17	1.70		36	0.381
18	1.51		37	0.360
19	1.36		38	0.342
20	1.23		39	0.324

V. Calculating number of converters bits

Is was found that when the sampling factor N for SS or CS is know and 2<N<64 we could calculate approximately the number of converters bits in order the converter to be considered as an "ideal converter" with the following formula:

$$n1>=\lg(N)+2=\lg(Fd/Fs)+2, [bit] \quad (9)$$

where lg is a logarithm in base 2.

When the amplitude error Emax (0<Emax<1) is known a more general formula given below could be used to calculate the minimum number of converter's bits in order the converter to be considered as an "ideal converter"

$$n2>=\lg(1/Emax)+2, [bit] \quad (10)$$

When signal to noise ratio (SNR) is known in decibels the well know formula for calculating the number of converters bits could be used

$$n3>= (SNR-1.76)/6.02, [dB] \quad (11)$$

When we could apply all of the three approaches mention before we should choose the maximum possible value of n, according to the formula:

$$n>=max(n1,n2,n3) \quad (13)$$

VII. A general approach for calculating the sampling factor N

Because SS and CS have five basic "parameters", we could say that five basic errors are introduced during the signal conversion:

- amplitude error Ea,
- function error Efn,
- frequency error Efr,
- phase error Eφ,
- direct current error Edc (Normally, Edc=0 when N=Fd/Fs=4*k, k=1, 2, 3, ...).

In order to calculate the total conversion factor N=Fd/Fs we could apply the following approach:

- We are evaluating the five basic errors: amplitude errors Ea, frequency error Efr, function error Efn, phase error Eφ and the direct current error Edc for the purposes of the application.
- We are calculating the five sampling (conversion) factors: amplitude sampling factor Na, function sampling factor Nfh, frequency sampling factor Nfn, phase sampling factor Nφ and direct current error sampling factor Ndc according to the corresponding errors.
- We are calculating the total sampling factor N total as a maximal value of the five sampling factor calculated before

  $$Ntotal= max(Na, Nfn, Nfr, N\varphi, Ndc) \quad (14)$$
- We are calculating the sampling frequency Fd according to the formula Fd=Ntotal*Fs.

The method discussed above is guaranteeing that the conversion error for each of the parameter is less than the limiting values (Ea, Efn, Efr, Edc and Eφ).

VIII. Conclusion

The paper is giving simple and practical approach for calculating during the SS and CS conversion several important parameters:

- the sampling factor N=Fd/Fs;
- the maximal amplitude error Emax due to non sampling the SS/CS into its maximal value;
- the sampling frequency Fd;
- the minimal number of converters bits n, in order to consider the converter as "an ideal converter" (in order to neglect the converter's error and to keep only the error from the sampling factor N=Fd/Fs).

The equations given in Table 2 are useful for evaluating the maximum amplitude error Emax when sampling a SS and CS analog signal which is not possible with the Theorem of Shannon-Kotelnikov-Whittaker.

Moreover, we have found that sampling factor N=Fd/Fs=4 is guaranteeing a maximum difference between the amplitude of the "original" SS or CS and corresponding maximal digital code (the produced approximated staircase function by the ADC) less than –29.3% or –3dB.

It is important to note that the maximal amplitude error E(N,n) and the root-mean-square error E(N,n)rms during the analog to digital (or staircase function) depends on two principal factors:

- the error E(N) from the sampling factor N=Fd/Fs;
- the error E(n) from the finite number of bits into the digital word n.

We could give the following two formulas:

$$E(N.n)max = E(N)+E(n) \quad (15)$$

and

$$E(N.n)rms = sqr(E(N)*E(N)+E(n)*E(n)) \quad (16)$$

The method and equipment for sampling and direct signal reconstruction is described in [1]. Several practical circuits with ADC and DAC are published in [2]. The theorem of Shannon-Kotelnikov-Whittaker may be found in many sources, e.g. [3 and 4].

IX. References

1. Petre Tzvetanov Petrov, Method and equipment for sampling and direct reconstruction of analog signals. Printed in Technical University-Sofia. 2003. Bulgaria.
2. Petre Tzvetanov Petrov. More than 111 electronic circuits. Sofia. Tehnika. 2001. Bulgaria.
3. C.E. Shannon. A mathematical Theory of Communication. The Bell System Technical Journal. Vol. 27, pp. 379-423, 623-656, July, October 1948. USA.
4. Oppenheim A.V., A.S.Willsky, I. T. Young., Signals and systems. Prentice-Hall, Inc., 1983 (Chapter 8). USA.

Equipment for Direct Digital Synthesis of Synchrounous Analog Test Signals.

Petre Tzvetanov Petrov

Abstract: **The paper is giving description of equipment for direct digital synthesis of synchronous analog signals with staircase function approximation. The board is EPROM-based with two 8-bits DACs and could generate simutaneously two analog signals with sampling factor N=Fd/Fs from 1 to 256. Also, it is producing up to 32 diffrenent preprogrammed test signals. Moreover, a set of synchronous pulses produced by additional board could be generated. Several bords with common clock and reset could be used to generate more than two synchronous analog test signals. The equipment is build for educational, research and testing purposes.**

Keywords: **direct digital synthesis of analog signals**

I. Introduction and advantages of the method

Sometimes during the testing of electronic equipment it is necessarily to generate simultaneously and sinchronously two analog test signal, eg. sinusoisdal signal (SS) and cosinusoidal signal (CS) or a SS with frequency F and SS with frequency 2*F, etc. One of the simpest and chipest method to do that is with the so-called method of "direct digital synthesis of analog signals" (DDAS). With this method the samples are directly read from a table and then put into a DAC data register without any additional calculations.

The method has the following advantages compared to the analog signal generation:

1. High precision and predictability of all parameters of the generated signal (frequency, amplitude, phase, total harmonic distortion (THD), intermodulation distortion (IMD) etc.)
2. Opportunity to generate almost every analog signal given by a formula or a table with digital codes.
3. Changing of all parameters of generated analog signal in a large scale.
4. Fully programmability of all parameters.
5. The equipment is useful for automatic test or control equipment.
6. Programmable and controlable spectrum of the produced analog signal.

Petre Tzvetanov Petrov is mith Microengeneering-Sofia, Bulgaria. Emails: ppetre@caramail.com , ptzvp@yahoo.fr

7. Large band of generated analog signals (from direct current to megahertz).
8. Possibility of simultaneous and synchronous independent generation of many analog signals.
9. The equipment based on the method is simple and low cost and could have a lot of implementations based on different programmable components.
10. The equipment is useful as a programmable function generator.
11. The equipment could be used as a prototype for building specialized programmable boards, blocks and integrated circuits.
12. The DDAS is the fastest possible digital method for analog signal generation because the programmable synchronous counter is the fastest programmable digital processor, for addressing a table with signal data.

All these advantages and many others are the main raisons to develop and implement several digital boards for DDAS and one of them is discussed in this article.

II. General description of the method and the board

The discussed board for DDAS, shown in Figure 1, is based on tables with analog samples and is built from the following blocks:

1. Table with pre-calculated samples. The samples could be put within any appropriate type of programmable memory devices. In this case two 8KByte EPROMs (one per output function) are used. The board is generating synchronously two output signals with 1 to 256 samples per period. Each sample could have from 1 to 8 bits ot data.
2. Address generation unit. This unit is generating the addressees within the tables with digital codes representing the analog signals to be generated. Synchronous binary or decimal counters could be used. A fast RISC microcontroller is a possible but not always acceptable alternative.
3. Output register to hold the codes read from the memory.
4. DAC to convert the digital codes read from the memory into an analog signal (current or voltage).

The equipment is intended to be used with:

1. Additional analog filters for adjusting the form (spectrum) of the generated analog signal.
2. Amplifiers in order to obtain higher voltage, current and power.
3. Clock generator with fixed or variable output frequency Fd between DC and several megahertz. In this case Fd is limited mainly by the access time of the memory and the convertion time ot the DACs.
4. Spectrum analyzers.
5. THD and IMD measurement equipment.

The used DAC AD558 has typical conversion time of 800ns (Tctyp=800ns, Fctypmax=1/Tctyp=1.25MHz). This is giving the opportunity to use clock frequency higher than 1 MHz in most of the cases.

In Table 1 are given the maximum frequencies of the generated output "analog" signal (a staircase function approximation (SF) of a SS) depending on the selected sampling frequency Fd and sampling factor N=Fd/Fs.

Table 1. Frequency of the output sinusoidal signal Fs, depending on the sampling frequency Fd and sampling factor N=Fd/Fs.

Fd=640KHz, Td=1.5625us							
N =Fd/Fs	4	8	16	32	64	128	256
Fs [KHz]	160	80	40	20	10	5	2.5

Notes: 1. Fd is the discretization (sampling, conversion) frequency. Fs is the output (analog) signal frequency, the frequency of the generated SF or SS. 3. N=Fd/Fs is the sampling factor or number of signal's samples per period.

III. Hardware implementation

The equipment has two principal units: 1/ function generator and 2/ synchronous pulses generator. Only the first part is shown in Figure 1 and a short explanation of the blocks in the unit is given below:

1. Input stage with Shmitt trigger and protection to produce square wave signal with good quality for the address counters. The sampling (discretization) frequency Fd shold be applied at the input Fd (external clock).
2. An 8-bit programmable synchronous binary counter built by two LSTTL ICs 74LS161/3 for address generation. The maximum number of addresses in one page is 256. Decimal counters 74LS160/2 could be used instead but in this case the size of one page is 100 bytes and the sampling factor N=Fd/Fs will be from 1 to 100. The initial value of the counters is programmed with mecanical switches. The counters could be stopped by stopping the external clock and cleared by external Reset.
3. EPROM 27XXX (in this case 2764 is used but this is not obligatory) with tables of digital codes representing the staircase functions of analog signals to be synthesized. Up to 32 pages (tables) are available in one memory 2764 (32pages x 256 bytes=8192 bytes). One table contains one or more periods of signal to be generated. For example one page could have one period with 256 samples, two periods with 128 samples each, four periods with 64 samples each, etc. Also, one period of the signal could contain any number of samples from 1 to 256 (N=Fd/Fs from 1 to 256) because the address counters are programmable. The contents of both EPROMs are independant and two-diferent sychronous signals are generated.
4. The output data registers 74ALS273 for writing and maintaining the code read from the EPROM in the end of each clock cycle Td. The register is obligatory in order to maintain the stability of the output voltage of the DAC and to reduce the dependability of the DAC output from the EPROM access time.
5. One eight bit DAC AD558 per output channel (analog signal), with typical conversion time (Tc) of 0.8us and with maximum conversion time Tcmax=1.5us.
6. The output code from the EPROM is brought to the connector and could be used from any suitable external DAC and synchronous pulses generation unit.
7. Block with switches for selection of the active page in the memory. Each page is 256 bytes long. The starting address of the page is $XX00 and the last address is $XXFF, where XX is the memory page number from 0 to 31 (from $00 to $1F).

The equipment is giving the opportunity to experiment with nimber of bits n from 1 to 8 bits and to simulate a DAC with the same number of bits. The used method could be masking (truncation) or rounding of the unused bits. This is giving the possibility to evaluate the parameters (form, spectrum, THD, etc) of the output signal in function of the selected number of bits n. The equipment could produce one fraction of the period, one or more periods of a periodic signal.

IV. Conclusion and field of application of the described method and equipment

The disscussed signal generation method and board are useful in the following research and educational areas:

1. Evaluation THD of the generated signal (in particular SS) in function of conversion factor N=Fd/Fs;
2. Evaluation THD of the generated signal (in particular SS) in function of number of digital bits n (from 1 to 8) of the code.
3. Selection of analog or digital filters in function of the parameters of the signal to be generated.
4. Digital synthesis of "analog" signal with almost any form.
5. Comparison between rounding and truncation of the digital codes during the signal generation.
6. Testing and selecting DACs for signal synthesis.

The principal method is based on pre-calcualted tables with digital codes representing a staircase function and has the following advantages:

1. The contents of the memory could be standardized and used for standard tests and calibration procedures in order to compare electronic equipment from different sources.
2. The highest frequency of the digitally generated analog signals because the synchronous counter is the simplest and perhaps the fastest processor able to address the memory table with the signal codes. The arithmetic methods are giving lower frequency range are more expensive and more complicated.

3. The method could generate the analog signals with almost any possible form described with formula or table.
4. The frequency of the output signal is from direct current (DC) to many megahertz, depending on the implementation.
5. The output signal could be unipolar (with or without offset) or bipolar depending on the used DAC and amplifiers.
6. The amplitude of the output signal could be adjusted in large range with additional DAC or digital potentiometers, voltage dividers, amplifiers etc.
7. The methods with tables is simple, clear and reliable and has two independant phases: 1/ Calculating the contents of the table, which could by done on a PC, MPU/MCU kit, MPU or MCU system and there is no need to be done in real time. 2/ real time generation of the analog signal with the digital codes in the table.
8. The proposed method and electronic boards could be implemented with low cost ICs. Moreover, the board could be realized as programmable peripheral board, block or specialized ICs, controlled by a MPU or MCU, or even to be incorporated in a MCU or digital processor as a programmable output block for signal synthesis.
9. The method is giving possibility to produce a standart memory IC with large volume e.g. 64Kx8bits EPROM 27512 (256 pages x 256 bytes) with many standard signals in order to evaluate and compare analog and digital equipment and to do a research in the field of sampling and filtering.
10. The memory size, the number of bits of the counters and number of bytes in one page could be easy augmented in order to produce SF with higher precision (number of bits) or samples per period.
11. The method is giving the possibility of simultaneous and synchronous synthesis of two or more analog signals with the same or difference frequencies and the same or different forms (e.g. sinusoid, square wave, triangular wave etc.) with the same or separate address counters, but with individual memories and DACs.
12. The boards could be used with digital frequency synthesizer in order to obtain more output frequencies.

The method is simple and flexible for application. It gives the opportunity not only to examine the results of discretization of analog signals but also to evaluate low frequency equipment such as amplifiers, filters, preamplifiers, loudspeakers, voltmeters etc.

The discussed electronic boards has the following main areas of application:

- didactic and research equipment for studding digital signal synthesis
- testing equipment for low frequency amplifiers, filters measurement systems, analog and digital filters etc.
- systems for special sound effects
- control equipment
- programmable peripheral block with MPU or MCU control.

More information about the integrated circuits in the equipment and a lot of useful application notes how to use them could be found in [1, 2, 3]

V. References:

1. Texas Instruments. Selection Guide and data Book. Logic CD ROM. February 2000. USA
2. Analog Devices, Integrated Circuits. 1984 Data Book. Volume 1.
3. Intel Corp. Memory components Handbook 1993. USA.

VII. Appendix

Schematic diagram of the electronic board for direct digital synthesis of two synchrounous staircase functions, representing analog signals (Figure 1)

Method and examples of calculating the sampling frequency when the maximum rate of change and amplitude of the signal are known

Petre Tzvetanov Petrov

Abstract: **The proposed method of calculating the sampling factor N and the sampling frequency Fd when the maximum amplitude error Emax and the maximum rate of change (the slew rate) Vamax are given is based on the following basic steps:**

1. **We are calculating the maximum frequency of interest Fsmax = Vamax /(π*2*Am), [Hz]**
2. **We are calculating the sampling factor N=180/(90-arcsin(1-Emax)), [-]**
3. **We are calculating the sampling frequency Fd=N*Fsmax.**

Keywords: **sampling factor, slew rate, amplitude error**

I. Introduction

From the practical point of view it is important to calculate in a simple, clear and verifiable way and with acceptable amplitude error Emax, the sampling factor N=Fd/Fs, the sampling frequency Fd and the number of the converter's bits n when a signal with "arbitrary" form (a "real" signal from a "real" sensor) is converted into digital codes.

Sometimes we know or we could find easily:

1. The maximum allowed rate of change (the slew rate) Vamax into the analog channel ending with analog to digital converter (ADC) or starting with digital to analog converter or (DAC). Vamax could be easily calculated, measured or is known from the technical parameters of the equipment;
2. The amplitude Am or the amplitude from peak to peak App of the analog signal to be sampled. We could use a spectrum analyzer, oscilloscope, AC voltmeter plus band pass filters, technical data sheets, etc. to evaluate Am or App of the frequency component of interest;
3. The maximum permissible amplitude error during the conversion Emax. Emax is the maximum difference between the amplitude value (the maximum) of the analog signal Am and the maximal digital code when an ideal converter with infinity number of bits is used.

Petre Tzvetanov Petrov in an engineer in radio-electronics with "Microengineering"-Sofia, Bulgaria. Emails: ppetre@caramail.com и ptzvp@yahoo.fr.

4. The reference voltage Vref and the full scale voltage Vfs of the converter.

In most of the cases with n-bit converter (ADC or DAC) we have the following equations:

$$n>=3 \text{ bit} \quad (1)$$

$$LSB=Vref/2exp(n) \quad (2)$$

$$LSB<<App<=Vfs \quad (3)$$

$$LSB<<Am<=Vfs/2 \quad (4)$$

where

- LSB is the least significant bit of the converter (ADC or DAC),
- n is the number of bits of the converter,
- Vref is the reference voltage the converter,
- Vfs is the full scale voltage of the converter.

II. The method

In [1] a parameter called "sampling (encoding) factor" N was introduced by the formulas

$$N=Fd/Fs \quad (5)$$

and

$$N=Fd/Fmax \quad (6)$$

where

- Fd is the sampling (discretization, encoding) frequency,
- Fs is the signal frequency when a sinusoidal signal (SS) or co-sinusoidal signal (CS) has to be converted,
- Fmax is the maximum signal frequency of interest if a band wide or multi-tone signal has to be converted into digital codes.

If the frequency component is an SS it is given by the equation:

$$A=Am*\sin(2*\pi*F*t+\varphi) +Bdc \quad (7)$$

We could find the maximum slew rate of a SS by differentiation:

$$Vamax = dA/dt=Am*d(\sin(2*\pi*F*t+\varphi))/dt \quad (8)$$

or

$$Vamax = dA/dt = 2*\pi*F*Am = \pi*F*App, [V/s] \quad (9)$$

In [2] a theorem of C.E. Shannon (1948) was given and could de used as general guidance for calculating the sampling frequency Fd. Here we will try more practical approach. We could calculate the sampling factor N and the sampling frequency Fd in the following steps:

1. We know the maximum slew rate Vamax and the amplitude of the signal Am (or the amplitude from peak to peak, for example App=2*Am). Consequently, we can calculate the frequency of the signal Fmax and we could admit that Fmax is the maximum frequency

in the spectrum of the signal that has to be converted into digital codes with amplitude error not greater than a given value Emax. Because that is only one signal (frequency) component we could use the next formula for a SS and CS:

$$Fsmax = Vamax /(\pi*2*Am), [Hz] \quad (10)$$

2. The maximum amplitude error Emax (0<=Emax<=1) is given and we can calculate the sampling factor N according to [1]:

$$N=180/(90-\arcsin(1-Emax))>0, [-] \quad (11)$$

3. Now, we can calculate the sampling frequency Fd with the next formula

$$Fd=N*Fsmax. \quad (12)$$

Normally, the maximum rate of change of the signal Vamax (slew rate) is measured in V/s or V/us. The following equations are applicable:

$$Vamax[V/us] = Vamax[V/s]/1000\ 000 \quad (13)$$

And

$$Vamax[V/s] = Vamax[V/us]*1000\ 000 \quad (14)$$

III. The method of calculating the sampling frequency Fd in function of the maximum slew rate Vamax in examples

Example 1:
Let us calculate the minimum frequency of sampling Fd for an analog signal with unknown form, for which we know that the slew rate could not be higher than Vamax = 500 000V/s=0.5V/us and the amplitude from peak to peak could not be higher than App=2*Am=1V. The amplitude error Emax during the analog to digital conversion due to the sampling factor N should be not greater than –3dB. Also we know that the equation 1*LSB<<App<=Vfs is satisfied. (The given Vamax could be the maximum slew rate of the analog channel between the source and the converter and could be equal to the maximum slew rate of the used amplifiers, sample and holds, multiplexers and filters. For example, Vatyp for operational amplifiers 741 and 1458 is approximately 0.5V/us.)

Solution:
We are admitting that Vamax=0.5V/us is for the frequency component with the maximum frequency Fmax, which could not have amplitude from peak to peak higher than 1V. This could be verified in practice by testing the channel with real signal. Moreover, we could admit that only one frequency component has slew rate Vamax=0.5V/us and it has sinusoidal or cosinusoidal form because it is only one frequency component.

Now, it is possible to calculate the frequency of the signal Fsmax with Vamax and the amplitude Am. For a SS we have the equation (10) and we are able to draw the conclusions that:

1. If we increase the frequency of the signal Fs that will increase proportionally its maximum slew rate Vamax;
2. If we increase the amplitude of the signal Am (or the amplitude from peak to peak App) that will increase its maximum slew rate Vamax.

Obviously, the amplitude of the signal from peak to peak is limited from the converters full scale voltage Vfs.

We are using the equation (10) in order to calculate the maximum frequency Fsmax in the spectrum of the signal to be sampled

$$Fsmax = Vamax[V/s] /(\pi*App) =$$
$$= 500\ 000V/s/(\pi*1V) = 159160 \text{ Hz} = 160KHz$$

As it was published in [1] the frequency component Fsmax with enough amplitude Am (LSB<<Am<Vfs/2) will be converted into digital codes with amplitude error less than –3dB, if we select the sampling frequency Fd according to the equation

$$Fd>=4*Fs \quad (15)$$

In this example we have:

$$Fd>=4*Fs>=4*160KHz >=642KHz$$

The equation above could be drawn from the basic equation (11) for calculating the sampling factor N in function of the maximum amplitude error Emax for a SS.

Example 2:
In the analog channel before the ADC are used blocks (filters, amplifiers, etc.), which are limiting the slew rate of the signal (for example from a temperature sensor) at the ADC input to Vamax=120 V/s and the amplitude from peak to peak App=2*Am=2.55Vpp.
a/ We have to calculate the sampling frequency Fd with a guarantee that the maximum difference between the maximal digital code and the amplitude value of the analog signal Am is less than 10% (or to any other applicable value between 0% and 100%) when we are using an ideal ADC with error close to zero;
b/ We have to choose a real ADC with number of bits n under the same conditions (amplitude error is less than 10%).

Solution:
a/ We are calculating the signal component with the maximum frequency Fsmax which has to be converted into digital codes. We will use the formula (10) and we have

$$Fsmax = 120V/s /(3.1416*2.55V) = 15 \text{ Hz}$$

We have the formula giving the relation between the sampling factor N and the maximum amplitude error Emax (11). If we apply this formula we will have:

$$N= 180/(90-\arcsin(1-0.1))=180/(90-64.16)= 7, [-]$$

We have found Fsmax and N and we are calculating Fd

$$Fd=7*15Hz=105Hz$$

In this case if we are sampling with frequency Fd=105Hz or higher, with infinity fast ADC with infinity high number of bits n ($n\rightarrow\infty$) and with infinity small conversion error Eadc we could guarantee that the maximum difference between the maximal digital code and the amplitude of the signal (or the amplitude error) is less than -10% or approximately –1dB.

b/ We will try to choose the real ADC with number of bits n less than the infinity and to maintain the total conversion error Econv according to the equation

$$Econv=Eadc+Emax<=10\% \quad (16)$$

In order to calculate the minimum number of bits of the ADC in function of the sampling factor N (and in function of the maximum amplitude error Emax) the author is proposing the simplified formula:

$$n>= lg(N) + (2\ bit),\ [bit] \quad (17)$$

where lg is the logarithm in base 2 and 2=<N<=48.

In this case

$$n>=lg(7)+(2\ bit) >= 2.73\ bit + (2\ bit) >= 4.73\ bit$$

We are choosing the effective number of converter bits n = 6 bit. It is known that the maximum conversion error Eadc introduced by an 6-bit ADC is

$$Eadc = +-0.5*100\%/(2exp(n))=$$
$$=+-0.5*100\%/(2exp(6)) = +-0.5*100\%/64 = +-0.78125\%$$

The root mean square error (Eadcrms) introduced by the 6-bit ADC is given by the widely used formula:

$$Eadcrms = 1*LSB\%/sqr(12) \quad (18)$$

We could calculate

$$Eadcrms=(100\%/64)/sqr(12) = 1.5625\%/3.464 =0.451\%.$$

If we apply the model of the maximum error (in this model we add all errors in order to obtain the maximum possible error) we will have the following error distribution in order to have a maximum conversion error less than 10%.

- Eadc = 0.78125% (error from the ADC);
- Emax=10%-0.78125% = 9.22% (error from the sampling factor N=Fd/Fs).

Now we have Emax and we could calculate the sampling factor N with the formula (10)

$$N= 180/(90-arcsin(1-0.0922))=180/(90-65.20)= 7.26\ [-]$$

We have calculated the sampling factor N and we could calculate the sampling frequency with (12)

$$Fd = N*Fs = 7.26*15=109Hz.$$

The solution of the Example 1 was found and we can draw the conclusions that:

1. The decreasing of the effective number of converter's bits n could be compensated only partially (in small degree) by the increasing of the sampling factor N;
2. The increasing of the sampling factor N from 4 to infinity will reduce the maximum amplitude error Emax from -29.3% (or -3dB) to 0% (when n→∞).

IV. How can we found the maximum slew rate Vamax?

There are many ways to know the maximum slew rate of the analog channel between the sensor (the source of information) and the ADC:

1. From the data sheet of the sensor.
2. From the data sheet of the operational amplifier(s) and filter(s) used to amplify and filter the signal from the sensor.
3. From the data sheets of the filters between the sensor and the ADC.
4. With an "almost ideal" square wave signal and oscilloscope we could measure the rise and the fail times between the levels of 10% and 90% of the maximum levels on the output of the analog channel. (Usually Trise=Tfall=Tr). Consequently, it is possible to calculate two slew rates (the rate of rise of the signal Vr and the rate of the fall of the signal Vf), to choose the greater from them (Vamax=max(Vr, Vf)) and to use it as a maximum slew rate of the channel. In most of the cases between the rise time Tr and the bandwidth of the analog channel BW(-3dB) we could apply the following equation [3]:

$$BW(-3dB)= 0.35/Tr \quad (19)$$

Table 1 is giving an idea about the maximum slew rate Vamax of some SS and CS with frequency Fs, Am=1V and App=2*Am=2V.

Table 2 is giving some basic values for the sampling factor N=Fd/Fs and the corresponding possible amplitude error during the SS and CS conversion with n→∞ if the formulas (11) is used for the calculation of Emax and the minimum number of the converter bits n, according to the equation (17). There is an obvious amplitude modulation, depending on the phase of the signal (SS or CS) to be converted into digital codes.

Table 1
The maximum slew rate of some SS and CS with frequency Fs, Am=1V and App=2*Am=2V.

Fs	Vamax		Fs	Vamax
1Hz	6.283V/s		2Hz	12.567V/s
1kHz	6283V/s		2kHz	12567V/s
1MHz	6.283V/us		2MHz	12.567V/us
1GHz	6283V/us		2GHz	12567V/us
1THz	6.283V/ns		2THz	12.567V/ns

Table 2
Some basic values of the sampling factor N=Fd/Fs and the possible amplitude error during the SS and CS conversion

N	Possible amplitude error (n→∞)	Variation of the phase	n, [bit] (nadc, ndac)	Eadc, +- LSB/2
2	0 to -100%	0 to 90 deg.	>3	6.2%
4	0 to –29.3%	0 to 45 deg.	>4	3.1%
7	0 to -10%	0 to 25.7 deg.	>4.8	1.8%
22.2	0 to -1%	0 to 8.1 deg.	>6.5	0.55%

V. Calculating the number of bits of the converter n

Once we have calculated the sampling factor N and the sampling frequency Fd we have to calculate the minimum acceptable number of bits for the converter (e.g. the ADC).

As a first step we are calculating the (minimal) number of converters bits n (in order to consider the converter as an "ideal" one) from the sampling factor N with simplified formula (17):

$$n1 >= \lg(N) + (2\ bit),\ [bit] \qquad (20)$$

As a second step the well known formula giving the Signal To Noise Ratio (SNR) in function of the effective number of converter's bits n could be applied [4]:

$$n2 = (SNR[dB] - 1.76dB)/6.02 \qquad (21)$$

Finally, we could choose the minimal acceptable number of the converter bits n, according to the formula

$$n = \max(n1, n2) \qquad (22)$$

If the signal amplitude from peak to peak App is less than Vfs/2 we are able to calculate the lost of the converter bits L using the following formula

$$L = \lg(Vfs/App),\ [bit], \qquad (23)$$

Where lg is a logarithm in base 2.

As we mention before the lost of converters bits L could be compensated only partially with higher than calculated sampling factor N (or sampling frequency Fd). This conclusion could be drawn from the following formula:

$$Emax = 1 - \sin(90 - 180/N)) \qquad (24)$$

VI. Conclusion

The paper is giving a simplified and useful approach for calculating:

1. The sampling factor N=Fd/Fs;
2. The sampling frequency Fd;
3. The minimal number of converters bits n;

when the maximal slew rate Vamax, the maximum amplitude Am of the signal and the maximum amplitude error during the conversion Emax are known.

The method discussed in the present paper could be easily tested with a direct current (DC) signal, SS or CS with a DC component and with a sum of SS and DC signals with or without a DC component.

The method proposed in the paper is very useful because every real signal has a finite slew rate Vamax and finite amplitude Am or App which could be measured or calculate easily and accurately. It should be noted that only real signals with finite slew rate could be represented accurately with Fourier series. The artificial signals with infinity high slew rate ($Vmax \rightarrow \infty$) like rectangular or saw-tooth signal (one or both of the edges of the signal are infinitely short or a part of the signal is infinitely short) cannot be represented fully with Fourier series.

VII. References

1. Petre Tzv. Petrov, Method and equipment for sampling and direct reconstruction of analog signals. Brochure 32p. TU-Sofia. August 2003. Bulgaria.
2. C.E. Shannon. A mathematical Theory of Communication. The Bell System Technical Journal. Vol. 27, pp. 379-423, 623-656, July, October, 1948. USA.
3. Tektronix. XYZ of Oscilloscopes. 2004. USA
4. Datel-Intersil Inc., Data Acquisition and Conversion handbook. Edited by Eugene L. Zuch. Third Printing, June 1980. USA.

Analysis of the Security Risks in the Windows 2000 Networks

Peter T. Antonov [1] and Valentina R. Antonova [2]

Abstract - **This paper reviews security problems in the Windows 2000 networks. An approach for the security risks estimation is offered, based on the idea of maximum using the potential of the security specialists. A technology for analysis and decision making to neutralization of the security risks is presented too.**

Keywords - **security, risks.**

I. INTRODUCTION

Modern computer nets are characterized by complex structures and are quite vulnerable to the attack of a great number of security risk factors. That is why at the same time with the development of these structures, problems with the protection of network sources and counteraction to the increasing "computer crimes" attain greater significance [1,2,3,4,6,7, etc.].

According to the accepted guidance and the Interpol classifier, developed by the European Community countries, all computer crimes are divided into the following basic groups [4, etc.]: illegal access and data tacking, changing computer programs and data; computer frauds; illegal copying; computer sabotage and so on.

In order to protect the network sources against the specified crimes corresponding methods and security means are used. Their efficiency depends mainly on the proper evaluation of the security risk factors.

The above-mentioned facts completely concern Microsoft Windows 2000 - based computer networks.

The security system in these networks allows users' identification and the management of the data and network sources access, control of the used files, folders and printers, realization of the Authenticity protocol Kerberos V5 and the infrastructure with public keys [2,3,4,7, etc.]. In Windows 2000 networks, as well as in the other networks, there exist security risks for data and services. The types of data and possible risks for their security are shown in Figure1 [7]. In relation to the risks for services, Windows 2000 nets are vulnerable to the so-called "Denial of Services Attacks" (DoS), which block the usual access to data and applications. The preliminary and periodic analysis of the pointed out risks is one of the main prerequisites for designing and supporting a highly efficient protection system against illegal access.

[1] Peter T. Antonov is with the Faculty of Computing and Automation at Technical University of Varna, 1 Studentska Str., 9010 Varna, Bulgaria, E-mail: peter.antonov@ieee.org

[2] Valentina R. Antonova is with the Faculty of Computing and Automation at Technical University of Varna, 1 Studentska Str., 9010 Varna, Bulgaria, E-mail: valyvarna@yahoo.com

In relation to the subject, this paper deals with security problems and develops an efficient approach to the risk evaluation in Windows 2000 networks, which uses in full value the maximum security experts' potential in a certain organization.

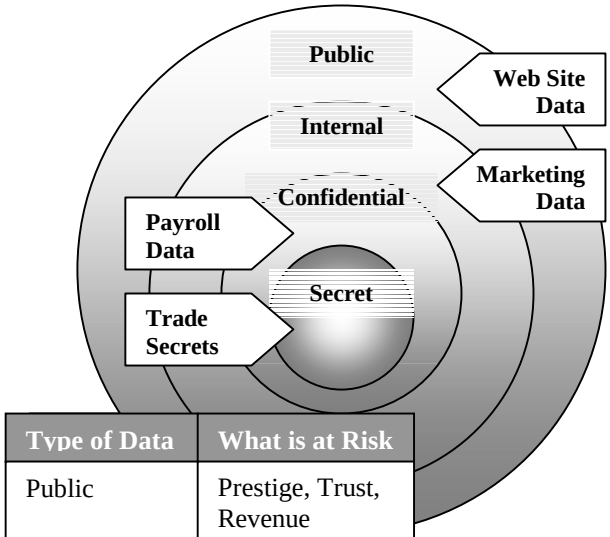

Type of Data	What is at Risk
Public	Prestige, Trust, Revenue
Internal	Operations
Confidential	Operations, Internal Trust
Secret	Intellectual Property

Figure 1

II. CONTENT AND GROUNDING OF THE APPROACH TO SECURITY RISK EVALUATION

The structures of Windows 2000 - based nets, as well as all modern information structures contain two main components: computational infrastructure and management infrastructure [8]. The main components of the computational infrastructure are: applications and services, support systems and communications systems. Those of the management infrastructure are: communications management and application and services management.

One of the most important tasks of the management infrastructure is connected to the organizing and accompanying the security system, providing efficient protection against illegal access to the network sources.

Developing a sufficiently operative system for complex security in Windows 2000 networks is a complicated and large-scale task, that can be solved with the help of a number of measures with organizational and program - technical characteristics. They can be set up as following basic groups [1,2,3,7, etc.]: development organization; management and control of the security system; physical and technical protection of the equipment and resources; protection of the data exchange process; users' and management-operators' authentication; management of the resource access.

All measures, connected to the security administration, i.e. to the design of the organization and implementation of the security system, as well as its management and control, are included in the first group. Human factor, or to be more precise - the qualification and motivation of the designers and maintenance personnel, has to be taken into consideration. The significance of this factor constantly increases as a result from the continuous growth of network complexity and security requirements. Besides that, current or ex-representatives of the personnel do nowadays about 50% of the criminal breach of the security regulations, which is another confirmation of the necessity in a thorough approach to these problems.

During the process of design of the security system the following basic steps should be followed: network analysis and classification of the vulnerable points according to their importance; evaluation of the real threats to an illegal access to the vulnerable points; analysis of the risks and the expected damage from each real threat; choice of the means and mechanisms for providing an efficient protection; evaluation of the necessary initial and exploitation expenses and planning the project implementation. The above-specified measures and infrastructure management problems can be considered as part of its main direction known as *security management*. As it has already been mentioned, one of the tasks of this direction is connected to the organizing and conducting of *control* of the developed security system, which, on its turn, compulsory includes a security audit.

The term *security audit* is comparatively new. It gained ground after 1995 and now there exist a number of company and international standards and specifications, the most famous of them being ISO 17799, BSI AND COBIT [6, etc.]. The security audit usually means a systems process for receiving real quality and quantitative evaluation of the current security state, according to certain criteria and indicators. The audit is carried out once - after the developing of the security system and then regularly- for example, once or twice a year.

At the present moment there are three main directions for evaluation and analysis of the current state of the security: analysis of the requirements for the security system, instrumental check of the security state and analysis of the security risks. The latter is considered to be the fullest and most efficient and for this reasons it is a subject this investigation.

At practical application of this direction familiar approaches have been used [6, etc.], which are implemented by the help of external auditors. In our opinion this does not allow using the personnel capabilities to the full in the field of networks security. That is why we are going to offer a new approach for security risks analysis, based on the known methodology [5, etc.] for working in *quality clubs*, that became world - popular in 80s of the last century.

In order to implement this approach it is necessary to organize groups from the personnel working in network security. These groups should include no less than 5 people and no more than 10 people, because that size is the most rational in concern with the efficiency of the discussion results.

The groups, collected with the pointed out purpose, are convenient to be called *groups for security risks* evaluation (GSRE). The discussions, held in GSRE, should be led by the managers with a highest rank in the separate groups. It is not advisable to for them to continue more than an hour, because after that time the fatigue decreases the efficiency of the work. The recommended methodology for holding the discussions themselves is the following:

Stage 1. Writing a list of security risks in a particular network.

For that purpose the group members sit in a circle, without observing the rank or leadership, and the leader addresses them consecutively and at each turn of the circle discussion individual participants formulate just one risk with a short grounding. The circle discussion continues until new different risks are generated and everyone writes them down in order of their suggesting.

Stage 2 : Ranging the risks, formulated on the previous stage.

This stage is held in three consecutive sub-stages, which combine the advantages of individual and team decisions.

2.1. Arranging the risks according to their importance

It is done individually by each participant and during it the advantages of the method of minimum mutual interaction can be observed. If, for example, the number of the mentioned risks is *n*, then to each of them a score of 1 to *n* can be opposed and the most important risk is denoted with *n*, the next according to its importance - with (*n*-1) and so on till the risk, considered by the last participant as the least important, is denoted with 1.

2.2. Receiving a total rating of the risks

It is done by the leader of the GSRE, who summarizes the grades given by different participants. For that purpose the given individual ratings of each risk are summed up and then a final arrangement of risks is done according to the level of their importance. During this process it is possible to receive equal total ratings of some of the risks, which will mean an equal level of importance of these risks in group members' opinion.

2.3. *Marking the security risks*

It is done as a teamwork under the leading of the group manager; each risk is separately discussed and marked with (*) if the help of the higher rank structures and managers is required for its elimination.

These stage aims at separating the risks that can be eliminated by the GSRE itself and the marked ones, which need a superior support.

After the end of the second stage each group member will have a list of generated risks for networks security, a ranging of these risks according to the level of their importance and marking.

Stage 3. Analysis of the reasons for security risks.

This stage with elements of brainstorm is held separately for each one of the risks included in the list, written on stage 2, starting with the most important one.

3.1. *Defining the reasons for the discussed risk.*

A list with possible reasons, causing the corresponding risk is comprised. This is done by the guiding of the GSRE manager, similarly to the technology used on stage 1. Each participant formulates one reason in each consecutive asking from the leader.

3.2. Ranging the reasons

It is done by each participant on his/her own as on sub-stage 2.1. Different reasons have ratings in dependence on the individual judgment on their importance.

3.3. Receiving a total rating of the reasons.

The GSRE leader, who summarizes the individual opinions from the stage 3.2, and then announces the received result, conducts it on analogy with 2.2.

Stage 4. Decision formulation and realization

The decision is generated by whole team and the discussion is led again by the group leader. The content of the decision is directed towards eliminating the reasons, causing the corresponding risk. It should include two points - first, what should each participant do and how long, and second, what help is needed from the superior officials.

Having taken the decision the group is back to stages 3 and 4, which are realized for the second risk according to the importance and so on.

The above-described approach can be used as an addition to the external audit, which is conducted after the initial development of the security system, as well as for a regular internal audit of the security during the operation of Windows 2000 networks. The internal audit, conducted by GSRE, in the common case, will be characterized by a greater efficiency than the external audit, conducted by a distant organization of experts-auditors. It does not interfere with the presented technology of an internal audit to be combined with a controlling external audit, conducted no more than once or twice a year.

III. New capabilities of Windows 2000 and Some Security Problems

It is widely known that the operating system of Windows 2000 is notable for its greater security comparing to Windows NT4. Although, it is not absolutely protected, that is true for every operating system.

The main capabilities of Windows 2000 in the field of security are expressed in the following: usage of the system of security on level IP (Internet Protocol) - IP Security, Encrypting File System (EFS), tools for Group Policy, a capability for Security Configuration and Analysis, Security Templates, the implementation of the popular authentication protocols like RADIUS (Remote Authentication Dial-in User Service) and Kerberos, etc.

It becomes obvious that Windows 2000 has all advantages and the typical security risks of the implemented new technologies. Therefore, the above-described GSRE have to consider and analyze the typical risks as well as the possible risks, caused by the particular conditions of implementation and operation of the network infrastructure.

For instance, a secure and fast cryptographic algorithm DESX (Extended Data Encryption Standard) is used in EFS. It has been offered by Ron Rivest and RSA Data Security Company as a version of the so far most popular cipher DES (Data Encryption Standard) and it uses the following formula for encryption [1]:

$$E_J = K_1 \oplus F_{DES}\left[K_E, (K_2 \oplus M_J)\right], \quad (1)$$

where F_{DES} denotes the familiar procedure for the encryption at DES with a secret key K_E, which has a size of 56 bits. The difference at DESX is in that initially the encryption block M_j is summed bit-by-bit according to mod 2 with a 64-bite key K_2 and then it is encrypted using the key K_E. The received cipher block is summed, on analogy, with the key K_1 and thus the final cipher block E_j is achieved. As it is known, the length of 56 bits of K_E at DES is already insufficient and for that reason a new federal standard for data encryption called AES (Advanced Encryption Standard) was adopted in the USA at the end of 2000. It uses a significantly bigger length of the secret key. DESX is offered, too, in order to overcome the pointed out drawback of DES, linked with the small length of the key. At DESX the actual encryption key becomes equal to 120 bits [56 bits (K_E) + 64 bits (K_2)= 120 bits]. K_1 is a 64-bit sequence, calculated according to a one-way hash function of that 120-bit key. In comparison to DES, DESX has significantly higher resistance to Brute Force Attack, as well as to a differential and linear cryptographic analysis. In recent years and now a 120-bit length of the secret keys has proved to be completely enough, concerning the capabilities of the modern cryptographic analysis and information technologies. Despite that, it is logical to expect a change of DESX in the next versions of Windows, since the most cryptographic

systems on the market have already used keys with a length bigger than 128 bits (≥128 bits).

A management system for the keys with symmetrical and asymmetrical (with public or secret keys) encryption and decryption is provided in Windows 2000. The components of the public key structure are shown in Figure 2 [7].

Figure 2

It is known that the most significant problem for the asymmetric encryption is due to the possibility for corrupting the public keys.

If the public key of a user Y is taken from an unspecified place U**,** there is no an absolute guarantee that it really belongs to Y, to whom the U claims to belong. It is possible to be a violator, for example - Z, who has corrupted, with or without the knowledge of U, Y's public key with his/her own public key and willfully intercepted all messages sent to Y. When a message is intercepted by Z, it can be decrypted by the secret key of the violator Z, read by him/her, even changed, and then encrypted with the real public key of Y and sent to Y from Z. Thus, the source X and the receiver of the message Y can not realized at all or for a certain time, that there has been an ill-intentioned interference. Besides, it is possible for Z to send X a false message - answer on the behalf of Y. Of course, X will find the substitution at the receiving of Y's message, but it can be too late.

Therefore, if X wants to establish a protected communication with Y using the cryptographic algorithm with public keys, he/she has to be absolutely sure he/she has entire disposal of the real public key of Y (if X is not sure in the authenticity of Y's key, the idea of encryption is preliminary discredited).

The above-mentioned problem can be solved only if X receives the public key of Y personally from Y or from a mediator U, who X and Y trust fully. The mediator U can sign the real public keys with his/her own secret key. Then those who receive public keys from the mediator will check the authenticity of the signatures, he/she has put on the keys, spread by him/her.

A significantly secure infrastructure for working with public keys has been developed in Windows 2000, but GSRE should have in mind the above-mentioned problem that can lead to security risks. Besides, it is useful to consider the well-formulated in [9] 10 common directions for decreasing the risk and increasing the security in the whole process of GSRE work.

IV. Conclusion

The offered approach for security risks evaluation allows using the personnel qualification in the field of security of Windows 2000 - based networks to its maximum. At the same time it motivates them to a higher degree of loyalty. Moreover, the discussions can be held with different regularity, particularly after each detected gap in the security system or at a smallest doubt for its existence.

References

[1] Антонов, П., С. Малчев. Криптография в компютърните комуникации. – Варна, 2000. – 315 с.

[2] (Microsoft). MCSE Training Kit. Microsoft Windows 2000 Server. Т1 и Т2. Прев. от англ. – София: СофтПрес, 2000. – 1102 с.

[3] (Microsoft). MCSE Training Kit. Microsoft Windows 2000. Администриране на мрежовата инфраструктура. Прев. от англ. – София: СофтПрес, 2001. – 566 с.

[4] Скамбрей, Дж. и др. Защита от хакерски атаки – тайни и техники на мрежовата сигурност. Прев. от англ. – София: СофтПрес, 2001. – 744 с.

[5] Рууни, Дж. (вицепрезидент по качеството на фирма Ролс Ройс – Англия). Цикъл лекции на семинар по управление на качеството. – София: ИСУ, октомври 1983 (ръкопис).

[6] Петренко, С., А. Петренко. Аудит безопасности INTRANET. – М: ДМК Пресс, 2002. – 416 с.

[7] (Microsoft). Designing a Secure Microsoft Windows 2000 Network. Course Number 2150A. – Microsoft Corp., 2000.

[8] Ray, P. Cooperative Management of Enterprise Networks. – NY: Kluwer Academic, 2000. – 187 p.

[9] (SUN Microsystems). 10 Ways to minimize Risk and maximize Security. – SUN Microsystems, 2003. – 27 p.

Using Genetic Algorithms to Solve Software Clustering Problem

Violeta T. Bojikova[1] and Milena M. Karova[2]

Abstract - **In this paper is presented a genetic algorithm (GA), which solves software clustering problem, using a fitness function that is based on maximizing the cohesiveness of clusters and minimizing inter-cluster coupling. Software clustering facilitates program understanding and reengineering. The presented approach differs strongly from other published genetic approaches because of the choice of the fitness function, genetic operator's realization and the presence of determinism.**

The goal of the developed genetic project is to produce better clustering results, with regard to the solution quality and the algorithm complexity. s.

Keywords – **search-based software clustering algorithms, software clustering, genetic algorithms, program reengineering**

I. INTRODUCTION

Most interesting software systems are large and complex, and as a consequence, understanding the structure of these systems is difficult [1,2,3]. Software Engineering books advocate the use of documentation as an essential tool for describing a system's intended behavior, and for capturing the system's structure. In practice, however, we often find that accurate and current design documentation does not exist. This problem is exacerbated because the original designers and developers of the system are often no longer available for consultation.

In the absence of advice or documentation about a system's structure, software maintainers are left with several choices. First, they can manually inspect the source code to develop a mental model of the system organization. This approach is often not practical because of the large number of dependencies between the source code components. Another alternative that is now becoming available to software maintainers is to use automated tools to produce useful information about the system structure. A primary goal of these tools is to analyze the low-level dependencies in the source code, and cluster them into meaningful subsystems.

A subsystem is a collection of source code resources that closely collaborate with each other to implement a high-level feature, or provide a high-level service to the rest of the system. Typical source code resources that are found in subsystems include modules, classes, packages, files. Subsystems facilitate program understanding by logically treating many low-level source code resources as a single high-level entity. Subsystems are not specified in the source code explicitly, as most programming languages do not support this kind of structuring yet. Because source code lacks the descriptiveness necessary to specify subsystems, we can use tools for automatically recovering the subsystems of a software system from the source code. Software designers use directed graphs to represent the structure of a software system and to make the structure of complex software systems more understandable.

The graph is formed by representing the modules of the system as nodes, and the dependencies between the modules as edges. We refer to this graph as the Module Dependency Graph (MDG) of a software system. Each partition of the MDG consists of a set of non-overlapping clusters that cover all of the nodes of the graph. The goal is to partition the MDG into meaningful subsystems.

Given an MDG with n components that are partitioned into k distinct clusters (subsystems), the number of ways to cluster the MDG grows exponentially with respect to the number of modules in the system. The general problem of clustering software systems is NP hard, however, the formal proof of this remains an open problem. Most researchers have addressed the software clustering problem by using heuristics to reduce the execution complexity to a polynomial upper bound.

Our approach treats clustering as an optimization problem, where the goal is to find a good (possibly optimal) partition. To explore the extraordinarily large solution space of all possible partitions for a given MDG, we use a Genetic Algorithm (GA).

II. GENETIC ALGORITHMS: ENCODING, OBJECTIVE FUNCTION, OPERATORS

Genetic algorithms apply ideas from the theory of natural selection to navigate through large search spaces efficiently [2]. GAs perform surprisingly well in highly constrained problems, where the number of "good" solutions is very small relative to the size of the search space.

GAs operate on a set (*population*) of strings (*individuals*), where each string is an encoding of the problem's input data. The number of strings in a population is defined by the *population size*. The larger the population size, the better the chance that an optimal solution will be found. Since GAs are very computationally intensive, a trade-off must be made between population size and execution performance. In the

[1] Violeta Bojikova is with the Department of Computer Science Varna Technical University, Bulgaria, e-mail: vbojikova2000@yahoo.com

[2] Milena Karova is with the Department of Computer Science Varna Technical University, Bulgaria, e-mail:mkarova@ieee.bg

case the population size is defined by the number of sequential algorithms that form the stating population [4,5].

Each string's *fitness* is calculated using an objective function. In each generation, a new population is created by taking advantage of the fittest individuals of the previous generation.

Genetic algorithms are characterized by attributes such as objective function, encoding of the input data, genetic operators, and population size. After describing these attributes, we describe the GA algorithm in Section III.

- The objective function

The objective function k is used to assign a fitness value to each individual in the population. In the case, it is designed so that an individual with a lower objective function value have a high fitness and represents a better solution to the problem.

The basic idea of this objective function is "well designed software systems are organized into cohesive clusters that are loosely interconnected".

The weight – Wk of each cluster $g_i \in$ MDG with $x_i \in X$ components (nodes) corresponds to the restrictive condition Wo, where w_i – is the label of node - x_i and presents the number of node's elements (i.e. modules):

The value of "k", where k_{ij} is the number of inter-edges (*i.e.*, external edges that cross cluster boundaries) between nodes x_i and x_j is calculated as follow:

$$k = \sum_{i=1..M} \sum_{j=1..M} k_{ij}, \forall i \neq j$$

M is the number of clusters in the current partition of the MDG.

- Encoding

GAs operate on an *encoding* of the problem's input data. The choice of the encoding is extremely important for the execution performance of the algorithm. A poor encoding can lead to long-running searches that do not produce good results.

Each node in the graph G=(X,U), where N=|X| has a unique numerical identifier assigned to it (*e.g.*, node x1 is assigned the unique identifier 1, node two is assigned the unique identifier 2, and so on). These unique identifiers define which position in the encoded string S will be used to define that node's cluster. We can use the next encoding string S:

$S=s_1\ s_2\ s_3\ \ s_N$, where $s_i \in \{1\ldots M\}$, $i \in \{1\ldots N\}$.

Therefore, the first character in the string S - s_1, indicates that the first node (x1) is contained in the cluster labeled s_1. Likewise, the second node (x2) is contained in the cluster labeled s_2, and so on.

- Genetic operators

GAs feature the following three basic operators, which are executed sequentially by the GA:

1. Selection
2. Crossover
3. Mutation

During **selection**, pairs of individuals are chosen from the population according to their fitness. We use in GA *competition selection*. The 2 individuals with the high fitness are selected from the old population to be included in the new population. This selection is complemented with *elitism*. Elitism guarantees that the fittest individual of the current population is copied to the new population.

Crossover is performed immediately after selection. The crossover operator is used to combine the pairs of selected strings (parents) to create new strings that potentially have a higher fitness than either of their parents.

During crossover, each pair of strings is split at a random position. Two new strings are then created by swapping these random characters of the selected individuals. Thus, two strings are used to create two new strings, maintaining the total population of a generation constant.

The **mutation** operator is applied if the strings resulting from the crossover process are identical. The mutation is applied over one of the string – random exchange of random number of nodes between the clusters of one of the solutions (one of the individuals).

After that, we can apply **restoring** – to satisfy the restrictive condition Wo.

III. THE GA ALGORITHM

GAs use the operators defined above to operate on the population through an iterative process, which is as follows:

1. Generate the initial population, creating a set of constructive sequential solutions (strings) of fixed size [4,5].
2. Create a new population by applying the selection operator to select pairs of strings.
3. Apply the crossover operator to the pairs of strings of the new population.
4. Apply the mutation operator to each string in the new population.
5. Apply the restoring operator, if the new strings are identical.
6. Replace the old population with the newly created population.
7. If the number of iterations is less than the maximum and the population is changed, go to step 2. Else, stop the process and display the best answer found.

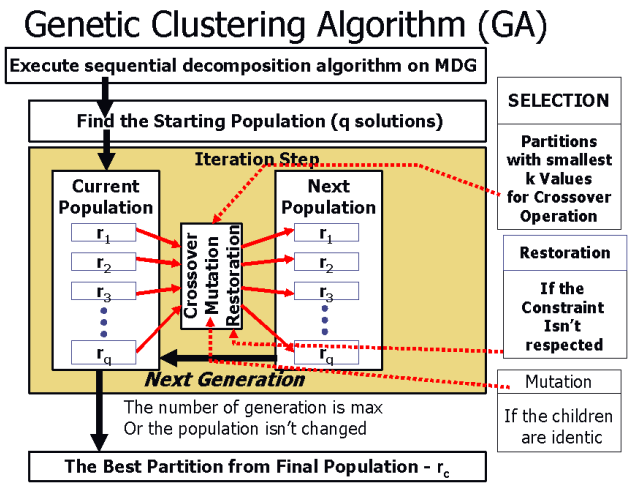

fig.1. Genetc Clustering algorithm

IV. CONCLUSION

In this paper we describe a Genetic Algorithm (fig.1) for software clustering. Over the past few years we have seen an increasing interest and activity in software clustering research [1,2,3]. Clustering has been applied in the fields of mathematics, social sciences, engineering and biology for many years. However, only within the last 25 years have researchers investigated and applied clustering techniques to the software domain. This work has resulted in new clustering techniques, as well as the adaptation of classical clustering techniques to the particularities of the software domain.

Improving Optimization Techniques is one of the new research directions in the area of software clustering. Genetic algorithms have been shown to produce good results in optimizing large problems. Although the initial results with the genetic realization in [2] are promising, additional study is needed. We are presented an GA algorithm that has an other goal function and apply alternative selection and mutation operators. Additional research is needed to proof the effectiveness of this algorithm.

REFERENCES

[1]. Comparing the Decompositions Produced by Software Clustering Algorithms using Similarity Measurements, Spiros Mancoridis and Brian Mitchell
IEEE Proceedings of the 2001 International Conference on Software Maintenance (ICSM'01). IEEE.

[2]. Spiros Mancoridis, Brian Mitchell, and Diego Doval, Automatic Clustering of Software Systems using a Genetic Algorigthm, , IEEE Proceedings of the 1999 International Conference on Software Tools and Engineering Practice (STEP'99)

[3]. Search Based Reverse Engineering", by B. S. Mitchell, S. Mancoridis, M. Traverso. In the ACM *Proceedings of the 2002 International Conference on Software Engineering and Knowledge Engineering (SEKE'02)*, Ischia, Italy, July, 2002. pp. 431-438.

[4]. Software Architecture Decomposition, Violeta Bojikova, M. Mitev, Proceedings of the 14th Int'l Conference SAER'2000, Varna, 2000, pp. 173-177.

[5]. An Approach to measure the Cost of Program restructuring, Violeta Bojikova, M. Karova, Proceedings of papers, Volume 2, pp 669-671, 2002, Nish, Yugoslavia

A Genetic Algorithm for a Student Timetabling Problem

Milena N. Karova[1] Violeta T. Bojikova[2] Radoslav E. Mladenov[3]

Abstract - **This paper introduces a flexible method for scheduling a timetable using a genetic algorithm. The timetabling problem comes up in every educational institution. It is a special kind of optimization problem. A timetable is explained as a schedule with constraints placed upon it. There had been many attempts to address this problem using classical methods, such as integer programming and graph theory algorithms without much success. These methods also are difficult to automate the process. The solution, which this paper offers, includes a genetic algorithm implementation in order to give a maximal approximation of the problem, modifying a generated solution with genetic operators.**

Keywords: **genetic algorithm, timetabling, scheduling, constraints, optimization, approximation, selection, genetic operator**

I. INTRODUCTION

The timetabling problems belong to the NP-hard problems class and it is quite difficult to solve them with conventional methods including iterative and recursive algorithms. These problems are generally characterized as constraint satisfaction problems. That's why we use two general categories of constraints – hard constraints and soft constraints. The basic objective in solving the problem is to allocate events to time slots while minimizing constraint violation. This approach needs robust heuristics which can evolve and evaluate the set of solution candidates called chromosomes. The scheduling doesn't mean just arranging events in the time slots but also observing some additional rules – teachers may be busy in certain weekdays, some events may require a specific time slot and so on.

II. CONSTRAINTS

The genetic algorithm which we use, observes two generic groups of constraints – soft constraints and hard constraints. Hard constraints are constraints which mustn't be broken in order to have a regular timetable. These include:

- a teacher giving two or more lessons at the same time
- a group attending two or more classes at the same time
- a room being occupied by two or more groups at the same time

[1]Milena N. Karova is with the department of Computer Science, Studentska 1, Technical University Varna Email: mkarova@ieee.bg
[2]Violeta T. Bojikova is with the department of Computer Science, Studentska 1, Technical University Varna Email:vbojikova2000@yahoo.com
[3]Radoslav Mladenov is student, department of Computer Science, Technical University Varna Email: radoslavmladenov@abv.bg

Such constraints include more sophisticated problems to be solved – room capacity problems, time violations etc. Hard constraints have to be taken into consideration very strictly because the timetables that violate just one of them are practically unusable. Soft constraints are not so important but they mustn't be belittled. They involve restrictions as:

- reducing the void time slots
- setting the lectures before seminaries
- selecting preferred time slots

Soft constraints offer more gentle options for constructing the timetable. Soft constraints are the tools for customizing a particular timetable without many efforts. The soft constraints' violations will not make a timetable unusable; it will only be more discursive. A comparison function is necessary, to define when a chromosome is better than another chromosome. Comparing two chromosomes (and thus obtaining the best individual) consists in choosing the individual with the best hard fitness (in case of ties, choosing the individual with the best soft fitness). Note that the best fitness means the lowest fitness factor (the fitness factor is decreasing with better individuals) and thus maybe a more appropriate name for this fitness factor would have been "conflict factor".

III. EVENTS AND SOLUTIONS

Every single solution generated by the algorithm is represented by a chromosome. The chromosome itself is an indivisible unit which forms the total amount of solutions called generation. Each chromosome is made up of a set of genes (the smallest information carrying unit of a chromosome). In our approach, inside the chromosome, there is a gene for each activity in the timetable. This gene represents the scheduled time of the corresponding event. So, a chromosome is actually an array of genes, each gene representing the starting day and hour of an event.

The chromosomes are built with direct encoding. This means that the chromosome is not a sequence of logical 0 and 1 but contains more meaningful information. The single most important attribute of the chromosome is its length. The length is determined from the total amount of events, taking part in the schedule. The event is a discrete container which includes a teacher, a group and a room. Each gene in the chromosomes represents the time slot for the corresponding event in the set of events. To reduce the space representation of the whole solution, we linearize the chromosome. We use 6 fixed time slots per day, so representing a single time slot we should need a matrix. Linearization removes the

indispensability of using a matrix. If there are 5 working days the matrix will be 6x5, but if we linearize, we will need only a vector with 30 fields. Then the generation would be a matrix (not a cube) and the total number of solution candidates would be a cube (not a 4-dimensional hypercube).

IV. GENETIC OPERATORS

The genetic algorithm we present uses three genetic operators to perform the evolution process. They are crossover, mutation and preserving. The crossover is a biological term which is widely used in the genetic algorithms theory. It is the phase in our algorithm where we produce new solution candidates from existing ones. Crossover is committed in two processes: one is the parent selection, where we select two chromosomes by following some criteria. In this process we try to give a better solution using old solutions. After the two parent chromosomes had been selected, we need to determine how to combine the two chromosomes to produce new better solutions. There are two common methods of doing so – single-point crossover or double-point crossover where we segment the chromosomes randomly and exchange their genetic information. We also offer another crossover variation – crossover with elitism. Elitism is the mechanism of evaluating and finding the best chromosome from certain population. We use a single-point crossover which consists of finding a point of division (it's randomly chosen) and then swapping the genetic information between the two adult chromosomes. The second genetic operator which is used in the algorithm is the mutation operator. It introduces a rapid change in the genetic material in a single chromosome. This operator must be used rarely because it brings unforeseen changes which are likely to deteriorate the chromosome's fitness value. Sometimes mutation surprisingly gives enormous improvements in the solution's overall structure. Mutation ratio should be kept small, often 5% or less because it is an irreversible process which may worsen the solution rather than improve it. The last genetic operator we use is the preserving. It is just copying one solution form the old population into the new generation.

V. SELECTION AND EVOLUTION

We offer two methods of selection. These are the three-tournament selection and semi-elitism method. The three-tournament selection involves selecting three absolutely random chromosomes from the current generation. They are evaluated and then sorted ascending. The worst of the three is eliminated from consequent evolution. In the crossover phase are used the better two chromosomes and in mutation and preserving is used only the best of the three randomly chosen chromosomes. The semi-elitism selection method is a variant of the classical elitism. It finds the best chromosome but does not find the next better chromosome. Instead it chooses randomly the second genetic operand. In mutation and preservation only the best chromosome of the whole population takes place. We do not use the best two chromosomes in crossover due to the aggregate violations avoiding. It is proven that in most cases the first two best chromosomes are almost identical and it is likely that swapping them will give no good result. That's why we do not use them.

Selection is not enough to retrieve the new solution candidates. Evolution is the process of choosing which genetic operator to execute. There are probabilities for each genetic operator to switch. The program allows the user to adjust these values according to the specific situation. We assign a probabilities area which is units 100 long (if we work in per cent). Consider the following situation: crossover probability: 85%, mutation probability: 5%, preserve: 10%. The probabilities area will be divided into three fields: (0,5], (5,90] and (90,100]. Then a random number between 1 and 100 is selected and according to the probabilities area, the genetic operator is chosen. The next step in the implementation of the genetic algorithm is the evaluation.

VI. EVALUATION

Evaluating the chromosomes is carried out in two phases – evaluating the hard fitness and the soft fitness of a particular chromosome. Hard constraints must not be violated in order to have a useable timetable, so the primary criterion in the evaluation is the hard fitness value. It is formed as a simple sum of penalty points. A penalty point is given if a certain hard constraint isn't obeyed. The total hard fitness is evaluated by the following formulae Eq. (1):

$$TotalHardFitness = \sum_{k=0}^{N} fi_k \qquad (1)$$

The total hard fitness helps as at evaluating the algorithm's overall efficiency. It is used in graphics, visualizing the sequence of population propagation. Each chromosome is evaluated with arithmetic sum of its individual time slot violations. This process looks like Eq. (2):

$$Fitness = \sum_{k=0}^{n} TimeSlotClash_k \qquad (2)$$

n is the total amount of events taking part in the timetable construction. This is very important because just one violation in time slots makes the schedule unusable without manual corrections, but the purpose of our algorithm is to avoid manual corrections of a generated solution. The soft constraints evaluation is the same, but when comparing two chromosomes the hard fitness factor is more important than the soft fitness factor. The purpose of the genetic algorithm at all is to fulfill the hard constraints and to reduce the soft constraints maximally.

VII. EXPERIMENTAL DATA

An experimental implementation was done as a C++ object oriented program. It directly uses the evolution data for the particular timetable and draws a graphic which shows how the

conflicts go down. The black line represents the hard constraints and the red line represents the soft fitness. Here we show how the population size affects the speed of finding a satisfactory solution. The following table presents the experiments Table I:

TABLEI

Population size	***Selection***
32	Tournament
32	Semi-elitism
128	Tournament
128	Semi-elitism

First, we experiment with a population of 32 solution candidates using tournament selection. The result is shown in the following figure Fig. 1:

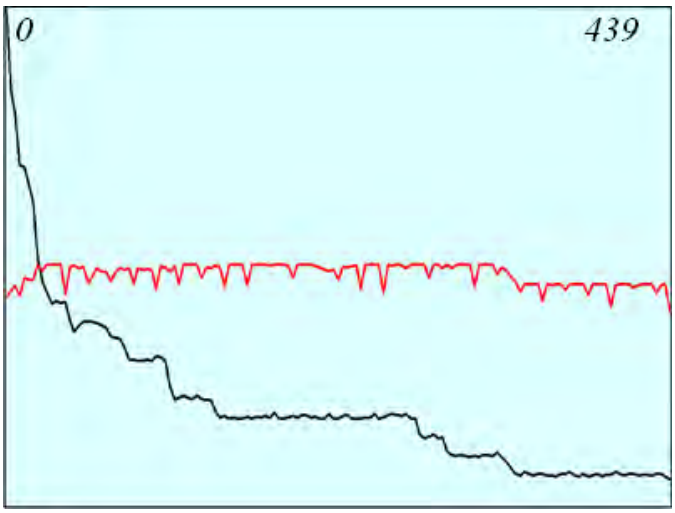

Fig. 1

The population number 439 contains a chromosome which is fulfilled every hard constraint in its set. The next figure shows the results of the same population size, but using elitism Fig. 2:

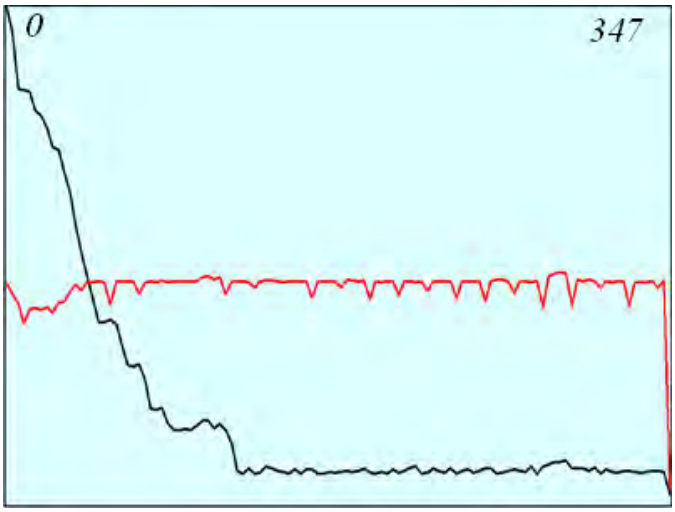

Fig. 2

It is obvious that using elitism reduces the total number of generations which are evolved. Also the better solution is found faster than the tournament selection. The population size here is more important than the selection method. The following two figures show how the solution improves faster and faster when the population size is 128. The time taken however increases as the population size increases, so when dealing with larger data sets it's necessary to choose the most appropriate population size. Fig. 3 shows that when the population size is bigger, the number of generations is lower. It's using a tournament selection.

Fig. 3

The fourth experiment is the same as the third experiment except for the selection method. Here is used elitism which reduces the generations Fig. 4.

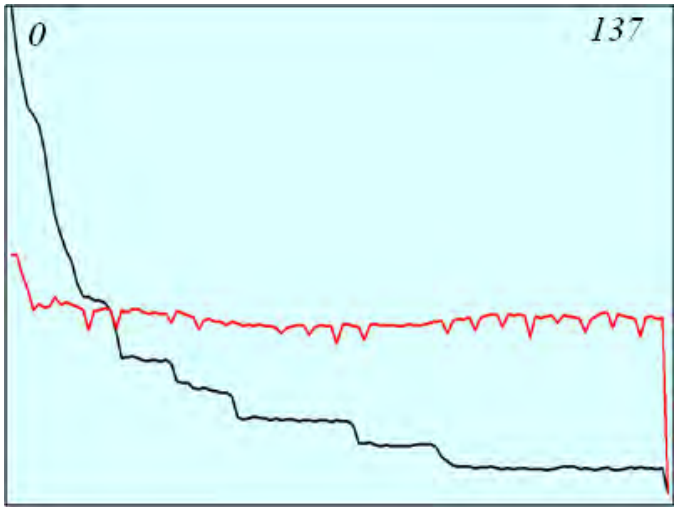

Fig. 4

All of the above experiments use these genetic operator probabilities:

Crossover – 87%

Mutation – 5%
Preserving – 8%

The program allows these values to be adjusted whenever the user wants to do so. For the bulk of data sets the above values give pretty good results and that's why we used them in the experiments.

VIII. CONCLUSION

We presented a algorithm for solving timetabling problems, which combines principles of the local search with other techniques for solving constraint satisfaction problems. The proposed principles can be applied to other constraints satisfaction problems; they can be easily extended to cover additional hard and soft constraints.

Further research is oriented both theoretically, to formalize the techniques and to put them in a wider context of constraint programming, and practically, to implement the above described genetic algorithm.

REFERENCES

[1] Abramson D., Abela, A Parallel genetic algorithm for Solving the school Timetabling Problem., Royal Melbourne Institute of technology, 1991

[2] Burke E., Ross P., Practice and Theory of Automated Timetabling. Lectures Notes In Computer Science Springer, Berlin 1996

[3] Michalewicz Z., Janikow C., Handling constraints in genetic algorithms. In Proceeding of the 4th International Conference in Gas. Morgan Kauffman, 1991.

[4] Michalewicz Z, Genetic Algorithms+ Data Structures = Evolution Programs, Springer Verlag, 1992.

[5] Syswerda G. Uniform crossover in genetic algorithms. Proceeding of Third International Conference of Genetic algorithms

[6] Corne D., Ogden J., Evolutionary Optimisation of Methodist Preaching Timetables, Selected papers from the Second International Conference on Practice and Theory of Automated Timetabling II, p.142-155, August 20-22 1997.

[7] Goldberg D., Web courses, http://www.engr.uiuc.edu/OCEE, 2000

VIP Customers Management System in Bulgarian Telecommunication Company

Daniela L. Yordanova-Todorova[1], Daniel A. Dankov[2] and Rositsa G. Hinova [3]

Abstract **- BTC have developed a CRM System guaranteeing the automation of all main processes related to the company's relations with corporate customers. CRM System is established as an integrated platform including following supports: Centralized Database of all Customers, Managing Sales Processes, Processing Customer Complaints and Giving Information. For centralization and automation of the relations with the Customers, CRM System develops IP Contact Center.**

Keywords **- Customer Relationship Management /CRM/, Internet Protocol Contact Center /IPCC/, Intelligent Contact Management /ICM/, Cisco Call Manager /CCM/, Interactive Voice Response /IVR/.**

I. INTRODUCTION

BTC is the incumbent operator in Bulgaria and provides telecommunications services with a national coverage. The company wishes to improve the way of key customer care in view of the retention of their loyalty throughout the forthcoming liberalization of the telecommunications market in Bulgaria.

The system covers a limited number of key customers of BTC in the first phase of the implementation. Subsequently the number of key customers will gradually increase till the system encompasses all business customers of the Company.

II. IPCC COMPONENTS

Using Cisco and Microsoft technologies, Cisco IPCC contains the following components:

ICM System

ICM system is dedicated to call routing and also logs calls to the main ICM database. This combined Router and Logger is called a "Rogger".

CCM

CCM software provides traditional PBX telephony features and functions (basic call processing, signalling, and connection services) to packet telephony devices such as Cisco IP phones and Voice over IP Gateways /VoIP Gateways/. Supplementary and enhanced services - including hold, transfer, forward, conference, automatic route selection, speed dial, last-number redial, and more - are also provided.

IVR

Within the IPCC, an IVR can act as a queue point, a routing client, as a managed resource and as an information source for consolidated real-time and historical reports. If an appropriate agent is not available when a call is received, the IPCC utilizes the IVR for call treatment such as playing announcements, collecting digits, or offering alternate routing options before redirecting the call to a targeted answering resource.

In our system the IVR is used to gather customer-profile information, to complete transactions, or to queue calls.

Peripheral Gateways

A Peripheral Gateway /PG/ provides an interface between ICM software and a system peripheral. Each PG tracks events on a per-agent and per-contact basis, ensuring the most accurate routing decisions possible.

The IPCC includes following PG software:

CCM PG

The CCM PG provides the interface to the CCM from the ICM. It provides information on incoming calls from the CCM into the ICM call router. It also provides information from the CCM to the ICM Controller, on the status of all Agents connected to the CCM.

IVR PG

The IVR PG provides the interface between the ICM system and the IVR subsystem and facilitates the routing of calls and data to or from the IVR system. The PG provides information to the Central Controller of the status of all IVR Ports /Agents/. In addition, it passes all the Customer entered data, collected at the IVR for the call, back to the ICM.

Computer Telephony Integration /CTI/, CTI Object Server /CTIOS/ PG

The CTI/CTIOS PG provides an interface between the ICM system and workstations or server-based applications, thereby facilitating the integration of calls and call-related data with these applications. The CTI/CTIOS PG runs the CTI/CTIOS Server component of ICM. Client applications that need to make use of the functions provided by the CTI/CTIOS Gateway, call these functions via a CTI/CTIOS Client component.

Call History System

The Call History System is configured to replicate a pre-defined set of call information from the main ICM Logger database and store it in the Historical database. This database can then be used to generate reports analysing call activity over time, performing trend analyses etc.

Agent Workstation Clarify Client

The Agent workstation Clarify client software provides the Agents with the application functionality that they require to process incoming customer calls. In order to utilize functions of the ICM system, these workstations run a program developed to communicate between the Clarify CRM desktop and the ICM via the CTI/CTIOS Server.

Admin Workstations

The Admin Workstations provide facilities for monitoring and administering the ICM System and for generating reports. Webview Admin Workstations are used to access

[1]Daniela L. Yordanova-Todorova is with BTC, 8 Haidushka poliana Str., 1612 Sofia, Bulgaria, E-mail: djordanova.cits@btc.bg

[2]Daniel A. Dankov is with BTC, 8 Haidushka poliana Str., 1612 Sofia, Bulgaria, E-mail: ddankov.cits@btc.bg

[3]Rositsa G. Hinova is with BTC, 8 Haidushka poliana Str., 1612 Sofia, Bulgaria, E-mail: rhinova.cits@btc.bg

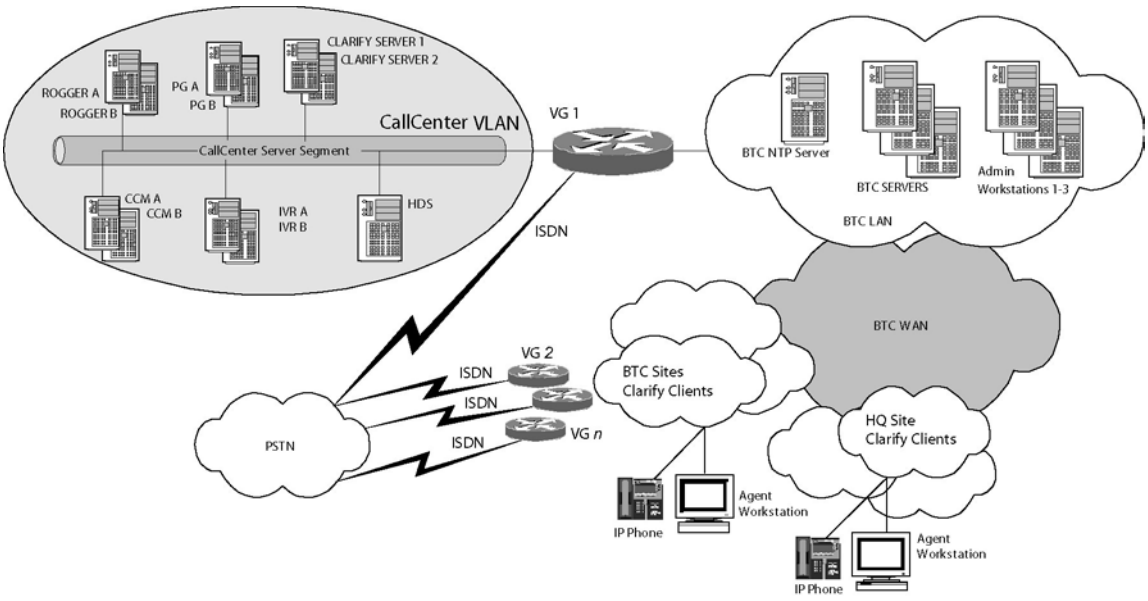

Fig. 1. IPCC Infrastructure

administration functions, including scripting and report generation, over an Intranet using a Web browser.

The Agents connected to the IPCC utilize the Cisco IP Telephone 7940. This full-featured, second-generation voice instrument uses IP transport technology to permit the consolidation of data and voice into a single network infrastructure.

VoIP Gateways

The VoIP Gateways are used as interfaces between Public Switched Telephone Network and IP Network.

III. IPCC Infrastructure

The network diagram of the IPCC structure is given in Fig.1. As shown in Fig. 1, a Failover IPCC System replicates all the components of the Primary system so that all data is also available in the event of a failover situation occurring.

IV. BTC Application Call Flow

The developed application consists of the following components:

Agent Logon/Logoff

The Agents "log on" to the Clarify desktop client application, which in turn notifies the ICM system which creates a real-time table associating the Agent number with the IP Phone handset IP address and the Desktop Workstation IP address. The Agents will have already been set up in the ICM with Agent ID, Name, skill sets and password.

ICM Call Routing

The ICM controls the incoming call from when it arrives at the Gateway to when the Customer disconnects. Cisco ICM software provides the central intelligence for call routing.

The routing are:

All calls requesting "Sales" are routed to an Agent with Sales as a primary skill set if available, if not route to Agent with Sales as secondary skills.

Cisco IP Telephones

All calls requesting "Complaints" are routed to an Agent with Complaints as a primary skill set if available, if not route to Agent with Complaints as secondary skills.

All calls requesting "Information" are routed to an Agent with Information as a primary skill set if available, if not route to Agent with Information as secondary skills.

All other calls are routed to an multi-skilled Agent.

IVR Functions

In this application the IVR is used to gather customer-profile information (via database lookup), to complete transactions, or to queue calls.

Database Lookup

As part of the process for gathering information on which to base call routing decisions, the ICM/IPCC needs to access suitable Customer records. The Clarify Oracle Database contains detailed records and history for all the Customers that will call the BTC Contact Center. This database could be accessed from either the ICM or the IVR. The IVR scripts that have been developed make a database lookup to Clarify Oracle Database based on a variety of information, either from the call context (ANI, DNIS…), or customer provided via Caller Entered Digits (CED).

Interface with Clarify Desktop

The Cisco IPCC (IP Contact Center) gathers information from a number of different sources:

From the telephony network: Caller number (ANI or CLI), called number (DNIS)…

From the caller themselves via IVR and Caller Entered Data (CED): e.g. Customer account number

From database lookups generated by either IVR or ICM call Routing scripts.

A Clarify CRM system uses Clarify desktop thick clients. The easiest, quickest and safest way to access this client from/to another application is by using Dynamic Data Exchange (DDE).

Clarify Driver has been developed as an interface

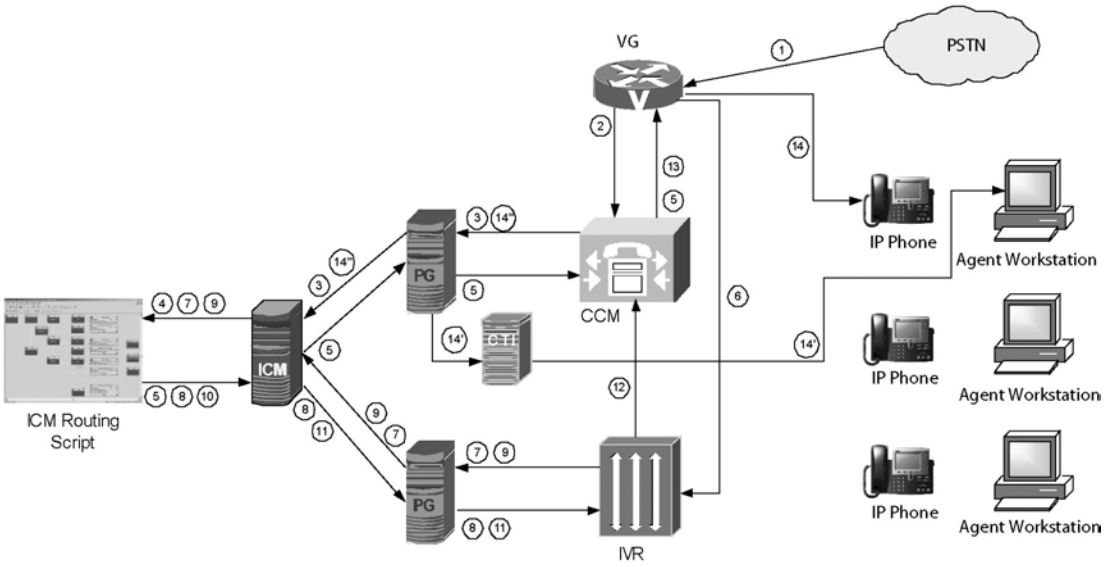

Fig. 2. Customer incoming call flow

application, accessing Cisco ICM through CTI OS ActiveX component and the Clarify desktop thick client via DDE.

Reporting

Enterprise wide Reporting is facilitated via Admin Workstations. The standard IPCC system reports, both real-time and historical, are available - info on specific skill groups, services, peripherals, routes end scripts. Historical data are stored in the ICM central database at five- and 30-minute intervals. In addition, tools are provided for developing custom reports.

Customer call follows the call flow shown in Fig. 2 and contents the steps described below.

Step 1: A customer dials a BTC telephone number that terminates on a port on Cisco 3660 VoIP Gateway.

Step 2: The VoIP Gateway forwards the customer call to CCM.

Step 3: The CCM, using ICM PG, sends a Route Request to ICM Rogger.

Step 4: The ICM Router, based on dialed number, and follow CallType CT_IncomingCall, runs script IncomingCall.

Step 5: The ICM script, using Translational Route, sends message to the VoIP Gateway (via PG and CCM) to transfer the call to one of IVR servers.

Step 6: The VoIP Gateway sends the customer call to the selected IVR server.

Step 7: The IVR sends a REQUEST_INSTRUCTION request to the ICM Router informing the ICM that a call has arrived at the IVR and is awaiting queue instructions.

Step 8: The ICM script sends a RUN_SCRIPT request to the IVR containing a script number that instructs the IVR what queue treatment should be provided to the caller.

Step 9: The IVR performs a database lookup on Customer ANI aqainst the Clarify Oracle database and sends a RUN_SCRIPT_RESULT message to the ICM Router indicating that the specified script has been executed and attaches the call variables with the results.

Step 8' and 9': The steps 8 and 9 are repeated so many times as the ICM script instructs.

Step 10: The ICM script decides to send the call to an available agent.

Step 11: The ICM Router sends a CONNECT request to the IVR containing the destination label of the device target.

Step 12: The IVR interprets the label and sends a re-direct request message to the CCM requesting the CCM to redirect the call to the particular extension (dialed number).

Step 13: The CCM finds the IP phone with the line that maps to the dialed number. The CCM associates the dialed number with an IP Address for the agent phone (all IP phones register with a CM and update it with their current IP address). The CCM will direct the VoIP Gateway to redirect the RTP stream to the agent's extension.

Step 14: The VoIP Gateway and IP Phone begin sending voice RTP streams to each other.

Step 14': CTI information is sent to Clarify Desktop through CTI server.

Step 14": Call information is returned back to ICM for some statistics.

V. CONCLUSION

In the next phases CRM System should have interfaces to and from BTC Systems associated with customer servicing: Regional Systems for Customer Care and Network Description (ISOM/RILA) and Regional Billing Systems (ISOA).

The IPCC can be extended and used for other BTC Systems. For example the IPCC service Customer Calls about Intelligent Network problems.

ACKNOWLEDGMENT

Hewlett-Packard Bulgaria

REFERENCES

[1] CCM ver. 3.2 Documentation
[2] ICM ver. 4.6 Documentation
[3] IVR Documentation

Monitoring of Processes in an Induction Heated Electro-Technological Installation

Stanimir Y.Yordanov[1], Nikolay D. Madzharov [2]

Abstract: **This paper describes a general structure of a computer-implemented, object-oriented software system is describe. The system uses artificial intelligence mechanisms and is intended for the control of technical objects that function both in predictable and random environments. The structural and regular nature of the suggested system can be use for creation dedicated computers which operate on non-Von Neumann's principles and mechanisms of generating neural-network structure.**

Keywords: **Real-Time problems; RTS System Kernel functions; Automatically programmed RTS, Neural network identification and control**

I. Introduction

Contemporary industry has at hand a wide spectrum of methods for ensuring quality of output. On the other hand technological process has a substantial impact on both the structure and the construction of active control systems. The questions here is the choice of the most appropriate method for the specific case. One possible solution for reducing quality assurance costs is the optimization and management of production processes by active monitoring of the basic production parameters [5].

In the basis of this direction is real time observation of production processes. Based on of the alteration of a certain number of quantities, one can judge about the final production output. This control method is characterized by high reliability, reduction of defects due to the possibility for an immediate reading of any change in the normal production progress, as well as the possibility for anticipating of the occurring changes [4]. For this purpose it is necessary to create specialized software for the realization of the active monitoring method. The present paper describes the application of an active monitoring system in an electro-technological installation for food processing industry.

II. Object Description

A number of contemporary electro-technological processes with inductive heating when producing packaging for food industry are characterized by a wide range of inductors, mainly low-impedance ones, working in a specific sequence of heating. Having in mind the high precision of processes and the quality of the end product, a strictly defined voltage should be supplied for the respective inductors. This condition places requirements to the power sources for the cases when it is necessary to rapidly switch from one inductor to the other with exact co-ordination of voltage and power.

[1] Stanimir Y.Yordanov is with the Technical University of Gabrovo, H.Dimitar str. 4, 5300 Gabrovo, Bulgaria e-mail: sjjordanov@tugab.bg Pfone: 0035966223571

[2]Nikolay D. Madzharov is with the Technical University of Gabrovo, H.Dimitar str. 4, 5300 Gabrovo, Bulgaria e-mail: madjarov@tugab.bg Pfone: 0035966223557, Fax: 003596624856

There exist several approaches to satisfy those specific requirements. Most often it is power supply represented by transistor power supply with autonomous inverters (AI) feeding the various inductors, according to the diagram on Figure 1, which is used in this paper

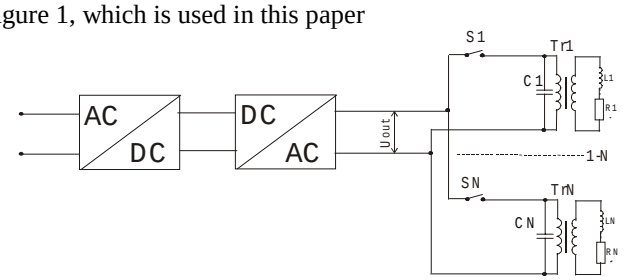

Fig 1: A principle diagram of a induction heating installation

Which consists of:

- AC/DC block– rectifier and DC/DC converter (PWM-type), intended to ensure necessary DC voltage of the AI.
- DC/AC high-frequency power supply, intended to convert direct into high frequency alternating energy about 550kHz
- the system with individual transformers and tank circuits

As it can be seen the supply source is switched by the electronic switches S1 – SN to the coils L1, R1 – LN, RN, which have their own output transformers Tr1–TrN and matching capacitors C1-CN. Individual power for a given inductor is specified by the autonomous inverter (AI) direct currency control. In this case the AI output voltage is invariable and is controlled in narrow limits and by the output transformers Tr1–TrN and the matching capacitors C1-CN is maintained the predefined value of the equivalent resistance of the tank circuit, working in resonance or near-resonance. More detailed information on the generator function can be found in [1 in 2].

Functional capabilities of the system with individual transformers and tank circuit are good, but the presence of appliance complexity is apparent, also exploitation inconveniences and in some cases reduced reliability. To solve the problem instead of a parallel, rather a parallel-serial tank circuit is used together with a system for active monitoring of processes.

III. Selection of analysis parameters

The object of production is cartons for liquid products. For their manufacturing it is necessary to be made three seams. Each seam is a volume of foil with thickness 0.008 mm, which has to be heated and also plastic which has to be melted. It is obvious that to have a quality seam i.e. to melt the plastic at the required temperature, a specific power

quantity has to be applied for a given time at the place of seaming. Power can be easily calculated if the parameters of the inductor are measured – the current, the voltage and the phase shift between them, i.e. $P = U.I.\cos\varphi$. The power depends on the mutual position of the inductor and the foil to be welded and obviously it is a major criterion, by which the quality of the manufactured carton can be judged. If P is less than necessary, an uneven, thin seam will be produced, if P is higher, the seam will overburn and again will not have the required quality. Less P occurs at a longer distance between the inductor and the foil, the reason for which could be simply mechanical.

Assessment of power is made on the basis of voltages of the secondary coil of the transformer and the inverter.

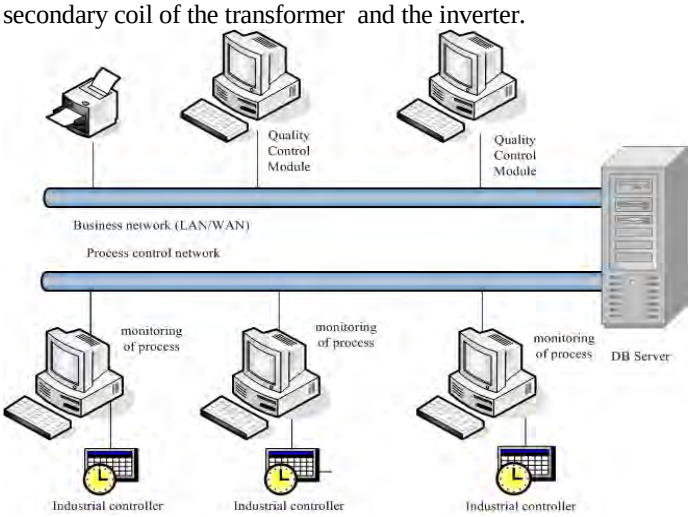

Fig.3. The structure of system.

Based on these arguments the system for quality assessment of cartons manufacturing is built, namely by measuring the principal electric parameters of the system *inductor-welded foil*, to calculate the power transmitted in each seam and by subsequent computer data processing to control the quality of cartons as a whole and to provide an estimation of its level.

IV. Structure of a software system for active monitoring.

The structure for active monitoring of processes is shown on Figure 3.

The system consists of the following modules:

- Operating control module – designed to collect data, during the manufacturing process up to their importing to the main database. The latter resides on the same computer as the Operating control module.
- Local Database – this keeps data received during production up to its import to the Main Database. It resides in the same computer as the Details Quality Control and Assessment Module.
- Main Database – it keeps data about the process flow of all manufactured details, as well as the data received after analysing the preceding data. The time for keeping the data is defined by the specific character of manufacturing and the corporative policy regarding this information. It is situated on a separate file server.
- Details Quality Control and Assessment Module – designed to perform an analysis of manufacturing data and yield a conclusion about production quality. Based on data received, an analysis of the tendency on quality managemnt and decisions are taken on the manufacturing process.
- Module for design of active processes monitoring – its purpose is to build up the topology of the monitoring system.

V. System Implementation

a) System Structure

The separate functions are realized bt three software modules: Active Monitoring and Process Management Module - *Control Manager*, Data Statistical Processing and Keeping - *Quality Manager* and a Module for Database Creation and Editing of supported technological processes - *Library Manager*. A key stage in system realization is the choice of platform for its realization.

The present system is realized on Windows NT. The prerequisites for the choice of this platform are:

- popular and easy to use graphic interface
- widely distributed applications, servicing and maintenance of devices (serial, parallel and network) and a specialized interface (for animation), which can be used to sell the new products and applications faster.
- Possibility for operating on a wide range of cheap PC platforms, which reduces application costs.
- a wide range of software instruments and a large number of experiences developers which reduces development costs
- whole and continuous interaction between the hardware elements, the OS and the software means RTS
- time necessary for developing of an efficient software application
- The necessary human working hours for RTS designing, adjustment and servicing
- Low-level drivers are already created
- Windows NT comprises all aspects of network integration and file management
- The known technologies and management algorithms allow for an easy implementation

The active monitoring system is designed for real-time operation. Hence a basic parameter in its implementation is the reaction time. After performing an analysis of the processes in the induction-heated electro-technological system for the food processing industry the following conclusions were reached at regarding the quantities, characterizing the manufacturing process. These are the power in the secondary coil of the output transformer and the inductor. With three seams it is apparent that to assess the suitability of the package four parameters of the welding operation need to be monitored.

The process of collecting and analysis of data is performed in a sequence, shown on figure 4.

The time for data processing is defined by the necessary technological period for each stage like transformation of analogue signals, data receiving and buffering T_o, data processing T_1; visualization and saving T_2; object feedback T_3.

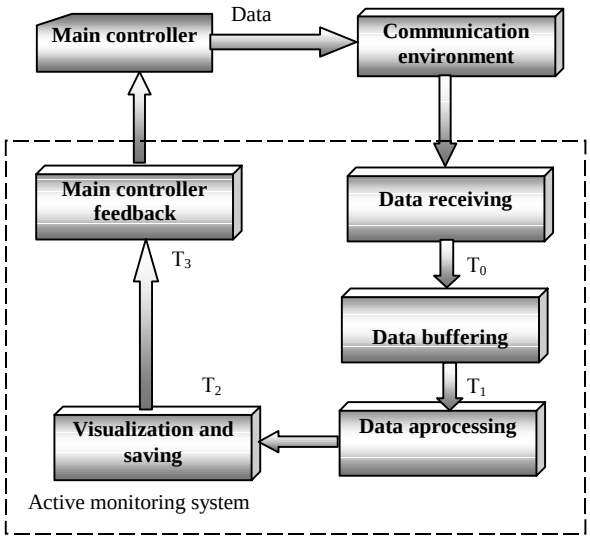

Fig. 4. Flowchart of data flow in the software system

b) Analysis of the system processes

The duration of a work cycle is in the order of 150 ms. Therefore the data analysis should be performed within this period. The *Quality Control* module (Fig 5) can function at 0.1 ms clock as timed by a PC.

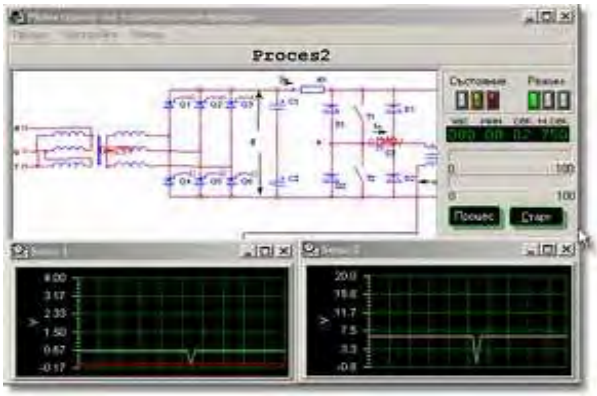

Fig 5. Quality Control module

Therefore 1500 quantity points will be available for process analysis. This data is pretty large and the processes are comparatively inertial. After the performed analysis, a conclusion is drawn that 10 quantity points are enough for processes identification or discreteness of 15 ms. For a higher precision the discreteness clock is set to 1 ms.

Two approaches for process analysis are used. With the first one the data is processed in real time by a module based on a neural network (Fig 6) and with the other the analysis is performed subsequently by the statistical control module *Quality Manager* (Fig 7).

The system operates with a huge quantity of data. From the analysis performed for a manufacturing cycle 57600 bytes will be necessary and for a twenty-four hour period about 33177600000 bytes or 30.8990 GB will be necessary.

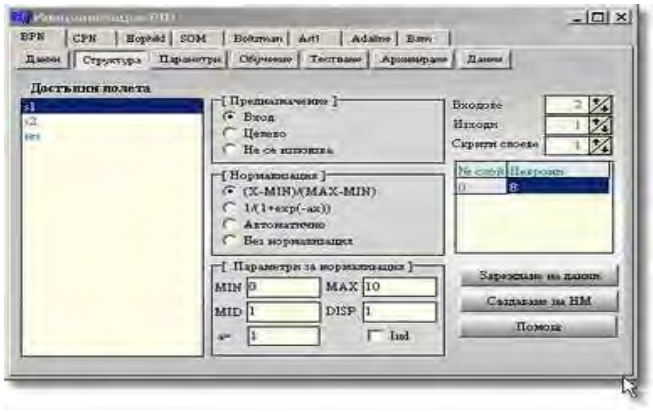

Fig 6. Choice of a neural network structure

Fig. 7. The Quality Manager module

To limit the quantity of data saved in the database several approaches are used. With the first of them in the database is written only data overflowing a given interval, set in the process of system calibration. It is obvious that this approach is suitable for evaluating of the *fit – unfit* type, however it is not suitable for to analyse the tendency of process alteration. The second approach is based on the introduction of a mechanism for data compression which consists of the following.

At discretisation (квантуване) of input processes $f(t)$ their discrete equivalents are formed $f^*(t)$ by special algorithms, allowing to remove the surplus information. We are speaking about those discrete amplitudes of $f^*(t)$, which could be excluded from input into the computer memory. In this way memory is saved without reducing the informative content of $f^*(t)$.For this case e so called compression coefficient is entered

$$K = \frac{N_c}{N} \qquad (1)$$

where $Nç$ is the number of essential amplitudes of $f^*(t)$, respectively $f(t)$, for a given interval [0,T], and N is the total amount of amplitudes of $f^*(t)$, within the same interval. These values are obtained with a set constant discretisation time Δt.

In the present system as meaningless are considered those amplitudes of $f^*(t)$, which differ insignificantly from the last amplitude considered as meaningful. If the amplitude $f^*(n)$s considered meaningful (it is the first amplitude of the process, for which it is obligatory), then $f^*(n+1)$ is also considered meaningful if the following

inequality is fulfilled:

$$\left| f^*(n) - f^*(n+1) \right| \geq \delta \qquad (2)$$

where δ is the significance level of the separate amplitudes one to another. In the course of a single time interval *t* after the moment $t=n.\delta$ *t* the zone limited by the quantity $f=\{f^*(n)+\delta, f^*(n)-\delta\}$, shows where should reside the following meaningless (insignificant) amplitude $f^*(n+1)$.

The algorithms by which it could be defined that a given amplitude is meaningful or not, are various. Though it is clear, that they should be based on the analysis of the dynamic properties of real time processes. As a conclusion it could be deducted that with a carefully selected data compression algorithm the effect from sparing computer memory when processing the information could be substantial. This effect is especially apparent with non- stationary processes, entering at the input of the active monitoring system. In the present system δ is chosen from the following dependency $\delta = (y(T_2) - y(T_1))/4$, where $y(T_1)$ and $y(T_2)$ are respectively the values of the signal at two pre-selected points when describing the borderline deflections.

c) Analysis of the processes by artificial neural networks.

To perform a real time analysis of the process an artificial neural network is used with backward distribution. This type of network is chosen regardless of the fact that the training process is very slow. This type of networks can function with a huge amount of data. For the purposes of the present idea this is very important. Moreover the training process itself is steady enough. That is, if in the training data a series of incorrect information is supplied and afterwards a series of corrected data is provided, the final result of the teaching will not be altered, with the exception that the training time will be changed. The applied training methods affect all data, which is why increasing training data will alter the training period. Besides that the backward distribution method does not give way to the other methods when dealing with a small data quantity; the precise training methods would yield a smaller error at the time of training but at operation time the error would be commensurable.

A major indicator for control quality is the error level. When having networks with equal error level it is advisable to select the one with a simpler structure. The necessity of multiple experiments leads to the fact the control set starts playing a key role as a correcting factor. This enforces the choice of a new control sequence. The network was tested with them to make sure that training is real, and is not an artifact of the training process. Of course the test set should be used only once. Its repeated usage turns it into a control set.

Working out of the network in the constructed system after choosing the input variables consists of the following steps:

- Choice of an initial network configuration (for example an intermediate layer of elements equal to half of the sum of inputs and outputs times three minus one).
- Performing a series of experiments with various configurations, keeping the best of them. In the package *Cunami Neural Networks* an automatic keeping the best network during the experiment. For each configuration several experiments have to be performed, to make sure that we haven't fallen into a local minimum.
- If at training it proves that the network is under-trained, additional neurons and intermediate layers are added.

If there is re-training (the control error starts going up), some of the elements have to be removed. Neural networks function with a certain amount of data, distributed in a given range. For this reason input data are scaled into a certain range and the missed data are replaced by average values.

VI.Conclusion

Quality management of production is a fundamental priority in industry. In the present article a method for achieving these aims is described. The high efficiency of this solution consists of the analysis of production based on the processes running during the production cycle. This allows for an immediate reaction to the alterations of processes, as well as for anticipating any change in the execution as a result of the alteration of some quantities. In this way it is possible to directly exert influence on processes during its run. The proposed solution functions on a Windows NT Platform, which is an additional prerequisite for the low price of the system. The software application, which ensures the efficiency of the execution is based on RTS Kernel, operating with regular constant objects. In this case a higher reliability and efficiency during operation is achieved. Using artificial neural networks in the control and management module makes the system exceptionally flexible and applicable with a wide range of electro-technological systems.

References

[1] Todorov T.S., Madzharov N.D., Aleksiev D.T., Ivanov P.T., Autonomous inverters, Gabrovo, 1996 – (in Bulgarian)

[2] Madzharov N.D., Development and research of the autonomous inverters with energy dosing. Dissertation on scientific degree "Doctor", Gabrovo, 1997.

[3] Todorov T.S., Madzharov N.D., Alexiev D.T., Ivanov P.T., Adaptive Resonant Inverter for Electrothermics, Proceedings PCIM'95, Power Conversion, Nurnberg, Germany, 1995, pp. 379-391

[4] Yordanov S., T. Todorov, System for quality control and monitoring of the main variables of electrothechnical systems, Int. Conf. ET2000 –Sozopol (in Bulgarian)

[5.] Yordanov S. The Real-Time Expert Control Systems International Conference on Computer Systems and Technologies - *CompSysTech'2002*

[6]. Yordanov S. Aplication of Self Organizing Maps-SOM in systems for active monoring quality. International scientific conference 2003, Gabrovo –(in Bulgarian)

[7.] Rudner V.I.,D.L.Laveles Modern power supplies, road matching, process control and monitoring. Inductoheat 1997

[8] By Ray L. Cook, R.L.Myers. Process monitoring for more effective induction handening control. MAN-Modern Application News, August 1995.

Failure Analysis of Semiconductor Devices

Neli G. Georgieva

Abstract - **This paper is devoted to problems, connected with failures of semiconductor devices. It is made a review of some fundamental requirements, which should be completed from semiconductor devices, reliability prediction approach, and prognostication methods. Some requirements, completed from the conditions by which the semiconductor devices and integral circuits should be tested, are presented by means of tables. Special attention is paid to the reliability problems, connected with the failures in some Insulated Gate Bipolar Transistors (IGBT). Failures of some power semiconductor devices are analyzed and their operated reliability is predicted.**

Keywords - **failure analysis, reliability of the electronic device.**

I. Some Requirements for the Reliability of the Semiconductor Devices

Reliability is the characteristic expressed by the probability that the part will perform its intended function for a specific period of time under defined usage conditions.

Every Company, producing semiconductors, should achieve best-in-class quality and reliability performance on all their products through a systematic approach that emphasizes quality at every phase of product development through manufacturing. From initial design conception to fabrication, test, and assembly; quality is built-in and assured through stringent SPC monitoring of fabrication and assembly processes, materials inspections, wafer level reliability, new product qualifications, reliability monitoring of finished product and strict change control management.

There are 2 basic types of failures, Early Failures and Wear Out Failures. These are reflected in the curve known as the Bathtub curve (fig. 1).

Companies, producing semiconductors, should use Reliability Testing to ensure all its products are below targets set for Early Failure Rates in PPM and Wear Out Failures in FITs.

Qualification. *New processes and new packages.* New processes and New Packages are qualified using a minimum 3 lot (77 units per lot) testing for: 1. Early Failure Testing (915 samples); 2. Operating Life Test; 3. Temp and Humidity Biased Test; 4. Temperature Cycling; 5. Auto-Clave; 6. ESD/ Latch-Up; 7. Board Level Temp Cycle (for packages). Power cycling and data retention testing is also done when applicable.

Smart quals. Products designed to process and package design rules and using qualified processes and packages are released using 168hr reliability data. This approach supports Time to Market needs without compromising reliability. In order to ensure there is no customer risk, it should be create a continuous reliability monitoring in place.

Reliability monitor program. An ongoing reliability mo nitor is in place to ensure that products manufactured to qualified processes under qualified reliability standards, has not drifted.

Dates of the reliability monitor program should be published in catalogs, reference book and handbook for semiconductor device; Test frequency is as posted below (Tab 1).

[1] ***Ph. D. Neli Gentcheva Georgieva, is with the Technical University - Varna, Departments of Electronic Engineering, str. Studentska 1, Varna, Bulgaria, e-mail: neligeorgieva@yahoo.com***

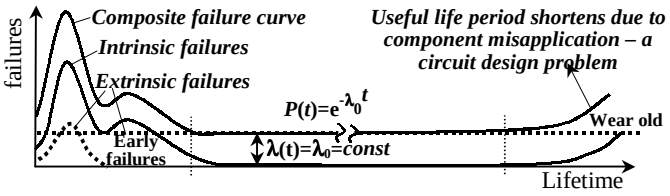

Fig.1 Illustration of intrinsic, extrinsic, and composite reliability curves for component hazard rate in a field-operating environment.

TABLE 1.

Test	Frequency
EFR (All major processes)	Every week
OPL (1000 hr)	Every 8 weeks
THBT (1000 hr)	Every 8 weeks
ACLV (96 hr)	Every 8 weeks
TMCL (1000 cycles)	Every 8 weeks

Fix reliability testing capabilities reliability test services and ESD and Latch-up testing labs are fully equipped to support the reliability qualification testing. Details of the lab equipment are listed in the following two tables. Reliability testing services equipment inventory.

TABLE 2. EQUIPMENT IN THE ESD/LATCH-UP LAB

	Keytek Zap Maste	RCDM	MK-2
Max Pins	256	N/A	768
HBM Voltage	25÷12000	50÷4000	50÷8000
MM Voltage	25÷2000	N/A	50÷2000
IEC 1000 Capable	Yes	No	No
On Board Clock	No	No	Yes
Vectored Latch-up	No	No	Yes

Failure mechanisms/failure models. Various failure mechanisms are tested during Reliability Testing. Major ones are listed below.

Determination of failure rate (point estimate). Failure rate can be determined by using actual test results. Determine "demonstrated" failure rate from actual test data as follows:

Failure Rate=No. rejects/sample size x no. hours.

Example 1. Assume a sample size of 13500, 2 failures and test duration of 500 hours. To calculate FR: FR=2 rejects/13500 devices x 500 hours; FR=2/6750000 device-hours=296.10^{-9} rejects per device-hour; 296 FITS (reciprocal of 296.10^{-9}) or 3375,000 hours MTBF.

In expressing failure Rate, the equivalent values below may be helpful.

Determination of failure rate (statistical estimates). In addition to point estimates, FR and MTBF may be estimated by using the chi-square statistic at 2(r+1) degrees of freedom. The 50% probability statistic would give the "best estimate"; the 60% or 90% probability statistic would give the upper confidence limit.

Acceleration factors. In order to express accelerated test results in terms of expected failure rate at actual use conditions, semiconductor manufacturers commonly use the Arrhenius model. The Arrhenius model assumes that degradation of a performance parameter is linear with time, with the rate of degradation depending on the temperature stress. To put it another way, the Arrhenius equation relates *t* where: he time rate of change of a process to the temperature at which the process

is taking place. If appropriate, the calculated acceleration factors listed in the following table may be used.

TABLE 3. FAILURE MECHANISM AND MODEL

Mechanism	Model
Failure Mechanism	Failure Model
Electromigration	Blacks Model
Excessive Intermetallics	Kidsons Model
Reverse Bias Breakdown	Tasca
Stress Dependent Diffusive Voiding	Okabayashi Model n NE 1, Okabayashi Model n EQ 1
Time Dependent Dielectric Breakdown	Fowler Nordhiem Tunnel Model
Slow Trapping	Positive Gate Voltage Model, Negative Gate Voltage Model
Metallization Corrosion	Plastic Metal Corrosion, Hermetic Metal Corrocion
Modular Case Fatigue	Shear Fatigue Model Case
Modular Case Fracture	Shear Fatigue Model Case
BGA Solder Fatigue	Time to fail by Creep,
Discrete Solder Fatigue	Dis Solder Jnt Cap 90pb10sn, Dis Soldr Jnt Fat Cap 63sn37pb
Flip Chip Solder Fatigue	Inner Flip Chip Revised, Hybrid Flip Chip Revised
Lead Seal Fracture	Principal Stress Model
Lead Solder Joint Fatigue	Thermal Cycle Fatigue Model
Lid Seal Fracture	Tensile Strength Model
Substrate Attach Fatigue	Substrate Attach Fracture Model, Substrate Attach Fatigue Model
Wire Bond Fatigue	Hu Pecht Dasgupta Model, Wirebond Pad Shear Failure, Bond Pad Fatigue Revised
Wire Fatigue	Hu Pecht Dasgupta Model
Electro Static Discharge	Wunsch and Bell Model, Wunsch and Bell Model, Wunsch and Bell Model

TABLE 4. RELIABILITY PARAMETERS

No. Failure Per Device-Hours	Failu Rat	% Per 000 Hour	PPM, Hours	FITS	MTBF Hours
$1/10^9$	10^{-9}	10^{-4}	10^{-3}	10^0	10^9
$1/10^8$	10^{-8}	10^{-3}	10^{-2}	10^1	10^8
$1/10^7$	10^{-7}	10^{-2}	10^{-1}	10^2	10^7
$1/10^6$	10^{-6}	10^{-1}	10^0	10^3	10^6
$1/10^5$	10^{-5}	10^0	10^1	10^4	10^5
$1/10^4$	10^{-4}	10^1	10^2	10^5	10^4
$1/10^3$	10^{-3}	10^2	10^3	10^6	10^3

Calculation of applicable junction temperature. Failure rates and MTBFs obtained from operating life tests pertain when the junction temperature is the same as the ambient test temperature. Temperatures used during OPL tests are usually T_A= 1250°C or T_A=1500°C. In most cases, these ambient temperatures are very close to the junction temperature T_J. However, when a significant difference between T_A and T_J exists, respective T_J must be considered. This would be the case with parts that dissipate significant amounts of power, such as certain linear and MOS devices.

To obtain FR and MTBF for a specific application where T_J differs significantly from T_A do the following: 1. Determine junction temperature for given application; 2. Calculate FR of MTBF at the applicable T_J, using the Arrhenius model. The equation for junction temperature for given application is:

$$T_J = T_A + P_D Q_{JA}, \quad (1)$$

where: T_J - junction temperature for given application; T_A - ambient temperature; P_D - power dissipated on the device (see datasheets for device); Q_{JA} - thermal resistance from junction to ambient (see datasheet).

TABLE 5. ACCELERATION FACTORS FOR COMMON JUNCTION TEMPERATURES AND COMMON ACTIVATION ENERGIES

Est. R_J accel. tests	Estimated TJ9 normal use application					Energies for Activation, eV
	25°C	35°C	45°C	55°C	35°C	
125°C	49	31	18	12	3.7	
130°C	58	35	22	14	4.3	0.4
150°C	89	60	37.4	24	7.3	
125°C	134	71	39.4	22.6	5.1	
130°C	160	85	47	27.1	6.1	0.5
150°C	317	169	92.6	53.4	12	
125°C	942	388	171	77.6	9.7	
130°C	1,218	500	219	101	12.6	0.7
150°C	3,159	1,300	569	259.1	32.7	
125°C	2,540	914	358	145	13.6	
130°C	3,377	1,221	476	193	18.1	0.8
150°C	10,041	3,632	1,414	575	53.8	
125°C	6,691	2,140	735	272	18.8	
130°C	9,174	2,964	1,006	370	26	0.9
150°C	31,256	0,10	3,429	1,261	88.2	

Example: Assume use condition for device LM741 is T_A= 50°C, V_S = ±20V. Determine T_J.

Solution: Datasheet for LM741 gives P_D = 150mW, and Q_{JA}= 150°C per walk. T_J = 50°C + 0,150 × 150°C = 72,5°C.

Confidence Factors. The failure rate resulting from a High Temperature Bias test is an average, or estimate, of the typical expected failure rate for a product or process; but has no statistical boundaries established.

Companies, that produce semiconductors, should use generally states the upper 60% confidence limit for failure rate estimate using the chi-squares statistic, per the following formula.

$$\lambda \max = \frac{\chi^2_{1-\alpha}[with\ df = 2(r+1)]}{2t} \quad (2)$$

where: λ_{max} - maximum failure rate or worst case; χ^2 - chi square distribution; r - number of failures; df - degrees of freedom; t - total number error test hours (number of devices x number of hours); α - statistical error expected in estimate (for 60% confidence α=0,6). α can then be interpreted to mean that we can state with statistical confidence of α (i.e., 60%) that the actual failure rate is equal to or less than the calculated max. failure rate (λ_{max}). Values of chi square are found in a number of statistical tables. A few more typical values are shown as follows (Table 6).

The fundamental theory governing the process of evidence evaluating is a principle of logic known as prediction (Bayes') theorem. The Bayes' prediction approach to reliability prognostication has been used for many years in specific applicati-

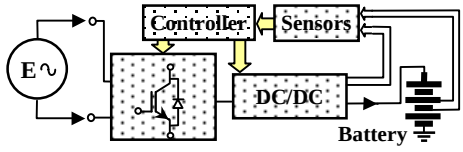

Fig. 1 The block diagram of a battery charger

ons due to certain advantages over traditional reliability analysis. Prognostication of the reliability is needed in the desing process to be able to build dependable systems that fulfill strict requirements regarding reliability and availability. Several models exist that are able to provide designers with an estimate of device or system reliability, however they have been found inadequate to predict the reliability of components in a number of situations, leaving the design engineer without a valuable tool for estimating the reliability of a system. The lace of accuracy of the models is usually related to the difference among the factors used to generate the model and the ones found in actual applications. Only when the application is very close to the one intended in the model, reliability prognostication can be done with a certain lover of confidence on the results.

Among the lots of components that are part of even the simplest electronic system, power devices play a fundamental role. These components are part of the power supply circuit that feeds the rest of the system, or part of the actuators that interact with the environment as outputs of the system. In each case, power devices have to work under heavy stress conditions; hence highly reliable components are required.

TABLE 6. PERCENTILES OF THE CHI^2 DISTRIBUTION. (VALUES OF CHI^2 CORRESPONDING TO CERTAIN SELECTED PROBABILITIES)

Typical Use		AQL	Best Estimate	50% Confidence	70% or 90% Confidence
Probability, %		5.0	50.0	60.0	90.0
1-α		0.05	0.50	0.60	0.90
df	Total Failures				
2	0	0.103	1.390	1.830	4.61
4	1	0.711	3.360	4.040	7.78
6	2	1.640	5.350	6.210	10.60
8	3	2.730	7.340	8.350	13.40
10	4	3.940	9.340	10.500	16.00
12	5	5.230	11.300	12.600	18.50
14	6	6.570	13.300	14.700	21.10
16	7	7.960	15.300	16.800	23.50
18	8	9.390	17.300	18.900	26.00
20	9	10.900	19.300	21.000	28.40
22	10	12.800	21.300	23.000	30.80
26	12	15.400	25.300	27.200	35.60
32	15	20.100	31.300	33.400	42.60
42	20	28.200	41.300	43.700	54.10

II. RELIABILITY OF THE POVER SEMICONDUCTOR DEVICES

Novadyes, the desing of highli efficient power supples can be accomplished using new power devices like Insulated Gate Bipolar Transistors (IGBTs). This kind of devices csn be directli connected to AC power supplies and can be used at switching frequencies of up to 40 kHz, whith allaws for the design of power supplies with very low harmonic distortion and high efficency. The general diagram of a battery charger that uses IGBTs in the rectifier stage shows in fig. 1, and table.7 shows some results from the reliability testing of IGBT.

Different current levels are supplied to the battery through an integrated modular DC/DC converter. The entire system is monitored and regulated by a controller that uses information from external sensors and an algorithm to perform an optimized charge.

High dependability is a fundamental requirement for this system, because of the potential harm to the environment (persons or machines) that can result from a failure. Our research focuses on the design of dependable systems through the use of highly reliable components and the application of design techniques that ensure correct operation or, in case of failure, safe outputs.

TABLE.7 RESULTS FROM THE RELIABILITY TESTING OF IGBT

Part Number Type		Package		Die Type	
HGT4E40N60B3S		TO-268		49052	
Stress	**Conditions**	**Duration**		**Results**	**Sample Size**
Drain Bias	Tc=150°C, Vds=80% Rated	1000	Hrs	2(1)	40
Thermal Fatigue	PD=40W, delta Tj=100°C	10,000	Cyc	INC	40
Temp Cycle	-65°C, +150°C, Air	1000	Cyc	2(1)	40
Relative Humidity	Ta=85°C, RH=85%	1000	Hrs	2(1)	40
Pressure Cooker	Ta=121°C, 15psi	168	Hrs	0	40
Operating LIfe	Tc=150°C, Vds=15V	500	Hrs	0	40
Note 1. High ICEs/IGEs due to cracked Nitride					

This paper describes our work on the first aspect, i.e., highly reliable components. The target device that we characterize is the IGBT because of its fundamental role in the system depicted in fig 1. IGBTs combine the best features of MOSFET and bipolar transistors, delivering high output impedance (insulated gate), and low conduction loss (bipolar transistor). Typical applications are AC/DC switch-mode power supplies, high voltage DC/DC, power factor correction stages, automotive ignition systems and motor drive systems.

A. Reliability tests and results

Design of dependable systems is done on the basis of accurate reliability prediction models that help the design engineer to choose the appropriate components for every application, and impose design c1onstraints of the system by providing the expected mean time to failure. Prediction models such as described by MIL-HDBK-217 are widely accepted in industry, however they do not provide accurate values in a number of situations. In this section we present the reliability tests that are part of the first phase of our research, where the goal is to determine degradation models for the power device presented in the previous section. Several environmental tests, as described in [4], have been applied to a set of ten IGBT pairs. Tab. 8 shows a short description of the tests and their characteristics.

Every test has a well-specified set of conditions, and a detailed application procedure. For instance, under test 103B, (Tab. 8) devices are exposed to high relative humidity (90 to 95 percent), at an elevated temperature (40°C), for a period of time that depends on the test condition. There are four conditions, *A*, *B*, *C*, and *D* that correspond to lengths of 96, 240, 504 and 1344 hours each. Materials that are sensitive to moisture can deteriorate rapidly under the mentioned conditions.

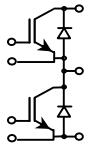

Fig. 2 Symbol of the IGBTs under test

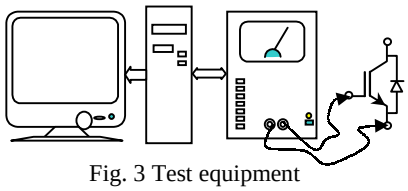

Fig. 3 Test equipment

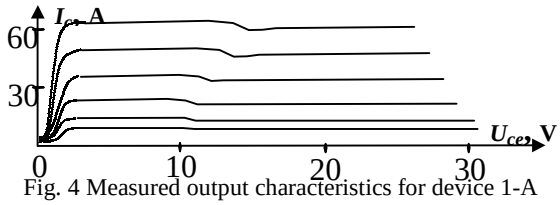

Fig. 4 Measured output characteristics for device 1-A

Fig. 2 shows symbol of the IGBTs under test, and Fig. 3 shows our current layout to carry out the tests Devices are placed in a climatic box, where accelerated tests take place. A programmable high-power curve tracer, attached to a PC for data analysis, is used to extract and compare the electrical characteristics of the power devices before after each test. We evaluate not only the number of components that pass/fail every test, but also the degradation of the characteristics of the devices with time. Several software packages - some developed in our group, are used to software packages - some developed in our group, are used to interact with the curve tracer, store and analyze experimental data.

B. Experimental results

The experiments were conducted using a sample of 12 IGBTs. These devices come in pairs enclosed in a ceramic package, which makes them very resistant to environmental stress as we observed throughout our tests. We numbered every device from 1 to 6 (six packages), A or B (two devices per enclosure); for instance, device 3-A would be the first device in package 3. Experiments took place over a period of 5 months. Environmental tests (Temperature and humidity) were applied to the devices in a climatic box for more than 1800 hours. The electrical characteristics of each device were measured before and after every test at an environment temperature of 20 °C (±5%). In addition, visual inspection was done to assess the degradation of the ceramic enclosure and metallic contacts.

TABLE 8 ENVIRONMENTAL TESTS

Test	Name	Description	
		Time, Hours	Temperature, °C
108A	**Humidity (steady state)**	**240 (*condition B*)**	**40**
	Humidity (steady state)	**504 (*condition C*)**	**40**
103B	**Life**	**96 (*condition A*)**	**70**
	Life	**504 (*condition C*)**	**70**
	Life	**504 (*condition C*)**	**150**

A set of measurements was done for every device, to verify if it failed, and to extract its electrical output characteristics. Using a power curve tracer, the device was characterized at six different gate voltages (*Uge* in Table 9). For every *Uge*, 40 measurements were taken for collector-emitter voltages (*Uce*) ranging from 2.5V to 63V, which rendered collector currents from 1A to 70A. Fig. 4 shows the measured output characteristics for device 1-A before any test was applied. The different curves correspond to several *Uge* values. Table 9 shows a summary of measurements for device 2-A before and after the second test (Test 103B condition C. See Table 8). The parameter *S* is defined as *Ic*/*Uge*.

After analyzing the collected date, we could realize of the excellent resistance of this devices to environmental stress. None of the devices failed, or even had a noticeable variation in its electrical characteristics. Therefore we could not conduct a more detailed analysis to obtain activation energy, mean time to failure, or degradation models, as it was our objective when we started this phase of our research. The devices result to be more reliable than expected, which changes our focus for the second phase of our research, where we are planning to conduct tests that stress the devices while in operation.

Another conclusion obtained from the data was related to the measurement process itself. The variation between the electrical characteristics of a device, measured before and after a test, is of the same order as the variation of the characteristics between two consecutive tests. This fact shows that the electrical characteristics of the devices were not affected by our environmental tests. It also surfaces a flaw in our measurement methodology. While we carefully planned the tests, characteristics to observe, and measurement conditions, we did not anticipate the small variations that the devices would show, therefore our measurement procedure was not precise enough to obtain accurate data. Fig. 5 shows an example of the variation between measurements. The figure shows the maximum variation of a measurement (*S*) between two consecutive tests, and within a particular test. Data for the figure is taken from device 4-A, tests 2 and 3.

TABLE 9 MEASUREMENTS FOR THE DEVICES BEFORE AND AFTER THE TEST

Voltages		After test		Before test		Distinction
J_{ge}, V	J_{ce}, V	I_c, A	S, Ω^{-1}	I_c, A	S, Ω^{-1}	ΔS
8,1	20,7	10,3	1,28	10,4	1,29	0,01
8,6	20,3	17,4	2,04	17,6	2,05	0,01
9,1	20,4	27,1	2,99	27,5	3,04	0,05
9,6	20,5	39,1	4,08	39,8	4,16	0,08
10,1	20,5	53,0	5,27	54,1	5,37	0,10
10,6	21,1	68,1	6,45	69,7	6,59	0,14

III. CONCLUSIONS

The maximum variation of the conductance is below 0.04 for any particular test, while the variation between the measurements after one test, and before the following, is also in the same range (0.025 in the example of Fig. 5). Because of this, we can not extract any conclusion about the possible degradation of the characteristics of the devices after applying the tests, however conductance seems to increase steadily for all devices.

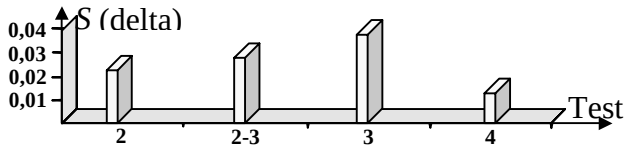

Fig. 5 Maximum variation of *S* within a test, and from test to test

Despite the aforementioned flaw in our methodology, we accomplished important objectives with our tests:

- Assess the resistance to environmental stress of the devices we selected. This is an important conclusion for our research in the design of reliable battery chargers.
- Establish and improve the flow for he second phase of our research, where we will be using the same equipment (climatic box, curve tracer, and analysis tools).

REFERENCES

[1] Intersil Press Release, "Intersil Completes 600-Volt Switch Mode Power Supply IGBT Family Targeting Internet File Servers and Telecom Switches", Palm Bay, FL, March 16, 2000.

[2] *JEDEC Standard 22 Series, Test Methods,* http://www.jedec.org

[4] *MIL-STD-202FM*. "Test methods for electronic and electrical component parts", http://www-library.itsi.disa.mil.

Utilization of the Serial Analysis Method of the Date for Reliability Evaluation of the Electronic Devices

Neli G. Georgieva[1] and Anton Sl. Georgiev[2]

Abstract **- In the contemporary manufacture of the semiconductor devices and integral circuits, the time is decreased from the idea to the realization of the ready production. Because of that, the time, for testing and estimating the reliability indicators of the manufactured semiconductor devices, should be decreased. Nowadays, that is one of the main reasons that we should pay attention to the statistical method for serial analysis of the dates, received when the devices are examined. In the presented paper, the possibilities, for serial statistical method application by reliability evaluation of the semiconductor devices, are examined. Its advantages and disadvantages are analyzed. It is shown the specified method application. It is also paid an attention to the risk of the consumer and the risk of the manufacturer.**

Keywords **- failure analysis, reliability of the electronic device.**

I. THEORY

When the determined statistical control limits are at least equal to or within the specification limits, a process is defined as capable and deemed incapable whenever the control limits lie outside of the specification limits. The capability index

$$C_P = \frac{USL - LSL}{6\sigma} \qquad (1)$$

where *USL* and *LSL* represent the upper and lower specification limits and σ the population standard deviation, is a handy measure of Process Capability.

If C_P<1, the process is deemed incapable, by convention; if C_P=1 or C_P>1, the process is considered *marginally* or *definitively capable* (Ex: $C_P \geq 1.33$). Hence, for a selected *USL-LSL* specification range, any sampling decision on whether a process is *capable* is dependent upon the process standard deviations σ_0 (C_P>1) σ_1 (C_P<1) and corresponding type *I* α and type *II* β errors for hypothesis acceptance or rejection. With the exception of double sampling, most accept/reject inspection decisions assume that the observational numbers are independent of the results and require a predetermined sample size. Serial test or inspection plan sample sizes are dependent on the outcome of the observations and require three decisions: (2) Accept the test hypothesis, (3) Take another observation, (4) Reject the test hypothesis.

In 1943, Serial testing results from the theory of serial analysis that was created by Wald for war time military equipment development and inspections. Numerous examples of the theory's practical applications and sampling saving economies were later published1 by the Statistical Research Group of Columbia University.

The basis for Wald's serial test are the probability inequality ratios:

$$\frac{P_{1N}}{P_{0N}} \leq \frac{\beta}{1-\alpha} \qquad (2)$$

$$\frac{\beta}{1-\alpha} < \frac{P_{1N}}{P_{0N}} < \frac{1-\beta}{\alpha} \qquad (3)$$

$$\frac{P_{1N}}{P_{0N}} \geq \frac{1-\beta}{\alpha} \qquad (4)$$

where P_{0N}, P_{1N} are the probability density functions corresponding to the test H_0 and alternate H_1 hypothesis for the serial set of observations $X_1 \ldots X_N$, and α, β are the selected type *I* (producer's risk) and type *II* (consumer's risk) errors. The test is continued when inequality ratio (3) applies and discontinued at the first occurrence of the ratios (2) or (4) resulting in the acceptance of hypotheses H_0 or H_1 respectively.

Consider the sequence of observations $X_1 \div X_N$, as an example of test principle usage, from a normally distributed process with a known mean μ and unknown standard deviation σ, where the test hypothesis is $\sigma \leq \sigma_0$ and the alternate $\sigma \geq \sigma_1$. For each value of *N*, the probability ratio P_{1N}/P_{ON} is calculated. Thus, the test hypothesis $\sigma \leq \sigma_0$ is accepted when (2) $P_{1N}/P_{ON} \leq \beta/(1-\alpha)$ and the alternate $\sigma \geq \sigma_1$ when (4) $P_{1N}/P_{ON} \geq (1-\beta)/\alpha$. The test is continued when (3) $\beta/(1-\alpha) < P_{1N}/P_{ON} < (1-\beta)/\alpha$. The expansion of inequality (3) results in expression (5) below:

$$\frac{2\log_e\left(\frac{\beta}{1-\alpha}\right) + N\log_e\left(\frac{\sigma_1^2}{\sigma_0^2}\right)}{\frac{1}{\sigma_0^2} - \frac{1}{\sigma_1^2}} < \sum_{i-1}^{N}(X_i - \mu)^2 < \frac{2\log_e\left(\frac{1-\beta}{\alpha}\right) + N\log_e\left(\frac{\sigma_1^2}{\sigma_0^2}\right)}{\frac{1}{\sigma_0^2} - \frac{1}{\sigma_1^2}} \qquad (5)$$

and further simplification results in the straight line forms that are used to create the table (Table 2) and/or graph (Figure 1) of a Wald serial test procedure for process variability:

Accept standard deviation σ_0 at step *N* if the summed observations (In the cases where the mean μ is unknown the sum of squares is replaced by the squares of the deviations from the sample mean and the limit *N* is replaced by *N*-1. Five useful points of both the operating characteristic $Pa(\sigma)$ and average sample number $ASN(\sigma)$ curves can be calculated from the formulas in Table 1) $\Sigma(X_i\ \mu)^2$ satisfy In 1943, Serial testing results from the theory of serial analysis that was created by Wald for war time military equipment development and inspections. Numerous examples of the theory's practical applications and sampling saving economies were later published1 by the Statistical Research Group of Columbia University.

[1] Ph. D. Neli Gentcheva Georgieva, is with the Technical University - Varna, Departments of Electronic Engineering, ul. Studentska 1, Varna, Bulgaria, e-mail: neligeorgieva@yahoo.com

[2] Ph. D. Anton Slavtchev Georgiev, is with the Technical University - Varna, Departments of Electronic Engineering, ul. Studentska 1, Varna, Bulgaria. georgiev_an@yahoo.com

$$\sum(X_i-\mu)^2 \le Y_0(N)= SN + h_0 \qquad (6)$$

or

$$\sigma_1 \quad \text{if} \quad \sum(X_i-\mu)^2 \ge Y_1(N)= SN + h_1 \qquad (7)$$

and continue sampling if

$$Y_0(N)< \sum(X_i-\mu)^2 < Y_1(N) \qquad (8)$$

where:

$$S=\frac{\log_e\left(\frac{\sigma_1^2}{\sigma_0^2}\right)}{\frac{1}{\sigma_0^2}-\frac{1}{\sigma_1^2}} \qquad h_0=\frac{2\log_e\left(\frac{\beta}{1-\alpha}\right)}{\frac{1}{\sigma_0^2}-\frac{1}{\sigma_1^2}} \qquad h_1=\frac{2\log_e\left(\frac{1-\beta}{\alpha}\right)}{\frac{1}{\sigma_0^2}-\frac{1}{\sigma_1^2}} \qquad (9)$$

TABLE 1: FIVE USEFUL POINTS

σ	0	σ_0	$\sqrt{S}$	σ_1	∞
$PA(\sigma)$	1	1-α	$h_2/(h_1+h_2)$	β	0
$ASN(\sigma$	$\frac{h_1}{S}$	$\frac{(1-\alpha)h_1-\alpha h_2}{S-\sigma_0^2}$	$\frac{h_1 h_2}{2S^2}$	$\frac{(1-\beta)h_1-\beta h_2}{\sigma_1^2-S}$	0

The Average Sample Number $ASN(\sigma)$ estimates the average number of samples required for a decision at a specified standard deviation *s* since the exact number is not known beforehand.

II. SERIAL STATISTICAL METHOD APPLICATION BY RELIABILITY EVALUATION OF THE SEMICONDUCTOR DEVICES

The method choice for examining is a serious task for the specialist in the area of reliability. In the presented paper is made a reliability estimation of the semiconductor devices with the help of the serial method. It is preferred because smaller sample and smaller duration are required. The volume of the examinations is decreased 50% in comparison with the another methods.

It should be selected one procedure, which requires the less time, from all the different procedures by which the serial analysis is made. As it is known [1], procedures possess these characteristics by which the decisive rule is based on the serial criteria of probability relation. With the help of the serial analysis of the results of the examinations is obtained a complete and accurate information. Actually, if $\underline{R}$ appears to be $\underline{R} < R_{specified}$, then it means that $R < R_{specified}$, so maybe the volume is still not enough and the upper written conditions will be met with the increase of the number of the conducting examinations K. A serial procedure for control of the conducting examinations with measured values of the function of the serviceability of the semiconductor devices will be presented in this paper. We may accept the hypothesis that *f* has a Gausov distribution, then:

$$R = P\{p>0\} = F^*\left\{\frac{m_f}{f_f}\right\} = F^*\{r\} \qquad (10)$$

We may accept that if $R=\overline{R}$, the semiconductor devices are capable, but if $R=\underline{R}$, then semiconductor devices are incapable. So, the serial analysis may be presented as 1. Test of the hypothesis R_0 $\{R=\overline{R}\}$ by alternative R_1 $\{R=\underline{R}\}$ and 2. The set reliability for an error of type *I* α (risk for the manufacturer) and of type *II* β (risk for the customer).

On account of the monotony of the function $F^*\{r\}$ in reference of *r*, the hypothesis R_0 and R_1 may be presented as R_0 $\{r = \overline{r}\}$ by alternative R_1 $\{r=\underline{r}\}$, where $\overline{r}$ and $\underline{r}$ are quintiles of the normal distribution corresponding to $\overline{R}$ and $\underline{R}$.

Let the sample, which is characterized with f_k and volume *k*, is defined. From the given sample $\overline{f_k}$, are defined the mathematical expectation $\hat{m}_f$ and the quadratic metan deviation $\hat{\sigma}_f$.

$$\hat{m}_f = \frac{\sum_i^k f_i}{n};$$

$$\hat{\sigma}_f = \sqrt{\frac{\sum_i^k (f_i-\hat{m}_f)^2}{k-1}}. \qquad (11)$$

It's obvious that the quantity $\hat{r}=\hat{m}_f/\hat{\sigma}_f$ is also random. In accordance with the serial criteria, the relation of the probabilities of the hypothesis R_0 may be accept if:

$$\lambda = \frac{\varphi\left(k-1, \overline{r}\sqrt{k}, y\right)}{\varphi\left(k-1, \underline{r}\sqrt{k}, y\right)} \le \frac{\beta}{1-\beta}, \qquad (12)$$

where $\hat{r}\sqrt{k}$ is the value found from the sample f_K.

The production is incapable if

$$\lambda = \frac{\varphi\left(k-1, \overline{r}\sqrt{k}, y\right)}{\varphi\left(k-1, \underline{r}\sqrt{k}, y\right)} \ge \frac{1-\beta}{\alpha}, \qquad (13)$$

and the examinations continue if

$$\frac{\beta}{1-\alpha} < \frac{\varphi\left(k-1, \overline{r}\sqrt{k}, y\right)}{\varphi\left(k-1, \underline{r}\sqrt{k}, y\right)} \le \frac{1-\beta}{\alpha}. \qquad (14)$$

We would analyze the problems connected with the serial control examinations by exponential distribution. We would examine the reliability with the help of the index - mean time to failure. For the plan development of testing, it should be given the levels for capability and incapability (corresponding T_0 and T_1) and the risks of the manufacturer (α) and the customer (β). It is evaluated after each failure whether the level of the reliability is too high in order to be accepted the elemnts for capable, or it is too low in order to be accpted for incapable. An index for the evaluation is the total mean time to failure of the elements of the sample.

The condition for capability or incapability of the elements is the following:

$$\frac{t_\Sigma}{T_0} \ge \frac{T_1}{T_0-T_1}\left[r\ln\frac{T_0}{T_1} - \ln\frac{\beta}{1-\alpha}\right] \qquad (15)$$

and

$$\frac{t_\Sigma}{T_0} \le \frac{T_1}{T_0 - T_1}\left[r \ln \frac{T_0}{T_1} - \ln \frac{1-\beta}{\alpha} \right], \quad (16)$$

where t_Σ is the total duration of the examination.

The lines of correspondence *II* and discrepancy *I* are made from the equations (15) and (16) (fig.1).

The control has the following algorithm. From the batch of elements is made a random sample where $N>r_0$. If at the initial moment of the examination failure $r>r_0$ elements, the batch is incapable. If failures occur in the process of examination, the graphic of the serial control of reliability is a steplike line (fig. 1).

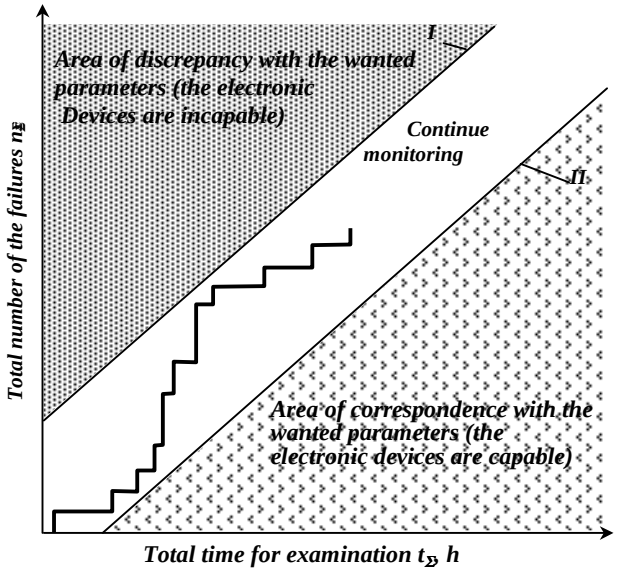

Fig.1. Graphical model of the serial method for examination

III. SAMPLE APPLICATION AND EXAMPLE RESULTS

In table 2, are registered sample data for application of the serial statistical method application by reliability evaluation of the semiconductor devices. The graphic model of the sample data, registered in table 2 is illustrated in fig. 2. The sample data corresponds to the starting data: Producer's risk 0,001, Consumer's risk 0,001, Group size 1, Cum. Samples 18, Standard deviation choices *Std1, Std*2 (Lowest *Std*1 12,5 and Highest Std2 24,3); starting condition: by $C_P \le 1 \rightarrow$ incapable, $1<C_P<1.33 \rightarrow$ continuing monitoring. Calculated Process Capability Indexes are the following: $C_P \ge 1.33 \rightarrow$ capable; C_P *Std*1 is 1,33, C_P *Std*2 is 0,686.

A Chi-square test X^2 is usually applied, when a classical test of significance is applied to question of whether the sample variance s^2 differs significantly from the desired population variance σ_0. The test hypothesis H_0 specifies the population variance as H_0: $s^2 = \sigma_0^2$ and the alternate hypothesis H_1: $\sigma_1^2 > \sigma_0^2$. If H_0 is correct, then X^2/f is the distribution for s^2/σ_0^2 for f degrees of freedom. Thus, a rejection of the test hypothesis H_0 occurs at some chosen significance level a such that

$$\frac{S^2}{\sigma_0^2} > \frac{X^2_{1-\alpha}}{f}. \quad (17)$$

TABLE 2: SERIAL SAMPLING PROCESS CAPABILITY DETERMINATION

ampl size	Calculated Criteria Sums				Deviation Sqr Value	Compare Deviation Sqr Sum (sum number of the failure n_Σ)
	:or:	Accept Std1	:or:	Accept Std2		
1	no	-2652	no	3216	2	2
2	no	-2369	no	3499	79	81
3	no	-2087	no	3781	106	187
4	no	-1804	no	4064	6	193
5	no	-1522	no	4346	3	196
6	no	-1239	no	4629	41	237
7	no	-957	no	4911	97	334
8	no	-674	no	5194	161	495
9	no	-392	no	5476	332	827
10	no	-109	no	5759	101	928
11	no	171	no	6041	21	949
12	no	454	no	6324	140	1089
13	no	736	no	6606	255	1344
14	no	1019	no	6889	62	1406
15	no	1301	no	7171	74	1480
16	no	1584	no	7454	199	1679
17	no	1866	no	7736	202	1881
18	**yes**	2149	no	8019	111	1992

The test's sample size can be estimated from the power of the discriminating test needed to distinguish between the population variances σ_1^2 and σ_0^2 at f degrees of freedom:

$$\frac{\sigma_1^2}{\sigma_0^2} = \frac{X^2_{1-\alpha}(f)}{X^2_{\beta}(f)} \quad (18)$$

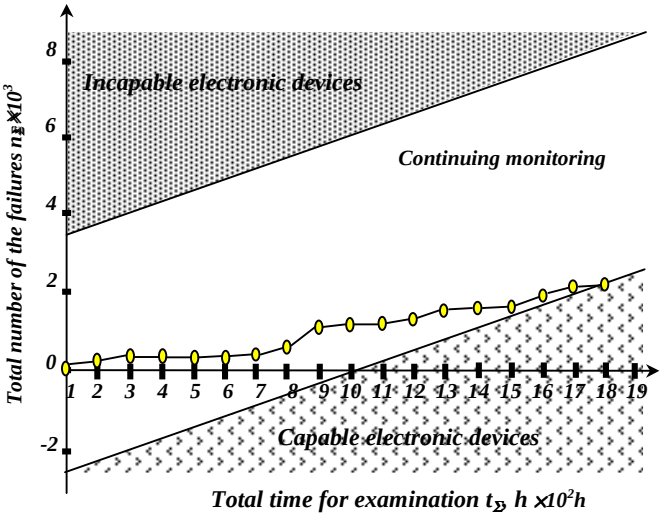

Fig.2. Graphical model of the serial statistical method application by reliability evaluation of the semiconductor devices

The substitution of the textile process parameters, σ_0=12.5, σ_1=24.3, α=0.001, β=0.001, in the discriminating test equation (18) yields $\sigma_1^2/\sigma_0^2=3.78=X^2_{.999}(f)/X^2_{.001}(f)$ at about 47 degrees of freedom, which translates into a required sample size of 48 for the classical test. The average sample number *ASN* requIred for a serial test decision at a standard deviation level of σ_0=12.5 is 23. For an unknown mean, the sample size is increased by one and the saving's percentage is reduced to 50%.

IV. CONCLUSION REMARKS

Compensations are not made for the effects of sample grouping on type *I* is a limitation of the Serial method, type *II* errors, *ASN* and *OC* curve values. When compared with single item serial plans, grouping by sample increments results in an increase in the number of items inspected and advantageously lower type *I* and type *II* errors. If the process is evaluated is very good or bad, expeditious decisions occur. However, these accept or reject decisions are dependent upon the closeness of the standard deviation parameters σ_0, σ_1 and the degree of risk α, β that the manufacturer or organization is willing to accept. Borderline processes often require indefinite sample sizes and a truncation point leading to an increased α or β risk has to be agreed upon. The method does not exempt the manufacturer or organization from continuous monitoring since processes do change in time. Also, the example discussed is based on the assumption of a centered normally distributed process.

The major advantage in the use of serial probability ratio test arises from the ease at which it can be automated, enhanced and extended to the Binomial, Poisson and Reliability Test areas. Algorithms can be devised that require only computer familiarity and data entry skills on the part of the user. AddItionally, hardware as simple as a programmable pocket calculator can be used for many of the applications.

REFERENCES:

[1] Wald A, Sequential Analysis, John Wiley & Sons, New York, NY. 1947.

[2] Additional Sequential Probability Ratio Test citations can be found at http://citeseer.nj.nec.com/context/78315/0 and Internet Interactive Wald Sequential Sampling Tables for Attributes can be generated at http://home.clara.net/sisa/sprthlp.htm.

[3] Hald, A, Statistical Theory with Engineering Applications, John Wiley & Sons, New York, NY , 1952.

[4] Филев В. Д., Ценкова М. К. Изпитване на надеждност в електроуредостроенето. София, Техника, 1980.

[5] Ненов Г. Д. Надеждност на радиоелектронните изделия. София, Техника, 1983.

[6] Braband J.Risk Assessment in Railroad Signaling: Experience Gained and Lessons Learned. *Proc. Reliability and Maintainability Symposium*, January 28-31, 2002.

[7] Braband J., F. Renpenning. Hazard and Risk Analysis for a Low-cost Train Control *System Proc. 19-th International System Safety Conference*, System Safety Society, 2001.

Analysis. Parameters. Characteristics and Circuits with PIN Photodiodes for Multielement Photodetectors

Ivan S. Kolev and Tsanko V. Karadzhov

***Abstract* – A photodiode is a photodetector which is characterized with an internal photoeffect and a PN junction without internal amplification of the photocurrent. It has the fastest response of all types of photodetectors. Photodiodes are mainly made of silicon – Si and germanium – Ge. They are usually divided into three types – photodiodes with PN junction, PIN photodiodes and avalanche photodiodes. A detailed classification of the photodiodes is shown in Application. 1.**

Keywords – Photodiode, Photodetector, Photocurrent, Dark current.

I. OPERATION MODES

Photodiodes operate in two main modes – photodiode and photogalvanic. At photodiode mode (Fig. 1), the photodiode is energized with inverse voltage from an external source. The reverse current through it depends upon the illuminance. At photogalvanic mode (Fig. 2), the photodiode generates photoelectromotive force at illuminance without availability of an external source.

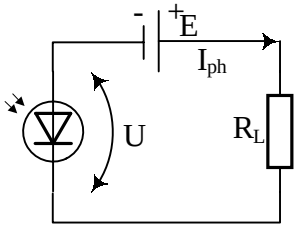

Fig. 1

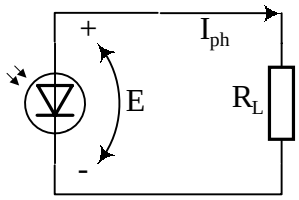

Fig. 2

Ivan S. Kolev. Department of Electronics, Technical University – Gabrovo, Street "Hadji Dimiter" No. 4, 5300 Gabrovo, Bulgaria, phone: +359 66 801064.

Tsanko V. Karadzhov. Department of Electronics, Technical University – Gabrovo, Street "Hadji Dimiter" No. 4, 5300 Gabrovo, Bulgaria, phone: +359 66 801064, e-mail: karadjov_st@abv.bg

In PIN photodiodes there is a layer with intrinsic conduction (i-layer) among the layers with different conduction. Therefore they have higher sensitivity, smaller barrier capacity and possess good frequency characteristics (limit frequency over 1GHz).

When operating in photodiode mode, it can be written down about the voltage upon the photodiode:

$$U = I_{ph}.R_L - E \qquad (1)$$

where I_{ph} – photocurrent;
U – inverse voltage on the photodiode;
R_L – load resistance.

The current through the photodiode is:

$$I = I_D\left(e^{\frac{U}{m.\varphi_T}} - 1\right) - I_{ph} \qquad (2)$$

where I_D – dark current;
M – coefficient (1÷1.5), showing the deviation from the ideal volt-ampere characteristic of the PN junction; φ_T – temperature potential.

$$\varphi_T = \frac{k.T}{q} \qquad (3)$$

where k – Boltzmann's constant;
T – temperature, °K;
q – electron charge

At photogalvanic mode (Fig. 2), the photoelectromotive tension is:

$$E_{ph} = m.\varphi_T \ln\left(1 + \frac{I_{ph}}{I_D}\right) \qquad (4)$$

where:I_{ph} – photocurrent generator;
I_D – dark current generator;

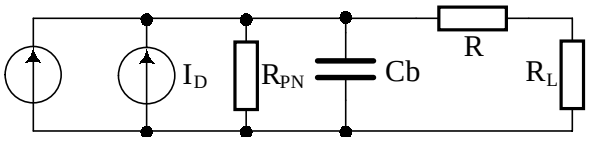

Fig. 3

An equivalent photodiode circuit is presented in Fig. 3
R_{PN} – non-linear incremental resistance of the PN junction;
Cb – barrier capacity;
R – base and junctions low-ohmic series resistance.

The incremental resistance of the photodiode depends on the applied inverse voltage and the illuminance and its value is $10^6 \div 10^9$ Ω. The diode capacity also depends on the applied inverse voltage.

The maximum limit frequency of the photodiode at $R << R_{PN}$ is:

$$f_{MAX} = \frac{1}{2\pi RCb\left(1+\frac{R}{R_{PN}}\right)} \approx \frac{1}{2\pi RCb} \quad (5)$$

There are three main types of photodiodes in accordance with the wavelength λ: (850÷940) nm – Si-photodiode, 1300 nm – Ge photodiode, 1550 nm – InGaAs photodiode.

II. FREQUENCY CHARACTERISTICS OF THE PHOTODIODES

The law, in accordance with which the output photodiode current is changed at switching on and switching off, is expressed through the following transition functions:

$$h_1(t) = K\left(1 - e^{-\frac{t}{\tau}}\right) \quad (6)$$

$$h_1(t) = K\left(e^{-\frac{t}{\tau}}\right) \quad (7)$$

where τ is the time constant of the photodiode.

III. TIPES OF PHOTODIODES

A. *PIN photodiodes with optical tails*

Fig. 4

The structure of such a photodiode is shown in Fig.4. It contains (20÷30) cm of optical fiber connected to the photodiode through an optical coupling. It finds application in optical communications by means of optical fibers and cables.

B. PIN photodiodes with a digital output

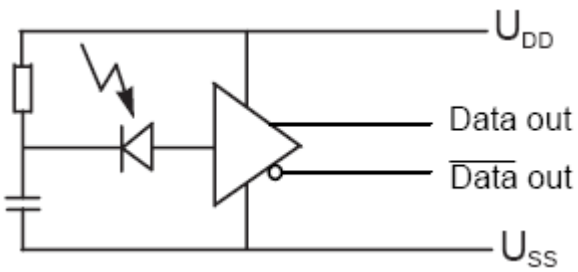

Fig. 5

They are used as photodetectors in optical lines or infrared channels for digital information transmission (Fig. 5).

B. *PIN photodiodes with an analogue output*

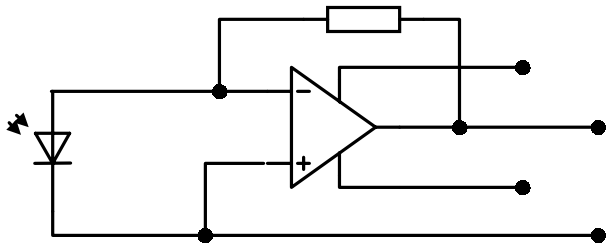

Fig. 6

They have a built-in operational amplifier with a feedback resistor in the diode case (Fig.6).

IV. CHARACTERISTICS OF THE PIN PHOTODIODES

The characteristics of a silicon PIN photodiode made by Telefunken are shown as an example.

- Lux-ampere (light) characteristic – it shows the dependence of the photocurrent upon the illuminance at constant supply voltage $I_{ph}=f(E_V)$ - Fig. 7;

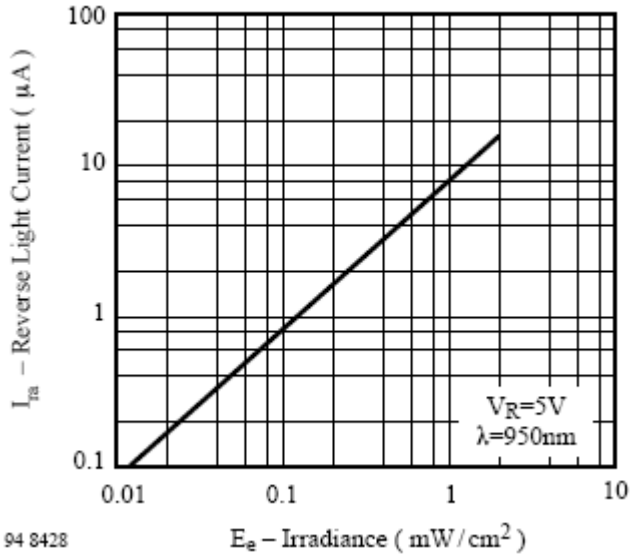

Fig. 7

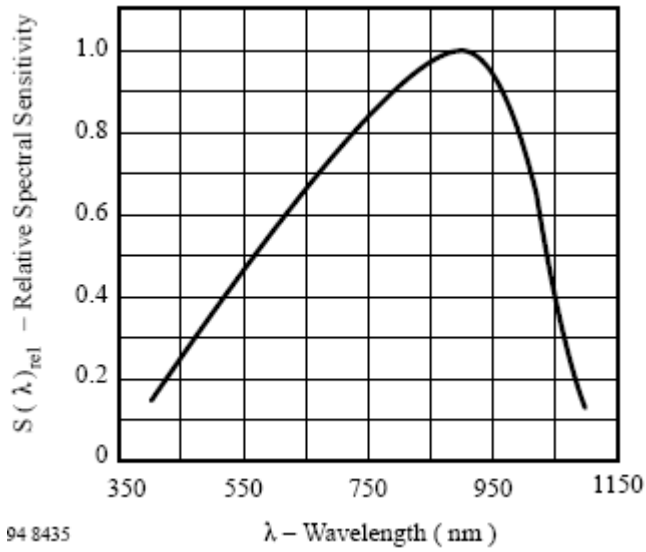

Fig. 8

- Spectral characteristic – it expresses the dependence of the photocurrent upon the wavelength at constant voltage and constant power of the irradiating luminous flux $I_{ph}=f(\lambda)$, Fig.8;
- Volt-ampere characteristic – it is a dependence of the photocurrent upon the applied voltage at a constant luminous flux $I_R=f(U_R)$ - Fig. 9;

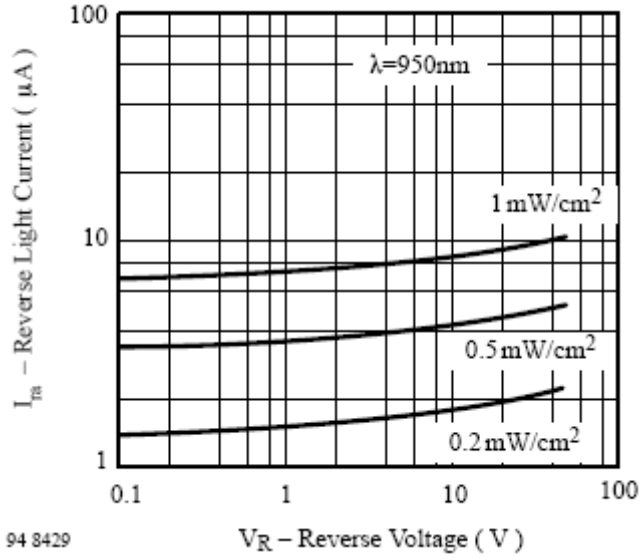

Fig. 9

- Dependence of the photoelectromotive voltage upon the illuminance $E_{ph}=f(E_V)$;
- Thermodependence of the photocurrent $I_{ph}=f(T)$;
- Thermodependence of the dark current $I_D=f(T)$;
- Thermodependence of the photoelectromotive voltage $E_{ph}=f(T)$;
- Dependence of the capacity upon the applied voltage.

V. MAIN PARAMETERS OF THE PHOTODIODES

Operating inverse voltage U_R, V	Voltage, at which the photodiode does not change its nominal parameters if it has operated long enough.
Dark resistance R_D, Ω	Photodiode resistance in the absence of the light falling upon it
Dark current I_D, A	Current flowing through the photodiode at a specific voltage and luminous flux absence
Light resistance R_{ph}, Ω	Resistance of the photodiode when irradiating it by luminoius flux in the range of its spectral sensitivity
Photocurrent I_{ph}, A	Current flowing through the photodiode at a specified voltage and luminous flux radiation upon the photodiode
Common current I, A	Photodiode current consisting of the photocurrent and the dark current
Integral sensitivity S, A/lm	Relationship between the photocurrent variation and the lunminous flux change
Spectral sensitivity S_λ	Dependence of the photodiode sensitivity upon the wavelength
Current impulse sensitivity S_{imp}, A/W	Relation of the photocurrent amplitude to the impulse power amplitude of the radiating luminous flux
Noise current I_{nois}, A	Mean square value of the photodiode dark current variation
Noise voltage U_{nois}, A	Mean square value of the photodiode dark voltage variation
Sensitivity threshold D, lm	Mean square value of the modulated fixed spectrum luminous flux acting upon the diode at which the mean square value of the photocurrent (voltage) is equal to the mean square value of the noise current (voltage)
Rise time t_r, s	Minimum time interval necessary for transition from (0.1÷0.9) of the fixed photocurrent or voltage value upon the photodiode
Decay time t_d, s	Minimum time interval necessary for transition from (0.9÷0.1) of the fixed photocurrent or voltage value to the photodiode
Limit frequency f_0, Hz	Frequency of the sinusoidal luminous flux, at which the photodiode sensitivity falls to level 0.707 of the sensitivity of constant luminous flux
Photodiode capacity C, F	Capacity of the photodiode PN junction

VI. CONCLUSION

The results of this paper will be used for lectures and seminars with students in the programmes of "Optoelectronics" и "Optoelectronics and Optical Communications".

REFERENCES

[1] Siemens. Si-Photodetectors and IR Emitters, Reference Book, 1995.
[2] Vishay Telefunken. Reference Book, 1999.
[3] И. С. Колев. Инфрачервена оптоелектроника. Габрово, Унив. изд. Васил Априлов, 2003.
[4] И. С. Колев, Т. С. Тодоров. Оптрони и приложението им. София, Техника, 1988.
[5] http://www.mitelsemi.com

Application 1

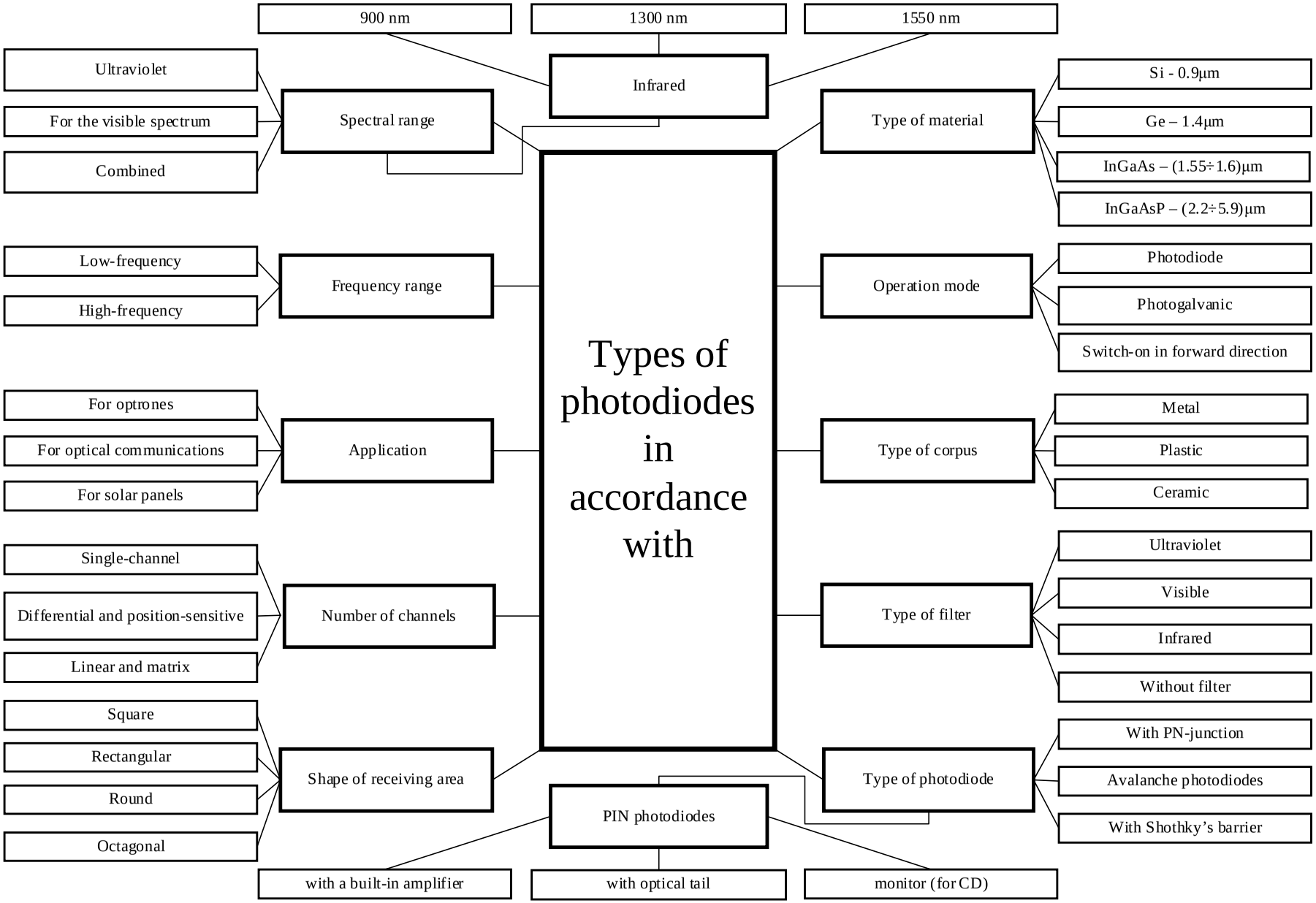

Design and Investigation of FPAA Square-wave Generator

Emil D. Manolov[1], Peter I. Yakimov[2] and Marin H. Hristov[3]

***Abstract* – In this paper a FPAA (field programmable analog array) square-wave generator with programmable frequency and duty cycle is designed. The synthesized circuit is investigated by using AN220D04 Evaluation Board from Anadigm®.**

***Keywords* – programmable analog IC, Field programmable analog array (FPAA), square-wave generator**

I. INTRODUCTION

The Field Programmable Analog Arrays (FPAAs) are one of the most contemporary and perspective products for fast and flexible implementation of different circuit and devices. Essentially, FPAAs are the analog equivalent of well-known digital Field Programmable Gate Arrays (FPGA). The most popular of them use switched-capacitor techniques, which ensure improved accuracy and consistency of time constants and give possibilities for dynamic programming of configuration and performance of the circuits [1].

Some of the most popular FPAAs are the chips of Anadigm Inc. [2]. They consist of switched-capacitor configurable analog blocks and SRAM. By changing the configuration data, stored in the memory, designer can control the functionality or parameters of the blocks. This programming procedure uses CAD tools that automate the process. Currently, different types of amplifiers, sample-and-hold circuits, integrators, differentiators, filters, etc. are available as library components (IP modules). Different complex analog systems can be implemented by using them. The simplicity and compactness of these solutions stimulate designers to synthesize and examine various circuits and systems by using FPAA.

The paper presents design and investigation of square-wave generator with programmable frequency and duty cycle by using FPAA from Anadigm®.

II. CLASSIC SQUARE-WAVE OSCILLATOR

Fig. 1 shows the classic square-wave oscillator circuit [3]. The circuit uses two op amps: first of them (A), together with the resistors R1 and R2, build up a symmetric Schmitt trigger; the second (B), together with the resistor R and capacitor C, build up an Integrator.

[1]Emil D. Manolov is with the Faculty of Electronic Engineering and Technologies, Dept. of Electronics, Technical University – Sofia, 1000 Sofia, Bulgaria, E-mail: edm@tu-sofia.bg

[2]Peter I. Yakimov is with the Faculty of Electronic Engineering and Technologies, Dept. of Electronics, Technical University – Sofia, 1000 Sofia, Bulgaria, E-mail: pij@tu-sofia.bg

[3]Marin H. Hristov is with the Faculty of Electronic Engineering and Technologies, Dept. of Microelectronics, Technical University – Sofia, 1000 Sofia, Bulgaria, E-mail: mhh@tu-sofia.bg

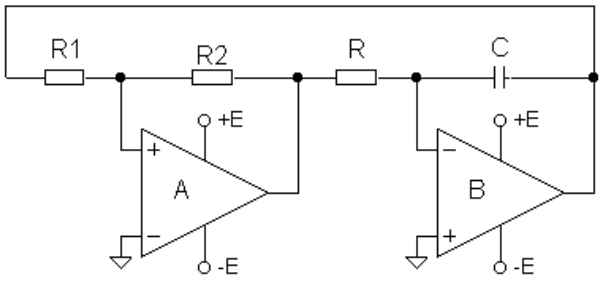

Fig. 1. Classic square-wave oscillator

The equations for pulse width T^+ and pause T^- are:

$$T^+ = \frac{H}{kU^+} \quad (1)$$

$$T^- = \frac{H}{kU^-} \quad (2)$$

where H is the hysteresis of Schmitt trigger, k is the constant of the integrator ($k=1/RC$), U^+ and U^- are the corresponding output values of positively and negatively saturated op amp A. Because of $U^+ \approx -U^-$, the duty cycle D is constant (about 50%).

In Fig. 2 is depicted the functional structure of improved square-wave oscillator [4]. To control duty cycle D and frequency of generation f, two independent voltage sources U^+ and U^- are added. Through analog multiplexer AMUX (controlled by Schmitt trigger output state), these voltage sources are switched alternatively to the input of the integrator. By changing their values, the duration of T^+ and T^- (and consequently the frequency f and duty cycle D) of the signal can be controlled.

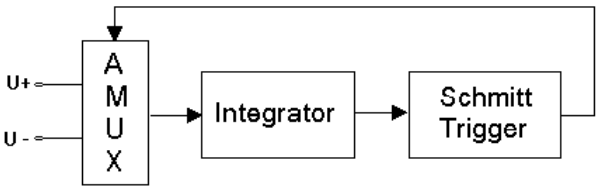

Fig. 2. Functional structure of square wave oscillator with independent control of frequency and duty cycle

III. FPAA SQUARE-WAVE OSCILLATOR CIRCUIT

Fig. 3 shows FPAA implementation of the oscillator from Fig. 2. The square waves appear between pins 3 and 4, and triangular waves - between pins 7 and 8. The circuit is designed by using specialized development software AnadigmDesigner2. The integrator *Int* is realized with standard IP module from the Anadigm® library. The Inverting

Schmitt trigger [5] uses Gain Stage with Switchable Inputs (*Comp1+PGA1*), Reference Voltage Source (*+3V*) and Inverting Gain Stage Amplifier (*IGS*). The analog multiplexer AMUX consists of second Gain Stage with Switchable Inputs (*Comp2+PGA2*) and two Reference Voltage Sources (*+3V* and *–3V*). The Gain Stage with Switchable Inputs is a standard library block of AnadigmDesign2 software [2]. It consists of comparator *Comp* and switchable input amplifier with low-pass filter *PGA*. The output of the comparator *Comp* controls the input switching of the amplifier. The gain of amplifier *PGA* can be programmed independently for each of the switchable signals.

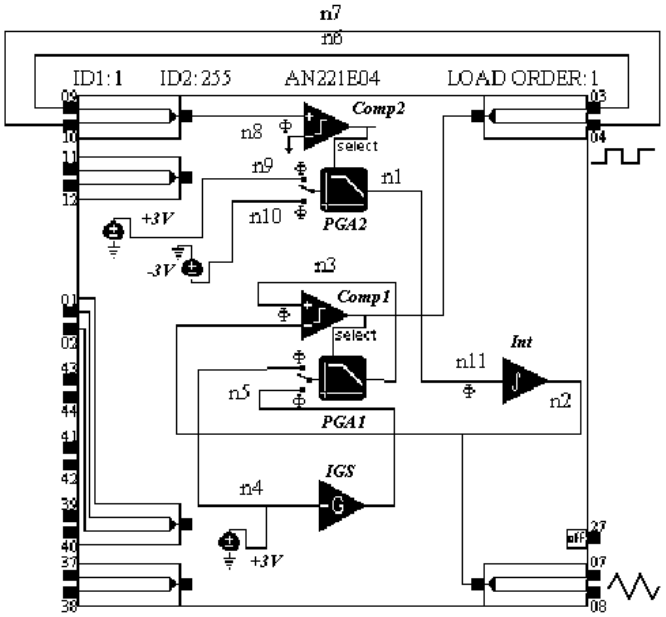

Fig. 3. Implementation of FPAA square wave generator with independent control of frequency and duty cycle

From (1) and (2), for the frequency *f* and duty cycle *D* of oscillations is obtained the following:

$$f = \frac{k}{H\left(\frac{1}{U^+} + \frac{1}{U^-}\right)} \tag{3}$$

$$D = \frac{U^-}{U^- + U^+}. \tag{4}$$

In the above formulas U^+ and U^- are the corresponding values of voltage at node n11 (the input of the Integrator) during the pulses and pauses of the signal. Their values are:

$$U^+ = +3G_1 \tag{5}$$

$$U^- = -3G_2 \tag{6}$$

where G_1 and G_2 are the gain for each of the channels of *PGA2*.

The value of hysteresis *H* depends on the gain parameters of the amplifier with low-pass filter *PGA1*, which is included in the Schmitt trigger [5].

Hence, the full scale values of the frequency and duty cycle could be adjusted by changing *k*, *H*, U^+ and U^-.

The discussed oscillator is examined by using AN220D04 FPAA Evaluation Board from Anadigm®. This board allows programming of FPAA integrated circuit AN220D04 via the serial port of the personal computer.

The synthesized circuit is examined for different combinations of values of *k* (between 0,04μS^{-1} and 4,05μS^{-1}), *H* (between 0.3*V* and 6*V*), U^+ (between 0.15*V* and 3*V*) and U^- (between 0.15*V* and 3*V*). As results, time intervals from 2μS to 400μS were obtained. The summarized results for four corner combinations of U^+ and U^- are shown in Table 1. To ensure better linearity of integration and higher accuracy of generated waveforms in discussed experiment, the values of *k* and *H* are chosen as follows: *k*=0.1μS^{-1} and *H*=6*V*.

TABLE 1
SUMMARIZED RESULTS FROM CIRCUIT EXAMINATION

U^+, *V*	U^-, *V*	*Frequency, Hz*		*Duty cycle*	
		Calculated	*Measured*	*Calculated*	*Measured*
0.3	0.3	2500	2500	0.5	0.4875
0.3	3	4545.5	4525	0.909	0.905
3	0.3	4545.5	4444	0.0909	0.0889
3	3	25000	23810	0.5	0.488

The analysis of results shows good predictability of the generated frequency and its duty cycle. Specific feature of the amplifiers, used in the circuit, is the possibility to regulate their gain with very small step (down to 0.01). Hence, the desired waveform parameters can be tuned more precisely by using simple interactive procedures based on the successive and purposefully changing of U^+ and U^- up to the achievement of the desired results.

IV. CONCLUSION

The paper proposes an implementation of square-wave oscillator with programmable frequency and duty cycle by using FPAA. To this aim, an analogy with classic oscillators is used to determine the functional structure of oscillator with external control of parameters. On this base, FPAA circuit, which uses specific functional blocks from the library of the FPAA device, is synthesized. The proposed circuit is practically implemented and examined with AN220D04 FPAA Evaluation Board from Anadigm®. It is characterized with good predictability, simple tuning and high precision in setting of the frequency and duty cycle of the generated waveforms.

The presented results will be used as a part of more complex analog and mixed-mode FPAA systems.

REFERENCES

[1] Harrold, Steve. Programmable Analog ICs. Sensors Online, April, 2003. www.sensorsmag.com.

[2] Anadigm Inc. Documentation. www.anadigm.com.

[3] Malvino, A. P., Electronic Principles. McGraw-Hill Book Company. 1998.

[4] Tietze, U., Ch. Schenk. Halbleiter-schaltungstechnik. Springer-Verlag. 1980.

[5] Manolov, E., P. Yakimov, M. Hristov. Design and Investigation of FPAA Modules with Hysteresis in a Transfer Characteristic. Proceedings of 04 Int'l Spring Seminar on Electronics Technology 27th (ISSE) 13-16 May, Sofia, Bulgaria (in press).

Design and Investigation of Pulse Width Modulator Using FPAA

Peter I. Yakimov[1], Emil D. Manolov[2] and Marin H. Hristov[3]

***Abstract* – The paper presents the design of a pulse width modulator using field programmable analog array (FPAA). The presented circuit is designed and implemented as integrated analog IP core using the FPAAs of Anadigm®. The operation of the designed pulse width modulator has been simulated using AnadigmDesigner2 software. The simulation results have been validated using Anadigm® evaluation board.**

The presented results will be used in further design of more complex analog and mixed-mode systems using FPAA.

***Keywords* – Pulse width modulator (PWM), Field programmable analog array (FPAA), Switched capacitor circuit, Analog IP core**

I. INTRODUCTION

Pulse width modulators (PWM) convert analog voltage $u_i(t)$ to square waves $u_{PWM}(t)$ with a constant frequency and a variable width, which is accurately proportional to the analog quantity as it is shown on the time diagrams in Fig. 1. The magnitude of the pulses is equal to the supply voltage. PWMs are used in the industrial measurement and in the automation and control, especially for motion control. Pulse width modulators are basic stages in the switching power supplies and power amplifiers [1].

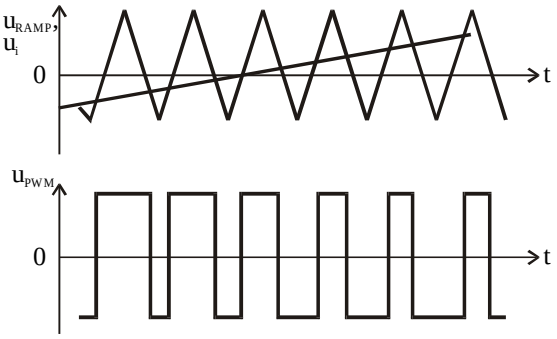

Fig. 1. Time diagrams of a pulse width modulator

The transfer function of the pulse width modulator is [4]:

$$U_{PWM} = \frac{U_{mid} - U_i}{U_{pk}} U_{CC}, \qquad (1)$$

[1]Peter I. Yakimov is with the Faculty of Electronic Engineering and Technologies, Dept. of Electronics, Technical University - Sofia, 1000 Sofia, Bulgaria, E-mail: pij@tu-sofia.bg

[2]Emil D. Manolov is with the Faculty of Electronic Engineering and Technologies, Dept. of Electronics, Technical University - Sofia, 1000 Sofia, Bulgaria, E-mail: edm@tu-sofia.bg

[3]Marin H. Hristov is with the Faculty of Electronic Engineering and Technologies, Dept. of Microelectronics, Technical University - Sofia, 1000 Sofia, Bulgaria, E-mail: mhh@tu-sofia.bg

where U_{PWM} is the average value of the output voltage $u_{PWM}(t)$, U_i is the average value of the input voltage $u_i(t)$, U_{mid} is the middle point of the ramp voltage $u_{RAMP}(t)$, U_{pk} is the peak value of the ramp voltage $u_{RAMP}(t)$, U_{CC} is the supply voltage [2].

PWM circuits are taking the same general course of development traveled by operational amplifiers and many other electronic functions. Concepts were brought to life using discrete components and were followed by modules, hybrids and then monolithics. In order to obtain a high accuracy and linearity they require stable voltage references and precise passive components. If the settings must be changed the used components have to be replaced by another with different values or to be used components with variable values.

Most of the disadvantages can be avoided by using field programmable analog arrays (FPAA) [3]. They are integrated circuits that possess the possibility of programming and dynamic reconfiguration of different analog and mixed-mode functions in one chip. These contemporary and very advanced products offer reducing of cost, size and complexity of electronic circuits. As the physical platform the FPAA architecture is built on the natural precision, generic form, and switching fabric of a CMOS-based switched-capacitor (SC) network. The analog circuits based on this array can perform multiple functions, adjust to different environmental conditions, or compensate for equipment aging.

II. BASIC CIRCUIT

The functional PWM circuit which operation corresponds to the above time diagrams is shown in Fig. 2. It comprises a ramp voltage generator and a comparator.

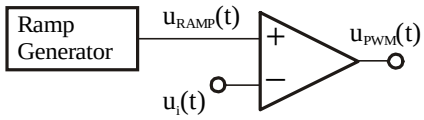

Fig. 2. Functional circuit of PWM

The accuracy depends on the offset of the comparator and the linearity of the ramp voltage. The peak value of the ramp voltage determines the range of the input voltage.

The circuit of the ramp voltage generator is based on the very popular self-oscillating functional generator [4], shown in Fig. 3 and consists of an integrator, a comparator (Schmitt trigger), an electronic switch and two voltage references. The output of the comparator makes the electronic switch to connect the input of the integrator either to the positive or to the negative reference voltage. R_1 and R_2 determine the thresholds (U_+ and U_-) which are the peak values of the ramp

voltage $u_{RAMP}(t)$. If the values of the voltage references are equal the duty-cycle will be 50%. The operation of the circuit is shown on the time diagrams in Fig. 4.

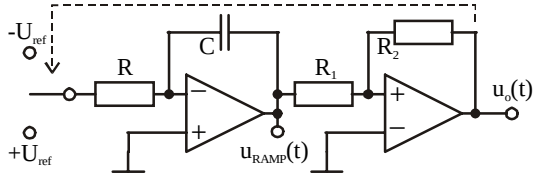

Fig. 3. The classic circuit of a functional generator

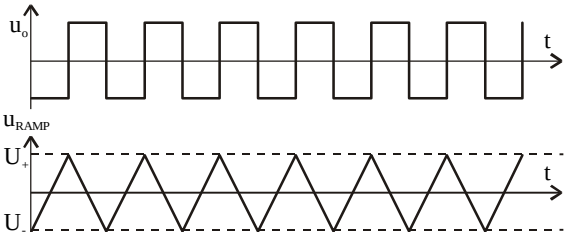

Fig. 4. Time-diagrams of the generator from Fig.3

So, the parameters of the ramp voltage depend on the values of R_1, R_2, the time-constant of the integrator and the voltage references. At the same time these components are error sources. The accuracy could be increased by introducing new technologies and integrated circuits like the FPAA.

III. Circuit Design using FPAA

Anadigm® brings platform-based design to the analog world with prequalified software and hardware components that allow complex analog circuits to be implemented in an analog equivalent to the FPGA [2].

Configurable Analog Modules (CAMs) are the functional building blocks for AnadigmDesigner®2-based designs.

The circuit implementation is shown in Fig. 5.

The input voltage is applied at node 6 (*n6*) of the circuit, which is the inverting input of the comparator. The ramp voltage is connected to the non-inverting input *n5* of it. The ramp voltage generator is designed according to the circuit in Fig. 3. There are used a positive voltage reference, two gain inverting stages (*-G*), an integrator and a CAM, which combines a gain stage with switchable inputs and a comparator. The comparator output controls which of the input signals will be switched on. The output signal *n2* of the gain stage with switchable inputs drives the inputs of the integrator and the first (*–G*). Changing the gain of the corresponding input with small steps adjusts every of the thresholds of the Schmitt trigger, consequently the peak value and the frequency of the ramp voltage in the integrator's output *n5*. In addition both thresholds could be adjusted by changing the gain of the first (*-G*). The frequency could be tuned changing the time constant of the integrator. The second (*-G*) is used to obtain negative voltage reference. Its value could be adjusted changing the gain of this stage. The output PWM signal is obtained from the output of the comparator *n7*. Thus the control of the all parameters mentioned above is available and high precision can be achieved.

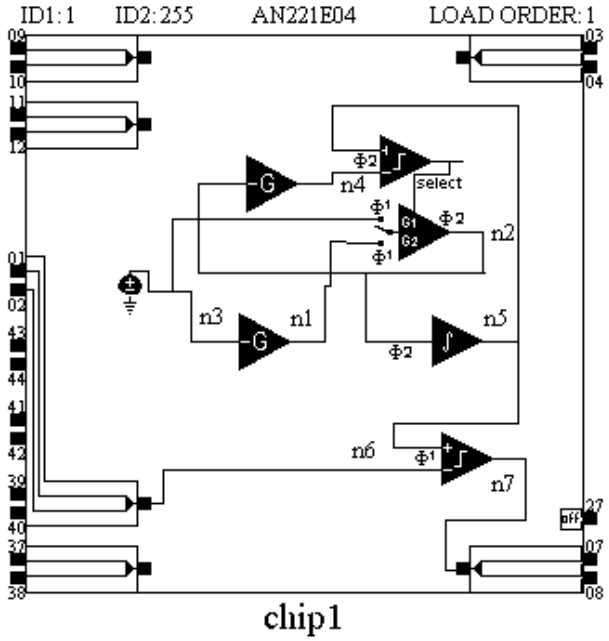

Fig. 5. FPAA implementation of the pulse width modulator

The operation of the designed circuit has been simulated using AnadigmDesigner2 software.

The simulation results have been validated using Anadigm® evaluation board. The obtained results confirm emphatically the above propositions.

IV. Conclusions

User-programmable and re-programmable attributes of FPAAs under software control assure flexibility in design and adjustment of analog circuits with different applications.

FPAAs are suitable for design of PWM circuits because of the independence on the components aging and tolerances.

Acknowledgements

This work is supported by ECAD Laboratory - Faculty of Electronic Engineering and Technologies at Technical University - Sofia.

References

[1] Malvino, A.P., Electronic Principles. McGraw-Hill Book Company. 1998.

[2] Pulse Width Modulation Amplifier, Application Note 30, Apex Microtechnology, Feb. 2001

[3] Anadigm Inc. Documentation. www.anadigm.com.

[4] Tietze, U., Ch. Schenk. Halbleiter-schaltungstechnik. Springer-Verlag. 1980.

Methodology for design of automatic orienting systems in bowl feeders

Ivo K. Malakov[1] and Mihail K. Todorov[2]

Abstract: **The objective of this paper is to introduce methods for design of automatic orienting systems of parts in bowl feeders. The performances of discernible stable positions of details are classified. Interaction forces and details recognition methods are classified and possibilities of combining are given. Simple orienting devices are chosen from working catalogue. The index number of every device was created in order to simplify work with catalogue. The example of application of above methods is shown.**

Keywords: **automation, design, automation orienting, supplying vibration containers and methodology.**

I. INTRODUCTION

One of the main goals in automating of discrete manufactory is design of effective and reliable automatic orienting systems [1,2]. To solve the above mentioned problem is complex task, which depends on number of factors as characteristics of details, designer experience, manufacture, technological processes, type of equipment, productivity, coast, etc.

In order to aid the design process number of methods is used [3,4,5,6]. Well known methods have some weaknesses, which make their application difficult. In most of then the choice of orienting system is based on classification of details according to detail characteristics. Despite discernible stable positions are with high priority in the design of automatic orientation systems. Besides this for some details included in classification decisions are not given. In those methods not all the ways of detail recognition and the interaction forces are observed. Which leads to limited solutions (often the solution is only one), in consequence of that it is difficult to reach optimal decision.

The aim of this paper is to describe methods for design of systems for automatic orientation of details in bowl feeders. In this methodology disadvantages of the known methodologies are eliminated.

II. DESCRIPTION OF METHODOLOGY

Algorithm of application of the methodology is shown on fig.1.

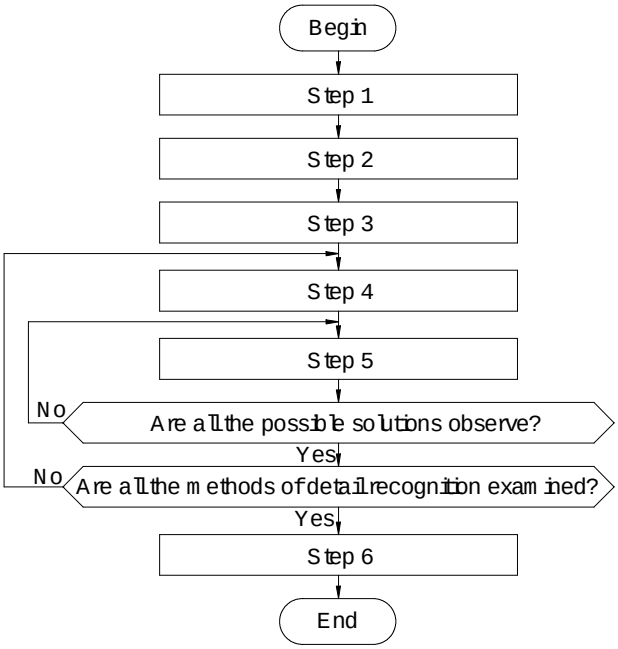

Fig.1. Algorithm of methodology

Step 1. Different discernible stable positions of objects (parts, assemblies) should be determined. Mathematical probability of stable positions of objects is determined empirically.

Step 2. The physical properties of the details are determined: material, color, transparency, weight, roughness, reflection capability, coefficient of friction, adhesion towards vibrating containers, relative magnetic permeability, relative permittivity, conductivity, etc.

Step 3. The differences between characteristics of discernible stable positions of details (vertical projection onto surfaces of orientation, physical properties, etc.). Moving direction of the details should be taken into account. Comparison between different projections and ignoring of them is unallowable, since this will cause unacceptable errors. Most frequently used parameters are shown bellow:

01 – size; 01/1 – height; 01/2 – width; 01/3 – length;

02 – outlines; 02/1 – contour; 02/2 – concentric circular contour, orthogonal to direction of moving; 02/3 - concentric eccentric contour, orthogonal to direction of moving;

03 – internal contour; 03/1 - contour; 03/2 - concentric circular hole, orthogonal to direction of moving; 03/3 - eccentric circular hole, orthogonal to direction of moving;

04 – outer cone surfaces; 04/1 – D>>H; 04/2 – D<H, D≈H;

[1] Assoc. Prof. Ph.D. Ivo K. Malakov, Department of "Automation of discrete manufacture", Technical University - Sofia, E-mail: ikm@tu-sofia.bg

[2] Master Eng. Mihail K. Todorov, Department of "Automation of discrete manufacture", Technical University - Sofia, E-mail: michael_krumov@yahoo.com

05 – guiding surfaces; 05/1 – grooves; 05/2 – ribs; 05/3 – cotters, pins, etc.

06 – chamfers; 06/1 – extruded surfaces; 06/2 - revolved surfaces;

07 – stepped surfaces; 07/1 - L>a (L>R); 07/2 - L<a (L<R);

08 – Obviously shifting of the center of mass; 08/1 – orthogonal to direction of moving; 08/2 – parallel to direction of moving; 08/3 – in height;

09 – color;

10 – coefficient of friction and etc.

The results of analyzes are summarized in the Table 1. Number of discernible stable positions is marked by n.

TABLE I

N	1	2	…	j	…	n
1	-	P_{12}	…	P_{1j}	…	P_{1n}
2	P_{21}	-	…	P_{2j}	…	P_{2n}
…	…	…	…	…	…	…
i	P_{i1}	P_{i2}	…	P_{ij}	…	P_{in}
...	…	…	…	…	…	…
n	P_{n1}	P_{n2}	…	P_{nj}	…	-

Step 4. Analyzes of the results from *Step 3* should be done as well as determination of the simple orienting devices, using working catalogue, which is no shown in this paper. The choice of the devices is based on method for recognition and characteristic of discernible stable position.

The choice of recognition method should be done according to *Step 2* and Table II. Recognition methods and interaction forces, used in the methodology and possible ways of method combining are shown in Table II.

Recognition method is defined as a way to distinguish characteristics of discernible stable positions of details. Various methods are: MM – mechanical; ME – electrical; MEM – electromagnetic; MP – pneumatic; MH – hydraulic; MG – gravitational; MO – optical; MT – television.

The interaction forces are: FG - gravitational; FI – force of inertia: centrifugal force; FF – friction force; FP - pneumatic force: FP1 – air drag, FP2 – aerodynamic drag, FP3 - blast pressure; FE – electric force: FE1- effect of capacitor, FE2- dielectric placed in non-uniform electrical field; FEM – magnetic force: FEM1 - electromagnetic force, FEM2 – diamagnetic and paramagnetic placed in non-uniform magnetic field; FM – mechanical force and FEL – elastic force.

TABLE II

	MM	ME	MEM	MP	MH	MG	MO	MT
FG	●	●	●			●		
FI	●			●		●		
FF	●		●					
FP1	●	●	●	●		●	●	●
FP2	●	●	●	●		●	●	●
FP3	●	●	●	●		●	●	●
FE1		●				●	●	●
FE2		●				●	●	●
FEM1	●	●	●	●		●	●	●
FEM2			●					
FM	●	●	●	●	●	●	●	●
FEL	●							

Step 5. Making systems using simple orienting devices. Compatibility between simple orientation devices should be taken into account. Compatibility is defined as possible way for simultaneous work of devices in common system. Combining of simple orientation devices which used different recognition methods is unacceptable, because is too expensive.

Interactive procedures for determining of multitude of possibilities for automatic orienting systems are included in this algorithm. Varying of possible recognition methods can approach different solutions.

Step 6. The optimal system for automatic orientation should be chosen. Evaluation of different solutions is done according to project.

A small passage of the working catalogue containing the simple orienting devices is shown on fig. 2.

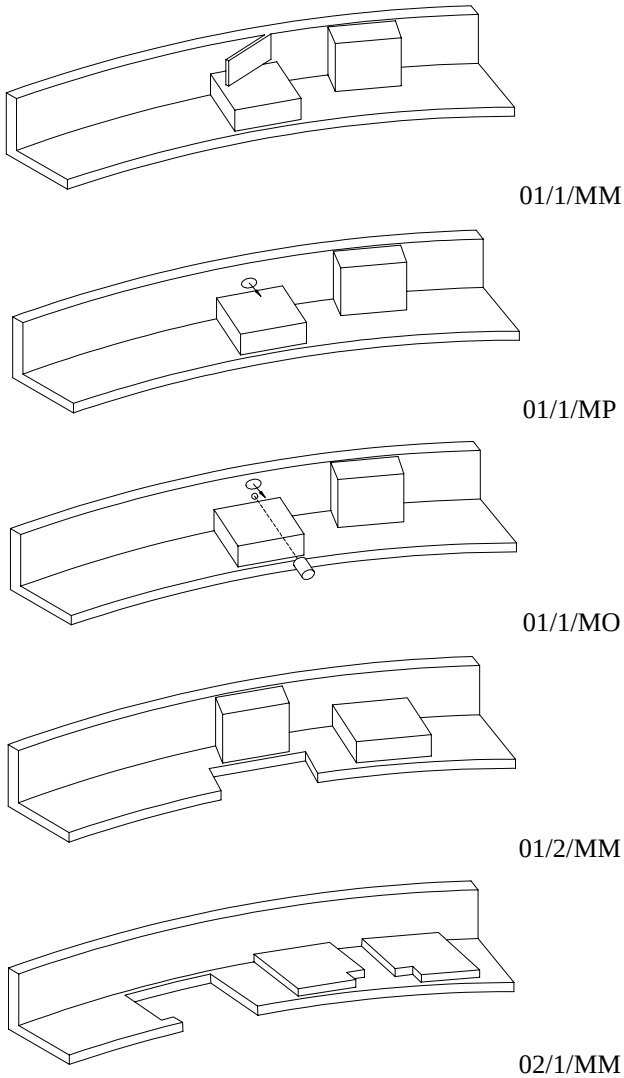

Fig. 2. Catalogue with simple orienting devices

III. APPLICATION OF THE METHODOLOGY

To illustrate how methodology of design of automatic orienting system in bowl feeders is applied in practice we shall consider the design of orientation system of prismatic part - type "Body" (shown on fig. 3).

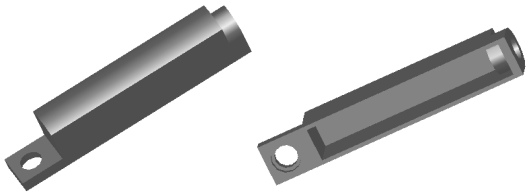

Fig. 3. Prismatic part type "Body"

Step 1. In table 3 are shown discernible stable positions of parts and empirical determined probabilities with which the various orientations of parts would occur after initial orientation.

TABLE III

N	Position	Probability	N	Position	Probability
1		9,4%	5		10,4%
2		14,6%	6		13,4%
3		14,5%	7		9,9%
4		16,4%	8		10,9%

Step 2. The main characteristics relative to the orientation process are shown in Table IV.

TABLE IV

Material	PE
Color	Cyan
Transparency	<5% (λ=500nm)
Weight	0,5g
Roughness	R_Z=40
Reflection capability	≈15% (λ=500nm)
Coefficient of friction	0,2
Relative magnetic permeability	≈1
Relative permittivity	2,2
Conductance	0

Step 3. Discernible stable positions in relation to basic orientating surface were compared. The result of the analyses is shown on Table V.

TABLE V

N	1	2	3	4	5	6	7	8
1	-	01/2	07/2	01/2	07/2 03/1 08/2	01/2 08/2	07/2 08/2	01/2 08/2
2	01/1	-	01/1	02/1	01/1 08/2	02/1 08/2	01/1 08/2	02/1 08/2
3	07/2 03/1	01/2	-	01/2	07/2 03/1 08/2	01/2 08/2	07/2 08/2	01/2 08/2
4	01/1	02/1	01/1	-	01/1 08/2	02/1 08/2	01/1 08/2	02/1 08/2
5	07/2 03/1 08/2	01/2 08/2	07/2 08/2	01/2 08/2	-	01/2	07/2	01/2
6	01/1 08/2	02/1 08/2	01/1 08/2	02/1 08/2	01/1	-	01/1	02/1
7	07/2 03/1 08/2	01/2 08/2	07/2 08/2	01/2 08/2	07/2 08/2	01/2	-	01/2
8	01/1 08/2	02/1 08/2	01/1 08/2	02/1 08/2	01/1	02/1	01/1	-

Step 4. The weight of the part is small. Material characteristics are: paramagnetic; relative permittivity is with small value; reflection capability is low; material is transparent for IR rays. Suitable recognition methods are: mechanical; electrical; pneumatic; optical (in visible light spectrum). Gravity method can be used in suitable conditions. The interaction forces are as follows: Gravity force; centrifugal force; pressure of fluid; capacitor effect; dielectric placed in non-uniform electrical field; mechanical force.

Simple orienting devices and recognition method are show in Table VI.

TABLE VI

Char.	Description	Method
02/1 (2,4,6,8)	Outlines – Contour	MM, MP, MO
07/2 (1,3,5,7)	Stepped surfaces - L<a	MM, MO
01/1	Size - Height	MM, MP, ME, MO
01/2	Size - Width	MM, MP, ME, MO
03/1	Internal contour - Contour	MM, MP, MO
08/1	Obviously shifting of the center of mass - Orthogonal to direction of moving	MM

Step 5. In this example are developed five different versions of automatic orienting systems, which consist of simple orienting devices shown in Table VII.

TABLE VII

N	5	7	5	6	8
1 (07/2)	-	-	-	-	-
3 (07/2)	-	-	-	-	-

5 (07/2)	MM	-	MO	-	-
7 (07/2)	-	MM	-	-	-
2 (02/1)	-	-	-	MM	-
4 (02/1)	-	-	-	MM	MM
6 (02/1)	-	-	-	-	-
8 (02/1)	-	-	-	MM	-
2, 4, 6, 8 (01/2)	-	-	-	-	-
1, 3, 5, 7 (01/1)	-	-	-	MM	-
1, 5 (03/1)	-	-	-	-	MM
1,2,3,4 (08/1)	-	-	-	-	-
5,6,7,8 (08/1)	-	-	-	-	-

Theoretically total number of solutions is 20, but in practice most of them are ignored due to higher costs, lower reliability, high complexity, etc.

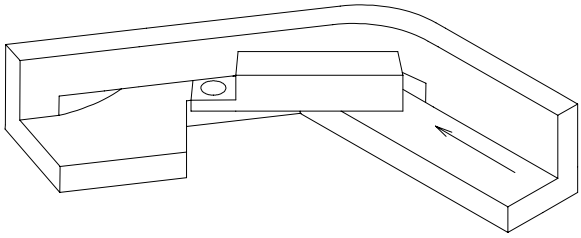

Fig. 4. Version one

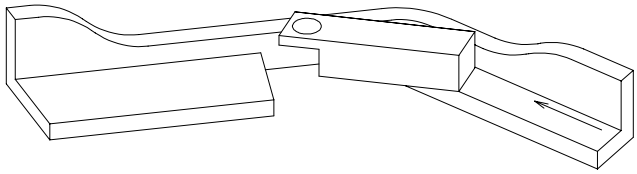

Fig. 5. Version two

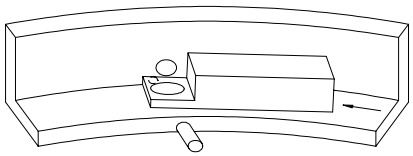

Fig. 6. Version three

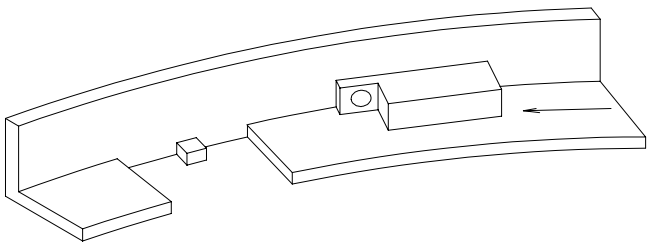

Fig. 7. Version four

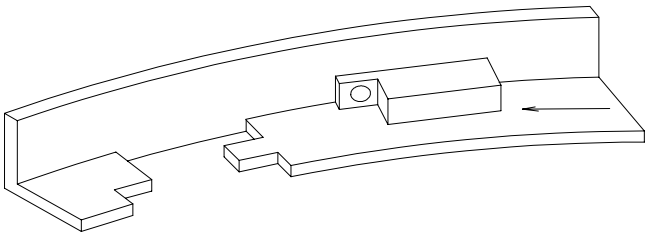

Fig. 8. Version five

IV. CONCLUSION

A methodology of design of automatic orienting systems in bowl feeders was described in this paper. The methodology is interactive and is based on combining of different simple orienting devices, performing common function. The choice of the devices is based on different discernible stable positions of the parts.

For determining of multitude of possibilities is used the method of "morphological box" and all the possible solutions are found out.

The discernible stable positions of parts are classified.

The interaction forces and recognition methods are classified.

Catalogue of simple orienting devices was made (a small passage of the catalogue is show in this paper). This catalogue can be updated. The index number of every device was created in order to simplify work with catalogue.

The example of design of orientation system of prismatic part - type "Body" is shown to illustrate application of the methodology in real conditions. After the analyses five versions were chosen out of twenty possible solutions.

REFERENCE

[1] Малаков, И.К., И.К. Милушев, М.К. Тодоров. Система за автоматично ориентиране на призматични асиметрични детайли тип "Тяло". Научни известия на НТС по Машиностроене, Година X, Бр. 3 (66), ISSN 1310-3946, октомври 2003, София, с. 97 ÷ 110.

[2] Дюкенджиев, Г. К., И. К. Малаков, Р. С. Йорданов. Система за нискостойностна автоматизация за сортиране на детайли тип "Конектор". Научни известия на НТС по Машиностроене, Година VII, Бр. 2 (53), ISSN 1310-3946, май 2000, Созопол, с. 157÷163.

[3] Handbook of Feeding and Orienting Techniques for Small Parts. Department of Mechanical Engineering, University of Massachusetts, Amherst, Massachusetts 01003.

[4] Бляхеров, И.С., Г.М.Варьяш, А.А.Иванов и др. Автоматическая загрузка технологических машин. Справочник. Под общ. ред. И.А.Клусова. Москва, Машиностроение. 1990.

[5] Делиев, С. Каталог на ориентиращи устройства. Печатна база при ВМЕИ – София, 1983.

[6] Витлиемов, В.Д. Автоматизация и роботизация на дискретното производство. Печатна база при Русенския университет "А.Кънчев", 1998.

The Influence of Power Converters Built with Power Semiconductor Devices on the Quality of the Electrical Energy

Kamen Seimenliyski[1], Tzanko Zanev[2], Pavlik Rahnev[1], Silvija Letskovska[1], M. Uscheva[1]

Abstract - **In the last years and in the present there is a tendency most of the produced electrical energy to be used in the converted type.**
In the process of the conversion of the energy the condition for regulation and stabilization of the parameters are realized, together with the possibility for automation of the technological processes. That is why the problems connected with power devices and converters built with them simultaneously arise.
In this work same of these problems are investigated as well as the factors generated them.

Key words - **regulator, converters, electromagnetic comp tability.**

I. Introduction.

One of the most serious problem, arising in the interaction between converter devices and power net is the harmonics generation of the supplied current. The reason of this is a nonlinear converters input as a result of that the current consumed from the net does not have sins form. The additional effects, depending on the peculiarity of converting net power are next:

- Distortion the voltage form in the connection point of the converting devises (converter);
- Lowing the power factor of the energy system;
- Radiating power low frequency and radio noise via the line and ether;
- Decreasing the pass capability of the lines;
- Additional losses in the net.

In this paper the results from the investigation the processes of interaction between semiconductor converters and AC supply net are described and particularly their influence on to the harmonics in the net current.

II. Description of the methodology.

In the correspondence with [1, 6] the numerical method for analysis and modeling is applied.

[1]Pavlik Rahnev is with of Burgas Free University, Alexandrovska 101, 8000 Burgas, Bulgaria, E-mail rahnev@bfu.bg
[1]Silvija Letskovska is with of Burgas Free University, Alexandrovska 101, 8000 Burgas, Bulgaria, E-mail silvia@bfu.bg
[1]Kamen Seimenliyski is with of Burgas Free University, Alexandrovska 101, 8000 Burgas, Bulgaria, silvia@bfu.bg
[2]Tzanko Zanev is with of Tehnical University Gabrovo, Bulgaria, tsanev@tugab.bg

The subject for investigation classical circuits of semiconductor converters are used. They are for alternative voltage converting in mono phase and three phase variant with opposite – parallel connected in the phase semiconductor devises and load, connected in star with or without zero cable and in three angle. With the agreement of the accepted method for analysis [4 - 6], the ratio between converter power and supplying transformer is calculated as well as the influence of the low voltage convection line parameters and load power factor.

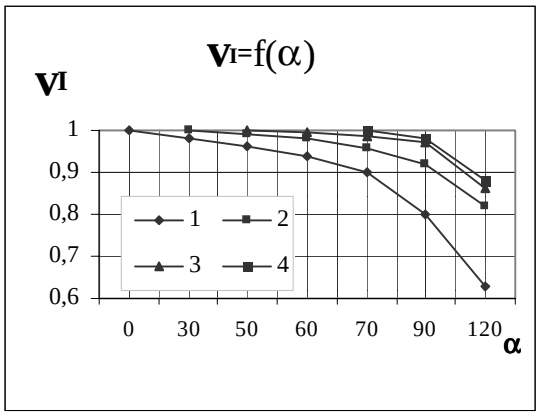

Fig 1. 1-cosφ = 1; 2 - cosφ = 0.9; 3 - cosφ = 0.7; 4 - cosφ = 0.4.

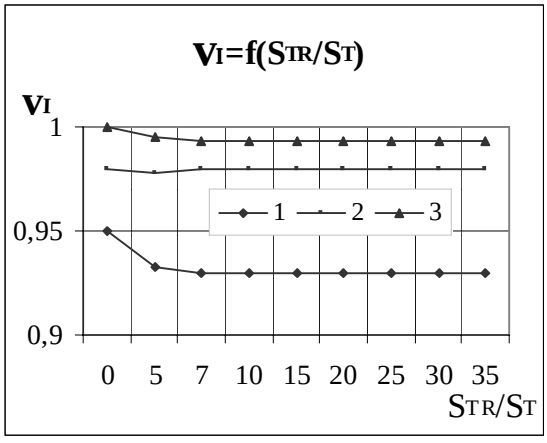

Fig 2. 1-cosφ = 1; 2 - cosφ = 0.9; 3 - cosφ = 0.7.

In the present work some of the results obtained related to the mode of phase regulation of the output power are described. From one side this method has wide application, but with strongly expressed back influence disadvantages.

The obtained results have an importance as base to compare in regulation with other methods and circuits.

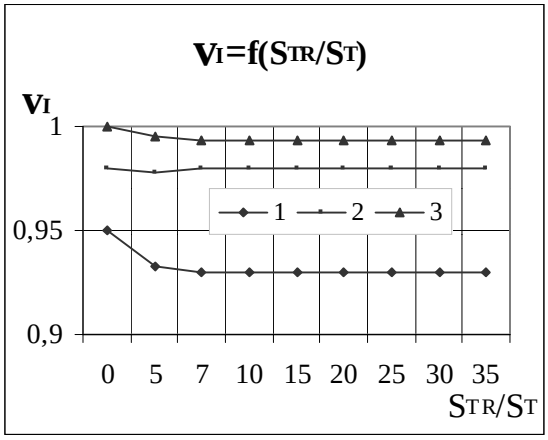

Fig 3. 1-cosφ = 1; 2 - cosφ = 0.9; 3 - cosφ = 0.7; 4 - cosφ = 0.4.

On Figures 1 - 5 the results are shown for part of the provided investigations for the dependence of distortions coefficient of the net current of the ν_I as a function of the regulating angle α and the relation between the supplied transformer power and the load S_{TR}/S_T for the parameter cosφ as follows:

1. Figures 1 – 3 – for mono phase and three phase converter with symmetrical load, star connected with presence of zero cable.
2. Figure 4 – 5 for circuits from p.1 with absence of zero cable.

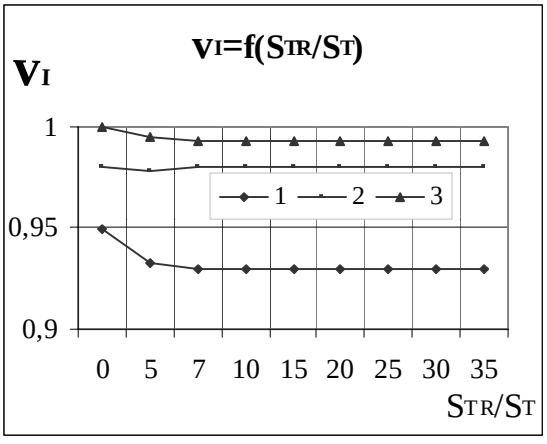

Fig 4. 1-cosφ = 1; 2 - cosφ = 0.9; 3 - cosφ = 0.7; 4 - cosφ = 0.4.

3. In Fig. 6 and Fig. 7 are shown for estimations respectively the dependence of power distortion D_0 from the regulating angle α.

From the present characteristics the next particularities could be established:

- The distortion coefficient ν_I strongly depends on the regulation angle α in the active load. In the circuit without zero cable the rate of ν_I change in is higher;
- Insignificant (up to 0.9) decreasing lowing the power factor cosφ leads to significant increasing of ν_I better seen in the circuit without zero cable. This effect could be reached using connected inductive filters;

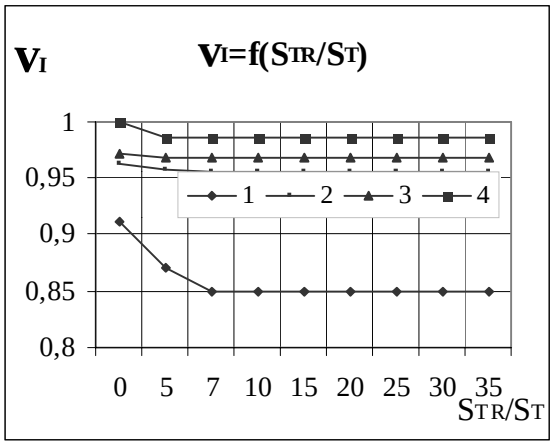

Fig 5. 1-cosφ = 1; 2 - cosφ = 0.9; 3 - cosφ = 0.7; 4 - cosφ = 0.4.

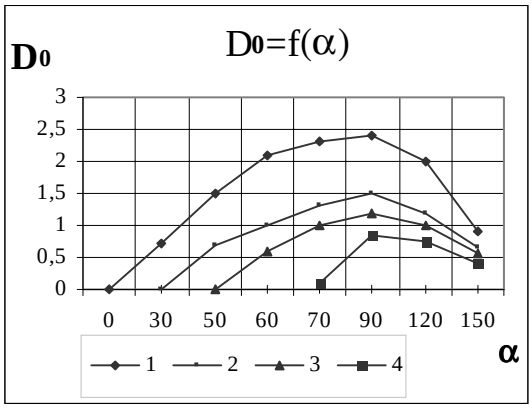

Fig 6. 1-cosφ = 1; 2 - cosφ = 0.9; 3 - cosφ = 0.7; 4 - cosφ = 0.4.

- The dependence $\nu_I = f(S_{TR}/S_T)$ appears more strong with high cosφ and small ratios S_{TR}/S_T (for $S_{TR}/S_T < 5$). The present characteristics relate

respectively for regulation angle $\alpha = 60^0$ and $\alpha = 90^0$.

The increasing influence of S_{TR} / S_T in low values on to ν_I is a result of the increasing role of the inductive resistance in the equivalent circuit, determined from transformer parameters and distribution line, connected in star without zero cable in the determined ratios between supply transformer power and a load.

- The comparison between different circuit shown that the values of ν_I for "star without zero cable" and "three angle" are almost equal and bigger than for "star without zero cable".
- The dependence $D_0 = f(\alpha)$ also shown that the disturbances in the circuit with zero cable are bigger than the other two circuit.

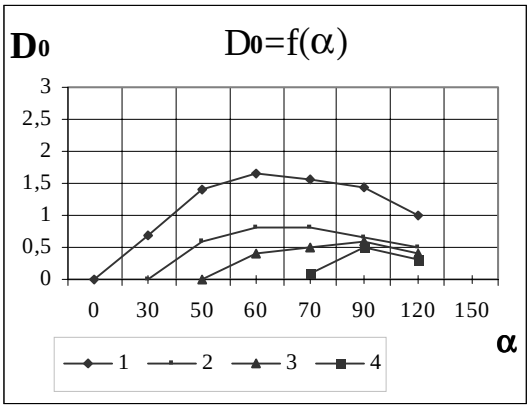

Fig 7. 1-cosφ = 1; 2 - cosφ = 0.9; 3 - cosφ = 0.7; 4 - cosφ = 0.4.

- The characteristics from Fig. 6. and Fig. 7. confirm the conclusions mode before.

III. Conclusions

The obtained results from the realized investigation, because of the its common character, have knowledge importance and in the some time ere concrete enough for practical use.

References

[1] IEC – Publ.146 Semiconductores converters. Genf 1993.
[2] TGL 200-0608/01 bis 29, Stromrichtenlagen, gerate und Stromrichter.
[3] DIN 41750 Bl. 1 bis 7, Stromrichter.
[4] DIN 57558, Halbleiter – Stromrichter.
[5] IEC–Publ., 146–2(1997), Part 2, Semiconductor selfcommutated converters.
[6] Kamen Seymenliyski, Tzanko Zanev, Silvija Letskovska, An equivalent circuit of the system power network – converter for technological purposes, Research work of BSU, Vol. 4, 2000.

Some Peculiarities Of Mass-Overall Dimensional Characteristics Of Brushless Motors

Dimitrina Koeva[1]

Abstract **-** Brushless motors (polyphased AC induction, synchronous and brushless DC motors) have no alternatives in modern electric drives. They possess highly efficient and very wide range of speeds. The objective of this paper is to represent some equations giving a relation between the basic parameters and magnitudes of electrical machines. This allows to be made a comparative analysis and a choice of motor concerning each particular case based not only on catalogue data or price for sale.

Keywords **-** Brushless DC motors, Brushless DC motors PM.

I. INTRODUCTION

Some different requirements such as high output power, high rotational frequency, full controllability, highest efficiency and low price could be insisted on modern high-speed brushless motors (AC, BLPM, SR motors). The selection of any type of motors for a particular application is a difficult task and is always accompanied with a compromise between price and quality.

II. RESULTS AND DISCUSSION

The analysis and juxtaposition of the mass-overall dimensional characteristics of these motors allows the possibility of their use in every particular case to be assessed. The mass-overall dimensional characteristics used frequently as criteria for comparison include: relative weight (motor weight per unit of useful power); relative weight of the active materials put in such as electrical sheet steel, wires, permanent magnets; torque per weight; power per unit of weight; price of the active materials put in per unit of power; developed torque per unit of price or weight, etc.

According the authors of Ref. [1] the relative power (p) characterizing the extent of use of the active materials is as following:

$$p = \frac{P'}{D^2.l_\delta} = \frac{m.I_n.E}{D^2.l_\delta}, \qquad (1)$$

where:

p is the relative power, $[W/m^3]$;

P' is calculated power, $[W]$;

m is the number of phases of stator winding;

I_n is the nominal current of the motor, $[A]$;

E is the electromotive force, $[V]$;

D is the stator diameter, $[m]$;

l_δ is the active length of the stator, $[m]$.

A more common criterion is the ratio between the developed motor torque and the volume of the active parts [1]. This ratio is called an utilization factor and can be expressed as:

$$f_u = \frac{P'}{D^2.l_\delta.\Omega}, \qquad (2)$$

where

f_u is utilization factor;

Ω is the angular velocity of the rotor, $[rad/s]$.

Another approach for estimation the technical level of each motor [1] is the determination of relative weight (m^*). This is the weight of motor per unit of motor volume.

Some cases occur, more frequently among motors with low power, when it is necessary the motor chosen to be insert in definite spaces of electric tools, kitchen and special appliances, etc. This necessitates, on the one hand, the chosen motor to be more compact, and on the other hand, as an object of operation to possess high reliability and energy indices, and to have comparatively low price.

As a specific case a comparison between three recently widely used motors such as asynchronous induction motor (AC), brushless DC motor with permanent magnets (BLPM) and brushless DC motor with reactive rotor (SR) was done [3, 4, 5]. The three mentioned above motors have identical overall dimensions and the same type of cooling. Their stators are made of one and the same kind of steel with equal external diameters and active lengths (Fig. 1).

All rest dimensions are optimized with the goal the use of copper wire for stator windings, electrical sheet steel, permanent magnets if they are put in motor construction and air gap to be relatively balanced.

[1] Dimitrina Koeva is with the Technical University of Sofia, Branch - Sliven, Department of Electronics and Electrical Engineering, e-mail: dkoeva@abv.bg

In order the comparison to be fairly done and the selection to be made using catalogue data and price for each motor has been approached individually.

Using the above-mentioned equal initial dimensions the data generalized are represented in Tables I-III.

Analyzing the results presented the following conclusions can be made. AC, BLPM and SR generate 3,7 kW, 10,5 kW and 6,6 kW output power, respectively. Thus, BLPM and SR generate 2,84 and 1,78 times higher power, respectively, in respect to the power that AC generates at equal stator dimensions and current density. AC motor has the biggest volume of stator and rotor, but generates the smallest torque and lowest power per unit of active materials weight. The data analysis presents an advantage of BLPM first and then of SR. The last possesses very good energy characteristics (η = 92 %) and because of the lowest price of the materials used it is the cheapest. BLPM possesses excellent energy characteristics (η = 94%) and electromagnetic parameters. The last motor is the most compact but is 8,17 and 6,5 times cheaper than SR motor and AC motor, respectively.

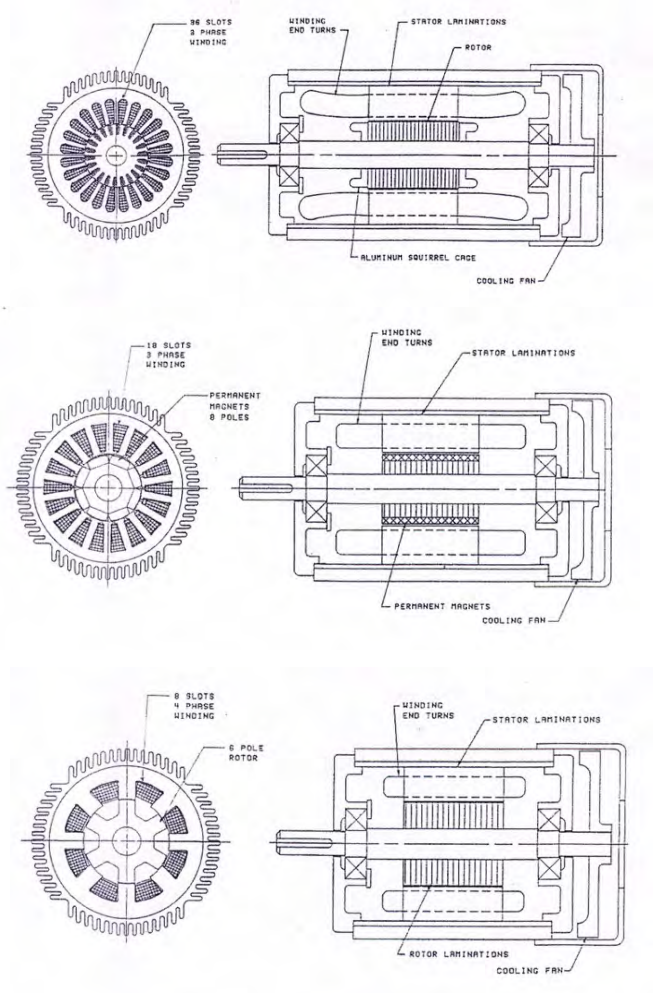

Fig. 1.

TABLE I

Motor type	Continuous torque (1800 rpm), Nm	Continuous power (1800 rpm), kW	η,%	Current density, A/mm^2
AC	19,78	3,7	90	7,8
BLPM	56,5	10,5	94	7,65
SR	36,6	6,6	92	7,7

TABLE II

Motor type	Stator		Rotor	Air gap, mm
	External diameter, mm	Internal diameter, mm	External diameter, mm	
AC	193,6	112,6	112,2	0,38
BLPM	193,6	96	95,6	0,38
SR	193,6	108,8	107,6	0,38

TABLE III

Motor type	m^*, kg/m	Torque per unit of weight, Nm/kg			Power per unit of weight, kW/kg		
		Rotor	Stator	Total	Rotor	Stator	Total
AC	4,04	2,31	1,35	0,9	0,43	0,25	0,2
BLPM	5,43	8,19	3,19	2,3	1,52	0,59	0,4
SR	5,18	5,3	2,57	1,7	0,98	0,48	0,3

III. CONCLUSION

Each of the motors considered has its peculiarities, which are defined by the selection of: electromagnetic materials; heat and mechanical loadings with reading the dynamic indices; use of permanent magnets; regime of regulation.

Recently the tendency is the optimal design of such motors to be orientated towards their weight minimization at optimal electromagnetic loadings and, investment of new materials and construction improvement .

The results illustrate an advantage of BLPM due to the use of highly energetic magnets (NdFeB, Sm-Co). This allows the device to be changed in principle. As a result the motor overall dimensions are reduced, the power per unit of active materials volume increases and the highest efficiency is considerably improved.

REFERENCES

[1] Kopilov I. P., “Design of electric machines”, I, M. E. 1993.
[2] Hendershot J. R., “AC, Brushless, Switched reluctance motor comparisons”, Magna Physics Corporation, Hillsboro, OH.
[3] Baldor Motors and Drives Catalogue.
[4] Maxon Motor Catalogue, 2001.
[5] PAPST DC Motion Catalogue, 2000.

Flux and Torque Ripple Minimization in DTC of Induction Motor

Nebojsa Mitrovic[1], Vojkan Kostic[2], Milutin Petronijevic[3] and Borislav Jeftenic[4]

***Abstract* – In this paper the torque ripple in Direct Torque Control schemes (DTC) is analyzed in detail. It is found that the torque ripple can be divided into two parts, one is only related to the motor parameter and the other is related to the applied voltage and the rotor angular velocity. Based on the analysis, a duty ratio modulation method is proposed. Simulation results indicate the effectiveness of the proposed torque ripple minimizing method.**

***Keywords* – induction motor drive, direct torque control, duty ratio modulation.**

I. INTRODUCTION

DTC schemes to become an alternative for the classic variable speed AC drives. A fast dynamic can be achieved by calculating the instantaneous torque and flux. Using switching table not only simplifies the control system, but also decrease computing time. With a three phase voltage source inverter, there are six non-zero voltage vectors and two zero voltage vectors which can be applied to the machine terminals. The stator flux can be estimated by integrating emf using measuring current and voltage vectors or DC link voltage. The torque can be calculated using *d-q* components of the estimated flux and measured currents [1, 2].

Besides its advantages in application, the conventional DTC system has its drawback. First, its switching frequency varies according to the motor speed and the hysteresis bands of torque and flux. Second, large torque ripple is generated especially in a low speed region. Third, in DTC the stator current contains much more harmonics than that fed with sinusoidal voltage [3–5].

In order to reduce the torque ripple and the current harmonics, high switching frequency is needed but this will bring high sampling frequency and increase the system cost. Multilevel inverter is another choice [6], which reduces the torque ripple and current harmonics by providing more selective voltage vectors. But this kind of topology needs more power devices and the control scheme becomes more complex, that make it only suitable for high power applications.

[1]Nebojsa Mitrovic is with the Faculty of Electronic Engineering, Beogradska 14, 18000 Nis, Yugoslavia, E-mail: nesa@elfak.ni.ac.yu

[2]Vojkan Kostic is with the Faculty of Electronic Engineering, Beogradska 14, 18000 Nis, Yugoslavia, E-mail: vkostic@elfak.ni.ac.yu

[3]Milutin Petronijevic is with the Faculty of Electronic Engineering, Beogradska 14, 18000 Nis, Yugoslavia, E-mail: milutin@elfak.ni.ac.yu

[4]Borislav Jeftenic is with the Faculty of Electrical Engineering, Bulevar Revolucije 73, 11000 Belgrade, Yugoslavia, E-mail: jeftenic@etf.bg.ac.yu

In this paper analysis work is done on the relationship between applied voltage and corresponding torque and stator flux variations. Based on the analysis, a new DTC strategy is introduced with torque ripple reduction by modulating the duty ratio of the applied voltage. Simulation results are presented to verify the effectiveness of the control algorithm.

II. PROPOSED DUTY RATIO MODULATION METHOD

The dynamic behavior of an induction machine is described by the equations written in a *d-q* stationary reference frame [7] as follows:

$$\begin{aligned} v_{ds} &= R_s i_{ds} + \frac{\mathrm{d}\varphi_{ds}}{\mathrm{d}t} \\ v_{qs} &= R_s i_{qs} + \frac{\mathrm{d}\varphi_{qs}}{\mathrm{d}t} \\ 0 &= R_r i_{dr} + \frac{\mathrm{d}\varphi_{dr}}{\mathrm{d}t} + \omega_r \varphi_{qr} \\ 0 &= R_r i_{qr} + \frac{\mathrm{d}\varphi_{qr}}{\mathrm{d}t} - \omega_r \varphi_{dr} \\ \varphi_{ds} &= L_s i_{ds} + L_m i_{dr} \\ \varphi_{qs} &= L_s i_{qs} + L_m i_{qr} \\ \varphi_{dr} &= L_r i_{dr} + L_m i_{ds} \\ \varphi_{qr} &= L_r i_{qr} + L_m i_{ds} \end{aligned} \tag{1}$$

where: v_{ds}, v_{qs}, i_{ds}, i_{qs}, i_{dr}, i_{qr}, φ_{ds}, φ_{qs}, φ_{dr}, φ_{qr}, R_s, R_r, L_s, L_r, L_m, ω_r *d-q* components of stator voltage vector, $\overline{v_s}$, *d-q* components of stator and rotor current vector, $\overline{i_s}$ and $\overline{i_r}$, *d-q* components of stator and rotor flux vector, $\overline{\varphi_s}$ and $\overline{\varphi_r}$, stator and rotor resistance and self inductance, mutual inductance and rotor angular speed expressed in electrical radians, respectively.

From (1), the induction machine can be modeled with stator and rotor flux as the state variables as:

$$\begin{aligned} \frac{\mathrm{d}\varphi_{ds}}{\mathrm{d}t} &= -\frac{1}{\sigma T_s}\varphi_{ds} + \frac{L_m}{\sigma T_s L_r}\varphi_{dr} + v_{ds} \\ \frac{\mathrm{d}\varphi_{qs}}{\mathrm{d}t} &= -\frac{1}{\sigma T_s}\varphi_{qs} + \frac{L_m}{\sigma T_s L_r}\varphi_{qr} + v_{qs} \\ \frac{\mathrm{d}\varphi_{dr}}{\mathrm{d}t} &= \frac{L_m}{\sigma T_r L_s}\varphi_{ds} - \frac{1}{\sigma T_r}\varphi_{dr} - \omega_r \varphi_{qr} \\ \frac{\mathrm{d}\varphi_{qr}}{\mathrm{d}t} &= \frac{L_m}{\sigma T_r L_s}\varphi_{qs} + \omega_r \varphi_{dr} - \frac{1}{\sigma T_r}\varphi_{qr} \end{aligned} \tag{2}$$

where: $\sigma = 1 - \frac{L_m^{\ 2}}{L_s L_r}$, $T_s = \frac{L_s}{R_s}$ and $T_r = \frac{L_r}{R_r}$ leakage coefficient, stator and rotor time constant, respectively.

The electromagnetic torque can be written in the terms of stator and rotor flux as:

$$T_e = \frac{3}{2} p \frac{L_m}{\sigma L_s L_r} \left(\varphi_{qs} \varphi_{dr} - \varphi_{ds} \varphi_{qr} \right) \tag{3}$$

where p is number of pole pairs.

From (1) stator flux can be written in the terms of stator voltage and stator current as:

$$\begin{aligned} \varphi_{ds} &= \int \left(v_{ds} - R_s i_{ds} \right) \mathrm{d}t \\ \varphi_{qs} &= \int \left(v_{qs} - R_s i_{qs} \right) \mathrm{d}t \end{aligned} \tag{4}$$

From (2), it can be seen that there is an inertia part between stator flux and rotor flux. The stator flux responses faster to the control action than the rotor flux does, and it can be assumed that the rotor flux does not change when the time interval is very small. So from (3) we can get that turning the stator flux can easily change the electromagnetic torque. Equation (4) indicates that the stator flux follows the stator voltage very quickly.

Because the value of sampling period, Δt, is very small, the stator and rotor flux state function in (2) can be expressed in discrete forms as (5).

$$\begin{aligned} \varphi_{ds_{k+1}} &= \varphi_{ds_k} + \left(-\frac{1}{\sigma T_s} \varphi_{ds_k} + \frac{L_m}{\sigma T_s L_r} \varphi_{dr_k} + v_{ds_k} \right) \Delta t \\ \varphi_{qs_{k+1}} &= \varphi_{qs_k} + \left(-\frac{1}{\sigma T_s} \varphi_{qs_k} + \frac{L_m}{\sigma T_s L_r} \varphi_{qr_k} + v_{qs_k} \right) \Delta t \\ \varphi_{dr_{k+1}} &= \varphi_{dr_k} + \left(\frac{L_m}{\sigma T_r L_s} \varphi_{ds_k} - \frac{1}{\sigma T_r} \varphi_{dr_k} - \omega_{rk} \varphi_{qr_k} \right) \Delta t \\ \varphi_{qr_{k+1}} &= \varphi_{qr_k} + \left(\frac{L_m}{\sigma T_r L_s} \varphi_{qs_k} + \omega_{r_k} \varphi_{dr_k} - \frac{1}{\sigma T_r} \varphi_{qr_k} \right) \Delta t \end{aligned} \tag{5}$$

Equation (5) clearly shows the variation of the stator flux due to the applied voltage vector, for given operating conditions. Neglecting the stator resistance effects, stator flux equation from (5) can be written as (6).

$$\begin{aligned} \varphi_{ds_{k+1}} &\cong \varphi_{ds_k} + v_{ds_k} \Delta t \\ \varphi_{qs_{k+1}} &\cong \varphi_{qs_k} + v_{qs_k} \Delta t \end{aligned} \tag{6}$$

From (6), it appears that the stator flux variation has the same direction of the applied voltage vector and an amplitude which is proportional to $\left| \overline{v_{s_k}} \right|$ and Δt.

The electromagnetic torque at (k+1) sampling time can be written as:

$$T_{e_{k+1}} = \frac{3}{2} p \frac{L_m}{\sigma L_s L_r} \left(\varphi_{qs_{k+1}} \varphi_{dr_{k+1}} - \varphi_{ds_{k+1}} \varphi_{qr_{k+1}} \right) \tag{7}$$

Substitute (5) into (7) and neglect the term proportional to the square of Δt, the torque at time of t_{k+1} is written as below:

$$T_{e_{k+1}} = T_{e_k} + \Delta T_{e1_k} + \Delta T_{e2_k} \tag{8}$$

where:

$$\Delta T_{e1_k} = -T_{e_k} \left(\frac{1}{T_s} + \frac{1}{T_r} \right) \frac{\Delta t}{\sigma} \tag{9}$$

$$\begin{aligned} \Delta T_{e2_k} = \frac{3}{2} p \frac{L_m}{\sigma L_s L_r} [& (v_{qs_k} - \omega_{r_k} \varphi_{ds_k}) \varphi_{dr_k} - \\ & (v_{ds_k} + \omega_{r_k} \varphi_{qs_k}) \varphi_{qr_k}] \Delta t \end{aligned} \tag{10}$$

Equation (8) indicates that the torque ripple can be composed into two parts, ΔT_{e1_k} i ΔT_{e2_k}. It is show in (9) that the applied voltage vector and rotor speed will not influence to ΔT_{e1_k}. It is only related to the motor parameters and its effect is to reduce the torque. The second part, ΔT_{e2_k}, represents the effect of the applied voltage vector on torque variation and is dependent on operating condition. For a given voltage vector this part is mainly affected by the rotor speed.

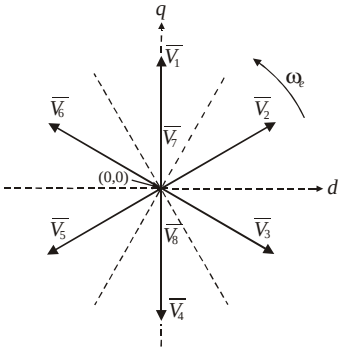

Fig. 1. The inverter output voltage vectors

In general DTC scheme, only one of eight voltage vectors is applied during each sampling period as shown in Fig. 1. And the torque ripple is unable to control during this time interval. If we can divide the sampling period into two parts and send different voltage vectors in the two parts, then the torque ripple can be controlled and reduced. From (8) it is easy to know that if we can make $\Delta T_{e2_k} = -\Delta T_{e1_k}$ then the average torque ripple of one sampling period is null. The torque ripple itself will be reduced too.

Assumung the sampling period is divided into two parts, $\Delta t = \Delta t_1 + \Delta t_2$. Voltage vector $\overline{v_{s1}}$ is applied during Δt_1, and $\overline{v_{s2}}$ during Δt_2, then:

$$\begin{aligned} \Delta T_{e2_k} = \frac{3}{2} p \frac{L_m}{\sigma L_s L_r} [& (v_{qs1_k} M_1 + v_{qs2_k} M_2 - \omega_{r_k} \varphi_{ds_k}) \varphi_{dr_k} - \\ & (v_{ds1_k} M_1 + v_{ds2_k} M_2 + \omega_{r_k} \varphi_{qs_k}) \varphi_{qr_k}] \Delta t \end{aligned} \tag{12}$$

where: $M_1 = \frac{\Delta t_1}{\Delta t}$ and $M_2 = \frac{\Delta t_2}{\Delta t}$ modulation ratio of $\overline{v_{s1_k}}$ and $\overline{v_{s2_k}}$, respectively.

In this DTC scheme, the voltage vector $\overline{v_{s1_k}}$ is decided by the conventional switching table to increase the torque. Voltage vector $\overline{v_{s2_k}}$ is selected to decrease the torque, and make $\Delta T_{e2_k} = -\Delta T_{e1_k}$. Because only the voltage vectors $\overline{V_7}$ (000) and $\overline{V_8}$ (111) will decrease flux and torque at any

condition, so $\overline{V_7}$ is selected to full fill Δt_2 to make the scheme simple. And we can get:

$$M_1 = \frac{T_{e_k}\dfrac{K_1}{K_2} + \omega_{r_k}\left(\varphi_{ds_k}\varphi_{dr_k} + \varphi_{qs_k}\varphi_{qr_k}\right)}{v_{qs1_k}\varphi_{dr_k} - v_{ds1_k}\varphi_{qr_k}} \qquad (13)$$

where: $K_1 = \left(\dfrac{1}{T_s} + \dfrac{1}{T_r}\right)\dfrac{1}{\sigma}$ and $K_2 = \dfrac{3}{2}p\dfrac{L_m}{\sigma L_s L_r}$.

Equation (13) indicates that M_1 is dependent on T_{e_k}, ω_{r_k}, motor parameters and other components. But all quantities from (13) are necessary for realization speed sensorless DTC algorithm.

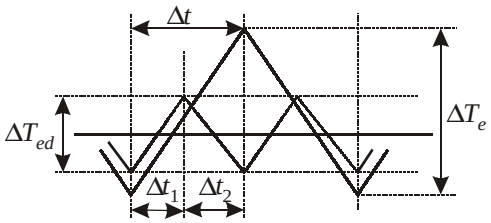

Fig. 2. The torque ripple with and without duti ratio

Fig. 2 present the graphic effectiveness of applying duty ratio modulation. Here ΔT_{ed} presents the torque ripple amplitude with duty ratio modulation, while ΔT_e presents the torque ripple without duty ratio modulation.

III. New DTC Scheme Configuration

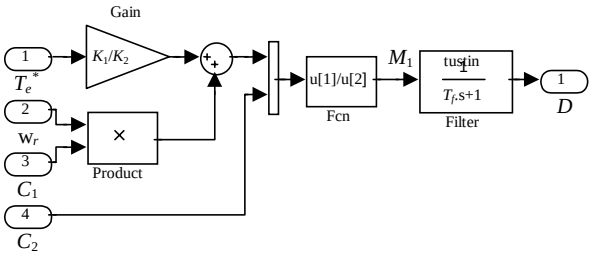

Fig. 3. Output voltage duty cycle ratio determination diagram

The strategy above gives the principle of a new DTC scheme with duty ratio modulation. In this scheme the selection of $\overline{v_{s1}}$ at k+1 sampling time is done by the conventional method as show in Fig. 1. But in practical system there must be some adjustments. Fig. 3 gives the diagram for determining the duty cycle of output voltage vector. In this figure D indicate the final output duty cycle ratio, T_f is a time constant for filtering (T_f =0.001-0.01), T_e^* is the given reference torque and ω_r is rotor angular speed expressed in electrical radians. Quantities C_1 i C_2 are parts of (13): $C_1 = \varphi_{ds_k}\varphi_{dr_k} + \varphi_{qs_k}\varphi_{qr_k}$, $C_2 = v_{qs1_k}\varphi_{dr_k} - v_{ds1_k}\varphi_{qr_k}$.

IV. Simulation Results

Simulations have been carried out for the comparison of a conventional and proposed DTC schemes. The simulations were conducted using Matlab/Simulink simulation package [8]. The hysteresis loop bands in both schemes are the same, 2.5 Nm for torque and 0.01 Vs for flux. The system is run under load torque of 15 Nm with DC bus voltage of 540 V. Torque limit is set to 45 Nm. During speed change duty ratio is set to 0.9. The system sampling frequency is 15 kHz and switching frequency is 7.5 kHz. The motor's parameter is listed in Table I.

TABLE I
INDUCTION MOTOR PARAMETER

Rated power	4 kW
Rated line to line voltage	400 V
Rated speed	1440 rpm
Rated torque	26.7 Nm
Rated stator flux	0.95 Vs
Pole pairs	2
R_s	1.13 Ω
R_r	0.9 Ω
L_s	0.142 H
L_r	0.143 H
L_m	0.13 H
Load inertia	0.06 kgm^2

In both cases the motor starts at t=0 s with speed reference of 720 rpm, and the reference speed is changed to 1080 rpm at t=0.7 s. Fig. 4 show the duty cycle ratio variation. During speed acceleration the modulation ratio is at set value, providing the maximum electromagnetic torque and less ripple than conventional DTC. When the rotation speed reaches the reference, the modulation ratio decrease to a certain value to reduce torque ripple.

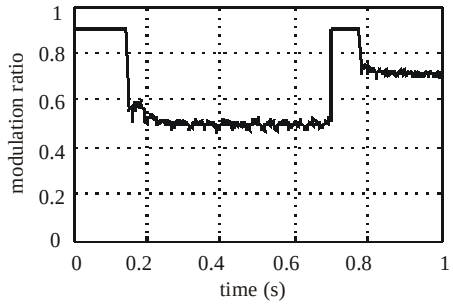

Fig. 4. Output voltage modulation ratio

Figs. 5 and 6 show the speed, torque, current and flux variance in the conventional and proposed DTC scheme. In steady state it can be found that with duty ratio modulation the torque ripple is reduced effectively but the ripple still will increase as speed raise up, according to (12). During speed change torque ripple is reduced because value of duty ratio modulation is set to 0.9. The stator flux ripple is reduced too, and ripple is less at lower speed. Another advantage of this DTC scheme is reduction of the current harmonics. So this kind of control scheme does not deteriorate the dynamic performance of DTC but at the same time the stable performance is improved.

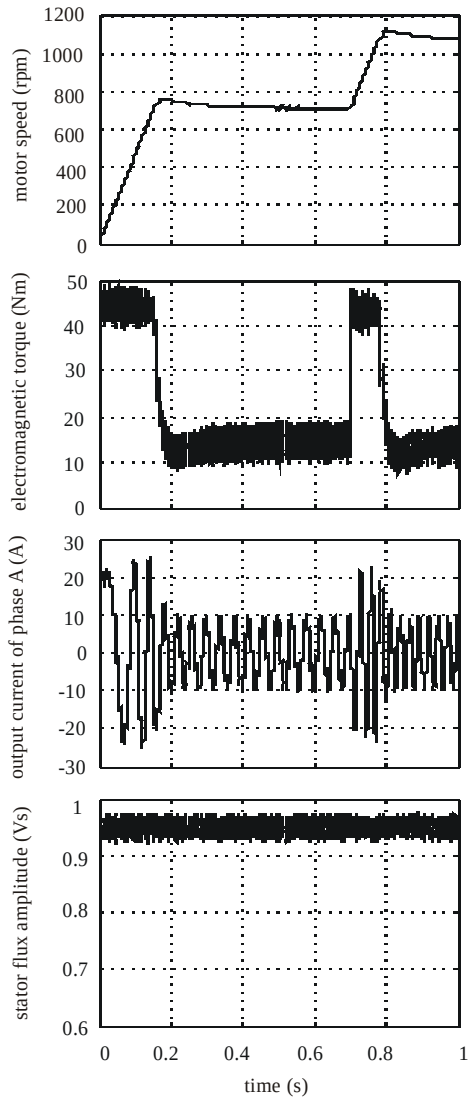

Fig. 5. The speed, torque, current and flux in conventional DTC scheme

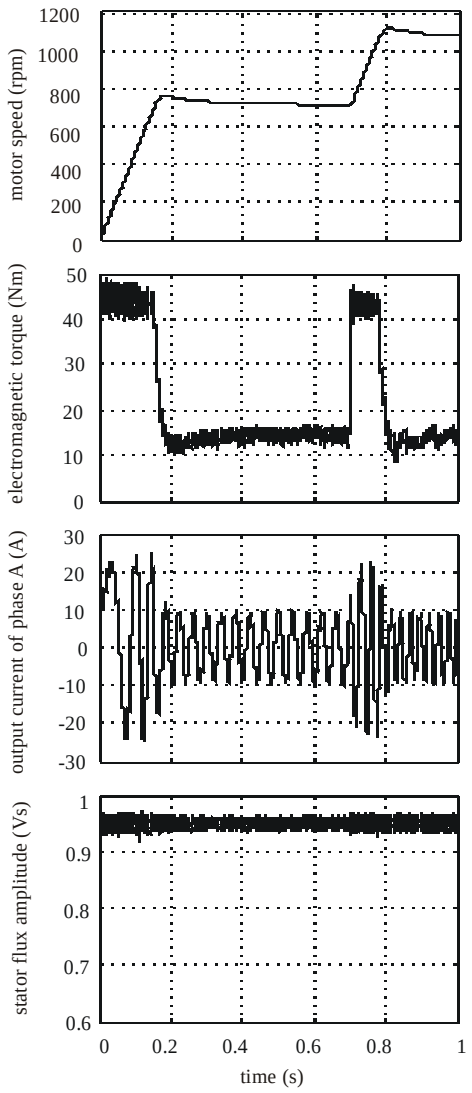

Fig. 6. The speed, torque, current and flux in the proposed DTC scheme

V. CONCLUSION

In this paper the torque ripple in DTC is analyzed in detail. The torque ripple minimization method based on duty ratio modulation of output voltage is described. This method does not deteriorate the dynamic performance of DTC but at the same time the stable performance is improved. The method is very easy to be embedded in conventional DTC scheme without increasing the system complexity greatly. Simulation results prove the advantages of this method.

REFERENCES

[1] R. Krishnan, *Electric Motor Drives, Modeling, Analysis, and Control*, Prentice Hall, New Jersey, 2001.

[2] Nebojsa Mitrovic, Vojkan Kostic, Milutin Petronijevic and Borislav Jeftenic, "Comparison by Simulation of Torque Control Schemes for Electric Drive Application", ICEST 2003, pp. 417-420, Sofia, Bulgaria, 16-18 October 2003.

[3] S. Kaboli, M. R. Zolghadri, S. Haghbin, A. Emadi, "Torque ripple minimization in DTC of induction motor based on optimized flux value determination", Proc. 29th Annual Conference of the IEEE Industrial Electronics Society, IECON03, Roanoke, VA, USA, pp. 431-435.

[4] D. Casadei, G. Serra, A. Tani, "Analytical investigation of torque and flux ripple in DTC schemes for induction motor", Industrial Electronics, Control and Instrumentation, IECON 97. 23rd International Conference, vol. 2, pp: 552-556, 1997.

[5] N.R.N. Idris and A.H.M. Yatim, "Reduced Torque Ripple And Constant Torque Switching Frequency Strategy For Direct Torque Control Of Induction Machine", In. Conf. Rec. IEEE-APEC, pp. 154-161, vol. 1, 2000.

[6] Kyo-Beum Lee, Joong-Ho Song, Ick Choy and Ji-Yoon Yoo, "Torque Ripple Reduction in DTC of Induction Motor Driven by Three-Level Inverter With Low Switching Frequency", IEEE Trans. on Power Electronics, Vol. 17, No. 2, March 2002.

[7] Paul C. Krause, Oleg Wasynczuk, Scott D. Sudhoff, *Analysis of Electric Machinery*, IEEE Press, New York, 1994.

[8] Tang L., Rahman M.F.,"A Matlab/Simulink Model based on Power System Blockset - A New Direct Torque Control Strategy for Permanent Magnet Synchronous Motor Drive System", Australasian Universities Power Engineering Conference, Perth, Australia, September, 2001, pp. 281-286.

Modeling The External Characteristic Of Cold-Plasma Reactors

Peter Dineff[1] and Dilyana Gospodinova[2]

Abstract – **The external or static volt-ampere characteristic describes the behavior of technological barrier discharge at diverse stages of development and application regimes. Various approaches to mathematical modeling of the external characteristic of cold plasma reactors creating plasma volumes and plasma surfaces for plasma surface modification of polymers and polymeric materials are examined.**

Keywords - **External characteristic, Cold-plasma reactor, One-atmosphere barrier discharge, Plasma surface modification.**

I. INTRODUCTION

Barrier discharges feature serious technological advantages determining their application to the technology of textiles and textile fibers, electronics and microelectronics, and printing industry [1].

Characteristic of all types of barrier discharges is the presence of one or two dielectric barriers separating the electrodes from the working medium.

This remains a purely external token of barrier discharges, as the dielectric barrier performs a quite essential part in discharge occurrence and burning, which is expressed by the following, [1, 2]:

❑ the barrier with its capacitance C_δ performs the part of a reactance, i. e. of a capacitive ballast reactance $X_C = \omega^{-1} C_\delta^{-1}$, that limits the increase of the electric current in the course of discharge burning;

❑ the barrier re-distributes the electric field intensity in the interelectrode space, loading electrically the working (gaseous or vaporous) medium, the intensity in this medium increasing ε_δ times with respect to the electric field intensity in the barrier, where ε_δ is the relative dielectric permittivity of the barrier material or it determines the critical parameters of barrier discharge: voltage of ignition U_{bd} and current of ignition I_{bd};

❑ the barrier determines the voltage of burning U_b of the discharge, which remains constant in the course of its burning and does not depend on the working voltage chosen.

! The multiple ionization-related and chemical processes going simultaneously during burning of the barrier discharge at atmospheric pressure present considerable problems not only in controlling of discharge, but also in describing its behavior, [2].

THE TASK of the present work is to use various approaches to modeling the behavior of a low-frequency (50 Hz) barrier discharge, which burns in the volume or on the surface of a cold-plasma generator system, under load or in the absence of a load, in air at atmospheric pressure (**760** ± 25 Torr, **1** atm), i. e. of a *one-atmosphere barrier discharge* (*OABD*).

The investigations are focused on two types of a cold-plasma reactor system:

♦ *the first one* representing two plane-parallel electrodes with a glass barrier between them, which create a plasma volume with relatively uniform distribution of the electric field between the glass barrier and one of the electrodes, i.e. a *one-atmosphere uniform barrier discharge* (*OAUBD*);

♦ *the second one* representing two plane-parallel electrodes, which embrace tightly the glass barrier in such a way, that solely on that side of the barrier, which looks at the comb-shaped electrode, there emerges a plasma surface with strongly non-uniform distribution of the electric field, i. e. a *one-atmosphere non-uniform barrier discharge* (*OANUBD*).

II. General formulation of the investigations

Our experimental investigations [2, 3, 5] performed during a continuous period of time allow to search for a new description of the behavior and control of the barrier discharge at atmospheric pressure, based on its external or static volt-ampere characteristic.

This characteristic expresses the relationship between the average value of current I_{gap} (*AV*) passing through the barrier discharge and the effective value of voltage U_{gap} (*RMS*) applied across discharge, Fig. 1.

Moreover, it turns out [2,3], that the external characteristic may be simulated by means of a broken-line polygon of three linear segments, each of them corresponding to one of the three development stages of the barrier discharge, Fig. 1:

♦ the stage preceding the ignition of the barrier discharge, namely the so-called free or non-operational regime;

♦ the first stage of burning, which corresponds to the formation of cold ozone- and oxygen-containing plasma;

♦ the second stage of burning, which corresponds to the formation of cold plasma mostly containing nitrogen oxides.

At high values of linear correlation factor r_{pc} the linear law describes very well the individual sections of the external characteristic of barrier discharge. However, the transitional regions of the characteristic remain outside the scope of this description, because there is a smooth transition between each two adjacent regions, while the polygon simulating the characteristic represents a broken line.

Do the latter two stages (or regimes) of burning of the barrier discharge really exist? The answer is positive, because the analysis of the elementary processes clearly separates from each other the two air media, in which ozone and products of its decomposition are generated, [1]:

[1]Peter Dineff is with the Faculty of Electrical Engineering, Technical University of Sofia, Kliment Ohridski 8, 1000 Sofia, Bulgaria, E-mail: dineff_pd@abv.bg.

[2]Dilyana Gospodinova is with the Faculty of Electrical Engineering, Technical University of Sofia, Kliment Ohridski 8, 1000 Sofia, Bulgaria, E-mail: dilianang@abv.bg.

♦ *one of these*, a medium depleted of energy, is created in electric fields of low relative intensity *E/p*, favoring processes with larger cross-section of impact interaction – about 10^{-16} cm^2, i. e. ozone generation from molecular ions O_2^+, where two molecules of ozone O_3 correspond to one molecular ion O_2^+. A product of its rapid decomposition under conditions of α-impact ionization are the exited, chemically active oxigen (O_2^*) molecules (the so-called singlet oxygen);

♦ *the other*, energy-rich medium, is created in electric fields of higher relative intensity *E/p* and favors processes with smaller cross-section of impact interaction – about 10^{-18} cm^2, i. e. the generation of ozone O_3 from atomic ions O^- and O^+ through intermediate synthesis of negative O_3^- and positive O_3^+ ozone ions.

The energy–richer medium of higher values of the relative electric-field intensity *E/p* and plasma temperature creates conditions not only for rapid decomposition of ozone, but also for its inhibition in reactions with negative atomic ions O^-, with atomic oxygen *O*, or with nitrogen oxides NO_x. Such a medium is characterized by rapid depletion as regards the ozone and products of its decomposition. It is enriched with nitrogen oxides, [1].

This thesis is supported by the direct measurement of the ozone obtained in ozone-air mixtures in the two regimes of burning of the barrier discharge, [4].

The mathematical model thus obtained is based on its real reasons, moreover that experiments in modifying low-energy polymeric surfaces indicate different physico-chemical relations of materials in these two cases, [4].

This comes to show that there exist physical, chemical and technological reasons that make this model very useful. One-atmosphere barrier discharge can be simulated and controlled as a voltage-controlled current source.

At the same time *Zhiyu Chen* and *J. Reece Roth* [5] propose a new model of behavior of one-atmosphere barrier discharge based not on the linear law, but on a power one. The discharge current follows a power law, a characteristic of the voltage-current behaviour of a normal glow discharge (in vacuum). For example, the current-voltage relationship of various normal glow discharges in vacuum was $I \propto U^2$, $I \propto U^3$, and $I \propto U^9$.

Its output current follows the power law given by the following equation

$$I = 0 \text{ , for } U_{gap} < U_{bd} \qquad (1)$$

$$I \alpha \left(U_{gap} - U_{bd}\right)^n \text{, for } U_{gap} \geq U_{bd} \qquad (2)$$

where *n* is an integer that may range from 1 to 12 in different types of glow or barrier discharge plasma devices, U_{bd} - the voltage of breakdown.

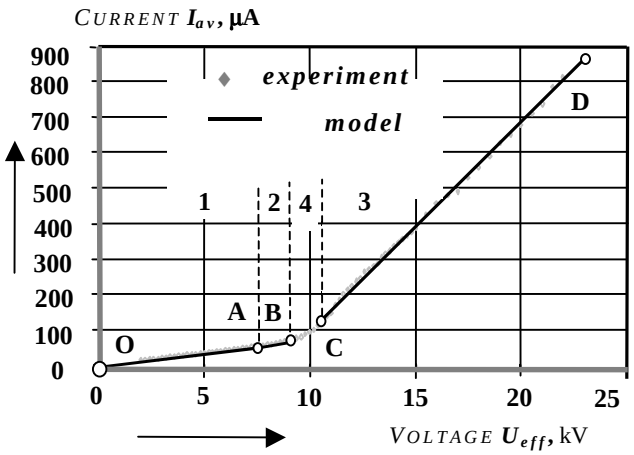

Fig. 1. Operating sectors on the external characteristic of one-atmosphere barrier discharge, namely the relationship between the average value of current I_{gap} and the effective value of applied voltage U_{gap}.

OA - non-operating sector; **AB** – first stage of burning – a cold technological plasma containing ozone and products of its decomposition; **CD** - second stage of burning – a cold technological plasma containing nitrogen oxides; **BC** – transient area.

A power law, for which $U_{gap} < U_{bd}$ is set equal to zero, does not adequately simulate the behaviour of the one-atmosphere barrier discharge. The power law relates to the whole region of burning of barrier discharge, i. e. for $U_{gap} \geq U_{bd}$.

Furthermore, the authors also assume that the voltage of burning U_b of barrier discharge remains constant, irrespective of the value of voltage U_{gap} applied across discharge gap, and for this reason they also speak for one-atmosphere *glow* discharge plasma (*OAGDP*).

In the present work it is made an attempt to transfer the new relationship found between the instantaneous values of current and voltage onto the simulation of the experimentally obtained external characteristic or between the average value of current I_{gap} and the effective value of voltage U_{gap}. This is a possibility of obtaining a unitary controlling model for the whole region of burning of barrier discharge.

The generalized model of burning of one-atmosphere barrier discharge is created under the following conditions:

❑ the barrier discharge, similarly to the normal glow discharge in vacuum, burns at a constant value of the voltage of burning, i. e. $U_b = const$;

❑ the ignition of barrier discharge represents a threshold process occurring for certain critical parameters – the voltage of ignition U_{bd} (*max*) and current of ignition I_{bd} (*AV*), this determining the necessity that the description of discharge in the stage of burning is governed by eq. 2;

❑ the barrier discharge may be described in the whole region of burning or individually in each of the two subregions of burning;

❑ the generalized equation of barrier discharge burning, governed by the power law, is of the following form:

$$\frac{I_{gap} - I_{bd}}{\left(U_{gap} - \frac{U_{bd}}{\sqrt{2}}\right)^n} = B \qquad (3)$$

where I_{gap} (*AV*) is the current through the barrier discharge; U_{gap} (*RMS*) – the voltage across discharge gap; I_{bd} (*av*) and U_{bd} (*max*) – the critical ignition parameters of discharge; $n \geq 1$ – the exponent; B – a constant determining the increase of discharge current.

❑ the generalized equation includes in itself the linear law of variation as a particular case at $n = 1$:

$$\frac{I_{gap} - I_{bd}}{\left(U_{gap} - \frac{U_{bd}}{\sqrt{2}}\right)} = B = tg\alpha \text{ , or} \qquad (4)$$

$$I_{gap} = B\,U_{gap} + A \text{ , at} \qquad (5)$$

$$A = I_{bd} - B\,\frac{U_{bd}}{\sqrt{2}}. \qquad (6)$$

II. RESULTS AND DISCUSSION

A. General presentation of the regions of burning

The experimental investigations are conducted with a barrier representing a plate of thickness $\delta = 3$ mm, made of alkaline silicate glass of dielectric permittivity $\varepsilon = 10$, volumetric specific resistance $\rho = 10^9$ Ωm and $tg\delta = 25$ (at 20 ^{0}C).

External characteristics of the type $I_{gap}\,(AV) = \varphi\,[\,U_{gap}\,(RMS)\,]$ are obtained experimentally for two types of plasma generator systems:

♦ *the first one* having a virtually uniform electric field of a one-atmosphere uniform barrier discharge – the so-called *OAUBDG*-system; and

♦ *the second one* having a non-uniform electric field of a one-atmosphere non-uniform barrier discharge – the so-called *OANUBDG*-system.

The *OAUBDG*-system creates a plasma volume between the glass barrier and one of the two planar metal electrodes of area $S = 651.5\ cm^2$ and shape reducing the edge effect, the thickness of the plasma region being $H = 6\ mm$. The barrier capacitance is $C_\delta = 1192\ pF$, measured at industrial frequency.

The *OANUBDG*-system creates a plasma surface on one of the two flat metal electrodes of area $S = 480\ cm^2$ that embrace tightly the glass barrier. The discharge burns on the side to the electrode made in the form of a comb with width of *4 mm* of its constituent elementary electrodes and a distance of *4 mm* between each two of them. The discharge burns on the dielectric barrier itself – between the elementary electrodes. The barrier capacitance is $C_\delta = 536\ pF$ measured at industrial frequency.

The experimentally obtained external characteristics (for both plasma systems) permit applying both approaches to modeling in no-load regime.

The linear model for the ozone-oxygen region of burning the barrier discharge has the following parameters in accordance with eq. 5, Table 1.

TABLE 1.

SYSTEM	**B**, μA/kV	**A**, μA	U_{bd}, kV	I_{bd}, μA	*Correlation Coefficient* r_{lc}, /
OAUBDG	19.58	- 0.55	7.700	151	0.999375
OAUNBDG	349.7	- 455	3.014	599	0.998380

The linear model for the second region (that of the nitrogen oxides) of discharge burning has the following parameters in accordance with eq. 5, Table 2.

TABLE 2.

SYSTEM	**B**, μA/kV	**A**, μA	U_{bd}, kV	I_{bd}, μA	*Correlation Coefficient* r_{lc}, /
OAUBDG	26.82	- 62.5	11.92	250	0.993858
OAUNBDG	399.0	- 1145	14.00	4441	0.998640

The model generalized according to the power law for the whole region of discharge burning has the following characteristical parameters in accordance with eq. 3, Table 3.

TABLE 3.

SYSTEM	U_{bd}, kV	I_{bd}, μA	INTEGER n, /	*Correlation Coefficient* r_{lc}, /
OAUBDG	7.700	151	1.5	0.99467
OAUNBDG	3.014	599	1.1	0.99934

In loading the *OAUBDG*-system almost the whole plasma volume is filled with the material to be treated; in this case this is a non-woven textile based on polyethylene terephthalate (PET) with area mass 500 g/m^2. For this type of textile load the external characteristic changes to a significant extent – the region of burning is a single one and corresponds to the first characteristic region of burning, Table 4.

TABLE 4.

SYSTEM - MODEL	**B**, μA/kV	**A**, μA	U_{bd}, kV	I_{bd}, μA	*Correlation Coefficient* r_{lc}, /
OAUBDG-Linear model	359.37	- 372	10.85	172	0.992730
SYSTEM - MODEL	**INTEGER** n, /		U_{bd}, kV	I_{bd}, μA	*Correlation Coefficient* r_{lc}, /
OAUBDG-Power law	1.47		10.85	172	0.999195

Analyzing the models obtained indicates that both approaches enable making a description of the process by regions of burning or for the whole region of burning at a relatively high value of the linear correlation factor. This makes possible the application of both approaches for the purposes of examining or controlling the technological process.

Describing fully the process of discharge burning by means of a single function is of great practical importance, as it allows investigating very easily the influence of various parameters of the plasma generator system upon exponent *n* as

well as upon two parameters critical for the ignition - I_{bd} and U_{bd} , Table 3.

Moreover, this characteristic may be made linear by taking the logarithm of both sides of eq. 3:

$$lg\left(I_{gap} - I_{bd}\right) = n\, lg\left(U_{gap} - \frac{U_{bd}}{\sqrt{2}}\right) + lg\ B\,. \qquad (6)$$

The linear model is suitable for making an individual description for each of the two characteristic regions of burning of the discharge. This is especially imperative in the case of realizing a technology in only one of the two technological regions of burning.

A. Using the power law model for describing the individual regions of burning of the discharge.

The values of the linear correlation factor are not always high, i. e. above 0.96, all over the investigated region, Fig. 2.

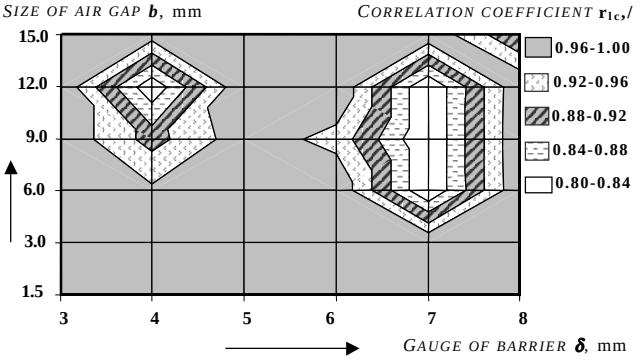

Fig. 2. There are regions in the space examined – thickness of the dielectric barrier δ and size of plasma volume *b*, of the first sub-region (or regime) of burning without load of the *OAUB*-discharge, in which linear correlation factor r_{lc} is of relatively low values, namely below 0.96.

This situation can be changed if using the generalized law for describing those individual regions of burning of the discharge, which are characterized by lower degree of linearity of the external characteristic.

As an example it is taken an *OAUBDG*-system with barrier thickness $\delta = 7$ *mm* and largest size of plasma volume $H = 9$ *mm*, operating in a regime under load: treating PET non-woven textile with area mass $500\ g/m^2$ and thickness *5 mm*. At $n = 1$ the linear correlation factor is relatively low, namely 0.9898, Table 6.

Verifying linear correlation factor r_{lc} for various values of exponent *n* indicates a new, higher value of $r_{lc} = 0.9960$ at $n = 1.66$, Table 6.

This is another possibility of describing more precisely the two technological sub-regions of burning of the one-atmosphere barrier discharge.

III. CONCLUSION

By using both methods investigated, it is possible to model successfully the experimentally obtained external characteristic of one-atmosphere barrier discharge with industrial frequency (*50* or *60* Hz) in the region of burning, either as a whole, or individually for each of its two parts.

TABLE 5.

SYSTEM - MODEL	**B**, μA/kV	**A**, μA	U_{bd}, kV	I_{bd}, μA	*Correlation Coefficient* r_{lc}, /
OAUBDG - Linear model	97.56	- 1079	12.56	146	0.9898
SYSTEM - MODEL	*Integer* n, /	**B**, μA/kV	U_{bd}, kV	I_{bd}, μA	*Correlation Coefficient* r_{lc}, /
OAUBDG - Power law	1.66	13.7	12.56	146	0.9960

The linear law that relates the average value of current I_{gap} through the discharge to the effective value of voltage U_{gap}, applied across discharge gap, is suitable for describing and controlling the burning of discharge in its two technological sub-regions, while the power law is more suitable for involving the whole region of burning of the barrier discharge.

However, the power law may be applied with the same success to certain cases, where a more precise description of behavior in the two sub-regions of burning is necessary.

In both cases, starting from the models of the external characteristic obtained as described and performing the necessary calculations, it is possible to determine the technological characteristic of the barrier discharge.

REFERENCES

[1] P. Dineff. Electrotechnology. Introduction to Electrotechnology. Technical University, Sofia, Bulgaria, **2000** (in Bulgarian).

[2] P. Dineff, D. Gospodinova. Energy-Effective Plasma-Chemical Surface Modification of Polymers and Polymeric Materials at Atmospheric Pressure. International Conference MEDPOWER'02, November 04-06, **2002**, Athens, Greece, Proceedings, pp. 1124-1128.

[3] P. Dineff, D. Gospodinova. Electric Characteristics of Barrier Discharge. XXXVI. International Scientific Conference on Information, Communication and Energy Systems and Technologies "ICEST '2003". Sofia, Bulgaria, October 16-18, **2003**. Proceedings, Heron Press. Ltd., pp.442-445.

[4] T. Vladkova, P. Dineff, D. Gospodinova. Wood Flour: A New Filler for Rubber Processing Industry. II. Cure Characteristics and Mechanical Properties of NBR Compounds Filled with Corona-Treated Wood Flour, J. Appl. Polym. Sci., **2003,** 91(2), p. 883-889.

[5] P. Dineff, R. Boshnakova**.** Production of Ozone-Air Gaze Mixture at Low Voltage Barrier Discharge. XI. Symposia with International Participation on Electrical Apparatus and Technologies "SIELA '95", Plovdiv, Bulgaria, June 01-02, **1995**. Proceedings, v.1, pp. 214-219 (in Bulgarian).

ACKNOWLEDGEMENT

This research was financially supported by Ministry of Education and Sciences (MON) - Project MU-TN-1201 / 02.

One Atmosphere Barrier Discharges With Electrode Edge Effect

Peter Dineff[1] and Dilyana Gospodinova[2]

Abstract - **A new development of the concept of using strongly non-uniform fields in the creation of technological plasma systems at atmospheric pressure is proposed.**

Experimental investigations showing the effectiveness of electrode systems, for which the length of the electrode corona-forming line is introduced as a parameter, are considered. In other words, the degree of influence exerted by the edge effect upon static characteristics of the discharge and electrical characteristics of the plasma system is taken into account.

Keywords - **Electrode edge effect, external characteristic, cold plasma reactor system, one atmosphere air barrier discharge, plasma surface modification.**

I. INTRODUCTION

Barrier discharges at atmospheric pressure (**760** ± 25 Torr, **1** atm) have serious technological advantages, which impose their application to the technology of textiles and textile fibers, electronics and microelectronics, printing industry [1, 4].

Characteristic to all types of barrier discharges is the presence of one or two dielectric barriers that separate the electrodes from the working medium. This remains a purely external trait of barrier discharges, as the dielectric barrier performs a very essential part in the occurrence and burning of the discharge, [1, 2]:

❏ the barrier with its capacitance C_δ plays the role of a reactance, i. e. of a capacitive, ballast reactance $X_C = \omega^{-1} C_\delta^{-1}$, that limits the increase in the electric current during discharge burning;

❏ the barrier re-distributes the electric field intensity in the inter-electrode space by electrically loading the working air gap and determining the critical parameters - ignition voltage U_{bd} and ignition current I_{bd} of the barrier discharge;

❏ the barrier defines the voltage of burning U_b of the discharge, which remains constant during its burning and does not depend on selected working voltage.

! The multiple ionization and chemical processes going simultaneously during barrier discharge burning at atmospheric pressure create considerable difficulties nor only in controlling the discharge, but also for the description of its behavior, [2].

The TASK of the present work consists in studying the behavior of low-frequency (50 Hz) air barrier discharge that burns without any load in the volume or on the surface of a cold-plasma generator system at atmospheric pressure - *one-atmosphere air barrier discharge* (*OAABD*).

The investigations are mainly focused on three types of cold plasma reactor systems:

❒ *the first one* representing two flat-parallel electrodes with a glass barrier between them, that creates a plasma volume with relatively uniform distribution of the electric field between the glass barrier and one of the electrodes, i. e. with suppressed electrode edge effect - *one-atmosphere uniform barrier discharge* (*OAUBD*);

❒ *the second one* representing a cold plasma reactor system, analogous to the *OAUBD*- reactor system, with a barrier and air gap placed in series between the two electrodes, but having a comb-shaped high-voltage electrode with strongly expressed electrode edge effect resulting from the increased length of the edge contour line - *one-atmosphere edge effect serial barrier discharge* (*OAEESBD*);

❒ *the third one* representing two flat-parallel electrodes that embrace tightly the glass barrier in such a way, that a plasma surface with the participation of the electrode edge effect is created only on that side of the barrier, which looks at the comb-shaped electrode, and the air gap turns out to be connected in parallel to the dielectric barrier - *one-atmosphere edge effect parallel barrier discharge* (*OAEEPBD*).

A comparative investigation is conducted by using the external static characteristic and the electric and technological characteristics of one atmosphere air barrier discharges, which result from the former one [3].

II. Experimental investigations

Experimental investigations [2, 3, 5], performed by us for a continuous period of time in connection with the manifestation of electrode edge effect in a cold plasma reactor system, allow to seek a new technical solution in using the electrode edge effect for creating an open (or single-side) cold plasma reactor system.

The *OAUBD*- plasma reactor system has electrodes, for which the electrode edge effect is neutralized by means of appropriately made chamfers along the external contour line of each electrode, i. e. by using the well-known *Rogovski's electrodes*.

In the other plasma reactor systems examined - *OAEESBD* and *OAEEPBD*– this effect is not compensated for. On the contrary, the edge effect is made stronger by introducing a comb-shaped high-voltage electrode consisting of alternating 4-millimeter-wide elementary electrodes separated from each other by an air gap of the same width, Fig. 1.

[1]Peter Dineff is with the Faculty of Electrical Engineering, Technical University of Sofia, Kliment Ohridski 8, 1000 Sofia, Bulgaria, E-mail: dineff_pd@abv.bg.

[2]Dilyana Gospodinova is with the Faculty of Electrical Engineering, Technical University of Sofia, Kliment Ohridski 8, 1000 Sofia, Bulgaria, E-mail: dilianang@abv.bg.

The *OAEESBD*- and *OAEEPBD*- plasma reactor systems differ from each other in the organization of the inter-electrode space – in the first case the barrier and plasma gap are placed in series between the electrodes, Fig. 1b, and in the second case – in parallel, Fig. 1c.

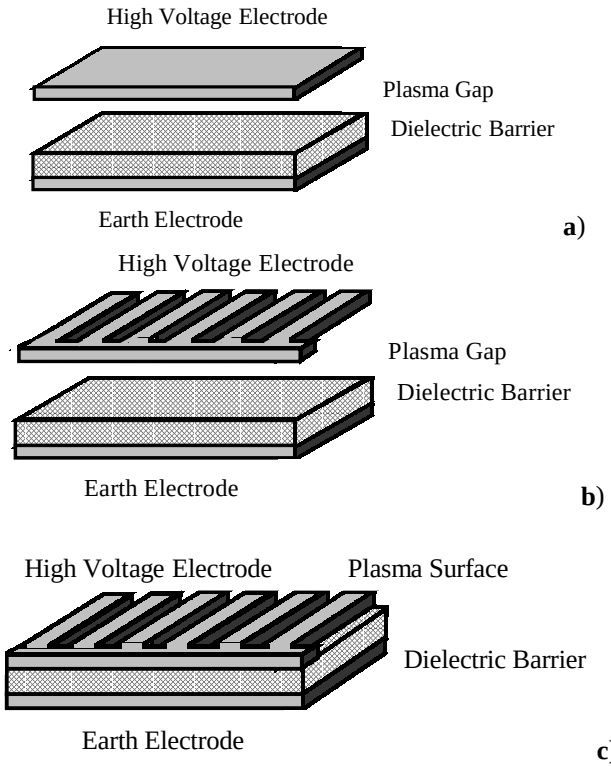

Fig. 1. Types of plasma reactor systems used in the experimental investigation: a - one atmosphere uniform barrier discharge (*OAUBD*); b - one atmosphere edge effect serial barrier discharge (*OAEESBD*); c - one atmosphere edge effect parallel barrier discharge (*OAEEPBD*).

The external or voltage-current characteristic of the barrier discharges is determined experimentally. It expresses the relationship between the average value of electric current I_{gap} (*AV*) flowing through the barrier discharge and the effective value of voltage U_{gap} (*RMS*) applied across the discharge gap - $I_{gap}\,(AV) = \varphi\,[\,U_{gap}\,(RMS)\,]$, Fig. 1.

The external characteristic is represented by a broken-line polygon of three linear sectors, each of them corresponding to one of the three development stages of the barrier discharge, Fig. 2 [2, 3]:

♦ the stage preceding the ignition of the barrier discharge, or the so-called free or non-operating regime;

♦ the first stage of burning, which corresponds to the formation of cold ozone- and oxygen-containing plasma;

♦ the second stage of burning, which corresponds to the formation of cold plasma containing mostly nitrogen oxides (NO_x).

For high values of linear correlation factor r_{pc} the linear law describes very well the individual sectors of the external characteristic of barrier discharge.

A generalized model of burning of the one atmosphere barrier discharge is created under the following conditions:

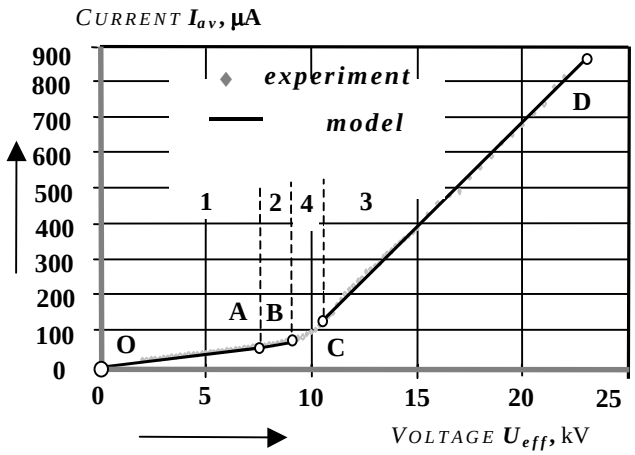

Fig. 2. Operating sectors of the external characteristic of one atmosphere barrier discharge, which represents the relationship between the average value of current I_{gap} and the effective value of applied voltage U_{gap}.

OA - non-operating sector; *AB* – first operating sector – cold technological plasma containing ozone and products of its decomposition; *CD* - second operating sector – cold technological plasma containing nitrogen oxides; *BC* – transient area.

❑ the barrier discharge, similarly to the normal glow discharge in vacuum, burns at a constant value of the voltage of burning, i. e. $U_b = const$;

❑ the barrier discharge ignition represents a threshold process that occurs at specific critical parameters - ignition voltage U_{bd} (*max*) and ignition current I_{bd} (*av*).

The external characteristic of one-atmosphere barrier discharges is used for determining the basic technological characteristic of discharges. As different plasma reactor systems are compared: on one hand *OAUBD* and *OAEESBD* creating plasma volumes, and on the other hand OAEEPBD that creates a plasma surface, the surface density of power p_S in W/m^2 is used as a basic technological characteristic for the purpose of comparison.

The experimental investigations are conducted with a barrier representing a plate of thickness δ = 3 mm, made of alkaline silicate glass and having dielectric permittivity ε = 10, volumetric specific electric resistance $\rho = 10^9$ Ωm and $tg\delta$ = 25 (at 20 ^{0}C).

II. RESULTS AND DISCUSSION

The basic parameters of first operating sector *AB* of the external characteristic are given in Table 1 for the three plasma reactor systems.

Table 1.

Plasma reactor system	Intercept A, μA	Slope B, μA/kV	Correlation coefficient r_C	C_{bar}, pF
OAUBD	- 716	119	0.97669	1922
OAEESBD	- 836	164 (38%)	0.99036	1922
OAEEPBD	- 455	350 (194%)	0.99838	536

The rate of relative increase of current *B* in μA/kV grows up considerably – with about 38 percent – as a result of increasing the electrode contour line or intensifying the edge effect, i. e. due

to the adoption of a comb-shaped electrode instead of the plane-shaped one, Figs. 1a and 1b.

The influence of the edge effect is more strongly expressed in the *OAEEPBD*- reactor system, where the rate increase observed is already 194 percent, Table 1.

The parameters of the second operating sector *CD* of the external characteristic of investigated plasma reactor systems are given in Table 2. The *OAEESBD*- plasma reactor system has no expressed second (*CD*) sector in the region of voltage investigation – up to 17 kV (*RMS*).

The rate of relative increase of the current in the second operating sector *CD* of the *OAEEPBD*- reactor system grows up with about 82 percent with respect to that of the basic *OAUBD*-reactor system.

Table 2.

Plasma reactor system	Intercept A, μA	Slope B, μA/kV	Correlation coefficient r_C
OAUBD	- 1580	219	0.99961
OAEESBD	-	-	-
OAEEPBD	- 1145	399 (82 %)	0.99864

The calculated values of the voltage of discharge burning for the first operating sector *AB* and the critical parameters of the first (*AB*) and second (*CD*) operating sectors of the external characteristic are shown in Table 3. Voltage of burning U_b of *OAB*- discharges decreases considerably with increasing the length of the electrode contour line and adopting the *OAEEPBD*- reactor system.

Table 3.

Plasma reactor system	U_b, kV	U_{bd} (1), kV	I_{bd} (1), μA	U_{bd} (2), kV	I_{bd} (2), μA
OAUBD	6.000	7.995	238	8.655	317
OAEESBD	5.088	5.700	101	-	-
OAEEPBD	1.302	3.014	599	14.002	4441

The calculated values of capacitance C_{pl} of the plasma region for the two operating regions of the external characteristic of the barrier discharges examined are given in Table 4.

Table 4.

Plasma reactor system	C_{pl} (*AB*), pF (mode of connection)	C_{pl} (*CD*), pF (mode of connection)
OAUBD	541 (serial)	1303 (serial)
OAEESBD	835 (serial)	-
OAEEPBD	705 (parallel)	879 (parallel)

For the established linear relationship between the average value of current I_{gap} (*AV*) and the effective value of applied voltage U_{gap} (*RMS*) capacitance C_{pl} of the plasma region may be calculated by first determining the total capacitance C_Σ, and then for a known, i. e. measured (at 50 Hz) capacitance C_{bar} of the glass barrier the capacitance C_{pl} of the plasma region is determined depending on the manner of connecting the barrier and plasma region, C_{bar} and C_{pl}: in series (eq. 2) or in parallel (eq. 3):

$$C_\Sigma = \frac{1}{2\sqrt{2}} \frac{\pi}{\omega} \frac{I_{gap}}{U_{gap}}, \ \omega = 2\pi f = 314\,(50\ Hz); \qquad (1)$$

$$C_{pl} = \frac{C_\Sigma C_{bar}}{C_{bar} - C_\Sigma}; \text{ or} \qquad (2)$$

$$C_{pl} = C_\Sigma - C_{bar} \qquad (3)$$

The basic technological characteristic of the discharge – the relationship between surface density of active power p_S and applied voltage U_{gap} – is obtained on the basis of the experimentally determined external characteristic.

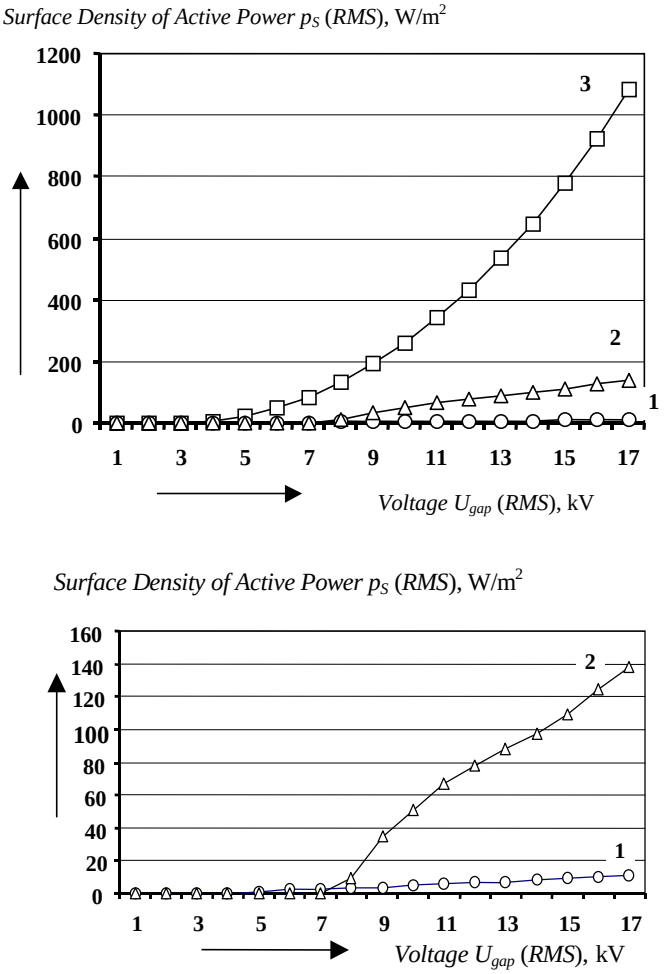

Fig. 3. Variation of surface density of active power p_S with applied voltage U_{gap}: **1** - *OAUBD*-reactor system; **2** -*OAEESBD*-reactor system; **3** - *OAEEPBD*-reactor system.

The surface density of active power p_S of the *OAEEPBD*-reactor system is conditionally determined for the geometrical area, on which the plasma layer is conditionally distributed. This means that the plasma active area includes also the areas between the elementary electrodes of the system. It is this approach only that allows making comparison between electrode systems with uniform and strongly non-uniform electric fields.

In such a way it is possible to compare different plasma generator systems, i. e. to compare plasma systems creating plasma volumes like the *OAUBD*- or *OAEESBD*- systems with plasma systems creating plasma surfaces like the *OAEEPBD*- system.

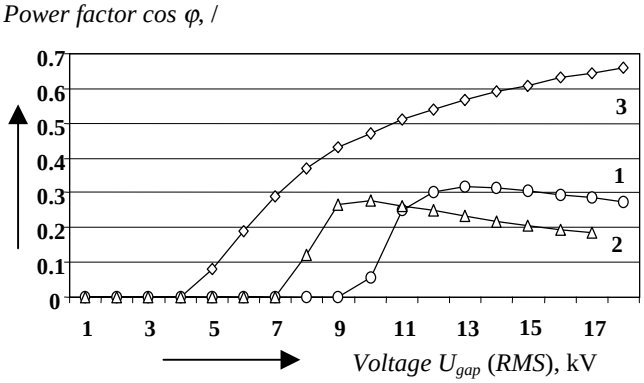

Fig. 4. Variation of power factor cos φ with the voltage applied across the discharge gap in different plasma generator systems: **1** - *OAUBD*; **2** - *OAEESBD*; **3** - *OAEEPBD*.

An even simplified analysis of technological characteristics clearly indicates that increasing the non-uniformity of the electric field in the discharge gap through the participation of an edge effect, i. e. through the increase of the high-voltage electrode perimeter – in the case of a comb-shaped electrode, Fig. 1, combined with adopting a parallel configuration of the dielectric barrier and plasma volume instead of the series scheme of placement of the dielectric barrier and plasma volume, provides the greatest possibilities for improving the external characteristic of the barrier discharge and the technological characteristic of the plasma generator system, Fig. 3.

The two plasma generator systems *OAUBD* and *OAEEPBD* are virtually incomparable: the value of surface density of active power p_S, which is acquired by *OAEEPBD* at voltage within $5 \div 6$ kV, is attained by *OAUBD* only at 17 kV (*RMS*), Fig. 3.

Increasing surface density p_S more than ten times, Fig. 3, may provide a much more intensive and energy-effective technological process of surface plasma-chemical modification of low-energy materials. In this case, the surface active power density represents a quantitative measure for the topological (etching) and chemical (activation, netting, polymerization) modifications of the surface of polymeric materials.

The energy-related effectiveness of plasma-chemical processes is different for the individual plasma generator systems, Fig. 4.

It is known that the power factor cos φ represents a measure for the effectiveness of the process of transforming the electric energy into another type of energy – in this case into the energy of chemical and physical modifications of the surface. The *OAEEPBD* technological plasma system ensures values of power factor, e. g. 0.65, which remain unattainable for the classical corona and barrier discharge plasma systems. Moreover, the energy-related effectiveness of technological regimes at relatively low voltages is strongly increased.

III. CONCLUSION

The experimentally plotted external characteristic of one atmosphere barrier discharge with industrial frequency (50 or 60 Hz) in the region of burning may be successfully used in the analysis of plasma generator systems, which are very different externally, even in the case when one system creates a plasma volume, and the other a plasma surface.

Increasing the degree of non-uniformity of the electrical field by changing the perimeter of the high-voltage electrode, i. e. by intensifying the impact of the edge effect, along with adopting a parallel circuit of connecting the dielectric barrier with the air gap, turns out to be an efficient way for magnifying the technological potentials and the energy-related effectiveness of plasma generator systems.

Using the *OAEEPBD*- plasma reactor system in the practice of plasma and plasma-assisted chemical surface modification of materials reveals a new opportunity for creating technologically effective plasma systems.

This type of reactors enables even more effective application not only at increased and high frequencies, but also at *RF*-frequencies.

REFERENCES

[1] P. Dineff. Electrotechnology. Introduction to Electrotechnology. Technical University, Sofia, Bulgaria, **2000** (in Bulgarian).

[2] P. Dineff, D. Gospodinova. Energy-effective plasma-chemical surface modification of polymers and polymeric materials at atmospheric pressure. International conference MEDPOWER'02, November 04-06, **2002**, Athena, Greece, Proceedings, pp. 1124-1128.

[3] P. Dineff, D. Gospodinova. Electric Characteristics of Barrier Discharge. XXXVI. International Scientific Conference on Information, Communication and Energy Systems and Technologies "ICEST '2003". Sofia, Bulgaria, October 16-18, **2003**. Proceedings, Heron Press. Ltd., pp.442-445.

[4] T. Vladkova, P. Dineff, D. Gospodinova. Wood Flour: A New Filler for Rubber Processing Industry. II. Cure Characteristics and Mechanical Properties of NBR Compounds Filled with Corona-Treated Wood Flour, J. Appl. Polym. Sci., **2003,** 91(2), p. 883-889.

ACKNOWLEDGEMENT

This research was financially supported by Ministry of Education and Sciences (MON) - Project MU-TN-1201 / 02.

Switched Mode Power Supply

Veselka M. Ivancheva[1], Dimitar K. Kraichev[2]

Abstract: In the paper is discussing switched mode power supply pulse-width-modulation (PWM) for PC, ensuring high security on exit voltage and protection of power supply in failure.

Keywords- switched mode power supply.

I.INTRODUCTION

Power supply source is the 'hearth' in the electronic apparatuses. For a long time in the field of sources had been used linear power supplies, but nowadays in practice are using power supply, working in switched regime or the so-called switched mode power supply.

In using of high fundamental frequency of switching the sizes of transformer or filtering elements decrease too much. That give us a chance to make many compact and light powers supply, which is one of the main requirement in most of the devices.

The main priority of switched mode power supply are the receiving for bigger capacity under the burden in smaller sizes and bigger coefficient of performance. The failings are the radiating of bigger radio frequency interference and more difficult projecting which needs more time.

The aim of this paper is to offer switched mode power supply pulse-width-modulation for PC, providing high quality of the outer voltages and protection for the power supplies in failure.

For this aim it must ensure following output constant voltages:

+3.3V in maximal current 18A and minimal current 1A;
+5V in maximal current 23Aand minimal current 1A;
+12V in maximal current 11A and minimal current 1A;
-5V 0.4A in maximal current and minimal current 0.1A;
-12V in maximal current 1A and minimal current 0.1A.
Pulsation of voltage ripple 50mV.
Instability of the output voltage ±2%.

The stabilizer will be supplied with variable voltage with value 220V and frequency-50/60Hz.

[1]Veselka M. Ivancheva is with the Technical University of Sofia/ Faculty of Engineering and Pedagogy in Sliven, Sliven 8800, 59, Bourgasko Shaussee Blvd, E-mail: vivancheva@yahoo.com
[2]Dimitar K. Kraichev, is with the Technical University of Sofia/ Faculty of Engineering and Pedagogy in Sliven, Sliven 8800, 59, Bourgasko Shaussee Blvd, E-mail: idj@mail.bg

II. SCHEME OF THE SWITCHED MODE POWER SUPPLY

Block diagram of the switched mode power supply is shown on figure 1.

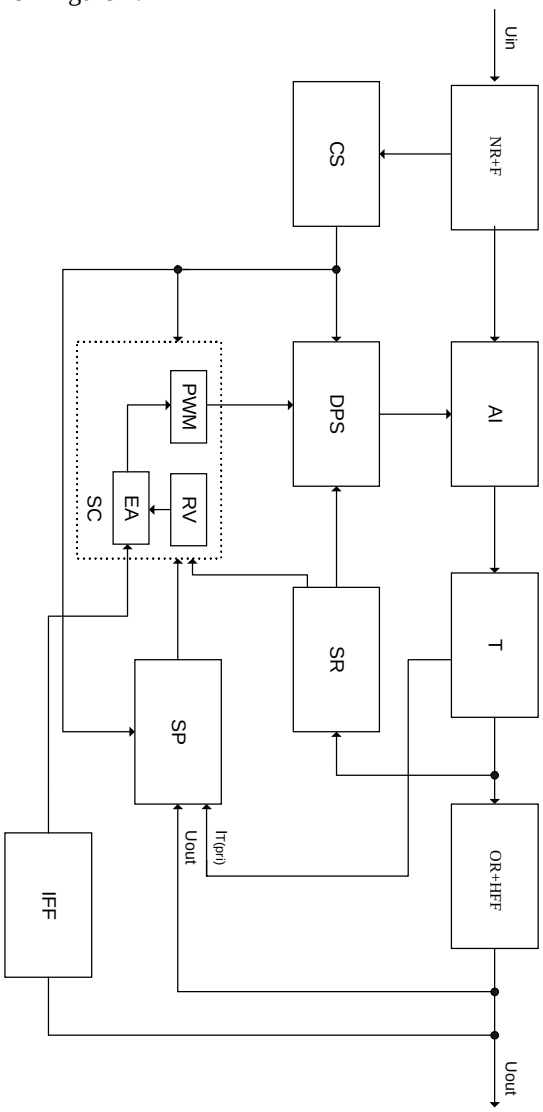

Fig.1. Block diagram

The symbols have the following meaning:
NR+F –network rectifier and filter;
AI –adjustable inverter;
T – transformer;
OR+HFF – output rectifier and high-frequency filter;
CS – circuit starting ;
DPS – driver of power switch;
SR – secondary rectifier;
SC – scheme for control;

SP – scheme for protection;
IFF – inverse feedback factor;
PWM-pulse-width-modulation;
RV-reference voltage;
EA-error amplifiers ;

Circuit diagram is shown on figure 2.

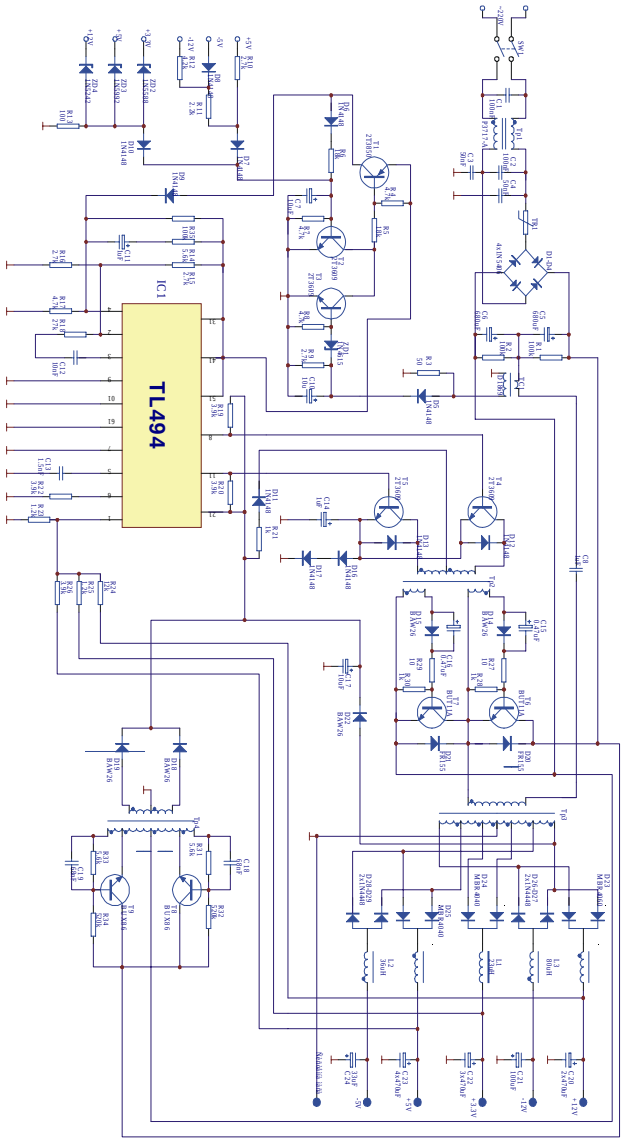

Fig.2. Circuit diagram

The hearth of the stabilizer is high-frequency control inverter. With the inventor output voltage is transforming in voltage with high frequency /20-200KHz for existing supplies/. After that is completing rectification and ripple smoothing, to be produced constantly voltage..

As scheme for controlling is using integrated circuit(IC) TL494.It is intended for designing switched mode power supply pulse-width-modulation (PWM) controlled with voltage. It contains: error amplifiers, inner adjustable oscillator, dead-time control comparator, control trigger , source of reference voltage and output-control circuit.

Output transistor's stages may work in common emitter scheme or as emitter follower. Output transistor's stage may work in single-ended or push-pull regime. The regime of work is chosen by detached pin. The inner scheme controls each of pins in process of working in push-pull regime. It don't permits supplying double impulses.

The transformer has two purposes–to ensure galvanic division in the entry and exit and to decrease the input pulse-width-modulation voltage.

Magnetic core is E35/18/10 type of 3C90 material made by Ferroxcube with 37 turns of primary winding and 2, 3,7 turns corresponding for 3,3; 5; 12 V.

The final stage includes the elements which ensure rectification and filtration of voltage.

The voltage in exit of the scheme for controlling intensifies its capacity by driver stage and in appropriate linkwork supply in base of power transistor.

The function of the linkwork for negative feed-back for voltage is to support constant value of output voltage. Its main part is Operational amplifier with big coefficient of amplification, called error amplifiers.

As a trigger circuit we use Self Oscillating transistor inverter in scheme with central tap.

The scheme for protection has the aim to provide protection of regulator in fault of load, or to safe the load, if the regulator damaged . Of the scheme depends regulator reliability.

Anti suction filter on input and inner rectifier consist of 3 to 5 blocks – anti suction filter against electromagnetic interference, eventually circuit starting with current limitation, scheme for suppressing of voltage overshoots, rectifier and input filtering capacitor.

III.CONCLUSION

In the paper is discussing switched mode power supply pulse-width-modulation (PWM) for PC, ensuring high security on exit voltage and protection of power supply in failure.

REFERENCES

1. Наръчник по токозахранващи устройства- ст.н.с. д-р.инж.Стефанов Николай.Йорданов, ст.н.с. д-р.инж. Атанасов Теодор Бойчев, инж. Маноилов, Атанас Георгиев. "Техника"-София.
2. Токозахранващи устройства - Браун Марти. "Техника" София 1997 г.
3. Справочник на радиолюбителя – Рачев Димитър.А. "Техника" София 1990г.
4. Интернет адреси: www.Philips.com; www.Ferroxcube.com; www.Rlocman.ru; www.Chipinfo.ru; www.Sbplan.narod.ru; www.Diode.com; www.Coilcraft.com;

A Unified Analysis and Characteristics of a DC-DC Converter Operating above or below the Resonance

Evgeniy I. Popov[1] and Michail H. Antchev[2]

Abstract - **A DC-DC converter with a serial resonant inverter is analyzed. The uniform expressions of the main parameters are given. The generalized transcendent equation for the devices conduction angles is numerically solved. The controlling characteristics are found. Computer simulations and experiments confirm the results. The study shows the advantages of the mode above the resonance frequency.**

Keywords - **Unified analysis, DC-DC converter, Resonant inverter, Conduction angles, Controlling characteristics.**

I. INTRODUCTION

The application of resonant power conversion implemented with a serial transistor inverter improves the efficiency of the DC-DC converters due to the zero current switching (ZCS) or/and zero voltage switching (ZVS) [1], [2], [3], [4], [5], [6]. Such a converter is analyzed separately in [1], [2] when operating at a frequency higher than the resonance one and in [4], [5] when operating at a frequency lower than the resonance one. But the converter controlling characteristics are not given in these publications because the transistor and diode conduction time intervals (and angles) are not determined for different values of the controlling frequency and the output voltage.

This paper is aimed at carrying out a unified analysis of a DC-DC converter implemented with a serial resonant transistor inverter operating at a frequency higher or lower than the resonance one. It is also aimed at obtaining the controlling characteristics related to the parameters of electrical energy conversion and component stress that will allow an adequate design of the power circuit.

II. ANALYSIS MAIN ASSUMPTIONS

A half-bridge (Fig.1) or a full-bridge converter are considered. The resonance frequency is $\omega_0 = 1/\sqrt{LC}$ and the characteristic impedance is $Z_0 = \sqrt{L/C}$. The circuit is analyzed in a normalized form: all voltages are divided by $V_d/2$ or by V_d for the half- or full-bridge configurations respectively (V_d is the supplying voltage); all currents are divided by $V_d/(2Z_0)$ or by V_d/Z_0 for the half- or full-bridge connections respectively.

[1]Evgeniy I. Popov is with the Faculty of Electronic Technique and Technologies, Technical University, Sofia – 1000, Bul. Kl. Ohridski 8, Bulgaria, email: epopov@tu-sofia.bg.

[2]Michail H. Antchev is with the Faculty of Electronic Technique and Technologies, Technical University, Sofia – 1000, Bul. Kl. Ohridski 8, Bulgaria, email: antchev@tu-sofia.bg.

At obtaining the controlling characteristics the independent variables are the normalized controlling frequency ω/ω_0 and the normalized output voltage $q = V_0/(V_d/2)$ or $q = V_0/V_d$ for the half- or full-bridge circuits respectively where $\omega=2\pi f$ is the controlling frequency and V_0 is the output voltage. The efficiency of the power circuit is considered close to unity. If $\alpha=\omega_0 t_D$ is the diode conduction angle and $\beta=\omega_0 t_Q$ is the transistor conduction angle then $\chi=\alpha+\beta=\pi\omega_0/\omega$.

For continious inverter current mode and $\omega>\omega_0$ we put $x=\beta$, $y=\alpha$, $x_{min}=0$, and the following constants are introduced $c=1$, $k=0$. When $\omega<\omega_0$ we put $y=\beta$, $x=\alpha$, $x_{max}=\pi$ and the constants are $c=-1$, $k=1$. In discontinuous inverter current mode ($\omega<0.5\omega_0$) $\alpha=\beta=\pi$, $\chi>2\pi$.

The main relations describing the converter operation at a frequency higher [1] or lower [4] than the resonance one taken into account in the paper are symmetrical in fact.

III. DETERMINATION OF TRANSISTOR AND DIODE CONDUCTION ANGLES

The conduction angles for continuous inverter current mode are determined according to the procedure described below (for discontinuous inverter current mode they are given above). The conduction angle x that has to fulfil the inequalities

$$cx < \cos^{-1}(-cq) \tag{1}$$

$$x > x_{min} \quad \text{for } \omega>\omega_0 \tag{2}$$

$$x < x_{max} \quad \text{for } \omega<\omega_0 \tag{3}$$

is found after solving the following transcendent equation when ω/ω_0 and q are known

$$x + k\pi + \tan^{-1}\frac{c(1-q^2)\sin x}{2q + c(1+q^2)\cos x} = \pi\frac{\omega_0}{\omega} = \chi \tag{4}$$

Then the other conduction angle y is

$$y = \chi - x \tag{5}$$

IV. INVERTER PARAMETERS

The main parameters of the inverter circuit can be expressed in a generalized and normalized form as follows:

The peak capacitor voltage is

$$V_{CPEAK} = \frac{(1-cq)(1-\cos x)}{q + c\cos x} \tag{6}$$

The peak output current (at primary of transformer) is

$$I_{PEAK} = \frac{1 - cq^2 - k2q\cos x}{q + c\cos x} \tag{7}$$

The average supplying current is

$$I_d = \frac{2q(1-cq)(1-\cos x)}{\chi(q+c\cos x)} \quad (8)$$

(in the half-bridge circuit this value has to be divided by 2).

The average output current (at primary of transformer) is

$$I_{AVG} = \frac{2(1-cq)(1-\cos x)}{\chi(q+c\cos x)} \quad (9)$$

The RMS output current (at primary of transformer) is

$$I_{RMS} = \{\frac{1}{\chi}[I_0^2(\frac{y}{2}+\frac{\sin 2y}{4}) + (1+cq+V_{C0})^2(\frac{y}{2}-\frac{\sin 2y}{4}) - cI_0(1+cq+V_{C0})\sin^2 y + (1-cq+V_{C1})^2(\frac{x}{2}-\frac{\sin 2x}{4})]\}^{\frac{1}{2}} \quad (10)$$

where I_0 is the initial output current (in the beginning of conduction of diodes at $\omega>\omega_0$ or transistors at $\omega<\omega_0$)

$$I_0 = \frac{(1-q^2)\sin x}{q+c\cos x} \quad (11)$$

The quantity V_{C0} is the initial capacitor voltage (in the beginning of conduction of diodes at $\omega>\omega_0$ or transistors at $\omega<\omega_0$)

$$V_{C0} = \frac{q(1-cq)(1-\cos x)}{q+c\cos x} \quad (12)$$

The quantity V_{C1} is the capacitor voltage in the beginning of conduction of transistors at $\omega>\omega_0$ or diodes at $\omega<\omega_0$

$$V_{C1} = \frac{c(1-cq)(1-\cos x)}{q+c\cos x} \quad (13)$$

The values determining the average transistor and diode currents can be calculated from

$$I_1 = \frac{(1-q^2)(1-\cos x)}{2\chi(q+c\cos x)} \quad (14)$$

$$I_2 = \frac{(1-cq)^2(1-\cos x)}{2\chi(q+c\cos x)} \quad (15)$$

When the converter operates at a controlling frequency higher than the resonance one ($\omega>\omega_0$) the average transistor current is $I_{QAVG} = I_1$ and the average diode current is $I_{DAVG} = I_2$. When the converter operates at a controlling frequency lower than the resonance one ($\omega<\omega_0$) the average transistor and diode currents are $I_{QAVG} = I_2$, $I_{DAVG} = I_1$.

V. Inverter characteristics

The independent variables namely the normalized controlling frequency ω/ω_0 and the normalized output voltage are varied (for instance ω/ω_0 *=0.1-1.9* with a step of *0.1* and *q=0.1-0.9* with a step of *0.2*). In the continuous inverter current mode the transcendent equation (4) is numerically solved by a computer program when the restrictions expressed by (1), (2), (3) are obeyed and the conduction angles *x*, and *y* (5) are determined. Then the main parameters of the inverter circuit expressed by (6), (7), (8), (9), (10), (14), (15) applying also (11), (12), (13) are calculated. The main converter characteristics after the calculation are graphically displayed in Fig. 2 – Fig. 10. These characteristics show the diode and transistor conduction angles, the peak capacitor voltage, the peak output current, the average supplying current, the average output current, the RMS output current, the average transistor and diode currents as functions from the independent variables ω/ω_0 and *q* respectively. They are applied for assessment of the appropriate mode of operation and adequate design of the converter elements. Of course the controlling characteristics can be very easily obtained for different values of ω/ω_0 and *q*. Discontinuity of the graphics is observed around the resonance frequency. There the operation is not recommended due to the larger stresses of the converter elements.

VI. Computer simulation

PSPICE computer simulations of the half-bridge converter are carried out with the following data V_0*=60 V*, V_d*=305 V*, *L=205 μH, C=33 nF, q=0.3934* in three cases: 1) ω/ω_0 *=1,362* (period $T=2\pi/\omega=12$ μS); 2) ω/ω_0 *=0,6537* ($T=2\pi/\omega=25$ μS); 3) ω/ω_0 *=0,3632* ($T=2\pi/\omega=45$ μS). The main results from the proposed method of calculation and from the PSPICE simulations in a power circuit with ideal switching devices are summarized in Table 1. The graphical results from the PSPICE simulations with real device models (power transistors IRF450) are shown in Fig. 11, Fig. 12 and Fig. 13 for cases 1, 2 and 3 respectively. The results from the proposed method of calculation and from the PSPICE simulations are in good agreement that confirms the correctness of the unified analysis and the characteristics. Fig. 12 and Fig. 13 also show the spikes of the currents through the semiconductor devices due to the simultaneous conduction of a diode and a transistor from opposite shoulders of the circuit and due to the discharge of the snubber capacitor right away after the transistor turns on. These effects are avoided when the converter operates at a controlling frequency higher than the resonance one.

VII. Experimental study

A number of experiments of the half-bridge circuit having the same data as stated above are carried out. The experimental results are close to these given in Table. 1. For instance Fig. 14 shows the waveforms of the transistor drain-source voltage and the output current at case 1 of the computer simulation. The measured values of the conduction angles of diodes and transistors, peak capacitor voltage, and peak output current are 44^O, 88^O, 188 V, 3.4 A respectively. They compare well to the calculated results from the proposed method and the PSPICE simulation.

VIII. Conclusions

A unified analysis of a DC-DC converter implemented with a half-bridge or a full-bridge serial resonant transistor inverter operating at a frequency higher or lower than the resonance one is carried out. Uniform mathematical expressions for the main

parameters of the power circuit are proposed. The conduction angles of diodes and transistors are determined by numerically solving a transcendent equation. The converter characteristics when the controlling frequency and the output voltage vary are calculated, and graphically displayed. They are applied for assessment of the appropriate mode of operation and adequate design of the converter elements. It can be concluded that the operation at a frequency higher than the resonance one should be preferred due to the smaller peak capacitor voltage and absence of current spikes through the semiconductor devices (smaller switching power losses at turn on). The converter is also studied by computer simulations and experimentally. There is a good agreement between the theoretical expressions and characteristics, the computer simulation and experimental results that shows the correctness of the proposed analysis.

REFERENCES

[1] M. H. Antchev, G. J. Maleev "Analysis of a transistor inverter operating at a frequency higher than the resonance one", Journal "Electrical Engineering and Electronics", vol. 5-6, 2000, pp. 12-17 (In Bulgarian).

[2] S. Valtchev, J. B. Klaasens "Efficient resonant power conversion", IEEE Transactions on Industrial Electronics, vol. 37, No. 6, December 1990, pp. 490-495.

[3] A. F. Witulski, R. W. Erickson "Design of the series resonant converter for minimum component stress", IEEE, Transactions on Aerospace and Electronic Systems, vol. AES-22, No. 4, July 1986, pp. 356-363.

[4] R. King, T. A. Stuart. "Modeling the full-bridge series-resonant power converter" IEEE, Transactions on Aerospace and Electronic Systems, vol. AES-18, No. 4, July 1982, pp. 449-459.

[5] R. King, T. A. Stuart. "Inherent overload protection for the series resonant converter", IEEE Transactions on Aerospace and Electronic Systems, vol. AES-19, No. 6, November 1983, pp. 820-829.

[6] M. Mohan, T. M. Undeland, W. P. Robbins. "Power electronics, converters, applications and design", 2nd ed., New York, Wiley, 1995.

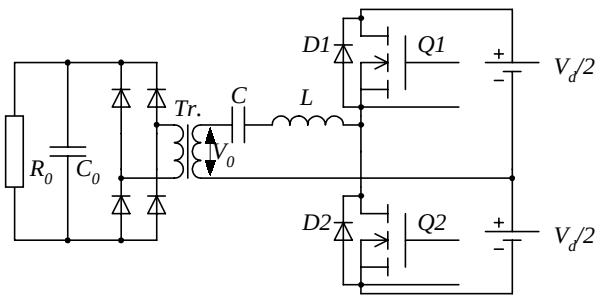

Fig. 1. Half-bridge resonant DC-DC converter.

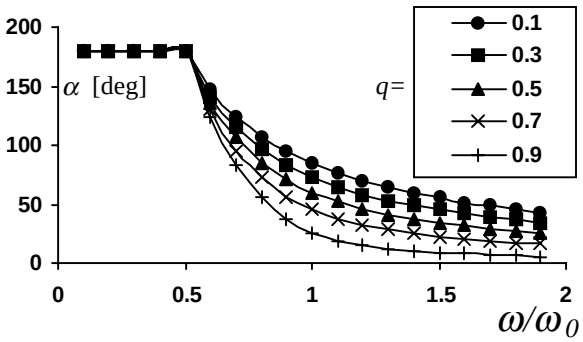

Fig. 2. Diode conduction angle.

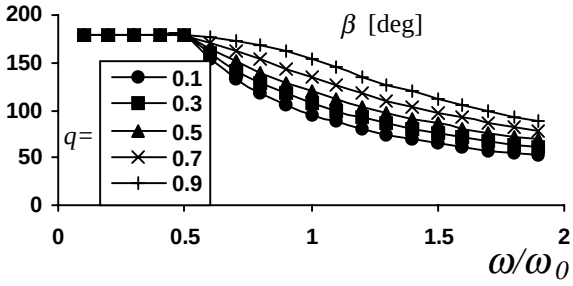

Fig. 3. Transistor conduction angle.

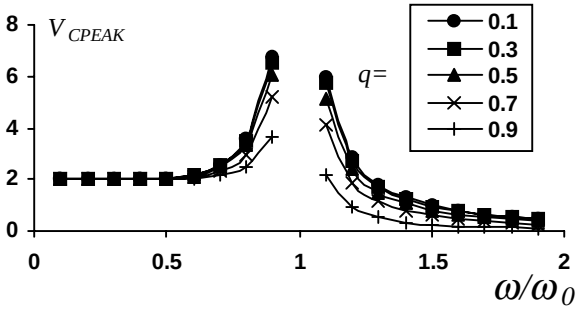

Fig. 4. Peak capacitor voltage.

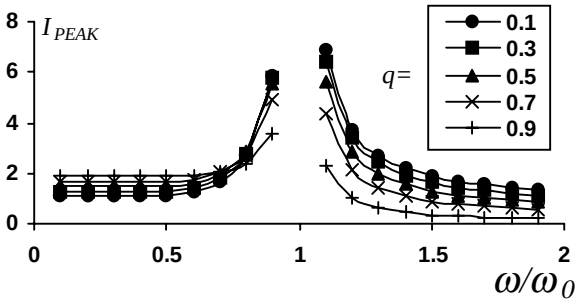

Fig. 5. Peak output current.

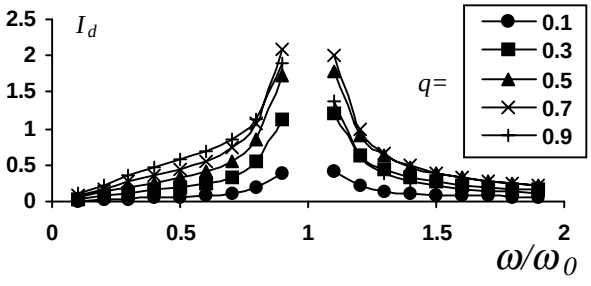

Fig. 6. Average supplying current.

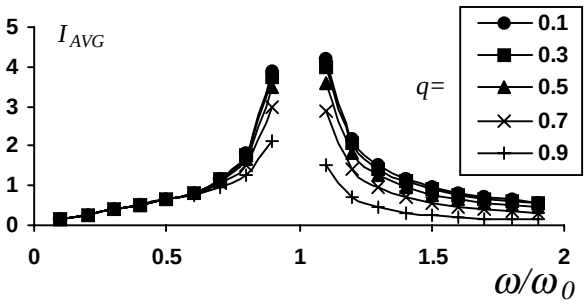

Fig. 7. Average output current.

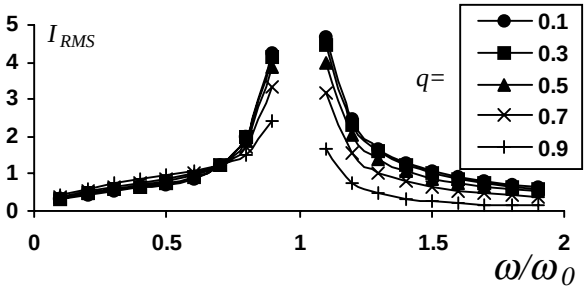

Fig. 8. RMS output current.

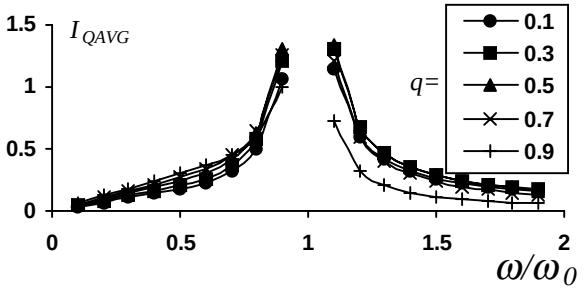

Fig. 9. Average transistor current.

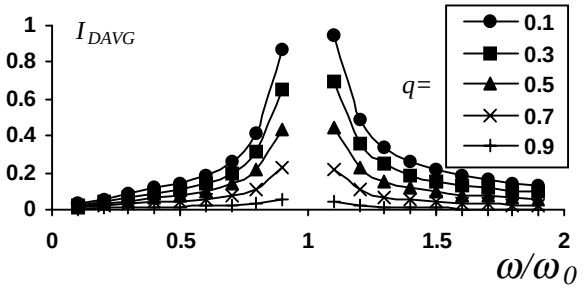

Fig. 10. Average diode current.

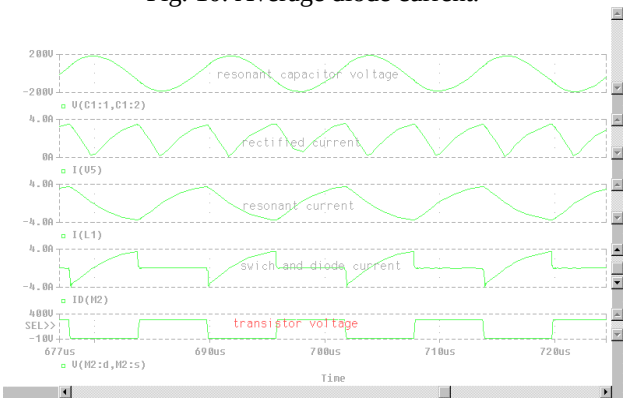

Fig. 11. Simulation results above the resonance.

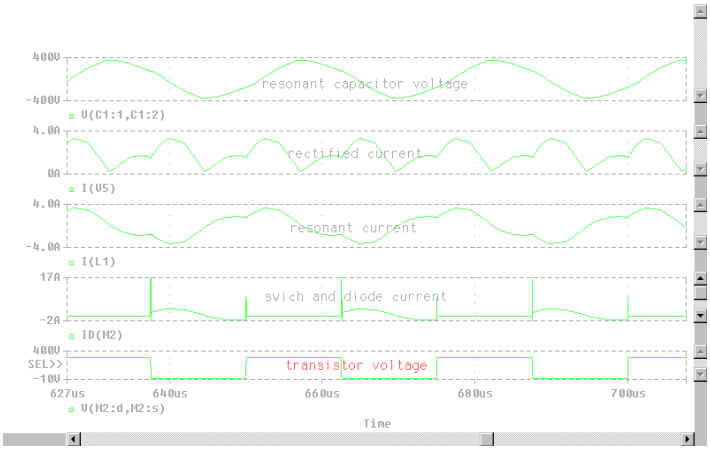

Fig. 12. PSPICE simulation results at a frequency lower than the resonance one and continuous output current.

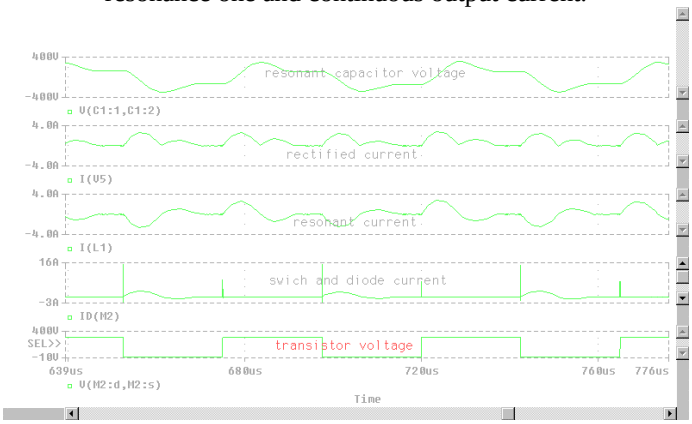

Fig. 13. PSPICE simulation results at a frequency lower than the resonance one and discontinuous output current.

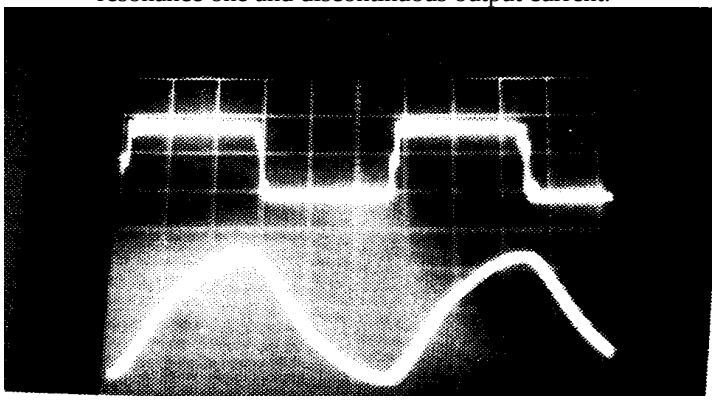

Fig. 14. Waveforms of the transistor drain-source voltage (150 V/div) and the output current (2 A/div). Time scale 2 μS/div.

TABLE 1. THEORETICAL AND SIMULATION RESULTS.

№	q	ω/ω_0	α	β	Method
	-	-	deg.	deg.	
1	0.3934	1.362	45 44.8	87.2 87.1	Proposed PSPICE
2	0.3934	0.6537	122 122	153 153	Proposed PSPICE
3	0.3934	0.3632	180 180	180 180	Proposed PSPICE

Effect of Extrusion Parameters on the Production and Characteristics of Reconstituted Tobacco

Venelina Popova[1], Ventzislav Nenov[2], Abdel Karim Omar[3]

Abstract – **The task of the current study is to analyze reconstituted tobacco sheet (RTS), made by the extrusion-and-rolling method. An all-factor experiment has been conducted to estimate the effect of extruder's mouth shape, level of compression, percentage of carboxyl methylcellulose (CMC) and propylene glycol (PG) on the production process. Best technological properties of the RTS are estimated with the following conditions: square shaped mouth, 1:1 compression, 6% CMC.**

Keywords **– reconstituted tobacco, extrusion, specific mechanic energy (SME)**

I. INTRODUCTION

The goals achieved through the usage of reconstituted tobacco sheet (RTS) have long ago exceeded the mere economical range of utilization of waste tobacco materials. It is estimated that during cigarette production about 8-12% of the basic tobacco blend turns into wastes, consisting mainly of tobacco dust, lamina particles and stems [1]. The approximate quantities of unused tobacco wastes in Bulgaria are said to be around 5000-6000 tons per year and despite ongoing improvement of technology this trend is expected to continue in the next years [11]. This situation turns out to be a significant ecological problem as well, with respect to finding way to dispose of wastes and needs special attention, as there is no operative technological solution for the moment.

Although there are certain scientific achievements in the utilization of tobacco waste materials – through extraction with different solvents, or isolation of specific constituents, these achievements have no significant application yet and the most suitable way of dealing with the problem remains the transformation of waste (or parts if it) into reconstituted (homogenized) tobacco and its consequent incorporation in the blends for tobacco products. Besides, with the use of RTS in the blends for cigarettes a number of technological problems are affected - those connected to improving the physical characteristics of the blend, controlling smoke output (tar and nicotine content), and maintaining the desired smoking and flavour properties of the product [2, 4, 5, 10].

There are various processes for the production of RTS, but most of them are modifications of the two basic methods – the paper method and the slurry (cast sheet) method [1, 2, 4]. The reconstituted tobacco achieved by the different ways of production vary in a wide range, as every process forms a product with specific structure properties, texture, physical and chemical characteristics [1, 2, 4, 5]. The final properties of the RTS depend to a great extent on the quantity and nature of the additives incorporated and on the treatment of the raw materials. A good process is considered to be that leading to a final product, which would go through all the stages and operations of cigarette production in a way, analogical to that of the genuine tobacco strips.

As advantages of the currently studied method for production of RTS through extrusion and rolling (stretching) could be considered the relatively low presence of non-tobacco additives (carboxyl methylcellulose and propylene glycol), as well as the compactness of the equipment, the little investments needed, etc.

The task of the current study is to determine the effect of some construction features of the extruder (mouth shape, level of compression) on the energy consumption and productivity of the process, as well as on certain technological and chemical characteristics of the final product – reconstituted tobacco sheet.

II. MATERIALS AND METHODS

The reconstituted tobacco sheet (RTS) studied in the current paper is made by the extrusion-and-rolling method, developed by a team of the University of Food Technologies – Plovdiv, Bulgaria [7]. The experimental equipment consists of a laboratory extruder Brabender 20 DN and a rolling (stretching) mechanism [7, 8]. As a raw material tobacco dust from the cigarette production of "Blagoevgrad BT" PLC is used, after sieving to obtain fraction with particle size below 400 μm. In the experimental blends are also included: carboxyl methylcellulose (CMC) as a binding agent, propylene glycol as a plasticizer and water [10]. The variants analyzed are designed up at the proportion tobacco dust: water ≈ 6, on the grounds that the above-mentioned proportion gives best hardiness and resistance of RTS [7].

The experiments are carried out under the following conditions: frequency of rotation of the active screw - 130min^{-1}; frequency of rotation of the feeding screw -80 min^{-1}; temperature throughout active screw's length – I zone – 30^0C, II zone – 50^0C, III zone –

[1]**Venelina Popova** is with the Technological Faculty, Department of Tobacco, Sugar and Essential Oils, University of Food Technologies, 26 Maritza blvd., 4002 Plovdiv, Bulgaria, E-mail: vpopova2000@yahoo.com

[2]**Ventzislav Nenov** is with the Technical Faculty, Department of Machines and Apparatuses for Food Industry, University of Food Technologies, 26 Maritza blvd., 4002 Plovdiv, Bulgaria, E-mail: vnenov2001@yahoo.co.uk

[3]**Abdel Karim Omar** is with the Technological Faculty, Department of Tobacco, Sugar and Essential Oils, University of Food Technologies, 26 Maritza blvd., 4002 Plovdiv, Bulgaria.

TABLE I
CHARACTERISTICS OF THE RECONSTITUTED TOBACCO SHEET

Sample variants				M_c, Nm	Q, kg/h	SME, Wh/kg	Nicotine, %	ρ_y, g/cm^3	Weight per area (air-dry matter), g/m^2	δ, mm
Mouth	Compression	CMC, %	PG, %							
Round	1:1	14	7	11,5	2,88	54,3	0.89	-	349	0.52
		14	3	13	2,52	77,6	0.86	-	353	0.53
		6	7	14	2,28	83,6	0.85	-	289	0.48
		6	3	16	2,4	90,7	1.08	-	392	0.50
	2:1	14	7	14,5	2,68	73,5	0.82	0.490	352	0.46
		14	3	15,3	1,95	107	0.79	0.490	346	0.44
		6	7	15,67	1,83	116	0.86	0.490	293	0.35
		6	3	16	1,44	151	1.09	0.498	382	0.45
Square	1:1	14	7	27,5	2,38	150,2	0.84	0.487	204	0.31
		14	3	30	2,4	162,5	0.89	0.462	233	0.33
		6	7	25	2,27	142,7	0.98	0.481	256	0.31
		6	3	27,5	2,25	158,6	1.05	0.475	198	0.32
	2:1	14	7	32,5	2,06	207,8	0.88	0.465	163	0.31
		14	3	38,5	2,3	221,2	0.86	0.451	236	0.34
		6	7	35	2,22	208,2	0.96	0.453	175	0.32
		6	3	33	2,55	171	1.06	0.484	212	0.37

80^0C; level of compression – 1:1 и 2:1; extruder' mouth shape – square with dimensions 20/1mm and round with diameter 5 mm. The diameter of the round mouth is chosen in compliance with the condition of equal cross section areas. The characteristics of the rolling mechanism are as follows: rollers' diameter – 100 mm; frequency of rotation of the rollers - 22÷100 min^{-1}; daylight between the rollers – 0.04÷0.08 mm.

There has been determined the following characteristics of the reconstituted tobacco sheet: nicotine content (%) – after the spectrophotometric method [9]; thickness (mm) – using a thickness-meter with extended area of the measuring pawls; density (relative) of cut tobacco shreds (g/cm^3)– by the press method with Borgwaldt density meter [9], after cutting with a laboratory cutter to shreds with δ=0.8-1.0 mm; weight per area (air-dried matter) (g/m^2)– by weighing 10 squares 20/20 mm and drying at 103±2°C. The values shown in tables I and IV are mean arithmetic values of different number of repetitions, as demanded by the corresponding method.

The specific mechanical energy (SME) is calculated according to the equation [3, 7]:

$$SME = \frac{M_c.\omega}{Q},\ Wh/kg \qquad (1)$$

where:

- M_c – resistance moment of the work screw in the process of extrusion, Nm;
- ω - frequency of rotation of the work screw rad/s. ω = (π.n_p)/30, where n_p – frequency of rotation of the work screw, min^{-1}.
- Q – mass productivity, kg/h.

The productivity (Q) is determined through measuring the weight of samples taken from the working extruder at a defined period of time. The time periods are read with mechanical chronometer "Slava" with precision 0.1 s, and the weight of the samples is measured with an electronic balance with precision 0.01 g.

III. RESULTS AND DISCUSSION

To evaluate the influence of the composition of the initial blend and the construction characteristics of the extruder on the production process and the parameters of the final product, the following experimental factors have been studied: degree of compression of the active screw; percentage of carboxyl methylcellulose (CMC); percentage of propylene glycol (PG) and shape of the extruder's mouth. The results obtained both for the process characteristics and the reconstituted sheet produced are presented in Table I.

The index SME expresses the mechanical energy spent for producing one unit of weight extruded matter. The low consumption of mechanic energy, when combined with good physical and chemical properties of the final product, proves to be an index for the economic efficiency of the process [7].

The data obtained show that maximum productivity, and respectively - minimum energy consumption, are observed with the variants of a round extruder's mouth, with 14 % CMC and 7 % PG. When considering the characteristics of the sheet produced, however, it should certainly be emphasized that with respect to the analyzed technological characteristics these samples are considerably inferior to that coming out from the square mouth. Furthermore, the reconstituted tobacco sheet from the variants with level of compression 1:1 and a round mouth turned out to be with highly deteriorated outlook and texture, and

TABLE III

MATRIX OF EXPERIMENT

№	Encoded values								Natural values		
	x_0	x_1	x_2	x_3	$x_1.x_2$	$x_1.x_3$	$x_2.x_3$	$x_1x_2x_3$	x_1, mm	x_2,%	x_3,%
1	+	-	-	-	+	+	+	-	1:1	6	3
2	+	+	-	-	-	-	+	+	2:1	6	3
3	+	-	+	-	-	+	-	+	1:1	14	3
4	+	+	+	-	+	-	-	-	2:1	14	3
5	+	-	-	+	+	-	-	+	1:1	6	7
6	+	+	-	+	-	+	-	-	2:1	6	7
7	+	-	+	+	-	-	+	-	1:1	14	7
8	+	+	+	+	+	+	+	+	2:1	14	7

hence we have been unable to cut them and evaluate their relative density. Data in Table I show that there are observed generally higher values for the indices thickness, weight per area and relative density of the RTS with the round mouth. The density of the analyzed RTS is greater as a whole, compared to that of reconstituted tobacco produced by using other methods: American by the paper method – 0.325 g/cm^3 [5]; AZ 8 – France (by the Schwietzer technology) – 0.225 g/cm^3; MCF – France (by the thick pulps' method) – 0.300 g/cm^3 [6]. The measured values for the thickness of the sheet coming out from the square mouth are slightly higher than the real situation, because there is a specific wrinkling of the sheet. From a technological point of view, such wrinkling is desired and sought for, because it results in an increase of the filling properties of the material when incorporated in the tobacco blends for cigarettes. The samples produced with the square mouth under both levels of compression show considerably lower values for the weight per area index compared to those coming out from the round mouth. With respect to nicotine content no significant differences attributed to the factors studied can be observed.

The above-stated considerations served as a basis to exclude the factor "mouth shape" from our further investigation and to carry out an all-factor experiment 2^3. The input factors: X_1 – level of compression at the active screw; X_2 – percentage of carboxyl methylcellulose; and X_3 – percentage of propylene glycol; as well as their maximum and minimum levels, and variation intervals, are presented in Table II.

TABLE II

INPUT FACTORS RANGE

Factor Level	Symbol	X_1	X_2	X_3
Basic level	x_{i0}	-	10	5
Interval of variation	Δx_i	-	4	2
Minimum level	$x_{i\,min}$	1:1	6	3
Maximum level	$x_{i\,max}$	2:1	14	7

Table III shows the experimental matrix of the input factors with their encoded and natural values.

The model of regression equation sought for the target function – the specific mechanic energy SME (Y) is of an incomplete quadratic type:

$$Y = B_0 + B_1.X_1 + B_2.X_2 + B_3.X_3 + B_{12}.X_1.X_2 + B_{13}.X_1.X_3 + B_{23}.X_2.X_3 + B_{123}.X_1.X_2.X_3 \quad (2)$$

In Table IV the results for the estimated SME of the analyzed sample variants are given (in three fold repetition).

TABLE IV

SPECIFIC MECHANIC ENERGY

№	X_1	X_2	X_3	SME, Wh/kg			SME_{cp}, Wh/kg
				1	2	3	
1	-	-	-	156.94	159.12	159.74	158.60
2	+	-	-	170.83	171.88	170.27	171.00
3	-	+	-	161.97	163.32	163.21	162.50
4	+	+	-	220.14	223.12	220.34	221.20
5	-	-	+	141.30	143.52	143.28	142.70
6	+	-	+	206.96	209.30	208.34	208.20
7	-	+	+	148.85	151.20	150.55	150.20
8	+	+	+	206.72	208.80	207.88	207.80

These results prove to be the basis for deriving the following adequate regression equation, depicting the dependence of the specific mechanic energy on the input variables: level of compression of the active screw of the extruder, percentage of carboxyl methylcellulose and propylene glycol:

$$Y = 177.8160 + 24.2325X_1 + 7.6925X_2 + 4.7572X_1X_2 + 6.5425X_1X_3 - 5.9175X_2X_3 \quad (3)$$

It could be seen that the variable X_3 – the percentage of propylene glycol, drop out of the equation as a separate factor. It affects the SME only in combination with the two other factors – X_1 and X_2.

Fig. 1 shows the response surface and Fig. 2 – the contours of equal response for the target function SME.

Fig. 1. Estimated response surface

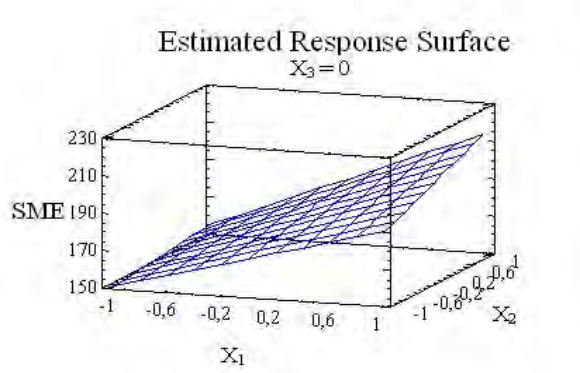

Fig. 2. Contours of estimated response surface

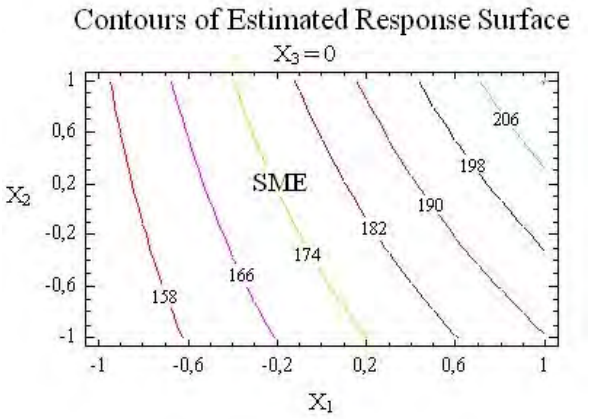

The estimated response area (Fig. 1) is approximated to a plain with a positive slope at higher level of compression and higher percentage of CMC. Similar information can be derived from Fig. 2.

IV. Conclusions

1. The reconstituted tobacco sheet made by applying the square-shaped mouth surpasses that made with the round mouth in basic technological indices (thickness and weight per area), despite the worse energetic parameters.

2. From the energetic point of view, with approximately equal physical and chemical properties, it is more favourable to extrude the tobacco sheet with
no compression at the active screw (volume ratio at the beginning and at the end of the screw 1 : 1) and percentage of CMC approx. 6 %.

References

[1] Anonymous, "The New Role of Reconstituted Tobacco", Bulg. Tutun, vol. 5, pp. 23-28, 2003.

[2] Browne C. L., *"The Design of Cigarettes"*, Hoechst Celanese Corp., 3rd edition, 1990.

[3] Das H. K., A. Lambrev, S. Tanchev, "Response Surface Methodology in the Control of Extrusion Texturing of Soya", Sci. Works of HIFFI -Plovdiv, vol. XXXVIII, part 1, pp. 201-212, 1991.

[4] Davis D. E. L., M. T. Nielsen, *"Tobacco: Production, Chemistry and Technology"*, Blackwell Science, N.A. Orders, UK, 1999.

[5] Gueorgiev S., *Technology of Tobacco Products*, Plovdiv, A. Gueorgiev Publ., 2002.

[6] Gutev N., G. Dimov, "Chemical and Technological Characteristics of Tobacco Sheet, Produced by Different Methods", Bulg. tutun, vol. 6, pp. 32-36, 1988.

[7] Djambazov V., A. Lambrev, V. Nenov, "Technology for Production of Reconstituted Tobacco by Extrusion and Stretching", "Food and Quality of Life – 2000", Conference Proceedings, Plovdiv, Bulgaria, 2000.

[8] Nenov V., V. Djambazov, A. Lambrev, "Optimizing Mixture Composition in the Production of Restored Tobacco through Extrusion and Stretching", 2nd Balkan Scientific Conference "Quality and Efficiency of Tobacco Production, Treatment and Processing", Conference Proceedings, pp. 322-328, Plovdiv, Bulgaria, 2002.

[9] Peeva S., *"Tobacco Technology – Students' Manual for Experimental Work"*, Plovdiv, HIFFI Publ., 1988.

[10] Popova V., V. Nenov, A. K. Omar, "Chemical and Technological Characteristics of Reconstituted Tobacco Sheet Made by the Extrusion-and-Rolling Method", Sci. Res. of the Union of Scientists – Plovdiv, series C, vol. III. Scientific Session "Technics, Agrarian Sciences and Technologies", pp. 182-186, 2004.

[11] Tasheva R., "Investigation of Tobacco Waste, as a Source for the Production of Reconstituted Tobacco", Bulg. Tutun, vol. 6, pp. 40-43, 1990.

Approaches for Obtaining Texture Images for Computer Vision Purposes

Daniela D. Ilieva[1]

Abstract - **In this paper is proposed an algorithm for generating synthetic texture with desired appearance and size and an algorithm for synthesizing texture from a photo. Also, is proposed a proper visualization process for using the received texture to obtain a realistic appearance of 3D surfaces which can by applied in geographic maps, for mapping of a vegetation and other special features onto terrains, to correct failings of a photo, video and satellite images.**

Keywords - **texture synthesis, texture generation, texture visualization.**

1. Introduction

The computer's generated images with textured surfaces are interesting and realistic. The texture mapping is a technique for adding details to the external appearance of the surface by wrapping or projecting the textured image onto the surface. The first step in working with textures is creating them. Often the source of textures is a photo or video image or a hand drawn picture and the resulting texture piece usually hasn't the desired shape and size. To cover a large object with the texture we must repeat it but that will produce unacceptable defects such like visible boundaries, visible repetitions or the both. To escape that defects there is necessity of synthesizing texture with desired size from a texture piece. There is no general approach for decision of this problem[1],[4],[6],[9].

Other alternative way is creating synthetic texture by algorithmic (procedural) manner that gives a possibility to receive many and various samples with different sizes. Such texture samples can be used for applications from decoration to creating complex 3D structures and motion.

Texture is related to qualitative properties of surfaces, but due to its complexity and great variety, there exists neither a unique definition of texture nor an accepted computational representation of it. One of the widely accepted definitions of texture is given by Pickett[10]. He states that a texture is an optical pattern that contains a large number of elements (spatial variations in intensity or wavelength), each visible to some degree, and, on the whole, densely and evenly arrayed over the field of view.

One of the many applications of textures consists in synthesizing realistic images of terrains. Such images pose a number of problems. The challenge stems from the visual complexity and diversity of the modelled scenes[7],[8]. They include natural ecosystems such as forests or grasslands, human-made environment, for instance parks and gardens, intermediate environments, such as lands recolonized by vegetation after forest fires or logging, visualization of models of ecosystems for research and educational purposes, and synthesis of scenes for computer animations, games, and computer art.

[1]Daniela D. Ilieva is with the Technical University of Varna, Faculty of Computer Sciences, 1, Studentska Str., 9010, Varna, Bulgaria, e-mail: dilieva@bitex.com

2. Definition of the problem

There is necessity of new ways and means to obtain surfaces with texture appearance with the aim of generating natural scenes in systems for visualization of spatial data. The texture sample must have a needed size to cover the surface without repetitions, a desired appearance and must be obtained quickly. The texture visualization system must be flexible and must allow the user quick changes of the appearance of the terrain (its texture) as well as of its shape.

3. Solution of the problem

The task assigned for texture visualizing is solved by means of a computer-generated texture and a synthesized texture

-computer generated texture

The advantage of generated textures in comparison with the synthesized ones consists in the rapid obtaining of image with previously given size and the avoiding the necessity of analyses when synthesizing textured image from a photo. The generated texture looks like vegetation with adequate color arrangement.

-synthesizing texture from a photo

The goal of texture synthesis can be stated as follows: to generate a new image from an example texture, such that the new image is sufficiently different from the original yet still appears as though it was generated by the same underlying stochastic process as was the original texture. If successful, the new image will differ from the original, yet have perceptually identical texture characteristics. This can be measured psychophysically in texture discrimination tests. To satisfy both criteria, a synthesized image should differ from the original in the same way as the original differs from itself.

Proposed solution of the defined problem is a system composed of a part for generation/synthesis the texture**,** a part for specification the terrain and a part for texture visualization of spatial data describing the terrain and the texture.

3.1 Generation of 2D texture sample

3.1.1. Algorithm

In this paper is proposed following algorithm for generation of texture images that is next map onto the terrain:

1. Input data: size of generated image determined by the coordinates of upper left and lower right corner **(x1, y1, x2, y2),** a scaling variable **scale**, a colour palette **pal**.

2.Output data: a computer-generated texture image possessing given size, scale and colour appearance.

3. Method: the proposed algorithm generates a texture image by determining the intensity of pixels in a small area and propagates it in its neighbourhood**.** The process starts with the given size of the image and decrease that size to reach the level of one pixel surrounded by eight neighbours. The initial setting of the intensity of the four pixels marking the four corners of the image is randomly. From the primary randomly assigning is determined pixels intensity, marked the corners of four new equal rectangles consist of the initial one.

The process continues recursively with determining the intensity of the following five pixels dividing the corresponding rectangle into four new pieces etc. until the level of one pixel is achieved. After that the algorithm continues by scanning the areas in reversed order until a complete image size is achieved. Scanning the pixels in generated image in the depicted manner is done in procedure divide. The function adjust determines the pixel's intensity.

1.1.1Experimental results and analyses

The proposed algorithm is tested with various colour palettes, scales and image sizes (fig 1.,2). By assigning the colour palette **pal** in the registers and interrupting of the monitor is achieved different and interesting colour arrangement. Figure 1a illustrates obtaining different colour combinations. The changes of the scaling variable **scale** lead to images in different scales independent of the image size. Figure 1b shows this scaling. The image size is 240 X 240 pixels. The algorithm generates an image with given size (the necessity of various size of texture piece follows from the various size and shape of the terrain). When the texture is little in size it must resized or repeated to cover the terrain. In both cases this results in undesirable defects. Receiving an image with arbitrary size eliminates this inconvenience. On the figure 2 is shown an image with size 480 X 640 pixels. The image size has no crucial effects in comparison with the algorithms for texture synthesis from a given texture sample where the size of piece is of great importance for the synthesis velocity [2].

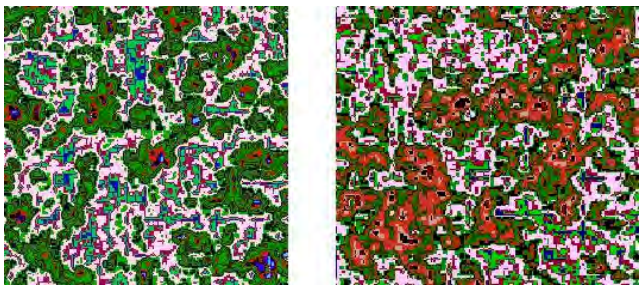

Fig. 1 (a) Texture images obtained with a various values of the color palette

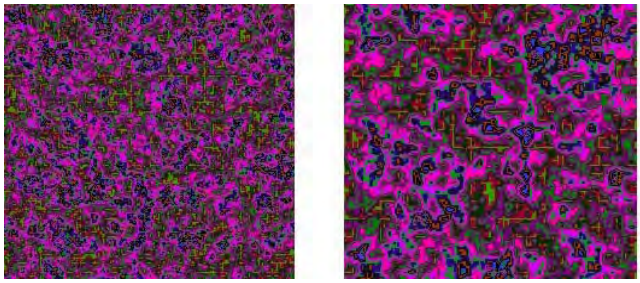

Fig. 1 (b) Texture images obtained with a various values of the scaling variable

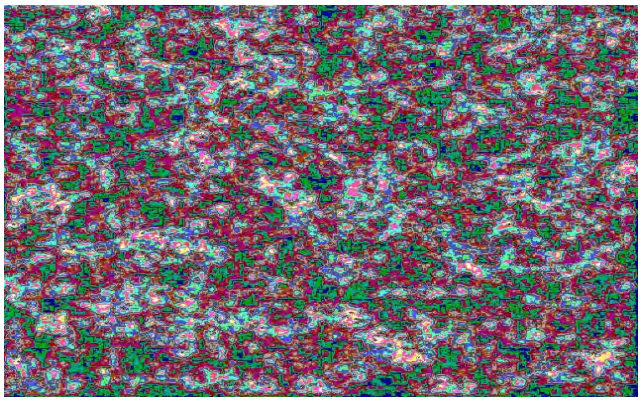

Fig. 2. Texture image obtained with given size- 480 x 640 pixels.

3.2 2D texture synthesis

3.2.1 Pyramidal methods for image analysis

The image pyramid data structure was originally developed for image coding. In this data structure an image is represented hierarchically, with each level corresponding to a reduced resolution approximation.

Wavelets have become a tool of choice in analyzing single and multidimensional signals, especially if the signal has information both at different scales and localizations [3]. A wavelet representation is a multiscale decomposition of the signal and can be viewed as a complete tree, where each level stores the projections of the signal, with the wavelet basis function of a certain resolution. A wavelet representation can be transformed back into the original signal using a fast hierarchical inverse transform. The computations proceeds from the root of the tree down to the leafs, using filters that are complementary to those used in wavelet transform.

3.2.2 Algorithm

1.Input data: texture sample (scanned photo image)

2.Output data: texture with given size and perceptually identical with the original.

3. Method The texture sample is a tree representing the wavelet based multiresolution analysis. From the point of view of the synthesis algorithm the image is a collection of pats from the root of the tree toward the leaves.

The task of the algorithm is to generate a tree whose pats are typical sequences generated by the most likely mutual source of the input tree. From the resulting tree a new image is reconstructed by applying an inverse wavelet transform. A measure of similarity is threshold. Two pats from nodes x and y are considered similar when the differences between their corresponding values are below a certain threshold. If two pats are similar we can continue one with values from the other, while still preserving the fact that they emerged from the same stochastic process. A level-dependent similarity criteria for tree pats is used. Lower resolution levels of the tree have looser similarity criteria than higher resolution levels and therefore a larger threshold is used at lower levels. This adaptive measure is chosen because the human visual system is more sensitive to high frequency information [5].

3.2.3. Experimental results and analyses

On the fig.3 are shown the results of the algorithm with various values of the threshold. The output image (synthesized texture) is four times larger than the input ones. The selection of the threshold has a big impact on the outcome of the algorithm. Selecting a larger threshold causes the outcome to differ more strongly from the input. On the other hand, a small threshold can cause the outcome to be a copy of the input. Thus, by leaving the threshold selection to the user, the user is supplied with a powerfull tool to achieve the desired outcome.

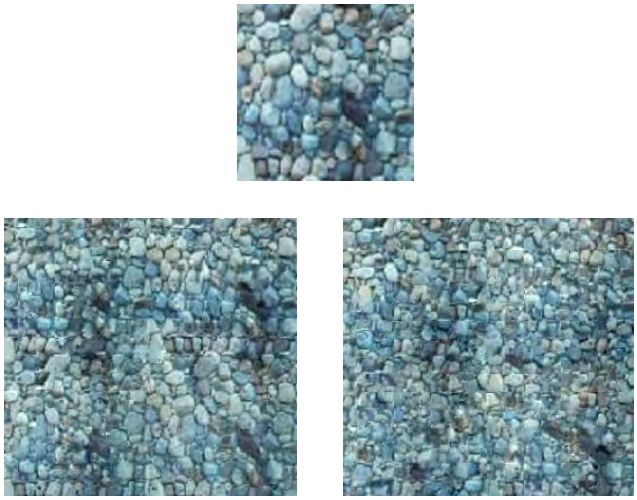

Fig. 3. Texture synthesis from a texture sample obtaining from a photo.

3.3 Terrain specification

The aim of this step is to determine shape and local orientation of the terrain. The surface representing a terrain covered with vegetation is generated by any equation of two variables or may be known in advance.

The generated surface can be edited for introducing new additional elements and for increasing the realism of the scene. The synthesizing algorithm gives a possibility of additional editing which increases the realism of the terrain. In the future it can be expanded with parameters controlling the roughness of the terrain, the rate of its changes, the expletive possibility of adding streams, roads and others.

4. Use of the proposed approach for computer visualization purposes.

The technique of texture mapping is based on mapping the synthesized image onto a surface. There are many works on the problem in the computer graphics literature. In our work we use a technique for standard texture mapping: the initial image (texture) is mapped onto the surface in a 3D object space (terrain) by mapping function and the surface is mapped onto the image space (display) by projection.

Extras like illumination, reflection and point of view are not subject of this work.

On a fig.4 is shown the visualization system and its components.

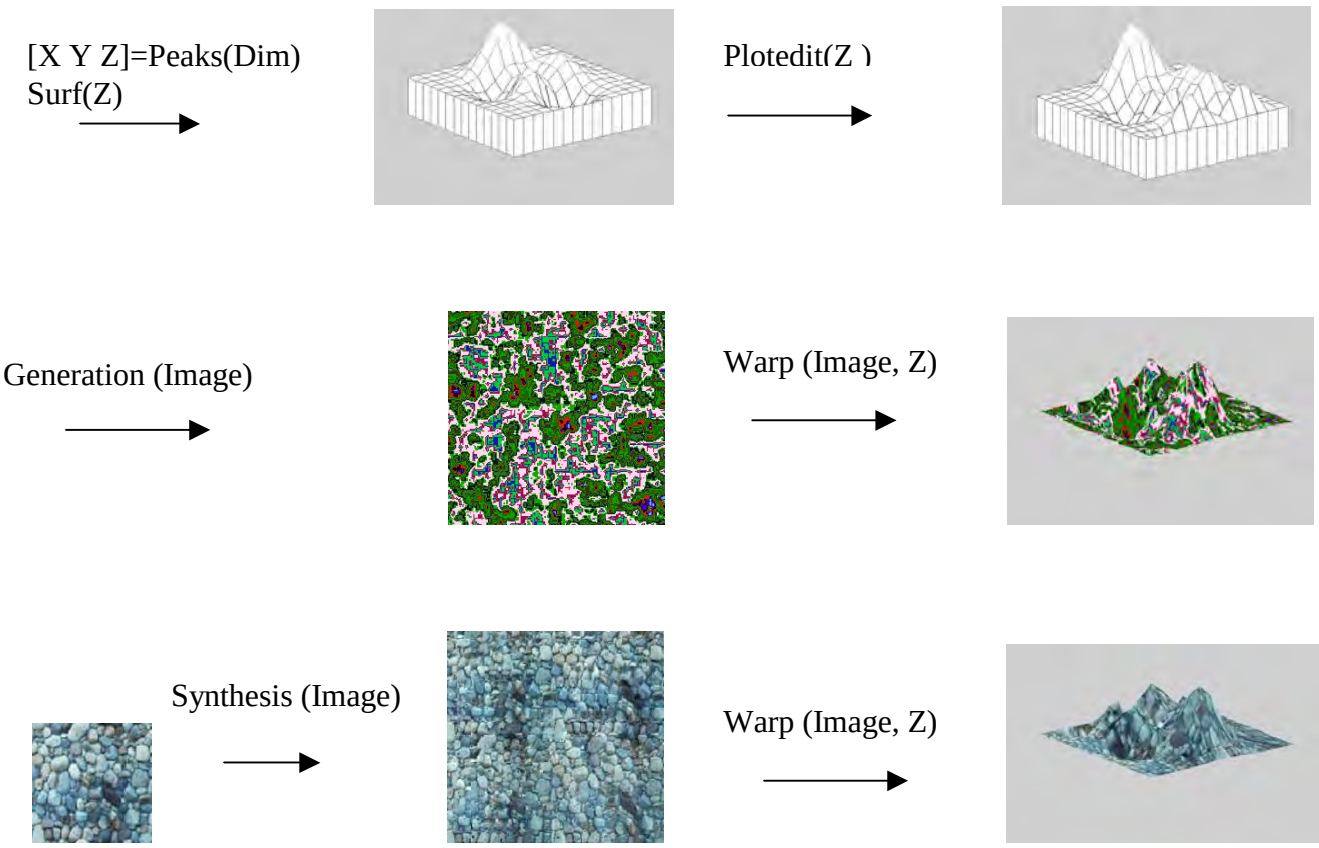

Fig. 4. System for texture visualization

5. Conclusions and future work

In this paper we show how computer generated/synthesized image (texture) can be used for mapping onto computer generated and hand edited surface (terrain) to receive a synthesized scene of terrain. Such scenes gives interesting possibilities for spatial data visualization. The texture image could be obtained from scanned photos or could be generated.

Increasing of realism of the scene could be obtained by introducing illumination and reflection.

By additional analyses the proposed approach can find an application in image correction by introducing a changes in the image so these changes remain invisible for the viewer. This is usually applied in the tasks for reconstructing damaged images and also for elimination of unneeded elements of the scene.

6. References

[1] Ashikhmin, M., " Synthesizing Natural Textures**",** The Proceeding of 2001 ACM Symposium of Interactive 3D Graphics, Research Triangle Park, North Carolina, pages 217-226, March, 2001.

[2] Rachev. B, Ilieva. D, "An approach for texture SDI visualization", International conference on computer systems and technologies CompSysTech' 2003, Sofia, Bulgaria, 19-20 June 2003,

[3] Stollnitz,E.J, T.D.De Rose and D.H.Salesin," Wavelet for Computer Graphics: Theoty and Applications", Morgan Kaufman,1996.

[4] Xu,Y., Guo,B. and Shum,H. "Chaos mosaic: Fast and memory efficient texture synthesis." Tech. Rep. MSR-TR-2000-32, Microsoft Research, 2000.

[5] Ilieva,D., Varbanov.,G.,"Pyramidal approach for analisis and synthesis of one class of images", International conference TELEKOM 2002, Varna, Bulgaria 9-11.Oct.,2002.

[6] Dischler,J., and Ghazanfarpour,D. "Interactive image-based modeling of macrostructured textures." *IEEE Computer Graphics and Applications 19*, 1 (January-February 1999), 66–74.

[7] House,D., Schmidt,G., Arvin,S. and Kitagawa-DeLeon. "Visualizing a real forest." *IEEE Computer Graphics and Applications*, 18(1): 12–15, 1998.

[8] Marshall,D., Fussel,D. and Campbell.A. "Multiresolution rendering of complex botanical scenes." In *Proceedings of Graphics Interface 97*, pages 97–104, May 1997.

[9] Praun,E., Finkelstein,A., and Hoppe,H. "Lapped textures." *Proceedings of SIGGRAPH 2000* (July 2000), 465–470.

[10] Pickett,R.M., "Visual Analysis of Texture in the Detection and Recognition of objects", *Picture Processing and Psychopictorics*, Ed. Academic Press, pp. 298-308, 1970.

Forming A Quadrature Signal By Using A Raster Algorithm

Miroslava Doneva

The purpose of algorithms for raster graphics is to service the visualization on raster devices. They are characteristics of good response time because of the simple arithmetic operations which they perform in order to make a decision for selection of the relevant point of the raster network.
Such an algorithm is used in this paper as a source of coordinates of points which later shall approximate sinusoidal and cosinusoidal signal. The advantage of using a raster algorithm for a circle is that both signals are simultaneously formed.
The algorithm for circle is Brenham's in which it is evaluated the error /m/ which is made at every step at the choice of one or another point of the raster /fig.1/. At a point chosen (x_i , y_i) the possible following one is : the horizontal (x_i+1 , y_i), vertical (x_i , y_i-1) or diagonal (x_i+1 , y_i-1) [1].

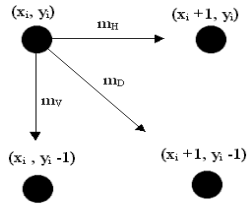

Fig.1

As a result of performance of the algorithm for a given radius, a file of integral values is obtained, which are the x and y coordinates of the separate pixels /points/. These selected points are discrete reports of a curve which approximates a central circle in an orthogonal system of coordinates. Each pair of coordinates of the i-th point (x_i,y_i) uniquely determine the angle formed between the radius-vector r_i and the ordinate axis (fig.1). The dependence is given with the formula (1).

(1) $$a = arctg(x_i / y_i)$$

Having in mind the parametrical circle equation (2) and the considerations stated above, it is ascertained that the algorithm provides digitalization by angles of signals determining curves which approximate sinusoidal or cosinusoidal signal (fig.2)[2].

(2) $$\begin{cases} x(t) = R * \sin a(t) \\ y(t) = R * \cos a(t) \\ a \in [0 \div 2\pi] \end{cases}$$

After rasterization the generated values of the sinusoidal and cosinusoidal signal have quadrilateral symmetry regarding the coordinate axes. This makes it possible both to rasterize only one fourth of the circle, and to consider and analyze the signals which approximate it in one of the quadrants.

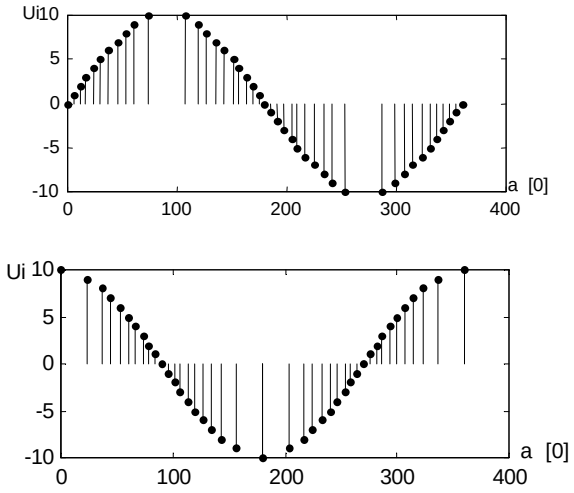

Fig. 2

Brenham's raster algorithm begins from a point having coordinates (0, R) , approximates a circle in the clockwise direction and calculates the pixels of the central circle for fourth quadrant. The obtained step-like approximating signals compared to the ideal calculated ones using (3) are given in (fig.3).

(3) $u(a)_{\sin} = R * \sin(a)$ and $u(a)_{\cos} = R * \cos(a)$, where $a \in [0 \div \pi/2]$

The approximation of the two signals after rasterization of the circle is a step-like approximation with even quantization by level and uneven quantization by angle /time/.
The ideal sinusoid $u(a)_{sin}$ and the rasterizing curve $\tilde{u}(a)_{sin}$ change within the range $[0 \div R]$. For the cosinusoid $u(a)_{cos}$ and its rasterizing curve $\tilde{u}(a)_{cos}$ the interval is $[R \div 0]$. Both ranges are broken into *n* equal increases. In this particular case *n* = *R*. At this quantization the height of each step is one and its length is different and is determined according to its position in the interval of forming. The ordinate of the separate steps is [1 ; 2 ;...i ; i+1 ;.....R-1 ; R] for the sinusoid and [R ; R-1 ;...i ; i+1 ;....2 ; 1] for the cosinusoid. The abscissa of the points of the approximation is determined by formulation (1).
The raster algorithm, the figures provided and the analysis below are implemented in the MATLAB 5.X media [3].
The deviation of the approximating curve from the ideal one is evaluated by a quadratic mean deviation. For its

evaluation a programme is created by which it is checked the position of the step-like curve to the calculated one (3), i.e. a check is made of the position of the abscissa of the intersection point of the two curves a^o_i as to the abscissa of the transition point a_i (fig.3).

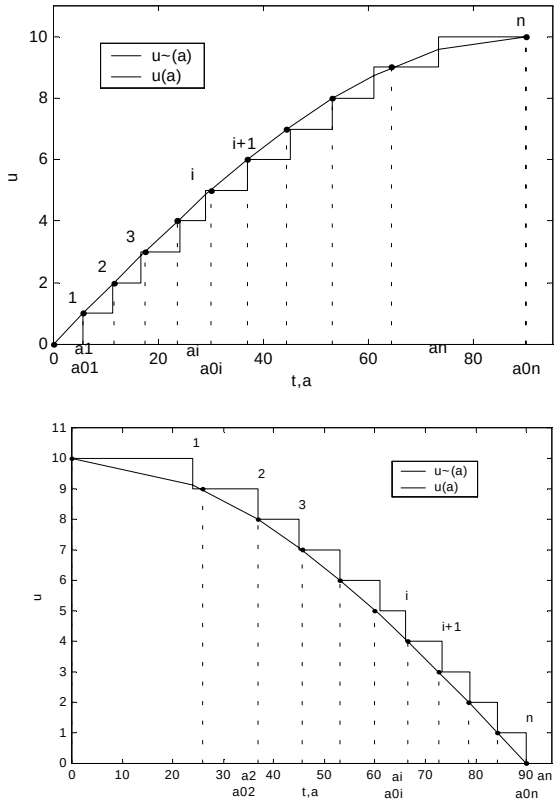

Fig.3

In order to calculate the quadratic mean deviation / QMD / of the approximating curve of the sinusoid it is necessary to consider its position as to the ideal one. In order to make a decision regarding the formulation for calculating QMD for each step (g_i), it is necessary to distinguish between four cases determined by the type of intersection of the two curves:

- $a^o_i < a_i$ и $a^o_{i+1} < a_{i+1}$

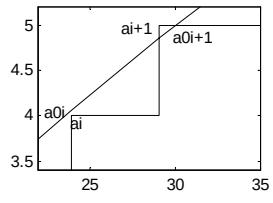

$$g_i = \int_{a_i^0}^{a_{i+1}} (R.\sin a - i)^2 da + \int_{a_{i+1}}^{a_{i+1}^0} (R.\sin a - (i+1))^2 da$$

- $a^o_i < a_i$ и $a^o_{i+1} < a_{i+1}$

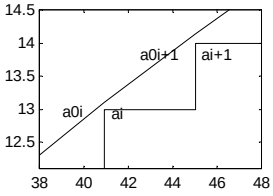

$$g_i = \int_{a_i^0}^{a_{i+1}} (R.\sin a - i)^2 da - \int_{a_{i+1}^0}^{a_{i+1}} (R.\sin a - (i+1)^2 da$$

- $a_i < a^o_i$ и $a_{i+1} < a^o_{i+1}$

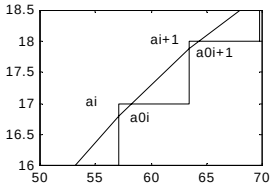

$$g_i = \int_{a_i^0}^{a_{i+1}} (R.\sin a - i)^2 da + \int_{a_{i+1}^0}^{a_{i+1}^0} (R.\sin a - (i+1))^2 da$$

- $a_i < a^o_i$ и $a^o_{i+1} < a_{i+1}$

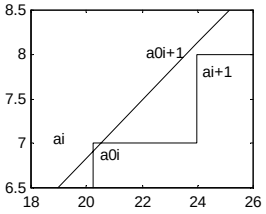

$$g_i = \int_{a_i^0}^{a_{i+1}} (R.\sin a - i)^2 da - \int_{a_{i+1}^0}^{a_{i+1}} (R.\sin a - (i+1)^2 da$$

At approximation of the cosinusoid, the step-like curve is always above the ideal one. This reduces the calculations of QMD to two cases because the condition $a^o_i < a_i$ is always true.

- $a^o_i < a_i$ и $a^o_{i+1} < a_{i+1}$

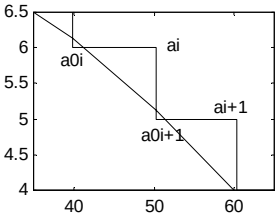

$$g_i = \int_{a_i^0}^{a_i} (R.\cos a - (R-i))^2 da + \int_{a_i}^{a_{i+1}^0} (R.\cos a - (R-i))^2 da$$

- $a^o_i < a_i$ и $a^o_{i+1} < a_i$

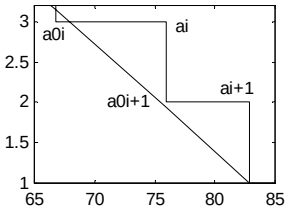

The result of the programme which calculates QMD for

$$g_i = \int_{a_i^0}^{a_i} (R.\cos a - (R-i))^2 da - \int_{a_{i+1}^0}^{a_i} (R.\cos a - (R-i))^2 da$$

each step is represented in the form of a table. The source of approximating signals is a raster algorithm of B for circle, applied for radius R=10 [the pixel].

Step [i]	**1**	**2**	**3**	**4**	**5**	**6**	**7**	**8**	**9**	**10**	**G**
QMD $\tilde{u}(a)_{sin}$	1.95	2.17	2.82	1.67	3.2	2.26	1.93	2.79	7.43	**26.67**	**52.89**
QMD $\tilde{u}(a)_{cos}$	**13.72**	6.15	3.04	3.84	2.35	2.18	2.48	2	1.95	1.93	**39.62**

Table.1

The highest QMD, i.e. the biggest inaccuracy of approximation for the sinusoid is on the last step and for the cosinusoid – on the first step. These are the intervals in which there are approximated the maximum values of the sinusoidal $u(a)_{sin}$ and the cosinusoidal $u(a)_{cos}$ signals.
The sum of QMD for each step gives the deviation of the whole approximating curve G (4).

$$(4) \quad G = \sum_{i=1}^{n} g_i$$

In order to reduce the total QMD (G) it is necessary to process the steps which lead to the greatest inaccuracy. The new algorithm for these steps is based on Brenham's algorithm but provides less increase in level.
Only the first fourth of the central circle, located in the first quadrant was considered. Lets assume that at the i-th step of this algorithm there was selected point $P_i = (x_i, y_i)$. This is the point after which it is necessary to reduce the

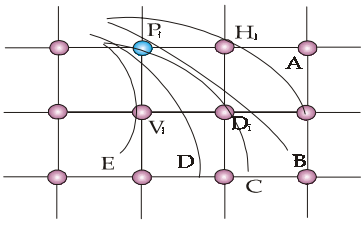

Fig.4

increase in level from 1 to a smaller step (st). The next choice should be only one of the points: $H_i = (x_i + st , y_i)$, $V_i = (x_i, y_i - st)$ or $D_i = (x_i + st, y_i - st)$, shown in fig.4. In the same figure there are shown the possible ways (A, B, C, D, E), in which the considered part of the one fourth of the circle may be positioned as to the points of the new raster. The step of increase of the more precise algorithm is defined according to formula (5).

(5) st = 1/ p, where p is an integer

The initial evaluation with which rasterization is commenced is calculation of the error at potential selection of a diagonally positioned point.
$\boldsymbol{\Delta_i} = D(\mathbf{D}_i) = (x_i + st)^2 + (y_i - st)^2 - R^2$
(6)

Case 1. Lets $\boldsymbol{\Delta_i < 0}$. Then the circle is positioned as in the cases A and B in the figure above and the reasonable selection is $H_i = (x_i + st , y_i)$ or $D_i = (x_i + st , y_i - st1)$. Another evaluation should be introduced in order to differentiate between these two options:
$\boldsymbol{\delta_i} = D(\mathbf{H}_i) + D(\mathbf{D}_i) = 2.(x_i + st)^2 + (y_i - st)^2 + y_i^2 - 2.R^2$ (7)

At $\boldsymbol{\delta_i < 0}$ / case A / **H** is always selected$_i$, because $D(\mathbf{H}_i) \le 0$ and $D(\mathbf{D}_i) < 0$, hence and $\delta_i < 0$.
At $\boldsymbol{\delta_i > 0}$ / case B / **D** is selected$_i$. Both terms of the sum $\boldsymbol{\delta_i}$ (7) have different signs, at $D(\mathbf{H}_i) > D(\mathbf{D}_i)$ the selected point is $\mathbf{D}_i$, i.e. the curve B.
At $\boldsymbol{\delta_i = 0}$, **D** is selected$_i$.

After selecting one of the two points, the new initial evaluation is:
$\boldsymbol{\Delta}_{i+1} = D(\mathbf{D}_{i+1}) = (x_{i+1} + st)^2 + (y_{i+1} - st)^2 - R^2$
Case 2. Now $\boldsymbol{\Delta_i > 0}$. This corresponds to positions D and E in fig.6 . As in the preceding case, a new evaluation is introduced in order to differentiate between these two options:

$\boldsymbol{\varepsilon_i} = D(\mathbf{V}_i) + D(\mathbf{D}_i) = (x_i + st)^2 + 2.(y_i - st)^2 + x_i^2 - 2.R^2$ (8)

The similar analysis of the options for selection between D and E , leads to the conclusion:
- at $\boldsymbol{\varepsilon_i > 0}$, **V** is selected$_i$
- at $\boldsymbol{\varepsilon_i < 0}$, $\mathbf{D}_i$ is elected
- at $\boldsymbol{\varepsilon_i = 0}$, $\mathbf{D}_i$ is selected.

After selecting one of the two points, the new initial evaluation is:
$\boldsymbol{\Delta}_{i+1} = D(\mathbf{D}_{i+1}) = (x_{i+1} + st)^2 + (y_{i+1} - st)^2 - R^2$
Case 3. As it is clear in fig.4 (position C), at $\boldsymbol{\Delta_i = 0}$, the circle passes exactly through the diagonally positioned point **D**i and it is the one to be selected.

The next initial evaluation is :
$\boldsymbol{\Delta}_{i+1} = D(\mathbf{D}_{i+1}) = (x_{i+1} + st)^2 + (y_{i+1} - st)^2 - R^2$
After performing the algorithm described above with step st = 0.2 applied for the last and first step relevantly for the

sinusoid and the cosinusoid, there are obtained approximating curves shown in (fig.5) .

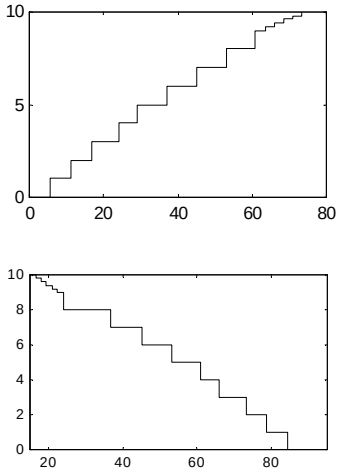

Fig. 5

After applying the new algorithm per one step of the approximating curves, the sum of QMD for the sinusoid is G_{sin}= 38.24, and for the cosinusoid G_{cos}= 29.68 . With decrease of the step through which a decision is made for the next point of the curve, its quality is improved, but the number of iterations of the raster algorithm is increased, which leads to decrease of its response time. The suggested algorithm may be applied for more than one, as well as for all steps of the curves.

REFERENCES

[1]Лукипудис Е, Компютърна графика и геометрично моделиране,Техника,1990.

[2]Халачев В,Теория на сигналите, Техника,1980.

[3]Потемкин В, Система инжинерных и научных расчетов MATLAB 5.x, Москва,1999.

Numerical Modelling of Dielectric Mixtures

Antoniya R. Georgieva

Abstract - **The present paper reports the results of a numerical analysis of electromagnetic fields in two component dielectric mixtures. The mixture consists of a homogeneous background in which circular cylinders are embedded. Both materials are lossless. Finite-difference time-domain method is used to simulate wave propagation through the mixture. The effective permittivity is determined from the reflection coefficient. The numerical results are compared with theoretical mixture models.**

Keywords - **Dielectric mixture, artificial dielectric, effective permittivity, FDTD method.**

I. INTRODUCTION

Materials encountered in nature are quite often inhomogeneous and complicated in structure. Many of them, like snow, sea ice and soil, consist of several phases with different electromagnetic properties. Such media are referred as dielectric mixtures in literature. One of the phases is usually considered as a background medium and the other are treated as inclusions.

The problem of interaction between electromagnetic waves and such a complex material object is quite a difficult one to solve. However, under certain conditions the dielectric mixture could be considered as a homogeneous medium characterized by only one macroscopic parameter - the effective permittivity (the components of the mixture are assumed non-magnetic).

The properties of dielectric mixtures depend on the internal structure of the medium i.e. the shape, the volume fraction, and the arrangement of the different components. This makes it possible to develop new artificial materials having desired electromagnetic properties.

The history of the study of heterogeneous mixtures dates back to 19th century and several analytical and empirical models have been proposed. The advances in computer technology in the recent years made it feasible to perform numerical predictions for the electrical parameters of mixtures.

This paper demonstrates an approach for determining the characteristics of a heterogeneous lossless two-phase mixtures numerically by means of the Finite Difference Time Domain (FDTD) method. This is a dynamic method to solve the full set of Maxwell equations in a finite region. For computational restrictions, a two-dimensional mixture is treated instead of the full three-dimensional case. The inclusions are two-dimensional spheres (cylinders). Both regular lattice and random location of inclusions are studied.

The effective permittivity of the material is deduced from the reflection coefficient at the surface of the mixture by transmission line analogy. The effective permittivity concept is defined to the permittivity of such a homogeneous sample from which the reflection coefficient is the same as from the mixture under study. The simulation is carried out in free space.

The results are obtained as a function of the volume fraction (the volume of inclusions to volume of background medium ratio) for various contrasts between permittivities of the ingredients.

The numerical results are compared to the most common mixing rule predictions such as the Maxwell-Garnett and Bruggeman models.

Antoniya R. Georgieva is with the Department of Radiotechnics, Technical University of Varna, 1 Studentska str., 9010 Varna, Bulgaria, e-mail: antonia_ross@yahoo.com

II. MIXING FORMULAS IN TWO DIMENSIONS

As mentioned previously, the attention in the following is limited to 2-D mixtures. In the literature, many mixing models can be found for the effective dielectric permittivity of mixtures. The major limitation of this models is that the inhomogeneities have to be of clearly smaller scale than the wavelength of the operating field. Otherwise scattering effects inside the medium cannot be neglected and the concept of the effective permittivity loses its physical meaning. Here are presented some of the commonest mixing formulas.

The oldest known mixing rule, the Maxell-Garnett formula, reads in two dimensions [2]:

$$\varepsilon_{eff} = \varepsilon_h + 2f\varepsilon_h \frac{\varepsilon_i - \varepsilon_h}{\varepsilon_i + \varepsilon_h - f(\varepsilon_i - \varepsilon_h)}, \qquad (1)$$

where circular inclusions (2-D spheres) of permittivity ε_i are embedded in homogeneous host medium (ε_h) and occupy a volume fraction f. It is to be noted that all permittivities in this paper are relative quantities.

Another famous mixing rule is the symmetric Bruggeman formula [2]:

$$(1-f)\frac{\varepsilon_h - \varepsilon_{eff}}{\varepsilon_h + \varepsilon_{eff}} + f\frac{\varepsilon_i - \varepsilon_{eff}}{\varepsilon_i + \varepsilon_{eff}} = 0. \qquad (2)$$

The approach presented in [2] collects dielectric mixing formulas in two dimensions into one family:

$$\frac{\varepsilon_{eff} - \varepsilon_h}{\varepsilon_{eff} + \varepsilon_h + v(\varepsilon_{eff} - \varepsilon_h)} = f\frac{\varepsilon_i - \varepsilon_h}{\varepsilon_i + \varepsilon_h + v(\varepsilon_{eff} - \varepsilon_h)}. \qquad (3)$$

For different values of the dimensionless parameter v, the previous mixing rules are recovered: $v = 0$ gives the Maxwell-Garnett rule, $v = 1$ gives the Bruggeman formula. The third approximation for $v = 2$ gives the Coherent Potential formula [2] known in solid state physics.

Different mixing models predict different effective permittivity values for a given mixture. However, there are theoretical bounds that limit the range of predictions. The loosest bounds are the so-called Wiener bounds [1,2]:

$$\varepsilon_{eff,\min} = \frac{\varepsilon_i \varepsilon_h}{f\varepsilon_h + (1-f)\varepsilon_i} \tag{4}$$

and

$$\varepsilon_{eff,\max} = f\varepsilon_i + (1-f)\varepsilon_h . \tag{5}$$

These two cases correspond to capacitors connected in parallel or series in a circuit. The bounds retain the minimum and maximum character independently of the type of the mixture, i.e. they are valid for both $\varepsilon_i > \varepsilon_h$ and $\varepsilon_i < \varepsilon_h$.

III. Principle of Numerical Calculation

The effective permittivity of a mixture is determined by calculation of the reflection coefficient from a sample. Both cases of a regular lattice and random positioned circular inclusions are studied. In the latter case overlapping of inclusions is allowed. The volume fraction of inclusions is controlled with their number keeping the radius constant.

Using a standard FDTD scheme [5], reflection from a sample of the mixture is simulated in free space. A case of parallel polarization is studied. The incident wave is a plain wave with components E_y and H_z coming from free space at an angle of 90^o to the sample surface. First order Mur's absorbing boundary conditions (ABC) are used to simulate infinite space outside the artificial computation domain borders. Fig.1 illustrates the simulation setup.

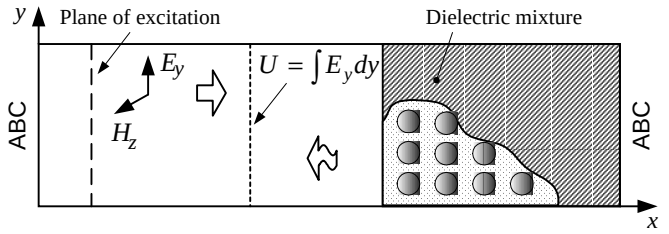

Fig.1. Schematics of the simulation setup. The dielectric mixture is formed of circular inclusions infinite in z-direction (cylinders). A plane wave is launched to travel in x-direction and reflection is studied. Electric field integrals are calculated in y-direction for each value of x to yield voltages.

The computational domain has a size of 150x50 cells. The used cell size is $\Delta x = \Delta y = 3$mm. The reflecting surface of the mixture is placed at $x = 65$. The diameter of inclusions is 6 cells. Excitation is performed at a distance of $10\Delta x$ from the left border of the computational domain. The time behavior of the excitation is a sinusoide of unit amplitude. One simulation is run as long as is needed to create a steady state.

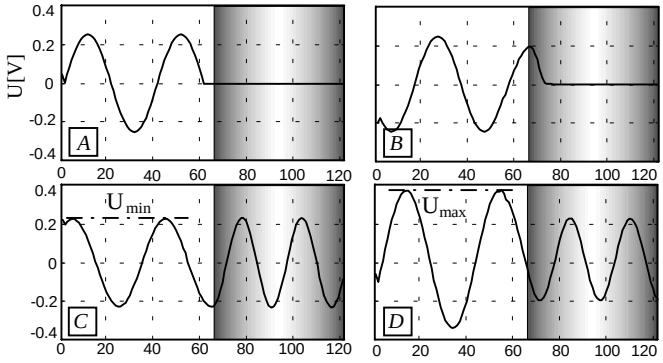

Fig.2. Reflection from dielectric mixture surface. Voltage is plotted as a function of x-coordinate, shown in spatial steps (one steps is equal to 3 mm). In A only the incident wave is shown, in B reflection starts, C and D show field pulses in time. Simulation is carried out at 1.5 GHz. The effective permittivity of the mixture is 2.4.

As results of the simulation, electric field integrals in y-direction are calculated for each time step. Each integral is equivalent to voltage between points with coordinates (x,0) and (x,50). The total field in front of the reflecting surface pulses, varying from a minimum ($U_{\min}$) to a maximum ($U_{\max}$) value as shown on Fig.2. The ratio of these values gives a voltage standing wave ratio (VSWR) defined by analogy with the transmission line theory:

$$VSWR = \frac{U_{\max}}{U_{\min}} = \frac{1+|R|}{1-|R|}.$$

where R is the reflection coefficient.

On the other hand the reflection coefficient can be determined from the Freshnel formulas. In the case of perpendicular incidence and parallel polarization we have:

$$R = \frac{1-\sqrt{\varepsilon_{eff}}}{1+\sqrt{\varepsilon_{eff}}} \quad \text{and} \quad |R| = \frac{\sqrt{\varepsilon_{eff}}-1}{\sqrt{\varepsilon_{eff}}+1}. \tag{7}$$

Substitution of (7) in (6) gives:

$$VSWR = \sqrt{\varepsilon_{eff}} . \tag{8}$$

Thus, the effective relative permittivity can be estimated by observing the total field variations in time in front of the reflecting surface.

An important issue in the simulation setup is incorporation of circular inclusions to the Cartesian square grid used for FDTD formulation of the Maxwell equations. Usually staircasing is used to represent curved boundaries provided that the grid cell is sufficiently smaller than the curved body. This technique, however, inevitably affects the accuracy of the simulation. To decrease this effect, in the current analysis weight coefficients are used for determining permittivity values between E field nodes when one of the nodes is inside an inclusion and the other lies in the background medium.

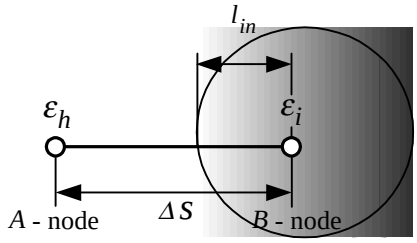

Fig.3. An estimation of the permittivity between two nodes lying in different media is based on geometry considerations.

Fig.3 illustrates this idea. The value of permittivity between the nodes "*A*" and "*B*" is:

$$\varepsilon_{A+B} = \frac{l_{in}}{\Delta s}\varepsilon_i + \frac{\Delta s - l_{in}}{\Delta s}\varepsilon_h , \qquad (9)$$

where l_{in} is the length of the cell edge part falling outside the inclusion boundary and Δs is the spatial step.

IV. Simulation Accuracy

The accuracy of the FDTD simulation can naturally be increased by decreasing the grid size (the spatial step). However, halving the cell size causes the computational time to grow by factor of four, and simulation must be run twice as long as before in terms on time steps.

A general rule in FDTD algorithm is to keep the spatial step much smaller (at least 20 times) than the shortest wavelength in the computational region [1]. At a frequency of 1,5 GHz within a region with maximum permittivity value of 10, the wavelength is 63 mm which is approximately 20 times larger than the grid size of 3 mm used in the simulation.

To test the influence of the grid size on the effective permittivity result, a number of simulation were performed in which inclusions were arranged in a regular lattice and their volume fraction was kept the same, but the cell size was varied. For mixtures with $\varepsilon_i < \varepsilon_h$ the results do not vary with the cell size. The composites with $\varepsilon_i > \varepsilon_h$, however, exhibit a slightly increasing trend in obtained permittivity value vs. cell size. Hence, for this type of mixture it is reasonable to use a denser grid.

The frequency of the simulation does not influence significantly the obtained effective permittivity. Simulations are carried out at three frequencies (700 MHz, 1 GHz and 1,5 GHz) and averaging is used to obtain a representative result.

V. Results

Effective permittivity was calculated for two types of mixtures - normal ($\varepsilon_i > \varepsilon_h$) and inverted ($\varepsilon_i < \varepsilon_h$). Both regular lattice and random distribution of inclusions are studied. Fig.4 illustrates field distribution inside such samples, detected at very low frequency (static case). There, contour plots of the electric field amplitude are given. Dark color corresponds to high values of electric field intensity. Light coloring marks the regions with low intensity values. The position of inclusions

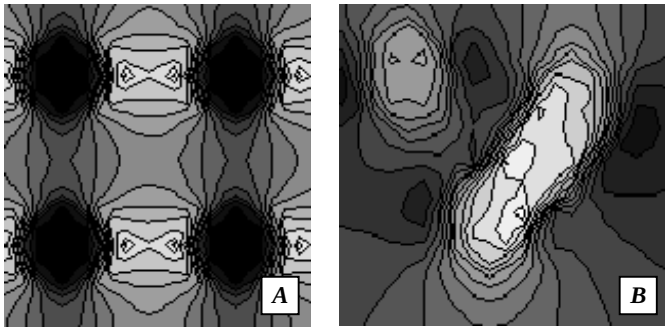

Fig.4. Electric field distribution in normal *(A)* and inverted *(B)* mixtures. In *A* a sample with regular lattice of inclusions is shown. In *B* the inclusions are randomly distributed. There are four inclusions, three of them are overlapping.

can be clearly seen. As expected, the field amplitudes are smaller in areas with higher dielectric permittivity.

The results for a medium with a regular lattice of inclusions are shown in Fig.5. The inclusion permittivity is ε_i = 2.5 and the host material is air (ε_h = 1). The cross sign denotes numerical results. Three analytical models are plotted too for volume fractions up to 1. However, the maximum volume fraction that could be achieved for regular lattice of inclusions is 0.78 (cylinders that do not overlap cannot fill the entire space).

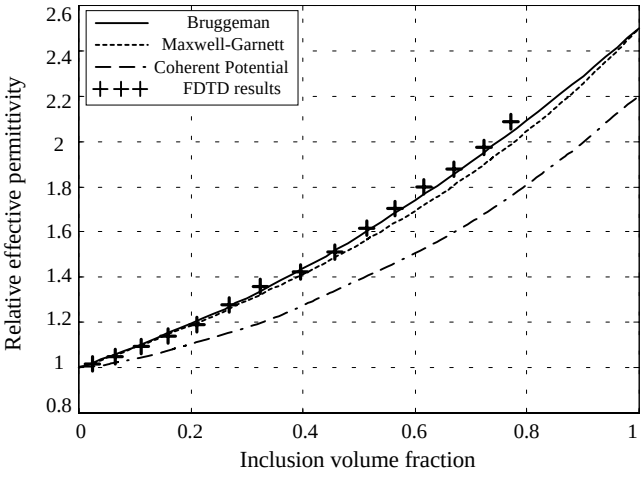

Fig.5. Effective permittivity of a mixture with $\varepsilon_i = 2.5$ and $\varepsilon_h = 1$ compared with theoretical models.

For low volume fractions the analytical results obtained from different formulas do not differ significantly. They all well coincide with numerical results. For high volume fractions Bruggeman model appears to be closest to the numerical results.

Fig.6 shows the results for inverted mixture with ε_i =1 and ε_h = 2.5 Comparison with Fig.5 shows that the results for a chosen volume fraction are not equal as Bruggeman symmetric formula predicts. Increasing of volume fraction and/or the difference between ε_i and ε_h causes this effect to become more significant.

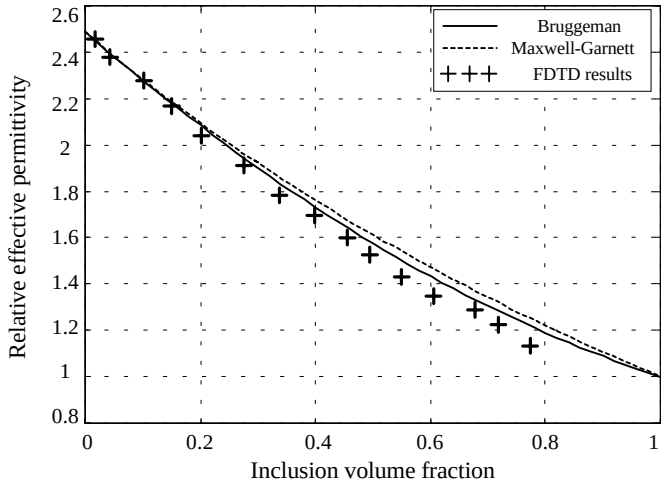

Fig.6. Effective permittivity of a mixture with $\varepsilon_i = 1$ and ε_h=2.5 compared with theoretical models.

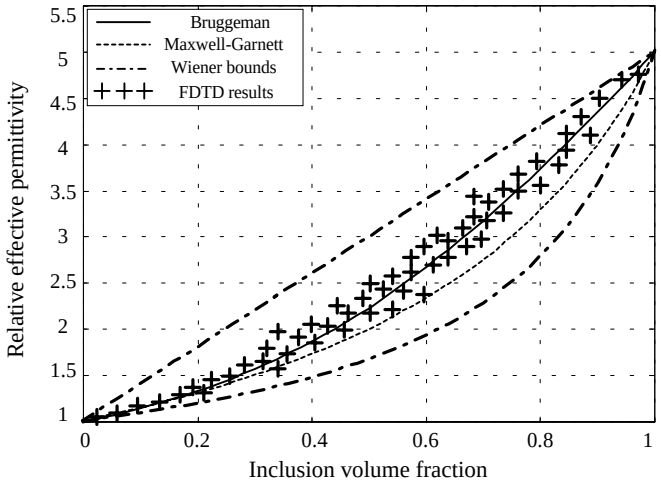

Fig.8. Effective permittivity of a mixture with $\varepsilon_i = 5$ and $\varepsilon_h = 1$ The inclusions are randomly distributed.

In Fig.7 one can see the results for a mixture with ε_i =20 and ε_h = 3.5. As the permittivity contrast grows, Bruggeman model predicts higher values of ε_{eff} than the numerical results for high volume fraction of inclusions (f > 0.5). Maxwell-Garnett rule can be used only for low volume fractions. This is natural, because the model is derived analysing a single inclusion not interacting with others, which is reasonable for low volume fractions.

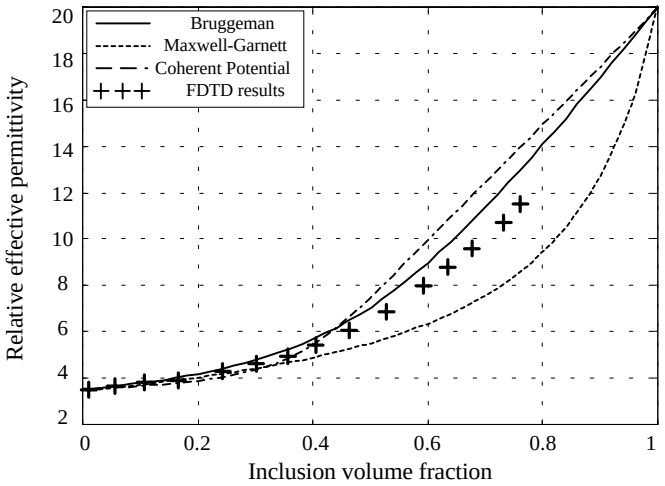

Fig.7. Effective permittivity of a mixture with $\varepsilon_i = 20$ and ε_h= 3.5 compared with theoretical models.

In Fig.8 a set of 50 simulation results for a mixture with randomly positioned inclusions are compared with Maxwell-Garnett and Bruggeman models. In every simulation both the volume fraction and positioning of inclusions were randomly chosen. Therefore, each sample has a permittivity that may differ from the value of another sample having an identical volume fraction because of their different structure. For low volume fractions results converge to a single value because the probability of inclusion overlapping and forming complex structures is low. This means that different samples do not differ in the type of their microstructure. The same happens in the case of high volume fractions when most of the inclusions overlap every time the simulation is carried out. Overlapping of inclusions allows volume fractions up to one to be achieved.

All the results in Fig.8 lie between the Wiener bounds. Numerical results are in very good agreement with the Bruggeman formula. The Maxwell-Garnett formula is applicable for low volume fractions and low contrast between the permittivities of the two phases.

VI. Conclusion

This paper presented a numerical approach based on the common Finite Difference Time Domain method for obtaining the effective permittivity value for two-phase lossless mixtures with periodical and random arrangements of inclusions. The numerical results were compared to the predictions of some well-known theoretical models. Best agreement was obtained with the Bruggeman rule.

The reported numeric technique can be easily extended to multiphase mixtures and various shapes of inclusions.

References

[1] O.Pekonen, K.Kärkkäinen, A.Sihvola and K. Nikoskinen, "Numerical testing of dielectric mixing rules by FDTD method", Journal of Electromagn. Waves Applicat., vol. 13, pp. 67-87, 1999

[2] A. Sihvola, *Electromagnetic Mixing Formulas and Applications*, London, IEE Electromagnetic Waves Series 47, 1999

[3] W.Merrill, R. Diaz, M.LoRe, M. Squires, N. Alexopoulus, "Effective Medium Theories for Artificial Materials Composed of Multiple Sizes of Spherical Inclusions in a Host Continuum", IEEE Trans. Antennas Propagat., vol.47, No.1, pp.142-148, Jan. 1999

[4] K.Kärkkäinen, A.Sihvola and K. Nikoskinen, "Effective Permittivity of Mixtures: Numerical Validation by the FDTD Method", IEEE Trans. Geoscience Remote Sensing, Vol.38, No.3, pp. 1303-1308, May 2000

[5] U.Andersson, "Time-Domain Methods for the Maxwell Equations", PhD theses, Royal Institute of Technology, Stockholm, Sweden, 2001

Influence of Heat Exchange over the Conditions of Combustion in the Initial Section of the Torch

Petar Kostov[1], Koycho Atanasov[2] and Neven Krystev[3]

***Abstract* - A diffusion process of burning on natural gas with a minimum coefficient of air-surplus is simulated in a cylindrical combustion chamber. Heat exchange from the torch is being shaped toward the walls of the chamber with different density of the thermal flow. A considerable influence with the cooling over the combustion zone is ascertained. With the increase of the intensity of heat exchange, the maximum temperature and the size of the high-temperature nucleus of the torch decrease.**

***Key words* – numerical modeling, injected turned stream, gas fuel**

I. INTRODUCTION

Aim of the present work is through numerical shaping to be received figures about temperature changes in the burning zone, with different density of the thermal torch flow. It is used a cylindrical combustion chamber with the following geometrical measurements: inner diameter D = 80 mm, length L = 350 mm , and diameter of the air opening behind the rotary apparatus d = 50 mm. The process of burning is simulated for fuel – natural gas, and conditions of a diffusion burning with a coefficient of air surplus α = 1,05. A program, which was composed in the Engineering-Pedagogical Faculty – Sliven, is applied [3]. It has a modifying computing procedure, which enables giving different density of the thermal flow on the borderline of the computing capacity. Three different densities of the thermal flow are accepted: q=107kw/m^2, q=180kw/m^2 and q=0 under adiabatic conditions.

II. NUMERICAL INVESTIGATION

It is known about the influence of the temperature over the speed of the chemical reactions during combustion and burning of a fuel-air mixture [1]. The hot torch is in a dynamic calorific interaction with the surrounding heat-receptive surfaces which defines the conditions of the process of burning.

In conformity with the Theory of spontaneous combustion, the thermal balance in the zone of burning as well as the temperature of the fuel-air mixture defines stability of the process of burning [2]. As far as the industrial combustible devices work under quite different temperature conditions (from thermal furnaces to gas heating apparatuses for invasive liquids), it is of great interest how the temperature in the zone of burning changes under different intensity of heat exchange from the torch towards the heat-exchanged surfaces of the equipment.

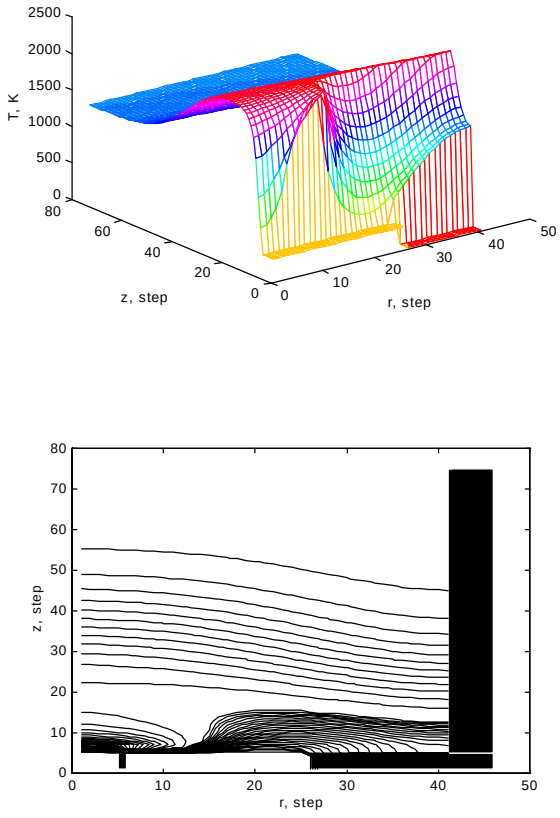

Fig. 1a. A temperature change and isotherms along the length of the combustion chamber at q=0 kW/m^2

[1] Petar St. Kostov – Engineering-pedagogical Faculty – Sliven at Technical university Sofia, No 59 "Burgasko shosse" Bld., 8800 Sliven, Bulgaria

[2] Koycho T. Atanasov – Engineering-pedagogical Faculty – Sliven at Technical university Sofia, No 59 "Burgasko shosse" Bld., 8800 Sliven, Bulgaria, E-mail: katanasov@tu-sliven.com

[3] Neven J. Krystev – Engineering-pedagogical Faculty – Sliven at Technical university Sofia, No 59 "Burgasko shosse" Bld., 8800 Sliven, Bulgaria, E-mail: nkrystev@tu-sliven.com

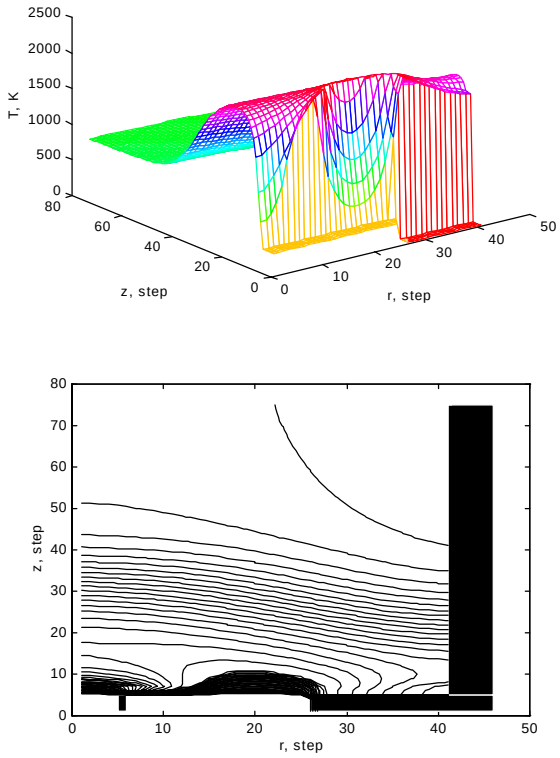

Fig. 1b A temperature change and isotherms along the length of the combustion chamber at q=107 kW/m^2

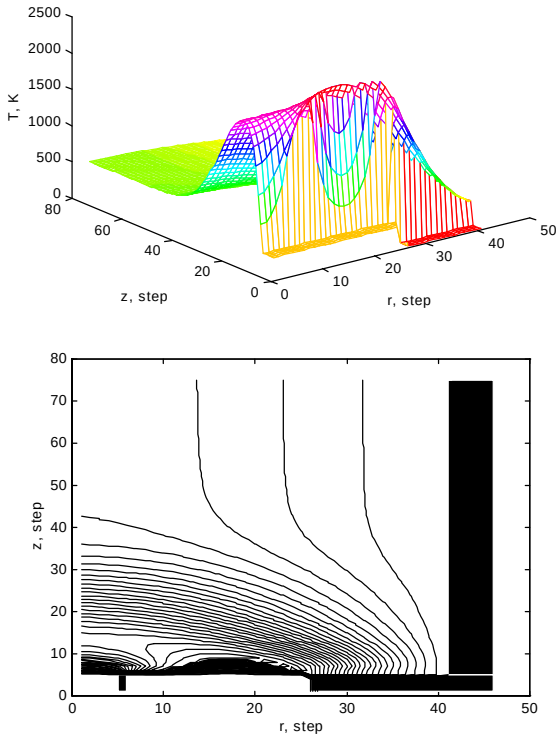

Fig. 1c A temperature change and isotherms along the length of the combustion chamber at q=180 kW/m^2

In the first figure there are images of the temperature surfaces represented, as well as the location of the isotherms along the length of the combustion chamber with different densities of the thermal flow. In the drawings, in the direction of the longitudinal axis of the chamber and on the radius, there are measurements given in a number of computing steps. The value of one step on the radius is 1 mm, and on the axis is 5 mm. The figures show the “deformation” of the temperature fields and the monotony of decreasing the temperature maximum while increasing the thermal flow from the torch towards the walls of the chamber.

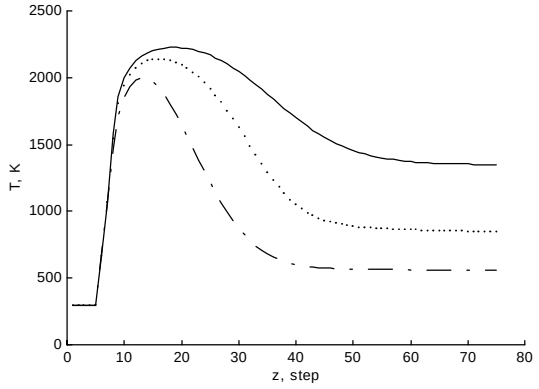

Fig. 2a. A temperature changes on the axis of the combustion chamber

—— - q=0 W/m2; · · · · · - q=107 kW/m2; · - · - · - q=180 kW/m2;

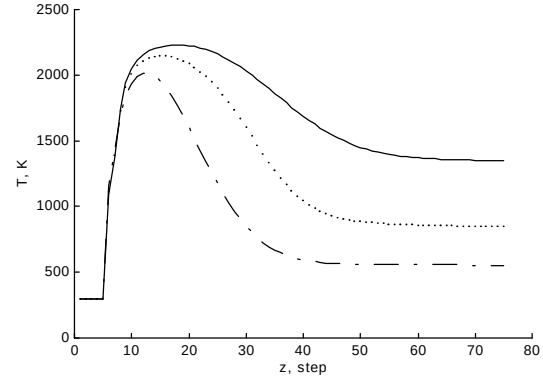

Fig. 2b A temperature changes in a plane at a distance of 5 steps from axis of the combustion chamber.

—— - q=0 W/m2; · · · · · - q=107 kW/m2; · - · - · - q=180 kW/m2;

In the second figure it is depicted the temperature change on the axis of the combustion chamber, as well as in a plane which is at a distance of 5 steps from its axis. The form and the location of the high-temperature zone are quite impressive. With the increase of the density of the thermal flow of the torch, the length and the capacity of the high-temperature zone decrease. At the same very time the temperature maximum goes down too. There is a tendency toward its moving into the beginning of the chamber, where starts the reaction between the fuel and the oxidizer.

The received results demonstrate the possibility to predict the dynamics of burning in the zone of combustion under assigned conditions on the walls of the combustion chamber. They are a precondition for following valuation to parameters, such as completeness of reaction to the fuel, maximum admissible mass output of the fuel-air mixture, as well as noxious emissions in the products of burning [4].

III. INFERENCES

1. Through numerical shaping are received temperature fields in the combustion zone of the torch.
2. With the increase of the density of the thermal flow of the torch, the maximum temperature in the burning zone goes down and the temperature maximum strives for the initial torch sections.
3. It is observed a capacity decrease of the high-temperature nucleus of the torch, which could be a reason for changed emission of the products of burning, and especially of the $N0_x$.

REFERENCES

1. Faler J.H., Leibovich S., The Physics of Fluids, 20 , 9, September, p.138 (1987)
2. Bonev B., Totev T., Combustion of Power Fuels, Publishing House “Kata”, Sofia 2002, p.84
3. Kostov P., Atanasov K., Computer Simulation of the Combustion of Gas Fuel in a Limited Turned Flow, “Energetics” Magazine, issues 6-7, 2002
4. Swithenbank J., Combustion Fundamentals, Report NJS 150, Dept. of Chemical Engineering and Fuel Technology, Sheffield University, England, 1980

Teaching Aspects of Contemporary Reprogrammable Devices

Nikolay I. Ivanov[1] Ivan S. Simeonov[2]

Abstract – **The present paper discusses some aspects of the process of learning the operation with modern re-programmable devices of CPLD and FPGA type. A possibility is shown to use the mathematic notion "algebra" in assembling the learning programme. Some aspects of the programme suggested are discussed.**

Keywords – **Education, Programmable logic, CPLD, FPGA**,

INTRODUCTION

One of the explanations for the great expansion of digital technique in different areas of practice is connected with the use of modern re-programmable devices of CPLD and FPGA type.

The reprogrammable logic structures are in their essence high technology devices that define, form and dictate the tendencies in the development of the basic elements of electronic industry [1]. They possess excluding flexibility, high speed, excellent electromagnetic compatibility, high reliability and low consumed power. The realization of a comparatively not complex project with their help from its idea up to its practical application, which used to take weeks, is now done for hours. All this locates these devices in close proximity to the knowledge and dreams of any person in the field of electronics.

Despite of it, the questions having the attitude to the problems and methods how to teach the nature of these devices, together with their practical application remain not well described. Precondition and caused for this purpose suffices.

The first one is the absence of appropriate literature (in bulgarian), which explains in detail their essence and removes the psychological barrier about the practical use of the re-programmable devices. The second one is the lack of suitable methodology for their teaching. The third one is the insufficient attention paid to problems connected with the technological specifics implied by these devices use.

By itself the decision of these problems is rather simple.

The solution of the problems thus set is simple. It is expressed in the discovery of a form that will unite and control the process of teaching in operation with re-programmable devices, independently on their essence(digita or analog) or kind (CPLD or FPGA) type. This solution, no matter how strange, is found and offered by mathematics, in one of its basic notions – the notion "algebra". It exists thanks to indisputable logic, which enables the introduction of the abstract branches of modern mathematics in different areas of knowledge. Hence the question whether it is possible to use this notion in re-programmable devices area, is logical. Our answer to this question is firm and unambiguous - yes.

TEACHING ACCENTS

The notion algebra can be regarded in the general case as a triple of objects, including a set of elements, a set of rules for action with the elements and a set of constraints. The practical application of this notion for the purposes of teaching in the area of re-programmable devices defines accents on three objects:

Elements basis;

Rules of action with the elements basis;

Constraints concerning the features of the elements basis.

Some devices of CPLD and FPGA families of Xilmix are appropriate for use as elements basis in teaching. The main motive for this orientation is their easy accessibility, attractive price and user-friendly environment.

The rules of action with the elements basis are dictated and defined by the characteristics of the developing environment. In this particular case we are oriented towards the integrated environment Web Pack 6.1 of Xilmix. At the first stage of teaching, when some main notions and concepts of the re-programmable devices are introduced, our

[1]Institute of Information Technologies BAS, acad. Georgi Bonchev street bl. 2,Sofia 1113,Bulgaria,
e-mail ivanovnikolay@hotmail.com

[2] Technical University Gabrovo, H. Dimitar street 4, Gabrovo 5300, Bulgaria
E-mail isim@mail.bg

preferences are connected with the application of a built-in schematic editor. Its accepting by the learners is of particular importance not only at the first stages of teaching, but also afterwards, when the functional connections of hierarchical and complex architectures are created.

The constraints, connected with the elements basis include all the features that can appear in the practical realization of a system with these devices. This category includes phenomena of the type parasite capacities, inference between channels, etc. Their incorporating in the lectures horrarium enables the direct connection with a number of other disciplines such as physics, electro techniques, signals theory, etc. Moreover, accounting the high speed of these devices, the surrounding logistic environment starts to play strong, and in some case dominating role. This defines the necessity to teach in parallel the discipline electronic apparatus construction and automation of the engineering job (circuit boards design). These considerations lie on the fact that the printed circuit board today is already not just a tool for mechanic mounting of the electronic components. Their location on the circuit board is not an exercise in topology, but a complicated problem requiring the solution of problems connected with amplitude and phase distortion, reflections, temperature modes, ways of elements mounting, etc.

The information concerning every of the directions above mentioned is presented in a graphical and tabular form in the teaching process. Due to the absence of a corresponding Bulgarian expression, word or notion, or in order to avoid any inaccuracy in the translation, the corresponding information is provided at many places in English. This will be a difficulty for everyone new in this area, but future doctors have to study Latin for a similar reason.

In order to enable the learners clear up the theoretic knowledge obtained in the area of modern re-programmable devices and also to develop their design abilities, several modifications of the apparatus tools have been developed (called kits). They are separated in several groups and allow the detail study of the properties of separate CPLD and FPGA devices.

The first kit enables the design of small, not complex projects with the help of CPLD devices of XC9500 series and Cool Runner-XPLA3. Their comparatively not high price enables wide access to a large group of users in and out of the University. The second group of kits is intended for students in a higher course of teaching. It is oriented towards CPLD devices from CoolRunner II series and allows the most complete and exact investigation, learning and application of all characteristics, realized at apparatus level. The third group of kits is intended for students in the last courses. It is oriented towards FPGA devices of Spartan II series and enables the investigation of software systems like Picoblase and Microblase, which is the first step towards the practical learning of the process of built-in systems design (SoC).

CONCLUSION

We believe that the model thus presented for constructing a system for learning the operation with re-programmable devices may be realized on the basis of an apriori built sequence of stages [4]. These stages are: organization, information, interface and product. Each one of them is a ranked hierarchical sequence of different sub-stages in the design of every system for electronic teaching [5]. It is appropriate to use the so-called flow diagrams and the step model of the flow diagram when constructing the suggested model for re-programmable devices teaching. The implementation of these stages and of the flow diagram will enable the direct transfer of the model to the sphere of distant Web-based learning.

REFERENCES

[1] Ivanov, N. CPLD – yesterday, today and tomorrow. IIT Working papers, IIT/WP-116B, November, 2001 (in Bulgarian).
[2] Ivanov, N. Modern re-programmable devices. Sofia, Anubis, 2002 (to be printed, in Bulgarian).
[3] Labunets, V. G. Algebraic theory of Signals and Systems. Izdatelstvo Krasnoiarskogo universiteta, Krasnoiarsk, 1984 (in Russian).
[4] Monov K. Ch., I. S. Simeonov. Modeling and construction of a multimedia script of a system for distance e-learning on “Analysis and Synthesis of Logic Circuits”. Advanced Control Theory and Applications, June 16 – 29, Plovdiv – Gabrovo, Bulgaria, 2003, pp. 119-123.
[5] Dette, K., Multimedia und Computeranwendungen in der Lehre, Springer Verlag, 1992.

AUTHOR INDEX